Synthesis and Analytics of Rigidified Peptide Architectures

Neuropeptide Y Dipeptide Scan

Ring-Chain-Equilibria of Iminopeptides

Thiazole Amino Acids for Thiopeptide Antibiotics

———

Synthese und Analytik fixierter Peptidarchitekturen

Dipeptid-*Scan* am Neuropeptid Y

Ring-Kette-Gleichgewichte von Iminopeptiden

Thiazol-Aminosäuren für Thiopeptid-Antibiotika

Dissertation

zur Erlangung des Doktorgrades

der Naturwissenschaften

(Dr. rer. nat.)

dem

Fachbereich Chemie

der Philipps-Universität Marburg

vorgelegt von

Sebastian Enck

aus München

Marburg / Lahn 2010

Vom Fachbereich Chemie

der Philipps-Universität Marburg als Dissertation angenommen am 16.07.2010.

Erstgutachter: Herr Prof. Dr. Armin Geyer

Zweitgutachter: Herr Prof. Dr. Mohamed A. Marahiel

Tag der mündlichen Prüfung am 13.08.2010.

Dedicated to my mother († 12/04/2000)

The experimental work described in this thesis was performed from August 2006 to June 2010 at the Department of Chemistry, Philipps-Universität Marburg.

I owe special thanks to

Prof. Dr. Armin Geyer

for his generous support of my Ph.D. thesis and the excellent scientific guidance, allowing me to work on several exciting projects with great flexibility.

“Wine?“

Feeb E. in *Guest House Paradiso*, 6th scene

“There are three stages of scientific discovery:

first people deny it is true;

then they deny it is important;

finally they credit the wrong person.”

Alexander von Humboldt

Abstract

The functional spectrum of naturally occurring peptides encompasses the role as hormones, neurotransmitters and as chemical warfare agents utilized by microorganisms for the purpose of defending their respective ecological niche. The action of peptide ligands relies on the interaction with binding partners by which a certain biological signal is triggered or inhibited. In order to be able to perform its dedicated task a peptide must exhibit a high affinity to a certain binding partner. This must occur with a minimum extent of selectivity, which means that binding to other partners (and, thereby, further biological effects) has to be excluded. These properties depend on the structure of the peptide, which in other words is the specific alignment of certain functional units. It is the rigidification of a structure in its biologically active conformation which is a key to the generation and enhancement of biological activity and selectivity.

In principle, there are three possibilities for the fixation of a molecular structure. By the formation of small rings local rigid structural motifs are generated, whereas macrocyclizations restrict the global flexibility. Finally, various examples are found in nature in which these both strategies are combined. Each of the three chapters of this thesis deals with one of these three options, thereby addressing questions that concern the analysis of rigid peptide structures and their preparation by chemical synthesis.

In the first chapter a novel scanning technique is described which by the incorporation of a rigid bicyclic dehydroalanine-thiaproline dipeptide (Dha=Tap) effects a local fixation of the peptide backbone and thus enables its structural analysis. The denotation "=" indicates the fixation of the backbone by a second covalent bond. The method was tested with Neuropeptide Y (NPY), a linear peptide whose various functions in the human organism result from its multiple receptor affinity. To understanding and control these binding processes is prerequisite for the development and application of therapeutic NPY analogs. In cooperation with the *Beck-Sickinger* group (University of Leipzig) a series of NPY analogs with systematically varied Dha=Tap single-, double-, and triple substitutions was examined with respect to the receptor binding properties. This enabled for the first time to identify trends in the receptor affinities and selectivities which depend on the number and the exact positions of the substitutions. For a series of NPY analogs, detailed structural studies were undertaken using NMR spectroscopy in the presence of a membrane mimetic. These investigations demonstrated the excellent applicability of the Dha=Tap unit as NMR label for structure elucidation and to determine details of the membrane coordination of a peptide.

The second part of this work deals with the thermodynamic characterization of macrocyclizations. The inclination of a linear precursor to form the corresponding macrocycle is dependent on its preferred conformations, but no details of the structural prerequisites are known, which is why one has to rely on empirical or computational data for the planning of this challenging synthetic step. Furthermore, no methodical approach exists which deals with this process and which quantifies the loss of flexibility of a peptide chain upon macrocyclization. A solution to this problem is given by peptides which macrocyclize by forming a reversible carbonyl bond and which thereby enable a thermodynamic analysis. In cooperation with the *Marahiel* group it was possible to quantify the pH- and temperature dependence of the ring-chain equilibria of various naturally occurring and synthetically modified iminopeptides. This allowed to identify structural determinants for the formation of a macrocycle as well as the first quantification of the entropy balance of such processes.

The third research project of this thesis encompassed the development of a novel synthetic strategy towards highly functionalized thiazole dipeptides. Thiazoles are generated by the cyclization of a Cysteine side chain with the N-terminally adjoining backbone amide and for example occur in the thiopeptide antibiotics. These natural products constitute complex three-dimensional peptide networks, and their high toxicity against microorganisms bases on the combination of macrocyclic structures and several thiazoles in the backbone. An efficient synthetic access towards the thiopeptide thiazole dipeptides which are linked up to four-fold to the backbone and which in addition carry a glycosylation site is the prerequisite for the total synthesis of these last-resort antibiotics and for the generation of analogs thereof. In the present work, a synthetic approach was developed which bases on condensation products of uronic acids and Cysteine and which enables a few-step stereoselective synthesis of polyhydroxylated thiazole depsidipeptides. Finally, by *N*/*O*-exchange a first synthetic pathway was established to the (2*S*,3*S*,4*S*)-dihydroxyglutamate dipeptide which constitutes the central linking motif in the nocathiacin and thiazomycin antibiotics. In addition, directed side chain functionalizations also allowed to obtain epimers and homologs of this compound.

Zusammenfassung

Die funktionelle Bandbreite natürlich vorkommender Peptide umfasst den Einsatz als Hormone, als Neurotransmitter sowie als Mittel zur biologischen Verteidigung, mit welcher sich Mikroorganismen ihre Existenz in der jeweiligen ökologischen Nische sichern. Die Wirkung von Peptidliganden beruht auf der Wechselwirkung mit Bindungspartnern, wodurch ein bestimmtes biologisches Signal ausgelöst oder inhibiert wird. Um seine spezifische Aufgabe erfüllen zu können, muss ein Peptid folglich eine ausreichend hohe Affinität zu einem bestimmten Bindungspartner besitzen. Dies muss mit einem Mindestmaß an Selektivität verbunden sein, was bedeutet, dass andere Bindungspartner (und damit unerwünschte weitere biologische Wirkungen) ausgeschlossen werden. Diese Eigenschaften werden durch die Struktur des Peptids – die spezifische Ausrichtung bestimmter funktioneller Einheiten – kontrolliert. Der Schlüssel zur Generierung und Erhöhung biologischer Aktivität und Selektivität beruht dabei auf der Rigidifizierung einer Struktur in ihrer biologisch aktiven Konformation.
Für die Fixierung einer molekularen Struktur bestehen drei grundsätzliche Möglichkeiten. Durch die Bildung kleiner Ringe werden lokale rigide Strukturmotive gebildet, wohingegen Makrocyclisierungen die globale Beweglichkeit einschränken. Schließlich findet man in der Natur auch viele Beispiele, in welchen diese beiden Strategien kombiniert werden. Jedes der drei Kapitel dieser Arbeit befasst sich mit einer dieser Varianten in Fragestellungen, welche auf die Analyse rigider Peptidstrukturen sowie auf ihre Herstellung durch chemische Synthese eingehen.

Das erste Kapitel beschreibt eine neuartige *scanning*-Methode, welche eine systematische lokale Rigidifizierung des Peptidrückgrats bewirkt und dessen Strukturanalyse ermöglicht. Dies geschieht durch den Einbau eines starren bicyclischen Dehydroalanin-Thiaprolin-Dipeptids (Dha=Tap; das Symbol "=" kennzeichnet die lokale Fixierung durch das doppelte Rückgrat des Bausteins). Getestet wurde das Verfahren am Neurotransmitter Neuropeptid Y (NPY), einem linearen Peptid, dessen vielfältige Funktionen im menschlichen Organismus aus seiner multiplen Rezeptoraffinität resultieren. Das Verstehen und die Kontrolle dieser Bindungsvorgänge ist Voraussetzung für die Entwicklung und Anwendung therapeutischer NPY-Analoga. In Kooperation mit der Arbeitsgruppe *Beck-Sickinger* (Universität Leipzig) wurde eine Reihe von NPY-Analoga mit systematisch variierter Dha=Tap-Einfach-, Zweifach- und Dreifachsubstitution am bisher kaum untersuchten N-Terminus bezüglich ihrer Bindungseigenschaften und Struktur charakterisiert. Dabei konnten erstmalig Trends in der Rezeptoraffinität und -selektivität festgestellt werden, welche von der Anzahl und der genauen Position der Substitutionen abhängen. Für eine Reihe von NPY-Analoga wurden detaillierte Strukturuntersuchungen mittels

NMR-Spektroskopie in Gegenwart eines Membranmimetikums durchgeführt, welche die hervorragende Eignung des Dha=Tap-Bausteins als NMR-Label zur Bestimmung der Struktur und der genauen Koordination des Peptids an die Membran zeigten.

Im zweiten Teil der Arbeit werden Macrocyclisierungen hinsichtlich ihrer thermodynamischen Charakterisierung behandelt. Wie gut ein linearer Vorläufer einen Macrocyclus bildet, hängt von dessen Vorzugskonformationen ab, doch die genauen strukturellen Voraussetzungen sind unbekannt, weshalb man sich in der Planung dieses anspruchsvollen Syntheseschritts auf empirische Daten verlassen muss. Ebensowenig existiert ein methodischer Ansatz, welcher die Thermodynamik dieses Prozesses behandelt und den damit verbundenen Verlust an Beweglichkeit der Peptidkette quantifiziert. Eine Lösung zu diesem Problem stellen Peptide dar, deren Macrocyclen über eine reversible Carbonylbindung geschlossen werden und welche deshalb eine thermodymanische Analyse erlauben. In Kooperation mit der Arbeitsgruppe *Marahiel* gelang es, mittels NMR-Spektroskopie die pH- und Temperaturabhängigkeit von Ring-Kette-Gleichgewichten verschiedener natürlicher und synthetisch modifizierter Iminopeptide zu quantifizieren. Dies erlaubte die Identifizierung struktureller Voraussetzungen für die Bildung eines Macrocyclus sowie die erstmalige Bestimmung der Entropiebilanzen derartiger Prozesse.

Als drittes bearbeitetes Forschungsprojekt wurde eine neuartige Synthesemethode zu hochfunktionalisierter Thiazol-Dipeptiden erschlossen. Thiazole werden durch Cyclisierung von Cystein-Seitenketten mit der nächsten N-terminalen Rückgrat-Amidbindung gebildet und finden sich beispielsweise in den Thiopeptid-Antibiotika. Diese Naturstoffe stellen komplexe dreidimensionale Peptidnetzwerke dar, und ihre hohe Toxizität gegenüber Mikroorganismen ist in der Kombination macrocyclischer Strukturen und mehrerer Thiazole im Rückgrat begründet. Ein effizienter synthetischer Zugang zu den in den Thiopeptiden enthaltenen Thiazol-Dipeptiden, welche bis zu vierfach mit dem Rückgrat verknüpft und zusätzlich glycosyliert sind, ist Voraussetzung für die Totalsynthese dieser *last resort*-Antibiotika und für die Generierung von Analoga. In der vorliegenden Arbeit wurde ein Syntheseansatz entwickelt, welcher, ausgehend von Kondensationsprodukten aus Uronsäuren und Cystein, in wenigen Stufen den stereoselektiven Aufbau polyhydroxylierter Thiazol-Depsidipeptide ermöglicht. Weiterhin wurde durch *N*/*O*-Austausch ein erster Synthesezugang zum (2*S*,3*S*,4*S*)-Dihydroxyglutamin-Thiazol-Dipeptid entwickelt, welches das zentral verknüpfende Motiv der Nocathiacin- und Thiazomycin-Antibiotika darstellt. Durch gezielte Seitenkettenmodifikationen sind außerdem epimere und homologe Verbindungen zugänglich.

State of publication

A part of the work presented here has been published:

- Michael Haack, **Sebastian Enck**, Harald Seger, Armin Geyer*, Annette G. Beck-Sickinger*:

  Pyridone Dipeptide Backbone Scan to Elucidate Structural Properties of a Flexible Peptide Segment.

  Journal of the American Chemical Society **2008**, *130* (26), 8326–8336.
  DOI: 10.1021/ja8004495

- **Sebastian Enck**, Florian Kopp, Mohamed A. Marahiel*, Armin Geyer*:

  The Entropy Balance of Nostocyclopeptide Macrocyclization Analysed by NMR Spectroscopy.

  ChemBioChem ***2008***, *9* (16), 2597–2601.
  DOI: 10.1002/cbic.200800314

- **Sebastian Enck**, Florian Kopp, Mohamed A. Marahiel*, Armin Geyer*:

  The Reversible Macrocyclization of Tyrocidine A Aldehyde: A Hemiaminal Reminiscent of the Tetrahedral Intermediate of Macrolactamization.

  Organic and Biomolecular Chemistry ***2010***, *8* (3), 559–563.
  DOI: 10.1039/b917549k

Table of contents

Abbreviations

[m=n]	pNPY with Dha=Tap substitution at positions m and n
1D/2D/3D	one-/two-/three-dimensional
4-MePro	(2*S*,4*S*)-methylproline
A	adenylation domain (NRPS)
Å	Ångström
abs	absolute
Ac	acetyl
Ac_2O	acetic acid anhydride
AcOH	acetic acid
Ahx	6-aminohexanoic acid
Aib	aminoisobutyric acid
All	allyl
aPP	avian pancreatic polypeptide
aq.	aqueous
Ara	D-arabinurono-
Bn	benzyl
BnOH	benzyl alcohol
Boc	*tert*-butyloxycarbonyl
br s	broad singlet (NMR)
b.r.s.m.	based on recovered starting material
$BrCCl_3$	bromotrichloromethane
C	condensation domain (NRPS)
cal	calories
CD	circular dichroism spectroscopy
$CDCl_3$	deuterochloromethane
CH_2Cl_2	dichloromethane
CH_3CN	acetonitrile
$CHCl_3$	chloroform
CoA	coenzyme A
COSY	COrrelated SpectroscopY
CSA	camphorsulfonic acid
Cy	heterocyclization domain (NRPS)
cycl	cyclic
d	day(s) / dublet (NMR)
DBU	1,8-diazabicyclo[5.4.0]undec-7-ene
dd	dublet of dublets (NMR)
ddd	dublet of dublets of dublets (NMR)
DEAD	diethylazodicarboxylate
Dha	dehydroalanine
Dha=Tap	dehydroalanine-thiaproline bicyclic dipeptide
DHPC	dihexanoylglycerophosphatidylcholine
DIAD	di-*iso*-propylazodicarboxylate
DIPEA	ethyl-di-*iso*-propylamine
DMAP	4-*N*,*N*-dimethylaminopyridine
DME	1,2-dimethoxyethane
DMF	*N*,*N*-dimethylformamide
DMP	2,2-dimethoxypropane
DMPC	dimyristylglycerophosphatidylcholine
DMSO	dimethyl sulfoxide

DMSO-d_6	hexadeutero dimethyl sulfoxide
DPC	dodecylphosphocholine
DPC-d_{25}	dodecylphosphocholine, perdeuterated
DPFGSE	Double Pulsed Field Gradient Spin Echo
dpt	dublet of pseudo triplets (NMR)
Dyg	2,3-dihydroxyglutamate
E	epimerization domain (NRPS)
eq	equivalent(s)
ESI-MS	electron spray ionization - mass spectrometry
Et	ethyl
et al.	and others (lat. *et alii*, *et aliae*)
Et_3N	triethylamine
EtOAc	ethyl acetate
EtOH	ethanol
Fmoc	9-fluorenylmethyloxycarbonyl
FRET	fluorescence resonance energy transfer
g	gram(s)
G	free energy
GFP	green fluorescent protein
gg	*gauche*/*gauche* (rotamer)
Glc	D-glucurono-
GPCR	G-protein coupled receptor
gt	*gauche*/*trans* (rotamer)
h	hour(s)
H	enthalpy
H_2SiF_6	hexafluoro silicic acid
$HC(OEt)_3$	triethyl orthoformate
HCOOH	formic acid
HEC-1-B hY_5	human endometrial adenocarcinoma cell line, expressing the NPY Y_5 receptor
HEPES	2-N'-[N-(2-hydroxylethyl)-piperazinyl]-ethanesulfonic acid
HMQC	Heteronuclear Multiple Quantum Coherence
hNPY	human Neuropeptide Y
HOBt	1-hydroxybenzotriazole
HPLC	high-performance liquid chromatography
hPP	human pancreatic polypeptide
HSQC	Heteronuclear Single Quantum Coherence
hY_n	human NPY receptor, subtype n (n = 1-5)
Hz	Hertz
IBX	2-iodoxybenzoic acid
*i*Pr	*iso*-propyl
*i*PrOH	*iso*-propyl alcohol
J	Joule
J	spin-spin coupling (NMR)
K	Kelvin / equilibrium constant
KHMDS	potassium tris(trimethylsilyl)amide
lin	linear
LP	leader peptide
m	minutes / multiplet (NMR)
M	molar
MARS	membrane-assisted receptor selection

MAS-NMR	magic angle spinning nuclear magnetic resonance
mccB17	microcin B17
MeI	methyl iodide
MeOH	methanol
min	minute(s)
MnO_2	manganese dioxide
MOM	methoxymethyl
MPR	2-methoxypropene
Ms	methanesulfonyl-
ms	milliseconds
NADPH	nicotinamide adenine dinucleotide phosphate
$NaIO_4$	sodium periodate
NaOMe	sodium methanolate
ncp	nostocyclopeptide
NiO_2	nickel dioxide
NMM	N-methylmorpholine
NMR	nuclear magnetic resonance
NOE	nuclear Overhauser enhancement
NOESY	Nuclear Overhauser Enhancement SpectroscopY
NPY	Neuropeptide Y
NRPS	non-ribosomal peptide synthethase
Ox	oxidation domain (NRPS)
PCP	peptidyl carrier protein (NRPS)
Pd/C	palladium on charcoal
PDB	protein data bank (file); www.pdb.org
PEG	polyethyleneglycol
PG	protecting group
Ph	phenyl
pNPY	porcine Neuropeptide Y
PP	pancreatic polypeptide
ppb	parts per billion
PP-fold	pancreatic polypeptide tertiary structure
PPh_3	triphenylphosphane
PPII	polyproline-II(-helical)
PS	polystyrol
pt	pseudotriplet (NMR)
*p*TosOH x H_2O	*para*-toluene sulfonic acid monohydrate
PyBOP	benzotriazole-1-yl-oxy-tris-pyrrolidino-phosphonium hexafluorophosphate
Pyr	pyridine
PYY	YY (Tyr-Tyr) peptide
R	residue / reductase domain (NRPS)
RB	rotatable bond(s)
RDF	rotational degree(s) of freedom
ref.	reference
res.	residue (amino acid)
Rib	D-riburono-
ROE	rotating frame nuclear Overhauser enhancement
ROESY	Rotating frame Overhauser Enhancement SpectroscopY
RT	room temperature / retention time (HPLC)
s	second(s), singlet (NMR)

S	entropy
SC	side chain
SDS	sodium dodecylsulfate
SDS-d_{25}	sodium dodecylsulfate, perdeuterated
SegA	Segetalin A
SK-N-MC hY_1	human neuronal epithelium cell line, expressing the NPY Y_1 receptor
SPPS	solid-phase peptide synthesis
t	time / triplet (NMR)
T	temperature
Tap	thiaproline
TBAF	tetrabutyl ammonium fluoride
TBS	*tert*-butyldimethylsilyl-
tert	tertiary
TES	triethylsilyl
Tf	trifluoromethanesulfonyl
TFA	trifluoroacetic acid
TFAA	trifluoroacetic acid anhydride
tg	*trans*/*gauche* (rotamer)
THF	tetrahydrofuran
Thz	thiazole
TLC	thin layer liquid chromatography
TMS	trimethylsilyl-
TOCSY	TOtal Correlation SpectroscopY
Tol	toluene
TPP	thiamine pyrophosphate
Ts	*para*-methylphenylsulfonyl-
Tuv	tubuvaline
TycA	tyrocidine A
Tyh	trihydroxy-homoglutamate
UV	ultraviolet
vs.	versus
WATERGATE	WATER suppression by GrAdient Tailored Excitation
Xaa	any amino acid
Xaa<Thz	dipeptide consisting of any amino acid and a thiazole
Y_n	NPY receptor, subtype n (n = 1-5)

1 Research scope: The role of structure rigidification in nature and chemistry

In spite of the size differences between technical machines and functional molecules, they exhibit similarities with respect to their modes of action. In both cases, the function is enabled by the controlled movement of intertwining parts. The single components and their linkages must exhibit a flexibility which allows the required motions, but as only specific motions are required, this flexibility must not be too high. The prerequisite of an adequate rigidity also plays a role in evolutionary processes. According to the induced-fit model, a molecular ligand and its dedicated receptor have to structurally accommodate to each other. The more the bioactive conformation is already stabilized in the unbound ligand, the higher will be its binding affinity and selectivity towards a single receptor.

In the case of polypeptides, which are among the most important classes of natural products, several biosynthetic strategies have been established by which the overall rigidity is tuned. This can be exemplarily demonstrated by the nocathiacin/thiazomycin thiopeptides shown in figure 1.1. On the one hand, local restraints are introduced by the formation of small rings, for example thiazoles (highlighted in blue) which lock single torsions along the backbone. On the other hand, a global restriction of molecular flexibility is obtained by the formation of macrocycles (highlighted in red). Especially if combined with each other, these structural modifications are an important source of biological activity and selectivity of lower-molecular weight substrates, and they are indispensable tools in medicinal chemistry and analytics.

This thesis deals with such rigidified peptidic architectures in three topics which are aimed at the synthesis and structural analysis of biologically relevant peptides. In figure 1.1, the synthetic modifications are demonstrated by an exemplaric Gly-Ala-Pro tripeptide, and they are related to the three sets of problems. One topic deals with the introduction of structural information by artificial rigid dipeptides to Neuropeptide Y (chapter 2). These systematic substitutions should enable conformational analysis and elucidation of topological prerequisites for the binding to different receptor subtypes. The second research project of the thesis concerns another option of synthetic chemistry which is the specific variation of functional groups. The substitution of an amide tether by a reversibly formed imine is key to the thermodynamic characterization of the fundamental macrocyclization process (chapter 3).

The synthetic access to natural products can be the bottleneck to structural analyses and modifications for potential therapeutic use, and this is the case for the complex nocathiacin/ thiazomycin thiopeptide antibiotics. This thesis deals with a synthetic pathway to highly functionalized thiazole peptides as they are present in this natural product class (chapter 4).

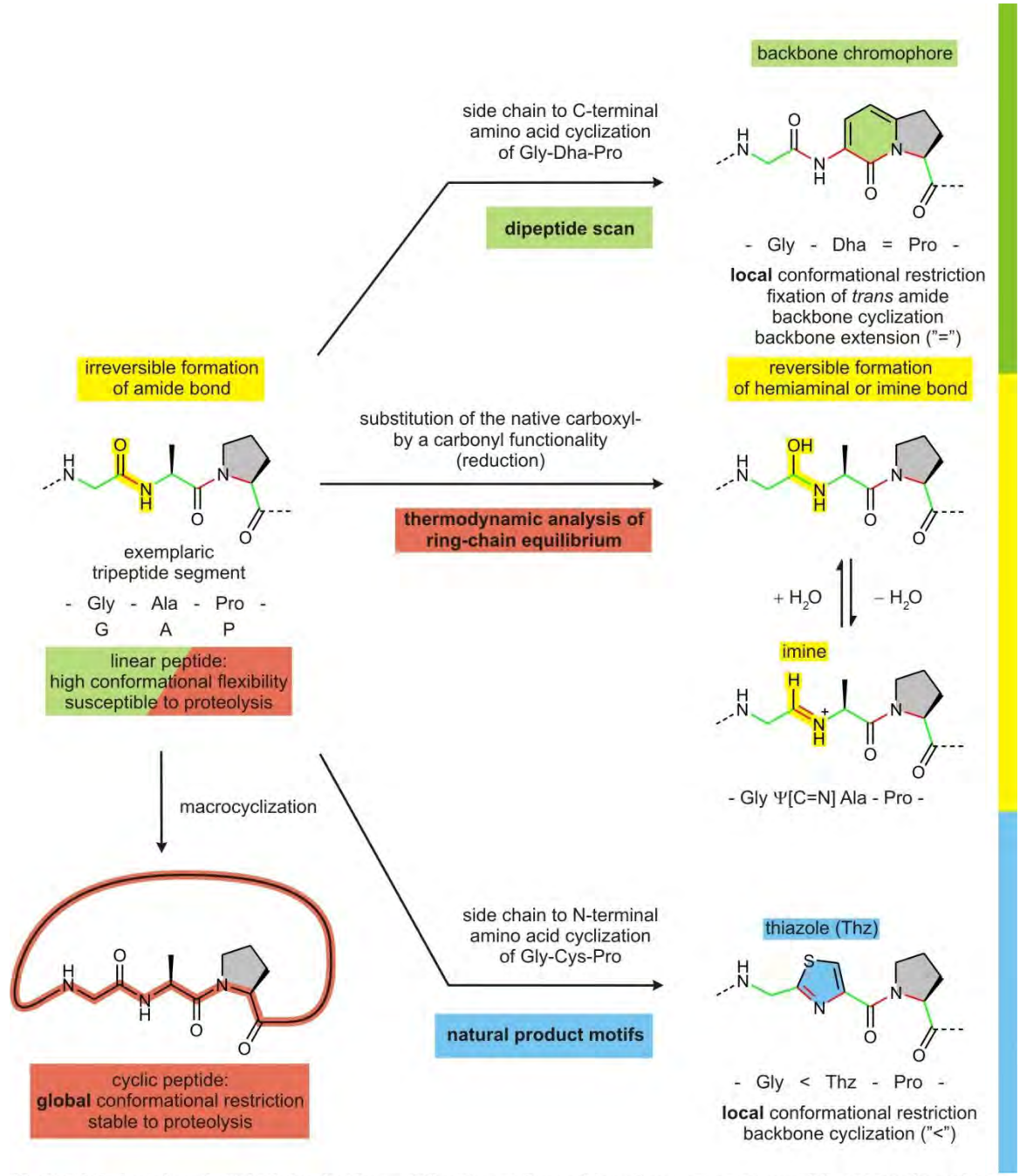

Figure 1.1 Local and global synthetic modifications of peptides give access to peptidic natural products and are the prerequisite for their structural and functional analysis. *The Gly-Ala-Pro tripeptide shown on the left contains the three differently flexible types of proteinogenic amino acids. The Gly lacks any side chain and is more flexible than Ala, and the pyrrolidine ring present in Pro (grey) fixes the ϕ torsion. All rotatable backbone torsions are marked in green and fixed torsions are highlighted in red. To obtain an overall (global) rigidification of a linear peptide it can be macrocyclized by a covalent tether between both termini (marked in red, left). On the right, local modifications which are the subject of this thesis are shown, with the colored bars indicating the three different research projects that are described in section 2, 3, and 4, respectively. On the next page, the respective research topics are indicated.*

For the analysis of Pro-rich peptide segments, structural information can be incorporated by a dehydroalanine (Dha, highlighted in green) as part of a dipeptide building block which extends the backbone by a second linkage (indicated by “=”). Systematic substitutions enable a novel backbone scan which was applied to the N-terminus of Neuropeptide Y. Selected analogs were structurally analyzed by NMR, and the full series was examined with respect to receptor affinities and selectivities (chapter 2).

These structural simplifications are in contrast to the introduction of more complexity (substitution of amides by reversibly formed functionalities) required for the examination of peptide macrocyclizations.

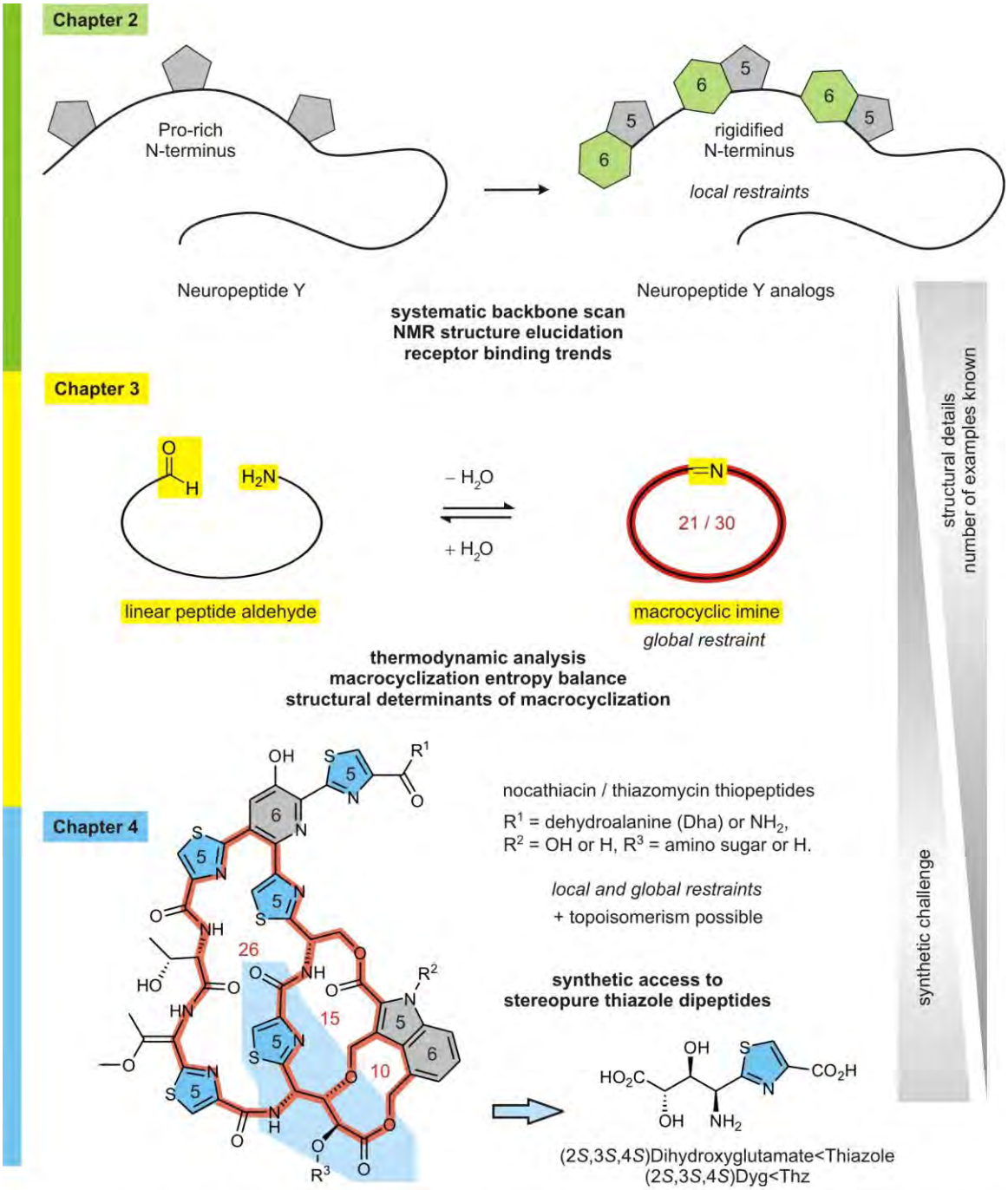

The stability of peptides in aqueous solution is related to the amide bond (yellow) which is formed irreversibly, and this feature has so far foreclosed thermodynamic analyses of peptide macrocyclizations. Substitution of the carboxyl functionality by its carbonyl analog does not effect structural changes, but the imino/hemiaminal linkage differs from the amide by its reversible formation in aqueous solution. If this leads to an observable and controllable equilibrium between the linear peptide (an ω-amino aldehyde) and its cyclic analog, this macrocyclization process can be analyzed thermodynamically (chapter 3).

While the backbone extension by a fused dehydroalanine (chapter 2) is only accomplished by chemical synthesis, the condensation of a Cys side chain with the adjacent N-terminal amide is widely applied in the biosynthesis of thiazoles (blue). This local conformational restriction fixes the Cys ϕ torsion (indicated by "<"). Thiazoles are important structural elements for example in the thiazomycin antibiotics which exhibit complex polycycles containing small, medium, and large rings. As the chemical synthesis of thiazole amino acids is problematic and as important motifs like the dihydroxyglutamate<thiazole dipeptide are not accessible by chemical synthesis yet, the third research topic comprised synthetic studies that aim to find an access to stereopure polyhydroxylated thiazole amino acids (chapter 4).

2. Establishing a Dha=Tap backbone scan in order to elucidate structural properties of the N-terminus of NPY

2.1 Introduction. A seemingly endless conundrum: understanding and controlling the receptor promiscuity of NPY

As one of the most abundant neurotransmitters in the human brain, neuropeptide Y (NPY) stands out by its ability to regulate various physiological processes by binding to several receptors. The evolutionary success of such a compound, which means the long-time defeating of numerous competitors, can only be explained by a superb physiological profile which makes it an indispensable part of the organism's metabolism. However, as vital as the roles of NPY obviously are, as difficult it turned out to shed light onto them. Since its discovery in 1982[1] this inconspicuous peptide has both fascinated and frustrated researchers due to its complex modes of action. Far from being completely understood after almost three decades of intensive studies, the roles of NPY have been extensively reviewed[2, 3] and due to the great complexity and amount of data, only a rough look at the "*universal soldier*"[3] NPY can be given here.

2.1.1 The NPY family

The NPY family (table 2.1) exhibits a group of physiologically relevant peptides which are present in vertebrates. All peptides have in common a sequence length of 36 amino acids and a C-terminal amidation. According to their sequences and physiological roles, the members can be classified into three groups.[2] From 20 different species of vertebrates, YY peptides (PYY) have been isolated which share sequential identity of at least 42%.[4] The term "YY" refers to the presence of tyrosine (Y) residues at the N- and C-terminus, a characteristic which is common to most of the NPY family members. From the group of pancreatic polypeptides (PP) more than 30 members are known, with a minimal identity of 20%. The PYY and PP members all act as hormones, a fact which distinguishes them from the third group of the neuropeptides Y (NPY) playing central roles as neurotransmitters. In fact, these peptides are among the most abundant neurotransmitters in the mammalian brain and the peripheral nervous system. Table 2.1 shows the sequences of selected members of each group, with conserved positions indicated by green letters. The residues Pro^{5}, Pro^{8}, Gly^{9}, Ala^{12}, Tyr^{27}, Arg^{33} and Arg^{35} have been found to be present in all members of the family, and the Y in NPY refers to the C-terminal tyrosine (Y) present in all of the 15 NPY analogs isolated to date. However, beyond that, more than 61% of the sequence is identical, which is why the NPY analogs hold the world record as the most conserved peptides

Table 2.1 Some members of the NPY family as present in different species.

peptide	acronym	sequence
porcine Neuropeptide Y	pNPY	YPSKPDNPGEDAPAEDLARYYSALRHYINLITRQRY-NH_2
human Neuropeptide Y	hNPY	YPSKPDNPGEDAPAEDSARYYSALRHYINLITRQRY-NH_2
Neuropeptide Y of *torpedo marmorata*		YPSKPDNPGEGAPAEDLAKYYSALRHYINLITRQRY-NH_2
porcine peptide YY	pYY	YPAKPEAPGEDASPEELSRYYASLRHYLNLVTRQRY-NH_2
avian pancreatic polypeptide [crystal structure: see figure 2.3]	aPP	GPSQPTYPGDDAPVEDLIRFYDNLQQYLNVVTRHRY-NH_2

Table 2.2 The cloned NPY receptor subtypes Y_1-Y_5.

Receptor subtype	Binding affinities	Localization	Physiological effects
Y_1	NPY ✓ PYY ✓ PP ✗	Brain Heart Kidneys Gastrointestinal tract	Vasoconstriction Anxiolysis Ethanol resistance Food intake
Y_2	NPY ✓ PYY ✓ PP ✗	Central nervous system, especially Hippocampus Sympathic and para-sympathic nerve fibres	Signaling: cAMP accumulation Norephedrine and Glutamate release suppression Cardial vagal action
Y_3	NPY ✓ PYY ✗ PP ✗	Neurons in *nucleus tractus solitarius* Brainstem	Inhibition of Catecholamine release Arterial blood pressure
Y_4	NPY ✗ PYY ✗ PP ✓	Colon Small intestine Prostate Pancreas	Inhibition of pancreatic secretion Gall bladder contraction
Y_5	NPY ✓ PYY ✓ PP ✗	Hypothalamus	Food intake

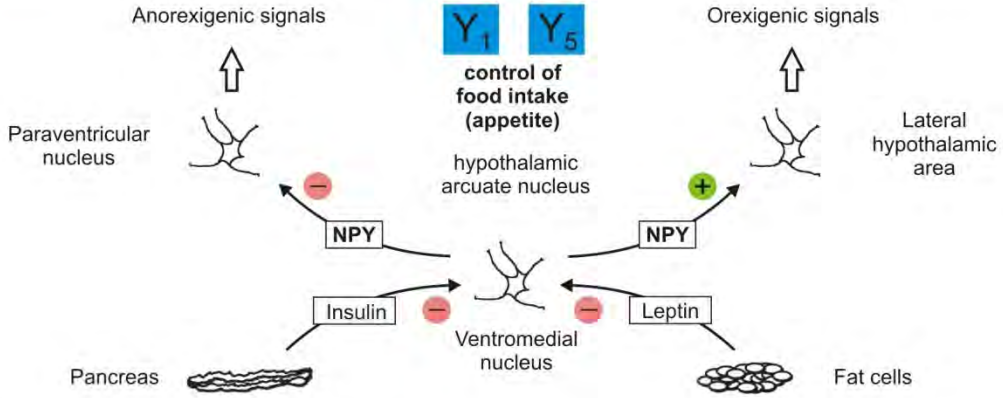

Figure 2.1 NPY and the control mechanism of appetite. *In the process of energy homeostasis, NPY is not the only regulatory substance but it plays a predominant role. The proteohormone insulin and the peptide hormone Leptin are released by pancreas and fat storages, respectively, and circulate in the blood in concentrations proportional to the content of body fat and the energy balance. In the ventromedial nucleus, which is the satiety center of the hypothalamus, they trigger the release of NPY. The less the amount of insulin and leptin, the more NPY is produced in the arcuate nucleus of the hypothalamus. NPY then acts as a stimulator of food intake in two ways. On the one hand, it increases the activity of anabolic pathways by causing orexigenic (appetite increasing) signals in the lateral hypothalamic area. On the other hand, it inhibits anorexigenic signals sent by the paraventricular nucleus that increase the activity of catabolic pathways. Both the Y_1 and the Y_5 receptor are involved in this pathway, and the understanding of how the promiscuitive binding of NPY works in this process and how it can be controlled can be the key for the development of obesity therapeutics. Figure according to ref. [3].*

known. For example, human NPY (hNPY) and its analog present in pigs (pNPY) only differ in one residue, and an even more stunning example is given by the comparison of human hNPY and its analog found in the sting ray *torpedo marmorata* (Table 2.1).[4, 5] In spite of the huge evolutionary distance between these two species, only three of the 36 residues are different, as indicated by red letters. In the course of this work, pNPY and analogs thereof have been used, but it can be assumed that identical or at least very similar results would have been obtained by the use of the human sequence (which is why the unspecified acronym "NPY" is commonly used). This is of high relevance as the research is aimed at the elucidation (and, as the next step, at the control) of the action of NPY especially in the human organism. The next section deals with these attempts and the difficulties associated therewith.

2.1.2 NPY in the human organism: perspectives and problems

2.1.2.1 The multi-talented NPY: receptor affinities and physiological roles

It is the receptor promiscuity of NPY which causes its ability to simultaneously carry out different physiological effects and which also is the pivotal problem in studying them. To date, five NPY binding receptor subtypes Y_1 to Y_5 with different localization profiles have been identified (table 2.2). Concerning the binding affinities to the subgroups of the NPY family, the Y_4 receptor stands out as it binds PP with higher affinity than NPY.[6, 7] The y_6 receptor exhibits another subtype but has, unlike the others, not been found in primates. Since it could not be related to physiologically relevant actions, it is denoted with a lower case y.[8] The binding of NPY to the other five subtypes is unambiguously related to fundamental processes, some of which are listed in table 2.2. Furthermore, NPY has been proven to control the circadian rhythm[9, 10] and to regulate the release of pituitary growth and sex hormones.[11-13] Some of the numerous effects of NPY could be related to a single receptor subtype, like the control of ethanol consumption and resistance which was effectively demonstrated with NPY deficient[14] as well as Y_1 knockout mice[15] voluntary consuming greatly enhanced amounts of ethanol and showing significantly reduced ethanol-induced sedative effects. In contrast, the food intake ("appetite") regulatory loops have been shown to be mediated by an interplay of Y_1 and the Y_5 subtype binding.[16, 17] Figure 2.1 gives an overview of the signaling pathways. The central involvement of NPY into what we commonly call our "appetite" makes it one of the hottest therapeutic candidates in the battle against obesity which exhibits a major threat to public health and which is well on the way to become a dominating cause of death in the developed countries by the associated heart diseases.[18] The not yet understood receptor promiscuity of NPY in the appetite regulatory

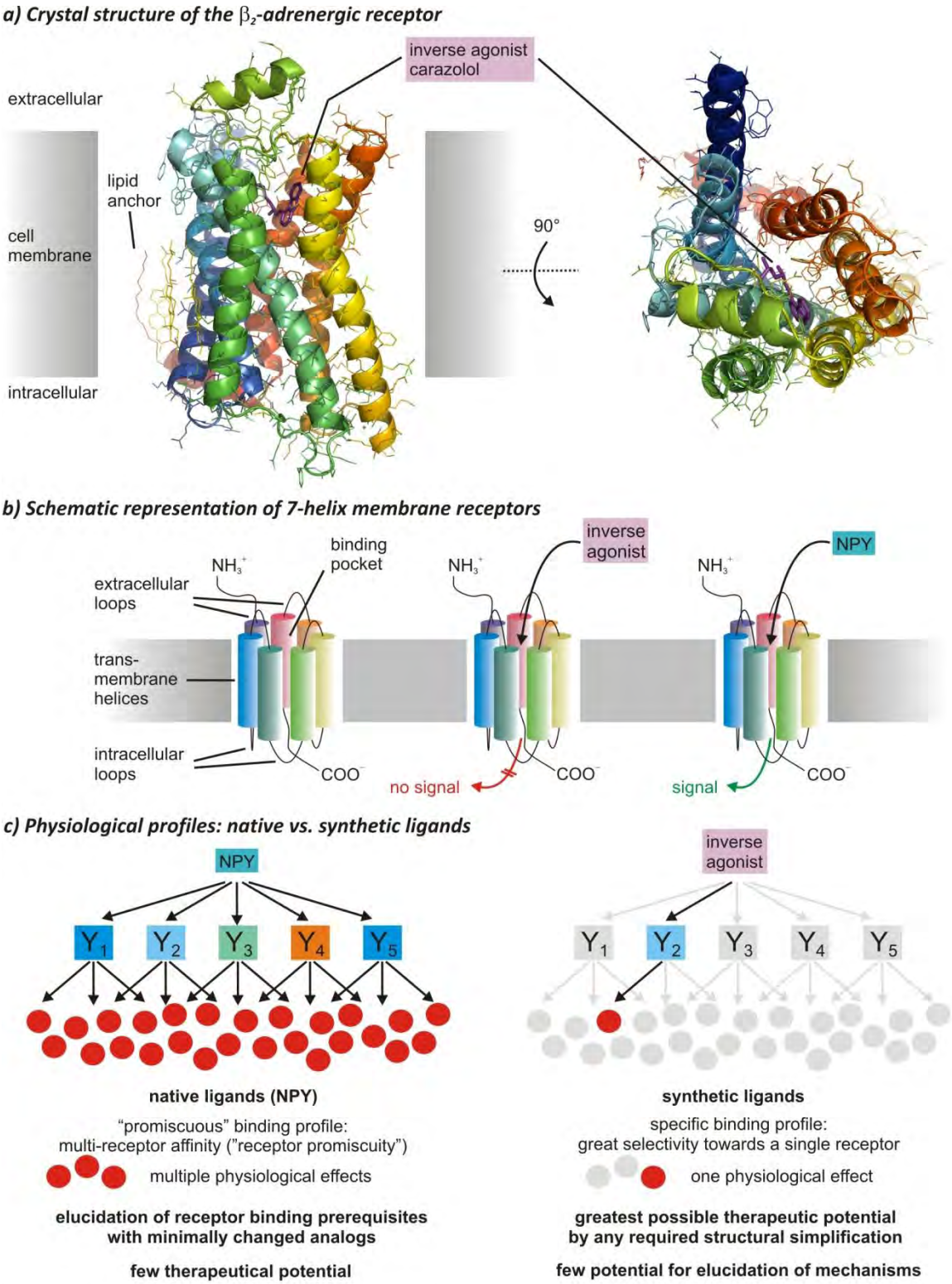

Figure 2.2 Membrane receptors: structure and ligand types. ***a)*** *In contrast to the NPY-binding receptors, the human β_2-adrenergic receptor could be crystallized in a lipid environment. To reduce conformational heterogeneity and to enhance crystal nucleation, one intracellular loop was replaced by a T4 lysozyme. The inverse agonist carazolol (shown in purple) was included to be able to investigate crucial interactions at the binding site. Left: view along the membrane plane, right: extracellular view perpendicular to the membrane showing the tunnel-like binding site.* ***b)*** *While an inverse agonist blocks the constitutive activity of the receptor, an agonist like NPY enhances the signal which is sent to the cell.* ***c)*** *A native receptor-promiscuous ligand like NPY exhibits a highly different profile from what is expected from a synthetic analog with potential as therapeutic (simplified schematic depiction).*

pathways illustrates the two major challenges which must be overcome to open the way to NPY-related therapeutic agents (figure 2.2). On the one hand, the comprehensive understanding of all details in the physiological pathways is a prerequisite to be able to develop safe and efficient therapeutics. The decisive puzzle piece hereby is the clarification of the NPY binding details at the respective receptors, a task which is still far from being accomplished (section 2.2.2). This problem has so far been tackled and can only be solved by evaluation of the binding properties of a multitude of accordingly modified NPY analogs.[2] There are many options to do this (section 2.2) and the work carried out within the scope of this thesis has established a novel promising methodology; however, the point is that near-native peptidic models with distinct minimal variation are needed. By contrast, as therapeutic agents they do not proove suitable for three reasons. First of all, the "soft", i.e. multiple receptor binding profile of the natural system, thereby always inducing more than one physiological effect in parallel, is in sharp contrast to the strict "one-to-one" prerequisite for a therapeutic agent which should address one single receptor with highest-possible affinity and selectivity, and which should trigger only a single effect (figure 2.2c). Second, the linear peptide chains of the native substrates and of their corresponding analogs are receptive towards proteolytic degradation and therefore their stabilities are far from the requirements to a (if possible orally) applicable therapeutic. Third, the structural and functional complexity of the native-like substrates, while being requested to elucidate all binding details, is not suited for medicinal chemistry which seeks to provide structurally simple, low-molecular weight molecular systems which are cost-efficient to produce on great scale.

2.1.2.2 NPY/receptor complexes: analytical options

The necessity to perform structure-affinity studies by modified analogs is also explained by the lack of crystallographic and NMR data of NPY bound to its receptors. All NPY receptors are members of the class of rhodopsin-like G-protein coupled receptors (GPCR) which have a seven-helix transmembrane structure as characteristic, with extracellular location of the N-terminus and intracellular location of the C-terminal segment (figure 2.2). GPCRs are extremely difficult to crystallize as functional complexes with their ligands due to their inherent structural flexibility, low natural abundance and insufficient stability in detergent solutions. Thus, bovine rhodopsin[19] and the human β_2-adrenergic receptor[20, 21] (the latter shown in figure 2.2) remain the only examples of successful X-ray analyses carried out so far. Furthermore, NPY-receptor complexes could not yet be isolated as functional complexes which would enable structure

a) aPP crystal structure: the monomer

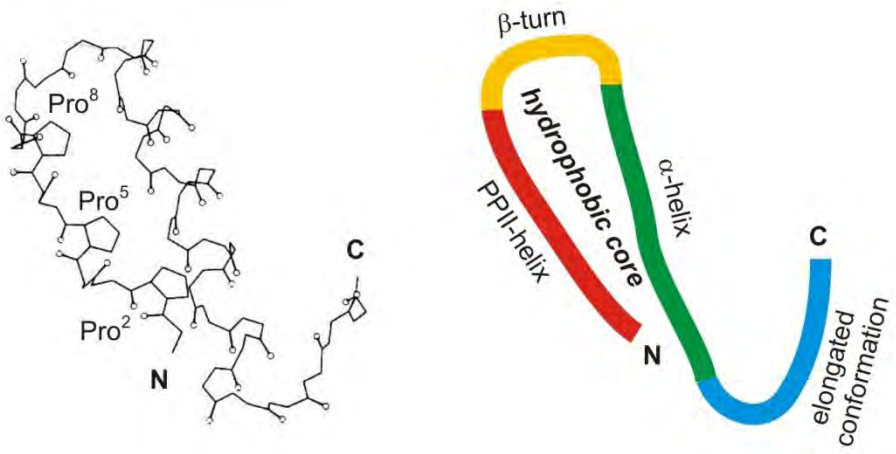

b) aPP crystal structure: the dimer

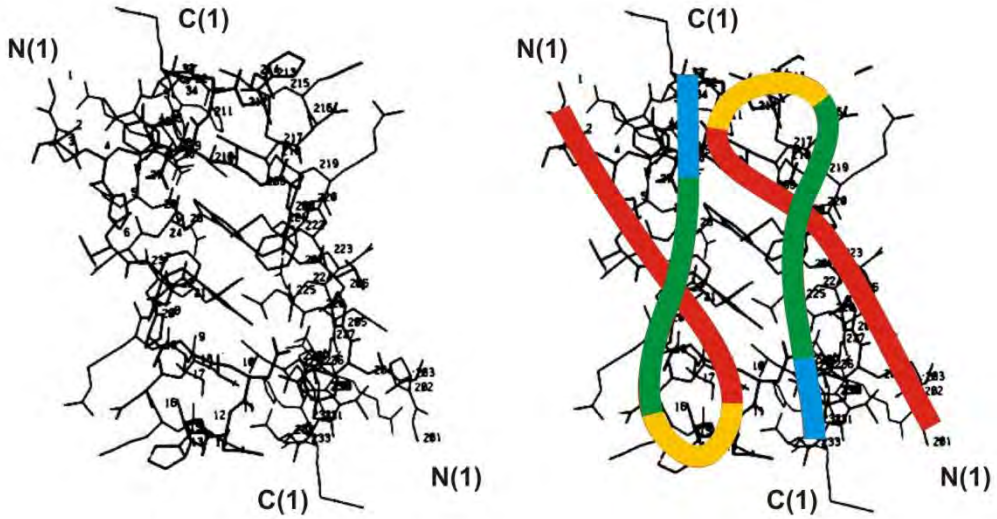

Figure 2.3 aPP crystal structure. ***a)*** *left: Depiction of a peptide unit (side chains except Pro residues are not shown for clarity); right: schematic illustration of the backbone (red: PPII-helical N-terminus, yellow: β-turn, green: α-helical segment, blue: C-terminus).* ***b)*** *Depiction of the dimer with all side chains (left) and again with the peptide backbone as colored line (right). The dimers are shown from another perspective which indicates the approx. 30° overlap of PPII- and α-helix of each monomer. In the dimer, both the PPII- as well as the α-helical segments also run antiparallel to each other and include angles of approx. 30°.*

elucidation via MAS-NMR methodology as it has already been successfully carried out for the peptidic ligands neurotensin[22] and bradykinin[23].

Without these methods being able to be exploited for NPY, receptor affinity studies with modified analogs have so far been the only possibility to elucidate the respective interactions at the distinct receptor types, and the methods and results are presented in section 2.2. The next section gives a short overview over studies concerning the conformation of NPY in the crystal and under solution conditions, the latter being of high relevance due to the receptor recognition process.

2.1.3 The aPP crystal structure and its transferability to NPY

For NPY or an analog thereof no crystal structure has been obtained so far, but the X-ray analysis of the aPP[24, 25] showed to be transferable to NPY due to the high sequential homology (figure 2.1) and indications from computational studies.[26, 27] Figure 2.3a gives an impression of the monomeric peptide. The most conspicuous characteristic is the formation of a distinct tertiary structure which is remarkable for a peptide sequence as short as 36 amino acids. This globular arrangement, commonly referred to as PP-fold, is realized by the antiparallel packing of two helical segments against each other. The Pro-rich N-terminus (residues 1-8) adopts a polyproline II (PPII) helical shape while an α-helix is formed by residues 14-31. Both helices are fixed in approx. 10 Å distance to each other by a type II β-turn with an extended chain conformation of residues 12-13. The C-terminal pentapeptide (residues 32-36) points away from the globular array by adopting a rather elongated conformation. The reason for the unusually strong short-sequence tertiary arrangement is explained by the distinct amphiphilicity of both helices. By the helix-packing, the hydrophobic half-spaces (Pro residues in the PPII helix and aromatic side chains in the α-helix) interact with each other and are buried in the core of the globular structure. The presence of further hydrophobic residues in the α-helical region (Ile, Leu) leads to the formation of dimers which are stabilized by additional interactions of these unpolar side chains. This is accomplished by the antiparallel arrangement of the α-helices of two aPP molecules in approx. 10 Å distance (figure 2.4b).

Structural characteristics obtained from crystallographic analysis are generally not transferable to the solution conditions, which are far closer to the conditions required to elucidate the conformation under physiological conditions. In the case of NPY (and also of other members of the entire NPY family), however, it turned out that some structural characteristics observed in

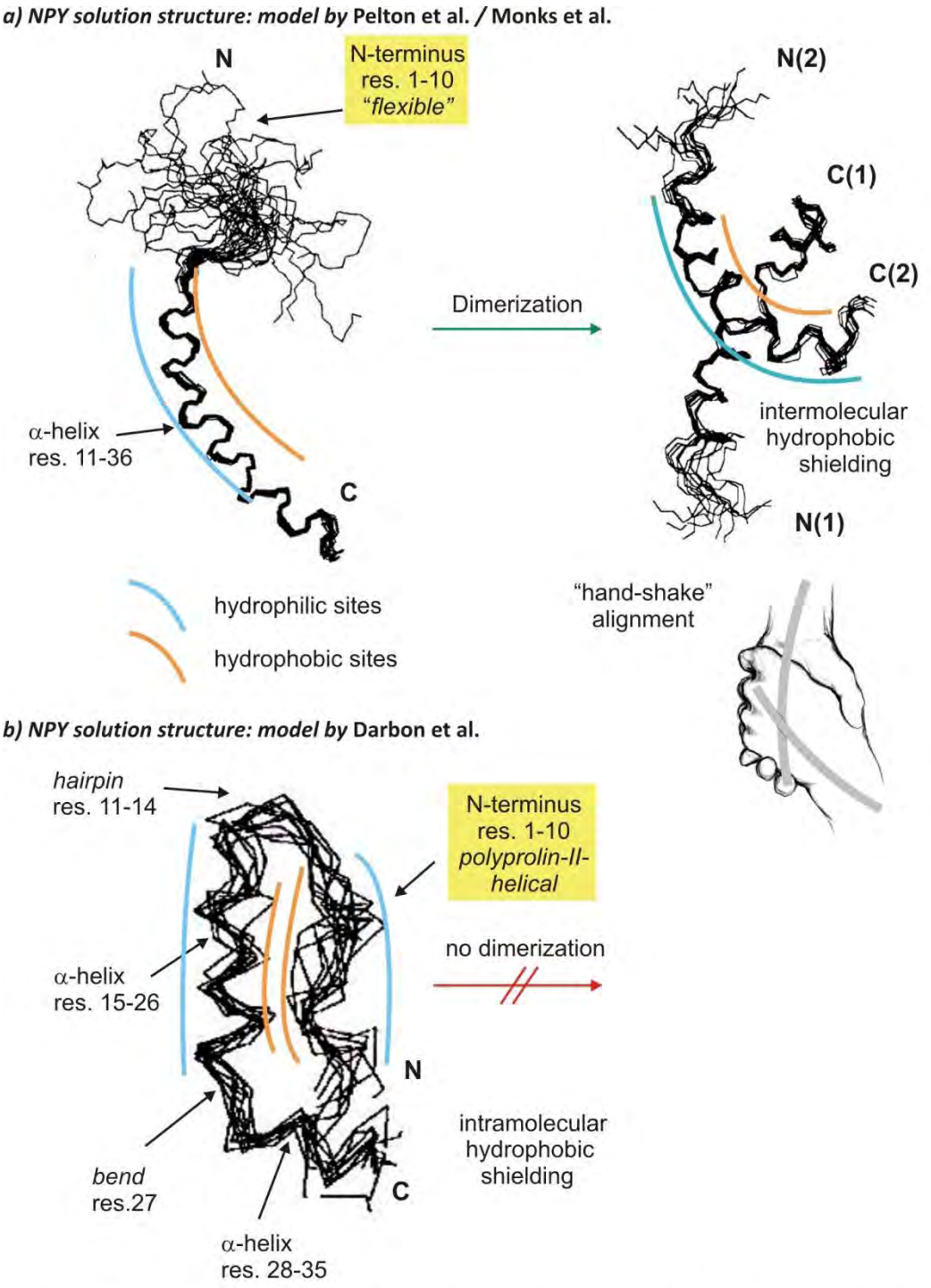

Figure 2.4 Disagreeing suggestions for the solution structure of NPY, published in the 1990s. *All structures are shown as superimposition of molecular modeling results.* ***a)*** *The structures obtained by* Pelton et al. *and* Monks et al. *do not show a backfolding as observed in the aPP crystal (figure 2.3), and instead the hydrophobic sites of the α-helices are shielded from the solvent by formation of antiparallel hand-shake dimers. The hydrophilic and hydrophobic site of the α-helix is indicated by blue and orange lines, respectively, and the N-terminal residues 1-10 assigned as "flexible" are not shown.* ***b)*** *The structure proposal by* Darbon et al.*, in contrast, based of an interpretation of long-range NOEs as being intramolecular and therefore comprises a backfolding of the N- towards the C-terminus similarly to the aPP crystal structure. The fact that the N-terminus was assigned to adopt a distinct PPII-helical conformation, in contrast to its flexibility as proposed by the other researchers (**a**) demonstrates the difficulty in obtaining reliable data about such a proline-rich peptide segment. Depictions according to ref. [29], [30] and [33].*

the aPP X-ray structure to some extent also apply for the structures formed in solution which were discussed controversially and which are described in the following.

2.1.4 The discussion of the NPY structure in solution

Saudek et al. were the first to present a near-complete NMR assignment and a solution conformation of NPY[28] which was also supported by investigations carried out from *Monks et al*.[29] Dissolved in a 4 mM concentration in D_2O, the peptide forms an α-helix which, in contrast to the crystal structure, already starts with Asp^{11} and continues to the C-terminal Tyr^{36} (Figure 2.4a). While an exclusive *trans* conformation of Pro^{13} was observed, which is essential for helix formation, other Pro residues at positions 2, 5, and 8 showed *cis*/*trans* isomerism and gave rise to several sets of signals. Concerning the conformation of the N-terminus, the identification of only sequential NOE contacts as well as the random coil like chemical shifts gave rise to assign this segment as being "flexible", which also was proposed by the majority of later structural works described in the following.

The more detailed investigations of some NOE contacts which could not be reconciled with the structural results were later on explained by the formation of NPY dimers.[30] These were named "hand-shake" alignments as the hydrophobic half-spaces of the α-helices of two peptides intertwine in an angle of approx. 30° (Figure 2.4a). The driving force of the dimerization is the shielding of the unpolar side chains from the aqueous environment, and this effect is maximized by a distinct bending of the helical axes towards each other. These results were also obtained by CD spectroscopic analyses under comparable conditions.[31] *Kessler et al*. investigated the structure of NPY in a trifluoroethanol/water mixture (9:1) which is known to induce helicity.[32] Under these conditions, no dimerization was observed, which was explained by the less polar solvent that does not require any dimerization to shield the unpolar side chains. As the α-helical segment was clearly shorter than in the dimer, with the α-helix starting only at residue 19, the aggregation was proposed to promote the larger helical content. Accordingly to the previous studies, no PPII-helical content was observed for the N-terminal segment, which is why this was stated to adopt "*no regular structure*".[32]

These results were in quite sharp contrast to results obtained by *Darbon et al.* who chose aqueous solution conditions similar to the previous work and reported a highly different structural model (figure 2.4b).[33] They proposed the NOE which had been explained by dimerization to be intramolecular and described a globular monomeric conformation quite similar to the aPP crystal structure. The N-terminal segment (residues 1-10) is now structured, featuring a PPII-helical conformation and by a hairpin (residues 11-14) being oriented onto the

Table 2.3. Structures found for NPY under various solution conditions.

Solution conditions	aqueous buffer solution	aqueous buffer solution	aqueous solution with DPC micelles
Concentration	nM *physiological concentrations*	μM-mM	μM-mM
Method	CD, FRET	CD, NMR	CD, NMR
Proposed structure(s)	monomer no PP-fold	equilibrium monomer/dimer (figure 2.5a)	equilibrium micelle on/off (figure 2.5b) no dimers
	decreased α-helicity "flexible" N-terminus	strong α-helicity "flexible" N-terminus	very strong α-helicity "flexible" N-terminus

a) NPY equilibrium in aqueous solution.

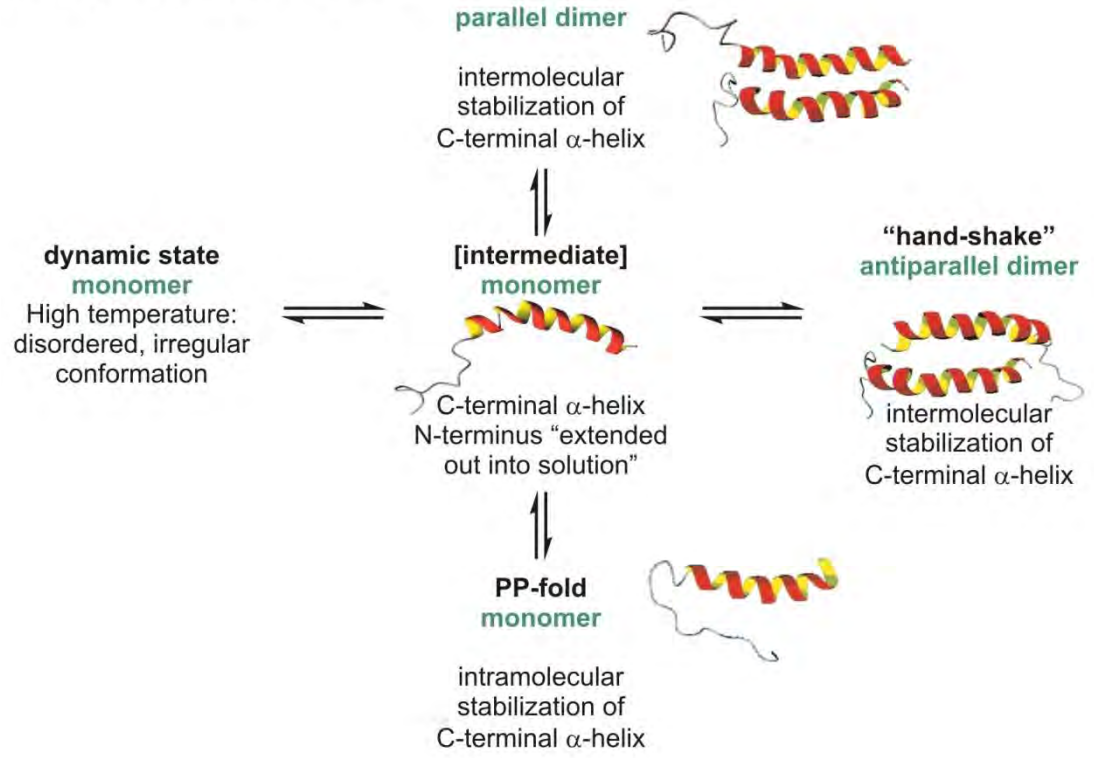

b) NPY equilibrium in the presence of a membrane mimetic.

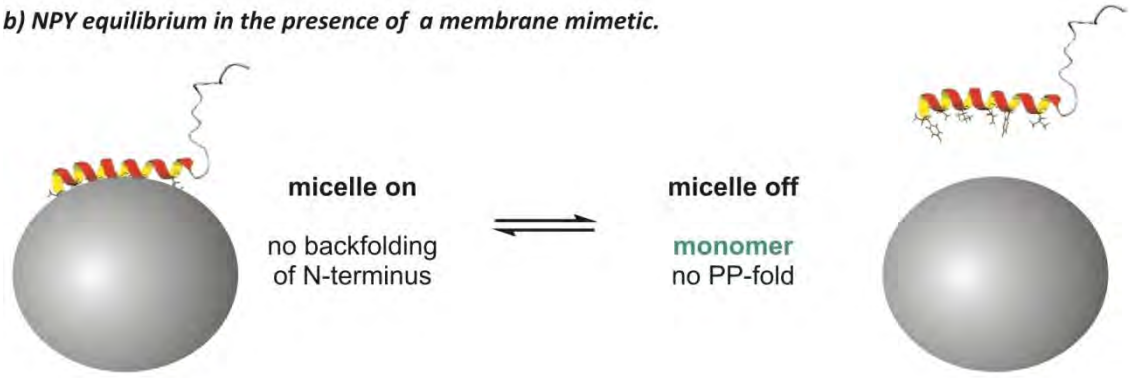

Figure 2.5 Today's conception of structural equilibria of NPY in aqueous solutions without (a) and with (b) membrane mimetic. *Depictions according to ref. [34] and [43].*

C-terminal part. The latter features two α-helical segments (residues 15-26 and 28-35) which are oriented to each other by a bend at residue 27. As another distinct difference to previous work, there is no aggregation observed as by the other studies because the peptide is able to shield its hydrophobic sites solely by intramolecular coordination.

In an attempt to resolve the greatly different observations by the research teams, *Nordmann et al.* finally proposed a conformational equilibrium of NPY in aqueous solution where the monomeric peptide with "unstructured" N-terminus appears as intermediate in the transition between a PP-fold-like monomer and a "hand-shake" dimer.[34] They also suggested the presence of self-associated NPY dimers in the organism which at high concentrations enable a slow release of physiologically active NPY monomers.

However, under physiological conditions, the NPY concentration do not exceed the nanomolar range, while all studies carried out so far were performed with µM to mM concentrations. Using fluorescence resonance energy transfer (FRET), *Beck-Sickinger et al.* showed that under these concentrations - which are outside the range of NMR techniques - neither PP-fold nor dimerization is observed (table 2.3 and figure 2.5).[35] Overall, the low concentrations lead to significant loss of secondary structural elements. This raises the important question of how the structurally highly disorded peptides are able to be recognized and to be bound by their receptors, leading to the concept of that the interaction with the membrane may exhibit a crucial step in this process (section 2.1.7). The following section will give an introduction to the options NMR spectroscopy in presence of membrane mimetic, which is an indispensable tool in the investigation of membrane proteins and membrane-coordinating peptides.

2.1.5 NPY in membrane-mimetic environment

If a peptide like NPY, which exerts its functions by binding to membrane proteins (and this apparently from a membrane-bound state), is examined in aqueous solution, this will ignore the presence of the cellular membrane as a significant part of the environment in the organism. Therefore it is reasonable to question the results due to their relevance and transferability to *in vivo* conditions. In order to enable the incorporation of membrane-mimetic systems to NMR spectroscopic investigations, several systems have been established over the last decades, the most recent milestone being the development of in-cell NMR techniques.[36, 37] In order to elucidate how the conformation of a peptide changes upon binding to a membrane (compared to the free solution conformation, these changes can be far from negligible), it has proven sufficient to relay on simplified systems enabled by membrane-mimetic detergents. Figure 2.6 gives an overview of substrates and aggregates used in comparison to a cellular membrane.

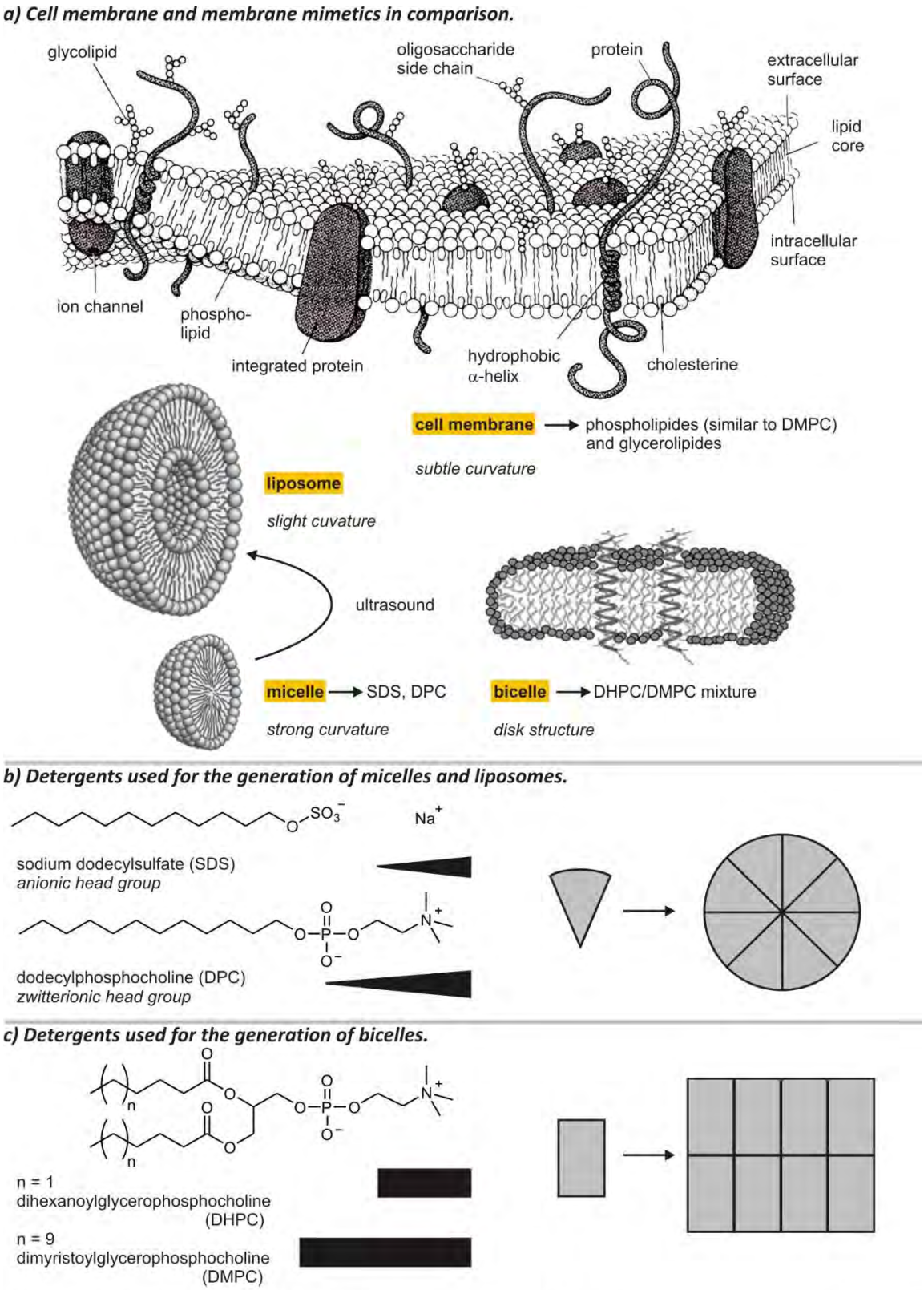

Figure 2.6 Artificial membrane surrogates. ***a)*** *In contrast to the complex cellular membrane, relatively small aggregates consisting of various detergents proved suitable for mimicking the membrane.* ***b)*** *Cone-shaped molecules like SDS (also used in this work for several purposes) or the larger DPC self-assemble to spherical micelles, and larger double-layered liposomes are obtained by treatment with ultrasound.* ***c)*** *In the aggregation of detergents with two fatty acid chains, the formation of bicelles whose size depends on the mixing ratio of molecules with longer and shorter alkyl chains is energetically favored. In perdeuterated form all these compounds are used for NMR spectroscopic measurements.*

According to their size and longitudinal shape, these detergents form spherical micelles, bigger double-layered liposomes or planar bicelles. For example, sodium dodecyl sulfate (SDS) has proven successful in several studies and also in the work carried out within the scope of this thesis.[38] The micelles which are formed if the critical micelle concentration of 8.0 mM SDS is exceeded[39] exhibit a diameter of 3-5 nm and contain approx. 80 SDS molecules.[40] In comparison to a cellular membrane whose curvature is negligible in relation to the dimension of a biomolecule (which is why a cellular membrane is conveniently pictured as a two-dimensional liquid) these aggregates first of all differ by their strong curvature. Furthermore, they exhibit rather a coordinative equilibrium than a permanent composition as the single SDS molecules join and dejoin with high rate. This implicates that SDS aggregates may be capable of adjusting their shape to the respective molecular ligand. The membrane charge is dependent on the polar head group of the mimetic. While the surface of an SDS aggregate is negatively charged (sodium ions as counter ions), phosphocholine membranes are zwitterionic (figure 2.6). The use of SDS also allows to investigate aqueous solutions of extremely unpolar or amphiphilic peptides which are otherwise insoluble at the concentrations required for NMR. Within the scope of this thesis, this option was utilized for the investigations of Tyrocidine A aldehyde.[41]

2.1.6 Water-suppression techniques

The choice of the appropriate solvent for investigations aimed to approach the *in vivo* conditions may appear trivial as all physiological processes run in salt water. Far from easy to assess, however, were the problems arising from using deuterated water for NMR spectroscopic investigations. Due to proton exchange, acidic positions will be occupied by abundant deuterons and therefore become invisible with standard ^{1}H based 1D and 2D NMR experiments. While these exchange processes are utilized to evaluate whether protons are oriented towards the solvent or shielded by hydrophobic cores or hydrogen bonds, these effects can lead to improper assignment and structure calculation results, or even abolish them. Therefore, much effort has been spent for the development of easy-to-use water suppression techniques which allow the use of undeuterated water (with approx. 10% D_2O for the lock signal). The *presaturation technique* and the *jump-and-return-sequence* exhibit simple methods to selectively irradiate the water resonance, but as they suffer from baseline distortions as well as from co-irratiation of exchanging protons and of other signals in proximity to the water resonance. This ultimately led to the development of WATERGATE techniques (*WATER suppression by GrAdient Tailored Excitation*), the latest and most powerful variant being the double WATERGATE DPFGSE

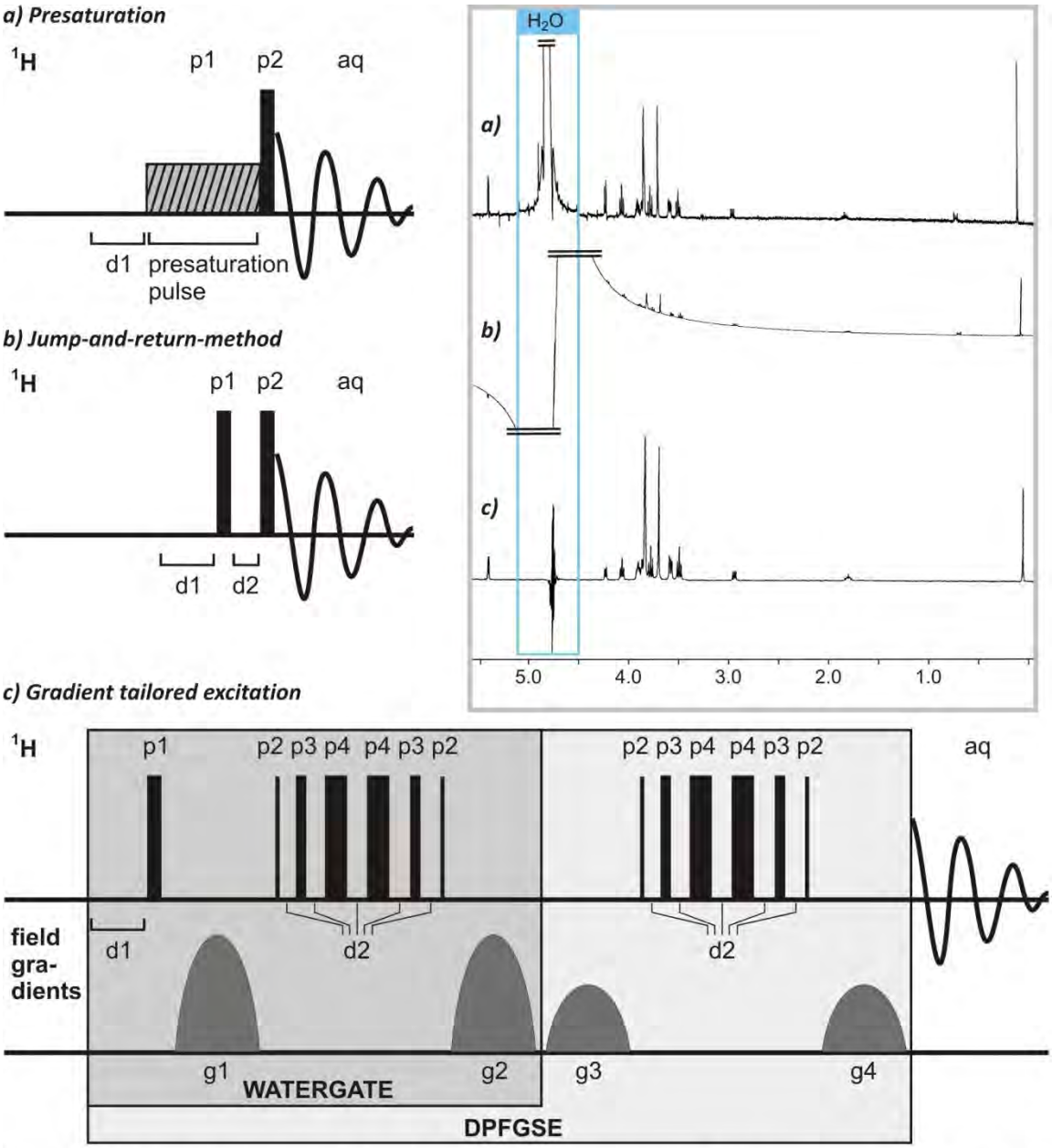

Figure 2.7 Water suppression techniques used for NMR spectroscopy. *Without water suppression, signals of the solute (mmolar concentrations) would be invisible next to the signal resulting from the 55 molar H_2O. In the diagrams, pulses (p), delays (d), field gradient pulses along the z axis (g) and the resulting FID (aq) are depicted in temporal order. For every sequence, the corresponding NMR spectra of 2 mmol sucrose (500 MHz, 300 K, H_2O/D_2O 9:1) are depicted.* ***a)*** *The presaturation differs from a standard ^1H experiment by a 2 s long presaturation pulse on the water resonance. This leads to a decrease of the H_2O signal; however, exchanging protons are also affected and become invisible.* ***b)*** *The jump-and-return sequence overcomes this problem, but the quality of the spectra is affected by a phase change at the H_2O (offset) resonance. After the first 90° pulse, a second pulse leads to zero transversal magnetization of the offset frequency only.* ***c)*** *The use of sinusoidal field gradients exhibits the most powerful method to suppress the H_2O signal, which is reduced to a signal of similar size compared to the sample signal, and which gives a plain baseline. Briefly, after a first 90° pulse (p1) that generates transverse magetization all spins are dephased by a field gradient (g1). The following binomial "pulse train" (similar to the spin echo sequence) excites all resonances except of the offset water resonance, and the second field gradient (g2) brings all resonances in phase again, only the offset resonance is getting further dephased. This sequence corresponds to the WATERGATE sequence. The DPFGSE technique applies this sequence a second time (with varied gradients g3 and g4), by which phasing problems and baseline distortions are overcome, resulting in a superior quality of the obtained spectra.*

sequence (*Double Pulsed Field Gradient Spin Echo*).[42] The pulse sequence is schematically depicted and explained in Figure 2.7.

Taken together, the combination of modern water-suppression methods that allow the use of undeuterated water with the use of perdeuterated SDS membrane-mimetics is a powerful method to investigate biomolecules under conditions that approach physiological environment as far as possible, and it also proved successful in this work. The first examination of NPY in a membrane-mimetic environment carried out by *Zerbe et al.*[43] was a significant progress towards understanding the conformation of NPY and its receptor binding mechanism. ^{15}N-labeled pNPY in 3 mM concentration in H_2O/D_2O (9:1) was used to exploit [^{15}N-^{1}H]-HSQC experiments which facilitate spectral assignment and which, according to the mixing time, provide information about ^{1}H homonuclear scalar and dipolar couplings. As a membrane mimetic, perdeuterated DPC (DPC-d_{38}) was used in 300 mM concentration, leading to a micelle concentration of approx. 5 mM. The peptide and detergent concentrations were in the range of the concentration applied within the scope of this work. Compared to the results obtained by *Saudek et al.*[28] and *Monks et al.*,[29] the NMR structure obtained under these conditions appeared to be quite similar (Figure 2.8a). However, the presence of DPC micelles has a stabilizing effect on the α-helix which is formed from residue 15 to 34 and becomes extended over two residues in each direction by adding DPC. Furthermore, there is no sharp transition between helical and non-helical segments as the adjoining segments 13-15 and 34-36 are in equilibrium between an α-helical and an extended conformation. These findings are supported by ^{15}N relaxation measurements which are shown in Figure 2.8b. Like in previous studies, the α-helix appeared to be bent with the hydrophobic side chains located towards the concave site. However, the significance of these studies by *Zerbe et al.* resulted from a first insight into the orientation of the peptide on the membrane surface. By performing proton exchange studies in pure D_2O it could be shown that the amide protons of some hydrophobic residues in the helical region (Leu^{24}, Arg^{25}, Tyr^{27}, Ile^{28} and Ile^{31}) were extremely slowly exchanged. As these residues are all located towards the same (hydrophobic) side of the α-helix, the observations were explained by the side chains penetrating the hydrophobic core of the micelle, which leads to a solvent-shielded localization of the amides on the micellular surface. These results were also supported by spin-label experiments (Figure 2.8). A spin-label contains an unpaired electron and thereby strongly reduces signal intensities of nuclei in less than approx. 10 Å distance. By adding small amounts of the spin-label 5-doxyl stearate which as a detergent gets incorporated to the DPC micelles all residues localized towards the membrane exhibited significantly reduced signal intensities compared to a reference sample without the spin-label.

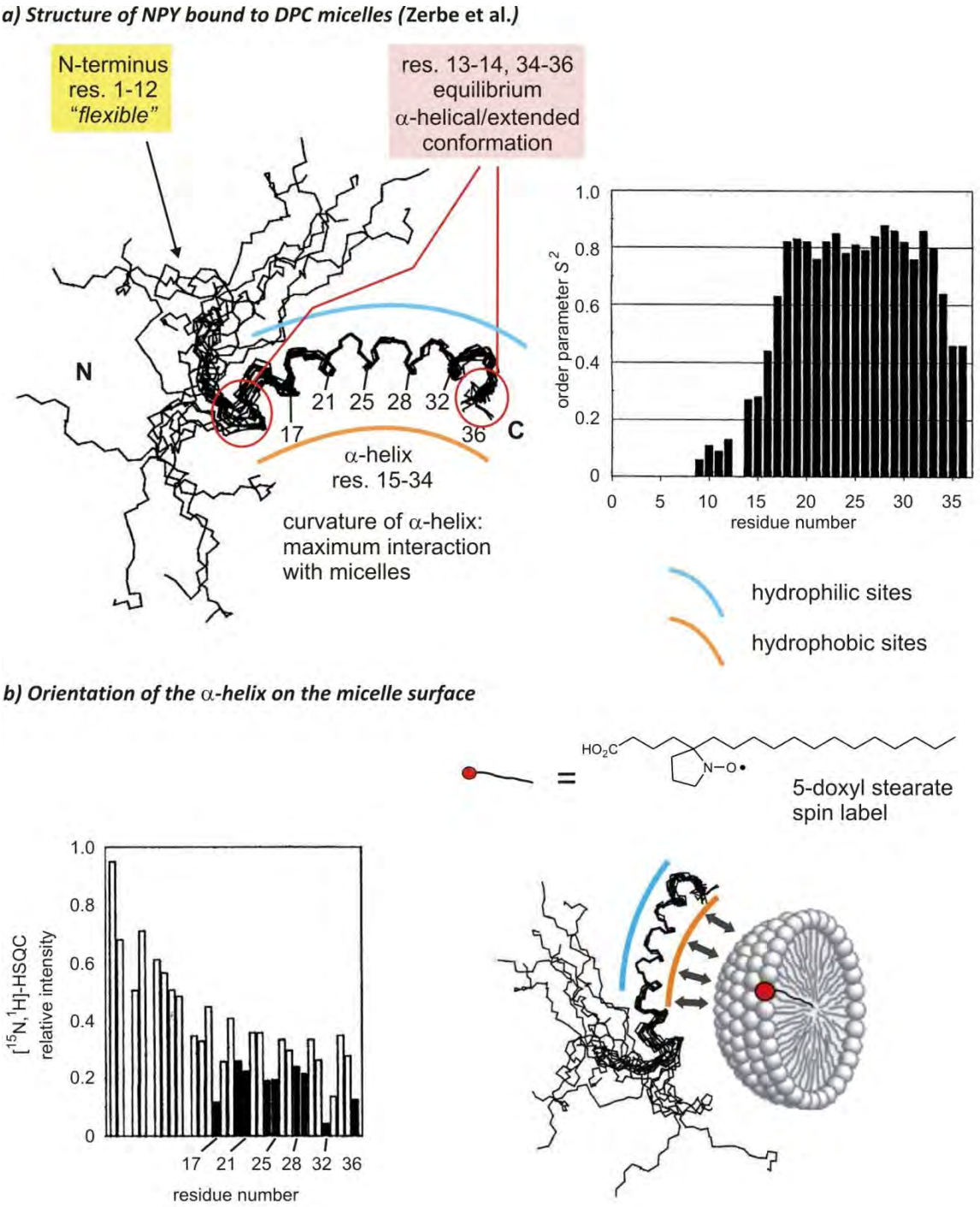

Figure 2.8 Investigations on micelle-bound NPY. ***a)*** *left: Depiction of the backbone atoms of 17 minimized structures of NPY bound to DPC micelles, as obtained by* Zerbe et al. *The structures are superimposed over the backbone atoms of residues 21-31. Like in figure 2.4, hydrophobic and hydrophilic sites of the α-helix are marked by an orange and blue line, respectively. Right: Determined by relaxation measurements of the ^{15}N backbone atoms, the order parameters S^2 revealed the range of the α-helix (S = 0 corresponds to full flexibility, S = 1 corresponds to perfect alignment as in an ideal crystal).* ***b)*** *The average relative orientation of the α-helix on the membrane surface was examined by comparing the signal intensities of NPY bound to micelles with and without the spin-label 5-doxyl stearate. The periodical high loss of intensity (marked by black bars) suggests a preferred orientation of the hydrophobic site towards the micelles. As schematically depicted on the right, the spin-labeled micelles contained on average one 5-doxyl stearate detergent molecule (head group highlighted in red). Depictions according to ref. [43].*

In addition to the antiparallel “hand-shake” dimers proposed in earlier work, investigations with spin-labeled NPY analogs indicated that also parallel dimers may be present which are in equilibrium with partially unfolded monomers and antiparallel dimers. Concerning the conformation of the N-terminal segment, the same results were obtained as in earlier works: it was denoted “flexible” with a rather extended conformation (Figure 2.8a). Furthermore, all experimental results indicated that no backfolding takes place, neither in solution nor at the membrane.

2.1.7 The theory of membrane-assisted receptor selection

The detailed results obtained by *Zerbe et al.* suggested that the receptor-binding mechanism of NPY (as well as of other members of the NPY family) may proceed according to a hypothesis by *Kaiser* and *Kedzy*[44] which is commonly referred to as *membrane assisted receptor selection* (figure 2.9).[43, 45] This means that certain ligands are not recognized from free solution but from the membrane-bound state, which reduces the diffusion from the three-dimensional aqueous solution to the “two-dimensional liquid” membrane, a fact which may significantly enhance the sensitivity concerning the low density of the receptors on the target cell membranes (approx. 80 000 to 100 000 per cell).[46] As the NPY with its amphiphilic helix appears to be the result of an evolutionary optimization process towards optimal membrane affinity, and as this binding occurs with a distinct orientation of the peptide on the membrane surface, the role of the membrane to induce a conformation and orientation which is already similar to what is required to successfully enter the binding pocket of the receptor. The C-terminal Tyr^{36} is supposed to serve as membrane anchor and thus, in interplay with the oriented α-helix, to induce a distinct orientation of the Arg^{33} and Arg^{35} side chains which obviously are the decisive receptor-binding element by being involved into electrostatic interplays. More recent studies concerning the following receptor-binding step also fit this theory.[47] They assume a role of the extracellular N-terminal domains in transferring the membrane-bound peptides into the binding pocket, which also proceeds by electrostatic interactions.

2.1.8 The underestimation of the role of the N-terminus: a motivation for a novel scan

As already mentioned, the work on NPY which was described in the previous sections greatly restricted the structural discussion to the C-terminal segments, which can be considered as a significant drawback in the efforts to obtain an overall picture of the conformational preference and of the receptor binding mechanisms. In fact, the dynamics of the proline-rich N-terminal

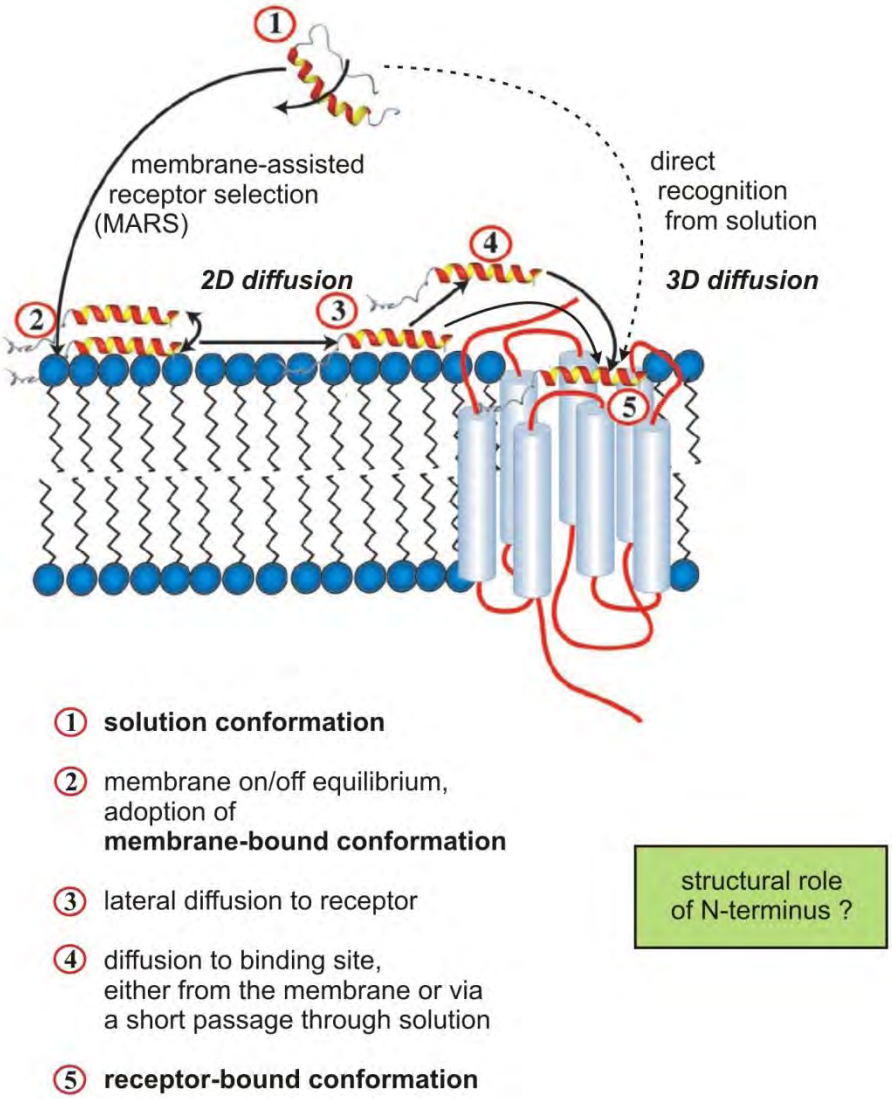

Figure 2.9 Schematic depiction of the steps in the hypothetic membrane-assisted receptor selection mechanism of NPY. *Figure according to ref. [45]. The obvious role of the N-terminus in receptor binding is in contrast to its structural underdetermination, which gives a main motivation for the research carried out within the scope of this thesis.*

segment are difficult to analyze which is why it mostly was assigned to be “unstructured”, or “flexible”. More important, due to the lack of information the term “flexibility” is often set equal with (or explained by) the absence of any distinct conformation, which is simply false. The lack of amide protons at the proline residues is a further complication as this leads to a significant restriction of information available by NMR analytics. Therefore, only few studies have been reported which explicitly rise questions about the role of the N-terminal segment of NPY.[48-50] Comparing CD and NMR data of N- and C-terminally truncated NPY analogs, a highly important role of the N-terminus could be proposed. First of all, a PPII-helical conformation of the N-terminus can generally not be excluded in solution as well as in the membrane-bound state of the peptide, and so it can contribute to the stabilization of the α-helix (as it is the case in the aPP crystal). Consequently, as a high α-helical content was proven to enhance the receptor affinity, this implicates a role of the N-terminus in triggering the proper conformation and orientation of the C-terminal part for entering the binding sites. A contribution of a PPII helical conformation was also suggested by the substitution of the highly conserved Pro^2, Pro^5 and Pro^8 residues against Ala which lead to significantly decreased receptor affinity.[2] Furthermore, a proper conformation of the N-terminus apparently helps to present and to orient the Tyr^1 which plays a further key role in receptor binding.[48] As every peptidyl-prolyl bond is to some extent subjected to *cis*/*trans* isomerization, the question whether the three respective amides in the N-terminal segment adopt the *cis* or *trans* conformation in the receptor-bound state has to be answered.[51]

In this context, the motivation of the research carried out within the scope of this thesis was the need to establish novel methodologies that overcome the existing deficiencies in the analysis of “flexible” peptide segments which are difficult to characterize. The N-terminus of NPY surely exhibits a prominent prime example of such a challenging fragment. In order to allow a closer look to the N-terminus with respect to conformational properties and associated roles in receptor affinity and selectivity, a “backbone scan” using a rigid dipeptide unit proved to be a successful strategy for structural analytics and for the evaluation of receptor binding trends.[38] The following section introduces this method and compares it to the numerous previous studies on NPY analogs which gave rise to today’s conception of how NPY binds to its receptors.

Possibilities to modify a peptide (continued on next page)

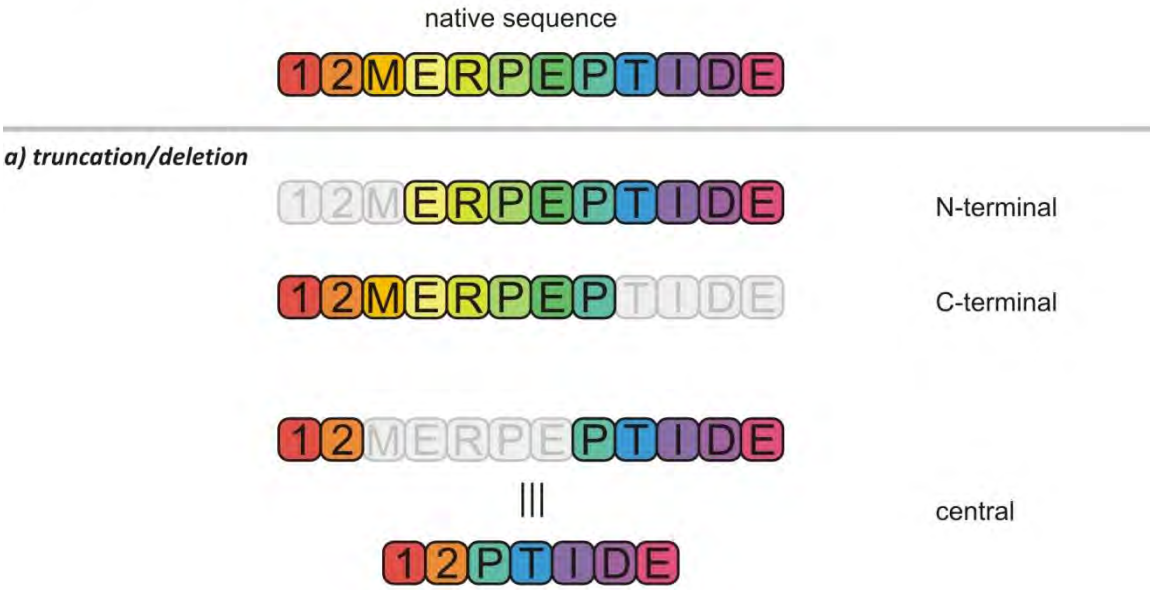

Figure 2.10 (continued on next page) Options to generate analogs of modular natural products. *In the exemplarily chosen dodecapeptide ("12merpeptide"), the single residues are schematically depicted as squares in prismatic colors to clarify the respective structural changes.* ***a)*** *Truncations and deletions can serve to investigate the importance of single residues or segments.* ***b)*** *Additions and insertions of further amino acids or segments conserve all functionalities of the native sequence but change the overall length.* ***c)*** *By artificial cyclizations it can be proven whether the substrate adopts a globular conformation in the receptor-bound state. However, this rigidification may hamper the entering of the binding pocket. Other cyclizations like side-chain-to-head/tail linkages or the tethering of residues in adjacent helix turns are not shown. Another established modification strategy is the inversion of the N- to C-terminal course of the backbone in the so-called retro- and retro-inversopeptides (not shown).*

2.2 The concept of the Dha=Tap backbone scan

2.2.1 Research context: The art to gain maximum information from designed peptide analogs

Medicinal chemists as well as biochemists seek to develop molecular ligands with maximum affinity for a single receptor in order to trigger just one physiological effect. From the view of medicinal chemistry, the quality of these selective ligands stands and falls with their potential as well-applicable and -producable therapeutics, and any structural change and simplification with respect to the native ligands is acceptable for the sake of a superb therapeutic profile. The identification for candidates is based on the screening of huge molecular libraries which are restricted according to the found candidate lead structures. In contrast, one must orient with the natural products to elucidate how they act in the organism, which is a prerequisite for a rational molecular design of synthetic ligands. Only the examination of analogs with high structural and functional analogy allows to draw conclusions for the native ligand under physiological conditions. In other words, the art to come to an understanding of how natural ligands like NPY react consists in choosing the proper minimum modifications for the designed systems which reveal precise information about the native system. The modularity of natural products like peptides, proteins, and glycosides serves as key to obtain analogs with systematic high diversity. In the case of the 36-mer peptide NPY, great effort has been made for this purpose, and common methods are schematically shown in figure 2.10 for a dodecapeptide.

In order to elucidate the importance of molecular segments, the molecule can be shortened by eliminating an N-terminal, C-terminal or central part of it (truncation, figure 2.10a). By contrast, additional segments can be attached to the termini or be inserted to central parts (addition/insertion, figure 2.10b). In order to prove a possible globular conformation (as for example the backfolding of the N- onto the C-terminus in NPY), the substrate can be macrocyclized by head-to-tail or sidechain cyclization (figure 2.10c). There are several options to perform systematic substitutions. On the one hand, the exchange of central sequences for a flexible α-aminohexanoic acid (Ahx) linker is performed to evaluate whether the importance specific overall conformations for receptor binding (figure 2.10d). However, isosteric substitutions are often easiest to interprete as they exhibit only small variations, and the greater the impact of such modifications, the more precise are the conclusions that can be drawn for the native system. The terminus “isosteric” is in this context not used in its original function as denoting the same number of atoms, number of electrons, and identical electron configuration.[52, 53] It is rather used in terms of “bioisosteric” which indicates similar spatial

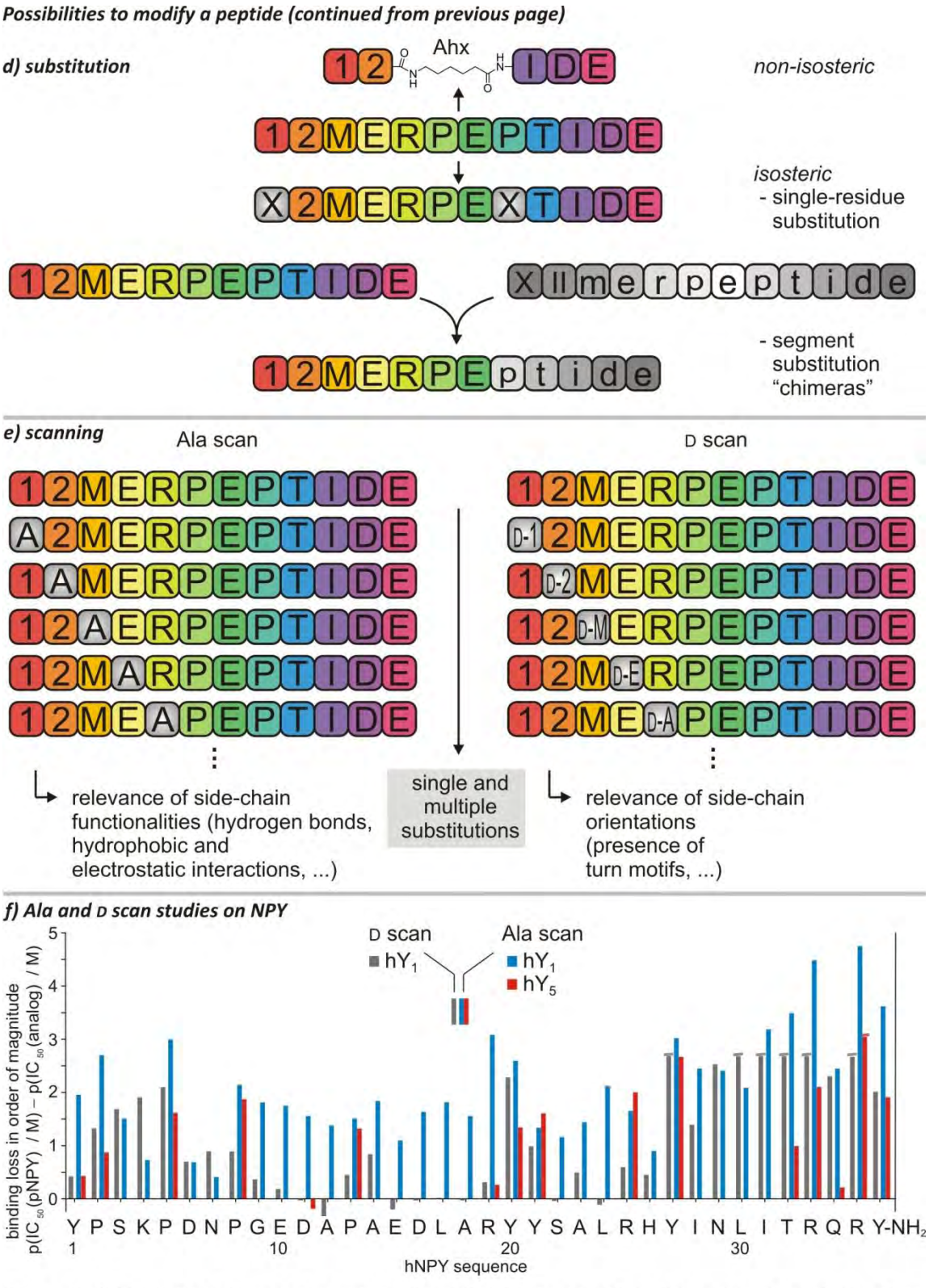

Figure 2.10 (continued from previous page) Substitution analogs of modular natural products. ***d)*** *In many cases, isosteric substitutions prove superior to non-isosteric changes as the lenght of the backbone is held constant.* ***e)*** *Systematic substitution studies (called scans) can be carried out in different ways; the shown substitution of all residues against Ala (native Ala residues are commonly substituted by Gly) or the enantiomeric amino acid (D scan) being the most used variants. Other possibilities are, for example, the scanning with flexible Gly or with charged side chains.* ***f)*** *No clear trends are visible from the Y_1 and Y_5 affinities determined for Ala- and D-scanning analogs of NPY. The affinity at the Y_5 subtype has not been determined for all substrates. Double lines over a bar indicate a loss at least equal to the shown value.*

extension and comparable biological action after the exchange of molecular parts and functionalities.[54] For peptides this is accomplished by changing single residues while maintaining the backbone with respect to its length, or by inserting segments from other substrates which results in so-called “chimeric” peptides. Most notably, it is the possibility to systematically vary the substitution position throughout the substrate, which is commonly referred to as “scanning”. One of the most used methods is the alanine (Ala) scan where replaces every residue is replaced by an Ala, leading to a series of n analogs for an n-mer peptide (figure 2.10e,f). Another important method is the D scan in which every amino acid is replaced by its enantiomer to evaluate the influence on the formation of secondary structure elements.
Instead of single-amino acid variations, multiple substitutions in different sections of the substrate or substitutions by oligopeptide sequences are further options. The incorporation of a dipeptide which has restrictional effects on the backbone (dipeptide backbone scan) and which was examined within the scope of this thesis (section 2.3) is a logical next step in NPY analytics. To bring this in context with earlier work, some examples are described below.

2.2.2 Earlier work accomplished for NPY analogs

Over the last decades, intensive research has been carried out which was dedicated to the search for peptidic NPY analogs that show decreased receptor promiscuity and therewith potentially shed light on prerequisites for the respective receptor affinities (figure 2.11). As there is still lack of crystal and NMR data concerning the conformations of NPY in the respective receptors (not to mention the topologies of the binding pockets and the single receptor-ligand interactions) our today’s conception of the binding situation in the single receptors is based on the multitude of structure-affinity relationship studies carried out so far. For the receptor subtypes Y_1, Y_2 and Y_5 which are examined best to date, the different contact sites have been described explicitly for the first time by *Beck-Sickinger et al.* in 2001[55] and they are shown in figure 2.11c. From the great number of studies which ultimately led to this conception and which have extensively been reviewed,[2] only a selection of instructive examples can be given here. For every receptor subtype, a peptidic high-molecular weight selective agonist is shown schematically in comparison to a low-molecular weight selective antagonist (figure 2.11b,d).
The Y_1 and Y_2 receptors were the first subtypes that could be differentiated,[56] and it turned out that a proper induction of the α-helix and the integrity of the N-terminus is of high relevance only for Y_1,[57, 58] while a close proximity of both termini is required at the Y_2 subtype.[59] The Y_1 receptor is very susceptible to changes and it took two decades of research until the first selective agonists were obtained by delicate single-residue variations, with [Phe^7,Pro^{34}]-pNPY

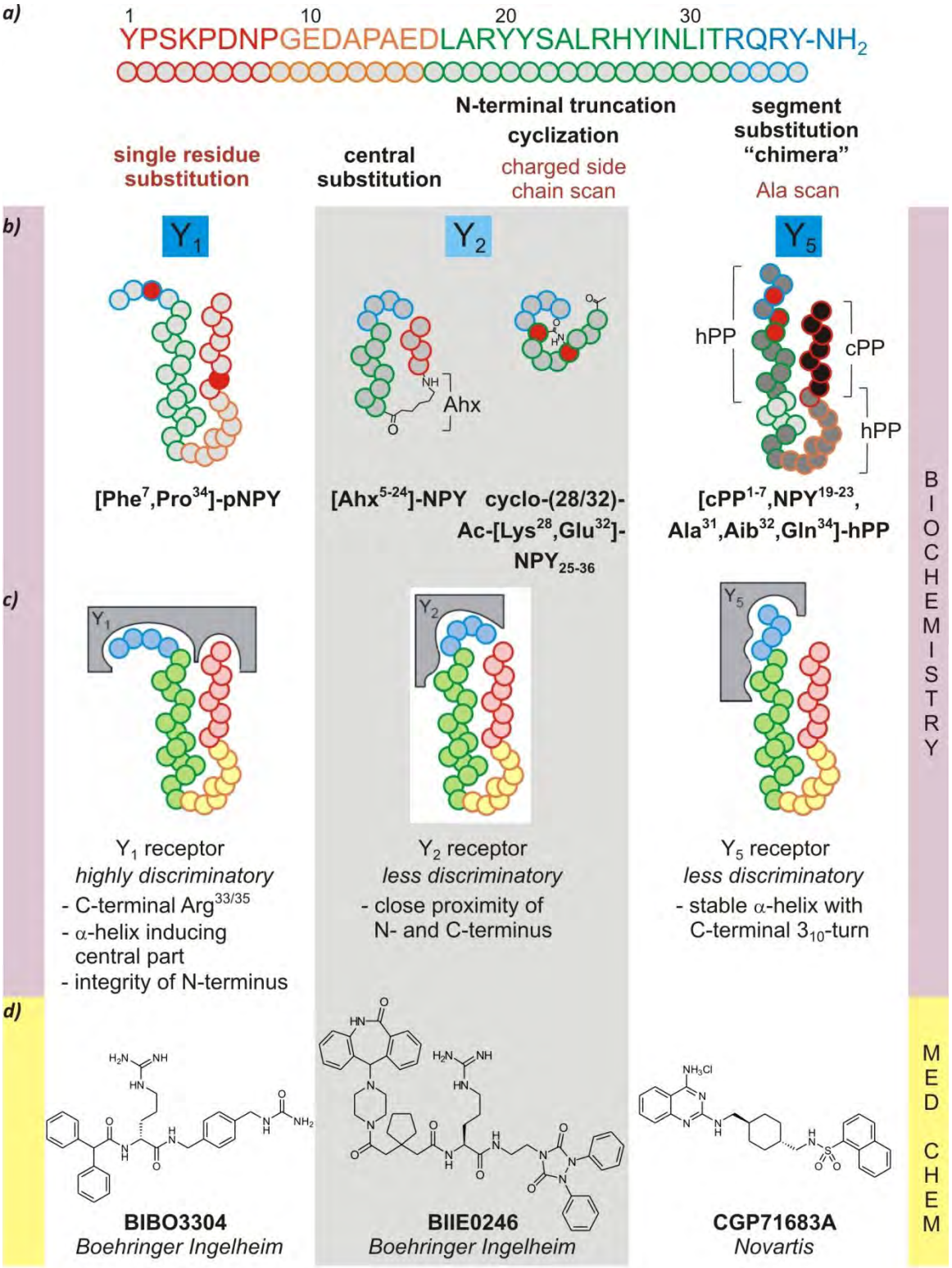

Figure 2.11. Comparison of selected NPY analogs: peptidic agonists and low-molecular weight antagonists. ***a)*** *Modifications applied to NPY, resulting in the analogs shown below for the elucidation of receptor binding. Every residue is represented by a circle in red (PPII-helical region 1-8), yellow (turn region 9-16), green (α-helical region 17-31), and blue (C-terminal tetrapeptide 33-36), respectively.* ***b)*** *Schematic representation of selective agonists at the Y_1 (left), Y_2 (middle), and Y_5 (right) subtype. Unmodified residues are marked grey, single substitutions are shown in red and hPP/cPP segments of the Y_5 selective chimera are marked in grey and black, respectively.* ***c)*** *Depiction of receptor binding prerequisites and of the assumed respective conformations of NPY.* ***d)*** *Structures of low-molecular weight selective antagonists.*

(figure 2.11b, left) showing the best binding profile.[60] In contrast, the first non-peptidic antagonist had already been identified several years before,[61] and figure 2.11d (left) shows the antagonist BIBO3304 discovered in 1998.[62] The comparison with the Y_2 selective antagonist BIIE0246 (figure 2.11d, center) developed in 1999[63] reveals some common structural details like the incorporation of an Arg residue as the only "peptidic" motif (although with different stereoconfiguration), while the perhaps most noticeable difference consists in the absence of the "C-terminal" iminocarbamate of BIBO3304 which mimics the essential Tyr^{36} amide. However, as already mentioned, such low-molecular weight compounds cannot serve to elucidate the configurations of the natural ligands. This can only be accomplished by near-native analogs, as shown by comparing the Y_1 and Y_2 agonists (figure 2.11b). In contrast to the requirement for Y_1 binding, the integrity of the peptide is not required any more at the Y_2 subtype and the intermediate segment can be substituted by a flexible Ahx, as accomplished in the case of the agonist [Ahx^{5-34}]-NPY. A superb Y_2 selectivity is also obtained by deletion of the section of residues 1-24 and cyclization of the introduced Lys^{28} and Glu^{32} side chains.[64] The lactam bridge causes a tight hairpin that orients both peptide parts closely to each other, which is very reminiscent of the proposed conformation of native NPY (figure 2.11b and c, center).

After the discovery of the Y_5 receptor and its important physiological functions[65, 66] researchers mainly focused on this subtype. It turned out that, like at the Y_1 and in contrast to the Y_2 receptor, the truncation of central segments is not tolerated[55] and that the stability of the α-helix is important but not the only prerequisite. By single amino acid replacements, the Ala^{31}-Aib^{32} motif (Aib = aminoisobutyric acid) which induces a 3_{10}-helical turn conformation of the C-terminus was identified as key to Y_5 selectivity.[67] The best results were finally obtained by combining the segments of several NPY family members to so-called "chimeras".[68] Figure 2.11b (right) schematically depicts the cPP/NPY/hPP chimera [cPP^{1-7},NPY^{19-23},Ala^{31},Aib^{32},Gln^{34}]-hPP which is among the best Y_5 selective agonists identified so far.[69] By extensive library screening, a non-peptidic Y_5 antagonist, CGP71683A, containing a quinazoline and an arylsulfonamide was identified in 1998 (Figure 2.11d, right).[70, 71] Another Y_5 antagonist, S-2367 developed by *Shionogi Ltd.*, is the first candidate for an NPY-based obesity therapeutic and is currently undergoing phase IIb clinical trials.[72]

2.2.3 Motivation: The need for novel scanning strategies

Complete Ala and D scans were performed to evaluate the importance of the single residues for binding at the Y_1 and Y_2 receptor (the Y_5 profile was only examined for a part of the substitutions)[55, 73, 74] and served as data source for the studies carried out so far. Figure 2.10

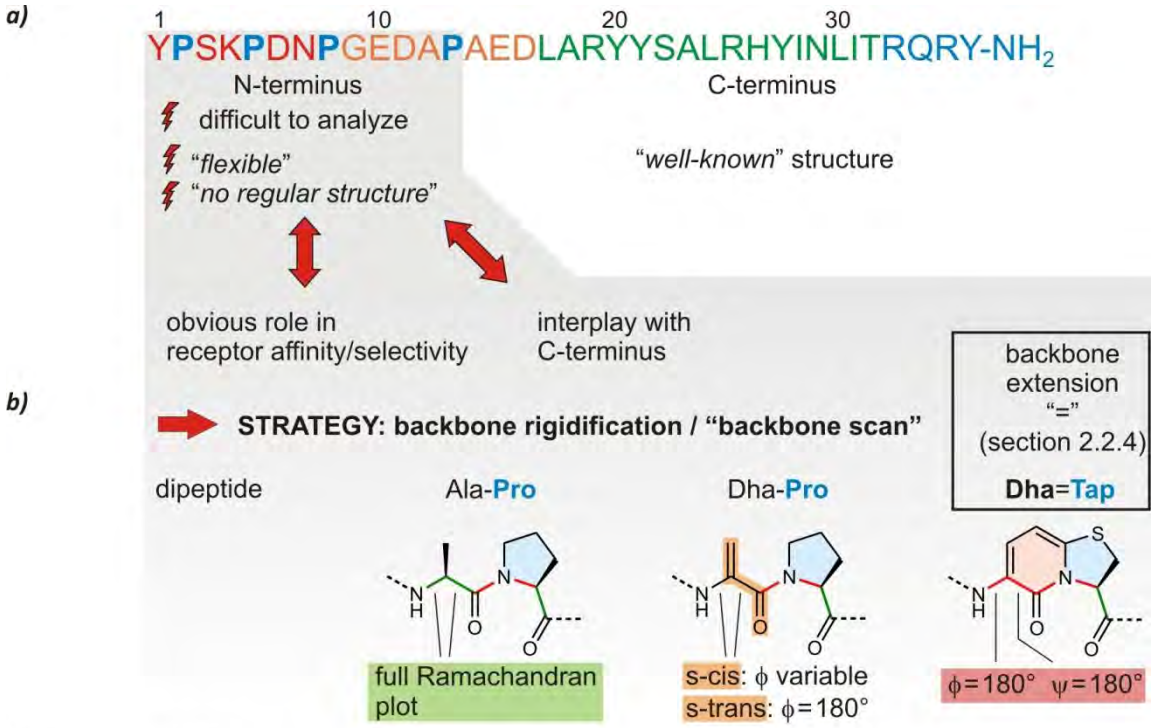

c)

	Ala/Dha		
ψ rotamers	72	72	1
ψ conformers	~25	2	1
	Ala/Dha		
ϕ+ψ rotamers	5184	5184	72
ϕ+ψ conformers	1008	73	1

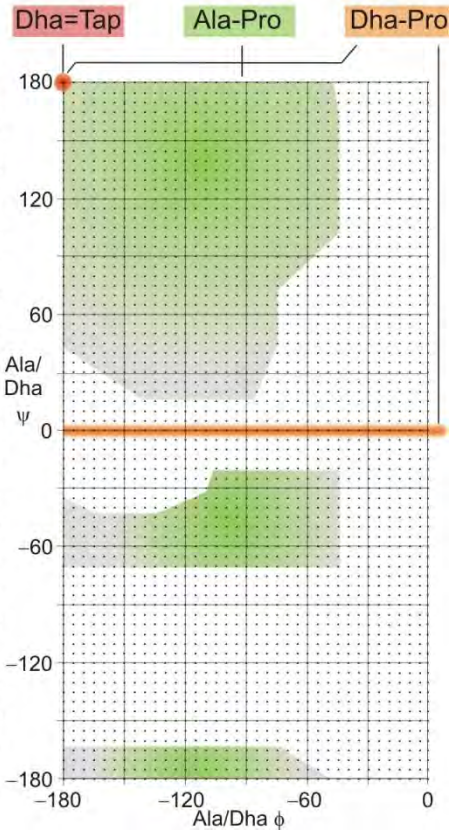

Figure 2.12 Backbone rigidification is a logical step to overcome the lack of information about Pro-rich peptide segments. *Our strategy to tackle this problem* ***(a)*** *is shown schematically by conformational fixation of an Ala-Pro dipeptide in two steps* ***(b)****. Rotatable bonds are marked green and freezed bonds in red, respectively.* ***c)*** *The three differently restrained dipeptides are compared with respect to their number of rotamers and conformers. This is carried out according to the procedure which is described in more detail in section 3.2.2. The number of rotamers is determined by 5° increment of the respective angle(s), which results in 72 rotamers for a single angle and in 5184 (= 72²) for a pair of angles, as it is the case for the Ala. The conformers exhibit the fraction of rotamers which are actually populated in the real system.* ***d)*** *For all three cases, the allowed conformational space of the ϕ/ψ pair is shown in the relevant part of the Ramachandran plot (green: Ala-Pro, orange: Dha-Tap, red: Dha=Tap). The 5° increments are symbolized by the dot matrix, and the number of dots in the populated areas resemble the allowed number of conformers. There is a great restriction of Dha in contrast to Ala (72 conformers in the case of s-cis (orange line) and one conformer in the case of s-trans (orange dot)), and the second tethering which leads to the Dha=Tap unit finally results in one single conformation with ϕ = ψ = 180°.*

schematically depicts the binding loss of the Ala- and D-substituted analogs at the Y_1 and Y_5 receptor. Clearly, in the light of the preparative effort, the gain of information by comparison of values for Y_1 and Y_5 at the single positions as well as by the evaluation of how the affinities change along the peptide sequence, is rather moderate. Indeed, essential residues like the N-terminal prolines or the arginines at position 32 and 34 can be identified by the above-average affinity loss associated with their substitution. Furthermore, the affinities are particularly susceptible if the C-terminal part is affected, especially in the case of D substitution. However, there is a lack of clear *trends* concerning the receptor affinities. It would be far more important if systematic preferences for one single receptor, according to the substitution pattern, could be revealed, which actually is the key to understanding the receptor discrimination and to utilize this knowledge for the successful development of NPY-based therapeutics (section 2.1.2.1). The fact that biochemistry must answer fundamental questions in order to serve as fundament for medicinal chemistry, has, in the light of the effort spent to date, been brought to the point in the case of the Y_1 receptor: "(…) *an agonist with high selectivity at the Y_1 receptor that may confirm or not the results obtained so far by using selective antagonists is still missing. The better the understanding of the NPY system the higher will be the chance for drug design*."[2] One important step towards this understanding would be the identification of distinct receptor trends, and it is clear that novel methodologies are required in order to gain a systematic picture of which structural details are responsible for selectivity towards the respective receptor subtypes.

These obstacles served as motivation for the research on NPY which has been done within the scope of this thesis. We thereby focused on the Y_1 and Y_5 receptor subtypes which are especially important to be understood and controlled with respect to ligand selectivity trends as they serve as appetite-controlling receptor pair in the organism. On the one hand, Y_5 selectivity turned out to be a key to possible therapeutics against obesity, and the first promising candidate is already under clinical trials (section 2.2.2).[72] On the other hand, as Y_1 receptors are overexpressed by more than 90% of all breast tumors and of 100% of the examined metastases,[75] Y_1 selectivity of radiolabelled NPY analogs has recently been proven to enable highly sensitive diagnosis of cancer tumors and metastases in first clinical tests and gives a perspective to apply similar peptides as carriers of chemotherapeutic agents.[76] The basic ideas that underlie the development of our novel peptide scanning method, as well as the characteristics and advantages of the artificial dipeptide unit, are specified in the next section.

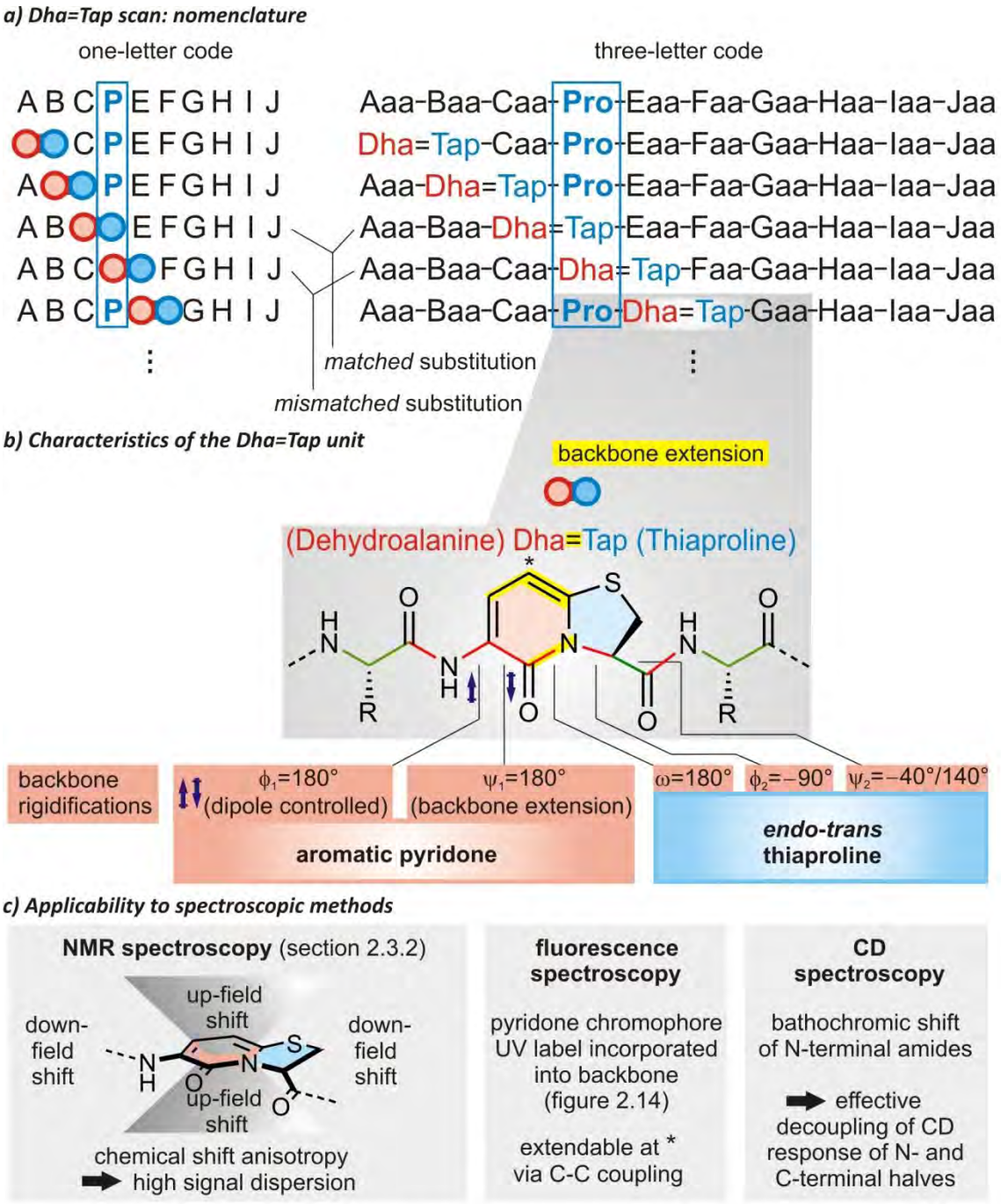

Figure 2.13 The Dha=Tap backbone scan. ***a)*** *Compared to the established single-residue scans like the Ala and D scan (figure 2.10f), the Dha=Tap scan replaces two adjacent amino acids. The chosen denotation of the dipeptide in the one-letter code (left) is a bicyclic symbol, while in the three-letter code the second link of both residues is emphasized by the use of a hyphen "=". The shown segment contains a Pro residue (blue) to emphasize the option to introduce the dipeptide at matched or mismatched positions. In the matched substitution, the native Pro is replaced by the Tap (thus, the position of the 5-membered prolyl ring is conserved) and the Dha substitutes the N-terminal adjacent residue. With the Dha=Tap in the mismatched position, the Dha is at the native Pro position, while the Tap substitutes the C-terminal adjacent amino acid.* ***b)*** *Structural formula of a Xaa-Dha=Tap-Xaa tetrapeptide. Rotatable backbone torsions are marked green, and all frozen bonds are marked red. The two covalent linkages of Dha and Tap which are descriptively denoted by the hyphen are highlighted by yellow bars. All torsional restrictions within the Dha (red) and the Tap (blue) are listed in red boxes.* ***c)*** *Because of its properties, the Dha=Tap dipeptide is an excellent label for NMR, fluorescence, and CD spectroscopy. In addition to the rigidfication of the modified peptide segment, Dha=Tap incorporation results in increased hydrophobicity.*

2.2.4 The dipeptide backbone scan: A consequent advancement of existing scanning strategies

The starting point for our synthetic work was the search for a peptide unit for the characterization of Pro-rich and flexible peptide and protein segments which, as they are difficult to analyze, can be the sore spot in the analysis of how the interaction of all parts finally causes biological activity and selectivity (section 2.1.8). The N-terminus of NPY which is a prime example of such segments, should thereby serve as test substrate, with the identification of receptor trends concerning the prominent Y_1 and Y_5 receptor pair (sections 2.1.2 and 2.2.3) being a desirable goal.

In the light of the necessity to cope with the "flexibility" of the N-terminus, the strategy of structural rigidification was considered as step towards the right direction. Concerning the possibilities to apply specific modifications to peptides and proteins, modern chemical synthesis can show its full strength as it provides an arsenal of amino acids as well as isosters thereof going far beyond what is available by the genetic code. For example, the Ala can be substituted against a dehydroalanine (Dha) which leads to a planarization of the backbone (Figure 2.12b). This has great implications for the rigidity of the backbone as the ψ torsion is now restricted to two conformations (s-*cis* and s-*trans*). While the ϕ torsion is still variable in the s-*cis* conformation, it will be restricted to one single value (180°) in the s-*trans* conformation due to dipole interactions. The next logical step and the experimental implementation are achieved by cyclization of the Dha side chain with the adjacent Pro δ-position, resulting in an aromatic pyridone ring. This motif fulfills a key role as it freezes the ϕ/ψ pair of the Dha to a single conformation, or, from another point of view, restricting the Pro amide (which is well-known to be inclined for *cis*/*trans* isomerization) to a *trans* amide. Furthermore, the pyridone ring serves as a chromophore, and there is no reactive Michael acceptor site present, in contrast to the un-fused Dha. If a thiaproline (sulfur at γ-position) is present this results in the bicyclic dipeptide unit which was used for the research within the scope of this thesis (Figure 2.12b). Its 6,5-bicycle corresponds to an aromatic 3-amino-2-pyridone ring which is fused with the thiaproline at position 1 and 6. The atom sequence of the backbone is conserved and thus a substitution of a dipeptide by this unit has the important feature to be bioisosteric (as outlined in section 2.2.1). As shown in Figure 2.13a, this dipeptide can be used for a novel scanning method which may conveniently be described as a "dipeptide backbone scan", and this strategy proved to be the right step for successful analysis of the NPY N-terminus (section 2.3). By shuffling the unit along the backbone, certain backbone torsions are systematically frozen and thus conformational information is included in the peptide segment. Furthermore, if Pro residues are present,

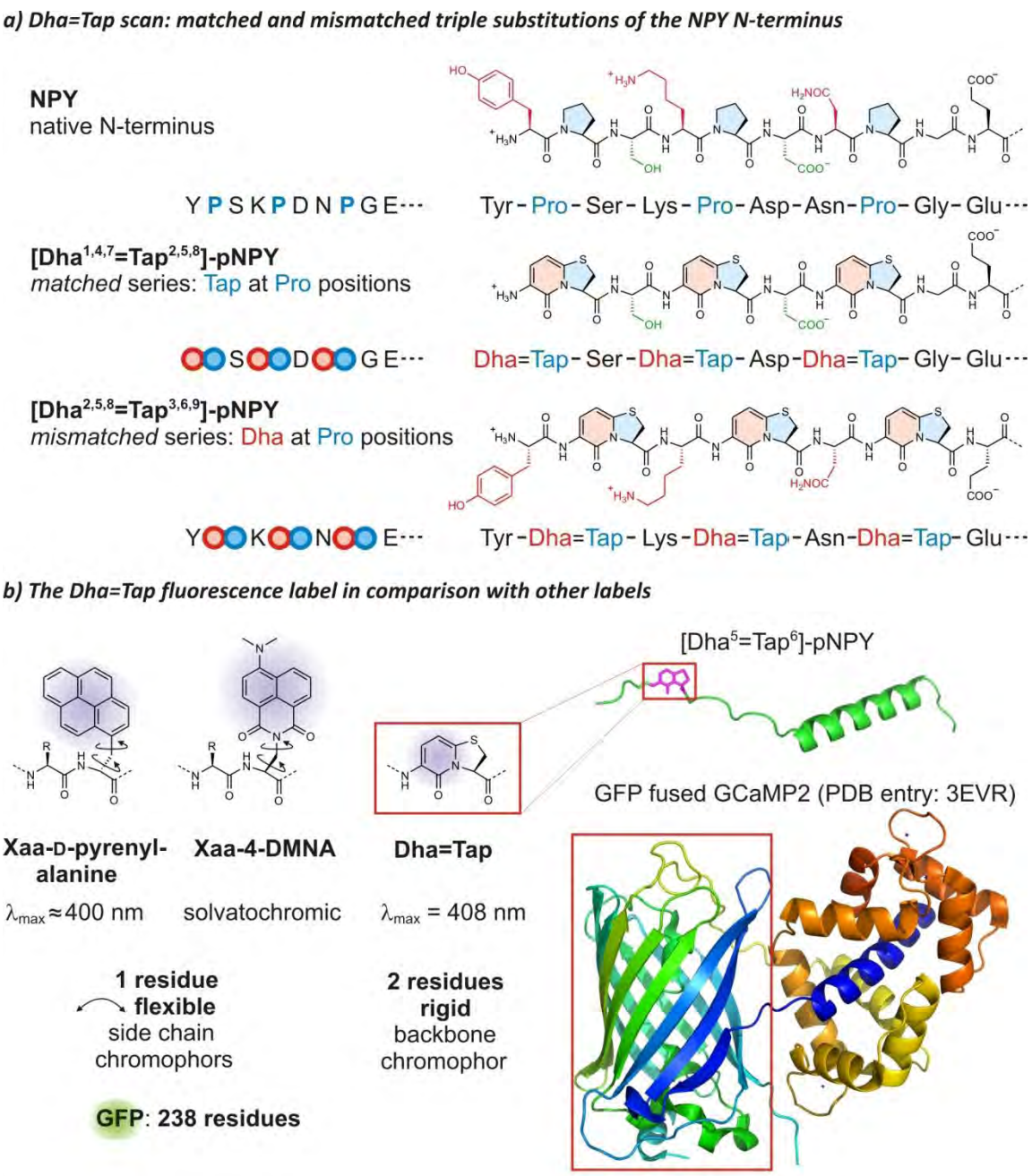

Figure 2.14 The Dha=Tap backbone scan: application in matched and mismatched substitution series and as flourescence label. ***a)*** *Comparison of matched and mismatched triple substitution of the N-terminus of NPY. The residues N-terminal to the Pro positions (marked in red) are substituted in the matched series, while all C-terminal residues (green) are not present in the mismatched series. In addition to the rigidification, the substituted segment is highly hydrophobized.* ***b)*** *Side-chain fluorescence labels (two examples are shown) suffer from the high steric demand of the bulky aromatic hydrophobic motifs which can greatly influence secondary and tertiary structures of modified peptides. Furthermore, the side chain position is associated with flexibility as indicated by the arrows. The Dha=Tap label shows comparable fluorescent properties but overcomes all these drawbacks by ist small size and fixation as a part of the backbone. On the right, the 36 residue NPY analog with one Dha=Tap unit at position 5-6 is compared with the 413 residue GCaMP2 (Ca^{2+} sensor protein calmodulin (CaM) fused with a green fluorescent protein (GFP)). Of course, any comparison of GFP with synthetic low-molecular weight must be made with care due to the highly different synthesis and application profiles (for example, the protein fluorophores are available by gene expression). The comparison of the Dha=Tap with the GFP fluorophore (red boxes) impressively demonstrates the different sizes of the fluorophores. 4-DMNA = 4-*N,*N-dimethyl-amino-1,8-naphthalimido-alanine.*

matched (Tap at Pro position) and *mismatched* (Dha at Pro position) analogs can be compared (figure 2.14a) which yields information on receptor binding trends in the examined case of the N-terminus of NPY (section 2.3). As in the one-letter code the common alphabet is almost completely required for the proteinogenic amino acids, other appropriate symbols are often used,[77] and the dipeptide can be descriptively symbolized by a bicyclic icon (figures 2.13 and 2.14). To indicate the double backbone linkage we introduced the equals sign "=" for the three-letter code in the respective publication.[38]

The Dha=Tap dipeptide unit has been developed by *Seger*, *Tremmel* and *Geyer*[78, 79] and is well available on gram scale as enantiomerically pure Fmoc-protected pyridone carboxylic acid which is ready for use in solid-phase peptide synthesis (SPPS). The gram-scale availability of an Fmoc-Xaa-Yaa-OH dipeptide does not apply for many other systems, but it is an important aspect as it allows a complete scan with a single batch. Furthermore, Dha=Tap can be coupled by SPPS standard protocols without the danger of racemization due to oxazolidinone formation. Within the scope of this thesis, the novel scanning method was successfully established for the analytics of the NPY N-terminus, a Pro-rich "flexible" (and therefore difficult to analyze, section 2.1.8) peptide segment. Figures 2.13 and 2.14 list the characteristics of the Dha=Tap unit which proved superior in various aspects. In addition to the decisive constriction of conformational space of the backbone by fixing three torsion angles and keeping the Tap amide in a *trans* conformation, it greatly enhances and facilitates the gain of information by NMR spectroscopy due to the high signal dispersion and chemical shift anisotropy caused by the aromatic pyridone ring. Furthermore, UV and CD spectroscopy profit from the extension of the amide chromophore of the peptide backbone toward an aromatic heterocyclic ring system which can be further extended by C-C couplings.[79] This direct incorporation of a fluorophore into the backbone is so attractive because it only requires a minimum change in the substrate's size and composition. Peptide-based sensors carrying fluorophores in their side chains have recently come into the focus of research[80, 81] as they exhibit an alternative to the fluorescent proteins (for example, green fluorescent protein (GFP)) without which protein tracking would be unimaginable today.[82] It is the much smaller size of such chromophores compared to the size of fluorescent proteins which makes them so attractive, as they should to a far less extent influence trafficking and binding of the substrates they are attached to. Here, organic chemistry again shows its strength because, as recently pointed out, "*the range of useful GFP variants pales in comparison with the commercially available synthetic fluorophores*".[83] The Dha=Tap unit exhibits another attractive option as here the fluorophore is not located in the side-chain but a fully integrated part of the backbone.

Table 2.4 Synthesized full-length NPY analogs. *The Dha=Tap units are displayed as red/blue bicyclic icons (section 2.2.4). The peptides are arranged according to the Dha=Tap position(s) and (with exception of the [12=13] analog) every mismatched substitution is written below the respective matched analog. Further N- and C-terminally truncated analogs are described in ref. [36]. The HPLC elution in % refers to the amount of solvent A (0.08% TFA in CH_3CN) in a gradient of 10 to 60% A over 30 min. Solvent B: 0.1% TFA in water. All shown peptides were synthesized by M. Haack (Beck-Sickinger Group, University of Leipzig). See ref. [38] for details.*

peptide	acronym	sequence	binding at SK-N-MC Y_1		binding at HEC-1-B Y_5		HPLC
			K_i [nM]	rel. to pNPY	K_i [nM]	rel. to pNPY	elution
native pNPY	pNPY	YPSKPDNPGEDAPAEDLARYYSALRHYINLITRQRY-NH_2	9.3 ± 3.2	1	23 ± 1.4	1	46 %
[Dha^{1}=Tap^{2}]-pNPY	[1=2]	⬤⬤SKPDNPGEDAPAEDLARYYSALRHYINLITRQRY-NH_2	78 ± 1	8.4	101 ± 27	4.4	46 %
[Dha^{2}=Tap^{3}]-pNPY	[2=3]	Y⬤⬤PDNPGEDAPAEDLARYYSALRHYINLITRQRY-NH_2	99 ± 8	10.6	57 ± 8	2.5	47 %
[Dha^{4}=Tap^{5}]-pNPY	[4=5]	YPS⬤⬤NPGEDAPAEDLARYYSALRHYINLITRQRY-NH_2	85 ± 3	9.1	211 ± 19	9.2	47 %
[Dha^{5}=Tap^{6}]-pNPY	[5=6]	YPSK⬤⬤PGEDAPAEDLARYYSALRHYINLITRQRY-NH_2	91 ± 10	9.8	91 ± 6	4.0	47 %
[Dha^{7}=Tap^{8}]-pNPY	[7=8]	YPSKPD⬤⬤EDAPAEDLARYYSALRHYINLITRQRY-NH_2	39 ± 7	4.2	130 ± 5	5.7	46 %
[Dha^{8}=Tap^{9}]-pNPY	[8=9]	YPSKPDN⬤⬤DAPAEDLARYYSALRHYINLITRQRY-NH_2	109 ± 5	11.7	196 ± 12	8.5	48 %
[Dha^{12}=Tap^{13}]-pNPY	[12=13]	YPSKPDNPGED⬤⬤AEDLARYYSALRHYINLITRQRY-NH_2	7.4 ± 1	0.8	30 ± 4	1.3	46 %
[Dha^{1,4}=Tap^{2,5}]-pNPY	[1=2,4=5]	⬤⬤S⬤⬤NPGEDAPAEDLARYYSALRHYINLITRQRY-NH_2	180 ± 35	19.4	241 ± 16	10.5	47 %
[Dha^{2,5}=Tap^{3,6}]-pNPY	[2=3,5=6]	Y⬤⬤K⬤⬤PGEDAPAEDLARYYSALRHYINLITRQRY-NH_2	201 ± 9	21.6	77 ± 16	3.3	48 %
[Dha^{1,7}=Tap^{2,8}]-pNPY	[1=2,7=8]	⬤⬤SKPD⬤⬤EDAPAEDLARYYSALRHYINLITRQRY-NH_2	76 ± 10	8.2	142 ± 11	6.2	50 %
[Dha^{2,8}=Tap^{3,9}]-pNPY	[2=3,8=9]	Y⬤⬤KPDN⬤⬤DAPAEDLARYYSALRHYINLITRQRY-NH_2	342 ± 32	36.8	175 ± 20	7.6	50 %
[Dha^{4,7}=Tap^{5,8}]-pNPY	[4=5,7=8]	YPS⬤⬤D⬤⬤EDAPAEDLARYYSALRHYINLITRQRY-NH_2	92 ± 4	9.9	188 ± 27	8.2	48 %
[Dha^{5,8}=Tap^{6,9}]-pNPY	[5=6,8=9]	YPSK⬤⬤N⬤⬤DAPAEDLARYYSALRHYINLITRQRY-NH_2	213 ± 54	22.9	86 ± 12	3.7	48 %
[Dha^{1,4,7}=Tap^{2,5,8}]-pNPY	[1=2,4=5,7=8]	⬤⬤S⬤⬤D⬤⬤EDAPAEDLARYYSALRHYINLITRQRY-NH_2	304 ± 62	32.7	286 ± 43	12.4	50 %
[Dha^{2,5,8}=Tap^{3,6,9}]-pNPY	[2=3,5=6,8=9]	Y⬤⬤K⬤⬤N⬤⬤DAPAEDLARYYSALRHYINLITRQRY-NH_2	326 ± 12	35.1	140 ± 18	6.1	50 %

2.3 Results and discussion

The research described in this chapter was performed in cooperation with the *Beck-Sickinger* group (*M. Haack*, University of Leipzig). Using the Dha=Tap building blocks which were provided by *H. Seger* (*Geyer* group, University of Marburg) as Fmoc-protected substrates ready for SPPS,[79] peptide synthesis as well as CD spectroscopic investigations and receptor binding experiments were done in the *Beck-Sickinger* group. The own work which was done within the scope of this thesis comprised contributions to the identification and discussion of the receptor trends, all NMR spectroscopic investigations and molecular modeling studies.

2.3.1 The backbone scan reveals distinct receptor trends

All synthesized full-length peptides (for further truncated analogs see ref.[38]) are listed in table 2.4 according to the Dha=Tap position. In the search for a readable and uncomplicated indication of the pyridone dipeptide position(s) we decided to use numbers in brackets (table 2.4, second column): for example, the single substituted [Dha^1=Tap^2]-pNPY is abbreviated to [1=2]. Multiple substitutions are indicated by commata between the pairs of numbers: instead of [$Dha^{2,8}$=$Tap^{3,9}$]-pNPY, for example, the acronym [2=3,8=9] is used. This nomenclature is used throughout the text and in the following figures concerning the receptor binding studies.

2.3.1.1 Overview: The Y_1 and Y_5 subtypes differentiate matched- and mismatched substitutions

In table 2.4, all analogs are brought to a first logic order according to the position and the number of substitutions. For clarity, all four Pro residues (positions 2, 5, 8, 13) are colored blue to emphasize the substitution by the Dha (shown as red circle, mismatched position) or Tap (shown as blue circle, matched position) motif of the Dha=Tap unit. The list starts with the native sequence and the seven single substitutions. All Pro residues have been matched-substituted (peptides [1=2], [4=5], [7=8], [12=13]), and the three positions within the segment capable for PPII-formation have also been mismatched-substituted (peptides [2=3], [5=6], [8=9]). The following multiple substitutions were made for Pro at positions 2, 5, and 8. All combinations of double substitutions were synthesized for the matched- and mismatched position, yielding three different combinations for matched and mismatched, respectively. Finally, a triple substituted matched substrate [1=2,4=5,7=8] and its mismatched analog [2=3,5=6,8=9] (see figure 2.14b for structural formula) were investigated. Table 2.4 also lists the K_i values at the Y_1 and the Y_5 receptor which were determined by competitive binding assays. Using cells which are

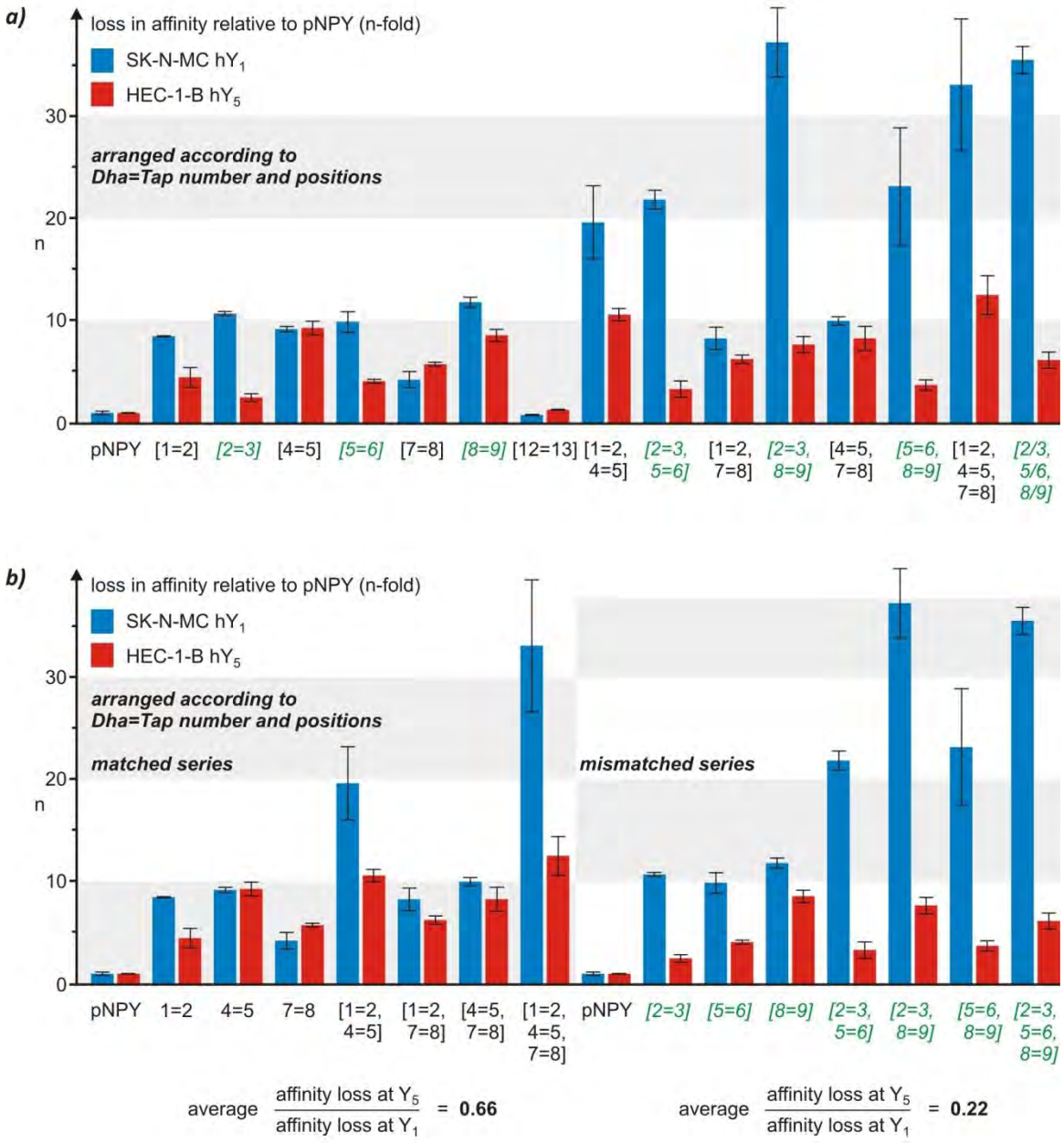

Figure 2.15 Receptor affinities: Overview and matched vs. mismatched substitutions. ***a)*** *Depiction in order according to table 2.4. To point out matched- and mismatched substitutions, the acronyms of the mismatched series are written green and in italic letters.* ***b)*** *Comparison of matched and mismatched analogs. There is a distinct preference of the mismatched substitutions at the Y_5 receptor. The matched analogs exhibit on average a 1.5-fold higher affinity loss at the Y_1 subtype, but a 4.5-fold higher loss is observed on average for the mismatched analogs.*

expressing the respective receptor types (hY_1: human neuroblastoma cell line SK-N-MC; hY_5: human endometrial carcinoma cell line HEC-1-B),[84] the single NPY analogs were tested for their ability to compete with radiolabeled native pNPY. Some analogs were also examined in a signal transduction assay which indicated receptor activation in an agonistic manner, which can also be assumed for the other analogs.[38] Compared to the K_i values, the relative loss of affinity (n-fold in comparison to the native ligand) exhibits a value more comfortable to use as it has no unit and does not require comparison with the reference value of native pNPY (Table 2.4). A consequent use of this value for diagrams has been made in this work because it yields descriptive pictures of the relative loss of receptor affinity: the higher the respective bar, the worse is the binding of the ligand. As the evaluation of binding selectivity (Y_1 vs. Y_5 receptor activity) should be the center of attention, a pair of bars is thoroughly used for all analogs, with the blue bar indicating the loss of affinity at the Y_1 receptor and the red bar showing the affinity for the Y_5 subtype.

The order of analogs chosen in Figure 2.15a is in accordance with the listing in Table 2.4. The first impression given by this overview is the extraordinary low affinity loss of all analogs compared to the results of other scans. At the Y_1 receptor, affinities are not reduced more than 37-fold, and it is even less at the Y_5 subtype (which is known as less discriminatory in comparison to Y_1)[2] where the reduction in affinity does not exceed 12-fold. These values must be seen in the light of the drastic effects obtained by the Ala scan: for example, the substitution of Pro^2 resulted in a 500-fold loss and the replacement of Pro^5 in a 1000-fold decrease of affinity at the Y_1 subtype while, the single substitutions by Dha=Tap are much better tolerated, with affinity losses as low as 7- to 11-fold. At the Y_5 subtype these differences are, though not that immense, still significant. Figure 2.10f (section 2.2.3) which depicts the losses of affinity in a logarithmic manner gives a good impression of these highly different consequences of Ala- and Dha=Tap substitutions, respectively.

Therefore, as a first result it turned out that each receptor accepts the impacts on rigidity and functionalization that are associated with the incorporation of Dha=Tap. A comparison of the profiles of single- and multiple-substituted analogs shows that an increasing number of Dha=Tap units in the N-terminus is tolerated at both receptor subtypes. On average, it leads to only slightly increased affinity losses at Y_1, and the binding at Y_5 is even less affected. With exception of the matched single-substituted [4=5], [7=8] and [12=13] analogs, all peptides show a (mostly moderate) preference for the Y_5 subtype. An growing number of Dha=Tap units also effects an increasing hydrophobization which is experimentally confirmed by the HPLC retention times (Table 2.4 and ref.[38]).

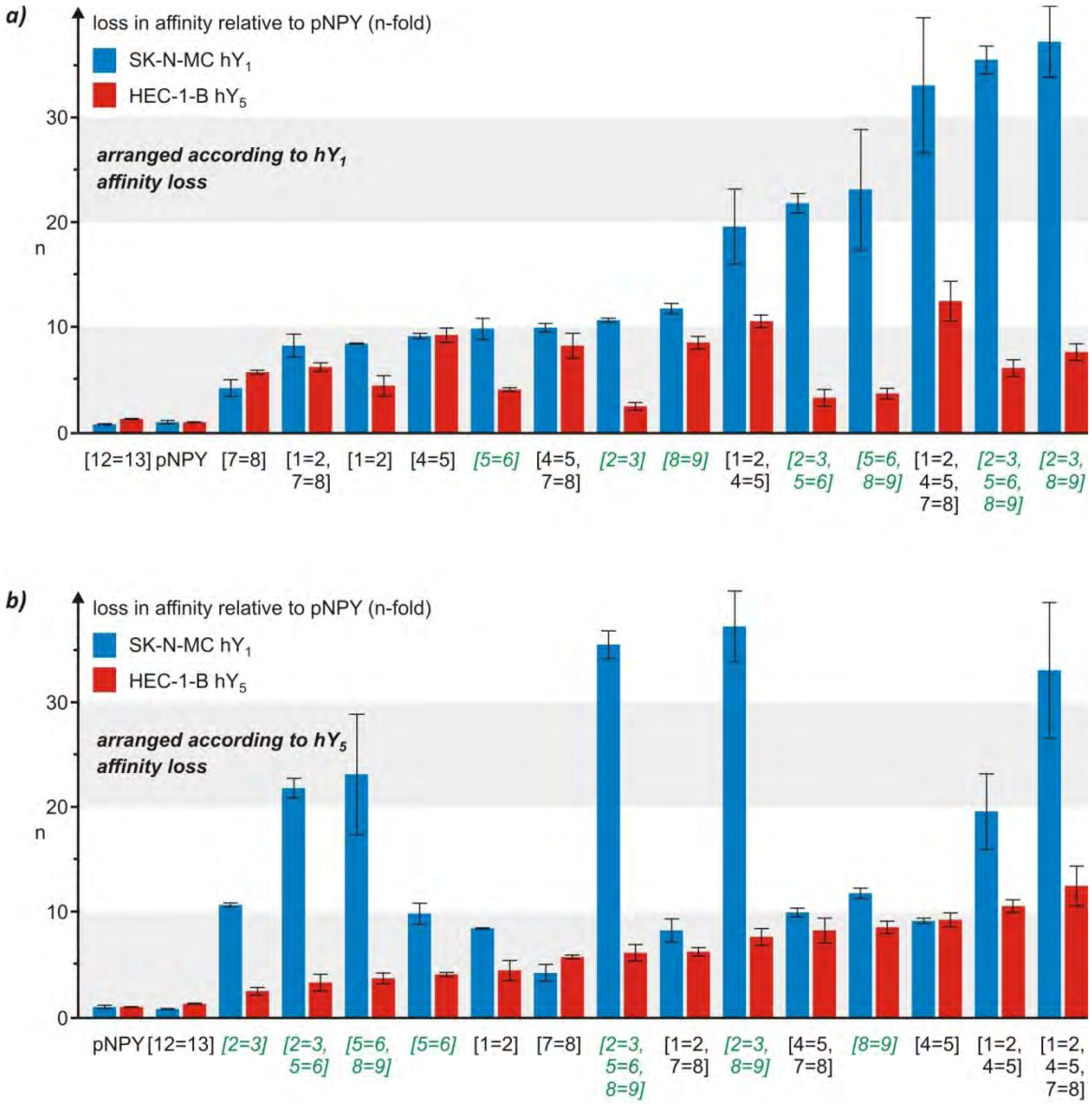

Figure 2.16 Receptor affinities: Order of affinity loss at the Y_1 (a) and Y_5 (b) receptor subtype. *Both orders greatly differ from each other as visible from the irregular binding loss variations at the respective other subtype. While the matched analogs on average bind better at the Y_1 subtype, they are rather distributed towards the analogs with worse binding at the Y_5 subtype.*

Figure 2.15b presents another overview of the binding profiles, again according to the position but now grouped into matched (left) and mismatched (right) substitutions. A comparison of the respective receptor profiles gives another significant result. The average affinity at the Y_1 receptor is significantly higher in the matched series while in contrast the Y_5 binding is on average better if Dha=Tap units are occupying mismatched positions. Furthermore, the preference of mismatched analogs for the Y_5 subtype is distinctly higher (except for [8=9], the quotient of Y_1/Y_5 affinity loss is greater than 2 for all analogs) while most of the matched substitutions lead to rather similar losses for each receptor. Overall, the exact position of the Dha=Tap units is more important for the Y_5 than for the Y_1 receptor binding ability. These different receptor binding patterns, with the Y_5 subtype clearly preferring the mismatched series, show that the placement of Dha=Tap at an – apparently – "wrong" position is far from being just an irrelevant "side option". Although the term "mismatched" in the light of these results is actually misleading, it will be further used in the text and solely refers to the position of the Tap with respect to the native Pro and not to any binding properties.

2.3.1.2 Further influences: Substitution number, total charge, and aromaticity of the N-terminus

Considering the effects of matched vs. mismatched substitutions on the receptor profiles, the next question concerns the influence taken by the number of substitution and by the deletion of certain side chains. In Figure 2.16, the single substitutions are arranged according to the binding loss at the Y_1 (a) and at the Y_5 (b) subtype. It is noticeable that the 12=13 substitution binds to the Y_1 subtype even better than native NPY, and that the Y_5 affinity is only slightly decreased (1.3-fold). This observation will be discussed in the context with the molecular modeling studies in section 2.3.2. Regarding the decreasing receptor affinities for each subtype, as depicted in figure 2.16, it is interesting to compare how the respective binding affinities at the other receptor subtype evolve. Clearly, neither the Y_5 nor the Y_1 affinity loss shows a regular increase as the respective other profile, which again demonstrates that only certain Dha=Tap substitutions lead to a more significant Y_5 preference. There is an interesting difference between the Y_1 and Y_5 series concerning the number of Dha=Tap units. The positions of single, double, and triple substitutions in the Y_1 sequence (a) are distributed as one may intuitively predict for an increasingly modified native structure: the single substitutions are rather among the more active analogs while the double and, above all, the triple substitutions concentrate in the group of substrates with lower affinity. The situation at the Y_5 subtype, however, is remarkably different. All substitution types are shuffled and distributed along the whole lineup, and there

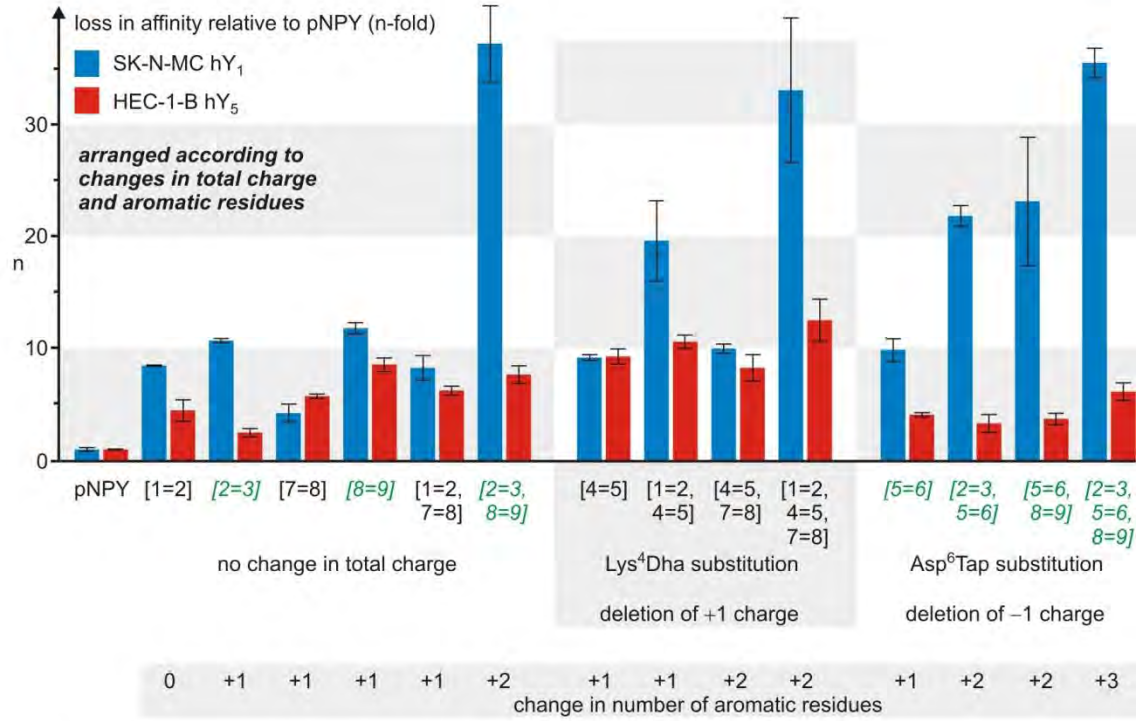

Figure 2.17 Receptor affinities: Influence of charge deletions. *All analogs (except [12=13]) in order according to the charge deletion, and within the groups according to the Dha=Tap number and positions. The deletion of the positively charged Lys^4 is not tolerated at the Y_5 subtype while the analogs with substitution of the negatively charged Asp^6 are among the substrates with highest Y_5 affinity.*

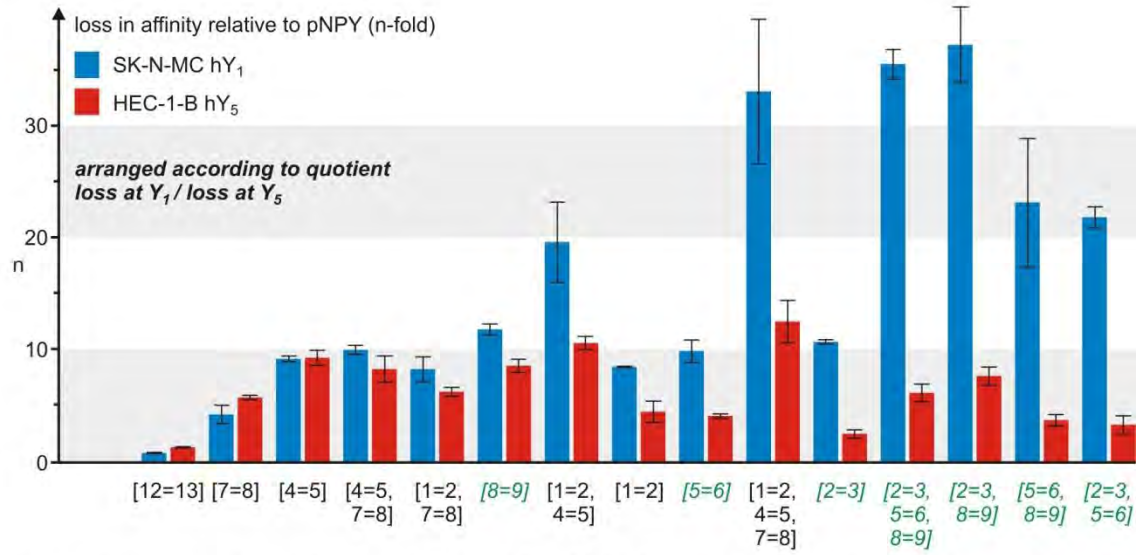

Figure 2.18 Receptor affinities: Quotients of Y_1/Y_5 affinity loss. *As already indicated by comparison of the average quotients of affinity losses in figure 2.15b, the highest Y_5 selectivities are observed for the mismatched analogs.*

are single substitutions ([8=9] and [4=5]) which are distinctively less tolerated than a triple incorporation of Dha=Tap ([2=3,5=6,8=9]).

In search for the origin of these different binding profiles it is worth to have a closer look at charges and polarities of the modified N-terminal segments. Therefore, in figure 2.17 all examined analogs are arranged in three groups according to the change in total charge (left: no change; center: deletion of one positive charge by substitution of Lys^4 by Dha (accomplished by a 4=5 matched position); right: deletion of one negative charge by substitution of Asp^6 by Tap (accomplished by a 5=6 mismatched position). Within these groups, the sequence follows the number and position of Dha=Tap units, as it also has been done for all other depictions described so far. Interestingly, this order within each group also corresponds to the total gain in aromaticity. Only the single Dha=Tap incorporation at position 1=2 keeps the number of aromatic residues constant (Tyr^1 is substituted by Dha^1) while all other substitution patterns result in the presence of one to three more aromatic motifs. No distinct affinity pattern becomes visible by these changes, but there seems to be a distinct influence of the varied N-terminal total charge on the Y_5 affinity. While the four peptides featuring deletion of the positively charged Lys^4 side chain exhibit the highest loss of affinity, the substitution of the negatively charged Asp^6 is associated with an only below-average affinity loss. At this point, it cannot be determined whether this effect results from the overall charge of the N-terminal segment or whether it is the side chain itself that plays a critical role in the receptor binding by, for example, participating in the ligand-receptor interplay via a distinct electrostatic interaction. However, the further results which are described in the following allow to assume that the interactions of single residues may be responsible for the “fine-tuning” of the respective overall conformation. Such subtle differences may be required for an individual receptor type and therewith be a decisive parameter for the ability of a substrate to differentiate the subtypes.

To further illustrate this, all substrates are rearranged with respect to their Y_5 receptor preference in figure 2.18. Also in this depiction a difference between matched- and mismatched series can clearly be made. While the Dha=Tap substitution at matched positions leads to mostly only slight Y_5 preferences or even effects the opposite, nearly all mismatched analogs bind clearly worse to the Y_1 subtype.

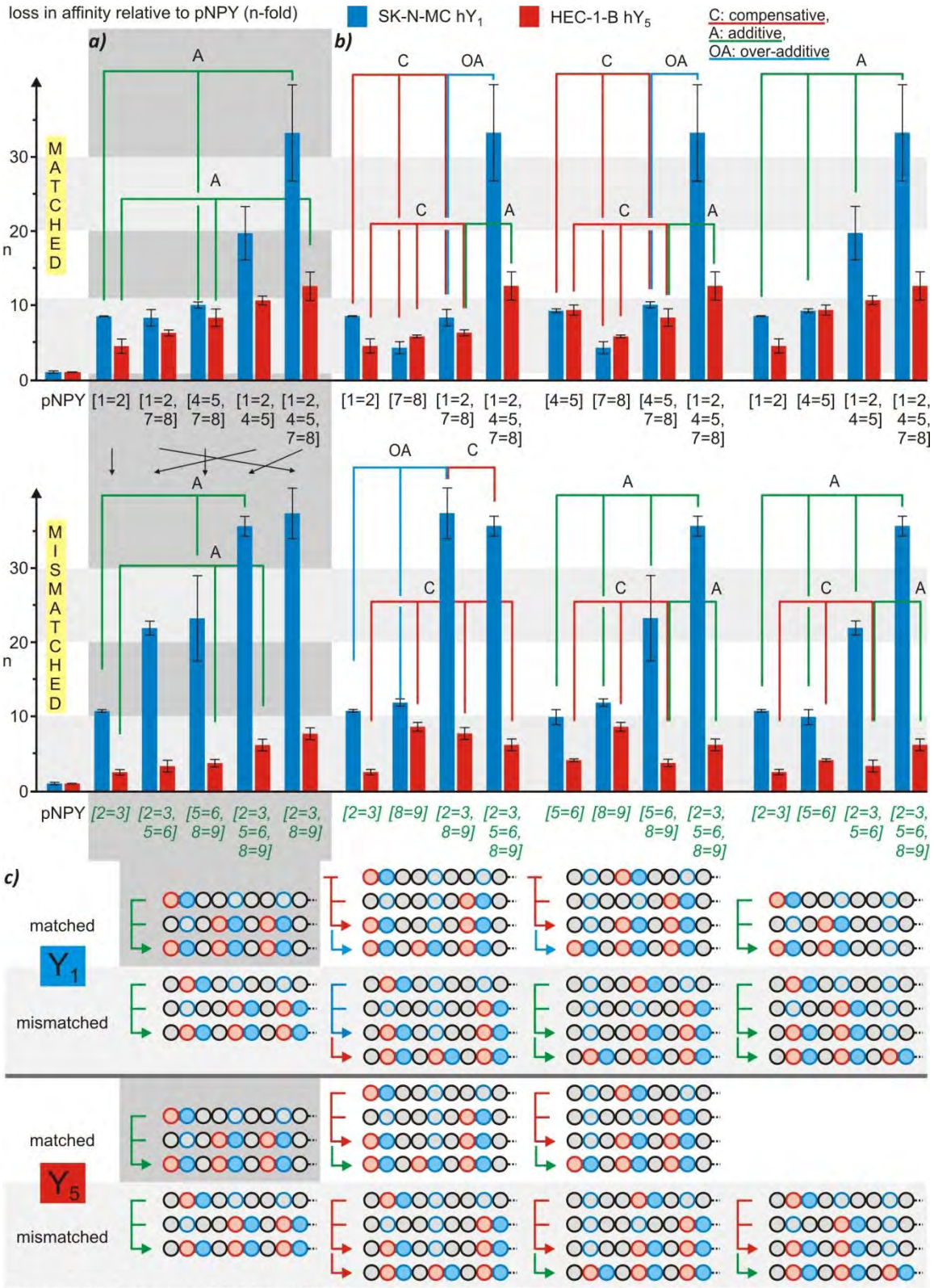

Figure 2.19 Receptor affinities: additive, over-additive and compensative effects caused by concomitant Dha=Tap introductions. ***a)*** *Comparison of series of matched (top) and mismatched (bottom) analogs with increasing loss of affinity at both receptors. The black arrows indicate how the order of analogs is rearranged.* ***b)*** *Comparison of identical substitution series of matched (top) and mismatched (bottom) analogs. In the mismatched series, several additive and over-additive effects observed at the Y_1 receptor are compensative at the Y_5 subtype, which demonstrates the high acceptance of multiple substituted mismatched analogs.* ***c)*** *Identical alignment of all effects shown above, with simplified depictions of the N-termini. Dha=Tap is symbolized by the bicyclic icon* ⬭.

2.3.1.3 Substitution variation patterns reveal additive, over-additive and compensative effects

These trends described in the preceding section encouraged us to have a closer look on certain substitution patterns. Starting with a single substitution, the effects of additional Dha=Tap units were examined, which revealed different systematic trends in receptor binding. Figure 2.19 shows some of the obtained receptor affinity profiles, wherein the matched substitution patterns (upper row) are consistently compared with their mismatched counterparts (lower row). Shown in the grey box (a) is a series with concurrent affinity loss at both receptors for the matched as well as for the mismatched substitutions. Both series start with the N-terminal single substitutions [1=2] and [2=3], respectively, but the sequence leading to concomitantly increasing Y_1 and Y_5 affinity loss is different, as indicated by the black arrows that link the matched with their respective mismatched analogs. A distinctive trend which similarly occurs in both series is an additive effect caused by the combination of the most N-terminal substitution with the complementary double substitution [4=5,7=8] and [5=6,8=9], respectively. As indicated by the green lines, this effect is observed for each receptor type and for the matched as well as for the mismatched substitution. All binding trends which are indicated in the diagrams are also pictured by schematics of the N-termini in figure 2.19c which are arranged according to the upper part of the figure.

The right part of figure 2.19b shows three quartets for each receptor which compare two single substitutions with the respective concomitant double introduction and the triple substitution. In the matched series, the Y_1 affinity is particularly affected by the concomitant introduction of Dha=Tap at positions [1=2] and [4=5] by an additive effect of both single substitutions (right). The other possible combinations, in contrast, give rather compensative effects (red lines) and it is only the triple substitution which leads to declined binding affinity (over-additive effect indicated by blue line). The Y_5 affinities evolve in a similar pattern, although it is not as pronounced as in the Y_1 binding.

In contrast, the trends at each receptor are highly different in the mismatched case, as shown by the identical line-up of the mismatched analogs in the lower right part of figure 2.19b. For example, the additive effect on Y_1 binding loss which was observed for the matched analogs occurs in a very similar manner by concomitant introduction at the mismatched positions [2=3] and [5=6]. Looking at the other possible combinations (figure 2.19b, left and center), in contrast, there are significant differences between matched and mismatched patterns as now additive and even over-additive effects (blue line) occur. Furthermore, the triple Dha=Tap incorporation in comparison to the [2=3,8=9] double substitution evokes a compensative effect (red line) in

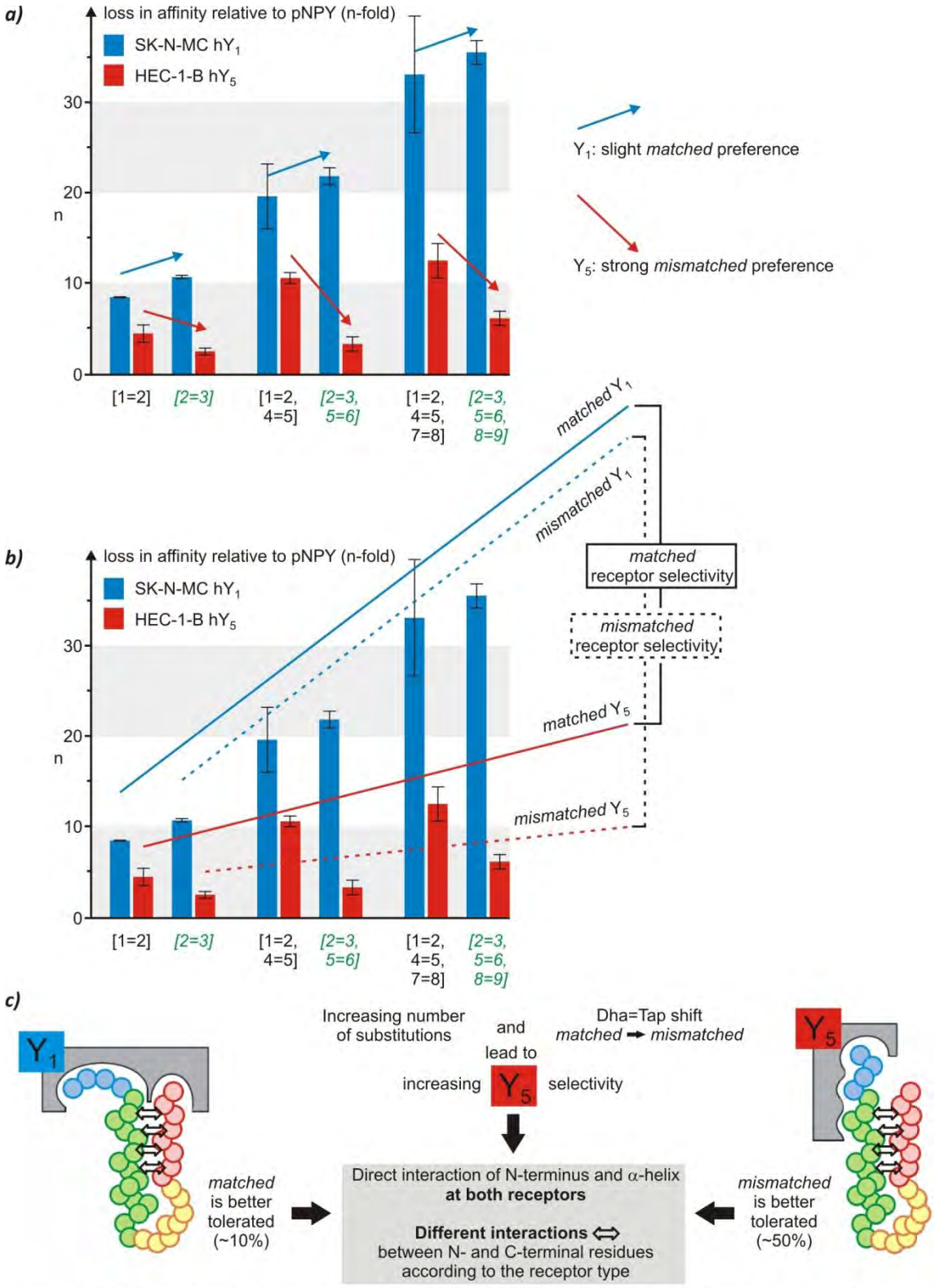

Figure 2.20 Receptor affinities: a possible strategy to high Y_5 selectivity. ***a)*** *In the series shown, all matched analogs lose approx. 10% affinity at the Y_1 subtype, while the mismatched analogs show significantly increased affinity at the Y_5 receptor (approx. 50%).* ***b)*** *The same series of analogs, now with indication of the increasing Y_5 selectivity according to the number of Dha=Tap units. In the mismatched case, this selectivity is considerably higher.* ***c)*** *Summary of the results with respect to the proposed receptor conformations (see also figure 2.11c). The unexpected high and systematic influence of the Dha=Tap position (matched or mismatched) suggests the interaction of certain residues according to the receptor subtype.*

sharp contrast to the high loss of Y_5 binding for the analogous matched analogs. The shown combinations of mismatched analogs are also highly different if the developments of Y_1 and Y_5 affinity are compared, which reveals the mismatched preference of the Y_5 receptor: the (over)additive effects observed at Y_1 are in contrast to the compensation at the Y_5 subtype evoked by double- or even triple substitution.

2.3.1.4 A key puzzle piece: Lining up Dha=Tap units towards the C-terminus results in Y_5 selectivity

The most valuable hints on the respective preference at each receptor subtype could be revealed by starting with the N-terminal single substitutions [1=2] and [2=3], respectively, and inserting further Dha=Tap units towards the C-terminus. Figure 2.20a shows the three matched and mismatched couples and indicates the preference of each receptor type by arrows. Clearly, the affinity losses at the Y_1 subtype do not differ to great extent within the couples, and the matched analogs bind with slightly better affinities (approx. 10%). In contrast, the exact position is rather important at the Y_5 receptor which shows a distinct preference for the mismatched analogs (approx. 50% reduced affinity loss). Concerning the number of substitutions, this alignment of analogs shows that the Y_1 subtype is far more susceptible. Figure 2.20b indicates the growing difference in affinities by solid and dashed lines for the matched and mismatched analogs, respectively. With increasing number of substitutions the receptor affinities become more different and, due to the differing acceptance of both substitution series, the mismatched triple substitution [2=3,5=6,8=9] finally shows the most distinct affinity. Although the mismatched double substitutions are quite similar and the term “selectivity” has to be used with care as the losses of affinity do not differ to more than 6.5-fold, these results are of relevance for the understanding of the structural requirements to be recognized from the single receptor subtypes as they exhibit the first distinct receptor binding trends that could be elucidated from one systematic scanning series (figure 2.20c). It is plausible to attribute the good acceptance of even triple Dha=Tap substituted NPY analogs to the increased hydrophobicity of the modified N-terminal segments, which gives a first hint on the possible important role of hydrophobic interactions between N-terminus and C-terminal α-helix. But why does the exact position of the unit have such an impact on Y_5 selectivity? This allows the assumption that, according to the receptor type, individual side chain contacts may be present between both termini, which can have hydrophobic or ionic character. The obvious decrease of Y_5 affinity associated with deletion of the Lys^4 side chain (section 2.3.1.2) also supports this hypothesis.

Table 2.5 NPY analogs examined by NMR spectroscopy. *Further details of the preparation of the NMR samples are given in section 5.2.4.*

			concentrations in H_2O/D_2O 5:1	peptide	SDS-d_{25}
peptide	acronym	sequence		[mM]	[mM]	rel. to peptide
native pNPY	pNPY	YPSKPDNPGEDAPAEDLARYYSALRHYINLITRQRY-NH_2	2.57	207	80.6
[Dha^2=Tap^3]-pNPY	[2=3]	Y⊙⊙KPDNPGEDAPAEDLARYYSALRHYINLITRQRY-NH_2	1.93	205	105.6
[Dha^5=Tap^6]-pNPY	[5=6]	YPSK⊙⊙NPGEDAPAEDLARYYSALRHYINLITRQRY-NH_2	2.25	206	91.2
[Dha^8=Tap^9]-pNPY	[8=9]	YPSKPDN⊙⊙EDAPAEDLARYYSALRHYINLITRQRY-NH_2	2.22	206	92.8
[$Dha^{1,4,7}$=$Tap^{2,5,8}$]-pNPY	[1=2,4=5,7=8]	⊙⊙S⊙⊙D⊙⊙GEDAPAEDLARYYSALRHYINLITRQRY-NH_2	0.63	60	95.4

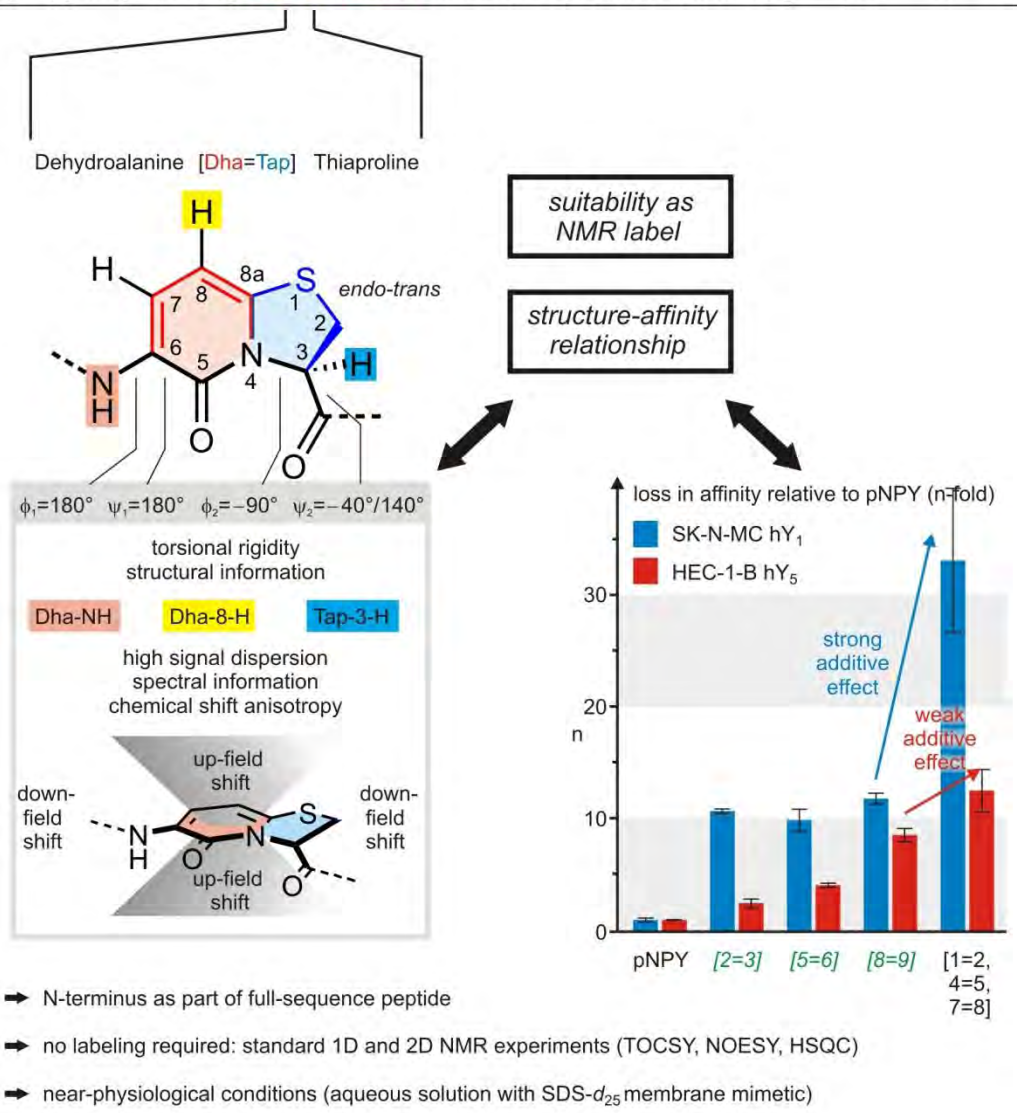

Figure 2.21 Characteristics of Dha=Tap as NMR label. *Within the scope of this thesis, the suitability of the Dha=Tap unit as NMR label should be tested by incorporation into the N-terminus of NPY. Furthermore, the NMR studies were aimed to identify determinants of the various receptor trends observed at the Y_1 and the Y_5 receptor type. For further details regarding the Dha=Tap dipeptide see figure 2.13.*

2.3.2 Probing the NPY receptor selectivity with NMR studies

In the light of the results concerning the receptor binding trends, the structure elucidation of the modified analogs turned out to be of particular interest, and this was accomplished by CD and NMR spectroscopy. The CD measurements were performed by *M. Haack* (*Beck-Sickinger* group, University of Leipzig) and are described in detail in the corresponding publication.[38] Briefly, all analogs showed α-helical content in the range of native NPY, and it turned out to be dependent on the Dha=Tap substitution. However, the extent of α-helicity does not correlate with the observed receptor binding profile. A particular important outcome of the CD studies was the observation of a significant mutual interaction of both N- and C-termini, which is in line with the NMR data and the interpretation of the receptor binding results discussed in section 2.3.1.4.

2.3.2.1 Peptide and protein structure elucidation by NMR: strategy and methodology

The evaluation process of a molecular structure by NMR is divided in several steps which base on each other. First, one-dimensional ^{1}H and ^{13}C spectra give an overview of the number of nuclei present by the counting of signals and their respective integrals. The next step is the assignment of every proton and carbon nucleus in the substrate with its respective chemical shift. As usually some types of amino acids are present more than one time it is important to identify all chemical shifts of the nuclei in the respective residue (which exhibits an isolated spin system). With this task accomplished, the connectivity of the single residues can be elucidated which finally leads to the primary structure. Now, the secondary and tertiary structural elements can be elucidated, and preferred conformations of the backbone and of side chains can be identified by dipolar and scalar couplings which indicates the dynamics of the respective segments. Finally, the NMR parameters also give information about intra- and intermolecular non-covalent interactions.

For this evaluation process, two-dimensional (2D) NMR techniques have become an indispensable tool in biomolecular NMR as they extend the crowded one-dimensional spectra (figure 2.22) to a second dimension. This greatly reduces the extent of signal overlap and facilitates evaluation. Even more important is the fact that, according to the experiment, specific additional information about spin pairs is made visible. Figure 2.23 shows the pulse sequences of the most-used homonuclear 2D experiments COSY, TOCSY and NOESY which, like all 2D NMR sequences, consist of four periods. The first “preparation” period generates transversal magnetization (coherences) by a 90° pulse (or by a pulse sequence, respectively) which is subsequently allowed to “evolve” during the time interval t_1 in the second period, which means

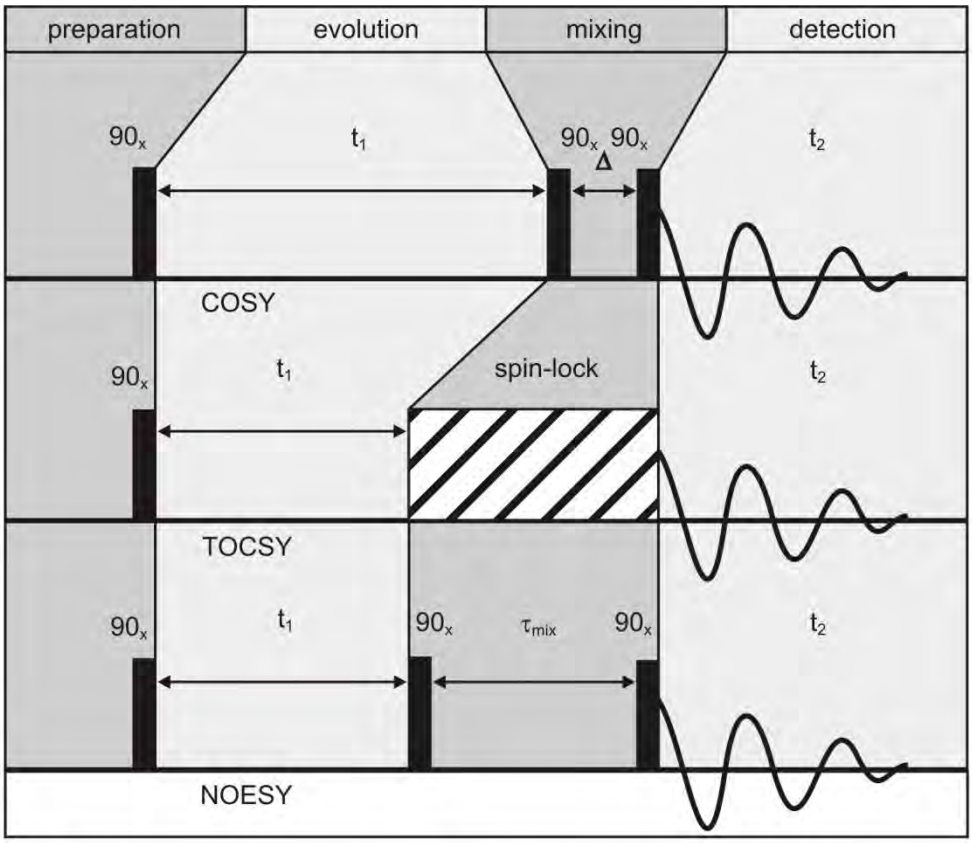

Figure 2.22 Pulse sequences of homonuclear 2D-NMR experiments. *All techniques consist of four parts termed preparation, evolution, mixing, and detection phase. The mixing periods are the crucial phases in every experiment as their composition determines which information will be made visible during the following detection period. The couplings which are determined by the respective methods are depicted in figure 2.23.*

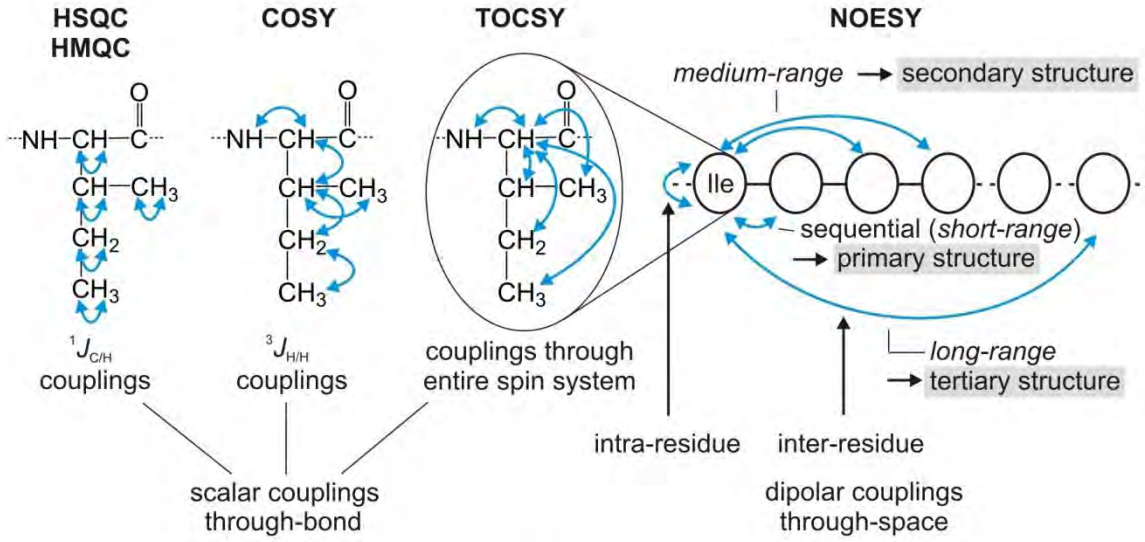

Figure 2.23 Coupling information provided by the HSQC/HMQC and the homonuclear experiments COSY, TOCSY, and NOESY, schematically shown for Isoleucine. *The HSQC/HMQC gives information about which protons are attached to which carbon nuclei, and the COSY shows all scalar H/H couplings over three bonds. In the TOCSY, all couplings within an isolated spin system are visible (for clarity, only couplings for the α-H are shown). In contrast, dipolar through-space couplings are identified by the NOESY experiment, which enables to identify the peptide sequence as well as secondary and tertiary structure elements.*

that couplings and different frequencies - information which later will be visible in the second indirect dimension - are generated and subjected to “evolution”. Before the final “detection” period (t_2), a “mixing” interval is necessary. This is different according to the experiment type, as the kind of information that is allowed to be transferred between single spins will determine the information that is finally visible as cross signals in the 2D spectrum. The generation process of the second dimension can best be seen with the DQF-COSY sequence. The “mixing” period consists of two 90° pulses separated by a certain time interval Δ. By stepwise increasing this interval with every repetition of the sequence, the FID of the second dimension is recorded point-by-point, and the cross-peaks in the resulting 2D spectrum indicate scalar ^3J couplings between single nuclei, which gives a linking matrice for the examined molecules (figure 2.23). For the assignment of peptides and proteins, the TOCSY sequence is a valuable alternative as it triggers scalar couplings between all spins within an isolated spin system (which can be an amino acid or a glycosyl residue) independent of the number of bonds between them. This is accomplished by applying a spin-lock field which “equalizes” all spins within the system and evokes strong scalar couplings between them (figure 2.23). The HSQC experiment (pulse sequence not shown) allows to identify the proton resonances by the attached carbon nuclei which exhibit chemical shifts that are less susceptible to exterior influences. It extends the ^{1}H NMR spectrum to the ^{13}C dimension and selectively shows all scalar ^1J couplings between the carbons and the attached protons.

In addition to these methods which give information on scalar “through-bond” couplings, the NOESY experiment makes dipolar “through-space” couplings visible by utilizing the Nuclear Overhauser Effect (NOE). As schematically depicted in figure 2.23, the couplings of protons in adjoining residues reveal the connectivity of the single spin systems (the primary structure), and the detection of NOESY cross signals between nuclei in residues that are located far from each other in the sequence is used to determine secondary and tertiary structural elements. This information about the linking of the single spin systems is of particular importance if some amino acids are present to high extent as it is the case in pNPY (for example, Ala, Arg, Glu, Pro and Tyr exhibit more than 50% of all residues). Owing to the high content of information, certain regions of the NOESY spectrum are commonly referred to as “fingerprint” regions. According to the secondary structure of a certain peptide segment, a specific pattern of NOE contacts is observed between nuclei which are located in residues of certain distances along the primary structure. The application of this procedure to NPY is described in detail in section 2.3.2.2.2. The greatest benefit of NOE couplings is given by the fact that the intensity *I* of a cross signal, in

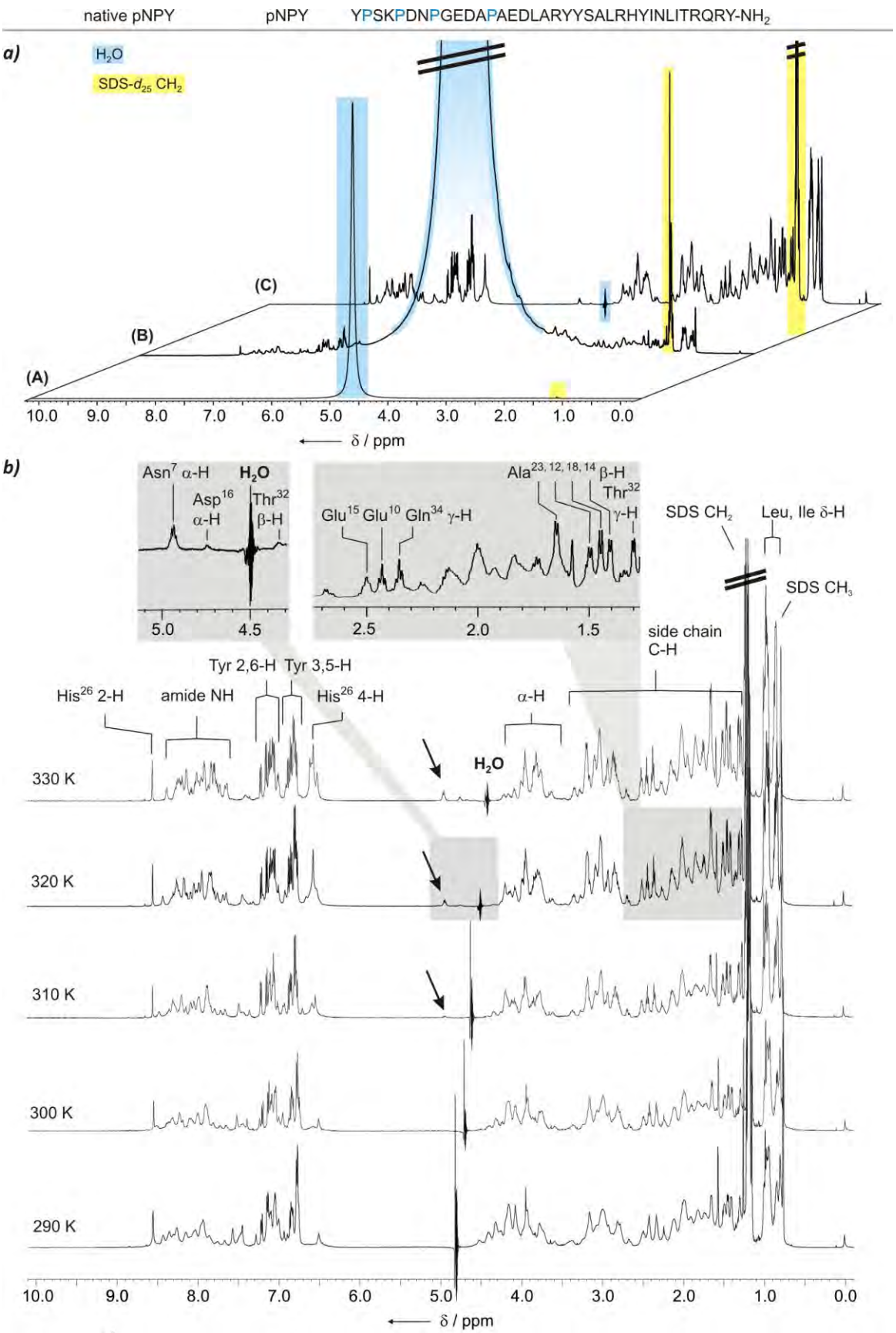

Figure 2.24 *^{1}H NMR spectra (H_2O/D_2O 5:1, 80 eq SDS-d_{25}, 600 MHz) of native pNPY.* ***a)*** *The effect of the DPFGSE water suppression technique. (A) Spectrum at 300 K without water suppression, (B) same spectrum shown with 160-fold increase or intensity, (C) spectrum with water suppression.* ***b)*** *Spectra at different temperatures. Two spectral regions are shown enlarged within the grey boxes.*

comparison to a reference signal, can be used to calculate the distance *d* between the respective two nuclei.

$$I = A\frac{1}{d^6} \qquad (A = \textit{scaling constant}) \qquad (1)$$

For the utilization of this relationship for protein structure elucidation, the Nobel Prize in Chemistry 2002 was awarded to *K. Wüthrich.*[85] This emphasized its impact on biosciences as it gave the possibility to calculate three-dimensional molecular structures in solution. Within the scope of this thesis, NOE-based molecular modeling was also carried out for the Dha=Tap substituted analogs and exhibited an indispensable part of the structural investigations.

The information which can be extracted from NMR spectra is always the result of an equilibrium of conformations which can be highly different from each other, especially in linear substrates like the NPY analogs described in this chapter. The averaging of single structures in molecular modeling corresponds just to this conformational equilibrium, and it is important to remember that the various average structures found in the literature and also obtained within the scope of this thesis exhibit no rigid conformations but rather describe the average conformational preference of the substrate. Consequently, taking the average structure and not only single snapshots of the molecular dynamics simulation as basis for interpretations and discussions is far more realistic in the view of structural dynamics.

2.3.2.2 NMR experiments: General considerations and experimental setup

The NMR spectroscopic investigations carried out within the scope of this thesis served as proof whether the incorporation of Dha=Tap units into peptide sequences (this scanning method was performed for the first time) exhibits an option to elucidate flexible peptide segments that are difficult to analyze with other scanning methods (section 2.2.3). In this context, the Dha=Tap unit itself which is a promising NMR label (figure 2.21, see section 2.2.4 for detailed description) should be examined with respect to its impact on the surrounding peptidic structure and the chemical shifts observed for nuclei in adjoining residues. NMR spectroscopy has potential for the structure elucidation as it provides geometric parameters for molecular modeling studies. A further advance of NMR spectroscopy is the option to tune the solution environment of the substrate, and in the present case the addition of perdeuterated sodium dodecyl sulfate (SDS-d_{25}) provided a membrane-like environment.

Besides the native NPY, four Dha=Tap substituted analogs were analyzed by NMR spectroscopy which are listed in table 2.5 and whose receptor binding profiles are shown in figure 2.21: the three single-substituted peptides [2=3], [5=6], [8=9] (section 2.3.2.3) and the triple-substituted

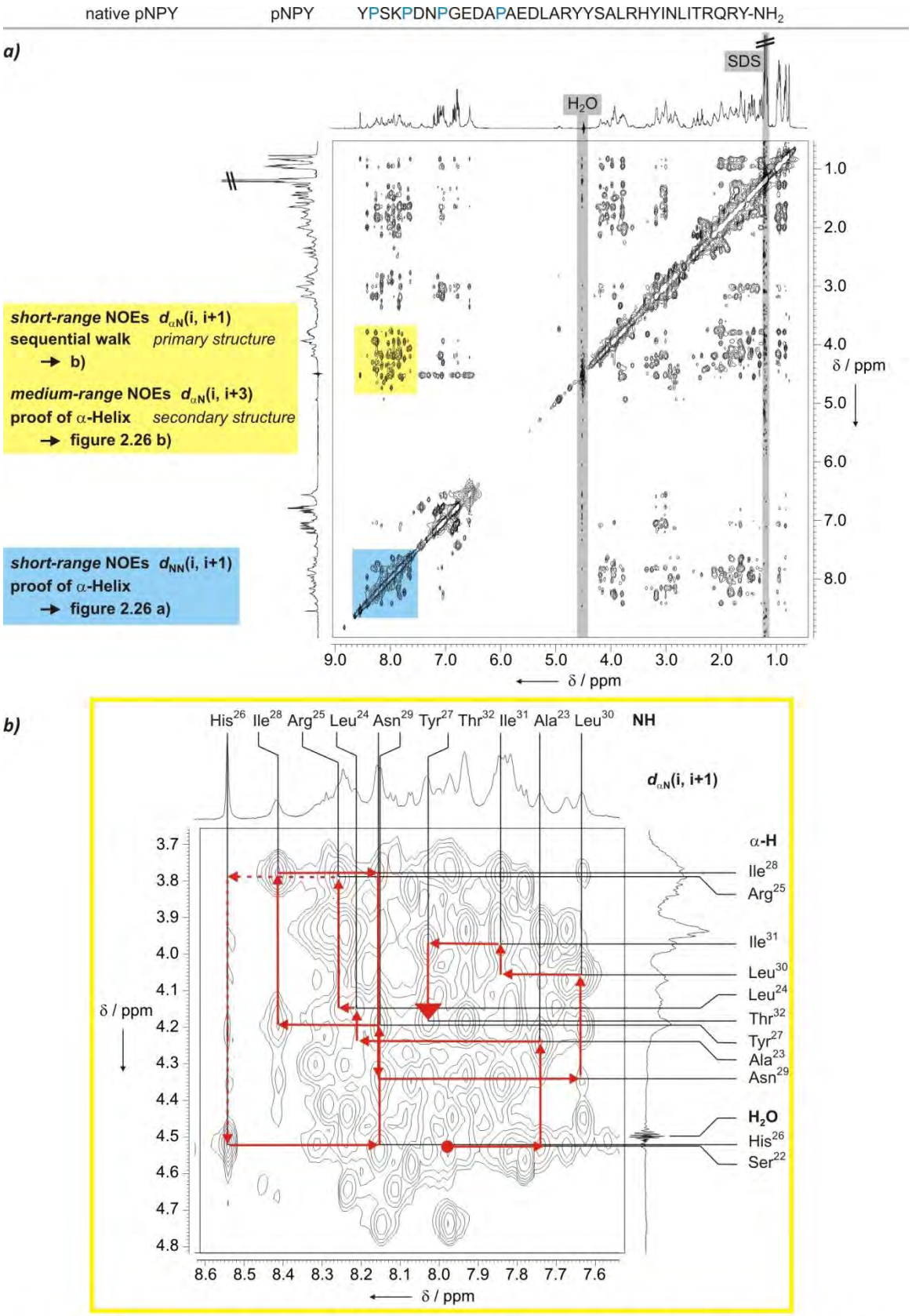

Figure 2.25 (continued on next page) Determination of pNPY primary and secondary structure from NOE contacts. ***a)*** *Complete NOESY spectrum (H_2O/D_2O 5:1, 80 eq SDS-d_{25}, 600 MHz, 320 K) with two fingerprint regions marked in yellow (α-H/NH cross peaks) and blue (NH/NH cross peaks).* ***b)*** *Enlarged α-H/NH fingerprint region. The sequential walk along the backbone NOE couplings from Ser[22] to Thr[32] is indicated by red arrows.*

matched analog [1=2,4=5,7=8] (section 2.3.2.4). The choice of mismatched analogs is justified by their (initially unexpected) high binding affinity as well as distinct selectivity towards the Y_5 receptor subtype (section 2.3.1). Furthermore, the only slight loss of affinity which is observed at the Y_5 subtype by inserting three instead of just one Dha=Tap units (in the mismatched case, a strong compensative effect even occurs) and which stands in contrast to the high affinity loss at the Y_1 receptor (figure 2.21) was expected to be explained by structural impacts caused by the increase of the number of Dha=Tap residues.

Several NMR evaluation strategies using different solvents and methods have been described in the literature. For the envisioned studies, the choice of a partially deuterated aqueous solution (H_2O/D_2O 5:1) together with the perdeuterated sodium dodecyl sulfate (SDS-d_{25}) as membrane mimetic was considered as a good option for three reasons. First of all, as the NMR studies should enable to explain the remarkable receptor binding trends of the analogs, it was desirable to approach the physiological conditions (or, at least the conditions of the binding assays) as much as possible. Second, similar solution conditions had already been proven as advancements in the structure elucidation of native NPY.[43] Third, the choice of SDS-d_{25} as the simplest membrane mimetic (the more complex and far more expensive DPC-d_{38} had been used by *Zerbe et al.*) should also be part of the intention to gain valuable information from an experimental setup that is as cost-effective and as easy to perform as possible. This implicates that, in contrast to the extensive labeling which was required for the experiments carried out by *Zerbe et al.*, the structure elucidation of the Dha=Tap scan analogs should be possible with completely unmarked substrates and be restricted to standard and time-efficient NMR experiments. To anticipate the results described in the following, this strategy proved successful in the case of the N-terminus of NPY. The NMR experiments comprised one-dimensional ^{1}H NMR experiments using the DPFGSE water suppression technique (section 2.3.2.2.1) and two-dimensional homonuclear (TOCSY, NOESY) as well as heteronuclear (HSQC) experiments (section 2.3.2.2.2). As for example visible from a section of the NOESY spectrum of the single substituted peptide [5=6] (figure 2.30) the spectra were of good quality and, as marked by colored bars, the chemical shift anisotropy of the Dha=Tap unit facilitated the assignments as some signals are located in otherwise “empty” regions of the spectra. For the Dha=Tap modified segment, this fact can in its impact be compared to the facilitation which is given by the labeling of the substrate. Furthermore, all measurements could be carried out with just one NMR sample of each analog.

To enable the measurements in undeuterated aqueous solution, the DPFGSE sequence for water suppression had to be set adequately by optimizing the field gradient strengths and the offset resonance. Without water suppression, the ^{1}H NMR spectrum of native pNPY

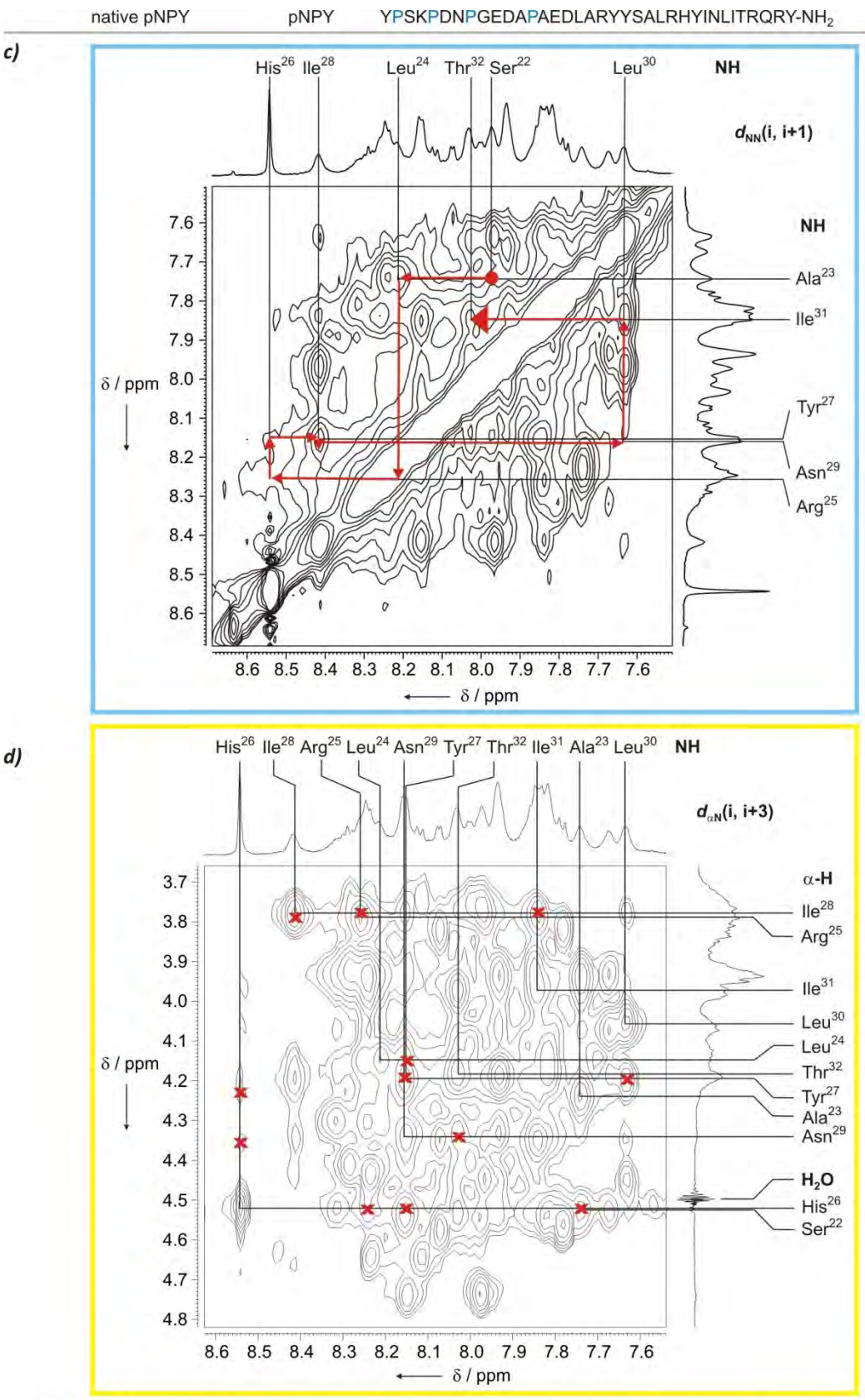

Figure 2.25 (continued from previous page) Determination of pNPY primary and secondary structure from NOE contacts. ***c)*** *Enlargement of the NN/NH fingerprint region. The sequential walk along the backbone NOE contacts of residues n and n+3 (red arrows) indicates the presence of an α-helix.* ***d)*** *Enlargement of the α-H/NH fingerprint region. The red crosses mark the α-H/NH NOE contacts of residues n and n+3 which are also typical for an α-helical structure.*

(2.57 mM in H_2O/D_2O 5:1) with 80 eq SDS-d_{25} at 320 K (the choice of temperature is reasoned below) is dominated by the huge peak originating from the abundant H_2O (figure 2.24a), and only the SDS methyl residual signal at 1.08 ppm (approx. 1/220 of the H_2O signal intensity) is visible. After increasing the intensity scale of this spectrum 160-fold, some signals of the peptide are well visible, but the H_2O signal abolishes even qualitative interpretation of an approx. 3 ppm area. The comparison of the ^{1}H NMR spectrum obtained under identical conditions using water suppression with the correctly set parameters shows the dramatic improvement. The huge H_2O signal is now reduced in intensity by a factor of approx. 11000 and appears as residual peak at 4.50 ppm which is comparable in size with the peptidic signals. Furthermore, a distortion-less baseline is obtained which allows for signal integration, and, in spite of the presence of large amounts of SDS-d_{25}, well-shaped signals are obtained.

A relevant question concerns the choice of the temperature which can have significant impact on the structure. As it is desirable to approach physiological conditions as far as possible, applying a measuring temperature of 310 K which corresponds to the human body temperature is reasonable. On the other hand, the NMR spectra themselves can dictate the temperature as the quality of multiplet splitting is often temperature dependent. Furthermore, problems with signal overlap due to temperature-dependent peak positions may occur. Therefore, the optimum temperature was determined by recording ^{1}H NMR spectra in 10 K steps from 290 to 330 K (figure 2.22b). As for example visible from the amide signals around 8 ppm, the choice of 320 K as measuring temperature turned out to be a good compromise between good signal shapes as well as multiplet resolutions and the proximity to the body temperature. The residual H_2O signal is subjected to a strong temperature-dependent high-field shift of approx. 250 Hz in the examined 40 K range (in contrast, the corresponding shifts of the peptidic signals did not exceed 20 Hz). To enable comparison of spectra recorded at different temperature, all spectra were calibrated on the SDS methyl (CD_2H) resonance at 0.772 ppm which appears temperature-independent (this assumption can be made by the fact that these methyl groups are in the core of the micelles and therefore hardly affected by the exterior conditions). As indicated by the arrow in figure 2.22b, signals become visible which are not detected at lower temperature due to overlap with the H_2O signal or due to close proximity. The DPFGSE water suppression affects such signals with respect to their intensities, which is why integration must not be used for the evaluation of signals close to the offset frequency.

These results led to the following experimental setup: After sufficiently long tempering in the spectrometer (at least 2 h) every peptide sample was analyzed by ^{1}H DPFGSE, TOCSY, ROESY and HSQC experiments at 320 K. As some important α-H signals were invisible in the HSQC spectra

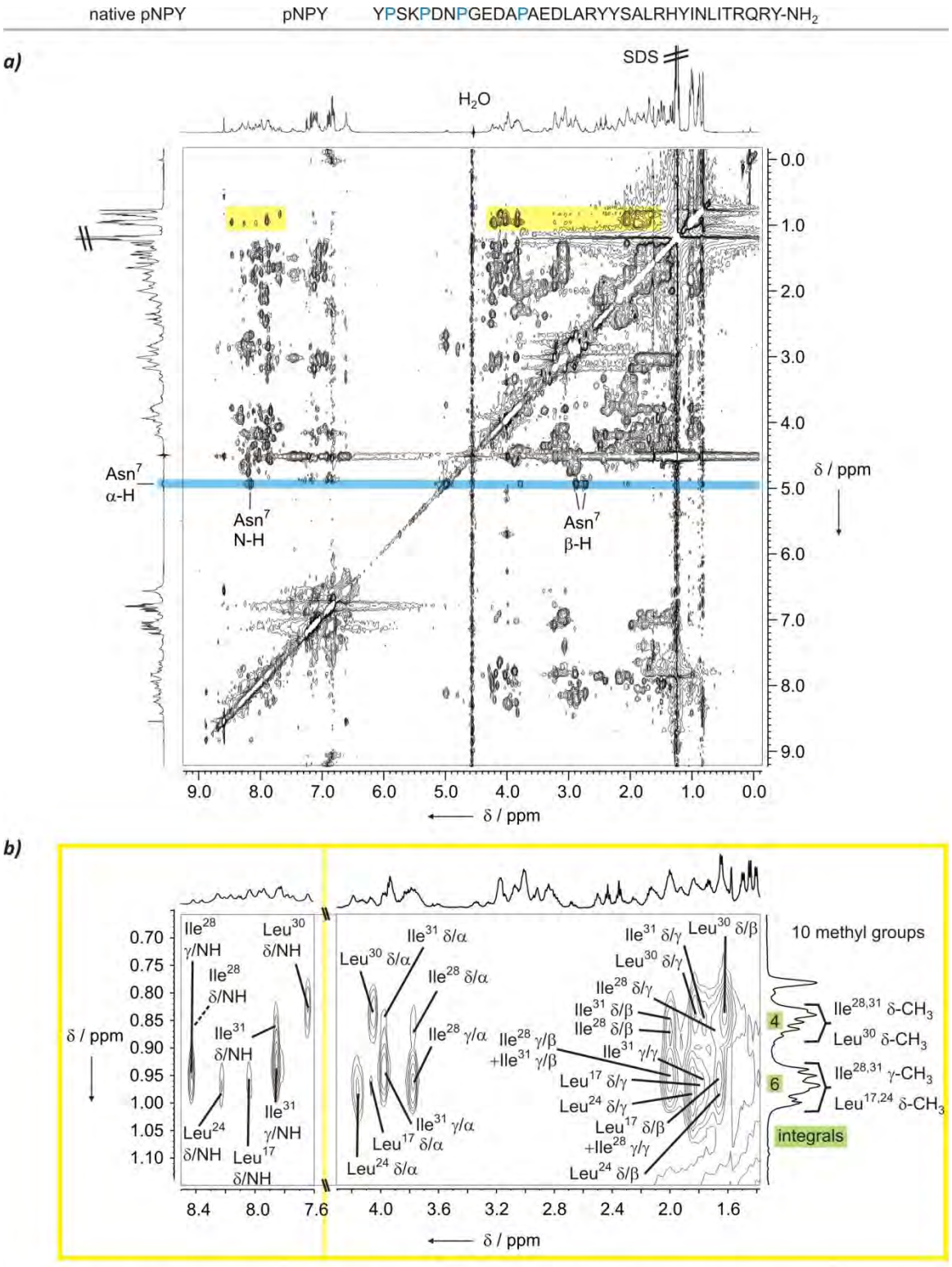

Figure 2.26 Side chain assignment from TOCSY cross peaks. a) *Complete TOCSY spectrum (H_2O/D_2O 5:1, 80 eq SDS-d_{25}, 600 MHz, 320 K) of native pNPY. In an ideal case, all chemical shifts within a single residue can be read from one line of signals, as indicated for the down-field Asn^7 α-H resonance with a blue bar.* ***b)*** *Enlarged depiction of the two regions which are highlighted yellow in a). The identification of all cross signals shown was the key for the complete assignment of the aliphatic side chains. For clarity reasons, the assignments of the cross peaks are abbreviated (for example, δ/γ indicates the cross peak between the δ-and the γ-CH_3 group. The different signal intensities of the NH/γ and NH/δ cross peaks of residues Ile^{28} and Ile^{31} demonstrate that the number of bonds between the coupling spins is influencing the signal intensity in the TOCSY spectrum.*

due to the water resonance line, a second series of HSQC measurements was carried out at 300 K which enabled to assign also these peaks. ^{1}H NMR experiments were also recorded before and after every 2D experiment in order to detect eventual changes and shim problems, which was not the case in all long-time measurements used for evaluation.

The signal assignment of native pNPY was the fundament for the subsequent evaluation of the impacts associated with the incorporation of Dha=Tap units. As the peptides were not isotope-labeled, the results obtained by *Zerbe et al.* could not be used as starting point. Former signal assignments (section 2.1.4) were obtained from different solution conditions and without membrane mimetics present, which has a great impact on the chemical shifts and does not enable to refer to these results. Therefore, *ab initio* assignment had to be carried out; however, it was not intended to provide a complete assignment of the peptides or to carry out kinetic analyses. The data obtained from native NPY should rather be the reference to evaluate the impact on structure associated with the incorporation of Dha=Tap units. As two side chains are deleted per Dha=Tap, the disappearance of the corresponding signals, which is directly visible by overlay of the corresponding 2D spectra, allows the precise assignment in native NMR and in analogs which are substituted at different positions. Furthermore, the NMR chemical shifts, as they are sensitive to changes, provide information about whether influences exerted by the Dha=Tap units are global (affect all or the majority of chemical shifts) or local (like the chemical shift anisotropy of the aromatic pyridone which is expected to have a position-selective influence on adjoining residues).

2.3.2.3 Native pNPY: signal assignment and secondary structure

2.3.2.3.1 ^{1}H DPFGSE-NMR spectrum

A close look at the ^{1}H NMR spectrum of native NPY already reveals lots of information in spite of the apparent signal overcrowding in the single dimension. As shown in figure 2.24b, a spectrum typical for a peptide is obtained, with the signal groups of aliphatic Leu/Ile, side chain CH, α-H, aromatic (Tyr) side chains and amide protons to be identified when going from up- to downfield shifts, and the 2-H of the His^{26} side chain finally appears separated at 8.54 ppm. Some other resonances which could be assigned by the 2D spectra and by comparison with the substituted analogs are assigned in the two boxed spectral sections. In proximity of the residual water signal, further resonances appear well-separated from each other (left). Here, the comparison of the Asn^{7} α-H and Asp^{16} α-H intensities clarifies how much the signals closer to the water resonance are affected due to the water suppression. The up-field section shown in the right box illustrates

native pNPY pNPY YPSKPDNPGEDAPAEDLARYYSALRHYINLITRQRY-NH_2

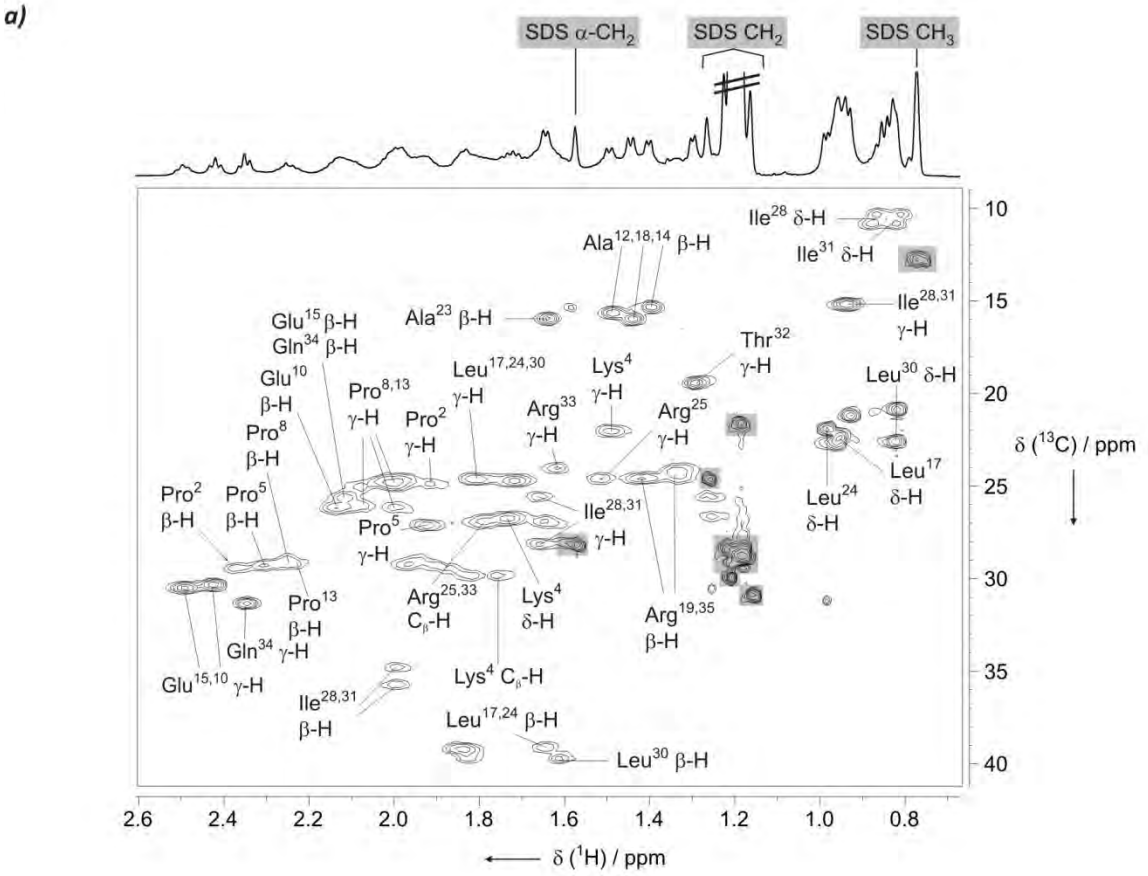

Figure 2.27 (continued on next page) Assigned HSQC spectrum (H_2O/D_2O 5:1, 80 eq SDS-d_{25}, 600 MHz, 320 K) of native pNPY. *The signals appear in three groups which are depicted in* ***a)*** *(up-field region; SDS cross signals marked in grey)* ***b)*** *(β/α region), and* ***c)*** *(down-field region). Compared to the homonuclear spectra depicted in the preceding figures, the heteronuclear HSQC features more clarity and there are only few overlapping signals. The informational benefit of this experiment is the connection of the proton resonances to characteristic carbon resonances which often allows to securely correlate these signals with certain types of residues. For example, the Asp and Leu β-H signals appear at crowded regions in the proton spectra, but in the HSQC they are easy to identify as the attached carbon resonances experience a down-field shift which is above-average for these proton shifts (approx. 40 ppm). Of course, all signal assignments can only be seen as unambiguous if they also fit the results from the homonuclear 2D spectra. Only the combination of several NMR techniques in signal assignment provides a secure basis which can serve as starting point for data interpretations and structure calculations. To enable the assignment of signals near the H_2O resonance (for example, Ser^3α-H), HSQC spectra were also recorded at lower temperature (300 K) which results in a down-field shift of the H_2O resonance (b).*

that, in spite of the peak crowding, some side chain signals resulting from Glu, Gln, Ala, and Thr residues can be identified by their well-resolved multiplets. The ^{1}H NMR spectrum even allows first suggestions concerning the secondary structure. One of the four characteristic Ala CH_3 dublets (Ala^{23}) appears separated from the other ones and is shifted down-field. This effect results from the incorporation of the Ala^{23} in the well-stabilized α-helix. Another highly important information that can already be extracted from the ^{1}H NMR spectrum is the presence of a single set of signals, which indicates that all Pro amides exist in a single conformation (probably *trans*) and that *cis* rotamers are present below detectability.

2.3.2.3.2 Signal assignment by 2D NMR experiments: NOESY, TOCSY, and HSQC

The evaluation of secondary structure elements in native pNPY is illustrated in figure 2.25. For clarity reasons, the complete NOESY spectrum (figure 2.25a) is shown with moderate signal intensity so that only signals of strong and medium intensities are visible. Two areas are emphasized which were particularly useful for the determination of the peptide sequence and the identification of the α-helix.

The upper highlighted region (yellow) contains NH/α-H cross signals which served as the proof of an α-helix. Before that, the primary structure had to be verified by a “sequential walk” along the backbone within this spectral region (figure 2.25b). This requires starting points which were unambiguously identified from the TOCSY and HSQC spectra. In the present case, the well-separated Thr^{32} β-H signal allowed to identify the Thr^{32} α-H/Ile^{31} NH cross signal (figure 2.25b). As shown by the red arrows, it was now possible to identify the chemical shifts of all backbone α-H and NH signals until Ser^{22} α-H. This enabled as next step to assign all protons in the segment Ser^{22} to Thr^{32} by identifying the side-chain resonances in the TOCSY and HSQC spectra. The adjoining segments of this region could not be identified unambiguously by this method because the N-terminally adjoining Tyr^{20,21} dipeptide as well as the C-terminal segment containing two Arg side chains were difficult to assign, which gave no sound basis for the assignment of further cross signals along the sequential walk. In the N-terminal segment, however, the Ala residues finally enabled a partial assignment, and towards the C-terminus all resonances until to Gln^{34} could be identified.

With the assignment of the primary sequence accomplished, the presence of an α-helix as secondary structural element could be identified from the NH/NH spectral region (highlighted blue in figure 2.25a), as shown in figure 2.25c. This sequential assignment from Ser^{22} to Thr^{32} (indicated by red arrows) identifies NH/NH NOE contacts between two residues at position n and

native pNPY pNPY YPSKPDNPGEDAPAEDLARYYSALRHYINLITRQRY-NH_2

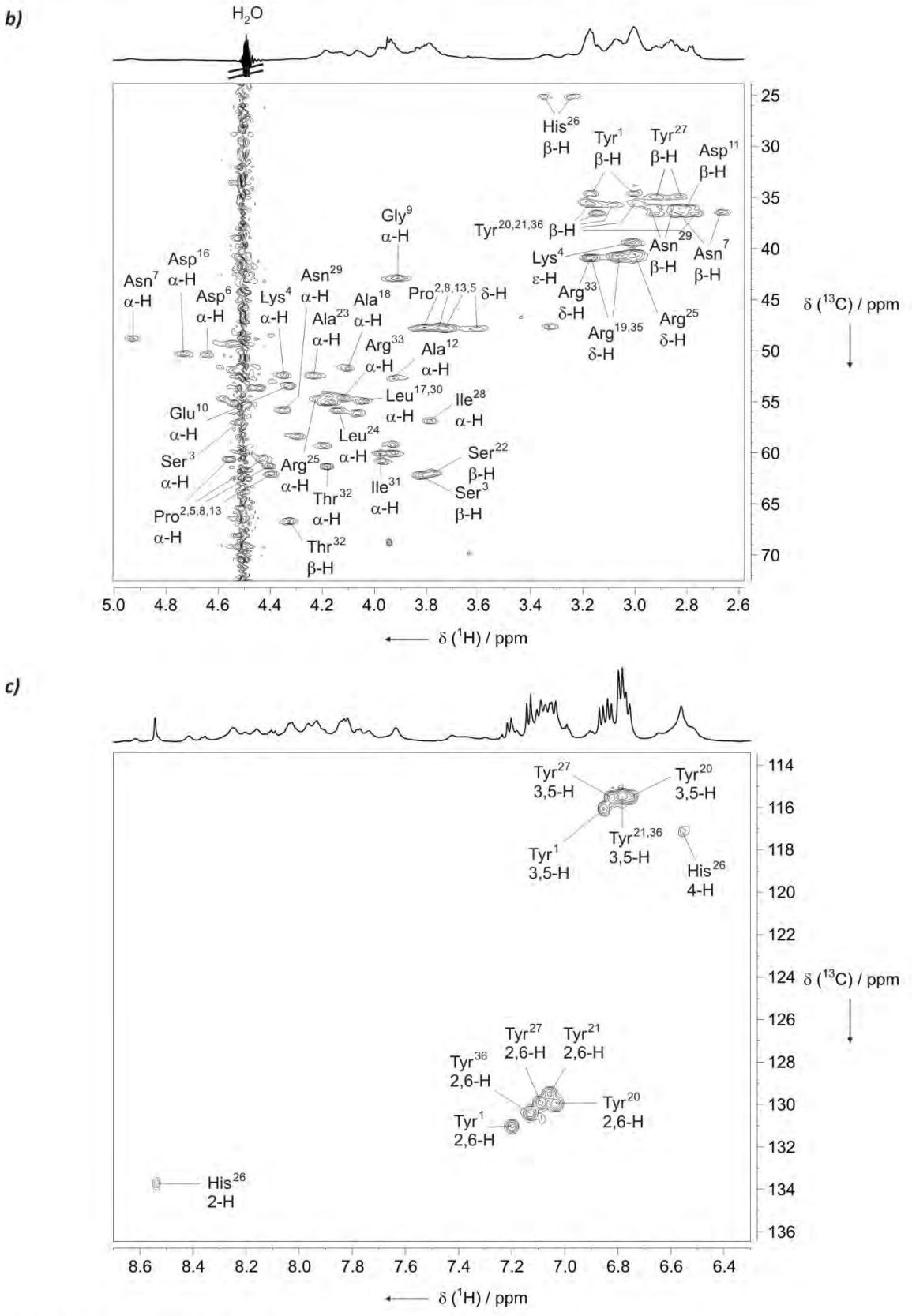

Figure 2.27 (continued from previous page)

n+3 which is a typical spectral fingerprint of α-helices. Another proof of this secondary structure is given by the identification of α-H/NH cross signals of adjoining residues. The corresponding region is shown enlarged in figure 2.25d, with all identified NOE contacts marked by red crosses. Finally, by investigation of the triple substituted matched analog [1=2,4=5,7=8], a stable α-helix turned out to start already from Ala^{18}, which was in agreement with the results obtained by *Zerbe et al.* (section 2.1.5).[43]

Figure 2.26a shows the complete TOCSY spectrum of native pNPY in the presence of SDS micelles. The signal intensity has been increased so that also weak cross signals are visible, which shows that especially in the side chain and α-H region there is a high signal density obtained. As all amino acid types show a characteristic set of side chain signals in the TOCSY due to the scalar coupling throughout the residue, this experiment is essential to prove the identity of the α-H and NH proton resonances which have been identified by the sequential walk in the NOESY spectrum or by characteristic ^{13}C resonances in the HSQC. As an example, the set of Asn^{7} cross signals which is well separated due to the low-field resonance of the α-H is emphasized by a blue bar. The five aliphatic side chain residues in the α-helical section ($Ile^{28,31}$ and $Leu^{17,24,30}$) had to be assigned in order to be able to elucidate the orientation of the α-helix on the micelle surface (section 2.3.2.4.1). In spite of the high extent of signal overlap in the corresponding up-field cross signal regions (marked yellow in figure 2.26a and shown enlarged in figure 2.26b) this could be accomplished by analyzing the TOCSY signal patterns on basis of the signal integrals obtained from the ^{1}H NMR spectrum. The high signal densities of the NOESY and TOCSY sections with high information content illustrate the need of heteronuclear 2D experiments to obtain reliable data from larger biomolecules. In the assigment of native NPY (and in the comparison to its analogs, as described in the next sections), the HSQC experiments greatly facilitated the assignment process by extending the ^{1}H dimension to the corresponding ^{13}C resonances. Figure 2.27 depicts the HSQC spectrum of native pNPY (divided in three sections). The comparison of ^{1}H and ^{13}C shift distributions (for example, of the Pro δ-H) shows that, while protons at identical positions but located in different residues can show highly different resonances, the ^{13}C shifts always appear within a narrow chemical shift range. It is this high extent of independence of ^{13}C shifts from exterior conditions which makes ^{13}C-relayed 2D experiments a reliable tool for signal assignment.

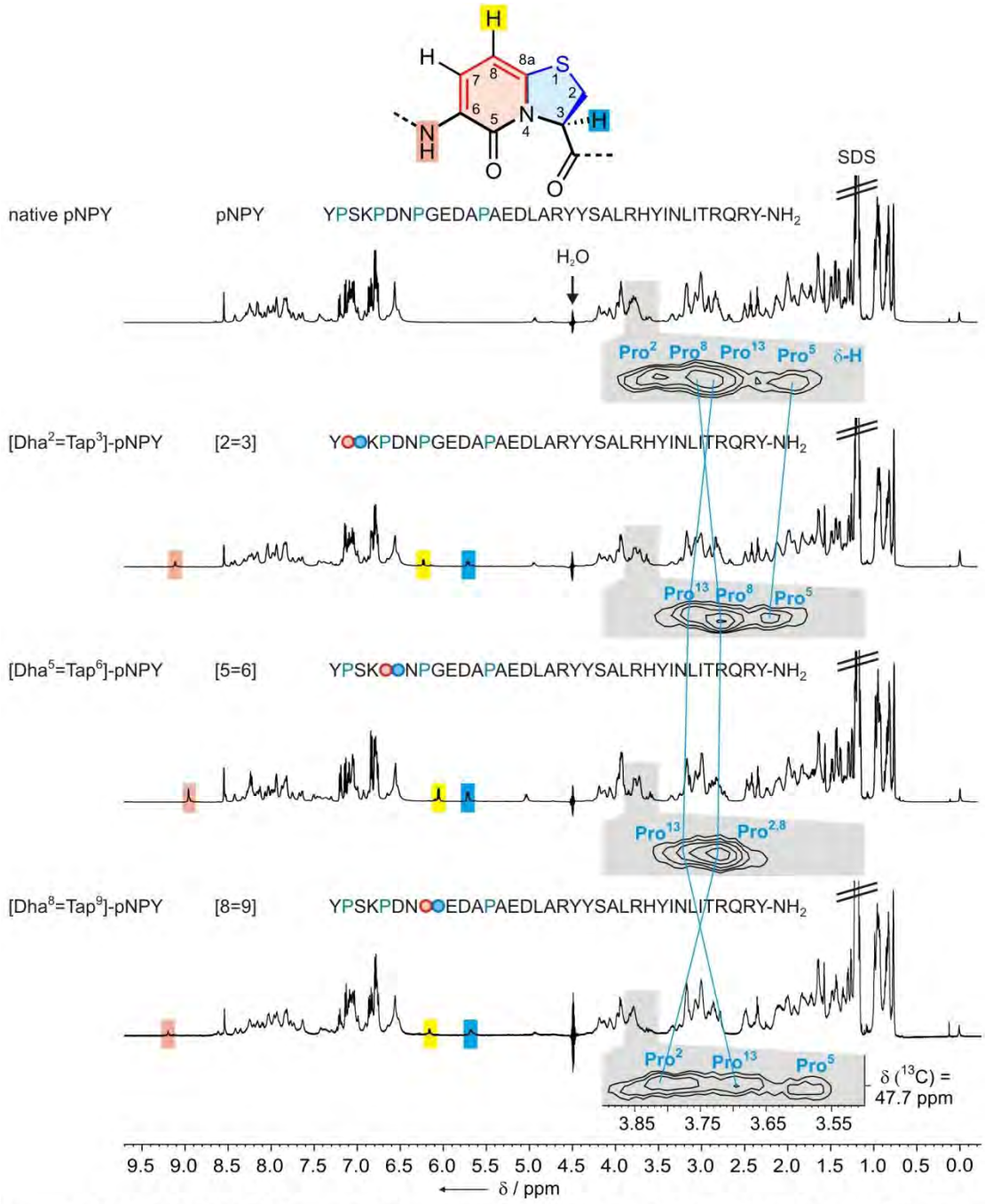

Figure 2.28 ***^{1}H DPFGSE-NMR and HSQC spectra (H_2O/D_2O 5:1, SDS-d_{25}, 600 MHz, 320 K) of single-substituted pNPY analogs in comparison with native pNPY.*** *For peptide and concentration details see table 2.5. Already the ^{1}H NMR spectra reveal the advantageous characteristic of the Dha=Tap label to show three proton resonances that appear in otherwise empty spectral regions: the Tap 3-H resonance (blue) as well as the Dha 8-H (yellow) and NH signal (red). These resonances facilitate the analyses of the spectra and provide a firm basis for data interpretation. A comparison of the three single-substituted analogs shows that the 8-H and NH proton resonances of the Dha=Tap units at position [2=3] and [8=9] are similar while they appear up-field shifted in [5=6]. This already gives a first hint on a position-dependent influence of the pyridone dipeptides; this is discussed in the main text. Below the ^{1}H NMR spectra, a section of the respective HSQC spectra containing the Pro δ-H cross peaks is shown (grey boxes). While the ^{13}C resonances always appear at approx. 47.7 ppm, the proton resonances of the three Pro residues which remain after a single substitution change according to the position of the Dha=Tap. This demonstrates the suitability of 2D spectra to identify which residues are exchanged and to quantify the influence of the aromatic pyridone ring, which is a valuable tool for the assignment of the peptide sequence in a demanding Pro-rich peptide segment. An example from the NOESY spectra is shown in figure 2.29.*

2.3.2.4 Single-substituted NPY analogs [2=3], [5=6], and [8=9]: The Dha=Tap unit influences the backbone conformation according to its position

2.3.2.4.1 Overview

The NMR samples of the single-substituted analogs were prepared with similar peptide and SDS concentrations as the sample of the native peptide (table 2.5). A significant facilitation of assignment and structure elucidation turned out by comparing the spectra of modified and native peptides. As the Dha=Tap label is "moved" along the N-terminus, two residues are substituted by the Dha=Tap dipeptide with its well-identifiable resonances. This enables to identify the resonances of the substituted residues, and it allowed to assign the proton shifts in the N-terminus of NPY which, in the many cases reported in the literature, was reluctant to spectral assignment if examined as part of the full-length peptide. The first characteristic visible from the comparison of the ^{1}H NMR spectra is the fact that some signals now appear within otherwise "empty" spectral regions, which correspond to Dha=Tap proton resonances (figure 2.28). The signals at approx. 5.7 ppm (marked blue) origin from the Tap 3-H, and the Dha 8-H signals appear at approx. 6.1-6.2 ppm (marked yellow). A strong down-field shift is observed for the Dha NH proton which is the only signal visible in the region beyond the other peptidic amide protons. These results are of great relevance for the suitability of the Dha=Tap unit as NMR label, as this signal dispersion into less crowded spectral areas gives safe starting points for signal assignment as well as for the identification of scalar and dipolar coupling cross peaks. It is also a benefit that these signals result from both residues of the dipeptide, and furthermore along the backbone (Dha NH, Tap 3-H) as well as in the side chain (Dha 8-H). In order to demonstrate this effect by a 2D spectrum, figure 2.29 shows a section of the NOESY spectrum of [Dha^{5}=Tap^{6}]-pNPY.

Furthermore, the comparison of the chemical shifts of residues adjoining to the Dha=Tap units directly illustrates the effect of the Dha=Tap neighbor with its aromatic pyridone ring. This is demonstrated for the Pro δ-H resonances by the insets of the corresponding HSQC sections in figure 2.28. This overview already suggests that the Dha=Tap unit, according to its position in the N-terminus, does not have identical effects on the adjoining residues. In the analog [2=3], the Pro^{5} δ-H resonances are subjected to a down-field shift, while the corresponding Pro^{8} δ-H resonances in analog [5=6], being in identical sequential distance to the Dha=Tap unit, are slightly shifted up-field.

In order to obtain a full picture of how the pyridone dipeptide affects the modified peptide segment in dependence of its position, the N-termini of the three single-substituted analogs were analyzed with respect to the chemical shift changes of adjoining residues. Furthermore, all

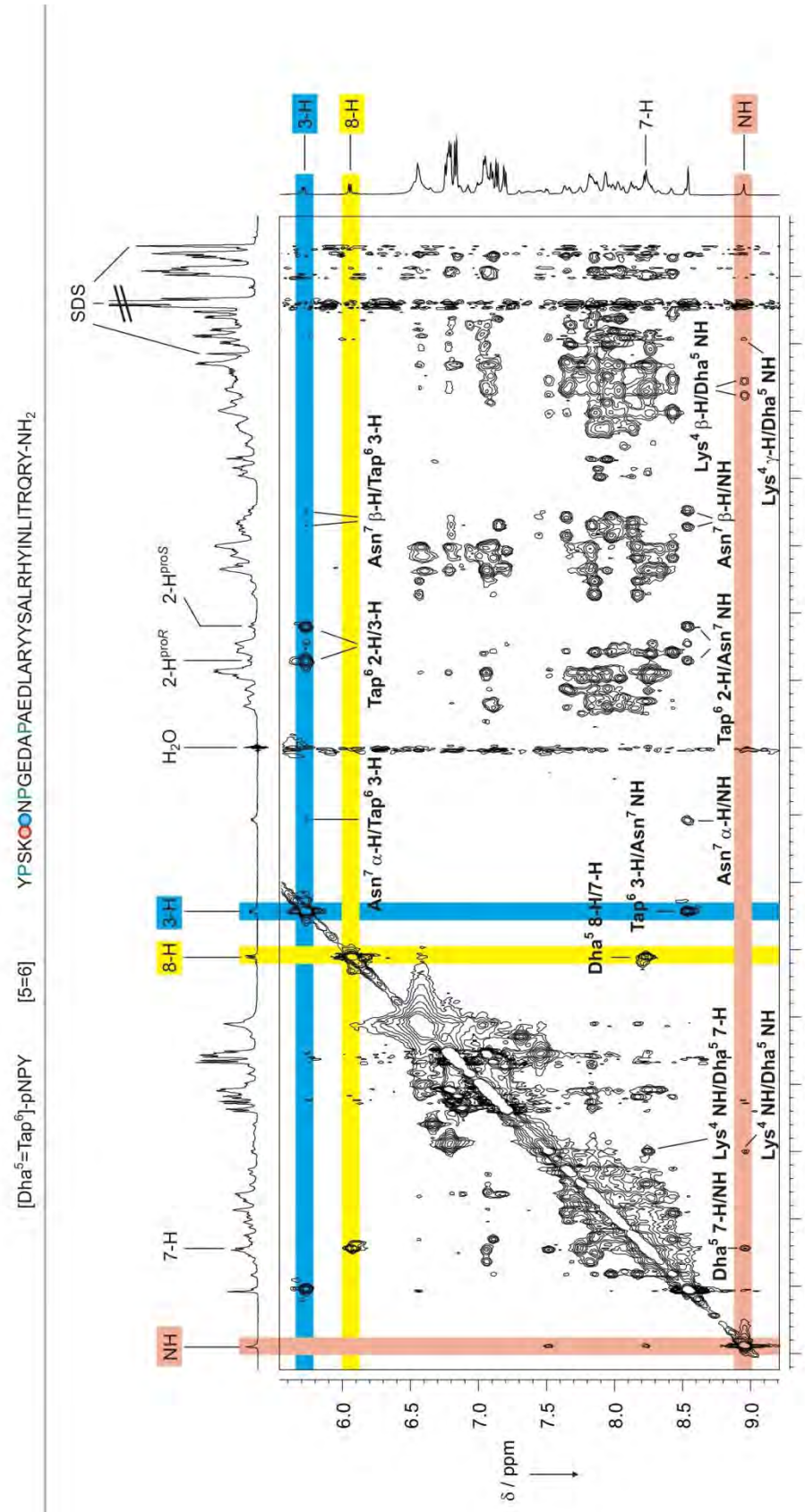

Figure 2.29 Section of the NOESY spectrum of [Dha^5=Tap^6]-pNPY (H_2O/D_2O 5:1, 90 eq SDS-d_{25}, 600 MHz, 320 K, mixing time 150 ms). *Some inter- and intra-residue cross peaks in less crowded spectral regions are assigned. The Dha=Tap unit exhibits a dipolar coupling barrier as no NOE contacts between the Dha and the Tap are observed. The discussion of these NOE and the comparison with the other analogs is described in the main text and in the following figures 2.30 and 2.31.*

NOE contacts were analyzed to enable structure calculations. In all analogs, the long-range chemical shift variations dropped below measuring uncertainty after the third residue in N-terminal as well as C-terminal direction. For the immediate surroundings of the Dha=Tap unit, however, precise data could be obtained, as described in the following.

2.3.2.4.2 The analog [5=6]

The substitution of residues Pro^5 and Asp^6 clearly had the greatest impact on the structure of the N-terminus, with very distinct NOE contacts and chemical shift changes also visible for the second amino acids in each direction (figure 2.30). Like for all following examples, the NOE contacts are shown in one structure while the other depiction contains the changes in proton chemical shifts compared to the native peptide. The most conspicuous detail shown from the NOE pattern is the fact that there are no dipolar couplings observed between Dha and Tap residue (in addition to the missing scalar couplings). This "coupling barrier" property of the dipeptide also facilitates data evaluation as an N-terminal as well as C-terminal spin system can be evaluated separately. This fact exhibits no problem for the structure calculation as the linking unit has a rigid structure with well-known geometry and torsion angles. The Dap^5 residue shows NOE contacts to the adjoining Lys^4 backbone and side chain, and from the Tap^6 dipolar couplings to all protons of Asn^7 can be quantified. The fact that the diastereotopic Dha 2-H can be assigned pro*R* and pro*S* is particularly useful to determine the exact position of adjoining residues. As there is a medium-range NOE contact between the Pro^8 γ-H and the Tap^6 2-$H^{pro S}$, while the pro*R* proton shows no contact, it can be concluded that the C-terminal backbone folds over the Dha=Tap plane. The most useful source of information, however, is the aromatic pyridone ring which causes down-field shifts of nuclei in the aromatic ring plane and leads to the up-field shifting of residues above or below the plane. This effect is so precise that it even allows for the position determination of individual positions within a single residue. While the Lys^4 backbone protons and β-H appear down-field shifted, indicating their position within the plane, the rest of the Lys^4 side chain protons, as well as the α- and β-H of the Ser^3 residue are positioned outside the plane. On the side of the Tap^6, in contrast, all positions are shifted down-field and there is an especially big influence observed for the Asn^7 α-C resonance which migrates almost 200 Hz. The only slight changes of chemical shifts observed for Pro^8 and Gly^9 demonstrate how the aromatic ring current decreases with growing distance.

The observed NOE contacts were, according to their intensities, converted into the corresponding interproton distances. These served as restraints for a molecular dynamics simulation of the N-terminal segment from Tyr^1 to Gly^9 using the program package

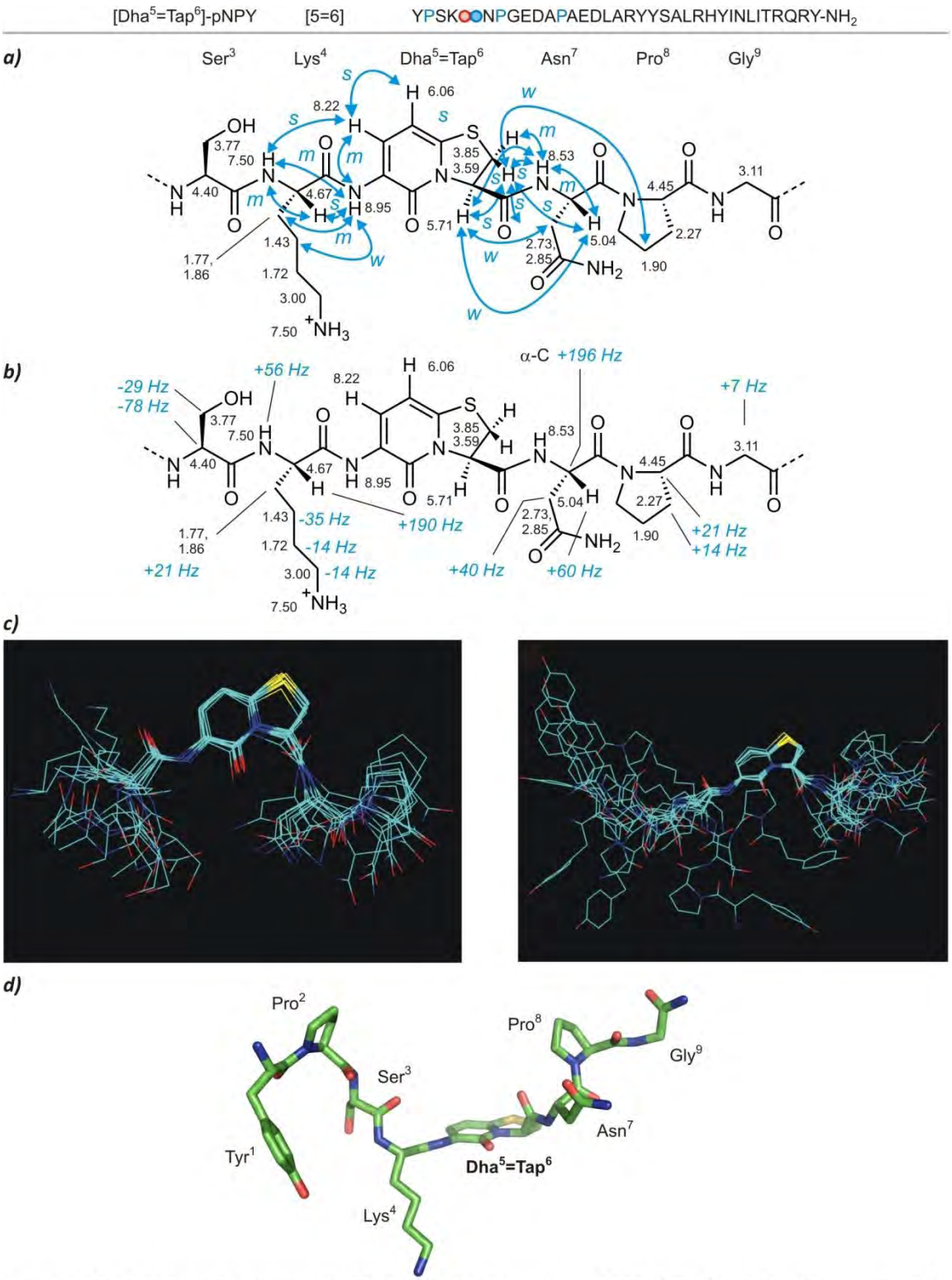

Figure 2.30 NMR-based structure elucidation of the N-terminus of [Dha^5=Tap^6]-pNPY. ***a)*** *Structure of the section for which influences of the Dha=Tap unit were identified (residues 3-9). The NOE contacts are indicated by blue arrows and assigned according to their intensities as strong (s), medium (m), and weak (w). All unambiguously assigned chemical shifts are written next to the respective positions.* ***b)*** *The same structure, now assigned with the chemical shift differences (in Hz) compared to native pNPY.* ***c)*** *Molecular dynamics simulation results: overlays of ten snapshots of residues 3-8 (left) and residues 1-9 (right). Carbons are shown in green, nitrogens in blue, oxygen in red, and sulfurs in yellow. The protons are not depicted for clarity reasons.* ***d)*** *Energy-minimized average structure of residues 1-9. All prolyl amides were kept in the* trans *conformation as the NMR spectra did not show any signals resulting from* cis *amides.*

HyperChem[86]. The overlay of the ten snapshots depicted in figure 2.30c gives an impression of the amplitude of the peptide dynamics. In the next step, the average structure was obtained by a common protocol which was used for all molecular modeling procedures carried out within the scope of this thesis. The snapshot structures were averaged and subsequently allowed to relax without the NOE restraints. If no significant differences are obtained (especially in the backbone geometry) this proves the plausibility of the structure obtained from the NOE data. This test is important as it detects eventual wrong assignment of NOE cross peaks. The longer the distance between two nuclei showing an NOE, the greater the impact on this restraint on the structure calculation, and already one single NOE contact which is falsely assigned as long-range coupling can constrain the structural defaults to such an extent that it results in a completely wrong overall conformation of the substrate.

The result obtained for the N-terminal nonapeptide of [5=6] after relaxation still fits the observed NOE contacts (figure 2.30d). At the N-terminal site of the Dha=Tap unit, the positions of the single Ser^3 and Lys^4 side chains relative to the aromatic plane of the pyridone are in good accordance with the chemical shift differences shown in figure 2.30b. The kink which takes the Lys side chain below and the N-terminal Ser^3 residue above the plane is mainly caused by the 133° ψ torsion of Lys^4. The modeling of the single substituted N-terminus already made an important effect of the Dha=Tap incorporation visible. With this dipeptide, a planar motif is introduced, but this does not result in a more planar average conformation of the total segment. The outcome seems to be quite the reverse, as the planarity of the dipeptide is apparently compensated by a distinct folding of the attached peptide strands out of this plane. In the triple-substituted NPY analog (section 2.3.2.4) this trend occurred even stronger.

2.3.2.4.3 The analogs [2=3] and [8=9]

The comparison of [5=6] to the other two single-substituted NPY analogs [2=3] and [8=9] indicates that the further course of the backbone geometry depends on the position of the Dha=Tap unit. Figure 2.31a shows all observed NOE contacts and changes in chemical shifts identified for the N-terminal tetrapeptide. The aromatic protons of the N-terminal Tyr^1 side chain are shifted up-field suggesting a preferred conformation with the Tyr aromatic ring positioned over the pyridone plane, possibly for the generation of hydrophobic π-stacking interactions. At this point it should be mentioned that for every analog a strong NOE was detected between the Tap NH and the α-H of the N-terminal amino acid, while the intra-residue Tap-NH/Tap^7-H NOE exhibited weak intensity. This proves the dipole-controlled Tap *trans* amide conformation and enables the comparison of N-terminal conformations in the various analogs.

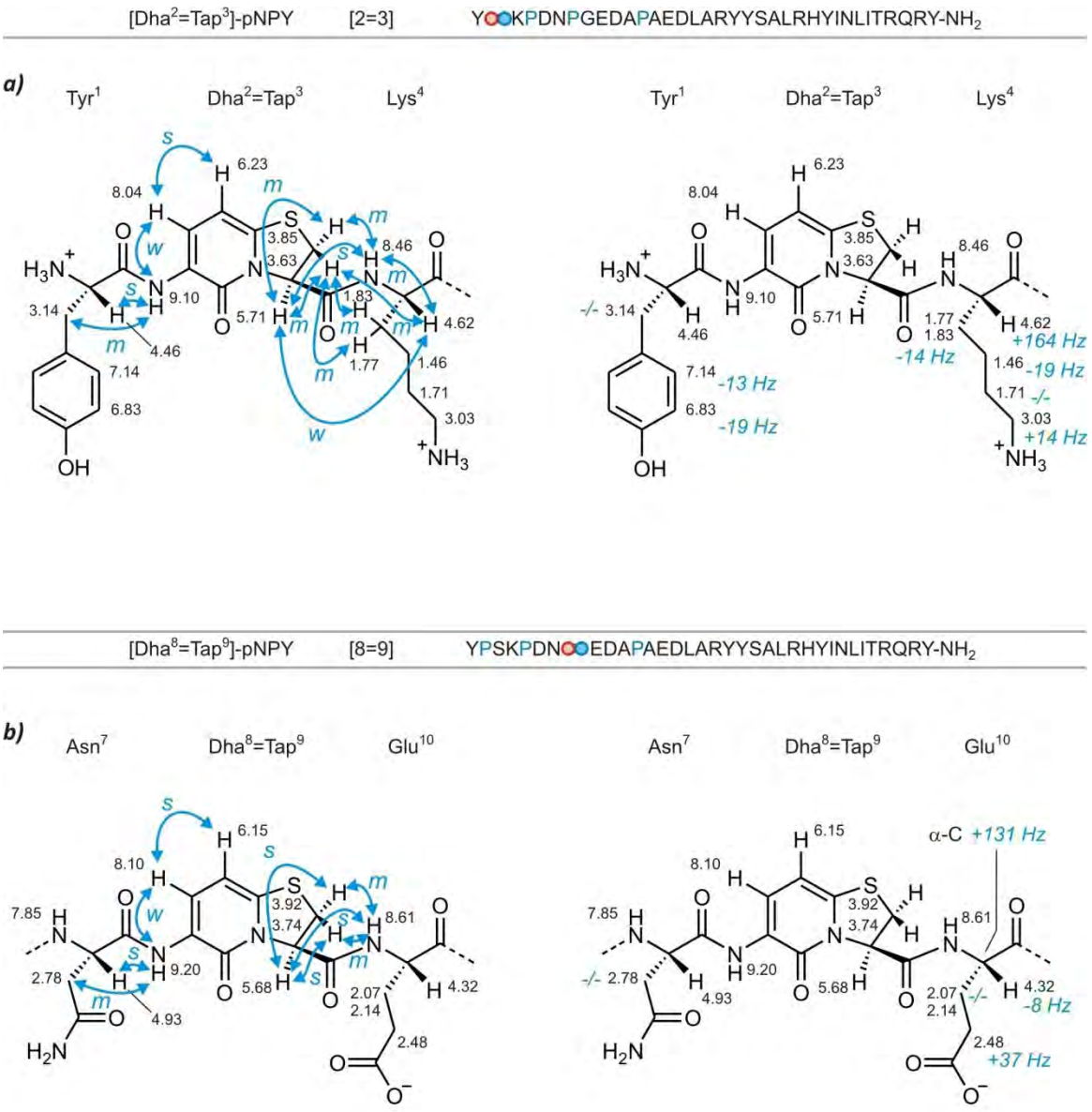

Figure 2.31 Structural analysis of the N-terminal segments of [Dha²=Tap³]-pNPY (a) and [Dha⁸=Tap⁹]-pNPY (b). *In comparison to [5=6] (figure 2.30), significant chemical shift changes and NOE contacts with Dha=Tap protons are only observed for the N- and C-terminally adjoining residues. While the NOE patterns of [2=3] and [5=6] are similar with respect to the contacting positions and the intensities, [8=9] differs by the lack of several dipolar couplings between Dha=Tap and adjoining residues. This indicates that the dipeptide position influences the configuration of the backbone. In addition, especially the substitution of the flexible hinge Gly⁹ plays a role for the dynamics of the N-terminal segment.*

At the respective C-terminal sites of the three analogs, different NOE patterns are observed between the diastereotopic 2-H and the adjoining C-terminal amide protons according to the Dha=Tap position. The chemical shift changes of the corresponding α-H are also highly different and decrease the more the Dha=Tap unit is located towards the C-terminus (+164 Hz for Lys^4 in [2=3], +60 Hz for Asn^7 in [5=6], and −9 Hz for Glu^{10} in [8=9]). This suggests that the conformational preferences of the C-terminal oligopeptide may be steered by the Dha=Tap position. The difference is particularly distinctive in [8=9] where a NOE between Tap^9 3-H and the α-H of the following residue is completely missing. It is reasonable to ascribe this to the substitution of the flexible Gly^9 residue as it may force the C-terminal part adjoining the Tap and possibly the N-terminus, too, into a conformative equilibrium which is different from the other analogs and from the native peptide. This hypothesis is supported by the lowered Y_5 receptor affinity loss compared to the other mismatched single substitutions, which may be ascribed to the fact that some requirements for fitting the binding pocket may not be fulfilled any more.

These results are especially relevant if the Y_5 binding property of the analog [1=2,4=5,7=8] is included into the considerations. In spite of the high degree of substitution, this analog shows only a moderate affinity loss. This apparently results from the fact that the lack of the Gly^9 hinge can be compensated by a greater backfolding tendency in the area of residues 10-13, caused by the extensively hydrophobized triple substituted N-terminus. In the case of the triple-substituted matched analog, which is described in the following section, this hydrophobization of the N-terminal segment turned out to be highly fruitful for detailed NMR analysis.

2.3.2.5 The triple-substituted analog [2=3,5=6,8=9]

The multiple incorporation of Dha=Tap units in the N-terminal segment results in strong hydrophobization of the NPY analogs, as it was visible from the increased HPLC retention times (Table 2.4 and ref.[38]). The NMR analysis of the matched triple-substituted NPY analog therefore should answer the question how and to what extent such a significant modification of the N-terminus influences the overall structure of the peptide. This is all the more relevant as we sought an explanation for the remarkable good binding properties of these analogs. Regarding the moderate Y_5 selectivities, the impact of the multiple Dha=Tap incorporation regarding peptide functionalization and hydrophibicity seems to fit the requirements especially at the Y_5 receptor where only a 12-fold and 6-fold affinity loss was obtained for the matched and mismatched analog, respectively.

The ^{1}H NMR spectrum of the triple-substituted analog [2=3,5=6,8=9] strikingly differs from the spectra of the other analogs by a position-selective line-broadening. This characteristic allowed

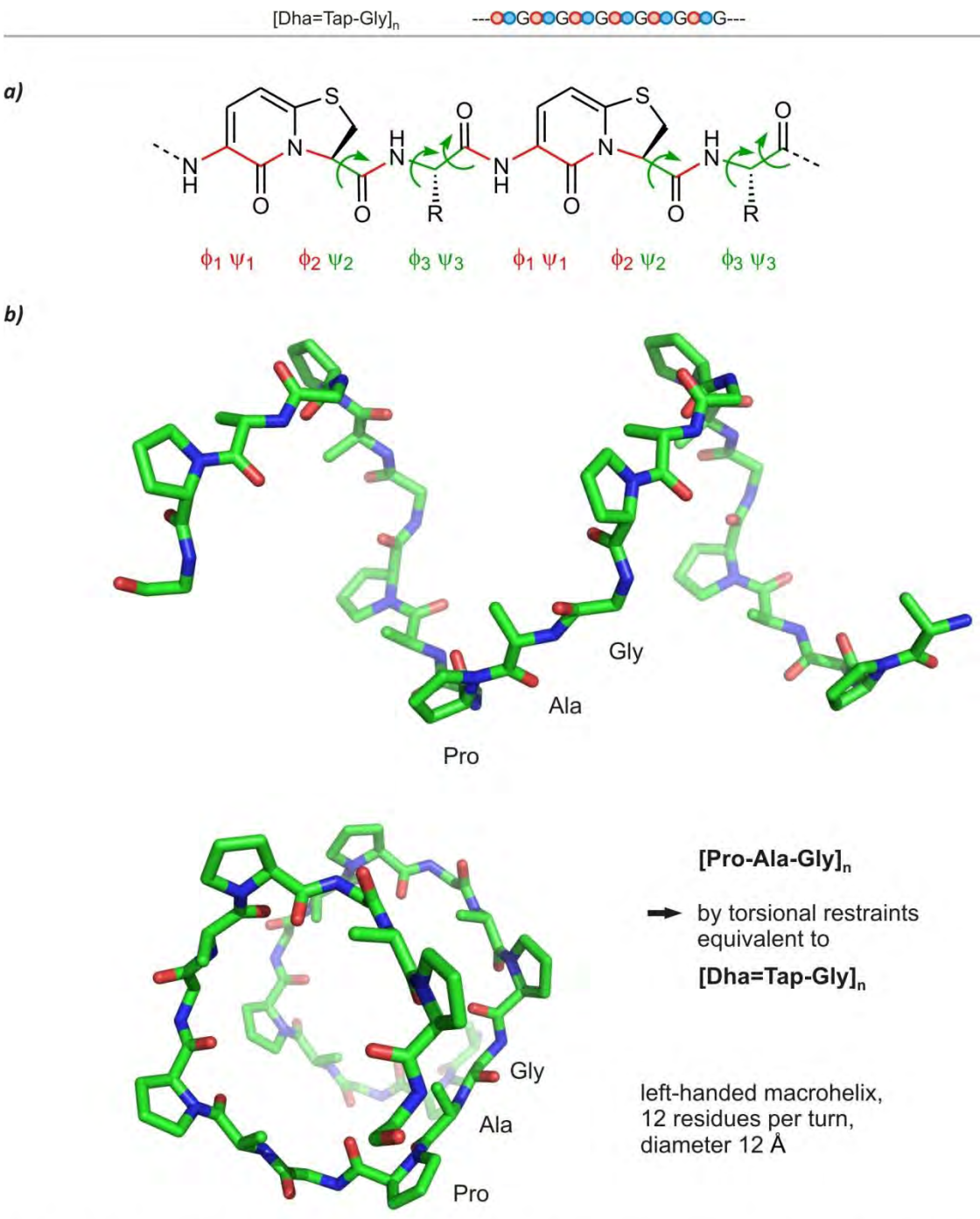

Figure 2.32. [Dha=Tap-Xaa] polymers: Rigidification of backbone torsions and structure calculations. ***a)*** *On average, half of the ϕ/ψ torsions are restricted in a [Dha=Tap-Xaa]$_n$ polypeptide as present in the examined triple-substituted NPY analogs [1=2,4=5,7=8] and [2=3,5=6,8=9]. Three frozen torsions (ϕ/ψ/ϕ; marked red) are followed by three rotatable angles (ψ/ϕ/ψ; marked green). R = amino acid side chain.* ***b)*** *Molecular modeling results of a [Pro-Ala-Gly]$_n$ polypeptide whose torsions were restrained as in a [Dha=Tap-Gly]$_n$ polypeptide. In comparison with an [Ala-Pro-Gly]$_n$ polypeptide with analogous restraints, the shown polymer converged best. Two helix turns equivalent to a [Gly-Pro-Ala] octamer are shown from two perspectives. If viewed exactly along the helical axis, all residues n+12 are exactly masked by the corresponding residues n. In the lower shown projection this can be seen from the identical orientations of the respective Pro rings in the two turns. This structure is different from the rather flat conformation obtained for the N-terminal [Dha=Tap-Gly] trimer in [Dha^{1,4,7}=Tap^{2,5,8}]-pNPY (figure 2.39), which may be the result from the presence of SDS micelles.*

to draw detailed conclusions about the coordination of the peptide to the membrane and its secondary structure, information which otherwise is only accessible by labeling studies and extensive experimental methodology. This great benefit of multiple [Dha=Tap] labeling is described in section 2.3.2.4.1.

By triple incorporation of Dha=Tap in the matched positions, this N-terminal nonapeptide is converted into a trimer with the sequence $[Dha=Tap\text{-}Xaa]_3$. Is the "flexible" segment by this modification turned into a rigid chain, and how do its preferred conformations look like? As shown in figure 2.32a, there are three types of ϕ/ψ pairs with different conformational restriction in a $[Dha=Tap\text{-}Xaa]_n$ polymer. While the Dha pair is frozen to 180°/180° due to the covalent tethering and the dipole interaction, there are two possibilities for the Tap pair in which the ψ torsion adopts two proposed angles (140° and −40°). The Xaa pair, in contrast, is not restricted and can adopt all angle combinations as marked in the Ramachandran plot (figure 2.12d, green area). Taken together, by fixation of two of three ϕ and of every third ψ angle, every second rotational degree of freedom is frozen, which results in a significant overall restriction. In order to evaluate the structural impact we performed molecular modeling studies of an [Ala-Pro-Gly] oligomer whose torsions had been frozen according to the restrictions given in a $[Dha=Tap\text{-}Xaa]_n$ chain. The outcome, as shown in figure 2.32b, is quite unexpected as the rigid and planar Dha-Pro units do not extend the persistent length of the polypeptide. They rather effect the opposite by inducing a left-winding macrohelix with a diameter of 15 Å and one helix turn corresponding to exactly four [Ala-Pro-Gly] units. In section 2.3.2.4.3 this structure will be compared to the modeling result of the analogous sequence in the triple-substituted NPY, which allows conclusions on interactions with the SDS micelles.

2.3.2.5.1 The position-selective line-broadening in the ^{1}H NMR: reasons and implications

Compared to the native peptide and to the three single-substituted analogs, only approx. one quarter of the amount were available from $[Dha^{1,4,7}=Tap^{2,5,8}]$-pNPY for NMR studies (1.59 mg, 0.38 µmol), resulting in a 0.63 mM solution. As no concentration dependences were observed in the case of the other investigated peptides, this also can be assumed for the triple-substituted analog. Therefore only one quarter of the SDS amount compared to the other samples was added, in order to obtain a similar ratio of peptide/SDS concentration. The resulting 60 mM SDS concentration (other samples: 200 mM) still greatly exceeded the critical micelle concentration of 8.0 mM.[39] Furthermore, this kept the option to add more SDS later if required. In spite of the low concentration, well resolved ^{1}H NMR spectra using the DPFGSE water suppression could be obtained, however, 512 scans were necessary to obtain sufficient signal intensities, and the

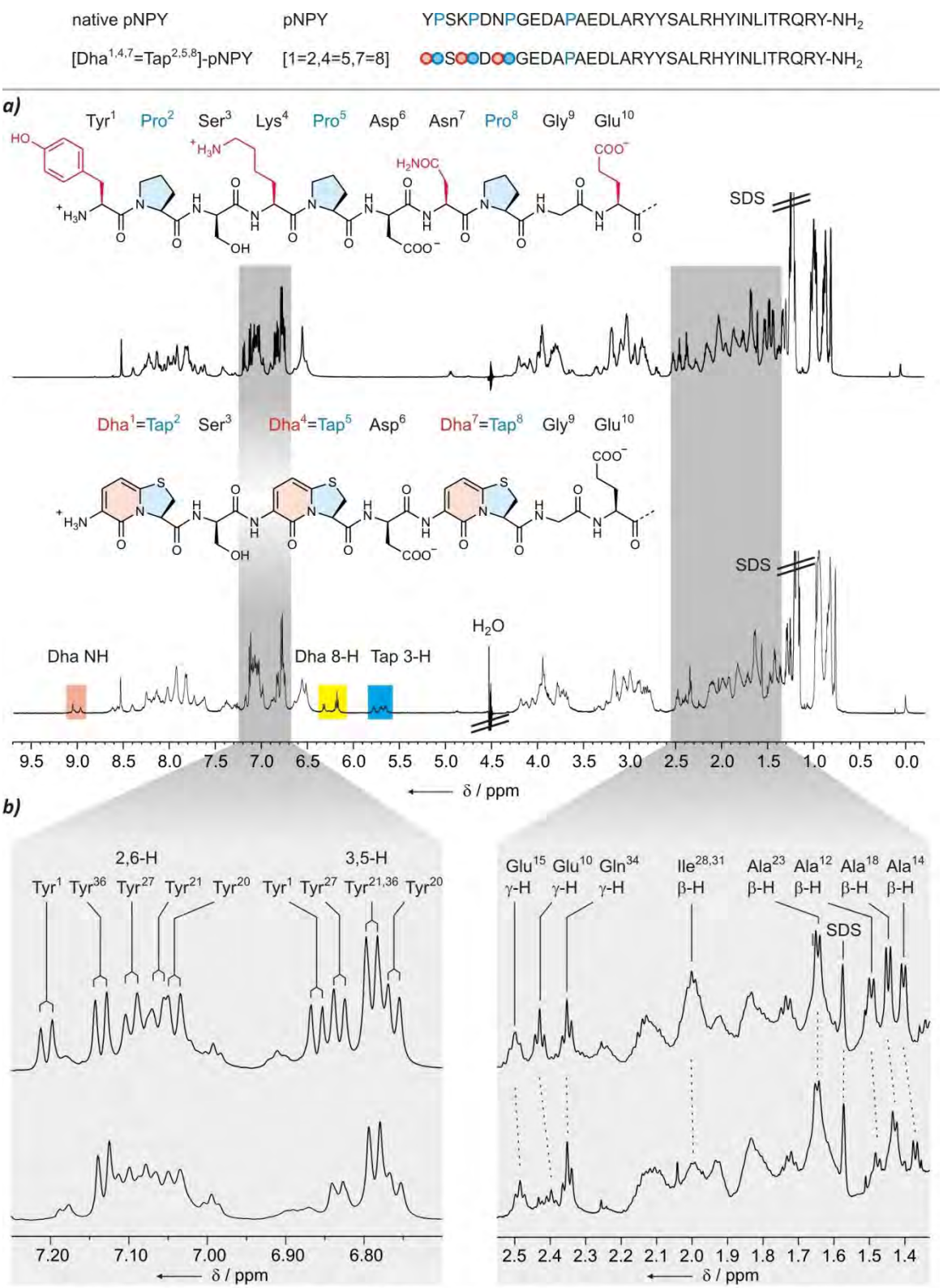

Figure 2.33 A residue-selective line-broadening within the ^{1}H NMR spectrum is obtained after increasing the hydrophobicity of the N-terminus with triple Dha=Tap substitution. ***a)*** *Depiction of the complete ^{1}H DPFGSE-NMR spectra (H_2O/D_2O 5:1, SDS-d_{25}, 600 MHz, 320 K) of native pNPY (top) and [Dha^{1,4,7}=Tap^{2,5,8}]-pNPY (bottom). The three Dha=Tap proton resonances which appear separated from the crowded regions are marked according to figure 2.21.* ***b)*** *Enlargements of the Tyr region (left) and of a high-field section (right) showing the different extent of line-broadening according to the residue in the triple-substituted analog (bottom). In table 2.6, all assigned side chain signals are listed together with the extent of broadening.*

2D spectra required longer acquisition times (approx. 36 h per experiment). Figure 2.33a compares the ^{1}H NMR spectra of native and matched triple Dha=Tap substituted pNPY and depicts the respective N-termini (residues 1-10). Most important, no impurities were determined and one single set of signals was also observed in this case, though no purification via HPLC had been carried out, which demonstrates the excellent applicability of the Dha=Tap dipeptide for solid phase peptide synthesis. A comparison of both spectra again reveals the advantageous signal dispersion associated with Dha=Tap incorporation. The three Tap 3-H signals appear separated from each other at 5.66, 5.71 and 5.79 ppm. Two of the Dha 8-H doublets overlap to a pseudotriplet at 6.19 ppm which can be resolved by *Lorentz*-to-*Gauss* transformation. Finally, the Dha^{4} and Dha^{7} amides are located at 8.97 and 9.05 ppm, respectively, in the otherwise empty spectral region, while the N-terminal Dha^{1} ammonium peak remains invisible, apparently due to strong signal broadening.

The comparison of the signal shapes in the ^{1}H NMR spectra of native and triple-substituted NPY revealed a detail which had not been observed for the single-substituted analogs. Many signals and signal groups, distributed over the entire spectrum, are significantly broadened, and this is associated with a decrease of the signal intensities. This effect is most apparent in the case of the Ala and Tyr side chains, as visible from the two spectral sections in figure 2.33b. Notably, the line-broadening occurs with varying intensity and only affects certain signals, which is why mistakes in the NMR experimental setup can be excluded. The fact that not only N-terminal residues are affected (the strongly broadened Ile^{31} being the most C-terminal one) shows a distinctive long-range effect of the Dha=Tap units over more than 20 residues. As much residues as possible were assigned by detailed comparison of the ^{1}H and 2D NMR spectra of native and the triple-substituted NPY, and all unambiguously identified residues are listed in Table 2.6, together with the respective chemical shifts and with the extent of broadening which was cataloged in strong, medium, and weak. The depiction of broadening intensities by the primary sequence of the NPY analog (figure 2.34) illustrates the distribution along the peptide. Although for some residues the extent of broadening could not be assigned due to strong signal overlap, the identified broadenings show a distinctive pattern. While exclusively strong broadenings are observed for all residues in the N-terminal section up to Ala^{14}, the signals of residues located in α-helical segment are differently affected. Finally, the signals assigned to the C-terminal residues Thr^{32}, Gln^{34}, and Tyr^{36} are not broadened.

[Dha^{1,4,7}=Tap^{2,5,8}]-pNPY [1=2,4=5,7=8] SSDDGEDAPAEDLARYYSALRHYINLITRQRY-NH_2

Table 2.6 Extent of signal broadening in the ^{1}H DPFGSE NMR spectrum after triple Dha=Tap substitution. *Only those signals are listed which were unambiguously identified and which are sufficiently separated.*

residue	position	chemical shift / ppm	extent of line-broadening
Ser^3	α-H	4.68	strong
	β-H	3.94	strong
Asp^6	α-H	4.88	strong
	β-H	2.92	strong
Gly^9	α-H	4.00	strong
Glu^{10}	γ-H	2.40	strong
Ala^{12}	β-H	1.48	strong
Ala^{14}	β-H	1.37	strong
Glu^{15}	γ-H	2.49	medium
Ala^{18}	β-H	1.43	low
Tyr^{20}	2,6-H	7.04	strong
	3,5-H	6.76	strong
Tyr^{21}	2,6-H	7.06	strong
	3,5-H	6.79	strong
Ala^{23}	β-H	1.65	none
Leu^{24}	α-H	4.19	medium
	δ-H	0.98	medium
His^{26}	2-H	8.53	none
Tyr^{27}	2,6-H	7.11	strong
	3,5-H	6.83	strong
Ile^{28,31}	β-H	2.00	strong
	γ-CH_2	1.73	medium
	γ-CH_3	0.93	medium
	δ-CH_3	0.86 (Ile^{28}), 0.83 (Ile^{31})	medium
Leu^{30}	γ-H	1.83	low
Thr^{32}	γ-H	1.30	none
Gln^{34}	γ-H	2.35	none
Tyr^{36}	2,6-H	7.13	none
	3,5-H	6.79	none

Figure 2.34 Graphical depiction of the extent of line-broadening in the ^{1}H DPFGSE NMR spectrum. *Analogously to figure 2.11 the four segments of NPY are colored red (N-terminus), orange (turn segment), green (α-helical segment) and blue (C-terminus). The distribution of the intensities of line-broadening along the sequence suggests a membrane coordination of the hydrophobized N-terminus and of the hydrophobic α-helical side. For all residues without bar no sufficiently separated signals were found which would allow an unambiguous characterization.*

Searching for the reason of this strongly position-selective broadening, the globular dynamics (*tumbling* motion) of the peptide/SDS aggregates can be excluded as these are still mobile enough so that anisotropic interactions are averaged out. Instead, it is plausible to assume that a chemical exchange process causes the observed signal broadening. If two species interconvert very slowly on the NMR time scale, one signal set for each species is observed. An increase of the exchange rate leads to signal broadening and finally to the coalescence to one single set of signals. If the exchange is not too fast, this set of signals appears broadened, and this also applies for the triple-substituted pNPY. Like every membrane-coordinating substrate, it is subjected to equilibrium between the micelle-bound state (micelle on) and the free solution state (micelle off). Obviously, the high content of Dha=Tap, which results in a higher hydrophobicity of the peptide, decreases the (de)coordination rate so that it becomes visible by the signal broadening. This is supported by the increasing HPLC retention times with the extent of Dha=Tap insertion (Table 2.4 and ref.[38]). Hydrophobic peptides generally tend to stronger membrane coordination in order to minimize the contact to the polar solution environment, and proteins can be "fine-tuned" with respect to their membrane permeability for example by attaching or removing fatty acid chains.[87] It is plausible to assume that not only the α-helical region interacts with the micelles (as proven by *Zerbe et al.*[43]) but also the hydrophobic Dha=Tap rich N-terminus. Described from another perspective, more detergent molecules are required to keep the lipophilic NPY in aqueous solution. This principle was also utilized within the scope of this work to enable the NMR spectroscopic characterization of cyclic Tyrocidine A aldehyde which tends to aggregate in water, as it was only soluble after adding a sufficient amount of SDS (section 3.5).

Concerning a visualization of peptide/SDS interaction, it must be remembered that SDS micelles do not resemble stable closed systems with constant and well-defined shape. They rather feature highly mobile self-organizational equilibria which can - in the other extreme - also be described as an increased concentration of detergent molecules at the hydrophobic contact sites of the biomolecules. Therefore, the depictions of SDS aggregates should only be seen as descriptive to illustrate the interactions. Modeling results of a SDS micelle containing 80 molecules (this has been determined as average number)[40] are shown in figure 2.35. To clarify the proportions, a native NPY molecule coordinating with its α-helix on the micelle surface is also depicted. The comparison of the peptide chain length (approx. 6.5 nm) with the diameter of the micelle (3.5 nm) shows that one aggregate alone is too small to enable simultaneous coordination with the helix and the N-terminus. This would require an unfavorable strong bending of the peptide around the aggregate. Consequently, it is plausible that two

[Dha^{1,4,7}=Tap^{2,5,8}]-pNPY [1=2,4=5,7=8] SSDGEDAPAEDLARYYSALRHYINLITRQRY-NH_2

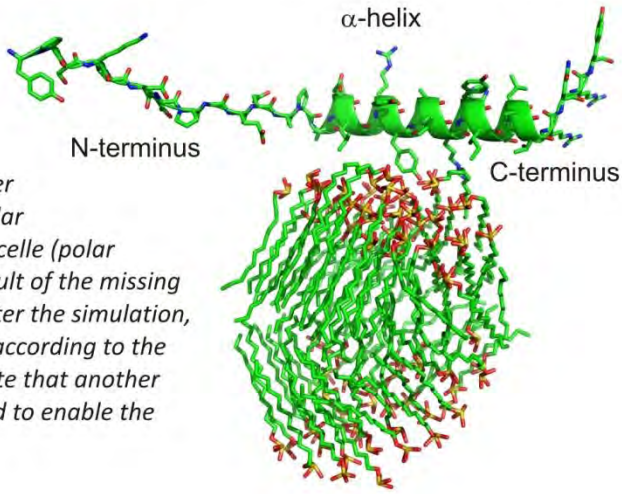

Figure 2.35 Coordination of native pNPY to an SDS aggregate. *The micelle containing 80 SDS molecules was calculated over 200 ps starting from a double-layered alignment. The aggregate adopted a spherical form, but the alignment of the single detergent molecules rather tended to resemble an intermediate form of regular (polar headgroups on the surface) and inverse micelle (polar headgroups in the center) which might be the result of the missing solvent (simulation under vacuum conditions). After the simulation, the calculated pNPY was attached to the micelle according to the results by* Zerbe et al.*[43]. The proportions indicate that another micelle or a rather tubular aggregate are required to enable the coordination of a hydrophobized N-terminus.*

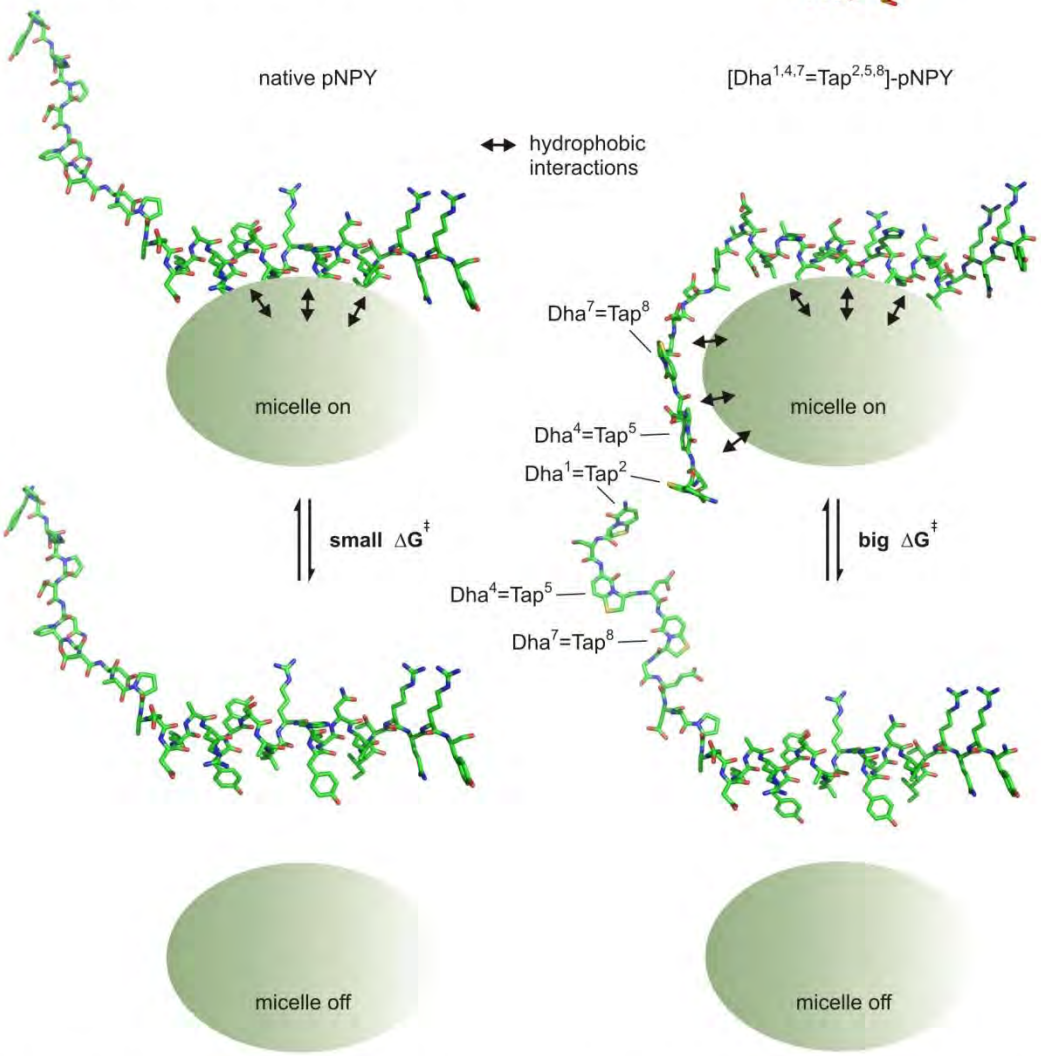

Figure 2.36 All membrane-coordinating molecules are in an equilibrium with a free-solution state. *Simplistic comparison of the micelle on/off equilibria of native (left) and hydrophobized pNPY (right). The SDS micelles are symbolized as grey spheres as no detailed picture can be given of these highly mobile aggregates. As the threefold Dha=Tap substituted N-terminus also interacts with the membrane mimetic, the free activation energy $\Delta G^{\ddagger}$ increases, which effects a slower (de)coordination rate that finally causes the line broadening in the ^{1}H NMR spectrum. The conformation of the N-terminus corresponds to the NOE-based modeling results which are in more detail shown in figure 2.39.*

SDS micelles may be involved to keep one NPY analog in solution. Regarding the mobile nature of the aggregates, it is imaginable that SDS molecules diffuse with high rate between them, which would lead to the conception of a rather tubular aggregate which is generated by fusing both micelles. However, it would be speculative to attempt a more detailed illustration of how this aggregate could look like. As the surroundings of the protons (and, consequently, their chemical shifts) change with membrane (de)coordination, the micelle-on/off equilibrium exhibits a chemical exchange. As shown in Figure 2.36, the triple Dha=Tap incorporation increases the peptide/micelle interactions (indicated by arrows) which again results in an increased free transition energy $\Delta G^{\ddagger}$ between the membrane-bound and the solution state. Finally, as a higher free energy barrier has to be overcome, the chemical exchange rate decreases, as visible by the broadened NMR signals. Protons which are oriented towards the solvent in the membrane-bound state will not show a measurable change in their chemical shifts, except if the conformation of the peptide is subjected to significant changes upon membrane binding. The results of *Zerbe et al.* showed that the only structural effect of membrane coordination of native NPY is an increased stability of the α-helix and its extension over more residues.[43] This fact allows to draw an important conclusion for the Dha=Tap modified NPY analog: the stronger the broadening of signals, the more are the corresponding protons oriented towards the micelle and away from the solution.

On basis of these considerations, the Dha=Tap insertion turned out to be an excellent method to elucidate the positions and conformations of the single peptide segments on the SDS aggregates. Notably, this can be read out directly from the ^{1}H NMR spectrum and does not require any other experimental techniques (which only enable indirect determination). In the hydrophobic N-terminus, all identified signals resulting from residues adjacent to a Dha=Tap unit (Ser^{3}, Asp^{6}, Gly^{9}) are strongly broadened which indicates that all Dha=Tap dipeptides interact with the membrane mimetic. For the following segment which tethers the two regions of high membrane affinity (the hydrophobic N-terminus and the α-helix starting at the latest from Ala^{18}), strong (Glu^{10}, Ala^{12}, Ala^{14}) and medium (Glu^{15}) signal broadenings could be determined. This suggests that also this segment is closely located to SDS aggregates, which is compatible with the conception of a tubular aggregate, or, with a high concentration of SDS molecules that are exchanged between the micelles coordinating the N-terminus and the α-helix, respectively.

The detailed examination of signal broadenings along the α-helical section should be particularly interesting. As already outlined in section 2.1.5, the hydrophobic site of the helix turned out to be located towards the micelle, with the unpolar Tyr, Leu, and Ile side chains penetrating the surface.[43] This alignment is shown in figure 2.37a for the fragment Ala^{18} to Ile^{31}. Consequently,

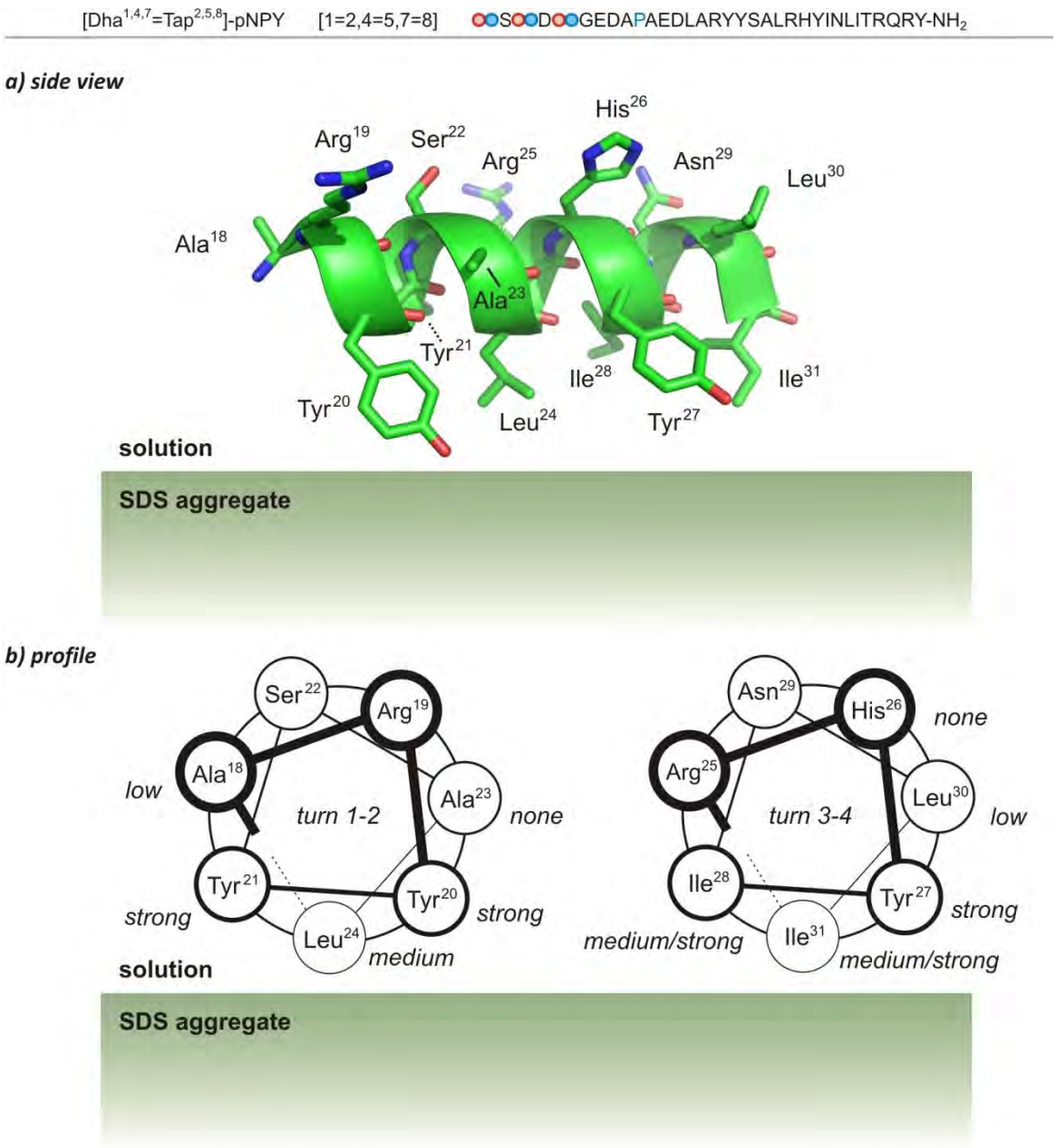

Figure 2.37 The ^{1}H DPFGSE-NMR line broadening data of residues located in the α-helical section of [Dha^{1,4,7}=Tap^{2,5,8}]-pNPY give direct evidence of the orientation of the α-helix on the micelle surface, in contrast to the intricate methods used in former works which give only indirect hints. a) *A part of the α-helical segment (residues 18-31) is shown as modeling result (HyperChem) perpendicular to the helical axis with the hydrophobic side of the helix oriented towards the micelle surface. The Tyr^{21} side chain which is also located towards the aggregate is covered by the helix cartoon and indicated by a dotted line.* ***b)*** *Schematic depiction along the helical axis together with the observed extents of line broadening. In this section, the α-helix adopts four turns. The first and the second turn (residues 18-24) are shown on the left, and the following two turns (residues 25-31) are shown on the right, with the line thicknesses indicating the respective distances from this perspective. For 10 of the 14 residues, sufficiently isolated signals were found which allowed to estimate the extent of line broadening. The hydrophobic side chains which are oriented towards the aggregate can penetrate the surface of the membrane. Consequently, their protons experience different chemical shifts in the membrane-on- and off-state, which causes the line broadening. In contrast, the side chains on the hydrophilic side are oriented towards the solution, independently of the membrane coordination. Therefore, their signals do not change upon strong hydrophobization by the triple Dha=Tap substitution.*

in our case the signal broadenings should be more distinct the closer the corresponding side chain is located towards the micelle-coordinating hydrophobic site of the helix, resulting in a periodicity of signal broadening along the backbone. As shown in the depiction of the helix profile for turns 1-2 (left) and 3-4 (right) in figure 2.37b, the signal broadenings greatly fit this conception. Finally, the signals of all identified residues along the C-terminal pentapeptide (Thr^{32}, Leu^{34}, Tyr^{36}) showed no broadening which indicates a rather extended conformation and would also be compatible with an equilibrium between α-helical and extended conformation according to the results of *Zerbe et al*.[43] The C-terminal Tyr^{36} amide was supposed to serve as membrane anchor which stabilizes the bioactive conformation. Interestingly, our data suggest no interaction of the Tyr^{36} side chain with the membrane, which may be required to allow for an optimum anchoring of the amide.

These results are remarkable as the secondary structure and the orientation of the peptide on the membrane are *directly* visible from ^{1}H NMR spectroscopy, without the need of performing cost-intensive labeling and time-consuming 2D NMR experiments and spin-relaxation measurements that must be interpreted *indirectly*.

2.3.2.5.2 The structural impact of triple Dha=Tap incorporation: Short-, medium- and longe-range effects

The low concentration of [1=2,4=5,7=8] in the NMR sample complicated the evaluation of the 2D NMR spectra, but finally a sufficient number of NOE contacts in the N-terminus was determined which enabled to gain a picture of its conformation. Figure 2.38 shows the N-terminal section (residues 1-10) with all NOE contacts (a) and with the chemical shift changes in comparison to the native peptide (b). The three Dha=Tap units could be assigned to their position which was enabled by the greatly separated 3-H signals (figure 2.33a). All signals of protons in the residues Ser^{3} and Asp^{6} linking two Dha=Tap units as well as the Gly^{9} α-H signal are significantly shifted down-field (between 60 and 148 Hz), as expected by the proximity to one or two aromatic pyridone motifs. Therefore, it can be concluded that all residues adjacent to one or two Dha=Tap units are located in the planes of the pyridones.

The comparison of the NOE pattern with the single-substituted analogs (figures 2.30a and 2.31) revealed differences on both the Dha and the Tap site. While the Dha^{4} and Dha^{7} amide protons show NOE contacts with the α-H and β-H of the residues at positions n−1, which corresponds to the observations that were made for all three single substitutions, all Dha 7-H show no NOE contacts at all. At the Tap units, the situation is even more different. In contrast to the many dipolar couplings observed between the Tap 2-H/3-H and the residues at positions n+1 in the

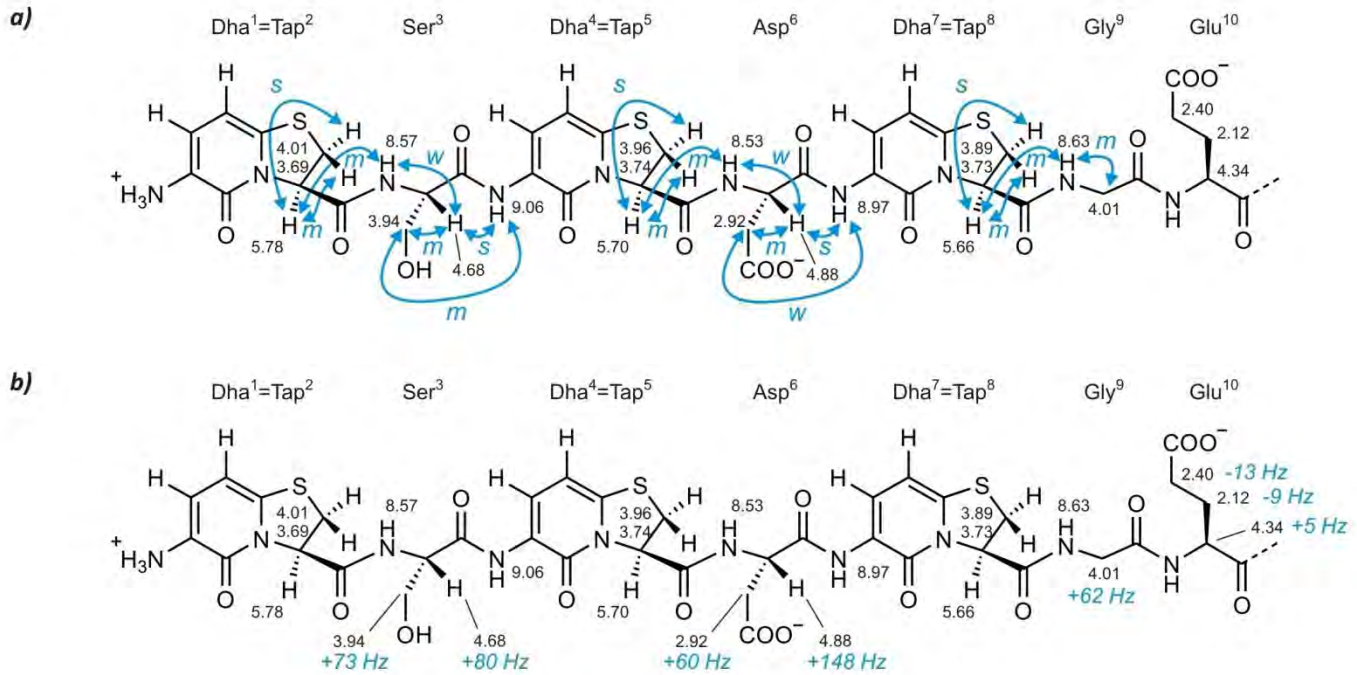

Figure 2.38 NOE contacts and chemical shift changes in the N-terminus of [Dha[1,4,7]=Tap[2,5,8]]-pNPY. ***a)*** *Structure of the N-terminal decapeptide with all assigned chemical shifts written next to the respective positions, and with all found NOE contacts indicated by blue arrows. According to their intensities the NOE couplings are classified as strong (s), medium (m), and weak (w). Compared to the single-substituted analogs, there are several weak and strong couplings which are not observed, which indicates that the hydrophobized N-terminus adopts a different geometry. Therefore, the three Dha 7-H/8-H pairs could not be assigned their respective positions (chemical shifts: 8.08/6.33 ppm, 8.14/6.19 ppm, 8.15/6.19 ppm). Interestingly, no conspicuous chemical shift differences are observed for the signals of the Dha=Tap protons compared with the single-substituted analogs.* ***b)*** *The same structure, now assigned with the chemical shift differences (in Hz) compared to native pNPY. All protons except those in the Glu[10] side chain are located in the plane of one or two aromatic pyridones and therefore down-field shifted. Molecular dynamics simulation results are shown in the following figure 2.38, and the up-field shift of the Glu[10] side chain protons is discussed in figure 2.39.*

single-substituted analogs, there are no Tap 2-H contacts at all, and the only contacts observed for Tap 3-H are towards the Tap NH. This absence of many weak and strong contacts which are present in the single-substituted analogs suggests a significant structural impact of the high density of Dha=Tap units. To evaluate this, the NOE contacts were used as restraints for a molecular modeling of the N-terminal decapeptide Dha^{1}=Tap^{2}-Ser^{3}-Dha^{4}=Tap^{5}-Asp^{6}-Dha^{7}=Tap^{8}-Gly^{9}-Glu^{10} which is shown in different overlays and from different directions of view in figure 2.39a-d. The chosen perspective in figure 2.39d reveals an interesting detail, as the Dha^{4}=Tap^{5} and Dha^{7}=Tap^{8} dipeptides assume a nearly parallel orientation during the entire molecular dynamics simulation. This conformational preference is remarkable in the light of the high overall amplitude of the adjoining peptide chains. Finally, this in-plane alignment was also obtained for the average structure which is depicted in figure 2.39e from two perspectives.

At first glance, these structural results are quite unexpected as they greatly differ from the macrohelical structure which was obtained for an analogous oligomer (figure 2.32). As a part of NPY in membrane mimetic environment, the overall conformation is different as the backbone adopts a rather zigzag-like course (view perpendicular to the pyridone planes) with a remarkable flat overall shape of the entire peptide (view along the pyridone planes). However, this matches very well with the increased membrane affinity of the triple substituted peptide as it allows an optimal coordination of the hydrophobic pyridone dipeptides with the membrane.

In section 2.3.2.3, the consequences of Gly^{9} deletion by mismatched Dha=Tap substitution were discussed. The triple matched substitution in [1=2,4=5,7=8] conserves this flexible hinge which links the rigidified, hydrophobic N-terminus (three Dha=Tap, one Ser, one Asp) to the rest of the peptide. As indicated in figure 2.39a, the chemical shift changes of Glu^{10} give important hints on the course of the backbone in this segment. While the α-proton of Glu^{10}, like the Gly^{9}, is still localized in the Dha^{7} plane (+5 Hz), the values turn negative for the side chain proton chemical shifts (β-H: -9 Hz, γ-H: -13 Hz). This can only be explained by a distinctive kink at the Gly^{9} by which the backbone folds out of the Dha^{7} (and also the Dha^{4}) plane. Molecular modeling studies support this finding as they always resulted in a backfolding of the N-terminal section. As the triple Dha=Tap introduction significantly increases the persistent length of the N-terminal segment, the role of the Gly^{9} becomes all the more important. First, it facilitates the population of globular conformations, and second, it serves as a source of entropic stabilization by allowing a multitude of orientations of the N-terminus with respect to the α-helical segment.

If there is a significant backfolding tendency, this may also be visible by chemical shift changes of residues which are located at greater distances to the aromatic pyridones. In fact, for almost all residues in the adjoining segment with sufficiently separated signals (Ala^{12}, Ala^{14}, Glu^{15}, Ala^{18})

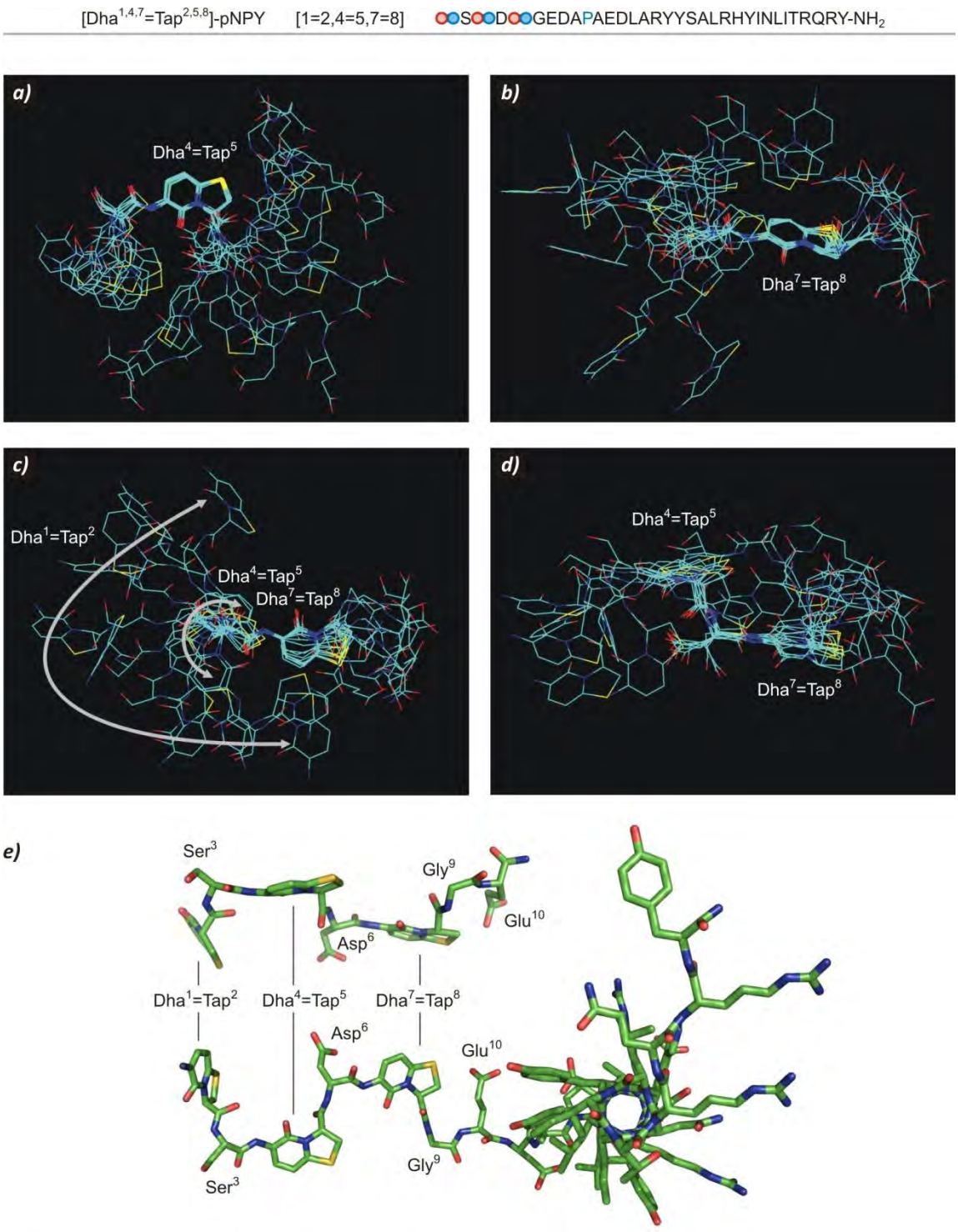

Figure 2.39 NMR-based structure elucidation of the N-terminus of [Dha^{1,4,7}=Tap^{2,5,8}]-pNPY. a)-d) *Overlay of ten snapshots of molecular dynamics simulation (residues 1-10). The dipeptide Dha =Tap served as basis for the overlay shown in a), and Dha =Tap is the basis for the overlays shown in b), c), and d). The white arrows in c) show the relative mobility range of the three Dha=Tap dipeptides within the simulation time span of 0.1 ns. The perspectice chosen in d) indicates the in-plane orientation of Dha^4=Tap^5 and Dha^7=Tap^8 which possibly is a preferred conformation as it effects an optimal coordination of the hydrophobic pyridones to the membrane. Carbons are shown in green, nitrogens in blue, oxygen in red, and sulfurs in yellow. The protons are not depicted for clarity reasons.* ***e)*** *Energy-minimized average structure of residues 1-10 shown from two perspectives: along the Dha=Tap planes (top) and as part of the full-length peptide (bottom) viewed perpendicular to the Dha=Tap planes and along the α-helical axis.*

an up-field shift was determined which suggests that these residues are located outside the pyridone planes. This is only compatible with a backfolding at Gly^{9} as in an extended conformation these residues would be in too big spatial distance to the Dha=Tap units to experience the chemical shift anisotropy. Table 2.7 lists the chemical shift changes of all unambiguously assigned positions starting from Glu^{10}. Notably, similar trends, though not as strong, can be seen for the single-substituted analogs, too. These data are compatible with a membrane-induced stabilization of the α-helix, and with the backfolding tendency of the hydrophobic N-terminal segment. If the α-helix already starts at Ala^{14}, with the orientation on the micelle surface according to figure 2.37, the radial positions are compatible to the signal broadening as well as to the down-field shifts, and the influence of the Dha=Tap units is decreasing towards the C-terminus (figure 2.40b).

Figure 2.40 summarizes the conception of the conformational preferences in a simplified illustration of the overall peptide. As the N-terminus is strongly hydrophobized, it also interacts with the SDS aggregates, and therefore the micelle on/off rate is decreased to such extent that it is visible by signal broadening in the ^{1}H NMR spectrum. Notably, this occurs selectively for the residues coordinating the membrane, and thus enables to determine the exact orientation of the α-helical segment on the aggregate. From the chemical shift anisotropy of the aromatic pyridones, the course of the backbone N-terminus with respect to the α-helical segment can be examined, and the data suggest a backfolding tendency of the hydrophobized N-terminus. The influence of the Dha=Tap unit on the chemical shifts is the second parameter which indicates the radial position of single residues in the α-helix, as only residues on the membrane-averted side experience the down-field shift of the pyridones. The more the residues are located towards the C-terminus, the weaker is this influence.

2.3.2.5.3 Molecular modeling: The role of Pro^{13} amide conformation and implications on the term “flexibility”

In order to obtain a picture of the full-length peptide, it was calculated with the N-terminal decapeptide frozen in the average conformation which was depicted in figure 2.38e. Two simulations were run, with the Pro^{13} amide being in the *cis* and in the *trans* conformation, respectively. The superimpositions (over the α-helical segment) are shown in figure 2.42. Most notably, the simulation in both cases revealed a distinct backfolding tendency of the triple-substituted N-terminus. As expected from the NMR data, the folding starts at the Gly^{9} hinge and the backbone of residues 10-12 takes a course out of the Dha=Tap planes. The Pro^{13} amide is the crucial determinant of the orientation of the entire N-terminal segment with respect to the

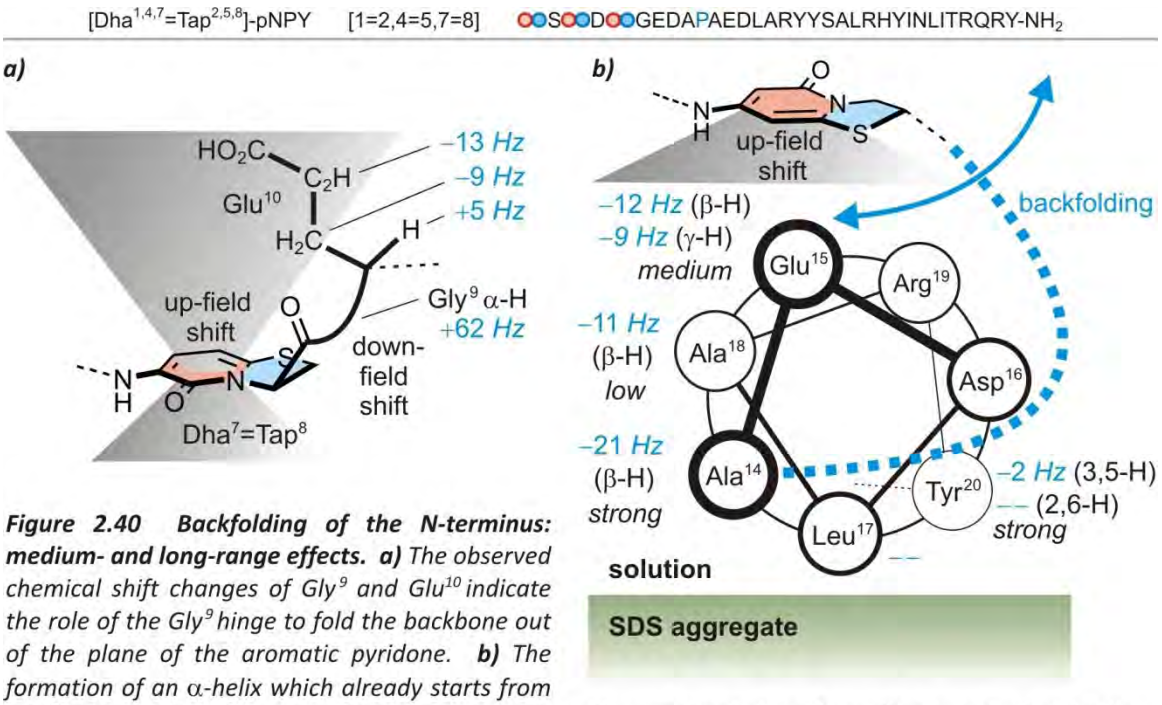

Figure 2.40 Backfolding of the N-terminus: medium- and long-range effects. a) *The observed chemical shift changes of Gly[9] and Glu[10] indicate the role of the Gly[9] hinge to fold the backbone out of the plane of the aromatic pyridone.* ***b)*** *The formation of an α-helix which already starts from Ala[14] and which in this segment is in equilibrium with an extended conformation is indicated by the experimental data: the signal broadening gives hints on the helix orientation on the micelle surface and the chemical shift changes show the extent of the up-field shifting influence of the Dha=Tap units in the N-terminus. The α-helix is depicted along the axis according to figure 2.37b, and the blue dotted line schematically indicates the backfolding tendency of the N-terminus. However, this takes place within an equilibrium (blue solid arrow) and the N-terminal segment probably moves within a great conformational space, as shown in the following figure 2.41a. The picture only represents the membrane-bound state, as in the solution state the α-helix is destabilized in the shown segment and the N-terminus in principle can also backfold on the hydrophobic side of the α-helix.*

Table 2.7 Changes in chemical shifts of ^{1}H DPFGSE NMR signals. *Only signals which were unambiguously assigned are listed. n.d. = not determined due to signal overlap.*

residue	position	chemical shift change relative to native NPY / Hz			
		[2=3]	[5=6]	[8=9]	[1=2,4=5,7=8]
Glu[10]	α-H	+7	+14	–7	–5
	β-H	–7	–7	–7	–9
	γ-H	–6	–6	–27	–13
Ala[12]	α-H	--	--	–14	–32
	β-H	--	–2	–8	–11
Ala[14]	β-H	–2	–7	–15	–21
Glu[15]	β-H	–6	–13	–6	–12
	γ-H	–2	–13	–7	–9
Leu[17]	δ-H	--	--	--	--
Ala[18]	β-H	–2	–4	--	–11
Tyr[20]	3,5-H	--	--	--	–2
	2,6-H	--	--	--	--
Ala[23]	α-H	--	--	--	–4
	β-H	–5	--	--	--
His[26]	4-H	–5	–7	–2	n.d.
	6-H	–3	–2	--	–4
Leu[30]	δ-H	+7	+7	--	+18
Gln[34]	γ-H	--	--	--	--

α-helix, as only the *trans* conformation enables a tight backfolding. This suggests a *trans* conformation of Pro[13] also in the receptor-bound state of native NPY and is supported by the superb affinities of [Dha[12]=Tap[13]]-pNPY which even binds better than native pNPY at the Y_1 subtype (25% increase of affinity) and shows the lowest affinity loss (1.3-fold) of all analogs at the Y_5 receptor. Here, a distinction between this tertiary structure and the backfolding in the presence of SDS must be made. The modeling results show an interaction with the hydrophobic site of the α-helix, which is reminiscent of the PP-fold (figure 2.41b). In the membrane-bound state, these interactions are not possible due to the membrane coordination, and only the hydrophilic side is experiencing the proximity of the Dha=Tap units, as suggested by the NMR data. The question to what extent the interaction of the hydrophilic side of the α-helix with the hydrophobic N-terminus is energetically favored remains to be answered. Obviously, the backfolding tendency of the triple-substituted N-terminus observed in the presence of SDS is rather the consequence of the Gly[9] hinge. It is important to distinguish between the inherent flexibility of the N-terminus and its overall flexibility as a peptide segment, and this for the first time can shed light on how the term "flexibility" may have to be used in the case of NPY and its analogs: "flexibility" is rather related to the entire segment which can rotate relatively independently of the α-helical axis. This, however, does not implicate that the segment *itself* is also flexible, as demonstrated by the NOE-based modeling results of the Dha=Tap rich analog. This may also fit the Pro-rich N-terminus in the native NPY which is capable of forming a PPII-helix. In other words, the flexibility which was interpreted from the low amount of data (resulting from the high Pro content of the native N-terminus) must not be mistaken for the lack of preferred conformations. It is the entire segment which is mobile, as for example enabled by the Gly[9] hinge, but this does not categorically exclude distinct secondary structures.

2.3.2.5.4 A hypothesis about the determinants of Y_1 and Y_5 receptor binding

The tertiary structure obtained for *trans*-Pro[13] shows a striking similarity to the proposed conformations at the Y_1 and Y_5 receptor subtypes (figure 2.43). As the N-terminus in both cases apparently adopts similar conformations and orientations, the question of interest concerns the reasons for the good acceptance of the Dha=Tap scanning analogs at the Y_5 subtype. In more detail, an explanation is demanded for the increasing Y_5 selectivity if more Dha=Tap units are inserted and shifted towards the mismatched positions. First of all, it must be stated that also the affinity losses at the Y_1 subtype are thoroughly low (maximum 37-fold) in comparison to the results of other scannings which mostly were one to three orders of magnitude higher (figure 2.10f). Therefore, as already mentioned, the term "selectivity" must be used with care if

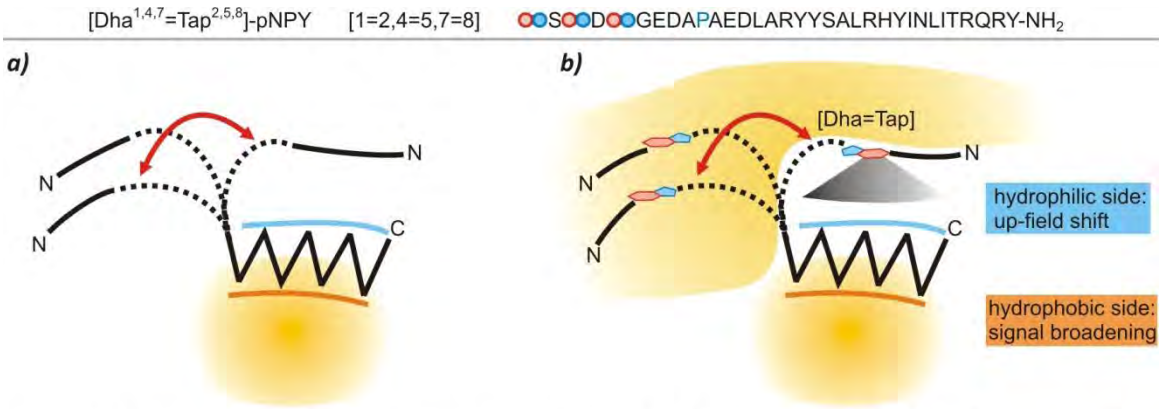

Figure 2.41 Comparison of native NPY (a) and triple Dha=Tap substituted NPY (b) with respect to membrane binding and effects on ^{1}H NMR signals. *SDS aggregates are indicated as orange spheres in this simplistic depiction which gives no detailed picture of the binding (see section 2.3.2.4.1 for further discussion). While in native NPY only the α-helix is coordinating an aggregate, the hydrophobization of the N-terminus by Dha=Tap substitution leads to an overall membrane affinity of the peptide. The resulting ^{1}H NMR signal broadening of coordinating side chains directly indicates the α-helical orientation, which in the case of the native peptide can only be proven indirectly. The backfolding tendency of the N-terminus is visible by the up-field shift of side chain signals at the other side of the α-helix. As indicated by the red arrow, in both native and modified NPY the N-termini feature rotational mobility, but this does not exclude the presence of preferred conformations within this segment (compare to figure 2.39).*

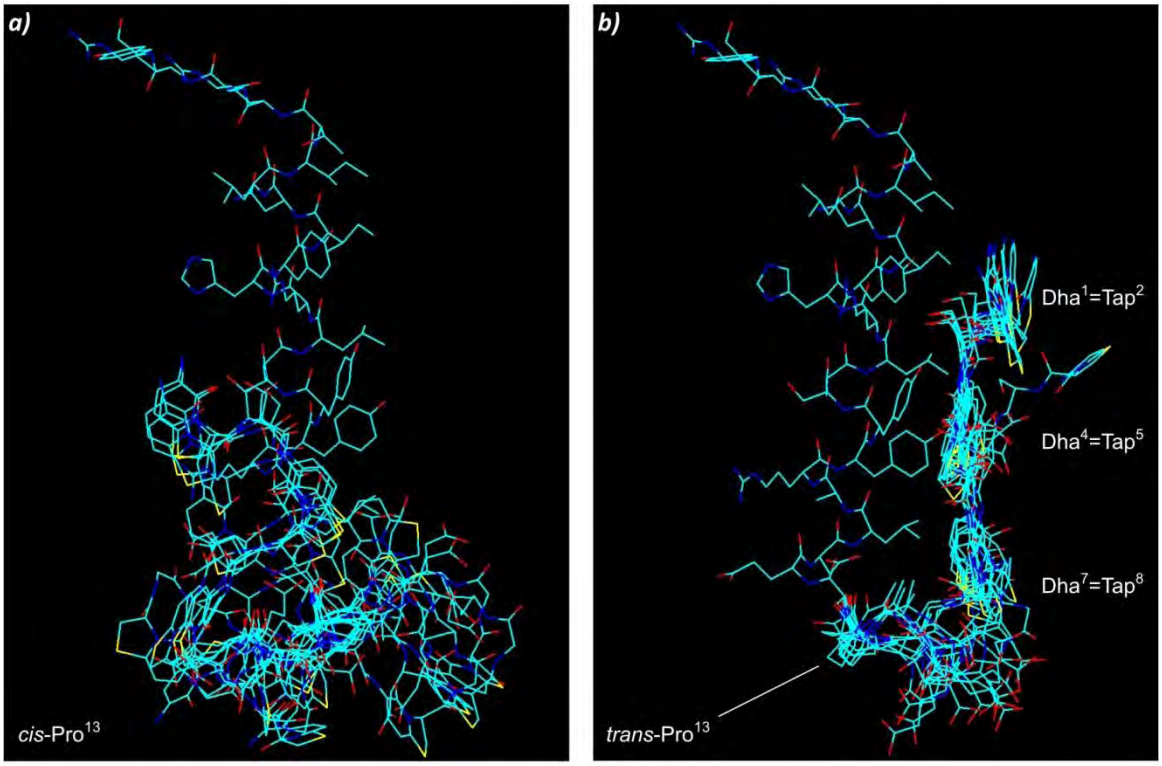

Figure 2.42 Molecular modeling results of triple Dha=Tap substituted pNPY [1=2,4=5,7=8]. *The average structure obtained for the N-terminal decapeptide (figure 2.39e) was frozen and attached to the full-length peptide with idealized α-helix. Ten snapshots from 10 x 10 ps molecular dynamics simulation (step size 1 fs, 300 K) are shown superimposed on the α-helix.* ***a)*** *With* cis-*Pro^{13} in the starting structure, the rigidified N-terminus rotates relatively independently of the C-terminal α-helix and no preferred orientation is adopted.* ***b)*** *trans-Pro^{13}, in contrast, effects a distinct conversion with the Dha=Tap units coordinating the side chains at the hydrophobic site of the α-helix. This globular trend is additionally pronounced under the vacuum simulation conditions applied to the modeling but can also be assumed for solution conditions, as supported by the NMR data (figure 2.41) and the receptor binding trends (figure 2.43).*

comparing the analogs of the Dha=Tap scan. However, this does not impair the success of the Dha=Tap scan as these modifications turned out to be a right way to identify trends in receptor affinities and to relate these on certain structural determinants.

The importance of N-terminal integrity for sufficient Y_1 affinity[2] is supported by the increasing affinity loss if more Dha=Tap units are incorporated according to series shown in figure 2.20. Although the exact positions are not as important as in the case of the Y_5 subtype, there is a slight matched preference. As the N-terminal residues presumably interact with the receptor binding pocket of the Y_1 receptor (figure 2.43), the substitution of Tyr^1 by Dha possibly conserves a π-stacking interaction of the first N-terminal residue with another aromatic side chain in the binding pocket, and therefore a part of the affinity that is lost by the Dha=Tap substitution of the other residues may be regained. The conservation of the native Pro motifs which is only the case in the matched substitutions (Tap at Pro positions) may be another reason. Furthermore, as already mentioned in section 2.3.1 (figures 2.17 and 2.20), other certain N-terminal side chain interactions with motifs in the α-helix or the receptor may play a role.

In contrast, the Y_5 subtype affinity is less susceptible to the deletion of such potential interactions between side chains, as demonstrated by a low influence of the number of substitutions. This supports the hypothesis that, in contrast to the situation at the Y_1 subtype, the N-terminus is not directly interacting with the receptor binding pocket. Instead, the stability of the α-helix (in addition to the C-terminal turn motif) is the main determinant of Y_5 binding ability (figure 2.11), and the main role of the N-terminus is to stabilize the important α-helical structure for the sake of maximizing its interactions with the binding pocket. The interaction between N-terminus and α-helix takes place by hydrophobic interactions, and especially the Pro residues turned out to be crucial as a PPII-helical structure obviously fits best as coordination partner of the hydrophobic site of the α-helix. Thus, the high affinity of the multiple Dha=Tap substituted analogs is the first proof for hydrophobicity as most important characteristic of the N-terminus at the Y_5 subtype. Furthermore, as visible from figure 2.43, the rigidified N-terminus with its increased persistent length is apparently capable of mimicking the PPII-helical conformation. In this case, the strong influence of the exact positions of the Dha=Tap units could also be reasonably explained. In the native structure, the Pro residues are not only most relevant for the conformation, but also for the interaction with the α-helix as they exhibit the only hydrophobic motifs in this segment, while all other residues are rather polar (Tyr^1, Ser^3, Asn^7) and charged (Lys^4, Asp^6). The substitution of all Pro positions by an even more hydrophobic motif, with concomitant conservation of the PPII-helical conformation, should lead to more affinity at the Y_5 subtype because the α-helix is further stabilized. This is just the case if the

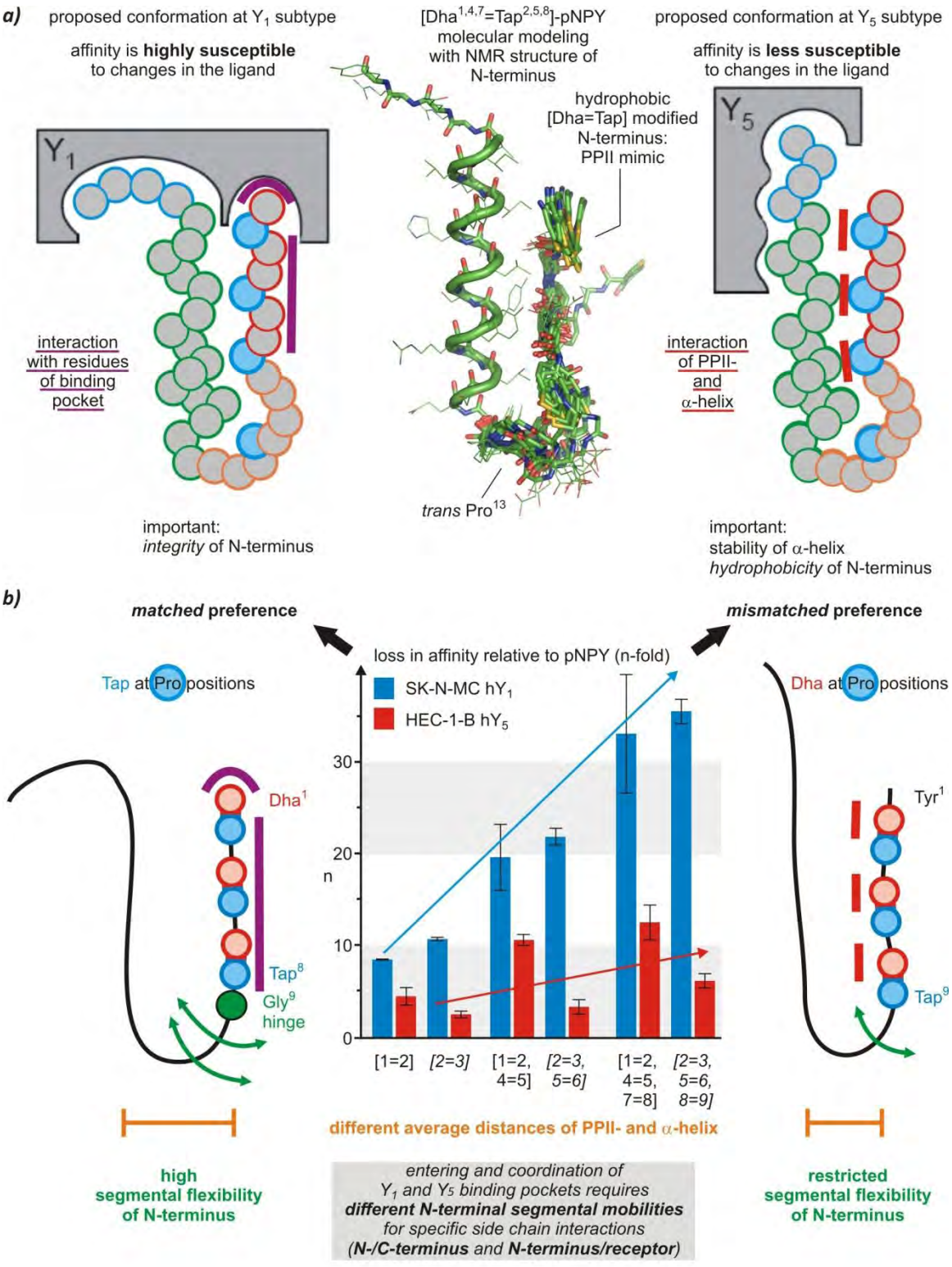

Figure 2.43 Determinants of Y_1 vs. Y_5 receptor affinity as suggested by the Dha=Tap backbone scan. ***a)*** *The molecular modeling result of [Dha^{1,4,7}=Tap^{2,5,8}]-pNPY with* trans-*Pro^{13} shows a noticeable similarity to the proposed conformation at both receptor subtypes.* ***b)*** *Combining the binding trends with the* matched *and* mismatched *substitution pattern of the triple-substituted analogs suggests that interactions between N-terminus and receptor (purple lines) are rather important at Y_1 while the stabilization of the α-helix by hydrophobic interactions (red lines) plays a key role at Y_5, which is why the substitution of Pro by the more hydrophobic Dha (mismatched) is well accepted at Y_5. The absence or presence of the Gly^9 hinge is a further determinant of receptor affinity as it determines the segmental mobility of the N-terminus relative to the α-helix.*

Dha=Tap units are shifted to the mismatched position: The substitution of the native Pro residues by the aromatic Dha motif leads to approx. 50% decreased losses of affinity compared to the matched analogs where the Tap is at the Pro positions. This also suggests that the aromatic side chains along the α-helix ($Tyr^{20,21,27}$) are crucially involved in the hydrophobic side chain interactions with the N-terminus.

By comparison of the modeling results and the receptor binding trends, the apparent importance of the backfolding raises further questions: How essential is the exact position of the backfolding-inducing elements, and finally, to what extent are the receptor affinities influenced by the distance between the PPII- and the α-helical axis? It is remarkable that the triple matched-substituted analog [1=2,4=5,7=8], which was calculated on basis of the NOE data and thus served as basis for these considerations, has the highest Y_5 affinity loss of all 15 examined analogs. However, the only slight increase of affinity loss compared to the single matched analogs demonstrates that the backfolding ability which bases on hydrophobic contacts profits from the Dha=Tap introductions. But one important factor has not been analyzed yet: the matched→mismatched shift in the triple-substituted analogs, which leads to 50% higher Y_5 affinity (only 6-fold loss compared to native pNPY), also deletes the flexible Gly^9 hinge. As suggested from the modeling results and the NMR data, the Gly^9 is important for the introduction of the turn, but its deletion does apparently not abolish the ability of the N-terminus to fold back. Instead, the frozen Tap ϕ torsion of $-90°$ which is well-known to induce β-turns may serve as the turn-inducing motif. The resulting tertiary structures with Gly^9 and Tap^9 as essential elements, respectively, can significantly differ from each other by mobility of the segments (the Gly^9 hinge exhibits one more rotational degree of freedom than the Tap^9 kink) and by different average distances of PPII- and α-helical axes. This may give further hints on the requirements at the respective receptor subtypes. All analogs with Pro^8-Gly^9→Dha^8=Tap^9 substitutions show low affinities at the Y_1 subtype, while at the Y_5 receptor the affinity loss due to single substitution [8=9] is significantly decreased by concomitant Dha=Tap introductions. As a hypothesis it can therefore be stated that the more rigid geometry of the turn induced by the Tap^9 effects a decreased rotational mobility of the N-terminus and thus a smaller average distance of both helices, which may enforce the hydrophobic stabilization of the essential α-helical motif. In contrast, the topology of the Y_1 binding pocket may require a different geometry of the turn region with a higher mobility of the N-terminal segment, so that (in addition to the hydrophobic interactions of both helices) crucial side-chain interactions of the N-terminus with the binding pocket are enabled. Finally, these differences of relative segmental

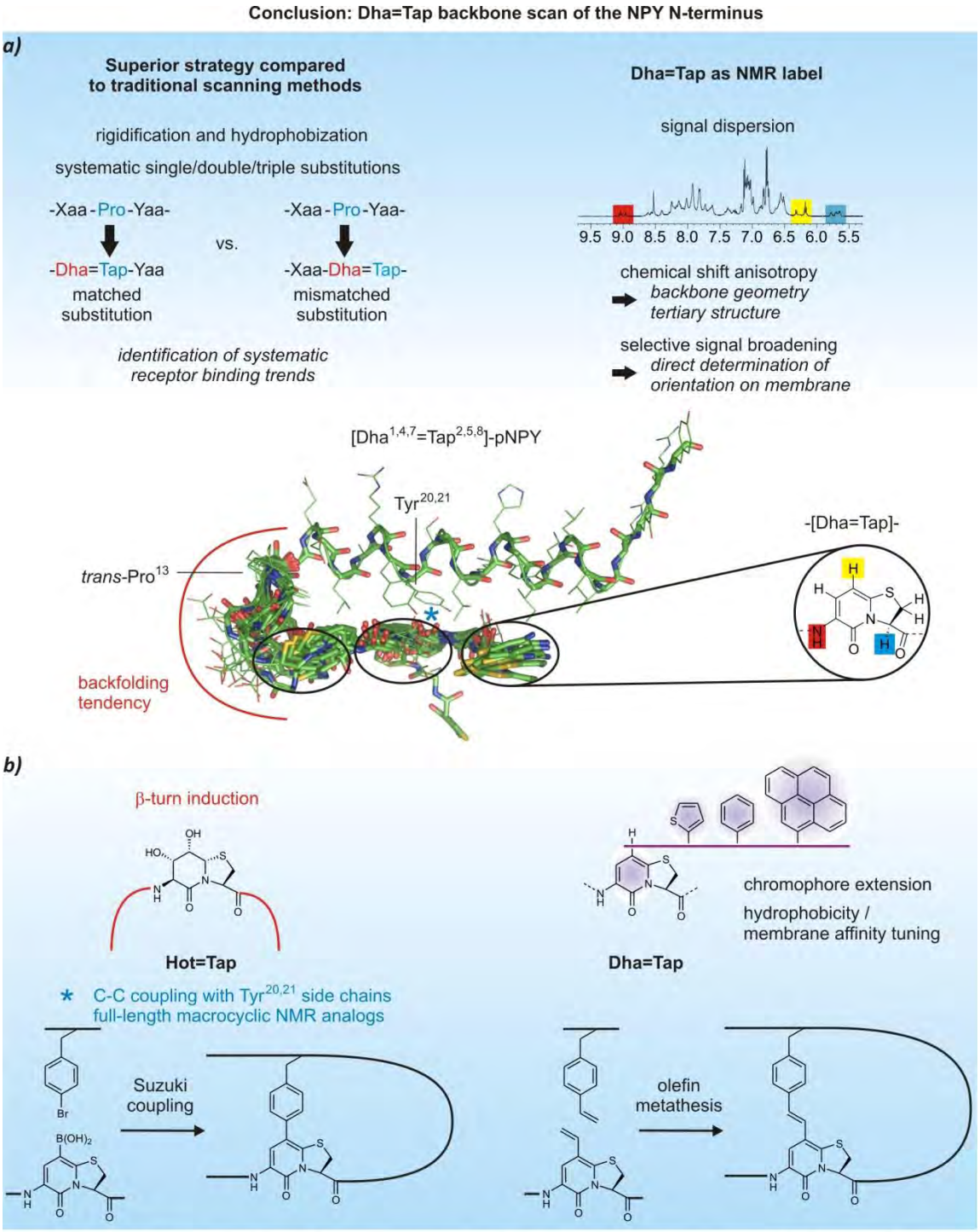

Figure 2.44 Dha=Tap backbone scan: summary and outlook. *In the center, the NMR-based modeled structure of the triple matched substituted NPY analog is shown which by its detailed NMR spectroscopic analysis revealed valuable hints on structural and functional prerequisites for the Y_1 and Y_5 receptor types.* ***a)*** *The research described in this chapter comprised the interpretation of receptor binding properties which were obtained from a systematic scanning series of single and multiple Dha=Tap substituted analogs. The comparison of matched and mismatched analogs was especially valuable as it for the first time revealed specific patterns in the receptor affinities. NMR studies of selected analogs showed that the incorporation of Dha=Tap units greatly enhances the information content of the spectra concerning secondary and tertiary structure as well as orientation on the membrane.* ***b)*** *Some further promising modifications to extend these studies: peptides with β-turn inducing Hot=Tap units (Hot = hydroxythreonine) and with Dha=Tap dipeptides containing extended chromophores (thiophenyl, phenyl, or pyryl residues have already been successfully attached by C-C couplings), and macrocyclizations.*

mobilities may not only affect the binding abilities themself, they may also be relevant for the process of entering the differently shaped binding pockets.

2.4 Summary and outlook

The Dha=Tap (dehydroalanine=thiaproline) dipeptide backbone scan is a novel scanning technique which proved superior to traditional scanning methods with single amino acid substitutions and mutations. It was successfully applied to the structural and functional analysis of the N-terminus of Neuropeptide Y (NPY), a segment which is relevant for receptor selection and binding but which, due to its high Pro content, had not been characterized in detail before (figure 2.43a). The systematic substitutions of two adjoining residues by Dha=Tap units increase structural rigidity and hydrophobicity, which turned out to be the right strategy as, in contrast to numerous previous studies, distinct Y_1 and Y_5 receptor subtype binding trends were identified. In this context, the differentiation of matched and mismatched substitution series (Dha or Tap at Pro positions) was particularly useful to highlight topological prerequisites for the single receptor subtypes. The control of Y_1 vs. Y_5 receptor selectivity is especially relevant for the development of therapeutics as they are involved in the control mechanisms of appetite.

In detailed NMR spectroscopic investigations the Dha=Tap dipeptide proved as an valuable NMR label as it brings signal dispersion into crowded spectral regions and can serve to directly identify secondary and tertiary structural motifs. By multiple substitution it is possible to tune the membrane affinity, and the residue-selective line-broadening allows to directly determine the peptide orientation on the membrane. The chemical shift anisotropy of the aromatic Dha pyridones indicated a backfolding tendency of the N-terminus towards the α-helix.

These results encourage to extend the studies by investigating further analogs via NMR. For example, the comparison of matched and mismatched triple substitutions with concomitant Dha=Tap incorporation at position 12-13 should reveal further details on how the substitution influences the conformational preferences of the N-terminus. The comparison with analogs containing locked *cis*-Pro amides will specify the role of the Pro residues for N-terminal backfolding. A project which is already in progress is the incorporation of Hot=Tap dipeptides which are superior in the induction of stable β-turn motifs (figure 2.43b). C-C coupling reactions at position 8 of Dha=Tap were already successfully applied and give access to intramolecular macrocyclizations and to chromophor extensions for fluorescence studies and to further tune the hydrophobicity of the N-terminus.

Taken together, utilizing the various options of systematic substitution with differently modified rigid dipeptides should contribute to the effort to characterize and to control the complex interplay of NPY and its receptors, and it will be interesting to apply the backbone scanning strategy to other Pro rich peptide segments of biologically relevant substrates.

3 Iminopeptides as key to the thermodynamic analysis of macrocylizations: The ring-chain equilibria of peptide aldehydes

3.1 Introduction: The role of macrocyclizations in biology and medicine

In contrast to *local* structural rigidifications, as they were described in the previous chapter, macrocyclizations, the formation of rings containing 12 or more atoms,[88] have a *global* conformational effect on the substrate. Rather than freezing single torsions they cut down the possibilities for the overall conformation as only certain combinations of backbone torsions in the cyclized segment are allowed. The research described in this chapter deals with the thermodynamic analysis of peptide macrocyclizations which are among the most abundant macrocyclic ring formations carried out in biosynthesis and synthetic chemistry.[89] The motivation for this project is given by the limited knowledge of factors that determine the inclination of a substrate to cyclize and, given the important role of macrocyclizations, it is desirable to establish methods that allow for their analysis.

No matter whether they fulfill roles as chemical warfare agents between microbes, cell-to-cell communication or signaling molecules, macrocycles often outmatch their linear analogs as they provide their functionalities in a fixed spatial arrangement which is evolutionary optimized for a specific role. Macrocyclization induces global conformational restriction to an open-chain ligand and thereby generally scales its receptor affinity and selectivity.[90-92] In the light of the induced-fit hypothesis for ligand/receptor interaction which states that the ligand as well as the receptor binding pocket structurally adapt themselves to each other for optimum binding,[93] this does not automatically imply that the binding properties are improved, as schematically shown in figure 3.1. Cyclization only has a beneficial effect if it results in an average solution conformation which already is similar to the bioactive conformation.[90] Macrocyclization is generally associated with an entropic penalty, but this pays off upon binding as the loss of conformational entropy associated with the adoption of the specific receptor-bound conformation is lower than in the case of an open-chain ligand (figure 3.1). In addition, macrocyclization can not only improve but also sustain biological activity as cyclic substrates lacking terminal C- or N-end groups are more stable towards proteolysis.

The role of macrocyclizations as source of biological activity and selectivity is demonstrated by the multitude of macrocyclic natural polyketides, peptides, and depsipeptides, and it has prompted chemists to develop synthetic strategies for a large number of valuable protein ligands.[88, 94, 95] In the following, selected macrocyclic peptidic natural products are described in order to demonstrate some ways of how peptides are rigidified by formation of large rings.

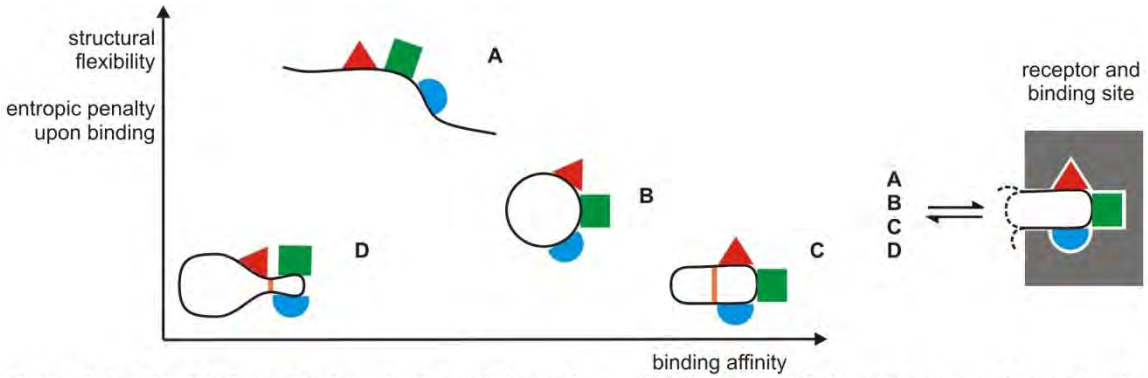

Figure 3.1. The binding affinity of a ligand depends on the similarity of the average conformation in solution to the bound conformation. *Three binding motifs of the ligand are schematically represented by colored shapes (red, blue, and green), and the receptor-bound conformation is shown on the right. The dashed lines indicate that linear as well as cyclic ligands are basically able to bind. As visible from the positions of the four ligand analogs in the diagram, structure rigidification of the linear ligand A is only increasing the binding affinity if the resulting topology still fits the requirements of the binding pocket. After head-to-tail cyclization (ligand B) a significantly lower entropic penalty is associated with adaption of the receptor-bound conformation. By another intramolecular linkage (orange) the rigidity and binding affinity can be further increased (ligand C). At a different position, however, this linkage fixes a topology which does not fit the binding site (ligand D) and which can result in an even lower affinity in comparison to the floppy linear ligand.*

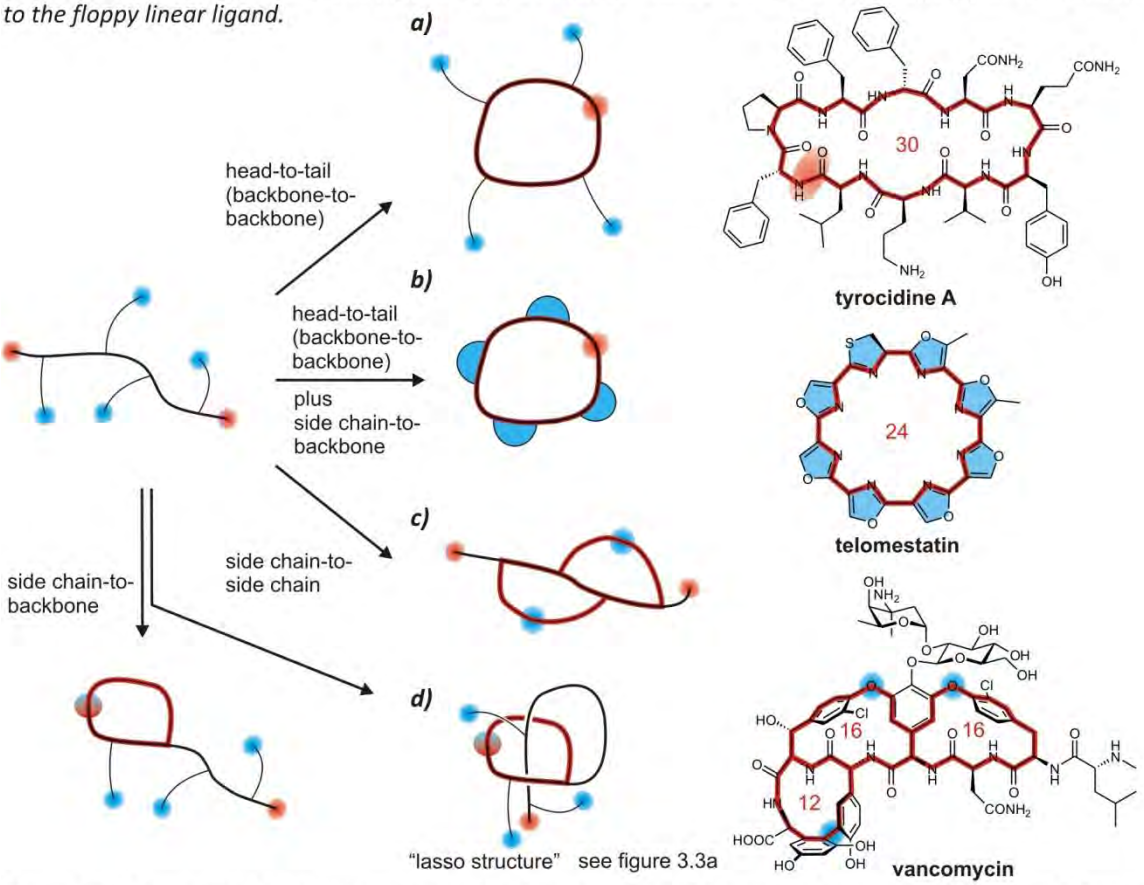

Figure 3.2. Examples of peptide macrocyclizations carried out by non-ribosomal peptide synthethases. *Three different strategies of structure rigidification are schematically shown on the left with the terminal backbone and side chain functionalities indicated in red and blue, respectively. The number of atoms in the macrocyclic rings (red lines) are written in the respective centers. A head-to-tail lactam formation generates the macrocycle of the antibiotic tyrocidine A* ***(a)****. The cyclized backbone can be further rigidified by side chain-to-backbone cyclizations which extensively takes place in telomestatin biosynthesis* ***(b)****. The overall rigidity of Vancomycin is generated solely by side chain-to-side chain linkages highlighed in blue* ***(c)****. An example of side chain-to-backbone cyclization* ***(d)*** *is given in figure 3.3a by the lasso peptide microcin J25.*

3.1.1 Examples of macrocyclizations in natural product biosynthesis

Nature has developed complex enzymatic machineries that promote the macrocyclization of linear precursors and provide a multitude of macrocyclic natural polyketides, peptides, and depsipeptides.[96, 97] These protein assembly lines referred to as non-ribosomal peptide synthethases (NRPS) are comprised of several consecutive modular sections that are responsible for the attachment of one building block to the nascent product.[98] Every module in turn consists of several domains which each catalyze a single step. The construction of a peptide chain from the single amino acids comprises the selection and activation of the monomer (adenylation domain) by attachment to a peptidyl carrier protein (thiolation domain) that carries the bound substrates between the catalytic sites, and subsequent condensation of the monomer to the growing chain of the product (condensation domain). The macrocyclization of the linear chain is in most cases accomplished by a final thioesterase domain which subsequently releases the mature cyclopeptide. NRPS provide cyclopeptides with vast chemical diversity as a big arsenal of non-proteinogenic amino acids can be utilized. Further domains along the assembly line can catalyze structural tailoring like epimerization of amino acids from L- to D-configuration.

Figure 3.2 shows three examples of non-ribosomally synthesized peptides which also represent various strategies of structure rigidification via ring formation.[99] A head-to-tail backbone cyclization between D-Phe^{1} and Leu^{10} is the final biosynthetic step of tyrocidine A (TycA, a).[100-102] This cyclodecapeptide exhibits high toxicity to many bacteria by perturbing the lipid bilayer of their membranes and it was the first commercially available antibiotic.[103] Two phenyl residues are D-configured and the peptide has a high antiparallel β-sheet content. In section 3.5, further characteristics of TycA are described in the context of the research of this thesis.

The combination of head-to-tail macrocyclization and side chain-to-backbone cyclization results in especially rigid structures with strong hydrophobicity due to the formed heterocycles. A prime example is given by the octapeptide telomestatin (b) which is a strong inhibitor of telomerase by mimicking a DNA G-quadruplex.[104, 105] Its structure exhibits a line-up of eight five-membered heterocycles (blue): five oxazoles, two methyloxazoles and one thiazoline. The macrocyclization site and details about the non-ribosomal synthesis are yet to be elucidated but it is assumed that its assembly starts with the construction of a linear octapeptide consisting of five serines, two threonines, and one serine. This octapeptide is subsequently macrocyclized and all side chains are backbone-cyclized to yield this impressively tailored natural product.[96, 97]

The side chain-to-side chain cyclization is another option which is utilized in nature to generate macrocycles from linear precursors. The antibiotic vancomycin is a prominent member of non-ribosomally synthesized peptides which are rigidified by oxidative couplings of aromatic side

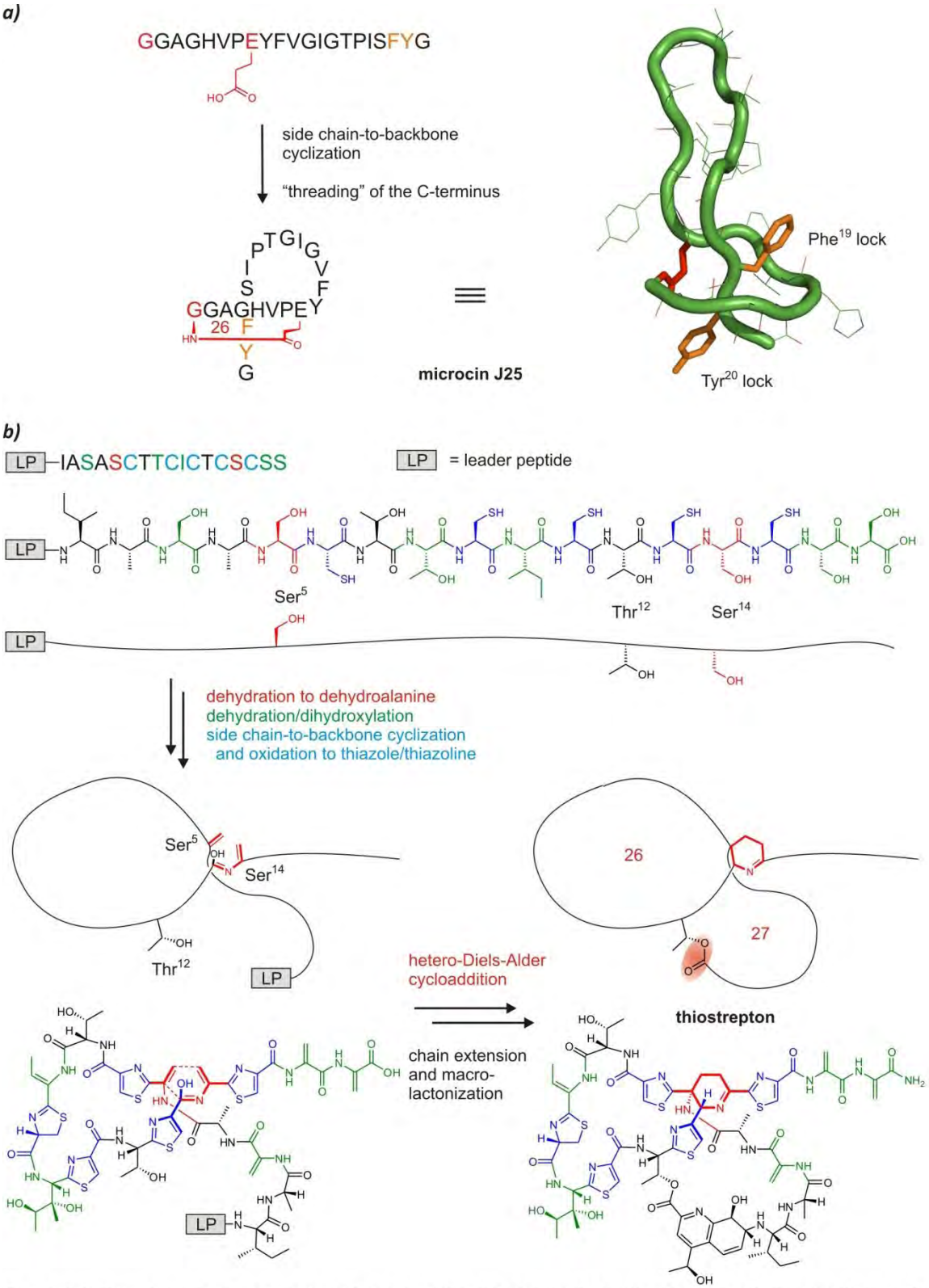

Figure 3.3 Two remarkable examples of macrocyclization strategies in the post-translational tailoring of ribosomally synthesized peptides. ***a)*** *The lassoed tail architecture of microcin J25 (shown in the one-letter-code and as average structure; PDB entry 1Q71) results from threading the C-terminus through a macrocycle formed by side chain-to-backbone tethering (red). The Phe[19] and Tyr[20] side chains (orange) act as steric locks and prevent unthreading.* ***b)*** *The complex topology of thiopeptide antibiotics (shown example: thiostrepton) is generated by an electrocyclic reaction between two dehydroalanine side chains and an amide (red) which yields a 26-mer macrocycle and the dehydropiperidine unit. The second macrocycle is closed by macrolactone formation.*

chains (figure3.2c).[89, 106] After the NRPS assembly of a linear heptapeptide which comprises five non-proteinogenic aromatic residues, two aryl-aryl ether and two C-C crosslinks are generated by the action of three oxygenases. Remarkably, this results in an overall structural rigidification of a dome-shaped architecture without any further covalent linkage of the linear peptide backbone. Finally, the vancomycin aglycon is released from the NPRS and glycosylated by further tailoring enzymes.

While research has provided a detailed picture about NRPS macrocyclization mechanisms over the last two decades, little has been known about how these are carried out for ribosomally synthesized peptides.[89, 97] Due to the restriction to the 20 proteinogenic amino acids these natural products are expected to be far less modified than NRPS products, but recent research has shown that the post-translational tailoring by enzymes can turn the linear peptides into vastly modified complex macrocyclic compounds.

The 21-residue peptide microcin J25 has antibacterial activity against Gram-negative bacteria where it interacts with RNA polymerase. The linear sequence is produced ribosomally, and originally it was proposed to be post-translationally head-to-tail cyclized.[107] Reinvestigations by three groups, however, independently revealed that this structure is incorrect. Instead, side chain-to-backbone cyclization of the Glu^8 side chain carboxyl function to the N-terminal Gly^1 amide takes place and the remaining linear segment of residues 9-21 is threaded through this macrocycle, which results in a noose-like structure and gave rise to the term “lariat peptides” for this class of peptides (figure 3.3a).[108-110] Remarkably, it is the contribution of non-covalent interactions which (in addition to the macrocycle) in this case causes overall rigidity.

Recent work on the biosynthesis of thiopeptide antibiotics (sulfur containing peptides; the most prominent member thiostrepton is shown in figure 3.3) has extended the conception of to what extent ribosomally produced linear peptides can be modified post-translationally.[111-113] Figure 3.3b gives an overview of the tailoring in the biosynthesis of thiostrepton.[114, 115] After 13 of the 17 side chains of the ribosomally synthesized linear peptide have been dihydroxylated, dehydrated (green), or backbone-cyclized to thiazoles (blue), a formal [4+2]-cycloaddition of two dehydroalanines and one amide (red) produces a dehydropiperidine core which links the formed 26-mer macrocycle to two linear peptide segments. In the final steps which are yet to be elucidated, the N-terminal tetrapeptide is elongated and linked to the Thr^{12} side chain which results in a 27-mer macrolactone and the remarkable mature thiostrepton peptide network.

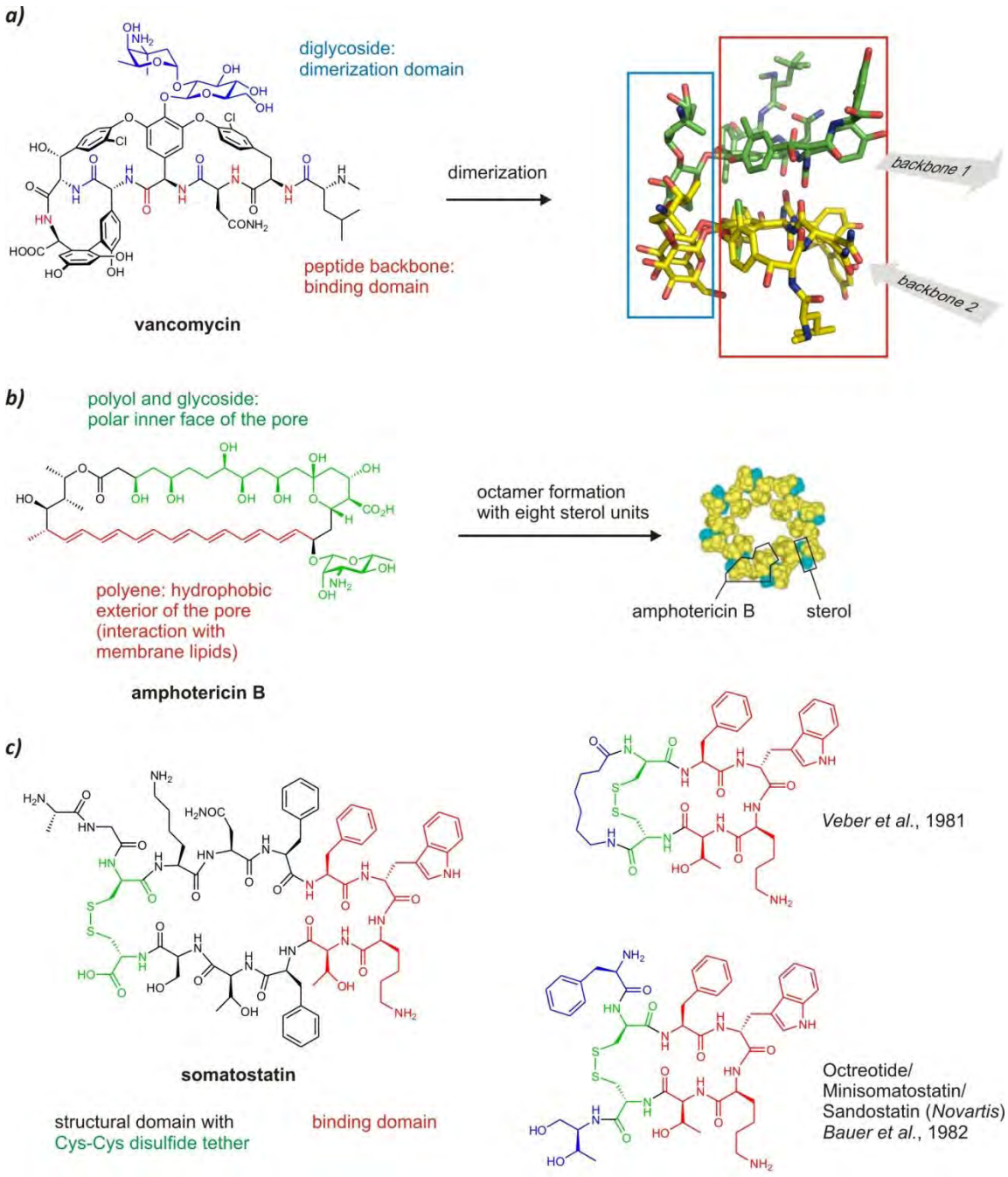

Figure 3.4 The modular composition of macrocycles. *As shown for three examples, the high biological activity and selectivity of macrocyclic compounds often relies on the presence of functionally independent sub-regions (domains) similar to the domains found in protein structures.* ***a)*** *Vancomycin forms dimers with the diglycoside and the peptide backbone as coordination sites (highlighted in blue). The peptide backbone forms a binding pocket, and the averted amide functionalities (red) bind to D-Ala-D-Ala motifs in peptidoglycan precursors. The antiparallel spatial arrangement of two backbones (indicated by grey arrows) is fixed by the dimer in such a distance that two peptidoglycan strands are simultaneously coordinated.* ***b)*** *Amphotericin B which is marketed as fungicide is evolutionary optimized for the formation of cell wall pores consisting of eight amhotericin B molecules (yellow) and eight sterol units (blue). For this purpose, the macrocycle has a hydrophobic polyene domain (red) which can interact with the hydrophobic membrane interior, and two hydrophilic sub-regions (green) which form the polar interior of the pore.* ***c)*** *The peptide hormone somatostatin consists of an active tetrapeptide (red) while the other part plays a structural role. In the search of simplified analogs (two examples are shown), the active part and the Cys-Cys disulfide tether was conserved and the rest of the stuctural domain was simplified as far as possible.*

3.1.2 Macrocyclizations in medicinal chemistry and chemical synthesis

An extensive cheminformatic study in 2005 showed that only approx. 3% of the more than 130 000 known secondary metabolites were macrocycles with 13 or more ring atoms.[116] This small fraction of natural products, however, includes especially bioactive and selective ligands.[88]

In spite of the more than 100 macrocyclic drugs which have already been marketed as successful therapeutics (e.g. as antibiotics, anti-infectives and for the treatment of tuberculosis and cancer), macrocycles are still under-explored as possible lead structures for drug discovery.[88] Reasons for this may be the insufficient accordance of macrocycles with commonly accepted guidelines for screening candidates (*Lipinski's* "rule of five"),[117] the structural complexity of the natural products and the synthetic difficulties which may be associated with the macrocyclization step. In the light of the growing urgency to tackle the health threat by drug-resistant pathogens, the pressure to explore new structural space increases, and this will bring macrocyclic natural products to the fore as basis for screenings.[88] As demonstrated by some successfully marketed therapeutics in the following, macrocycles outmatch their linear analogs in many respects.

Macrocycles can be considered as the smallest examples of biomolecules with functional subdomains that allow for non-covalent aggregation. This is a prerequisite for certain modes of action, as shown for two examples in Figure 3.4a and b. Vancomycin (marketed for example as Vancocin®, *Ely Lilly Pharm.*)[118] is used as last-resort antibiotic against Gram-positive bacteria where it binds with high affinity to peptidoglycan chains in the cell walls.[119, 120] Its diglycoside acts as dimerization domain and the peptidic part as binding domain. The resulting aggregate is able to span two peptidoglycan chains in the bacterial cell wall, each of which is coordinated by one peptide backbone.[121, 122] The fungicide amphotericin B (marketed by several companies, for example by *Pfizer* as Amphocin®)[123] employs its mode of action by formation of an octameric pore in the membrane of the target cell. This is enabled by the amphiphilic character of the macrocycle consisting of one hydrophobic domain, which in the pore is located towards the membrane, and of two polar domains which are oriented to the formed channel.[124] As the sub-regions are functionally independent, they can be modified separatedly, a fact which accommodates with the requirements of chemical synthesis. For example, while the evolutionary optimized binding domain is maintained, the structural domain can be simplified and varied by incorporation of synthetic building blocks in order to cut down the number of work steps and the complexity of the synthesis. A prime example for this strategy is the development of therapeutic analogs of somatostatin, a 14 amino acid peptide which is

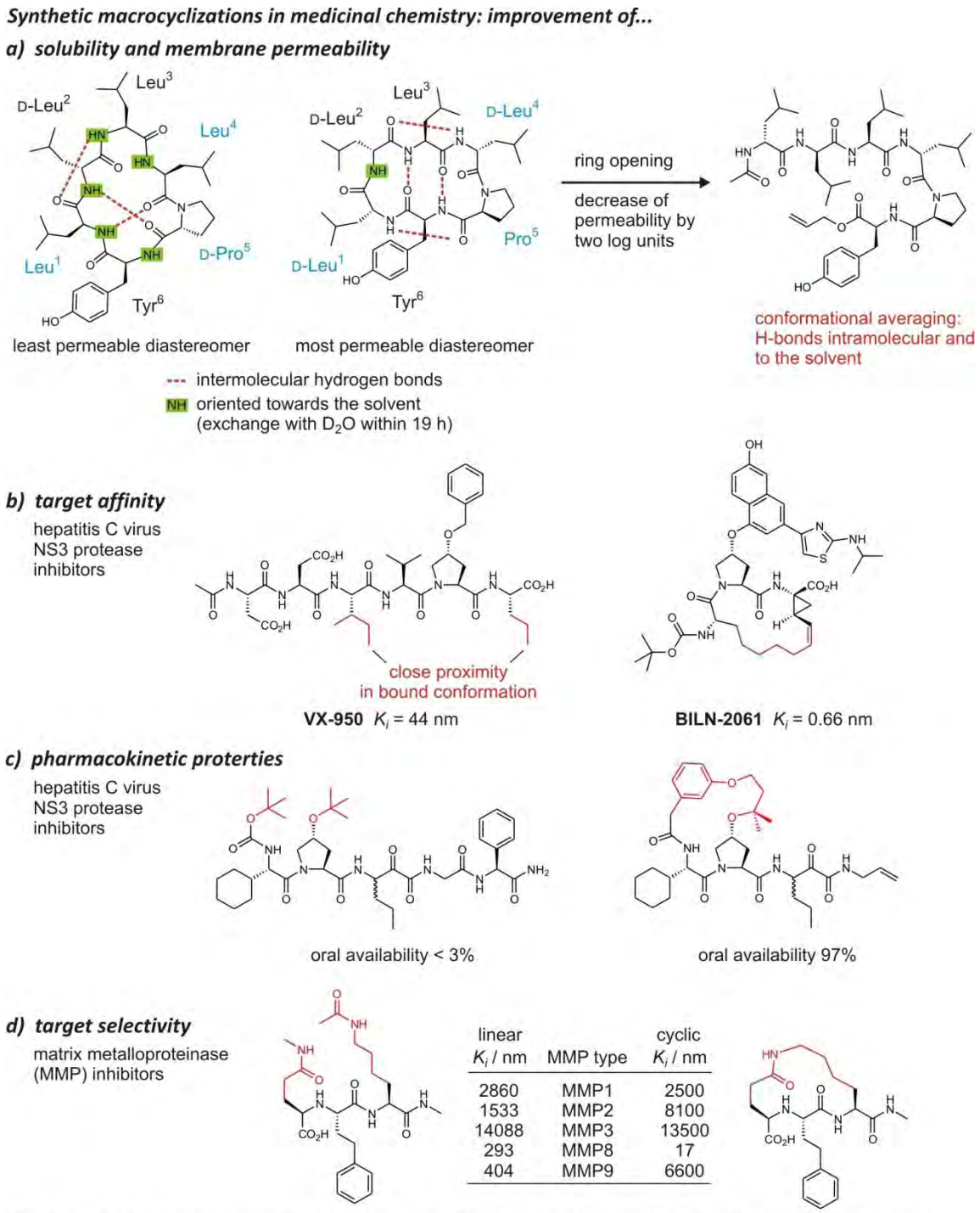

Figure 3.5 Medicinal chemistry profits from artifical ring closures in various ways. ***a)*** *A sufficient membrane permeability is of high relevance for whether a substrate is suitable as therapeutic. For a series of cyclo[(Leu)$_4$-Pro-Tyr] hexapeptide diastereomers, the membrane permeability was determined. The red dotted lines indicate intramolecular hydrogen bonds. While the macrocycle on the left exhibits a twisted irregular conformation, a pseudo-symmetric conformation is obtained by inverted stereoconfiguration of three residues (blue) and minimzes hydrogen-bonding interactions with the solvent.* ***b)*** *An inhibitor with sub-nanomolar affinity towards the hepatits C virus (HCV) NS3 protease, BILN-2061, was obtained by structural tailoring of the ligand VX-950 by macrocyclization of two aliphatic side chains (red).* ***c)*** *The oral availability of α-ketoamide HCV inhibitors was greatly enhanced by macrocyclization of a hydroxyproline side chain to the C-terminus.* ***d)*** *A side chain-to-side chain macorcyclization also proved successful for the improvement of the target selectivity of matrix metalloproteinase (MMP) inhibitors. As visible from the K_i values in the table, a promiscuous linear tripeptide is turned into a ligand with high selectivity towards the MMP8 subtype by covalent tethering of the Gln^1 and the Lys^3 side chain.*

macrocyclized via a Cys-Cys disulfide bridge (figure 3.4c) and which inhibits the release of hormones such as insulin, glucagon, and growth hormone. Due to the short half-time (< 3 min), the natural peptide cannot be applied as a therapeutic, which is why simple analogs with increased metabolic stability were developed.[125, 126] The shown agonists (figure 3.4 c) have in common that the binding domain, a β-turn containing the D-Trp-Lys pharmacophore (red), is maintained while the structural domain (black) is shortened. In both cases, the disulfide bridge directly adjoins the binding motif. The analog developed by *Veber et al.* features a further covalent link by 7-aminohexanoic acid, which leads to a [21.16.6] macrobicycle.[127] Studies by *Bauer et al.* revealed that the second tether is not required and that attachment of Phe to the N-terminal Ser and capping of the C-terminus by threoninol also leads to a sufficiently stable (half-life approx. 90 min) and bioactive analog.[128] This octapeptide called octreotide is marketed by *Novartis* as Sandostatin® for the treatment of gastrointestinal tumors and acromegaly.

Medicinal chemistry especially has to rely on macrocycles if complex macromolecular targets like interaction surfaces of proteins are to be modulated.[88] This is, for example, the case for cancer therapies that base on disturbing the cell division by affecting microtubule dynamics,[129] and, in addition to the already marketed paclitaxel (Taxol®),[130] the epothilones are promising lead structures for the development of further therapeutics.[131]

Chemical synthesis can show its strength by providing synthetic macrocyclic analogs which can show significantly improved properties, and some recent successes are described in the following. Linear peptides often exhibit limited therapeutic applicability not only due to their metabolic instability but also by their low membrane permeability. By comparison of several linear and cyclic Leu-rich hexapeptides *Pande et al.* demonstrated that macrocyclization can increase the membrane permeability by two log units if, by proper residue composition and configurations, a maximum number of hydrogen bonds are formed intramolecularly and not with the solvent (figure 3.5a).[132, 133] In search of potent hepatitis C virus (HCV) NS3 protease inhibitors, the target affinity of the linear hexapeptide ligand VX-950 (figure 3.5b) was increased by side chain-to-side chain cyclization of two aliphatic residues (marked in red) which exhibit close proximity in the bound conformation. In combination with further modifications this led to the macrocycle BILN-2061 which was the first HCV protease inhibitor to be moved forward into clinical development.[134-136] For a different series of HCV protease inhibitors, it was the the search for improved oral availability which prompted to investigate side chain-to-side chain macrocyclized analogs (figure 3.5c). In many cases, however, not the biological activity but the selectivity of the ligand is a serious problem which can foreclose a therapeutic use. As shown in

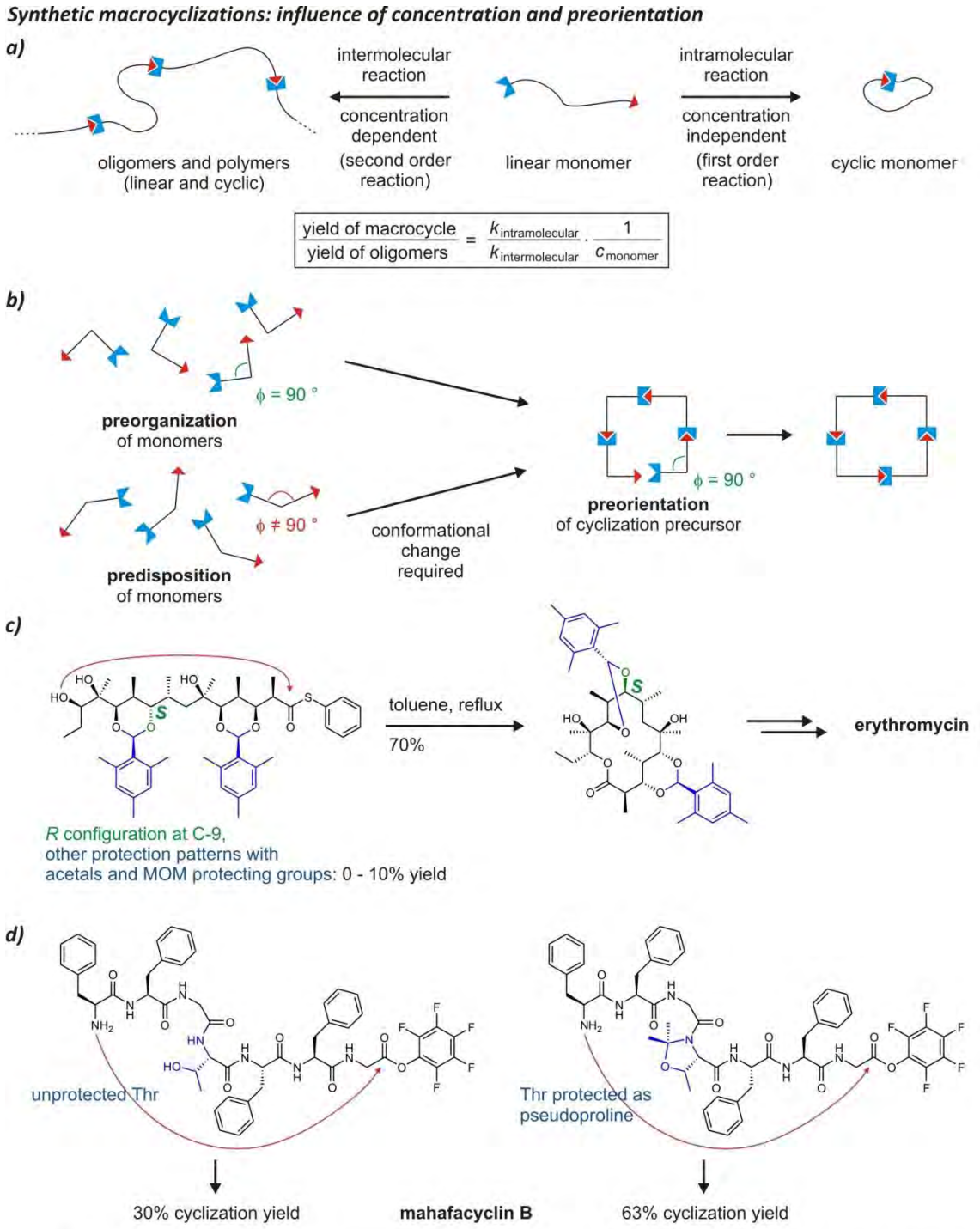

Figure 3.6 ***a)*** *Intramolecular macrocyclizations generally compete with intermolecular oligomer formation. The higher the monomer concentration the higher is the probability that the reactive ends of two different molecules react with each other. In contrast, the average time of a reactive end to get located close enough to the other end of the same molecule is concentration independent. In order to suppress oligomerizations, the reaction has to be run at low concentrations. k = reaction rate, c = concentration.* ***b)*** *The inclination of a precursor to cyclize is influenced by whether and to what extent structures with close proximity of the reacting ends are populated (preorientation). This also depends on the geometry of the monomers.* ***c)*** *The OH group protection pattern in the cyclization precursor of erythromycin takes influence on its extent of proper preorientation and was prerequisite of a successful macrocyclization step. Furthermore, the stereocenter at C-9 which was annihilated at a later stage in the synthesis had to be in the S configuration.[143-145]* ***d)*** *Bridging of a Thr side chain with its amide by an acetal (pseudoproline) fixes its Φ torsion. This improved the yield in the cyclization step of the mahafacyclin B total synthesis.[146]*

figure 3.5d, macrocyclization proved successful to overcome the binding promiscuity of tripeptidic inhibitors towards several closely related matrix metalloproteinase subtypes.[137]

The discovery of natural products containing carbon macrocycles of various sizes has evoked great efforts to develop efficient chemical macrocyclization methods since the 1920s. The main problem of these reactions, first described by *Ruzicka et al.*,[138] were the low yields, and today the macrocyclization step still is the bottleneck of many syntheses. In a pioneering work, *Ziegler et al.* provided as explanation that the desired intramolecular ring closure is outmatched by intermolecular reactions that lead to oligomers and polymers (figure 3.6a).[139] Consequently, a low concentration of the linear precursor is necessary, which is achieved practically by slow addition to an excess of activating reagent (*Ruggli-Ziegler dilution method*).[140]

While irreversible reactions are preferred in total synthetic pathways, the research field of Dynamic Covalent Chemistry is aimed at the characterization and utilization of reversible reactions under equilibrium conditions.[141, 142] The most important outcome for macrocyclization reactions was the observation that the conformational preferences of the linear precursor determine its inclination to cyclize, as schematically demonstrated in figure 3.6b. As there is a high possibility of the end groups of the shown tetramer to be located near to each other, it is *preoriented* for cyclization. This can either be due to a monomer conformation which already corresponds to the geometry required for the cyclizing tetramer, and this case is termed *preorganization*. If the monomers are not adopting this conformation but if the incorporation into the precursor triggers a conformational change, this case is termed *predisposition*.[142] The role of an appropriate precursor *preorientation* (this term is used as more general description) has exerted influene on many chemical macrocyclizations which could be significantly improved by the design of the precursor.[95] Figure 3.6c depicts the key cyclization steps of two natural product total syntheses where the the precursor was preoriented by an appropriate selection of protecting groups. In the total synthesis of erythromycin by *Woodward et al.*,[143-145] several macrolactonization precursors were tested for their inclination to cyclize. Only the concomitant acetal protection of the hydroxyl groups at positions 3/5 and 9/11, respectively, and the *S*-configuration at position 9 (this stereocenter is destroyed at the end of the synthesis), gave a good cyclization yield.[144] In the total synthesis of mahafacyclin B, an acetal protection of a Thr residue as pseudoproline led to a more than two-fold increase of yield.[146]

In spite of the important role of macrocyclizations for the generation of conformationally constrained biological and artificial ligands, as described in this section, our knowledge of factors that determine the inclination of a substrate to cyclize is low. This problem which was the motivation for the research of this thesis is described in the following.

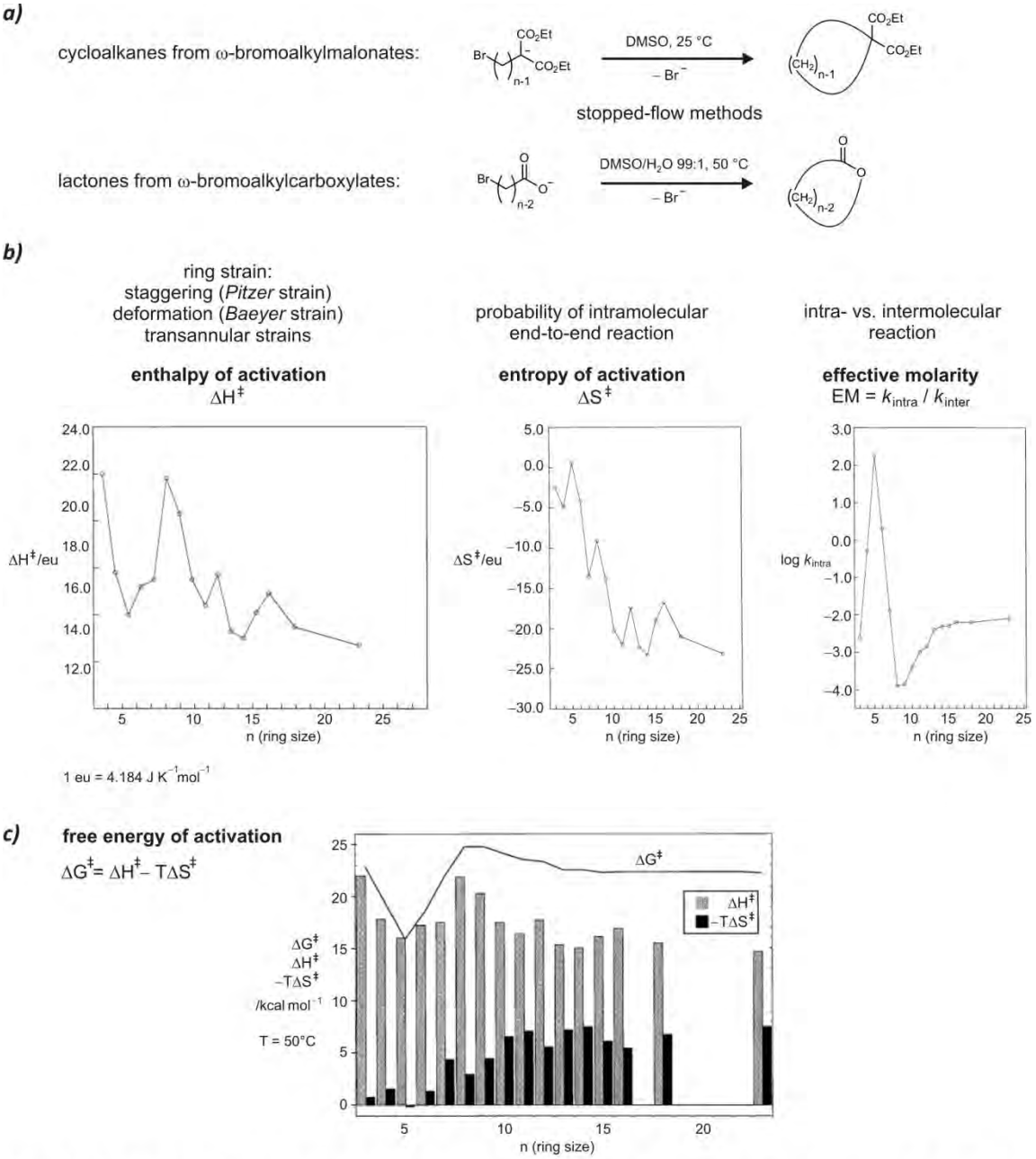

Figure 3.7 Kinetic macrocyclization experiments. ***a)*** *Two reaction types have been examined so far, which are the formation of cycloalkanes by C-C bond formation and the macrolactonization of functionalized alkyl chains.* ***b)*** *For the lactonization experiments, the kinetic parameters of interest are plotted against the ring size n (see a). The enthalpy of activation (left) depends on different kinds of strains occurring if a cyclic structure is adopted. 5-membered rings are the most favored small rings, and with growing ring size the ring strains first increase (maximum: 8-membered rings) and then decrease towards macrocyclic rings. The dependence of the entropy of activation (center) from the ring size shows that the entropy loss roughly increases with growing ring size, confirming the hypothesis of* Ruzicka *that the probability of both ends to be located near each other decreases with growing chain length.[138] In the range of small ring sizes, the added amount of lost entropy can be set equivalent of the entropy associated with one CH_2-CH_2 rotor that is restricted in its mobility. At larger ring sizes, this effect decreases due to the inherent flexibility of the cyclized chain. The effective molarity (EM, right) is the quotient of intra- and intermolecular reaction rate and serves as quantitative measure of the inclination to cyclize ("intramolecular reactivity").[151] It strongly depends on the ring size for small and medium rings but changes less for macrocycles.* ***c)*** *Depiction of the dependence of the free energy of activation from the ring size (solid line), calculated from the Gibbs-Helmholtz equation. The contributing enthalpy and entropy terms are shown as bars. The data were collected from the series of lactone formations at T = 50°C (a). Figures according to ref. [153].*

3.2 The lack of experimental setups for the thermodynamic characterization of biological macrocyclizations

3.2.1 Previous work: kinetic experiments

The successful syntheses and application of macrocyclic substrates in medicinal chemistry and total synthesis, however, hide the fact that macrocyclization processes are far from being *understood*. This means that the inclination of a linear substrate to cyclization cannot be predicted, and that the optimization of its structure must be made empirically or on the basis of computer modeling.[147] This makes a the optimization of macrocyclic ligands with respect for their target affinities and selectivities a difficult task for medicinal chemists. Also in total syntheses, the key macrocyclization steps must be exploited by extensive computational studies or they have to be approached empirically.[95] Regarding the problem of inter- vs. intramolecular head-to-tail reaction of a bifunctional substrate (figure 3.6a), *Jacobson* and *Stockmayer* contributed pioneering work with their theoretical model,[148] and *Flory's* work on the statistical mechanics of molecular chains has had great impact on polymer sciences.[149] As a synthetic chemist seeks to obtain products which are as stable as possible, macrocyclizations are normally run irreversibly. In this field, especially *Mandolini et al.* have contributed to the investigation of ring closures under kinetic conditions.[150, 151] Figure 3.7a gives an overview of the exploited reaction types (cycloalkane and lactone formations with ring sizes from 3 to 23 atoms) which give the effective molarity and enthalpy/entropy of activation as kinetic information. Further influences like the presence of double bonds along the cyclizing chain have also been investigated.[152] As these experiments give information about the transition state, the question arises whether and to what extent this allows to draw conclusions about the cyclization product.[151] Furthermore, changes in solvation may be big as ionic species react to uncharged and unpolar products. The exact sources of the individual reaction rates rate are still discussed[153] and computational studies have to be employed for these simple systems.[154, 155]
In summary, these studies provide useful information about the kinetics of macrocyclizations, but the access to data about a wide range of ring sizes has so far been limited to simple cycloalkanes, and they allow only limited conclusions for the cyclization of the complex biopolymers like peptides which are composed of a variety of building blocks and which contain various stereocenters and functional groups. Furthermore, as the difference between linear and cyclic species with respect to their structural features is of interest, thermodynamic analyses are necessary. However, these have also so far been restricted to model systems (examples are described in section 3.2.3) which, in spite of their simplicity, show complex behavior and which are not transferable to biological substrates.[142, 156]

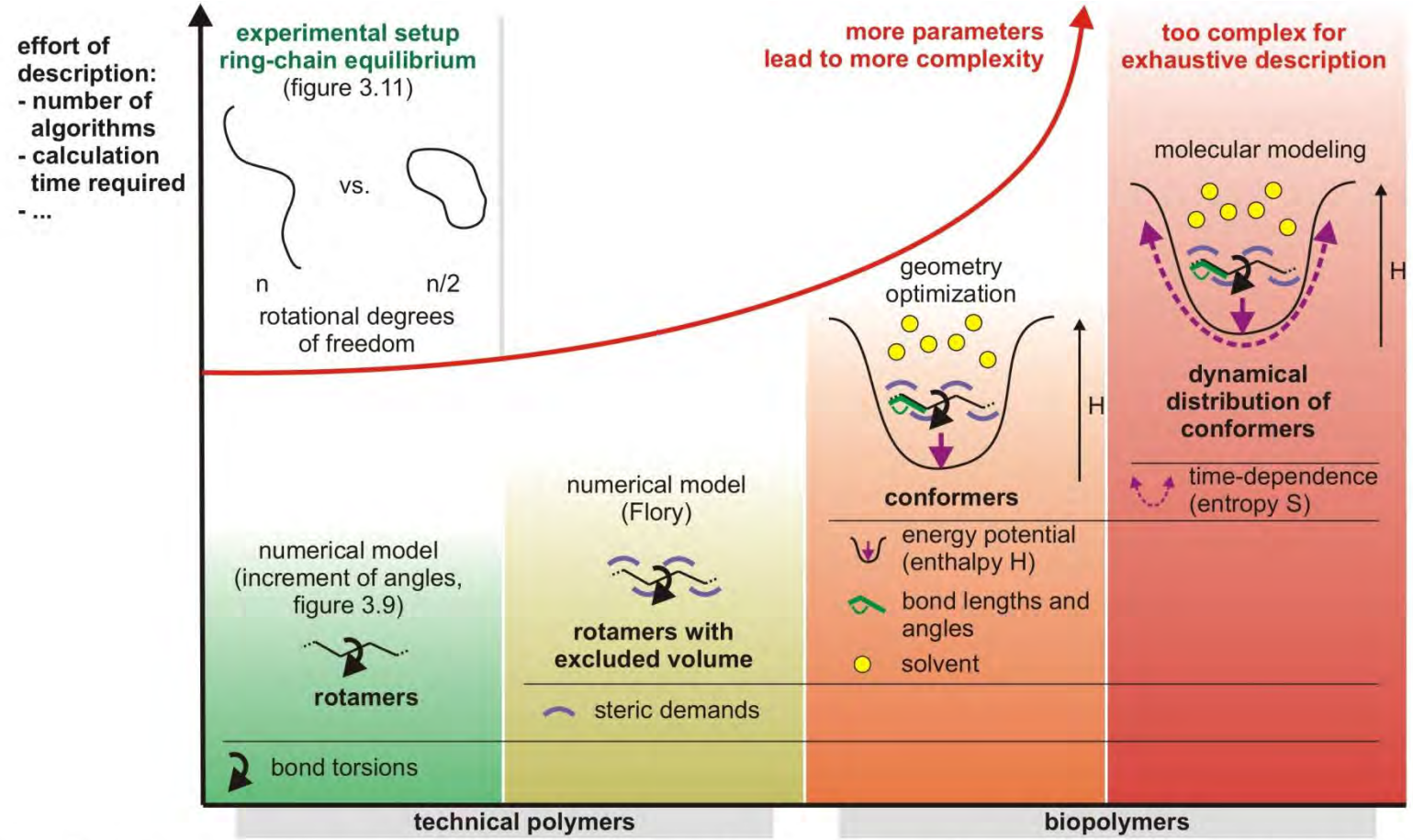

Figure 3.8 The more parameters are included in the characterization of a molecular system, the more complicated is the mathematical description. *The four columns show models which describe molecular structure with increasing details. In each column, a schematic representation of the included parameters is given and explained below. The knowledge of structure (green, yellow and orange column) does not include the knowledge of dynamics, and these time-dependent aspects like frequencies finally make the systems too complex to describe and do not lead to the prediction of physical properties. Furthermore, an increased detailedness is always associated with more sources of error. Therefore, we rely on the simple numerical model as only this provides a theoretical basis of the experiments with ring/chain equilibria (green column). This is based on the systematic increment of angles and suggests a halving of the number of rotational degrees of freedom upon macrocyclization. The context with the experimental setup is further illustrated in figures 3.11 and 3.12.*

3.2.2 Rotamer incrementation as theoretical basis for an experimental setup

As the structural complexity of biological macrocyclization substrates prohibits an exhaustive theoretical description, experimental approaches are needed which, in turn, address the questions given by the theory. In this context, the research of the thesis was aimed at the characterization of thermodynamic differences between linear and cyclic peptides. Initially, the lack of experimental methodologies was not the only aspect of the problem: there was also need of a simple theoretic model by which the experimental results can be explained and which gives general conclusions to predict physical parameters of other systems. In the following, this model is described and related to the envisioned experimental setup.

3.2.2.1 The complexity of molecular systems: from rotamers to conformers to dynamics

To predict physical parameters of molecular species in a model-based approach, at least four steps of increasing complexity of description can in principle be distinguished, as depicted in figure 3.8. The simplest way of description is restricted to rotational motions (green bar), and its advantage is the applicability of a numerical model. A systematic incrementation of the torsion angle of every rotatable bond by a defined value gives the number of rotamers which is equivalent to all physically possible and impossible spatial arrangements. This model will be applied to peptides of different length later in the text (table 3.1). The next step to gain a more complete picture is to consider the excluded volume of the chain (yellow bar). This is accomplished in the theory by *Flory et al.* which provides a precise mathematical description of synthetic polymers.[149] However, these calculations reach their limits if sequence-specific biomolecules are considered which by their multiple side-chain functionalization greatly exceed in complexity any homo- and copolymers of technical interest. Therefore, it also cannot serve as a discussion basis for experimental data obtained from ring-chain equilibria.

Attractive and repulsive intramolecular interactions contribute to the total enthalpy H of every single rotamer and therewith determine to what extent a rotamer is actually populated under the respective conditions. Therefore, only a fraction of the rotamers is enthalpically favored, and they are referred to as conformers. In a two-dimensional depiction, a conformer is defined by an enthalpy well of an ascertained minimum depth (figure 3.8, orange bar), and the cut-off value must always be defined by the experimenter. The total number of conformers, however, cannot be calculated without effort as the total enthalpy of every single rotamer must be determined. Therefore, molecular modeling must be used, and the exhaustive calculation of rather rigid and simple systems is already a formidable challenge. The conformational analysis of possible cyclization precursors of dendroamide A is one of the few complete examinations which are

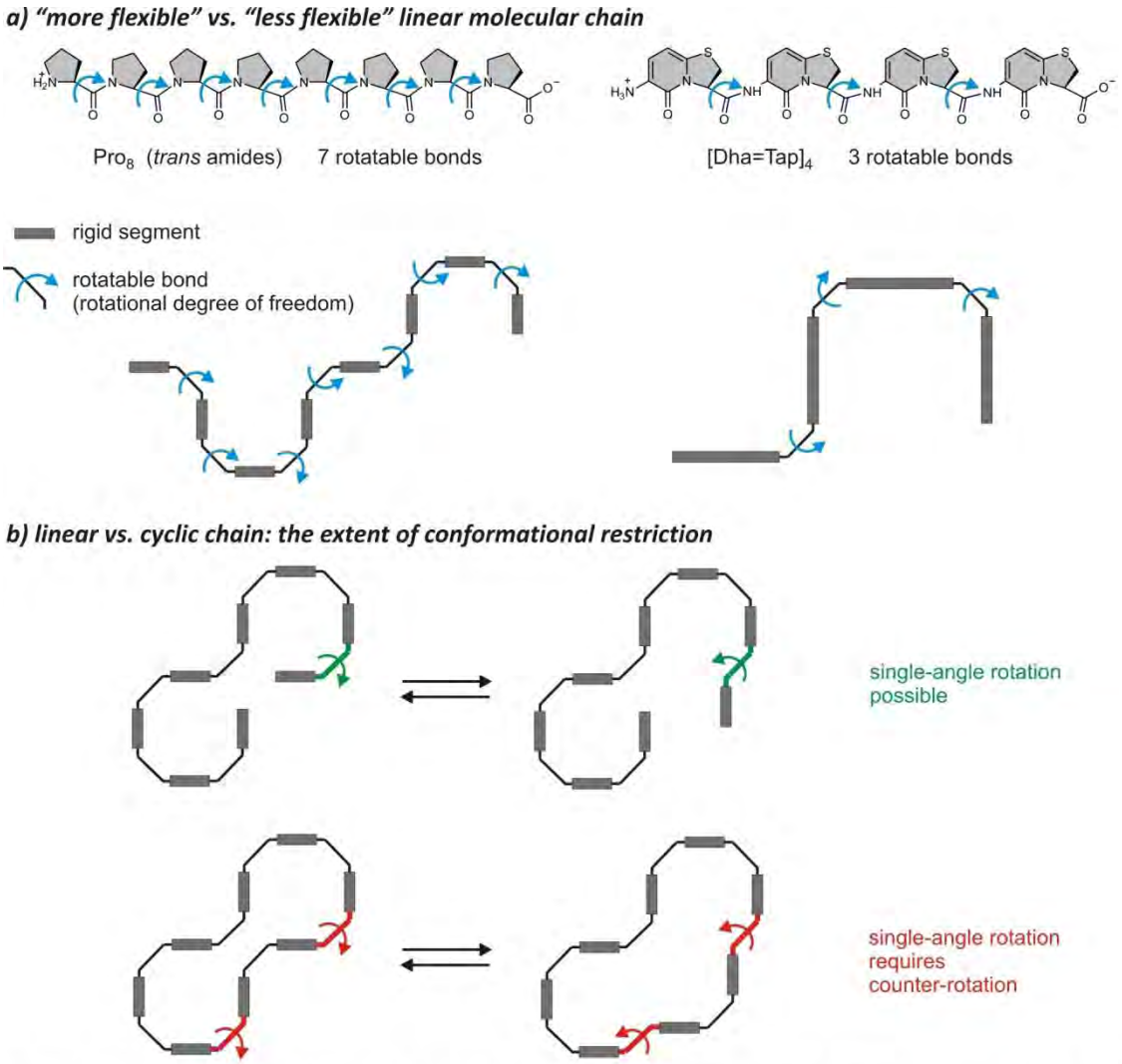

Figure 3.9. The use of the term "flexibility" explained by model peptides. ***a)*** *Comparison of two linear peptides of identical length, with the macroscopic models shown below the structural formula. A Pro octamer has seven rotatable backbone ψ bonds (left) which are indicated by blue arrows (the C-terminal bond is not included). If every second Pro is theoretically exchanged by a fused dehydroalanine (Dha), this results in a Dha=Pro tetramer with only three rotatable bonds (right). As visible from the macroscopic illustrations, the reduced number of rotatable bonds can be described as a reduction of flexibility. Therefore, the macroscopic term of "flexibility", if used for microscopic systems, is proportional to the number of rotational degrees of freedom.* ***b)*** *Comparison of allowed conformational flexibility of the Pro octamer in its linear (left) and cyclic form (right). The covalent tethering of both ends prohibits any single-angle rotation. As only pairs of angles can be moved in the ring, this suggests that the number of rotational degrees of freedom is halved. The impossibility of any single-angle variation corresponds to a significant cut of rotational flexibility, as shown in the following table 3.1 and figure 3.10.*

Table 3.1 The number of rotatable bonds (RB), rotational degrees of freedom (RDF), and rotamers (n_{rota}) for proline-free peptides comprising two to ten amino acid residues. *The overall number of rotamers was calculated by applying 5° increments on the rotatable torsions.*

	residues	2	3	4	5	6	7	8	9	10
linear	RB = RDF	3	5	7	9	11	13	15	17	19
	n_{rota}	$3.7 \cdot 10^5$	$1.9 \cdot 10^9$	$1.0 \cdot 10^{13}$	$5.2 \cdot 10^{16}$	$2.7 \cdot 10^{20}$	$1.4 \cdot 10^{24}$	$7.2 \cdot 10^{27}$	$3.8 \cdot 10^{31}$	$1.9 \cdot 10^{35}$
cyclic	RB	4	6	8	10	12	14	16	18	20
	RDF	2	3	4	5	6	7	8	9	10
	n_{rota}	5184	$3.7 \cdot 10^5$	$2.7 \cdot 10^7$	$1.9 \cdot 10^9$	$1.4 \cdot 10^{11}$	$1.0 \cdot 10^{13}$	$7.2 \cdot 10^{14}$	$5.2 \cdot 10^{16}$	$3.7 \cdot 10^{18}$

found in the literature.[157] To depict the distribution of enthalpies about the rotamers, “energy landscapes” can be used which for example describe the total enthalpy as a function of all torsion angles. Every conformer corresponds to an “energy well”, and its population increases with the depth of the minimum. To name two extremes, the energy landscape of a floppy polyethylene chain consists of a multitude of shallow energy minima while a protein chain folds into its native state which is resembled by a single deep well and which exhibits the global minimum. Much effort has been spent to answer the question how this native state is reached on short time scale.[158] A linear polypeptide chain is somewhere between these extremes, and the Ramachandran plot is a well-known 2D projection of the 3D energy landscape for the ϕ/ψ angle pair of a single residue (depicted in figure 2.12). However, the simultaneous consideration of more than two angles prohibits a descriptive graphical depiction as the 3D space is not sufficient anymore, and therefore potential hypersurfaces must be used.

The most complex description of molecular chains finally includes the development of the system over time, with the entropy S as central factor (figure 3.8, red bar), but at this level of complexity an exhaustive description is not possible. Therefore, molecules in the solution state which requires consideration of pH value, salts, and possible membranes must basically be considered under-determined as spectroscopic methods only provide a small window of time- and spatial resolution. For example, the processes in proteins comprise 15 orders of magnitude on the time scale, from picoseconds (librational motions) to hours (global folding). It must therefore be concluded that the increasing complexity of the models as outlined in figure 3.8 does not lead to the goal to predict physical parameters of biomolecules and to understand biomolecular macrocyclizations, which is motivation to our solution approach.

3.2.2.2 “Flexibility” and “rigidity”: How to use terms from the macroscopic world for microscopic systems

The description of microscopic molecular architectures generally suffers from the use of terms from the macroscopic world. To characterize molecular “shape” or “structure”, the terms “flexibility” and “rigidity” are commonly used, and it is questionable how they are applicable to the microscopic world in order to classify molecular properties. Thinking of the term “flexibility” on the molecular level, one may bear in mind a linear molecular chain which adopts various conformations by rotation of its backbone torsions. Microscopic “flexibility” therefore may be described by the accessible space while “rigidity” in contrast scales with the height of energy barriers that have to be overcome for a spatial rearrangement. It is important to be able to quantify these macroscopic terms, which is demonstrated by two model peptides shown in

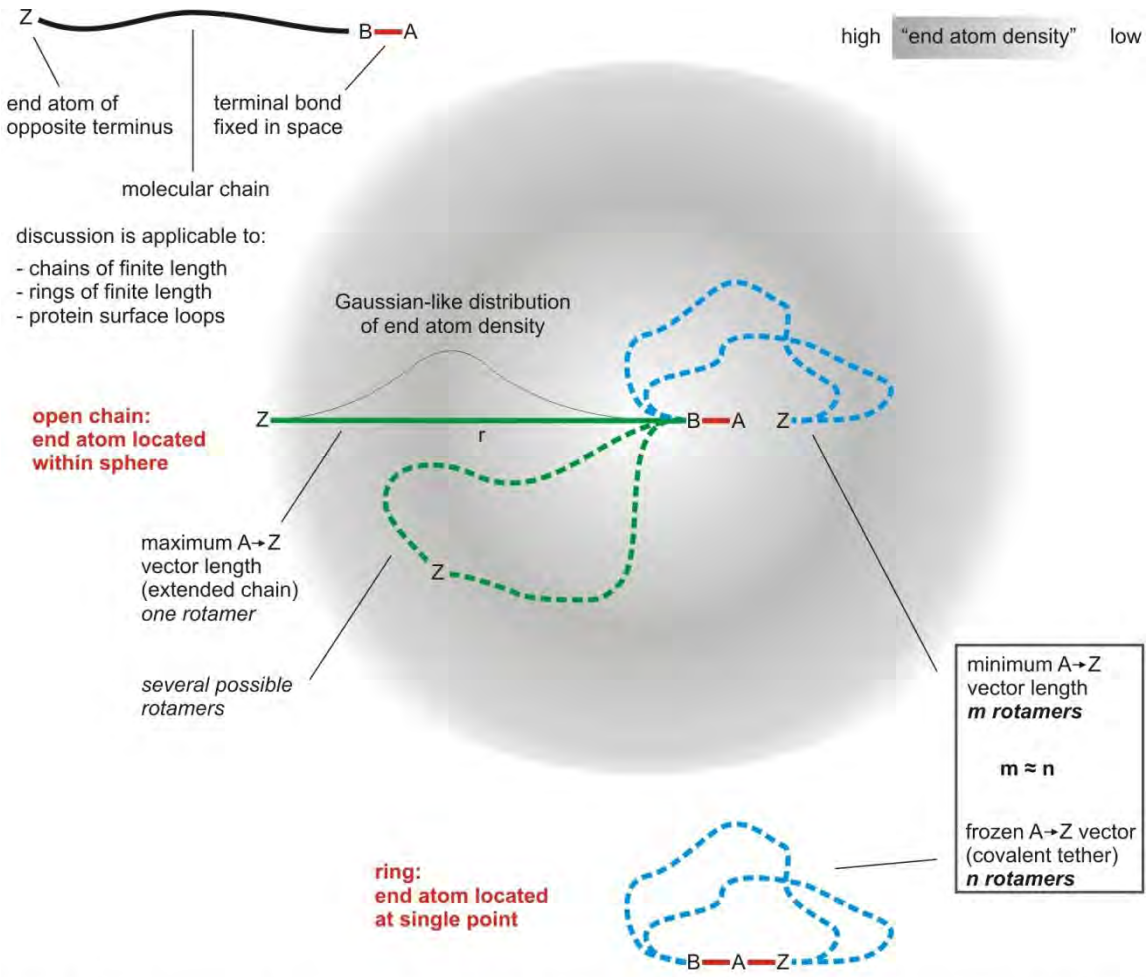

Figure 3.10 Illustration of the conformational restriction upon macrocyclization: the sum of backbone bond vectors. *If the first backbone bond of a linear chain is fixed in space (A-B bond, red) the end atom (Z) is localized within a sphere of maximum radius r which is equal to the length of the fully extended chain (green solid line). This "orbital" is not symmetric as the maximum distance between A and Z decreases the more the chain is bent. For every position of the end atom within this sphere, the number of rotamers can be determined by the calculation of all spatial arrangements of the chain and of their respective energies (for one point, two rotamers are indicated by green dashed lines). This leads to a certain probability of the end atom to be localized at a certain position, and the "terminal atom density" distribution will adopt a Gaussian-like shape with the maximum slightly greater than r/2. Approaching the center of the sphere, the probability will quickly go towards zero due to sterical repulsions. However, there is a minimum distance of both terminal atoms with significant probability to be populated: this is equivalent to a single point and located along the covalent bond which would link both terminal atoms in the macrocycle. There are m rotamers which are accessible by the linear chain with the end atom Z at this position, and two are depicted as blue dashed line. Now, a comparison of linear and cyclic species with respect to the reduction of rotamers is possible. For this purpose, the length of the covalent tether (A-Z bond indicated by red line) is in an approximation set equal to the minimum distance of the two terminal atoms in the open chain. The number and populations of allowed cyclic rotamers n are then equal to the number and population of linear rotamers m. In other words, the number of cyclic rotamers n is equal to the small fraction of linear rotamers in which the distance of both terminal atoms resembles this minimum distance. This demonstrates the high extent of conformational restriction as the three-dimensional spherical orbital of the linear chain end is restricted to one single point.*

To be expressed in a numerical way, the possible positions of the linear chain end can be described as a three-dimensional dot matrix. After cyclization, only one of these dots remains, which corresponds to the distance of both end atoms fixed by the covalent tether. In figure 2.12 such a scenario is described for a pair of angles which is restricted to one single conformation: in this case it is not a 3D but a 2D dot matrix which is finally restricted to one single dot.

figure 3.9a which exhibit the same length but different numbers of rotatable backbone torsions. The comparison of their macroscopic models below shows that the term “flexibility” on the microscopic level refers to the number of rotatable bonds, or, to the number of rotational degrees of freedom.

3.2.2.3 From chains to rings: the macrocyclization process

The examples shown in figure 3.9a are described only with respect to rotations of backbone bonds, which corresponds to the simplistic model already discussed (figure 3.8, green bar). Also concerning an equilibrium between a linear and a cyclic peptide, this has the advantage that it allows to exhaustively quantify molecular flexibilities and thereby to compare different molecular systems. For example, the increment of a torsion by 5° gives 72 possible rotamers, and consequently for a molecule with n rotatable bonds 72^n rotamers are obtained. As shown for linear peptides consisting of two to ten residues in table 3.1, this method enables quantitative comparison of the flexibility of any system.

Assuming that a molecular linear chain and its cyclic analog exhibit similar local flexibilities (which is fulfilled if the ring is large enough), the difference of rotamers gives a quantitative comparison. A cyclic molecule has roughly the same number of rotatable bonds but obviously exhibits a greatly restricted flexibility. As discussed later, this can also be expressed by the sum of all backbone vectors which is restricted to one single value in a cycle (figure 3.10). The restriction results from the covalent tethering of both ends and has significant implications on the calculation of rotamers. The increment of a single angle is not possible any more as it would break the cyclic structure, and the ring is only conserved by counter-rotation of (at least) one another angle (figure 3.9b). Setting every rotational backbone bond equal to one rotatable degree of freedom, we propose a simplistic rule-of-thumb: if a linear chain is macrocyclized, the number of rotational degrees of freedom is halved. Consequently, in the case of 5° torsion increments as already described for linear species, the total number of rotamers of a cyclic molecule with n rotatable backbone torsions is calculated by $72^{n/2}$. The halving of the exponent represents a considerable restriction of flexibility. Table 3.1 lists the numbers of rotamers obtained of cyclic peptides consisting of 2 to 10 amino acid residues and compares them to their respective linear analogs.

This working hypothesis is conclusive by its simplicity but must be verified by an experiment. Furthermore, the fact that already the simplest numerical model used for linear molecules cannot be transferred to macrocycles without applying a rule-of-thumb demonstrates the difficulty to compare chains and rings with respect to their flexibility. Based on the random chain

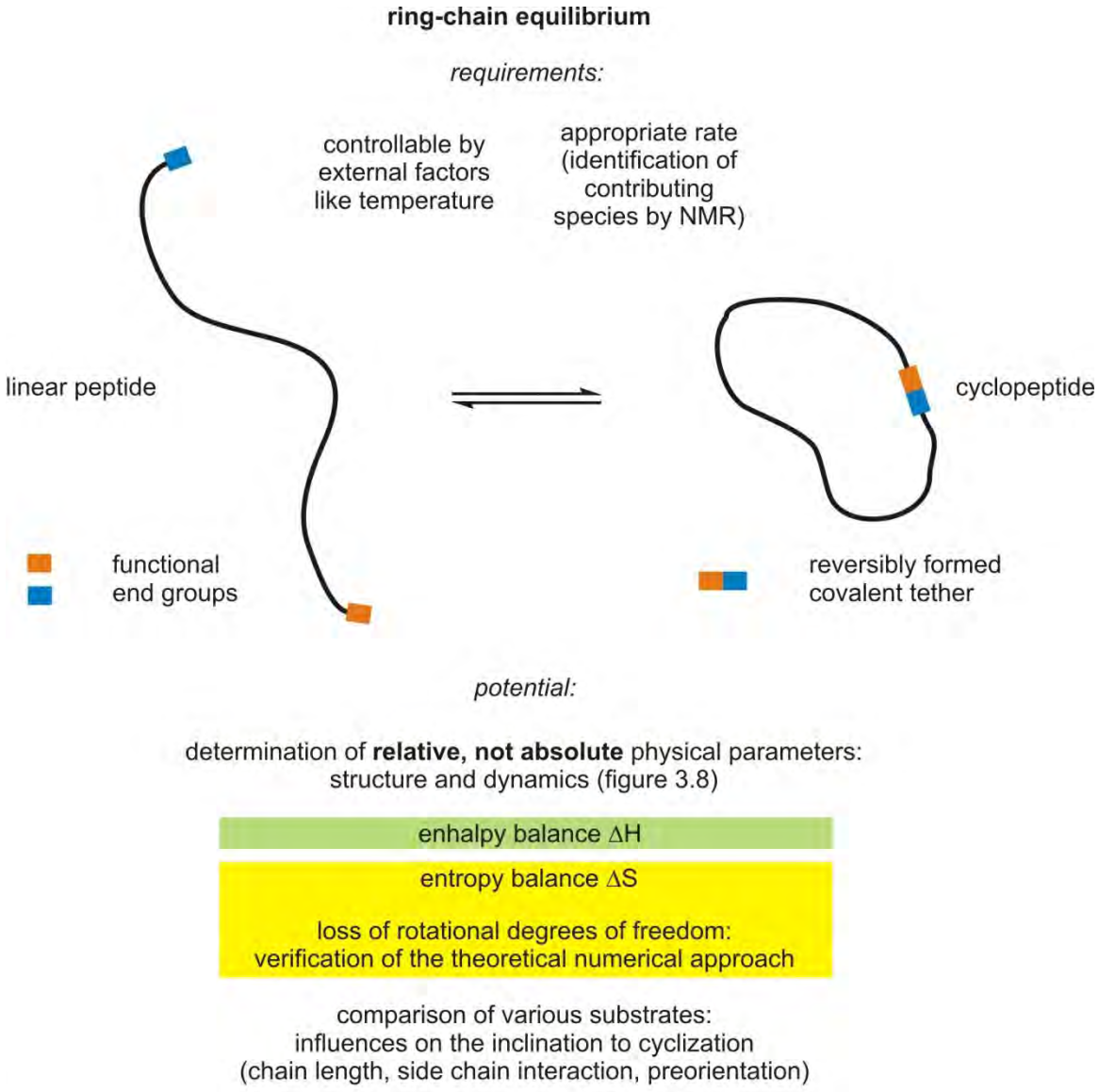

Figure 3.11 Experimental setup for the thermodynamic characterization of peptide macrocyclizations: requirements and potential. *The peptides must be modified in such way that the ring closure is reversible and that the composition of the equilibrium is controllable by the experimenter. Appropriate rates of interconversion are required to enable observation by NMR spectroscopy. The experimental values obtained from such an equilibrium characterize the differences between linear and cyclic species in structure and dynamics and thus cover the whole band width of physical factors as depicted in figure 3.8. The entropy balance, which can be calculated from the temperature dependence of the equilibrium, quantifies the loss of rotational degrees of freedom upon macrocyclization. For the understanding (and, as the next step, the prediction) of the processes it is important to know which factors to what extent determine the inclination of a linear substrate to cyclize. Such information can be made accessible by the comparison of several equilibrium systems with distinct structural modifications of the substrates.*

concept developed by *Flory et al.* we propose an illustration of the rigidification by considering the vector sum of all backbone bonds (figure 3.10). If the terminal bond of a molecular chain is fixed in space, the terminal atom at the other chain end is located within a spherical “orbital”. In dependence on the population of the possible rotamers at each position, every point within this sphere is associated with a certain possibility of the end atom to be localized. If the macrocycle is closed, the sphere is reduced to a single point: the position of the end atom which is covalently bound to the other terminus. The number and relative population of cyclic rotamers are similar to the accessible linear species where both end atoms are in the minimum distance to each other without forming a bond. This reduction of the accessible space of the end atom from a 3D sphere to a point also demonstrates the extent of global conformational restriction which occurs upon macrocyclization.

3.2.2.4 Our approach: an experimental setup combined with the simple numerical model

The central problem in the determination of molecular thermodynamic parameters is that their absolute values cannot be measured. For the characterization of a macrocyclization, however, it is rather the difference between linear and cyclic species which is of interest, or, in other words, the conformational restriction which is associated with macrocyclic ring closures, and this finally constitutes the dominant role of macrocyclizations in evolution as a source of biological activity and selectivity. An experimental setup which establishes a controllable equilibrium between a linear molecular chain and its cyclic analog would be a key to this information and allow to determine the balance of enthalpy and entropy (figure 3.11). Furthermore, the results can be used to test the validity of the theoretical proposal that the number of rotational degrees of freedom is halved upon macrocyclization. Though only outlined for rotamers (table 3.1), this rule-of-thumb should likewise be applicable to the number of conformers (and therefore allow to calculate the number of lost rotational degrees of freedom) by the following consideration. Every intramolecular interaction is energetically likewise favored or disfavored, no matter whether the chain ends are covalently linked or not. In other words, any *local* conformations which contribute to the stabilization of a *global* linear conformation (and therefore cause an energy well in the hypersurface) will comparably benefit the stability of the corresponding macrocycle. Therefore, the quotients of linear/cyclic rotamers and conformers should be similar. The experimental data of the equilibrium, however, do not only comprise differences in structure but also in dynamics and thus cover the full range of factors outlined in figure 3.8.

Establishing an experimental setup which allows to control a ring-chain equilibrium would provide the entropy balance of the macrocyclization process. This key term quantifies the

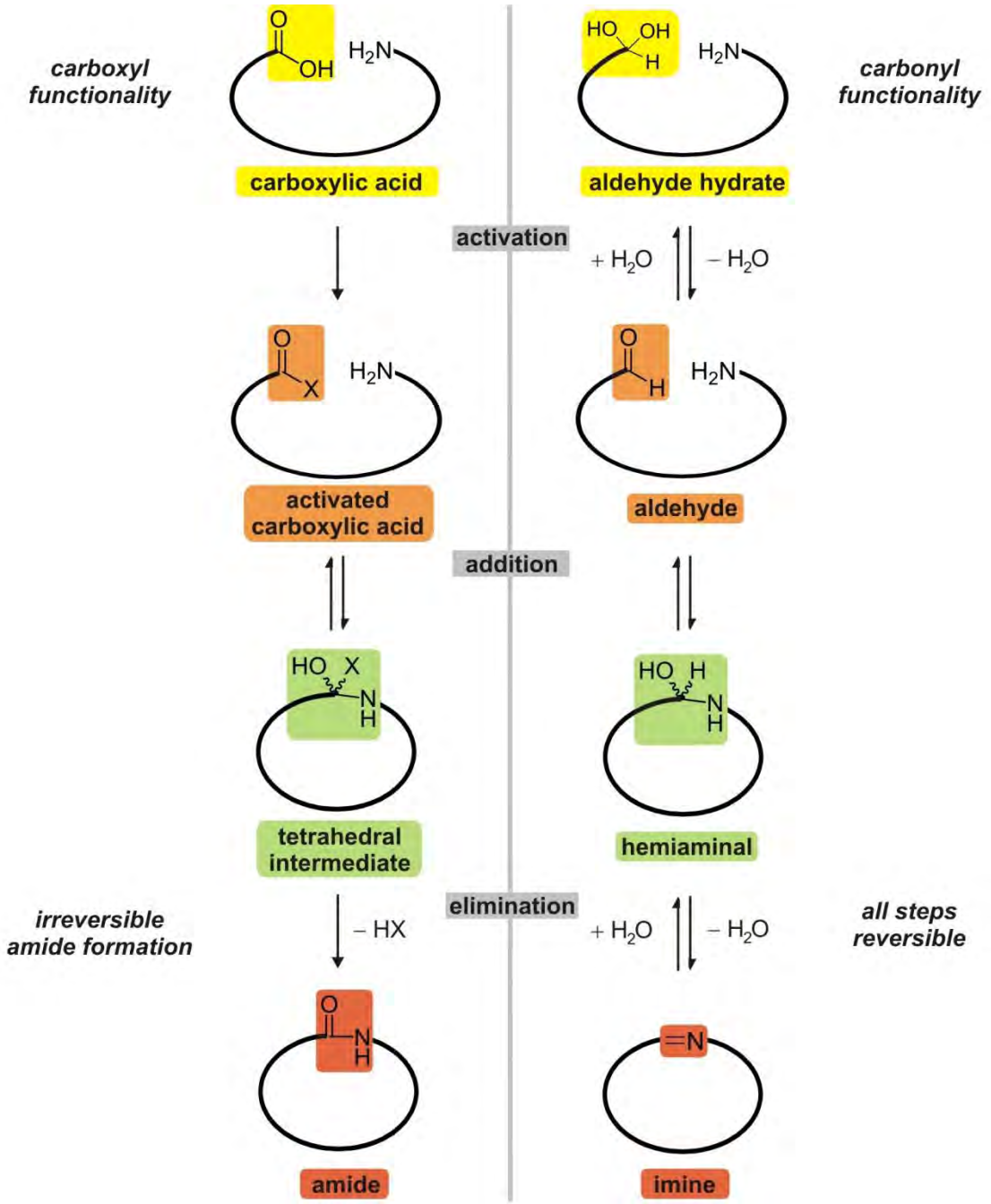

Figure 3.12 Peptide macrocyclizations can be made reversible by substituting the C-terminal carbonyl- by a carboxyl functionality. *Amides condense irreversibly in aqueous solution while all steps of macrocyclic imine generation are reversible. Both pathways have in comon the same sequence of intermediates, as the carboxylic acid or aldehyde hydrate (yellow) first has to be activated to yield an activated carboxylic acid or an aldehyde, respectively (orange). The following ring closure (addition reaction) to a tetrahedral intermediate or a hemiaminal (green) is reversible in both routes. The decisive step is the subsequent elimination which gives the macrolactam or the macrocyclic imine. While the amide is generated irreversibly from the tetrahedral intermediate, the imine is in equilibrium with a hemiaminal. This suggests that the utilization of peptides with an aldehyde- instead of a carboxylic acid function at the C-terminus could be a key to establish a reversible cyclization equilibrium.*

conformational difference between linear and cyclic species and determines the inclination of a substrate for cyclization. Finally, it resembles the thermodynamic expression for the biological purpose of peptide macrocyclization, which is to turn floppy linear peptides with low biological activity into rigid scaffolds that can act as efficient functional molecules in the organism.

NMR spectroscopy is a method of choice as it can be used to quantitatively analyze the ratio of all dominant contributing ring-chain isomers and therefore allows the direct monitoring of the equilibrium. In order to obtain signal sets for linear and cyclic species, the rate of ring-chain interconversion must be slow on the NMR time scale, but not too slow as a long time span until the equilibrium state may abolish its characterization. On the other hand, if the equilibrium rate is too high, only one set of signals is obtained, which makes NMR spectroscopy inappropriate for evaluation. So far, no such experimental setup has been described for two reasons. First of all, there are no enzymes known which can trigger such equilibrium. Second, as evolutionary processes result in structures which are as stable as possible for the sake of proper biological function, all macrocyclization processes are irreversible in aqueous solution, and this also applies for cyclopeptides which are irreversibly closed by an amide bond. In order to be able to characterize a peptide macrocyclization, the ring closure must be modified in a way that it features reversibility in aqueous solution. This can be accomplished by extending the functional group repertoire beyond the irreversible amide and ester tethers found in natural cyclo(depsi)peptides, and the exchange of these carboxyl functionalities by carbonyl groups is an obvious option (figure 3.12). As all steps of macrocyclic imine formation are reversible in aqueous solution, it should be possible to establish a ring-chain equilibrium between linear peptide aldehydes and the corresponding cyclopeptides which exhibit a covalent imine tether (they are in the following named cycloiminopeptides). Furthermore, such a modification implicates only a minimum change of the overall peptide structure and conserves the number of atoms as well as the atom sequence of the backbone, which is important as conclusions on the native peptides should be made. As imine formation is pH-dependent, the change of pH could be a key to control the composition of the equilibrium.

In this context, the recently discovered nostocyclopeptides, which are the only known natural cyclopeptides with an imino function in the backbone, turned out to be suitable candidates. Before the results are described, previous work about these remarkable natural products is summarized in an overview in the next section.

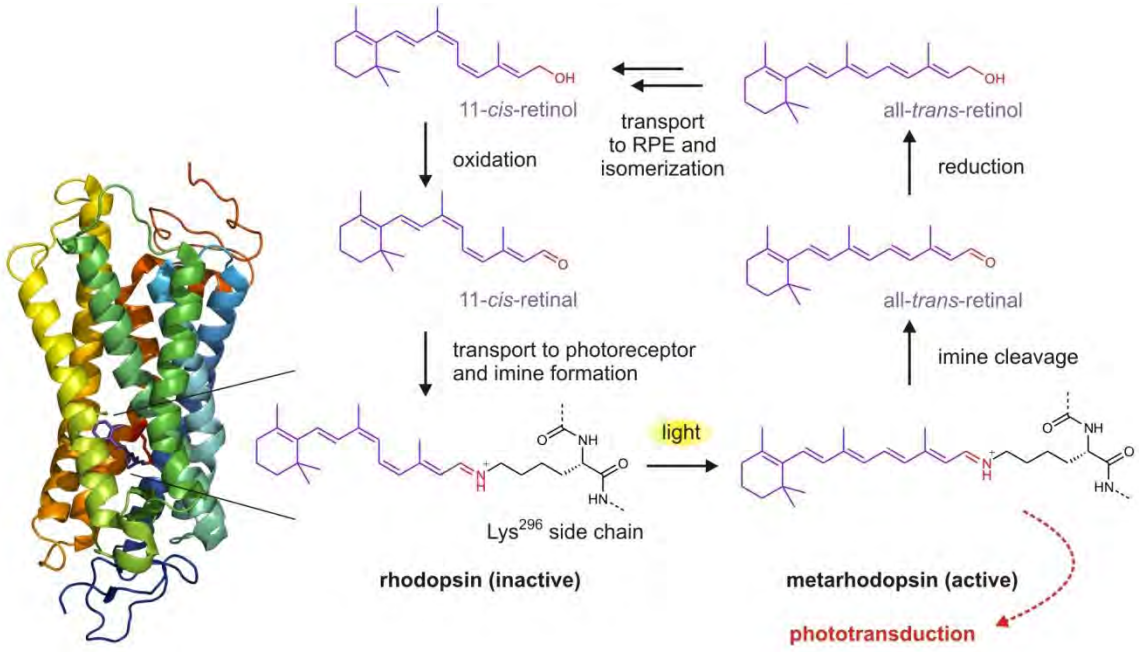

Figure 3.13 Imine functions in natural products: rhodopsin. *In rhodopsin (X-ray structure of the monomer shown on the left, PDB entry 2G87) retinal (purple) is bound as* trans*-imine to the Lys*^{296} *side chain. Photoactivation of the chromophore effects isomerization of the 11-*cis *double bond to* trans*. As this conformation does not fit the binding pocket, the protein undergoes a conformational change to the active metarhodopsin which starts the further phototransduction cascade (overall, the conversion into a electrical signal which is sent to the visual cortex). The reversibility of the imino tether is crucial as the active all-*trans*-retinal must be cleaved off immediately in order to prevent light desensitization of the rod. After reduction to the less active all-*trans*-retinol it is transported to the retinal pigment epithelium (RPE) where it is isomerized in several steps to the 11-*cis *form and subsequently oxidized to 11-*cis*-retinal. After the transport back to the photoreceptor the chromophore is tethered again as imine which reconstitutes the photosensitive rhodopsin.*

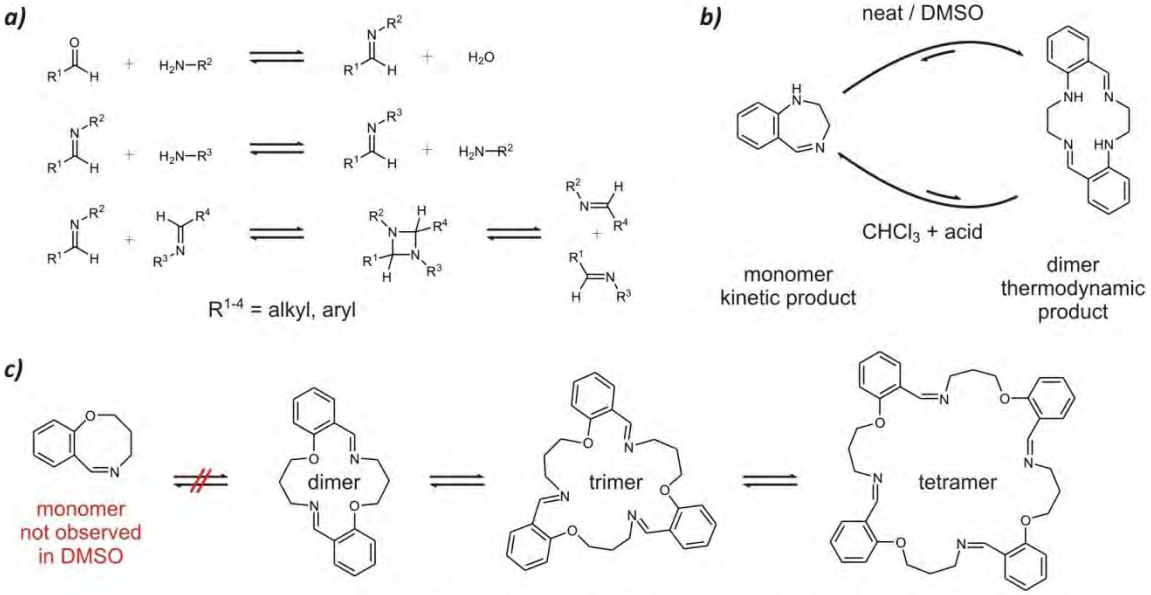

Figure 3.14 Imine functions in dynamic combinatorial libraries. ***a)*** *Types of reversible reactions with imino functions involved: imine formation/hydrolysis (top), imine exchange (center), and imine metathesis (bottom).* ***b)*** *The equilibrium between a 7,6-bicyclic imine monomer (intramolecular imine formation, kinetic product) with the thermodynamically favored dimer depends from the conditions. In this case, the conversions proceed via imine exchange and not via metathesis.* ***c)*** *A longer alkyl chain effects a more complex equilibrium. In many cases, the presence of diverse linear oligomers further complicates analysis.*

3.2.3 The Nostocyclopeptides: rare examples of natural products with imino functions

3.2.3.1 Imines in natural products and in dynamic covalent chemistry

In the course of evolution, only a few functional groups like esters, amides and acetals gained importance as structure-generating linkages. Imines are by comparison rather inappropriate, as they are generated reversibly under aqueous conditions (figure 3.12).[159, 160] Complete imine formation only occurs within a narrow pH range which depends on the pKa and HOMO energy of the amine and from the LUMO energy of the aldehyde, and even in that pH range the kinetic barrier for hydrolysis towards the primary amine and the aldehyde is low.[161] Therefore, they remain in spite of a significant role as metabolic intermediates[162] a great exception as stable structural units in functional molecules. A prominent example is the imino linkage between the retinylidene chromophore and the Lys^{296} side chain in rhodopsin (figure 3.13).[163] After light-induced *cis*→*trans* isomerization of the imino-bound retinal, which is the primary visual process in the eye, the *trans*-retinal is cleaved in order to be enzymatically recycled to the *cis* form.[164] The reversible imino linkage is a prerequisite for this cycle as it enables facile hydrolysis of the chromophore from the rhodopsin.

It is just this reversibility that makes imines valuable structural compounds in dynamic covalent molecular libraries (see also section 3.1.2).[142, 165] During the past two decades, research has been concentrated on methods which allow to generate imine (*Schiff* base) macrocycles without the presence of metal ions that can act as templates, which also distinguishes this research from the numerous studies concerning *Schiff* base metal complexes. In addition to the imine formation and hydrolysis (equilibrium with aldehyde and amine), two other reversible reactions can occur, which are transimination and imine metathesis[166] (figure 3.14a). As shown by numerous examples in the literature, the equilibria are mostly far from simple as monomeric, dimeric and oligomeric linear speices are co-existent with their cyclic analogs, and the exact compositions are very susceptible to changes in concentration and pH value.

A rather simple example of such an equilibrium of cyclic imines is shown in figure 3.14b. The bicyclic monomer can be isolated as kinetic product, whereas the thermodynamically stable dimer is formed in DMSO. Treatment of the dimer with acidic chloroform, in contrast, effects formation of the monomer.[167] The extension of the alkyl chain by one methylene group has significant effects on the equilibrium (figure 3.14c) as no monomers are detected in DMSO (appararently due to the thermodynamically unstable 8-membered ring) but tri- and tetrameric macrocycles are formed.[168] The higher the concentration, the more the equilibrium is shifted towards the largest rings.

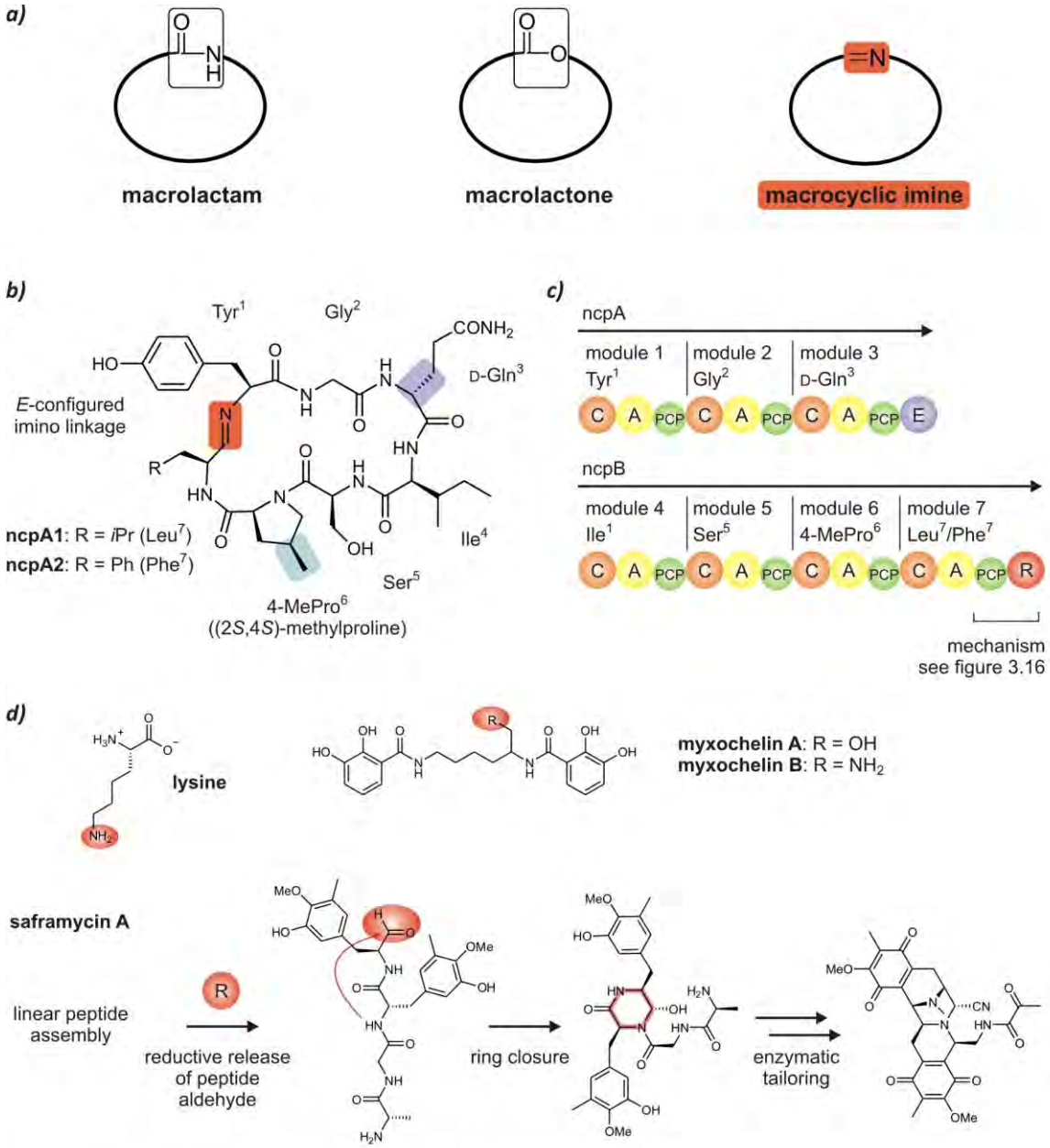

Figure 3.15 Macrocyclic imine formation in biosynthesis: the ncp imine macrocycles and the role of reductase domains. ***a)*** *The macrolactam and macrolactone formations are widely used as macrocyclizations in natural product synthesis and are generally irreversible in aqueous solutions. In contrast, macrocyclic imine formation is reversible and the nostocyclopeptides (ncp) remain the only hitherto known natural products that contain this linkage.* ***b)*** *Structure of the two known cycloiminopeptides, ncpA1 (C-terminal Leu[7]) and ncpA2 (C-terminal Phe[7]). Besides the imine, the rarely found (2S,4S)-methylproline and the D-Gln are highlighted.* ***c)*** *Depiction of the ncp gene cluster with the domains indicated by colored spheres (orange: condensation (C) domain; yellow: adenylation (A) domain, green: peptidyl carrier protein (PCP); blue: epimerization (E) domain; red: reductase (R) domain). The biosynthesis of the peptide is secluded by the reductive release of a linear peptide aldehyde from the R domain. This release triggers the cyclization to the imine (figure 3.16).* ***d)*** *Depiction of some of the rare examples of natural products in which reductase domains are involved in biosynthesis. In most known cases, amines and alcohols are produced, like in the case of lysine and myxochelin synthesis (top). Besides the ncp, only in saframycin biosynthesis (bottom) an aldehyde is released from the synthethase. In this linear tetrapeptide, backbone-to-backbone cyclization of the C-terminal aldehyde to an amide NH results in a six-membered ring with an N-acyl-hemiaminal linkage. Further enzymatic tailoring results in the tetrahydroisoquinolidine core present in all saframycins.*

3.2.3.2 Previous work on nostocyclopeptide biosynthesis and *in vitro* macrocyclization

Before the discovery of the nostocyclopeptides (ncp) by *Golakoti et al.* in 2001,[169] two macrocyclization strategies were known for the numerous macrocyclic non-ribosomal peptides (NRPs), which are macrolactamization and macrolactonization.[97] With the nostocyclopeptides (ncp), which exhibit the only known NRPs with an imino linkage in the backbone, the macrocyclic imine formation added as third possibility of peptide backbone cyclizations in biosynthesis (figure 3.15a). The two ncp known so far, ncpA1 and ncpA2, are cyclohexapeptides which only differ in the C-terminal amino acid (ncpA1: Leu^7, ncpA2: Phe^7; figure 3.15b). Both contain a D-configurated Gln which apparently induces a β-turn and the rare nonproteinogenic amino acid [2*S*,4*S*]-methylproline (4-MePro) which is biosynthesized from Leu.[170] The peptides have been isolated from the terrestrial cyanobacterium *Nostoc* sp. ATCC53789 which, together with *Nostoc* sp. GSV224, has come into the focus of research as it also produces the antitumor agent cryptophycin.[171-173] The ncp, however, displayed only weak cytotoxicity against several tested cell lines and showed no antifungal, antibacterial or protease-inhibiting activity,[169] and their biological role still remains unknown.

After the primary structure had been elucidated,[169] the involved NRPS was characterized in order to clarify from which precursor the imino linkage is formed and what kinds of NRPS domains are involved.[174] Figure 3.15c depicts the domain organization of the ncp biosynthetic complex which consists of two subunits, ncpA and ncpB. Instead of the commonly found thioesterase domain at the end of the complex, a reductase (R) domain was identified which was assumed to release a linear peptide aldehyde which is subsequently macrocyclized to the imine. Such R domains are rarely found and they catalyze the reductive release of alcohols and amines (for example in the biosynthesis of lysine in yeast[175] and of the myxochelines[176]). The only other known example where an aldehyde is released is the biosynthesis of the saframycin antibiotics (figure 3.15d).[177] However, details of how the R domain in the ncp biosynthesis works and whether the macrocyclization step is assisted by a yet unidentified protein remained speculative.

The characteristics of the R domain were specified by *Marahiel et al.* who showed that the recombinant peptidyl carrier protein (PCP)-R domain in the presence of NADPH efficiently catalyzed the reduction and subsequent cyclization of the peptidyl-CoA substrate, while the isolated R domain displayed lower activity (figure 3.16).[178] This demonstrated that no additional protein is involved in the macrocyclic imine formation.

In order to specify the role of the R domain in the macrocyclization step, the peptide aldehydes were synthesized on solid phase and subsequently incubated in HEPES buffer at pH 6 with and

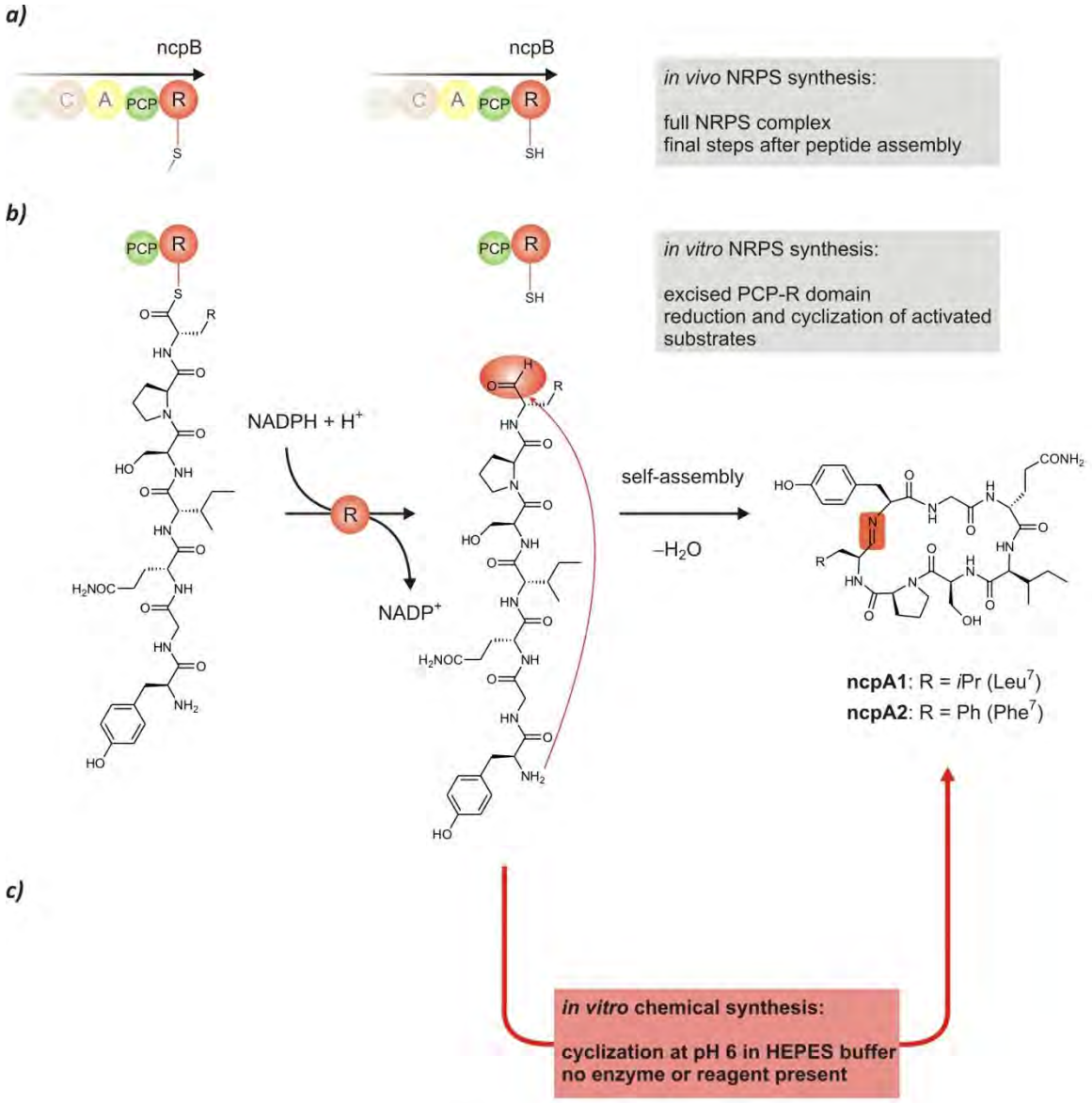

Figure 3.16 The macrocyclic imine formation of the ncp occurs enzyme-independently. ***a)*** *Simplified depiction of the final steps of ncp biosynthesis (only the final NRPS domains are shown, see figure 3.15b for the complete NPRS complex). The linear peptide is attached as thioester to the terminal R domain and then in the presence of NADPH subjected to reductive release from the domain. The peptide aldehyde finally self-assembles to the cycloiminopeptide, and no further enzyme is required for this step.* ***b)*** *The excised PCP-R domain accepts thioester-activated linear peptides and also triggers macrocycle formation after reductive release of the cyclization precursor.* ***c)*** *The decisive experiment which revealed the ability of the ncp to self-cyclize was carried out by incubating the artificially synthesized peptide aldehydes (figure 3.17) in HEPES buffer solution at pH 6. Under these conditions, the macrocyclic imines were also formed quantitatively. The fact that this process occurs quickly and highly selectively (no intermolecular imine formation is observed, in contrast to the dynamic combinatorial libraries described in figure 3.14) suggests an important role of preorientation of the linear peptides. This question was adressed by the NMR spectroscopic investigations described in the following section 3.3.*

without the recombinant PCP-R domain. It turned out that the PCP-R domain is not required for the macrocyclic imine formation as in both cases a complete conversion to the macrocycle was observed. Consequently, the linear peptide aldehyde cyclization precursors, after being released from the R domain, are able to self-cyclize independently of an enzyme (figure 3.16c). Remarkably, the cyclized ncp were the only species observed after the self-cyclization. Recalling the complex mixtures of monomers as well as linear and cyclic oligomers which are generally observed for imine-based dynamical combinatorial libraries,[142, 165] a pronounced preorientation of the linear peptide aldehydes was assumed as reason for the high selectivity.

3.2.4 Task of this study

These findings suggested the ncp as ideal substrates for NMR spectroscopic experiments which are aimed at the thermodynamic investigation of a peptide macrocyclization and which finally should serve to validate our simple theoretical model which quantitatively describes the entropy loss accompanied by macrocyclization processes (section 3.2.2).

The self-cyclization as observed in the case of ncp is a remarkable process, and it is rarely observed. Regarding that the macrocyclic ring closure step often exhibits the crucial step of chemical syntheses, the ability of a substrate to form a macrocycle in high yield and without any enzyme or reagent is of immense value. Therefore, the first task to be accomplished by the NMR studies should be the identification of structural features of the linear precursors which effect this selectivity, as well as the average conformation of the macrocyclic imine.

In the following, appropriate solution conditions which allow the self-cyclization to take place in the NMR tube should be evaluated. This would also be the first step towards our goal to establish a ring-chain equilibrium which - also at best in the NMR tube - must be controllable in its composition according to pH value and temperature, as this is essential for the determination of thermodynamic parameters of the cyclization process. The prerequisite, however, of such studies is a full reversibility of the ncp ring closure, which also has to be proven by NMR.

As the two ncp exhibit the only hitherto known examples of cycloiminopeptides, further studies should examine whether other peptidic substrates which are modified by substitution of an amide by an imino tether can also be utilized. This is essential as ideally other parameters like different ring sizes must be included in the study to gain a comprehensive picture of the structural determinants of macrocyclizations.

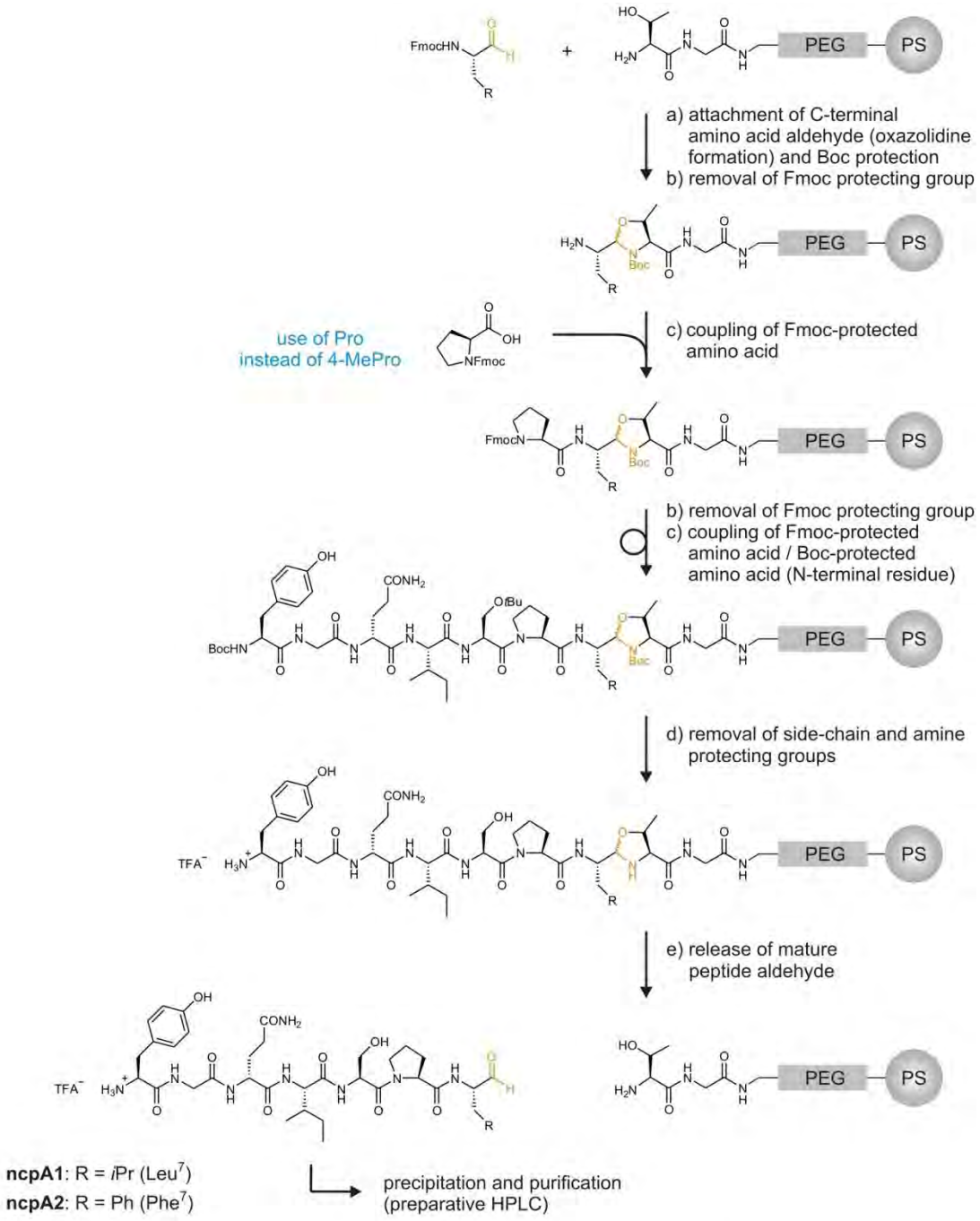

Figure 3.17 Solid phase synthesis of the ncp aldehydes (performed by* F. Kopp*). *During peptide chain assembly the C-terminal amino acid aldehyde is masked as an oxazolidine which is formed by reaction with a Thr. The solid phase consists of a polyethylene (PEG) grafted polystyrene (PS) resin functionalized with a Thr-Gly dipeptide. An aldehyde-loaded resin is commercially available with a number of residues (*Novabiochem*), including Leu and Phe as required for ncp synthesis. The peptide chain is now assembled by standard Fmoc protocols (automated or manual synthesis). After coupling with the respective N-terminally adjoining Fmoc-protected amino acid, the Fmoc-protecting group is removed for the next coupling step. The last residue is attached with Boc-protected amine, which yields the resin-coupled hepta-peptide. With 100% TFA all remaining protecting groups are removed without affecting the oxazolidine linker. Under aqueous acidic conditions, the peptide aldehyde finally is cleaved from the resin as TFA salt and subjected to precipitation and further purification.* Reagents and conditions: a) Fmoc-amino aldehyde (5.0 eq), 1% AcOH in CH_2Cl_2/MeOH 1:1, RT, then Boc_2O (5.0 eq), NMM (5.0 eq); b) DBU/piperidine/DMF 2:2:96; c) Fmoc/Boc-protected amino acid (3.0 eq), PyBOP (3.0 eq), HOBt (0.5 eq), DIPEA (6.0 eq); d) 100% TFA; e) AcOH/H_2O/CH_2Cl_2/MeOH 10:5:63:21.

3.3 Results and discussion: Ring-chain equilibria of the nostocyclopeptides[179]

3.3.1 Synthesis of the peptide aldehydes

The linear cyclization precursors of ncpA1 and ncpA2 were synthesized by *F. Kopp* on solid phase as described in earlier work[178] according to a protocol by *Novabiochem*.[180] The procedure is described in detail in section 5.3 and outlined in figure 3.17. In brief, NovaSyn® TG resin (*Novabiochem*) with the C-terminal Leu (ncpA1) and Phe (ncpA2) aldehyde immobilized as oxazolidine was used and the linear peptide chains were assembled by automated Fmoc solid phase synthesis. After the last peptide coupling and removal of all protecting groups, the peptide aldehydes were cleaved from the resin, precipitated, and purified by preparative HPLC. After lyophilization, the linear peptide aldehydes were obtained as colorless solids (ncpA1 precursor: 11.1 mg, ncpA2 precursor: 9.9 mg) ready to use for NMR spectroscopic experiments. As the naturally occurring 4-MePro is tedious to synthesize, especially in the amounts needed for solid-phase peptide synthesis, it was replaced by Pro.[181] This small structural change is justified in the light of the great reduction of experimental effort and time. None of the experiments gave hints on that the presence of the methyl group in the Pro^6 side chain would significantly effect the cyclization. Therefore, the experimental outcomes described in the following likewise apply, in a well-applicable approximation, for the artificially synthesized desmethylated analogs as well as for the natural heptapeptides.

3.3.2 NMR assignment and structure elucidation

3.3.2.1 General considerations: nomenclature and experimental setup

Due to the replacement of the 4-MePro by Pro (see above) all experiments were performed with the Pro^6-γ-desmethyl analogs of ncpA1 and ncpA2, respectively. For the sake of simplification, these will be abbreviated to ncp throughout this chapter.

A nomenclature had to be conceived which can be used in the text and by which linear and cyclic peptide species can be clearly discriminated. As the macrocyclic peptides are termed ncpA1 and ncpA2, respectively, we decided to add the characteristic C-terminal functional groups to these abbreviations to assign the corresponding linear peptides. The cyclization precursors of ncpA1 and ncpA2 with the aldehyde functions at the C-terminus are therefore abbreviated ncpA1-CHO and ncpA2-CHO, respectively (figure 3.18b).

As it should be possible to perform multiple measurements at different pH values with one NMR sample, finding appropriate solvent conditions was an important task at the beginning. In order

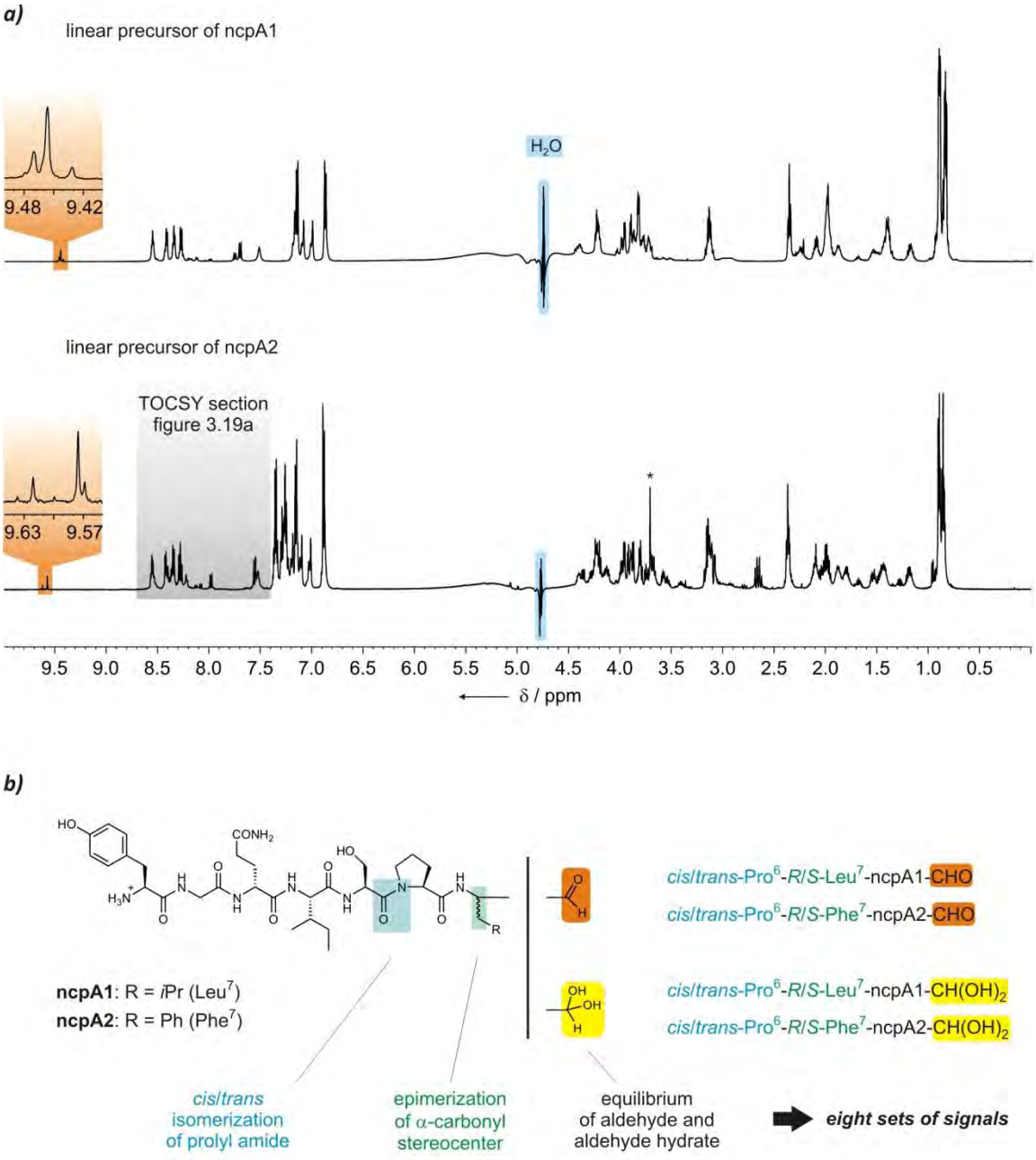

Figure 3.18 NMR spectroscopic analysis of the ncpA1 and ncpA2 cyclization precursors. a) *^{1}H DPFGSE-NMR spectra (H_2O/D_2O 5:1, H_3PO_4/KH_2PO_4, pH 3.0, 600 MHz, 300 K) of linear ncpA1 (top) and ncpA2 precursor (bottom). The suppressed H_2O signals are highlighted blue and the asterisks * mark a signal caused by residual PEG from the SPPS resin (figure 3.17). The spectra were calibrated on the H_2O resonance (4.80 ppm at 300 K). The well-separated aldehyde signals (diastereomers) are highlighted in orange and depicted with magnification. The appearance of several aldehyde signals and their low intensities indicate the presence of several species.* ***b)*** *The aldehydes (orange) are only present to approx. 5% as they are mostly hydrated (yellow) under the applied solution conditions. As* cis/trans *isomerization of the prolyl amide bond occurs (blue) and the C-terminal amino acid is subjected to racemization (green), up to eight different linear species are expected in the case of ncpA1 and ncpA2, respectively. On the right, the nomenclature of the linear peptides which is used throughout this chapter is shown. The indication of the carbonyl functional group at the C-terminus marks the species as linear, while the sole ncpA1 and ncpA2, respectively, denote the cycloiminopeptides. The down-field region highlighted in grey in a) is shown as section of a TOCSY spectrum in the following figure 3.19.*

to effect the reversibility of imine formation, which is the prerequisite to establish an equilibrium of linear and cyclic species, an aqueous solution is necessary. As the amide protons should be visible, non-deuterated solvent is required, and in most cases approx. 10% of D_2O are added (H_2O/D_2O 9:1) for the deuterium lock signal. More D_2O is usually neither necessary nor desirable as it leads to a reduction of the signal intensity of exchanging protons. However, we decided to use a deuterium-rich mixture of H_2O/D_2O 5:1 in order to ensure a fast and stable solvent locking in the NMR experiments which can be crucial for performing reaction kinetics, as for example required for the envisioned pH series of measurements.

This also suggests the use of buffered solutions as it must be possible to slightly and precisely change the pH value, at best by direct addition of acid or base to the sample in the NMR tube. HEPES buffer solution had been used by *F. Kopp* for the ncp cyclizations at pH 6,[178] but this is not optimal for NMR spectroscopic experiments as the buffer molecules would give rise to several strong NMR signals that may complicate the analyses. For the same reason, TRIS buffer was not chosen either. We therefore considered a phosphate buffer solution which is invisible in the NMR spectra as more suitable. More important, while HEPES and TRIS buffer solutions are applied at near-neutral pH values, the use of phosphate buffer also allows to precisely set the pH in the acidic range, which is crucial as the linear peptide aldehydes should be analyzed and therefore must be kept from cyclizing. For the investigation of the pH dependence of the ring-chain equilibria, the pH can be increased or decreased within a large pH range covering acidic, neutral, and basic conditions by addition of solid Na_2CO_3 or aqueous H_3PO_4, respectively.

3.3.2.2 The linear peptides

As outlined in section 3.2.4, an important task to be tackled by NMR experiments was the structure elucidation of the linear peptide aldehydes in order to identify the reasons for their efficient and selective ring closures which take place in the absence of any enzyme or reagent. 3.0 mg of the linear peptide aldehydes ncpA1-CHO and ncpA2-CHO, respectively, were dissolved in H_3PO_4/NaH_2PO_4 buffer solutions at pH 3.0 (no insoluble residues were observed), yielding approx. 5 mM peptide solutions (see section 5.3 for details).

The suppression of the water signal in the ^1H NMR spectra was accomplished by excitation sculpting (WATERGATE DPFGSE method, see section 2.3.2.1).[182] The spectra which were obtained after optimization of the acquisition parameters, are shown in figure 3.18a. Under acidic conditions (pH 3.0) imines are not stable and only linear species are expected to be present. As the prolyl amide is usually present in the *trans* as well as in the *cis* conformation, two sets of signals are expected. However, as can be seen in figure 3.18a,

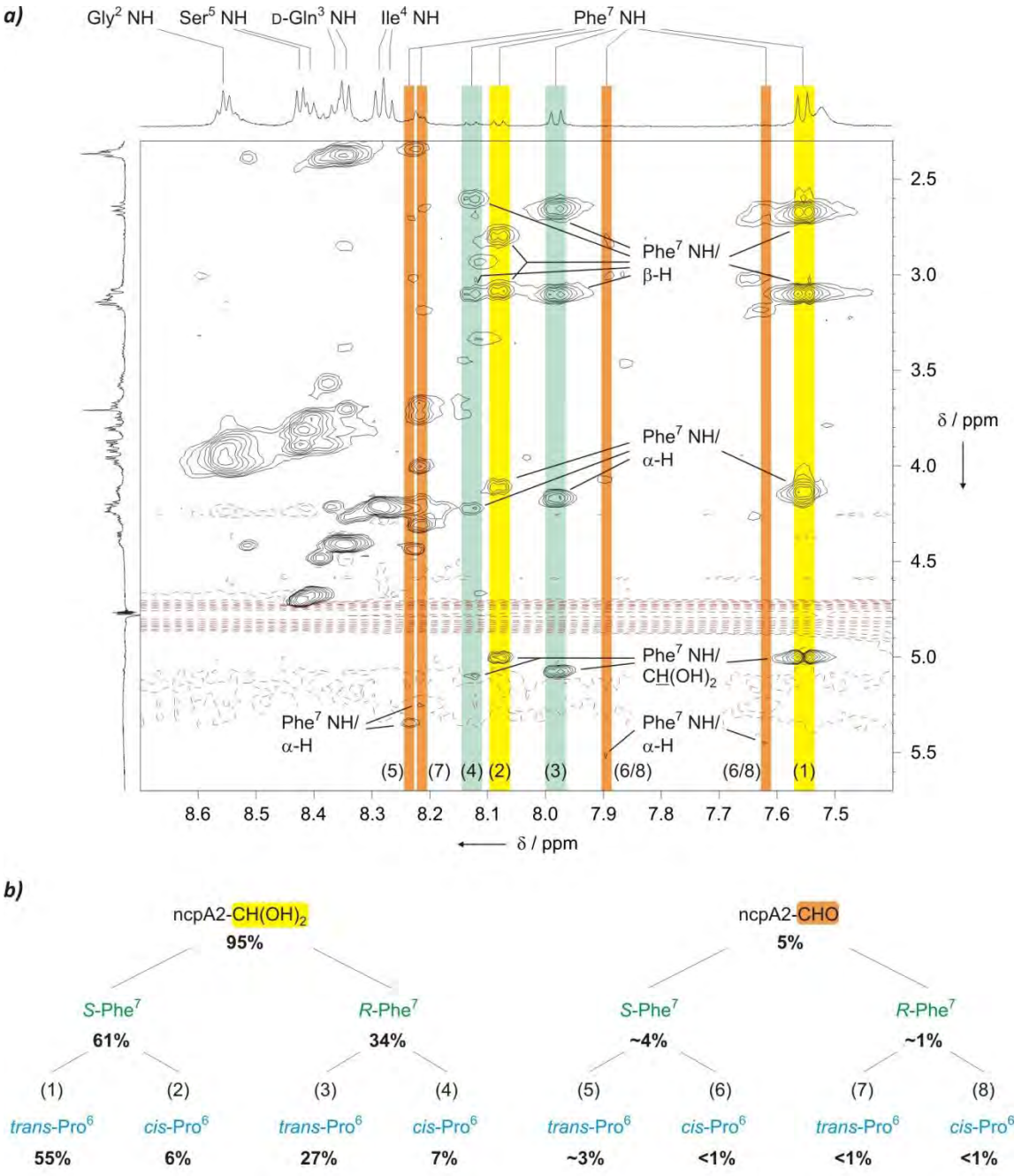

Figure 3.19 Eight linear ncpA2 species are in equilibrium with each other at pH 3.0 and can be assigned by 2D NMR experiments. ***a)*** *Section of the TOCSY spectrum of linear ncpA2 precursor (H_2O/D_2O 5:1, H_3PO_4/KH_2PO_4, pH 3.0, 600 MHz, 300 K). In the 1D projection at the top, the amide proton signals are assigned. While the D-Gln[3], Ile[4] and Ser[5] NH signals only allow to distinguish* S- *and* R-*configured aldehyde hydrates (discussed in detail in section 3.3.2.3), the Phe[7] NH signals are subjected to a high chemical shift dispersion. The respective positions are marked in the spectrum by colored bars (yellow: aldehyde hydrates with* S-*Phe[7], green: aldehyde hydrates with* R-*Phe[7], orange: aldehydes) and the visible TOCSY cross peaks of the NH protons are marked.* ***b)*** *Depiction of the relative percentages of all contributing linear ncpA2 peptides. Every species is assigned a number in order to mark the respective bar in the TOCSY spectrum (a). While the percentages of the four aldehyde hydrate species could be quantified by the signal intensities (*S/R-*Phe[7] epimer) and [13]C chemical shifts (*cis/trans-*Pro[6]), the low intensities of the peptide aldehydes signals only gave few cross signals and therefore the* cis-*Pro[6] species (6) and (8) can not be unambiguously identified. The linear species of ncpA1 can be assigned analogously by the Leu[7] signals, but in this case much lower chemical shift dispersions were observed. This possibly indicates a lower extent of peptide preorientation and is discussed in section 3.4.2.*

more than two species are present, and the well-separated aldehyde signals (marked in orange) are of low intensity. In fact, the peptide aldehydes constitute only approx. 5% of all species, and the C-terminal aldehyde hydrates ncpA1-CH(OH)$_2$ and ncpA2-CH(OH)$_2$ dominate under these solution conditions (figure 3.18b).

Evaluation of the ^{13}C chemical shifts in the HSQC spectrum showed that the two sets of signals with highest intensity are not caused by *cis*/*trans* isomerization of the prolyl amide but rather by the epimerization of the α-stereocenter of the C-terminal amino acid. For both peptides, the ratio of epimers was determined to be 64:36 (*cis* as well as *trans* prolyl amides included). At this stage the absolute stereoconfigurations remained unclear, but cyclization experiments (section 3.3.3) finally enabled us to identify the *S*-configuration as the dominating one. The amount of *cis*-Pro is low, constituting 20% of *R*-Phe-ncpA2-CH(OH)$_2$ and only 10% of *S*-Phe-ncpA2-CH(OH)$_2$ and *R*/*S*-Phe-ncpA1-CH(OH)$_2$, respectively. Overall, the presence of aldehydes and aldehyde hydrates which exist as epimeric mixtures and, moreover, exhibit *cis* and *trans* prolyl amide configurations, results in the presence of eight sets of signals. Figure 3.19a shows a section of the TOCSY spectrum of ncpA2-CHO/ncpA2-CH(OH)$_2$ from which signals of each species can be identified, and the respective percentages are shown in figure 3.19b.

The chemical shift influences of aldehyde/aldehyde hydrate functionalization, epimerization and prolyl amide isomerization are mainly restricted to the three C-terminal residues and drop below spectral resolution in the N-terminal tetrapeptide. On the one hand, this facilitates evaluation of the NMR spectra which are less crowded, but on the other hand this restricts the possibilities to observe changes in the composition of the equilibrium as only few signals are separated to sufficient extent. As shown in figure 3.19a, the Phe^7 amide proton of ncpA2-CH(OH)$_2$ is the only amide proton which can be identified clearly for all four aldehyde hydrate species. The corresponding Leu^7 amide proton signals of ncpA1-CH(OH)$_2$ are also well separated but due to significant signal overlap less proton shifts were identified for the linear ncpA1 species. However, the percentages shown in figure 3.19b for ncpA2-CHO/ncpA2-CH(OH)$_2$ apply for the corresponding ncpA1 equilibrium, too.

In the case of both ncp subtypes, the two dominating species are the respective epimers of the *trans*-Pro^6 aldehyde hydrates and they add up to 82% of all equilibrating species. For these compounds, all ^{1}H and non-quarternary ^{13}C chemical shifts were identified by 2D NMR experiments (TOCSY, HSQC, ROESY; fully assigned ^{1}H NMR spectra in figures 3.25 and 3.26; chemical shift tables in section 5.3). Well-separated signals could also be identified for most of the *cis*-Pro and aldehyde species. This provided the basis for structure elucidation (section 3.3.2.5) and cyclization experiments.

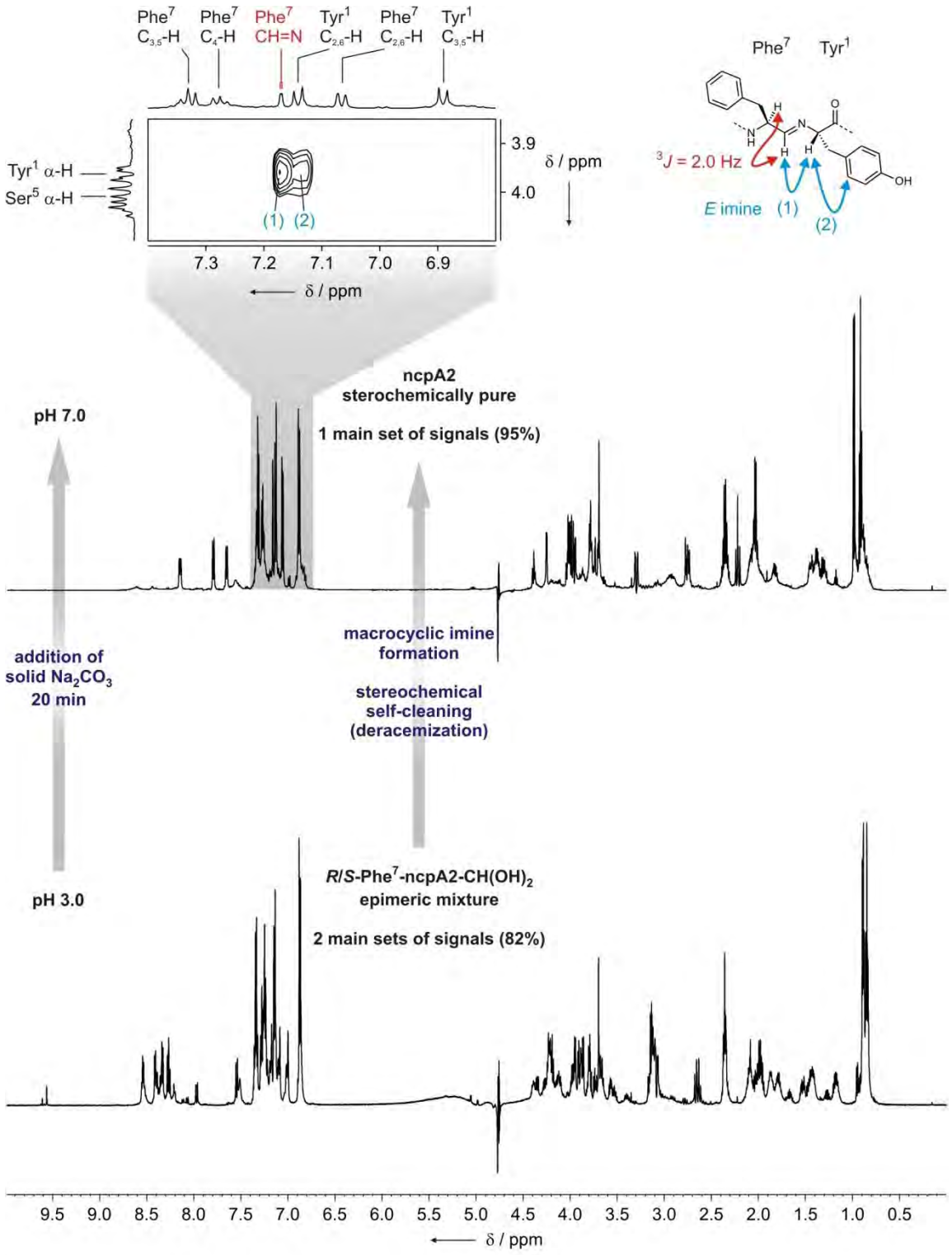

Figure 3.20 Within 20 min. the epimeric mixture of ncpA2 cyclization precursors (R/S)-Phe^7-ncpA2-CH(OH)$_2$ macrocyclizes in the NMR tube and simultaneously deracemizes to one single configuration. *The two main signal sets of the linear peptides at pH 3.0 (lower spectrum) have disappeared and one new main set of signals is obtained 20 min. after the pH has been increased from 3.0 to 7.0 by addition of solid Na_2CO_3 (upper spectrum). All spectra were recorded in partially deuterated phosphate buffer (H_2O/D_2O 5:1, H_3PO_4/KH_2PO_4) at 600 MHz and 300 K using the DPFGSE-WATERGATE water suppression technique. As indicated in the projection of the shown region of the ROESY spectrum, the imine proton is identified by a 2.0 Hz scalar coupling to the Phe^7 α-H in agreement with the literature. The shown ROESY cross signals indicate the* E *configuration.*

3.3.2.3 Macrocyclic imine formation: pH dependence of the equilibria

3.3.2.3.1 Spontaneous cyclizations: monitoring the selective macrocyclization process by NMR

Having elucidated the equilibrium of linear species at pH 3.0 by NMR assignment, attention was concentrated on whether it was possible to perform a macrocyclic imine formation directly in the NMR tube. For this purpose, the pH of the ncpA2 NMR sample was increased from 3.0 to 7.0 by addition of solid Na_2CO_3. 20 min after the pH increase a ^{1}H NMR spectrum was recorded, and the comparison with a spectrum recorded at pH 3.0 showed that the signal sets of linear species had disappeared (figure 3.20). A striking characteristic of the spectrum at pH 7.0 was the presence of one main set of signals, in contrast to the two main sets of signals which were observed at pH 3.0 and which originate from the *S*- and *R*-Phe^7 epimeric aldehyde hydrates (figure 3.21). When the experiment was analogously carried out for the linear precursor of ncpA1, the same observations could be made, and complete macrocyclization is observed after 60 min (time of the first spectrum recorded after pH increase).

In accordance with the literature,[169] the imino tethers formed upon macrocyclization are well-identifiable from the ^{1}H, HSQC and NOESY spectra by the chemical shifts (C<u>H</u>=N: 7.07/7.17 ppm, <u>C</u>H=N 167.4/165.8 ppm (ncpA1/A2) and a small scalar coupling (^3J = 2.0 Hz) to the Leu^7 and Phe^7 α-H, respectively. Furthermore, the *E* configurations of the imines are indicated by a dipolar coupling to the Tyr^1 α-H.[169] Under all temperature and pH conditions applied in later experiments, no other imine signals were observed from the ^{1}H and 2D NMR spectra.

These observations show that the macrocyclization processes of ncpA1 and ncpA2 in buffered aqueous solution (which resembles the pH at physiological conditions) occur quickly and selectively. More importantly, epimeric mixture of linear peptide precursors (which had not been observed in earlier work, presumably due to different solution conditions) are by macrocyclization converted to stereochemically pure cyclic products. This means that the peptides undergo a stereochemical self-cleaning upon macrocyclic imine formation. Figure 3.21 schematically shows the ring-chain tautomerism of the nostocyclopeptides in dependence of the pH, comparing all transformations which are theoretically possible and those that are actually observed. A multitude of NMR experiments with variation of temperature and pH were required to gain this comprehensive picture, and these series of measurements will be described and discussed below.

The presence of only one cyclization product shows a great selectivity for the head-to-tail intramolecular macrocyclization and the reluctance to form dimers or other linear or cyclic oligomerization byproducts. This is remarkable, as intermolecular oligomerization always

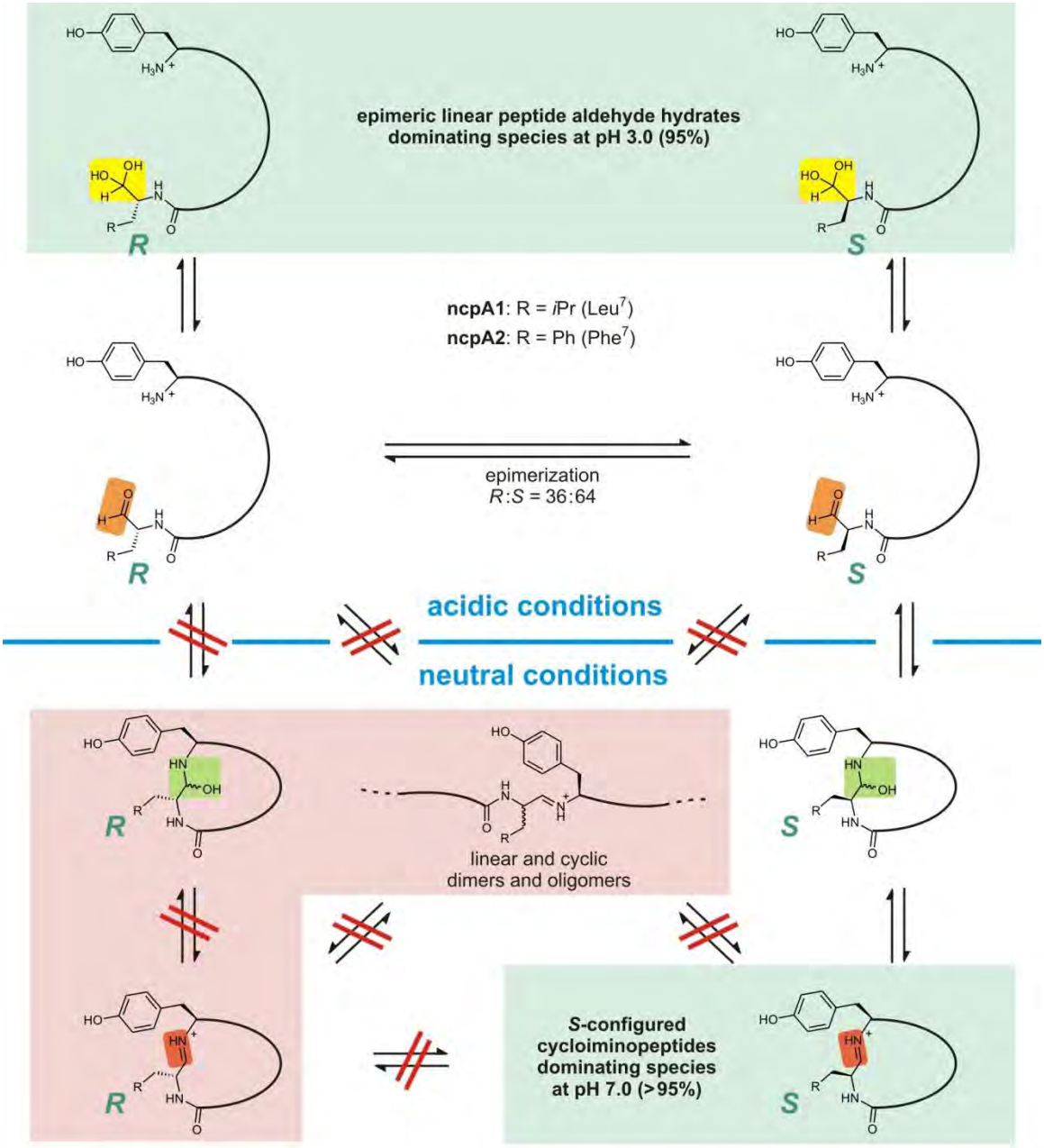

Figure 3.21 Overview of all possible equilibrium transformations in the dynamic covalent linear/cyclic ncp systems. *The scheme identically applies for ncpA1 as well as ncpA2 substrates. Peptides with the* R *configuration at the C-terminal residue are shown on the left, and the column on the right contains all substrates with the dominating* S *configuration. The alignment of linear and cyclic species has been chosen in accordance with the cyclization pathway shown in figure 3.12.*
The NMR experiments suggest that the cycloiminopeptides are exclusively formed by head-to-tail cyclization of the S*-configured aldehyde. All transformations which are not observed are indicated by crossed-out equilibrium arrows. The species which dominate the equilibrium according to the acidic or neutral conditions are highlighted in green, and all species which are theoretically possible to be formed but which are not detected in the NMR spectra are highlighted in red. The epimeric aldehydes exhibit only approx. 5% of all species at pH 3.0, and the* S*-configured cyclic peptide hemiaminal only occurs as unstable intermediate as it has not been indentified in the NMR spectra. In overall, this scheme illustrates the remarkably selective head-to-tail cyclization of the ncp which is accompanied by stereochemical self-cleaning, thus highlighting these peptides as highly optimized evolutionary systems.*

competes with intramolecular ring closure[141, 142] and normally occurs for macrocyclic imines, like the numerous examples studied in the field of supramolecular chemistry.[165] In contrast, the ncp, though highly decorated with stereocenters and functional groups, exhibit simple ring-chain equilibria that are concentration independent in the range studied.

In fact, some low-intensity sets of signals (which at low pH result from *cis*-Pro and aldehyde species, figure 3.19b) are also visible after cyclization, and it cannot be excluded that products of intermolecular imine formations are also present. However, the low intensity of all further signal sets (see also figures 3.25 and 3.26) allows to assume a total amount of byproducts below 5% of all peptide species in the neutral pH range. This is important for NMR evaluation as the comparison of the ^{1}H NMR signal integrals allows to analyze the ratio of all contributing ring-chain isomers quantitatively,[156] which makes the direct monitoring of the equilibria possible. As already outlined in section 3.2.2, the interconversion rates of interest must be slow, but not too slow, on the NMR time scale. This applies for the epimerization of the Leu^7 and Phe^7 stereocenters, the aldehyde/aldehyde hydrate conversions and the *cis*/*trans* isomerization of the Pro^6 amides, as visible from the spectrum depicted in figure 3.19a which shows well-resolved sets of signals for all major contributing species.

In order to determine how fast ncp macrocyclization actually occurs, another 5mM sample of ncpA1-CHO in phosphate buffer was prepared as described in section 3.3.2.1. After optimization of all NMR acquisition parameters, a ^{1}H NMR spectrum was recorded to ensure the presence of only linear species. An amount of solid Na_2CO_3 which was expected to increase the pH from 3.0 to approx. 7.0 was subsequently added, the sample was sealed immediately, shaken for mixing (3 s), and bubbles were removed by ultrasound (3 s). After insertion into the NMR spectrometer, *no* solvent locking, tuning/matching and shimming procedures were applied but a short ^{1}H NMR spectrum (4 pulses, duration 16 s) was recorded as soon as possible. This enabled us to obtain spectral information as early as 110 s after the Na_2CO_3 had been added to the sample. As shown in figure 3.22, by recording spectra at periodical points of time, it was possible to monitor the formation of the stereopure macrocyclic imine from the epimeric mixture of linear aldehyde hydrates. To our knowledge, this is the first example of tracking a biomolecular macrocyclization by NMR. Due to the low signal-to-noise ratio and signal overlap at this pH, the spectra only provide semiquantitative information. Figure 3.22 shows three representative spectral regions (down-field aldehyde and NH region as well as down-field α-H region) and lists all pH changes and the recording time of the spectra (passed time since the last pH change). The NMR signals are assigned yellow (*S*-Leu^7-ncpA1-CH(OH)$_2$), green (*R*-Leu^7-ncpA1-CH(OH)$_2$), red (ncpA1), and grey (further signal sets), respectively. At the beginning, only signals of the linear species are

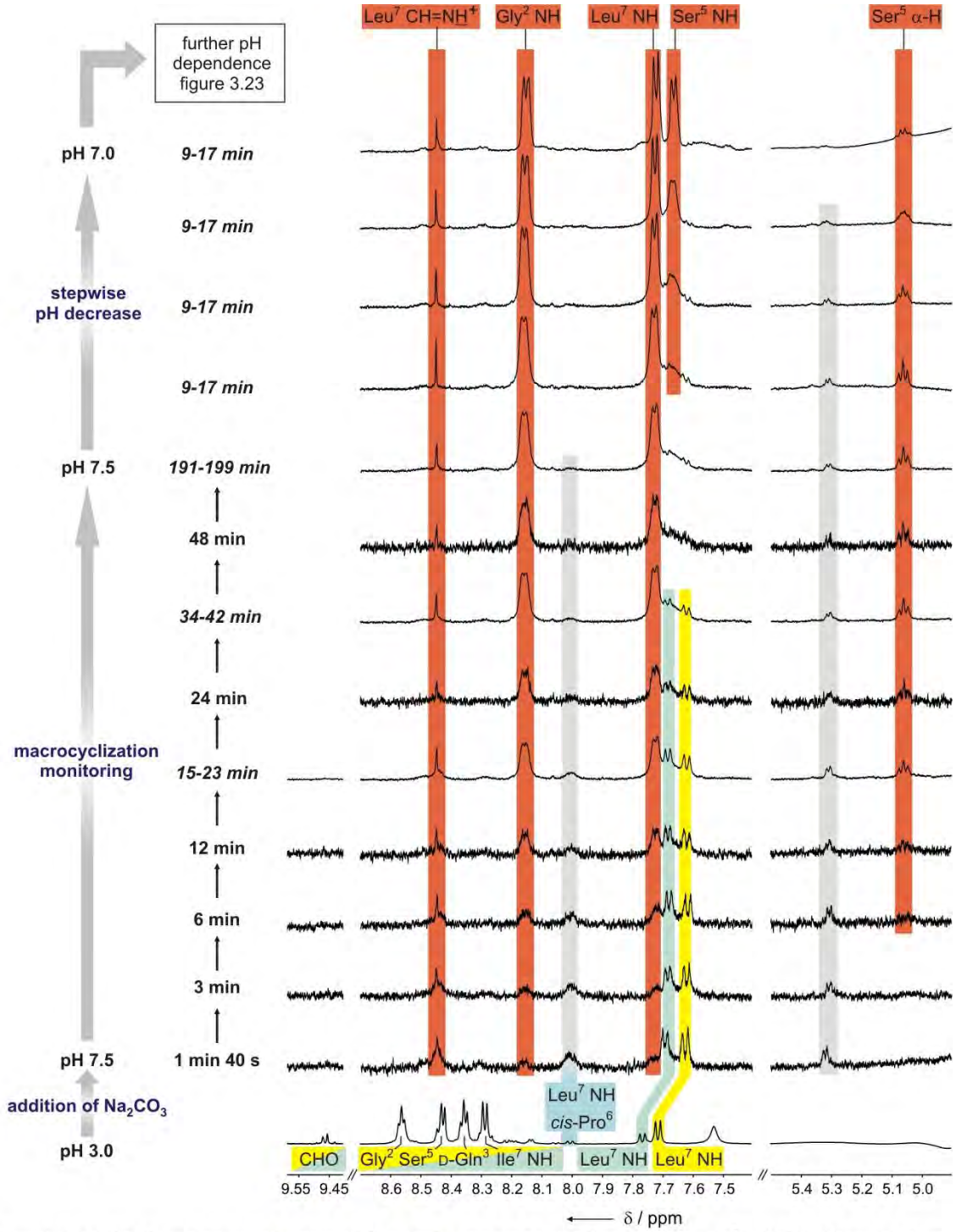

Figure 3.22 Real-in-time monitoring of the ncpA1 macrocyclization process via ^{1}H NMR. *After addition of solid Na_2CO_3 to a sample of the epimeric mixture of linear peptides (spectrum shown at the bottom) ^{1}H DPFGSE-NMR spectra (H_2O/D_2O 5:1, H_3PO_4/KH_2PO_4, 600 MHz, 300 K) were recorded at periodical points of time which are shown in three sections and in temporal order from the bottom to the top. The passed times since the addition of Na_2CO_3 and H_3PO_4, respectively, are written on the left, and for the long-time measurements (identifiable by the lower spectral noise; 128 instead of 4 scans, duration 8 min) the respective time intervals of aquisition are given (italic letters). The signals are highlighted green (linear* R *epimer), yellow (linear* S *epimer), blue (linear* S *epimer with* cis*-Pro^6), red (cyclopeptide) and grey (cyclization byproduct), respectively. The NH signals of the linear species (except Leu^7) are not identifiable after pH increase due to signal broadening. The high pH also causes broadening of the NH signals of the cyclopeptide, as can be seen by the spectra obtained during pH decrease. The* D*-Gln^3 and Ile^4 NH signals are still broadened at pH 7.0 and appear upon further acidification, as visible in the following figure 3.23.*

visible, and the Leu^7 NH dublets are well-separated to quantify the amount of both epimers (64:36). After pH increase, only the Leu^7 NH signals remain visible as the other signals appear strongly broadened. The first measurement (1:40 min) shows that both Leu^7 NH signals (which are slightly shifted up-field upon the pH change) are now similar in intensity, which indicates that one epimer is more quickly removed from the equilibrium than the other one. Though more detailed pH series of measurements (described in the next section) were required to unambiguously assign the stereoconfigurations, this indicates that the up-field signal (yellow) corresponds to the *S* epimer which macrocyclizes to the stereopure cycloiminopeptide. The signals of the macrocycle are already visible after 1:40 min and then increase in intensity as the signals of the linear species decrease in intensity. To obtain a better spectral resolution, a 128 scan ^{1}H NMR experiment (duration 8 min) was started after the first four 4 scan experiments, covering the time span of 15-23 min after pH increase. The signal intensities show that after more than 15 min the macrocyclic imine exhibits the dominating species in the equilibrium, and finally (195 min) the residual signals of the linear peptides disappear within the spectral noise. In the following, the sample was acidified stepwise in order to establish a pH of 7.0. This resulted in a decrease of signal broadening as the Ser^5 NH signal and the dublet structures of the Gly^2 and Leu^7 NH signals become visible.

As can be seen in figure 3.22, no aldehyde species are deteced after pH increase (or the signals are of too low intensity to be visible in the 4 scan ^{1}H NMR spectra) but in addition to the signal set of the cycloiminopeptide, two other weak signals are identified in the spectral region shown (highlighted by grey bars). These signals appear with highest intensity directly after pH increase and subsequently decrease until they are not detectable any more approx. 4 h after pH increase (spectrum at the top). One signal appears at the resonance frequency of the Leu^7 NH signal of *cis*-Pro^6-*S*-Leu^7-ncpA1-CH(OH)$_2$ (8.00 ppm, marked in blue) but it is too strong in intensity to result from a *cis*-Pro^6 species after pH increase. The temporal shift of the intensities suggests another cyclic species which is quickly formed upon pH increase and then slowly is converted to the cyclic main product. Due to the low intensity, no 2D NMR cross signals which could provide further information were obtained. Regarding all possible equilibrium transformations which are theoretically possible, this set of signals possibly results from intermolecular condensation products or *R*-Leu^7 configured macrocycles. The immediate formation after pH increase adds a hemiaminal intermediate as third possibility, and the observed chemical shift (5.31 ppm) in the otherwise empty region is similar to what was observed for the C(OH)NH hemiaminal resonance of Tyrocidine A (section 3.4). Analogous observations were made for ncpA2 where a low signal was detected at 5.43 ppm. However, as the amount of this (and all other) side products did not

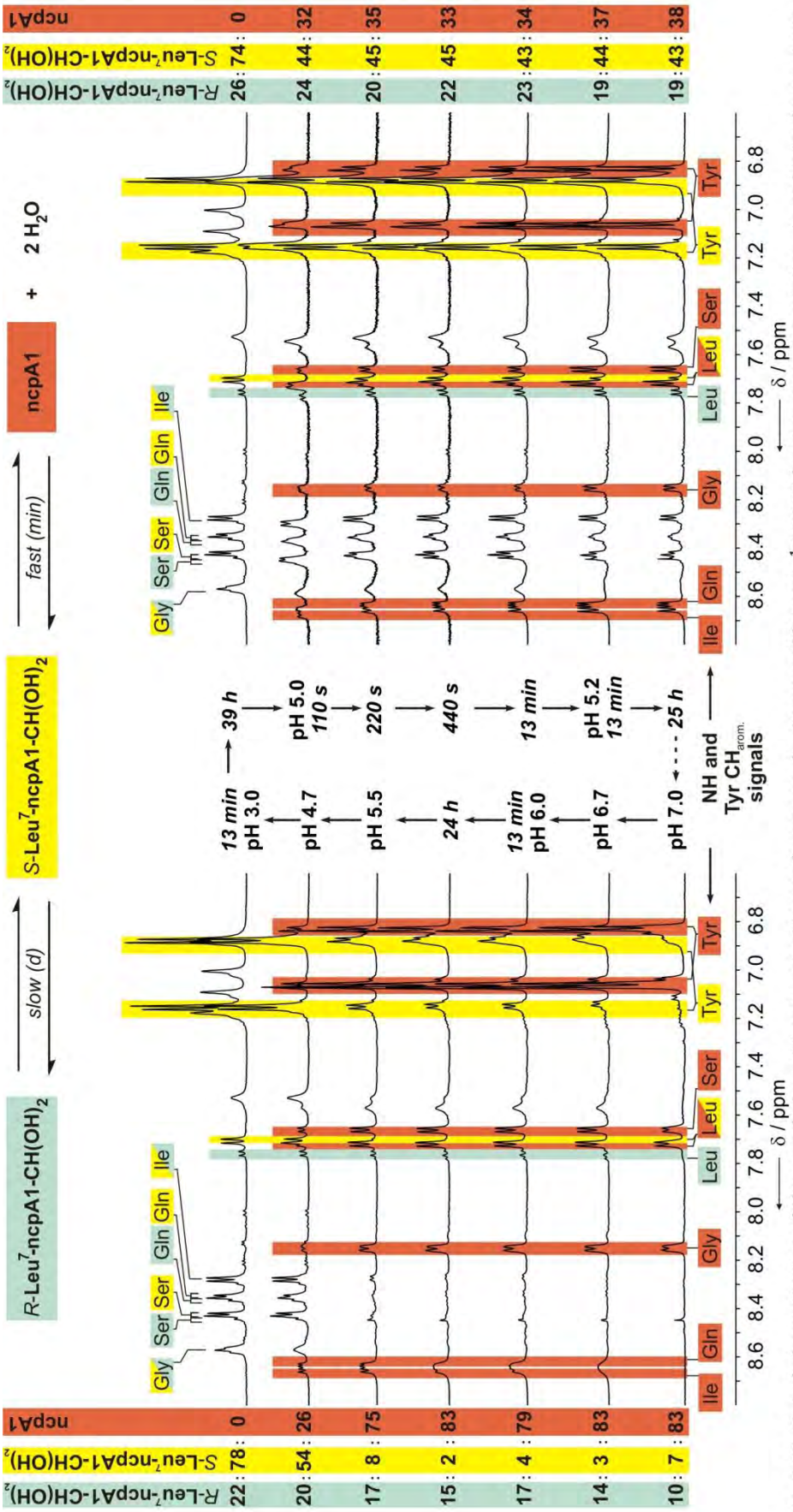

Figure 3.23 ***Detailed monitoring of the coupled ncpA1 epimerization and macrocyclization equilibria via ^{1}H NMR by stepwise pH variation.*** *In order to demonstrate the reversibility of the system, a near-complete pH increase/decrease cycle was performed. Acidification was accomplished by addition of 0.01 M H_3PO_4, and the pH was increased by adding solid Na_2CO_3. Only the NH region of the ^{1}H DPFGSE-NMR spectra containing well-separated signals which can be integrated for a quantitative determination of the equilibrium composition are shown (H_2O/D_2O 5:1, H_3PO_4/KH_2PO_4, 600 MHz, 300 K). The change of relative signal intensities (listed as percentages) shows the existence of two equilibria which are reached on minute (cyclization) and day timescales (epimerization). Low sets of signals are not included in the percentages, and the indication of 0% states that eventual residual amounts of the respective species are below the detection sensitivity. In the following figure 3.24, an analogous investigation of the ncpA2 system is shown.*

exceed 5% during the relevant pH and temperature series of measurements, only the main species had to be considered.

3.3.2.3.2 Quantitative investigations: The pH dependence of ncpA1 and ncpA2 equilibrium

The next task was to determine whether the linear and cyclic ncp species observed so far are in equilibrium with each other. Furthermore, it had to be explored whether the contributing species are interconvertible in a fully reversible equilibrium, which for example implies that the pH value can be changed repeatedly and in different directions. This is important for the experimental planning and for the ability to quantify the percentages of all main contributing species even after several series of measurements. For the investigation of the ncpA1 system, the sample at pH 7.0 investigated for the spontaneous cyclization study (figure 3.22) was subjected to further experiments. In contrast to this experiment, the pH was now increased or decreased step-by-step and 128 scan ^{1}H NMR experiments were subsequently recorded 13 min after pH change. For ncpA1, a near-complete pH cycle (7.0 →3.0 → 5.2) is shown in figure 3.23. Only the NH spectral region is depicted as it exhibits well-separated signals. These allow us to quantify the amount of the three major contributing species within the two coupled equilibrium reactions. The linear peptides *R*- and *S*-Leu^{7}-ncpA1-CH(OH)$_2$ (signals highlighted green and yellow, respectively) slowly epimerize, depending on the pH, within several days. Only the *S* epimer is capable of forming the macrocyclic imine (signals highlighted in red), and the ring-chain equilibrium is established on a minute timescale.

For the quantification of the equilibrium composition it is crucial to identify appropriate signals for every species allows their comparison in terms of their integrals. In the case of both ncpA1 and ncpA2, only the NH signals turned out to be suitable as in the up-field region no separated signals of the *R* epimer exist. For the ncpA1 equilibrium, only the Leu^{7} and Ser^{5} NH signals were compared as signal overlaps and pH dependent signal broadening was observed for the other NH signals (the latter being especially pronounced in the case of D-Gln^{3} and Ile^{4} NH). The calculation procedure is described in detail in section 5.3.

110, 220 and 440 s after every pH change, short control ^{1}H NMR experiments (8 pulses) were recorded before the 128 scan experiments were started. The comparison always showed that upon these slight pH changes the cyclization equilibrium is reached within the 110 s as no differences were observed in the respective series of spectra. As shown in figure 3.23, the stepwise pH decrease from 7.0 to 5.5 did not yield considerable changes in the composition. Below pH 5.5, however, the ncp cyclization equilibria are highly susceptible to pH variation. By decreasing the pH to 4.7, the amount of cyclioiminopeptide drops from 75% to 26%, and 13 min

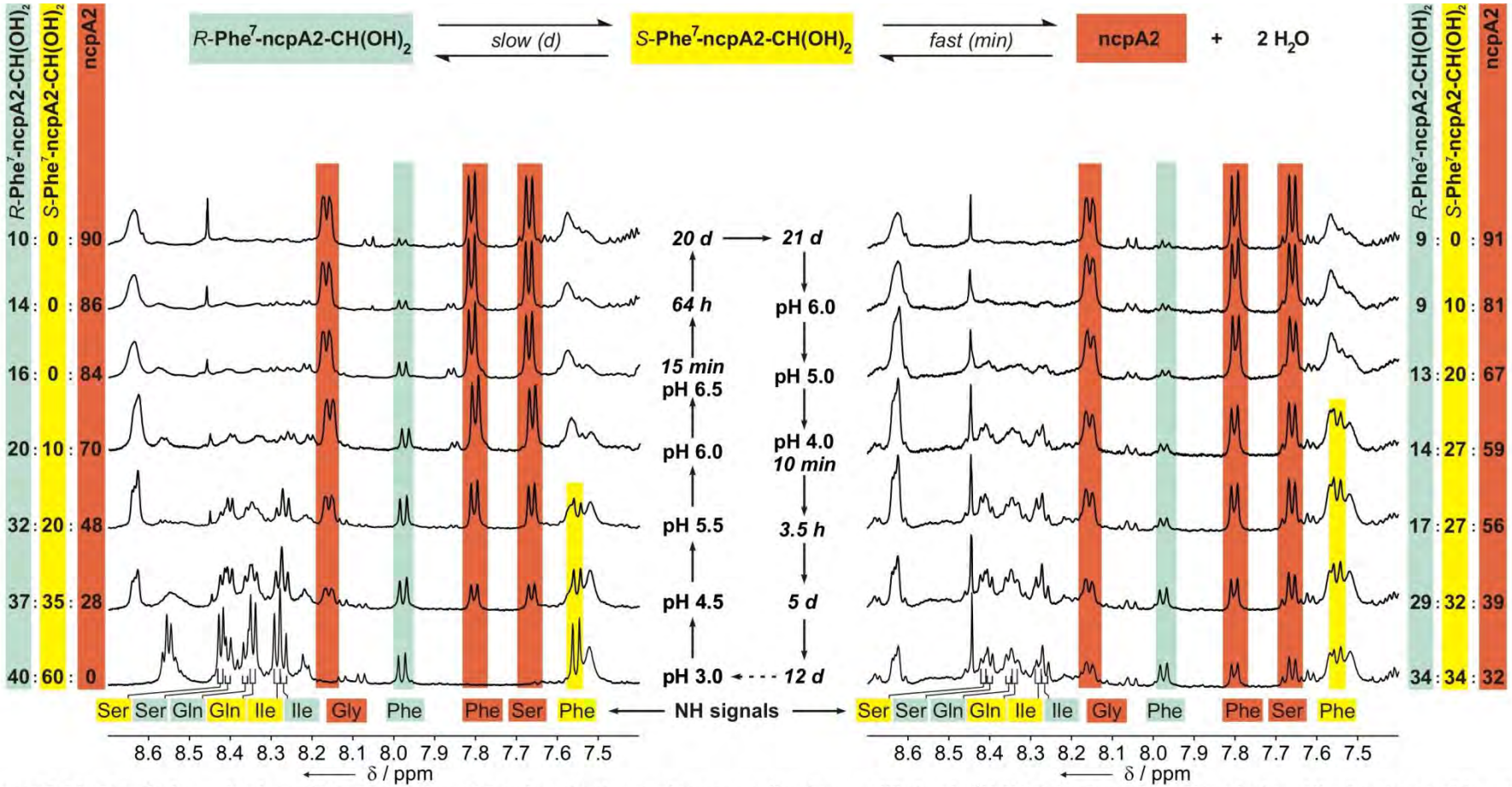

Figure 3.24 Detailed monitoring of the coupled ncpA2 epimerization and macrocyclization equilibria via ^{1}H NMR by stepwise pH variation. *Like for the ncpA1 system (preceding figure 3.23) a near-complete pH increase/decrease cycle was performed in order to demonstrate the reversibility of the system. This series of measurements was carried out in reverse order (increase of the pH and subsequent re-acidification). Only the NH/aromatic proton region of the ^{1}H DPFGSE-NMR spectra containing well-separated signals which can be integrated for a quantitative determination of the equilibrium composition are shown (H_2O/D_2O 5:1, H_3PO_4/KH_2PO_4, 600 MHz, 300 K). The change of relative signal intensities (listed as percentages) shows the existence of two equilibria which are reached on minute (cyclization) and day timescales (epimerization). Low-intensity signal sets are not included in the percentages, and 0% indicates that possible residual amounts of the respective species are below detection sensitivity. The sample at the final pH 5.2 was used for the investigation of the temperature dependence of the ring-chain equilibrium, as shown in figures 3.32 and 3.33.*

after the pH has been set to 3.0 no macrocycles are detected any more. The ring opening has increased the amount of *S*-configured linear peptides to 78%, and only 22% of the epimeric linear peptides are present. During the following hours the slow epimerization equilibrium is shifting towards 74:26 ratio (*S*:*R*), and after 39 h it has effected a 4% increase of the amount of *R* epimer. The opposite process can now be monitored by increasing the pH from 3.0 to 5.0. As only the *S* epimer is capable of macrocyclization, the amount of *R* epimer remains (within measuring uncertainty) constant and does not change during the minutes after pH change. The pH was finally set to 5.2 (identical to an analogously examined ncpA2 sample) so that all contributing main species are present to a sufficient extent in order to compare the signal integrals in a temperature series of measurements (section 3.4.3). As indicated by the dotted arrow, by further decrease of the pH value it is possible to reestablish the starting conditions, resulting in identical NMR spectra. This shows that the system is fully reversible. The only change comparing the conditions before and after this series of measurements is a slightly decreased peptide concentration (due to the addition of aqueous H_3PO_4 for pH decrease). The composition of the equilibria, however, turned out to be concentration independent in the range studied.

The ncpA2 equilibrium system was examined analogously and the spectra are depicted in figure 3.24. In this case, the measurements were started at pH 3.0 and the pH was incrementally increased to 6.5 and subsequently decreased to 4.0. In comparison to the ncpA1 spectra, the NH signals are better separated from each other, which allows to use the Ile^4 and Ser^5 NH signal integrals of the linear peptides. More importantly, the dublets of the epimer signals (D-Gln^3, Ile^4 and Ser^5) are separated from each other far enough to identify the corresponding absolute stereoconfigurations. Upon pH increase, the up-field shifted dublets of D-Gln^3 and Phe^7 NH as well as the down-field shifted dublets of Ile^4 and Ser^5 NH decrease considerably faster in intensity which indicates that these signals correspond to the *S*-Phe^7 configured linear peptide which macrocyclizes to ncpA2. To show how slow the epimerization actually occurs, the composition of the equilibrium at pH 6.5 was observed over 21 d. 15 min after the pH increase, all *S* epimer has been consumed and 16% of the *R* epimer are left. In the following, the amount of *R* epimer further decreases until it reaches 9% after 21 d. No *S* epimer is detected over this time span as it immediately cyclizes to the imine. The slow epimerization process is also well visible after acidification (pH 6.0 → 5.0 → 4.0). As the freshly formed *S* configured linear peptide epimerizes and therefore is slowly removed from the cyclization equilibrium, the amount of cyclopeptide further decreases over several days.

In summary, the ncpA1 and ncpA2 epimerization/macrocyclization equilibria were demonstrated to be fully reversible, and it is possible to regulate the equilibrium compositions by pH variation.

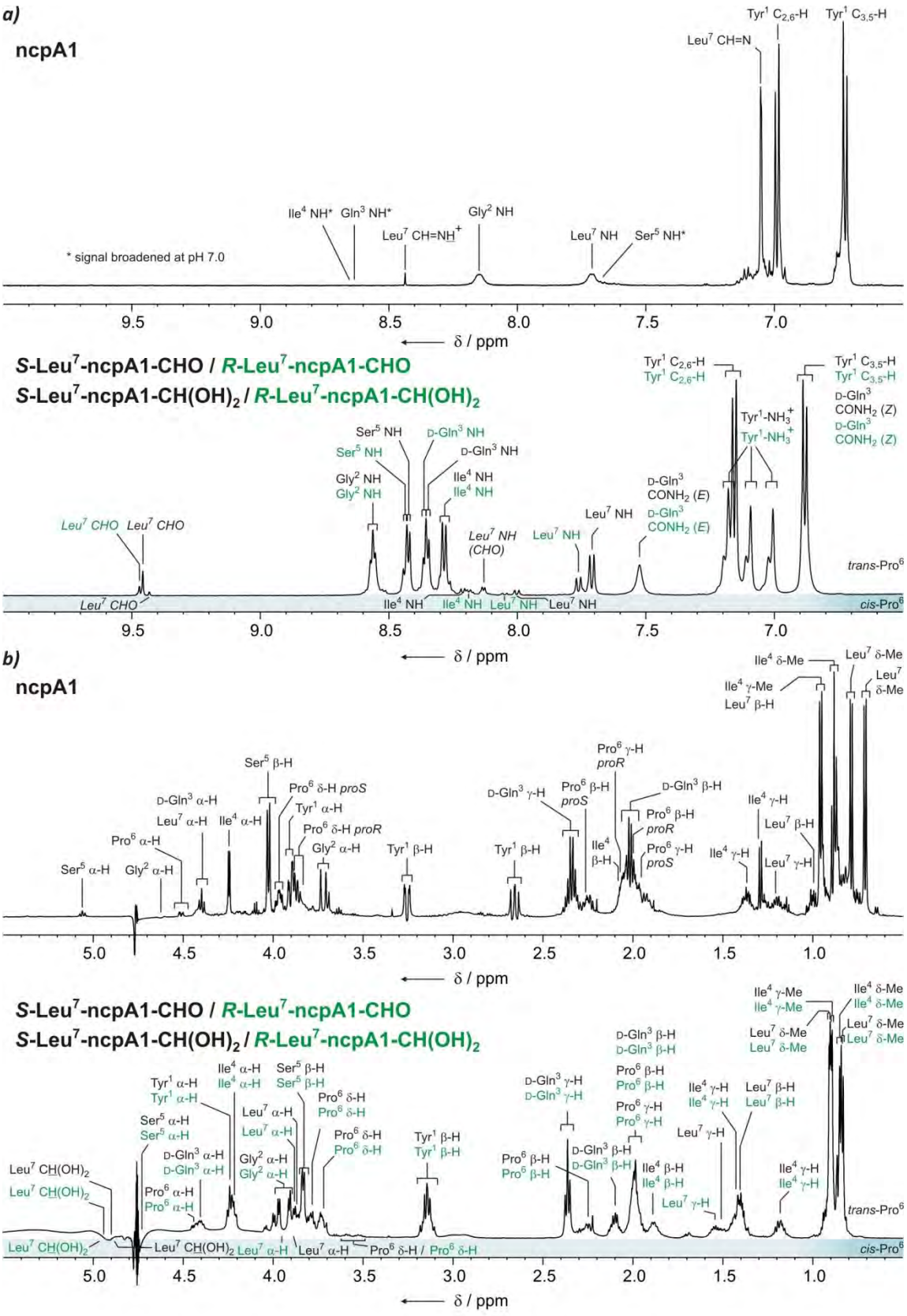

Figure 3.25. *Assigned ^{1}H DPFGSE-NMR spectra (H_2O/D_2O 5:1, H_3PO_4/KH_2PO_4, 600 MHz, 300 K) of* R/S-*Leu*^{7}*-ncpA1-CHO/CH(OH)*$_2$ *(pH 3.0) and ncpA1 (pH 7.0).* ***a)*** *down-field range,* ***b)*** *up-field range.* R *epimer signals are designated green and* S *epimer signals are designated black. Some signals of the linear* cis-*Pro*^{6} *peptides are also assigned in the blue bars.*

Under comparable conditions, both peptide systems appear to be very similar with respect to their compositions and to the timescales on which the equilibria are reached. However, the simultaneous observation of both the ncpA1 and ncpA2 system in one single NMR sample would be required for direct comparison. This option was not tested as the resulting NMR spectra would be too crowded, and no sufficiently separated signals would be available for quantitative investigations. An option for this could be the ^{15}N labeling of the peptides and the integration of $^{15}N/^{1}H$ cross signals in far less crowded 2D NMR specta. This was not tested within the scope of this thesis as it was our intention to work with unlabeled substrates and standard NMR techniques only (which was also the case for the NPY analytics described in section 2).

3.3.2.4 Structure elucidation

In order to examine structural determinants of the remarkable selective cyclization behavior of the nostocyclopeptides, complete NMR assignment and determination of further NMR parameters (scalar and dipolar couplings as well as temperature coefficients) were performed for all major contributing species. Figures 3.25 and 3.26 show the fully assigned ^{1}H NMR spectra of the major contributing ncpA1 and ncpA2 species, respectively. All separated signals of aldehyde and *cis*-Pro^{6} peptides are assigned, too. The corresponding spectral sections at pH 3.0 and 7.0 are always shown stacked in order to allow a direct comparison of the chemical shifts. Furthermore, in section 5.3 all chemical shifts and scalar coupling constants are listed in tables.

3.3.2.4.1 Hydrogen bonding

The temperature dependence of chemical shifts $\Delta\delta/\Delta T$ of amide ^{1}H NMR signals which is given in ppb K^{-1} (ppb = parts per billion) is an important NMR parameter for peptide structure elucidation.[90] The extent of signal shifting gives information about whether the amide protons are located towards the solvent or whether they are shielded by intramolecular hydrogen bonds. So far, most studies have used DMSO-d_6, and under these conditions temperature coefficients greater than approx. 5 ppb K^{-1} indicate solvent coordination while small coeffients (< 2 ppb K^{-1}) are found for amide protons which are located in stable intramolecular bonds.[183] Values in the intermediate region also suggest an intramolecular coordination but which is disturbed by conformational averaging. Only few studies describe the determination of temperature coefficients from aqueous solutions, but it has turned out that similar ranges of temperature coefficient values compared to DMSO are monitored.[184-186]

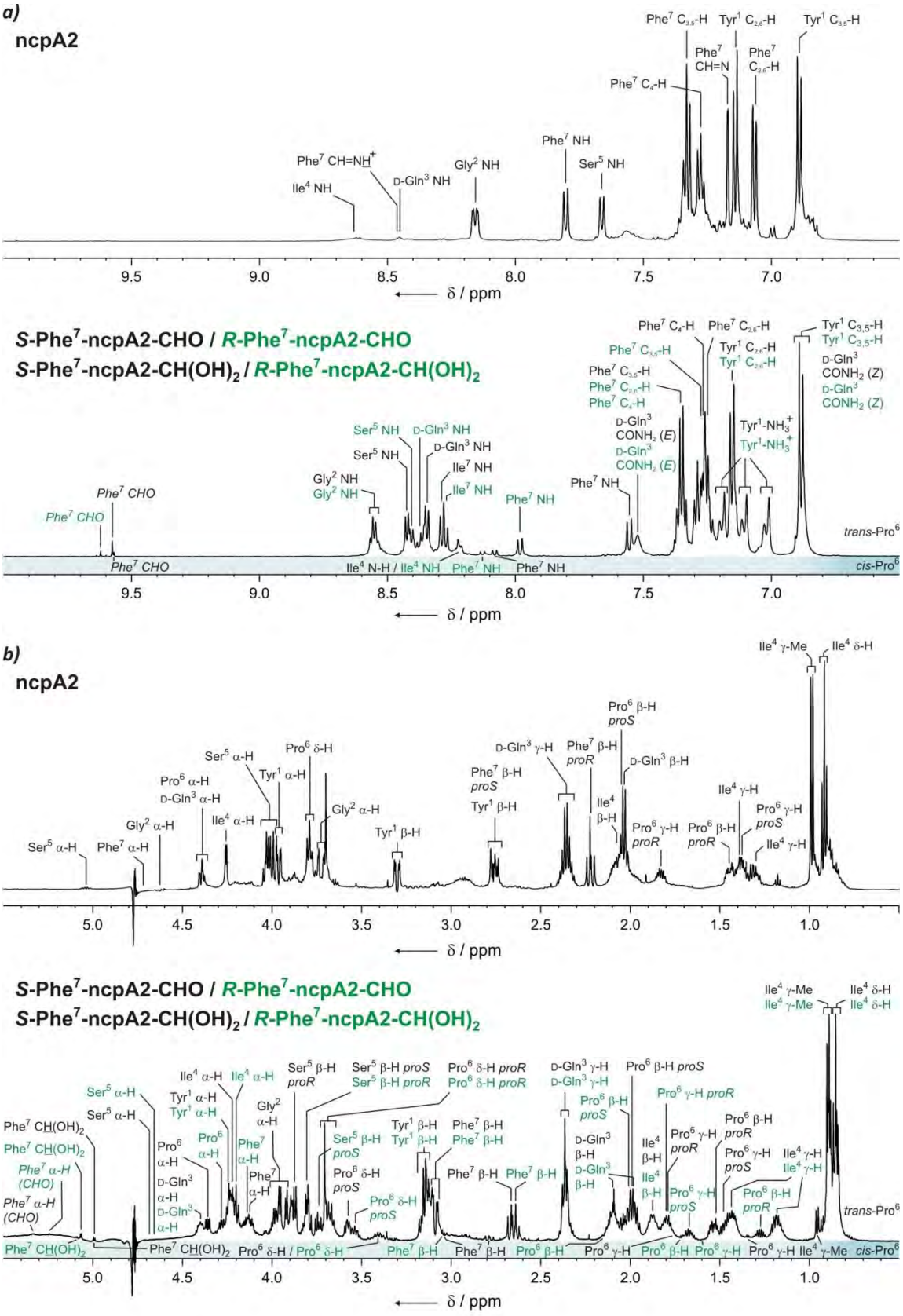

Figure 3.26. *Assigned ^{1}H-DPFGSE NMR spectra (H_2O/D_2O 5:1, H_3PO_4/KH_2PO_4, 600 MHz, 300 K) of* R/S-*Phe^7-ncpA2-CHO/CH(OH)$_2$ (pH 3.0) and ncpA2(pH 7.0).* ***a)*** *down-field range,* ***b)*** *up-field range.* R *epimer signals are designated green and* S *epimer signals are designated black. Some signals of the linear* cis-*Pro^6 peptides are also assigned in the blue bars.*

Therefore, in this work the determination of temperature coefficients could be utilized to identify intramolecular hydrogen bonds in the nostocyclopeptides. For this purpose, spectra of linear as well as cyclic ncpA1 and ncpA2 were recorded at various temperatures (290-320 K in 10 K steps). Figure 3.27a depicts the amide proton regions of the ^{1}H NMR spectra of linear ncpA2 peptide aldehyde (pH 3.0, left) and ncpA2 (pH 7.0, right). By comparison of the extent the signals are shifted upon temperature change, it can be seen that all NH resonances resulting from the linear peptides are similarily susceptible, showing temperature coefficients between −6.1 and −9.3 ppb K^{-1}. In contrast, two of the three identifiable cyclopeptide signals experience lower shifts (Gly^{2} NH: −3.6 ppb K^{-1}, Ser^{5} NH: −3.1 ppb K^{-1}). In figure 3.27b, all determined NH temperature coefficients of ncpA1 and ncpA2 species are written next to the respective positions in the structural formulas. With exception of the C-terminal amide in the linear and the imino tether region in the cyclic peptide, identical or similar values are found for both ncp subtypes. The cyclic structure as it is depicted already interprets the small temperature coefficients of Gly^{2} NH and Ser^{5} NH as a β-turn which is stabilized by the D-configured Gln^{3} in the *i*+1 position.[127] This effects a Ser^{5} NH→Gly^{2} CO as well as a Gly^{2} NH→Ser^{5} CO hydrogen bonding (indicated by red bars) and explains the small temperature coefficients of the respective ^{1}H NMR signals. As values greater that 2 ppb K^{-1} are obtained, the conformation probably is in equilibrium with other backbone geometries that do not exhibit a stable turn motif, but it is plausible to ascribe the shown conformation to the preferred one.

The high temperature coefficients obtained for all NH resonances of the ncpA1 and ncpA2 cyclization precursors indicate the absence of stable intramolecular hydrogen bonding, which is expected for a linear peptide in aqueous solution. Due to the multitude of populated conformations, all amide protons are mainly coordinated towards the abundant solvent molecules, which is why no effect of temporary intramolecular bondings is visible. Regarding the question concerning the extent of structural rigidification upon macrocyclization, the decrease of certain temperature coefficients after ring closure indicates a considerable restriction of conformational flexibility. However, this does not automatically imply that no β-turn can be adopted within the conformation equilibrium of the linear chain. This issue is further investigated in the discussion of the NOE-based calculated structures (section 3.3.2.4.4).

3.3.2.4.2 Conformational differences of the C-termini in the ncpA1 and ncpA2 cyclization precursor

Temperature dependent shifts were also observed for some signals of carbon-attached protons which are neither expected to coordinate with the solvent nor with intramolecular binding

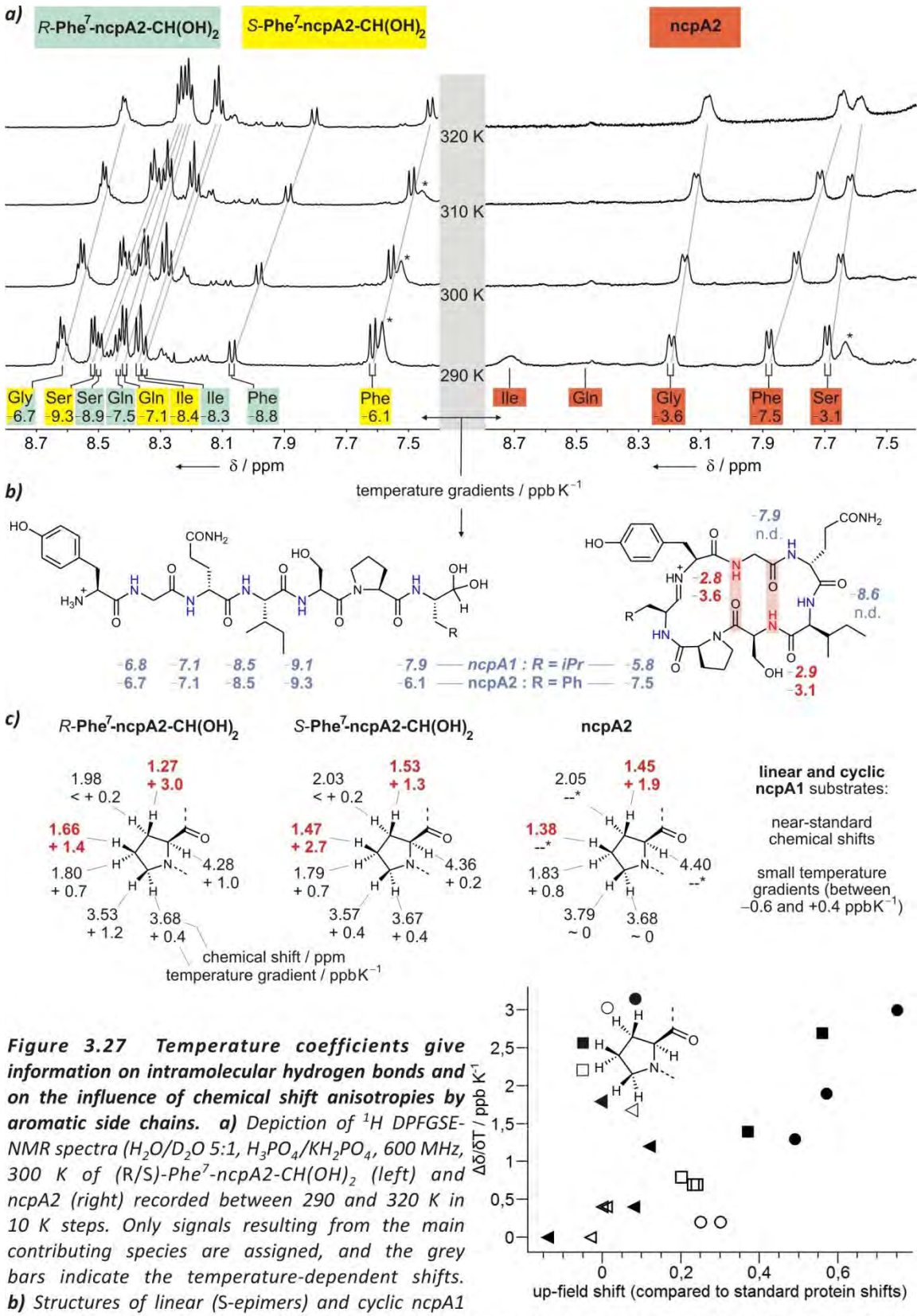

Figure 3.27 Temperature coefficients give information on intramolecular hydrogen bonds and on the influence of chemical shift anisotropies by aromatic side chains. ***a)*** *Depiction of ^{1}H DPFGSE-NMR spectra (H_2O/D_2O 5:1, H_3PO_4/KH_2PO_4, 600 MHz, 300 K of (R/S)-Phe^{7}-ncpA2-CH(OH)$_2$ (left) and ncpA2 (right) recorded between 290 and 320 K in 10 K steps. Only signals resulting from the main contributing species are assigned, and the grey bars indicate the temperature-dependent shifts.* ***b)*** *Structures of linear (S-epimers) and cyclic ncpA1 and ncpA2 assigned with all identified temperature coefficients. The low coefficients obtained for Gly^{2} and Ser^{5} NH indicate the presence of two internal hydrogen bonds.* ***c)*** *Assignment of chemical shifts and temperature gradients in linear and cyclic ncpA2. Plotting the chemical shift deviations from the standard shifts against the temperature coefficients reveals linear dependences. The distinctly greater effect on the "upper" prolyl ring half-space protons (filled icons) can be seen clearly. These results are interpreted in the following figure 3.28.*

partners. The comparison of the temperature coefficients of Pro^6 side chain proton signals with the respective chemical shifts revealed a distinct pattern which is only found for linear and cyclic ncpA2 substrates. Figure 3.27c schematically depicts the Pro^6 side chains of all three main ncpA2 species for which a complete assignment of the pro*R* and pro*S* positions was possible by evaluation of the ROESY spectra. Each proton is assigned with its chemical shift (in ppm, top line) and its temperature coefficient (in ppb K^{-1}, bottom line). Remarkably, all β-H and γ-H protons as well as all δ-H protons in the cyclopeptide are shifted up-field compared to standard chemical shifts.[187] On temperature increase, however, this influence decreases as visible from the positive temperature coefficients, and their magnitudes correlate with the observed extents of up-field shifts, as indicated in figure 3.27c. Interestingly, this effect is especially pronounced for the β-H pro*R* and γ-H pro*S* protons which are located in the same half-space of the prolyl ring (pointing towards the reader in the shown perspective). The Phe^7 stereoconfiguration apparently has some influence as the β-H pro*R* proton is most affected in *R*-Phe^7-ncpA2-CH(OH)$_2$ while the γ-H pro*S* position shows the biggest influence in the *S* epimer. As none of these effects is observed in the linear and cyclic ncpA1 substrates (all Pro^6 proton signals show near-standard chemical shifts and only small temperature coefficients are observed), an influence of the C-terminal Phe^7 is suggested, as shown in Figure 3.28a. It is reasonable to ascribe the effects to the chemical shift anisotropy of the aromatic Phe^7 side chain which interacts with the Pro^6 residue by hydrophobic stacking. This also gives an explanation for the restriction of the strong up-field shifts to the protons located in one half-space of the ring. As the temperature rises, an increased conformational averaging may result in a decreased population of the shown preferred conformation, which leads to a decrease of the up-field shifting influence of the Phe^7 aromatic ring. The presence of a hydrophobic stacking is also suggested by NOE contacts between the Pro^6 and Phe^7 side chains which are, as expected, only observed for the protons located in one half-space of the Pro^6 ring.

To summarize these results with respect to a comparison of ncpA1 and ncpa2, the cyclization precursor of ncpA2 exhibits a preferred conformation of the hydrophobic residues at the C-terminus which may contribute to the preorientation of the linear peptide. The substitution of Phe^7 by Leu^7 in ncpA1, in contrast, leads to the absence of hydrophobic stacking interactions (figure 3.28b). Regarding the envisioned cyclization entropy measurements, it will be interesting to see whether these different extents of preorientation of the C-termini influence the cyclization process (section 3.4.2).

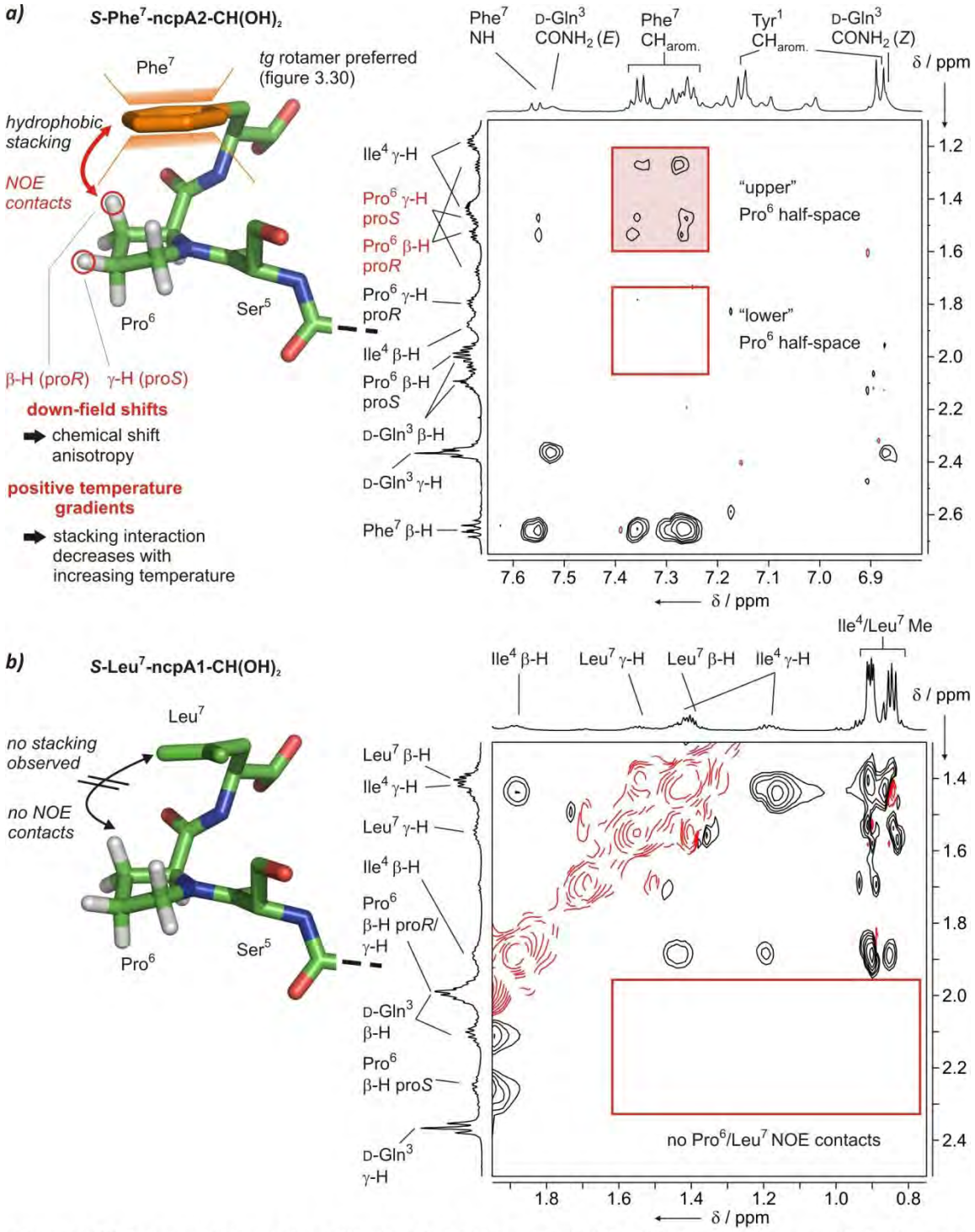

Figure 3.28 Interpretation of the different Pro⁶ CH chemical shifts and temperature coefficients in the linear ncpA1 and ncpA2 substrates. ***a)*** HyperChem *modeled structure (see section 3.3.2.4.4) of the C-terminus of S-Phe⁷-ncpA2-CH(OH)₂. The results obtained by the NOE-based structure elucidation also resulted in a Pro⁶/Phe⁷ hydrophobic stacking, and a preferred population of the* tg *(*trans/gauche*) side chain rotamer of Phe⁷ (section 3.3.2.4.3). The chemical shift anisotropy of the Phe⁷ side chain which decreases at higher temperature upon increased rotational side chain mobility gives an explanation for the observed chemical shifts and temperature coefficients. On the right, the section of the ROESY spectrum containing the Pro⁶/Phe⁷ cross signals is shown (H_2O/D_2O 5:1, H_3PO_4/KH_2PO_4, pH 3.0, 600 MHz, 300 K). The filled red box contains the signals of the Pro⁶ β-H proR and γ-H proS protons, and no NOE contacts are observed for the protons located at the other half-space of the prolyl ring.* ***b)*** *These effects are not observed for the ncpA1 analog (S-Leu⁷-ncpA1-CH(OH)₂, only the side chain has been changed in the calculated ncpA2 structure) and the ROESY spectrum shows no NOE contacts between Pro⁶ and Leu⁷ signals.*

3.3.2.4.3 Side-chain orientations in the cyclopeptides determined by rotamer distributions

The hydrophobic Pro^6/Phe^7 side chain stacking is also observed after cyclization, as indicated by the blue arrows in figure 3.29a. While no NOE contacts were observed between the terminal residues Tyr^1 and Phe^7 in the epimeric linear peptides, after cyclization a spatial proximity of the aromatic protons of Tyr^1 and only one of the two diastereotopic Phe^7 β protons is indicated by NOE contacts (figure 3.29a). This suggested a preferred alignment of the Tyr^1 as well as Phe^7 side chain. In contrast, the absence of Pro^6 and Leu^7 side chain interactions in case of the ncpA1 cyclization precursors also applies for the cyclopeptide. Analogously to ncpA2, NOE contacts indicate the proximity of both terminal side chains but both Leu β-H show contacts with comparable intensity (figure 3.29b).

These side chain interactions were further investiged by analysis of the vicinal scalar coupling constants (^3J). These NMR parameters are important for conformational analysis as they depend on the corresponding torsion angle θ. This relation is given by the *Karplus* equation (figure 3.30a):[188-190]

$$^3J(\theta) = A\cos^2\theta - B\cos\theta + C \qquad (2)$$

The coefficients A, B, and C depend on the substituents and their electronegativites, which is why they actually have to be determined for every molecular surrounding.[191, 192] In an approximation, their values, once they have been determined, can also be used for similar systems. By this approximation and by the ambiguity of the *Karplus* function, however, a torsion angle can only be determined within certain ranges, as indicated by the blue area in figure 3.30a). The interpretation of coupling constants in the medium range must be made with care as such values are often the result of conformational averaging.

By the $^3J_{\beta\text{-H}/\alpha\text{-H}}$ coupling constants the rotational isomerism of amino acid side chains can be analyzed, which is a valuable addition to the information given by the NOE parameters. In contrast to the NOE contacts which can be compared to a “long-term exposure” of the averaging, the coupling constants exhibit a real numeric averaging. Side chains are in most cases subjected to an (on the NMR time scale) quick equilibrium of several conformations. It is possible to determine their relative populations if in an approximation it is assumed that only the three energetically favored staggered rotamers are populated (*gauche*/*trans* (*gt*), *trans*/*gauche* (*tg*), *gauche*/*gauche* (*gg*); figure 3.30b). For the H^β-C^β-C^α-H^α torsion, the constants A = 9.5, B = 1.6 and C = 1.8 are used[191] and the *Karplus* equation gives the minimum (*gauche*,

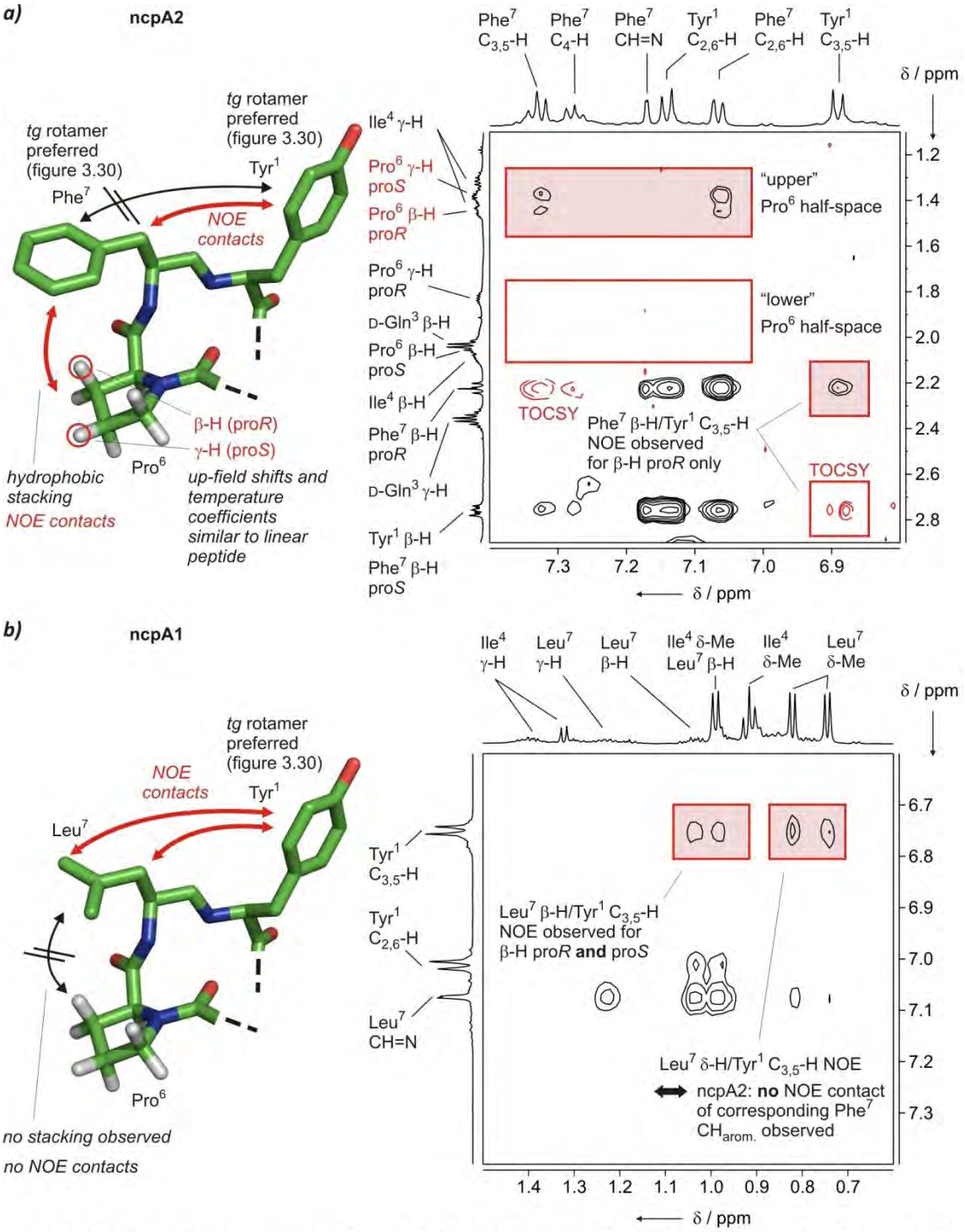

Figure 3.29 Interpretation of the different Pro⁶ CH chemical shifts and temperature coefficients in the cyclic ncpA1 and ncpA2 substrates. ***a)*** HyperChem *modeled structure (see section 3.3.2.4.4) of the C-terminus of ncpA2. Like in the case of the linear peptide, the NOE contacts show a hydrophobic stacking of Pro⁶ and Phe⁷. After cyclization, NOE contacts are also observed between Tyr¹ and Phe⁷. The conformational fixation of the Phe⁷ side chain is indicated by the fact that only one of the diastereomeric Phe⁷ β-H shows an NOE cross peak to the Tyr¹ $C_{3,5}$-H. Like in the preceding figure 3.28, NOE contacts are symbolized by red arrows while the black arrows indicate the lack of NOE cross signals, and corresponding sections of the ROESY spectra are shown on the right (H_2O/D_2O 5:1, H_3PO_4/KH_2PO_4, pH 7.0, 600 MHz, 300 K).* ***b)*** *In ncpA1 (modeled structure of ncpA2 with changed side chain shown) no Pro⁶/Leu⁷ hydrophobic stacking is observed. Instead, the Leu⁷ side chain shows a more pronounced interaction with the Tyr¹ side chain than the corresponding Phe⁷ in ncpA2 and features rotational flexibility, which is visible by the NOE contacts of both diastereotopic protons.*

60°/−60°) and maximum (*trans*, 0°/180°) ^3J coupling constants of 4.3 Hz (^3J_g) and 12.9 Hz (^3J_t), respectively, for the angles present in these rotamers. More detailed analyses allowed specific values to be identified for single amino acid residues. Due to the approximations which are *a priori* included in these considerations, however, it turned out that it is sufficient to use two pairs of minimum/maximum values which are 2.60/13.56 Hz[193] for non-aromatic side chains and 3.55/13.85 Hz[194] for aromatic residues, respectively.[195] This results in a three-equation system which finally gives the populations *p* of the three staggered rotamers:[191, 193]

$$p\,(gt) = \frac{^3J_{\beta-H(proS)/\alpha-H} - {}^3J_g}{^3J_t - {}^3J_g} \tag{3}$$

$$p\,(tg) = \frac{^3J_{\beta-H(proR)/\alpha-H} - {}^3J_g}{^3J_t - {}^3J_g} \tag{4}$$

$$p\,(gg) = 1 - p\,(gt) - p\,(tg) \tag{5}$$

For the Phe[7] residue in ncpA2, the up-field shifted β-H signal (2.22 ppm, $^3J_{\beta\text{-H}/\alpha\text{-H}}$ = 10.7 Hz) was assigned to result from the pro*R* protons while the other signal (2.76 ppm, $^3J_{\beta\text{-H}/\alpha\text{-H}}$ = 4.9 Hz) is generated by the pro*S* protons. The hydrophobic stacking of the Pro[6] and Phe[7] side chains as well as the fact that a NOE contact between the Tyr[1] side chain and exclusively the pro*R* proton is visible, indicates the preferred conformation of the *tg* rotamer (as depicted in figure 3.30b). In fact, the equation system (3)-(5) yields a 69% population for this rotamer while the *gt* and *gg* rotamers are only populated to 13% and 18%, respectively (table 3.2). Due to signal overlap in the spectra of the linear ncpA2 precursor, only the coupling constant of the pro*S* protons could be determined. Yet, these were very similar to the cyclic species (4.7 Hz in both epimers). Using equation (3), a similarly small *gt* population of 11% is calculated, and it is plausible to assume that the *tg* conformation is also preferred in the linear peptides. While no coupling constants could be unambiguously identified for the Leu[7] side chain β protons in linear and cyclic ncpA1, the Tyr[1] β-H/α-H scalar coupling was determined for all linear and cyclic substrates (section 5.3) which revealed a considerable difference in rotational mobility of the side chain before and after ring closure (table 3.2). Coupling constants of 7.3 Hz indicate a conformational averaging in the linear peptides, but within the macrocycle, side chain rotation is restricted, and the non-averaged coupling constants of 3.4/11.6 Hz (ncpA1) and 3.5/11.2 Hz (ncpA2) suggest a 78% (ncpA1) and 74% (ncpA2) population of the *tg* rotamer while the *gt* conformation is hardly adopted.

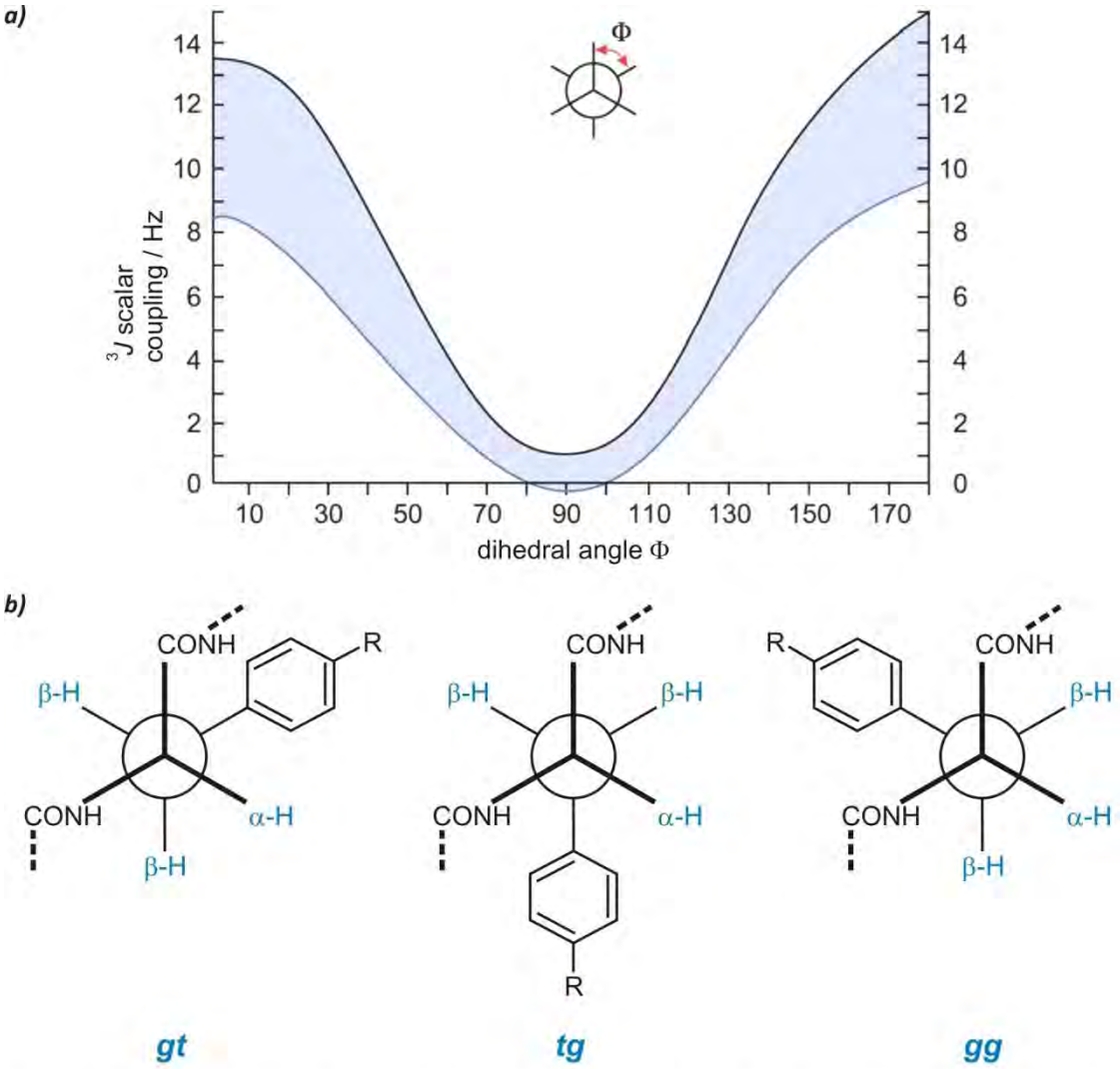

Figure 3.30 Determination of aromatic side chain rotamer distributions from scalar coupling constants. ***a)*** *Graphical depiction of the* Karplus *relation (equation (2)) for saturated hydrocarbons (according to ref. [189]). The lower curve (blue) corresponds to the calculated values and the blue area indicates the range in which the values are actually found. While a torsion can be determined within a single range for small (approx. lower than 2 Hz) and big (approx. larger than 9 Hz) scalar couplings, it can be within two possible ranges for intermediate values. In addition, such coupling constants can also represent averaged values due to conformational dynamics.* ***b)*** Newman *projections of the staggered side chain rotamers of Phe (R = H) and Tyr (R=OH). The scalar coupling constants between α and β protons (highlighted in blue) can be used to calculate the populations if it assumed that only these three staggered conformations are adopted (equations (3)-(5)). The results obtained for the aromatic side chains of ncpA1 and ncpA2 are listed in the table below.*

Table 3.2 Rotamer distributions (gt : tg : gg) of linear and cyclic ncpA1 and ncpA2 species.
The corresponding scalar coupling constants are given in tables 5.7 and 5.8.

position	*R*-Leu^7-ncpA1-CH(OH)$_2$	*S*-Leu^7-ncpA1-CH(OH)$_2$	ncpA1	*R*-Phe^7-ncpA2-CH(OH)$_2$	*S*-Phe^7-ncpA2-CH(OH)$_2$	ncpA2
Tyr^1	averaged [1)]	averaged [1)]	0 : 78 : 22	averaged [1)]	averaged [1)]	0 : 74 : 26
Phe^7	--	--	--	restricted [2)]	restricted [2)]	13 : 69 : 18

1) Both protons showed average coupling constants of 7.3 Hz (ncpA1 species) and 7.2 Hz (ncpA2 species), respectively, which results from unhindered side chain mobilities with equal population of all three rotamers.

2) Only the pro*S* coupling constant could be determined, which only differs in 0.2 Hz from the respective value of the cyclic species. Thus, similar rotamer populations as in ncpA2 can be assumed.

3.3.2.4.4 NOE-based molecular modeling

As the remarkable cyclization behavior of the ncp was expected to correlate with their amino acid composition, the solution conformations of *S*-Phe^7-ncpA2-CH(OH)$_2$ and ncpA2 were determined by molecular modeling. For this purpose, NOE contacts as determined from the ROESY spectra were converted to the corresponding interproton distances which served as restraints for molecular dynamics simulations using the program package *HyperChem*[86] (section 2.3.2.2; calculation details given in section 5.3). Due to signal overlap and low signal intensities, the structure of the linear *R* epimer was not calculated. Figure 3.31a shows the overlay of ten snapshots obtained for *S*-Phe^7-ncpA2-CH(OH)$_2$ (left) and for ncpA2 (right) which gives an impression of the relative side chain mobilities. A conspicuous detail of the linear overlay is the greatly reduced rotational mobility of the C-terminal Phe^7 side chain (hydrophobic stacking to Pro^6) in contrast to the Tyr^1 side chain at the N-terminus. As it was also suggested by the Pro^6 side chain CH temperature coefficients, the Pro^6/Phe^7 stacking occurs similarly in the linear as well as the cyclic peptide. The Tyr^1 side chain is restricted in its rotation after cyclization but still more flexible than the Phe^7 side chain. This is in accordance with the ROESY spectra which, in addition to the spatial proximity of the Tyr^1 aromatic ring to the Phe^7 pro*R* β-H, showed a weak transannular coupling to the Ser^5 β position.

After the average structures had been calculated, they were allowed to relax without the restraints in order to verify the plausibility of the structures. The final energy-minimized average structures are shown in figure 3.31b (left: *S*-Phe^7-ncpA2-CH(OH)$_2$, right: ncpA2). Importantly, the outcome of the calculations supports the presence of the β-turn in the cyclopeptide which effects a planarized alignment of the Gly^2-D-Gln^3-Ile^4-Ser^5 tetrapeptide. In a cyclohexapeptide, the remaining two residues could be incorporated into this structure by another β-turn. As in the ncp one additional amino acid has to be included, the peptide backbone kinks at the Ser^5 ψ torsion which introduces an α-turn fixed by the hydrogen bond between Ser^5 CO (*i* position) and Gly^2 NH (*i*+4 position). This turn motif is also supported by the positions of Pro and Tyr which are often found to be localized in α-turns at the *i*+1 and *i*+3 position, respectively.[196] In principle, an additional interaction of the iminium proton (CH=N<u>H</u>) with the Ser^5 CO is also conceivable.

The backbone geometry of the macrocycle effects a non-uniform spatial distribution of the side chains. While the Tyr^1 and Ser^5 side chains are oriented above the plain which can be defined by the β-turn, the three unpolar Ile^4, Pro^6 and Phe^7 motifs are rather located along one long side of the antiparallel backbone alignment (in the foreground from the perspective depicted in

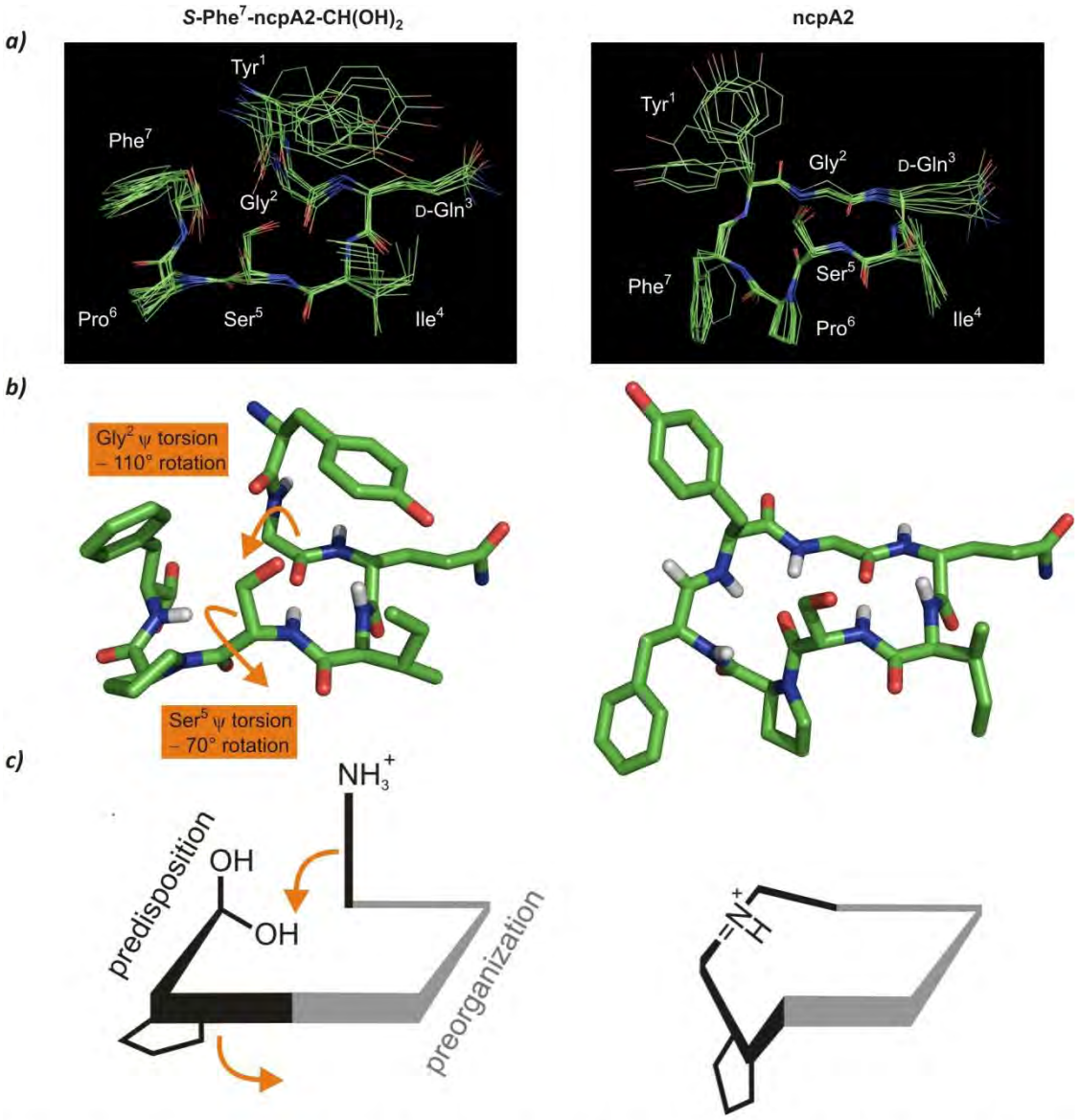

Figure 3.31 Comparison of the NOE-based calculated structures of S-Phe^7-ncpA2-CH(OH)$_2$ (left) and ncpA2 (right). ***a)*** *Overlays of ten snap shots (taken in 10 ps steps) of the molecular dynamics simulations with the NOE contacts as structural restraints (see section 5.3 for details) showing the relative rotational mobilities of the side chains.* ***b)*** *Energy-minimized average structures shown from the same perspective as in a). Carbon atoms are shown in green, oxygen atoms in red, and nitrogen atoms in blue. For clarity reasons, only the backbone protons are depicted (in white). Only few considerable differences before and after energy minimization were observed, and these mainly resulted from distances with the terminal and thus more mobile Tyr^1 or Phe^7 side chains involved, which speaks for the plausibility of the structures obtained (all values listed in tables 5.13 and 5.14). The conformational reorganization which is required for macrocyclization is accomplished by the change of two backbone torsions which are indicated by orange arrows in the linear structure.* ***c)*** *Schematic illustration of peptide backbone, Pro residue and reacting functional groups of S-Phe^7-ncpA2-CH(OH)$_2$ and ncpA2. The changes in backbone geometry upon cyclization give evidence of two distinguishable areas. The intermediate segment does not change its shape notably and is thus already preorganized for cyclization (shown in grey). In contrast, the alignment of both terminal segments (shown in black) changes, as the backbone kinks at Gly^2 and Ser^5 to sterically allow the heptapeptide macrocycle formation. Therefore, they are predisposed for cyclization as they, embedded in the hook-like main conformer, can adopt a certain preferred conformation which finally enables ring closure. As Pro^6 was used instead of the naturally occurring 4-MePro^6, the calculations were also performed with this modification. The presence of a methyl group at the Pro^6 γ position possibly further strengthens the hydrophobic stacking interaction with the Phe^7 side chain.*

figure 3.31b). This leads to a highly solvent-exposed backbone in the segment from Tyr[1] to D-Gln[3], and the alone-standing D-Gln[3] side chain with the amide function appears as an extension of the backbone functionality. In the light of the still unknown biological function of the ncp, this raises the question whether the exposed backbone section can exert any binding function or whether an amphiphilic character might be important.

Comparison of the geometry of the macrocycle to the average structure of the linear precursor (figure 3.31b, left) reveals that the β-turn motif is already preformed to some extent. This was not suggested by the temperature coefficients but the backbone NOE restraints as well as the absence of any D-Gln[3]/Ile[4] side chain/side chain NOE contacts indicate that, within the inherent conformational flexibility of the linear chain, a β-turn-like geometry is favored as an effect of the specific amino acid composition. To transfer the terminology used in Dynamic Covalent Chemistry,[142] this segment is *preorganized* for macrocyclization as it already exhibits the geometry which is required for the covalent tethering of both chain ends (figure 3.31c, see also sections 3.1.2 and 3.2.3). The two terminal dipeptides, in contrast, adopt significantly different average spatial orientations before and after ring closure. The kink at the Ser[5] ψ torsion is not present, and instead the N-terminal Tyr[1] is oriented above the β-turn plane by an approx. −90° Gly[2] ψ torsion. The alignment of the aldehyde hydrate (in relation to the preorganized β-turn motif) is already similar to the position of the imino tether after ring closure. This orientation is possibly crucial for the efficient and selective macrocyclization, and the backbone rigidification induced by the Pro[6] residue may play an important role. Further contributions may result from the Pro[6]/Phe[7] hydrophobic stacking. As this is missing in the ncpA1 precursor, this should result in a less distinctive alignment of the C-terminus.

Overall, a globular geometry is found for the linear peptide where both chain ends are already located close to each other. The macrocyclization is primarily triggered by two torsional changes in the backbone. In order to place the seventh amino acid within the antiparallel mini β-sheet structure, the backbone kinks at the ψ torsion of Ser[5] which gets apparent by the over 70° change of this angle. Importantly, this does not affect the position of the aldehyde hydrate and now allows the N-terminal Tyr[1] to snap into the emerging macrocycle. The Gly[2] is crucial for this process as it acts like a hinge, and the head-to-tail tethering is enabled by a 110° change of its ψ torsion. According to this, the terminal dipeptides are *predisposed* for cyclization (figure 3.31c). This means that they, being embedded in the hook-like main conformer, can adopt a certain preferred conformation which finally enables the ring closure. The depicted backbone geometries obtained for the ncpA2 substrates also apply for the

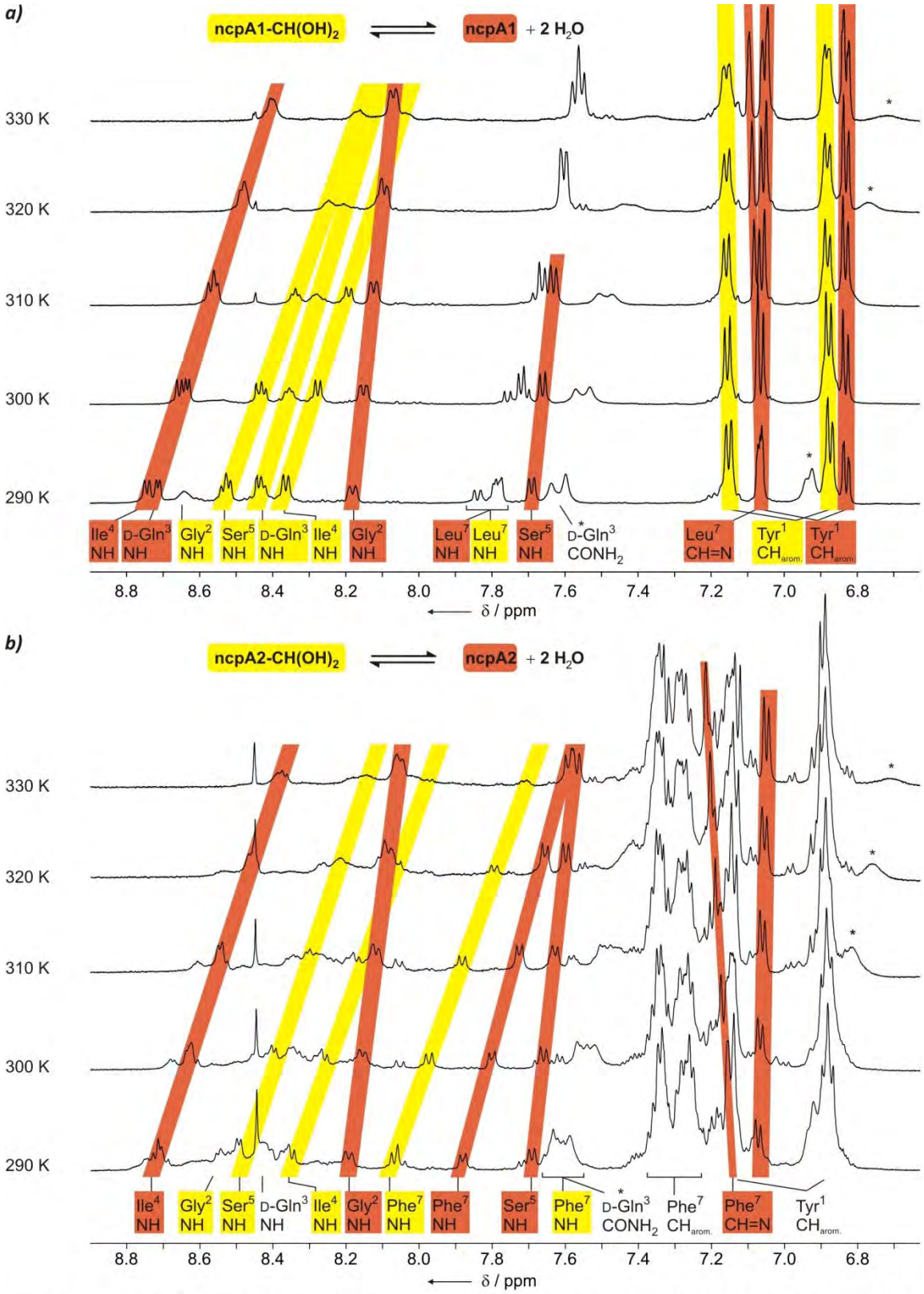

Figure 3.32 (see also next page) Monitoring of the temperature dependence of the ncp ring-chain equilibria via NMR. *The aromatic side chain and amide proton section of ^{1}H DPFGSE-NMR spectra (H_2O/D_2O 5:1, H_3PO_4/KH_2PO_4, pH 5.2, 600 MHz, 290-330 K in 10 K steps) are shown for the equilibrium of ncpA1* ***(a)*** *and ncpA2* ***(b)****. Signals resulting from linear peptides (*R *as well as* S *epimers) are marked yellow and cyclopeptide signals are marked red. Due to crowding and temperature-dependent shifts of the NH signals, this spectral section was not used for quantitative evaluation. The comparison of the signal intensities, however, indicates that more cyclopeptide is formed at higher temperature.*

respective species of ncpA1, as no noticeable differences in the NMR parameters were found. Taken together, the results reveal that an effective cyclization process as it is observed for the ncp relies on an appropriate combination of preorganized and predisposed areas. The preorganized β-turn motif induces a globular conformation which reduces the average distance between the reactive ends of the linear chain within the conformational equilibrium. However, the flexibility of the predisposed terminal dipeptides is equally important as conformational changes are the prerequisite to close the seven-residue macrocycle by adding an α-turn motif to the mini-β-sheet geometry. While the β-turn is preorganized to a comparable extent in the linear cyclization precursors of both ncpA1 and ncpA2, the difference with respect to the C-terminal segments is far from negligible as the Pro^6/Phe^7 hydrophobic stacking observed for *R*/*S*-Phe^7-ncpA2-$CH(OH)_2$ is absent in the ncpA1 analogs where Phe^7 is substituted by Leu^7.

3.3.3 The entropy balance of ncp macrocyclization

3.3.3.1 General considerations and experimental setup

With respect to the different preorientation levels of the ncpA1 and ncpA2 cyclization precursors, the question arises how much influence is exerted on the cyclization entropy balance by non-covalent interactions. This served as another motivation to use the ncp ring-chain equilibria for the first thermodynamic analysis of a biological macrocyclization. As it was described in the previous section, NMR parameters give a detailed picture of mediated *local* relative orientations and the dynamics of side chains. Yet, they can by themselves not provide the desired thermodynamical data of macrocyclization which affects the *global* mobility of the peptide by linking both backbone ends: it is the temperature dependence of the ring-chain isomerism which is key to a quantitative insight into the cyclization process. This can be accomplished by comparing the percentages of linear and cyclic species from ^{1}H NMR signal integrals. Consequently, a pH value should be chosen at which both linear and cyclic species are present to considerable extent. This is important as the integration of low-intensity signals (and comparison with signals of higher intensity) is more prone to errors, especially if, as in the case of the ncp systems, low-intensity sets of signals are present. Furthermore, sufficiently separated signals are required for each species. This turned out to be far from trivial as the presence of three main species (linear *R* and *S* epimer as well as macrocycle) leads to a high signal density of the ^{1}H NMR spectrum. Finally, the fact that an epimerization equilibrium is coupled with the ring-chain tautomerism also has to be included in the evaluation.

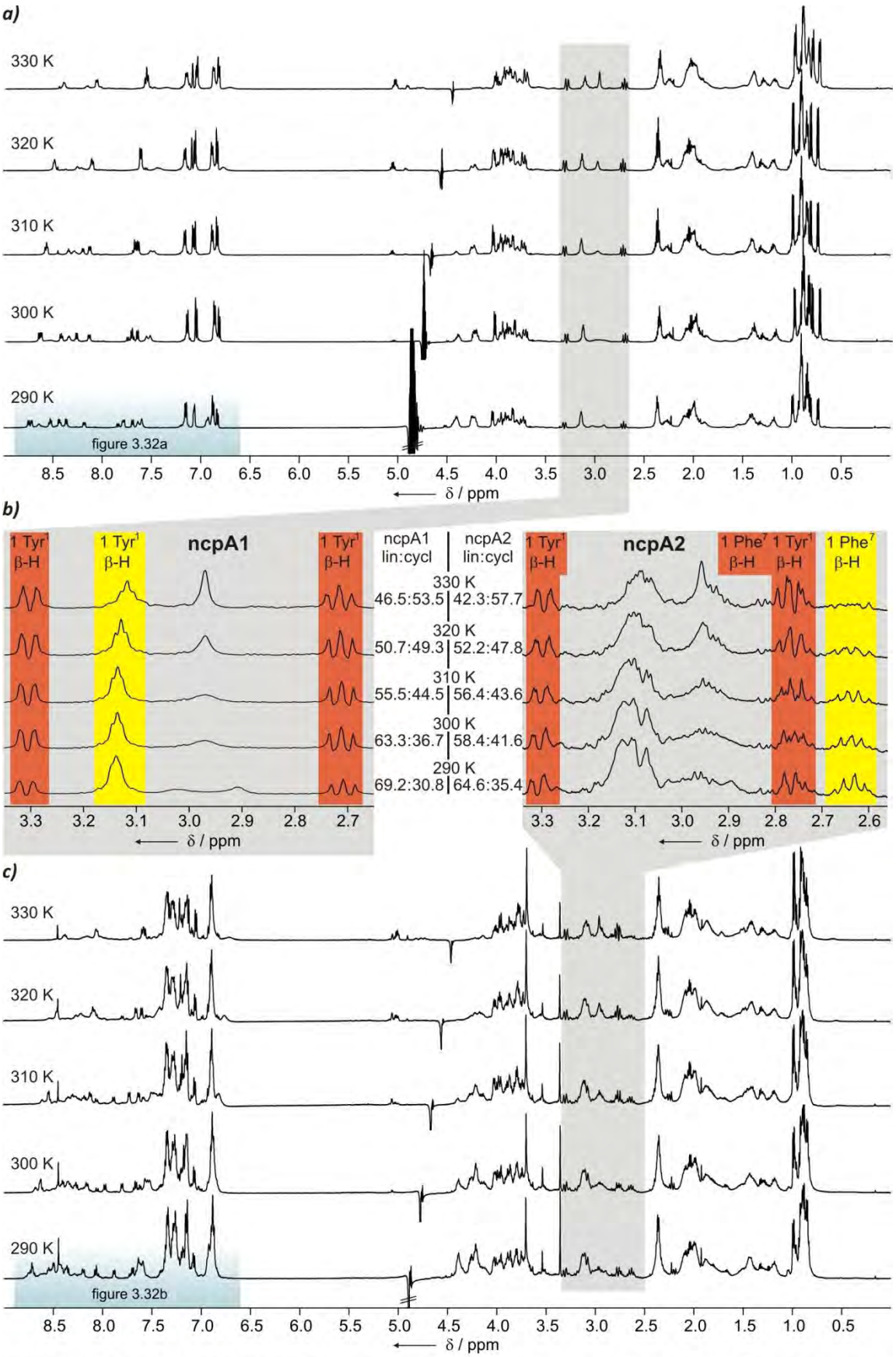

Figure 3.33 (see also previous page) Monitoring of the temperature dependence of the ncp ring-chain equilibria via NMR. *The complete ^{1}H-DPFGSE NMR spectra are shown in* ***(a)*** *for the ncpA1 and in* ***(c)*** *for the ncpA2 system. The sections with the β-H signals used for integration and the percentages are shown in* ***(b)****.*

3.3.3.2 Experiments and results

3.3.3.2.1 Determination of the temperature-dependent equilibrium compositions

Two samples of ncpA1 and ncpA2, respectively, were brought to pH 5.2 at the end of the series of measurements which concerned the pH dependence of the equilibria (figures 3.32 and 3.33). This pH value was chosen because sufficient amounts of both linear and cyclic species are present. The samples were allowed to equilibrate for 1 h at the respective temperature (10 K steps between 290 and 330 K), and ^{1}H NMR spectra were subsequently recorded and analyzed for suitable signals that allow for comparison of the corresponding ^{1}H NMR signal integrals. The NH regions of the spectra at the different temperatures are compared in figure 3.32. All signals resulting from the cyclopeptides are marked red and signals of the linear peptides are highlighted yellow (no difference is made between the *R* and *S* epimers, which will be explained later in the text). In fact, the qualitative comparison shows that upon temperature increase the intensities of the cyclopeptide signals grow while the signals resulting from the linear peptides are decreasing. The temperature dependent shifts of the NH chemical shifts, however, hamper the identification of low-intensity signals, and there are no signals and hardly any signal groups which are well-separated at all temperatures, which precludes the use of NH signal integrals for the quantitative determination of the linear/cyclic ratio. As an accurate comparison of ncpA1 and ncpA2 is only possibly by using analogous signals, Tyr^{1} side chain signals (which appear separated in the ncpA1 spectra) cannot be utilized as the presence of another aromatic side chain in ncpA2 (Phe^{7}) leads to high crowding in this area. This is further complicated by the presence of broad D-Gln^{3} primary amide signals (marked by *).

Based on these considerations, the relatively empty spectral regions around 3 ppm containing the Tyr^{1} and Phe^{7} β-H signals were chosen for evaluation (figure 3.33). For ncpA1 as well as ncpA2 the comparison of one linear peptide and two cyclopeptide signal integrals was possible at all temperatures (see section 5.3 for details), and the obtained ratios of linear/cyclic species are written next to the β-H spectral sections (figure 3.33b). For ncpA1, the percentages were compared to the results obtained by the integrals of the Tyr^{1} aromatic proton signals (figure 3.32a), and the deviations were found to be within the measuring uncertainty of approx. 5%.

The equilibrium compositions indicate that both peptides, in spite of the different local dynamics at the C-termini, exhibit almost identical cyclization behaviour. With increasing temperature, the amounts of cyclopeptides grow almost at the same rate and in a near linear manner, yielding approx. 6% more cyclopeptide per 10 K. In both cases, an approx. 1:1 mixture of linear and

a) ncpA1, pH 5.2

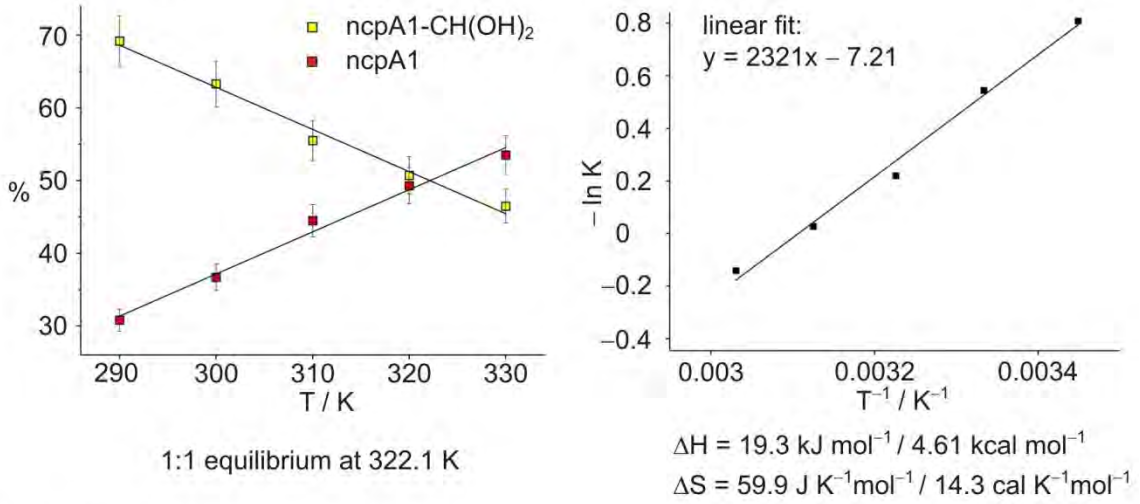

b) ncpA2, pH 5.2

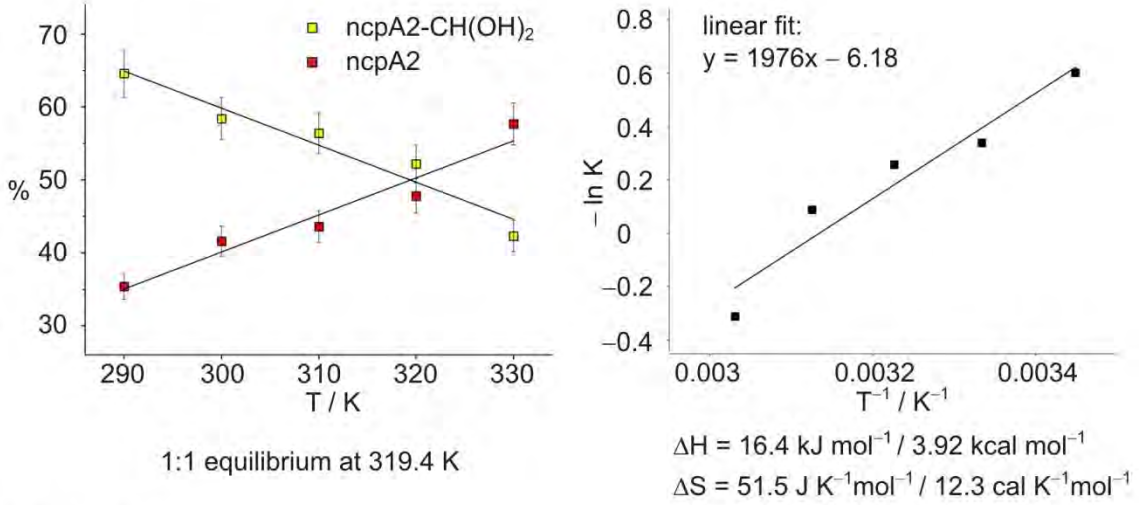

c) ncpA2, pH 4.0

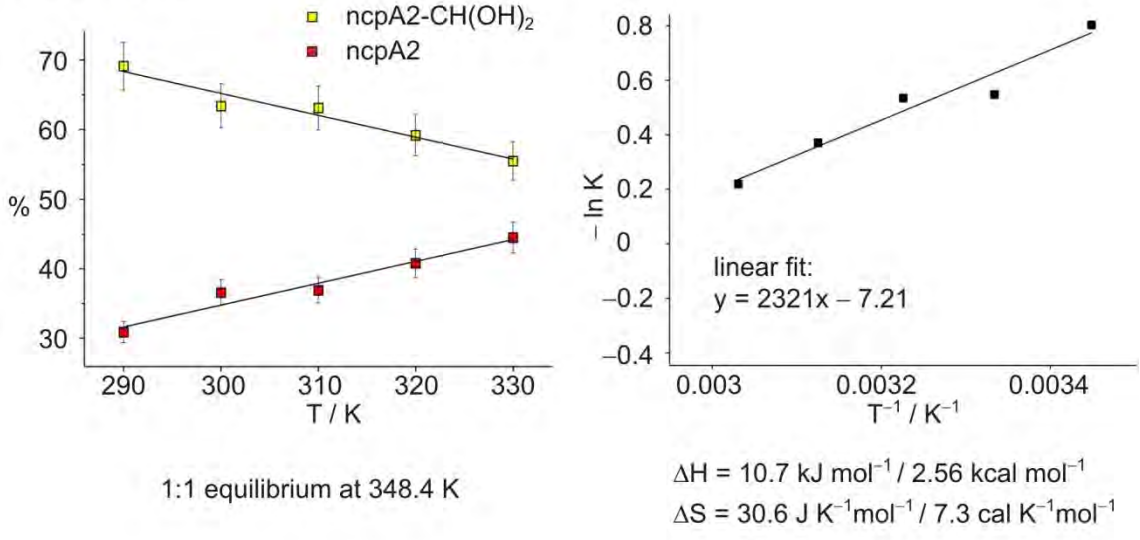

Figure 3.34 Temperature dependence (left) and* Van't Hoff *plots of the ring-chain equilibria of ncpA1 at pH 5.2 (a), ncpA2 at pH 5.2 (b) and ncpA2 at pH 4.0 (c).

cyclic species was obtained at about 320 K (figure 3.34a and b, left). In order to investigate the influence of the pH, the temperature dependence of the ncpA2 ring-chain equilibrium was also examined at pH 4.0. Under these conditions, temperature increase has less influence as the amount of cyclopeptide grows by no more than approx. 3% per 10 K, and approx. additional 10 K are required to reach a 1:1 ratio compared to pH 5.2 (figure 3.34c, left).

3.3.3.2.2 Calculation of the macrocyclization enthalpy and entropy balances

As more cyclic product is formed upon temperature increase, ncp macrocyclization exhibits an endothermic process which is promoted by the increase of the system entropy.[197] With the data obtained, the macrocyclization enthalpy ΔH can be calculated by the *Gibbs-Helmholtz* equation which describes the influence of temperature on the equilibrium constant K:

$$\frac{d \ln K}{d 1/T} = -\frac{\Delta H}{R} \qquad \left(K = \frac{\%\,(cycl)}{\%\,(lin)} \right) \tag{6}$$

Figure 3.34 (right) shows the plots of $-$lnK versus 1/T for the three series of measurements. The linear fit gradients are equivalent to $-\Delta$H/T and give cyclization enthalpies of 19.3 kJ mol^{-1}/4.61 kcal mol^{-1} (ncpA1, pH 5.2), 16.4 kJ mol^{-1}/3.92 kcal mol^{-1} (ncpA2, pH 5.2) and 10.7 kJ mol^{-1}/2.56 kcal mol^{-1} (ncpA2, pH 4.0), respectively. At the temperatures with a 1:1 ring-chain equilibrium (K = 1) the Free Energy ΔG is equal to zero according to:

$$\Delta G = -RT \ln K \qquad (R = gas\ constant) \tag{7}$$

The *Gibbs-Helmholtz* equation finally gives the entropy balances of the macrocyclizations:

$$\Delta G = \Delta H - T\Delta S \tag{8}$$

While the macrocyclization of ncpA2 at pH 4.0 is associated with an entropy gain of 30.6 J K^{-1} mol^{-1}/7.3 cal K^{-1} mol^{-1}, significantly higher values are obtained at pH 5.2. They do not differ to great extent according to the variation of the C-terminal residue (ncpA1: 59.9 J K^{-}1mol^{-1}/ 14.3 cal K^{-1} mol^{-1}, ncpA2: 51.5 J K^{-1} mol^{-1}/12.3 cal K^{-1} mol^{-1}). Generally, the macrocyclization of both peptides, in spite of their different C-terminal compositions and preorientations, is associated with a similar entropy balance of approx. 54 J K^{-1} mol^{-1}/ 13 cal K^{-1} mol^{-1}, and this value will be used for the further discussion of both peptides. It describes the *difference* between linear and cyclic substrates, and it includes all structural and

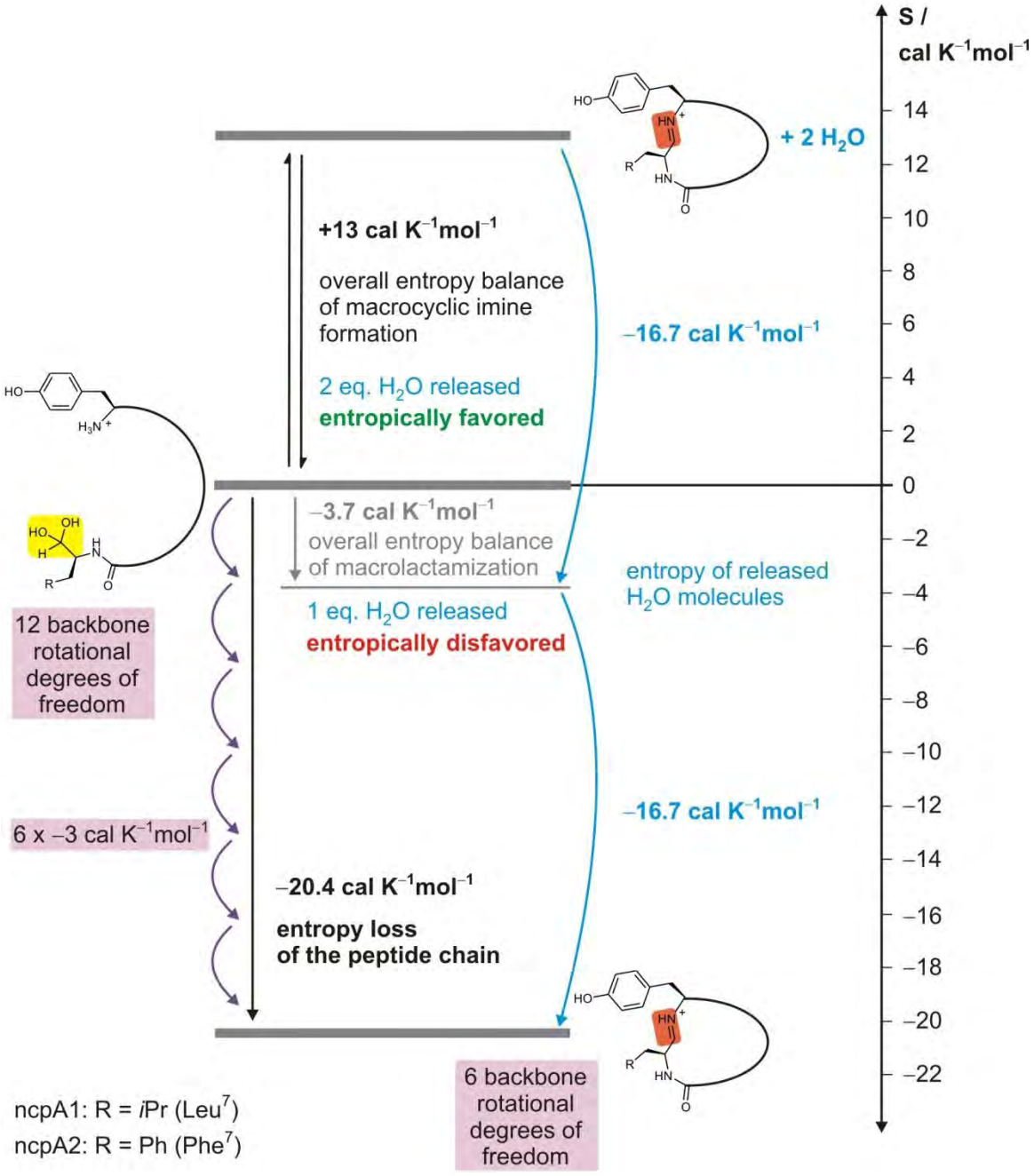

Figure 3.35 Estimation of the entropy loss of the ncp peptide chains. *For both peptides, an overall entropy balance of approx. +13 cal K^{-1} mol^{-1} was experimentally obtained from the temperature dependence of the ring/chain equilibria. If in an approximation a constant number of H_2O molecules in the hydration shell is assumed before and after cyclization, the entropy of the two released H_2O molecules has to be subtracted from the overall entropy balance (blue arrows). This allows to estimate the entropy loss of the peptide chain (–20.4 cal K^{-1} mol^{-1}) which can be explained by the reduction of 12 backbone rotational degrees of freedom in the linear peptide chain by half (purple arrows). An analogous macrolactamization which is accompanied by the release of only one equivalent of H_2O would not be entropically favored any more (overall entropy balance –3.7 cal K^{-1} mol^{-1}).*

dynamic parameters of the system as described in figure 3.8. Furthermore, as the signals of linear *R* as well as *S* epimers were integrated, the calculated thermodynamic parameters also include the epimerization equilibria. However, epimerization does not contribute to the entropy balance, and the changes in linear/cyclic compositions which would have occurred due to further epimerization after the 1 h equilibration at the respective temperature can be regarded as being within the 5% measuring uncertainty for two reasons. First, the samples were allowed to come to cyclization as well as epimerization equilibrium at pH 4.0 and 5.2, respectively, prior to the first measurements. Second, the temperature changes in equilibrium compositions upon 10 K increase had significantly lower influence than the pH variations depicted in figures 3.23 and 3.24. As the linear precursors of ncpA1 and ncpA2 show comparable epimerization behavior, the equilibria can be compared to each other (which is the subject of interest) if they, as it was the case, are examined under identical conditions.

3.3.3.2.3 The entropy balances of the peptide chains

The overall entropy of a system is comprised of various contributions, and in the present case it was of interest to identify the contribution of the peptide chain.[198] The experimentally obtained macrocyclization entropy *balances* (figure 3.35) represent the total entropy changes occurring upon cyclization with the two released water molecules and the changes in hydration included. In order to find out to which extent the peptidic structures are restricted upon ring closure, the task was to estimate the entropy balance of the mere peptide chains on basis of these experimental results.

The relative solvation of linear and cyclic species also influences the macrocyclization entropy as the reduced mobility of bound solvent molecules contributes to the total entropy.[199-201] The hydration state is a complex factor which can significantly affect the total entropy balance.[202, 203] In the case of the ncp, the observation of only minor chemical shift changes as well as the structure calculations give evidence of only small changes in hydration upon macrocyclization. The nostocyclopeptides keep their positive charge upon cyclization and, as the two polar end groups already interact with each other in the linear peptides, the condensation of the aldehyde hydrate with the amine should not have great impact on hydration.[204] Thus, allowing the approximation of neglecting entropic and enthalpic contributions, a constant number of molecules in the hydrating shell can be assumed and two main factors remain which influence the observed temperature dependence and the total entropy balance. One contribution is given by the loss of rotational degrees of freedom within the peptide backbone, which is the thermodynamic parameter of interest. The fact that the number of time-averaged NMR coupling

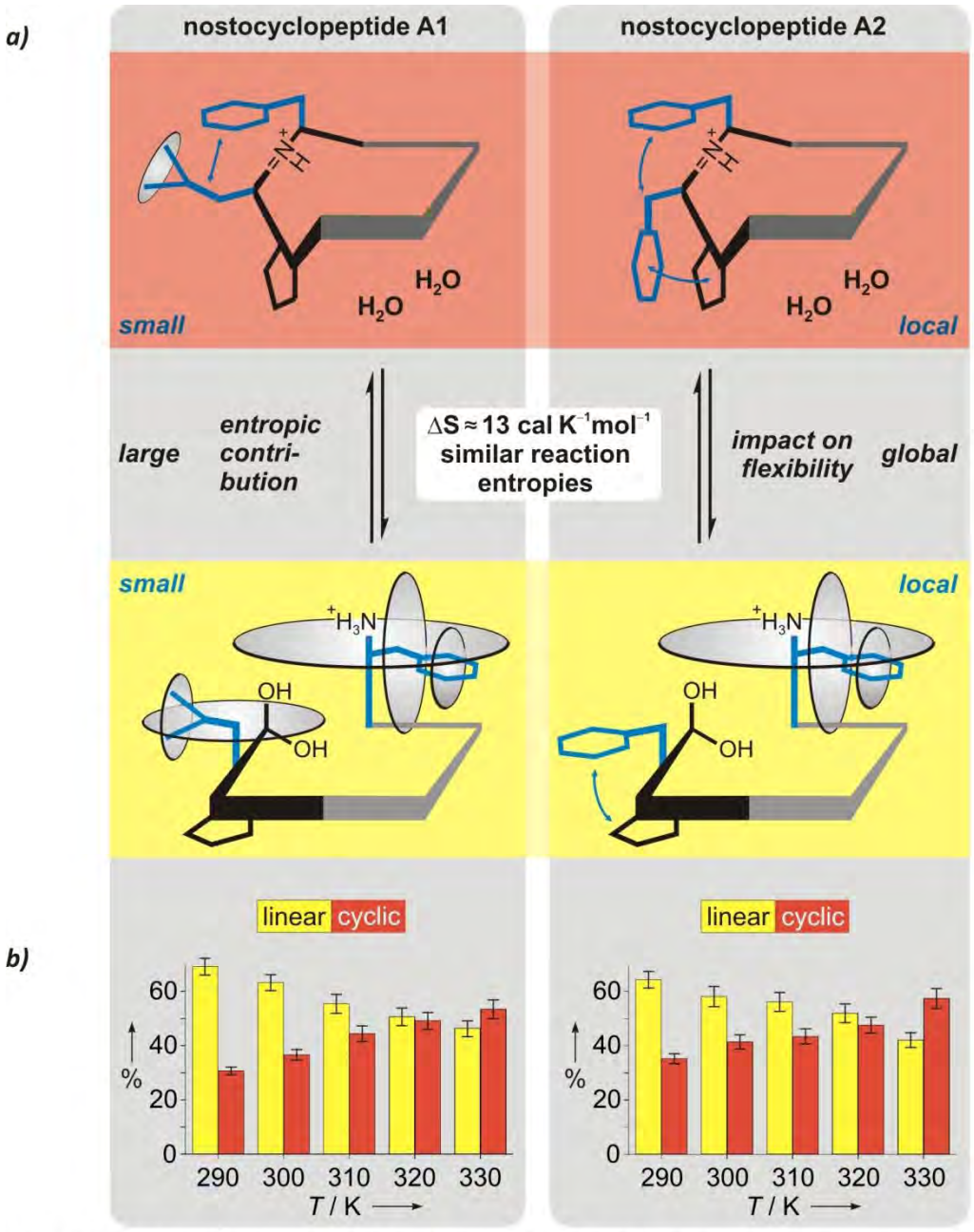

Figure 3.36 Identification of structural determinants of the ncp macrocyclization entropy balance. ***a)*** *Depiction of cooperative stabilization in the peptide termini that result from hydrophobic side chain interactions in ncpA1 (left) and ncpA2 (right). Peptide segments and side chains that appear differently in the linear and cyclic peptides and in ncpA1 and ncpA2 are marked blue. The presence of NOE contacts is indicated by blue arrows, while the presence of rotational mobility is indicated by grey disks. To obtain quantitative pictures of the side chain mobilities, scalar coupling constants were used to calculate the respective rotamer populations. For example, in the case of rotation of the Tyr side chain around the C-α/C-β bond in ncpA1, equal populations of all three rotamers (*gauche-trans, trans-gauche, gauche-gauche*) in the linear peptide indicate unhindered side chain mobility; this is in contrast to the 0:78:22 population obtained for the cyclic species. The Leu side chain exhibits complicated spin systems, which prevent the calculation of rotamer populations. However, the complete absence of sequential NOE contacts (linear peptide) in contrast to the large number of dipolar couplings towards the Tyr[1] side chain (cyclic peptide) give a qualitative picture of the interactions and mobilities displayed.* ***b)*** *Diagrams showing the temperature dependencies of the ncpA1 (left) and ncpA2 (right) macrocyclization equilibria. In spite of the differences in preorientation, the macrocyclization in both cases involves a similar entropy gain of approx. 13 cal $K^{-1}mol^{-1}$, which reveals that the entropic effects of local nonpolar interactions are small as compared to the cyclization entropy change.*

constants is restricted after cyclization gives sound evidence of a reduced conformational freedom and suggests that the cyclizing peptide chains loose entropy. Consequently, the overall *positive* entropy balance is caused by the release of two equivalents of water, which apparently compensates for the entropically unfavourable macrocyclization step and leads to an entropy gain as three molecules are generated out of one.

If the entropy of the two released water molecules (2 x +16.7 cal $K^{-1}mol^{-1}$)[200, 205] is subtracted from the overall entropy balance of +13 cal $K^{-1}mol^{-1}$, an entropy loss of –20.4 cal $K^{-1}mol^{-1}$ is obtained (figure 3.35). This value represents the loss of entropy of the peptide chains due to their conformational restriction upon ring closure.

3.3.3.2.4 Discussion of the entropy values: implications for the role of preorganization

In section 3.2.2 the rule-of-thumb was postulated that cyclization divides the number of rotational degrees of freedom by a factor of two. In a peptide chain, the entropy loss accompanied with the restriction of a single torsion is approx. –3 cal $K^{-1}mol^{-1}$.[151, 206, 207] As the linear ncp aldehyde hydrates exhibit 12 rotatable backbone bonds (the N-terminal C-NH_3^+ rotation is not considered), a loss of 6 rotational degrees of freedom is expected, which is equivalent to approx. –18 $K^{-1}mol^{-1}$. As illustrated in figure 3.35, this value fits well with the results obtained on basis of the experimentally obtained overall entropy gain of approx. +13 cal $K^{-1}mol^{-1}$. As no comparable entropy data of a biomolecular macrocyclization have been obtained so far, these outcomes give the first experimental evidence that this theoretical rule is actually applicable.

The positive overall entropy balance of ncpA2 macrocyclization is reduced under more acidic conditions (figure 3.34c), and the subtraction of the water entropy gives a slightly increased entropy loss of the peptide chain (–26.1 cal $K^{-1}mol^{-1}$). As the pH does not influence the peptide chain dynamics to measurable extent, pH dependent hydration effects may be the reason for this. However, more detailed interpretations may lead too far at this point, and further experiments are required to elucidate this correlation. The comparison of the ncpA1 and ncpA2 system under identical solution conditions, in contrast, gives valuable hints on the role of preorientation for the macrocyclization process (figure 3.36). Considering the different extent of C-terminal predisposition (figure 3.28) one may expect that the linear cyclization precursor of ncpA2, which features a distinct hydrophobic stacking interaction that apparently orients the aldehyde hydrate towards the N-terminal reaction partner, loses a considerably lower amount of entropy than the ncpA1 analog. However, the experiments show that both macrocyclizations

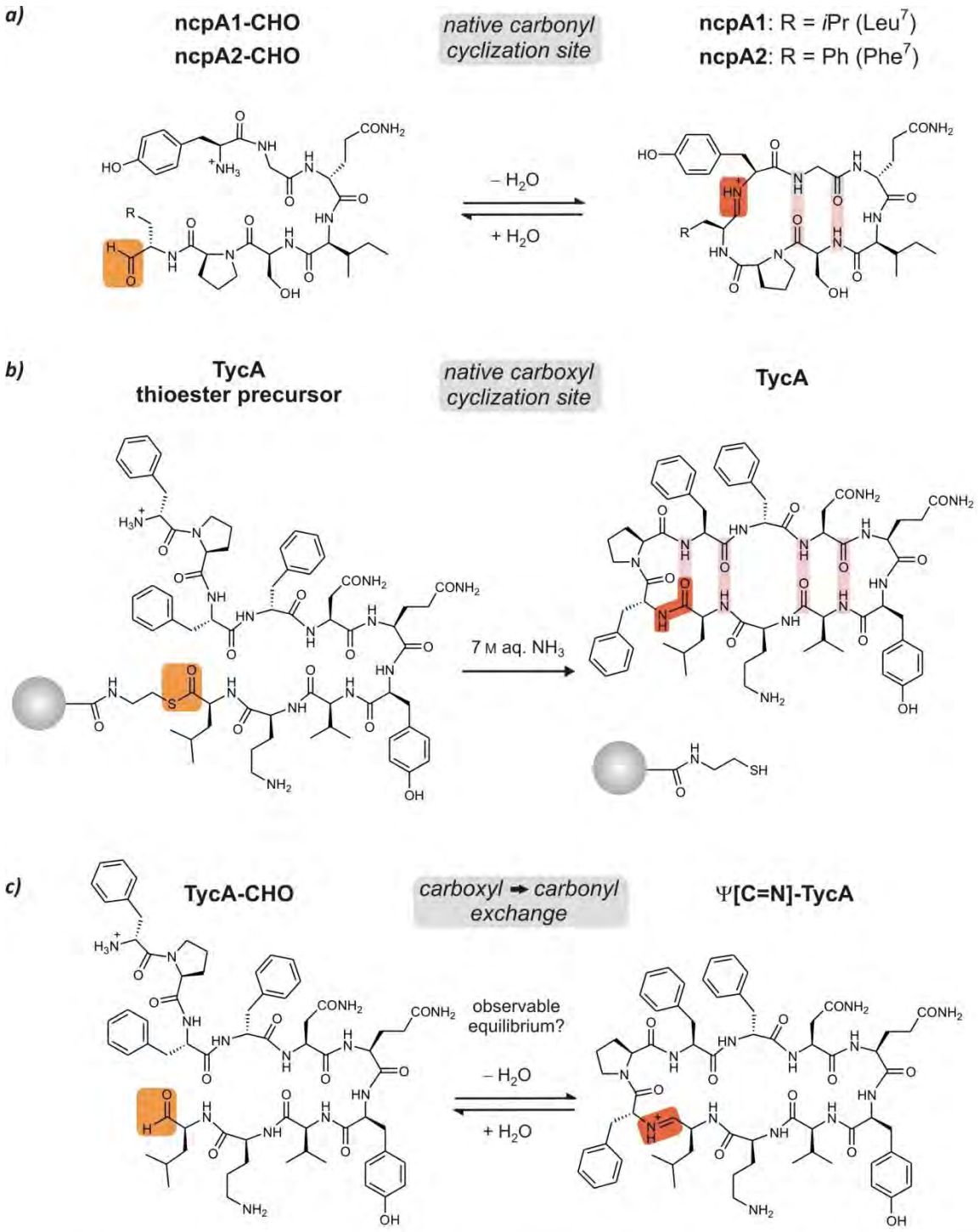

Figure 3.37 The substitution of a native amide cyclization site against a reversibly closing imino functionality enables to extend the analytical options given by cycloiminopeptides. ***a)*** *The carbonyl tether of the ncp was the prerequisite to observe a fully reversible ring/chain equilibrium which enabled thermodynamic analysis.* ***b)*** *The decapeptide tyrocidine A (TycA) shares with the ncp the remarkable characteristic of considerable preorientation of the cyclization precursor (hydrogen bonds indicated by red bars) and of self-cyclization. In aqueous ammonia, quantitative cyclization of the resin-bound thioester is observed.* ***c)*** *This makes TycA a promising substrate to test the isosteric substitution of the native C-terminal carboxylic acid function against an aldehyde (TycA-CHO) which would after cyclization result in the cycloimino analog (Ψ[C=N]-TycA, the chosen nomenclature is explained in the main text) which possibly also leads to an observable macrocyclization equilibrium. As the imine is geometrically similar to the amide, conclusions can be made for the cyclization of the native system.*

exhibit very similar entropy balances (and, in fact, the slight differences obtained speak against this influence of the C-terminal alignment in ncpA2 as a higher entropy loss is obtained). They rather indicate that side chain interactions operate on *local* segments yet do not measurably influence the *global* backbone mobility which is the result of the sum of all intramolecular interactions. This indicates that the preorientation of a peptide chain by non-covalent interactions and its subsequent cyclization determine mobility and therewith entropy on different scales. A well-defined solution conformation as it is observed by spectroscopic methods therefore must not be mistaken for rigidity, as only the covalent tethering of both ends can effect a global restriction of the conformational space. In other words, the experimental evidence that cyclization restricts the number of rotational degrees of freedom by a factor of two indicates that the entropy balance of macrocyclization mainly depends on chain length and is largely independent of peptide conformation. The extent of preorientation, however, has an essential function in the macrocyclization process: The exceptionally selective ncp ring closures illustrate the importance of preorientation for preventing polymerization or other side reactions. The macrocyclization reaction of the ncp is essentially promoted by the release of *two* equivalents of water. An analogous macrolactam formation with the release of one equivalent of water, in contrast, would be associated with an unfavored overall entropy *loss* of approx. -3.7 cal $K^{-1}mol^{-1}$. Therefore, it is the release of an additional water molecule upon imine formation which is driving the overall entropy balance in the positive range and makes the entire process entropically favored (figure 3.35). This makes the ncp whose biological function still remains unknown the more interesting and raises the question to what extent and for which purpose they appear as evolutionary optimized exceptional cases.

3.4 Interim conclusion: The carbonyl substitution as logical next step

In the preceding section it was demonstrated that cycloiminopeptides are a key to the thermodynamic investigation of peptide macrocyclizations and that NMR is the method of choice as it gives quantitative information about the ring-chain equilibrium compositions. The obtained experimental data were used to test our theoretical model about to what extent dynamical restrictions occur for a peptide chain upon ring closure, which was described in section 3.2.2. As the postulate was supported that half of the rotational degrees of freedom are lost upon macrocyclization, this encourages that our theroretical proposal of a simple numerical description of the macrocyclization process may show common validity and be transferable to any cyclopeptide formation. The valuable data on the structural determinants of macro-

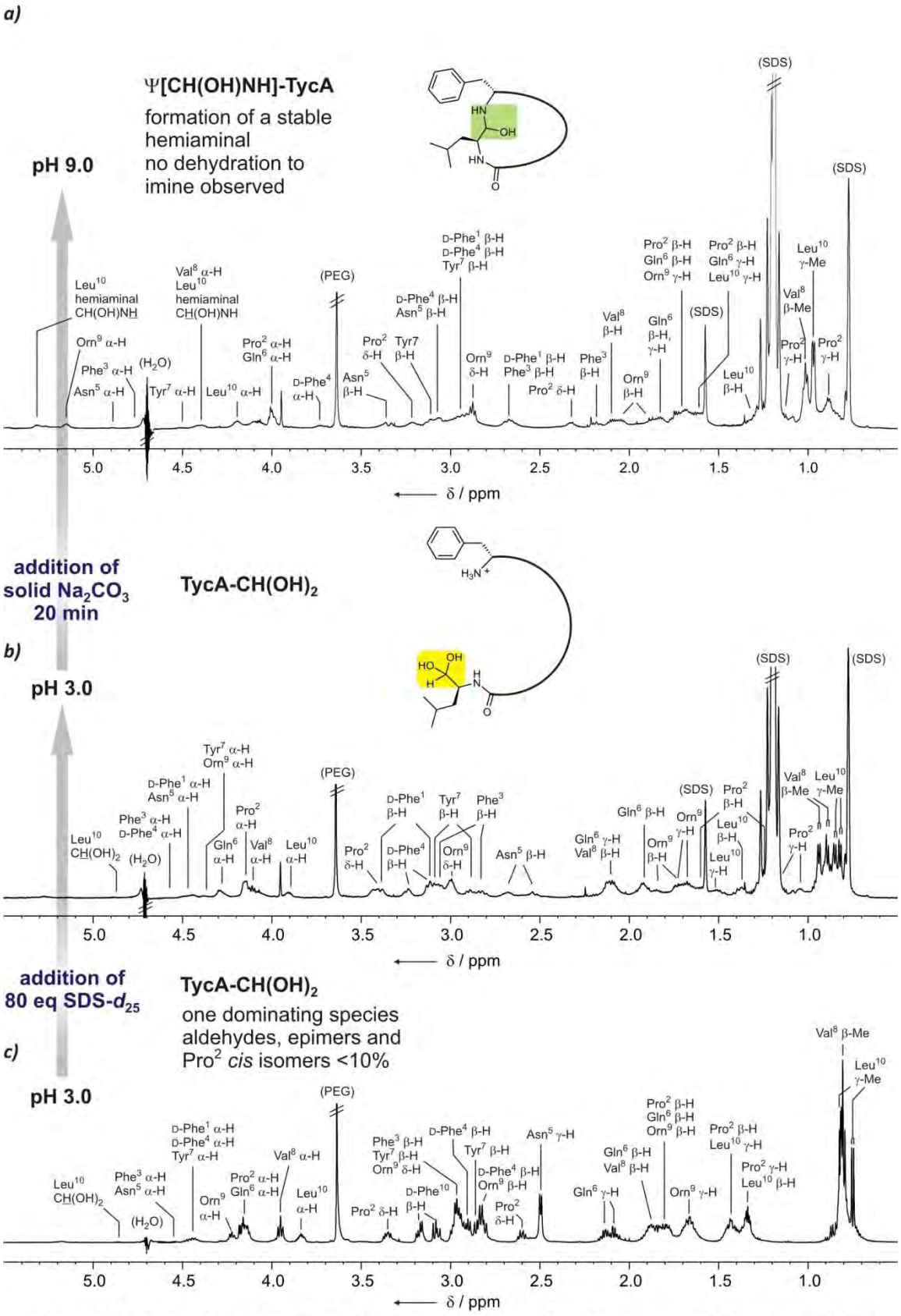

Figure 3.38 Upon pH increase, TycA-CHO spontaneously cyclizes to a macrocyclic hemiaminal. *The up-field ranges of assigned ^{1}H DPFGSE-NMR spectra (600 MHz, 300 K, H_3PO_4 /KH_2PO_4 buffer, H_2O/D_2O 5:1), are shown.* ***a)*** *Ψ[CH(OH)NH]-TycA in the presence of SDS-d_{25} (80 eq, 0.19 mol L^{-1}) at pH 9.0.* ***b)*** *TycA-CH(OH)$_2$ in the presence of SDS-d_{25} (80 eq, 0.19 mol L^{-1}) at pH 3.0.* ***c)*** *TycA-CH(OH)$_2$ without SDS-d_{25} at pH 3.0. The corresponding down-field sections are shown in the next figure.*

cyclization, as enabled by the described experiments, were obtained by the comparison of two peptides with identical chain length but different composition. As no further natural cycloiminopeptides were known to date, the question to be answered was whether the isosteric substitution of an amide ligation site of a cyclopeptide by an imine can be used to greatly extend the established experimental setup to the multitude of naturally occurring cyclopeptides (figure 3.37) and to gain thermodynamic data of the cyclization process. Such studies are essential to confirm the further validity of the found correlations, as they for example allow to include the influence of factors like chain length into the investigations. The proof-of-principle that this carboxyl→carbonyl exchange is applicable could be demonstrated by the decapeptide antibiotic Tyrocidine A (figure 3.2), which is described in the next section.

3.5 Results and discussion: The ring-chain equilibrium of Tyrocidine A aldehyde[41]

3.5.1 Tyrocidine A as test substrate for carbonyl functionalization

The cyclodecapeptide antibiotic Tyrocidine A (TycA, section 3.1.1) has been intensively studied with respect to its structure[208-213] and non-ribosomal biosynthesis[100]. By the demonstration that the excised terminal thioesterase domain is able to catalyze the ring closure of various linear peptidic precursors the way was opened for the engineered semienzymatic synthesis of cyclopeptides.[101, 214] The high antibacterial potency of TycA has in recent years led to various studies aimed at the synthesis of analogous peptides[102, 215-217] and glycopeptides[218, 219] with improved therapeutic scope. TycA appeared to be a promising first candidate for the substitution of the amide against an imine functionality not only because of its relevance as lead structure for the development of peptide antibiotics. It also shares some structural similarities with the ncp. The TycA macrocycle features one Pro residue and a mini β-sheet structure with a β-turn, and a considerable degree of preorientation has been identified for its linear cyclization precursor (figure 3.37b).[214] Furthermore, TycA as well as the ncp stand out by the ability to cyclize spontaneously and without the need of an enzyme in aqueous solution.[215] The linear TycA peptide chain is assembled on solid phase with the C-terminal Leu attached as thioester substrate, and in the last step it can be cleaved from the resin and concomitantly cyclized in aqueous ammonia solution. Of course, the (irreversible) formation of the macrolactam from a completely deprotected ω-amino carboxylic acid in aqueous solution is not possible due to the zwitterionic structure, so the first task was to examine whether after the exchange of the carboxylic acid against an aldehyde the (reversible) macrocyclic imine formation can be triggered analogously to the ncp (figure 3.37c).

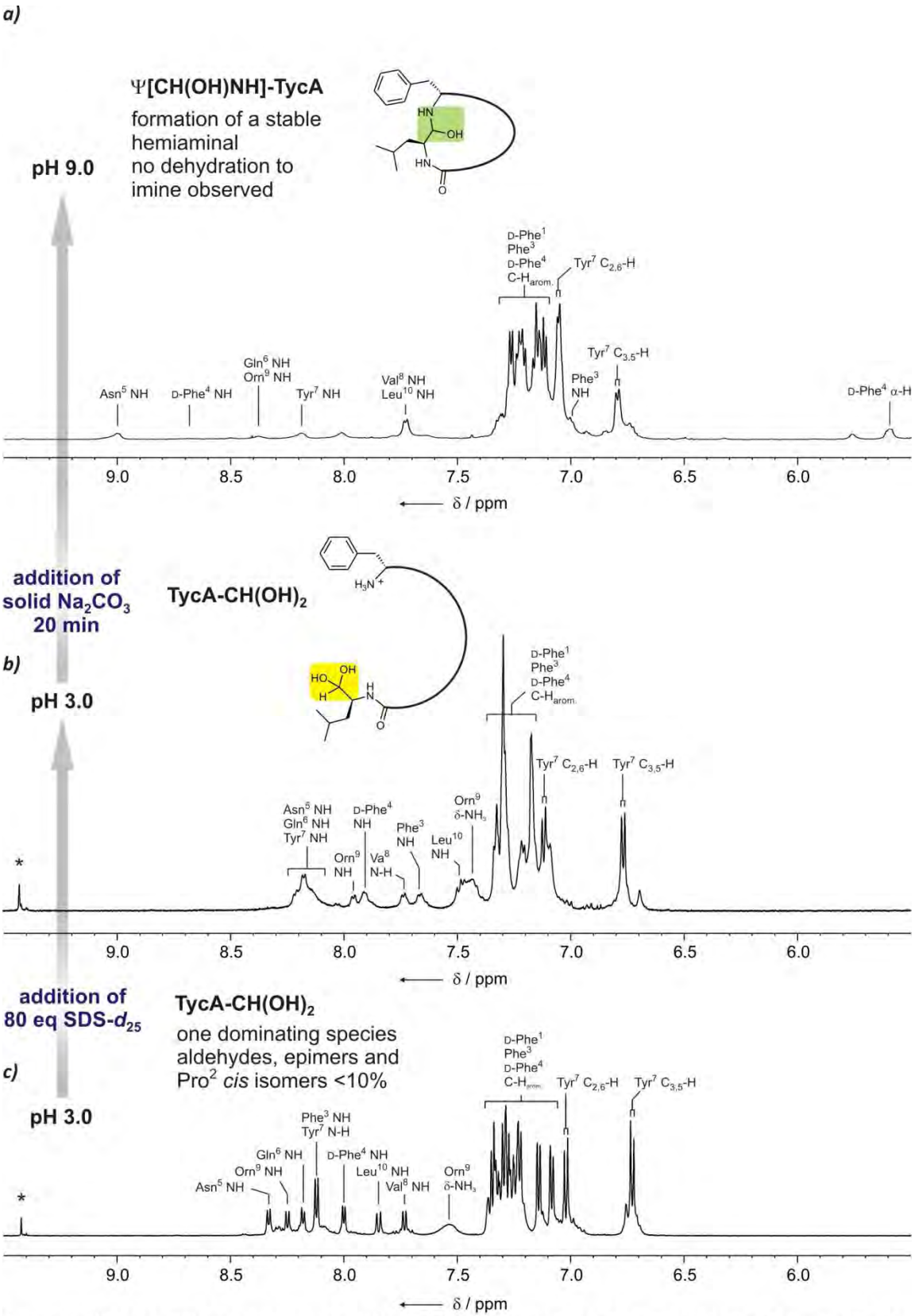

Figure 3.39 Upon pH increase, TycA-CHO spontaneously cyclizes to a macrocyclic hemiaminal. *The down-field ranges of assigned ^{1}H DPFGSE-NMR spectra (600 MHz, 300 K, H_3PO_4 /KH_2PO_4 buffer, H_2O/D_2O 5:1), are shown.* ***a)*** *Ψ[CH(OH)NH]-TycA in the presence of SDS-d_{25} (80 eq, 0.19 mol L^{-1}) at pH 9.0.* ***b)*** *TycA-CH(OH)$_2$ in the presence of SDS-d_{25} (80 eq, 0.19 mol L^{-1}) at pH 3.0.* ***c)*** *TycA-CH(OH)$_2$ without SDS-d_{25} at pH 3.0. The asterisks * mark the Leu^{10}-CHO peaks resulting from the linear peptide aldehyde. The corresponding up-field sections are shown in the preceding figure.*

3.5.2 Experimental setup

We envisioned to use the experimental protocol which was established by the examination of the ncp (section 3.4). After analysis of the linear substrates by ^{1}H and 2D NMR experiments at low pH, cyclization is triggered in the NMR tube and, if successful, the cyclization products are characterized. With the signal assignment of all major contributing species completed, the equilibrium is finally analyzed for its pH and temperature dependence. In the case of TycA it should also be examined whether all these measurements can be carried out with one single NMR sample. The linear TycA cyclization precursor analog with an aldehyde instead of a carboxylic acid function at the C-terminus (TycA-CHO) was synthesized by an Fmoc-based solid phase synthesis protocol which was also employed for the synthesis of the ncp precursors (figure 3.17). While in TycA biosynthesis D-Phe^{1} and Leu^{10} are covalently tethered by an amide, cyclization of the aldehyde precursor should result in reversible formation of the TycA imino analog cyclo(Asn^{5}-Gln^{6}-Tyr^{7}-Val^{8}-Orn^{9}-Leu$^{10}\Psi$[C=N]D-Phe^{1}-Pro^{2}-Phe^{3}-D-Phe^{4}). We suggest to abbreviate this modified TycA as Ψ[C=N]-TycA. The fact that no position for the modified tether is given indicates that the native cyclization position is retained.

A first NMR sample was prepared by dissolving 3.50 mg (2.75 µmol) of TycA-CHO in 0.72 ml of a partially deuterated H_3PO_4/KH_2PO_4 buffer solution (H_2O/D_2O 5:1) at pH 3.0 (TycA-CHO concentration: 3.82 mmol/l). Under these conditions, only the linear peptide could be examined as precipitation was observed when rising the pH. This likely resulted from formation of the cyclopeptide which is well-known to aggregate in aqueous solution due to its ten amino acid sequence (4n+2 residues) [220] with a high antiparallel amphipathic β-sheet content[209, 210, 221] and is inclined to self-aggregation in aqueous solution, a fact which hampers its handling. The combination of perdeuterated sodium dodecyl sulfate (SDS-d_{25}) micelles and aqueous phosphate buffer prevented precipitation when the pH was increased from 3.0 to 9.0 which is necessary for the NMR spectroscopic observation of cyclic species and of cyclization equilibria. The new NMR sample was prepared by dissolving 1.80 mg (1.41 µmol) of TycA-CHO and 36 mg (80 eq, 115 µmol) of SDS-d_{25} in 0.6 ml of a partially deuterated H_3PO_4/KH_2PO_4 buffer solution (H_2O/D_2O 5:1) at pH 3.0 (TycA-CHO concentration: 2.35 mmol/l, SDS-d_{25} concentration: 0.19 mol/l). Under these conditions, no precipitation was observed in the pH range between 3.0 and 9.0. For some further measurements, additional 1.40 mg (1.10 µmol) of TycA-CHO were added, resulting in a peptide concentration of 4.18 mmol/l. The completely assigned ^{1}H DPFGSE-NMR spectrum of TycA without SDS-d_{25} is shown in figure 3.38/3.39c, and the spectrum obtained after the addition of the detergent is depicted in figure 3.38/3.39b.

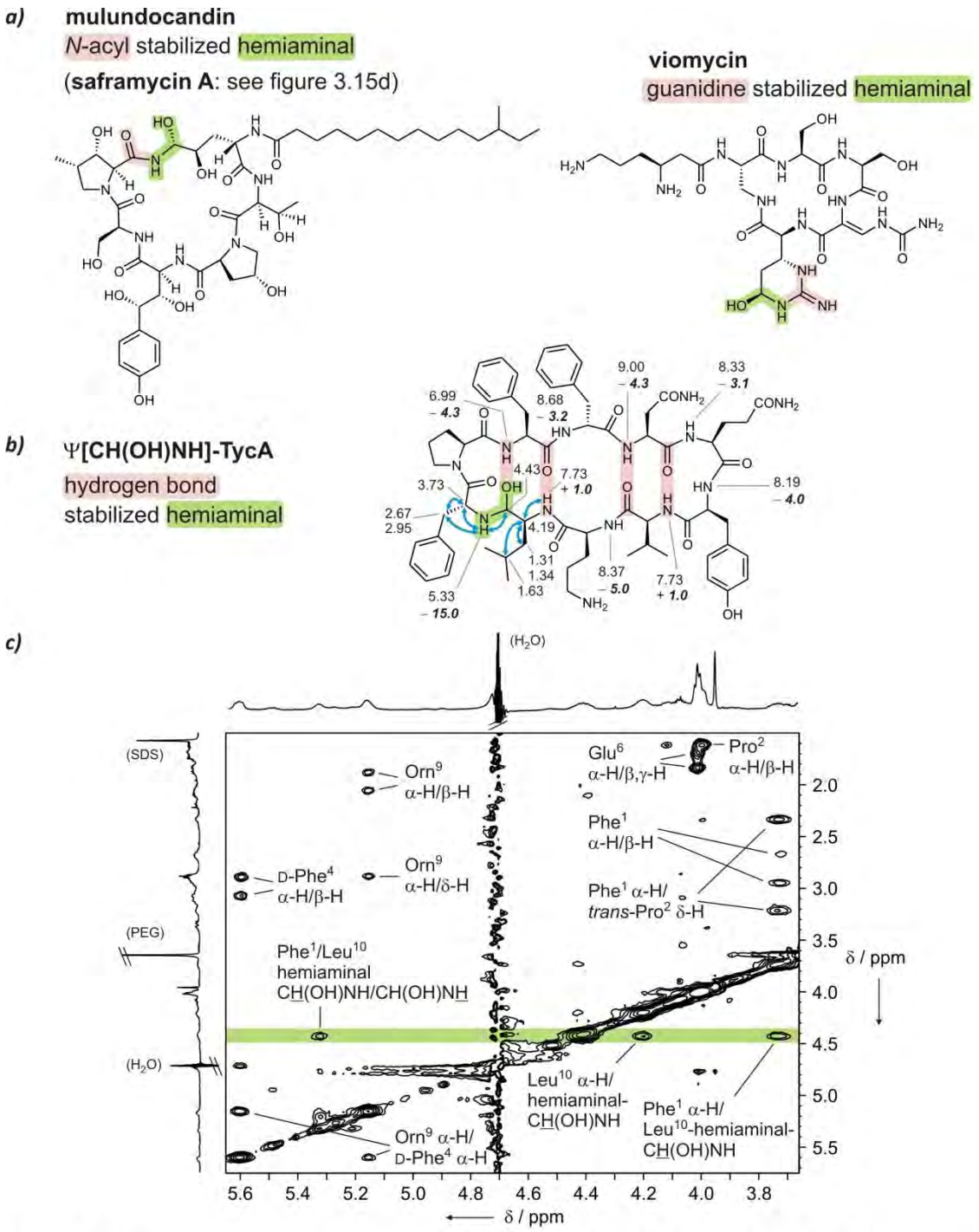

Figure 3.40 Hemiaminals in natural products rarely occur and they are always stabilized by conjugation. In contrast, the hemiaminal observed in cyclized TycA-CHO is the first example of a non-conjugated hemiaminal which is stabilized by hydrogen bonding. ***a)*** *Two examples of peptidic natural products that contain a hemiaminal. The lipopeptide mulundocandin (left) is a member of the echinocandin family and its* N*-acyl stabilized hemiaminal is formed in a side chain-to-tail macrocyclization of a dihydroxy ornithine side chain. In viomycin, the hemiaminal is located within a side chain as part of a guanidine unit.* ***b)*** *In contrast, the main cyclization product of TycA-CHO exhibits a hemiaminal which is instead stabilized by incorporation into the hydrogen bonding network of the antiparallel* β*-sheet. TOCSY correlations in the hemiaminal segment are indicated by blue arrows, and chemical shifts in the hemiaminal wegment and of the amide protons are written next to the respective positions. The bold numbers indicate the amide proton temperature coefficients (in ppb/*K^{-1}*).* ***c)*** *NOESY region (600 MHz, 300 K,* H_3PO_4/KH_2PO_4 *buffer,* H_2O/D_2O *5:1 with 80 eq (0.19 mol* L^{-1}*) SDS-*d_{25}*, pH 9.0) of cyclized* Ψ*[CH(OH)NH]-TycA showing correlations in the hemiaminal region (green bar), the trans-Pro*^{2} *configuration, and the* β*-sheet.*

3.5.3 Cyclization studies

As in the case of the nostocyclopeptides, at pH 3.0 only linear species are observed and the C-terminal aldehyde is mostly hydrated (amount of aldehyde < 10%).[179] The appearance of several low-intensity sets of signals which all together do not account for more than 10% of all species may also result from the Pro^2 *cis*/*trans* isomerism as well as from the epimerization of the aldehyde, as it was observed in the case of the ncp. However, while a considerable amount of ncp epimerization products was observed (36:64 ratio of *R* and *S* aldehyde hydrates), the C-terminal α-stereocenter of TycA-CHO shows much less inclination to epimerize although it is, like ncpA1, also functionalized with a Leu side chain. As an explanation for this we suggest a coordination of the aldehyde oxygen to the Phe^3 NH which decreases its basicity and consequently inhibits the enolization of the aldehyde.

A ^{1}H NMR spectrum recorded 20 min after raising the pH to 9.0 indicated the formation of one main product and only traces (< 5%) of linear species (figure 3.38/3.39a). This fast response of TycA-CHO to pH increase, as well as the high signal dispersion of the new set of signals showed that cyclization had occurred. The temperature gradients of the NH protons are characteristic for the Tyc macrocycles, and the strong long-range D-Phe^4 α-H/Orn^9 α-H NOE indicates the formation of the β-sheet. Furthermore, the *trans* conformation of the Pro^2 amide was confirmed by the strong sequential D-Phe^4 α-H/Pro^2 δ-H NOE.[212] A covalent linkage of D-Phe^1 and Leu^{10} is proven by NOESY and TOCSY spectra, but no imine signals of N=CH which are expected at chemical shifts of approx. 7 ppm (^{1}H) and 165 ppm (^{13}C) were detectable in the ^{1}H and 2D NMR spectra. In fact, the spectral information identifies a hemiaminal linkage (Ψ[CH(OH)NH]-TycA) with the hemiaminal-CH signal at 4.43 ppm and the NH signal at 5.33 ppm, respectively, as the dominating species at pH 9.0. Thus, the cyclization product of TycA-CHO is the first example of a macrocyclic peptide with a hemiaminal which was expected to be unstable in aqueous solution.

Hemiaminals are rarely found in natural products, and they always occur stabilized by N-acylation (for example in saframycin S,[177] anthramycin and sibiromycin[222]) or by the nitrogen being part of a guanidine unit in viomycin[223] (figure 3.40). N-acyl hemiaminals are also found in few peptidic natural products (for example in micropeptin T-20[224] and in the echinocandins[225]) but an unstabilized hemiaminal moiety as it is observed in the cyclized TycA aldehyde has not been described yet. Also in organic synthesis non-stabilized hemiaminals have only been characterized in very special cases as they generally either quickly are dehydrated to the imines

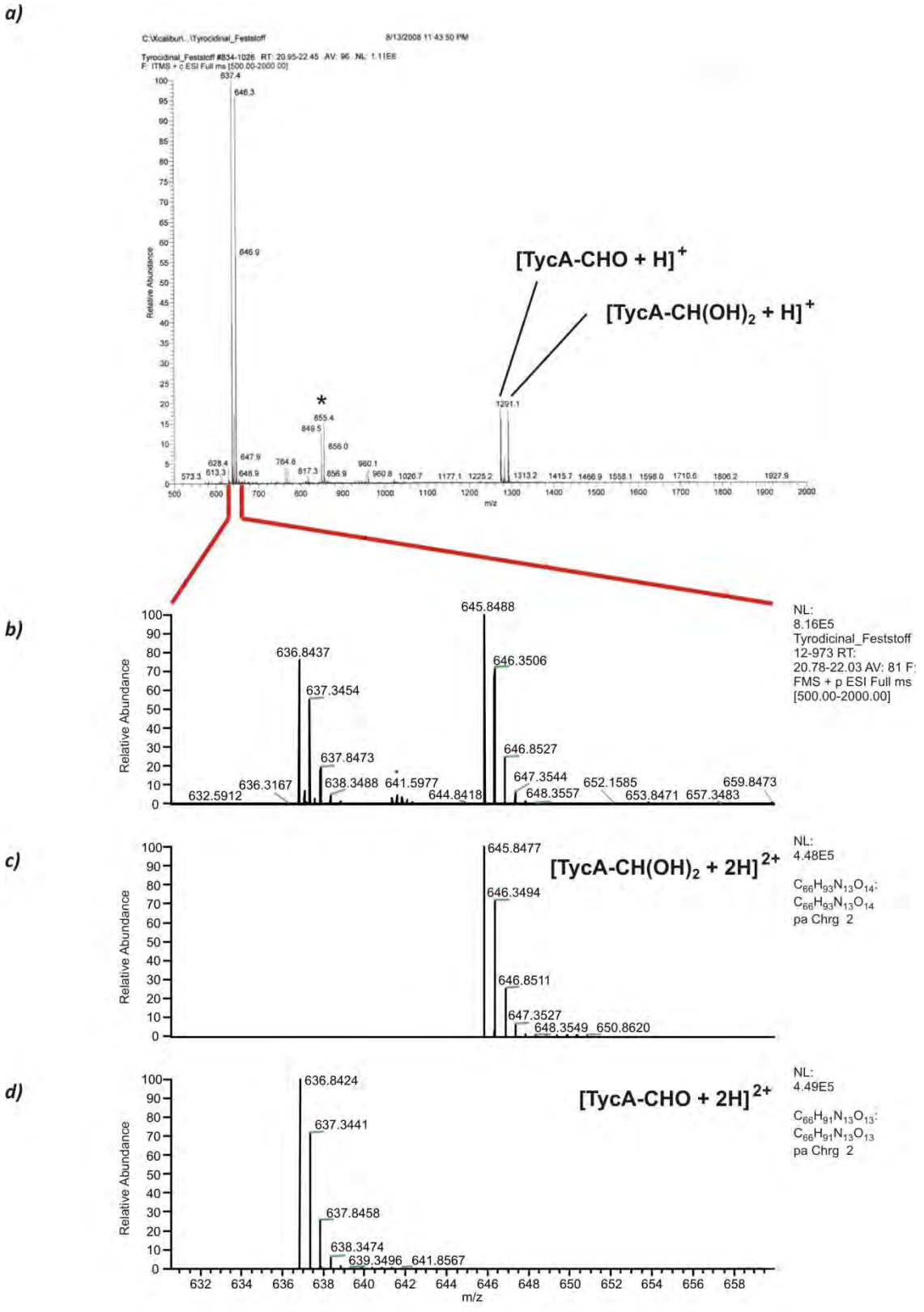

Figure 3.41 Integrated mass spectra (retention time: 20.78 - 22.03 min, figure 5.2) of HPLC-ESI-MS analysis of TycA-CHO under acidic conditions. ***a)*** *Overview of ESI spectrum.* ***b)*** *High-resolution ESI spectrum of area m/z = 630 - 660.* ***c)*** *Calculated high-resolution ESI spectrum of [TycA-CH(OH)$_2$ + 2H]$^{2+}$.* ***d)*** *Calculated high-resolution ESI spectrum of [TycA-CHO + 2H]$^{2+}$. The asterisks * mark signals which are caused by small amounts (< 10%) of dimers.*

or

dissociate to the starting reactants.[226-228] However, due to the relevance of hemiaminals as reaction intermediates much effort has been spent to be able to detect them by shielding with deep cavitands.[229] The cyclization product of TycA-CHO now enables to observe a free hemiaminal within a peptidic structure. Recalling the discussion of the ncp cyclizations (section 3.3.2.3.1), the possible presence of low amounts of hemiaminals (< 5%) has already been mentioned. However, the ncp and TycA-CHO are very different with respect to their macrocyclization step as imines are the only main species observed in the case of the ncp while possible amounts of analogous Ψ[C=N]-TycA species are below detection sensitivity.

As the α-position of the Leu^{10} aldehyde is subjected to racemization and a new stereogenic center is generated by formation of Ψ[CH(OH)NH]-TycA, four possible diastereomers can emerge from the cyclization reaction. The presence of only one cyclic main species, however, demonstrates that cyclization proceeds along a single reaction path and that the hemiaminal is incorporated into a structurally optimized cyclic structure which can be dominated by a distinct main stereoconfiguration. This remarkable behavior is reminiscent of the nostocyclopeptides which also deracemize upon cyclization, yielding stereopure macrocyclic *E*-configured imines from a mixture of *S*- and *R*-configured aldehydes (section 3.4).[179]

3.5.4 Stability of the hemiaminal

An important question concerns the origin of the unprecedented stability of the hemiaminal Ψ[CH(OH)NH]-TycA. The main difference to the corresponding imine Ψ[C=N]-TycA is the sp^3 hybridization and the presence of a hydroxyl function which is stabilized as part of the hydrogen bonding network of the antiparallel TycA β-sheet, thereby suppressing the dehydration step which would yield the imine. If the hemiaminal oxygen acts as electron donor for Phe^3-NH (temperature gradient: -4.3 ppb K^{-1}), a hydrogen bond analogous to the Phe^3-NH/Leu^{10}-CO interaction in native TycA is present, though the hemiaminal oxygen is expected to be weaker in its electron-donating ability than the amide oxygen. Of course the conditions applied in this case are different as TycA is investigated in a membrane mimetic environment in water, while DMSO and MeOH have been used in earlier works.[213] However, the similar pattern of temperature gradients $\Delta\delta/\Delta T$ of the NH protons (figure 3.45a) which give information on the antiparallel β-sheet indicates that, in spite of the modifications of TycA and of its environment, the β-sheet with the four hydrogen bonds is maintained.[212]

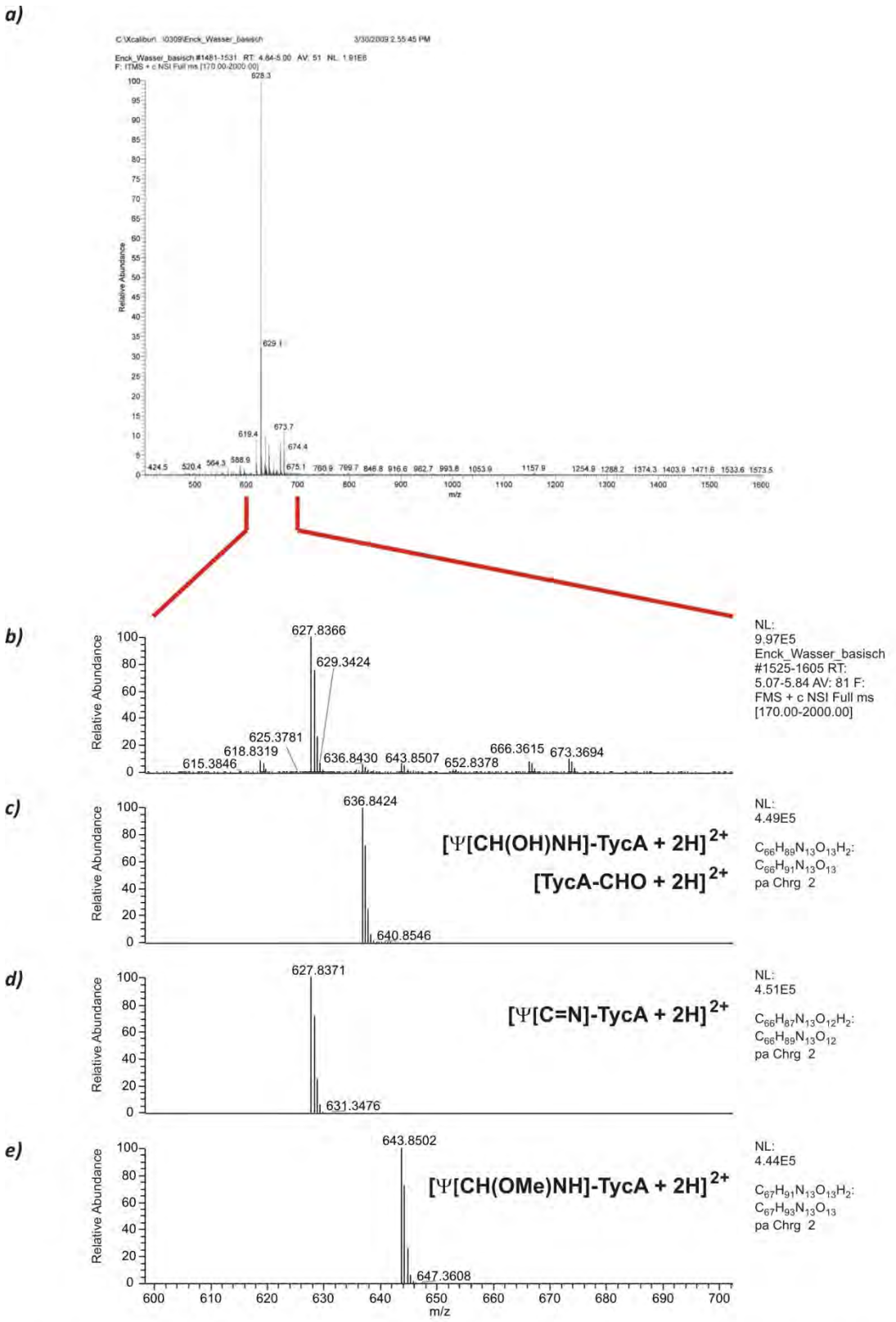

Figure 3.42 HR-ESI-MS analysis of an aqueous basic peptide solution after treatment with MeOH. ***a)*** *Overview of ESI spectrum.* ***b)*** *High-resolution ESI spectrum of area m/z = 598-702.* ***c)*** *Calculated high-resolution ESI spectrum of* $[\Psi[CH(OH)NH]\text{-}TycA + 2H]^{2+}$ *(and* $[TycA\text{-}CHO + 2H]^{2+}$*).* ***d)*** *Calculated high-resolution ESI spectrum of* $[\Psi[C=N]\text{-}TycA + 2H]^{2+}$*.* ***e)*** *Calculated high-resolution ESI spectrum of* $[\Psi[CH(OMe)NH]\text{-}TycA + 2H]^{2+}$*. The presence of the methyl aminal after evaporation of the MeOH and subsequent solution in* H_2O *(pH 9) suggests the stability of an aminal at the head-to-tail ligation site.*

The NOEs served as interproton restraints for molecular dynamics simulations of Ψ[*R*-CH(OH)NH]-TycA and Ψ[*S*-CH(OH)NH]-TycA, and the results are shown in figure 3.43 (see chapter 5 for the modeling protocol). The sp^3 hybridized carbon of the hemiaminal reminds of the geometrically similar tetrahedral intermediate of amide formation (Figure. 3.12). Hence, Ψ[CH(OH)NH]-TycA for the first time allows to observe the carbonyl analog of this species formed during a macrocyclic amide formation (figure 3.40b,c). In previous studies concerning the cyclization process of native TycA it was postulated that the tetrahedral intermediate may be involved in a stabilizing hydrogen bridge to Phe^3-NH which in turn is a result of the pronounced precursor preorganization.[214] The unexpected hemiaminal stability fits into this picture as it shows that the preorganization of the linear chain brings together both termini and thus facilitates ring closure. As visible from the structure shown in figure 3.43b, the hydrogen bonding should result in an orientation of the hemiaminal-NH to the solvent which is supported by the large temperature coefficient of -15.0 ppb K^{-1}. The stability of the hemiaminal may also be supported by the surrounding hydrophobic residues as the side chains of Leu^{10}, D-Phe^1, Pro^2, Phe^3 and D-Phe^4 are able to form a cavity which is shielding the hemiaminal oxygen from the solvent.

In addition to the NMR measurements, extensive ESI-MS studies were also carried out with peptide samples dissolved in acidic and basic media. The spectrum obtained from an acidic aqueous solution is shown in figure 3.41. The results obtained from basic aqueous samples (figure 3.42) demonstrated that the conditions of NMR spectroscopic analysis cannot be transferred to ESI-MS analysis in the case of ring-chain equilibrating iminopeptides. Under the high-vacuum conditions, the dehydration of the hemiaminal takes place and the imine Ψ[C=N]-TycA is also observed. As the macrocyclic hemiaminal Ψ[CH(OH)NH]-TycA and the linear aldehyde Tyc-CHO have identical molecular weight ($[M + 2H]^{2+} = 636.84$) they cannot be distinguished and therefore, no direct evidence of the presence of a hemiaminal can be given by ESI-MS. As a cyclic methyl aminal (Ψ[CH(OMe)NH]-TycA) in contrast would be identifiable ($[M + 2H]^{2+} = 643.85$) we performed an additional experiment. A small amount of basic aqueous solution was evaporated and the residue was subsequently dissolved in MeOH. The residue obtained after evaporation of the MeOH was finally dissolved in basic aqueous solution at pH 9 and subjected to ESI-MS analysis, and a weak methyl hemiaminal signal could be identified (figure 3.42e). Besides a further weak signal which originates from the cyclic hemiaminal and/or the linear aldehyde, the main signal represents the cyclic imine Ψ[C=N]-TycA. The fact that small amounts of Ψ[CH(OMe)NH]-TycA are still present is in accordance with the observed great inclination of TycA-CHO to form a stable hemiaminal in H_2O.

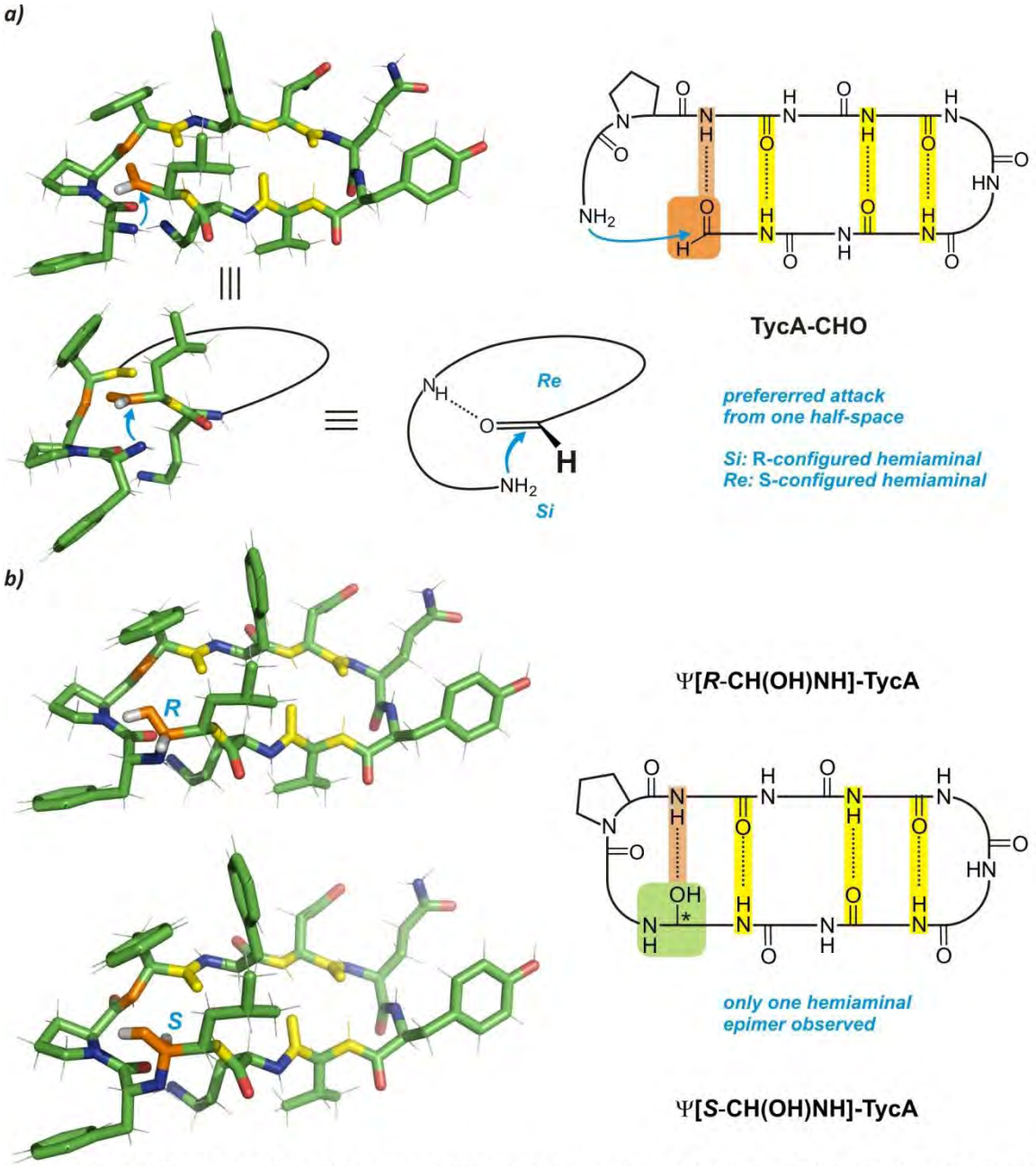

Figure 3.43 Hydrogen bond-assisted macrolactamization of TycA: Molecular modeling studies of cyclized TycA-CHO suggest the origin of the stereoselective hemiaminal formation. *On basis of the NOE data, both hemiaminal epimers were modeled using the program package* HyperChem *(see section 5.3 for details). The energy-minimized average structures of both the* R *epimer (**b**, top) and the* S *epimer (**b**, bottom) show an antiparallel* β*-sheet similar to native TycA. Carbons are shown in green, oxygens in red, and nitrogens in blue. The three amide hydrogen bonds are marked in yellow, and the hemiaminal hydrogen bonds are marked in orange. On the right, schematic representations of backbone, Pro[2] residue and hydrogen bonds are shown. The structure of the cyclization precursor shown by four differently simplified depictions in **a)** was obtained by cleaving the hemiaminal tether in order to obtain a perception of the geometries directly before macrocyclization. While the predisposed N-terminal segment features increased conformational flexibility, the residues 3-9 are preorganized for cyclization by the presence of three hydrogen bonds in combination with hydrophobic interactions. This enables a precoodination of the aldehyde by a hydrogen bond to Phe[3] NH (orange) which makes one of the half spaces better accessible for the amine. Although it can not be unambiguously determined, the obtained backbone geometries suggest that the* Re *half space is shielded by hydrophobic residues and that the nucleophile attacks from the* Si *side, which results in the* R *configured hemiaminal. In the cyclization precursor which yields the* S *configured hemiaminal (b, bottom) the aldehyde oxygen would not be capable of hydrogen bonding.*

3.5.5 Stereopurity of the hemiaminal

The selective formation of only one out of four possible diastereomers upon cyclization raises the question of the absolute stereochemistry of the cyclization site. The NOE data of Ψ[CH(OH)NH]-TycA are consistent with the NH temperature gradients and support the β-sheet formation under the NMR conditions. As they are similar compared to native TycA, they suggest the *S*-configuration of Leu^{10} like in the linear precursor. However, neither the Leu^{10} nor the hemiaminal stereoconfigurations could be unambiguously identified as more stable because similar geometries are obtained and the hemiaminal oxygens are capable of hydrogen bonding with Phe^{3}-NH.

The presence of a single stereoconfiguration results from the preference of one of the two half-spaces of the aldehyde by the amine nucleophile. This apparently arises from the steric shielding by the surrounding side chains in combination with a precoordination of the aldehyde to the Phe^{3}-NH (figure 3.43a). Although the modeling results of the cyclopeptide cannot safely determine which hemiaminal epimer is formed, the obtained backbone geometry suggests that the precoordinating aldehyde is attacked from the *Si* side which is the lower half-space in the perspective shown in figure 3.43a. This would result in the *R* configured hemiaminal.

30 min after cyclization, a low-intensity second set of signals (< 10%) is visible which grows during the following hours, finally reaching approx. 25% after 38 h (figure 3.44). The signal intensities are also reversibly changing upon temperature variation (figure 3.45a). As no imine or further linear species is detected, and as this set of signals is only visible if Ψ[CH(OH)NH]-TycA is present (figure 3.44), the corresponding peptide most likely is another macrocycle which slowly and reversibly emerges from the hemiaminal main product. Either this secondary set of signals results from the epimeric hemiaminal slowly formed via an imine intermediate by dehydration and subsequent addition of water which occurs less stereocontrolled than the addition of the amine to the aldehyde. Alternatively, a slow epimerization of Leu^{10} may also be the reason for the emerging second set of signals.[179] The formation of dimers in principle is also possible but was never observed in cyclization studies of native TycA.[215]

3.5.6 Thermodynamics of TycA macrocyclization

The composition of the TycA-CHO/Ψ[CH(OH)NH]-TycA macrocyclization equilibrium can, as in the case of the ncp, be controlled reversibly by variation of pH (addition of solid Na_2CO_3 or aq. H_3PO_4). In order to elucidate the entropy balance of the cyclization process we investigated the pH and temperature dependence (figures 3.44 to 3.46) of the cyclization equilibrium. In spite

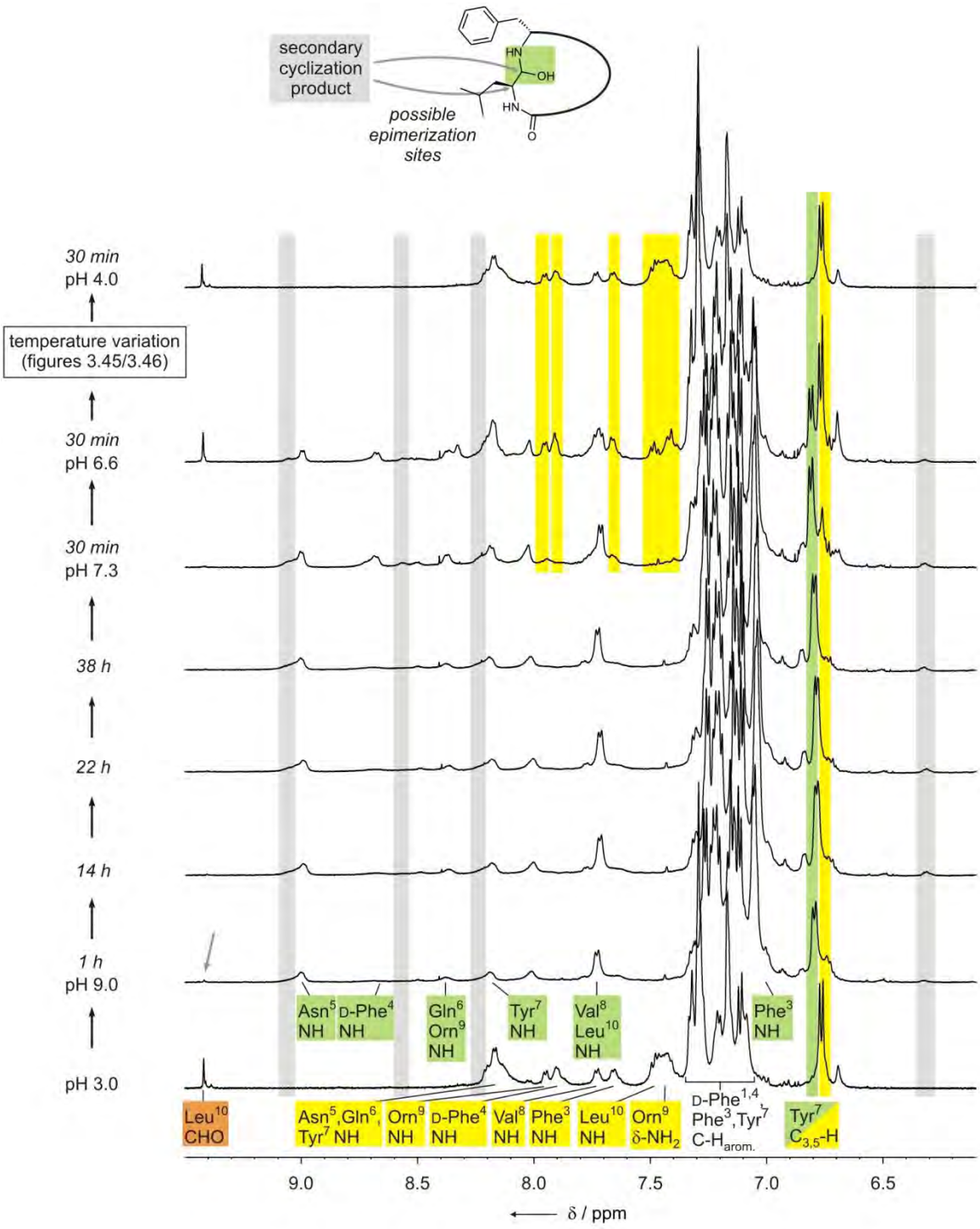

Figure 3.44 Monitoring of the pH dependence of the TycA-CHO ring-chain equilibrium. *The shown downfield ranges of ^{1}H DPFGSE NMR spectra (600 MHz, 300 K, H_3PO_4/KH_2PO_4 buffer, H_2O/D_2O 5:1, 80 eq (0.19 mol L^{-1}) SDS-d_{25}) demonstrate the fully reversible equilibrium between TycA-CH(OH)$_2$ (signals assigned yellow; amount of aldehyde < 10%) and Ψ[CH(OH)NH]-TycA (signals assigned green). The respective changes in pH and temperature are shown on the left. 1 h after rising the pH to 9.0 there is a weak aldehyde signal left (marked by grey arrow). The spontaneous cyclization yields one single hemiaminal diastereomer, and after several hours a second minor cyclic species is formed (signals assigned grey). This may result from the epimerization of the hemiaminal or the Leu^{10} α stereocenter. After the measurement at pH 6.6, the temperature dependence was examined as shown in figures 3.45 and 3.46. Subsequent setting of the pH to 4.0 yields only linear peptide, which demonstrates that the system is fully reversible.*

of high signal density (two main sets of decapeptide signals) and the line broadening caused by the SDS-d_{25}, the Val^{8} and Leu^{10} methyl signals are well enough resolved to be integrated and thus to give information about the composition of the equilibrating system (figure 3.46a). The thermodynamic parameters are determined from the temperature dependence of the percentages of linear (TycA-CH(OH)$_2$) and cyclic species (Ψ[CH(OH)NH]-TycA), respectively. As the composition of the linear/cyclic peptide mixture at pH 6.6 does not change significantly between 290 and 330 K (variations of < 5% are within measuring uncertainty) the balance of cyclization enthalpy ΔH can be set to zero according to the *van't Hoff* equation (6). The amounts of linear and cyclic species are approx. 50% each, which indicates that the free energy ΔG can in an approximation also be set to zero (equation (7)). Consequently, the *Gibbs-Helmholtz* equation (7) gives the entropy balance of the macrocyclization reaction which is equal to zero. This value represents the total entropy change which also includes the released water molecule.

In order to estimate the entropy loss of the peptide chain, several contributions must be taken into account, as already discussed for the case of nostocyclopeptide macrocyclization.[179] The changes in the solvation sphere are neglected in a first approximation in comparison to the water released upon condensation, which is supported by mostly slight changes of the chemical shifts (section 5.3). While two equivalents of water are released upon imine formation,[179] hemiaminal formation is accompanied by the loss of only one equivalent of water. Subtracting the entropy of one released water molecule (16.7 cal K^{-1} mol^{-1})[205] from the obtained entropy balance of approx. 0 cal K^{-1} mol^{-1} gives an entropy loss of the TycA peptide chain of approx. 17 cal K^{-1} mol^{-1}. The rule of thumb that half of the rotational degrees of freedom are lost upon cyclization proved to be a well applicable approximation.[179] Concerning the cyclization of the decapeptide TycA-CHO possessing 18 rotational degrees of freedom in the backbone we should expect an entropy loss of 27 (9 x 3) cal K^{-1} mol^{-1} which by 10 cal K^{-1} mol^{-1} exceeds the experimentally obtained value. Hence, the overall entropy balance of a decapeptide cyclization with the release of one equivalent of water should be in the range of approx. –10 cal K^{-1} mol^{-1} and thus entropically disfavored. This demonstrates that the linear precursors of the Tyrocidine peptides feature such an extraordinary pronounced preorientation that the cyclization entropy balance is shifted from a negative to an approx. neutral value. The reduction by 10 cal K^{-1} mol^{-1} observed for TycA-CHO cyclization is equivalent to approx. three rotational degrees of freedom and the cyclizing substrate acts more like a hepta- than a decapeptide. These results are in agreement with former qualitative investigations on native TycA in which its outstanding ability to self-cyclize without reagent was demonstrated[215] and now add a quantitative estimate of the TycA preorientation and cyclization tendency.

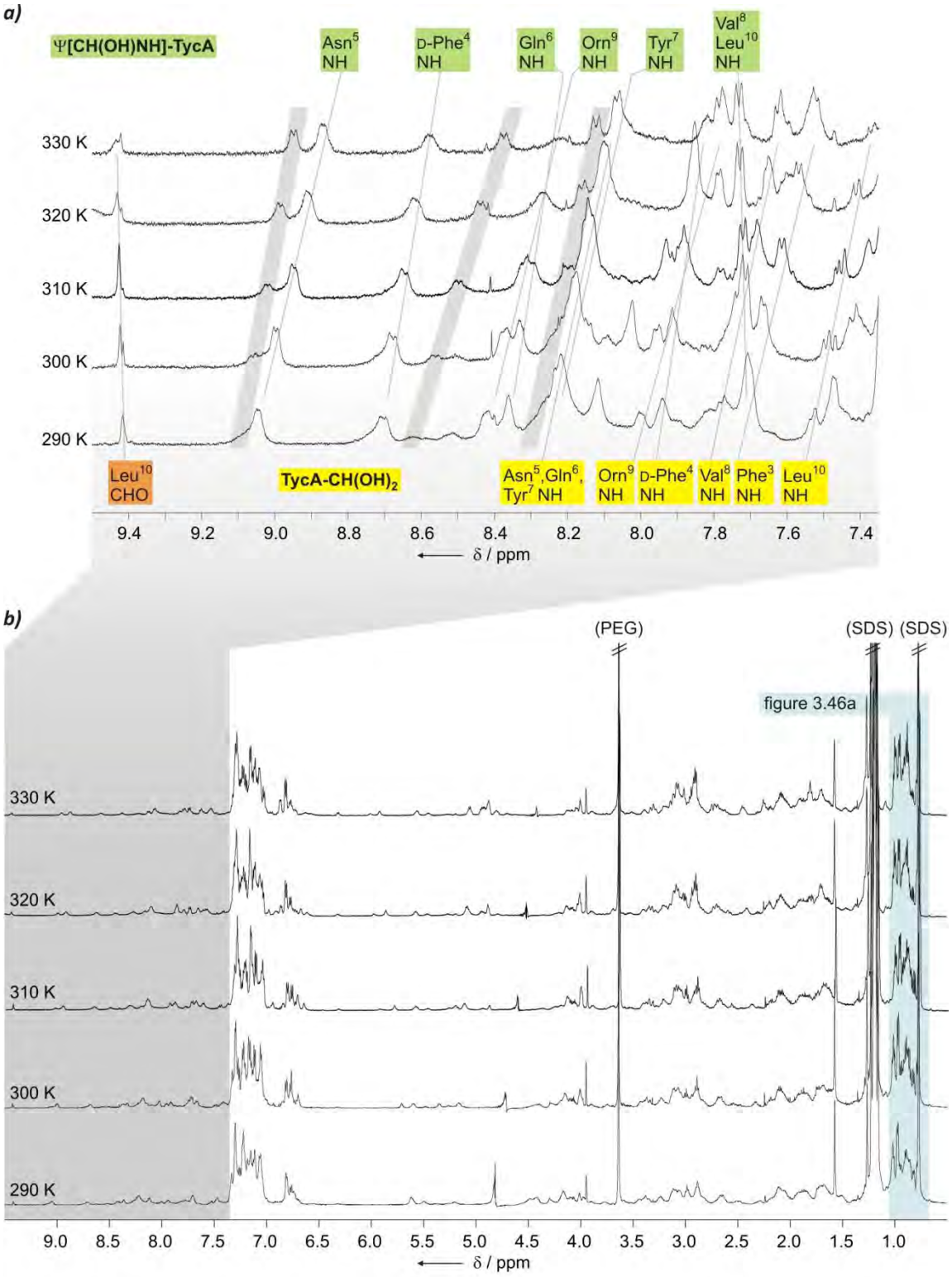

Figure 3.45 Monitoring of the temperature dependence of the TycA-CHO ring-chain equilibrium. ***a)*** *Down-field ranges of ^{1}H DPFGSE-NMR spectra (600 MHz, 290 to 330 K in 10 K steps, H_3PO_4/KH_2PO_4 buffer, H_2O/D_2O 5:1, pH 6.6, 80 eq (0.19 mol L^{-1}) SDS-d_{25}) with all resolved signals assigned. Under these conditions, TycA-CH(OH)$_2$ (signals assigned yellow) and Ψ[CH(OH)NH]-TycA (signals assigned green) are present to similar extents. The intensity of the signal set caused by the secondary cyclization product (marked in grey, see also figure 3.44) increases at higher temperatures.* ***b)*** *Complete spectra of TycA-CH(OH)$_2$/Ψ[CH(OH)NH]-TycA equilibrium system. Due to the crowding and the different extents of NH signal line broadening, the Val^{8} and Leu^{10} signals in the up-field section were used for quantitative determination of the equilibrium composition (marked in blue, see figure 3.44).*

3.6 Structural determinants of macrocyclization entropy

3.6.1 Comparison of the ncp and TycA-CHO macrocyclization processes

The three examined peptidic ring-chain equilibrium systems allow to draw several conclusions about which structural features determine the inclination of a substrate to cyclize.

With the ncp, two naturally occurring cycloiminopeptides were compared which feature identical chain lengths and similar extents of preorientation of the linear precursors. Upon cyclization, both peptide chains lose approx. 20 cal K^{-1} mol^{-1} of entropy. This is in well accordance with our hypothesis that the number of rotational degrees of freedom of a chain is divided by two upon cyclization, which is equivalent to an expected entropy loss of 18 cal K^{-1} mol^{-1} for a heptapeptide (figure 3.46b). Analogously, an entropy loss of approx. 27 cal K^{-1} mol^{-1} is expected for the decapeptide chain of the TycA-CHO precursor. However, the experimentally obtained entropy loss of only approx. 17 cal K^{-1} mol^{-1} is considerably smaller.

The ncp as well as the TycA-CHO precursors can be seen as exceptional cases for two reasons. First, they are able to self-cyclize without an enzyme and reagent, and second, they feature great selectivity of intramolecular cyclization vs. intermolecular oligomerization. These characteristics can be ascribed to their remarkable extent of preorientation as visible from the NMR spectroscopic studies, and it is the appropriate combination of preorganized and predisposed segments which allows for the efficient and selective macrocyclization (figure 3.31c). However, the next question is why the preorientation has no effect on the entropy balance in the case of the ncp while it shows a measurable influence for TycA. In principle, the preorientation of a linear peptide bases on two effects which are hydrophilic and hydrophobic interactions. In all three cases examined, hydrogen bonding of backbone amides (which performs a β-turn motif) takes place, but there is a considerable difference. While the NMR data suggest one single hydrogen bond in the case of the ncp, up to four bonds can be formed within the conformational equilibrium of the TycA-CHO precursor. However, it is questionable whether these differences account for the observed entropic effects as the peptides are examined in an aqueous environment. In presence of a multitude of hydrophilic interactions with the abundant solvent molecules, any effects by the (in comparison) sparse possibilities of intramolecular hydrogen bondings should not affect the conformational space of the linear chain to such extent that they effect a more than 30% restriction of the overall entropy loss upon macrocyclization as it is observed for TycA-CHO.

Apparently, it is rather the presence of several hydrophobic side chain interactions by which TycA-CHO differs from ncp precursors and which has the great influence on the entropy balance.

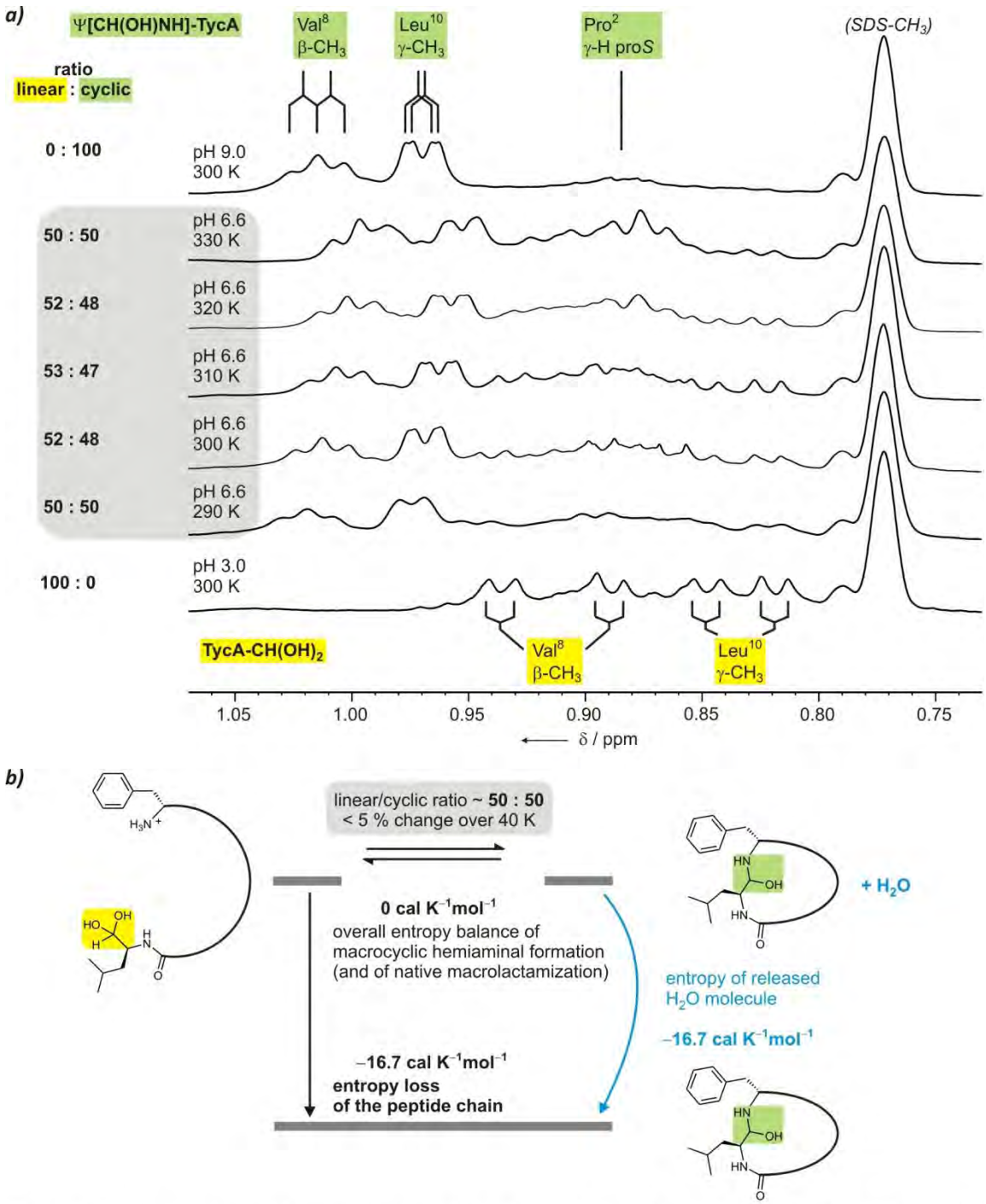

Figure 3.46 Monitoring of the temperature dependence of the TycA-CHO ring-chain equilibrium: the entropy loss of the TycA chain upon macrocyclization. a) *Up-field ranges of ^{1}H DPFGSE-NMR spectra (600 MHz, 290 to 330 K in 10 K steps, H_3PO_4/KH_2PO_4 buffer, H_2O/D_2O 5:1, pH 6.6, 80 eq (0.19 mol L^{-1}) SDS-d_{25}). The spectra at pH 6.6 (grey box) show the presence of an approx. 50:50 (linear/cyclic) mixture, which is temperature-independent of composition. The percentages of TycA-CH(OH)$_2$ and Ψ[CH(OH)NH]-TycA were determined by the integrals of the Val^8 and Leu^{10} methyl groups. For comparison, the spectrum of TycA-CH(OH)$_2$ at pH 3.0 and 300 K is shown at the bottom, while at the top the respective section of the freshly cyclized macrocyclic hemiaminal Ψ[CH(OH)NH]-TycA at pH 9.0 and 300 K, showing only one main set of signals, is depicted.* ***b)*** *As a 50:50 ratio independent of the temperature is observed, the thermodynamic parameters ΔG, ΔH and the overall entropy balance ΔS are approx. equal to zero. If, like in the case of the ncp, negligible changes in the hydration are assumed (section 3.4.3.2.3), the entropy loss of the peptide chain can be estimated by subtracting the entropy associated with the release of the H_2O molecule. The obtained value of −16.7 cal K^{-1} mol^{-1} also applies to the native macrolactam formation.*

In aqueous solution, the aggregation of hydrophobic side chains which minimizes their contact with the polar surroundings is expected to have far more implications on the conformational space of the peptide chain. In contrast to the ncp, the TycA macrocycle features a distinct amphipathic β-sheet content which evokes its aggregation tendency in aqueous solution.[230] It is conceivable that analogous side chain interactions are also present within the linear peptide chain and that these hydrophobic forces and the hydrogen bondings reinforce each other, which finally results in the remarkable reduction of entropy loss. In other words, our results suggest that it is the combination of hydrophobic and hydrophilic interactions *throughout the linear peptide chain* which effects a measurable influence on macrocyclization thermodynamics, and TycA surely exhibits an exceptional case in this respect.

In contrast, the NMR modeling studies suggest that in the ncpA2 precursor the only hydrophobic interaction is represented by the C-terminal Pro^6/Phe^7 stacking, and the ncpA1 precursor completely lacks any comparable interactions. In comparison with TycA this shows that the absence or presence of local hydrophobic forces does not measurably affect the macrocyclization entropy balance. Only if these are, in combination with polar interactions, present to such extent that they influence the overall backbone mobility they can reduce entropy loss upon the global restriction of macrocyclization.

In this context, the number of released H_2O molecules also has to be considered, adding another interesting perspective to the comparison of ncp and TycA. As it can be seen from figure 3.48, the release of one equivalent of H_2O upon TycA macrocyclization - and this applies for the formation of the hemiaminal as well as of the native amide - results in an approx. zero overall entropy balance and compensates the approx. 17 cal K^{-1} mol^{-1} entropy loss of the peptide chain alone. Consequently, the especially pronounced preorientation of the precursor may serve the purpose of reducing the entropy loss to such extent that a zero instead of an unfavorable negative overall entropy balance (–10 cal K^{-1} mol^{-1}) is obtained. In the case of the ncp, in contrast, the macrocyclization gets energetically favored by the release of two (imine formation) instead of only one (hemiaminal/amide formation) equivalents of H_2O. Thus, TycA and the ncp may represent two different evolutionary strategies to generate entropically favored macrocyclization processes. On the one hand, this can occur by the optimization of precursors with respect to their composition, leading to such an extent of preorientation that the entropy balance is influenced (TycA). The other option is the improvement of the molecular balance by functional modifications (one additional equivalent of water released by imine instead of amide formation). In figure 3.48 these experimental results are shown in the context of the proposed rule that macrocyclization reduces the number of rotational degrees of freedom by half.

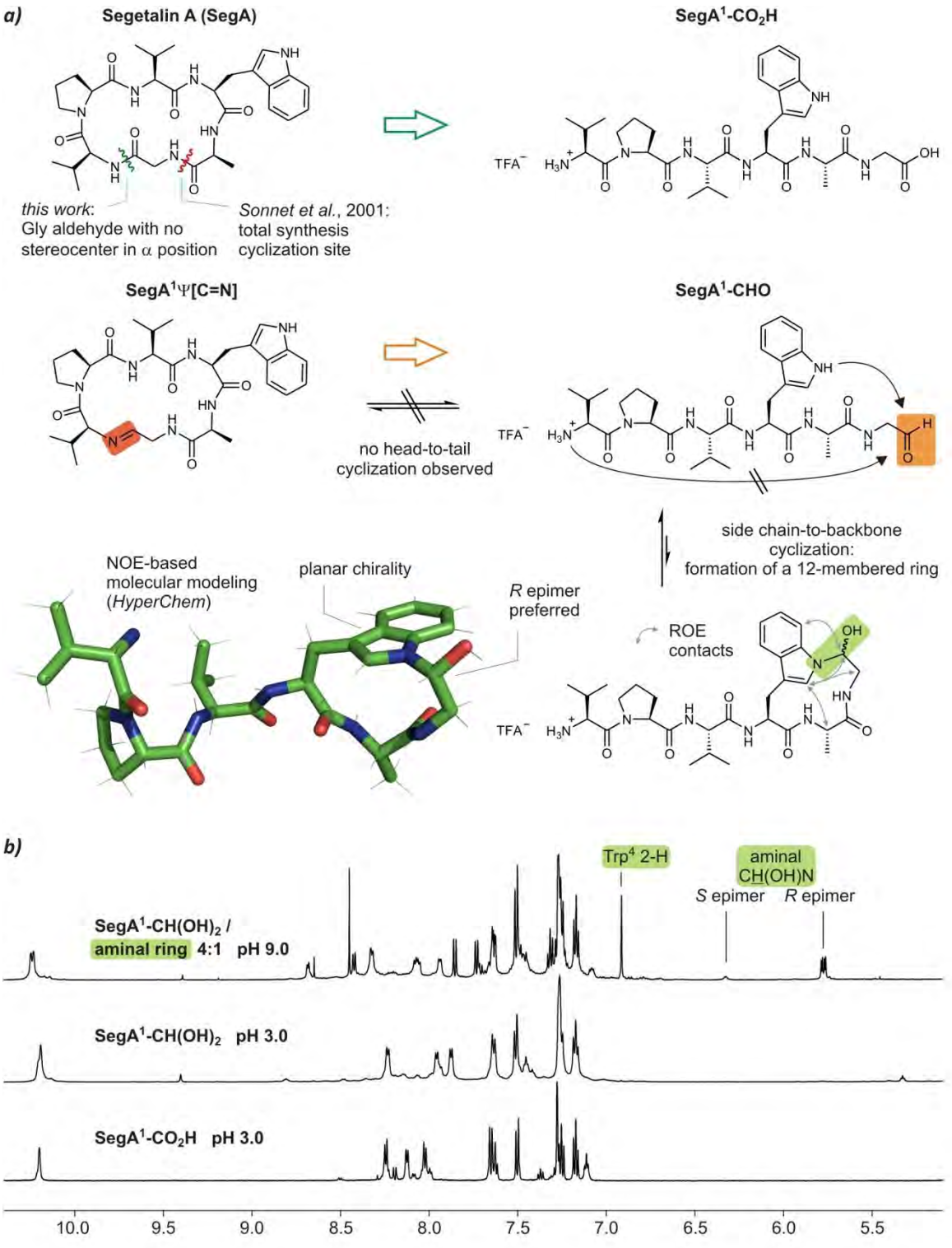

Figure 3.47 Cyclization studies with Segetalin A (SegA) aldehyde. ***a)*** *For the total synthesis of native SegA,* Sonnet et al. *chose the Ala[6]-Gly[1] junction as cyclization site (red). The Gly[1]-Val[2] junction (green) is suitable for a carboxyl/carbonyl exchange as the corresponding linear precursor SegA[1]-CHO contains a Gly aldehyde without an α-stereocenter. Consequently, no epimerization occurs which considerably reduces the signal crowding in the NMR spectra. In aqueous solution at neutral and basic pH, SegA[1]-CHO does not close the 18-membered macrocycle by head-to-tail cyclization. Instead, the linear peptide is in equilibrium with a side chain-to-backbone cyclization product containing a 12-membered ring.* ***b)*** *^{1}H DPFGSE-NMR spectra (H_2O/D_2O 5:1, H_3PO_4/KH_2PO_4, 600 MHz, 300 K) of SegA[1]-CO_2H at pH 3.0 (bottom), SegA[1]-$CH(OH)_2$ at pH 3.0 (center) and 1 h after the pH has been risen to 9.0 (top).*

3.6.2 Preliminary studies: The side chain-to-backbone cyclization of segetalinal A

These results motivate to extend the studies to further substrates with different chain lengths that have not been investigated yet (figure 3.48). As the ncp and TycA by their self-cyclization tendency exhibit quite particular cases, a logical further step is the examination of substrates that are not known to be particularly preoriented. We chose the cyclohexapeptide segetalin A (SegA; cyclo(Gly^1-Val^2-Pro^3-Val^4-Trp^5-Ala^6)) as target of carboxyl→carbonyl substitution (figure 3.47a). This natural product is isolated from the seeds of *Vaccaria segetalis* and plays an important role in traditional Chinese medicine due to its estrogen-like activity.[231, 232] In contrast to TycA and the ncp, SegA is probably produced ribosomally and its native cyclization site is not known. The characteristics of its solution structure in DMSO[233] are the *cis* conformation of Pro^3 and the presence of two β-turns. In a chemical total synthesis the macrocycle was closed between Ala and Gly; however, no reason was given for the choice of the cyclization site.[234]

For the carboxyl→carbonyl substitution we chose the adjacent Gly^1-Val^2 amide as the corresponding cyclization precursor features a C-terminal Gly aldehyde which, due to the lack of the α stereocenter, eliminates the problem of eventual racemization. The peptide synthesis was carried out by the same protocol used for ncp and TycA synthesis (figure 3.17),[180] but in this case all steps were carried out manually. As resin-bound Gly aldehyde is not commercially available, Fmoc-Gly-H was synthesized and subsequently loaded to H-Thr-Gly-NovaSyn® TG resin.[235] For the conversion of an N-protected amino acid to the corresponding aldehyde, several methods exist[236] which for example employ ethyl esters,[237] TMS esters,[238] morpholine amides,[239] and alcohols[240] as intermediates. The reduction of a *Weinreb* amide with LAH[240, 241] gave the best results and Fmoc-Gly-H was obtained in two steps from Fmoc-Gly-OH in 99% yield.

After cleavage from resin, a raw yield of 12% (5.0 mg) of the peptide aldehyde H-Val^2-Pro^3-Val^4-Trp^5-Ala^6-Gly^1-H (SegA^1-CHO, the superscript "1" indicates the position of the aldehyde) was obtained which already showed good purity by LCMS (section 5.3) and therefore, due to the low amount, was not further purified by preparative HPLC. For comparison, another hexapeptide with identical sequence but with the carboxyl function at the C-terminus (SegA^1-COOH) was also synthesized by manual SPPS using a standard Fmoc protocol.

Figure 3.47 shows the ^{1}H DPFGSE NMR spectra of SegA^1-COOH (c) and SegA^1-CHO (b) under identical solution conditions at pH 3.0. With exception of the amide proton signals, the carboxyl→carbonyl exchange only has small effects on the chemical shifts. In both cases, a low-intensity set of signals is caused by the presence of a *cis*-Pro^3 isomer, and the aldehyde occurs, as in the case of the ncp and Tyc-CHO, mostly hydrated under these conditions (SegA^1-CH(OH)$_2$), which gives rise to another low-intensity signal set caused by 5-10% of peptide aldehyde.

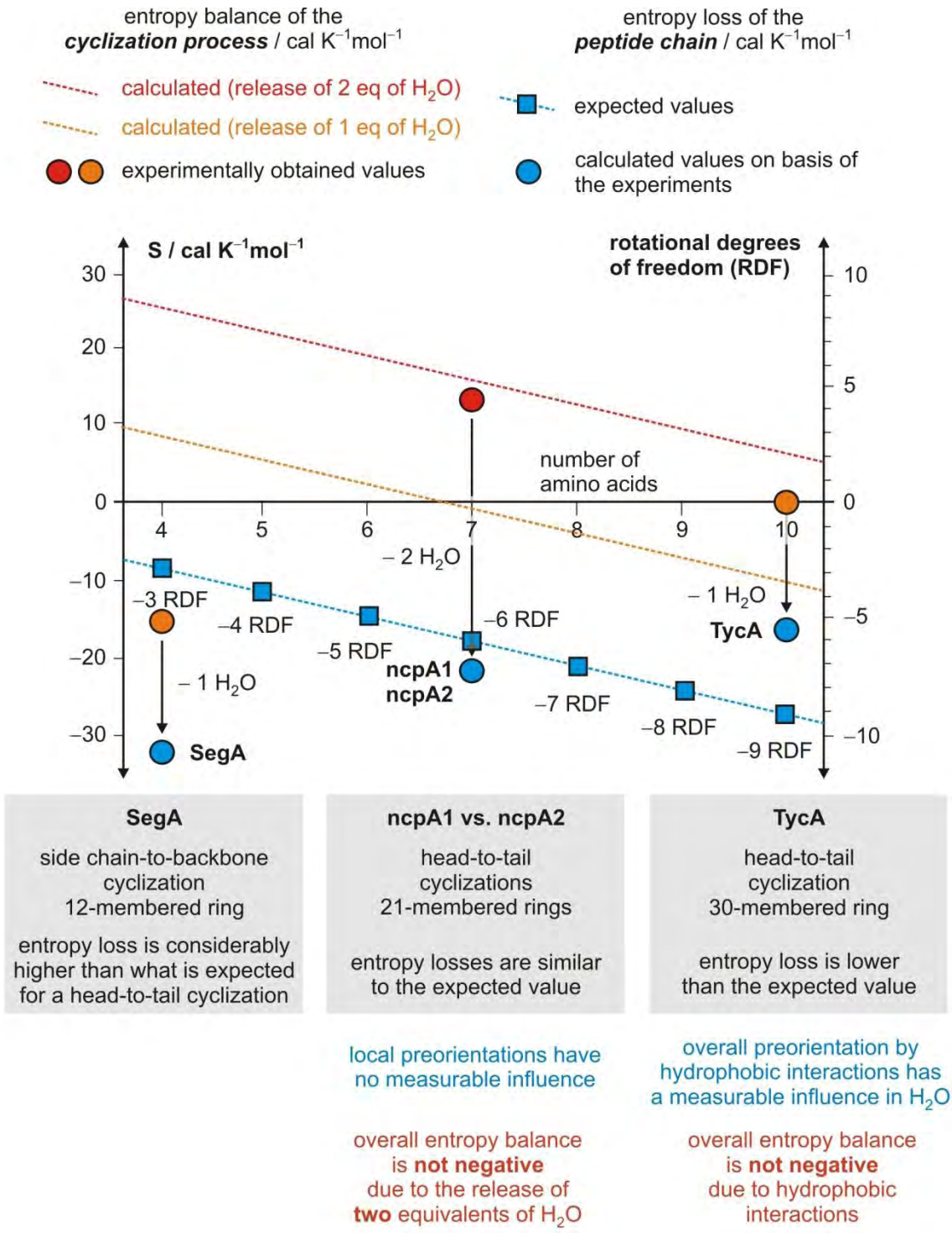

Figure 3.48 Summary and comparison of the experimentally obtained cyclization entropies and conclusions about structural determinants. *The diagram shows the entropy balances of peptide cyclizations which are expected on basis of the proposed rule that macrocyclization reduces the number of rotational degrees of freedom by half (discussed in section 3.2.2). The red and the orange dashed line shows the expected values of the overall entropy loss of if one equivalent or two equivalents of H_2O are released, respectively. After subtraction of the water entropies, the entropy balances of the peptide chains are obtained which are indicated by the blue dashed line and the blue squares. The red and orange dots show the experimentally obtained values, and the blue dots indicate the entropy losses upon the ring formations of SegA (side chain-to-backbone) as well as ncpA1/A2 and TycA (head-to-tail). The lower part of the figure summarizes the observations and the suggested influence of the various determinants on the entropy balance.*

Figure 3.47a shows the spectrum of SegA^1-CH(OH)$_2$ approx.the pH has been risen to 9.0 (spectra were also recorded at pH 7.0 which did not reveal any differences). Clearly, no head-to-tail cyclization was observed under these conditions, and the peptide aldehyde hydrate still remains the dominating species (the changes in the down-field region are evoked by the signal broadening of the amide proton signals). However, a new set of signal is well visible due to the high signal dispersion, and its intensity reaches approx. 1/4 of the main set of signals approx. 6 h after pH increase. By evaluation of the 2D NMR spectra the corresponding species could be unambiguously identified as a side chain-to-backbone cyclization product that is formed by addition of the Gly^1 aldehyde to the Trp^5 side chain NH (figure 3.47a). As the nitrogen is incorporated in the aromatic indole, no dehydration to the iminium function occurs and therefore a hemiaminal (indole carbinol) function can be observed. The strong up-field shift of the indole 2-H (6.92 ppm) and the appearance of the hemiaminal CH at 5.78 ppm are in accordance with comparable low-molecular weight indole carbinols,[242] and the restriction of mobility within the 12-membered ring is visible by non-mediated coupling constants and the highly differing chemical shifts of the diastereotopic Trp^5 β-H compared to the linear peptide.

These preliminary studies on SegA point out that a carboxyl→carbonyl substitution does not necessarily result in a near-quantitative head-to-tail macrocyclization as it was observed for TycA and the ncp. In fact, the substitution always leads to a precursor which is *basically* able to spontaneous formation of an intramolecular tether without any enzyme or reagent required. However, the results demonstrate that the exact position of the retrosynthetic cut is of relevance also for this reversible reaction type, and that the preorientation must play a key role in the cyclization process. In the case of SegA^1-CHO the conformational equilibrium obviously does not result in a spatial proximity of both ends, and instead the Trp^4 side chain nucleophile reacts with the carbonyl function. In the other substrates observed, analogous reactions also can occur (ncp: Ser^5 OH; TycA: Leu^9 NH$_2$) but have not been observed to measurable extent.

Macrocycles with side chains involved rigidify certain segments and effect a distinctive alignment of the side chains and their functionalities, which is why they are often introduced in Medicinal Chemistry for the improvement of biological activity and selectivity of a ligand (examples shown in figure 3.5). In contrast to TycA and the ncp, the amount of cyclic species increases at higher temperature as the released one equivalent of H_2O cannot compensate the entropy loss of the SegA chain (figure 3.48). However, the identification and examination of further side chain cyclizing substrates is required in order to show to whether and to what extent such a side chain-to-backbone cyclizations - especially if smaller rings are formed - are comparable to the corresponding head-to-tail tethering.

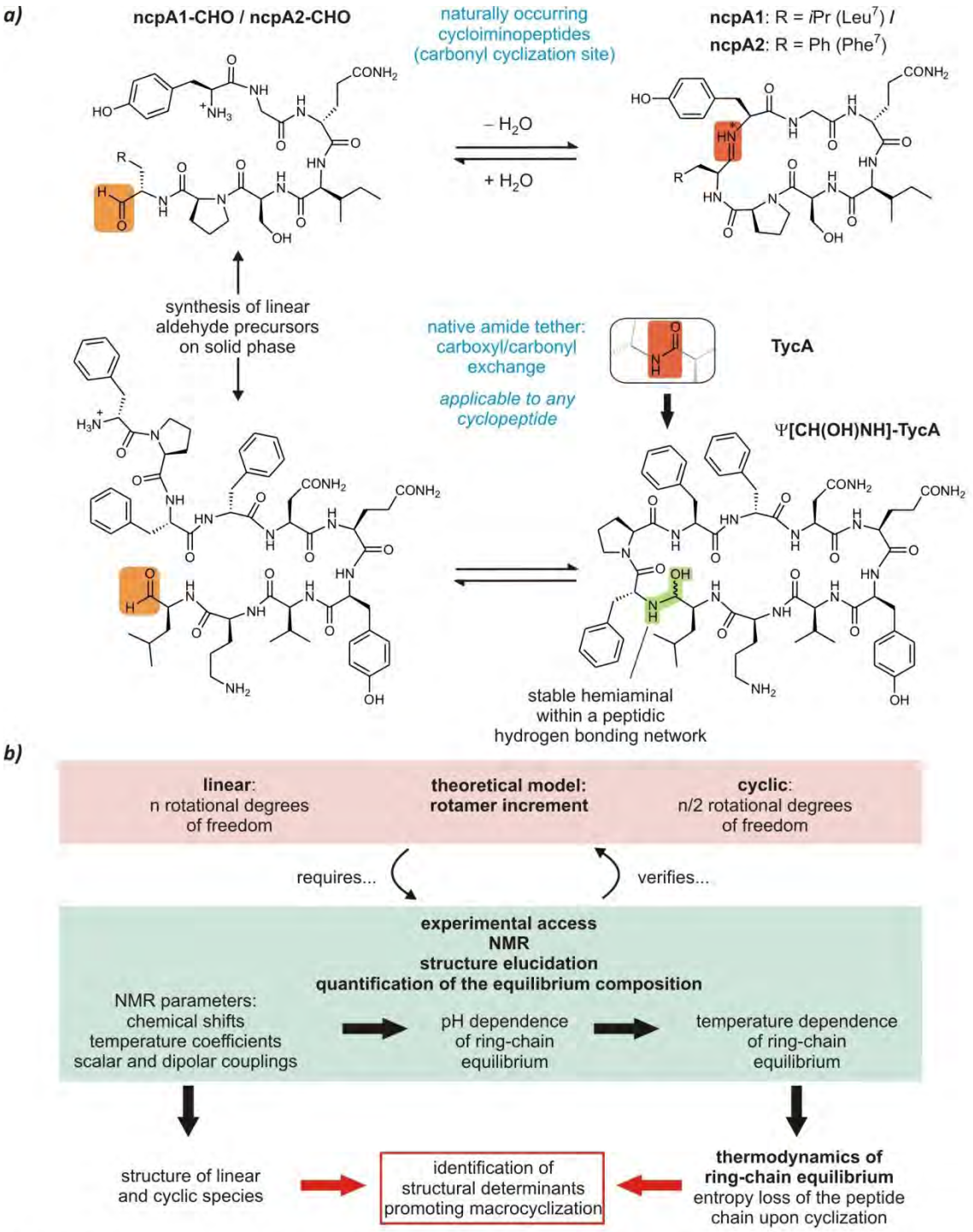

Figure 3.49 Summary of the established experimental access to elucidate the thermodynamics of biological macrocyclizations. a) *The nostocyclopeptides (ncp), which exhibit the only known cycloiminopeptides in nature to date, enabled by the reversibility of cyclization the first determination of a macrocyclization entropy balance. By exchanging the irreversibly closing amide, virtually every cyclopeptide can be investigated as its carbonyl analog, and this carboxyl/carbonyl substitution strategy was tested for TycA. In this case, no imine but a stable hemiaminal could for the first time be investigated within a peptidic environment (see also figure 3.40).* ***b)*** *The experimental studies also served to verify a proposed theoretical model which relates the macrocyclization entropy to the change of rotational degrees of freedom (section 3.2.2). The NMR protocol allows to obtain all parameters required for structure calculations as well as for the determination of the thermodynamic parameters with one single peptide sample. Finally, the comparison of the obtained structures and entropies allows to identify which factors increase or decrease the inclination of a substrate to cyclize (see also figure 3.48).*

3.7 Summary and outlook

In this work, the ring-chain equilibria of cycloiminopeptides have been shown as a key to the quantification of the entropy balances of macrocyclizations. This has given rise to a novel field of research as it allows to identify structural determinants which increase or decrease the inclination of a linear substrate to cyclize, which is of relevance due to the significance of the macrocyclization process in biosynthesis and medicinal chemistry. The results demonstrate the importance and ubiquity of biological macrocycles, supporting the concept that linear substrates can populate preferred conformations, but that only cyclization generates selective ligands for the interaction with the dedicated molecular receptors.

A measuring protocol was established which only requires one NMR sample and, according to the peptide length, not more than 3-5 mg of the substrate (figure 3.49b). Several ring sizes (six, seven, and ten amino acid residues) with different extent of preorientation of the linear cyclization precursors were included in the investigations. Furthermore the effect of single amino acid substitutions was examined. By comparison of the two nostocyclopeptides (ncp, figure 3.39a and section 3.3), being the only known naturally occurring cycloiminopeptides so far, it could be demonstrated that the appropriate combination of preorganized and predisposed segments can promote the macrocyclization process by preventing intermolecular oligomerization reactions, but such local effect do not decrease the entropy loss of the cyclizing chain. Consequently, preorientation of a peptide chain and its subsequent cyclization determine mobility and therewith entropy on different scales, and a well-defined solution conformation as it is observed by spectroscopic methods should not be mistaken for rigidity.

As there is the lack of a theoretical model for the prediction of the entropy loss of peptide chains, we propose a simplistic rule-of-thumb that the entropy loss upon macrocyclization can be estimated by reduction of the number of rotational degrees of freedom by half. In this context we also discuss how to use terms from the macroscopic world for the description of molecular dynamics (section 3.2.2). Although macroscopic terms like “mobility” or “rigidity” have only limited applicability on the molecular level, they are descriptive for the complex concept of “conformational space”. In fact, the ncp showed a restriction of conformational space which corresponds to what we would expect on basis of our theoretical model (figure 3.48).

By the investigation of the ring-chain equilibrium of tyrocidine A aldehyde (TycA-CHO, section 3.5) it was shown that the substitution of the native amide cyclization site against a reversibly closing imino function gives the possibility to examine the macrocyclization thermodynamics of virtually every cyclopeptide (figure 3.49a). It turned out that TycA-CHO features such a distinct extent of preorientation that the overall entropy balance is considerably

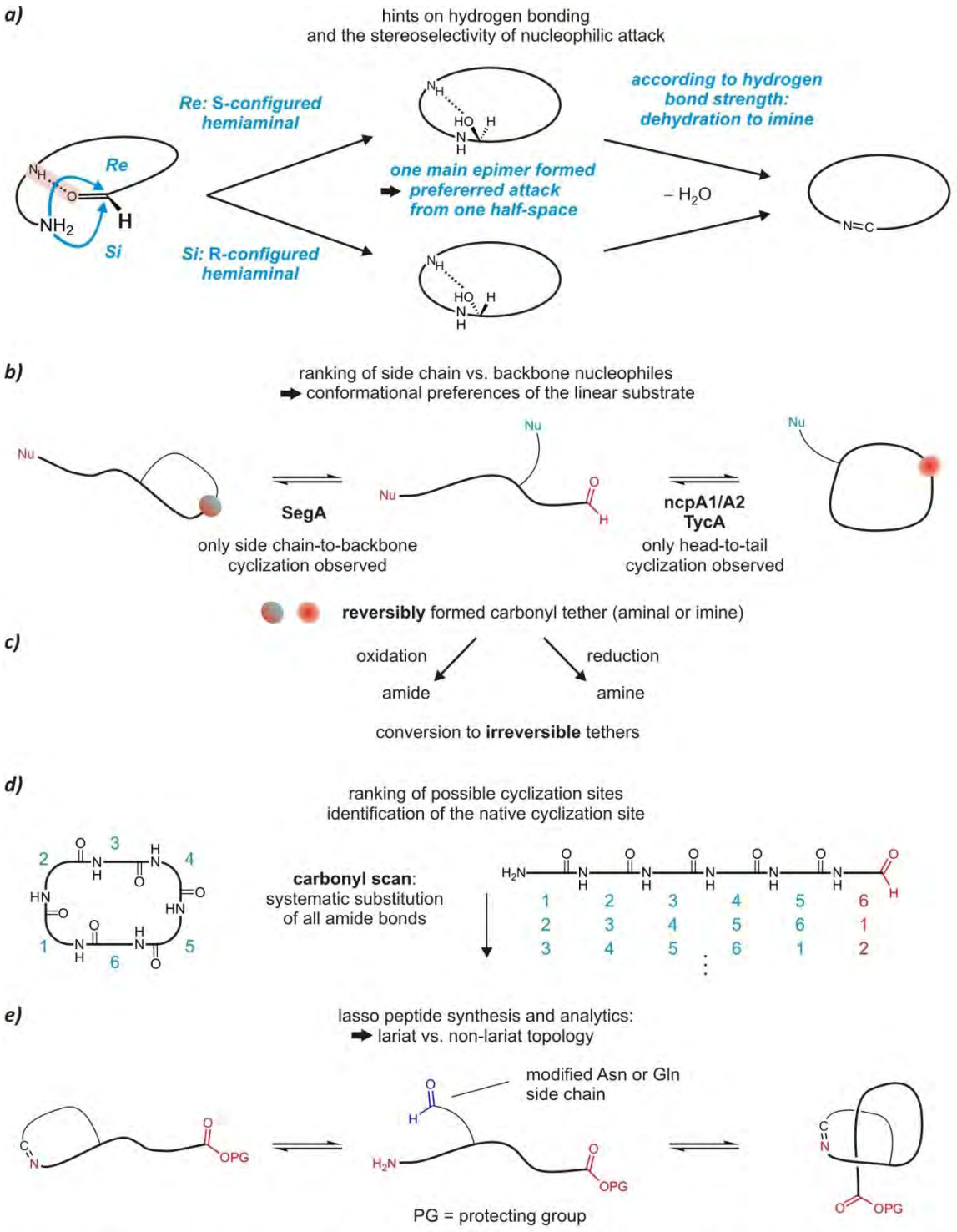

Figure 3.50 Summary and outlook: The scope of the carbonyl substitution in peptides. ***a)*** *The formed carbonyl tether allows to draw conclusions about whether hydrogen bonding partners are located around the cyclization site. The stereoselectivity of hemiaminal formation depends on the selectivity of the nucleophilic attack from the* Re *or* Si *half space, which indicates the extent of molecular preorientation.* ***b)*** *As shown by the examination of SegA, a side chain functionality can outrule the N-terminal amine as nucleophile, and the selectivity of side chain-to-backbone vs. head-to-tail cyclization indicates conformational preferences of the precursor.* ***c)*** *The subsequent conversion of the carbonyl function into an amide or amine exhibits an option for macrocycle synthesis.* ***d)*** *Concept of the carbonyl scan shown for a cyclohexapeptide.* ***e)*** *The elucidation of how the lariat protoknot of the lasso peptides is generated exhibits an especially attractive option of carbonyl substitution. By introducing the carbonyl function to the side chain, it can be investigated to what extent the ring is formed with the C-terminus threaded through (right) or not (left).*

restricted. The comparison with the ncp (section 3.6) suggests the presence of several strong hydrophobic interactions throughout the linear peptide chain as the reason and, consequently, that polar interactions in linear substrates in an aqueous environment must not be overestimated. However, further substrates have to be analyzed in order to show whether TycA (and, for example, the closely related gramicidin S) exhibit exceptional cases.

The hydrogen bonding network within the antiparallel TycA β-sheet had great implications on the formed carbonyl tether as no dehydration to the imine was observed and for the first time a stable hemiaminal function could be observed within a peptidic structure. This functional group is of analytical value as it corresponds to the tetrahedral intermediate of macrolactam formation, and it allowed to experimentally confirm the theories about how TycA macrocyclization is promoted by hydrogen bonding. Consequently, the propensity of imine vs. hemiaminal formation upon ring closure gives information about the localization of amide proton binding partners around the cyclization site (figure 3.50a). As a new stereocenter is generated in the hemiaminal, information is given about the stereoselectivity of the attack and therewith about whether the cyclization site is structurally well-defined. In the case of TycA-CHO, only one stereoisomer is formed and the NOE-based molecular modeling studies suggest a selective ring closure at the *Si* site of the precoordinating aldehyde.

By examination an aldehyde precursor of segetalin A (SegA, section 3.6.2) it was shown that also side chain-to-backbone cyclization products can be observed within an equilibrium, which allows for the synthesis of smaller rings (figure 3.50b). A logical next step to investigate is the conversion of the carbonyl tethers into irreversible linkages, which, especially if applicable under equilibrium conditions, is a possible option for the synthesis of macrocycles (figure 3.50c).

In this context, a systematic “carbonyl scan” of all amide bonds in a cyclopeptide could allow the ranking of different precursors with respect to their inclination to cyclize, and the comparison of native with non-native ligation sites. It also has potential for the determination of the native cyclization site if it is not known (figure 3.50d). Another promising target class is given by the lasso peptides (section 3.1.1) which by their unique structure feature high proteolytic stability and are promising novel lead structures for drug discovery.[243, 244] The carbonyl substitution of the side chain-to-backbone cyclization site could, in addition to the thermodynamic characterization, open a way how to synthesize these peptides by chemical methods (figure 3.50e).

Finally, it is desirable to derive conclusions about proteins from these studies. The linear peptides are reminiscent of the molten globule state of proteins, which is highly dynamic in spite of the presence of numerous secondary structural elements.[245] In contrast, protein surface

loops may be unstructured, but as they are fixed at the positions emerging from the stiffened membrane-bound protein segment they can perform important tasks. This recalls an analogy to the cyclopeptides which, even if they exhibit conformational averaging, experience a considerable restriction of mobility due to the covalent tethering of both termini.

4 Synthesis of polyhydroxylated thiazoles from sugar/amino acid condensation products

In addition to the macrocyclization processes described in the preceding chapter, the local side chain-to-backbone cyclization is another process employed for the structural tailoring of natural products. This generates a five-membered heterocycle which, as integrated in the backbone, introduces a local rigidity. While the amide bond is symbolized by the hyphen "-", we suggest the use of the hyphen "<" in order to indicate the second linkage generated by the cyclization. If for example a Cys side chain is cyclized onto the N-terminal amide function, a thiazole (Thz) ring is formed and the Cys ϕ torsion is locked. This is depicted in the following for an Ala-Cys dipeptide which is converted to an Ala<Thz dipeptide:

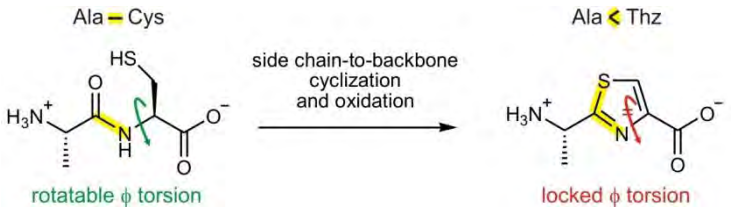

The tailoring by formation of thiazole as well as oxazole rings (figure 4.1a) also decreases the polarity of the substrate as it substitutes two hydrophilic functionalities (an amide and a polar side chain) by a hydrophobic motif. In the light of the high polarity of unmodified peptides this transformation appears all the more important as the hydrophobization opens up new possible modes of action of the biomolecule. It is therefore not surprising that "*heterocycles are a recurring motif in Nature's medicinal chemistry toolbox*",[246] being found in a multitude of peptides and polyketides of varying molecular weight and synthesized by different organisms.

4.1 Thiazole units in peptidic natural products

4.1.1 Ribosomal and non-ribosomal heterocycle formation

Figure 4.1a schematically shows the constitutive steps of thiazole and oxazole formation in biosynthesis. Every heterocycle in a peptide originates from a dipeptide **1** with any residue (Xaa) at the N-terminal position (red) and a Thr, Ser, or Cys residue at the C-terminal position (blue). Base activation of the side chain OH or SH nucleophile at the binding site of a heterocylization catalyst (heterocyclase) is followed by attack the amide carbon, resulting in the tetrahedral

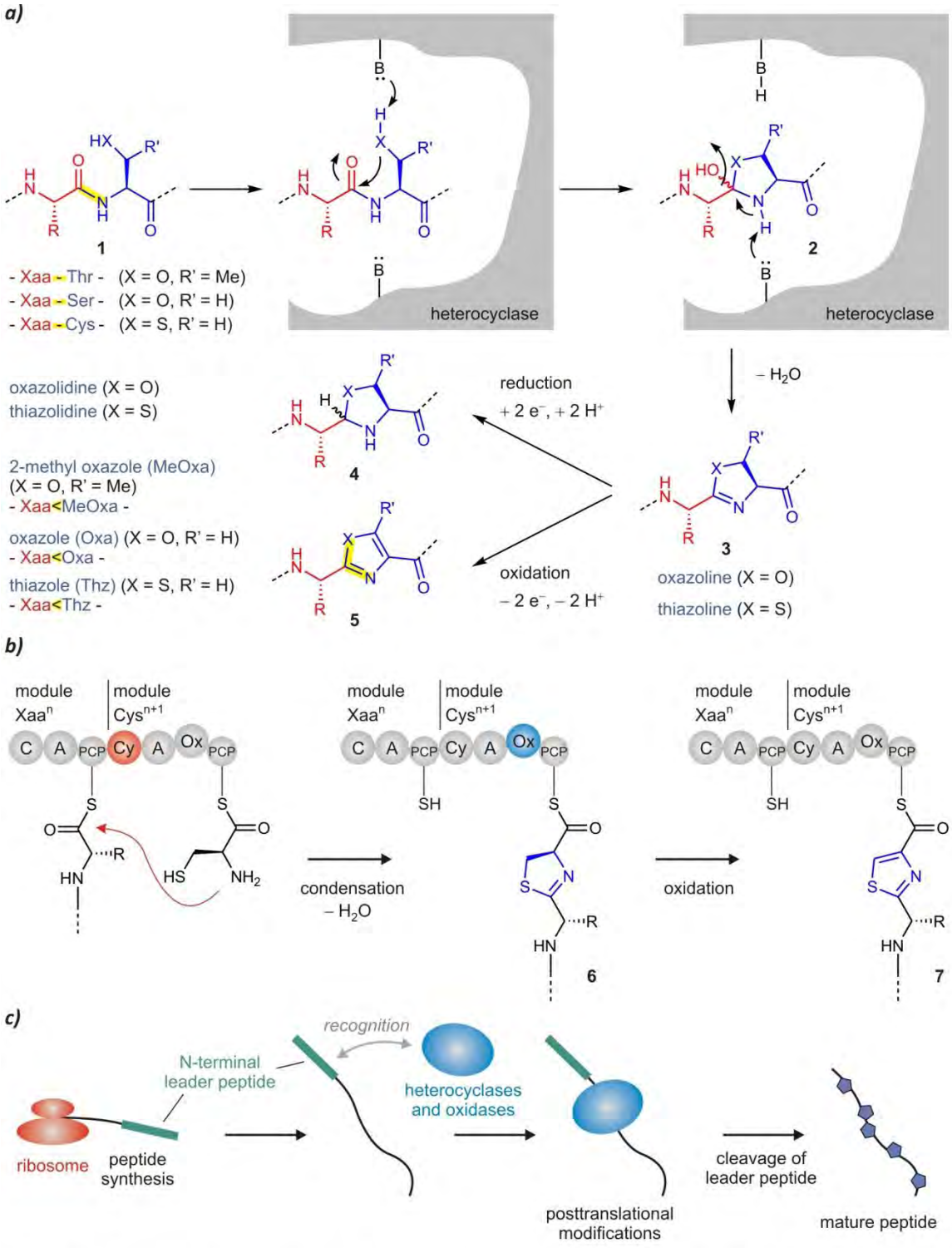

Figure 4.1 Thiazole biosynthesis. a) *Schematic depiction of the biosynthetic side chain-to-backbone cyclization leading to backbone five-membered heterocycles. At the active site of the enzyme (shown in grey), two basic side chains (B) trigger the nucleophilic attack of the side chain and the subsequent dehydration. According to the residue, this leads to oxazolines or thiazolines* ***3*** *which can be further modified by reduction or oxidation. The hyphen "<" in the three-letter nomenclature of the peptides has been chosen in order to indicate the additional covalent linkage.* ***b)*** *The thiazole construction in non-ribosomal peptide synthesis already occurs during peptide assembly, and the peptide chain containing the C-terminal thiazole (****7****) is either cleaved from the synthetase of subjected to further elongation.* ***c)*** *Thiazole units present in ribosomal peptides are generated post-translationally by dedicated heterocyclases and oxidases (blue) which recognize their target by a N-terminal leader sequence (green).*

intermediate **2**. Another basic function triggers dehydration which leads to a thiazoline or oxazoline heterocycle **3**. These structural motifs still exhibit the stereocenter of the former Thr, Ser, or Cys residue and they are widely occurring in natural products, from which the antibiotic bacitracin is among the most prominent ones (marketed for example as Nebacetin® (*Sandoz*) or Polyspectran® (*Alcon Pharma*, market volume 120 million USD).[247-249]

The semi-saturated heterocycles **3** can be subjected to further enzymatic tailoring. The reduction to the oxazolidine and thiazolidine motifs **4** is rarely observed, apparently due to their easy hydrolysis. The bacterial siderophore yersiniabactin is one of the few examples of natural products carrying a saturated heterocycle.[250, 251] In contrast, the oxidative transformation to unsaturated oxazoles and thiazoles **5** is carried out for the majority of oxazolines and thiazolines. This increases the stability of the heterocycle which is not inclined to hydrolysis any more, and it generates an aromatic motif within the backbone. In analogy to the suggested nomenclature of Xaa<Thz for a thiazole dipeptide, the corresponding oxazole and methyl oxazole dipeptides can be termed as Xaa<Oxa and Xaa<MeOxa, respectively. This nomenclature will be used throughout this chapter. As the synthetic work within the scope of this thesis concerned thiazoles, further introduction will concentrate on this structural unit.

Thiazole peptides can be synthesized by non-ribosomal peptide synthethases (NRPS, sections 3.1.1 and 3.2.3.2, figure 3.15) as well as by post-translational tailoring of ribosomal natural products.[246, 252] As shown in figure 4.1b, non-ribosomal thiazole synthesis occurs already during the assembly of the peptide (or polyketide) chain.[253] If a Cys residue is not only supposed to be amide-coupled but also cyclodehydrated to the nascent peptide, a heterocyclization (Cy) domain (highlighted in red) replaces the typically occurring cyclization (C) domain in the assembly line. This leads to formation of a peptidyl carrier protein (PCP) bound thiazolidine **6** which is subsequently converted to the thiazole **7** by an oxidation (Ox) domain (highlighted in blue).[254-256] This domain can be inserted into the adenylation (A) domain, as shown in figure 4.1b, but it can also occur C-terminally fused to the peptidyl carrier protein (PCP) of the module.[253] The fact that the heterocycle is tailored during the construction of the peptide chain is in contrast with the modification of ribosomal products where thiazoles can only be generated by post-translational modification (figure 4.1c).[257] The peptide chain is first assembled by the ribosome and subsequently released into the cytoplasm. For further structural modifications the substrate must be recognized by respective tailoring enzymes which is enabled by a specific leader peptide sequence (highlighted in green). In analogy to the non-ribosomal modifications, heterocyclases first catalyze the condensation reaction to thiazolidines while the oxidative aromatization leading to the thiazoles is accomplished by oxidases.[258]

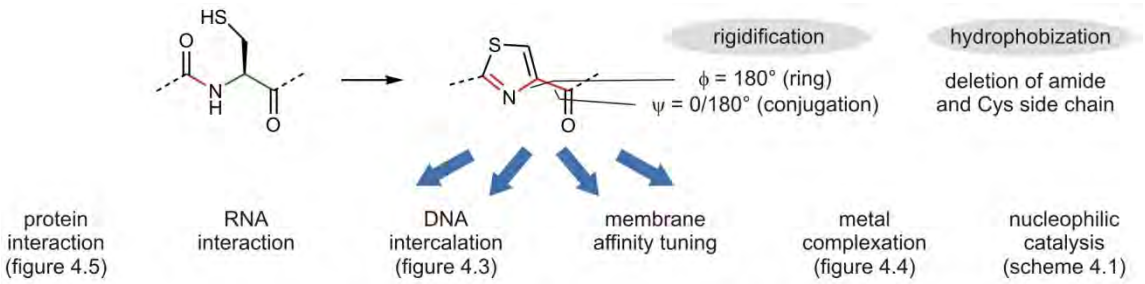

Figure 4.2 Impact of thiazole incorporation on structure and function of natural products. *Some biological modes of action which are the consequence of thiazole incorporation are shown by examples in scheme 4.1 and in figures 4.4 to 4.6.*

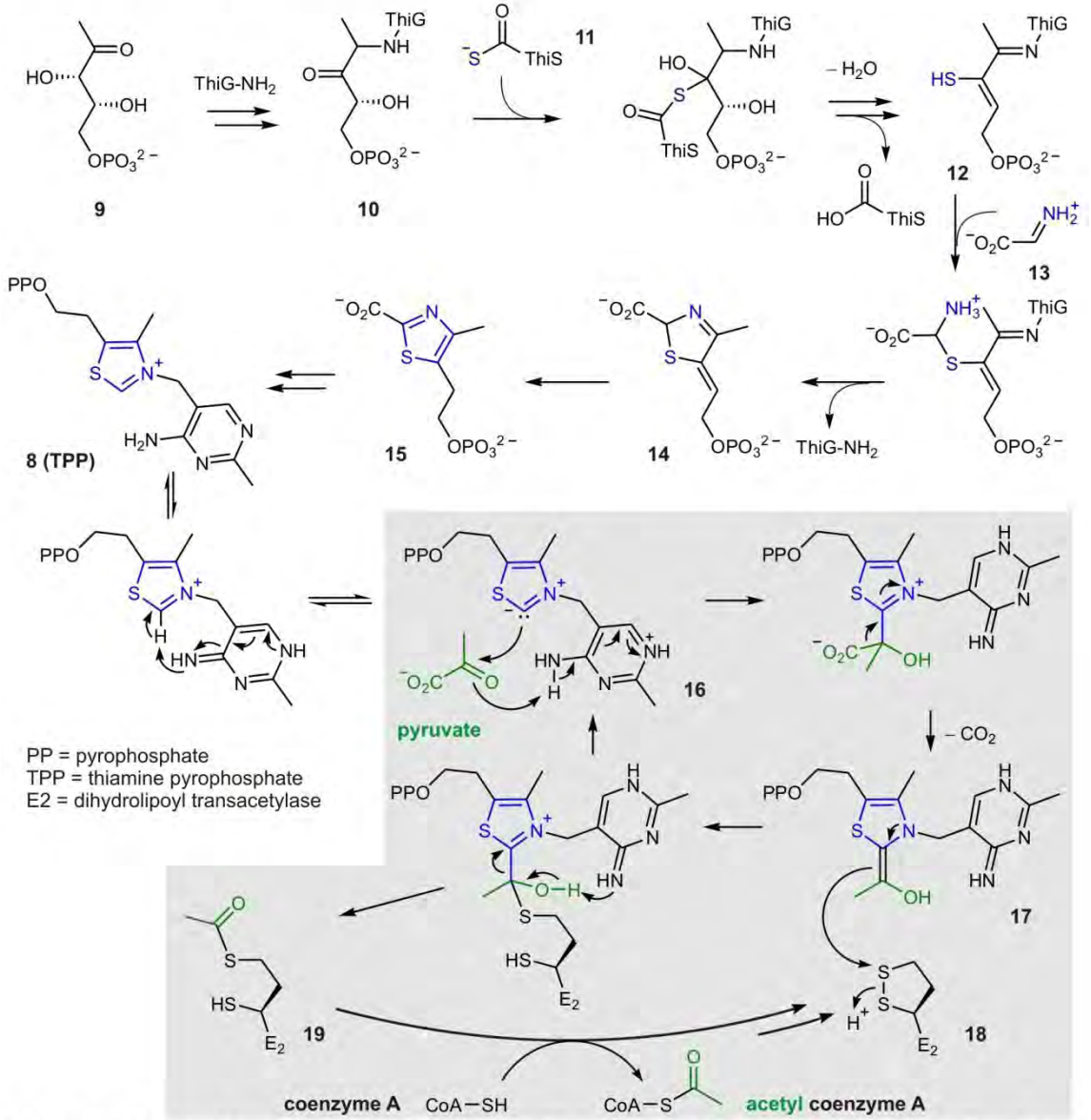

Scheme 4.1 Proposed mechanism for the biosynthesis of the thiazole ring of thiamine (not colored) and its role in the synthesis of acetyl coenzyme A (colored grey). *1-deoxy-D-xylulose-5-phosphate* ***9*** *(DXP) is adequately modified by two synthetases (ThiG and ThiS) and subsequently reacted with glycine imine* ***11****. The thiazole nitrogen and sulfur as well as the mature thiazole ring are highlighted in blue. In contrast to the thiazole units found in peptides and polyketides, the thiamine thiazole exhibits a quarternary nitrogen which is why it can act as nucleophilic catalyst. One biological role is the pyruvate decarboxylation as cofactor of the pyruvate dehydrogenase complex. Pyruvate and the acetyl groups are highlighted in green.*

4.1.2 Biological roles of thiazoles

The thiazole motif is found in such a great number of natural products as its impact is far beyond constraining the backbone geometry to conformations associated with increased biological activity and selectivity. By thiazole formation, the peptide backbone is not only rigidified by the restriction of two torsions, but a hydrophobic aromatic motif is generated (figure 4.2). This extends the possibilities of biological functions carried out by peptides as they now exhibit a hydrophobic contact site which enables specific interactions with proteins,[259] RNA,[260] and DNA.[261] The increased lipophilicity of the substrate also effects a higher membrane affinity which can turn peptides into membrane-disrupting toxins.[258] Furthermore, the nitrogen atoms within the heterocycles can serve as coordination sites for metal ions.[262] In the following, some examples of natural products and their biological roles will be illustrated.

4.1.2.1 Thiamine (Vitamin B1): nucleophilic catalysis

The cofactor thiamine pyrophosphate **8** (TPP, scheme 4.1) is the most prominent thiazole-containing biomolecule and it is essential for the nervous system as well as for the catabolism processes in organisms.[162] Its dephosphorylated form (thiamine/Vitamin B1) can be synthesized by prokaryotes and some eukaryotes (fungi and plants), but not by the human organism, which is why it has to be ingested by food.[263, 264] In the light of the artificial thiazole syntheses developed within the scope of this thesis, the biosynthesis of the thiamine thiazole shows an analogy as it is also generated by reaction of a sugar with an amino acid (scheme 4.1).[265] The sugar component bases on 1-deoxy-D-xylulose-5-phosphate **9** (DXP) which is converted to the α-aminoketone **10** by thiazole synthase ThiG. The ketone is subsequently attacked by the thiocarboxylate of thiazole synthase ThiS **11**, and three further steps (*S*/*O* acyl shift of ThiS, dehydration and elimination of ThiS) yield the thiol **12**. After addition of glycine imine **13** a transiminiation takes place which closes the five-membered ring **14** and which releases the substrate from ThiG. Protonation/deprotonation yields the thiazole carboxylate **15**, and by phosphorylation, decarboxylation and reaction with a pyrimidine the product **8** (TPP) is finally obtained. Its role as nucleophilic catalyst bases on the positively charged nitrogen of the thiazolium ring which, in combination with the acidic pyrimidine, has a low energetic barrier to form the ylide **16**. The lower part of scheme 4.1 shows the role of TPP in the glucose catabolism.[162, 266] The negatively charged ylide carbon attacks pyruvate (green) and thus enables its decarboxylation. The resulting species **17** attacks the cyclic disulfide of dihydrolipoyl-transacetylase **18** (E_2) which is acylated (**19**) and which in the next step transfers the acyl group to coenzyme A. This generates acetyl coenzyme A which is channeled into the citric acid cycle.

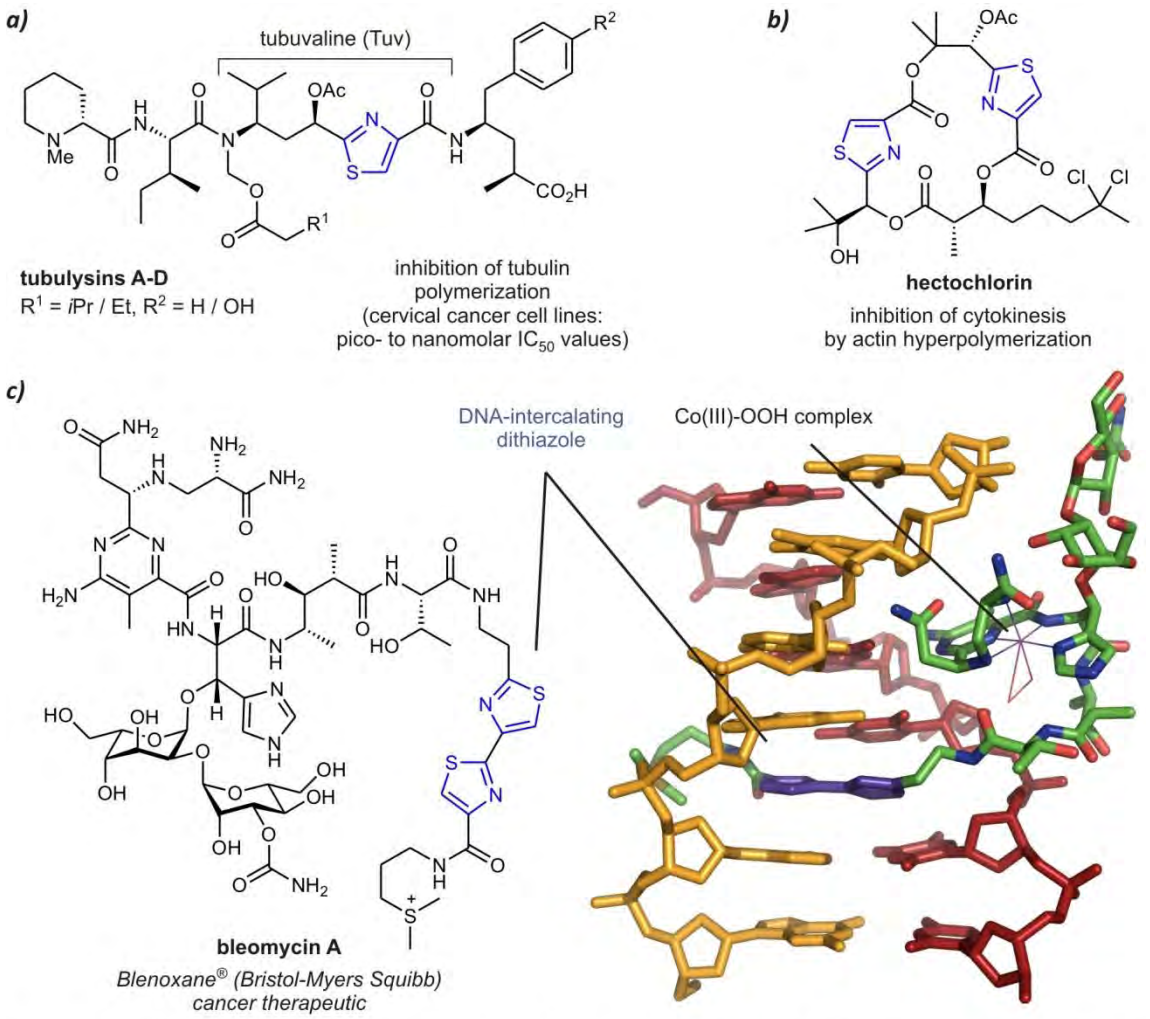

Figure 4.3 Examples of nonribosomally produced natural products with thiazole units: a) *tubulysins,* ***b)*** *hectochlorin,* ***c)*** *bleomycin A. All thiazoles are highlighted in blue. In the depiction of the DNA-intercalating bleomycin A (PDB entry: 1MTG), the DNA strands are colored orange and red. The narrow sticks indicate the Co(III)-OOH which is coordinated by an imidazole and pyrimidine nitrogen.*

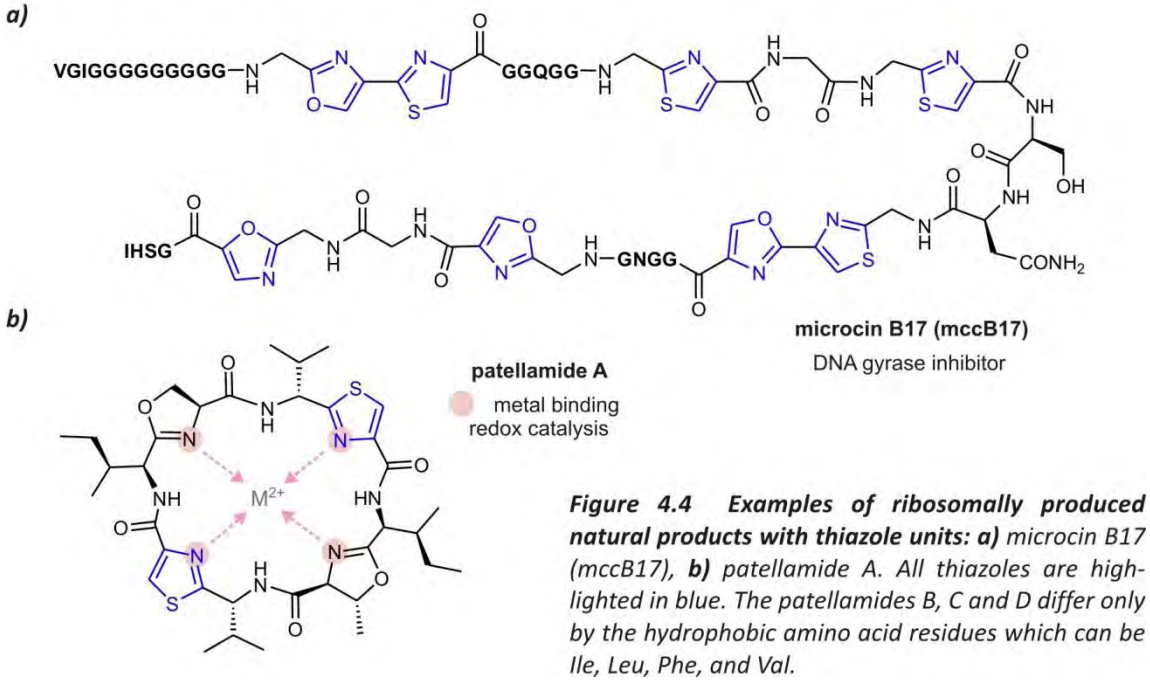

Figure 4.4 Examples of ribosomally produced natural products with thiazole units: a) *microcin B17 (mccB17),* ***b)*** *patellamide A. All thiazoles are highlighted in blue. The patellamides B, C and D differ only by the hydrophobic amino acid residues which can be Ile, Leu, Phe, and Val.*

4.1.2.2 Tubulysins, hectochlorin and microcin B17: protein interaction

The linear tubulysin tetrapeptides (figure 4.3a) are non-ribosomally produced by two myxobacteria species and they are among the most cytotoxic peptides known to date.[267, 268] Their antimitotic properties rely on binding to tubulin and effient depletion of the cell microtubules which induces cell death.[269, 270] Although binding details are not known yet, the thiazole dipeptide tubuvaline (Tuv) turned out to be essential for high activity.[271] In the past years, great effort has been spent on the synthesis of simplified analogs that for example lack the synthetically challenging Tuv aminal function[272] as well as on the development of tubulysin-folic acid conjugates[273] and nanoparticles for cancer therapy.[274]

The majority of thiazole-containing peptides is represented by macrocycles, and marine organisms like the cyanobacteria strain *Lyngbya majuscula* produce a multitude of these compounds.[275, 276] Figure 4.3b shows as an example the depsipeptide/polyketide hybrid hectochlorin which exhibits two identical thiazole units that are differently linked to the adjoining backbone.[277, 278] By inducing actin hyperpolymerization, hectochlorin arrests cells at cytokinesis and thus inhibits the cell division process.

The polypeptide microcin B17 (mccB17, figure 4.4a) also exerts its biological action by protein binding. In contrast to the tubulysins and hectochlorin it is synthesized ribosomally and exhibits the best-studied example of how the heterocyclic thiazole and oxazole functions are installed post-translationally (see also figure 4.1c).[279-282] The antibiotic activity of mccB17 results from binding to DNA gyrase, a protein that controls the supercoiling of DNA during the replication process. As mccB17 traps the double-strand cleaved DNA/protein complex it causes an accumulation of double-strand breaks and thereby induces apoptosis.[259, 283]

4.1.2.3 Bleomycin A and the patellamides: DNA intercalation and redox catalysis

In contrast to mccB17, the glycopeptides antibiotic bleomycin A is able to induce DNA douple-strand cleavage (figure 4.3c), and it is successfully applied as chemotherapeutic, e.g. against testicular cancer. The imidazole and pyrimidine serve as coordination sites for redox-active iron and copper ions which lead to the formation of oxygen radicals that attack the DNA.[284-287] The 4,2'-fused dithiazole at the C-terminus is able to intercalate between stacked DNA base pairs (figure 4.3c, right) and thus serves as DNA anchor which crucially increases the bleomycin A

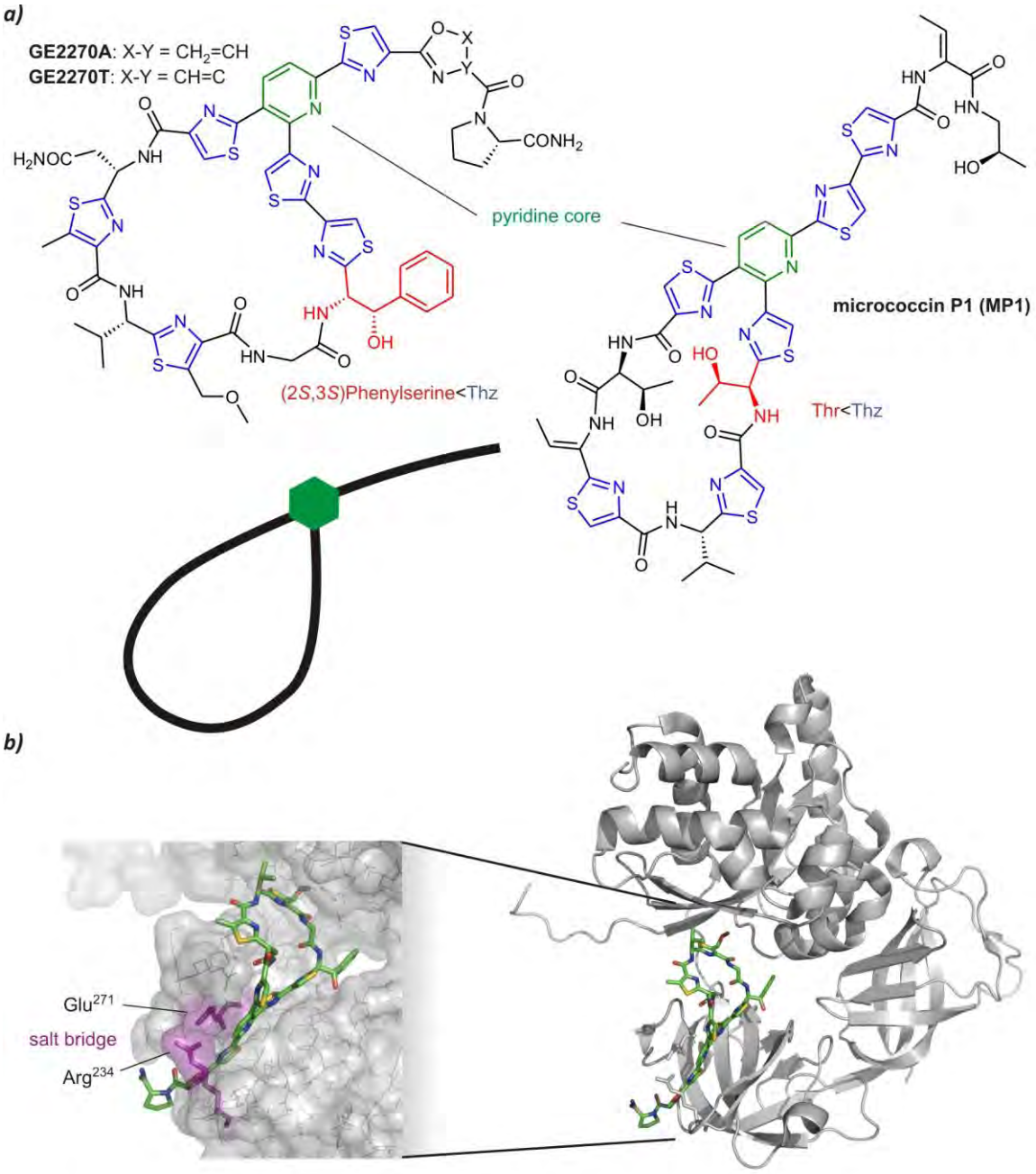

Figure 4.5 (c-e continued on next page) Members of the thiopeptide antibiotics, which represent the most complex thiazole-containing natural products and which feature highly functionalized Xaa<Thz dipeptides (highlighted in red). *The six-membered heterocycle core motifs are colored green, thiazoles and thiazolines are colored blue. The backbone networks are schematically shown next to the structural formulas.* ***a)*** *Structures of the GE2270 antibiotics (left) and of micrococcin P1 (MP1, right).* ***b)*** *Depiction of GE2270A bound to its biological target, the EF-Tu elongation factor of the bacterial ribosome (X-ray structure, PDB entry 2C77; right: ribbon depiction of the protein, left: enlargement of space-filling depiction with the residues bound by a salt bridge highlighted in purple).* ***c)*** *Structure of thiostrepton (see figure 3.3, section 3.1.1 for biosynthetic steps).* ***d)*** *Structure of the indole-containing thiopeptides multhiomycin (nosiheptide) and philipimycin.* ***e)*** *Structure of the hydroxyindole-containing nocathiacins and thiazomycins which feature the most complex framework and the highest functionalized thiazole dipeptide known to date with a dihydroxyglutamate (Dyg) side chain (Dyg<Thz, highlighted in red) which is linked to the peptide backbone, the indole and a glycoside at all five functionalities. The research described in this chapter gives a first synthetic access to this core motif. In addition to the three compounds shown here, further nocathiacins and thiazomycins have been isolated but which possibly are intermediates in biosynthesis.*

concentration at its target.[261] It is assumed that the 4,2'-fused oxazole/thiazole units in mccB17 (figure 4.4a) exert the same function and thus lead to a high local mccB17 concentration at the DNA gyrase protein.[252]

Redox catalysis activity is also enabled by the patellamide cyclopeptides (figure 4.4b),[288, 289] but in this case the thiazole and oxazolines nitrogens serve as metal-coordinating sites. The specific biological functions still remain unclear, however, it has been suggested that the patellamides enable specific electron transfer processes in the marine milieu.[262] The peptide precursors are ribosomally produced by ascidians, and the post-translational tailoring comprises the heterocycle formation and the macrocyclization as final step.[290-292]

4.1.3 Thiopeptide antibiotics

The natural products presented in the preceding chapter have in common that they exhibit simple unbranched linear or macrocyclic backbone geometries. Moreover, the Xaa residues of the Xaa<Thz dipeptides are - with exception of the tubulysins and hectochlorin - restricted to unpolar proteinogenic amino acids. The members of the class of thiopeptides show a considerably higher level of structural complexity and perhaps exhibit the most striking examples of how ribosomally produced "standard" linear peptides are converted to micro-biological warfare by ingenious combination of post-translational modifications.[111, 293, 294] Figure 4.5 shows some representative examples of these heterocyclic peptides in order of increasing structural complexity. For every substrate the backbone network is also schematically depicted.

All thiopeptides exhibit a six-membered nitrogen heterocycle (highlighted in green) which, as core motif of the network, links at least three peptide backbone strands to each other. In micrococcin P1 (MP1)[295] and the GE2270 antibiotics,[112, 296] which are among the members with the simplest backbone geometry, it is represented by a pyridine which at positions 2 and 3 connects one peptide strand, thus creating a 26-membered (MP1) or 30-membered (GE2270) macrocycle, and which is further linked to a linear sequence at position 6 (figure 4.5 a). The peptide chains are rich in thiazole heterocycles (some members like the GE2270 antibiotics also feature oxazoles or oxazolines) which are particulary densely present in proximity of the six-membered core ring, and a further characteristic of most thiopeptides is the presence of numerous dehydroamino acids derived from Ala and Thr. These extensive post-translational structural modifications increase the rigidity and hydrophobicity of the peptides and are responsible for their high toxicity towards Gram-positive bacteria, among them several multiple drug resistant strains like methicillin-resistant *S. aureus*. Furthermore, they do not harm

Figure 4.5 (continued from previous page)

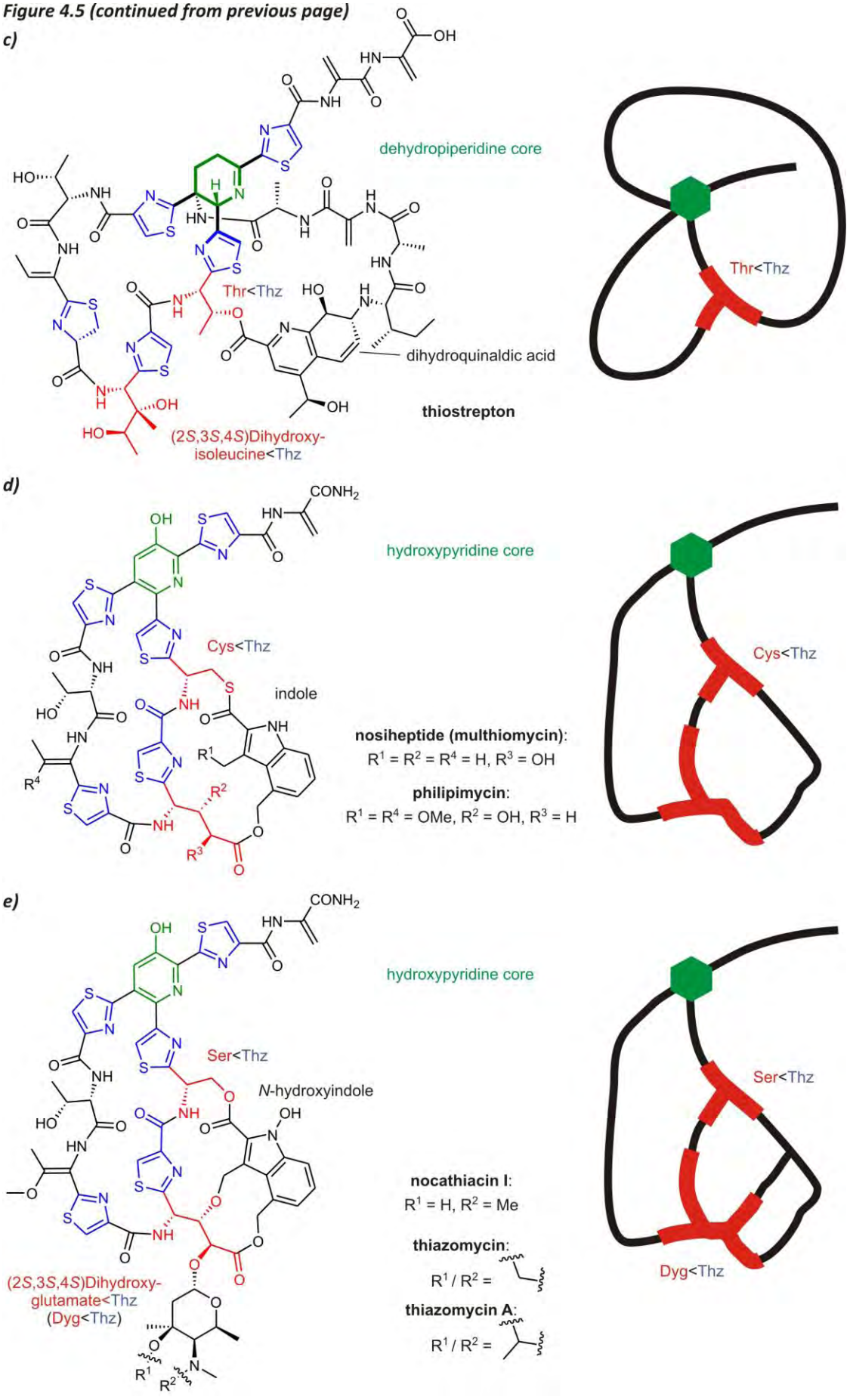

mammalian cells while exhibiting antibacterial activity comparable to that of the penicillins. This has over the past decade triggered great effort in research aimed at the establishment of thiopeptides as lead structures for a novel class of applicable antibiotics.[293, 294]

The toxicity of the thiopeptides (all synthesized by bacteria of the *Streptomyces* genus) largely bases on the efficient inhibition of bacterial protein biosynthesis, and two groups of thiopeptides can be distinguished according to the mode of action. The members of one group bind to a region of the 23S rRNA of the bacterial ribosome,[260, 297, 298] while the others show high affinity towards the elongation transfer factor EF-Tu, a protein which is essential as it recognizes and transfers aminoacyl-tRNA to the A site of the ribosome.[112, 299] Figure 4.5b depicts an X-ray structure of GE2270A bound to EF-Tu.[300] In addition to *van-der-Waals* interactions, GE2270A establishes a salt bridge between an Arg and a Glu residue (colored in purple in the depiction on the left), which probably evokes the strong binding affinity. The binding of the antibiotic abolishes essential conformational changes of the protein to perform its taks and thus disrupts the activity of the ribosome.

Thiostrepton (figure 4.5c) was the first known thiopeptide (discovered in 1955)[301] and exhibits significantly higher structural complexity. Instead of a simple loop, the peptide backbone forms a three-dimensional network connected by the dehydropiperidine core. The recent findings of how this network is obtained in biosynthesis *"push the limits of current biosynthesis paradigms"*,[111] and some key steps are shown in figure 3.3 (section 3.1.1). In addition to the 1,2-dihydroquinaldic acid moiety, the structure stands out by a Thr<Thz dipeptide which is not only linearly linked to the adjoining backbone but which serves as second core motif (highlighted in red). In addition, a highly functionalized (2*S*,3*S*)-dihydroxy-isoleucine<Thz dipeptide is present.

Multhiomycin (nosiheptide)[302] and philipimycin[303] (figure 4.5d) contain a hydroxypyridine and a Glu<Thz dipeptide as core motif, the latter being hydroxylated either in the 2- or the 3-position. They are structurally similar to the nocathiacins[304] and thiazomycins[305] (figure 4.5e) which represent the thiopeptides with the most complex backbone network comprising a 10-, 15- and 26 membered ring.[306] They also contain the most complex thiazole dipeptide known to date: a (2*S*,3*S*)-dihydroxyglutamate (Dyg)<Thz (highlighted in red) which exhibits four linkages to a *N*-hydroxyindole and to the peptide backbone and which in addition serves as glycosylation site at 3-OH.

The structural and functional complexity of the thiopeptide antibiotics exhibits challenges for their chemical syntheses, and this is strikingly demonstrated by the fact that, in spite of the research effort spent, only seven of the approx. 80 members of the thiopeptide class have so far succumbed to total synthesis.[294, 307] In this context, the highly functionalized thiazole dipeptides,

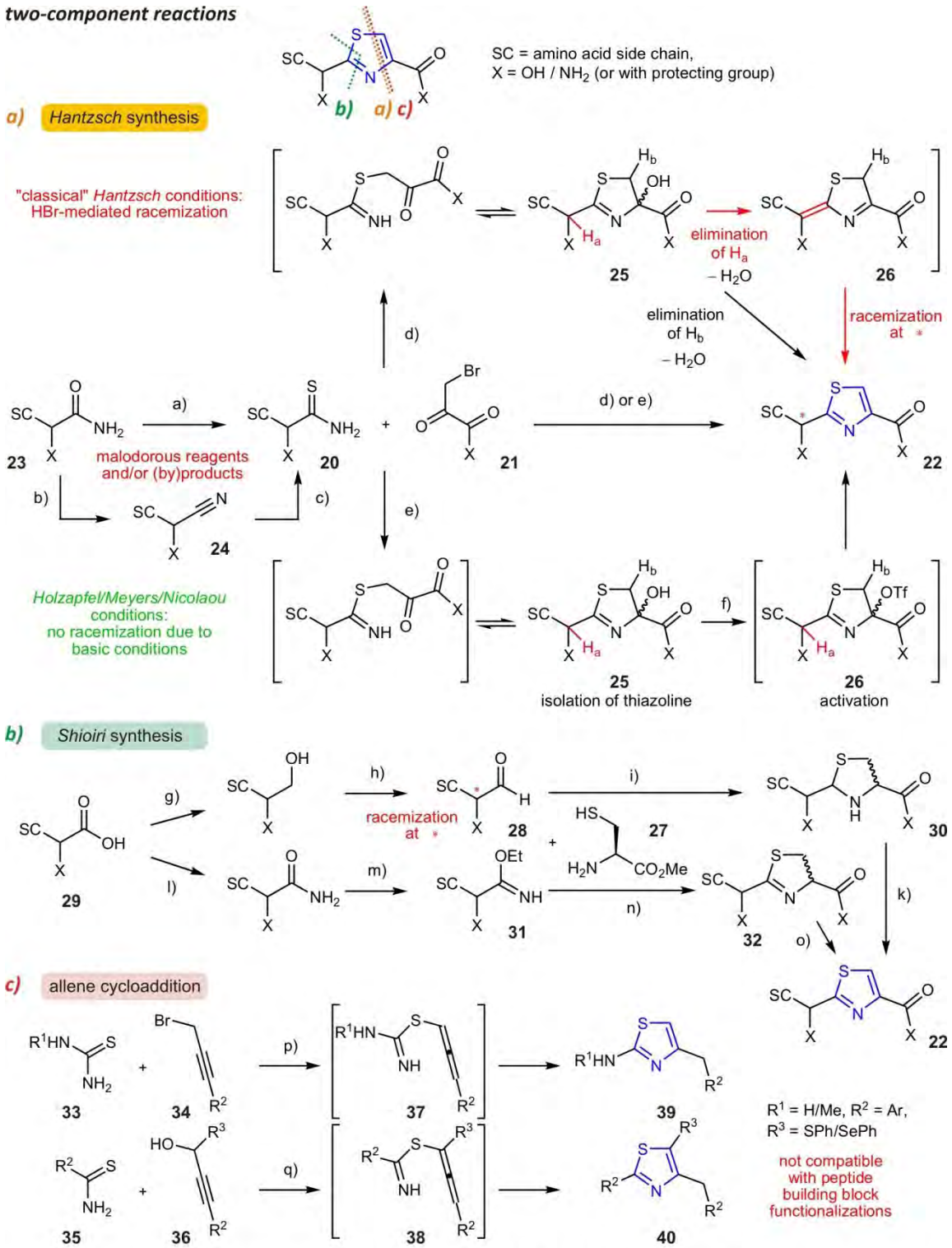

Scheme 4.2 Thiazole syntheses employing the coupling of two components. a) Hantzsch *synthesis and modified protocols according to* Holzapfel*,* Meyers*, and* Nicolaou. ***b)*** *Condensation reactions according to* Shioiri. ***c)*** *[3+2] cycloadditions of allenes and thiourea derivates or thioamides. Some problems associated with the syntheses are highlighted in red.* Reagents and conditions: a) *Lawesson's* reagent, dioxane, RT; b) Tf_2O, Pyr, 0 °C; c) H_2S, triethanolamine, EtOH, RT; d) EtOH, reflux; e) $KHCO_3$, DME, 0 °C (*Holzapfel*)/ –40 to –20 °C (*Meyers*)/ $NaHCO_3$, DME, RT (*Nicolaou*); f) Tf_2O, 2,6-Lu, DME, 0 °C (*Holzapfel*)/ –40 to –20 °C (*Meyers*)/ TFAA, Et_3N, Pyr, 0 °C (*Nicolaou*); g) CH_3I, $KHCO_3$, DMF, RT, then $NaBH_4$, LiCl, THF, RT; h) Pyr x SO_3, NEt_3, DMF, RT; i) NEt_3, Tol, RT; k) MnO_2, Tol, 50 to 70 °C; l) EEDQ, NH_4HCO_3, $CHCl_3$, RT; m) Et_3OPF_6, CH_2Cl_2, RT; n) MeOH, $CHCl_3$, 0 °C to RT; o) $BrCCl_3$, DBU, CH_2Cl_2, 0 °C; p) K_2CO_3, DMF, microwave, 130 °C; q) $Sc(OTf)_3$, $MeNO_2$, reflux.

in spite of their small size, turned out to be especially difficult to be accessed, which served as motivation for the synthetic work carried out within the scope of this thesis. In order to generate a context with already accomplished work, chemical syntheses of thiazole dipeptides will be presented in the following.

4.2 Chemical thiazole synthesis: Strategies and problems

4.2.1 Two-component reactions

The condensation reaction of a thioamide **20** and an α-bromocarbonyl compound **21** discovered by *Hantzsch*[308] exhibits the longest-known synthetic access to thiazoles dipeptides (**22**) and it is, with some modifications, still the most used reaction type for the synthesis of thiazole dipeptides (scheme 4.2a). In the first step, a primary amide **23** is transferred to the corresponding thioamide **20** either by using *Lawessons's* reagent[309] (a) or by dehydration to the α-amino nitrile **24** (b) and subsequent addition of H_2S (c).[310] These first preparation steps as well as the purification of the products are already associated with difficulties as the reaction with *Lawessons's* reagent suffers from the difficulty of removing phosphorus-containing byproducts, and the use of toxic and malodorous H_2S is problematic as well and not suitable for reactions on larger scale. The "classical" *Hantzsch* condensation procedure, which is the simple heating of the condensation partners (d), leads in the case of α-chiral thiazoles to a complete racemization of the product by elimination of the α-proton (**25→26**).[311] Therefore, modified reaction protocols were developed by *Holzapfel et al.*[312] and *Myers et al.*[313] which allow for the synthesis at RT. Under basic conditions (e), the hydroxythiazoline **25** can be isolated and subsequently be activated as triflate **26** which undergoes selective β-elimination and thus retains the stereochemistry at the α-position. Further modifications of the procedure by *Nicolaou et al.* led to a significant improvement of yields on larger reaction scales[314] and thus promoted the use of the *Hantzsch* synthesis within the scope of the landmark total synthesis of thiostrepton.[315, 316]

The thiazole formation developed by *Shioiri et al.*, in contrast, is similar to the biosynthetic condensation as it employs cysteine **27** as sulfur-delivering compound which reacts with an amino acid aldehyde **28** (scheme 4.2b).[317] For this purpose, an amino acid (**29**) is converted to the aldehyde by a reduction/oxidation sequence. These aldehydes, however, are the weak point of the approach as they often suffer from partial racemization. Condensation with cysteine finally yields the thiazolidine **30** which has to be oxidized in order to obtain the thiazole dipeptide target **22**. This step can also be problematic as harsh oxidative conditions are required,

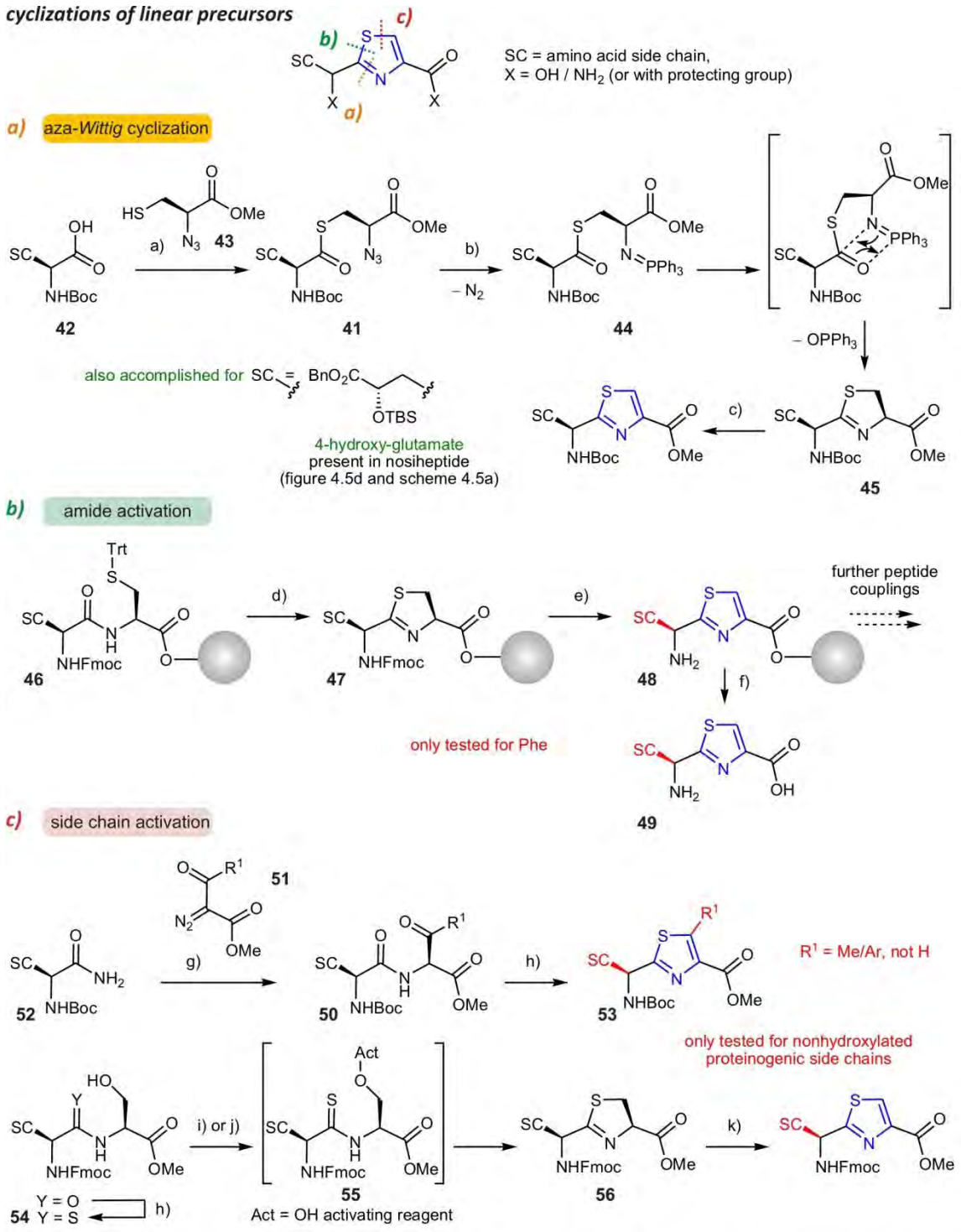

Scheme 4.3 Thiazole syntheses employing the cyclization of linear precursors. a) *Intramolecular aza-*Wittig *cyclization starting from an azido thioester* ***41****. This approach could be utilized for one of the few syntheses of thiazole dipeptides with non-proteinogenic hydroxylated side chains (scheme 4.5).* ***b)*** *Biomimetic approach by* Kelly et al. *which was established for solid-phase peptide synthesis by* Kessler et al.*: Cys side chain-to-backbone cyclization triggered by amide activation.* ***c)*** *Synthetic strategies which employ the intramolecular cyclization of thioamides to activated side chains: Rh carbene coupling yielding a dipeptide intermediate which an "activated" (oxidized) Thr side chain (top) and activation of the Ser hydroxy function with the* Burgess *reagent or DAST.* Reagents and conditions: a) DIC, DMAP, CH_2Cl_2, 0 °C to 20 °C; b) PPh_3, THF, −20 °C to RT; c) $BrCCl_3$, DBU, CH_2Cl_2, 0 °C to 20°C; d) PPh_3, Tf_2O, CH_2Cl_2, RT; e) $BrCCl_3$, DBU, CH_2Cl_2, RT; f) TFA/H_2O/TIS 95:2.5:2.5 (v/v), RT; g) Rh_2Oct_4, CH_2Cl_2, reflux; h) *Lawesson's* reagent; THF, reflux; i) *Burgess* reagent, THF, reflux; j) DAST, CH_2Cl_2, −78 °C; k) $BrCCl_3$, DBU, CH_2Cl_2, 0 °C.

and also in recently published syntheses the yields do not exceed 65%[318-321] and often are in the range of only 50%.[322-324] For the majority of the reactions published to date, activated MnO_2 (freshly precipitated and dried at high temperatures) is used.[325-327] An alternative is NiO_2 which is more active and therefore can be used at RT, in contrast to MnO_2 which requires temperature between 50 and 80 °C in most cases. However, NiO_2 has only been used successfully for a few systems to date.[328, 329] An alternative approach is the conversion of the amino acid **29** to an imidate **31** which after condensation yields the thiazoline **32**.[330] In contrast to thiazolidines, the already partially oxidized thiazolines are less problematic to oxidize to the corresponding thiazoles as treatment with activated MnO_2 at RT is sufficient.[331] Further methods for the oxidation step employ the reagent combinations of NBS/DBPO[332] or $BrCCl_3$/DBU,[333, 334] or molecular oxygen.[335]

A promising novel two-component coupling methodology which yields thiazoles in one single step is the cycloaddition of a thiourea derivate **33** with an α-bromo alkyne **34** (scheme 4.2c)[336] or of a thioamide **35** with an α-hydroxy alkyne **36** (bottom).[337] In both cases, an allene intermediate **37**/**38** is formed which subsequently cyclizes to a thiazole **39**/**40**.[338] However, this synthetic approach is restricted to few functionalities (R^1-R^3) and not yet suitable for the synthesis of peptide fragments.

4.2.2 Cyclizations of linear precursors

Over the past years, several strategies have been developed which allow for the construction of thiazole dipeptides under mild conditions. In all cases, the heterocycle is closed by nucleophilic attack of a sulfur functionality. In the efficient aza-*Wittig* based thiazole peptide synthesis developed by *Arndt et al.* (scheme 4.3a)[339] the sulfur is, as in the *Shioiri* synthesis (scheme 4.2a), introduced by thioester formation (**41**) of an N-terminal amino acid **42** with an azidocysteine **43**. Upon addition of PPh_3 an iminophosphorane **44** is formed which reacts to the thiazoline **45**. This strategy also proved suitable for the synthesis of bisthiazoles as for example present in bleomycin (figure 4.3c) and was successfully utilized in synthetic studies towards nosiheptide.[340]

Kelly et al. described a biomimetic approach in which, similarly to thiazole biosynthesis (figure 4.1a), ring formation occurs in a prepeptide **46** upon nucleophilic attack of the Xaa-Cys amide bond by the sulfur of the Cys side chain (scheme 4.3b).[331] In *Kelly's* synthesis, however, not the thiol but the amide is activated (with PPh_3, d) and also in this case a thiazoline **47** is obtained which is easily oxidized to the thiazole peptide **48**.[341] *Kessler et al.* demonstrated that this synthesis can be extended to solid phase-bound substrates, as shown in scheme 4.3b, with

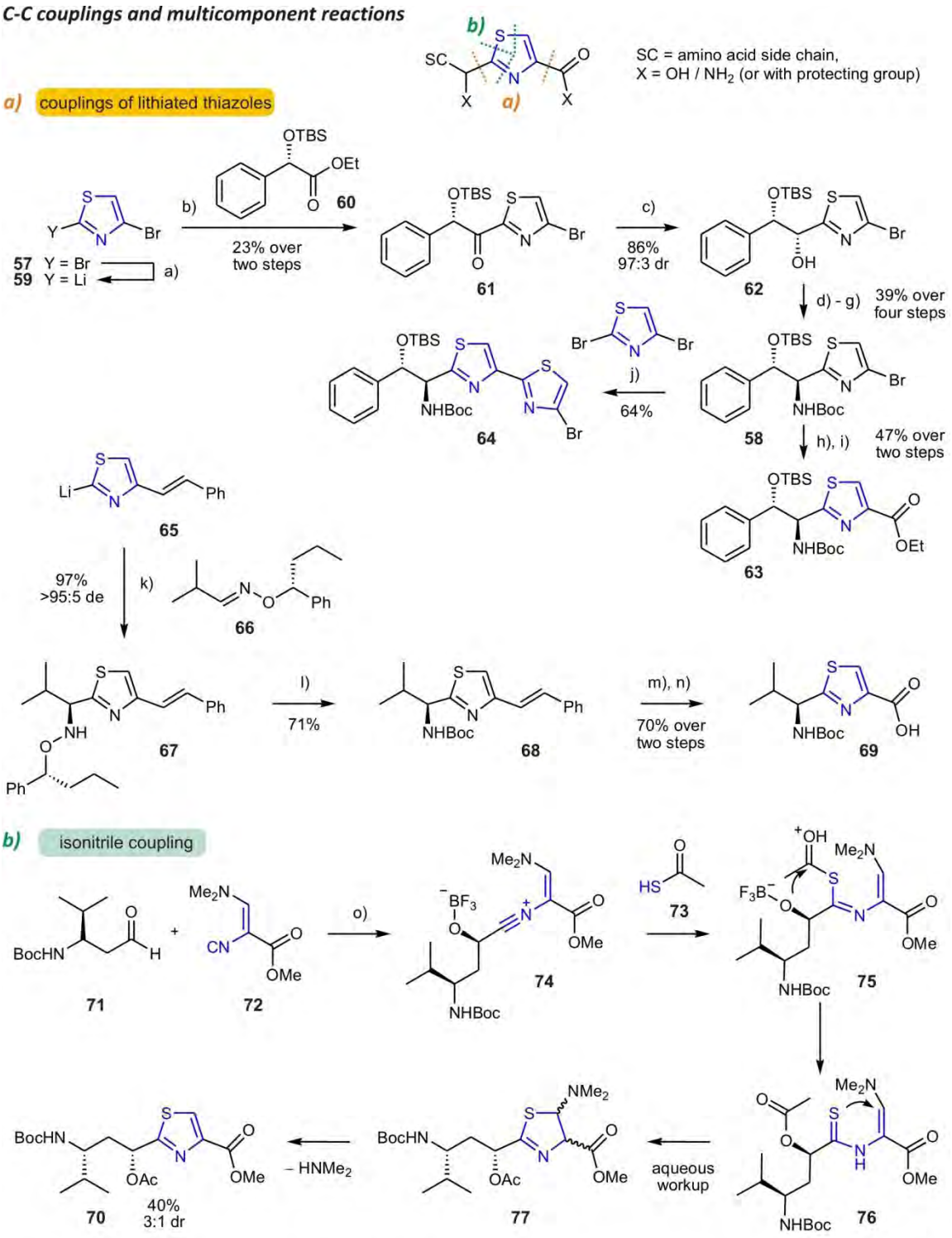

Scheme 4.4 Thiazole syntheses employing C-C couplings and multicomponent reactions. a) *C-C coupling reactions of lithiated thiazoles. Top: synthesis of (2S,3S)-phenylserine dipeptides (present in the GE2270 antibiotics) by* Bach et al. *Bottom: asymmetric synthesis of a Val<Thz dipeptide by coupling of a chiral oxime ether developed by* Moody et al. ***b)*** Lewis-*acid catalyzed three-component coupling of an isocyano-acrylate, an aldehyde and a thiocarboxylic acid developed by* Dömling *and* Wessjohann *for the total synthesis of the tubuvaline unit present in the tubulysines (figure 4.3a).* Reagents and conditions: a) *n*BuLi, Et_2O, –78 °C; b) Et_2O, –78 °C; c) L-selectride, THF, –78 °C; d) MsCl, NEt_3, –78 °C; e) NaN_3, DMSO, 90 °C; f) PPh_3, H_2O, RT; g) Boc_2O, CH_2Cl_2, RT; h) *t*BuLi, Et_2O, –78 °C, then solid CO_2; i) EtI, K_2CO_3, DMF; j) *t*BuLi, $ZnCl_2$, –78 °C; k) BF_3 x OEt_2, Tol, –78 °C; l) $[Mo(CO)_6]$, CH_3CN; then Boc_2O; m) O_3, CH_2Cl_2, –78 °C; then Me_2S; n) $NaClO_2$, CH_3CN, aq. H_2O_2/NaH_2PO_4; o) THF, –78 °C to RT.

good overall yields.[342] After the thiazole **48** is obtained, the peptide chain can be further extended on solid phase or the deprotected Xaa<Thz dipeptide **49** can be cleaved from resin.

Other strategies exploit the activation of the side chain which is subsequently attacked by an N-terminally located thioamide (scheme 4.3c, top). In this context, *Moody et al.* described an efficient synthesis of α-acylamino ketones **50** by coupling of a rhodium carbenoid **51** with a primary amide **52**.[343] The thiazole **53** then can be formed in one step with *Lawessons's* reagent.[344] This approach was successfully applied for the synthesis of the Asn<2-methyl-Thz unit present in the thiopeptide antibiotic amythiamycin;[345] however, it is restricted to thiazoles with alkyl and phenyl substitutions (R^1) at position 5.

The intramolecular nucleophilic attack by a thioamide can also be triggered in a Xaa-Ser dipeptide **54** (scheme 4.3c, bottom) if the Ser side chain hydroxyl function is adequately activated (**55**) and thus be turned into a leaving group. This can be accomplished with the *Burgess* reagent[346] or with DAST[347] and yields the thiazoline dipeptide **56**.

4.2.3 C-C couplings and multicomponent reactions

The methods described in the preceding two sections for the synthesis of Xaa<Thz dipeptides have in common the disadvantage that they are rather restricted to unpolar proteinogenic Xaa side chains. In order to be able to construct more complex thiazole units as they are present for example in the thiopeptides (section 4.1.3), further strategies were developed. One option which has been exploited for the incorporation of non-proteinogenic Xaa side chains is given by C-C couplings of lithiated thiazoles (scheme 4.4a). *Yamanaka et al.* described for the first time thiazole functionalizations by Pd catalyzed couplings,[348] and *Bach et al.* demonstrated that the different reactivity of 2,4-bromothiazole **57** can be utilized for the synthesis of the phenylserine<Thz scaffold **58** present in the GE2270 antibiotics.[349-351] The first metalation selectively occurs at position 2 (insertion of Mg or lithiation to **59**)[352] and treatment with the chiral pool mandelic acid ester **60** incorporates the first stereocenter, yielding the thiazolyl ketone **61**. Under *Felkin-Anh* control, reduction to the *threo* diol **62** takes place and a four-step *O*,*N*-exchange sequence yields the Boc-protected thiazolyl amine **58**. With the construction of the side chain completed, the adequate thiazole functionalization at position 4 can now be accomplished. By lithiation and carboxylation, the fully protected phenylserine<Thz dipeptide **63** is obtained. Alternatively, a *Negishi* coupling with a second Thz yields the bisthiazole **64** which was successfully used to accomplish the GE2270A total synthesis.[351]

Moody et al. utilized the C-C coupling of a styryl thiazole **65** and a chiral oxime ether **66** for the asymmetric synthesis of the Xaa stereocenter.[294, 353] The N-O bond of the alkoxyamine **67** is

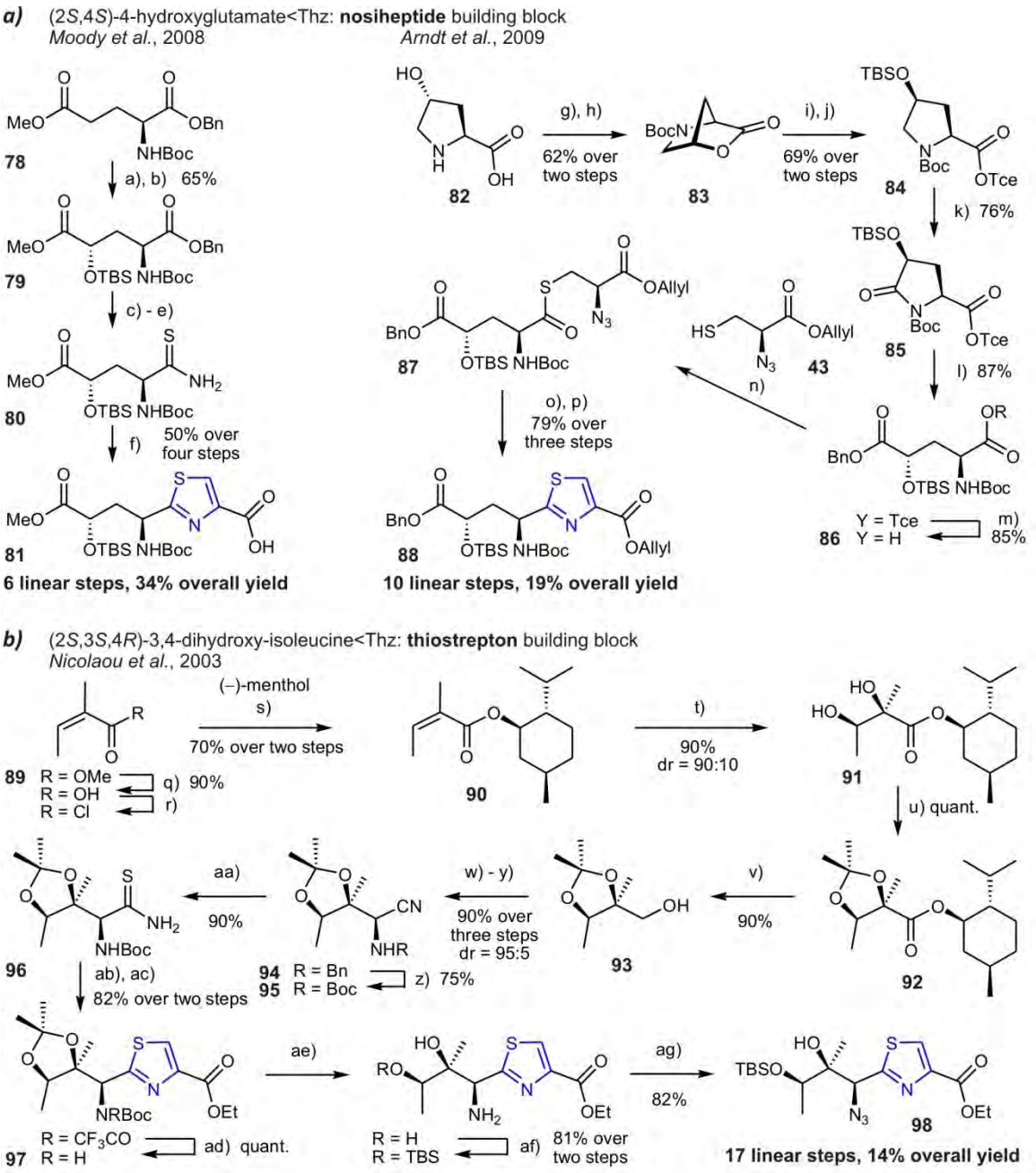

Scheme 4.5 Syntheses of hydroxylated thiazole dipeptides present in thiopeptides. a) *Total syntheses of the (2S,4S)-4-hydroxy-glutamate<Thz dipeptide present in nosiheptide by* Moody et al. *(*Hantzsch *synthesis, left) and* Arndt et al. *(*aza-Wittig *thiazole formation, right). A total synthesis of nosiheptide has not been accomplished yet.* ***b)*** *Synthesis of (2S,3S,4R)-3,4-dihydroxy-isoleucine<Thz within the scope of thiostrepton total synthesis by* Nicolaou et al. *This substrate exhibits the most complex thiazole dipeptide which is accessible by chemical synthesis so far.* Reagents and conditions: a) LHMDS, *Davis* oxaziridine, THF, –78 °C; b) TBSCl, imidazole, DMF, RT; c) Pd/C, H_2, MeOH, RT; d) Et_3N, EtO_2CCl, THF, RT; then NH_4OH, THF, RT; e) *Lawesson's* reagent, THF, reflux; f) $BrCH_2COCO_2Et$, $CaCO_3$, EtOH, RT; g) Boc_2O, K_2CO_3, 1,4-dioxane, 0 °C to RT; h) DIAD, PPh_3, THF, 0 °C; i) TceOH, NaH, THF, –78 °C; j) TBSCl, DMF, RT; k) $RuCl_3$, $NaIO_4$, $CCl_4/CH_3CN/H_2O$ 1:9:15 (v/v), 0 °C; l) BnOH, NaH, THF, –78 °C; m) Zn, THF, NaH_2PO_4, ultrasound, RT; n) EDC, HOBt, CH_2Cl_2, RT; o) PPh_3, THF, –20 °C to RT; p) $BrCCl_3$, DBU, CH_2Cl_2, RT; q) LiOH, MeOH/H_2O 1:1 (v/v), reflux; r) KOH, $(COCl)_2$, Et_2O, DMF, RT; s) Et_2O, RT; t) AD-mix-β, $MeSO_2NH_2$, *t*BuOH/H_2O 1:1 (v/v), 0 °C; u) DMP, *p*TsOH, RT; v) DIBAL-H, CH_2Cl_2, –78 °C; w) *Dess-Martin* periodinane, $NaHCO_3$, CH_2Cl_2, RT; x) $BnHN_2$, $Yb(OTf)_3$, CH_2Cl_2, RT; y) TMSCN, CH_2Cl_2, RT; z) $Pd(OH)_2$, H_2, EtOAc, RT; then Boc_2O, EtOAc, RT; aa) H_2S, Et_3N/EtOH/Pyr 1.7:1.7:1 (v/v), RT; ab) $BrCH_2COCO_2Et$, $NaHCO_3$, DME, RT; ac) Tf_2O, Pyr, 0 °C; ad) NaOEt, EtOH, 0 °C; ae) TFA/EtOH/CH_2Cl_2, 0 °C to RT; af) TBSCl, Et_3N, CH_2Cl_2, 0 °C to RT; ag) TfN_3, Et_3N, $CuSO_4$, $MeOH/H_2O/CH_2Cl_2$ (3.3:1:1), RT.

subsequently cleaved, the amine Boc-protected (**68**), and ozonolysis of the 4-styryl residue finally affords the thiazolyl dipeptide **69**. This approach, however, has so far only been proven successful for simple unpolar Xaa side chains like Val shown in scheme 4.4a.

Tubuvaline **70** (Tuv), a key part of the tubulysins (section 4.1.2.2), differs from the multitude of known Thz dipeptides by its nitrogen functionalization in the γ instead of the α-position of the side chain and by carrying an α-acyl group (scheme 4.4b), and it has contributed to the difficulties associated with total syntheses of the tubulysins.[268, 354, 355] In the first total synthesis of tubulysin derivates, *Dömling, Wessjohann et al.* utilized a *Lewis*-acid catalyzed three-component coupling of an aldehyde **71**, a *Schöllkopf* isonitrile **72**,[356] and a thiocarboxylic acid **73**.[357, 358] After formation of the isonitrile adduct **74**, reaction with **73** yields the hetero anhydride **75** which, in analogy to the mechanism of the *Passerini* multicomponent reaction, undergoes transacylation towards **76**.[359] Upon aqueous workup, the acrylic acid is attacked by the thioamide (**77**), and elimination of dimethylamine finally yields the C- and N-terminally protected thiazole dipeptide **70**.

4.2.4 Total syntheses of Xaa<Thz dipeptides present in thiopeptide antibiotics

The difficulty to access thiazole dipeptides with stereopure and highly functionalized non-proteinogenic side chains becomes especially apparent in the case of the few total syntheses of thiopeptides published so far, and much effort has been spent on the construction of these units which in some examples also serve as core motifs, linking several backbone segments and a hydroxyindole with each other. The total synthesis of nosiheptide, which exhibits the simplest member of the indole-containing thiopeptides, is the subject of current research. Its 4-hydroxy-glutamate<Thz core dipeptide is already accessible by two different strategies (scheme 4.5a, left). The synthesis by *Moody et al.*[360, 361] starts with the protected Glu **78** and stereoselectively introduces the 4-hydroxy function using the *Davis* oxaziridine (a, b).[362, 363] The benzyl ester of **79** is subsequently converted to the thioamide **80** which is converted to the thiazole dipeptide **81** by *Hantzsch* condensation (scheme 4.2a).

The alternative approach by *Arndt et al.*, in comparison, exhibits a longer sequence and a lower overall yield, yet it avoids the problems associated with the *Hantzsch* synthesis by a modern aza-*Wittig* mediated thiazole ring closure (scheme 4.5a, right). It utilizes the stereocenters of (2*S*,4*R*)-4-hydroxyproline **82** which is inverted in its configuration at position 4 via the lactone **83** and adequately protected (**84**). Oxidation at position 5 furnishes the lactam **85** which is opened and Tce-deprotected to yield the desired 4-hydroxy glutamic acid **86**. This reacts with the

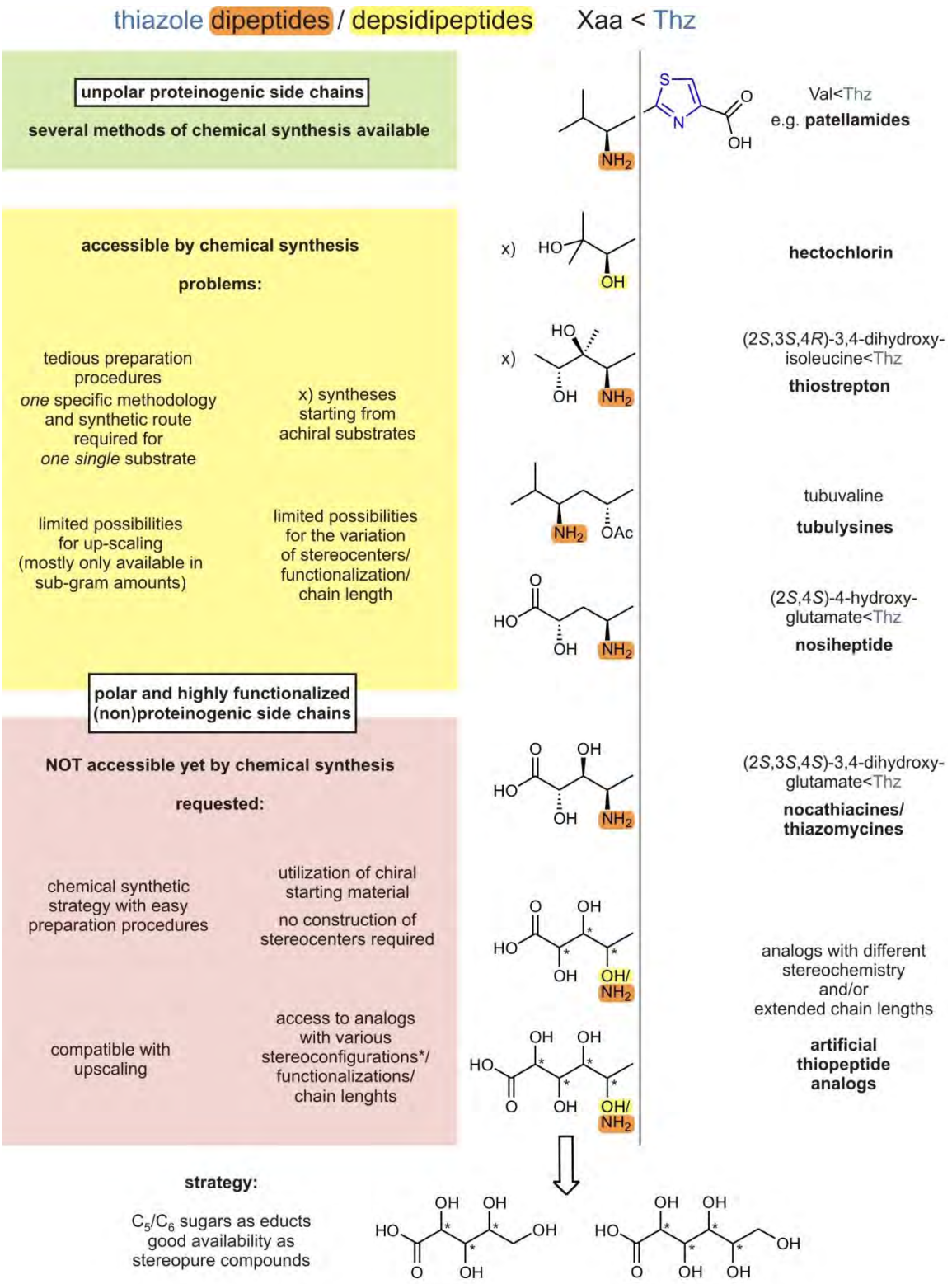

Figure 4.6 Summary of current possibilities and problems in thiazole dipeptide synthesis as motivation of the research carried out within the scope of this thesis. *On the right, some naturally occurring peptide and depsipeptide units are shown in order according to the ease of their preparation by chemical synthesis which is outlined on the left. While the synthesis of compounds with unpolar proteinogenic side chains is well feasible (green), the preparation of more complex substrates with higher functionalization is far from routine due to four main problems (yellow). The third group thiazole dipeptides is represented by those who have not been synthesized yet, like Dyg<Thz (red). This served as motivation to develop a novel synthetic methodology which utilizes the structural similarity of the side chains to sugars, as presented in figure 4.7.*

azidocysteine **43** to the thioester **87**, and the synthesis is accomplished by the aza-*Wittig* reaction (scheme 4.3a) and oxidation of the thiazolidine to the thiazole **88**.

A prerequisite of the total synthesis of thiostrepton by *Nicolaou et al.* [315, 316, 364, 365] was the successful construction of the (2*S*,3*S*,4*R*)-3,4-dihydroxy-isoleucine<Thz, the most complex thiazole dipeptide which is accessible by artificial synthesis so far (scheme 4.5b).[366] Remarkably, the sequence starts with an achiral substrate, (*Z*)-2-methylbut-2-enoic acid methyl ester **89** which is converted to the chiral (−)-menthyl ester **90** and then bishydroxylated to the diol **91** with 90:10 diastereoselectivity. After diol protection, yielding the acetonide **92**, and reduction of the ester to the alcohol **93**, the chain is extended by one carbon and the third stereocenter is introduced. For this purpose, a one-pot procedure was carried out in which the alcohol is oxidized to the aldehyde that is reacted with benzylamine, and the resulting imine is converted to the *Strecker* addition product **94**. The stereocontrol of the substrate thereby leads to the correct stereochemistry, as proven by X-ray crystallography.[366] After benzyl/Boc exchange, the nitrile **95** is converted to the thioamide **96** which is subjected to *Hantzsch* condensation. The use of Tf_2O for the dehydration to the thiazole leads to the TFA-protection of the Boc carbamate, and the TFA-group has to be removed (ad), which yields the dipeptide **97**. With the construction of the carbon skeleton completed, removal of the Boc group and exchange of the hydroxy protecting groups (ae, af) as well as a diazo transfer (ag)[367] yielded the thiazole dipeptide **98**.

4.3 Motivation and aims of this study

The efforts taken and the various synthetic methodologies developed in order to obtain thiazole dipeptides by chemical syntheses, some of which have been shown in the preceding sections, demonstrate the importance to gain access to these natural product building blocks for total synthesis and medicinal chemistry. Furthermore, they demonstrate that the synthesis of even structurally simple thiazole dipeptides, especially on a larger scale, is far from being a standard procedure. Most published syntheses only provide the compounds on the mg scale, and thiazole dipeptides are still not commercially available.

Figure 4.6 outlines the motivation of the research carried out within the scope of this thesis by giving an overview of the current scope of thiazole dipeptide (Xaa<Thz) synthesis. Clearly, the problems increase with complexity of the Xaa side chain, and the most difficult task is given by the introduction of the hydroxyl groups at the right position and with proper stereo-configuration. Most notably, some naturally occurring Xaa<Thz dipeptides, like the core motifs of the members of the nocathiacin and thiazomycin antibiotics, are not available yet. The known

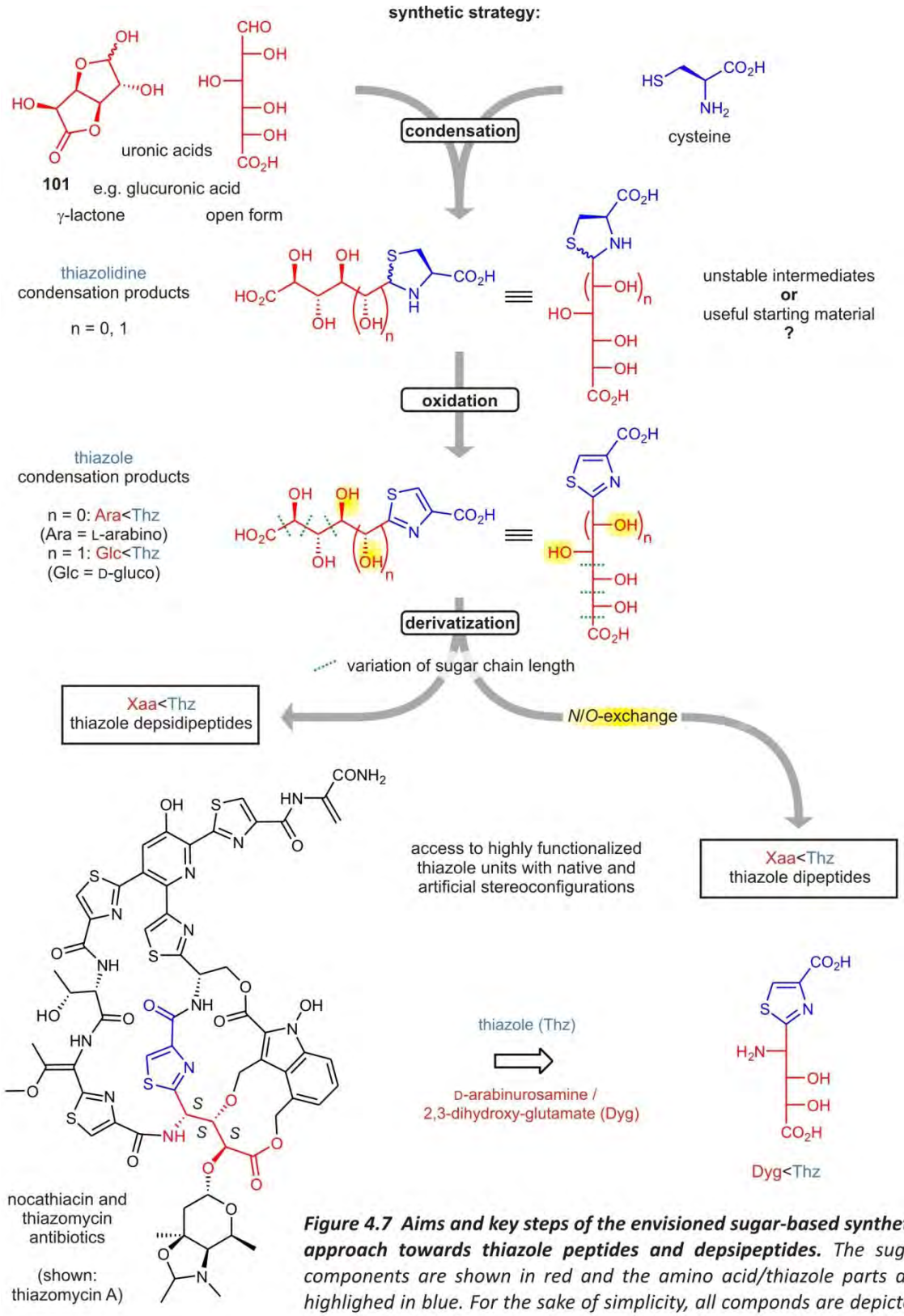

Figure 4.7 Aims and key steps of the envisioned sugar-based synthetic approach towards thiazole peptides and depsipeptides. *The sugar components are shown in red and the amino acid/thiazole parts are highlighted in blue. For the sake of simplicity, all componds are depicted in unprotected form; however, appropriate carboxyl and hydroxyl protection will be required. Starting from an uronic acid and cysteine, the first aim is given by the successful isolation of their thiazolidine condensation products, which in the second key step have to be oxidized to the corresponding thiazoles. Using glucuronic acid, this can lead to thiazole depsidipeptides with* L*-arabino- and* D*-gluco-configured side chain. With this accomplished, further studies concern the modification of the sugar chain, especially by* N/O*-exchange, in order to obtain naturally occurring dipeptides like the Dyg<Thz core motif of the nocathiacin and thiazomycin antibiotics which are not yet accessible by known methods.*

methodologies enforce individual coupling strategies and reaction sequences in order to obtain one single substrate, and they show limited possibilities for the synthesis of analogs with varying functionalization and stereoconfiguration.

This served as motivation for us to develop a methodology which is aimed at the construction of thiazole dipeptides with such polyhydroxylated side chains. Regarding the composition of these side chains, they can also be seen as fragments of glycosides. Consequently, a synthetic access which utilizes the stereopurity, high functionality and good availability of sugars as starting material for thiazole dipeptide synthesis, which has not been exploited yet, exhibits a logical proposal.

The general considerations and aims of our synthetic strategy are summarized in figure 4.7. In preliminary work by *Geyer et al.* it has been shown that uronic acids like γ-glucuronolactone **101** undergo condensation reactions with cysteine to thiazolidines.[368-370] The first task to accomplish was to examine whether these compounds, which occur as reaction intermediates in the formation of thiazolidine lactams and which were considered as unstable, can be isolated in acceptable yields in order to be subsequently subjected to successful oxidation. As the oxidation of thiazolidines to thiazoles generally requires harsh oxidative conditions, it was necessary to elucidate whether this affords polyhydroxylated thiazoles without spoiling the sugar's stereoconfiguration. Another important point then would be the investigation whether the syntheses allow for the preparation on a gram scale. The obtained polyhydroxylated thiazoles resemble highly functionalized thiazole depsidipeptide units, and the next aim is given by the exploration of the side (sugar) chain modifications. First of all, selective hydroxyl protections must be viable as prerequisite for controlled chain tailoring and transfunctionalization. The main focus of the studies should thereby be set on the exchange of the oxygen by a nitrogen functionality at the position adjoining the thiazole (highlighted in yellow) which affords thiazole dipeptides.

By choosing an adequate sugar precursor, this should finally allow for the first synthesis of the Dyg<Thz dipeptide which exhibits a core motif in the nocathiacin and thiazomycin antibiotics. In addition, it should also be investigated whether artificial analogs with different stereo-configurations, chain lengths, and functionalization are accessible without extensive modifications of the reaction sequences, which is a weak point of existing methodologies. This should be possible by the utilization of the diverse sugar starting materials available as well as of directed modifications of the polyhydroxylated side chains, and it is of relevance for the future construction of natural product analogs which potentially exhibit improved therapeutic profile compared to the natural compounds.

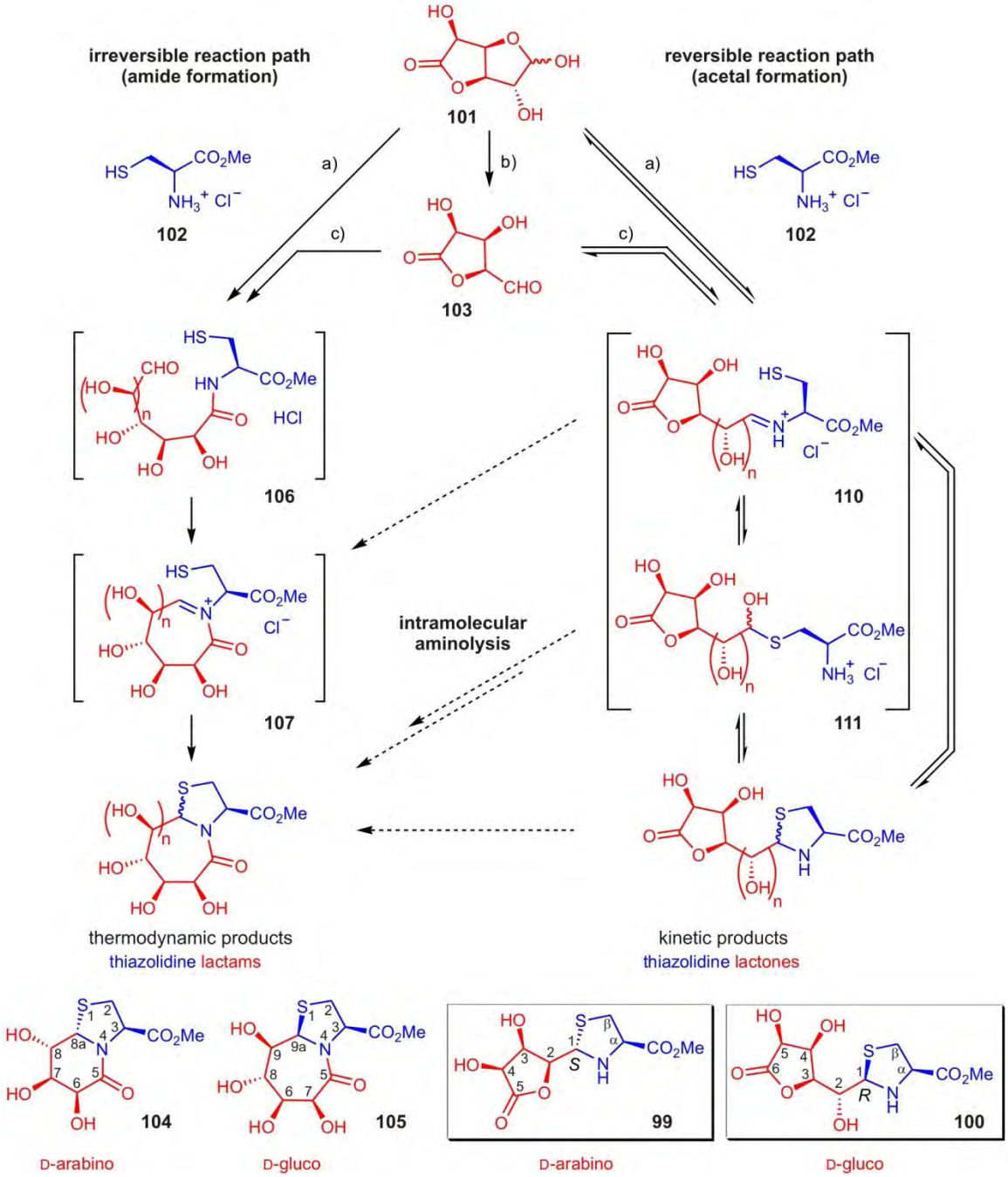

Scheme 4.6 Condensation reactions of D-gluco- and D -arabino configured uronic acids and cysteine. *The left side depicts the irreversible reaction pathway (initiated by formation of the lactam* **106***) which leads to the bicyclic thiazolidine lactams* **104** *and* **105***. They constitute the thermodynamic products and they are exclusively obtained after several days. In contrast, the reversible condensation reactions (initiated by attack of the Cys nucleophile at the carbonyl center of* **101** *and* **103***) proceed fast, which leads to a maximum concentration of the kinetic thiazolidine lactone products after a few minutes (***100***) and hours (***99***), respectively, before they are slowly converted to the thermodynamic products by intramolecular (dashed arrows) or intermolecular (solid arrows) aminolysis. As the lactams have proven to be difficult to be converted back to corresponding lactones, the thiazolidine lactone intermediates have to be isolated from the reaction mixture. This is accomplished by precipitation from the reaction mixture which is effected by running the condensations at high concentrations. Tables 4.1 and 4.2 list the examined reaction conditions for the isolation of* **99** *and* **100***, respectively, in detail.*

4.4 Results and discussion

4.4.1 Synthesis and isolation of the thiazolidine condensation products

The synthetic strategy relies on the thiazolidine lactones **99** and **100** which occur as kinetic products in condensation reactions of a sugar and an amino acid (scheme 4.6, mechanism discussed below). In one or two steps, complex carbon scaffolds with high functionalization and uniform stereochemistry are obtained. However, this occurs at the expense of a selective protection, and the challenge of sugar-based syntheses is given by the fact that neighboring group effects dominate the selectivity of the single functionalities. Therefore, the envisioned synthetic pathways can only be successfully implemented if the (de)protecting operations require a minimum effort, and consequently several of the numerous possible protecting group patterns have to be evaluated which, after developing of appropriate protocols for the isolation of the thiazolidine lactones, exhibited an essential part of this work.

Condensations of reducing sugars with amino acids have been subject of research[371] as they occur as first step of the *Maillard* reaction. This term stands for a highly complex sequence of reactions which cause the browning of food under high temperatures (roasting) and which finally furnish the flavor compounds like melanoidins.[372, 373] While the scope and the enormous number of intermediates and end products of the *Maillard* reaction are far from being completely elucidated, the condensation of uronic acids and cysteine at low temperature, in contrast, is well controllable. Research accomplished by the *Geyer* group showed that under appropriate conditions polyhydroxylated thiazolidine lactams are obtained as final products (scheme 4.6) which can be further converted to dipeptide surrogates,[374] β-turn mimetics[375] with protein-stabilizing function,[376, 377] fluorescence labels,[78, 79] and metal-chelating agents.[370]

A dipeptide which has already been discussed within the scope of this thesis is represented by the Dha=Tap unit which was incorporated into NPY analogs for the elucidation of structure and receptor binding properties (section 2).[38]

Scheme 4.6 shows the different reaction paths and intermediates leading to the lactam products. γ-glucuronolactone **101** was directly subjected to condensation with L-cysteine methyl ester hydrochloride **102**. In order to obtain D-arabino instead of D-gluco configured compounds, the C_6 chain of **101** can be shortened by diol cleavage, yielding D-arabinuronolactone **103** which reacts analogously with cysteine. The condensation reactions are generally carried out in H_2O/Pyr mixtures, and after several days at RT the thiazolidine lactams **194** (D-arabino) and **105** (D-gluco), respectively, are isolated as main producs. The exact reaction mechanism is still not completely understood and can rely on several pathways.[368, 369] In any case, the lactams are

generated by aminolysis of the lactone by the Cys amino function. This can either occur intermolecularly (scheme 4.6, left) by formation of the lactam **106** which is attacked by the aldehyde to yield the *N*-acyl iminium ion **107**, followed by closure of the thiazolidine heterocycle. However, when the reactions were performed at high concentrations, precipitates formed after few minutes to hours but which dissolved again after certain time spans.[369, 370] These turned out to be the thiazolidine lactones **99** (D-arabino) and **100** (D-gluco), respectively, which occur as reaction intermediates in a reversible reaction sequence (scheme 4.6, right). Upon attack of the Cys amine at the carbonyl function of the uronic acid, an iminium species **110** is formed which can be in equilibrium with a postulated thioacetal **111**. Both intermediates are capable of thiazolidine formation by attack of the remaining nucleophile.

The observations suggest that the thiazolidine lactones **99** and **100** are formed quickly, with a maximum concentration after a few minutes (D-arabino) and hours (D-gluco), respectively. In both cases they are generated as epimeric mixtures at position 1 (atom numeration shown in scheme 4.6), however, only the *S* epimer **99** and the *R* epimer **100**, respectively, precipitate due to higher concentration and/or lower solubility. In the following, they are slowly converted to the thermodynamic lactam products which, as suggested by marking experiments,[369] does not proceed via dissociation to the starting substrates **101** and **102** and subsequent intermolecular aminolysis but rather by intramolecular attack of the Cys nitrogen which in principle may occur in all compounds (indicated by dashed arrows).

For all previous studies which used condensation products of glucuronic acid and cysteine, the thermodynamic products **104** and **105** were used as starting material. NMR monitoring of the condensation reactions indicated that the thiazolidine lactams are formed in near-quantitative yield over several days, and 65% of **104** as well as 98% of **105** can be obtained by synthesis and crystallization on the multigram scale.[368, 378] In the present case it was the first task to identify reaction conditions for the isolation of a maximum amount of the lactones **99** and **100**, respectively. The difficulty of this step results from the fact that they do not appear as thermodynamic products but rather as labile kinetic intermediates (scheme 4.6). By extensive optimization studies, however, protocols were developed which allow to obtain the lactones **99** as well as **100** in more than 50% yield on the multigram scale, and the results are summarized in table 4.1 and 4.2. In the case of the D-gluco thiazolidine **100**, it turned out that a narrow time window of only a few minutes was available in order to obtain acceptable yields. Under the reaction conditions reported by *Tremmel et al.* (entry 1), the amount of precipitate, which appeared approx. 3-5 min after dissolving the starting material, decreased after approx. 15-20 min and no thiazolidine was isolated after stirring overnight (entry 2). As a 5 min cooling

period did not improve the yield (entry 3), the amount of solvent was further reduced as much as possible which resulted in improved yields (entry 5) also on larger scale (entry 4: 11.8 g of **100** isolated).

Table 4.1 *Condensation reactions of* **101** *and* **102** *to* **100**.

entry	reaction batch	solvent		conditions and duration	yield
1 [1)]	8.50 mmol	H_2O/Pyr 10:1	11 mL	RT, 10 min	36%
2	4.25 mmol	H_2O/Pyr 10:1	5.5 mL	RT, overnight	-- [2)]
3	26.2 mmol	H_2O/Pyr 10:1	33 mL	RT, 10 min → 5 °C, 10 min	31% [3)]
4	93.7 mmol	H_2O/Pyr 10:1	88 mL [4)]	RT, 10 min → 5 °C, 10 min	43%
5	26.2 mmol	H_2O/Pyr 10:1	22 mL [4)]	RT, 10 min → 5 °C, 10 min	51%
6	26.2 mmol [5)]	H_2O/Pyr 10:1	13 mL [4)]	RT, 5 min → 5 °C, 5 min	56%
7	26.2 mmol [5)]	H_2O/Pyr 10:1	13 mL [4)]	35 °C, 3 min → 5 °C, 15 min	32%
8	11.0 mmol [5)]	H_2O/MeOH/Pyr 15:5:1	20 mL [4)]	0 °C, 15 min	29%

1) original procedure described by *P. Tremmel*[369]; 2) only thermodynamic product **105** was isolated by subsequent workup; 3) 20% of thermodynamic product **105** were also isolated by subsequent workup; 4) minimium amount of solvent was used; 5) educts were thoroughly mixed and grinded prior to dissolving.

Table 4.2 *Two-step periodate cleavage/condensation reactions of* **99** *and* **102** *to* **99**. *The batch described in entry 1 was 50.2 mmolar, all other batches were 56.8 mmolar.*

entry	solvent		conditions and duration	washing of precipitate	yield
1 [1)]	H_2O/Pyr 10:1	100 mL	RT, 16 h	MeOH	17%
2	H_2O/Pyr 10:1	30 mL	RT, 12 h	MeOH	17%
3	H_2O/MeOH/Pyr 15:5:1	100 mL	RT, 10 h	H_2O/MeOH/Pyr 15:5:1	34%
4	H_2O/MeOH/Pyr 15:5:1	90 mL	RT, 2 h → 5 °C, 12 h	EtOH	39%
5	H_2O/MeOH/Pyr 15:5:1	90 mL	RT, 15 h	EtOH	53%
6	H_2O/MeOH/Pyr 15:5:1	55 mL [2)]	RT, 2 h	MeOH	26%
7	H_2O/MeOH/Pyr 15:5:1	55 mL [2)]	RT, 17 h	MeOH	36%

1) original procedure described by *S. Eckhardt*[370]; 2) minimium amount of solvent was used.

The yield could be further increased by thoroughly grinding the starting material which allowed a further reduction of solvent (entry 6). Further modifications like the variation of reaction temperature (entry 7) or solvent (entry 8; this mixture proved successful for the synthesis of **99**) did not further improve the yield. However, in all cases it was possible to isolate up to 20% of the thermodynamic product by following the respective procedure after filtration.

In the case of the D-arabino thiazolidine **99**, which is formed more slowly and which exhibits a longer time span for its isolation, the original solvent mixture in all cases led to low yields

(table 4.2, entries 1 and 2). Therefore, extensive studies concerning the variation of solvents were carried out, and the best results were obtained with a 15:5:1 mixture of MeOH/ H_2O/Pyr (entry 3). While cooling of the reaction mixture was not required, the use of EtOH as washing solvent of the precipitate further increased the yield, leading to a more than threefold amount of isolated product compared to the original procedure (entry 5). Other modifications like reduction of the amount of solvent and/or decreased reaction times, however, did not effect further improvements.

When sufficiently dry, both thiazolidine lactones can be stored for several months at low temperatures. In solution, they are prone to epimerization at the C-1 stereocenter, a process which occurs considerably faster in the case of **100** than of **99**. By making them accessible on a large scale in acceptable yields with quick and easy preparation procedures, the basis was provided for further investigations concerning the oxidation to the thiazoles, which is described in the following section.

4.4.2 Hydroxyl protection and oxidation to the thiazole lactones

Two synthetic strategies are possible to obtain thiazole dipeptides and depsidipeptides starting from the thiazolidines **99** and **100** (scheme 4.7). Either, the oxidation of the heterocycle is carried out at an early stage before the side chain diversifications (path A). Alternatively, the sugar chains can be modified first and the oxidation to the thiazole can be performed at a later stage (path B).

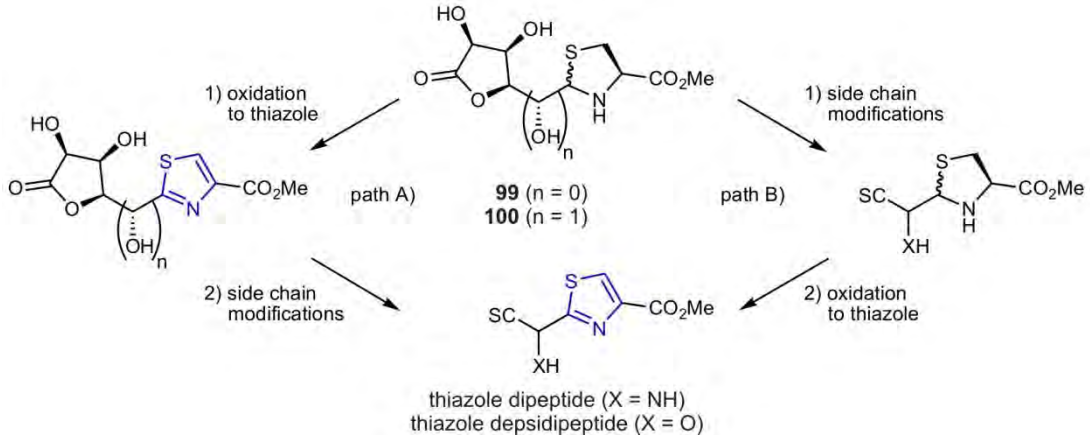

Scheme 4.7 Comparison of general synthetic strategies. *The key oxidation step can either occur at the beginning with adequately protected sugar chains as part of a minimal protection strategy (path A) or after the tailoring of the sugar residue (path B, see also figures 4.6 and 4.7). In both cases, the high polarity of the unprotected substrates, which makes them difficult to handle, must be included into the considerations. SC = (modified) sugar chain.*

Recalling the fact that the thiazolidine is a reversibly formed functionality which may be subjected to hydrolysis (scheme 4.6), a strategy which converts the thiazolidine into the stable aromatic heterocycle as quickly as possibly (path A) appeared to be more promising. In addition, nucleophilic attack of the thiazolidine secondary amine, if not protected, can lead to irreversible lactam formation (scheme 4.6), which has to be prevented in any case. A third fact which suggests to follow way A is the oxidation itself which may be a bottleneck of synthesis and which, as it requires harsh conditions, may lead to high optimization effort if carried out for many substrates after the side chain modifications (path B). Last but not least, some modifications of the sugar chains, like hydroxyl activation and *O*,*N*-exchange may be facilitated by the presence of the aromatic ring, because this influences the reactivity especially at position 2 where the exchange should take place.

In order to evaluate experimentally which strategy is the best option, we tested some transformations which are summarized in figures 4.8 and 4.9 for thiazolidine **100** and **99**, respectively. Concerning way B, these encompassed various oxidation protocols in order to evaluate whether the sugar chains can be selectively shortened by diol cleavage, activations with MsCl, and protections of the thiazolidine amine. Other experiments were aimed at the generation of adequately protected substrates (free thiazolidine amine, protected hydroxyl groups) for the early stage thiazolidine→thiazole oxidation according to way A.

The first experiments were performed with the D-gluco thiazolidine **100** (figure 4.8a), and it turned out that this substrate is difficult to handle due to its high polarity (well soluble only in H_2O, DMF, DMSO, and Pyr) and its instability under various reaction conditions. All tested oxidations resulted in complete decomposition of the substrate, however, an exception was observed when treating **100** with activated MnO_2 at RT which yielded small amounts of the 5,5-bicyclic thiazolidine lactam **112** with L-threo configuration of the residual sugar chain. A diastereomeric compound (with inverted C-7 and C-7a stereocenters corresponding to a D-erythro configuration) had already been obtained by *P. Tremmel*, yet by a multistep procedure starting from L-gulonic acid.[369] The isolation of this species allowed to draw conclusions about the oxidative effect of MnO_2 which leads to a diol cleavage between C-4 and C-5. By subsequent nucleophilic attack of the thiazolidine amine and oxidation of the hemiaminal the lactam **112** is finally formed. The relative stereoconfiguration was confirmed by ROE contacts, as indicated in figure 4.8b.

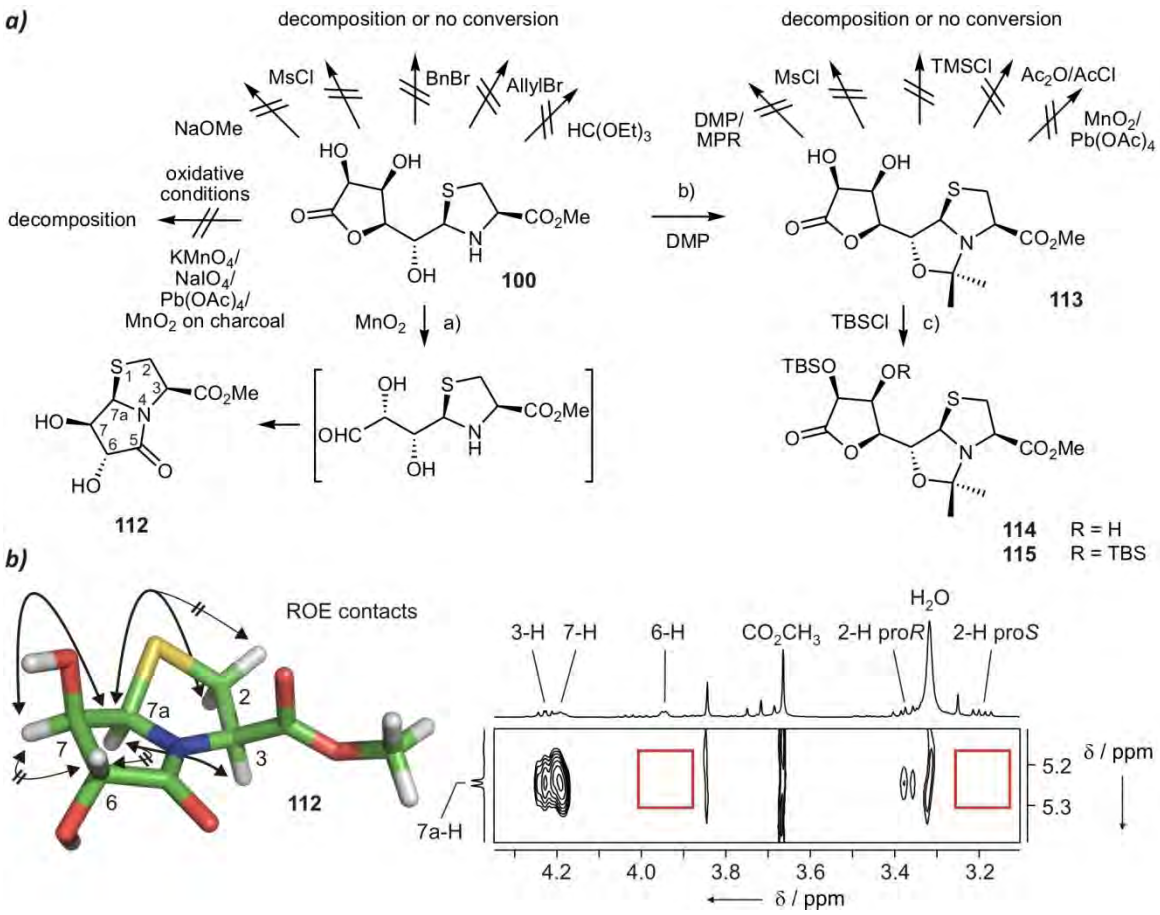

Figure 4.8 ***a)*** *Attempts to oxidize and protect the thiazolidine lactones* **100** *and* **113**. ***b)*** HyperChem *modeled structure of the diol cleavage product* **112** *with the presence and absence of some dipolar* ^{1}H-^{1}H *couplings (ROE contacts) indicated by arrows. On the left, a section of the ROESY spectrum of* **112** *is shown (DMSO-*d_6*, 500 MHz, 300 K). Missing ROE cross signals are indicated by red squares.* Reagents and conditions: a) MnO_2 (activated, 20 eq), CH_3CH/Pyr 1:1, RT, 43 h, 6.3%; b) DMP (8.0 eq), $CaSO_4$ x 1/2 H_2O (4.0 eq), CSA (cat.), DMF, RT, 22 h, 98%; c) TBSCl (2.5 eq), imidazole (2.5 eq), DMF_{abs}, 35 °C, 20 h, 28% of **114** and 38% of **115**.

Consequently, protection of the 4,5-diol, for example as acetonide, would be required in order to enable MnO_2-mediated oxidation of the thiazolidine according to way A (scheme 4.7). Treatment with DMP or MPR under several tested reaction conditions, however, effected selective formation of the *N*,*O*-acetal **113** (figure 4.8a) without any protection of the 4,5-diol observed, obviously due to restriction of space by the acetonide. Recalling the possible synthetic strategy employing a late-stage oxidation to the thiazole (way B, scheme 4.7), **113** is a promising starting substrate for tailoring of the sugar chain as the reactive thiazolidine amine is protected. First attempts to cleave the C-4/C-5 bond, however, effected decomposition, and only the TBS protection of the remaining diol was successful (**114**, **115**). After acetonide cleavage, this would result in the desired protection pattern; this option, however, was not further investigated as it turned out that all hydroxyl groups of **100** can be readily protected as silyl ethers (scheme 4.8).

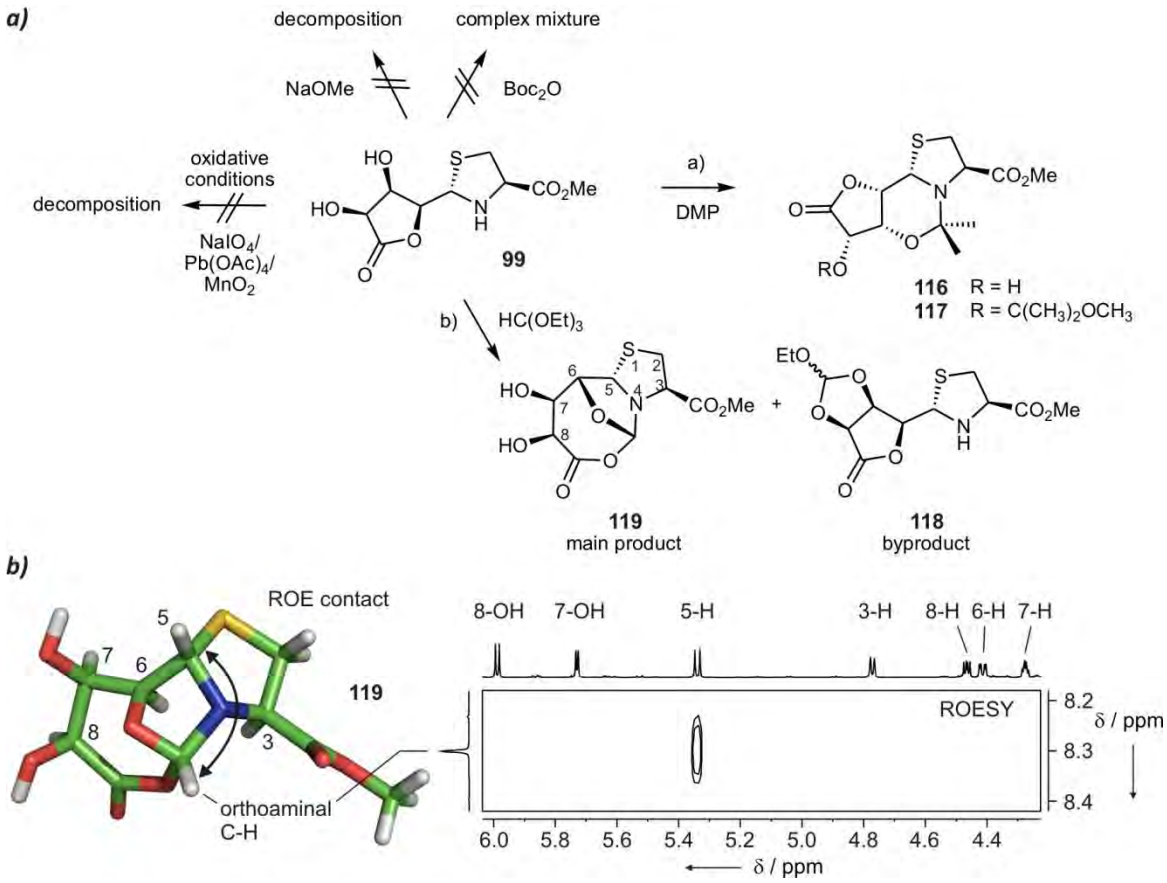

Figure 4.9 ***a)*** *Attempts to oxidize and protect the thiazolidine lactone* **99**. ***b)*** HyperChem *modeled structure of the tricyclic orthoaminal* **119** *with the ROE contact between the orthoaminal proton and the 5-H indicated by an arrow. On the left, a section of the ROESY spectrum of* **119** *is shown (DMSO-*d_6*, 600 MHz, 300 K). The orthoaminal proton shows an ROE contact only to the 5-H as, with exception of 2-H pro*S*, all other protons are located at the other side of the tricycle.* Reagents and conditions: a) DMP (10 eq), CSA (cat.), DMF, RT, 4 h, 54% of **116** and 10% of **117**; b) $HC(OEt)_3$ (1.6 eq), *p*TosOH x H_2O (cat.), DMF, RT, 26 h, 19% **119** and 2.5% **118**.

When applying the tested reaction conditions to the D-arabino configured thiazolidine **99**, similar observations were made (figure 4.9a). Again, treatment with DMP led to formation of an *N*,*O*-acetal (**116** and **117**) without protection of the 3,4-diol observed. In contrast to **100**, treatment with triethylorthoformiate led to a main product; however, the desired ortho-ester **118** was only isolated in traces. Instead, the thiazolidine amine reacted and lactone opening occurred which resulted in formation of the tricyclic orthoaminal **112**. This exhibits another promising starting point for sugar chain modification, similarly to the protected D-gluco analog **113** as the reactive thiazolidine amine is protected and the terminal diol allows selective tailoring of the sugar chain. However, further investigations concentrated on the strategy employing an early-stage oxidation to the thiazole. The prerequisite for this strategy is the selective protection of all hydroxyl groups while the thiazolidine amine has to remain unprotected. This could be accomplished by protection with TBS and TES groups. As first

attempts using the TMS group were not successful, the more stable TBS group was chosen (scheme 4.8, left). Several reaction conditions were tested, among them the use of KH/ 18-crown-6[379] as reagents; however, only the protection under *Corey* conditions[380] proved successful. This is carried out in DMF at high concentrations, using the silylchloride and imidazole, the latter acting as nucelophilic catalyst as well as a base which neutralizes the stoichiometrically generated HCl. In order to prevent irreversible lactam formation, the silyl protections of the D-arabino configured diol **99** must not be carried out at temperatures above 35 °C. When applying the *Corey* conditions at 60 °C, only the tri- and disilylated 6,5-bicycles were isolated (**120** and **121**). At 35 °C, aminolysis can be suppressed and the silylated lactones **122** and **123** are obtained, although long reaction times are required for the silylation of both hydroxyl groups. In contrast, no lactam formation was observed in the case of the D-gluco configured diol **100** at higher temperatures, which is why the reaction could be run at 50 °C. However, the close proximity of the three hydroxyl positions leads to longer reaction times also in this case, and 85 h were required in order to obtain a moderate 46% yield of the trisilylated compound **124**. However, this compound could be purified solely by extraction and crystallization on the 20 g scale. The X-ray structure of **124** gives a perception of the steric crowding caused by the three TBS groups (scheme 4.8). The stereoconfiguration corresponds to the starting material **100** and all silylation reactions of **99** and **100** yielded consistent configurations at position 1 which allows the assumption that epimerization of the thiazolidines, if at all, occurs to negligible extent under the silylation conditions (scheme 4.6). The isolation of the disilylated compound **125** suggested that, in consistence with the isolated products **120** and **121**, the α-carboxyl hydroxyl positions are the most reactive ones in both the D-arabino and the D-gluco configured thiazolidines.

Finally, switching from the TBS to the TES protecting group was rewarding as this led to significantly increased yields combined with shorter reaction times (scheme 4.8, right). After 3-4 h under *Corey* conditions, 78% of the disilyated thiazolidine **126** (with traces of the monosilylated compound **127**) were obtained, and the trisilylated D-gluco configured triol **128** was obtained in 97% yield. An excess of silyl chloride was required, probably due to silylation of the amine and subsequent cleavage of the N-Si bond which is susceptible to hydrolysis.[381, 382]

With the thiazolidine lactones available on multigram scale with suitable protection (silyl protected hydroxyl groups, unprotected thiazolidine amine), the next task that had to be accomplished was the crucial oxidation to the corresponding thiazoles. The most important question was whether this transformation would be possible without affecting the configurations of the stereocenters. As MnO_2[325, 326] and NiO_2[329] are the only suitable reagents,

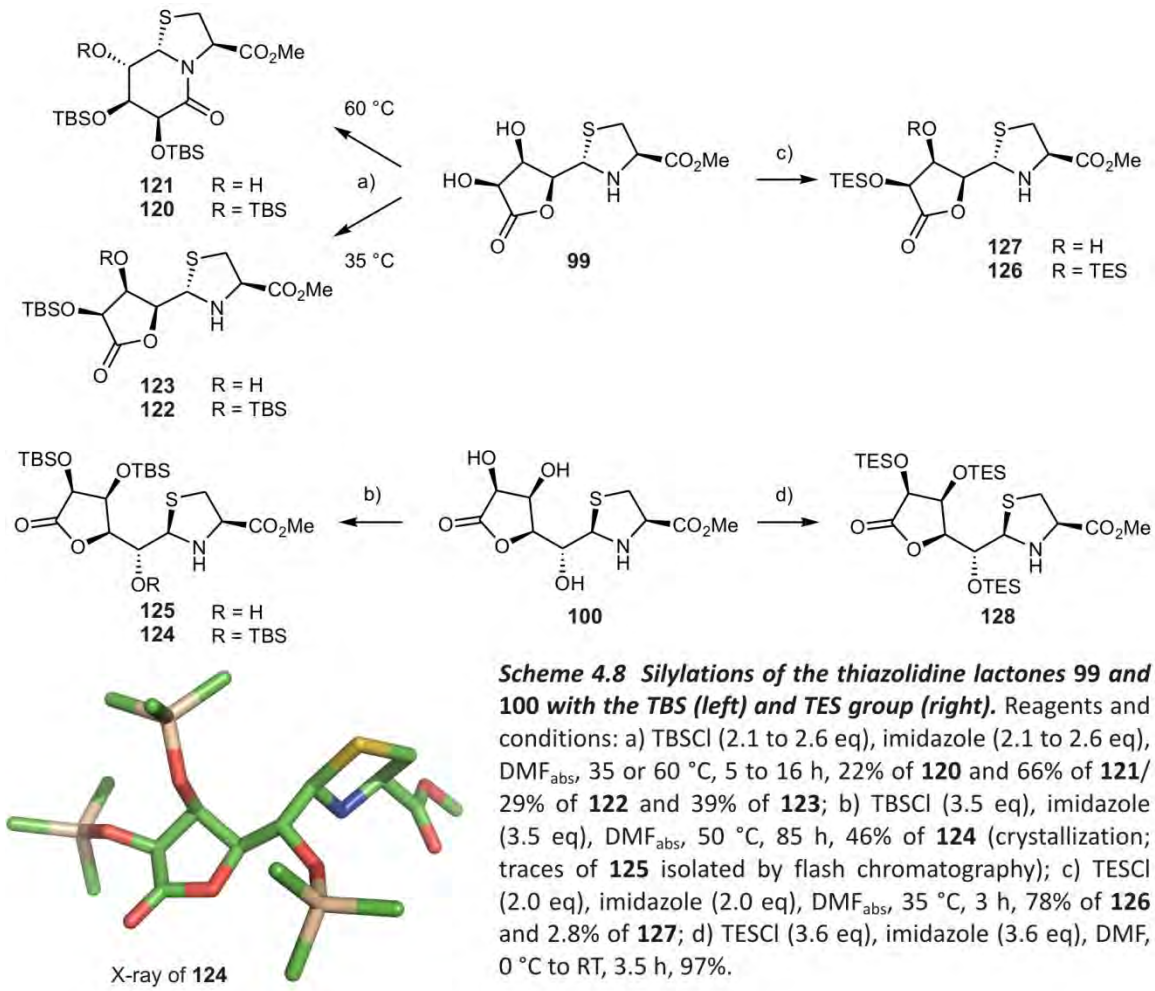

X-ray of **124**

Scheme 4.8 Silylations of the thiazolidine lactones* 99 *and* 100 *with the TBS (left) and TES group (right). Reagents and conditions: a) TBSCl (2.1 to 2.6 eq), imidazole (2.1 to 2.6 eq), DMF_{abs}, 35 or 60 °C, 5 to 16 h, 22% of **120** and 66% of **121**/ 29% of **122** and 39% of **123**; b) TBSCl (3.5 eq), imidazole (3.5 eq), DMF_{abs}, 50 °C, 85 h, 46% of **124** (crystallization; traces of **125** isolated by flash chromatography); c) TESCl (2.0 eq), imidazole (2.0 eq), DMF_{abs}, 35 °C, 3 h, 78% of **126** and 2.8% of **127**; d) TESCl (3.6 eq), imidazole (3.6 eq), DMF, 0 °C to RT, 3.5 h, 97%.

and as elevated temperatures as well as high excess of the reagents are required, this exhibited a “make-or-break” situation. While silyl protection groups had already been proven to be stable under the harsh oxidative conditions,[320, 383] polyol compounds had been described to be problematic due to elimination reactions[384, 385] and they had rarely been used.[325, 326] The thiazolidine lactones **122**, **124**, **126** and **128** represented the most complex substrates to be subjected to this oxidation procedure, and they are sterically demanding due to the multiple silyl protection.

20 eq of activated MnO_2 (purchased from *Merck* or *Fluka*) and Tol as solvent at 70 °C exhibited the first conditions tested for the oxidation of TBS- and TES-protected thiazolidines **122** and **126**, and in fact thiazole products without epimerization were obtained.

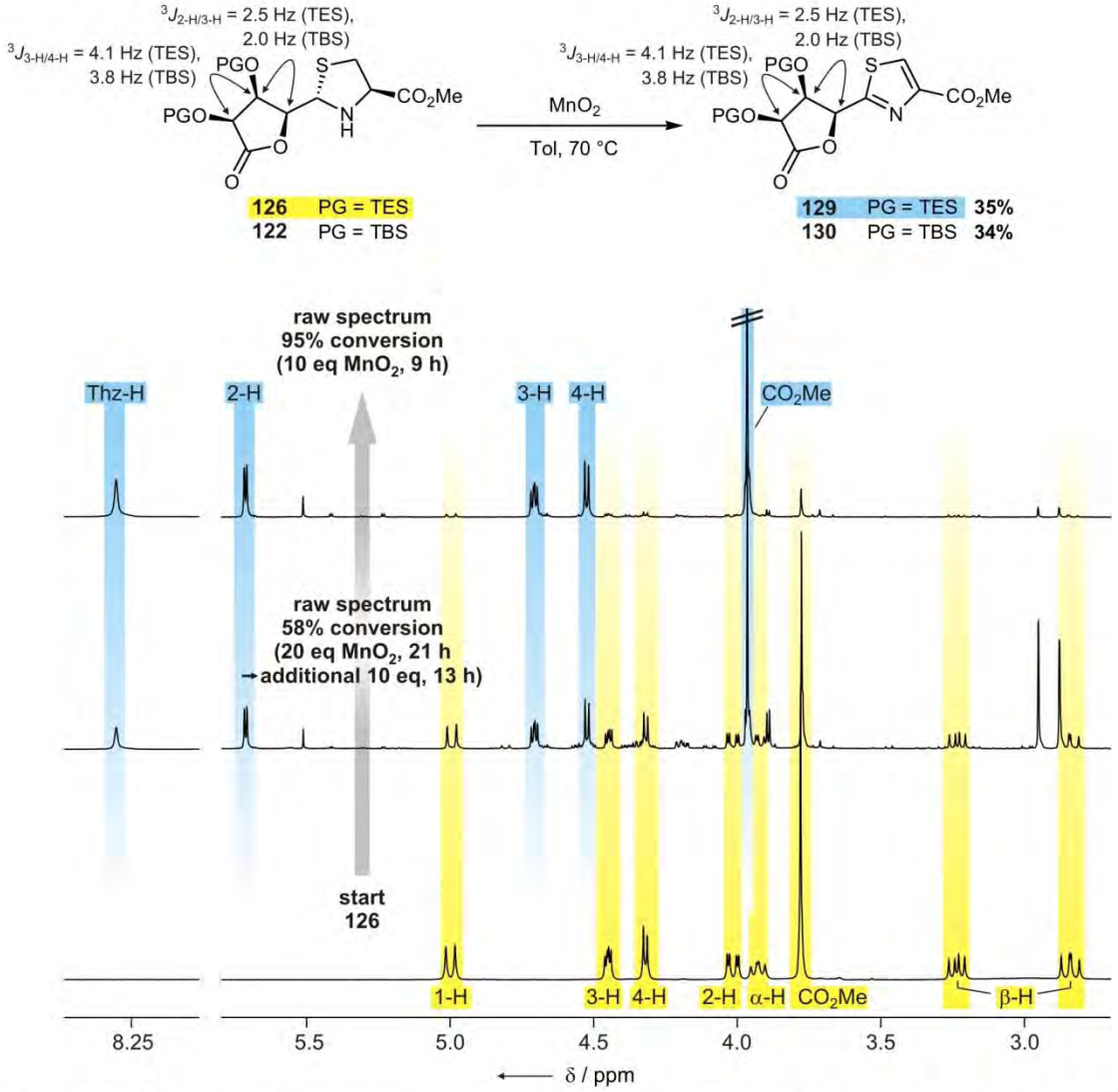

Figure 4.10 Oxidation of the D-arabino configured thiazolidine 126 with MnO_2: monitoring by ^{1}H NMR (DMSO-d_6, 300 MHz, 300 K). *Signals resulting from the starting material are marked yellow, and product signals are highlighted in blue. The down-field region containing the signals resulting from the TES protons is not shown. One single thiazole main product is obtained and no racemization of the three sugar chain stereocenters is observed, as visible from the similar scalar H/H couplings before and after oxidation (written next to the respective positions).*

Figure 4.10 illustrates the progression of the oxidation of **126** by ^{1}H NMR spectra. Control via TLC could be performed in all cases, however, it is not suited to quantify the amount of conversion or eventual intermediates and side products. After 21 h reaction time with 20 eq of MnO_2 and further 13 h with additional 10 eq of MnO_2, a raw spectrum of the concentrated reaction mixture (after removal of the MnO_2 by filtration) shows a 58% conversion to one single main product **129**. The addition of a second portion during the reaction is a commonly used procedure as the MnO_2 becomes less active upon longer stirring.[386] Further weak signals are visible in the ^{1}H NMR spectrum but they do not account for more than 5%. After additional 9 h of heating with

10 eq of fresh MnO_2, one single thiazole product is obtained, and the minor sets of signals visible in the raw spectrum again exhibit less than 5% in intensity. The thiazole products can easily be distinguished from unoxidized material in the ^1H NMR spectra by the thiazole singlet at down-field (usually > 8.0 ppm), the strong down-field shift of the 2-H in α-position to the aromatic thiazole (in the present case, it accounts for more than 1.7 ppm), and the down-field shift of the methyl ester protons. As the scalar coupling constants within the lactone ring (written next to the respective positions) do not change to great extent, the stereoconfiguration of the product can be assumed to be identical with that of the educt.

Having shown that a standard MnO_2 oxidation protocol[325, 326] is applicable to the thiazolidine lactones **122** and **126**, attention had to be paid to upscaling and to the optimization of the reaction to the thiazoles **129** and **130** (table 4.3). While the variation of temperature did not effect an improvement (70 °C were therefore used in all cases), the use of activated MnO_2 purchased from *Fluka* instead of *Merck* led to an increased yield of 34% instead of 30% (entries 1 and 2). Furthermore, it turned out that 20 eq of MnO_2 are sufficient and that no additional oxidant is required (entry 3). The change of the solvent from Tol to CH_3CN (more solvents were tested for the oxidation of a different substrate, table 4.14) led to slow conversion (entry 4). It was also attempted to reactivate used MnO_2 according to the *Goldman* method by azeotropic removal of H_2O[320, 387] but, curiously, this oxidant displayed low activity (entries 5 and 6). MnO_2 with small particle sizes (< 5 µm) purchased from *Aldrich* did not effect any conversion (entries 7 and 8).

The maximum yield of 35% may seem low, however, it is acceptable if compared to analogous oxidations reported in the literature. Although the substrates are far simpler concerning structure and functionalization, yields of not more than 50% have been often obtained.[322-324] The details of the MnO_2 oxidation mechanism remain obscure, and few is also known about the oxidative degradations caused by MnO_2 which are responsible for the generally moderate yields. However, the advantages of this reagent compensate these drawbacks. MnO_2 is a non-toxic low-cost oxidant which is easily removed from the mixture by filtration and which, in dependence of the substrate, can be reused.

Table 4.3 *One-step oxidations of the* D*-arabino thiazolidines* **122→130** *(PG = TBS) and* **126→129** *(PG = TES).*

entry	PG	solvent	reaction batch	MnO_2 type	conditions and duration[1)]	con-version	isolated yield[2)]
1	TBS	Tol	0.10 mmol	*Merck (90%)*	20 eq, 44 h → 40 eq, 19 h	complete (TLC)	30%
2	TBS	Tol	0.10 mmol	*Fluka (90%, fresh)*	20 eq, 16 h → 40 eq, 11 h	complete (TLC)	34%
3	TES	Tol	0.29 mmol	*Fluka (90%, fresh)*	20 eq, 22 h	complete (TLC)	35%
4	TBS	CH_3CN	3.04 mmol	*Fluka (90%, fresh)*	30 eq, 46 h	23%[3)] (^{1}H NMR)	n.d.
5	TBS	Tol	1.13 mmol	*Fluka (90%, aged, reactivated by azeotropic dist.)*	30 eq, 16 h	2% (^{1}H NMR)	n.d.
6	TES	Tol	0.56 mmol	*Fluka (90%, aged, reactivated by azeotropic dist.)*	30 eq, 16 h	30% (^{1}H NMR)	n.d.
7	TBS	Tol	1.13 mmol	*Aldrich (85%, <5 µm size)*	20 eq, 22 h	none (^{1}H NMR)	n.d.
8	TES	Tol	0.56 mmol	*Aldrich (85%, <5 µm size)*	20 eq, 22 h	none (^{1}H NMR)	n.d.

1) 70 °C reaction temperature was chosen in all cases; 2) isolated yield after flash chromatographic purification; 3) partial decomposition of educt observed (three thiazolidine signal sets).

Table 4.4 *Two-step silyl protection/oxidation protocol of the* D*-arabino thiazolidine* **99→129***: upscaling and optimization of the oxidation step. The silylation was always carried out in the same way as described in scheme 4.8, and the products were subjected to oxidation without purification.*

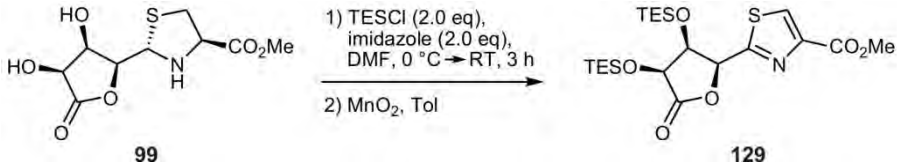

entry	solvent	reaction batch	MnO_2 type	conditions and duration[1)]	con-version[2)]	isolated yield over two steps[3)]
1	Tol	20.2 mmol	*Fluka (90%, fresh)*	20 eq, 21 h → 30 eq, 13 h* → filtration →10 eq, 9 h**	58% after *[4)] >95% after **[4)]	19%
2	Tol	20.0 mmol	*Fluka (90%, aged)*	20 eq, 30 h → filtration → 10 eq, 12 h → 20 eq, 19 h*	>99% after *	16%
3	Tol	39.6 mmol	*Fluka (90%, fresh)*	20 eq, 36 h* → filtration → 20 eq, 15 h**	40% after * >99% after **	33%

1) 70 °C reaction temperature was chosen in all cases; 2) determined by ^{1}H NMR; 3) isolated yield after flash chromatographic purification; 4) spectrum depicted in figure 4.10.

The synthesis of the thiazole **129** could be further optimized as it turned out that the purification of the TES-protected thiazolidine **126** (carried out by flash chromatography) is not required for the oxidation step. Instead, the raw product obtained from the silylation step (**99** → **126**) can be directly subjected to oxidation, and the protocol is applicable to batches on the multigram scale (table 4.4). Initially, only 19% of **129** were obtained (entry 1), which is less than what would be expected by the two-step procedure (27%). However, this was apparently caused by a considerable amount of TESOH which had not been removed from the raw product and which, like every alcohol, is well-known to compete with the substrate for the active coordination sites at the MnO_2 particles.[325] By drying the silylation raw product for a longer time *in vacuo* (approx. 24 h), this problem was avoided. While MnO_2 that had been stored under air for several months gave rise to low yields (entry 2), 33% of the thiazole **129**were finally obtained using fresh oxidant (entry 3). Thus, the simplified silylation/oxidation protocol is superior to the two-step procedure. As the yield is lowered by only 2% in comparison with the one-step oxidation of purified **126**, this suggests that it is the chromatographic purification which causes the loss of product in the silylation of **99** (78%, scheme 4.8). The fact that longer reaction times as well as more MnO_2 are required can be explained with residerable TESOH which cannot be removed completely after silylyation. The size of the batch could be further increased which led to 6.3 g of purified thiazole **129** (entry 3).

In the case of the D-gluco configured thiazolidines **124** and **128**, the oxidation conditions could also be successfully applied, furnishing the thiazoles **131** and **132**, respectively (figure 4.11). However, the reaction monitoring by ^{1}H NMR revealed a considerable difference. In contrast to the oxidations of the D-arabino configured substrates, where no other main species than thiazolidine and thiazole were detected (figure 4.10), the thiazoline intermediates **133** (shown) and **134** (TES-protected) accumulate in the reaction mixture as the second oxidation step occurs slower. The ^{1}H NMR spectrum obtained after 22 h heating with 20 eq of MnO_2 at 60 °C is shown in figure 4.11a with the percentages of the main species. The thiazolidine **124** has been consumed almost completely (8%) in the fast first oxidation step to yield the thiazoline **133** (68%), and only a small amount has already been further oxidized to the thiazole target compound **131** (24%).

As a consequence, long reaction times as well as the addition of further amounts of MnO_2 were required to effect complete conversion to the thiazoles **131** (TBS-protected) and **132** (TES-protected), respectively, and the isolated yields were low, not exceeding 23% although several

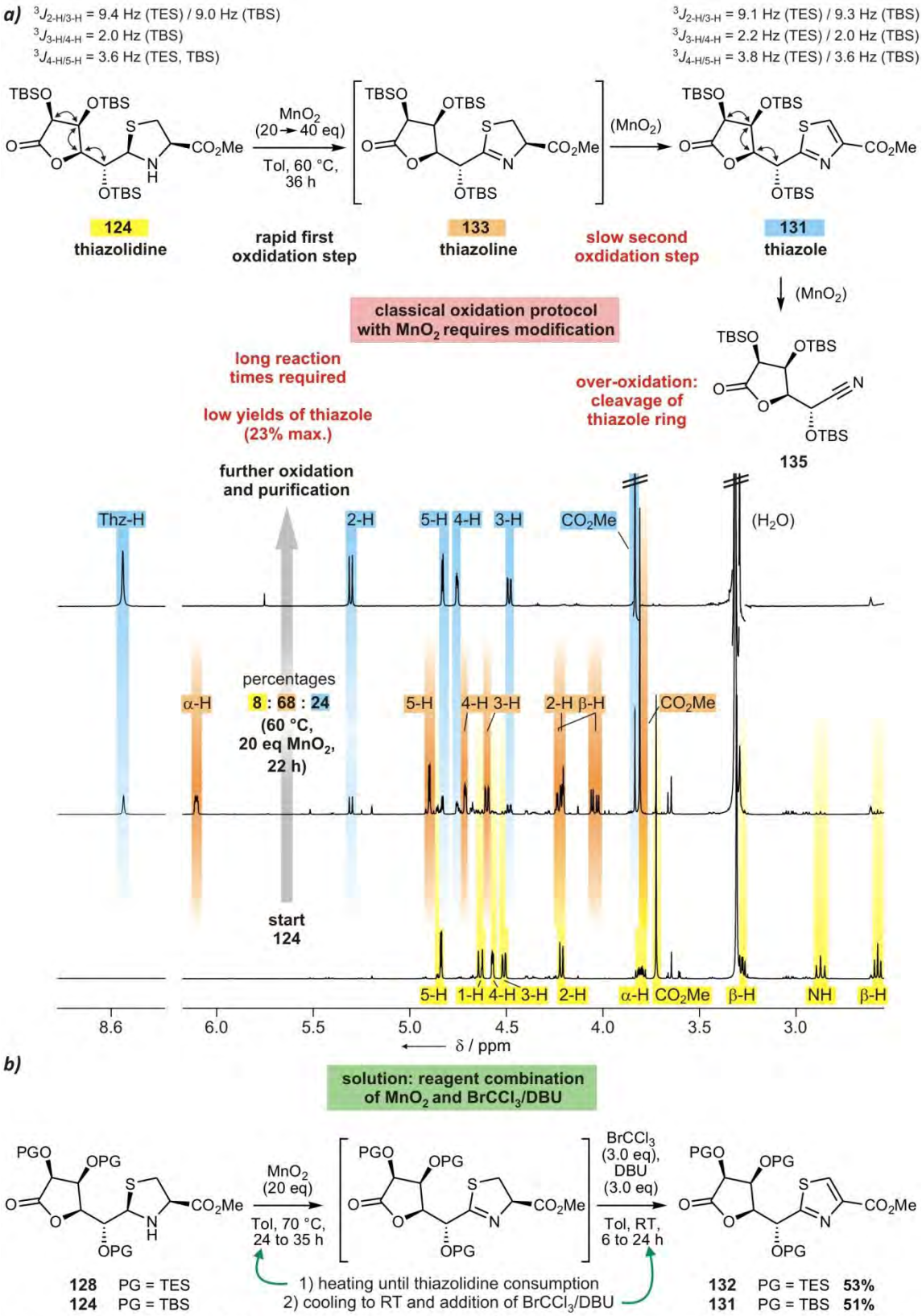

Figure 4.11 Oxidation of the* D*-gluco configured thiazolidine* 124 *with* MnO_2.** ***a) *Monitoring by* ^1H *NMR (DMSO-*d_6*, 300 MHz, 300 K). Signals are marked yellow (thiazolidine), orange (thiazoline) and blue (thiazole), respectively. The down-field region containing the TBS proton signals is not shown. Again, no racemization is observed within the sugar chain as visible from the scalar H/H couplings before and after oxidation.* ***b)*** *By using* $BrCCl_3$ *and DBU for the second reaction step, reaction times were reduced and the yields significantly increased.*

MnO_2 types, different solvents, and different temperatures were tested. The low yield is also caused by the formation of considerable amounts of the over-oxidation product **135** which is apparently formed by oxidative cleavage of the thiazole ring. No comparable oxidative thiazole degradation has been described in the literature and the mechanism remains speculative; however, the nitrile functionality could either be formed directly[388, 389] or from a primary amide which is subsequently dehydrated.[390] The latter hypothesis is supported by a primary nitrile oxidation product (obtained from another thiazole substrate) which was characterized by X-ray crystallography within this thesis (section 4.4.8.2).

Table 4.5 *One-and two-step oxidations of the* D*-gluco thiazolidines* **124→131** *(PG = TBS) and* **128→132** *(PG = TES). Tol was used as solvent in all cases.*

entry	PG	reaction batch	MnO_2 type	temp.	conditions and duration	second step with $BrCCl_3$/DBU[1)]	isolated yield[2)]
1	TBS	0.15 mmol	*Merck (90%, fresh)*	60 °C	20 eq, 22 h[3)] → 40 eq, 19 h	no	23%
2	TBS	19.5 mmol	*Alfa (58%, fresh)* →*Fluka (90%, fresh)*	70 °C	20 eq, 15 h (*Alfa)* → filtration →20 eq, 4 h (*Fluka*)	yes	38%
3	TBS	2.94 mmol	*Fluka (90%, fresh)*	70 °C	20 eq, 35 h	yes	51%[4)]
4	TES	0.14 mmol	*Fluka (90%, fresh)*	70 °C	20 eq, 24 h	yes	53%[5)]
5	TBS	3.71 mmol	*Fluka (90%, aged, reactivated by azeotropic dist.)*	70 °C	30 eq, 16 h	no	educt reisolated
6	TBS	1.13 mmol	*Aldrich (85%, <5 µm size)*	70 °C	20 eq, 22 h	no	educt reisolated
7	TES	0.08 mmol	*Sigma (90%, battery grade, <10 µm size)*	70 °C	20 eq, 20 h	no	educt reisolated

1) conditions: $BrCCl_3$ (3.0 eq), DBU (3.0 eq), Tol, RT, 6 to 24 h; 2) isolated yield after flash chromatographic purification; 3) ^{1}H NMR spectrum shown in figure 4.11; 4) 4.3% of the nitrile **135** were also isolated; 5) purified by extraction.

In order to avoid these drawbacks associated with the slow conversion of the thiazoline intermediates the combined use of different reagents was investigated and led to significant improvement (figure 4.11b). For the first reaction step (thiazolidine→thiazoline), MnO_2 was used as oxidant, and the solution was heated at 70 °C until TLC control showed complete conversion of the thiazolidine. The reaction mixture, which at this step mainly contained thiazoline next to small amounts of the thiazole target compound, was cooled to room temperature, and $BrCCl_3$ as well as DBU were added which smoothly converted the thiazoline to

the thiazole. As shown in table 4.5, this procedure increased the yield to 51% (TBS-protection) and 53% (TES-protection), respectively (entries 3 and 4 vs. entry 1). The amount of over-oxidation product remained low, and only 4.3% were isolated by flash chromatographic purification (entry 4). MnO_2 purchased from *Alfa* was also usable but effected lower yields (entry 2). MnO_2 purchased from *Fluka* again gave the best results, and the addition of a second portion of the oxidant was not required. After reactivation, however, it did not show oxidizing activity any more (entry 5), and MnO_2 with < 5 µm particle size as well as battery grade MnO_2 purchased from *Sigma* did not effect oxidation either (entries 6 and 7).

Table 4.6 *Two- and three-step silyl protection/oxidation protocols of the* D*-gluco thiazolidines* **100→131** *(PG = TBS) and* **100→132** *(PG = TES): upscaling and optimization of the oxidation step. The silylations were always carried out in the same way as described in scheme 4.8, and the products were subjected to oxidation without purification. Tol was used as solvent for all oxidations.*

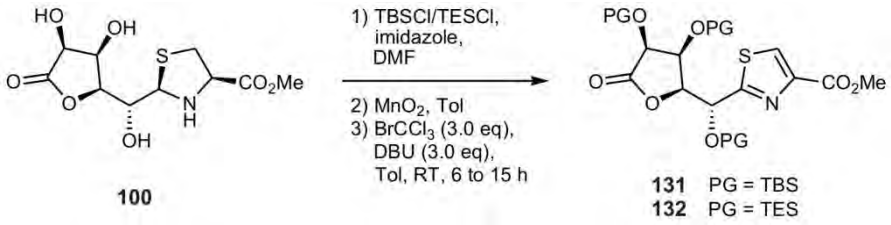

entry	PG	reaction batch	MnO_2 type	conditions and duration[1)]	third step with $BrCCl_3$/DBU	isolated yield over three steps[2)]
1	TBS	1.34 mmol	*Merck (90%, fresh)*	20 eq, 27 h → 33 eq, 24 h	no	22%
2	TBS	11.3 mmol	*Merck (90%, fresh)*	10 eq, 24 h → 15 eq, 22 h	no	29%
3	TBS	18.3 mmol	*Fluka (90%, fresh)*	20 eq, 10 h → 30 eq, 13 h	yes	34%
4	TES	13.2 mmol	*Fluka (90%, aged)*	20 eq, 19 h	yes	38%
5	TES	22.6 mmol	*Fluka (90%, fresh)*	20 eq, 28 h	yes	48%

1) 70 °C reaction temperature was chosen in all cases; 2) isolated yield after flash chromatographic purification.

As in the case of the D-arabino configured compounds, the procedure and overall yields were finally further optimized by subjecting the silylation raw product to oxidation without chromatographic purification (table 4.6). This two- or three step procedure (without and with $BrCCl_3$/DBU aided oxidation, entries 1-2 and 3-5, respectively) was also compatible with upscaling of the reaction batches and afforded the TBS-protected thiazole **131** in 34% overall yield (entry 3). In comparison with the 23% obtained if the silylation raw product is purified

before oxidation, this again demonstrates the considerable loss of substrate associated with crystallization (**124**) or chromatographic purification (**128**). Residual silyl alcohol which, in spite of 24 h drying *in vacuo*, was still present did not lower the oxidation activity of the MnO_2, and in the case of TES-protected substrate, no second addition of MnO_2 was required (entries 4 and 5). Interestingly, the use of MnO_2 purchased from *Fluka* which had been stored under air for several months required a shorter reaction time until consumption of the thiazolidine was complete, however, it also increased the oxidative degradation (entry 4). With fresh MnO_2, an overall yield of 48% was obtained, and running a 22.6 mmol reaction batch finally afforded 6.91 g of purified thiazole **132**.

In additional experiments it was investigated whether the 7,5-bicyclic thiazolidine lactam, which is the thermodynamic condensation product (scheme 4.6), can be converted to a thiazolidine with linear sugar chain by opening of the lactam (scheme 4.9). For this purpose, the tetraol **105** was protected as bisacetonide (**136**)[369, 391] and subjected to various lactam opening conditions which would furnish a fully protected thiazolidine that in the next step could be oxidized to the thiazole. While the lactams of analogous compounds with D-manno configuration or with benzothiazolidines had been shown to be readily opened under basic or oxidative conditions, respectively,[392] the lactam of **136** was stable against KCN/MeOH,[393, 394] NaOMe and $CsCO_3$ in MeOH,[395] and only epimerization at the C-3 stereocenter was observed (**137**).

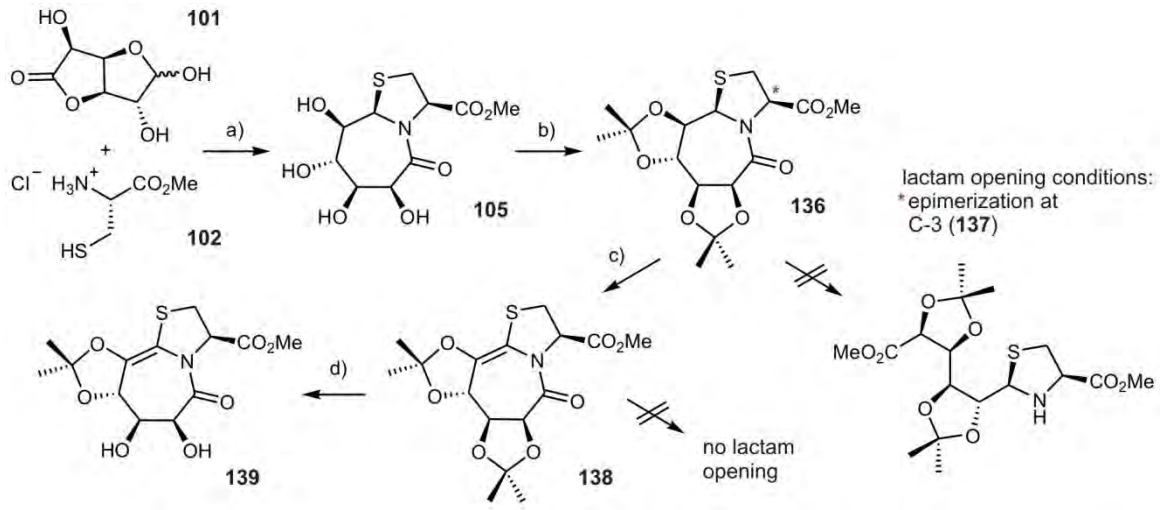

Scheme 4.9 Evaluation of the 7,5-bicyclic lactam* 136 *as starting point for thiazole polyol synthesis.
Reagents and conditions: a) H_2O/Pyr 9:1, RT, 4 d, 52%; b) DMP (10 eq), *p*TosOH x H_2O (cat.), DMF, 60 °C, 38 h, 93%; c) MnO_2 (20 eq), Tol, 70 to 80 °C, 8.5 h, 40%; d) TFA, EtOAc, RT, 24 h, 36%.

Therefore, it was examined whether the thiazolidine in **136** can be oxidized with MnO_2 to yield a species which in the next step can be converted to a *N*-acyl iminium ion, followed by cleavage of

the C-N bond.[392] In fact, treatment with MnO_2 led to formation of a single product, but the C9-C9a instead of the C2-C3 bond was selectively converted to a double bond (**138**, c). This compound turned out to be stable against oxidation with MnO_2, DDQ,[396] and Pd/C/cyclohexene.[397] Another option to investigate was the cleavage of the 8,9-acetonide, which would furnish an enol that, after isomerization to the corresponding ketone, eventually could be oxidized to an *N*-acyl iminium ion. However, the acetonide could not be removed under conditions which did not effect the decomposition of the substrate, and only the 6,7-diol was deprotected (**139**). Although these experiments with D-gluco configured compounds were not successful, the lactam opening products of thiazolidine lactams with D-manno configuration[392] are promising substrates to obtain thiazole polyols with stereoconfigurations different than the compounds obtained within the scope of this work.

4.4.3 Deprotection and lactone opening

The next task concerned the removal of the silyl groups and the evaluation of conditions that are suitable to effect the opening of the lactone rings. Numerous methods exist which allow for the mild cleavage of TES and TBS protecting groups, and some of them were initially tested for **131** as substrate which, with its three TBS groups in close spatial proximity to each other, is the most demanding one of the four synthesized compounds. The results are summarized in table 4.7 and the structures are shown in figure 4.12. TBAF in THF, which is the most common cleaving reagent for TES and TBS groups,[380] effected complete conversion of **131** to **140** also on a large scale, but the purification of the product from the tetrabutylammonium salts turned out to be difficult and time-consuming (table 4.7, entry 1). Therefore, some recently developed fluoride-free silyl deprotections were investigated, namely the use of catalytical amounts of AcCl in MeOH,[398] hydrogenation with Pd/C,[399] and the use of the $TiCl_4$/EtOAc complex as *Lewis* base,[400] but in all cases only educt was reisolated after the workup procedure (entries 2-4). Therefore, attention was concentrated to HF as reagent which is commercially available in various solvents and concentrations. 10% HF in CH_3CN[401] effected complete deprotection, but several products were isolated (entry 5). However, when HF in Pyr[402] instead of CH_3CN was applied, the reaction proceeded smoothly, and after 48 h the product was isolated in 91% yield (entry 6), ^{1}H NMR spectrum shown in figure 4.12a). Most important, the stereoconfiguration of the sugar chain was completely retained, as proven by X-ray crystallographic analysis (figure 4.12a). However, although leading to satisfactory results, the use of HF at high concentrations, should be avoided whenever possible as this exhibits an extremely toxic chemical which in the past has caused several fatal accidents by skin contact.[403] Therefore, the

applicability of the much less toxic reagent H_2SiF_6 was examined,[404, 405] and it turned out that quantitative desilylation equally occurs within significantly reduced reaction times (entry 7). H_2SiF_6 was also successfully applied for the desilylation of the TES-protected D-gluco and D-arabino configured lactones **132** and **129**, respectively, and the deprotected lactones **140** and **141** were isolated in 98% and 94% yield, respectively, with no chromatographic purification required (entries 8 and 9). Figure 4.12b shows an ^{1}H NMR spectrum of **141** obtained by this method.

Table 4.7 *Cleavage of TBS (***131→140***) and TES protecting groups (***132→140***,* **129→141***).*

entry	substrate	reaction batch	conditions and duration	result	isolated yield
1	**131**	up to 2.88 mmol	TBAF (3.0 eq), THF_{abs}, 0 °C, 3 h	complete conversion, but difficult to purify	n.d.
2	**131**	36 µmol	AcCl (cat.), $MeOH_{abs}$, 0 °C → 45 °C, 48 h	no conversion	educt reisolated
3	**131**	32 µmol	Pd/C, H_2, MeOH, RT, 3 d	no conversion	educt reisolated
4	**131**	29 µmol	$TiCl_4$ (6.0 eq), EtOAc (6.0 eq), $CH_2Cl_{2\ abs}$, 0 °C → reflux, 48 h	no conversion	educt reisolated
5	**131**	35 µmol	HF (10% in CH_3CN), RT, 28 h	complex mixture of products obtained	n.d.
6	**131**	4.00 mmol	HF (70% in Pyr), Pyr_{abs}, 0 °C → RT, 42 h	complete conversion (TLC)	91%[1)]
7	**131**	0.19 mmol	H_2SiF_6 (1.66 M in H_2O), CH_3CN, 45 °C, 8.5 h	complete conversion (TLC)	n.d.[2)]
8	**132**	3.30 mmol	H_2SiF_6 (1.66 M in H_2O), CH_3CN, 0 °C → RT, 4.5 h	complete conversion (TLC)	98%[1)]
9	**129**	3.30 mmol	H_2SiF_6 (1.66 M in H_2O), CH_3CN, 0 °C → RT, 4.5 h	complete conversion (TLC)	94%[1)]

1) isolated yield after crystallization from CH_3CN; 2) yield was not determined as inorganic salts were present.

Five-membered lactones, especially if all-*cis* configured, possess low inclinations to opening, which is visible by the difficulties associated with their polymerizations.[406] This problem also occurred in the attempts to open the D-gluco and D-arabino lactones (scheme 4.10). For initial methanolysis studies the TES protected compounds **132** and **129** were chosen as the silyl groups should be cleaved under the reaction conditions (basic with NaOMe in MeOH (a), and acidic with catalytical amounts of CSA in MeOH (b), respectively), which should allow to obtain the deprotected methanolysis products in one single step. In fact, both conditions, when applied to **132**, led to silyl cleavage as well as lactone opening; however, it was not possible to isolate the tetraol **142** as pure compound due to a ring-chain equilibrium with the lactone **140**

(scheme 4.10a). Addition of excess of NaOMe or acid never furnished the open species as dominating species, and, instead, a 1:1 mixture of both compounds was obtained. The separation of both compounds from each other was not successful, neither by column chromatography nor by crystallization, and **142** showed a high inclination to cyclize to the lactone **140**.

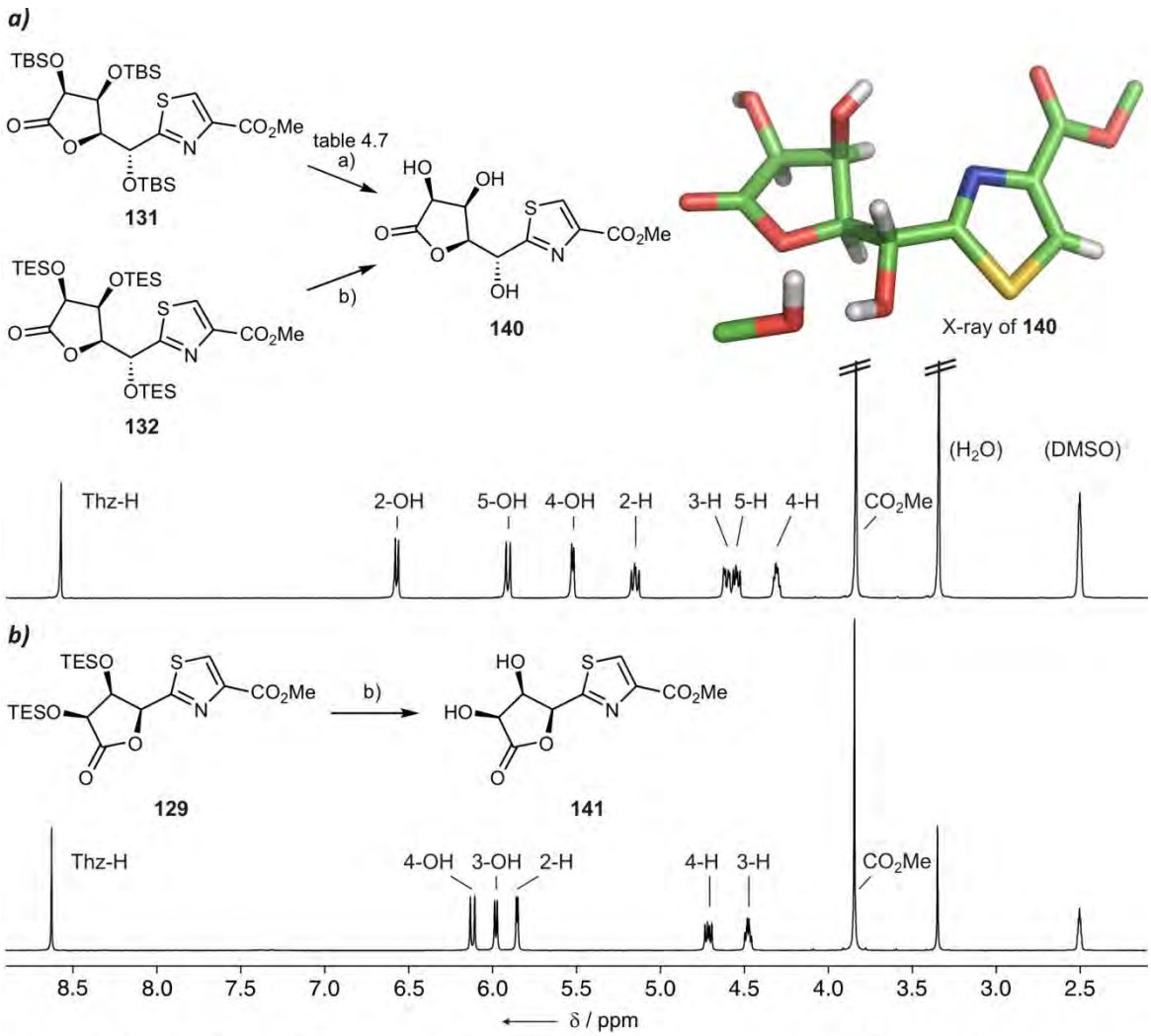

Figure 4.12 Synthesis of the unprotected* D*-gluco and* D*-arabino configured thiazole lactones* 140 *(a) and* 141 *(b). *The X-ray crystal structure of* **140** *obtained from crystals grown in MeOH shows the incorporation of one equivalent of MeOH into a three-dimensional hydrogen bonding network.* ^{1}*H NMR spectra of the products* **140** *and* **141** *are also depicted (DMSO-*d_6*, 300 MHz, 300 K).* Reagents and conditions: a) HF (70% in Pyr, 12 eq), Pyr_{abs}, 0 °C to RT, 42 h, 91%; b) H_2SiF_6 (1.65 M in H_2O, 2.0 eq), CH_3CN, 0 °C to RT, 4.5 h, 98% of **140**/94% of **141**.

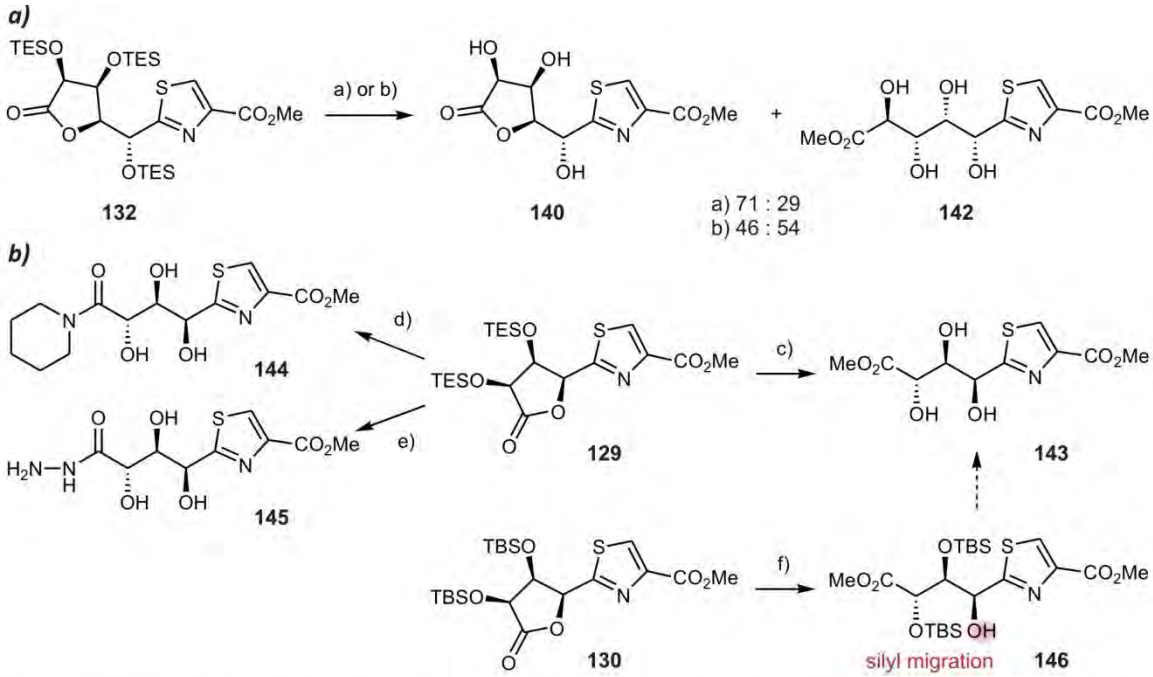

Scheme 4.10 Lactone opening: methanolysis and aminolysis reactions. a) *The* D*-gluco configured thiazole tetraol* **142** *could only be isolated together with the deprotected lactone* **140***, apparently as both compounds equilibrate under the applied reaction conditions.* ***b)*** *In contrast, the* D*-arabino analog* **143** *was isolated as pure compound. Aminolyses yielding the piperidine amide* **144** *and the hydrazide* **145** *were also possible. Unlike the TES groups, the TBS protection groups of* **130** *were stable towards the methanolysis conditions, but due to migration the alcohol* **144** *could not be isolated in acceptable purity.* Reagents and conditions: a) NaOMe (0.3 eq), $MeOH_{abs}$, 0 °C to RT, 23 h, 55% of **140**/22% of **142**; b) CSA (cat.), $MeOH_{abs}$, RT, 2.5 h, 46% of **140**/54% of **142**; c) NaOMe (0.1 eq), $MeOH_{abs}$, 0 °C to RT, 17 h, 50%; d) piperidine (7.5 eq), NEt_3 (cat.), DMF, 50 °C, 28 h; e) hydrazine hydrate (1.2 eq), MeOH, RT, 4.5 h; NaOMe (1.2 eq), $MeOH_{abs}$, 0 °C, 5 h, 85% (**146** 3,4-/2,4-/2,3-silyl/**130** 46:24:15:15).

When subjecting the TES-protected D-arabino configured lactone **129** to similar basic methanolysis conditions, an analogous equilibrium was also observed, but in this case it was possible to isolate the open chain product **143** by extraction (EtOAc/H_2O) in 50% yield after the reaction mixture had been neutralized (scheme 4.10b, conditions c). However, **143** also easily forms the corresponding lactone in solution, which limits its synthetic utility. The problem was solved at a later stage by the conversion of **129** to the benzyl ester (figure 4.13). Furthermore, aminolysis reactions were tested with the TES-protected lactone **129**, and syntheses of the piperidine amide **144** as well as of the hydrazide **145** were performed.

The reason why, up to this stage, the synthesis of the TBS-protected thiazoles was further investigated (although the TES-protected analogs were obtained in higher yields), was that these more stable protecting groups should not be cleaved under the conditions required for lactone opening, thereby affording thiazole depsipeptide units which are selectively deprotected at C-2. This would allow to perform an *O/N*-exchange sequence at this position, resulting in the desired α-amino thiazole dipeptide units (figure 4.19 and section 4.4.9). However, several attempts to open the lactone with aqueous and non-aqueous work-up procedures always gave product

mixtures as the migration of the silyl group in the desired alcohol **146** could not be avoided (scheme 4.10b, conditions f). This suggests the use of more stable silyl groups like TIPS or TBDPS which are less inclined to migrate.[407]

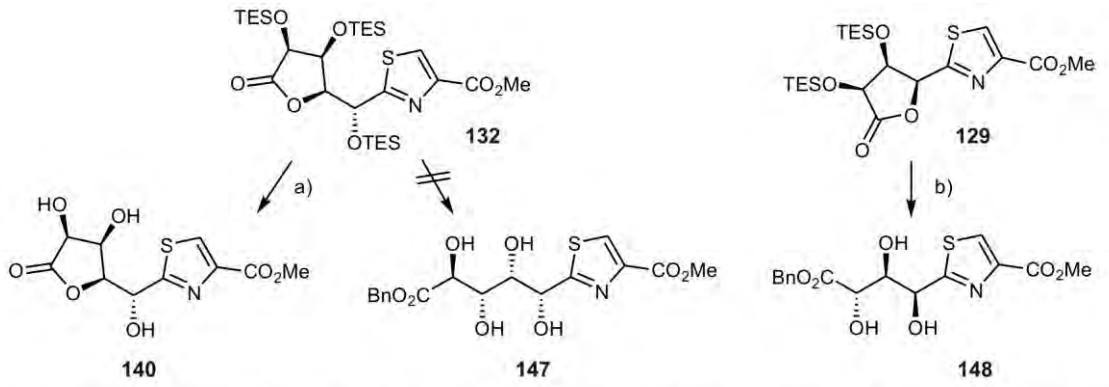

Scheme 4.11 Lactone opening with BnOH as nucleophile. *While the lactone of the* D*-gluco configured thiazole* **132** *is not opened even when refluxed in bulk BnOH, the* D*-arabino analog* **129** *readily reacts at 50 °C and the benzyl ester* **148** *be isolated in 81% yield directly from the reaction mixture as precipitate. The reaction is put into further context in figure 4.11.* Reagents and conditions: a) BnOH (bulk), CSA (cat.), 50 °C, 2 d; b) BnOH (bulk), CSA (cat.), 50 °C, 67 h, 81%.

Due to the disadvantages associated with the open chain methyl esters **142** and **143** (low yields and instability) further attempts were concentrated on the synthesis of benzyl ester analogs which would be of greater synthetic utility as both carboxyl functions are orthogonally protected. The D-gluco lactone **132**, when dissolved in BnOH (serving as reagent and solvent) with a catalytical amount of CSA, could not be opened to the desired benzylic ester **147** and only the deprotected lactone **140** was obtained (scheme 4.11) even after heating of the solution for 2 d. The lactone proved to be exceptionally stable under various conditions, and further experiments with protected substrates under various conditions are described in section 4.4.5.3. In contrast, upon stirring of the D-arabino lactone **129** in BnOH with traces of acid at 50 °C, a precipitate could be isolated directly from the reaction mixture which in fact turned out to be the desired benzyl ester **148** (scheme 4.11 and figure 4.13). This could be isolated in good purity (^{1}H NMR spectrum shown in figure 4.13b) by filtration of the reaction mixture and washing with Tol. This allowed to isolate the product as colorless powder in reproducable yields (varying between 75% and 81%) and in multigram amounts (the biggest reaction batch was 12.9 mmolar and furnished 3.69 g of the product). Figure 4.13a relates **148** to the Dyg<Thz core dipeptide of the nocathiacin and thiazomycin antibiotics. It exhibits the depsipeptide analog of the naturally occurring unit (hydroxyl instead of amine functionality at C-2) and the proper (2*S*,3*S*,4*S*) stereoconfiguration. This makes it a promising substrate to be incorporated into synthetic

analogs of these antibiotics. For this purpose, the three hydroxyl functions must be distinguishable in selective (de)protection reactions, a topic which will be described in section 4.4.5.2. Alternatively, the lactone **141** can also be a possible starting substrate for the assembly of the antibiotic analogs or fragments thereof, as the lactone serves as intramolecular protection of the 2-OH as well as of the sugar carboxyl functionality.

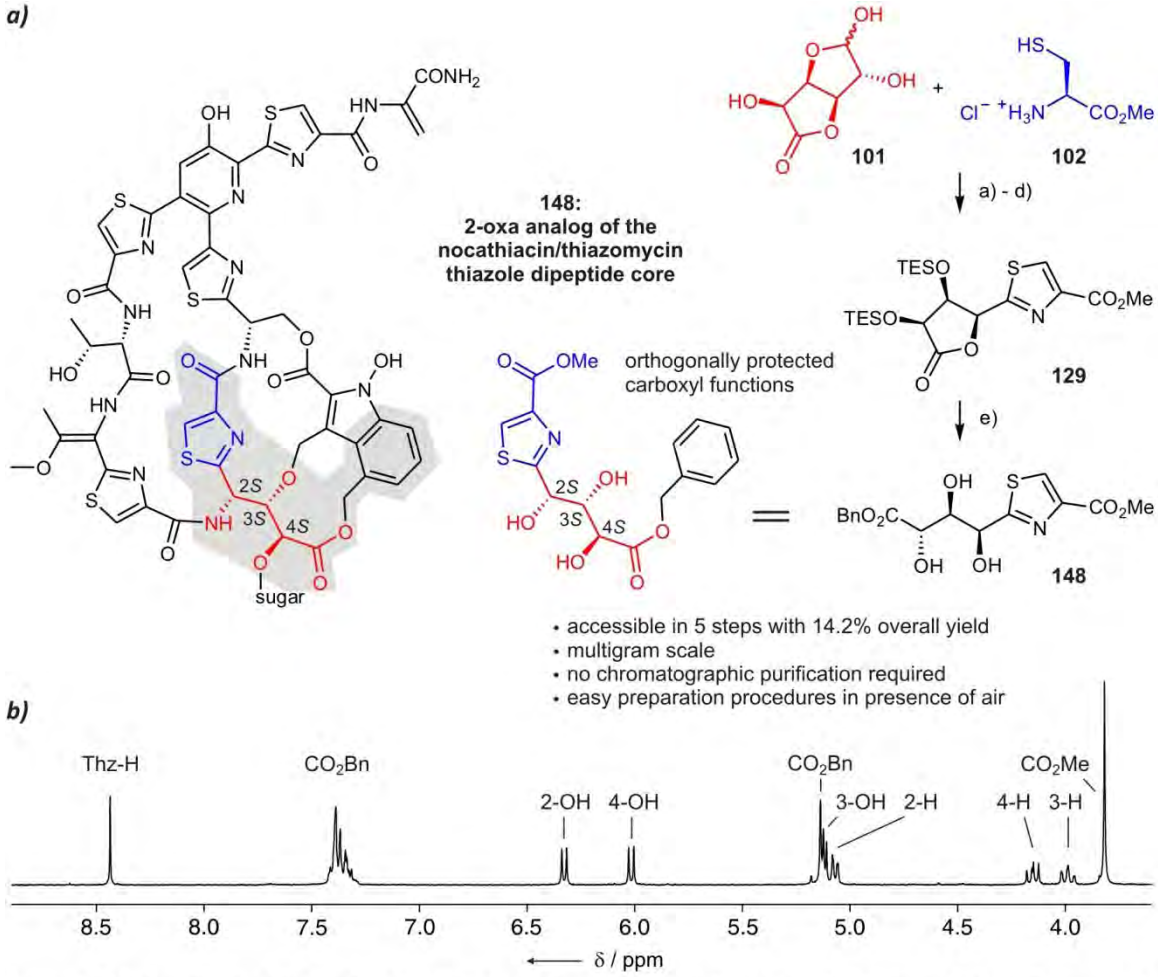

***Figure 4.13 Synthesis of the thiazole triol* 148. *This substrate differs from the Dyg<Thz dipeptide core of the nocathiacins and thiazomycins only by its functionality at C-2.* a)** *Overview of the five-step synthetic procedure starting starting from γ-glucuronolactone* **101** *and* L*-cysteine methyl ester hydrochloride* **102**. **b)** *^{1}H NMR spectrum of* **148** *(DMSO-d_6, 300 MHz, 300 K).* Reagents, conditions, and purification procedures: a) **101**, $NaIO_4$ (1.0 eq), Na_2HPO_4 (aq., 0.05 M), 0 °C, 1 h, no purification required; b) **102**, MeOH/H_2O/Pyr 15:5:1, RT, 15 h, crystallization, 53% over two steps; c) TESCl (2.4 eq), imidazole (2.4 eq), DMF, RT, 3 h, no purification required; d) MnO_2 (20+10 eq), Tol, 70 °C, 79 h, silica gel filter column, 33% over two steps; e) BnOH (bulk), CSA (cat.), 50 °C, 67 h, precipitation from reaction mixture, 81%.

The thiazole depsipeptide **148** also fulfills the important requirement of being available on large scale by an easy preparation procedure, starting from readily available educts. Figure 4.13a summarizes the five reaction steps which avoid any complicated purification procedures and the use of dry solvents and inert gas. The cleavage of the benzyl ester is accomplished by

hydrogenolysis (H_2 pressure of 1 bar is sufficient), affording the thiazole **149** with a fully deprotected sugar chain in 90% yield (scheme 4.12). No lactone formation was observed under these conditions as well as under the various hydroxyl protection experiments described in section 4.4.5.2.

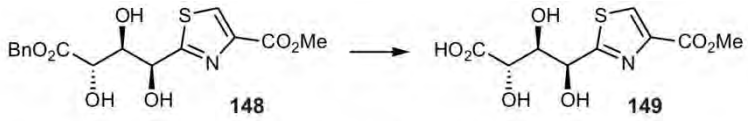

***Scheme 4.12 Cleavage of the benzyl ester* 148.** Reagents and conditions: Pd/C (5%, wet, *Degussa*), H_2 (1 bar), MeOH, RT, 3 d, 90%.

With its good availability, the triol **148** also represents a logical starting point for studies concerning the *O/N*-exchange at C-2, which has to occur with retention of the stereocenter in order to obtain the native stereoconfiguration of Dyg<Thz. The corresponding experimental work is discussed in chapter 4.4.9.3.

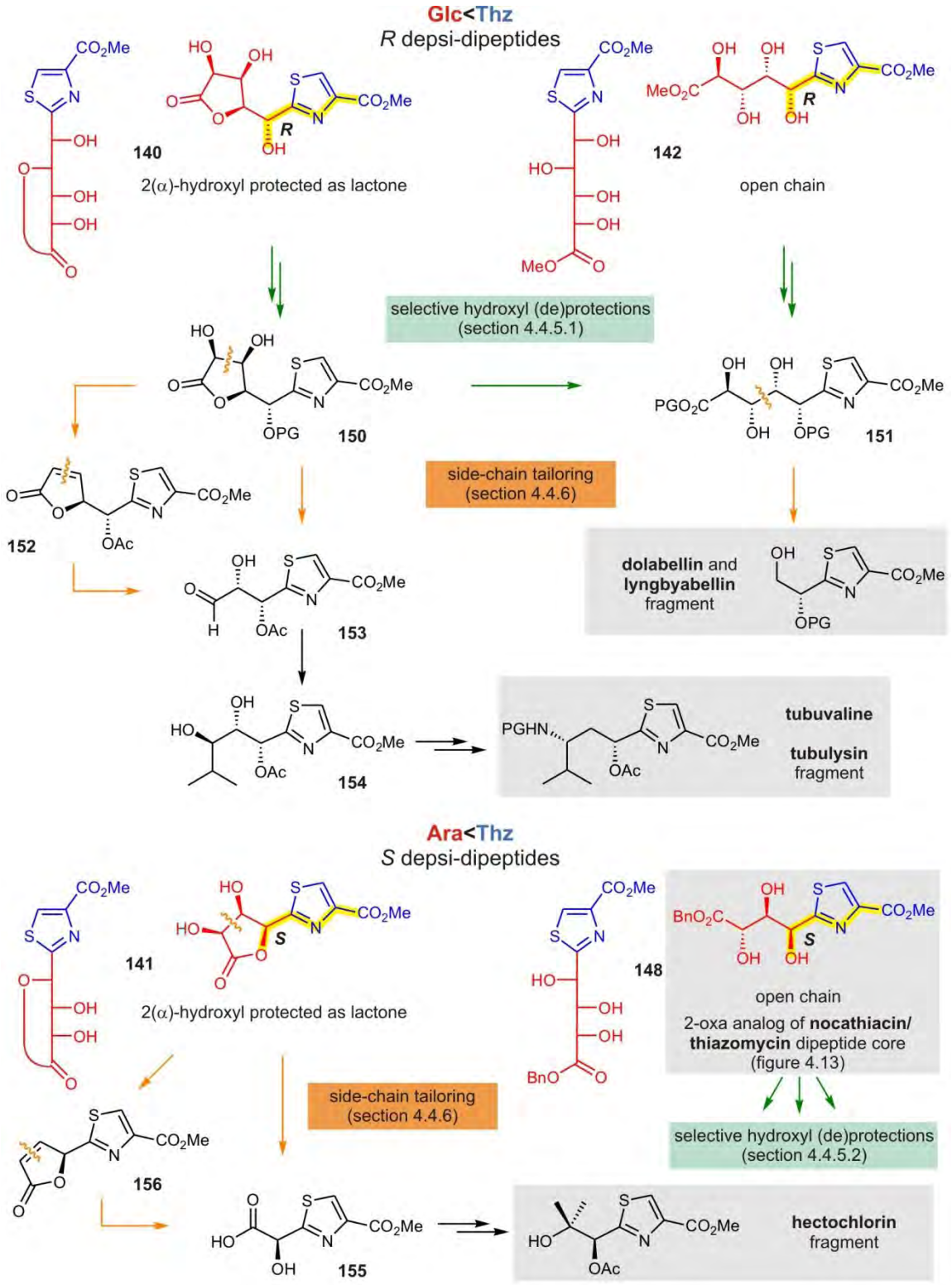

Figure 4.14 Interim summary and outlook: synthesized thiazole depsidipeptides and possible natural product targets. *The thiazole polyols which are accessible by the syntheses described in section 4.4.3 are shown in red and blue, highlighting the sugar chains and the thiazoles, respectively. As shown by the backbone (yellow), the* D*-gluco side chains correspond to* R *configured depsipeptides, while an* S *configuration is present in the* D*-arabino analogs. Both series of polyols also differ in the stereoconfiguration at C-3(β). The green and orange reaction arrows indicate further tailoring steps which encompass selective (de)protection of the hydroxyl groups and tailorings of the sugar chain by C-C bond cleavage. Such further modifications open the way to a variety of naturally occuring thiazole depsidipeptides.*

4.4.4 Interim summary and outlook: depsidipeptide targets

Figure 4.14 shows the obtained deprotected D-gluco and D-arabino thiazole polyols (shown in red/blue: Glc<Thz, top and Ara<Thz, bottom) which are accessible by the synthetic strategies described in the preceding sections. The course of the backbone is highlighted in yellow, and the *Fischer* projections (compare to figure 4.7) emphasize the glycosidic origin of the structures, reminiscent of the thiazole protecting methodology developed by *Dondoni et al.* in which the thiazole ring (without a carboxyl functionalization) serves as latent formyl group.[408] According to whether it is part of the glucurono or the arabinurono polyol, the C-2(α)-stereocenter is in the *R* (Glc<Thz) or *S* (Ara<Thz) configuration. Because of their functional groups, these unis are promising starting points for the construction of naturally occurring thiazole depsidipeptides by controlled tailoring of the sugar chain (orange reaction arrows). For this purpose, the possibilities of selective hydroxyl protection have to be explored for the D-gluco depsidipeptides (green reaction arrows) which is described in the following section. The selective protection of the α-hydroxyl group (**150**, **151**) is prerequisite for a possible synthesis of the depsidipeptide fragments which are present in the tubulysins,[267, 268] in dolabellin and in the lyngbyabellins (highlighted in grey).[275] By cleaving the C-4/C-5 bond of **150**, either directly with $NaIO_4$ or by ozonlysis of the substrate **152** which should be accessible by a *Corey-Winter* olefination, the aldehyde **153** is obtained. This could subsequently be subjected to a *Cram* chelate addition of *i*Pr, yielding the triol **154**. If an acyl groups has been chosen as protecting groups of the α-hydroxyl, this compound can be converted to the tubuvaline dipeptide by *O/N*-exchange at the γ position and deoxygenation at the β position. The dolabellin/lyngbyabellin diol is accessible from the open-chain compound **151** by cleavage of the C-3/C-4 bond and subsequent reduction.

In the D-arabino lactone **141**, the α-hydroxyl function is already protected by the intramolecular acylation. Under appropriate conditions, the cleavage of the C-2/C-3 bond should be possible, yielding the α-hydroxy carboxylic acid **155** either by periodate cleavage or ozonlysis of the *Corey-Winter* product **156**, respectively, and subsequent oxidation. Finally, the hectochlorin fragment could be accessible in a small overall number of steps. In contrast, by the accomplished synthesis of the triol **148** an analog of the Dyg<Thz dipeptide is already accessible (figure 4.13). In order to investigate its suitability for the construction of nocathiacin/thiazomycin analogs, its three hydroxyl functions must be distinguishable, and the resulting experiments are described in section 4.4.5.2.

Concerning the side chain tailoring reactions, some preliminary experiments were performed with D-gluco as well as D-arabino compounds, as outlined in section 4.4.5.4.

4.4.5 Selective hydroxyl protections and further lactone opening experiments

4.4.5.1 D-gluco configured substrates

The selective protections of the 4,5-diol and the 2-hydroxyl function of the D-gluco configured lactone **140** were obtained in different ways (figure 4.15a, reagents and conditions described in tables 4.8 and 4.9). Protections of the diol as acetonide (dimethylacetal, **157**)[409] using DMP and catalytical amounts of acid at 40 °C led to low yields in acetone/DMF (entry 1), and increasing the temperature promoted the formation of the undesired acetonide with MOP-protected 2-hydroxyl **158**. In absolute DMF, the yield could be increased and shorter reaction times were sufficient (entry 2). Rising the reaction temperature to 60 °C in DMF (absolute DMF was not necessary) did not promote the 2-hydroxyl protection, and using *p*TosOH x H_2O instead of CSA as acid finally afforded the acetonide **157** in an acceptable yield of 59% (entry 3). The selective protection of the 4,5-diol was proven by the HMBC correlation of the remaining hydroxyl proton and Thz-H, both showing a scalar heteronuclear ^3J coupling to C-1 (figure 4.15b).

As the yields of the acetonide protection could not be further increased, the alternative use of an ethoxymethylene acetal (ethyl orthoester) was investigated, a protective group which has widely been used in polynucleotide synthesis.[410] This diol protection group is also cleaved off under acidic conditions, but, in contrast to the acetonide, milder conditions are sufficient. The drawback of the orthoester, however, is the presence of a stereocenter if (as in the present case) an unsymmetric diol is protected, which leads to two sets of signals in the ^{1}H NMR spectra and therefore complicates evaluation. Using ethyl orthoformiate as reagent as well as solvent, the orthoester **159** could be isolated in much better yield (94%) that the acetonide, and 2-hydroxyl protection (**160**) occurred only to minor extent (entry 4).

In the next step, the remaining 2-hydroxyl functions were protected as acetates (**161** and **162**) and TBS ethers (**163** and **264**) in acceptable yields. The acetate was chosen as it is present in the naturally occurring tubuvaline unit (figure 4.14), and the TBS group is stable to conditions required for acetonide and orthoester removal. However, under the acyl protection conditions, a considerable extent of epimerization at C-2 occurred (**165**, entries 5 and 7), and the epimers were not separable by column chromatography. By shortening the reaction time,

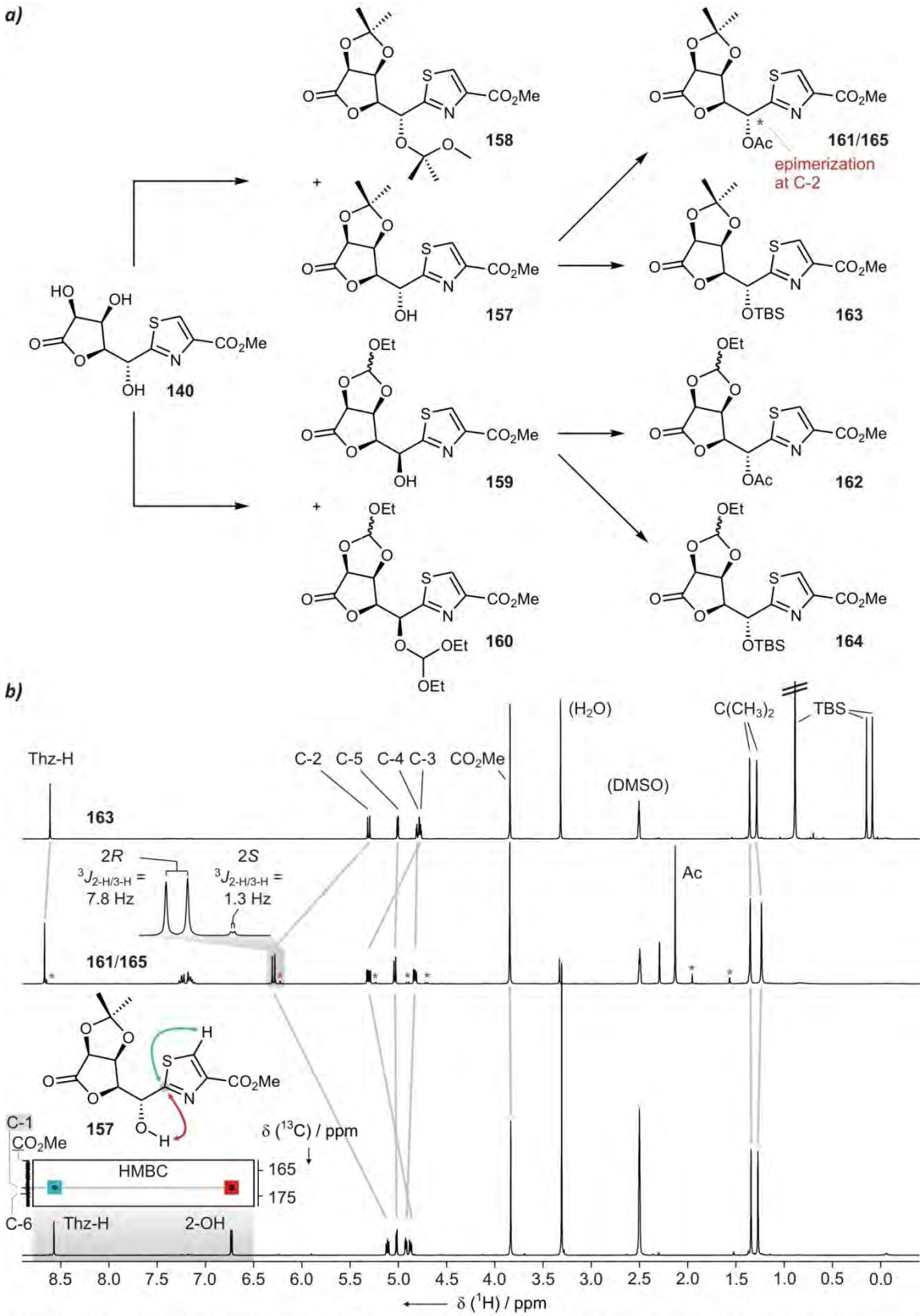

Figure 4.15 Hydroxyl protections of the D-gluco configured thiazole lactone* 140.** ***a) *The diol was protected as acetonide and ethyl orthoester, and the remaining 2-hydroxy functionality was protected as acetate or silyl ether. Table 4.8 lists the tested as well as optimized reaction conditions for the single steps.* ***b)*** *^{1}H NMR spectra of the acetonide protected diols* **157** *(bottom),* **161/165** *(middle),* and **163** *(top; DMSO-d_6, 600 MHz (***161/165***: 500 MHz), 300 K). A HMBC section of* **157** *is also shown, proving the selective protection of the 4,5-diol. Red stars indicate the C-2 epimerization product after acetylation.*

epimerization could be reduced but not suppressed completely (entry 6). In the spectrum of **161** (figure 4.15b), the signals resulting from the epimer are marked by red stars, and both stereoconfigurations at C-2 are well distinguishable by the different $^{3}J_{2\text{-}H/3\text{-}H}$ couplings. The TBS protections of **163** and **164** under *Corey* conditions[380] proceed without epimerization and in good yields (entries 8 and 9; spectrum of **163** shown in figure 4.15b).

With the 2-hydroxyl function orthogonally protected, removal of the acetonide or the orthoester should afford the deprotected 4,5-diol as starting substrate for chain tailoring experiments (figure 4.14). In the case of the 2-acyl protected thiazole lactone **161**, this turned out to be problematic as acyl migration occurred under the chosen acidic conditions, and only 28% of the desired product **166** were isolated (TFA/H_2O 99:1, table 4.9, entry 1). Increasing the amount of H_2O in the reaction mixture did not shorten the reaction time but led to a near 1:1:1 distribution of the acyl group to the three hydroxyl functions (migration products **167** and **168**, entry 2). This problem could be solved by using aqueous formic acid instead of TFA, which reduced the acyl migration to 10% (entry 3).

Table 4.8 *Diol protections of* **140** (→*acetonide:* **157**/→*orthoester:* **159**) *and subsequent acyl/TBS protection steps (***157**→**161**/**163**, **159**→**162**/**164**) *in comparison. See also figure 4.15a.*

entry	protection step	reaction batch	conditions and duration	extent of epimerization	isolated yield[1)]
1	**140→157**	7.95 mmol	DMP (5.0 →10 eq), $acetone_{abs}$ /DMF_{abs} 5:1, CSA (cat.), 40 °C, 24→42 h	no epimerization observed	25%[2)]
2	**140→157**	3.46 mmol	DMP (5.0 →20 eq), DMF_{abs}, CSA (cat.), 40 °C, 22→26 h	no epimerization observed	47%
3	**140→157**	4.21 mmol	DMP (20 eq), DMF, *p*TosOH x H_2O (cat), 60 °C, 20 h	no epimerization observed	59%
4	**140→159**	8.02 mmol	$HC(OEt)_3$ (bulk), *p*TosOH x H_2O (cat), RT, 41 h	no epimerization observed	94%[3)]
5	**157→161**	0.61mmol	Ac_2O (2.0 eq), DMAP (cat.), Pyr_{abs}, 0 °C, 3 h	13:1 (2*R*/2*S*)	67%
6	**157→161**	2.36 mmol	Ac_2O (2.0 eq), DMAP (cat.), Pyr_{abs}, 0 °C, 1.5 h	39:1 (2*R*/2*S*)	88%
7	**159→162**	0.47 mmol	Ac_2O (1.5 eq), DMAP (cat.), Pyr_{abs}, 0 °C→RT, 2 h	13:1 (2*R*/2*S*)	65%
8	**157→163**	0.44 mmol	TBSCl (3.0 eq), imidazole (3.0 eq), DMF, 50 °C, 8 h	no epimerization observed	90%
9	**159→164**	7.56 mmol	TBSCl (2.0 eq), imidazole (2.0 eq), DMF, 50 °C, 7 h	no epimerization observed	86%

1) isolated yield after flash chromatographic purification; 2) plus 4.4% of **158**; 3) 8:1 mixture of orthoester epimers, traces of **160** were also isolated.

Table 4.9 *Acetonide cleavage of* **161** *to the diols* **166** *and* **167**/**168**.

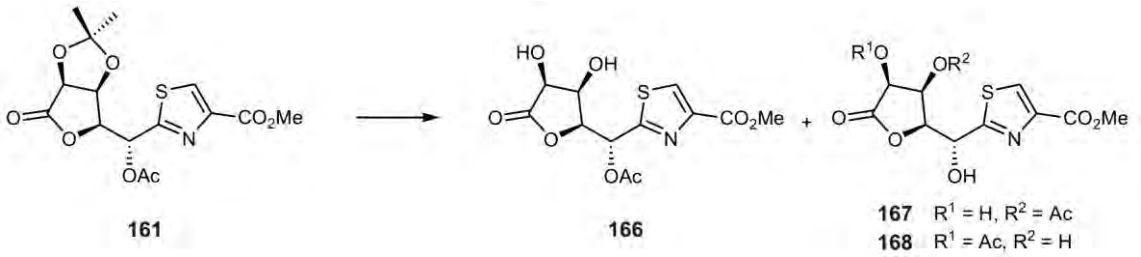

entry	reaction batch	conditions and duration	ratio 166/167/168	isolated yield of 166[1)]
1	0.35 mmol	TFA/H_2O 99:1, CH_2Cl_2, 0 °C, 1.5 h	63 : 24 : 13	28%
2	3.46 mmol	TFA/H_2O 9:1, CH_2Cl_2, 0 °C, 1.5 h	37 : 26 : 37	--[2)]
3	0.17 mmol	HCOOH (60% in H_2O), 65 °C, 40 min	90 : 8 : 2	77[3)]

1) isolated yield after flash chromatographic purification; 2) the isomers were not separated, overall yield after flash chromatographic purification 88%; 3) combined yield.

The acetonide cleavage with aqueous formic acid was also tested for the TBS-protected substrate **163** (table 4.10, entry 1). In this case, however, a longer reaction time was required (compare to table 4.9, entry 3) and the TBS group was partially cleaved, leading to a 55:45 mixture of the desired TBS ether **169** and the fully deprotected triol **140**. Therefore, catalyst and solvent were changed to CSA and MeOH, respectively, which should also allow to investigate whether lactone opening occurs. The acetonide, however, turned out to be too stable to be cleaved off at RT (entry 2), and longer reaction times and elevated temperatures effected cleavage of the TBS group.

Consequently, the analog **164** which is accessible in higher yields (table 4.8), protected by the less stable orthoester, was examined under identical conditions, and in this case the 4,5-diol could be quantitatively deprotected at RT (entry 3). However, as the silyl group readily migrated under these conditions the reaction was carried out using dry MeOH and omitting the aqueous workup procedure. By these changes, silyl migration could be suppressed and, in addition, a partial opening of the lactone ring to **170** was effected (entry 4), while only traces of this triol were obtained by the aforementioned protocol (entry 3).

Table 4.10 *Diol deprotections of* **163**/**164** *and attempts to open the lactone.*

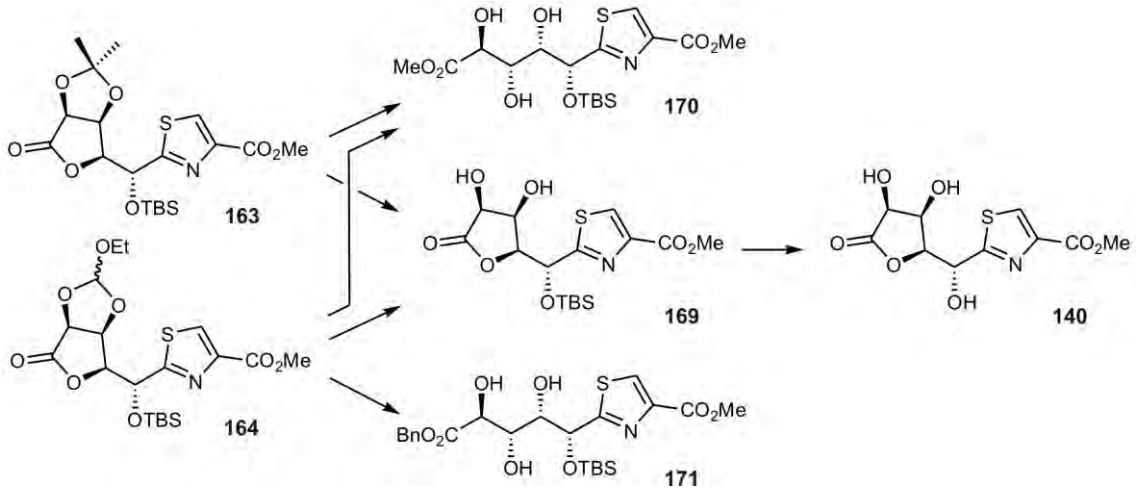

entry	deprotection step	reaction batch	conditions and duration	result	isolated yields[1)]
1	**163→169**	85.7 µmol	HCOOH (60% in H_2O), 65 °C, 5 h	**169**/**140** 55:45	--
2	**163→169**	0.23 mmol	CSA (cat.), MeOH, RT, 26 h	educt reisolated	--
3	**164→ 169/170**	0.28 mmol	CSA (cat.), MeOH, RT, 17 h	**169** and silyl group migration products; traces of **170**	--
4	**164→ 169/170**	70.0 µmol	CSA (cat.), $MeOH_{abs}$, RT, 23 h	**169** and **170**, no silyl migration observed	16% **169** 18% **170**
5	**164→ 169/171**	1.63 mmol	CSA (cat.), BnOH, 50 °C, 3 d	**169** and **140**, traces of **171**	35% **169** 17% **140**
6	**164→169**	82.7 mmol	aq. HCl (pH 2), 1,4-dioxane, RT→50 °C, 3 h	**169**/**140** 72:28	--

1) isolated yields after flash chromatographic purification.

The near 1:1 ratio of the lactone **169** and the lactone methanolysis product **170** (entry 4) suggests an equilibrium between these two species under the applied reaction conditions, as it is also observed in the case of the analog with unprotected hydroxyl functions (scheme 4.10, conditions b), and the low yields due to TBS deprotection make further optimization of the lactone opening reaction necessary. When using BnOH instead of MeOH as solvent and nucleophile, only traces of the lactam opening product **171** are obtained even after 3 d at 50 °C (entry 5). Concerning the selective cleavage of the orthoester, the best result was finally obtained by treatment with aqueous HCl (pH 2), which after neutralization with basic ion exchange resin afforded a 72:28 mixture of **169** and **140** and no further species, as determined from the raw product ^{1}H NMR spectrum (entry 6).

In summary, the experiments concerning the selective hydroxyl (de)protection of the D-gluco configured lactones show that this polyol chain is difficult to handle, and further attempts are necessary especially to optimize the opening of the stable lactone ring. The use of different silyl protecting groups which are more resistant to acidic or basic conditions should also be evaluated. Nevertheless, it could be shown that by a protection/deprotection sequence compounds with selective protection of the 2(α) hydroxyl function are accessible, which is a prerequisite for further studies of sugar-chain tailoring for the synthesis of thiazole depsidipeptide units of interest (figure 4.14).

4.4.5.2 D-arabino configured substrates

The opening of the D-arabinurono lactone had already been accomplished successfully by the multigram synthesis of the benzyl ester **148** (figure 4.13). In order to be applicable as a building block in the synthesis of thiopeptide analogs, as well as starting substrate for *O,N*-exchange studies, the three hydroxyl functions must be selectively addressable by (de)protection operations. For the unambiguous determination of the number and exact positions of attached protection groups, NMR spectroscopy is the method of choice as it gives a unique linking matrix between proton and carbon nuclei for every protection pattern (figure 4.16).

Scheme 4.13 summarizes the experiments aimed at the selective protection of one single hydroxyl group and subsequent (de)protections, and table 4.11 compares different silylation procedures. Acylation turned out to be suitable for complete protection of the triol only, as, by treatment with only 1.3 eq of Ac_2O, considerable amounts of the triacylated compound **172** were obtained, in addition to a mixture of single- and double substituted substrates (a). Silylation with 1.5 eq of TESCl under *Corey* conditions [380] was not regioselective as a mixture of single protected products was isolated (conditions b and table 4.11, entry 1). However, the hydroxyl function at position 4 was most readily silylated (**173**), and switching from TES to TBS led to a significant increase in yield and selectivity (conditions c and table 4.11, entry 2). In the first step, the silyl ether is regioselectively formed at position 4, yielding the diol **174**. In the case of excess of the protecting reagent, the second silylation occurs selectively at position 2, apparently due to steric reasons, furnishing **175** which exhibits the hydroxyl function at position 3 as the only unprotected functionality. The use of 2.2 eq of TBSCl led to the isolation of 48% and 40% of **174** and **175**, respectively, and by further increasing the amount of reagent the double silylation product is expected to become the main species.

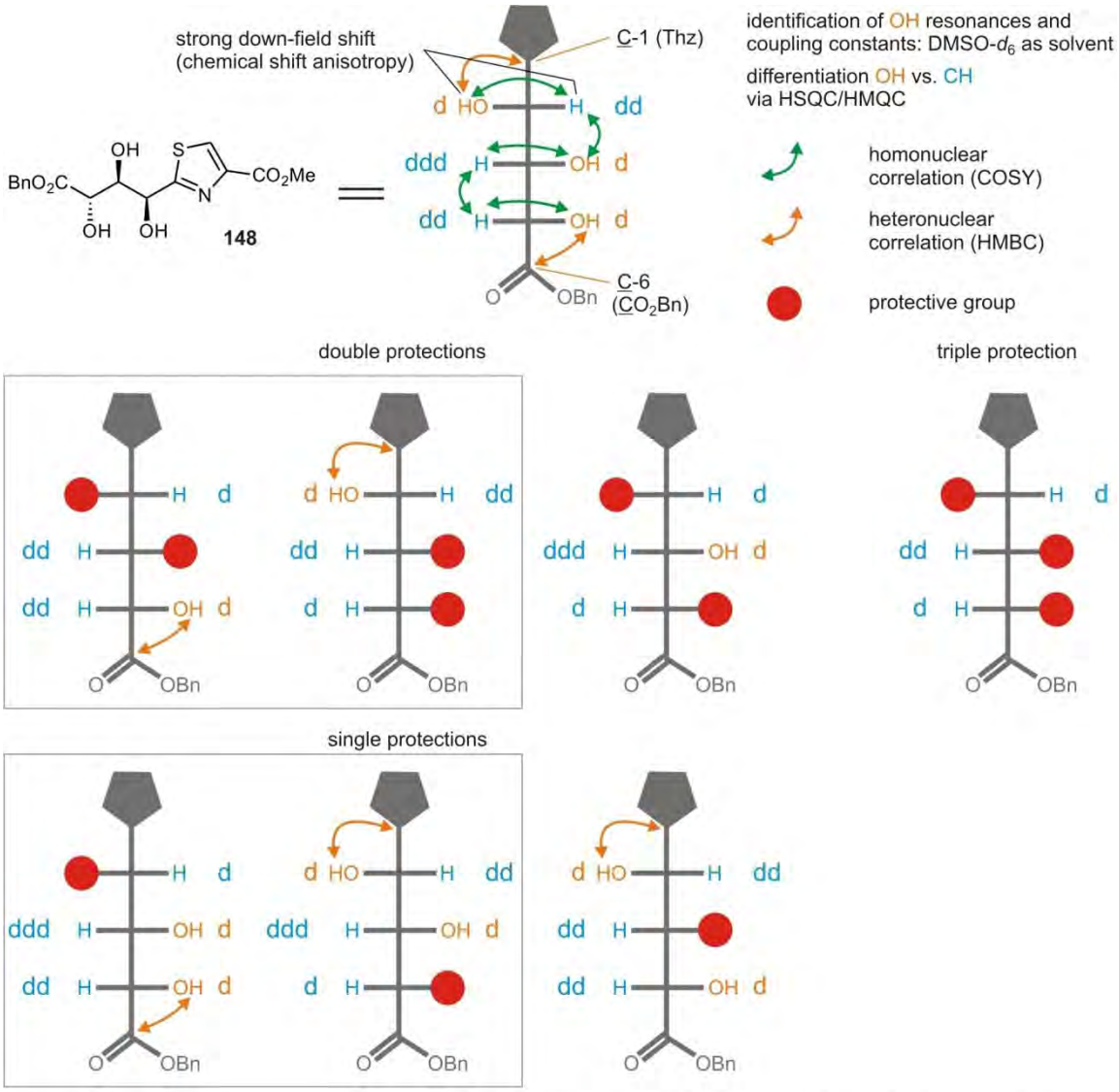

Figure 4.16 The seven protection patterns of an unsymmetric 1,2,3-triol and their identification by NMR. *Some structural details are listed which aid in the determination of the protection pattern. The oxygen-bound protons (orange) are easily distinguished from the carbon-bound protons (blue) by the absence of a heteronuclear ^{1}J HSQC or HMQC correlation. The homonuclear ^{3}J couplings in the COSY spectrum (green arrows) then allow to construct the linking matrice of the protons and lead to a characteristic number of dublets (d), dublets of dublets (dd), and dublets of dublets of dublets (ddd; according to the coupling constants other shapes like pseudotriplets are also possible). For a complete assignment it is crucial to use DMSO-d_6 as NMR solvent as this slows down chemical exchange and thus leads to well-resolved OH dublet signals. In order to determine whether a CH or OH proton showing a dd signal is located at C-2 or 4-H, further experiments are required. "Weak" information is for example given by the down-field shift of the aromatic thiazole ring which normally leads to a separation of the 2-H and 2-OH signals from the other peaks of the sugar chain (for example visible in the spectra of* **161**/**165** *and* **163** *shown in figure 4.15b. As this effect is dependent on the functionalization (the spectrum of* **157** *in figure 4.13b is one of the few examples; all four sugar CH signals are located closely to each other), additional NMR experiments are necessary. The HMBC experiment shows heteronuclear correlations to quarternary carbons (indicated by orange arrows) and thus allows to distinguish the 2-OH and 4-OH protons (and therewith the CH protons, too) which both show a homonuclear correlation to a dd CH signal. In the HMBC, they differ from each other as the 2-OH shows a ^{3}J HMBC correlation to C-1 and the 4-OH to C-5, respectively.*
For the identification of the protection pattern, it can be sufficient to determine the number of d, dd, and ddd signals in the ^{1}H NMR spectrum. The two rows show all possible single-, double- and triple hydroxyl protections of the triol (symbolized by red circles) with the resulting signal multiplets assigned to the respective OH and CH positions. Only one pair of single- and one pair of double protections (within the grey squares) can not be unambiguously identified, but the determination of the HMBC correlation of the remaining unprotected 2-OH or 4-OH group is sufficient to complete the required spectral information.

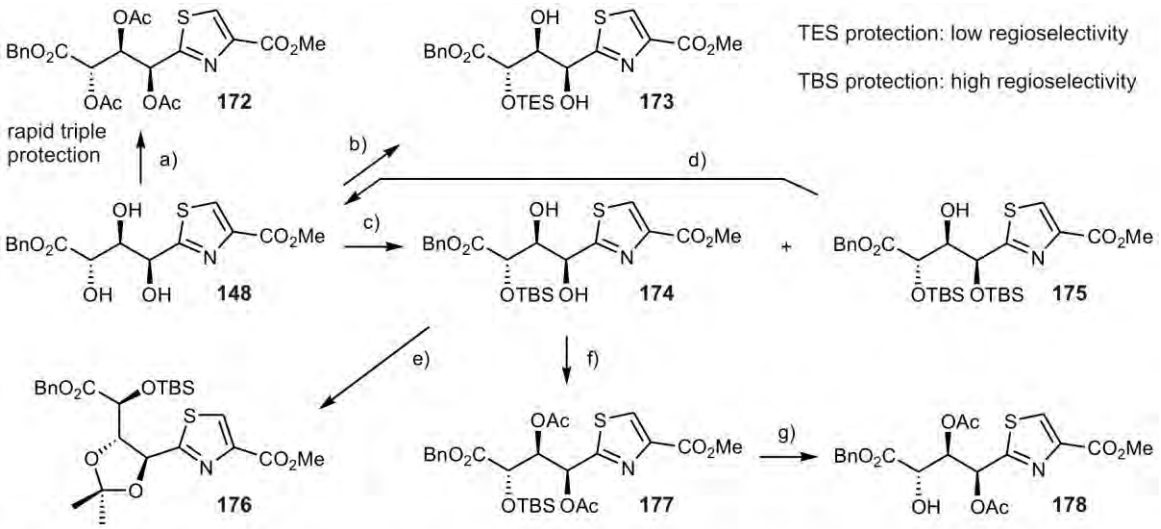

Scheme 4.13 Regioselective protection of the open chain* D-*arabino thiazole* 148*: reactions with monovalent protecting groups. *Selective protection of 4-OH, 2- and 4-OH, as well as 2- and 3-OH is possible.* Reagents and conditions: a) Ac_2O (1.3 eq), DMAP (cat.), Pyr_{abs}, 0 °C to RT, 15 h, 14% plus further di- and monoprotected species; b) TESCl (1.5 eq), imidazole (1.5 eq), DMF_{abs}, 0 °C to RT, 15 h, 16% plus further monoprotected species; c) TBSCl (1.2 eq), imidazole (1.2 eq), DMF_{abs}, 0 °C to RT, 24 h, 82% of **174** and 13% of **175**; d) H_2SiF_6 (1.66 M in H_2O, 1.0 eq), CH_3CN, 83%; e) DMP/DMF 1.7:1, *p*TosOH x H_2O (cat.), RT to 50 °C, 23 h; f) Ac_2O (2.5 eq), DMAP (cat.), Pyr_{abs}, 0 °C, 1.5 h, 85%; g) H_2SiF_6 (1.66 M in H_2O, 3.0 eq), CH_3CN, 63%.

Table 4.11 *Regioselective protections of* **148** *as silyl ethers.*

entry	PG	reaction batch	conditions and duration	result	isolated yields[1)]
1	TES	0.22 mmol	TESCl (1.5 eq), imidazole (1.5 eq), DMF_{abs}, 0 °C→RT, 15 h	unselective silylation	14% **173** 20% **148**[2)]
2	TBS	0.15 mmol	TBSCl (1.1→2.2 eq), imidazole (2.2→3.3 eq), DMF_{abs}, 0 °C→RT, 26→14 h	selective silylation 4-OH→2-OH	48% **174** 40% **175**
3	TBS	1.74 mmol	TBSCl (1.2 eq), imidazole (1.2 eq), DMF_{abs}, 0 °C→RT, 24 h	selective silylation 4-OH→2-OH	82% **174** 13% **175**
4	TBS	9.77 mmol	TBSCl (1.2 eq), imidazole (1.2 eq), DMF, 0 °C→RT, 18 h	selective silylation 4-OH→2-OH	74% **174** 9.6% **175** 16% **148**[2)]

1) isolated yields after flash chromatographic purification; 2) isolated yield after precipitation.

The remarkable selectivity of the protection at position 4 could be further utilized in order to obtain the single silylated compound **174** in 82% yield (table 4.11, entry 3). The procedure can be carried out on a multigram scale, and further optimization studies showed that the use of "peptide grade" instead of absolute DMF is also possible, and residual amounts of educt are reisolated from the crude product by precipitation (table 4.11, entry 4). If the double silylated

product **175** (which is still obtained in small amounts) is not needed it can be recyclized by treatment with H_2SiF_6 which allows to reisolate the triol **148** in 83% yield (d). It was also investigated whether the silyl group at position 2 can be cleaved selectively, but these attempts always resulted in the exclusive isolation of the fully deprotected compound. The remaining 2,3-diol of **174** is readily protected as an acetonide (**176**) or with acetate groups (**177**), and in the latter case the 4-hydroxyl group was selectively deprotected without considerable extent of acyl migration, yielding the alcohol **178**.

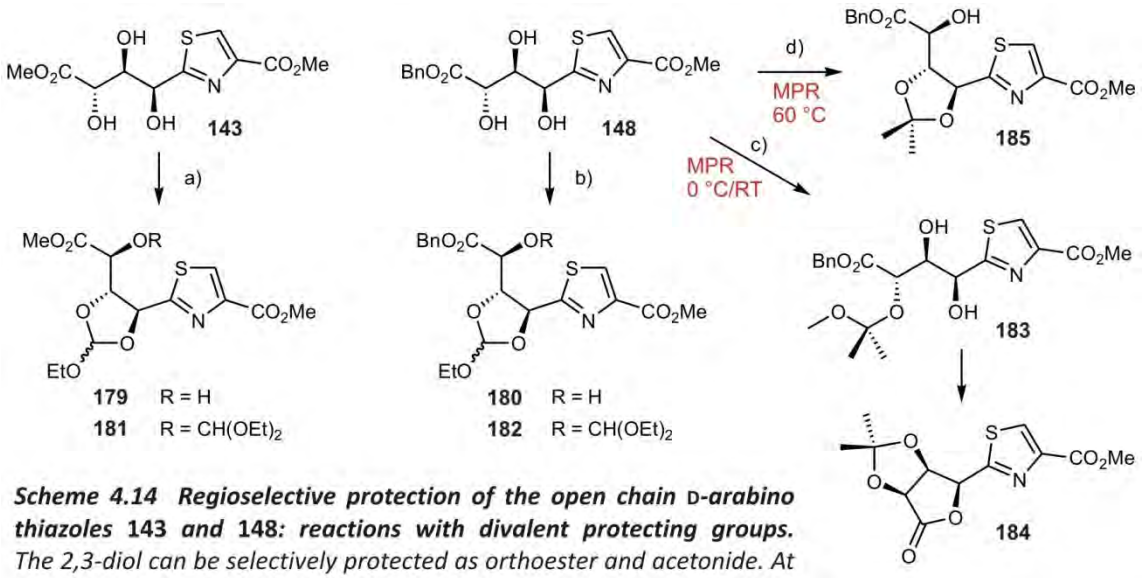

Scheme 4.14 Regioselective protection of the open chain D-arabino thiazoles* 143 *and* 148*: reactions with divalent protecting groups. *The 2,3-diol can be selectively protected as orthoester and acetonide. At low temperature, the reagent MPR used for acetonide formation attacks exclusively the 4-OH group, yielding the 4-MOP protected diol* **183**. Reagents and conditions: a) $HC(OEt)_3$ (bulk), *p*TosOH x H_2O (cat.), RT, 16 h, 83% of **179** and 5.5% of **181** (each 65:35 mixture of epimers); b) $HC(OEt)_3$ (bulk), *p*TosOH x H_2O (cat.), RT, 1.5 h, 61% of **180** and 39% of **182** (each 55:45 mixture of epimers); c) MPR/DMF 1:1, CSA (cat.), 0 °C to RT, 25 h, 33% of **183** and 18% of **184**; d) MPR/DMF 2:1, CSA (cat.), 60 °C, 12 h, 81% of **185** and 14% of **184**.

Subsequent experiments were aimed at the investigation of the reactivity towards diol protecting groups. The protection pattern of **178** turned out to be more easily accessible in only one synthetic step by attachment of an ethyl orthoester (scheme 4.14), and this reaction was performed with the methyl ester **143** as well as with the benzyl ester **148**. In addition to the alcohols **179** and **180** which are obtained in good yields, the fully protected compounds **181** and **182** are also isolated in varying amounts, presumably according to the amount of acid used.

Attempts to install an acetonide protection group in the triol **148** furnished different products according to the reaction temperature (scheme 4.14, conditions c and d). The reagents DMP and MPR are among the most used for this purpose, and the former is known to yield rather thermodynamic products while the latter rather furnishes kinetically controlled acetonides.[407] Interestingly, the use of DMP under different conditions was not successful in the case of **148** as

low conversion and several products were observed. With MPR as the reagent, in contrast, distinctive products could be isolated, but the outcome of the reaction turned out to be highly temperature dependent. At 0 °C and RT, the reagent selectively reacted with the hydroxyl group at position 4 (analogously to the TBS protection), leading to the 4-MOP protected compound **183**. In fact, the 3,4-acetonide was closed to small extent but apparently this instantly triggers a nucleophilic attack of the hydroxyl at position 2, which furnishes the lactone **184** as second product. At 60 °C, low amounts of the lactone **184** are also isolated but the reaction proceeds as in the case of the orthoester formations, yielding the 2,3-acetonide **185** as main product in 81% yield. Consequently, the hydroxyl group at position 4 exhibits the highest nucleophilicity under kinetic conditions, while the hydroxyl at position 2 attacks most readily under thermodynamic control. In principle, the orthoester and acetonide formation can also be initiated by the hydroxyl nucleophile at position 3, but this is less plausible as the nucleophilicity is increased at position 2 because of the α-position to the thiazole. A viable explanation of this behavior is yet to be made, but from the perspective of possible future syntheses where the triol **148** has to be incorporated into complex (depsi)peptidic networks this control of the nucleophilicity by temperature variation may allow to perform coupling reactions without the need of hydroxyl protecting groups.

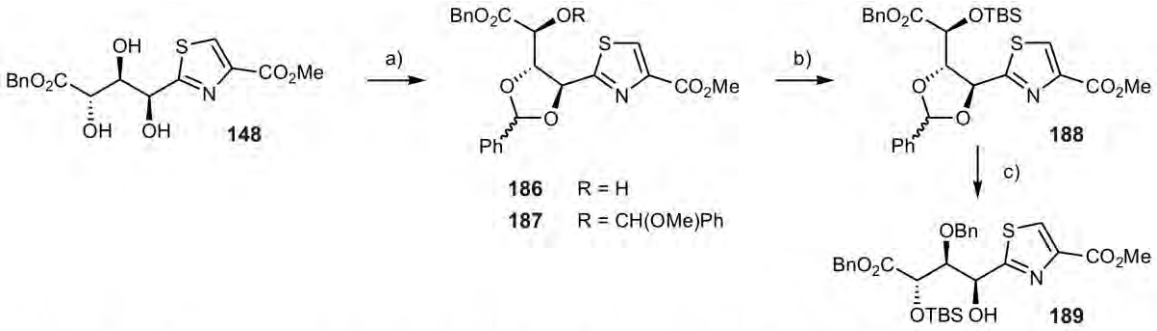

Scheme 4.15 Regioselective protection of the open chain* D-*arabino thiazole* 148*: selective protection of the 3,4-diol by regioselective cleavage of a benzylidene acetal. *With* **189** *the reaction sequence furnishes a starting substrate for selective* N/O*-exchange reactions at C-2 in order to obtain thiazole peptides.* Reagents and conditions: a) $PhCH(OMe)_2$/DMF 1:1, CSA (cat.), 60 °C, 50 h, 68% of **186** and 25% of **187**; b) TBSCl (1.5 eq), imidazole (1.5 eq), DMF_{abs}, 0 °C to 50 °C, 22 h, 72% of **188** plus 17% of starting material reisolated; c) BH_3 x SMe_2 (2.0 eq), BF_3 x OEt_2 (2.0 eq), $CH_2Cl_{2\ abs}$, 0 °C to RT, 3 h, 27% of **189** plus 10% of starting material reisolated.

When treated with benzaldehyde dimethylacetal at 50 °C, a selective protection of the 2,3-diol as benzylidene acetal **186** also occurred, with the fully protected compound **187** isolated as byproduct (scheme 4.15). This is remarkable as 1,2,3-diols are normally protected as six-membered acetals under these conditions.[407] The use of etheric HBF_4 instead of CSA as catalyst,

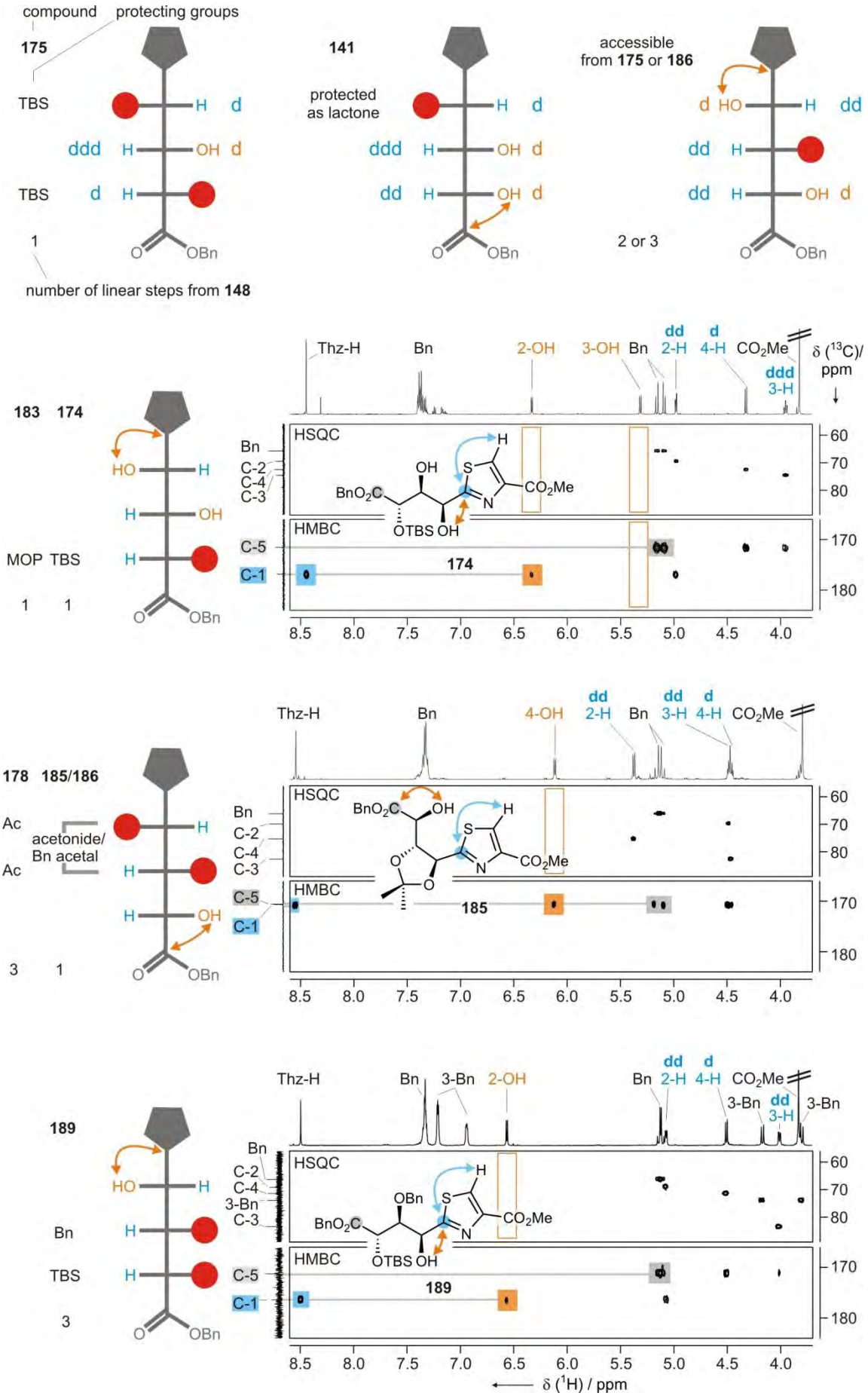
compound
protecting groups
175
TBS
ddd
TBS
1
number of linear steps from 148
141
protected as lactone
accessible from 175 or 186
2 or 3
183 174
MOP TBS
1 1
178 185/186
Ac
Ac
acetonide/ Bn acetal
3 1
189
Bn
TBS
3
Thz-H
Bn
2-OH
3-OH
2-H
4-H
CO2Me
3-H
δ (13C)/ ppm
HSQC
HMBC
C-5
C-1
174
4-OH
185
3-Bn
189
8.5 8.0 7.5 7.0 6.5 6.0 5.5 5.0 4.5 4.0
δ (1H) / ppm

which promotes formation of 1,3-diols,[411] effected no conversion. However, the selective formation of the 2,3-benzylidene acetal could be utilized for the synthesis of a 3,4-protected compound by selective cleavage of one of the two acetal C-O bonds (scheme 4.15). Which of these bonds is cleaved is usually dependent on steric and electronic factors, and in many cases the less sterically hindered alcohol is released.[412] Therefore, the hydroxyl function at position 4 was protected with a sterically demanding TBS group (**188**) and the acetal was subsequently treated with BH_3 and BF_3 to effect C-O bond cleavage.[413] In fact, one single product was obtained, with the hydroxyl at position 2 being released and the remaining benzyl group located at position 3 only (**189**). The low yield of this step apparently must be ascribed to partial decomposition as, apart from the desired alcohol **189**, only polar species were identified which could not be purified and characterized. Therefore, this transformation has yet to be optimized by testing different reaction conditions, which may be rewarding as this synthetic pathway is the only one found so far that provides a D-arabino configured thiazole polyol containing the hydroxyl group at position 2(α) as the only unprotected functionality. Thus, **189** exhibits a promising substrate for selective *O*,*N*-exchange reactions which, if successful, lead to thiazole dipeptides as present in the nocathiacines and thiazomycins (section 4.4.8).

Figure 4.17 connects the described results to figure 4.16 by giving a summary of protection group patterns which have been made accessible starting from the thiazole triol **148**. Except for the single protection at position 3, all variants were synthesized (the missing should be accessible in two steps from **175** or by regioselective cleavage of the acetal in **186**). For three differenty protected substrates (**174**, **185** and **189**) sections of the HSQC and HMBC spectra are shown which allowed to identify the signals of the remaining unprotected hydroxyl protons and their position in the chain.

Figure 4.17 (on the left) Synthesized D-arabino thiazole protection patterns. *As introduced in figure 4.16, the molecular scaffold is depicted in a* Fischer *projection. For every protection pattern except the triple protections, the obtained compounds are listed with the respective protecting groups and the number of linear steps that are required for the synthesis starting from the unprotected triol* **148**. *The lower part of the figure also shows sections of the HSQC and HMBC spectra for three examples, together with the respective one-dimensional ^{1}H and ^{13}C NMR projections (DMSO-d_6, 500 MHz (***174**: *600 MHz), 300 K). The orange squares indicate the absence of heteronuclear couplings which in the HSQC allow to identify a proton as being bound to carbon or to a heteroatom, and the OH protons at position 3 stand out by the lack of a strong $^{3}J_{C\text{-}H}$ coupling to C-1 as well as to C-5. The type and number of CH multiplets (d, dd, ddd; written next to the respective positions) are characteristic for every protection pattern, but they can not indicate whether a single unprotected hydroxyl is located at position 2 or 4 (see also figure 4.16), as it is the case for compounds* **185** *and* **189**. *The missing information is provided by the HMBC $^{3}J_{C\text{-}H}$ couplings to the quarternary carbons C-1 and C-5. As the remaining OH proton in* **185** *shows a cross peak at the same carbon chemical shift as the CH_2 protons of the benzyl ester, the respective carbon is identified as C-5, and consequently it is corresponding to the 4-OH. In contrast, the OH proton in* **189** *and the thiazole proton couple with the same carbon nucleus, which is only compatible with an unprotected 2-OH.*

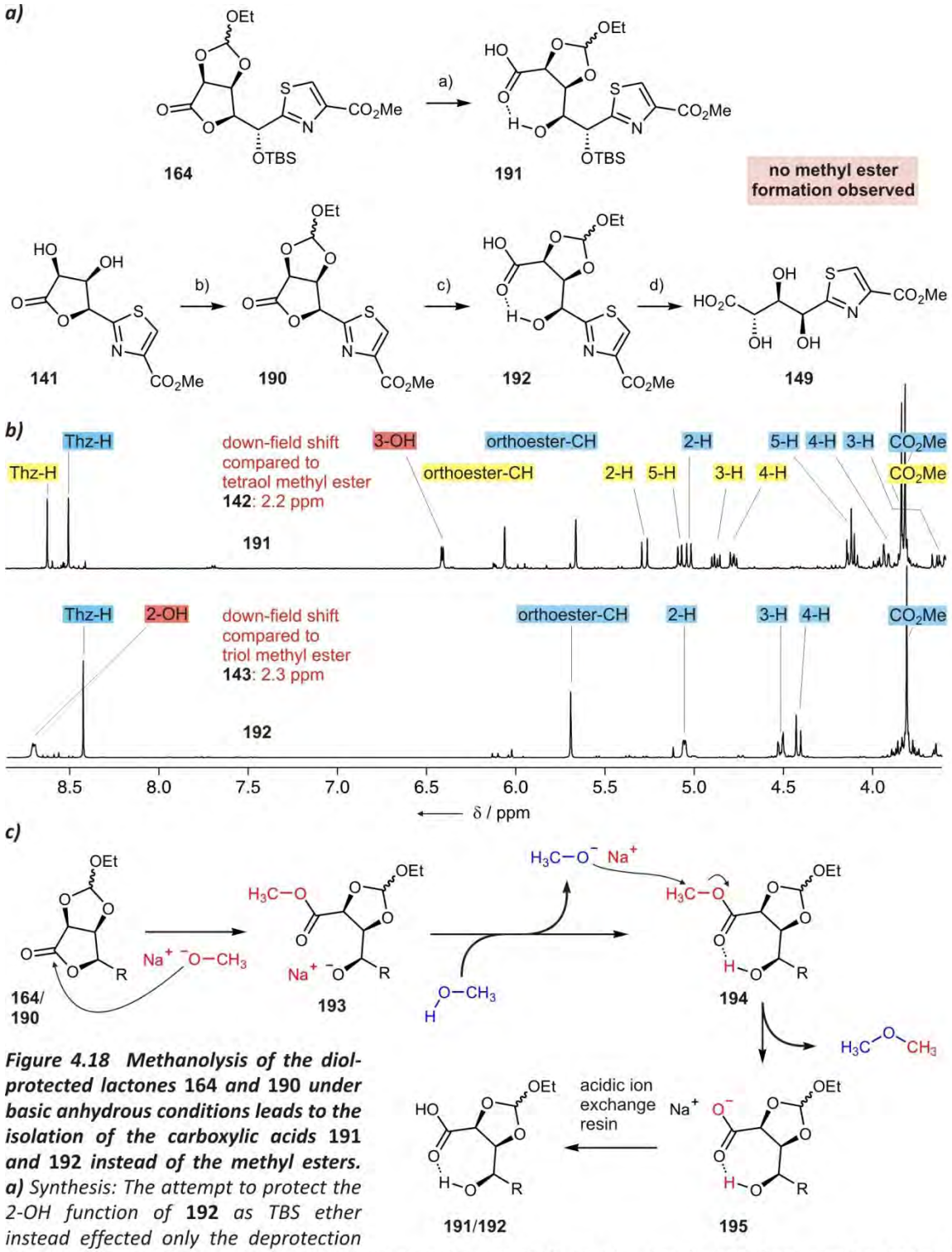

Figure 4.18 Methanolysis of the diol-protected lactones* 164 *and* 190 *under basic anhydrous conditions leads to the isolation of the carboxylic acids* 191 *and* 192 *instead of the methyl esters. ***a)*** *Synthesis: The attempt to protect the 2-OH function of* **192** *as TBS ether instead effected only the deprotection of the diol, leading to the trihydroxy carboxylic acid* **149** *which already had been synthesized via another pathway (scheme 4.12).* ***b)*** *Section of the ^{1}H NMR spectra (DMSO-d$_6$, 300 MHz, 300 K) of the* **191/164** *mixture (top) and* **192** *(bottom). The signals are marked yellow (educt) and red (product), respectively. The OH proton signals (marked in red) are down-field shifted to similar extent in comparison to the respective methyl esters with all OH positions deprotected. This suggests a comparable strength of the intramolecular hydrogen bond in both substrates.* ***c)*** *The formation of the carboxylic acids can be explained by the shown mechanism of the cleavage of the initially formed methyl ester* **194**. Reagents and conditions: a) NaOMe (0.3 eq), $MeOH_{abs}$, 0 °C to RT, 23 h, **191/164** 53:47; b) $HC(OEt)_3$ (bulk), *p*TosOH x H_2O (cat.), RT, 18 h, quantitative (12:1 mixture of epimers); c) NaOMe (0.3 eq), $MeOH_{abs}$, 0 °C to RT, 5 h; d) TBSCl (1.0 eq), imidazole (1.0 eq), DMF_{abs}, 0 °C to RT, 15 h. The yields of compounds **191**, **192** and **149** could not be determined as the highly polar compounds are difficult to purify.

4.4.5.3 Lactone opening of protected substrates

As attempts to open fully protected D-gluco configured lactones under acidic conditions (table 4.10) had not been successful yet, basic conditions were also investigated for the orthoester/TBS protected substrate **164**. As the selective protection of the hydroxyl groups at position 3 and 4 hitherto had only been achieved by the synthesis of **189**, with a low yield in the last step (scheme 4.15), the lactone diol **141** was protected as orthoester, affording **190** as D-arabino analog of the test substrate **164** (figure 4.18a). If the lactones can be opened under conservation of the protecting groups, open-chain compounds with the 2-OH (D-arabino) and 3-OH (D-gluco) position selectively unprotected are available.

When both lactones were treated with NaOMe in $MeOH_{abs}$ (0 °C to RT), reaction control by TLC showed that highly polar products were obtained exclusively. In fact, the lactone was opened in both cases without deprotection of the orthoester and the TBS group, but instead of the methyl esters the carboxylic acids **191** and **192** were isolated (figure 4.18a). Due to their high polarity, the compounds could not be purified by extraction or column chromatography so that only the raw products (obtained after neutralization of the reaction solution with acidic ion exchange resin and evaporation of the MeOH) were analyzed.

Figure 4.18b shows sections of the assigned ^{1}H NMR spectra of **191** (top) and **192** (bottom). Also in this reaction the D-gluco configured lactone proved more stable than the D-arabino analog. While 5 h reaction time are sufficient to furnish a < 95% opening of the lactone in **190**, only 53% yield is obtained in the case of the D-gluco configured lactone in **164** after 23 h under identical conditions (signal assignments are yellow (educt) and blue (product), respectively). The OH proton signals (highlighted in red) appear at down-field shifts (3-OH of **191**: 6.41 ppm, 2-OH of **192**: 8.60 ppm), which exhibits a considerable difference (more than 2 ppm) to the shifts which were observed for the other open-chain compounds synthesized within the scope of this work. Such down-field shifts can be ascribed to hydrogen bonding. In both cases, a seven-membered ring has to be formed in order to enable the intramolecular hydrogen bond, as shown in figure 4.18a, and with a single sp^2 bond (C=O) it exhibits a favorable chair geometry. As similar down-field shifts are observed for both substrates in comparison to the open-chain methyl esters **143** and **142**, the strength of the hydrogen bonds can be assumed as comparable.

The presence of the hydrogen bond can also give an explanation for the unprecedented formation of the carboxylic acid products instead of the methyl esters. Figure 4.18c shows the proposed mechanism which starts with the nucleophilic attack of a methanolate ion (red) at the lacton carboxyl function of **164** or **190**. This results in the methylester **193** which, after

protonation of the alcoholate by methanol (blue), should give **194** which corresponds to the expected reaction product. The inclination of the substrate to adopt the shown seven-membered ring conformation with a stable hydrogen bond promotes this protonation step. As electron density is subtracted from the methyl ester functionality, the methyl carbon is easily attacked by nucleophiles. By attack of a methanolate ion, a substitution at the methyl carbon occurs, yielding the sodium carboxylate **195** and $(CH_3)_2O$ as volatile byproduct. An analogous substitution reaction is also part of a known deprotection method of methyl esters which employs iodide nucleophiles and allows to selectively deprotect methyl- in presence of other esters.[414] In principle, the involvement of adventitious moisture is also possible as hydroxide ions can open the lactone or deprotect the methyl ester **194** instead of the (well solvated) methanolate ion.

Table 4.12 *Attempted alkylations of* **191**.

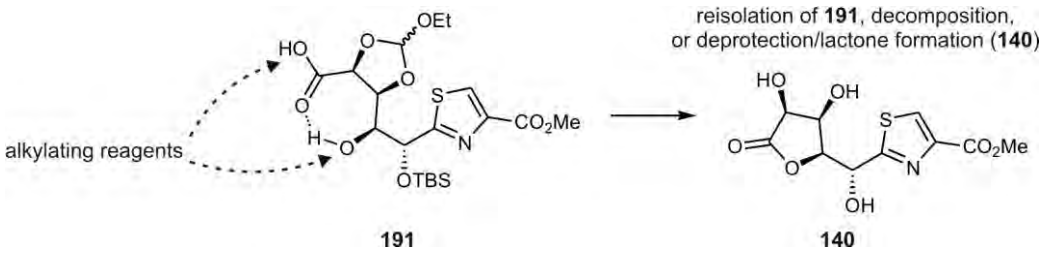

entry	conditions and duration	result
1	BnBr (2.0 eq), NaH (2.5 eq), THF_{abs}, 0 °C→RT, 6 h	educt reisolated
2	BnBr (2.0 eq), NaH (2.5 eq), THF_{abs}/DMF_{abs} 2:1, RT, 6 h	educt reisolated, decomposition
3	MeI (10 eq), acetone, RT, 2 d	formation of **140**
4	MeI (10 eq), DMF, RT, 2 d	formation of **140**, decomposition
5	EtI (10 eq), acetone, RT, 24 h	formation of **140**
6	EtI (20 eq), NEt_3 (cat.), THF_{abs}, RT, 2 d	educt reisolated
7	AllBr (10 eq), acetone, RT, 24 h	formation of **140**
8	AllBr (10 eq), NEt_3 (cat.), THF_{abs}, RT, 2 d	educt reisolated
9	AllBr (10 eq), NEt_3 (cat.), THF_{abs}/NMO 1:1, RT, 2 d	educt reisolated

Upon treatment of the reaction mixture with acidic ion exchange resin, the carboxylate **195** can be protonated to yield the carboxylic acid **191**/**192**. However, this functionality is expected to have a low pK_a due to the hydrogen bonding, and it is also possible that the isolated compounds correspond to the sodium salts equivalent to **195**. No carboxylic acid proton signal could be identified in the NMR spectra, but this can also be effected by extensive line broadening.

In order to be utilizable for synthesis, the obtained lactone opening products must be converted to less polar compounds which can be purified and which are compatible also with rather unpolar reaction media. Consequently, the carboxyl function must be protected, which should decrease the polarity of the substrate and lead to a weaker hydrogen bond. Alternatively, the protection of the hydroxyl function would remove the hydrogen bond and thus furnish a more reactive carboxyl function. Therefore, in first experiments it was attempted to protect the hydroxyl function of **192** as TBS ether. The applied *Corey* conditions, however, did not afford silylation but instead the cleavage of the orthoester, and the carboxylic acid **149** was isolated (figure 4.18a, condition d) which already had been obtained by cleavage of the benzyl ester of **148** (scheme 4.12). Several attempts were also made to protect the carboxyl or the hydroxyl function of **191**, but the proposed hydrogen bond proved to be exceptionally stable as none of the functional groups could be alkylated under various conditions (table 4.12). The only transformation which occurred was the cleavage of the TBS groups and the orthester, concomitant with closure of the lactone ring which yielded **140**.

4.4.6 Chain tailoring experiments

Various experiments were also performed in order to investigate possibilities of selective C-C cleaving reactions that lead to shortened sugar chains. In the light of the future synthesis of thiazole units embedded in natural products, the ability to vary the length of the polyol chain further extends the synthetic utility of these compounds as for example tubuvaline or the thiazole depsipeptide present in the hectochlorin macrocycle become accessible (figure 4.14). The results of experiments aimed at tailoring the sugar chains of the unprotected thiazole lactones **140** and **141** with $NaIO_4$ are summarized in scheme 4.16.

A typical procedure applied for sugar compounds is the treatment with 1.0 eq of $NaIO_4$ in aqueous phosphate buffer solution, as it is successfully applied for the cleavage of the C1-C2 bond in γ-glucuronolactone (scheme 4.6).[378] When the lactones **140** and **141** were subjected to

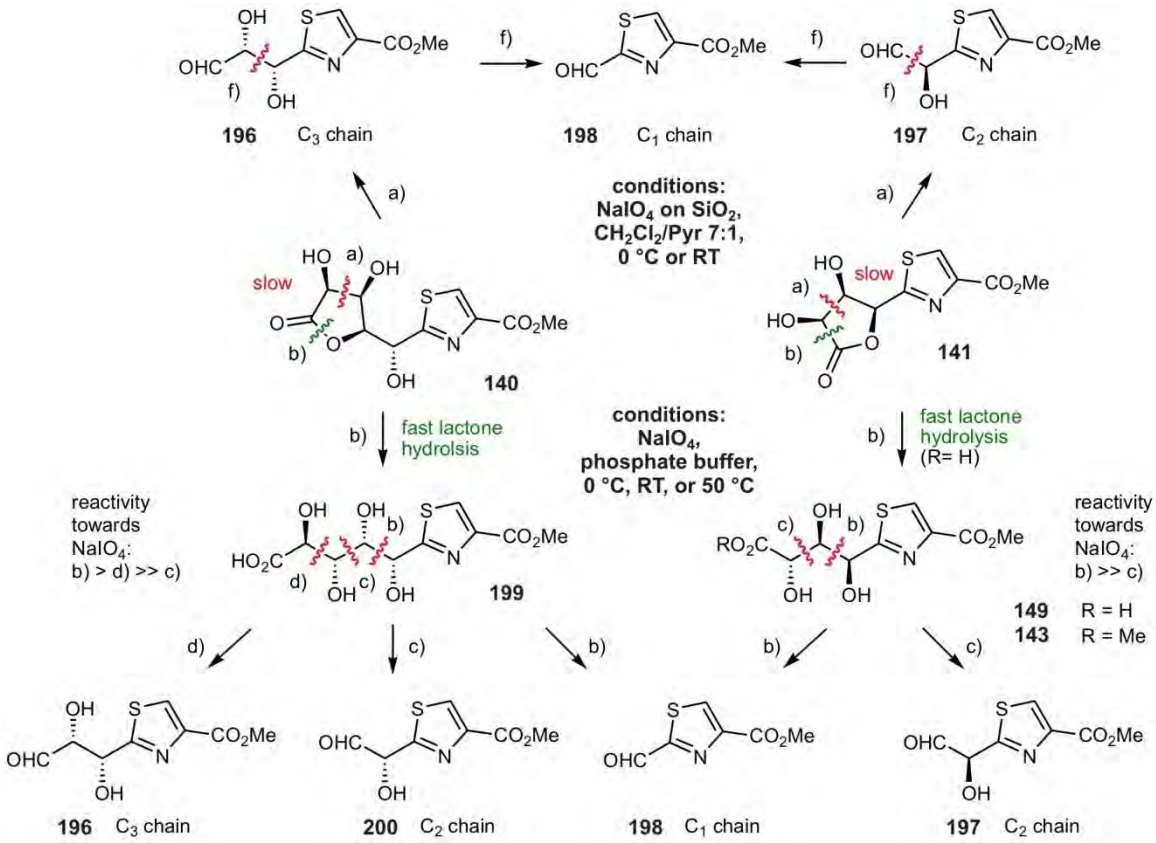

Scheme 4.16 Periodate cleavage reactions of unprotected thiazole polyols. *The use of $NaIO_4$ under anhydrous conditions (adsorbed on silica gel, top) as well as in buffered aqueous solution (Na_2HPO_4 buffer) led to the formation of the C1 thiazole* **198** *as main product by cleavage of the C2-C3 bond. This is effected by a further C-C bond clevage of the initially formed compounds* **196** *and* **197**, *respectively (a, f). Under aqueous conditions, the fast hydrolysis of the lactones (b) outrules the diol cleavage (a) which provides the polyol carboxylic acids* **199** *and* **149**, *and The high nucleaophilicity of the 2-OH functions is presumably responsible for the formation of* **198** *as main product.*

identical reaction conditions, however, the expected C_3 and C_2 chain products **196** and **197** were not obtained at all, or only minor amounts were formed (scheme 4.16). Instead, the C_1 thiazole **198** was obtained as main aldehyde product in most cases, which suggests an opening of the lactones that occurs faster than the reaction with $NaIO_4$, yielding the linear polyol carboxylic acids **199** and **149** in which the 3-OH and 2-OH, respectively, is not protected any more by the carboxyl function. In fact, these compounds were identified in most cases by NMR and mass spectra as the periodate cleavage proceeded at slow rates, and only at 50 °C a complete consumption was observed after several hours. The carboxylic acid **149** was easily identified as it had also been synthesized by another reaction pathway (scheme 4.12). An analogous reaction has already been observed by *P. Tremmel* in the case of γ-gulonuronolactone where lactone hydrolysis led to the release of the 3-OH function followed by a cleavage of the C3-C4 instead of the C2-C3 bond.[369] The lactone opening of **141** leads to the triol **149** which can be attacked at the 2-OH/3-OH (b) or the 3-OH/4-OH diol (c). The almost exclusive formation of

the C_1 thiazole **198** indicates that the reaction of the 2-OH/3-OH diol occurs more readily which may be explained by a stronger nucleophilicity of the 2-OH function. This result fits the observations made in all diol protections where the 1-OH/2-OH exhibited the highest reactivity (schemes 4.14 and 4.15). Similar results were also observed when the methyl ester **143** (R = Me) was subjected to the same reaction conditions. In the case of **199**, the product formed by hydrolysis of the lactone **140** three C-C bonds can be cleaved, and the C2-C3 bond also proved most reactive. While only traces of the C_2 thiazole **200** were observed, a partial (<30%) cleavage of the C4-C5 bond, yielding the C_3 chain of **196** occurred (d) when the reaction was run at 0 °C.

Because of these selectivity problems, the use of silica-supported $NaIO_4$ appeared as a promising alternative among the several protocols known for diol cleavage,[415] because it exhibits a more moderate reactivity and allows the use of a variety of organic solvents, which facilitates workup and the separation from inorganic salts.[416, 417] Furthermore, it is compatible with anhydrous conditions so that the formation of aldehyde hydrates is suppressed. **140** and **141** are not soluble in pure CH_2Cl_2 which had been proven as the best solvent for this reaction, but instead a 7:1 mixture of CH_2Cl_2/Pyr could be used. However, although lactone hydrolysis is not possible under these conditions, all performed reactions also yielded the C_1 thiazole **198** as main cleavage product. Even after only 15 min at 0 °C it is isolated as main product besides unreacted starting material. As shown in scheme 4.16, the C_2 and C_3 thiazoles **197** and **198** are presumably formed by (desired) cleavage of the lactone diols and subsequent decomposition of the 2-OH bound formyl ester. In the final step the C2-C3 bonds are cleaved by nucleophilic attack of the reactive 2-OH functions. The second step (f) occurs faster than (b) as also in the presence of equimolar amounts of $NaIO_4$ the C_2 and the C_3 species are, if all, only present in traces. The formation of **198** from **197** can be explained by reaction of the aldehyde function with the 2-OH bound periodate ion, and this reaction pathway possibly also occurs under aqueous conditions to some extent.

The conclusion which can be drawn from these experiments is that the protection of the reactive 2-OH function is a prerequisite for more selective C-C cleavage reactions. Preliminary tests with the 2-acyl protected thiazole lactone **161** were successful as the C_3 thiazole **153** was obtained under aqueous conditions by cleavage of the C4-C5 bond (scheme 4.17, a). This can either occur by cleavage of the lactone diol or by hydrolysis of the lactone to the carboxylic acid **201** which exhibits two possible cleavage sites (a and b). The fact that no C_2 thiazole species could be identified in the mass spectrum indicates that, as in the case of the fully deprotected tetraol **199**, the C3-C4 diol is much less inclined to form the diester with the iodate ion. Minor amounts of the C_1 thiazole **198**, however, were visible in the ^{1}H NMR spectrum which suggests that acyl

migration or deprotection takes place. Therefore, alternative protecting groups and anhydrous reaction conditions are to be investigated in order to optimize this reaction which affords a possible starting substrate for the synthesis of tubuvaline (figure 4.14).

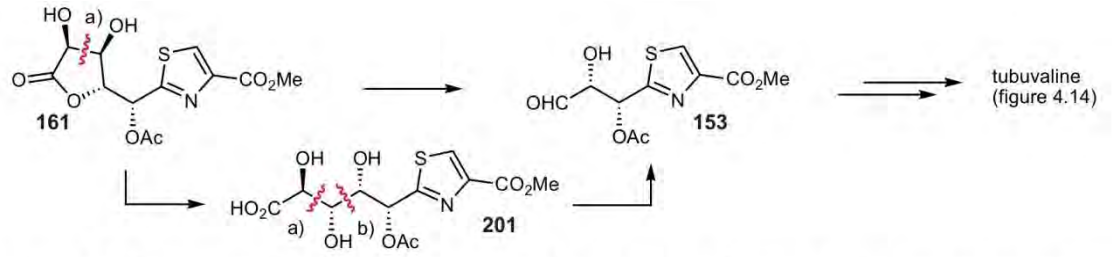

***Scheme 4.17 Regioselective C4-C5 bond cleavage of the 2-acylated thiazole* 161.** Reagents and conditions: $NaIO_4$ (1.0 eq), Na_2HPO_4 (aq., 0.05 N), 0 °C, 40 min.

As already shown in figure 4.14, the shortening of the sugar chains can in principle also be accomplished by ozonolysis of the thiazole butenolides **202** and **156** (scheme 4.18). Starting from the lactone diols **140** and **141**, several methods exist which allow to convert a diol to an olefin. For this purpose, the free diols must be converted to the corresponding thiocarbonates (**203** and **204**), orthoesters (**159** and **190**), or DMF acetals (**205** and **206**), which subsequently are activated in order to trigger the deoxygenation to the olefins. The thiocarbonates **203** and **204**, which are reqired as substrates for the classical *Corey-Winter* procedure[418] and variants of this protocol,[419-421] turned out to be unstable, which was dermined by carrying out the reaction in the NMR tube and monitoring by ^{1}H NMR experiments. The linear thiazole triol **143** could not be converted to thiocarbonates either (**207** or **208**, scheme 4.18, bottom).

Therefore, some of the alternative protocols were tested, and for this purpose the ortho-esters **159** and **160** as well as the DMF acetals **205** and **206** were prepared, which proceeded smoothly in all cases (conditions a-f, for the preparation of the orthoesters see also scheme 4.14). The orthoester can be treated with Ac_2O according to a protocol by *Ando et al.*[422] or with Tf_2O (protocol by *Yang et al.*)[423] in order to afford the olefin. For the DMF-acetal as substrate, a procedure employing Ac_2O has been developed by *Eastwood et al.*,[424] and MeI is used in the protocol by *Hanession et al.*[425].

However, none of these methods led to the formation of the desired butenolides **202** or **156**, and the results are summarized in table 4.13. While decomposition was observed in most reactions using the DMF-dimethylacetals as educts, the orthoesters proved exceptionally stable even under harsh conditions (for example, reflux in Ac_2O). To draw a conclusion from the experiments, the formation of a butenolide starting from a stable all-*cis* γ-lactone apparently is energetically strongly disfavored, which is in accordance with the few comparable syntheses

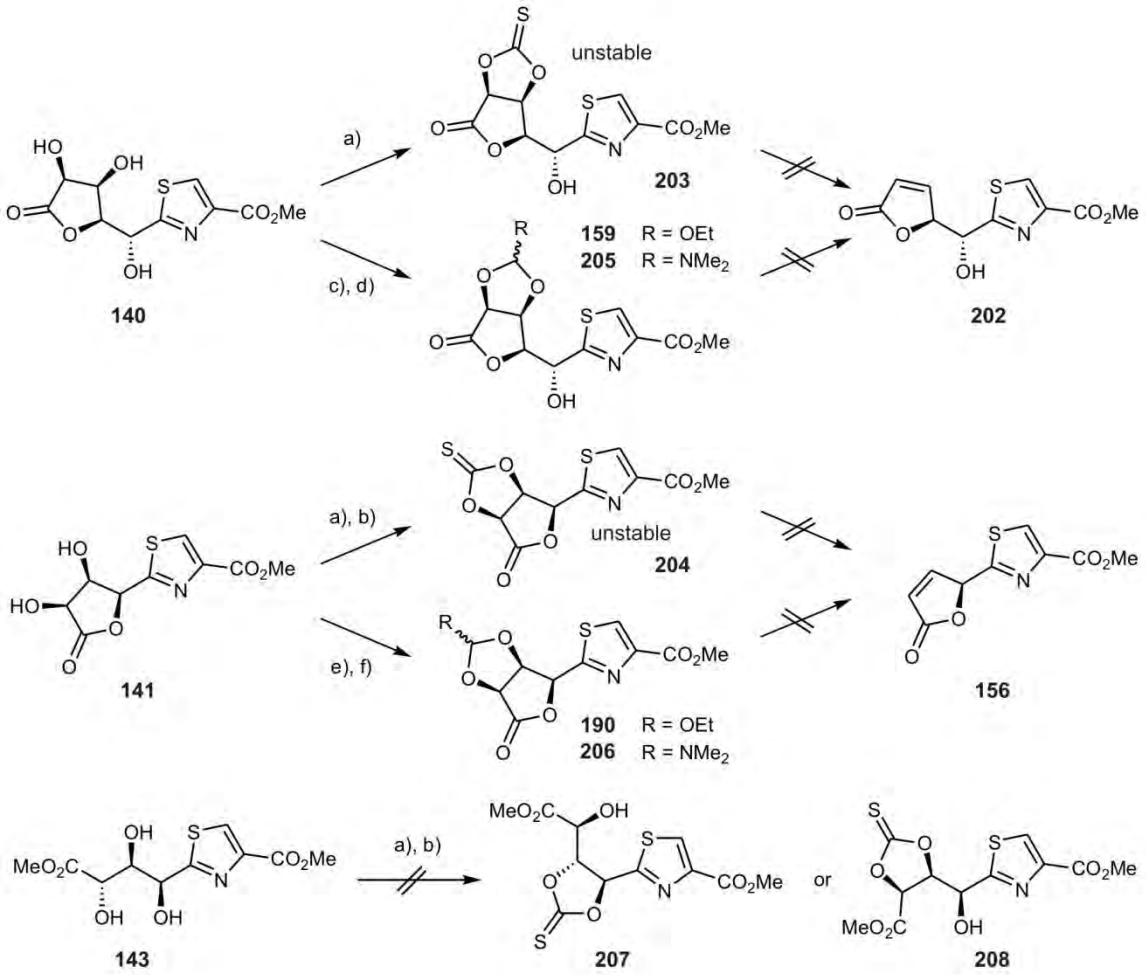

Scheme 4.18 Preparation of precursors for* Corey-Winter *olefin synthesis. *The attempts to obtain the olefins* **202** *and* **156** *are listed in table 4.13.* Reagents and conditions: a) 1,1'-thiocarbonyl diimidazole (1.3 eq), Pyr_{abs}, RT to 60 °C, 3 h; b) thiophosgene (1.2 eq), DMAP (2.4 eq), $CH_2Cl_{2\ abs}$ or DCM_{abs}/Pyr_{abs} 10:1, 0 °C to RT, 2.5 to 15 h; c) $HC(OEt)_3$ (bulk), *p*TosOH x H_2O (cat.), RT, 41 h, 94% (**159**, 4:3 mixture of epimers), d) DMF dimethylacetal (20 eq), CH_2Cl_2, RT, 25 min (**205**, raw product was directly used for the next step); e) $HC(OEt)_3$ (bulk), *p*TosOH x H_2O (cat.), RT, 18 h, quantitative (**190**, 12:1 mixture of epimers); f) DMF-dimethylacetal (20 eq), $CH_2Cl_{2\ abs}$, RT, 5 min (**206**, raw product was directly used for the next step).

described in the literature.[426-428] However, these mostly result in a C-C double bond which is still oxygen functionalized. Further methods which could not be tested within the scope of this thesis differ by utilizing no cyclic diol activation groups,[429-431] but it is questionable whether they will be successful as all experimental conditions employed so far did not even yield traces of the desired butenolides. Therefore, focusing on periodate cleavage reactions with adequately protected substrates exhibits the more promising option to obtain thiazole depsipeptides with shortened polyol chains.

Table 4.13 *Attempted olefination reactions of* **140***,* **141***, and* **143**. *The reaction batches were between 0.14 and 0.19 mmolar.*

entry	substrate	procedure	conditions and duration	result
1	**203**/**204**	classical *Corey-Winter* olefination	$P(OMe)_3$, Tol, reflux,	**203** and **204** unstable (NMR experiments)
2	**159**	*Ando* olefination	Ac_2O (bulk), DIPEA (4.0 eq), reflux, 5 h	educt reisolated
3	**205**	*Eastwood* olefination *(Hanessian* variant)	MeI (40 eq), Tol_{abs}, RT→reflux, 2 h	decomposition
4	**190**	*Ando* olefination	Ac_2O (bulk), DIPEA (4.0 eq), reflux, 10 h	mainly educt reisolated[1)]
5	**190**	*Ando* olefination (*Yang* variant)	Tf_2O (2.0 eq), DIPEA (2.0 eq), Tol_{abs}, 0 °C→60 °C, 20 h	educt reisolated
6	**206**	*Eastwood* olefination *(Hanessian* variant)	MeI (40 eq), Tol_{abs}, RT→reflux, 1 h	decomposition
7	**206**	*Ando* olefination (*Yang* variant)	Tf_2O (2.0 eq), DIPEA (2.0 eq), Tol_{abs}, RT, 30 min	formation of lactone diol **141**

1) two new signal set was observed after workup in the ^{1}H NMR spectrum (11% and 20%) but no double bond formation had occurred.

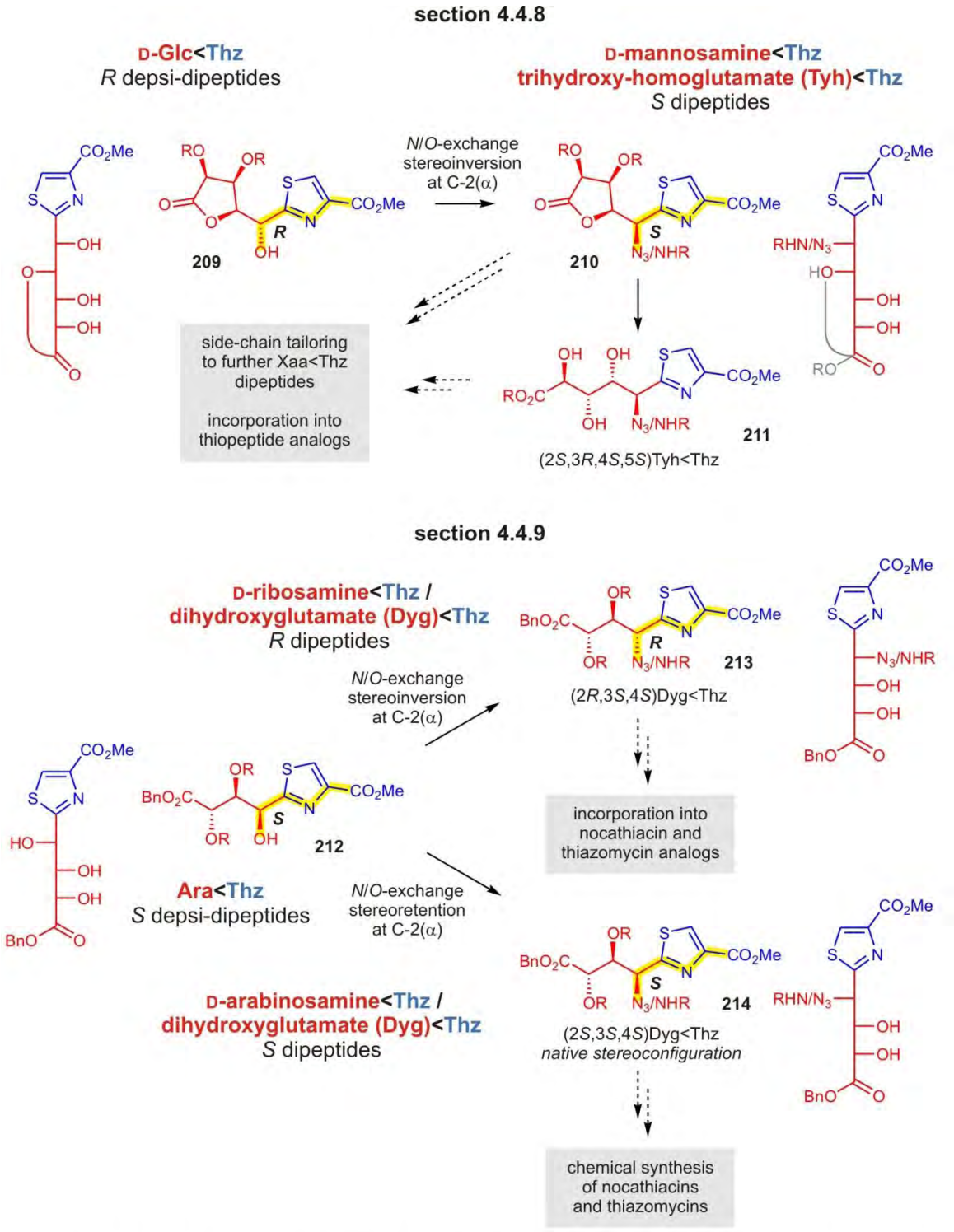

Figure 4.19 Interim summary and outlook: synthesis of thiazole dipeptides by N/O-exchange reactions. *As in figure 4.14, the sugar chains are shown in red and the thiazoles in blue, respectively. The synthesis of substrates with the 2(α) hydroxyl function selectively unprotected (described in the preceding sections) was the prerequisite for* N/O*-exchange experiments which are discussed in the following section 4.4.8 (*D*-gluco side chains) and 4.4.9 (*D*-arabino side chains), respectively. If the introduction of the nitrogen functionality occurs with inversion of the stereocenter,* R *as well as* S *configured thiazole dipeptides are accessible (***211***,* **213***). The retention of the α stereoconfiguration starting from* **212** *is another topic of interest as it furnishes the Dyg<Thz dipeptide core present in the nocathiacin and thiazomycin antibiotics with all three stereocenters in the native* S *configuration (***214***). R = H or protecting group.*

4.4.7 Interim summary and outlook: dipeptide targets

As described in the preceding sections, the thiazole sugar chains turned out to be challenging with respect to selective hydroxyl (de)protections, and considerable optimization work was required. As partially protected D-gluco as well as D-arabino configured polyols with the free 2(α)-OH could be obtained, studies concerning the synthesis of Xaa<Thz dipeptides by *O*/*N*-exchange at this positions were possible (figure 4.19). The following section 4.4.8 describes the attempts performed with Glc<Thz substrates (**209**). As in figure 4.12, all substrates are depicted in the *Fischer* projection which indicates the sugar nature of the polyol chain, as well as in a projection which emphasizes the (depsi)dipeptide character, with the course of the backbone highlighted in yellow. By an *N*/*O*-exchange with inversion of the α stereocenter, the nitrogen functionality with the desired *S* configuration (corresponding to the naturally found thiazole dipeptides) would be installed (**210**). As linear D-gluco configured polyols turned out to be difficult to obtain in acceptable yields, the *N*/*O*-exchange should be accomplished for the lactones. After the installation of the amine (which, as depicted, is masked as azide[366] or protected (R)) the mannosamine-configured lactone can be opened (**211**), furnishing a trihydroxy-homoglutamate (Tyh)<Thz dipeptide. The Tyh side chain is a C_1 extended homolog of the Dyg side chain present in the nocathiacin and thiazomycin antibiotics, and it exhibits more functionalities than all naturally occurring thiopeptide amino acid side chains, which makes it an attractive substrate for the synthesis of thiopeptide analogs where for example further structural motifs like glycosides and oligopeptides can be attached (grey box). In addition, the controlled tailoring of the side chain should be more controllable as the C2-C3 bond cannot be cleaved any more, as it was always the case for the unprotected polyols (scheme 4.16).

In contrast, the *N*/*O*-exchange with stereoinvestion at the 2(α) position of Ara<Thz substrates (**212**) yields ribosamine sugar chains with *R* configuration (**213**). As the sterocenters at C-4 and C-5 are both in the *S* configuration and therewith correspond to the native Dyg<Thz dipeptide core of the nocathiacins and thiazomycins, **213** resembles its α epimer. From the standpoint of a possible total synthesis of these thiopeptides, it is desirable to access the natural stereoconfiguration, but the option to investigate analogs with altered stereoconfiguration may lead to analogs with improved therapeutic profile and to more detailed insights into the modes of action. The impact of stereoconfiguration can be especially high in the case of Dyg<Thz which connects several parts of the antibiotic with each other.

Finally, the native (2*S*,3*S*,4*S*) configuration of Dyg<Thz could be accessible by introducing the amino function under stereoretention, leading to **214** with an arabinosamine sugar residue. All experiments aimed at the synthesis of these Dyg<Thz dipeptides are described in section 4.4.9.

4.4.8 Thiazole dipeptide synthesis with hexose sugar chain substrates

4.4.8.1 Experiments with D-gluco derivatives

The acetonide **157** with the 2-OH as the only unprotected functionality was examined as substrate for *Mitsunobu* type amination reactions (scheme 4.19),[432, 433] and in table 4.14 all applied experimental conditions are listed. Neither with phthalimide (entry 1) nor with zinc azide (entries 2-3)[434] as nucleophiles a conversion was observed, which apparently can be resoned by the limited space at the 2-OH position that hampers the attack of the bulky PPh_3 and DIAD reagents. The use of highly reactive HN_3 which had been successfully applied for sterically congested polyols[435] led to decomposition of the starting material (entry 4). In contrast, the hydroxyl activation as a sulfonate could be accomplished in good yields (scheme 4.19) using tosyl- (**215**) or mesyl chloride (**216**). Triflation was not successful as the initially formed triflate **217** was presumably subjected to elimination (see also scheme 4.21) and decomposition.

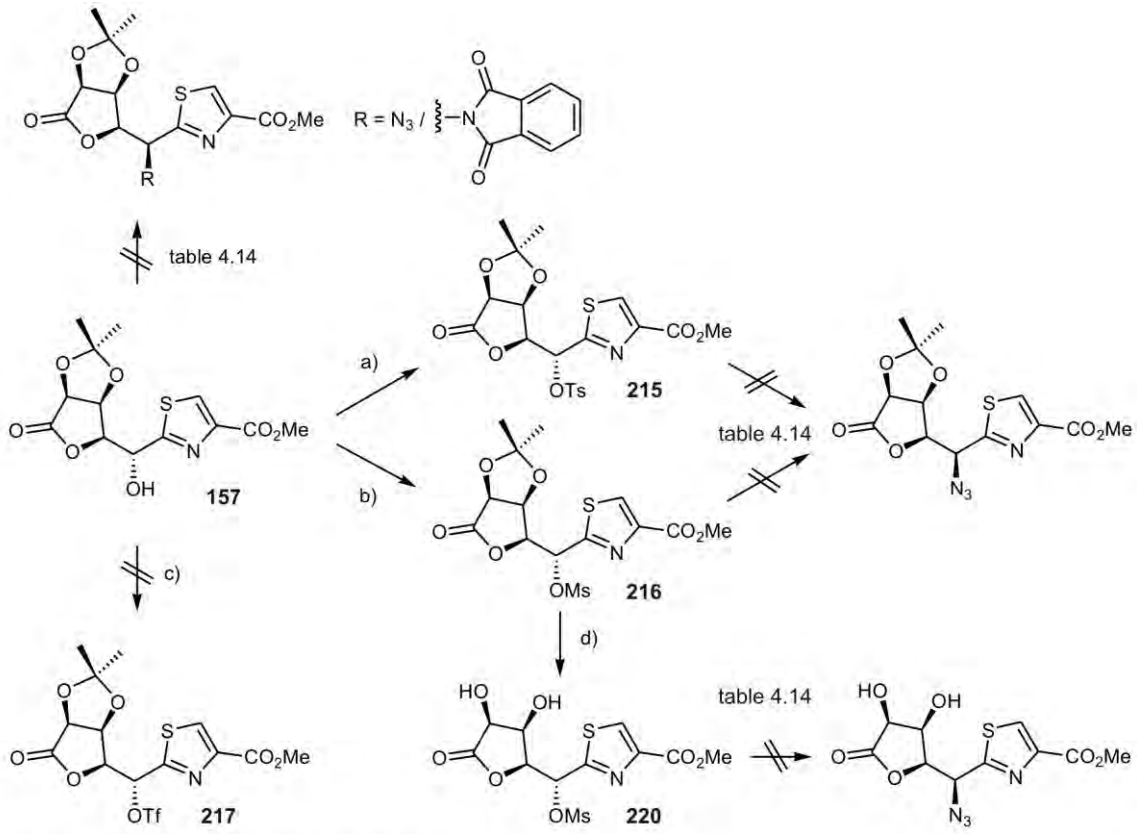

Scheme 4.19 Activation of the 2-OH function of* 157 *and* N/O*-exchange experiments. *All tested exchange reaction conditions are listed in table 4.13.* Reagents and conditions: a) TsCl (5.0 eq), DMAP (cat.), Pyr_{abs}, RT, 24 h, quantitative; b) MsCl (3.0 eq), DMAP (cat.), Pyr_{abs}, 0 °C to RT, 4 h, 84%; c) Tf_2O (2.0 eq), DMAP (cat.), Pyr_{abs}, 0 °C to RT, 3 h (decomposition); d) aq. HCl (1.0 M), THF, 40 °C, 24 h.

Table 4.14 *Attempted* N/O-*exchange reactions at the C-2 position of* **157** *(entries 1-4,* Mitsunobu *inversions) and* **215**/**216**/**220** *(entries 6-13, azidations of activated substrates). The mesylate* **216** *proved stable in DMSO at 80 °C, which is why the decomposition must arise from the presence of the azide (entry 5).*

entry	substrate	conditions and duration	result	isolated yields[1)]
1	**157**	DIAD (2.2 eq), PPh_3 (2.4 eq), phthalimide (1.2 eq), THF_{abs}, 0 °C to 40 °C, 18 h	no conversion	--
2	**157**	DIAD (2.0 eq), PPh_3 (2.0 eq), $Zn(N_3)_2$ x 2 Pyr (1.0 eq), Tol_{abs} 0 °C to 40 °C, 18 h	no conversion	--
3	**157**	DIAD (2.0 eq), PPh_3 (2.0 eq), $Zn(N_3)_2$ x 2 Pyr (1.0 eq), THF_{abs} 0 °C to 40 °C, 18 h	no conversion	--
4	**157**	DIAD (3.0 eq), PPh_3 (3.0 eq), HN_3 (3.0 M in Tol_{abs}, 3.0 eq), Tol_{abs}, 0 °C→RT, 1.5 h	decomposition	--
5	**216**	DMSO-d_6, 80 °C, 15 h	no decomposition	--
6	**215**	NaN_3 (2.0 eq), DMF, 50 to 80 °C °C, 15 h	no conversion	--
7	**215**	NaN_3 (2.0 eq), DMSO-d_6, 50 °C, 15 h	decomposition	--[2)]
8	**216**	NaN_3 (2.0 eq), DMF, 50→80 °C °C, 15 h	no conversion	--
9	**216**	NaN_3 (2.0 eq), DMSO-d_6, 50 °C, 15 h	decomposition	--[2)]
10	**216**	$Zn(N_3)_2$ x 2 Pyr (2.0 eq), DMSO-d_6, 80 °C, 45 h	hydrolysis to **218** and **219**	--[2)]
11	**216**	$Zn(N_3)_2$ x 2 Pyr (2.0 eq), DMF, 80 °C, 24 h	hydrolysis to **157**, **218**, and **219**	41% **157** (educt) 26% **218** 5.0% **219**
12	**216**	$Zn(N_3)_2$ x 2 Pyr (2.0→4.0 eq), DMF_{abs}, 80 °C, 48 h	no conversion, partial decomposition	--
13	**220**	NaN_3 (2.0 eq), DMF_{abs}, 40→70 °C, 48 h	decomposition	--

1) isolated yields after flash chromatographic purification; 2) the reaction was run in the NMR tube and monitored by ^{1}H NMR.

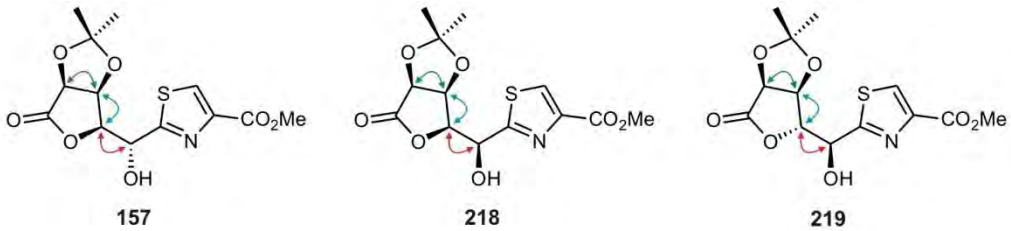

	157	218	219
2-H/3-H	3.0 Hz	6.6 Hz	2.0 Hz
3-H/4-H	3.6 Hz	3.5 Hz	< 1 Hz (not resolved)
4-H/5-H	5.2 Hz	5.2 Hz	5.7 Hz

Scheme 4.20 Scalar $^3J_{H/H}$ coupling constants ($CDCl_3$, 300 MHz, 300 K) of* 157 *(starting configuration) and of the hydrolysis products* 218 *and* 219 *(table 4.14, entries 10 and 11).

Various attempts to introduce the azide by substitution of the activated 2-OH function were made (using NaN_3 and zinc azide) but the desired *N*/*O*-exchange product could not be identified in any case (table 4.13, entries 6-13).[436] While the starting material could be reisolated in the case of DMF, the use of DMSO-d_6 (for monitoring of the reaction by NMR, entries 7, 9, and 10) effected decomposition which can be ascribed to the azide salts as the starting substrate **216** itself proved stable under the applied reaction conditions (entry 5). When zinc azide was used in combination with peptide grade DMF as solvent (which contains traces of H_2O) a partial hydrolysis of the mesylate was observed (entry 11). In addition to **157** with unaltered stereoconfiguraiton, a product was identified as the 2*S* alcohol **218** (scheme 4.20) by the altered 2-H/3-H scalar coupling constant compared to the 2*R* epimer **157**. In small amounts, a further epimerization product occurred which in addition exhibits an altered stereoconfiguration at C-3, corresponding to **219**. Although not having been successful with respect to the desired azidation, the formation of **218** as main product shows a possible pathway how to convert the D-gluco side chain of **157** into the D-manno configuration, a reaction which may be improved in its yield by varying the conditions. By analogous activation and azidation, **218** could serve as precursor of α*R* configured thiazole dipeptides.

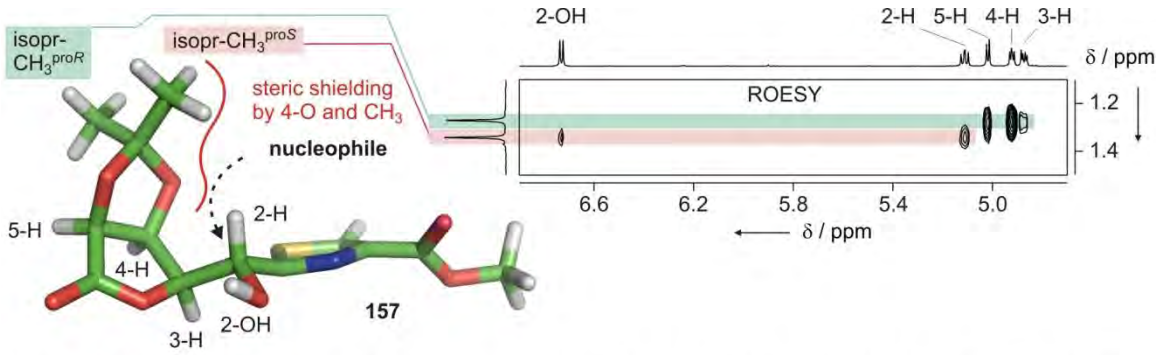

Figure 4.20 Possible explanation of the unreactivity of the D-gluco configured thiazole lactones against nucleophilic substitution at C-2. *The section of the ROESY spectrum of* **157** *(DMSO-*d_6*, 500 MHz, 300 K) shows the spatial proximity of the proS acetonide* CH_3 *group with the 2-OH and 2-H protons while the proR group undergoes strong dipolar couplings with the 4-H and 5-H protons. This is in accordance with the molecular modeling result (*HyperChem*) and suggests the steric shielding of the 4-O and the* CH_3^{proS} *group of the space required for a nucleophile to attack at C-2 under inversion of the stereocenter. As in the substrates with activated 2-OH function similar scalar coupling constants between 2-H and 3-H were found, this depiction also reflects the geometry of the substrates* **215** *and* **216** *which were subjected to various substitution conditions (table 4.14).*

Figure 4.20 shows the *HyperChem* modeled structure of **157** and the observed ROESY contacts of the diastereotopic acetonide CH_3 groups which give a possible explanation why the 2-OH function of **157** can be readily protected (figure 4.15a) and activated even with bulky substituents, while no nucleophilic substitution is possible although the α-position to the

aromatic thiazole ring should promote such processes. The modeling results are in accordance with the observed ROE contacts of the acetonide CH_3 groups, suggesting a steric shielding of the space required for the approach of the nucleophile. In contrast, the 2-OH is well accessible for bulky protecting reagents like TBSCl and for activating agents like TsCl. In order to investigate whether the acetonide is the only shielding element, it was cleaved from the mesylated lactone **216**, yielding the diol **220** which was subjected to azidation (table 4.14, entry 13). However, also in this case no azide was detected and decomposition occurred, which suggests that the lactone ring itself also contributes to the steric congestion.

As the removal of the acetonide of **216** proceeded with partial decomposition, it was further evaluated whether the unprotected triol **140** can be regioselectively activated (scheme 4.21). Tosylation first occurs at 5-OH (**221**), and only by using 3.6 eq of TsCl the 2-OH is also activated (**222**). Remarkably, treatment with the same amount of MsCl under otherwise identical conditions in contrast effects a twofold elimination of MsOH, yielding the planar conjugated thiazole butenolide **223**. Several syntheses of similar compounds, although without a thiazole and consisting of a sugar residue only, have been reported,[437-439] and a benzothiazole conjugated butenolide has been shown to be accessible by mesylation of a D-gluco configured 7,5-bicyclic thiazolidine lactam similar to **105** (scheme 4.6) by *R. Hörger*.[392] The *Z* configuration of the C2/C3 double bond in **223** results from the configuration of the sugar chain, and when dissolved in DMSO-d_6 the isomerization to the more stable *E* double bond (**224**) is observed over several days (scheme 4.21c) which is in accordance with the results of *R. Hörger*.

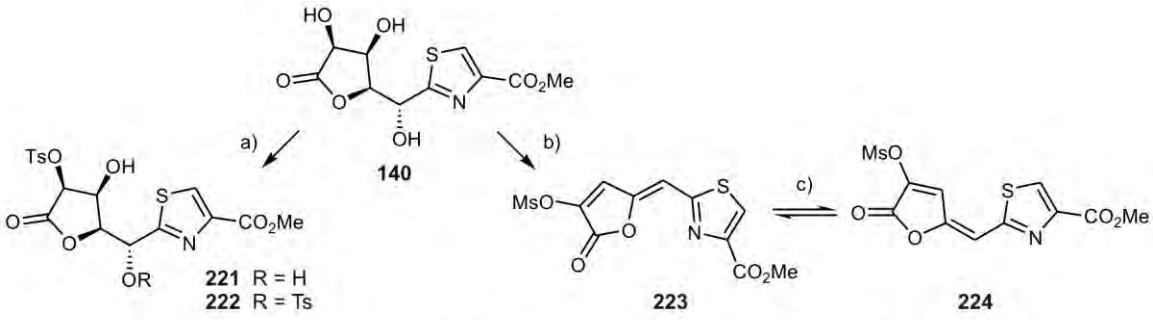

Scheme 4.21 Activation experiments of the thiazole* 140 *with unprotected sugar chain lactone. Reagents and conditions: a) TsCl (3.6 eq), DMAP (cat.), Pyr_{abs}, 0 °C to RT, 21 h, 48% of **222** and 19% of **221**; b) MsCl (3.6 eq), DMAP (cat.), Pyr_{abs}, 0 °C to RT, 18 h, 73% of **223**; c) DMSO-d_6, RT, ratio **223**/**224** 99:1 after 2 h, 68:32 after 13 d, 35:65 after 32 d.

An alternative method of amine synthesis starting from **157** is given by a reductive amination sequence (scheme 4.22). For this purpose, the alcohol **157** has to be oxidized to the ketone **225**, which could be accomplished in near-quantitative yield by refluxing with IBX in EtOAc.[440] In the

next step, the ketone can be transferred to a hydrazone (for example with Boc functionalization, **226**), a methyl oxime (**227**), or to various other C=N containing compounds. The crucial conversion is the reduction of the C=N double bond which (re)establishes the amine stereocenter (marked by *, **228**/**229**).[441-443] In the case of prochiral substrates this is accomplished by functionalization with stereocontrolling residues, as established for oxime ethers by *Moody et al*.[353] Chiral hydrazones are also employed for stereoselective α-alkylation (*Enders* method employing *S* or *R* configured aminoprolinol methyl ether hydrazones (SAMP/RAMP)).[444] In chiral substrates like **226** and **227**, the bulky lactam substituent will controle the stereoselectivity of reduction, and if the orientation of the lactam and the acetonide in the ketone **225** is comparable to the alcohol **157** (figure 4.17) the hydration is expected to occur from the *Re* half space which yields the desired *S* stereoconfiguration in **228** and **229**. The last steps encompass cleavage of the N-N or N-O bond (d, e) with Zn[353] or metal carbonyl complexes,[445, 446] and subsequent protection can for example afford the Boc protected amine **230**.

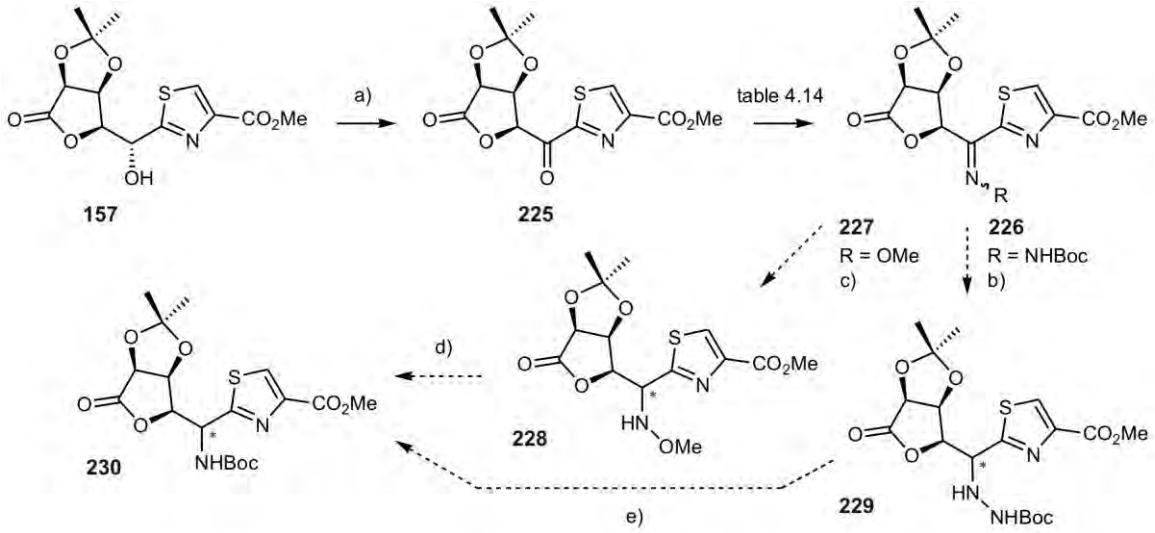

Scheme 4.22 Oxidation of the 2-hydroxy function of* 157 *and possible synthetic routes via reductive amination. *Attempts to introduce the nitrogen functionality are listed in table 4.15.* Reagents and conditions: a) IBX (4.0 eq), EtOAc, 80 °C, 12 h, 99%; b) Pd/C, H_2, MeOH, RT or BH_3, THF; c) $NaBH_3$, THF; d) $[Mo(CO)_6]$, CH_3CN or Zn, AcOH, then Boc_2O; e) $[Ru_3(CO)_{12}]$, CH_3CN, then Boc_2O.

Table 4.15 lists the various attempts performed to install the C=N functionality starting with the ketone **225**. In order to evaluate the reactivity of the ketone it was also treated with an alkyl as well as an aryl amine (entries 1 and 2), with hydrazine (entries 3-6) and with *tert*-butyl carbamate (entry 7). The majority of the reactions was performed directly in the NMR tube in order to allow facile monitoring by ^{1}H NMR. While no reaction was observed with *para*-

methoxyaniline and *tert*-butyl carbamate (entries 2 and 7) complex mixtures were obtained after treatment with the more reactive reagents propylamine and hydrazine (entries 1, 3-6) and no product could be identified in all cases.

In contrast, treating the ketone **225** with *tert*-butyl carbazate or methoxylamine hydrochloride in methanol led to formation of one main product, as observed from the NMR monitoring (entries 8 and 9). This indicates that the formation of one C=N bond isomer is considerably preferred. The compounds proved to be unstable towards aqueous workup and the ketone **225** was reisolated. As another route to thiazole amines (described in the following section) was successful, this reductive amination pathway was not further examined, but the Boc hydrazone **226** as well as the oxime methyl ether **227**, if they can be isolated or directly subjected to the reduction step, should enable to obtain thiazole dipeptides with a side chain in the D-mannosamine configuration (such as **230**, if the reduction step yields an *S* configured amine). The substrates obtained by the alternative access described in the following are epimeric at position 3 and thus correspond to thiazole dipeptides with a side chain in the D-altrosamine configuration.

Table 4.15 N/O-*exchange experiments with the ketone* **225** *(reductive amination pathway, scheme 4.22) to obtain substrates with C=N double bonds (***226***,* **227** *and further compounds). The respective residue R is given in column 2.*

entry	R	conditions and duration	result	remarks
1	Pr	propylamine (excess), Tol, RT, 20 min	several signal sets, no product identified	
2	*para*-methoxy-benzyl	*para*-methoxyaniline (excess), *p*TosOH x H_2O (cat.), DMSO-d_6, RT→80°C, 12 h	no conversion	monitoring by ^{1}H NMR
3	NH_2	hydrazine acetate (1.0 eq), $MeOH_{abs}$, 4 Å MS, 0 °C→RT, 5 h	complex mixture	
4	NH_2	hydrazine hydrate (1.0 eq), $MeOH_{abs}$, 4 Å MS, 0 °C, 1.5 h	complex mixture	
5	NH_2	hydrazine hydrate (1.0 eq), $CDCl_3$, RT, 8 h	complex mixture	monitoring by ^{1}H NMR
6	NH_2	hydrazine hydrate (1.0 eq), MeOD-d_4, RT, 6 h	complex mixture	monitoring by ^{1}H NMR
7	Boc	*tert*-butyl carbamate (1.0 eq), *p*TosOH x H_2O (cat.), $CDCl_3$, RT→70°C, 3 d	no conversion	monitoring by ^{1}H NMR
8	NHBoc	*tert*-butyl carbazate (4.0 eq), MeOD-d_4, RT, 40 h	86% conversion to **226**	monitoring by ^{1}H NMR; product is sensitive to aqueous workup
9	OMe	methoxylamine hydrochloride (1.0 eq), *p*TosOH x H_2O (cat.), MeOD-d_4, RT, 3 h	72% conversion to **227**	monitoring by ^{1}H NMR; product is sensitive to aqueous workup

4.4.8.2 A thiazolidine lactam as synthetic back-door: synthesis of altrosamine<Thz dipeptides

In earlier work accomplished in the *Geyer* group, *P. Tremmel* evaluated possible strategies for the selective variation of sugar configurations.[369] This bases on the concept that an uronic acid is "clamped" in a rigidified structure which allows to selectively modify single positions and thus to convert a sugar into another. The 7,5-bicyclic thiazolidine lactams which exhibit the thermodynamic condensation products of γ-glucuronolacone and cysteine have already been discussed in another context (schemes 4.6 and 4.9) and they allow for such operations, as shown in work by *P. Tremmel*.[369] Looking for the synthesis of nitrogen-functionalized substrates, the reactivity of the epoxide **231** towards NaN_3 was investigated, and it turned out that nucleophilic attack selectively occurs at position 9, leading to the azide **232** (scheme 4.23).

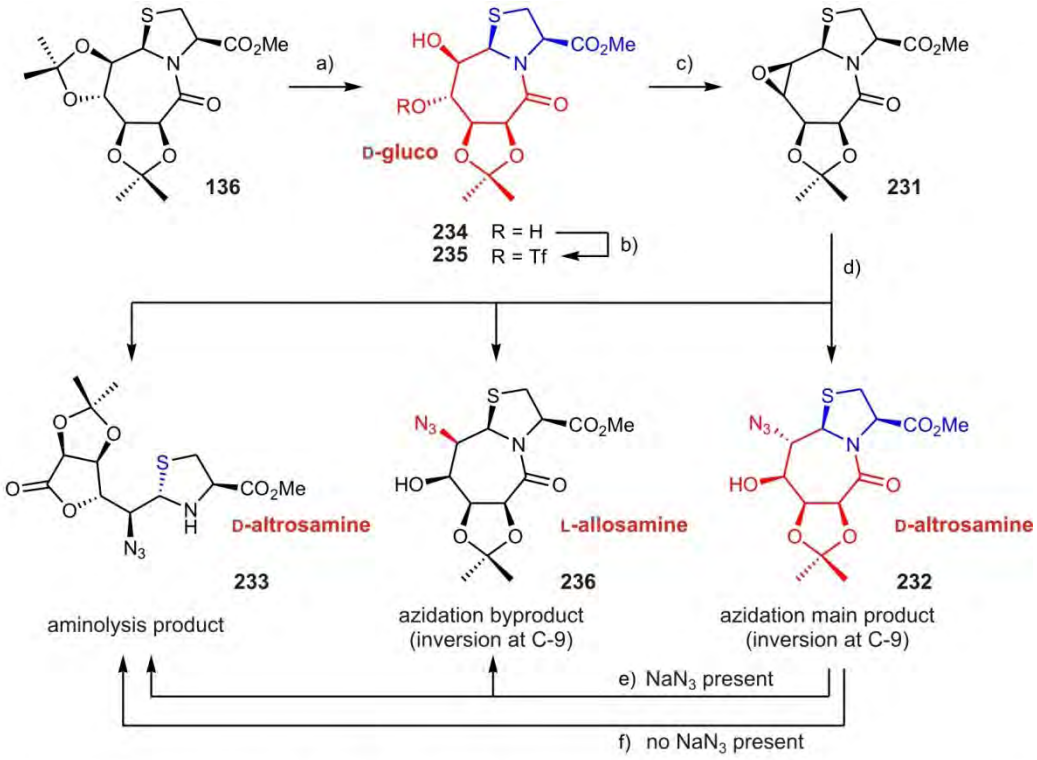

Scheme 4.23 Synthetic route to the 2(α)-azidated thiazolidine lactone* 233 *which is a precursor of thiazole dipeptides such as Tyh<Thz (figure 4.19). *Steps a) to d) were established in earlier work by* P. Tremmel. *The proposed mechanism of the formation of the three azidation products is shown in scheme 4.25.* Reagents and conditions: a) *p*TosOH x H_2O (cat.), MeOH, RT, 17 h, 67%; b) Tf_2O (1.2 eq), $CH_2Cl_{2\ abs}/Pyr_{abs}$ 3:1, 0 °C to RT, 4.5 h, 94%; c) NEt_3 (7.0 eq), DMF, 60 °C, 27 h, 81%; d) NaN_3 (1.7 eq), DMF/AcOH 130:1, 45 to 55 °C, 74 h, 39% of **233** / 33% of **232** / 12% of **236** / 4% of educt; e) NaN_3 (1.7 eq), DMF/AcOH 130:1, 45 to 55 °C; f) DMF/AcOH 130:1, 50 °C, 72 h, 33% of **233** plus starting material reisolated.

Thus, it was possible to convert the starting D-gluco into a D-altrosamine configuration. This was not the only reaction product as formation of the thiazolidine **233** (apparently by intramolecular

alcoholysis of the lactam) was also observed. As the reaction proceeded with low yields, this pathway was not further investigated by *P. Tremmel*. However, in the light of the current research project, it was decided to further investigate the reaction as the thiazolidine **233** is not only already functionalized with an azide at the 2(α) position, but as it also exhibits the desired *S* configuration. If it is possible to isolate the (originally undesired) side product **233** in acceptable yields and to perform the oxidation to the corresponding thiazole, this would exhibit a first synthetic pathway to trihydroxy-homoglutamate(Tyh)<Thz dipeptides (figure 4.19). Moreover, the C-3 stereocenter is also *S* configured which, in contrast to the dipeptides that are in principle accessible from the D-gluco configured substrates, corresponds to the native Dyg<Thz configuration and thus can be seen as a "real" C_1-extended homolog.

The synthesis of the epoxide precursor **231** was accomplished on the multigram scale according to the protocols by *P. Tremmel*,[369] and some purification procedures were improved. The bisacetonide **136** (see also scheme 4.9) was deprotected at position 8 and 9 to yield the diol **234** (69%) which was selectively triflated at position 8 in 97% yield (**235**). The formation of the epoxide **231** was accomplished by heating the triflate **235** in DMF with NEt_3, and the product can be isolated by crystallization in 81% yield (up to 6 g of product were obtained per reaction batch). The following azidation reaction (step d) is carried out by heating the epoxide **231** in DMF with NaN_3 and AcOH, and several variations of the reaction parameters were tested in order to improve the yield of the desired alcoholysis product **233**. It turned out that a third reaction product is formed which had not been described before and which corresponds to the epimeric azide **236** with an L-allosamine configuration. Its constitution as well as configuration was determined by NMR spectroscopy, and in scheme 4.24 the scalar $^1H/^1H$ coupling constants within the 7-membered rings are compared for different substrates.

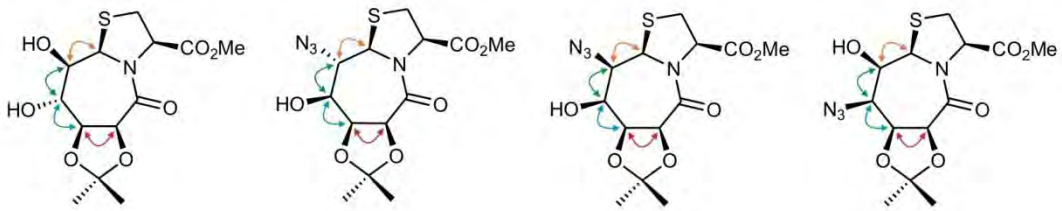

^3J	**234**	**232**	**236**	**237**
6-H/7-H	8.0 Hz	8.8 Hz	9.3 Hz	8.5 Hz
7-H/8-H	9.9 Hz	1.7 Hz	1.7 Hz	2.0 Hz
8-H/9-H	7.2 Hz	1.3 Hz	8.0 Hz	6.0 Hz
9-H/9a-H	3.1 Hz	10.4 Hz	3.7 Hz	2.5 Hz

Scheme 4.24 The comparison of the scalar $^3J_{H/H}$ coupling constants (DMSO-d_6, 300 MHz, 300 K) aided to determine the stereoconfiguration of the byproduct* 236 *by comparison with other substrates. *Similar coupling constants were observed in the case of the isomer* **237** *which is azidated at position 8 but which exhibits identical stereoconfiguration (synthesized by* H. Seger*).*

As the amount of **233** never exceeded 40% after workup (which can be reasoned with a lactam/lactone equilibrium between **232** and **233**, as discussed in the following) it was examined whether the other products can be further converted to the thiazolidine. If the lactam **232** is subjected to the same reaction conditions as the epoxide **231** (conditions e vs. d), **236** as well as **233** are formed. In contrast, if only AcOH and no NaN_3 is present, **233** is the only product, which suggests that the lactam **236** is generated from its epimer **232** by azide/azide exchange undergoing inversion of the stereocenter. **236** proved to be a stable "dead end" compound in the reaction sequence as it could not be reacted back to **232** even with great excess of NaN_3 at high temperatures, and no lactone formation was observed. As a consequence, the reaction has to be run under conditions which lead to a minimal formation of **236**. This could be accomplished by moderate reaction temperatures (stepwise increase from 45 to 50 °C and then to 55 °C), by using only 1.7 eq of NaN_3, and by reducing the amount of AcOH (DMF/AcOH mixture of 130:1), which results in the formation of not more than 12% of **236**. For the separation of the desired thiazolidine **233** from the lactams **232** and **236** as well as residual amounts of educt, an effective preparation procedure was established which employs a short silica gel column. Due to its reduced polarity, **233** can be separated in good purity from the mixture by elution with EtOAc/Tol 1:1 (39% yield), and in the next step the other compounds are quickly eluted with pure EtOAc. This mixture which mainly consists of **232** can be treated with a DMF/AcOH mixture (conditions f) to afford more **233**, resulting in an overall 66% yield which can be further increased by additional reaction cycles.

Scheme 4.25 depicts the proposed mechanism of the formation of the azidation products **232**, **236**, and **233** on basis of the experimental observations. The primary product **232**, resulting from the opening of the epoxide **231**, can either be attacked by another azide ion, which inverts the stereocenter at C-9 and leads to the thermodynamically stable lactam **236**. In contrast, an epimerization must occur at the *S*,*N*-acetal stereocenter (C-9a) in order to afford the thiazolidine **233** which is *S* configured in contrast to all isolated lactams. Under acidic conditions, the thiazolidine ring can be opened to yield the *N*-acyl iminium ion **238** which is in equilibrium with not only **232** but, as the sulfur can attack from both sides, also with the epimeric thiazolidine lactam **239**. This compound is not stable as the conformation of its 7-membered ring effects a close proximity of the 8-OH to the lactam functional group, and the amide can now be opened to the thiazolidine lactone **233**. As the thiazolidine amine apparently is not able to attack the lactone due to geometrical reasons (see also scheme 4.6), the observed equilibrium with **232** must result from the formation of the iminium ion **240** and subsequent attack of the nitrogen at the lactone, which reproduces the *N*-acyl iminium ion **238**.

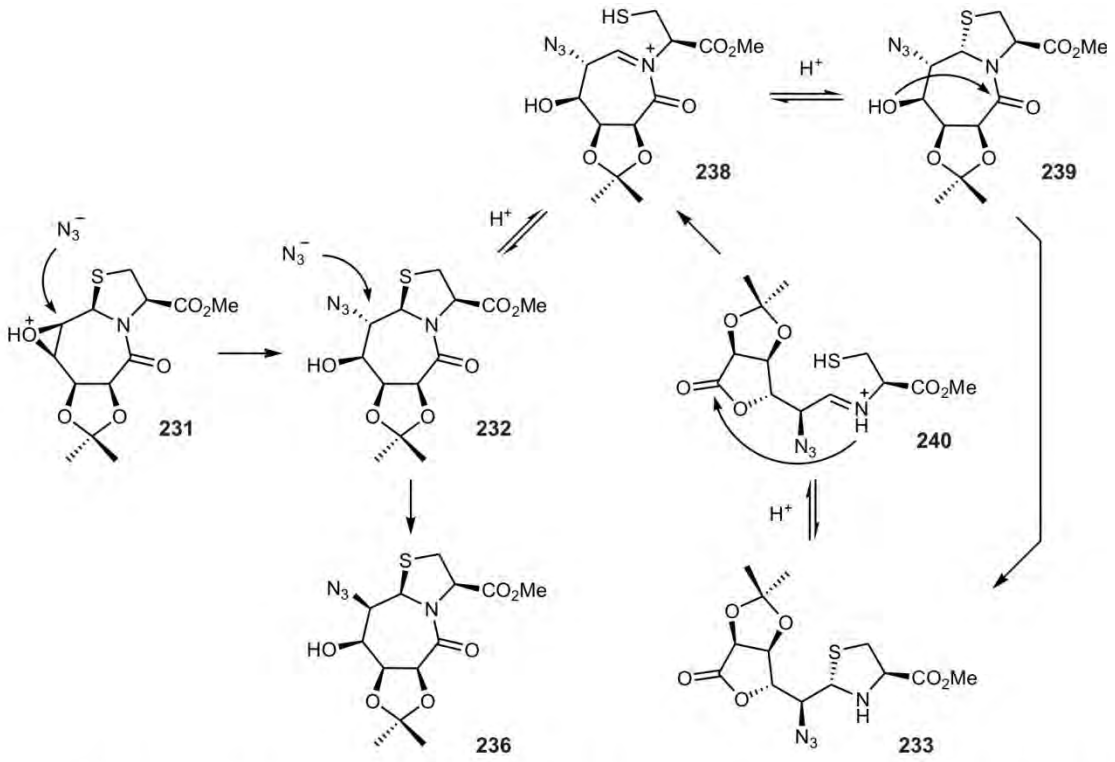

***Scheme 4.25 Proposed mechanism of the formation of the epimeric 7,5-bicyclic azides* 232 *and* 236 *as well as of the thiazolidine lactone* 233.** *The mechanism gives a possible explanation for why only the thiazolidine lactone* **233** *with* S *configuration at the stereocenter of the* S,N*-acetal is observed, whereas all isolated 7,5-bicyclic lactams are* R *configured at this position. The inversion of this stereocenter (*239*) is prerequisite for the intramolecular alcoholysis (8-OH) of the lactam.*

With the thiazolidine **233** available on the multigram scale, the crucial oxidation to the thiazole was examined in the next step. In the literature, several thiazolidine→thiazole oxidations are described where the thiazolidine is α-functionalized with a protected amino group,[321-323, 447] but no oxidation of an α-azido substituted thiazolidine has been reported yet. Figure 4.21 shows ^{1}H NMR spectra by which the oxidation of **233** was monitored. Gratifyingly, the azide can be subjected to the same oxidation conditions (20 to 30 eq of MnO_2 at 70 °C) as the protected thiazolidine polyols (figures 4.10 and 4.11) and one main product is obtained which corresponds to the thiazole **241**. Further signal sets of unidentified byproducts are of low intensity. Most important, also in this case no racemization of the product occurs, and the small scalar coupling constants between 2-H and 3-H in both substrates (written next to the respective positions) indicate that the relative configuration of the stereocenters at C-2 and C-3 is conserved. A single over-oxidation product, which is the thiazole carbamic acid **242**, could be identified and characterized by X-ray chrystallography (typically it was isolated in approx. 10% yield). As it is obviously formed by cleavage of the C1-C2 bond, it is generated in a different way than the nitrile **135** isolated from the oxidation reactions of a D-gluco configured thiazolidine

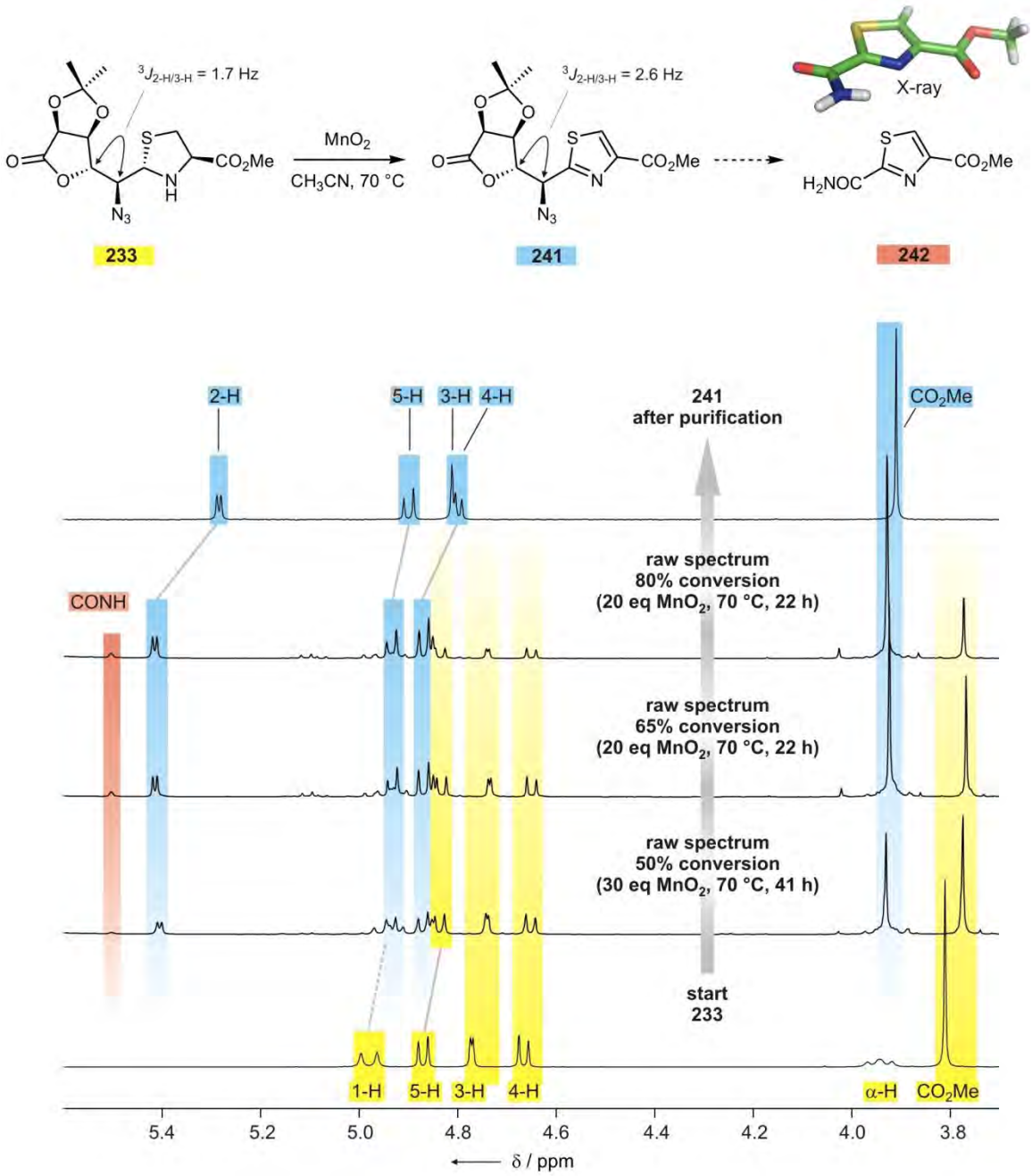

Figure 4.21 Oxidation of the azido configured thiazolidine* 233 *with MnO_2: monitoring by ^{1}H NMR ($CDCl_3$, 300 MHz, 300 K). *Signals resulting from the starting material are marked yellow, product signals are highlighted in blue, and the up-field amide proton signal of the over-oxidation product* **242** *is marked in red (the signal resulting from the CO_2CH_3 protons is not visible due to overlap with the corresponding signal of* **233***). Educt signals which overlap with product signals have not been marked. The shift of the signals in the raw spectra compared to the spectra of the purified substrates apparently results from the presence of a considerable amount of acetamide which is generated by oxidation of the solvent CH_3CN. One single thiazole main product is obtained, and the presence or only weak further signal sets suggests that racemization of the four sugar chain stereocenters (especially of the sensitive azidated benzylic C-2 stereocenter) occurs, if at all, only to low extent. The conservation of the relative configuration at C-2 and C-3 is indicated by the similar scalar H/H couplings before and after oxidation (written next to the respective positions).*

which still exhibits the C1-C2 bond and which must be a product of oxidative decomposition of the heterocycle (figure 4.11). As, in turn, none of such oxidation byproducts could be identified and isolated from all reactions of the D-arabino configured polyols, this suggests that the main mechanisms of oxidative decomposition may be dependent on functionalization of the sugar chain and on the steric shielding of the respective carbon-carbon bonds.

A thiazoline intermediate as it was observed in the oxidation process of the D-gluco configured thiazolidine polyols (figure 4.11) could not be identified in this case, which suggests that the first oxidation step (thiazolidine→thiazoline) is the rate-determining step. As visible from figure 4.21, long reaction times (85 h) and three batches of MnO_2 (30+20+20 eq) were required in order to effect a conversion of 80%. This led to low overall yields in the initial experiments and required extensive optimization studies which are summarized in table 4.16. As already mentioned in section 4.2.1, NiO_2 is also known to effect thiazolidine→thiazole oxidations, although examples of successful application are few,[328, 329] and it was also tested for the oxidation of **233** (entries 1-4). However, no conversion was observed, and the application of grinded NiO_2 (the commercially available substance is very coarse compared to the MnO_2 particles) only effected partial decomposition of the thiazolidine. No conversion was also observed in the case of the polyols (section 4.4.2). Therefore, the next experiments concentrated on commercially available MnO_2 (*Fluka*) which effected the fastest conversion rate, and different solvents were tested (entries 5-11) by stopping the reaction after 20 h and determining the extent of conversion by ^{1}H NMR. Interestingly, Tol was not the most effective solvent in this case, and instead CH_3CN (which was not suitable in the case of the polyols) gave the best results as it almost doubled the oxidation rate in comparison to Tol (entries 10 and 11). The reaction conditions also lead to a partial conversion of CH_3CN to acetamide (CH_3CONH_2) but which can be completely removed from the raw product in the flash chromatographic purification.

With the best oxidant and solvent determined, the purification procedure was improved in that the product **241** and unreacted thiazolidine **233** could be separated from each other by a short flash column. Thus, the reaction could be stopped before complete conversion and the long reaction times which led to low yields (< 10% of product) by a great extent of decomposition were avoided (entries 12-14). After heating of the reaction mixture for 30 h with 20 eq of MnO_2, 23% of **241** and considerably higher amounts of the starting material (33%) were isolated, which means that 45% of the substrate had been decomposed (entry 12). The increase of the reaction time (48 h) and of the amount of MnO_2 (30 eq) effected a slightly higher extent of decomposition (51%) but more product (28%) than starting material (21%) was obtained (entry 13). Therefore, the reaction time was reduced to 20 h which gave the best results, with

31% of **241** and 27% of **233** obtained in good purity (42% decomposition, entry 14). This procedure was successfully applied to a 3.73 mmolar reaction batch which finally yielded 309 mg of the thiazole **241** after chromatographic purification. Considering the high functionalization of the substrate, these results are acceptable in the context of the yields which are reported for the oxidation of significantly simpler thiazolidines.

Table 4.16 *Thiazolidine→thiazole oxidation experiments with* **233***. The first section (entries 1-4) shows the tests using NiO_2 as alternative oxidant, the second part lists the used solvents for MnO_2 oxidation (entries 5-11), and the third section contains the results employing short reaction times (entries 12-14). 70 °C was used as rection temperature in all cases as lower temperatures effected considerably slower conversion while higher temperatures increased the decomposition rate. The oxidant and solvent screening experiments (entries 1-11) were performed with 0.1 mmolar reaction batches, while the batches of entries 12-14 were up to 3.73 mmolar.*

entry	solvent	oxidant	conditions and duration	conversion to **241**[1]; result	isolated yields[2]
1	Tol	NiO_2 (*Fluka*)	20 eq, RT to 70 °C, 26 h	no conversion	--
2	CH_3CN	NiO_2 (*Fluka*)	20 eq, RT to 70 °C, 26 h	no conversion	--
3	Tol	NiO_2 (*Fluka*, grinded)	20 eq, 70 °C, 24 h	no conversion; partial decomposition	--
4	CH_3CN	NiO_2 (*Fluka*, grinded)	20 eq, 70 °C, 24 h	no conversion; partial decomposition	--
5	Pyr	MnO_2 (*Fluka*)	30 eq, 70 °C, 20 h	< 5%	--
6	DMF	MnO_2 (*Fluka*)	30 eq, 70 °C, 20 h	< 5%	--
7	1,4-dioxane	MnO_2 (*Fluka*)	30 eq, 70 °C, 20 h	15%	--
8	CCl_4	MnO_2 (*Fluka*)	30 eq, 70 °C, 20 h	18%	--
9	EtOAc	MnO_2 (*Fluka*)	30 eq, 70 °C, 20 h	18%	--
10	Tol	MnO_2 (*Fluka*)	30 eq, 70 °C, 20 h	19%	--
11	CH_3CN	MnO_2 (*Fluka*)	30 eq, 70 °C, 20 h	36%	--
12	CH_3CN	MnO_2 (*Fluka*)	20 eq, 70 °C, 30 h	reaction was stopped early	23% of **241** 33% of **233** (55% total)
13	CH_3CN	MnO_2 (*Fluka*)	30 eq, 70 °C, 48 h	reaction was stopped early	28% of **241** 21% of **233** (49% total)
14	CH_3CN	MnO_2 (*Fluka*)	30 eq, 70 °C, 20 h	reaction was stopped early	31% of **241** 27% of **233** (58% total)

1) determined by ^{1}H NMR; 2) isolated yields after flash chromatographic purification.

In order to evaluate possible pathways that allow for the tailoring of the azidosugar side chain, the lactone **241** was subjected to similar lactone opening and deprotection procedures which had also been tested in the case of the D-gluco configured polyol thiazoles (section 4.4.5), and

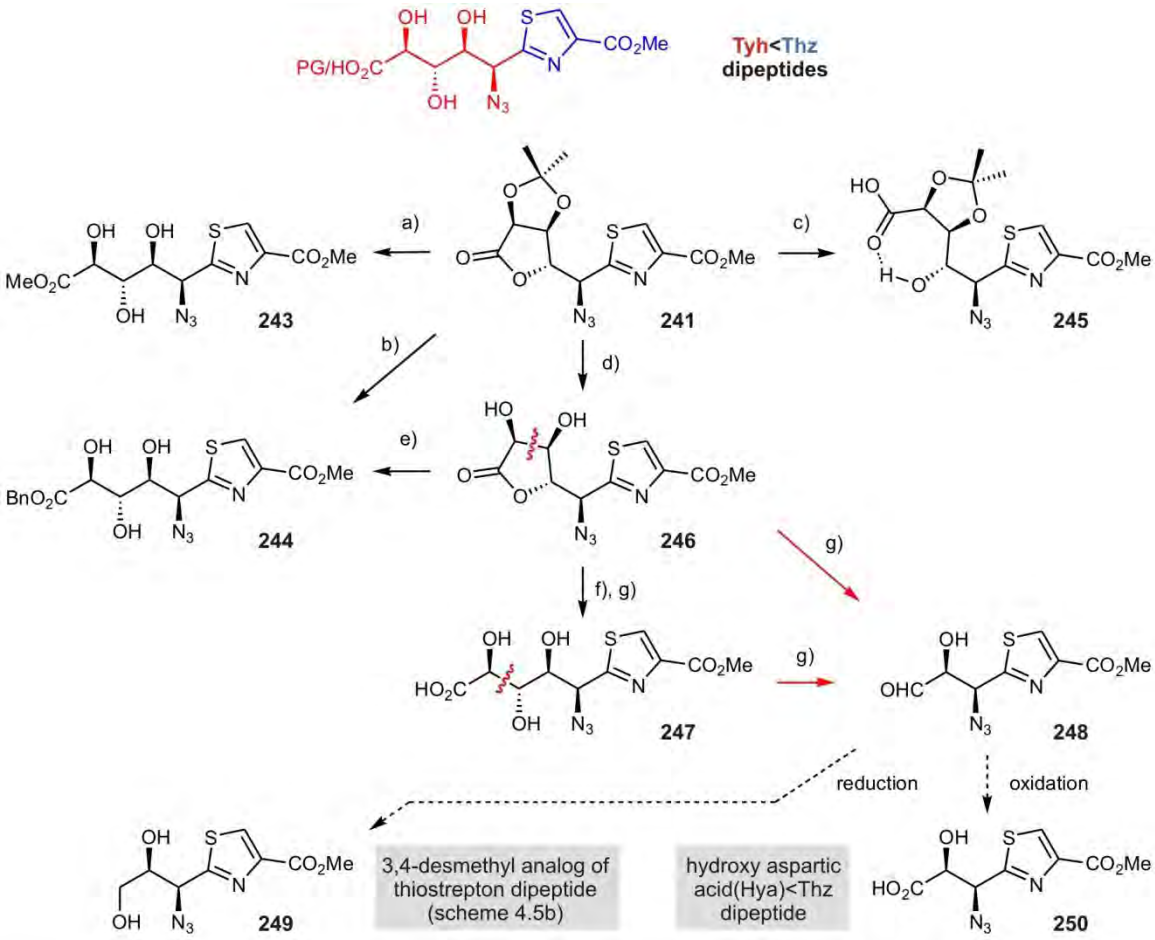

Scheme 4.26 Conversion of the lactone* 241 *to differently protected Tyh<Thz precursors. *A route to the amine- instead of azide functionalized substrates is shown in the following figure 4.22. Due to time restrictions, some reactions have only been tested with respect to their practicability, which is why only the conversion (determined from the raw NMR spectra) instead of an isolated yield is given.* Reagents and conditions: a) CSA (cat.), MeOH, 50 °C, 7 h, 38% of **243** and 12% of **246**; b) CSA (cat.), BnOH/Tol 1:1, RT, 4 d, 70% conversion to **244** and 30% conversion to **246** (no isolated yield was determined due to residual BnOH); c) NaOMe, $MeOH_{abs}$, 0 °C, 2.5 h, quant.; d) HCOOH (60% in H_2O), 65 °C, 40 min, 69%; e) CSA (cat.), BnOH, 60 °C, 36 h, 60% conversion (no isolated yield was determined due to residual BnOH); f) HCOOH (60% in H_2O), 65 °C, 15 h, > 50% conversion; g) $NaIO_4$ (1.0 eq), aq. Na_2HPO_4 (0.05 M)/Pyr 5:3, 0 °C to RT, 2.5 h, approx. 20% conversion (main product: **247**).

the results are summarized in scheme 4.26. While the lactone opening of the all-*cis* configured lactones had been problematic (table 4.10), the epimeric lactone ring present in **241** could be opened as methyl ester (**243**) as well as benzyl ester (**244**) under acidic conditions with concomitant cleavage of the 4,5-diol protecting group. Compared to the D-gluco configured lactone opening products, the linear polyols **243** and **244** were less problematic to handle as they were not inclined to recyclize to the lactone. Treatment of **241** with NaOMe yielded a highly polar main product which was identified as the carboxylic acid **245** which apparenty is formed from the methyl ester by the same mechanism which leads to the analogous D-gluco and D-arabino configured methanolysis products **191** and **192** (figure 4.18). In contrast to the esters

243 and **244**, the carboxylic acid **245** readily cyclizes in solution, yielding the diol lactone **246**. This compound is also accessible in one step and in acceptable yield from **241** by treatment with aq. HCOOH at 65 °C. The carboxylic acid **247** could be identified as byproduct in this reaction, and with an extended reaction time and/or temperature it should be possible to obtain this compound as a main product. The diol **246** was also tested with respect for its reactivity towards $NaIO_4$. As it had also been observed in the case of the other substrates, the lactone opening to **247** occurred faster than the diol cleavage of the lactone substrate (marked in red). However, the 4,5-diol of **247** reacted faster than the 3,4-OH (analogously to **199**, scheme 4.16), and therefore the thiazole with a C_3 chain (**248**) is observed as the only chain tailoring product. Optimizing the yields and the preparation procedure which has not been accomplished yet should be rewarding as the aldehyde **248** can serve as starting substrate for thiazole dipeptides with C_2 side chain. For example, the reduction of the aldehyde can lead to the diol **249** which reminds of the 3,4-dihydroxy isoleucine dipeptide present in thiostrepton (scheme 4.5b). By oxidation, a hydroxyl aspartic acid (Hya) side chain is installed (**250**), and this Hya<Thz dipeptide joins the homologous series of hydroxylated thiazole amino acids (Dyg<Thz, section 4.4.9; Tyh<Thz, this section) synthesized within the scope of this thesis.

Another topic which was examinated concerned the conversion of the azide (which can be seen as masked amine) to the amino function. When the azide **241** was subjected to a *Staudinger* reduction using PPh_3 in a THF/H_2O 10:1 mixture, a mixture of several products was obtained. In contrast, reduction with H_2 (Pd/C as catalyst) in EtOAc/MeOH 2:1 afforded one single product but which is not the expected primary amine **251** (scheme 4.27). In fact, **251** is not isolated at all due to an intramolecular aminolysis of the lactone which yields the six-membered lactam **252** in 88% yield. Due to time limitations, further studies about this reduction step could not be performed any more, but by for example choosing an acidic reaction milieu which ensures the immediate protonation and therewith deactivation of the nascent amine nucleophile, the lactamization of **251** should be able to be suppressed. Anyway, the obtained product **252** exibits a useful starting substrate. First, it can be converted to the desired Tyh<Thz amino acid with the free amino function at C-2, which is described below (figure 4.22). Second, it can possibly enable a novel access to thiazole tripeptides (Xaa-Yaa<Thz), as outlined in scheme 4.27. One the one hand, the lactam **252** can be seen as a Tyh<Thz dipeptide with the Tyh side chain carboxyl function cyclized to the N-terminal function. As indicated by the coloring of the bonds in scheme 4.27, however, **252** also exhibits a depsi-tripeptide (backbone marked in yellow) with the 5-OH als “N”-terminal function, the newly formed amide bond linking residues 1 and 2, and the Thz being the third residue. The sugar side chain diol (C-3 and C-4, marked in blue) links the

α-positions of the first two residues. By cleavage of a C-C bond of this tether (possible sites shown in red) this bridged dipeptide can be converted to a linear depsi-tripeptide **253** with *S* configuration at both α stereocenters. The high functionalization of the side chains should enable to obtain a variety of side chains. For example, periodate cleavage of the C3-C4 bond (after removal of the acetonide) is expected to result in two formylglycine (FGly)[448-450] residues which can be further modified. By exchanging the terminal alcohol function by an amine, the depsi-tripeptides can be converted to the corresponding tripeptides (**254**).

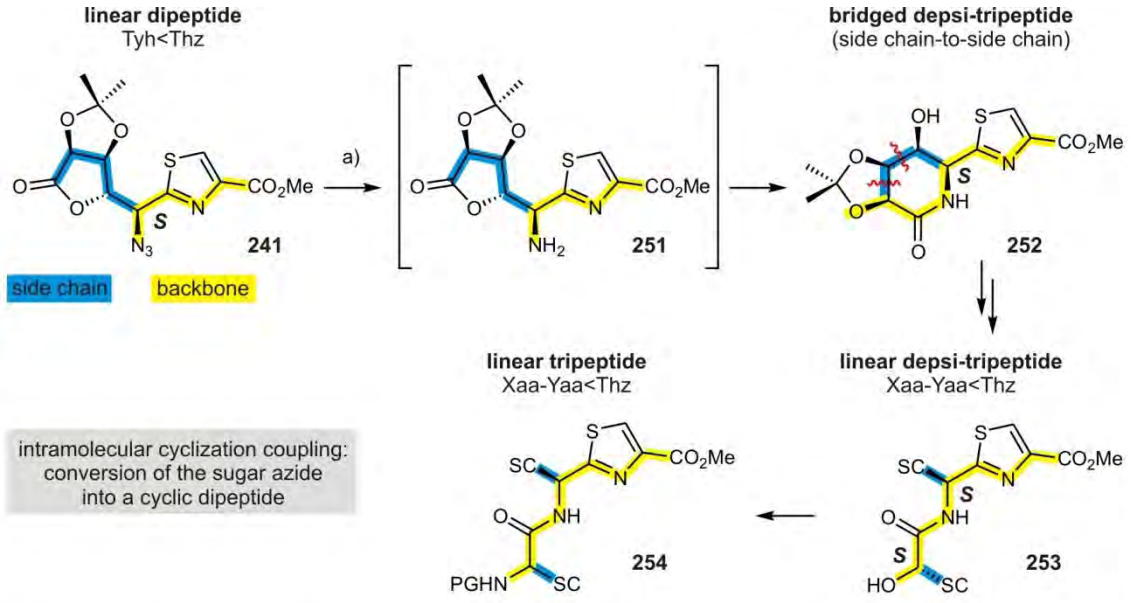

Scheme 4.27 Conversion of the lactone* 241 *to the six-membered lactam* 252 *and outline of a possible synthetic route to linear Xaa-Yaa<Thz peptides and depsipeptides. *The backbones are highlighted in yellow and the side chains (SC) are marked in blue. The intramolecular aminolysis of the lactone turns the sugar chain (C-3 to C-6) of the dipeptide* **241** *into an additional N-terminal amino acid residue (C-6 as amide proton) which is side chain-to-side chain cyclized with the adjoining C-terminal residue (C-2 to C-5). The triol tether can be subjected to C-C bond cleavage (possible positions marked in red) and to further tailoring which yields linear depsi-tripeptides (***253***). By N/O-exchange of the N-terminal alcohol a tripeptide* **254** *can be obtained.* Reagents and conditions: a) Pd/C (5%, wet, *Degussa*), H_2 (1 bar), EtOAc/MeOH 2:1, RT, 45 h, 88%.

In order to remove the acetonide protecting group in the lactam **252** it was treated with *p*TosOH in MeOH at 50 °C. In the two reactions run so far the acetonide exhibited high stability towards the tested conditions and 66 h of reaction time were required to effect a conversion more than 50% to the triol **255** (figure 4.22). The addition of NEt_3 for the neutralization of the reaction before workup instantly effected the formation of a colorless precipitate which could be separated by filtration and which turned out to be the lactam methanolysis product **256**. This exhibits the first Tyh<Thz dipeptide synthesized with an unprotected α-amino function and thus corresponds to an amine as it originally was expected to be accessible directly (as lactone **251**,

scheme 4.27) by reduction of the azide **241**. No acetonide protected linear amine was identified from ESI- and NMR spectra which suggests that the acetonide is cleaved before the lactam is opened. As no precipitate was observed prior to the addition of NEt_3, it can be assumed that it is the free amine, and not an ammonium salt, which is isolated. This is confirmed by the ^{1}H NMR spectrum of **256** which shows the NH_2 signal as broad singlet at 2.28 ppm (figure 4.22; scalar coupling to the 2-H visible in the COSY spectrum). The precipitation and filtration virtually removes all **256** from the reaction mixture as no residual amounts were visible in the ^{1}H NMR spectrum of the filtrate. In the test reaction, 22% of **256** were obtained and the filtrate contained a 7:3 mixture of triol **255** and starting material **252**. The yields are yet to be improved, and upon more harsh conditions the methanolysis is expected to be further promoted. Further experimental conditions are yet to be investigated which on the one hand allow for the synthesis of analogs of **256** with an orthogonally protected 6-carboxyl function, and which on the other hand enable to suppress the lactam opening so that the lactam triol **255** as starting substrate for thiazole tripeptide syntheses (scheme 4.27) is obtained as the only product.

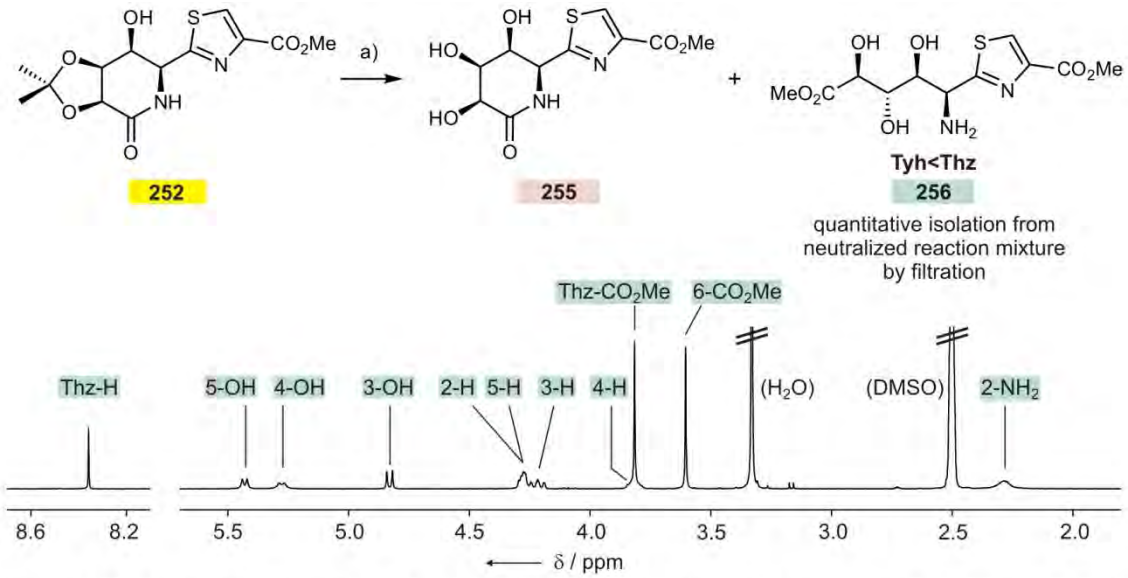

Figure 4.22 Acetonide deprotection of the lactam* 252 *to* 255 *and methanolysis to the Tyh<Thz dipeptide* 256 *with unprotected amino function. *The amine* **256** *precipitates from the reaction mixture upon neutralization with NEt_3 and the filtrate contains only the deprotected lactam* **255** *and residual unreacted starting material. The ^{1}H NMR spectrum of* **256** *(DMSO-d_6, 300 MHz, 300 K) also shows the NH_2 signal at 2.28 ppm which is a typical shift of an unprotected primary amine in DMSO. The presence of the amine is also indicated by the strong down-field shift of the C-2 signal (54.0 ppm) which is approx. 20 ppm below the usually observed shifts.* Reagents and conditions: a) *p*TosOH x H_2O (cat.), MeOH, 50 °C, 66 h, 22% of **256** (isolated yield after crystallization); filtrate: **255**/**252** 70:30.

4.4.9 Thiazole dipeptide synthesis with pentose sugar chain substrates

For the D-arabino configured thiazole polyols it has been shown that a variety of protection patterns is accessible (figure 4.17). The ability to control the selective (de)protection of the densely functionalized uronic acid chain turned out to be crucial for the desired *N*/*O*-exchange at position 2(α). As shown in the following, the Ara<Thz depsipeptides enable the synthetic access to the Dyg<Thz dipeptide which serves as central linking motif in the complex three-dimensional network of the nocathiacin and thiazomycin thiopeptide antibiotics and which has not been made accessible yet by chemical synthesis.

4.4.9.1 The stereoconfiguration of Dyg<Thz in nocathiacin I

The lack of a synthetic pathway to Dyg<Thz dipeptides also forecloses a total synthesis of members of the nocathiacins and thiazomycins. After the completion of the thiostrepton total synthesis in 2004,[315, 316, 364, 365] the successful construction of a member of these antibiotics would set another landmark in thiopeptide research. In contrast to other members of the thiopeptide family, the nocathiacins and thiazomycins are especially relevant as potential therapeutics because of their higher solubility, and great effort is spent in order to obtain nocathiacins by fermentation processes[451] and to modify their functionalization semi-synthetically.[452-460] Besides the Dyg<Thz core, it is especially the triple linked hydroxyindole unit which exhibits a challenging target.[461] The connecting of the hydroxyindole to the Dyg<Thz unit (at the Dyg 3-OH and 5-carboxyl unit) and to the Ser<Thz dipeptide C-terminally adjoining the Dyg<Thz (figure 4.11) closes a 10- and a 15-membered ring and will be crucial for the success of the total synthesis. Concerning the formation of the ether connection with the Dyg 3-OH, extensive studies have already been undertaken; however, due to the lack of an access to the native Dyg<Thz dipeptide the couplings had to be carried out with Ser<Thz dipeptides which are much simpler in complexity.[462] Only the use of Dyg<Thz substrates which exhibit both hydroxyindole coupling sites will enable to investigate the synthetic possibilities and problems associated with the construction of this part of the antibiotics.

The utility of a synthetic access to Dyg<Thz dipeptides also depends on whether non-natural diastereomers can also be synthesized. On the one hand, diastereomeric nocathiacin and thiazomycin analogs possibly exhibit better biological activity and selectivity, which increases the chances for the application of these thiopeptides as novel last-resort antibiotics. On the other hand, a total synthesis will serve as proof of the absolute stereoconfiguration but which has been proposed on the basis of few data.[463-465] The conformation of nocathiacin I has been determined on basis of NMR restraints which were used for molecular modeling studies

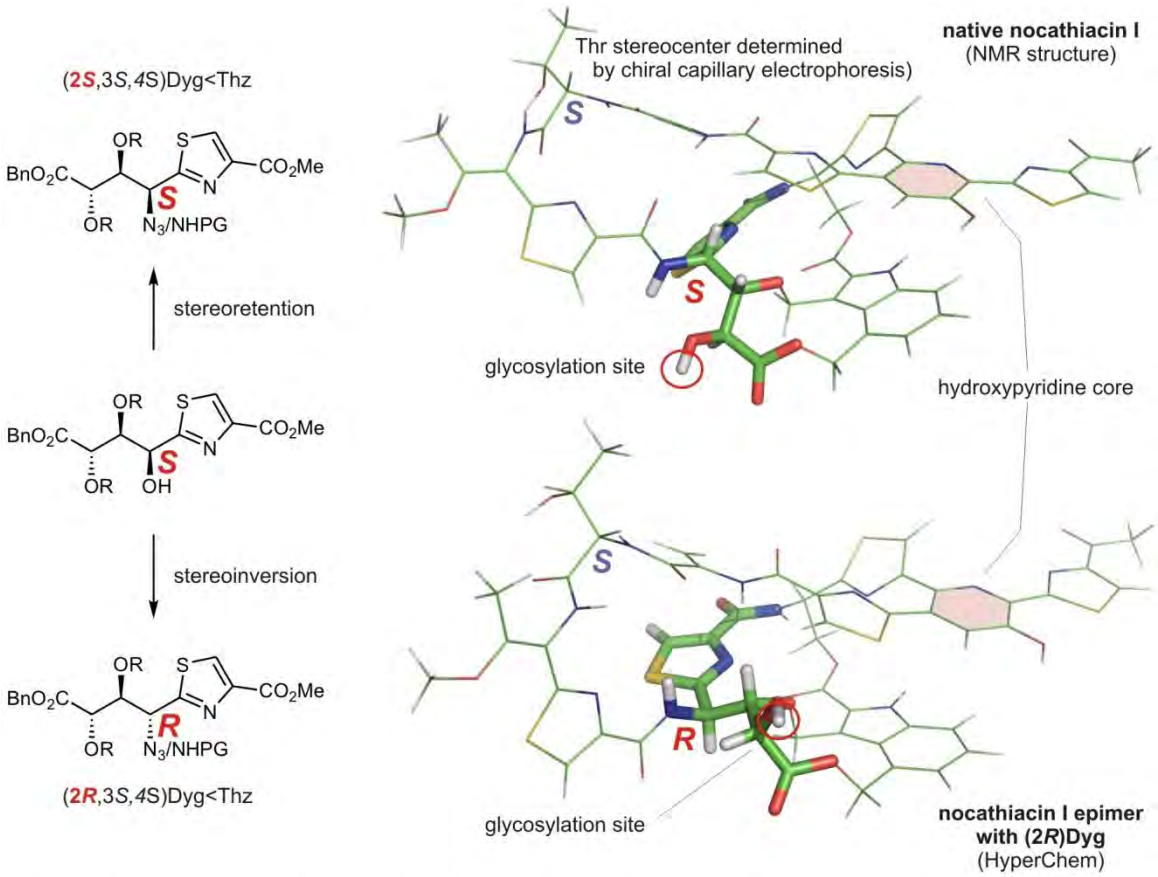

Figure 4.23 Comparison of nocathiacin I structures containing the 2S and 2R epimer of the Dyg<Thz core dipeptide. *The three-dimensional network of this antibiotic exhibits high rigidity and axial as well as planar chirality motifs. The Dyg<Thz units are emphasized by depiction as sticks while the rest of the thiopeptide is shown as lines. The glycosyl residue at the Dyg 5-OH is not depicted for clarity. The absolute configuration of native nocathiacin (top) has been elucidated by combination of chiral capillary electrophoresis (determination of the Thr stereocenter as S, purple), and NMR-based molecular modeling which suggested a single combination of the configuation of all ten stereocenters as energetically favored. This also resulted in the proposal of a (2S,3S,4S) configuration of the Dyg<Thz dipeptide. Apart from the fact that the results of this study (which exhibits the only work concerned with the structure of the nocathiacins and thiazomycins so far) must be accepted with caution, the question remains whether the incorporation of non-natural epimers (and homologs such as Tyh<Thz, section 4.4.8) can lead to thiopeptide analogs with improved affinity and selectivity. A synthetic access to the Dyg<Thz core and to stereoisomers thereof is the prerequisite for the validation of the proposed stereoconfiguration and for the comparison of analogs. The structure of the nocathiacin I epimer with the Dyg in 2R configuration was calculated on basis of the native structure using* HyperChem*. The comparison shows that the glycosylation site (red circle) is located towards another direction and that the relative orientation of the single parts is slightly changed. In order to obtain 2S as well as 2R configured Dyg<Thz building blocks, the 2-OH of the triol (center) must be exchanged against a nitrogen functionality with retention and inversion of the stereocenter, which is described in section 4.4.9.3. R = H or protecting group.*

(simulated annealing with X-PLOR). This resulted in the strong energetical preference of one single combination of the ten stereocenters present in the molecule (relative configuration). However, as this could not answer the question about the absolute stereoconfiguration, chiral capillary electrophoresis of the Thr residue (obtained by hydrolysis) was performed which indicated that nocathiacin I contains L-Thr. Thus, the absolute configuration of the other nine stereocenters was determined solely from the result obtained for the Thr residue, and for the

Dyg side chain the (2*S*,3*S*,4*S*) configuration was suggested. Figure 4.23 (top) depicts a structure of nocathiacin I obtained with *HyperChem* on basis of the published NMR data.[463, 464] The Dyg<Thz core in its (assumed) native (2*S*,3*S*,4*S*) configuration is highlighted as sticks while the rest of the molecule is shown as lines, and the glycosyl residue is not shown for clarity. The thiopeptide exhibits a rather rigid three-dimensional peptide network which is influenced by the configuration of the three Dyg<Thz core stereocenters. For comparison, the lower shown structure in figure 4.23 shows the *HyperChem* molecular modeling result of a nocathiacin I epimer with the Dyg α-stereocenter in the *R* configuration. This change in stereochemistry slightly influences the relative orientation of the single segments and leads to an altered overall topology of the antibiotic. As the dihedral angles within the Dyg side chain are considerably influenced, the alignment of the glycosylation site (4-OH) and thus of the glycosyl residue also changes. This example illustrates that the incorporation of Dyg<Thz diastereomers may be rewarding as the resulting thiopeptide analogs possibly exhibit improved affinity and selectivity. As outlined in the left part of figure 4.23, a step towards stereochemical diversification is the ability to introduce the nitrogen functionality at C-2 either by retention or inversion of the stereocenter, which was an essential topic of the experimental studies described in the following.

4.4.9.2 Activation and azide introduction: Identification of the appropriate protection pattern

Several differently protected Ara<Thz substrates were examined with respect to the selective activation of the 2-OH position and the subsequent azidation (scheme 4.28). All tested substrates which are protected at 3-OH as well as 4-OH proved not suitable which apparently can be reasoned by the steric shielding of the 2-OH position before and after activation. The 3- and 4-TBS protected substrate **146** obtained after opening of the lactone **130** (scheme 4.10) could not be isolated as pure compound but as mixture of three isomers due to silyl migration. Nevertheless, as all compounds could be assigned in the ^{1}H NMR spectrum the reactivity towards MsCl was examinated, and it occurred with complete conversion to **257** (and to the other two isomers with the 3- and 4-OH group mesylated, respectively) as determined from the ^{1}H NMR spectrum of the raw product mixture. However, upon treatment with NaN_3 no conversion to **258** and its isomers occurred. The same observations were made in attempts to invert the C-2 stereocenter by a *Mitsunobu* reaction.[433, 466] Experiments were performed with **189** as substrate which is Bn- instead of TBS protected at position 3, and the sterically less congested diol **174** was also tested. However, no conversion was observed or only traces of the

inversion products **259** were obtained even by using 2-chloroacetic acid as nucleophile which has proven successful for the inversion of other sterically congested alcohols (c).[467, 468]

The unprotected triol **148** was also tested for its reactivity in a *Mitsunobu* inversion using *p*-nitrobenzoic acid[469, 470] but only the starting material could be reisolated (d). Furthermore, a complex mixture of products was obtained when **148** was treated with MsCl for hydroxyl activation (e), and consequently the unprotected triol also cannot be used for activation and inversion of the C-2 stereocenter. In fact, the selective protection of the 4-OH function turned out to be the only pattern which allowed to selectively activate the hydroxyl at position 2 and also to introduce the nitrogen functionality. Once again these results demonstrate the difficulties associated with the adequate functionalization of the thiazole polyol chains, and they justify the extensive studies carried out within the scope of this thesis that were aimed at the selective (de)protection of the hydroxyl functions (section 4.4.5.2). The experiments leading to Dyg<Thz dipeptides starting with the silyl ether **174** are described in the next section.

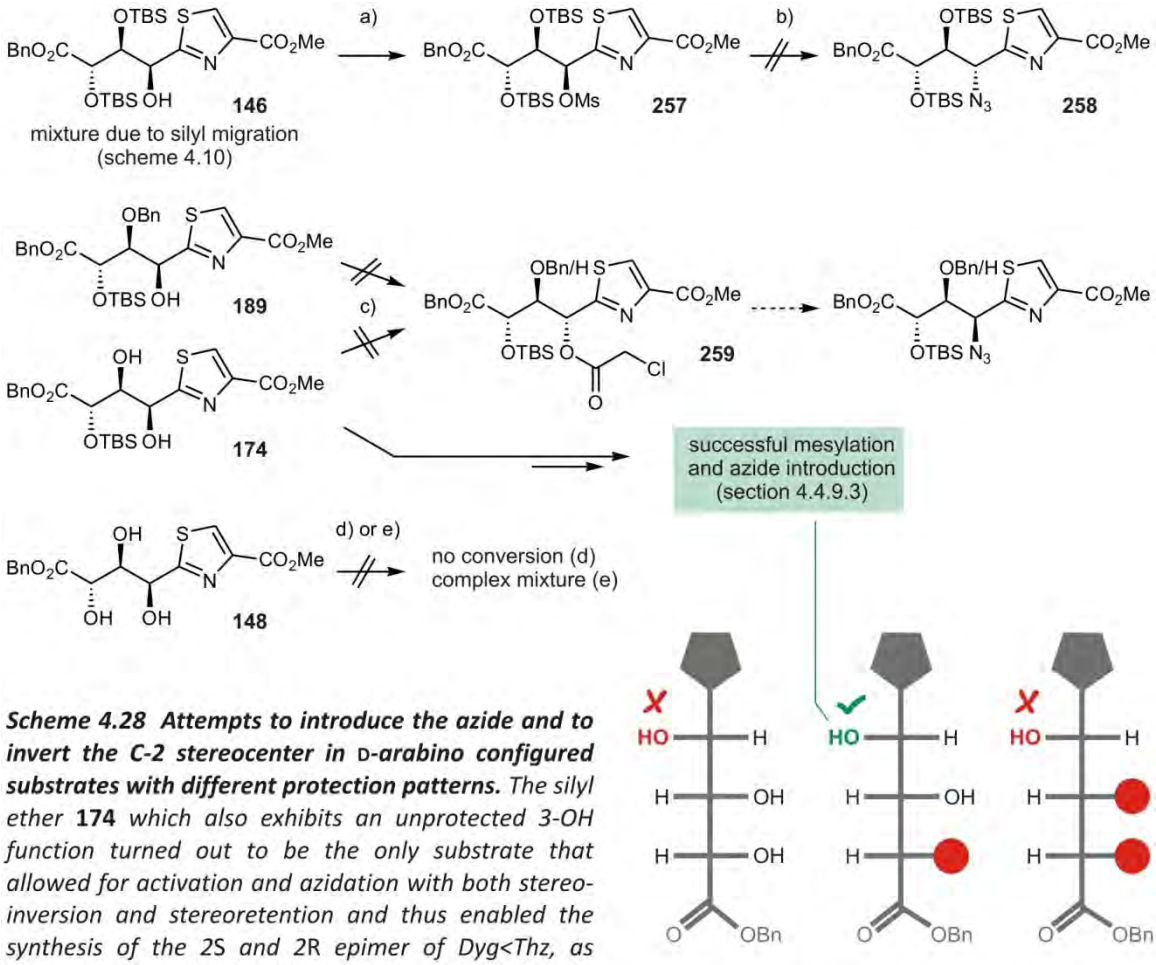

Scheme 4.28 Attempts to introduce the azide and to invert the C-2 stereocenter in D-arabino configured substrates with different protection patterns. *The silyl ether* **174** *which also exhibits an unprotected 3-OH function turned out to be the only substrate that allowed for activation and azidation with both stereo-inversion and stereoretention and thus enabled the synthesis of the 2S and 2R epimer of Dyg<Thz, as described in section 4.4.9.3.* Reagents and conditions: a) MsCl (3.0 eq), DMAP (cat.), Pyr_{abs}, 0 °C to RT, 4 h; b) NaN_3 (3.0 eq), DMF, 70 to 80 °C, 2 d; c) 2-chloro-acetic acid (2.0 eq), PPh_3 (2.0 eq), DEAD (2.0 eq), Tol_{abs}, RT, 15 h; d) *p*-nitrobenzoic acid (1.5 eq), PPh_3 (2.0 eq), DEAD (2.0 eq), THF_{abs}, RT, 15 h; e) MsCl (1.2 eq), DMAP (cat.), Pyr_{abs}, 0 °C to RT, 21 h.

4.4.9.3 Synthesis of 2*S* and 2*R* configured Dyg<Thz dipeptide motifs

If an azide function can be introduced at the activated 2-OH position of **174** under inversion, this will result in the unnatural 2*R* configuration (analogously to the conversion of **257** to **258**, scheme 4.28). In order to obtain a 2*S* configured azide, a double inversion is required, which can be accomplished by inversion of the alcohol at position 2, activation, and final *N*/*O*-exchange. The sugar chain in the thiazole triol obtained after the first step would also add to the synthesized polyols as a novel depsipeptide building block, now containing a D-ribose chain (Rib<Thz). As shown in figure 4.24a, this 2-OH inversion could be successfully accomplished by a two-step oxidation/reduction sequence. Such reactions have already been described by *Dondoni et al.* for polyol chains, and they used $KMnO_4$ for the oxidation step.[471] However, this work was restricted on sugars which were fully hydroxyl protected (except at the inversion site), and therefore $KMnO_4$ can not be used for the oxidation of **174** as it is also known to cleave the C-C bonds of diols. Instead, IBX in EtOAc was investigated as oxidant,[440] and in fact the oxidation occurred selectively at position 2, yielding the thiazolyl ketone **260**. The required reaction temperature of 80 °C also leads to a partial decomposition of starting material as well as product, and it turned out that a 5-fold excess of IBX in combination with a short reaction time (1.5 h) gives the best results. In fact, the isolated yield of **260** after chromatographic purification is moderate (29%) but 53% of the educt are also reisolated, which means that 18% of the material had decomposed. Longer reaction times (also until complete conversion) did not afford more than 36% of **260**, and considerably minor amounts of starting material were reisolated. Therefore, in the light of the easy separation of **174** and **260**, the short reaction time was the best choice.

Dondoni et al. performed the subsequent reduction with hydride reagents such as $NaBH_4$ or Li-selectride and they used ketones with protected amines or alcohols in the α-position. By *Felkin-Anh* control the resulting 1,2-diols and 1,2-aminodiols were in the *syn* configuration (dr between 70:30 and 95:5 according to the substrate and the reagent) which was desired as *anti*-configured diols and aminodiol starting material should be subjected to stereoinversion. In the present case, a *syn*-diol should be converted to the corresponding *anti* isomer, which is expected to be the main product under *Cram* chelate control. The ketone **260** fits this requirement by the coordinating hydroxyl group in α-position. The reagent combination of $BF_3 \times OEt_2$ and Bu_3SnH[472] turned out to be well applicable and the desired *anti*-diol **261** was obtained in a reproducible 75% yield and with a virtually complete stereoselectivity (no further diol species were isolated). The stereoinversion is visible from the optical rotations and the

scalar couplings along the sugar chain (figure 4.24a), and the ^{1}H NMR spectra showing the sugar chain signals of the *syn*- and *anti*-diol are compared in figure 4.24b.

In the next step, the diastereomeric diols **261** and **174** were examined with respect to the regioselective activation of the 2-OH group by mesylation. According to the stereoconfiguration the activations proceeded differently under comparable conditions. In fact, the 2-OH group was selectively mesylated first in both cases, but the *syn*-diol **174** was considerably more inclined to mesylation also of the 3-OH group than its *anti*-isomer **261** which required extensive optimization studies of the reaction protocol. The results are summarized in table 4.17 (mesylation of **261**) and table 4.18 (mesylation of **174**), respectively.

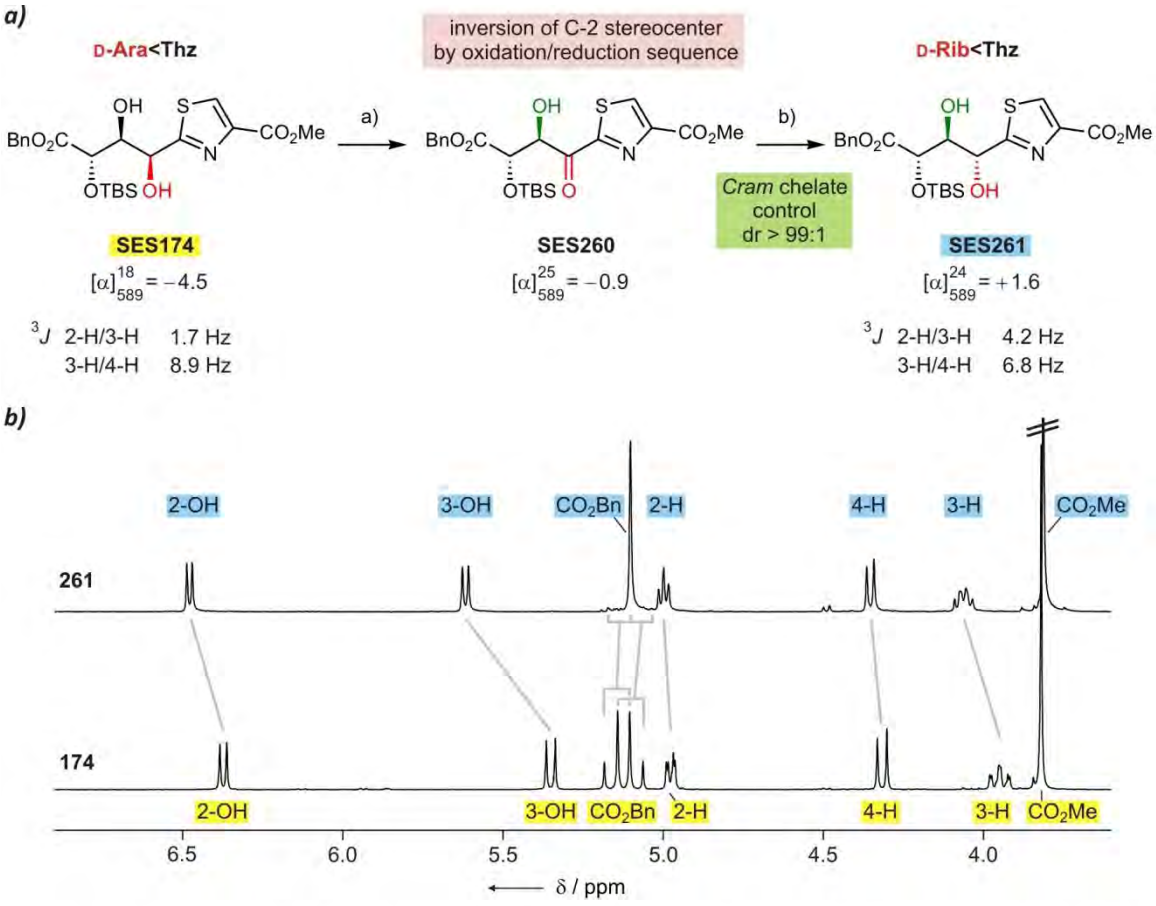

***Figure 4.24 Inversion of the 2(α) configuration in* 174 *by an oxidation/reduction sequence.* a)** *The* Cram *selectivity of the reduction step is enabled by the unprotected 3-OH function and leads to formation of the* anti-*diol* **261** *with excellent diastereoselectivity.* **b)** *Sections of the ^{1}H NMR spectra (DMSO-d_6, 300 MHz, 300 K) of the* syn-*diol* **174** *(bottom, signals assigned in yellow), and of the* anti-*diol product* **261** *(top, signals assigned in blue). The shape of the signals resulting from the diastereotopic protons of the benzyl ester significantly changes as two peaks of the two dublets appear at virtually the same chemical shift, which leads to an extreme roof effect (positions of the outer peaks indicated by the grey lines).* Reagents and conditions: a) IBX (5.0 eq), EtOAc, 80 °C, 1.5 h, 29% of **261** plus 53% of **260** reisolated; b) BF_3 x OEt_2 (2.2 eq), Bu_3SnH (2.2 eq), Tol_{abs}, –78 °C to RT, 32 h, 75%.

Table 4.17 *Mesylation experiments with the* D*-ribo configured diol* **261***. The arrows indicate the treatment with additional amounts of MsCl. In all cases, the additions of MsCl were carried out at 0 °C and the reaction mixtures were subsequently allowed to warm to RT.*

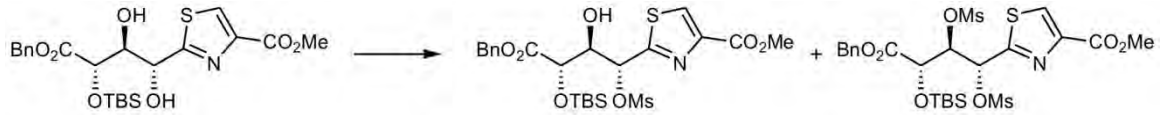

261 **262** **263**

entry	reaction batch	amount of MsCl, reaction time	base/catalyst and solvent	result and isolated yields[1)]
1	approx. 6 µmol	1.5 eq, 2 h →1.5 eq, 5 h →3.0 eq, 18 h	NEt_3 (2.0 eq), $CH_2Cl_{2\ abs}$	no conversion
2	0.40 mmol	1.2 eq, 12 h →1.0 eq, 24 h	DMAP (cat.), DMF_{abs}/Pyr_{abs} 1:1	50% of **262**, plus several unpolar byproducts
3	0.40 mmol	1.0 eq, 14 h →0.5 eq, 3 h	DMAP (cat.), Pyr_{abs}	73% of **262**, 25% of **263**

1) isolated yields after flash chromatographic purification.

The mesylation with NEt_3 as base in CH_2Cl_2 which was successfully applied by *Bach et al.* for the synthesis of phenylserine<Thz dipeptides (GE2270 total synthesis, figure 4.4a)[350] did not effect any conversion in the case of **261** (table 4.17, entry 1). The change of the solvent to a DMF/Pyr mixture and the use of DMAP as catalyst led to a 50% conversion to the desired mesylate **262**, but several byproducts were also identified and a considerable excess of MsCl as well as a long reaction time were required (entry 2). The use of Pyr as the only solvent finally allowed to obtain **262** in an acceptable 73% yield with a reduced amount of MsCl and within a reduced reaction time (17 h instead of 36 h, entry 3). However, the formation of the dimesylate **263** could not be suppressed (25% yield), and the use of lower amounts of MsCl led to long reaction times with strongly reduced yields also of the monomesylate **262**.

For the epimeric *cis*-diol **174**, the reaction was more difficult to optimize as the second mesylation of the 3-OH function occurred more readily (table 4.18). The use of 2.0 eq of MsCl effected a low 32% yield of the monomesylate **264** while the dimesylate **265** was isolated as main product (53%, entry 1). Attempts to add the MsCl in smaller portions lowered the amount of **265** but the yield of the desired product **264** was not considerably increased as the first mesylation did not exclusively occur at 2-OH, furnishing 13% of a monomesylate with the Ms group located at 3- instead of 2-OH (**266**, entry 2). In another experiment the first portion of MsCl was added at −78 instead of 0 °C using a CH_2Cl_2/Pyr mixture, but a very low conversion was observed at lower temperature than 0 °C and the variation of the solvent apparently promoted

the mesylation of the 3-OH function, leading to an 80% yield of the dimesylate **265** (entry 3). The best (although still moderate) result was finally obtained by running the reaction without DMAP catalyst in Pyr (entry 4). In this case, only 1.0 eq of MsCl and 13 h of reaction time were required in order to effect a 48% conversion to **264** and to reduce the formation of **265** (20%). In addition, 23% of the starting material could be reisolated.

Table 4.18 *Mesylation experiments with the* D-*arabino configured diol* **174***. The arrows indicate the treatment of the reaction with additional amounts of MsCl. In the case of the batch described in entry 3, the first addition of MsCl was carried out at −78 °C. In all other cases, the additions of MsCl were carried out at 0 °C and the reaction mixtures were subsequently allowed to warm to RT.*

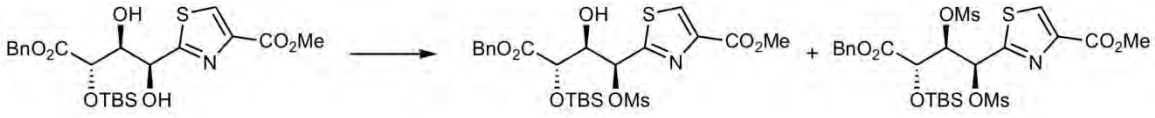

entry	reaction batch	amount of MsCl, reaction time	base/catalyst and solvent	isolated yields[1)]
1	0.64 mmol	1.0 eq, 5 h →1.0 eq, 12 h	DMAP (cat.), Pyr_{abs}	32% of **264**, 53% of **265**
2	1.42 mmol	0.6 eq, 2 h →0.6 eq, 18 h →0.3 eq, 8 h	DMAP (cat.), Pyr_{abs}	39% of **264**, 33% of **265**[2)]
3	0.37 mmol	1.0 eq, −78 °C →0 °C, 22 h →1.0 eq, 14 h	DMAP (cat.), $CH_2Cl_{2\ abs}/Pyr_{abs}$ 2:1	12% of **264**, 80% of **265**
4	2.05 mmol	1.0 eq, 13 h	*no DMAP*, Pyr_{abs}	48% of **264**, 20% of **265**, 23% of **174**

1) isolated yields after flash chromatographic purification; 2) in addition, 13% of the monomesylation product with the Ms group at position 3 were obtained (**266**).

For **174** the activations of the 2-OH group as nosylate (with NsCl) and as triflate (with Tf_2O) were also tested in order to examine whether these alternative reagents effect a lower extent of the undesired double activated compound (scheme 4.29). Using NsCl and Tf_2O in Pyr, however, effected no conversion, and treatment with Tf_2O in CH_2Cl_2/Pyr yielded the butenolide **267** as the only product.

With the monomesylates **262** and **264** available, the next experiments concerned the crucial azide introduction, and they are summarized in figure 4.25. It is important to mention that the dimesylates **263** and **265** could not be azidated in several experiments, and instead a complex mixture of polar decomposition and hydrolysis products was observed by TLC, NMR and HPLC

control of the reactions. This explains why considerable efforts were undertaken to reduce the extent of double mesylation of **261** as well as **174**, as described above (tables 4.17 and 4.18).

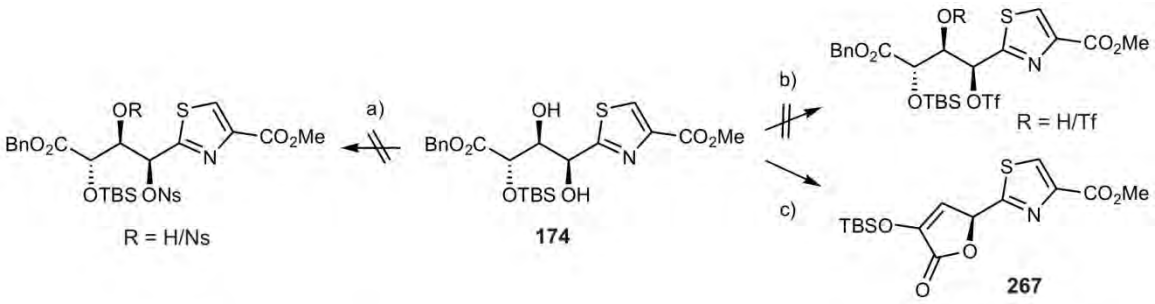

Scheme 4.29 Attempts to activate the 2-OH function of the diol* 174 *as nosylate and triflate. Reagents and conditions: a) NsCl (1.1+1.4 eq), Pyr_{abs}, 0 °C to RT, 2 d, no conversion; b) Tf_2O (1.0+1.0 eq), Pyr_{abs}, 0 °C to RT, 24 h, no conversion; c) Tf_2O (1.1+2.2 eq), $CH_2Cl_{2\ abs}/Pyr_{abs}$ 9:1, 0 °C to RT, 22 h, 30% of **267**.

In contrast, the azidations of **262** and **264** were successful under standard conditions with an excess of NaN_3 in DMF at 85 °C. No matter whether the *R* or *S* configured mesylate was used, an identical main- as well as byproduct was obtained, and in all cases the ESI spectrum revealed a molecular mass of 605 which is equivalent to the (expected) azide/mesylate exchange product with one TBS group. As visible from the 2D NMR spectra, however, these two compounds did not exhibit epimerization products which could have been formed by another attack of an azide ion to the primary products. Instead, they differed by the position of the TBS group which migrated during the reaction, yielding **268** as main- and **269** as byproduct. Consequently, as an identical stereoconfiguration was obtained independently of the stereoconfiguration of the mesylate, different reaction mechanisms must be assumed. The configurations of the starting material suggest a neighboring group effect by the 3-OH group which can form an epoxide by nucleophilic attack at C-2 (figure 4.25). This mechanism also suggests the 2*R* configuration of the products. In the *syn*-diol **264**, the conformation with the required *trans*-diaxial alignment of 3-OH and 2-OMs required for the attack is disfavored due to sterical congestion (red lines). Therefore, the epoxide **270** is not formed but the (expected) attack of the azide takes place (blue arrow), effecting a stereoinversion and yielding the *R* configured azide **268**. In contrast, the conformer required for epoxide formation starting from **262** is favored as the bulky substituents are located towards different directions, and thus the 3-OH outrules the azide as attacking nuceophile, yielding the *trans*-epoxide **271**. This is in the next step attacked by an azide ion which results in **268**, and consequently a double inversion (retention) of the C-2 stereocenter of **262** has taken place.

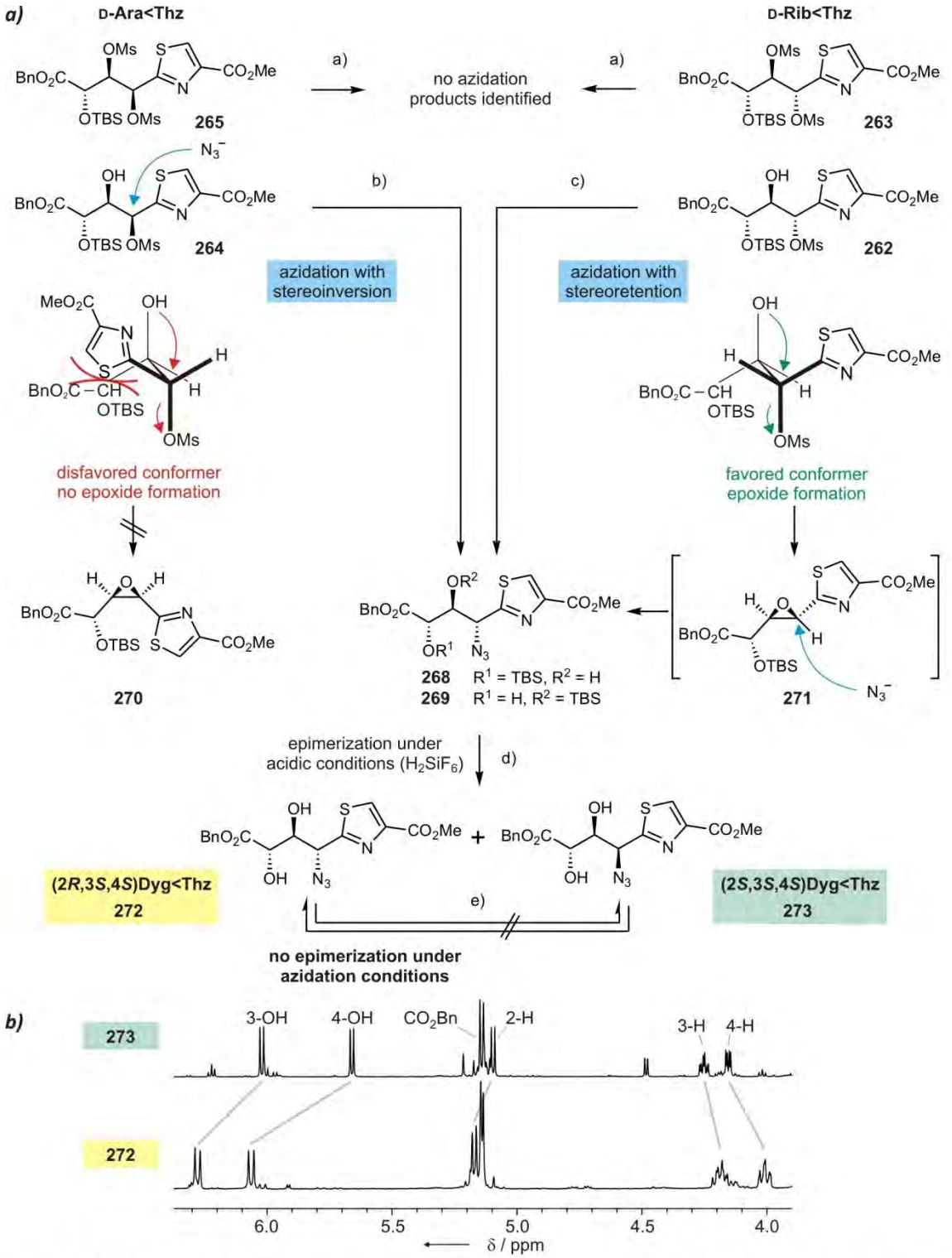

Figure 4.25 Azidation experiments with TBS-protected mesylates. ***a)*** *The single mesylated epimers* **264** *and* **262** *are converted to the same main product* **268** *by azidation. The identical stereoconfiguration can be explained by a neighboring group effect in the case of* **262** *which effects a double inversion (retention) of the stereocenter, while* **264** *is directly attacked by the azide. This mechanism suggests the 2*R *configuration of the products. Upon TBS cleavage epimerization takes place and the native configuration (2*S*) is also obtained.* ***b)*** *Section of ^{1}H NMR spectra (DMSO-d$_6$, 300 K) of the epimeric azides* **273** *(500 MHz, top) and* **272** *(300 MHz, bottom).* Reagents and conditions: a) NaN_3 (4.0 eq), DMF_{abs}, 85 °C; b) NaN_3 (1.5 eq), DMF_{abs}, 85 °C, 2.5 h, 12% of **268** and 8.4% of **269**; c) NaN_3 (1.5+1.5 eq), DMF_{abs}, 85 °C, 2.5+1.0 h, **268**/**269** 75:25 (raw product); d) H_2SiF_6 (2.0 eq), CH_3CN, RT, 24 h, 13% of **273** and 12% of **272** (over two steps from **262**); e) NaN_3 (10 eq), DMSO-d_6, 85 °C.

When the mixture of **268** and **269** was treated with H_2SiF_6 in order to cleave the TBS groups, epimerization of the azide stereocenter occurred and the diols **272** and **273** were isolated as an approx 1:1 mixture. The compounds can be separated from each other by column chromatography and they are obtained in acceptable purity, as shown by the sections of the ^{1}H NMR spectra in figure 4.25b. In order to prove the stability of the C-2 configuration under azidation conditions, each azide was heated with excess of NaN_3 in DMSO-d_6 and ^{1}H NMR spectra were recorded repeatedly. In both cases, no epimerization was observed, and prolonged heating only led to decomposition of the products, which supports the postulated reaction pathways that lead to identical azidation products.

At this stage, the identification of which of the diols **272** and **273** corresponds to the (2*R*) and (2*S*)Dyg<Thz epimer, respectively, was not possible yet. This suggested as next experiments the cleavage of the TBS group in the mesylates **262** and **264** and subsequent azidation, which should result in the formation of either **272** or **273** and thus allow to identify which one corresponds to the native 2*S* configuration. Furthermore, as the azidations of the TBS protected mesylates had occurred with low yields, the removement of the bulky TBS group was expected to lead to improved azidation yields. This had already been observed by *Bach et al*. during the construction of (2*S*,3*S*)phenylserine<Thz, a dipeptide present in the GE2290 antibiotics (scheme 4.30).[350] While the azidation of the TBS protected diol **274** afforded the product **275** in only 42% yield, 76% of azidation product were isolated in the conversion of **276** to **277**. As the diol **276** is *syn*-configured, the azide is introduced with stereoinversion and no epoxide is formed.

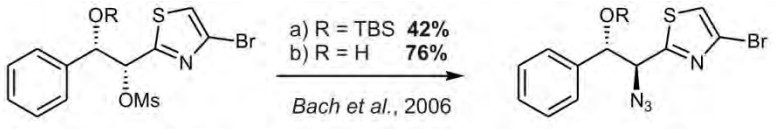

274 R = TBS
276 R = H

275 R = TBS
277 R = H

Scheme 4.30 Removal of bulky protection groups in proximity to azidation sites can considerably increase the yield of azidated product. *In the synthesis of (2S,3S)phenylserine<Thz almost the twofold yield was obtained after cleavage of the TBS group.* Reagents and conditions: a) **274**, NaN_3 (2.5 eq), DMSO, 90 °C, 14 h, 42% of **275**; b) **276**, NaN_3 (1.5 eq), DMSO, 65 °C, 2.0 h, 76% of **277**.

In the present case of Dyg<Thz synthesis the TBS group is not located in α but in β position to the azidation site, and the question was whether and to what extent its presence would influence the reaction. In the case of the D-arabino configured dimesylate no azidation was observed also after cleavage of the TBS group to **278** (scheme 4.31). In contrast, the examination of the D-arabino and D-ribo configured monomesylates was rewarding not only with respect to the azidation yields but also as the proposed mechanism could be confirmed. Cleavage of the

TBS group of **262** under acidic conditions with H_2SiF_6 led to hydrolysis of the mesylate and afforded the D-ribo configured triol **279**. The use of TBAF as reagent, in contrast, led to the formation of the *trans*-epoxide **280** as the only isolated product. This corresponds to the

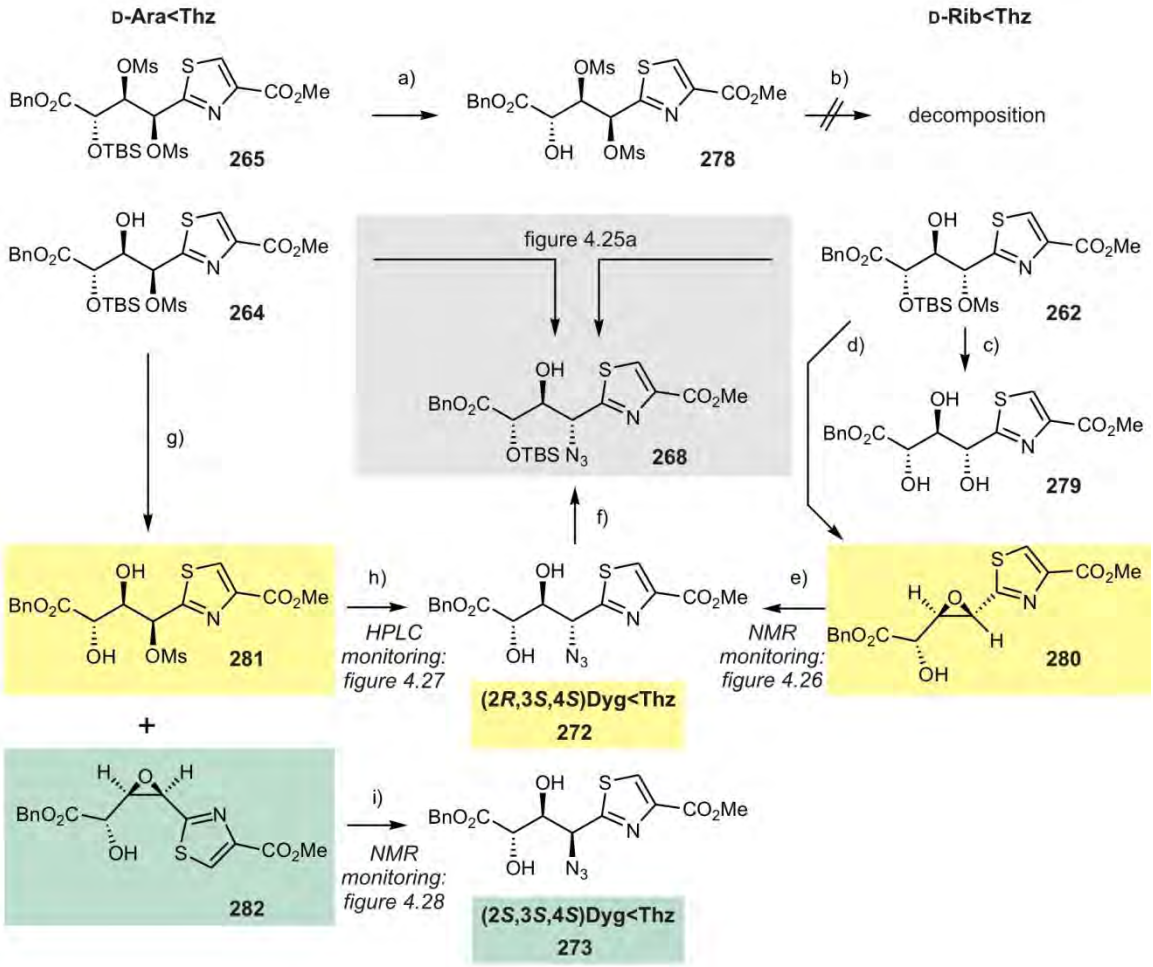

Scheme 4.31 TBS deprotection experiments and subsequent azidations. *The products obtained by treating the single mesylated epimers* **264** *and* **262** *with TBAF in order to remove the TBS group are in accordance with the proposed azidation mechanisms (figure 4.25) as epoxide formation takes place also under these conditions. In the case of the* anti-*diol* **262**, *the proposed epoxide intermediate of the azidation reaction (though TBS-deprotected) exhibits the only isolated product (***280***). Azidation subsequently furnishes the azide diol* **272** *which already had been obtained as part of an epimeric mixture (figure 4.25, conditions d) and which now could be assigned as 2*R *configured. By TBS protection, a 4-TBS protected main product is isolated which is identical to* **268** *(figure 4.25). As expected, the diol* **281** *was obtained by removal of the TBS group in* **264**, *and it is converted to (2*R*)Dyg<Thz (***271***) in 70% yield, which greatly exceeds the 20% conversion obtained with the TBS-protected analog (***264*** to* **268**, *figure 4.25, conditions b), in accordance with the results obtained by* Bach et al. *(scheme 4.30). Most important, the TBS deprotection of* **264** *also affords the epoxide* **282** *which gives the first controlled synthetic access to the Dyg<Thz dipepide in the native (2S) configuration.* Reagents and conditions: a) TBAF (1.3 eq), THF_{abs}, 0 °C, 2.5 h, 38%; b) NaN_3 (3.0 eq), DMF_{abs}, 85 °C, 30 min; c) H_2SiF_6 (2.0 eq), CH_3CN, RT, 20 h, 67%; d) TBAF (1.3 eq), THF_{abs}, 0 °C, 45 min, 42%; e) NaN_3 (5.0 eq), CSA (cat.), DMF_{abs}, 70 °C, 4 h, complete conversion (TLC), yield not determined; f) TBSCl (1.2 eq), imidazole (1.2 eq), DMF_{abs}, 40 °C, 6 h, 45%; g) TBAF (1.3 eq), THF_{abs}, 0 °C, 1.5 h, 21%; of **281** and 23% of **282**; h) NaN_3 (3.0 eq), DMF_{abs}, 85 °C, 2 h, 70%; i) NaN_3 (5.0 eq), DMSO, *p*TosOH x H_2O (cat.), 70 °C, 9 h, 16%.

epoxide **271** (figure 4.25) which has been postulated to occur as intermediate in the azidation of the TBS-protected monomesylate **262**. In the next step, the epoxide can be opened by selective azidation at position 2 which results in the 2*R* configured Dyg<Thz unit **272**. The reaction can be run DMF as well as in DMSO, and it was also performed in the NMR tube in order to allow monitoring by ^{1}H NMR spectra (figure 4.26). After 3.5 h at 70 °C the azide diol **272** can be identified as main product. The spectrum shown at the top was obtained from purified **272** which had been obtained from the alternative reaction pathway described in figure 4.25a in which the TBS group was removed after azidation (step d). The configuration of the main product **268** obtained by azidation of the mesylates **262** and **263** was confirmed by TBS-protection of **272** which yielded a substrate identical to **268** (scheme 4.31, step f; compare to figure 4.25, steps b to d).

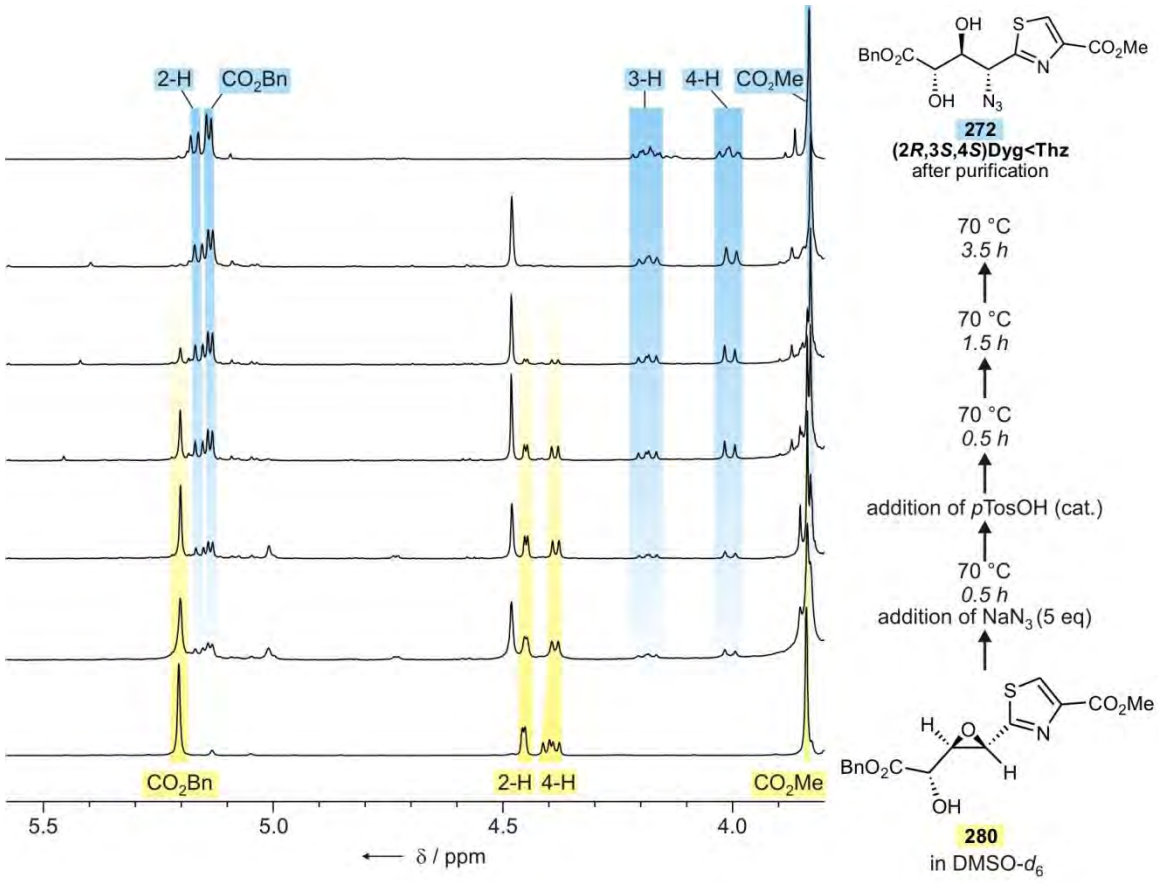

Figure 4.26 NMR monitoring of the azidation reaction of the epoxide 280 to the (2R) configured Dyg<Thz unit 272. *The reaction was performed in the NMR tube, using DMSO-d_6 as solvent, at 70 °C, and ^{1}H NMR experiments (300 MHz, 300 K) were subsequently recorded after the respective heating times given on the right. The spectrum at the top was obtained from purified* **272** *obtained by TBS cleavage of* **268** *(figure 4.22, conditions d). The simpler multiplet structures of the 3-H and 4-H signals in comparison with the NMR spectra of starting material* **280** *and purified product* **272** *result from the presence of acid which leads to a broadening of the OH proton signals.*

In contrast to **262**, the analogous TBS deprotection of **264** furnished a diol (**281**) as expected due to the less favored conformation which is required for epoxide formation. The azidation to **272** could be accomplished with an acceptable yield of 70% which is far better than the result obtained with the TBS-protected analog **264** (20%, figure 4.25, step b). As shown in figure 4.27, the reaction was monitored by analytical HPLC, and in addition to the starting material **281** and the product **272** only small amounts of polar hydrolysis and/or decomposition products were observed. In accordance with the results of *Bach et al.* (scheme 4.30), a lower temperature (70 instead of 85 °C) was also sufficient.

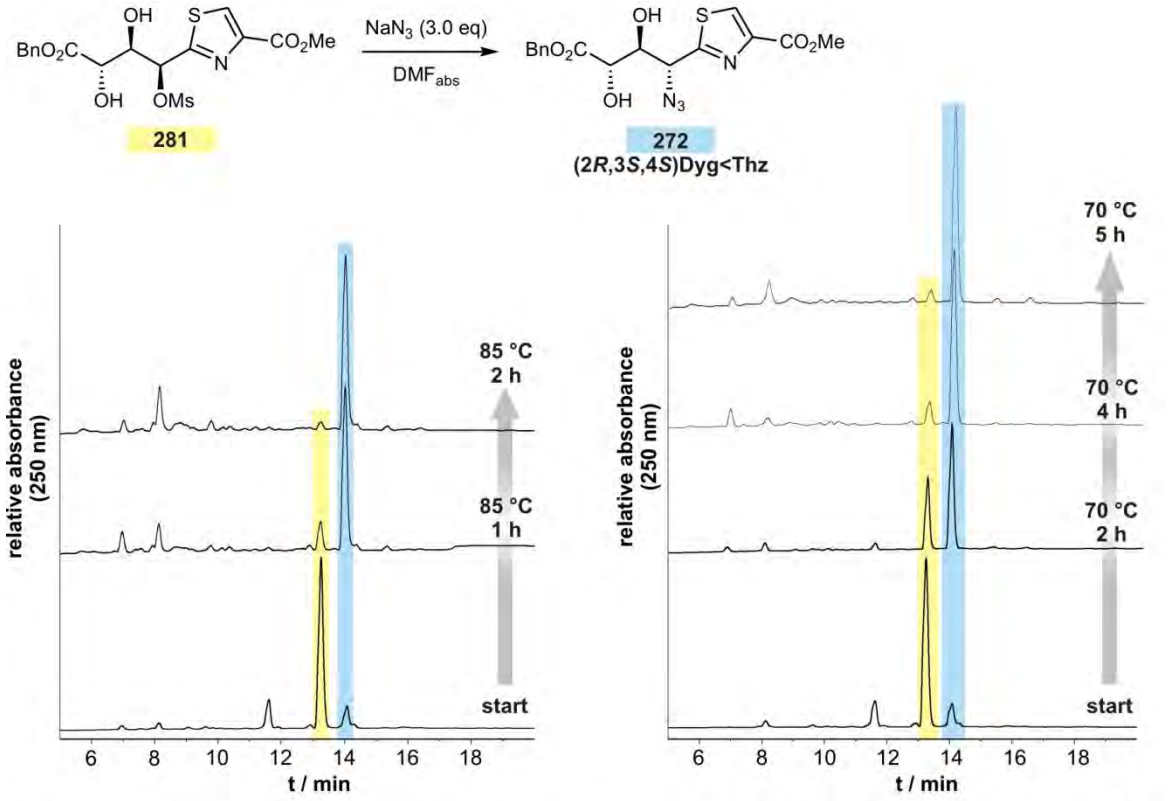

Figure 4.27 Monitoring of the mesylate/azide exchange (281 to 272) by analytical HPLC. *On the left, the HPLC diagrams obtained from the reaction at 85 °C are depicted, and the right side shows the monitoring of the reaction at lower temperature (70 °C). Peaks resulting from starting material and product are highlighted in blue and yellow, respectively. At lower temperature, a longer reaction time is required in order to obtain a > 90% conversion, but less hydrolysis and decomposition products are formed (peaks around 8 min elution time).*

Finally, the TBS deprotection of the D-arabino configured mesylate **264** also turned out to be a key to the first directed synthesis of the naturally occurring 2*S* configured Dyg<Thz (which at that time was accessible solely by epimerization of **268** under acidic conditions; figure 4.25, conditions d). In addition to the diol **281**, the *cis*-epoxide **282** was also obtained upon treatment

of **264** with TBAF, and both products could be easily separated from each other by column chromatography. In contrast to the *trans*-epoxide **280**, the azidation could not be carried out in DMF as solvent, but DMSO proved successful. The reaction was also carried out in the NMR tube in order to allow monitoring by ^{1}H NMR spectra (figure 4.28). As in the case of the conversion of **280** to **272** (figure 4.26), one single main product is obtained although a longer reaction time is required. The product is identical to the azide diol **273** which had been obtained as epimerization product after cleavage of the TBS ether of **268**.

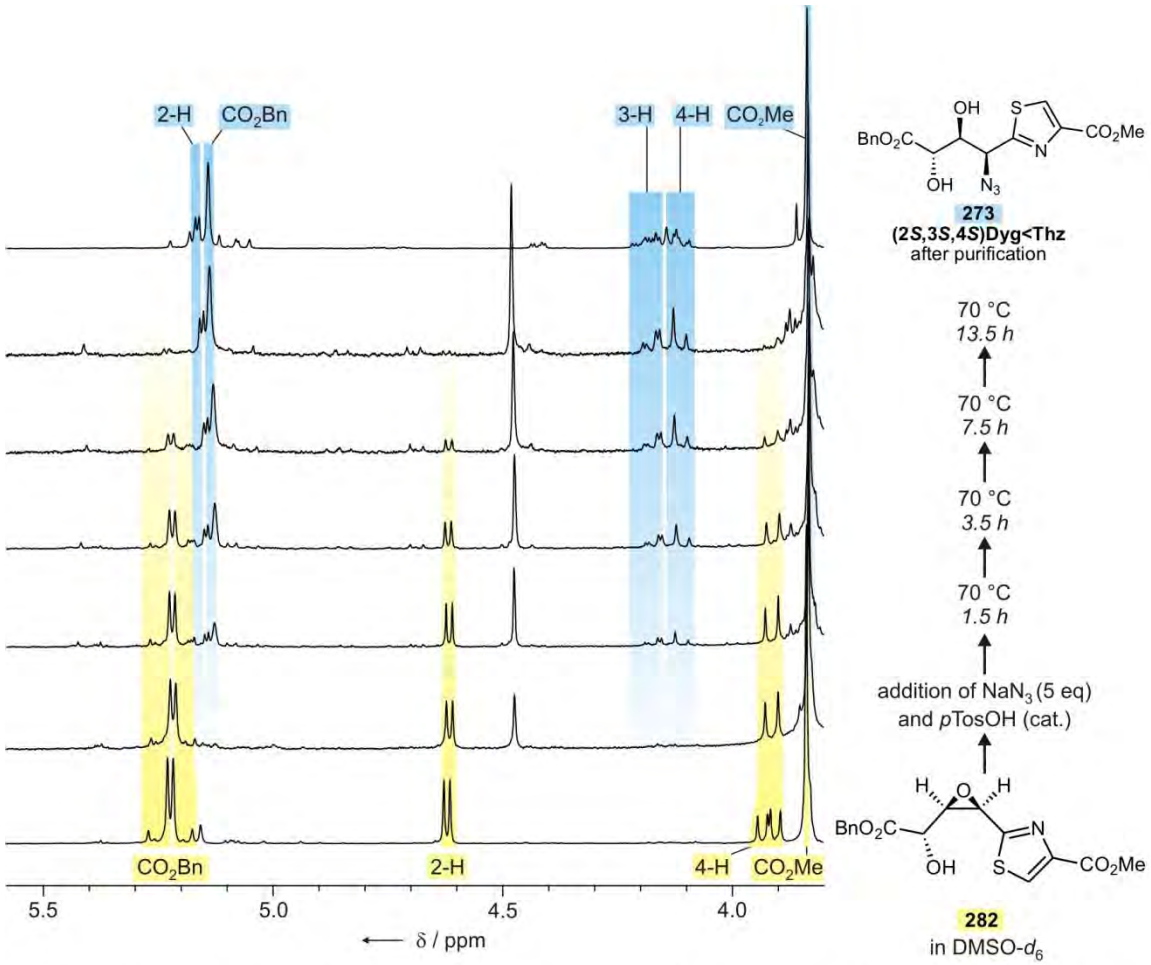

Figure 4.28 NMR monitoring of the azidation reaction of the epoxide 282 to the Dyg<Thz unit 273 with native 2S configuration. *The reaction was performed in the NMR tube, using DMSO-*d_6 *as solvent, at 70 °C, and* ^{1}*H NMR experiments (300 MHz, 300 K) were subsequently recorded after the respective heating times given on the right. The spectrum at the top was obtained from purified* **273** *which was obtained due to epimerization during the TBS cleavage of* **268** *(figure 4.25, conditions d). The different multiplet structures of the 3-H and 4-H signals in comparison with the NMR spectra of starting material* **282** *and purified product* **273** *result from the presence of acid which leads to a broadening of the OH proton signals and therefore simplifies the multiplets of the CH signals.*

In addition to the proposed azidation mechanisms, the absolute values of the optical rotations also allow to draw conclusions on the configurations at C-2 (figure 4.29).[473]

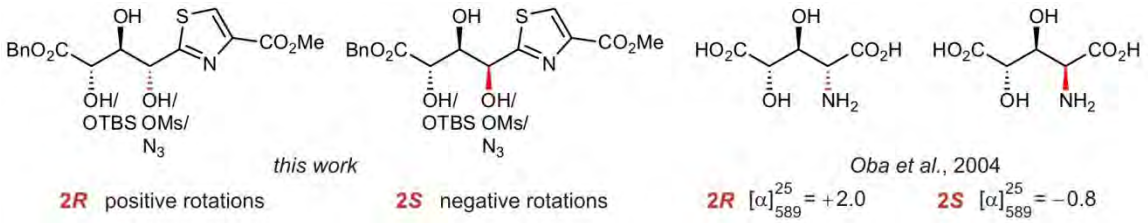

Figure 4.29 Comparison of optical rotations. *All synthesized* D*-ribo configured substrates (2*R*,3*S*,4*S*) showed positive values, while negative rotations were obtained for all* D*-arabino analogs independently of the hydroxyl functionalization and the presence of a hydroxyl or azido function at C-2. These observations were also made by* Oba et al. *in the case of fully deprotected 3,4-dihydroxyglutamic acids.*

Taken the results described in this section together, the regioselective activation of D-arabino and D-ribo configured thiazole triols can be used for the first synthetic access to the Dyg<Thz dipeptide core in the native (2*S*,3S,4*S*) configuration (**273**) and as 2*R* epimer (**272**). In the case of the TBS-protected substrates, the stereoselectivity of azide introduction is controlled by the absence or presence of a neighboring group (3-OH) effect which results in the formation of the 3*R* epimer independently of the starting configuration at C-2 (figure 4.25). As the presence of the bulky TBS group effected low azidation yields, the azidation reaction was also performed with the deprotected *trans*-epoxide **280** and with the diol **281**, which led to a clean conversion to the 2*R* epimer **272** which was monitored by HPLC and NMR (figures 4.26, 4.27 and 4.28), and the isolated yield was improved from 20% to 70%.

As the TBS deprotection of **264** also effected the formation of the *cis*-epoxide **282**, a route to the native 2*S* configured Dyg<Thz was also found (NMR monitoring in figure 4.28). However, additional studies are required to increase the yield of the epoxide **282** and to improve the azidation yield, which in the light of the good conversion as visible from the NMR monitoring may be caused by the workup procedure. In some preliminary experiments it was investigated whether the key *cis*-epoxide is accessible by another route. A possible alternative turned out to be the treatment of the TBS-protected mesylate **264** with KHMDS, which (in low yield, apparently due to partial decomposition) furnished the *cis*-epoxide **270** (scheme 4.32, a). The use of NaH as base afforded a complex product mixture, and K_2CO_3 as base in MeOH also effected epoxide formation, but a transesterification of the 6-benzyl- to the methylester also took place. Several attempts to generate the 4-OH deprotected epoxide **282** starting from the diol **281** were not successful (scheme 4.32).

However, the fact that the precursors of 2*S* as well as 2*R* configured Dyg<Thz (**282** and **281**, respectively) are both accessible from one single substrate, which is the D-arabino configured triol **264**, is advantageous from the standpoint of total synthesis as the oxidation/reduction sequence from the D-arabino to the D-ribo sugar chain (figure 4.24) is not required any more.

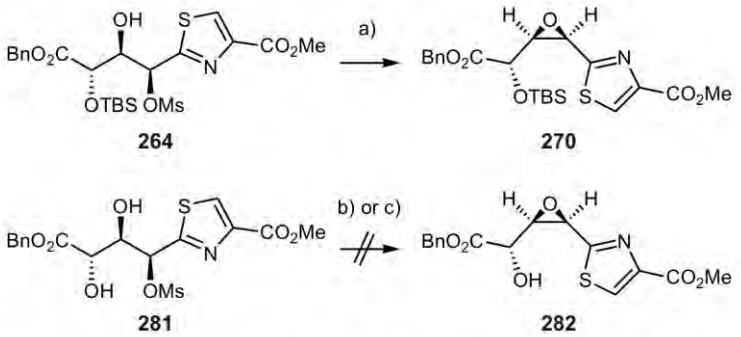

Scheme 4.32 Further attempts to selectively obtain* cis*-epoxides. Reagents and conditions: a) KHMDS (1.0 eq), THF_{abs}, −78 °C, 1 h, 16%; b) K_2CO_3 (1.0 eq), THF/H_2O 50:1, 0 °C to RT; c) KHMDS (1.0 eq), THF_{abs}, −78 °C, 1 h.

The next step in synthesis which has to be investigated concerns the reduction of the azides and their subsequent protection for example as Fmoc carbamates and the release of the thiazole carboxylic acid in order to obtain Dyg<Thz building blocks suitable for peptide synthesis protocols. The reduction of the azide in **272** was tested using *Staudinger* conditions,[474-476] and it turned out that the obtained amine **283** is difficult to handle as it readily cyclizes to the stable 5-membered lactam **284** under basic or neutral conditions (scheme 4.33). In addition, these compounds turned out to be highly polar. As determined by HPLC-ESI-MS, lactam formation can be suppressed by acidic workup which affords the ammonium salt **285**. In the next step, the side chain could be tailored adequately so that no lactam can be formed any more, and the amine should the be able to be protected in order to obtain dipepide building blocks with sufficiently lowered polarity.

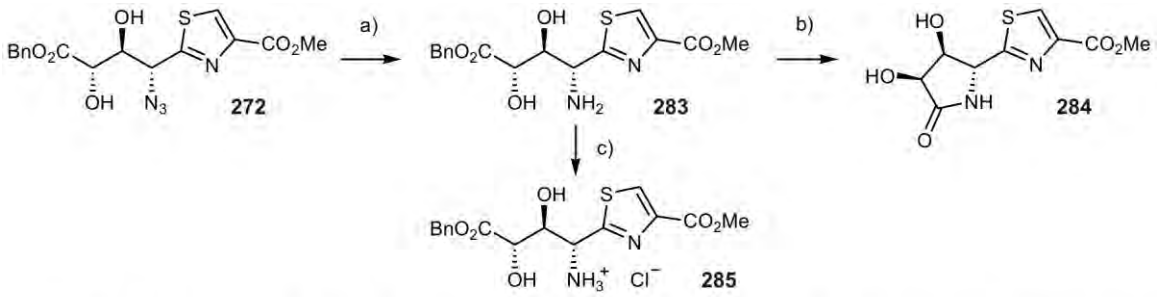

***Scheme 4.33 Preliminary studies concerning the reduction of the azide* 272.** Reagents and conditions: a) PPh_3 (2.0 eq), H_2O (2.0 eq), THF, 50 °C, 5 h; b) aqueous workup (neutral pH); c) aqueous workup (pH 4.5).

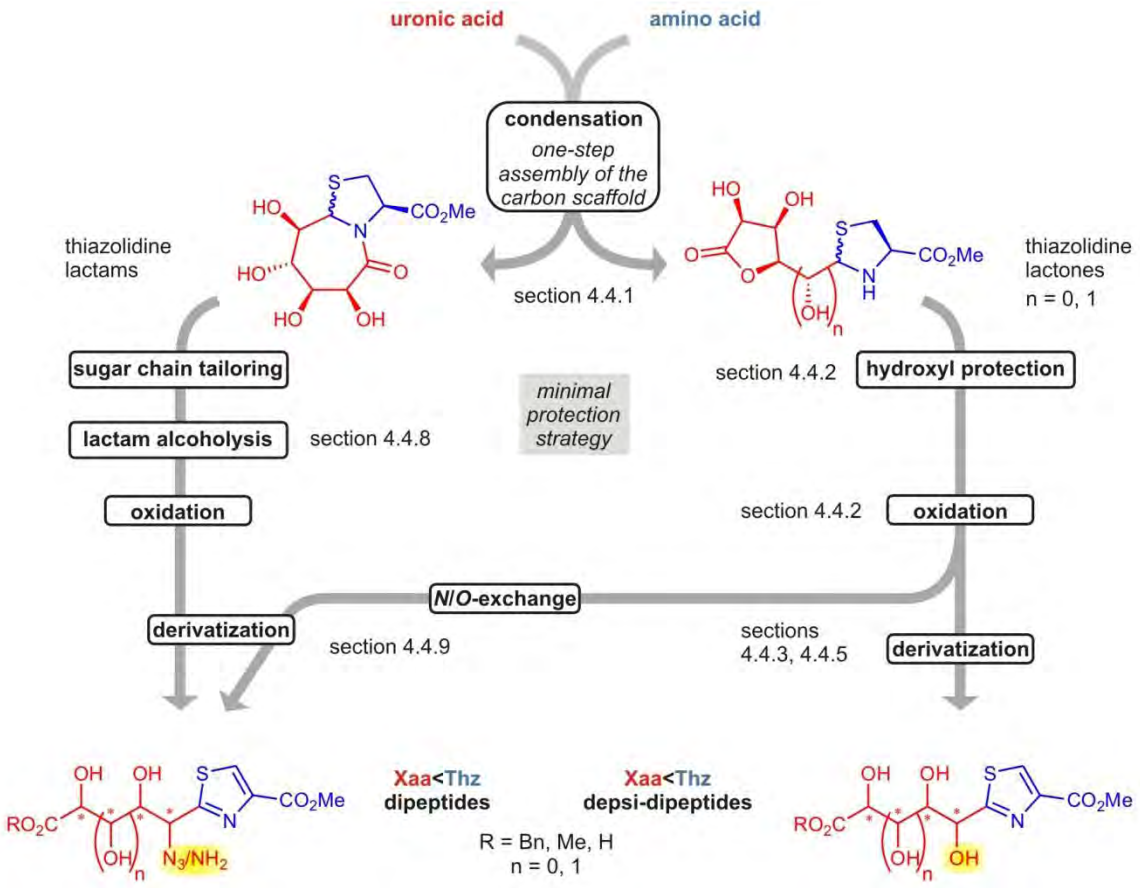

Figure 4.30 Synthesis of polyhydroxylated thiazole building blocks: strategy and general synthetic steps. *The stereopure and highly functionalized scaffolds of the thiazolidine lactams (left) and lactones (right) are already obtained in the first synthetic step and no protection of the sugar chains is required. The further pathway to the thiazole units follows a minimal protection strategy. Only two protecting group operations are required to obtain a thiazole dipeptide starting from the shown thiazolidine lactam (left), the lactone polyol shown on the right can be oxidized after a single protetion step. The sugar chain of the resulting thiazole polyol can in the following be tailored for the synthesis of various differently modified thiazole depsi-dipeptides. Alternatively,* N,O*-exchange operations afford further thiazole dipeptides.*

4.5 Summary and outlook

Within the scope of this work a synthetic access to thiazole depsipeptides and peptides was established which adds a reasonable new option to the various existing methodologies. For the construction of biologically relevant thiazole units with polyhydroxylated side chains this method proves superior as the high functionalization is already installed at the first stage of the synthesis. This is accomplished by using stereopure uronic acids and cysteine as starting material (figure 4.30) which is condensated to thiazolidine lactams and lactones. Remarkably, the high structural and functional complexity is generated in one single condensation step and, except for the methyl ester function of Cys, no protecting groups are required. It could be demonstrated that the resulting lactones, which had been considered as unstable intermediates in the lactam synthesis, can be adequately protected and subsequently oxidized to afford stereopure polyhydroxylated thiazole depsipeptides with different chain lengths and stereoconfigurations on the multigram scale (D-Glc<Thz (**140**), D-Ara<Thz (**148**), D-Rib<Thz (**279**), figure 4.31).

In order to exploit the structural complexity of these compounds, extensive studies concerning the selective protection and deprotection of the hydroxyl functions, requiring as few steps as possible, were performed. The various obtained protection group patterns and the options to tailor the sugar chain, the thiazole polyols have potential as precursors of Xaa<Thz depsipepdide motifs in natural products like the tubulyins.

The exchange of the hydroxyl against a nitrogen functionality, which gives access to the corresponding dipeptides, was shown to be viable in two ways (figure 4.30). The direct exchange proved to be dependent on neighboring group effects, and it was possible to install the azido function with inversion as well as retention of the C-2 stereoconfiguration of D-Ara<Thz. This enabled a first synthesis of the Dyg<Thz dipeptide with the amino function protected as an azide (**272**, **273**) which is of interest because of its function as central linking motif in the complex nocathiacin and thiazomycin thiopeptide antibiotics.

Due to the difficulties involved with the *N*/*O*-exchange in the case of the D-gluco configured thiazoles, an alternative strategy of azide introduction was established which bases on tailoring of the thiazolidine lactam sugar chain, intramolecular alcoholysis of the lactam, and final oxidation. The products exhibit the D-altrosamine configuration and thus the identical configuration as the native Dyg<Thz dipeptide, but they carry an additional CH(OH) functionality (highlighted in red) which could serve as additional functionalization site in corresponding

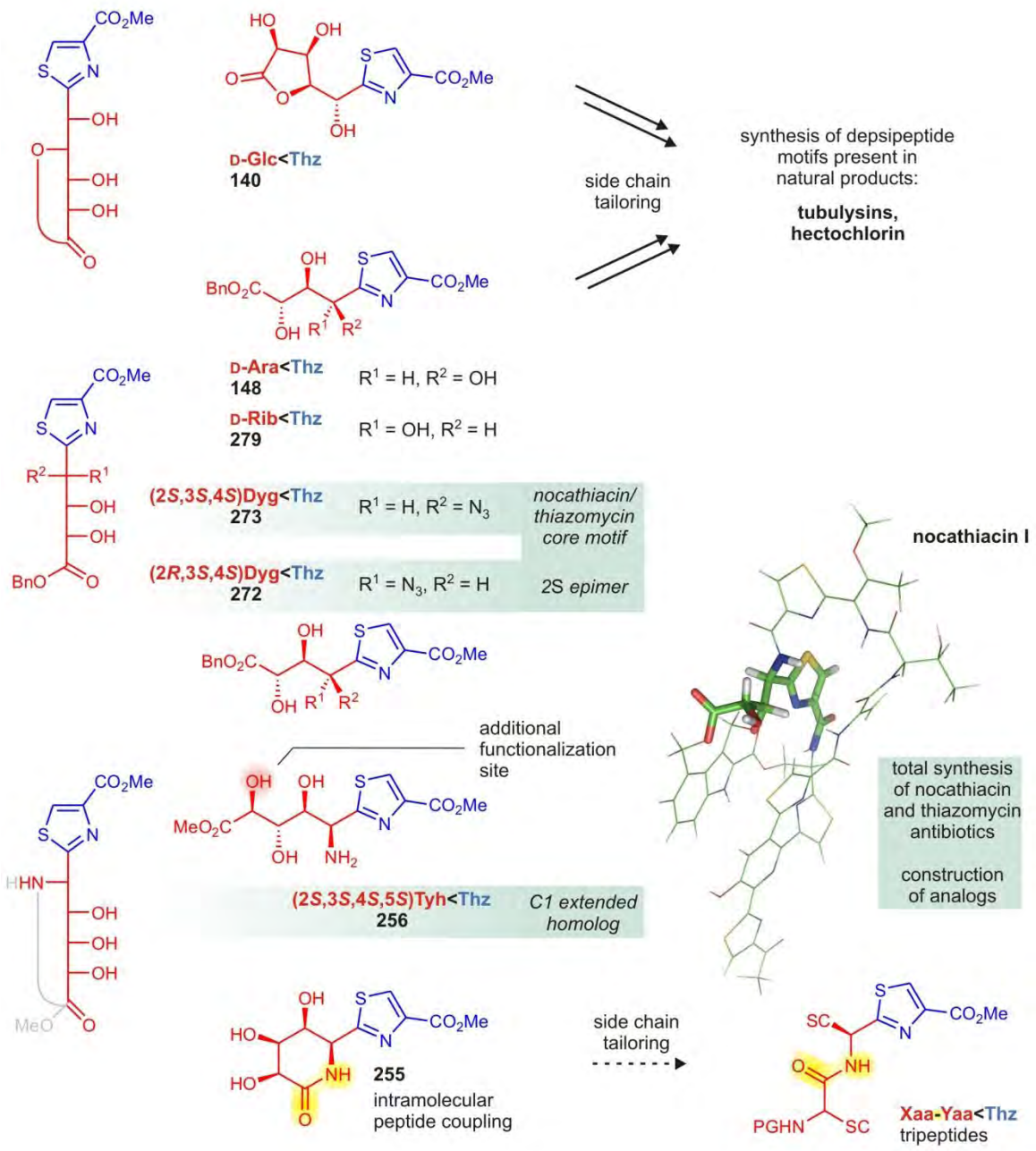

Figure 4.31 Comparison of synthesized thiazole depsi-dipeptides and dipeptides. *On the left, the various substrates are compared with respect to their chain lengths, functionalizations, and stereoconfigurations. Possible further synthetic modifications and applications are shown on the right. The Dyg<Thz and Tyh<Thz dipeptides (highlighted in green) can be used for the construction of nocathiacin and thiazomycin thiopeptide antibiotics and analogs thereof. In the shown NMR structure of nocathiacin I, the central Dyg<Thz core is emphasized by the depiction as sticks. In addition, the α-hydroxyl functionalized thiazols, which in this work have been shown to be available on the multigram scale, can in principle also be incorporated into depsipeptide analogs of thiopeptides.*

analogs of the nocathiacin/thiazomycin antibiotics (Tyh<Thz, **256**). Therefore, the established synthetic strategy does not only provide a structural key part of the antibiotics, the accessability of analogs thereof may lead to the synthesis of artificial thiopeptides with altered topology and/or functionalization, which is a prerequisite of characterizing and improving their biological activity and selectivity. In addition to the synthesized dipeptides, a possible access to thiazole tripeptide Xaa-Yaa<Thz is enabled by the lactam **255** (figure 4.31).

Finally, on basis of these results, the employment of further natural or artificially modified aldoses and uronic acids should enable to further extend the library of thiazole amino acids and polyols as building blocks for natural product synthesis.

5 Experimental section

5.1 General: Materials and methods

Solvents, reagents, inert gas

All solvents were distilled prior to use. For reactions which were sensitive to oxygen and moisture, absolute solvents were prepared as follows: CH_2Cl_2 was dried over CaH_2 and distilled in a nitrogen atmosphere directly prior to use; THF was dried over K/Na alloy and distilled in a nitrogen atmosphere directly prior to use; MeOH was dried over Mg, distilled, and stored over 4 Å molecular sieves; Tol was dried over Na, distilled, and stored over 4 Å molecular sieves.
DMF_{abs} and Pyr_{abs} were purchased from *Acros* and not further dried. If no DMF_{abs} was required, *peptide grade* DMF (purchased from *Iris Biotech*) was used.

All purchased reagents were not further purified prior to use.

Reactions with substrates, reagents, and catalysts sensitive to oxygen and moisture were run in a nitrogen atmosphere as inert gas. In addition, the reaction apparatus was baked out at 630 °C with a heat gun.

Analytical thin layer chromatography (TLC)

For reaction control by analytical TLC aluminium plates coated with silica gel 60 F_{254} were used (purchased from *Merck*). The chromatograms were processed by fluorescence extinction (UV lamp, λ = 254 nm) as well as by staining with one of the following solutions and subsequent heating to 260 °C (heat gun):

Mostain solution:	20.0 g of ammonium molybdate 400 mg of cerium(IV)sulfate in 400 mL of 10% aq. H_2SO_4.
Ninhydrin solution:	4.00 g of ninhydrin in 400 mL of EtOH.

Preparative flash chromatography

For the purification of synthesized compounds on the preparative scale, flash silica gel 60 (*Merck*, particle size 0.04-0.06 mm) was used. Elution was carried out at RT with compressed air. The length and diameter of the column as well as the fraction volume were determined individually according to the TLC of the raw product.

Preparative high-performance liquid chromatography (HPLC)

Purifications of crude pNPY and its Dha=Tap modified analogs by preparative HPLC (performed by *M. Haack*, *Beck-Sickinger* research group) were achieved on a *Shimadzu* HPLC system with a *Vydac* Protein & Peptides C18 column (218TP1022, 10 μm particle size, 300 Å pore diameter, 22 mm × 250 mm). A linear gradient 30%-60% of 0.08% TFA/CH_3CN in 0.1% TFA/H_2O was applied over 50 min (10 mL min^{-1}, 25 °C).

Purifications of crude peptide aldehydes by preparative HPLC were run by *F. Kopp*, *U. Linne* (*Marahiel* research group) or by the author using an *Agilent* 1100 HPLC system with diode array detection, vacuum degasser, quaternary pump, auto sampler, and HP-chemstation software. As HPLC column a reversed-phase Nucleodur C-18 (*Macherey & Nagel* 250/21, particle size 5 µm, pore diameter 100 Å) was used. A linear gradient 5%-55% of 0.1% TFA/CH_3CN in 0.1% TFA/H_2O was applied over 30 min (20 mL min^{-1}, 25 °C).

Analytical high-performance liquid chromatography (HPLC)

Analytical HPLC operations were run by the author using a *Dionex* system with diode array detection, a *Dionex* P680 dual gradient pump, auto sampler, and *Dionex Chromeleon* software. As HPLC column a reversed-phase *Dionex Acclaim* 120 (C-18, particle size 5 µm, pore diameter 120 Å, 4.6 x 150 mm) was used with a flow rate of 0.6 mL min (CH_3CN in 0.06% TFA/H_2O) and varying gradients (specified for the respective substrates).

Liquid chromatography-mass spectrometry (HPLC-ESI-MS)

HPLC-ESI-MS characterizations of the peptide aldehydes were run by *Dr. U. Linne* using an *Agilent* 1100 HPLC system with diode array detection, vacuum degasser, quaternary pump, auto sampler, and HP-chemstation software. As HPLC column a reversed-phase Nucleodur C-18 (*Macherey & Nagel* 125/2, particle size 3 µm, pore diameter 100 Å) was used. A linear gradient 10%-95% of 0.05% HCO_2H/CH_3CN in 0.05% HCO_2H/H_2O was applied over 50 min (0.2 mL min^{-1}, 45 °C).

Nuclear magnetic resonance (NMR) spectroscopy

The following spectrometers were used:

Routine measurements:

- *Bruker* DPX 250: 5 mm BBI dual probe head; 1D ^{1}H (250.13 MHz) and 1D ^{13}C (62.90 MHz) spectra;
- *Bruker* AV 300 A: 5 mm BBOF probe head; 1D ^{1}H (300.13 MHz) and 1D ^{13}C (100.61 MHz) spectra;
- *Bruker* AV 300 B: 5 mm BBI probe head; 1D ^{1}H (300.13 MHz) and 1D ^{13}C (100.61 MHz) spectra.

2D homo- and heteronuclear measurements for assignment and structure elucidation:

- *Bruker* DRX 400: 5 mm TXI probe head; 1D ^{1}H (400.06 MHz), 1D ^{13}C (100.61 MHz), and 2D spectra;
- *Bruker* DRX 500: 5 mm TXI probe head; 1D ^{1}H (500.13 MHz), 1D ^{13}C (125.76 MHz), and 2D spectra;
- *Bruker* AV 500: 5 mm BBFO probe head; 1D ^{1}H (500.20 MHz), 1D ^{13}C (125.79 MHz), and 2D spectra.

Peptide analytics with water suppression using excitation sculpting with gradients (DPFGSE-WATERGATE technique), as well as 2D homo- and heteronuclear measurements for assignment and structure elucidation:

- *Bruker* AV 600: 5 mm BBI probe head; 1D ^{1}H (600.13 MHz), 1D ^{13}C (150.90 MHz), and 2D spectra.

All NMR measurements were carried out at 300 K unless otherwise noted. The measurements at the DRX 400 and DRX 500 spectrometers were performed by members of staff of the NMR department, and the measurements at the AV 500 and AV 600 spectrometers were performed either by the author or by members of staff of the NMR department. The chemical shifts δ are given in parts per million (ppm) and they were determined from the center of the respective coupling pattern. The solvent signals were used as internal standard ($CDCl_3$: $\delta(^{1}H)$ = 7.26 ppm, $\delta(^{13}C)$ = 77.16 ppm; DMSO-d_6: $\delta(^{1}H)$ = 2.50 ppm, $\delta(^{13}C)$ = 39.52 ppm; D_2O: $\delta(^{1}H)$ = 4.80 ppm).
All ^{13}C spectra were recorded using broadband decoupling. The ^{1}H/^{1}H coupling constants are given in Hertz (Hz). All coupling patterns were characterized according to their actual appearance (phenomenological data) and not according to the multiplicity which is theoretically expected. The coupling constants were identified from *Lorentz-to-Gauss* transformed ^{1}H NMR spectra. The multiplicities are indicated as follows: s = singlet, d = dublet, t = triplet, dd = dublet of dublets, ddd = dublet of dublet of dublets, pt = pseudo triplet, dpt = dublet of pseudo triplet, m = multiplet, br = broad signal. Diastereomeric proton pairs which could not be assigned as pro*R* and pro*S* are marked with the index ^{u} for the up-field shifted and ^{d} for the down-field shifted proton. The assignment of ^{1}H and ^{13}C resonance signals was carried out by using 2D NMR experiments (homonuclear: COSY, TOCSY, NOESY, ROESY; heteronuclear: HSQC, HMQC, HMBC). All data were recorded and analyzed using *Bruker TopSpin* software.
For temperature series of NMR measurements, the temperature was increased from 280 K or 290 K to 320 K or 330 K in 10 K steps. The samples were allowed to equilibrate in the spectrometer 1 h prior to the first measurement.

Mass spectrometric analysis

All (–)ESI and (+)ESI measurements were performed by members of staff of the analytics department using a *Finnigan* MAT 95 spectrometer. In all cases, the high-resolution spectra were compared to a spectrum calculated on basis of the molecular formula.

Infrared spectroscopy (IR)

The IR spectra were either recorded on a *Bruker* interferometer IFS 88 by members of staff of the analytics department or on a *Bruker* Alpha spectrophotometer by *Y. Raeva* (*Geyer* research group) or by the author.

Optical rotation measurements

All optical rotation values were determined on a *Perkin-Elmer* 241 polarimeter by *Y. Raeva* (*Geyer* research group) or by the author. The values $[\alpha]_{\lambda}^{T}$ (T = temperature, λ = wave length) are given in [mL (mg dm)$^{-1}$]. The length of the used vessel was 1.0001 dm.

Melting points

The melting points were determined on a *Dr. Tottoli* apparatus by *Y. Raeva* (*Geyer* research group) or by the author.

Molecular modeling procedures

Interproton-distance restraints were derived from homonuclear NOESY or ROESY experiments and classified into three categories strong (approx. 2.2 Å), medium (approx. 3 Å), and weak (approx. 4 Å), serving as distance restraints for the structure calculations. For all calculations the program package *HyperChem* was used using MM+ force field without explicit water included, and no explicit parametrization was used. Ten snapshots were taken from the 10 x 10 ps molecular dynamics simulations (step size 1 fs, 300 K) and averaged. In order to prove the plausibility of the average structures obtained, they were subjected to energy minimization after the NOE constraints had been removed, and controlled for major changes in the distances. The structures obtained by this operation are shown in the main section. The program package *PyMol* (*DeLano Scientific*) was used for the visualization of the results.

5.2 Experimental data: chapter 2

5.2.1 Synthesis of the Dha=Tap building block

The synthesis of (3*R*)-6-amino-5-oxo-2,3-dihydro-5*H*-[1,3]thiazolo[3,2-α]pyridine-3-carboxylic acid (Dha=Tap) was performed by *H. Seger* and it has been described recently.[79] In brief, bicyclic condensation of D-aldurono-2,5-lactone and L-cysteine methylester hydrochloride led to a precursor whose α-hydroxy group had been activated and substituted by azide. Elimination of two hydroxyl groups in the presence of MsCl and NEt_3 followed by immediate hydrogenation (H_2 and Pd/C) in MeOH and subsequent protection with Fmoc-OSu in acetone and acidic ester hydrolysis led to the N^{α}-Fmoc-protected pyridone carboxylic acid.

5.2.2 Peptide synthesis and purification

The synthesis of pNPY and Dha=Tap modified analogs was performed by *M. Haack* (*Beck-Sickinger* research group, University of Leipzig) and details have been described in the corresponding publication.[38] The peptides were assembled by automated multiple solid phase peptide synthesis using the orthogonal Fmoc/*t*Bu strategy and coupling on Rink amide resin (30 mg, loading 0.6 mmol g^{-1}) to obtain C-terminally amidated peptides. The Dha=Tap building block and the N-terminally preceding amino acid were introduced by a manual coupling step. The peptides were precipitated from ice-cold diethyl ether, collected by centrifugation, washed four times, and finally dissolved in *tert*-butanol/water 1:3 and lyophilized.

After purification by preparative HPLC, characterization of the peptides was performed by matrix-assisted laser desorption/ionization (MALDI) mass spectrometry on a *Voyager* DE-RP workstation and by analytical HPLC on a *Merck-Hitachi* D/L-7000 HPLC system (*Hitachi*, Tokyo, Japan) with a reversed-phase *Vydac* Protein & Peptides C18 column (218TP54, 5 μm particle size, 300 Å pore diameter, 4.6 mm × 250 mm) A linear gradient 10%-60% of 0.08% TFA/CH_3CN in 0.1% TFA/H_2O was applied over 30 min (0.6 mL min^{-1}, 25 °C).

Table 5.1 Mass spectrometric data of synthesized pNPY and its analogs. *The nomenclature [m=n] indicates the substitution of residues m and n by a Dha=Tap unit. See table 2.4 and figure 2.13 for structural details.*

compound	**calculated mass** $[M+H]^+$ / Da	**observed mass** $[M+H]^+$ / Da
pNPY	4254.7	4254.6
[1=2]	4188.7	4188.7
[2=3]	4264.8	4264.9
[4=5]	4223.7	4224.3
[5=6]	4236.8	4236.7
[7=8]	4237.7	4237.7
[8=9]	4294.8	4295.0
[12=13]	4280.8	4280.9
[1=2,4=5]	4157.6	4157.6
[2=3,5=6]	4246.8	4246.9
[1=2,7=8]	4171.7	4171.3
[2=3,8=9]	4304.8	4304.7
[4=5,7=8]	4206.7	4206.6
[2=3,8=9]	4276.8	4276.6
[1=2,4=5,7=8]	4140.6	4140.3
[2=3,5=6,8=9]	4286.8	4287.2

5.2.3 Binding assays

The binding assays using $N^{\varepsilon 4}$-[propionyl-^{3}H]-pNPY as radioligand were performed by *M. Haack* (*Beck-Sickinger* research group, University of Leipzig) and details have been described in the corresponding publication.

5.2.4 NMR measurements and data

The peptides were dissolved in 0.6 mL of H_2O/D_2O (5:1) containing 80 to 100 eq of perdeuterated sodium dodecyl sulfate (SDS-d_{25}, peptide concentrations listed in table 2.5). All measurements were performed on a *Bruker* AV 600 spectrometer with a 5 mm BBI probe head. Water suppression was achieved by excitation sculpting with gradients (DPFGSE-WATERGATE technique).[182] Homonuclear 2D spectra (TOCSY, NOESY) were recorded at 320 K in the phasesensitive mode as data matrices of 512 (t_1) real × 2048 (t_2) complex data points; 48 scans (TOCSY) and 80 scans (NOESY), respectively, were used per t_1 increment. The used spectral widths were between 6602 and 9014 Hz. Mixing times of 100 ms (TOCSY) and 150 ms (NOESY) were applied. Heteronuclear 2D HSQC experiments of native NPY and monosubstituted derivatives were performed at 300 and 320 K in the phase-sensitive mode with data matrices of 512 (t_1, ^{13}C) real × 2048 (t_2, ^{1}H) complex data points and 80 scans per t_1 increment. The used spectral width was 7211 (^{1}H) and 24146 Hz (^{13}C). The HSQC measurement of [1=2,4=5,7=8] was carried out at 320 K with data matrices of 384 (t_1, ^{13}C) real × 2048 (t_2, ^{1}H) complex data points, 160 scans were performed per t_1 increment, and spectral widths of 8013 (^{1}H) and 12073 Hz (^{13}C) were chosen. All data were recorded and analyzed using Bruker TopSpin software. The spectra were calibrated on the well-separated SDS-CH_3 signal which appears temperature-independent at 0.772 ppm. This chemical shift is related to sodium 3-(trimethylsilyl)propionic acid as an internal reference with δ = 0.00 ppm.

The assignment of the spectra obtained from native pNPY is described in the main section. Identified chemical shifts observed in the Dha=Tap modified analogs are given in figure 2.30 for [5=6], figure 2.31a for [2=3], figure 2.31b for [8=9], and figure 2.38 as well as table 2.6 for [1=2,4=5,7=8], respectively.

Table 5.2 ^{1}H chemical shifts of native pNPY (H_2O/D_2O 5:1, 80 eq SDS-d_{25}, 600 MHz, 320 K).
n.d. = not determined due to signal overlap.

residue	NH	α-H	β-H	γ-H	δ-H	other
Tyr[1]	n.d.	4.20	3.00	--	--	6.86 (3,5-H), 7.21 (2,6-H)
			3.17			
Pro[2]	--	4.56	2.38	1.89	3.81	
				1.91		
Ser[3]	n.d.	4.53	3.82	--	--	
Lys[4]	7.40	4.34	1.75	1.49	1.73	7.95 (ε-NH_3^+)
Pro[5]	--	4.44	2.23	1.91	3.60	
				2.00		
Asp[6]	n.d.	4.63	2.80	--	--	
			2.83			
Asn[7]	8.11	5.00	2.68	--	--	
			2.83			
Pro[8]	--	4.40	2.25	1.99	3.73	
				2.09		
Gly[9]	n.d.	3.91	--	--	--	
Glu[10]	n.d.	4.33	2.13	2.42	--	
Asp[11]	n.d.	n.d.	2.82	--	--	
Ala[12]	7.93	3.94	1.50	--	--	
Pro[13]	--	4.39	2.23	n.d.	3.73	
Ala[14]	7.98	4.53	1.40	--	--	
Glu[15]	n.d.	n.d.	2.12	2.50	--	
Asp[16]	n.d.	4.73	n.d.	--	--	
Leu[17]	8.03	4.06	1.65	1.79	0.95	
Ala[18]	7.99	4.12	1.45	--	--	
Arg[19]	n.d.	n.d.	n.d.	n.d.	n.d.	
Tyr[20]	n.d.	n.d.	n.d.	--	--	6.76 (3,5-H), 7.04 (2,6-H)
Tyr[21]	n.d.	n.d.	n.d.	--	--	6.79 (3,5-H), 7.06 (2,6-H)
Ser[22]	7.98	4.52	3.78	--	--	
Ala[23]	7.74	4.24	1.64	--	--	
Leu[24]	8.21	4.16	1.65	1.84	0.98	
Arg[25]	8.26	4.23	1.79	1.52	3.00	
His[26]	8.54	4.52	3.25	--	--	6.57 (4-H), 8.54 (2-H)
			3.35			

(continued on next page)

(continued from previous page)

Tyr[27]	8.15	4.20	2.99	--	--	6.82 (3,5-H), 7.09 (2,6-H)
			3.08			
Ile[28]	8.41	3.78	2.00	1.76	0.86	0.95 (γ-CH_3)
Asn[29]	8.16	4.34	2.84	--	--	
			2.94			
Leu[30]	7.64	4.06	1.62	1.83	0.83	
Ile[31]	7.84	3.98	2.00	1.76	0.83	0.95 (γ-CH_3)
Thr[32]	8.03	4.18	4.33	1.30	--	
Arg[33]	7.81	4.13	1.80	1.60	3.14	
Gln[34]	7.93	4,18	2.12	2.35	--	
Arg[35]	n.d.	4.12	1.80	1.62	n.d.	
Tyr[36]	n.d.	n.d.	n.d.	--	--	6.79 (3,5-H), 7.13 (2,6-H)

5.2.5 Molecular modeling

The NOE contacts and their intensities which were used as restraints for the molecular modeling studies are shown by assigned blue arrows in figure 2.30a for [5=6], figure 2.31a for [2=3], figure 2.31b for [8=9], and figure 2.38 for [1=2,4=5,7=8], respectively.

5.3 Experimental data: chapter 3

5.3.1 Peptide aldehyde syntheses and purification procedures

5.3.1.1 Preparation of ncpA1-CHO, ncpA2-CHO, and TycA-CHO

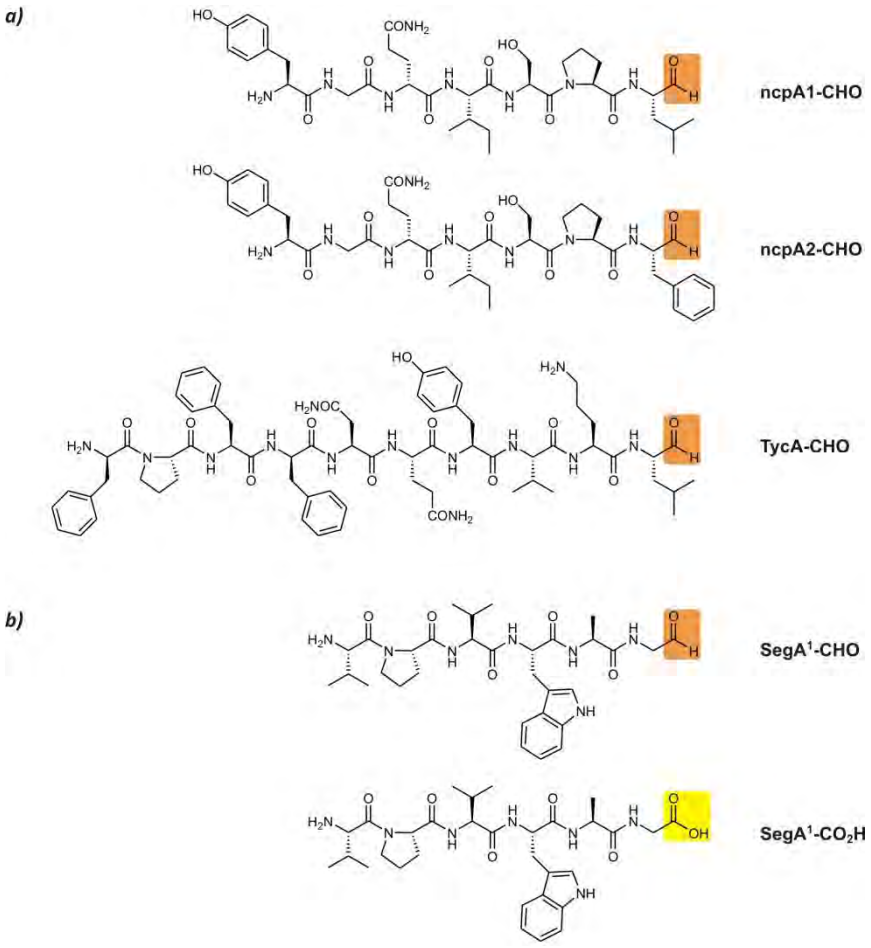

Figure 5.1 Peptide aldehydes and peptides synthesized by automated SPPS (a) and manual SPPS (b).

The syntheses of the linear cyclization precursors ncpA1-CHO, ncpA2-CHO and TycA-CHO (scheme 5.1a) were carried out by *F. Kopp* (*Marahiel* research group) on an automated peptide synthesizer (APEX 396 synthesizer, *Advanced ChemTech*) using a solid phase peptide synthesis (SPPS) protocol (0.1 mmol scale) which has been described previously.[178] As solid support, NovaSyn TG resin (*NovaBiochem*) with the C-terminal aldehyde immobilized as oxazolidine was used (see figure 3.17; for ncpA1-CHO and TycA-CHO: L-Leu aldehyde; for ncpA2-CHO: L-Phe aldehyde). The crude peptide aldehydes were precipitated in hexane, dissolved in CH_3CN/H_2O

and purified by preparative HPLC. After lyophilization, the peptide aldehydes were obtained as a colorless solids.

Yields (based on resin loading):
ncpA1-CHO: 14.6% (11.1 mg, 14.6 µmol);
ncpA2-CHO: 12.5% (9.9 mg, 12.5 µmol);
TycA-CHO 7.2% (9.1 mg, 7.2 µmol).

The peptides were subsequently characterized by HPLC-ESI-MS (table 5.3).

Table 5.3 *ESI-MS analysis of peptide aldehydes synthesized by automated SPPS.*

compound	molecular formula	calculated mass $[M+H]^+$ / Da	observed mass $[M+H]^+$ / Da
ncpA1-CHO	$C_{36}H_{56}N_8O_{10}$	761.4	761.4
ncpA2-CHO	$C_{39}H_{54}N_8O_{10}$	795.4	795.4
TycA-CHO	$C_{66}H_{89}N_{13}O_{13}$	1272.7	1272.7

The HPLC-ESI-MS analyses of ncpA1-CHO, ncpA2-CHO and the respective cyclization products were performed by *U. Linne* and *F. Kopp* (*Marahiel* research group) and they have been described elsewhere.[178]

The characterizations of TycA-CHO and the cyclization products were carried out by *U. Linne* (*Marahiel* research group) and the author. The identity of the peptide aldehyde obtained after preparative HPLC and lyophilization was confirmed by analytical HPLC-ESI-MS. Figure 5.2 shows the UV trace of the HPLC-ESI-MS analysis (a) as well as the FTMS ion chromatograms for the masses corresponding to TycA-$CH(OH)_2$ (b) and TycA-CHO (c).

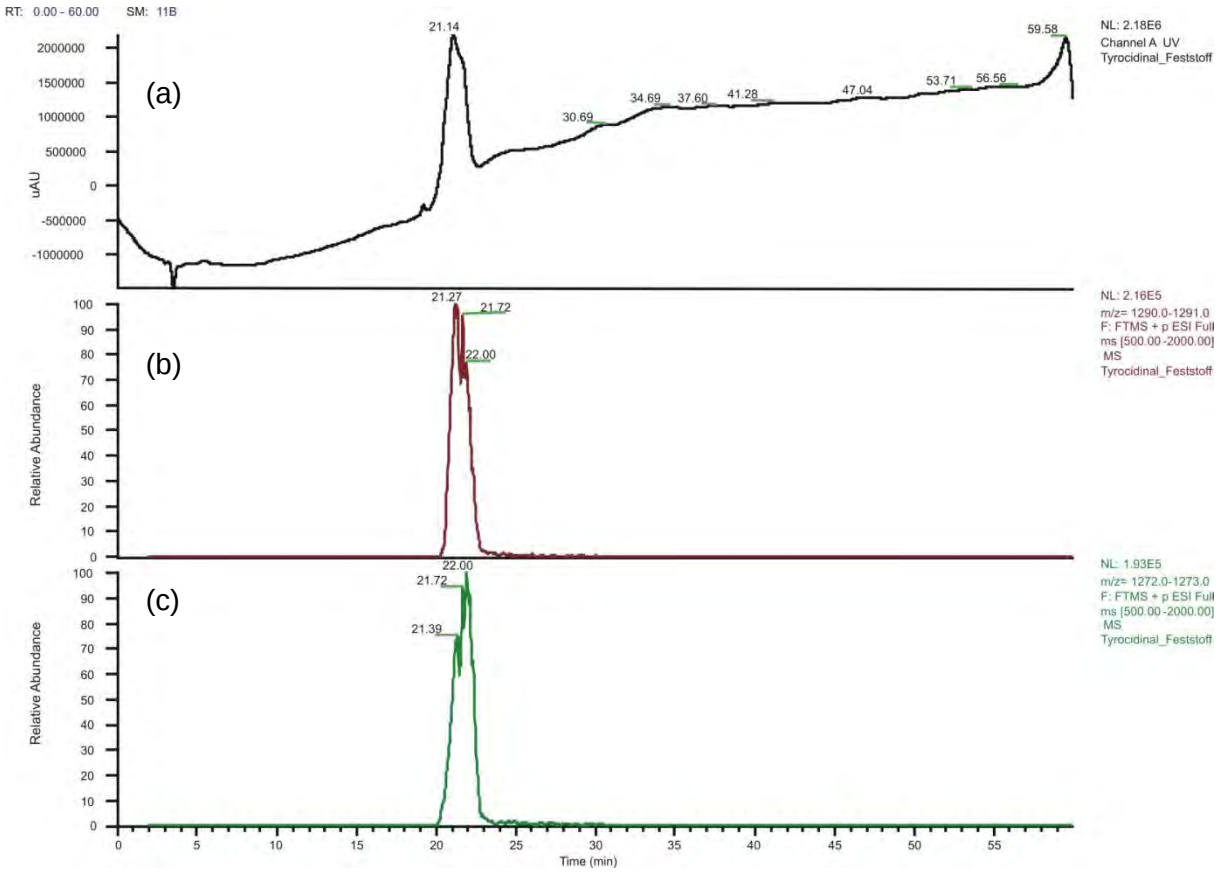

Figure 5.2 *HPLC-ESI-MS analysis of TycA-CHO. (a) UV trace (215 nm). (b) FTMS spectrum for m/z = 1290.0 - 1291.0 (Tyc-CH(OH)$_2$). (c) FTMS spectrum for m/z = 1272.0 - 1273.0 (TycA-CHO).*

The integrated mass spectrum over the main peak retention time (20.78 - 22.03 min) is shown in section 3.5, figure 3.41 and the section of m/z = 630 - 660 is shown in section 3.5, figure 3.42. The macrocyclic hemiaminal Ψ[CH(OH)NH]-TycA and the linear aldehyde Tyc-CHO have identical molecular weight ($[M + 2H]^{2+}$ = 636.84). As a cyclic methyl aminal (Ψ[CH(OMe)NH]-TycA) in contrast would be identifiable by its $[M + 2H]^{2+}$ = 643.85 signal an additional experiment was performed in order to detect this species, which is described in section 3.5. Table 5.4 summarizes calculated and observed masses of all linear species (pH 3.0) and of the cyclization products (pH 9.0).

Table 5.4 *ESI-MS analysis of TycA-CHO and its cyclization products.*

compound	molecular formula	calculated mass $[M+2H]^{2+}$ / Da	observed mass $[M+2H]^{2+}$ / Da
TycA-CHO	$C_{66}H_{89}N_{13}O_{13}$	636.8424	636.8437
TycA-$CH(OH)_2$	$C_{66}H_{91}N_{13}O_{14}$	645.8477	645.8488
Ψ[C=N]-TycA	$C_{66}H_{87}N_{13}O_{12}$	627.8371	627.8366
Ψ[CH(OH)NH]-TycA	$C_{66}H_{89}N_{13}O_{13}$	636.8424	636.8430
Ψ[CH(OMe)NH]-TycA	$C_{67}H_{91}N_{13}O_{13}$	643.8502	643.8507

5.3.1.2 Preparation of $SegA^1$-CHO and $SegA^1$-CO_2H

The syntheses of the linear segetalin precursors $SegA^1$-CO_2H and $SegA^1$-CHO (scheme 5.1b) were carried out by the author by manual SPPS protocols using glass frits. Fmoc-Gly-H was synthesized in two steps from Fmoc-Gly-OH (section 5.3.1.3 and 5.3.1.4) and subsequently loaded on H-Thr-Gly-NovaSyn® TG resin (*NovaBiochem*) according to protocol A (section 5.3.1.4.1). Using this Fmoc-Gly-H coupled resin, the manual SPPS of $SegA^1$-CO_2H was performed according to protocol B (section 5.3.1.4.2). For the synthesis of $SegA^1$-CO_2H, Fmoc-Gly-loaded 2-chlorotrityl resin (provided by *A. Jansen de Salazar*, *Geyer* research group) was used and the SPPS protocol C (section 5.3.1.4.3) was applied.

5.3.1.3 Synthesis of N^{α}-Fmoc-Gly *N*,*O*-dimethylhydroxamic acid

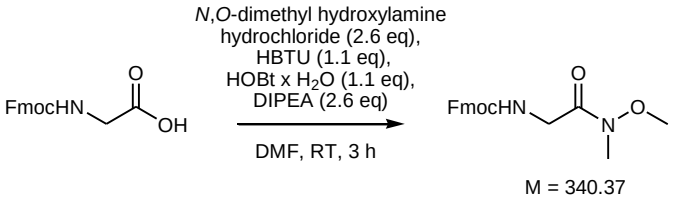

Preparation:

N^{α}-Fmoc-Gly-OH	M = 297.31 g mol^{-1}	1.0 eq	6.29 mmol	1.87 g
HBTU	M = 379.25 g mol^{-1}	1.1 eq	6.92 mmol	2.62 g
HOBt x H_2O	M = 153.14 g mol^{-1}	1.1 eq	6.92 mmol	1.06 g
DIPEA	M = 129.25 g mol^{-1}, ρ = 0.76	2.6 eq	16.4 mmol	2.78 mL (2.11 g)
N,*O*-dimethylhydroxylamine hydrochloride	M = 97.55 g mol^{-1}	2.6 eq	16.4 mmol	1.60 g
DMF				20 mL

1.87 g of Fmoc-Gly-OH (6.29 mmol, 1.0 eq) were dissolved in 20 mL of DMF. To this solution were added (in the following order) 2.62 g of HBTU (6.92 mmol, 1.1 eq), 1.06 g of HOBt x H_2O (6.92 mmol, 1.1 eq), 2.78 mL of DIPEA (2.11 g, 16.4 mmol, 2.6 eq), and finally 1.60 g of *N*,*O*-dimethylhydroxylamine hydrochloride (16.4 mmol, 2.6 eq). After stirring at RT for 3 h, the mixture was diluted with 200 mL of EtOAc, washed three times with 5% aq. $NaHCO_3$, two times with 10% aq. citric acid, and three times with brine. The organic phase was dried over $MgSO_4$, filtered, and concentrated *in vacuo* to afford the *Weinreb* amide in quantitative yield (2.14 g, 6.29 mmol) as pale yellow waxy solid. The analytical data are in accordance with the literature.

TLC: R_f = 0.59 (EtOAc/Tol 7:1).

ESI-MS: *m*/*z* = 363 $[M+Na]^+$.

HRMS: $[M+Na]^+$: $C_{19}H_{20}N_2O_4Na$, calculated: 363.1315, found: 363.1317.

^{1}H-NMR: 300 MHz, $CDCl_3$: δ = 3.23 (s, 3 H, NCH_3), 3.73 (s, 3 H, OCH_3), 4.17 (d, 2 H, $^3J_{\alpha\text{-H/NH}}$ = 4.5 Hz, α-H), 4.24 (t, 1 H, $^3J_{\text{Fmoc-CH/Fmoc-CH2}}$ = 7.2 Hz, Fmoc-CH), 4.39 (d, 2 H, $^3J_{\text{Fmoc-CH2/Fmoc-CH}}$ = 7.2 Hz, Fmoc-CH_2), 7.29-7.34 (m, 2 H, Fmoc-$CH_{arom.}$), 7.37-7.43 (m, 2 H, Fmoc-$CH_{arom.}$), 7.61-7.63 (m, 2 H, Fmoc-$CH_{arom.}$), 7.75-7.78 (m, 2 H, Fmoc-$CH_{arom.}$).

^{13}C-NMR: 75 MHz, $CDCl_3$: δ = 32.6 ($N\underline{C}H_3$), 42.3 (α-C), 47.3 (Fmoc-$\underline{C}$H), 61.7 ($O\underline{C}H_3$), 67.3 (Fmoc-$\underline{C}H_2$), 120.1, 125.3, 127.2, 127.8 (each Fmoc-$\underline{C}H_{arom.}$), 141.5, 144.1 (each Fmoc-$C_{arom., quart.}$), 156.5 (Gly-$\underline{C}$O). Fmoc-$\underline{C}$O invisible.

5.3.1.4 Synthesis of N^{α}-Fmoc-Gly-H

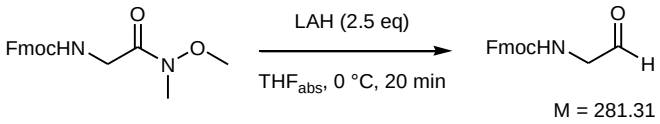

M = 281.31

Preparation:

N^{α}-Fmoc-Gly *N*,*O*-dimethylhydroxamic acid	M = 340.37 g mol^{-1}	1.0 eq	0.50 mmol	170 mg
LAH	M = 37.95 g mol^{-1}	2.5 eq	1.25 mmol	47 mg
THF_{abs}				1.5 mL

170 mg of N^{α}-Fmoc-Gly *N*,*O*-dimethylhydroxamic acid (0.05 mmol, 1.0 eq) were dissolved in 1.5mL of THF_{abs} in a nitrogen atmosphere and cooled to 0 °C. To this solution were added 47 mg of LAH in small portions over 15 min under vigorous stirring. The mixture was stirred for 5 min at 0 °C, carefully diluted with 5 mL of EtOAc and 4 mL of 10% aq. citric acid, and stirred for another 15 min at RT. The phases were separated and the aqueous phase was extracted three times with 1.5 mL of EtOAc. The combined organic phases were washed with 2.5 mL of 5% aq. $NaHCO_3$, 2.5 mL of H_2O, and 2.5 mL of 1 N HCl. After drying with brine (2 x 3 mL) and over $MgSO_4$, the solution was filtered and concentrated *in vacuo* to afford the Gly aldehyde in quantitative yield (141 mg, 0.50 mmol) as a colorless solid.

TLC: R_f = 0.64 (EtOAc/Tol 3:1).

ESI-MS: *m*/*z* = 336 $[M+MeOH+Na]^+$ (formation of methyl acetal in MeOH).

HRMS: $[M+MeOH+Na]^+$: $C_{18}H_{19}NO_4Na$, calculated: 336.1206, found: 336.1199.

IR: pellet; $\tilde{\nu}$ = 3337, 1686, 1535, 1449, 1409, 1282, 1255, 1167, 1104, 1010, 993, 869, 797, 757, 735 cm^{-1}.

^{1}H-NMR: 300 MHz, $CDCl_3$: δ = 4.17 (d, 2 H, $^{3}J_{\alpha\text{-H/NH}}$ = 5.0 Hz, α-H), 4.24 (t, 1 H, $^{3}J_{\text{Fmoc-CH/Fmoc-CH2}}$ = 7.1 Hz, Fmoc-CH), 4.43 (d, 2 H, $^{3}J_{\text{Fmoc-CH2/Fmoc-CH}}$ = 7.1 Hz, Fmoc-CH_2), 7.30-7.35 (m, 2 H, Fmoc-$CH_{arom.}$), 7.39-7.44 (m, 2 H, Fmoc-$CH_{arom.}$), 7.59-7.61 (m, 2 H, Fmoc-$CH_{arom.}$), 7.76-7.79 (m, 2 H, Fmoc-$CH_{arom.}$), 9.67 (s, 1 H, CHO).

^{13}C-NMR: 75 MHz, $CDCl_3$: δ = 47.3 (Fmoc-CH), 51.8 (α-C), 67.4 (Fmoc-CH_2), 120.2, 125.7, 127.2, 127.9 (each Fmoc-$CH_{arom.}$), 141.5, 143.9 (each Fmoc-$C_{arom., quart.}$), 196.4 (CHO). Fmoc-CO invisible.

5.3.1.4.1 SPPS protocol A*:* Loading of H-Thr-Gly-NovaSyn TG resin with C-terminal amino acid aldehyde and capping of oxazolidine nitrogen as Boc carbamate.

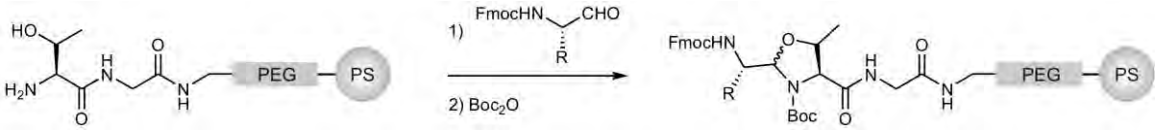

Scheme 5.2 *Loading of H-Thr-Gly resin with amino acid aldehyde and oxazolidine capping. R = amino acid side chain.*

a) 30 min swelling of the resin in 1% AcOH in CH_2Cl_2/MeOH 1:1;
b) addition of Fmoc-protected amino acid aldehyde (5.0 eq) in CH_2Cl_2;
c) 4 h incubation at RT;
d) washing with CH_2Cl_2, DMF, and THF (each 3 x 2 min);
e) 3 h incubation with Boc_2O (5.0 eq) and NMM (5.0 eq) in THF at 50 °C;
f) washing with CH_2Cl_2, DMF, and THF (each 3 x 2 min).

5.3.1.4.2 SPPS protocol B*:* Manual synthesis of peptide aldehydes.

a) 30 min swelling of amino acid aldehyde-loaded resin (protocol A) in DMF;
b) Fmoc-deprotection: 1 x 10 min and 1 x 20 min incubation with DBU/piperidine/DMF 2:2:96;
c) washing with DMF, *i*PrOH, THF, and MeOH (each 3 x 2 min);
d) chain elongation: 60 min incubation with the Fmoc-protected amino acid (3.0 eq), PyBOP (3.0 eq), HOBt (0.5 eq), and DIPEA (6.0 eq) in DMF;
e) washing with DMF, *i*PrOH, THF, and MeOH (each 3 x 2 min);

[repeat steps b) to e) until assembly of the target sequence except the N-terminal residue]

f) coupling of Boc-protected N-terminal amino acid (3.0 eq): 60 min incubation with PyBOP (3.0 eq), HOBt (0.5 eq), and DIPEA (6.0 eq) in DMF;
g) removal of Boc and side chain protecting groups: 2 x 10 min incubation with 100% TFA;
h) washing with CH_2Cl_2, (1 x 2 min);
i) cleavage of peptide aldehyde: 30 min incubation with AcOH/H_2O/CH_2Cl_2/MeOH 10:5:63:21.

5.3.1.4.3 SPPS protocol C: Manual synthesis of peptides.

a) 30 min swelling of Fmoc-Gly-loaded resin (provided by *A. Jansen de Salazar*, *Geyer* research group) in DMF;
b) Fmoc-deprotection: 1 x 10 min and 1 x 20 min incubation with DBU/piperidine/DMF 2:2:96 or 25% piperidine in DMF;
c) washing with DMF, MeOH, and CH_2Cl_2 (each 3 x 2 min);
d) chain elongation: 60 min incubation with the Fmoc-protected amino acid (2.0 eq), HBTU (3.0 eq), HOBt (2.0 eq), and DIPEA (4.0 eq) in DMF;
e) washing with DMF, *i*PrOH, THF, and MeOH (each 3 x 2 min);

[repeat steps b) to e) until assembly of the target sequence]

f) removal of side-chain protecting groups and cleavage of peptide: 60 min incubation with 95% TFA in H_2O, then washing with MeOH (3 x 2 min).

5.3.1.4.4 Peptide purification and analysis

The peptide solutions obtained after cleavage from the resin were concentrated *in vacuo* to a volume of approx. 0.5 mL and the peptides were subsequently precipitated from dry Et_2O at −20 °C, and lyophilized after centrifugation. SegA^1-CO_2H was characterized by analytical HPLC and ESI-MS, and SegA^1-CO_2H was characterized by HPLC-ESI-MS. In both cases, an approx. 80% purity was determined and the products were not further purified prior to NMR spectroscopic analysis.

SegA^1-CO_2H: 49% (17.3 mg, 27.6 µmol) based on resin loading, colorless solid.

RT (HPLC): 5%-70% CH_3CN in 0.08% TFA/H_2O (25 min, 25 °C): 12.11 min.

ESI-MS: m/z = 628 $[M+H]^+$.

HRMS: $[M+H]^+$: $C_{31}H_{45}N_7O_7H$, calculated: 628.3453, found: 628.3445.

The HPLC analysis of SegA^1-CHO (dissolved in MeOH/H_2O with a trace of TFA) showed two main signals. The ESI of the first fraction showed the presence of mainly aldehyde hydrate (SegA^1-$CH(OH)_2$), methyl acetal (SegA^1-CH(OMe)OH) and aldehyde (SegA^1-CHO) while the dimethyl acetal SegA^1-$CH(OMe)_2$ was the only product identified from the second fraction. All calculated and observed masses are listed in table 5.5.

SegA^1-CHO: 11.3% (5.0 mg, 8.2 µmol), pale yellow solid.

RT (HPLC-ESI-MS): 5%-70% 0.05% HCOOH/CH_3CN in 0.05% TFA/H_2O (50 min, 45 °C): 12.55 min (fraction 1) and 14.42 min (fraction 2).

Table 5.5 *HPLC-ESI-MS analysis of SegA^1-CHO and further linear species.*

fraction	compound	molecular formula	calculated mass $[M+H]^+$ / Da	observed mass $[M+H]^+$ / Da
1	SegA^1-CHO	$C_{31}H_{45}N_7O_6$	612.3504	612.3504
1	SegA^1-$CH(OH)_2$	$C_{31}H_{47}N_7O_7$	630.3609	645.3604
1	SegA^1-CH(OMe)OH	$C_{32}H_{49}N_7O_7$	644.3766	644.3768
2	SegA^1-$CH(OMe)_2$	$C_{33}H_{51}N_7O_7$	658.3923	658.3915

5.3.2 NMR measurements and data

All measurements were performed on a *Bruker* AV 600 spectrometer with a 5 mm BBI probe head. The peptide and SDS-d_{25} concentrations in the samples are given in table 5.6.

Table 5.6 *Prepared peptide NMR samples. In all cases, a partially deuterated H_3PO_4/KH_2PO_4 buffer solution (H_2O/D_2O 5:1) at pH 3.0 was used as solvent (sample 4: 0.6 mL, all other samples: 0.72 mL).*

sample no.	compound	amount of peptide/ mg	peptide concentration/ mmol L^{-1}	amount of SDS-d_{25}/ mg	SDS-d_{25} concentration/ mmol L^{-1}	concentration ratio SDS-d_{25}/ peptide
1	ncpA1-CHO	3.0	5.48	--	--	--
2	ncpA2-CHO	3.0	5.25	--	--	--
3	TycA-CHO	3.5	3.82	--	--	--
4	TycA-CHO	1.8	2.35	36	190	80
		+ 1.4[1)]	4.18			45
5	SegA[1]-CHO	5.0	11.4	--	--	--
6	SegA[1]-CO_2H	3.0	6.64	--	--	--

1) the additional amount was added at later stage for the determination of the temperature-dependence of the equilibrium.

Water suppression was achieved by using excitation sculpting with gradients (DPFGSE-WATERGATE technique).[182] Homonuclear 2D spectra (TOCSY, NOESY) were recorded in the phase-sensitive mode as data matrices of 512 (t_1) real x 2048 (t_2) complex data points; 16 or 32 scans were used per t_1 increment. The used spectral widths were 6010 Hz in each dimension for both TOCSY and NOESY experiments. Mixing times of 100 ms (TOCSY) and 150 to 200 ms (ROESY) were applied. Heteronuclear 2D HSQC experiments were performed in the phase-sensitive mode with data matrices of 512 or 1024 (t_1, ^{13}C) real x 2048 (t_2, ^{1}H) complex data points and 16 to 32 scans per t_1 increment. The used spectral widths were 6010 (^{1}H) / 22640 Hz (^{13}C). All data were recorded and analyzed using *Bruker TopSpin* software. The spectra of the samples 1, 2, 5 and 6 were calibrated on the H_2O resonance (4.80 ppm at 300 K).[187] The spectra of the TycA sample 4 containing SDS-d_{25} were calibrated on the residual SDS methyl signal which appears temperature independent at 0.772 ppm. The spectra obtained from the TycA sample 3 (without SDS-d_{25}) were calibrated on the polyethylene glycol (PEG) signal (residual PEG from resin) which occurs at 3.637 ppm in the spectra calibrated on the residual SDS methyl signal. All identified proton chemical shifts are listed in the following tables. Assigned spectra are shown in

figure 3.25 (ncpA1 species), figure 3.26 (ncpA2 species), and in figures 3.38 and 3.39 (TycA species), respectively. In tables 5.10 and 5.11 the temperature coefficients of the amide proton signals are listed for ncpA1/A2 and TycA species, respectively.

Table 5.7 *^{1}H chemical shifts (in ppm) and $^{3}J_{H/H}$ scalar coupling constants (in Hz) of ncpA1 species (600 MHz, 300 K) in H_3PO_4/KH_2PO_4 buffer (H_2O/D_2O 5:1). Linear peptides: pH 3.0; ncpA1: pH 7.0.*

position		***R*-Leu^{7}-ncpA1-CH(OH)$_2$**	***S*-Leu^{7}-ncpA1-CH(OH)$_2$**	**ncpA1**
Tyr^{1}	NH_3^+	7.02-7.20 m	7.02-7.20 m	--
	α-H	4.24 *t* (7.3)	4.24 *t* (7.3)	3.91 *dd* (3.4, 11.6)
	β-H	3.12 *dd* (7.3, 14.1)	3.12 *dd* (7.3, 14.1)	2.76 *dd* (11.6, 14.2)
		3.17 *dd* (7.3, 14.1)	3.17 *dd* (7.3, 14.1)	3.30 *dd* (3.4, 14.2)
	2,6-H	7.15 *d* (8.6)	7.15 *d* (8.6)	7.01 *d* (8.6)
	3,5-H	6.88 *d* (8.6)	6.88 *d* (8.6)	6.75 *d* (8.6)
	OH	invisible	invisible	invisible
Gly^{2}	NH	8.57 *t* (6.0)	8.57 *t* (6.0)	8.16 *dd* (3.3,10.0)
	α-H	3.90 *dd* (6.0, 16.7)	3.90 *dd* (6.0, 16.7)	3.73 *dd* (3.3, 17.2)
		3.98 *dd* (6.0, 16.7)	3.98 *dd* (6.0, 16.7)	4.63 [1)]
D-**Gln^{3}**	NH	8.36 *d* (7.2)	8.35 *d* (7.2)	8.63 *d* (5.9)
	α-H	4.41 *m*	4.41 *m*	4.39 *m*
	β-H	1.99 *m*	1.99 *m*	2.04 *pq* (8.1)
		2.11 *m*	2.11 *m*	
	γ-H	2.37 *t* (7.6)	2.37 *t* (7.6)	2.36 *m*
	$CONH_2$ (*Z*)	6.87 *br s*	6.87 *br s*	6.88 *br s*
	$CONH_2$ (*E*)	7.53 *br s*	7.53 *br s*	7.57 *br s*
Ile^{4}	NH	8.29 *d* (8.2)	8.29 *d* (8.2)	8.65 *d* (7.7)
	α-H	4.22 *t* (8.0)	4.22 *t* (8.0)	4.25 *m*
	β-H	1.89 *m*	1.89 *m*	2.08 *m*
	γ-Me	0.90 *d* (7.0)	0.90 *d* (7.0)	0.99 *d* (7.2)
	γ-H	1.18 *m*	1.18 *m*	1.30 *m*
		1.43 *m*	1.43 *m*	1.39 *ddd* (4.6, 7.8, 13.6)
	δ-H	0.86 *t* (7.6)	0.86 *t* (7.6)	0.91 *t* (7.7)
Ser^{5}	NH	8.44 *d* (6.6)	8.42 *d* (6.6)	7.66 *d* (8.7)
	α-H	4.74 [1)]	4.74 [1)]	5.06 *pq* (8.6)
	β-H	3.83 *m*	3.83 *m*	4.03 *d* (8.1)
	OH	invisible	invisible	invisible
Pro^{6}	α-H	4.45 *d* (4.1)	4.45 *d* (4.5)	4.52 *dd* (3.5, 9.5)
	β-H	1.99 *m*	1.99 *m*	2.00 *m* (pro*R*)
		2.25 *m*	2.25 *m*	2.28 *m* (pro*S*)
	γ-H	1.99 *m*	1.99 *m*	2.07 *m* (pro*R*)
				1.95 *m* (pro*S*)
	δ-H	3.73 *m*	3.73 *m*	3.88 *m* (pro*R*)
		3.79 *m*	3.79 *m*	3.98 *m* (pro*S*)
Leu^{7}	NH	7.76 *d* (9.6)	7.71 *d* (9.6)	7.73 *d* (9.1)
	α-H	3.90 *m*	3.87 *m*	4.43 *m*
	β-H	1.40 *m*	1.41 *m*	0.98 *m*
				1.03 *m*
	γ-H	1.50 *m*	1.55 *m*	1.23 *m*
	δ-H	0.84 *d* (6.9)	0.84 *d* (6.9)	0.74 *d* (7.2)
		0.91 *d* (6.9)	0.91 *d* (6.9)	0.82 *d* (7.2)
	CHO	9.57 *s*	9.62 *s*	--
	C<u>H</u>$(OH)_2$	4.93 [1)]	4.90 [1)]	--
	CH$(O$<u>H</u>$)_2$	invisible	invisible	--
	CH=N	--	--	7.07 *d* (2.0)

1) no coupling constants were obtained due to weak or broad signals.

Table 5.8 *^{1}H chemical shifts (in ppm) and $^{3}J_{H/H}$ scalar coupling constants (in Hz) of ncpA2 species (600 MHz, 300 K) in H_3PO_4/KH_2PO_4 buffer (H_2O/D_2O 5:1). Linear peptides: pH 3.0; ncpA2: pH 7.0.*

position		***R*-Phe^{7}-ncpA2-CH(OH)$_2$**	***S*-Phe^{7}-ncpA2-CH(OH)$_2$**	**ncpA2**
Tyr^{1}	NH_3^+	7.01-7.20 m	7.01-7.20 m	--
	α-H	4.24 *t* (7.3)	4.24 *t* (7.3)	3.96 *dd* (3.6, 11.3)
	β-H	3.12 *dd* (7.2, 14.1)	3.12 *dd* (7.2, 14.1)	2.76 *dd* (11.2, 14.1)
		3.16 *dd* (7.2, 14.1)	3.16 *dd* (7.2, 14.1)	3.30 *dd* (3.5, 14.1)
	2,6-H	7.15 *d* (8.6)	7.15 *d* (8.6)	7.14 *d* (8.6)
	3,5-H	6.88 *d* (8.6)	6.88 *d* (8.6)	6.89 *d* (8.6)
	OH	invisible	invisible	invisible
Gly^{2}	NH	8.56 *dd* (6.0, 6.4)	8.56 *dd* (6.0, 6.4)	8.16 *dd* (3.3,10.0)
	α-H	3.91 *m*	3.91 *m*	3.73 *dd* (3.3, 17.4)
		3.96 *m*	3.96 *m*	4.63 [1)]
D-**Gln^{3}**	NH	8.35 *d* (7.2)	8.35 *d* (7.2)	8.45 [1)]
	α-H	4.40 *m*	4.40 *m*	4.39 *t* (8.0)
	β-H	1.99 *m*	1.99 *m*	2.04 *m*
		2.11 *m*	2.11 *m*	
	γ-H	2.37 *t* (7.6)	2.37 *t* (7.6)	2.36 *m*
	$CONH_2$ (*Z*)	6.87 *br s*	6.87 *br s*	6.88 *br s*
	$CONH_2$ (*E*)	7.52 *br s*	7.52 *br s*	7.57 *br s*
Ile^{4}	NH	8.29 *d* (8.1)	8.29 *d* (8.1)	8.61 [1)]
	α-H	4.20 *t* (8.1)	4.22 *t* (8.1)	4.26 *d* (4.6)
	β-H	1.88 *m*	1.88 *m*	2.06 *m*
	γ-Me	0.89 *d* (7.0)	0.89 *d* (7.0)	0.99 *d* (7.1)
	γ-H	1.18 *m*	1.18 *m*	1.30 *ddd* (7.6, 9.7, 13.5)
		1.43 *m*	1.43 *m*	1.39 *ddd* (4.6, 7.6, 13.5)
	δ-H	0.85 *t* (7.5)	0.85 *t* (7.5)	0.92 *t* (7.6)
Ser^{5}	NH	8.40 *d* (6.7)	8.42 *d* (6.4)	7.66 *d* (8.9)
	α-H	4.66 *m*	4.69 *m*	5.04 *ddd* (6.7, 8.9, 9.6)
	β-H	3.74 *dd* (7.3, 11.0) (pro*R*)	3.81 *dd* (7.5, 11.0) (pro*R*)	3.99 *dd* (9.6, 10.6)
		3.80 *dd* (7.5, 11.0) (pro*S*)	3.88 *dd* (6.4, 11.0) (pro*S*)	4.03 *dd* (6.7, 10.6)
	OH	invisible	invisible	invisible
Pro^{6}	α-H	4.28 *d* (9.8)	4.36 *d* (9.6)	4.40 *d* (3.7, 9.1)
	β-H	1.27 *m* (pro*R*)	1.53 *m* (pro*R*)	1.45 *m* (pro*R*)
		1.98 *m* (pro*S*)	2.03 *m* (pro*S*)	2.05 *m* (pro*S*)
	γ-H	1.80 *m* (pro*R*)	1.79 *m* (pro*R*)	1.83 *m* (pro*R*)
		1.66 *m* (pro*S*)	1.47 *m* (pro*S*)	1.38 *m* (pro*S*)
	δ-H	3.68 *m* (pro*R*)	3.67 *m* (pro*R*)	3.79 *m*
		3.53 *m* (pro*S*)	3.57 *m* (pro*S*)	
Phe^{7}	NH	7.98 *d* (9.8)	7.55 *d* (9.6)	7.80 *d* (9.3)
	α-H	4.15 *m*	4.13 *m*	4.72 [1)]
	β-H	2.64 *m*	2.66 *m* (pro*R*)	2.22 *dd* (10.7, 14.2) (pro*R*)
		3.09 *dd* (4.7, 14.5)	3.09 *dd* (4.7, 14.5) (pro*S*)	2.76 *dd* (4.9, 14.2) (pro*S*)
	2,6-H	7.35 *d* (7.5)	7.25 *d* (7.5)	7.07 *m*
	3,5-H	7.29 *t* (7.5)	7.35 *t* (7.5)	7.33 *m*
	4-H	7.35 *d* (7.5)	7.28 *d* (7.5)	7.27 *m*
	CHO	9.57 *s*	9.62 *s*	--
	$C\underline{H}(OH)_2$	5.07 *d* (4.3)	4.99 *d* (4.9)	--
	$CH(O\underline{H})_2$	invisible	invisible	--
	CH=N	--	--	7.17 *d* (2.0)

1) no coupling constants were obtained due to weak or broad signals.

Table 5.9 *^{1}H chemical shifts (in ppm) of TycA species (600 MHz, 300 K) in H_3PO_4/KH_2PO_4 buffer (H_2O/D_2O 5:1).*
Left: TycA-CH(OH)$_2$ without SDS-d$_{25}$ at pH 3.0.
Middle: TycA-CH(OH)$_2$ in the presence of SDS-d$_{25}$ (80 eq, 0.19 mol L^{-1}) at pH 3.0.
Right: Ψ[CH(OH)NH]-TycA in the presence of SDS-d$_{25}$ (80 eq, 0.19 mol L^{-}) at pH 9.0.

position		TycA-CH(OH)$_2$	TycA-CH(OH)$_2$ SDS-d_{25}	Ψ[CH(OH)NH]-TycA SDS-d_{25}
D-	NH_3^+	1)	1)	--
Phe^1	hemiaminal-NH	--	--	5.33
	α-H	4.46	4.49	3.73
	β-H	3.07	3.13	2.67
		3.17	3.39	2.95
	2,6-H	2)	2)	2)
	3,5-H	2)	2)	2)
	4-H	2)	2)	2)
Pro^2	α-H	4.17	4.14	3.99
	β-H	1.43	1.24	1.62
		1.81	1.60	1.74
	γ-H	1.35	1.04	0.86
			1.15	1.13
	δ-H	2.60	3.39	2.33
		3.35	3.42	3.22
Phe^3	NH	8.12	7.66	6.99
	α-H	4.54	4.58	4.77
	β-H	2.82	2.82	2.18
		2.95	3.05	2.68
	2,6-H	2)	2)	2)
	3,5-H	2)	2)	2)
	4-H	2)	2)	2)
D-	NH	8.00	7.90	8.68
Phe^4	α-H	4.43	4.58	5.60
	β-H	2.82	3.11	2.89
		2.90	3.23	3.07
	2,6-H	2)	2)	2)
	3,5-H	2)	2)	2)
	4-H	2)	2)	2)
Asn^5	NH	8.33	8.18	9.00
	α-H	4.53	4.49	4.89
	β-H	2.49	2.54	3.04
			2.68	3.35
	$CONH_2$	1)	1)	1)
Gln^6	NH	8.18	8.17	8.33
	α-H	4.15	4.27	4.00
	β-H	1.82	1.91	1.68
		1.87		1.83
	γ-H	2.09	2.12	1.60
		2.14		1.82
	$CONH_2$	1)	1)	1)

(continued on next page)

(continued from previous page)

Tyr[7]	NH	8.12	8.20	8.19
	α-H	4.48	4.44	4.50
	β-H	2.84	2.88	2.91
		2.98	3.07	3.13
	2,6-H	7.02	7.11	7.05
	3,5-H	6.73	6.78	6.79
	OH	1)	1)	1)
Val[8]	NH	7.73	7.73	7.73
	α-H	3.95	4.12	4.39
	β-H	1.88	2.09	2.10
	β-Me	0.81	0.90	1.01
			0.94	
Orn[9]	NH	8.25	7.96	8.37
	α-H	4.22	4.43	5.16
	β-H	1.79	1.74	1.88
			1.85	2.04
	γ-H	1.66	1.67	1.67
			1.73	1.71
	δ-H	2.96	3.00	2.87
	δ-NH_3^+	7.53	7.44	1)
Leu[10]	NH	7.84	7.49	7.73
	α-H	3.83	3.91	4.19
	β-H	1.33	1.37	1.31
				1.34
	γ-H	1.45	1.52	1.63
	γ-Me	0.75	0.82	0.97
		0.83	0.85	
	CHO	9.42	9.42	--
	C<u>H</u>$(OH)_2$	4.86	4.88	--
	CH$(O$<u>H</u>$)_2$	1)	1)	--
	C<u>H</u>(OH)NH	--	--	4.43
	CH(O<u>H</u>)NH	--	--	1)

1) precise assignment was not possible due to fast chemical exchange with H_2O; 2) The Phe aromatic protons could not be precisely assigned due to signal overlap.

Table 5.10 *^{1}H chemical shifts (in ppm) and $^{3}J_{H/H}$ scalar coupling constants (in Hz) of SegA species (600 MHz, 300 K) in H_3PO_4/KH_2PO_4 buffer (H_2O/D_2O 5:1) at pH 9.0. The shifts of the N-terminal tripeptide are similar in the linear species and in the cyclization product and could not be precisely determined due to signal overlap.*

position		SegA[1]-CH(OH)$_2$	side chain(Trp[4] NH)-to-backbone cyclization product (*R* epimer)
Val[1]	NH_2	invisible	
	α-H	3.80	
	β-H	2.06	
	β-Me	0.93, 1.01	
Pro[2]	α-H	4.39	
	β-H	1.39, 2.07	
	γ-H	1.89	
	δ-H	3.54, 3.71	
Val[3]	NH	8.17	
	α-H	4.00	
	β-H	2.04	
	β-Me	0.92, 0.96	
Trp[4]	NH	7.93	8.59
	α-H	4.68	4.40
	β-H	3.28	3.00 (pro*S*), 3.35 (pro*R*)
	2-H	7.26	6.92
	4-H	7.64	7.73
	5-H	7.18	7.27
	6-H	7.26	7.31
	7-H	7.51	7.86
	NH	10.20	--
Ala[5]	NH	7.88	invisible
	α-H	4.23	4.26
	β-H	1.21	1.23
Gly[6]	NH	7.45	6.96 *dd* (5.5, 7.5)[1)]
	α-H	3.17	3.58, 3.92
	CHO	9.41	--
	C<u>H</u>(OH)$_2$	4.86	--
	CH(O<u>H</u>)$_2$	invisible	--
	C<u>H</u>(OH)N	--	5.78 *dd* (4.7, 10.0)
	CH(O<u>H</u>)N	--	invisible

1) the signal resulting from the *R*-epimer appears at 6.32 ppm.

Table 5.11 *Temperature gradients (in ppb K^{-1}) of linear and cyclic ncpA1 and ncpA2 species.*

position	*R*-Leu^7-ncpA1-CH(OH)$_2$	*S*-Leu^7-ncpA1-CH(OH)$_2$	ncpA1	*R*-Phe^7-ncpA2-CH(OH)$_2$	*S*-Phe^7-ncpA2-CH(OH)$_2$	ncpA2
Gly^2 NH	– 6.8	– 6.8	– 2.8	– 6.7	– 6.7	– 3.6
D-Gln^3 NH	– 7.3	– 7.1	– 7.9	– 7.5	– 7.1	-- [1)]
Ile^4 NH	– 8.5	– 8.5	– 8.6	– 8.3	– 8.5	-- [1)]
Ser^5 NH	– 9.3	– 9.1	– 2.9	– 8.9	– 9.3	– 3.1
Leu^7 NH	– 7.8	– 7.9	– 5.8	--	--	--
Phe^7 NH	--	--	--	– 8.8	– 6.1	– 7.5

1) no data were obtained due to weak signals.

Table 5.12 *Temperature gradients (in ppb K^{-1}) of TycA-CH(OH)$_2$ and Ψ[CH(OH)NH]-TycA.*

position	TycA-CH(OH)$_2$	Ψ[CH(OH)NH]-TycA
D-Phe^1 hemiaminal-NH	--	– 15.0
Phe^3 NH	– 4.7	– 4.3
D-Phe^4 NH	– 2.5	– 3.2
Asn^5 NH	– 3.3	– 4.3
Gln^6 NH	--[1)]	– 3.1
Tyr^7 NH	– 4.3	– 4.0
Val^8 NH	– 3.0	+ 1.0
Orn^9 NH	– 4.7	– 5.0
Leu^{10} NH	– 4.0	+ 1.0

1) no data were obtained due to signal overlap.

5.3.3 Molecular modeling data

The following tables list the ROE intensity derived restraints (target distance column) used for the molecular dynamics (MD) simulations discussed in chapter 3 as well as the distances obtained after the calculation (MD column). The distances resulting from the energy minimization (EM) are shown in the EM columns. For the MD and EM experiments, all differences to the target distances are listed (diff.). The column on the right show all changes in distances from the NOE-derived structures to the energy minimized structures (difference EM–MD).

Table 5.13 *ROE restraints and acquired distances (in Å) for S-Phe^7-ncpA2-CH(OH)$_2$.*

ROE	target distance	MD	diff.	EM	diff.	difference EM–MD
Phe^7 β-H^{proR} / Phe^7 C<u>H</u>(OH)$_2$	2.50	2.40	– 0.10	2.65	0.15	0.25
Phe^7 β-H^{proS} / Phe^7 C<u>H</u>(OH)$_2$	2.50	3.00	0.30	3.50	1.00	0.50
Phe^7 α-H / Phe^7 C<u>H</u>(OH)$_2$	3.00	3.00	0.00	3.00	0.00	0.00
Phe^7 2,6-H / Pro^6 β-H^{proR}	3.00	3.50	0.50	3.20	0.20	– 0.30
Phe^7 3,5-H / Pro^6 δ-H^{proS}	3.00	2.60	– 0.40	4.15	1.15	1.55
Phe^7 NH / Phe^7 β-H^{proR}	2.50	2.65	0.15	2.65	0.15	0.00
Phe^7 NH / Phe^7 C<u>H</u>(OH)$_2$	3.00	3.10	0.10	2.60	– 0.40	– 0.50
Phe^7 NH / Phe^7 α-H	3.00	3.00	0.00	3.05	0.05	0.05
Phe^7 NH / Pro^6 δ-H^{proS}	3.50	3.45	– 0.05	3.50	0.00	0.05
Phe^7 NH / Ser^5 β-H^{proR}	3.50	3.50	0.00	3.15	– 0.35	– 0.35
Ile^4 α-H / Ser^5 NH	2.50	2.60	0.10	3.00	0.50	0.40
Ile^4 δ-H / Tyr^1 δ-H	4.00	4.00	0.00	5.80	1.80	1.80
Ile^4 NH / Ile^4 α-H	3.00	3.00	0.00	3.00	0.00	0.00
Ile^4 NH / Ile^4 γ-Me	3.00	3.75	0.75	5.10	2.10	1.35
Pro^6 δ-H^{proS} / Ser^5 α-H	2.30	2.20	– 0.10	2.20	– 0.10	0.00
Pro^6 δ-H^{proS} / Ser^5 β-H^{proR}	2.50	2.40	– 0.10	2.25	– 0.25	– 0.15
Pro^6 α-H / Phe^7 NH	2.50	3.40	0.90	3.20	0.70	– 0.20
D-Gln^4 α-H / Ile^4 NH	2.50	2.40	– 0.10	2.15	– 0.35	– 0.25
D-Gln^4 NH / D-Gln^4 α-H	2.50	2.50	0.00	2.40	– 0.10	– 0.10
D-Gln^4 NH / Tyr^1 α-H	3.00	3.75	0.75	3.75	0.75	0.00
Ser^5 β-H / Phe^7 NH	3.50	3.60	0.10	3.00	– 0.50	– 0.60
Ser^5 β-H / Tyr^1 2,6-H	4.00	4.00	0.00	4.25	0.25	0.25
Ser^5 NH / Ser^5 α-H	3.00	3.00	0.00	3.00	0.00	0.00
Ser^5 NH / Ser^5 β-H^{proS}	2.50	2.60	0.10	2.45	– 0.05	– 0.15
Tyr^1 α-H / Phe^7 2,6-H	4.00	4.60	0.60	5.75	1.75	1.15
Tyr^1 α-H / D-Gln^4 NH	2.50	2.50	0.00	2.25	– 0.25	– 0.25

Table 5.14 *ROE restraints and acquired distances (in Å) for ncpA2.*

ROE	target distance	MD	diff.	EM	diff.	difference EM–MD
Phe^7 2,6-H / Pro^6 β-H^{proR}	3.00	3.15	0.15	5.55	2.55	2.40
Phe^7 2,6-H / Pro^6 δ-H^{proS}	3.00	2.95	– 0.05	3.95	0.95	1.00
Phe^7 NH / Gln^3 NH	3.50	3.55	0.05	3.95	0.45	0.40
Phe^7 NH / Phe^7 α-H	3.00	3.00	0.00	3.05	0.05	0.05
Phe^7 NH / Pro^6 δ-H^{proS}	3.50	3.45	– 0.05	3.40	– 0.10	– 0.05
Phe^7 NH / Ser^5 β-H	3.50	3.45	– 0.05	3.80	0.30	0.35
Gln^3 NH / Ser^5 β-H	3.50	3.70	0.20	4.00	0.50	0.30
Ile^4 α-H / Ser^5 NH	3.00	3.05	0.05	3.00	0.00	– 0.05
Pro^6 δ-H^{proR} / Ser^5 α-H	2.30	2.25	– 0.05	2.30	0.00	0.05
Gln^3 NH / Gln^3 α-H	2.50	2.65	0.15	2.75	0.25	0.10
Ser^5 β-H / Phe^7 NH	3.50	3.45	– 0.05	3.80	0.30	0.35
Ser^5 NH / Ser^5 α-H	3.00	3.05	0.05	3.05	0.05	0.00
Ser^5 NH / Ser^5 β-H	2.50	2.50	0.00	2.60	0.10	0.10
Phe^7 α-H / Phe^7 CH=N	2.30	2.45	0.15	2.80	0.50	0.35
Phe^7 CH=N / Tyr^1 α-H	2.50	2.30	– 0.20	2.65	0.15	0.35

Table 5.15 *ROE restraints and acquired distances (in Å) for Ψ[R-CH(OH)NH]-TycA.*

ROE	target distance	MD	diff.	EM	diff.	difference EM–MD
Asn^5 CO / Val^8 NH	2.00	2.10	0.10	2.30	0.30	0.20
Asn^5 NH / Val^8 CO	2.00	2.10	0.10	2.15	0.15	0.05
Phe^3 CO / Leu^{10} NH	2.00	1.90	– 0.10	1.95	– 0.05	0.05
Phe^3 NH / Leu^{10} CH(OH)NH	1.80	2.30	0.50	3.25	1.45	0.95
D-Phe^1 α-H / Leu^{10} CH(OH)NH	2.50	2.65	0.15	2.85	0.35	0.20
Pro^2 α-H / Phe^3 NH	3.50	3.55	0.05	3.60	0.10	0.05
D-Phe^4 α-H / Asn^5 NH	2.50	2.45	– 0.05	2.45	– 0.05	0.00
D-Phe4 α-H / Orn^9 NH	2.50	2.30	– 0.20	2.20	– 0.30	– 0.10
Tyr^7 NH / Val^8 NH	2.50	2.60	0.10	2.70	0.20	0.10
Tyr^7 α-H / Val^8 NH	3.50	3.50	0.00	3.50	0.00	0.00
Orn^9 α-H / Leu^{10} NH	2.20	2.10	– 0.10	2.20	0.00	0.10

Table 5.16 *ROE contacts used for the modeling of the 12-membered ring of the Trp^4 side chain-to-backbone cyclization product. Intensities are indicated as strong (s), medium (m), and weak (w).*

ROE	intensity
Trp^4 2-H / Trp^4 β-H^{proS}	m
Trp^4 2-H / Ala^5 α-H	w
Trp^4 2-H / Gly^6 α-H^{proR}	m
Trp^4 2-H / Gly^6 α-H^{proS}	m
Trp^4 2-H / Gly^6 C<u>H</u>(OH)N	s
Trp^4 7-H / Gly^6 C<u>H</u>(OH)N	w

5.3.4 pH and temperature dependence of the macrocyclization equilibria

The pH of the NMR samples was regulated by addition of solid Na_2CO_3 or aq. H_3PO_4 directly into the NMR tube. The solution was thoroughly mixed by shaking and air bubbles were removed by ultrasound in order to be able to perform the next NMR measurement as soon as possible after pH change. The pH values of the solutions were determined using pH-indicator strips (*Merck*; pH ranges: 2.5-4.5/4.0-7.0/6.5-10.0).

5.3.4.1 ncpA1 and ncpA2 equilibria

The pH-dependence of the ncp ring/chain equilibria was determined from the integrals of well-separated NH signals. The integrals of up-field signals (which were used for the determination of the temperature dependence) were not suitable as at low concentrations of one species (which is the case in the pH but not in the temperature series of measurements) due to base line distortions.

For the ncpA1 species the following signals were used and the following procedure was applied:

- *R*-Leu^7-ncpA1-$CH(OH)_2$: Leu^7 NH signal (10% of intensity have to be added in order to include the amount of *cis*-Pro amide);
- ncpA1: Ser^5 NH signal;

  ➔ determination of ratio *R*-Leu^7-ncpA1-$CH(OH)_2$/ncpA1;

➔ comparison with the signal multiplet of *S*-Leu^7-ncpA1-CH(OH)$_2$ Leu^7 NH and ncpA1 Leu^7 NH signal.

For the ncpA2 species the following signals were used and the following procedure was applied:

- *R*-Phe^7-ncpA2-CH(OH)$_2$: Phe^7 NH signal (20% of intensity have to be added in order to include the amount of *cis*-Pro amide);
- ncpA2: Gly^2 NH, Phe^7 NH, and Ser^5 NH signal;

➔ determination of ratio *R*-Phe^7-ncpA2-CH(OH)$_2$/ncpA2;

➔ determination of ratio *S*/*R*-Phe^7-ncpA2-CH(OH)$_2$ from the Ser^5 NH and Ile^4 NH signal pairs.

The temperature dependence of the ncp ring/chain equilibria could not be determined from the amide proton signals due to their temperature-dependend shifts and line broadening. Instead, it was determined from the integrals of the following well-separated up-field signals:

S/*R*-Leu^7-ncpA1-CH(OH)$_2$: both signals of the diastereotopic Tyr^1 β-H;
ncpA1: both signals of the diastereotopic Tyr^1 β-H.

S/*R*-Phe^7-ncpA2-CH(OH)$_2$: Phe^7 β-H (pro*R*) signal;
ncpA2: signal multiplet of Tyr^1 β-H and Phe^7 β-H (pro*S*), as well as the second Tyr^1 β-H signal.

5.3.4.2 TycA ring/chain equilibrium

For the quantification of the composition of the TycA ring/chain equilibrium, all percentages were determined by comparison of the following signals (see also figure 3.46):

TycA-CH(OH)$_2$: Val^8 β-Me and Leu^{10} γ-Me signals (the intensity of the Pro^2 γ-H (pro*S*) has to be subtracted);
Ψ[CH(OH)NH]-TycA: Val^8 β-Me and Leu^{10} γ-Me signals.

5.3.4.3 SegA side chain-to-backbone cyclization equilibrium

The quantification of the equilibrium between SegA^1-CH(OH)$_2$ and both aminal epimers formed by Trp^4 side chain-to-backbone cyclization was accomplished by comparing the integrals of the signal resulting from the *S*-epimer hemiaminal-CH (6.32 ppm) with the Trp^4 2-H signal resulting from the *R*-epimer (6.92 ppm) and the signal group from 7.18 to 7.31 ppm (containing the Trp^4 2-H, 5-H and 6-H signals of the linear peptide as well as the Trp^4 5-H and 6-H signals of the cyclization product).

Table 5.17 *Temperature-dependent composition (in %) of the SegA ring/chain equilibrium.*

T / K	SegA^1-CH(OH)$_2$	ring (*R* epimer)	ring (*S* epimer)
280	72.7	23.2	4.1
290	72.2	22.3	5.5
300	74.8	18.6	6.6
310	76.9	16.4	6.7
320	75.5	15.8	8.7

5.4 Experimental data: chapter 4 - synthetic procedures

5.4.1 (2*S*)-[(3*R*,4*S*)-dihydroxy-5-oxo-tetrahydro-furan-(2*S*)-yl)-(1*R*)]-1,3-thiazolidine-(4*R*)-carboxylic acid methyl ester (99)

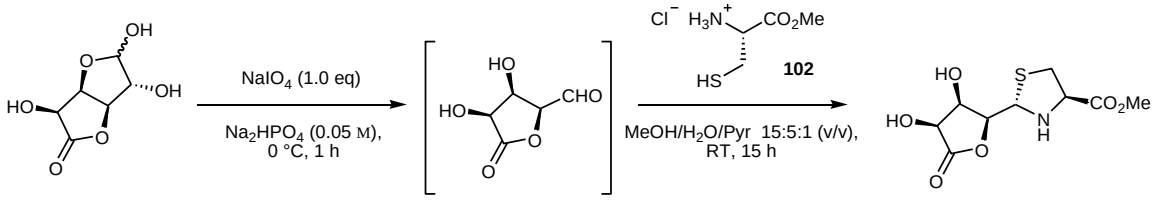

101 **103** **99**
M = 263.27

Preparation:

D-glucurono-3,6-lactone **101**	M = 176.12 g mol^{-1}	1.0 eq	56.8 mmol	10.0 g
L-cysteine methylester hydrochloride **102**	M = 121.16 g mol^{-1}	1.0 eq	56.8 mmol	9.77 g
$NaIO_4$	M = 291.51 g mol^{-1}	1.0 eq	56.8 mmol	16.6 g
Na_2HPO_4 (aq., 0.05 M)				100 mL
MeOH/H_2O/Pyr 15:5:1				90 mL

A) Periodate cleavage

10.0 g of D-glucurono-3,6-lactone **101** (56.8 mmol, 1.0 eq) were dissolved in 100 mL of aq. Na_2HPO_4 (0.05 M), the solution was cooled to 0 °C and 16.6 g of $NaIO_4$ (1.0 eq, 56.8 mmol) were added. The solution was vigorously stirred for 1 h at 0 °C and 100 mL of MeOH were subsequently added. After 30min the precipitated salts were filtered and the intensively yellow filtrate was concentrated *in vacuo*. Upon this procedure, iodine was removed with the solvent, and a colorless or pale yellow oil was finally obtained. The raw lactone aldehyde **103** was always directly further used for the condensation reaction.

B) Condensation

The oil was dissolved in 90 mL of MeOH/H_2O/Pyr 15:5:1, 9.77 g of L-cysteine methylester hydrochloride **102** (56.8 mmol, 1.0 eq) were added and the solution was stirred at RT for 15 h. A precipitate formws which was filtered, washed with cold EtOH, and dried *in vacuo* to yield 42% of the thiazolidine lactone **99** (6.26 g, 23.3 mmol) as a colorless solid. The filtrate was concentrated *in vacuo*, 50 mL of EtOH were added and the resulting suspension was placed in the fridge (5 °C) for 30 min. The precipitate was filtered, washed with cold EtOH, and dried *in vacuo* to yield additional 11% of the thiazolidine lactone **99** (1.67 g, 6.36 mmol) as a colorless solid. This resulted in an overall yield of 53% (7.93 g, 30.1 mmol).

TLC: R_f = 0.26 (pure EtOAc).

ESI-MS: m/z = 286 $[M+Na]^+$.

HRMS: $[M+Na]^+$: $C_9H_{13}NO_6SNa$, calculated: 286.0356, found: 286.0354.

^{1}H-NMR: 500 MHz, DMSO-d_6: δ = 2.69 (dd, 1 H, $^2J_{\beta\text{-H}}{}^{pro\mathit{R}}{}_{/\beta\text{-H}}{}^{pro\mathit{S}}$ = 10.0 Hz, $^3J_{\beta\text{-H}}{}^{pro\mathit{R}}{}_{/\alpha\text{-H}}$ = 8.2 Hz, β-H$^{pro\mathit{R}}$), 3.11 (dd, 1 H, $^2J_{\beta\text{-H}}{}^{pro\mathit{S}}{}_{/\beta\text{-H}}{}^{pro\mathit{R}}$ = 10.0 Hz, $^3J_{\beta\text{-H}}{}^{pro\mathit{S}}{}_{/\alpha\text{-H}}$ = 6.2 Hz, β-H$^{pro\mathit{S}}$), 3.67 (dd, 1 H, $^3J_{NH/1\text{-H}}$ = 7.8 Hz, $^3J_{NH/\alpha\text{-H}}$ = 11.3 Hz, NH), 3.70 (s, 3 H, CO_2CH_3), 3.93-3.98 (m, 1 H, α-H), 4.13 (ddd, 1 H, $^3J_{3\text{-H}/2\text{-H}}$ = 2.9 Hz, $^3J_{3\text{-H}/3\text{-OH}}$ = 4.2 Hz, $^3J_{3\text{-H}/4\text{-H}}$ = 4.6 Hz, 3-H), 4.24 (ddd, 1 H, $^3J_{2\text{-H}/3\text{-H}}$ = 2.9 Hz, $^3J_{2\text{-H}/1\text{-H}}$ = 9.7 Hz, $^4J_{2\text{-H}/3\text{-OH}}$ = 0.9 Hz, 2-H), 4.40 (dd, 1 H, $^3J_{4\text{-H}/3\text{-H}}$ = 4.6 Hz, $^3J_{4\text{-H}/4\text{-OH}}$ = 7.3 Hz, 4-H), 4.82 (dd, 1 H, $^3J_{1\text{-H}/NH}$ = 7.8 Hz, $^3J_{1\text{-H}/2\text{-H}}$ = 9.7 Hz, 1-H), 5.47 (dd, 1 H, $^3J_{3\text{-OH}/3\text{-H}}$ = 4.2 Hz, $^4J_{3\text{-OH}/2\text{-H}}$ = 0.9 Hz, 3-OH), 5.87 (d, 1 H, $^3J_{4\text{-OH}/4\text{-H}}$ = 7.3 Hz, 4-OH).

^{13}C-NMR: 125 MHz, DMSO-d_6: δ = 36.1 (C-β), 52.1 ($CO_2\underline{C}H_3$), 63.6 (C-α), 67.4 (C-1), 69.7 (C-3), 70.8 (C-4), 80.1 (C-2), 171.1 ($\underline{C}O_2CH_3$), 176.1 (C-5).

Melting point: 120 °C (decomposition).

Opt. rotation: $[\alpha]_{589}^{23}$ = −107.6, $[\alpha]_{578}^{23}$ = −112.5, $[\alpha]_{546}^{23}$ = −128.6, $[\alpha]_{436}^{23}$ = −227.4, $[\alpha]_{365}^{23}$ = −366.8

(c = 0.97 g/100 mL DMSO).

5.4.2 (2*R*)-[(3*S*,4*S*)-dihydroxy-5-oxo-tetrahydro-furan-(2*S*)-yl)-(1*R*)-hydroxymethyl]-1,3-thiazolidine-(4*R*)-carboxylic acid methyl ester (100)

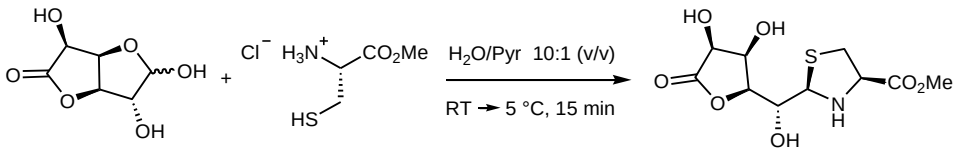

101 **102** **100**
M = 293.29

Preparation:

D-glucurono-3,6-lactone **101**	M = 176.12 g mol^{-1}	1.0 eq	26.2 mmol	4.61 g
L-cysteine methylester hydrochloride **102**	M = 121.16 g mol^{-1}	1.0 eq	26.2 mmol	4.50 g
H_2O/Pyr 10:1				13 mL

4.61 g of D-glucurono-3,6-lactone **101** (26.2 mmol, 1.0 eq) and 4.50 g of L-cysteine methylester hydrochloride **102** (26.2 mmol, 1.0 eq) were thoroughly grinded and placed in a 100 mL glass beaker. Under vigorous stirring, the mixture was dissolved in a minimum amount of H_2O/Pyr 10:1 so that a clear solution was obtained after 5 min. (approx. 13 mL required). A voluminous precipitate formed within approx. 10 min. and the mixture was subsequently placed in the fridge for 5 min. The product was filtered, washed with cold EtOH and dried *in vacuo* to yield 56% (4.39 g, 15.0 mmol) of the thiazolidine **100** as a colorless solid.

TLC: R_f = 0.30 ($CHCl_3$/MeOH 9:1).

ESI-MS: m/z = 316 $[M+Na]^+$.

HRMS: $[M+Na]^+$: $C_{10}H_{15}NO_7SNa$, calculated: 316.0461, found: 316.0459.

^{1}H-NMR: 300 MHz, DMSO-d_6: δ = 2.70 (pt, 1 H, $^2J_{\beta\text{-H}^{proS}/\beta\text{-H}^{proR}}$ = 9.8 Hz, $^3J_{\beta\text{-H}^{proS}/\alpha\text{-H}}$ = 9.8 Hz, β-H^{proS}), 2.89 (pt, 1 H, $^3J_{NH/\alpha\text{-H}}$ = 12.7 Hz, $^3J_{NH/1\text{-H}}$ = 12.7 Hz, NH), 3.22 (dd, 1 H, $^2J_{\beta\text{-H}^{proR}/\beta\text{-H}^{proS}}$ = 9.8 Hz, $^3J_{\beta\text{-H}^{proR}/\alpha\text{-H}}$ = 6.9 Hz, β-H^{proR}), 3.71 (s, 3 H, CO_2CH_3), 3.84 (ddd, 1 H, $^3J_{\alpha\text{-H}/\beta\text{-H}^{proR}}$ = 6.9 Hz, $^3J_{\alpha\text{-H}/\beta\text{-H}^{proS}}$ = 9.8 Hz, $^3J_{\alpha\text{-H/NH}}$ = 12.7 Hz, α-H), 3.98 (ddd, 1 H, $^3J_{2\text{-H}/1\text{-H}}$ = 1.1 Hz, $^3J_{2\text{-H}/2\text{-OH}}$ = 5.6 Hz, $^3J_{2\text{-H}/3\text{-H}}$ = 8.7 Hz, 2-H), 4.13 (m, 1 H, 4-H), 4.32 (dd, 1 H, $^3J_{3\text{-H}/4\text{-H}}$ = 2.7 Hz, $^3J_{3\text{-H}/2\text{-H}}$ = 8.7 Hz, 3-H), 4.51 (dd, 1 H, $^3J_{5\text{-H}/4\text{-H}}$ = 4.5 Hz, $^3J_{5\text{-H}/5\text{-OH}}$ = 7.3 Hz, 5-H), 4.70 (dd, 1 H, $^3J_{1\text{-H}/2\text{-H}}$ = 1.1 Hz, $^3J_{1\text{-H/NH}}$ = 12.7 Hz, 1-H), 5.45 (d, 1 H, $^3J_{4\text{-OH}/4\text{-H}}$ = 3.9 Hz, 4-OH), 5.85 (d, 1 H, $^3J_{2\text{-OH}/2\text{-H}}$ = 5.6 Hz, 2-OH), 5.90 (d, 1 H, $^3J_{5\text{-OH}/5\text{-H}}$ = 7.3 Hz, 5-OH).

^{13}C-NMR: 75 MHz, DMSO-d_6: δ = 37.0 (C-β), 52.3 ($CO_2\underline{C}H_3$), 65.1 (C-α), 67.7 (C-2), 69.1 (C-4), 69.5 (C-1), 70.7 (C-5), 81.5 (C-3), 171.4 ($\underline{C}O_2CH_3$), 176.0 (C-6).

Melting point: 144 °C.

5.4.3 (2*S*)-[(3*S*,4*S*)-dihydroxy-5-oxo-tetrahydro-furan-(2*S*)-yl)-(1*R*)-hydroxymethyl]-1,3-thiazolidine-(4*R*)-carboxylic acid methyl ester (100a)

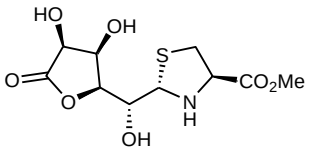

100a
M = 293.29

The thiazolidine lactone **100a** is formed by epimerization of **100** in solution (DMSO, DMF, H_2O).

TLC: R_f = 0.18 ($CHCl_3$/MeOH 9:1).

^{1}H-NMR: 300 MHz, DMSO-d_6: δ = 2.94 (dd, 1 H, $^2J_{\beta\text{-H}^{proR}/\beta\text{-H}^{proS}}$ = 10.3 Hz, $^3J_{\beta\text{-H}^{proR}/\alpha\text{-H}}$ = 4.9 Hz, β-H^{proR}), 3.03 (dd, 1 H, $^2J_{\beta\text{-H}^{proS}/\beta\text{-H}^{proR}}$ = 10.3 Hz, $^3J_{\beta\text{-H}^{proS}/\alpha\text{-H}}$ = 6.8 Hz, β-H^{proS}), 3.64 (s, 3 H, CO_2CH_3), 3.96 (dd, 1 H, $^3J_{2\text{-H}/3\text{-H}}$ = 4.5 Hz, $^3J_{2\text{-H}/2\text{-OH}}$ = 5.9 Hz, 2-H), 4.11-4.19 (m, 2 H, 3-H, 4-H), 4.38 (m, 1 H, α-H), 4.55 (m, 1 H, 5-H), 4.71 (br s, 1 H, 1-H), 5.52 (d, 1 H, $^3J_{2\text{-OH}/2\text{-H}}$ = 5.9 Hz, 2-OH), 5.55 (d, 1 H, $^3J_{4\text{-OH}/4\text{-H}}$ = 3.6 Hz, 4-OH), 5.88 (d, 1 H, $^3J_{5\text{-OH}/5\text{-H}}$ = 7.4 Hz, 5-OH). NH signal invisible.

^{13}C-NMR: 75 MHz, DMSO-d_6: δ = 36.7 (C-β), 52.0 ($CO_2\underline{C}H_3$), 64.2 (C-α), 69.6 (C-2), 70.1 (C-1, C-4), 70.7 (C-5), 81.9 (C-3), 171.8 ($\underline{C}O_2CH_3$), 175.9 (C-6).

5.4.4 (3*R*,6*S*,7*S*,8*S*,9*R*,9*aR*)-methyl octahydro-6,7,8,9-tetrahydroxy-5-oxothiazolo[3,2-*a*]azepine-3-carboxylate (105)

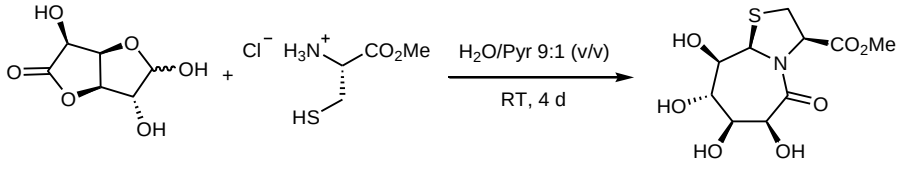

101 **102**

105
M = 293.29

Preparation:

D-glucurono-3,6-lactone **101**	M = 176.12 g mol^{-1}	1.0 eq	68.1 mmol	12.0 g
L-cysteine methylester hydrochloride **102**	M = 121.16 g mol^{-1}	1.0 eq	68.1 mmol	11.6 g
H_2O/Pyr 9:1				13 mL

12.0 g of D-glucurono-3,6-lactone **101** (68.1 mmol, 1.0 eq) and 11.6 g of L-cysteine methylester hydrochloride **102** were dissolved in 13mL H_2O/Pyr 9:1 and stirred for 4 d at RT. The solvents were removed *in vacuo*, the residue was dissolved in H_2O and the solution was allowed to stand for several days at RT in a crystallizing dish. The 7,5-bicyclic diol **105** was obtained in 52% yield (10.3 g, 35.1 mmol) as colorless crystals.

TLC: R_f = 0.25 (EtOAc/MeOH 10:1).

ESI-MS: m/z = 316 $[M+Na]^+$.

HRMS: $[M+Na]^+$: $C_{10}H_{15}NO_7SNa$, calculated: 316.0461, found: 316.0457.

IR: pellet; $\tilde{\nu}$ = 3371, 3303, 3257, 1715, 1651, 1436, 1371, 1340, 1231, 1180, 1110, 1073, 1010, 810 cm^{-1}.

^{1}H-NMR: 300 MHz, DMSO-d_6: δ = 3.27 (dd, 1 H, $^2J_{2\text{-}H^u/2\text{-}H^d}$ = 11.0 Hz, $^3J_{2\text{-}H^u/3\text{-}H}$ = 7.2 Hz, 2-H^u), 3.31 (dd, 1 H, $^2J_{2\text{-}H^d/2\text{-}H^u}$ = 11.0 Hz, $^3J_{2\text{-}H^d/3\text{-}H}$ = 7.8 Hz, 2-H^d), 3.54 (ddd, 1 H, $^3J_{9\text{-}H/9\text{-}OH}$ = 10.9 Hz, $^3J_{9\text{-}H/8\text{-}H}$ = 3.6 Hz, $^4J_{9\text{-}H/7\text{-}H}$ = 1.4 Hz, 9-H), 3.64 (s, 3 H, CO_2CH_3), 3.77-3.84 (m, 2 H, 7-H, 8-H), 4.30 (d, 1 H, $^3J_{9\text{-}OH/9\text{-}H}$ = 10.9 Hz, 9-OH), 4.51 (d, 1 H, $^3J_{6\text{-}OH/6\text{-}H}$ = 6.6 Hz, 6-OH), 4.68 (d, 1 H, $^3J_{6\text{-}H/6\text{-}OH}$ = 6.6 Hz, 6-H), 4.71 (pt, 1 H, 3-H), 5.33 (d, 1 H, $^3J_{7\text{-}OH/7\text{-}H}$ = 5.2 Hz, 7-OH), 5.42 (s, 1 H, 9a-H), 5.64 (d, 1 H, $^3J_{8\text{-}OH/8\text{-}H}$ = 3.4 Hz, 8-OH).

^{13}C-NMR: 75 MHz, DMSO-d_6: δ = 31.4 (C-β), 52.2 ($CO_2\underline{C}H_3$), 61.1 (C-9a), 64.0 (C-3), 69.3 (C-6), 70.1 (C-8), 76.1 (C-7), 77.0 (C-9), 170.5 ($\underline{C}O_2CH_3$), 170.7 (C-5).

Melting point: 117 °C.

Opt. rotation: $[\alpha]_{589}^{21}$ = –63.6, $[\alpha]_{578}^{21}$ = –66.1, $[\alpha]_{546}^{21}$ = –75.9, $[\alpha]_{436}^{21}$ = –137.7, $[\alpha]_{365}^{21}$ = –230.4 (c = 1.00 g/100 mL H_2O).

5.4.5 (3*R*,6*R*,7*R*,7*aR*)-methyl hexahydro-6,7-dihydroxy-5-oxopyrrolo[2,1-*b*]thiazole-3-carboxylate (112)

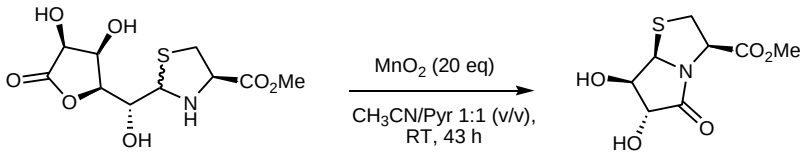

100 **112**
M = 323.24

Preparation:

Compound **100**	M = 293.29 g mol^{-1}	1.0 eq	1.02 mmol	300 mg
MnO_2, activated (*Merck*)	M = 86.94 g mol^{-1}	20 eq	20.4 mmol	1.78 g
CH_3CN/Pyr 1:1				30 mL

To a solution of 300 mg of **100** (1.02 mmol, 1.0 eq) in 30 mL CH_3CN/Pyr 1:1 were added 1.78 g of MnO_2 (activated, *Merck*; 20.4 mmol, 20 eq). The suspension was vigorously stirred for 43 h at RT, filtered over Celite, and concentrated. Residual Pyr was removed by coevaporation with Tol. The brown residue was dissolved in EtOAc (100mL) and H_2O (20 mL), the phases were separated and the aqueous phase was extracted two times with EtOAc. The combined organic phases were dried with brine and $MgSO_4$, filtered, and concentrated *in vacuo*. After purification with flash chromatography ($CHCl_3$/MeOH 9:1) 6.3% of the 5,5-bicyclic diol **112** (15 mg, 64.3 μmol) were obtained as a pale yellow oil.

TLC: R_f = 0.47 ($CHCl_3$/MeOH 9:1).

ESI-MS: *m*/*z* = 256 $[M+Na]^+$.

HRMS: $[M+Na]^+$: $C_8H_{11}NO_5SNa$, calculated: 256.0250, found: 256.0250.

IR: KBr; $\tilde{\nu}$ = 3349, 2955, 1739, 1700, 1438, 1347, 1275, 1218, 1179, 1099, 1069, 1008, 885, 777, 664 cm^{-1}.

^{1}H-NMR: 500 MHz, DMSO-d_6: δ = 3.18 (dd, 1 H, $^{2}J_{2\text{-H}}{}^{proS}{}_{/2\text{-H}}{}^{proR}$ = 11.4 Hz, $^{3}J_{2\text{-H}}{}^{proS}{}_{/3\text{-H}}$ = 5.6 Hz, 2-H^{proS}), 3.37 (dd, 1 H, $^{2}J_{2\text{-H}}{}^{proR}{}_{/2\text{-H}}{}^{proS}$ = 11.4 Hz, $^{3}J_{2\text{-H}}{}^{proR}{}_{/3\text{-H}}$ = 7.3 Hz, 2-H^{proR}), 3.66 (s, 3 H, CO_2CH_3), 3.94 (dd, 1 H, $^{3}J_{6\text{-H}/7\text{-H}}$ = 4.3 Hz, $^{3}J_{6\text{-H}/6\text{-OH}}$ = 6.1 Hz, 6-H), 4.19 (brm, 1 H, 7-H), 4.23 (dd, 1 H, $^{3}J_{3\text{-H}/2\text{-H}}{}^{proS}$ = 5.6 Hz, $^{3}J_{3\text{-H}/2\text{-H}}{}^{proR}$ = 7.3 Hz, 3-H), 5.24 (d, 1 H, $^{3}J_{7a\text{-H}/7\text{-H}}$ = 5.2 Hz, 7a-H), 5.69 (d, 1 H, $^{3}J_{7\text{-OH}/7\text{-H}}$ = 4.3 Hz, 7-OH), 6.07 (d, 1 H, $^{3}J_{6\text{-OH}/6\text{-H}}$ = 6.1 Hz, 6-OH).

^{13}C-NMR: 125 MHz, DMSO-d_6: δ = 35.0 (C-2), 52.1 ($CO_2\underline{C}H_3$), 58.0 (C-3), 70.5 (C-9a), 70.7 (C-7), 77.1 (C-6), 168.1 ($\underline{C}O_2CH_3$), 173.1 (C-5).

Opt. rotation: $[\alpha]_{589}^{18}$ = +32.5, $[\alpha]_{578}^{18}$ = +33.8, $[\alpha]_{546}^{18}$ = +38.6
(c = 0.92 g/100 mL MeOH).

5.4.6 (6*R*)-[(3*S*,4*S*)-dihydroxy-5-oxo-tetrahydro-furan-(2*S*)-yl]-4,4-dimethyl-tetrahydro-5-oxa-1-thia-3*a*-aza-pentalen-(3*R*)-carboxylic acid methyl ester (113)

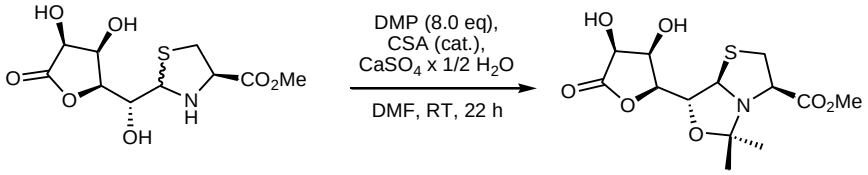

100 **113**
M = 333.36

Preparation:

Compound **100**	M = 293.29 g mol^{-1}	1.0 eq	0.51 mmol	150 mg
DMP	M = 104.15 g mol^{-1}, ρ = 0.85	8.0 eq	4.08 mmol	0.5 mL (42.5 mg)
CSA	M = 232.30 g mol^{-1}			cat.
$CaSO_4$ x 1/2 H_2O	M = 145.15 g mol^{-1}	4.0 eq	2.04 mmol	300 mg
DMF				9 mL

150 mg of compound **100** (0.51 mmol, 1.0 eq) were dissolved in 9 mL of DMF and 0.5 mL of DMP (42.5 mg, 4.08 mmol, 8.0 eq). After the addition of a catalytic amount of CSA and 300 mg of $CaSO_4$ x 1/2 H_2O (2.04 mmol, 4.0 eq) the solution was stirred for 22 h at RT. The reaction was neutralized by addition of NEt_3, filtered over Celite and concentrated *in vacuo*. Residual amounts of DMF were removed by coevaporation with Tol. The residue was subjected to flash chromatography ($CHCl_3$/MeOH 9:1) which yielded 98% (140 mg, 0.50 mmol) of the *O*,*N*-acetal **113** as a colorless oil.

TLC: R_f = 0.44 ($CHCl_3$/MeOH 9:1).

ESI-MS: m/z = 356 $[M+Na]^+$.

HRMS: $[M+Na]^+$: $C_{13}H_{19}NO_7SNa$, calculated: 356.0774, found: 356.0774.

IR: KBr; $\tilde{\nu}$ = 3402, 3287, 2950, 1783, 1402, 1657, 1437, 1389, 1201, 1149, 1005, 903, 856, 781 cm^{-1}.

^{1}H-NMR: 500 MHz, DMSO-d_6: δ = 1.27 (s, 3 H, Isopr-CH_3^{proS}), 1.30 (s, 3 H, Isopr-CH_3^{proR}), 3.03 (dd, 1 H, $^2J_{\beta\text{-H}^{proS}/\beta\text{-H}^{proR}}$ = 10.8 Hz, $^3J_{\beta\text{-H}^{proS}/\alpha\text{-H}}$ = 7.6 Hz, β-H^{proS}), 3.20 (dd, 1 H, $^2J_{\beta\text{-H}^{proR}/\beta\text{-H}^{proS}}$ = 10.8 Hz, $^3J_{\beta\text{-H}^{proR}/\alpha\text{-H}}$ = 2.2 Hz, β-H^{proR}), 3.65 (s, 3 H, CO_2CH_3), 4.15 (dpt, 1 H, $^3J_{4\text{-H}/3\text{-H}}$ = 2.8 Hz, $^3J_{4\text{-H}/4\text{-OH}}$ = 4.6 Hz, $^3J_{4\text{-H}/5\text{-H}}$ = 4.6 Hz, 4-H), 4.46 (dd, 1 H, $^3J_{3\text{-H}/4\text{-H}}$ = 2.8 Hz, $^3J_{3\text{-H}/2\text{-H}}$ = 8.2 Hz, 3-H), 4.51-4.56 (m, 2 H, 2-H, 5-H), 4.71 (dd, 1 H, $^3J_{\alpha\text{-H}/\beta\text{-H}^{proR}}$ = 2.2 Hz, $^3J_{\alpha\text{-H}/\beta\text{-H}^{proS}}$ = 7.6 Hz, α-H), 5.08 (d, 1 H, $^3J_{1\text{-H}/2\text{-H}}$ = 3.8 Hz, 1-H), 5.72 (d, 1 H, $^3J_{4\text{-OH}/4\text{-H}}$ = 4.6 Hz, 4-OH), 5.97 (d, 1 H, $^3J_{5\text{-OH}/5\text{-H}}$ = 7.5 Hz, 5-OH).

^{13}C-NMR: 125 MHz, DMSO-d_6: δ = 24.2 (Isopr-CH_3^{proR}), 29.4 (Isopr-CH_3^{proS}), 36.2 (C-β), 52.2 ($CO_2\underline{C}H_3$), 65.1 (C-α), 69.5 (C-4), 70.1 (C-5), 72.6 (C-1), 76.2 (C-2), 80.8 (C-3), 96.8 (Isopr-$C_{quart.}$), 171.7 ($\underline{C}O_2CH_3$), 175.8 (C-6).

Opt. rotation: $[\alpha]_{589}^{18}$ = –83.5, $[\alpha]_{578}^{18}$ = –87.2, $[\alpha]_{546}^{18}$ = –98.8, $[\alpha]_{436}^{18}$ = –166.8, $[\alpha]_{365}^{18}$ = –253.2 (c = 0.61 g/100 mL MeOH).

5.4.7 (6*R*)-[(3*S*)-hydroxy-(4*S*)-(*tert*-butyl-dimethylsilyl)oxy-5-oxo-tetrahydro-furan-(2*S*)-yl]-4,4-dimethyl-tetrahydro-5-oxa-1-thia-3*a*-aza-pentalen-(3*R*)-carboxylic acid methyl ester (114) and (6*R*)-[(3*S*,4*S*)-bis[(*tert*-butyl-dimethylsilyl)oxy]-5-oxo-tetrahydro-furan-(2*S*)-yl]-4,4-dimethyl-tetrahydro-5-oxa-1-thia-3*a*-aza-pentalen-(3*R*)-carboxylic acid methyl ester (115)

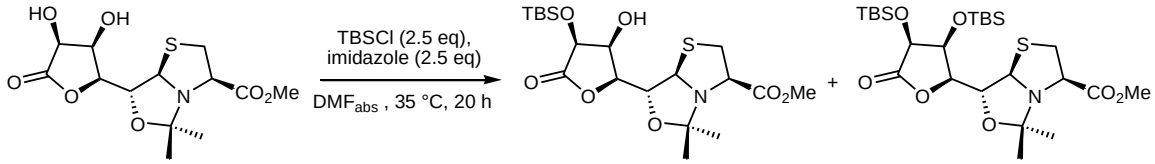

113 **114** M = 447.62 **115** M = 561.88

Preparation:

Compound **113**	M = 333.36 g mol^{-1}	1.0 eq	0.44 mmol	148 mg
TBSCl	M = 150.72 g mol^{-1}	2.5 eq	1.10 mmol	167 mg
Imidazole	M = 68.08 g mol^{-1}	2.5 eq	1.10 mmol	76 mg
DMF_{abs}				0.25 mL

A solution of 148 mg of **133** (0.44 mmol, 1.0 eq) in 0.25 mL of DMF_{abs} in a nitrogen atmosphere was treated with 76 mg of imidazole (1.10 mmol, 2.5 eq) and 167 mg of TBSCl (1.10 mmol, 2.5 eq) and stirred for 20 h at 35 °C. After cooling to RT and dilution with 10 mL of CH_2Cl_2 the reaction was quenched with 5% aq. $NaHCO_3$ (2 mL), the phases were separated and the aqueous phase was extracted two times with CH_2Cl_2. The combined organic phases were dried with brine and over $MgSO_4$, filtered, and concentrated *in vacuo*. Residual amounts of DMF were removed by coevaporation with Tol. The crude product was purified by flash chromatography (Tol/EtOAc 7:1) to yield 28% of the monosilylated product **114** (56 mg, 0.13 mmol) and 38% of the disilylated product **115** (95 mg, 0.17 mmol) as a colorless oils.

Compound **114***:*

TLC: R_f = 0.54 (Tol/EtOAc 5:1).

ESI-MS: m/z = 562 $[M+H]^+$.

HRMS: $[M+H]^+$: $C_{25}H_{47}NO_7SSi_2H$, calculated: 562.2685, found: 562.8692.

IR: film; $\tilde{\nu}$ = 2953, 2930, 2857, 1798, 1743, 1471, 1362, 1252, 1234, 1200, 1134, 1065, 1021, 1002, 983, 942, 878, 860, 836, 808, 778 cm^{-1}.

^{1}H-NMR: 500 MHz, DMSO-d_6: δ = 0.10, 0.10, 0.14, 0.15 (each s, 3 H, $SiCH_3$), 0.84, 0.92 (each s, 9 H, $SiC(CH_3)_3$), 1.31 (s, 3 H, Isopr-CH_3^{proR}), 1.34 (s, 3 H, Isopr-CH_3^{proS}), 3.08 (dd, 1 H, $^{2}J_{\beta\text{-}H^{proS}/\beta\text{-}H^{proR}}$ = 10.8 Hz, $^{3}J_{\beta\text{-}H^{proS}/\alpha\text{-}H}$ = 7.5 Hz, β-H^{proS}), 3.20 (dd, 1 H, $^{2}J_{\beta\text{-}H^{proR}/\beta\text{-}H^{proS}}$ = 10.8 Hz, $^{3}J_{\beta\text{-}H^{proR}/\alpha\text{-}H}$ = 2.0 Hz, β-H^{proR}), 3.63 (s, 3 H, CO_2CH_3), 4.41 (dd, 1 H, $^{3}J_{4\text{-}H/3\text{-}H}$ = 2.2 Hz, $^{3}J_{4\text{-}H/5\text{-}H}$ = 3.9 Hz, 4-H), 4.55 (dd, 1 H, $^{3}J_{2\text{-}H/1\text{-}H}$ = 3.9 Hz, $^{3}J_{2\text{-}H/3\text{-}H}$ = 8.4 Hz, 2-H), 4.61 (dd, 1 H, $^{3}J_{3\text{-}H/4\text{-}H}$ = 2.2 Hz, $^{3}J_{3\text{-}H/2\text{-}H}$ = 8.4 Hz, 3-H), 4.71 (dd, 1 H, $^{3}J_{\alpha\text{-}H/\beta\text{-}H^{proR}}$ = 2.0 Hz, $^{3}J_{\alpha\text{-}H/\beta\text{-}H^{proS}}$ = 7.5 Hz, α-H), 4.93 (d, 1 H, $^{3}J_{5\text{-}H/4\text{-}H}$ = 3.9 Hz, 5-H), 5.15 (d, 1 H, $^{3}J_{1\text{-}H/2\text{-}H}$ = 3.9 Hz, 1-H).

^{13}C-NMR: 125 MHz, DMSO-d_6: δ = −5.2, −4.8, −4.7, −3.7 (each $SiCH_3$), 18.0, 18.3 (each $Si\underline{C}(CH_3)_3$), 24.2 (Isopr-CH_3^{proS}), 25.7, 25.9 (each $SiC(\underline{C}H_3)_3$), 30.6 (Isopr-CH_3^{proR}), 36.6 (C-β), 52.1 ($CO_2\underline{C}H_3$), 64.8 (C-α), 72.5 (C-1), 72.6 (C-5), 72.9 (C-4), 75.6 (C-2), 80.7 (C-3), 96.9 (Isopr-$C_{quart.}$), 171.6 ($\underline{C}O_2CH_3$), 174.0 (C-6).

Opt. rotation: $[\alpha]_{589}^{18}$ = −77.6, $[\alpha]_{578}^{18}$ = −81.0, $[\alpha]_{546}^{18}$ = −91.8, $[\alpha]_{436}^{18}$ = −155.6
(c = 2.05 g/100 mL $CHCl_3$).

Compound **115***:*

TLC: R_f = 0.39 (Tol/EtOAc 5:1).

ESI-MS: m/z = 448 $[M+H]^+$.

HRMS: $[M+Na]^+$: $C_{19}H_{33}NO_7SSiH$, calculated: 448.1820, found: 448.1837.

IR: film; $\tilde{\nu}$ = 2952, 2930, 2857, 1791, 1738, 1464, 1437, 1385, 1363, 1297, 1253, 1200, 1145, 1062, 1007, 978, 940, 908, 866, 837, 802, 780 cm^{-1}.

^{1}H-NMR: 500 MHz, DMSO-d_6: δ = 0.12, 0.13 (each s, 3 H, $SiCH_3$), 0.90 (s, 9 H, $SiC(CH_3)_3$), 1.28 (s, 3 H, Isopr-CH_3^{proR}), 1.31 (s, 3 H, Isopr-CH_3^{proS}), 3.05 (dd, 1 H, $^2J_{\beta\text{-H}^{proS}/\beta\text{-H}^{proR}}$ = 10.8 Hz, $^3J_{\beta\text{-H}^{proS}/\alpha\text{-H}}$ = 7.5 Hz, β-H^{proS}), 3.21 (dd, 1 H, $^2J_{\beta\text{-H}^{proR}/\beta\text{-H}^{proS}}$ = 10.8 Hz, $^3J_{\beta\text{-H}^{proR}/\alpha\text{-H}}$ = 2.0 Hz, β-H^{proR}), 3.65 (s, 3 H, CO_2CH_3), 4.18 (ddd, 1 H, $^3J_{4\text{-H}/3\text{-H}}$ = 3.0 Hz, $^3J_{4\text{-H}/5\text{-H}}$ = 4.8 Hz, $^3J_{4\text{-H}/4\text{-OH}}$ = 5.4 Hz, 4-H), 4.50 (ddd, 1 H, $^4J_{3\text{-H}/4\text{-OH}}$ = 0.5 Hz, $^3J_{3\text{-H}/4\text{-H}}$ = 3.0 Hz, $^3J_{3\text{-H}/2\text{-H}}$ = 8.2 Hz, 3-H), 4.55 (dd, 1 H, $^3J_{2\text{-H}/1\text{-H}}$ = 3.8 Hz, $^3J_{2\text{-H}/3\text{-H}}$ = 8.2 Hz, 2-H), 4.71 (dd, 1 H, $^3J_{\alpha\text{-H}/\beta\text{-H}^{proR}}$ = 2.0 Hz, $^3J_{\alpha\text{-H}/\beta\text{-H}^{proS}}$ = 7.5 Hz, α-H), 4.79 (d, 1 H, $^3J_{5\text{-H}/4\text{-H}}$ = 4.8 Hz, 5-H), 5.12 (d, 1 H, $^3J_{1\text{-H}/2\text{-H}}$ = 3.8 Hz, 1-H), 5.61 (dd, 1 H, $^4J_{4\text{-OH}/3\text{-H}}$ = 0.5 Hz, $^3J_{4\text{-OH}/4\text{-H}}$ = 5.4 Hz, 4-OH).

^{13}C-NMR: 75 MHz, DMSO-d_6: δ = –5.1, –4.8 (each $SiCH_3$), 18.1 (each $Si\underline{C}(CH_3)_3$), 24.3 (Isopr-CH_3^{proS}), 25.7 ($SiC(\underline{C}H_3)_3$), 29.4 (Isopr-CH_3^{proR}), 36.2 (C-β), 52.2 ($CO_2\underline{C}H_3$), 65.1 (C-α), 69.7 (C-4), 71.4 (C-5), 72.6 (C-1), 76.3 (C-2), 80.9 (C-3), 96.9 (Isopr-$C_{quart.}$), 171.7 ($\underline{C}O_2CH_3$), 174.6 (C-6).

Opt. rotation: $[\alpha]_{589}^{18}$ = –88.8, $[\alpha]_{578}^{18}$ = –92.3, $[\alpha]_{546}^{18}$ = –104.6, $[\alpha]_{436}^{18}$ = –181.8
(c = 1.03 g/100 mL $CHCl_3$).

5.4.8 (2*S*)-[(3*R*,4*S*)-dihydroxy-5-oxo-tetrahydro-furan-(2*S*)-yl)-(1*R*)]-1,3-thiazolidine-(4*R*)-carboxylic acid methyl ester 3*O*-*N* dimethylacetal (116)

99 **116**
M = 303.33

Preparation:

Compound **99**	M = 263.27 g mol^{-1}	1.0 eq	0.40 mmol	104 mg
DMP	M = 104.15 g mol^{-1}, ρ = 0.85	10 eq	4.00 mmol	0.49 mL (42 mg)
CSA	M = 232.30 g mol^{-1}			cat.
DMF				4.0 mL

104 mg of the thiazolidine **99** (0.40 mmol, 1.0 eq) were dissolved in 4.0 mL of DMF and 0.5 mL of DMP (42 mg, 4.0 mmol, 1.0 eq). After the addition of a catalytic amount of CSA the solution was stirred for 4 h at RT. The reaction was neutralized by addition of NEt_3 and concentrated *in vacuo*. Residual amounts of DMF were removed by coevaporation with Tol. The residual oil was subjected to flash chromatography (EtOAc/Tol 5:1) which yielded 55% (66 mg, 0.22 mmol) of the *O*,*N*-acetal **116** as a colorless waxy solid.

TLC: R_f = 0.61 (EtOAc/MeOH 10:1).

ESI-MS: m/z = 326 $[M+Na]^+$.

HRMS: $[M+Na]^+$: $C_{12}H_{17}NO_6SNa$, calculated: 326.0669, found: 326.0773.

IR: pellet; $\tilde{\nu}$ = 3438, 2172, 1765, 1735, 1436, 1357, 1326, 1295, 1227, 1195, 1182, 1141, 1022, 983, 967, 898, 831, 786, 725 cm^{-1}.

^{1}H-NMR: 500 MHz, DMSO-d_6: δ = 1.25 (s, 3 H, Isopr-CH_3^{proS}), 1.53 (s, 3 H, Isopr-CH_3^{proR}), 2.91 (dd, 1 H, $^2J_{\beta\text{-H}^{proS}/\beta\text{-H}^{proR}}$ = 11.1 Hz, $^3J_{\beta\text{-H}^{proS}/\alpha\text{-H}}$ = 3.5 Hz, β-H^{proS}), 3.51 (dd, 1 H, $^2J_{\beta\text{-H}^{proR}/\beta\text{-H}^{proS}}$ = 11.1 Hz, $^3J_{\beta\text{-H}^{proR}/\alpha\text{-H}}$ = 9.7 Hz, β-H^{proR}), 3.64 (s, 3 H, CO_2CH_3), 4.10 (dd, 1 H, $^3J_{\alpha\text{-H}/\beta\text{-H}^{proS}}$ = 3.5 Hz, $^3J_{\alpha\text{-H}/\beta\text{-H}^{proR}}$ = 9.7 Hz, α-H), 4.18 (dd, 1 H, $^3J_{2\text{-H}/3\text{-H}}$ = 2.0 Hz, $^3J_{2\text{-H}/1\text{-H}}$ = 2.5 Hz, 2-H), 4.47 (dd, 1 H, $^3J_{3\text{-H}/2\text{-H}}$ = 2.0 Hz, $^3J_{3\text{-H}/4\text{-H}}$ = 4.0 Hz, 3-H), 4.55 (dd, 1 H, $^3J_{4\text{-H}/3\text{-H}}$ = 4.0 Hz, $^3J_{4\text{-H}/4\text{-OH}}$ = 7.6 Hz, 4-H), 5.12 (d, 1 H, $^3J_{1\text{-H}/2\text{-H}}$ = 2.5 Hz, 1-H), 5.82 (d, 1 H, $^3J_{4\text{-OH}/4\text{-H}}$ = 7.6 Hz, 4-OH).

^{13}C-NMR: 125 MHz, DMSO-d_6: δ = 24.2 (Isopr-CH_3^{proR}), 28.0 (Isopr-CH_3^{proS}), 34.2 (C-β), 52.0 ($CO_2\underline{C}H_3$), 60.4 (C-α), 60.9 (C-1), 70.1 (C-3), 70.8 (C-4), 73.4 (C-2), 86.3 (Isopr-$C_{quart.}$), 173.7 ($\underline{C}O_2CH_3$), 175.5 (C-5).

Opt. rotation: $[\alpha]_{589}^{24}$ = −63.0, $[\alpha]_{578}^{24}$ = −74.0

(c = 0.82 g/100 mL DMSO/$CHCl_3$ 1:1).

5.4.9 (2*S*)-[(3*R*)-hydroxy-(4*S*)-(methoxydimethyl)methoxy-5-oxo-tetrahydro-furan-(2*S*)-yl)-(1*R*)]-1,3-thiazolidine-(4*R*)-carboxylic acid methyl ester 3*O*-*N* dimethylacetal (117)

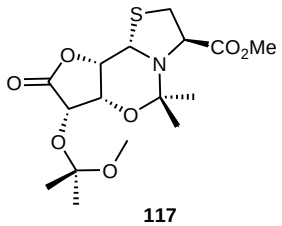

117
M = 375.44

The *N*,*O*-acetal **117** was isolated as side product of the synthesis of the *N*,*O*-acetal **116** (section 5.4.8). Flash chromatography (EtOAc/Tol 5:1) yielded 9.4% (14 mg, 37.3 µmol) of **117** as colorless powder.

TLC: R_f = 0.80 (EtOAc/MeOH 10:1).

ESI-MS: *m*/*z* = 398 $[M+Na]^+$.

HRMS: $[M+Na]^+$: $C_{16}H_{25}NO_7SNa$, calculated: 398.1244, found: 398.1248.

IR: pellet; $\tilde{\nu}$ = 3430, 3272, 1765, 1737, 1436, 1354, 1326, 1287, 1223, 1199, 1178, 1136, 1120, 1020, 985, 964, 899, 830, 787, 770, 722 cm^{-1}.

^{1}H-NMR: 600 MHz, DMSO-d_6: δ = 1.25 (s, 3 H, Isopr-CH_3^{proS}), 1.31, 1.32 (each s, 3 H, $C(C\underline{H}_3)_2OCH_3$), 1.52 (s, 3 H, Isopr-$CH_3^{proR}$), 2.91 (dd, 1 H, $^2J_{\beta\text{-}H^{proS}/\beta\text{-}H^{proR}}$ = 11.1 Hz, $^3J_{\beta\text{-}H^{proS}/\alpha\text{-}H}$ = 3.4 Hz, β-H^{proS}), 3.17 (s, 3 H, $C(CH_3)_2OC\underline{H}_3$), 3.51 (dd, 1 H, $^2J_{\beta\text{-}H^{proR}/\beta\text{-}H^{proS}}$ = 11.1 Hz, $^3J_{\beta\text{-}H^{proR}/\alpha\text{-}H}$ = 9.6 Hz, β-H^{proR}), 3.64 (s, 3 H, CO_2CH_3), 4.11 (dd, 1 H, $^3J_{\alpha\text{-}H/\beta\text{-}H^{proS}}$ = 3.4 Hz, $^3J_{\alpha\text{-}H/\beta\text{-}H^{proR}}$ = 9.6 Hz, α-H), 4.18 (dd, 1 H, $^3J_{2\text{-}H/3\text{-}H}$ = 2.0 Hz, $^3J_{2\text{-}H/1\text{-}H}$ = 2.5 Hz, 2-H), 4.52 (dd, 1 H, $^3J_{3\text{-}H/2\text{-}H}$ = 2.0 Hz, $^3J_{3\text{-}H/4\text{-}H}$ = 3.9 Hz, 3-H), 4.79 (d, 1 H, $^3J_{4\text{-}H/3\text{-}H}$ = 3.9 Hz, 4-H), 5.13 (d, 1 H, $^3J_{1\text{-}H/2\text{-}H}$ = 2.5 Hz, 1-H).

^{13}C-NMR: 150 MHz, DMSO-d_6: δ = 24.1 (Isopr-CH_3^{proR}), 24.4, 24.7 (each $C(\underline{C}H_3)_2OCH_3$), 28.1 (Isopr-$CH_3^{proS}$), 34.1 (C-$\beta$), 48.5 ($C(CH_3)_2O\underline{C}H_3$), 52.0 ($CO_2\underline{C}H_3$), 60.5 (C-$\alpha$), 60.8 (C-1), 70.0 (C-4), 70.1 (C-3), 73.5 (C-2), 86.4 (Isopr-$C_{quart.}$), 101.3 ($\underline{C}(CH_3)_2OCH_3$), 173.6 ($\underline{C}O_2CH_3$), 174.0 (C-5).

Opt. rotation: $[\alpha]_{589}^{24}$ = –76.9, $[\alpha]_{578}^{24}$ = –80.3, $[\alpha]_{546}^{24}$ = –90.8

(c = 0.73 g/100 mL DMSO/$CHCl_3$ 2:1).

5.4.10 9a(*S*)H-6-oxo-(7*S*,8*S*)-dihydroxy-octahydro-5,10-epoxy-thiazolo[3,2-*a*]-3-oxazocine-(3*R*)-carboxylic acid methyl ester (119)

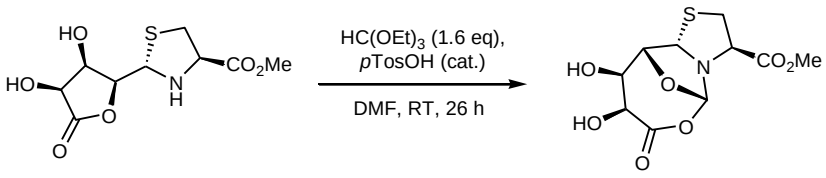

99 **119**
M = 291.28

Preparation:

Compound **99**	M = 263.27 g mol^{-1}	1.0 eq	0.38 mmol	100 mg
$HC(OEt)_3$	M = 148.20 g mol^{-1}, ρ = 0.90	1.6 eq	0.61 mmol	100 µL (90 mg)
*p*TosOH x H_2O	M = 190.22 g mol^{-1}			cat.
DMF				1.0 mL

100 mg of the thiazolidine **99** (0.38 mmol, 1.0 eq) were dissolved in 1.0 mL of DMF and 100 µg of $HC(OEt)_3$ (90 mg, 0.61 mmol, 1.6 eq) as well as a catalytic amount of *p*TosOH x H_2O were added. The solution was stirred for 26 h at RT, neutralized with NEt_3, and concentrated *in vacuo*. Residual amounts of DMF were removed by coevaporation with Tol. The resulting yellow oil was dissolved in *i*PrOH and the precipitate was filtered, which yielded 20% of reisolated starting material (20 mg, 76 µmol). The filtrate was concentrated *in vacuo* and the crude product was purified by flash chromatography (pure EtOAc) to yield 19% of the orthoaminal **119** (21 mg, 72 µmol) as a colorless oil.

TLC: R_f = 0.18 (pure EtOAc).

ESI-MS: *m*/*z* = 314 $[M+Na]^+$.

HRMS: $[M+Na]^+$: $C_{10}H_{13}NO_7SNa$, calculated: 314.0305, found: 314.0305.

^{1}H-NMR: 600 MHz, DMSO-d_6: δ = 3.26 (d, 1 H, $^{2}J_{\beta\text{-H}^{proS}/\beta\text{-H}^{proR}}$ = 12.6 Hz, β-H^{proS}), 3.55 (dd, 1 H, $^{2}J_{\beta\text{-H}^{proR}/\beta\text{-H}^{proS}}$ = 12.6 Hz, $^{3}J_{\beta\text{-H}^{proR}/\alpha\text{-H}}$ = 7.8 Hz, β-H^{proR}), 3.66 (s, 3 H, CO_2CH_3), 4.28 (dpt, 1 H, $^{3}J_{3\text{-H}/2\text{-H}}$ = 3.9 Hz, $^{3}J_{3\text{-H}/4\text{-H}}$ = 4.5 Hz, $^{3}J_{3\text{-H}/3\text{-OH}}$ = 4.5 Hz, 3-H), 4.41 (ddd, 1 H, $^{3}J_{2\text{-H}/3\text{-H}}$ = 3.9 Hz, $^{3}J_{2\text{-H}/1\text{-H}}$ = 9.8 Hz, $^{4}J_{2\text{-H}/3\text{-OH}}$ = 0.8 Hz, 2-H), 4.46 (dd, 1 H, $^{3}J_{4\text{-H}/3\text{-H}}$ = 4.5 Hz, $^{3}J_{4\text{-H}/4\text{-OH}}$ = 7.5 Hz, 4-H), 5.34 (d, 1 H, $^{3}J_{1\text{-H}/2\text{-H}}$ = 9.8 Hz, 1-H), 5.73 (dd, 1 H, $^{3}J_{3\text{-OH}/3\text{-H}}$ = 4.5 Hz, $^{4}J_{3\text{-OH}/2\text{-H}}$ = 0.8 Hz, 3-OH), 5.99 (d, 1 H, $^{3}J_{4\text{-OH}/4\text{-H}}$ = 7.5 Hz, 4-OH), 8.30 (s, 1 H, orthoaminal-CH).

^{13}C-NMR: 150 MHz, DMSO: δ = 31.6 (C-β), 52.3 ($CO_2\underline{C}H_3$), 59.4 (C-α), 60.7 (C-1), 69.5 (C-3), 71.0 (C-4), 79.7 (C-2), 161.0 (orthoaminal-CH), 169.2 ($\underline{C}O_2CH_3$), 175.5 (C-5).

5.4.11 (2*S*,4*R*)-methyl-2-((3*aS*,6*S*,6*aR*)-2-ethoxy-tetrahydro-4-oxofuro[3,4-*d*][1,3]dioxol-6-yl)-thiazolidine-4-carboxylate (118)

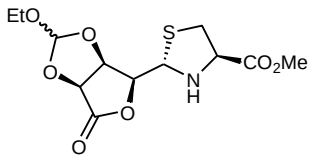

118
M = 319.33

The thiazolidine orthoester **118** (72:28 mixture of epimers) was isolated as byproduct of the synthesis of the orthoaminal **119** (section 5.4.10). Flash chromatography (pure EtOAc) yielded 2.5% (3.0 mg, 9.4 µmol) of **118** as a colorless solid.

ESI-MS: m/z = 320 $[M+H]^+$.

HRMS: $[M+H]^+$: $C_{12}H_{17}NO_7SH$, calculated: 320.0798, found: 320.0799.

Major epimer:

TLC: R_f = 0.67 (pure EtOAc).

^{1}H-NMR: 600 MHz, DMSO-d_6: δ = 1.07 (t, 3 H, $^{3}J_{OCH2CH3/OCH2CH3}$ = 7.1 Hz, OCH_2CH_3), 2.69 (dd, 1 H, $^{2}J_{\beta\text{-}H^{proS}/\beta\text{-}H^{proR}}$ = 10.0 Hz, $^{3}J_{\beta\text{-}H^{proS}/\alpha\text{-}H}$ = 8.3 Hz, β-H^{proS}), 3.14 (dd, 1 H, $^{2}J_{\beta\text{-}H^{proR}/\beta\text{-}H^{proS}}$ = 10.0 Hz, $^{3}J_{\beta\text{-}H^{proR}/\alpha\text{-}H}$ = 8.3 Hz, β-H^{proR}), 3.42-3.51 (m, 2H, OCH_2CH_3), 3.69 (s, 3 H, CO_2CH_3), 3.83 (dd, 1 H, $^{3}J_{NH/\alpha\text{-}H}$ = 11.2 Hz, $^{3}J_{NH/1\text{-}H}$ = 7.8 Hz, NH), 4.01-4.05 (m, 1 H, α-H), 4.51 (dd, 1 H, $^{3}J_{2\text{-}H/3\text{-}H}$ = 4.5 Hz, $^{3}J_{2\text{-}H/1\text{-}H}$ = 10.0 Hz, 2-H), 4.76 (dd, 1 H, $^{3}J_{3\text{-}H/2\text{-}H}$ = 4.5 Hz, $^{3}J_{3\text{-}H/4\text{-}H}$ = 6.4 Hz, 3-H), 4.79 (dd, 1 H, $^{3}J_{1\text{-}H/2\text{-}H}$ = 10.0 Hz, $^{3}J_{1\text{-}H/NH}$ = 7.8 Hz, 1-H), 5.07 (d, 1 H, $^{3}J_{4\text{-}H/3\text{-}H}$ = 6.4 Hz, 4-H), 6.06 (s, 1 H, orthoester-CH).

^{13}C-NMR: 150 MHz, DMSO: δ = 14.5 (OCH_2CH_3), 36.1 (C-β), 52.1 (CO_2CH_3), 60.2 (OCH_2CH_3), 63.7 (C-α), 67.9 (C-1), 74.0 (C-4), 76.7 (C-3), 81.2 (C-2), 115.4 (orthoester-CH), 170.9 (CO_2CH_3), 173.3 (C-5).

Minor epimer:

TLC: R_f = 0.60 (pure EtOAc).

^{1}H-NMR: 600 MHz, DMSO-d_6: δ = 1.04 (t, 3 H, $^{3}J_{OCH2CH3/OCH2CH3}$ = 7.0 Hz, OCH_2CH_3), 3.08 (dd, 1 H, $^{2}J_{\beta\text{-}H^{proS}/\beta\text{-}H^{proR}}$ = 10.5 Hz, $^{3}J_{\beta\text{-}H^{proS}/\alpha\text{-}H}$ = 5.8 Hz, β-H^{proS}), 3.12 (dd, 1 H, $^{2}J_{\beta\text{-}H^{proR}/\beta\text{-}H^{proS}}$ = 10.5 Hz, $^{3}J_{\beta\text{-}H^{proR}/\alpha\text{-}H}$ = 6.6 Hz, β-H^{proR}), 3.42-3.51 (m, 2H, OCH_2CH_3), 3.67 (s, 3 H, CO_2CH_3), 3.89 (pt, 1 H, $^{3}J_{NH/\alpha\text{-}H}$ = 9.9 Hz, $^{3}J_{NH/1\text{-}H}$ = 9.9 Hz, NH), 4.17-4.20 (m, 1 H, α-H), 4.57 (dd, 1 H, $^{3}J_{2\text{-}H/3\text{-}H}$ = 4.2 Hz, $^{3}J_{2\text{-}H/1\text{-}H}$ = 9.9 Hz, 2-H), 4.72 (pt, 1 H, $^{3}J_{1\text{-}H/NH}$ = 9.9 Hz, $^{3}J_{1\text{-}H/2\text{-}H}$ = 9.9 Hz, 1-H), 4.84 (dd, 1 H, $^{3}J_{3\text{-}H/2\text{-}H}$ = 4.2 Hz, $^{3}J_{3\text{-}H/4\text{-}H}$ = 6.2 Hz, 3-H), 5.09 (d, 1 H, $^{3}J_{4\text{-}H/3\text{-}H}$ = 6.2 Hz, 4-H), 6.06 (s, 1 H, orthoester-CH).

^{13}C-NMR: 150 MHz, DMSO: δ = 14.5 (OCH_2CH_3), 36.2 (C-β), 52.0 (CO_2CH_3), 59.9 (OCH_2CH_3), 64.9 (C-α), 67.7 (C-1), 74.2 (C-4), 76.9 (C-3), 82.7 (C-2), 115.4 (orthoester-CH), 172.1 (CO_2CH_3), 172.9 (C-5).

5.4.12 (8*aS*)H-(6*S*,7*R*,8*S*)-tris[(*tert*-butyl-dimethylsilyl)oxy]-5-oxo-hexahydro-thiazolo[3,2-a]pyridine-(3*R*)-carboxylic acid methyl ester (120) and (8*aS*)H-(6*S*,7*R*)-bis[(*tert*-butyl-dimethylsilyl)oxy]-(8*S*)-hydroxy-5-oxo-hexahydro-thiazolo[3,2-a]pyridine-(3*R*)-carboxylic acid methyl ester (121)

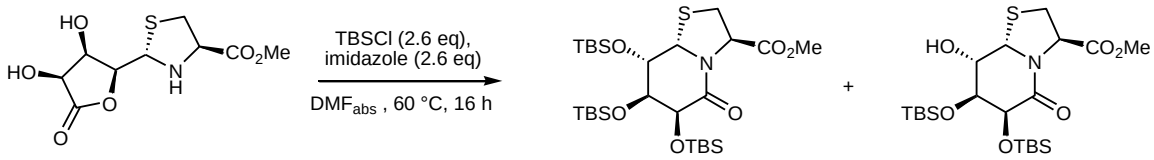

99 **120** M = 606.05 **121** M = 491.79

Preparation:

Compound **99**	M = 263.27 g mol^{-1}	1.0 eq	0.76 mmol	200 mg
TBSCl	M = 150.72 g mol^{-1}	2.6 eq	1.98 mmol	301 mg
Imidazole	M = 68.08 g mol^{-1}	2.6 eq	1.98 mmol	272 mg
DMF_{abs}				0. 50 mL

200 mg of the diol **99** (0.76 mmol, 1.0 eq), 301 mg of imidazole (1.98 mmol, 2.6 eq) and 272 mg of TBSCl (1.98 mmol, 2.6 eq) were dissolved in 0.50 mL of DMF_{abs} in a nitrogen atmosphere and the resulting solution was stirred for 16 h at 60 °C. After cooling to RT, the solution was diluted with 70 mL CH_2Cl_2 and 5% aq. $NaHCO_3$ was added under vigorous stirring until complete solution of the precipitate. The phases were separated and the aqueous phase was extracted two times with CH_2Cl_2. The combined organic phases were dried with brine and over $MgSO_4$, filtered, and concentrated *in vacuo*. Residual amounts of DMF were removed by coevaporation with Tol. The crude product was purified by flash chromatography (Tol/EtOAc 7:1) to yield 22% of trisilylated product **120** (101 mg, 0.17 mmol) as a colorless solid and 66% of disilylated product **121** (247 mg, 0.50 mmol) as colorless crystals.

The TLC identified only traces of the silylated thiazolidine lactones **122** and **123** which are obtained as main products at lower reaction temperatures (section 5.4.13).

Compound **120***:*

TLC: R_f = 0.86 (Tol/EtOAc 5:1).

ESI-MS: m/z = 628 $[M+Na]^+$.

HRMS: $[M+Na]^+$: $C_{27}H_{55}NO_6SSi_3Na$, calculated: 628.2950, found: 628.2955.

^{1}H-NMR: 600 MHz, DMSO-d_6: δ = 0.06, 0.09, 0.10, 0.11, 0.11, 0.15 (each s, 3 H, $SiCH_3$), 0.87, 0.88, 0.89 (each s, 9 H, $SiC(CH_3)_3$), 3.08 (dd, 1 H, $^2J_{2\text{-H}^{proS}/2\text{-H}^{proR}}$ = 11.4 Hz, $^3J_{2\text{-H}^{proS}/3\text{-H}}$ = 4.6 Hz, 2-H^{proS}), 3.29-3.32 (m, 1 H, 2-H^{proR}, H_2O), 3.65 (s, 3 H, CO_2CH_3), 4.08 (m, 2 H, 7-H, 8-H), 4.43 (d, 1 H, $^3J_{6\text{-H}/7\text{-H}}$ = 1.9 Hz, 6-H), 5.00 (dd, 1 H, $^3J_{3\text{-H}/2\text{-H}^{proS}}$ = 4.6 Hz, $^3J_{3\text{-H}/2\text{-H}^{proR}}$ = 7.8 Hz, 3-H), 5.20 (d, 1 H, $^3J_{8a\text{-H}/8\text{-H}}$ = 2.0 Hz, 8a-H).

^{13}C-NMR: 150 MHz, DMSO-d_6: δ = –5.3, –5.1, –5.1, –5.1, –4.7, –4.5 (each $SiCH_3$), 17.6, 17.7, 18.3 (each $Si\underline{C}(CH_3)_3$), 25.5, 25.5, 25.8 (each $SiC(\underline{C}H_3)_3$), 31.5 (C-2), 52.3 ($CO_2\underline{C}H_3$), 59.8 (C-3), 64.4 (C-8a), 68.6 (C-6), 69.2, 74.4 (C-7, C-8), 167.0 (C-5), 170.2 ($\underline{C}O_2CH_3$).

Compound **121***:*

TLC: R_f = 0.50 (Tol/EtOAc 5:1).

ESI-MS: m/z = 514 $[M+Na]^+$.

HRMS: $[M+Na]^+$: $C_{21}H_{41}NO_6SSi_2Na$, calculated: 514.2085, found: 514.2087.

^{1}H-NMR: 600 MHz, DMSO-d_6: δ = 0.08, 0.08, 0.10 (each s, 3 H, $SiCH_3$), 0.86, 0.90 (each s, 9 H, $SiC(CH_3)_3$), 3.05 (dd, 1 H, $^2J_{2\text{-H}^{proS}/2\text{-H}^{proR}}$ = 11.5 Hz, $^3J_{2\text{-H}^{proS}/3\text{-H}}$ = 5.5 Hz, 2-H^{proS}), 3.38 (dd, 1 H, $^2J_{2\text{-H}^{proR}/2\text{-H}^{proS}}$ = 11.5 Hz, $^3J_{2\text{-H}^{proR}/3\text{-H}}$ = 8.1 Hz, 2-H^{proR}), 3.64 (s, 3 H, CO_2CH_3), 3.94-3.95 (m, 1 H, 8-H), 4.15 (dd, 1 H, $^3J_{7\text{-H}/6\text{-H}}$ = 2.8 Hz, $^3J_{7\text{-H}/8\text{-H}}$ = 5.0 Hz, 7-H), 4.42 (d, 1 H, $^3J_{6\text{-H}/7\text{-H}}$ = 2.8 Hz, 6-H), 4.88 (d, 1 H, $^3J_{3\text{-H}/2\text{-H}^{proS}}$ = 5.5 Hz, $^3J_{3\text{-H}/2\text{-H}^{proR}}$ = 8.1 Hz, 3-H), 5.17 (d, 1 H, $^3J_{8a\text{-H}/8\text{-H}}$ = 3.1 Hz, 8a-H), 5.88 (d, 1 H, $^3J_{8\text{-OH}/8\text{-H}}$ = 5.0 Hz, 8-OH).

^{13}C-NMR: 150 MHz, DMSO-d_6: δ = –5.1, –5.1, –4.7, –4.4 (each $SiCH_3$), 17.7, 18.3 (each $Si\underline{C}(CH_3)_3$), 25.5, 25.9 (each $SiC(\underline{C}H_3)_3$), 31.3 (C-2), 52.2 ($CO_2\underline{C}H_3$), 59.8 (C-3), 65.2 (C-8a), 66.8 (C-8), 69.3 (C-6), 74.3 (C-7), 167.2 (C-5), 170.5 ($\underline{C}O_2CH_3$).

5.4.13 (2*S*)-[(3*R*,4*S*)- bis[(*tert*-butyl-dimethylsilyl)oxy]-5-oxo-tetrahydro-furan-(2*S*)-yl)-(1*R*)]-1,3-thiazolidine-(4*R*)-carboxylic acid methyl ester (122) and (2*S*)-[(3*R*)-hydroxy-(4*S*)-(*tert*-butyl-dimethylsilyl)oxy-5-oxo-tetrahydro-furan-(2*S*)-yl)-(1*R*)]-1,3-thiazolidine-(4*R*)-carboxylic acid methyl ester (123)

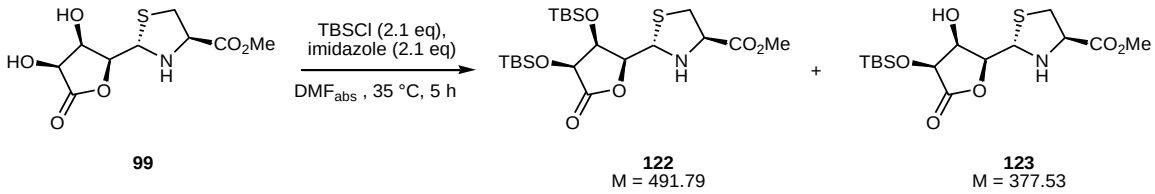

99

122
M = 491.79

123
M = 377.53

Preparation:

Compound **99**	M = 263.27 g mol^{-1}	1.0 eq	0.76 mmol	200 mg
TBSCl	M = 150.72 g mol^{-1}	2.1 eq	1.60 mmol	241 mg
Imidazole	M = 68.08 g mol^{-1}	2.1 eq	1.60 mmol	109 mg
DMF_{abs}				0. 50 mL

200 mg of the diol **99** (0.76 mmol, 1.0 eq), 109 mg of imidazole (1.60 mmol, 2.1 eq) and 241 mg of TBSCl (1.60 mmol, 2.1 eq) were dissolved in 0.50 mL of DMF_{abs} in a nitrogen atmosphere and the resulting solution was stirred for 5 h at 35 °C. After cooling to RT, the solution was diluted with 50 mL CH_2Cl_2 and 5% aq. $NaHCO_3$ was added under vigorous stirring until complete solution of the precipitate. The phases were separated and the aqueous phase was extracted two times with CH_2Cl_2. The combined organic phases were dried with brine and over $MgSO_4$, filtered, and concentrated *in vacuo*. Residual amounts of DMF were removed by coevaporation with Tol. The crude product was purified by flash chromatography (Tol/EtOAc 7:1→3:1) to yield 29% of the disilylated product **122** (108 mg, 0.23 mmol) as a colorless foam and 39% of the monosilylated product **123** (113 mg, 0.30 mmol) as a colorless solid.

The reaction temperature must not exceed 35 °C in order to suppress intramolecular aminolysis of the lactone which leads to the bicyclic thiazolidine lactams **120** and **121** (section 5.4.12).

Compound **122***:*

TLC: R_f = 0.30 (Tol/EtOAc 5:1).

ESI-MS: m/z = 514 $[M+Na]^+$.

HRMS: $[M+Na]^+$: $C_{21}H_{41}NO_6SSi_2Na$, calculated: 514.2085, found: 514.2091.

IR: pellet; $\tilde{\nu}$ = 3450, 2927, 2855, 1765, 1729, 1463, 1440, 1345, 1331, 1279, 1232, 1205, 1180, 1162, 1124, 1030, 980, 906, 861, 838, 778, 721 cm^{-1}.

^{1}H-NMR: 500 MHz, DMSO-d_6: δ = 0.09, 0.13, 0.13, 0.15 (each s, 3 H, $SiCH_3$), 0.86, 0.92 (each s, 9 H, $SiC(CH_3)_3$), 2.76 (dd, 1 H, $^2J_{\beta\text{-H}^{proR}/\beta\text{-H}^{proS}}$ = 10.0 Hz, $^3J_{\beta\text{-H}^{proR}/\alpha\text{-H}}$ = 8.2 Hz, β-H^{proR}), 3.17 (dd, 1 H, $^2J_{\beta\text{-H}^{proS}/\beta\text{-H}^{proR}}$ = 10.0 Hz, $^3J_{\beta\text{-H}^{proS}/\alpha\text{-H}}$ = 6.5 Hz, β-H^{proS}), 3.69 (s, 3 H, CO_2CH_3), 3.80 (dd, 1 H, $^3J_{NH/1\text{-H}}$ = 7.6 Hz, $^3J_{NH/\alpha\text{-H}}$ = 11.2 Hz, NH), 3.94 (ddd, 1 H, $^3J_{\alpha\text{-H}/\beta\text{-H}^{proS}}$ = 6.5 Hz, $^3J_{\alpha\text{-H}/\beta\text{-H}^{proR}}$ = 8.2 Hz, $^3J_{\alpha\text{-H/NH}}$ = 11.2 Hz, α-H), 4.38 (dd, 1 H, $^3J_{3\text{-H}/2\text{-H}}$ = 2.0 Hz, $^3J_{3\text{-H}/4\text{-H}}$ = 3.8 Hz, 3-H), 4.33 (dd, 1 H, $^3J_{2\text{-H}/3\text{-H}}$ = 2.0 Hz, $^3J_{2\text{-H}/1\text{-H}}$ = 10.0 Hz, 2-H), 4.73 (d, 1 H, $^3J_{4\text{-H}/3\text{-H}}$ = 3.8 Hz, 4-H), 4.85 (dd, 1 H, $^3J_{1\text{-H/NH}}$ = 7.6 Hz, $^3J_{1\text{-H}/2\text{-H}}$ = 10.0 Hz, 1-H).

^{13}C-NMR: 125 MHz, DMSO-d_6: δ = −4.9, −4.9, −4.8, −3.7 (each $SiCH_3$), 18.1, 18.3 (each $SiC(CH_3)_3$), 25.9 (each $SiC(CH_3)_3$), 36.5 (C-β), 52.2 (CO_2CH_3), 63.5 (C-α), 66.9 (C-1), 73.4 (C-3, C-4), 79.6 (C-2), 170.9 (CO_2CH_3), 174.5 (C-5).

Compound **123***:*

TLC: R_f = 0.19 (Tol/EtOAc 5:1).

ESI-MS: m/z = 400 $[M+Na]^+$.

HRMS: $[M+Na]^+$: $C_{15}H_{27}NO_6SSiNa$, calculated: 400.1221, found: 400.1226.

^{1}H-NMR: 600 MHz, DMSO-d_6: δ = 0.11, 0.12 (each s, 3 H, $SiCH_3$), 0.90 (s, 9 H, $SiC(CH_3)_3$), 2.69 (dd, 1 H, $^2J_{\beta\text{-H}^{proR}/\beta\text{-H}^{proS}}$ = 10.0 Hz, $^3J_{\beta\text{-H}^{proR}/\alpha\text{-H}}$ = 8.2 Hz, β-H^{proR}), 3.12 (dd, 1 H, $^2J_{\beta\text{-H}^{proS}/\beta\text{-H}^{proR}}$ = 10.0 Hz, $^3J_{\beta\text{-H}^{proS}/\alpha\text{-H}}$ = 6.2 Hz, β-H^{proS}), 3.66-3.70 (m, 4 H, NH, CO_2CH_3), 3.94 (ddd, 1 H, $^3J_{\alpha\text{-H}/\beta\text{-H}^{proS}}$ = 6.2 Hz, $^3J_{\alpha\text{-H}/\beta\text{-H}^{proR}}$ = 8.2 Hz, $^3J_{\alpha\text{-H/NH}}$ = 11.3 Hz, α-H), 4.15 (ddd, 1 H, $^3J_{3\text{-H}/2\text{-H}}$ = 2.9 Hz, $^3J_{3\text{-H}/4\text{-H}}$ = 4.8 Hz, $^3J_{3\text{-H}/3\text{-OH}}$ = 4.9 Hz, 3-H), 4.27 (ddd, 1 H, $^3J_{2\text{-H}/3\text{-H}}$ = 2.9 Hz, $^3J_{2\text{-H}/1\text{-H}}$ = 9.8 Hz, $^4J_{2\text{-H}/3\text{-OH}}$ = 0.9 Hz, 2-H), 4.63 (d, 1 H, $^3J_{4\text{-H}/3\text{-H}}$ = 4.8 Hz, 4-H), 4.82 (dd, 1 H, $^3J_{1\text{-H/NH}}$ = 7.8 Hz, $^3J_{1\text{-H}/2\text{-H}}$ = 9.8 Hz, 1-H), 5.42 (dd, 1H, $^3J_{3\text{-OH}/3\text{-H}}$ = 4.9 Hz, $^4J_{3\text{-OH}/2\text{-H}}$ = 0.9 Hz, 3-OH).

^{13}C-NMR: 150 MHz, DMSO-d_6: δ = –5.1, –4.9 (each $SiCH_3$), 18.1 ($SiC(CH_3)_3$), 25.7 ($SiC(CH_3)_3$), 36.0 (C-β), 52.1 (CO_2CH_3), 63.7 (C-α), 67.4 (C-1), 70.0 (C-3), 72.2 (C-4), 80.1 (C-2), 171.0 (CO_2CH_3), 174.5 (C-5).

Opt. rotation: $[\alpha]_{589}^{21}$ = –98.1, $[\alpha]_{578}^{21}$ = –103.0, $[\alpha]_{546}^{21}$ = –117.4, $[\alpha]_{436}^{21}$ = –184.1 (c = 1.05 g/100 mL $CHCl_3$).

5.4.14 (2*R*)-[(3*S*,4*S*)-bis[(*tert*-butyl-dimethylsilyl)oxy]-5-oxo-tetrahydro-furan-(2*S*)-yl)-(1*R*)-(*tert*-butyl-dimethylsilyl)oxymethyl]-1,3-thiazolidine-(4*R*)-carboxylic acid methyl ester (124)

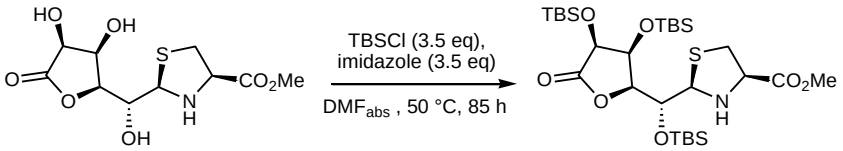

100 **124** M = 636.08

Preparation:

Compound **100**	M = 293.29 g mol^{-1}	1.0 eq	66.4 mmol	19.5 g
TBSCl	M = 150.72 g mol^{-1}	3.5 eq	232 mmol	35.0 g
Imidazole	M = 68.08 g mol^{-1}	3.5 eq	232 mmol	33.9 g
DMF_{abs}				40 mL

19.5 g of the triol **100** (66.4 mmol, 1.0 eq), 35.0 g of imidazole (232 mmol, 3.5 eq) and 33.9 g of TBSCl (232 mmol, 3.5 eq) were dissolved in 40 mL of DMF_{abs} in a nitrogen atmosphere and the resulting solution was stirred for 85 h at 50 °C. After cooling to RT, the solution was divided in three fractions. Every fraction was extracted with 700 mL pentane and the pentane phase was reextraced with 50 mL MeOH in order to remove the precipitate. The combined MeOH phases were extracted with pentane and the combined pentane phases were dried over $MgSO_4$, filtered, and concentrated *in vacuo*. The resulting oil was dried *in vacuo* at 40 °C for 24 h in order to remove the TBSOH. 90 mL *i*PrOH and 40mL H_2O were added and the resulting suspension was stirred overnight at RT and filtered to yield 42% of trisilylated thiazolidine **124** (17.5 g, 27.6 mmol) as colorless crystals. The filtrate was concentrated *in vacuo*, 16 mL MeOH were added and the solution was placed in the fridge (5 °C) overnight, yielding additional 4 % of **124** (1.63 g, 2.56 mmol) as colorless crystals and resulting in an overall yield of 46% (19.1 g, 30.2 mmol).

For the next step, the oxidation to the thiazole **131**, the raw product could be directly further used without crystallization (section 5.4.21).

TLC: R_f = 0.55 (Tol/EtOAc 7:1).

ESI-MS: m/z = 658 $[M+Na]^+$.

HRMS: $[M+Na]^+$: $C_{28}H_{57}NO_7SSi_3Na$, calculated: 658.3956, found: 658.3079.

IR: pellet; $\tilde{\nu}$ = 2955, 2929, 2849, 1780, 1737, 1462, 1455, 1417, 1364, 1251, 1186, 1150, 1134, 1106, 1022, 987, 953, 886, 836, 811, 778 cm^{-1}.

^{1}H-NMR: 600 MHz, $CDCl_3$: δ = 0.11, 0.15, 0.16, 0.17, 0.20, 0.21 (each s, 3 H, $SiCH_3$), 0.87, 0.93, 0.94 (each s, 9 H, $SiC(CH_3)_3$), 2.66 (pt, 1 H, $^2J_{\beta\text{-H}}{}^{pro S}{}_{/\beta\text{-H}}{}^{pro R}$ = 10.1 Hz, $^3J_{\beta\text{-H}}{}^{pro S}{}_{/\alpha\text{-H}}$ = 10.1 Hz, β-$H^{pro S}$), 3.07 (pt, 1 H, $^3J_{NH/1\text{-H}}$ = 12.9 Hz, $^3J_{NH/\alpha\text{-H}}$ = 12.9 Hz, NH), 3.26 (dd, 1 H, $^2J_{\beta\text{-H}}{}^{pro R}{}_{/\beta\text{-H}}{}^{pro S}$ = 10.1 Hz, $^3J_{\beta\text{-H}}{}^{pro R}{}_{/\alpha\text{-H}}$ = 6.2 Hz, β-$H^{pro R}$), 3.73-3.78 (m, 1 H, α-H), 3.79 (s, 3 H, CO_2CH_3), 4.31 (dd, 1 H, $^3J_{2\text{-H}/1\text{-H}}$ = 0.8 Hz, $^3J_{2\text{-H}/3\text{-H}}$ = 9.0 Hz, 2-H), 4.35 (dd, 1 H, $^3J_{3\text{-H}/4\text{-H}}$ = 2.0 Hz, $^3J_{3\text{-H}/2\text{-H}}$ = 9.0 Hz, 3-H), 4.38 (d, 1 H, $^3J_{5\text{-H}/4\text{-H}}$ = 3.6 Hz, 5-H), 4.44 (dd, 1 H, $^3J_{4\text{-H}/3\text{-H}}$ = 2.0 Hz, $^3J_{4\text{-H}/5\text{-H}}$ = 3.6 Hz, 4-H), 4.59 (dd, 1 H, $^3J_{1\text{-H}/2\text{-H}}$ = 0.8 Hz, $^3J_{1\text{-H}/NH}$ = 12.9 Hz, 1-H).

^{13}C-NMR: 150 MHz, $CDCl_3$: δ = –4.8, –4.6, –4.6, –4.4, –4.0, –3.2 (each $SiCH_3$), 18.6, 18.7, 18.9 (each $Si\underline{C}(CH_3)_3$), 26.1, 26.2, 26.3 (each $SiC(\underline{C}H_3)_3$), 38.9 (C-β), 52.7 ($CO_2\underline{C}H_3$), 66.1 (C-α), 69.2 (C-1), 70.1 (C-2), 72.9 (C-4), 74.3 (C-5), 81.6 (C-3), 171.3 ($\underline{C}O_2CH_3$), 173.6 (C-6).

Melting point: 98 °C.

Opt. rotation: $[\alpha]_{589}^{18}$ = –25.0, $[\alpha]_{578}^{18}$ = –26.3, $[\alpha]_{546}^{18}$ = –30.2, $[\alpha]_{436}^{18}$ = –53.8, $[\alpha]_{365}^{18}$ = –85.6 (c = 0.99 g/100 mL $CHCl_3$).

X-ray: Suitable crystals of **124** were grown from an *i*PrOH solution. See scheme 4.8.

5.4.15 (2*R*)-[(3*S*,4*S*)-bis[(*tert*-butyl-dimethylsilyl)oxy]-5-oxo-tetrahydro-furan-(2*S*)-yl)-(1*R*)-hydroxymethyl]-1,3-thiazolidine-(4*R*)-carboxylic acid methyl ester (125)

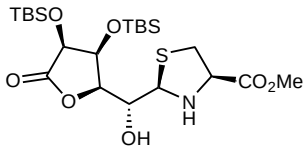

125
M = 521.82

The disilylated thiazolidine **125** can be isolated in small amounts from the TBS-protection reaction of **124** (section 5.4.14) by chromatographic purification (Tol/EtOAc 7:1).

TLC: R_f = 0.23 (Tol/EtOAc 7:1).

ESI-MS: *m*/*z* = 554 $[M+Na]^+$.

HRMS: $[M+Na]^+$: $C_{22}H_{43}NO_7SSi_2Na$, calculated: 554.2191, found: 554.2196.

IR: pellet; $\tilde{\nu}$ = 2955, 2930, 2856, 1798, 1741, 1467, 1454, 1353, 1251, 1205, 1136, 1061, 1018, 984, 943, 835, 808, 778 cm^{-1}.

^{1}H-NMR: 600 MHz, DMSO-d_6: δ = 0.00, 0.02, 0.08, 0.08 (each s, 3 H, $SiCH_3$), 0.85, 0.87 (each s, 9 H, $SiC(CH_3)_3$), 3.26 (dd, 1 H, $^2J_{\beta\text{-H}^{proS}/\beta\text{-H}^{proR}}$ = 11.0 Hz, $^3J_{\beta\text{-H}^{proS}/\alpha\text{-H}}$ = 8.4 Hz, β-H^{proS}), 3.28-3.31 (m, 1 H, β-H^{proR}, H_2O), 3.53 (dd, 1 H, $^3J_{1\text{-H}/2\text{-H}}$ = 3.6 Hz, $^3J_{1\text{-H}/NH}$ = 12.8 Hz, 1-H), 3.65 (s, 3 H, CO_2CH_3), 3.77 (m, 1 H, 2-H), 3.85 (d, 1 H, $^3J_{NH/1\text{-H}}$ = 12.8 Hz, 1-H), 3.93 (d, 1 H, $^3J_{3\text{-H}/2\text{-H}}$ = 4.8Hz, 3-H), 4.68 (dd, 1 H, $^3J_{\alpha\text{-H}/\beta\text{-H}^{proR}}$ = 7.0 Hz, $^3J_{\alpha\text{-H}/\beta\text{-H}^{proS}}$ = 8.4 Hz, α-H), 4.92 (s, 1 H, 4-H), 5.48 (s, 1 H, 5-H), 5.69 (d, 1 H, $^3J_{2\text{-OH}/2\text{-H}}$ = 4.0 Hz, 2-OH).

^{13}C-NMR: 150 MHz, DMSO-d_6: δ = –5.9, –5.8, –5.0, –4.7 (each $SiCH_3$), 18.0, 18.1 (each $Si\underline{C}(CH_3)_3$), 26.5, 26.6 (each $SiC(\underline{C}H_3)_3$), 31.3 (C-β), 52.1 ($CO_2\underline{C}H_3$), 60.6 (C-5), 63.6 (C-α), 71.1 (C-2), 71.2 (C-4), 76.9 (C-1), 78.8 (C-3), 81.6 (C-3), 168.5 (C-6), 171.2 ($\underline{C}O_2CH_3$).

Opt. rotation: $[\alpha]_{589}^{18}$ = –97.6, $[\alpha]_{578}^{18}$ = –101.8, $[\alpha]_{546}^{18}$ = –115.6, $[\alpha]_{436}^{18}$ = –193.9 (c = 0.82 g/100 mL $CHCl_3$).

5.4.16 (2*S*)-[(3*R*,4*S*)-bis[(triethylsilyl)oxy]-5-oxo-tetrahydro-furan-(2*S*)-yl)-(1*R*)]-1,3-thiazolidine-(4*R*)-carboxylic acid methyl ester (126)

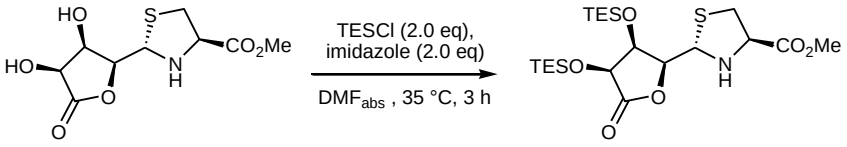

99 **126** M = 491.79

Preparation:

Compound **99**	M = 263.27 g mol^{-1}	1.0 eq	0.38 mmol	100 mg
TESCl	M = 150.72 g mol^{-1}, ρ = 0.90	2.0 eq	0.76 mmol	128 µL (115 mg)
Imidazole	M = 68.08 g mol^{-1}	2.0 eq	0.76 mmol	52 mg
DMF_{abs}				0. 25 mL

100 mg of the diol **99** (0.38 mmol, 1.0 eq) and 109 mg of imidazole (0.76 mmol, 2.0 eq) were dissolved in 0.25 mL of DMF_{abs} in a nitrogen atmosphere. 128 µL of TESCl (115 mg, 0.76 mmol, 2.0 eq) were added and the solution was stirred for 3 h at 35 °C. After cooling to RT, the solution was diluted with 50 mL CH_2Cl_2 and 5% aq. $NaHCO_3$ was added under vigorous stirring until complete solution of the precipitate. The phases were separated and the aqueous phase was extracted two times with CH_2Cl_2. The combined organic phases were dried with brine and over $MgSO_4$, filtered, and concentrated *in vacuo*. Residual amounts of DMF were removed by coevaporation with Tol. The crude product was purified by flash chromatography (Tol/EtOAc 4:1) to yield 78% of disilylated product **126** (108 mg, 0.23 mmol) as a pale yellow oil.
The reaction can also be carried out at RT as described for the two-step protection/oxidation procedure in section 5.4.19.

TLC: R_f = 0.52 (Tol/EtOAc 2:1).

ESI-MS: m/z = 514 $[M+Na]^+$.

HRMS: $[M+Na]^+$: $C_{21}H_{41}NO_6SSi_2Na$, calculated: 514.2085, found: 514.2091.

^{1}H-NMR: 500 MHz, $CDCl_3$: δ = 0.67-0.79 (m, 12 H, $SiC\underline{H}_2CH_3$), 0.94-1.01 (m, 18 H, $SiCH_2C\underline{H}_3$), 2.85 (dd, 1 H, $^2J_{\beta\text{-H}}{}^{pro\mathit{R}}{}_{/\beta\text{-H}}{}^{pro\mathit{S}}$ = 10.4 Hz, $^3J_{\beta\text{-H}}{}^{pro\mathit{R}}{}_{/\alpha\text{-H}}$ = 8.6 Hz, β-$H^{pro\mathit{R}}$), 3.01 (br s, 1 H, NH), 3.26 (dd, 1 H, $^2J_{\beta\text{-H}}{}^{pro\mathit{S}}{}_{/\beta\text{-H}}{}^{pro\mathit{R}}$ = 10.4 Hz, $^3J_{\beta\text{-H}}{}^{pro\mathit{S}}{}_{/\alpha\text{-H}}$ = 6.3 Hz, β-$H^{pro\mathit{S}}$), 3.78 (s, 3 H, CO_2CH_3), 3.93 (m, 1 H, α-H), 4.01 (dd, 1 H, $^3J_{2\text{-H/3-H}}$ = 2.5 Hz, $^3J_{2\text{-H/1-H}}$ = 9.5 Hz, 2-H), 4.45 (dd, 1 H, $^3J_{3\text{-H/2-H}}$ = 2.5 Hz, $^3J_{3\text{-H/4-H}}$ = 4.1 Hz, 3-H), 4.32 (d, 1 H, $^3J_{4\text{-H/3-H}}$ = 4.1 Hz, 4-H), 5.00 (d, 1 H, $^3J_{1\text{-H/2-H}}$ = 9.5 Hz, 1-H).

^{13}C-NMR: 125 MHz, $CDCl_3$: δ = 4.9, 5.4 (each $Si\underline{C}H_2CH_3$), 6.8, 7.0 (each $SiCH_2\underline{C}H_3$), 37.0 (C-β), 52.8 ($CO_2\underline{C}H_3$), 63.8 (C-α), 66.8 (C-1), 72.9 (C-3), 73.3 (C-4), 81.2 (C-2), 171.3 ($\underline{C}O_2CH_3$), 174.0 (C-5).

Opt. rotation: $[\alpha]_{589}^{18}$ = –131.6, $[\alpha]_{578}^{18}$ = –137.9, $[\alpha]_{546}^{18}$ = –157.0, $[\alpha]_{436}^{18}$ = –273.0, $[\alpha]_{365}^{18}$ = –430.9
(c = 0.81 g/100 mL $CHCl_3$).

5.4.17 (2*S*)-[(3*R*)-hydroxy-(4*S*)-(triethylsilyl)oxy-5-oxo-tetrahydro-furan-(2*S*)-yl)-(1*R*)]-1,3-thiazolidine-(4*R*)-carboxylic acid methyl ester (127)

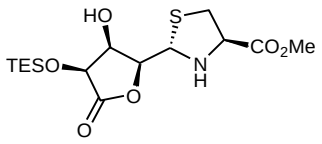

127
M = 377.53

The monosilylated thiazolidine lactone **127** was isolated in the synthesis of the disilylated compound **126** (section 5.4.16) in 2.8% yield (4.0 mg, 10.6 µmol).

TLC: R_f = 0.36 (Tol/EtOAc 2:1).

ESI-MS: m/z = 400 $[M+Na]^+$.

HRMS: $[M+Na]^+$: $C_{15}H_{27}NO_6SSiNa$, calculated: 400.1221, found: 400.1223.

^{1}H-NMR: 500 MHz, $CDCl_3$: δ = 0.68-0.77 (m, 6 H, $SiC\underline{H}_2CH_3$), 0.94-1.01 (m, 9 H, $SiCH_2C\underline{H}_3$), 2.86 (dd, 1 H, $^2J_{\beta\text{-H}^{proR}/\beta\text{-H}^{proS}}$ = 10.3 Hz, $^3J_{\beta\text{-H}^{proR}/\alpha\text{-H}}$ = 8.4 Hz, β-H^{proR}), 3.03 (br s, 1 H, NH), 3.26 (dd, 1 H, $^2J_{\beta\text{-H}^{proS}/\beta\text{-H}^{proR}}$ = 10.3 Hz, $^3J_{\beta\text{-H}^{proS}/\alpha\text{-H}}$ = 6.2 Hz, β-H^{proS}), 3.79 (s, 3 H, CO_2CH_3), 3.96 (dd, 1 H, $^3J_{\alpha\text{-H}/\beta\text{-H}^{proS}}$ = 6.2 Hz, $^3J_{\alpha\text{-H}/\beta\text{-H}^{proR}}$ = 8.4 Hz, α-H), 4.10 (dd, 1 H, $^3J_{2\text{-H}/3\text{-H}}$ = 2.9 Hz, $^3J_{2\text{-H}/1\text{-H}}$ = 9.2 Hz, 2-H), 4.36 (dd, 1 H, $^3J_{3\text{-H}/2\text{-H}}$ = 2.9 Hz, $^3J_{3\text{-H}/4\text{-H}}$ = 4.7 Hz, 3-H), 4.45 (d, 1 H, $^3J_{4\text{-H}/3\text{-H}}$ = 4.7 Hz, 4-H), 5.07 (d, 1 H, $^3J_{1\text{-H}/2\text{-H}}$ = 9.2 Hz, 1-H). 3-OH signal invisible.

^{13}C-NMR: 125 MHz, $CDCl_3$: δ = 4.8 ($Si\underline{C}H_2CH_3$), 6.7 ($SiCH_2\underline{C}H_3$), 36.9 (C-β), 52.8 ($CO_2\underline{C}H_3$), 63.8 (C-α), 66.5 (C-1), 69.8 (C-3), 71.6 (C-4), 81.0 (C-2), 171.3 ($\underline{C}O_2CH_3$), 173.5 (C-5).

5.4.18 (2*R*)-[(3*S*,4*S*)-bis[(triethylsilyl)oxy]-5-oxo-tetrahydro-furan-(2*S*)-yl)-(1*R*)-(triethylsilyl)oxymethyl]-1,3-thiazolidine-(4*R*)-carboxylic acid methyl ester (128)

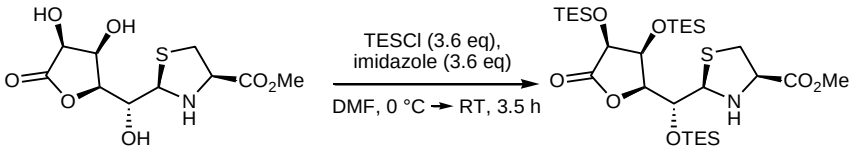

100 **128**
M = 636.08

Preparation:

Compound **100**	M = 293.29 g mol^{-1}	1.0 eq	0.52 mmol	153 mg
TESCl	M = 150.72 g mol^{-1}, ρ = 0.90	3.6 eq	1.88 mmol	315 µL (283 mg)
Imidazole	M = 68.08 g mol^{-1}	3.6 eq	1.88 mmol	128 mg
DMF				0.5 mL

153 mg of the triol **100** (0.52 mmol, 1.0 eq) were dissolved in 0.5 mL of DMF and cooled to 0 °C. 128 mg of imidazole (1.88 mmol, 3.6 eq) and 315 µL of TESCl (283 mg, 1.88 mmol, 3.6 eq) were added, the solution was stirred for 3.5 h and thereby allowed to warm to RT. The solution was diluted with 50 mL CH_2Cl_2 and 5% aq. $NaHCO_3$ was added under vigorous stirring until complete solution of the precipitate. The phases were separated and the aqueous phase was extracted two times with CH_2Cl_2. The combined organic phases were dried with brine and over $MgSO_4$, filtered, and concentrated *in vacuo*. Residual amounts of DMF were removed by coevaporation with Tol. The crude product was purified by flash chromatography (CH_2Cl_2/pentane 4:1) to yield 97% of trisilylated thiazolidine **128** (321 mg, 0.50 mmol) as a colorless oil.
For the next step, the oxidation to the thiazole **132**, the raw product could be directly further used without purification (section 5.4.22).

TLC: R_f = 0.47 (Tol/EtOAc 7:1).

ESI-MS: m/z = 658 $[M+Na]^+$.

HRMS: $[M+Na]^+$: $C_{28}H_{57}NO_7SSi_3Na$, calculated: 658.3956, found: 658.3053.

^{1}H-NMR: 500 MHz, DMSO-d_6: δ = 0.64-0.69 (m, 18 H, 9 x SiC<u>H</u>$_2$CH$_3$), 0.89 (t, 9 H, $^3J_{SiCH2CH3/SiCH2CH3}$ = 8.0 Hz, 3 x SiCH$_2$C<u>H</u>$_3$), 0.92-0.97 (m, 18 H, 6 x SiCH$_2$C<u>H</u>$_3$), 2.61 (pt, 1 H, $^2J_{\beta\text{-H}^{proS}/\beta\text{-H}^{proR}}$ = 9.8 Hz, $^3J_{\beta\text{-H}^{proS}/\alpha\text{-H}}$ = 9.8 Hz, β-H^{proS}), 2.86 (pt, 1 H, $^3J_{NH/1\text{-H}}$ = 12.7 Hz, $^3J_{NH/\alpha\text{-H}}$ = 12.7 Hz, NH), 3.28 (dd, 1 H, $^2J_{\beta\text{-H}^{proR}/\beta\text{-H}^{proS}}$ = 9.8 Hz, $^3J_{\beta\text{-H}^{proR}/\alpha\text{-H}}$ = 6.5 Hz, β-H^{proR}), 3.72 (s, 3 H, CO$_2$CH$_3$), 3.81-3.86 (m, 1 H, α-H), 4.22 (d, 1 H, $^3J_{2\text{-H/3-H}}$ = 9.4 Hz, 2-H), 4.44-4.46 (m, 2 H, 3-H, 4-H), 4.38 (d, 1 H, $^3J_{1\text{-H/NH}}$ = 12.7 Hz, 1-H), 4.79 (d, 1 H, $^3J_{5\text{-H/4-H}}$ = 3.6 Hz, 5-H).

^{13}C-NMR: 125 MHz, DMSO-d_6: δ = 4.1, 4.6, 4.7 (each Si<u>C</u>H$_2$CH$_3$), 6.4, 6.6, 6.6 (each SiCH$_2$<u>C</u>H$_3$), 37.4 (C-β), 52.3 (CO$_2$<u>C</u>H$_3$), 64.9 (C-α), 68.6 (C-1), 70.1 (C-2), 72.3 (C-4), 72.3 (C-5), 80.6 (C-3), 171.2 (<u>C</u>O$_2$CH$_3$), 174.9 (C-6).

Opt. rotation: $[\alpha]_{589}^{23}$ = –26.2, $[\alpha]_{578}^{23}$ = –27.4, $[\alpha]_{546}^{23}$ = –31.3, $[\alpha]_{436}^{23}$ = –55.5, $[\alpha]_{365}^{23}$ = –89.1 (c = 1.18 g/100 mL CHCl$_3$).

5.4.19 [(3*R*,4*S*)-bis[(triethylsilyl)oxy]-5-oxo-tetrahydro-furan-(2*S*)-yl)-(1*R*)]-1,3-thiazole-carboxylic acid methyl ester (129)

Method A) oxidation of purified thiazolidine **126**

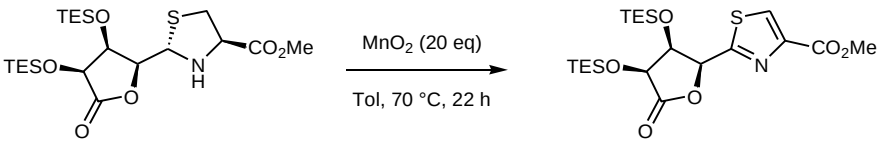

126 **129**
M = 487.76

Preparation:

Compound **126**	M = 491.79 g mol^{-1}	1.0 eq	285 µmol	140 mg
MnO$_2$, activated (*Fluka*)	M = 86.94 g mol^{-1}	20 eq	5.69 mmol	495 mg
Tol				6 mL

To a solution of 140 mg of thiazolidine **126** (285 µmol, 1.0 eq) in 6 mL of Tol were added 495 mg of MnO_2 (activated, *Fluka*; 5.69 mmol, 20 eq) and the suspension was vigorously stirred for 11 h at 70 °C. After cooling to RT, additional 495 mg of MnO_2 (activated, *Fluka*; 5.69 mmol, 20 eq) were added and the suspension was further heated to 70 °C under vigorous stirring for 11 h. After cooling to RT the suspension was filtered over a short Celite column and concentrated *in vacuo* to obtain 36% of the thiazole **129** (50 mg, 103 µmol) as a pale yellow oil.

Method B) two-step protection/oxidation of **99**

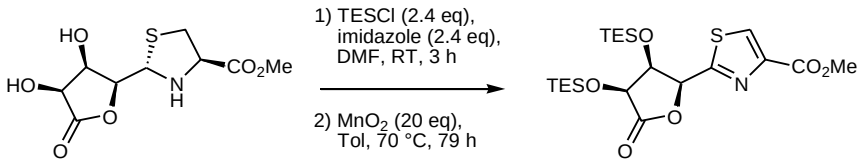

99 **129** M = 487.76

Preparation:

Compound **99**	M = 491.79 g mol^{-1}	1.0 eq	39.6 mmol	10.4 g
TESCl	M = 150.72 g mol^{-1}, ρ = 0.90	2.4 eq	95.0 mmol	16.5 mL (14.8 g)
Imidazole	M = 68.08 g mol^{-1}	2.4 eq	95.0 mmol	6.47 g
DMF				50 mL
MnO_2, activated (*Fluka*)	M = 86.94 g mol^{-1}	20 eq	792 mmol	68.8 g
Tol				250 mL

10.4 g of the thiazolidine **99** (39.6 mmol, 1.0 eq) and 6.47 g of imidazole (95.0 mmol, 2.4 eq) were dissolved in 50 mL of DMF in a nitrogen atmosphere. The solution was cooled to 0 °C and 16.5 mL of TESCl (14.8 g, 95.0 mmol, 2.4 eq) were slowly added over 3 min. The solution was stirred for 3 h at 0 °C, diluted with 200 mL CH_2Cl_2, and 5% aq. $NaHCO_3$ was added under vigorous stirring until complete solution of the precipitate. The phases were separated and the aqueous phase was extracted two times with CH_2Cl_2. The combined organic phases were dried with brine and over $MgSO_4$, filtered, and concentrated *in vacuo*. Residual amounts of DMF were removed by coevaporation with Tol. The sample was dried *in vacuo* for 24 h in order to remove the TESOH.

The resulting yellow oil was dissolved in 250 mL Tol, 68.8 g of MnO_2 (activated, *Fluka*; 792 mmol, 20 eq) were added and the suspension was vigorously stirred for 36 h at 70 °C. After cooling to RT, the suspension was filtered over a short Celite column and concentrated *in vacuo*. The residue was dissolved in 200 mL Tol, 51.6 g of MnO_2 (activated, *Fluka*; 594 mmol, 15 eq) were added and the suspension was heated to 70 °C under vigorous stirring for 28 h. After cooling to RT, additional 34.4 g of MnO_2 (activated, *Fluka*; 396 mmol, 10 eq) were added and the suspension was vigorously stirred for further 15 h at 70 °C. The mixture was cooled to RT, filtered over Celite and concentrated *in vacuo*. Flash chromatography (Tol/EtOAc 6:1→4:1) yielded 33% of the thiazole **129** (6.30 g, 12.9 mmol, over two steps) as a pale yellow oil.

TLC: R_f = 0.67 (Tol/EtOAc 2:1).

ESI-MS: m/z = 510 $[M+Na]^+$.

HRMS: $[M+Na]^+$: $C_{21}H_{37}NO_6SSi_2Na$, calculated: 510.1772, found: 510.1776.

IR: film; $\tilde{\nu}$ = 2954, 2912, 2877, 1811, 1732, 1485, 1458, 1436, 1413, 1379, 1345, 1327, 1216, 1184, 1131, 1097, 989, 941, 920, 843, 813, 784, 727, 683 cm^{-1}.

^{1}H-NMR: 500 MHz, $CDCl_3$: δ = 0.32-0.45 (m, 6 H, 3 x Si$\underline{H}_2$CH$_3$), 0.73-0.80 (m, 15 H, 3 x Si$\underline{H}_2$CH$_3$ and 3 x SiCH$_2$C$\underline{H}_3$), 1.01 (t, 9 H, $^3J_{SiCH2CH3/SiCH2CH3}$ = 7.9 Hz, 3 x SiCH$_2$C$\underline{H}_3$), 3.96 (s, 3 H, CO_2CH_3), 4.53 (d, 1 H, $^3J_{4\text{-}H/3\text{-}H}$ = 3.9 Hz, 4-H), 4.71 (dd, 1 H, $^3J_{3\text{-}H/2\text{-}H}$ = 2.7 Hz, $^3J_{3\text{-}H/4\text{-}H}$ = 3.9 Hz, 3-H), 5.71 (d, 1 H, $^3J_{2\text{-}H/3\text{-}H}$ = 2.7 Hz, 2-H), 8.26 (s, 1 H, Thz-H).

^{13}C-NMR: 125 MHz, $CDCl_3$: δ = 4.8, 4.9 (each Si$\underline{C}$H$_2$CH$_3$), 6.6, 6.8 (each SiCH$_2\underline{C}$H$_3$), 52.7 ($CO_2\underline{C}H_3$), 73.0 (C-4), 74.1 (C-3), 79.3 (C-2), 129.0 (Thz-H$\underline{C}$=C), 146.5 (Thz-HC=$\underline{C}$), 161.8 ($\underline{C}O_2CH_3$), 166.2 (C-1), 173.3 (C-5).

Opt. rotation: $[\alpha]_{589}^{20}$ = –46.6, $[\alpha]_{578}^{20}$ = –48.6, $[\alpha]_{546}^{20}$ = –54.9, $[\alpha]_{436}^{20}$ = –92.1, $[\alpha]_{365}^{20}$ = –137.9 (c = 0.92 g/100 mL $CHCl_3$).

5.4.20 [(3*R*,4*S*)-bis[(*tert*-butyl-dimethylsilyl)oxy]-5-oxo-tetrahydro-furan-(2*S*)-yl)-(1*R*)]-1,3-thiazole-carboxylic acid methyl ester (130)

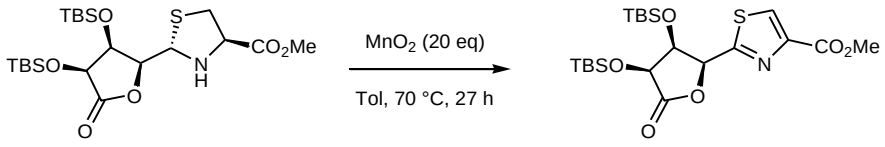

122 **130**
M = 487.76

Preparation:

Compound **122**	M = 491.79 g mol^{-1}	1.0 eq	0.10 mmol	50 mg
MnO_2, activated (*Fluka*)	M = 86.94 g mol^{-1}	20 eq	2.00 mmol	177 mg
Tol				2 mL

To a solution of 50 mg thiazolidine **122** (0.10 mmol, 1.0 eq) in 2 mL Tol were added 177 mg of MnO_2 (activated, *Fluka*; 2.00 mmol, 20 eq) and the suspension was vigorously stirred for 16 h at 70 °C. After cooling to RT, additional 177 mg of MnO_2 (activated, *Fluka*; 2.00 mmol, 20 eq) were added and the suspension was further heated to 70 °C under vigorous stirring for 11 h. After cooling to RT the suspension was filtered over a short Celite column and concentrated *in vacuo* to obtain 35% of the thiazole **130** (17 mg, 35 µmol) as a pale yellow solid.

TLC: R_f = 0.36 (Tol/EtOAc 5:1).

ESI-MS: m/z = 510 $[M+Na]^+$.

HRMS: $[M+Na]^+$: $C_{21}H_{37}NO_6SSi_2Na$, calculated: 510.1772, found: 510.1775.

IR: pellet; $\tilde{\nu}$ = 2951, 2929, 2857, 1815, 1730, 1471, 1333, 1252, 1224, 1180, 1125, 1095, 1028, 983, 941, 920, 899, 836, 783, 761, 694 cm^{-1}.

^{1}H-NMR: 400 MHz, $CDCl_3$: δ = –0.41, 0.02, 0.19, 0.23 (each s, 3 H, $SiCH_3$), 0.66, 0.96 (each s, 9 H, $SiC(CH_3)_3$), 3.95 (s, 3 H, CO_2CH_3), 4.57 (d, 1 H, $^3J_{4\text{-H}/3\text{-H}}$ = 3.9 Hz, 4-H), 4.72 (dd, 1 H, $^3J_{3\text{-H}/2\text{-H}}$ = 2.6 Hz, $^3J_{3\text{-H}/4\text{-H}}$ = 3.9 Hz, 3-H), 5.73 (d, 1 H, $^3J_{2\text{-H}/3\text{-H}}$ = 2.6 Hz, 2-H), 8.23 (s, 1 H, Thz-H).

^{13}C-NMR: 100 MHz, $CDCl_3$: δ = –5.3, –4.8, –4.6, –4.5 (each $SiCH_3$), 18.1, 18.8 (each $SiC(CH_3)_3$), 25.6, 26.1 (each $SiC(CH_3)_3$), 52.7 (CO_2CH_3), 73.6 (C-4), 74.1 (C-3), 79.2 (C-2), 128.7 (Thz-HC=C), 146.8 (Thz-HC=C), 161.7 (CO_2CH_3), 166.4 (C-1), 173.1 (C-5).

Melting point: 158 °C.

Opt. rotation: $[\alpha]_{589}^{20}$ = –70.5, $[\alpha]_{578}^{20}$ = –72.8, $[\alpha]_{546}^{20}$ = –83.0, $[\alpha]_{436}^{20}$ = –140.7, $[\alpha]_{365}^{20}$ = –212.0 (c = 0.98 g/100 mL $CHCl_3$).

5.4.21 [(3*S*,4*S*)-bis[(*tert*-butyl-dimethylsilyl)oxy]-5-oxo-tetrahydro-furan-(2*S*)-yl)-(1*R*)-(*tert*-butyl-dimethylsilyl)oxymethyl]-1,3-thiazole-carboxylic acid methyl ester (131)

Method A) oxidation of purified thiazolidine **124**

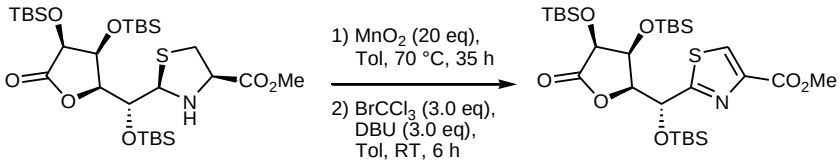

124 **131**
M = 632.04

Preparation:

Compound **124**	M = 636.08 g mol^{-1}	1.0 eq	2.94 mmol	1.87 g
MnO_2, activated (*Fluka*)	M = 86.94 g mol^{-1}	20 eq	58.8 mmol	5.11 g
$BrCCl_3$	M = 198.28 g mol^{-1}, ρ = 2.01	3.0 eq	8.81 mmol	0.87 mL (1.74 g)
DBU	M = 152.24 g mol^{-1}, ρ = 1.02	3.0 eq	8.81 mmol	1.32 mL (1.34 g)
Tol				50 mL

To a solution of 1.87 g thiazolidine **124** (2.94 mmol, 1.0 eq) in 50 mL Tol were added 5.11 g of MnO_2 (activated, *Fluka*; 58.8 mmol, 20 eq) and the suspension was vigorously stirred at 70 °C until TLC (Tol/EtOAc 7:1) showed complete consumption of the thiazolidine (35 h). After cooling to RT, 0.87 mL of $BrCCl_3$ (1.74 g, 8.81 mmol, 3.0 eq) and 1.32 mL of DBU (1.34 g, 8.81 mmol, 3.0 eq) were added and the suspension was stirred at RT until no thiazoline intermediate **133** (section 5.4.23) was shown any more by TLC (approx. 6 h, Tol/EtOAc 7:1). After filtration over Celite, the suspension was extracted once with sat. $NaHCO_3$ and once with sat. NH_4Cl, dried with brine and over $MgSO_4$, and concentrated *in vacuo*. Purification by flash chromatography (CH_2Cl_2/pentane 4:1) yielded 51% of the thiazole **131** (956 mg, 1.51 µmol) as a colorless oil.

Method B) three-step protection/oxidation of **100**

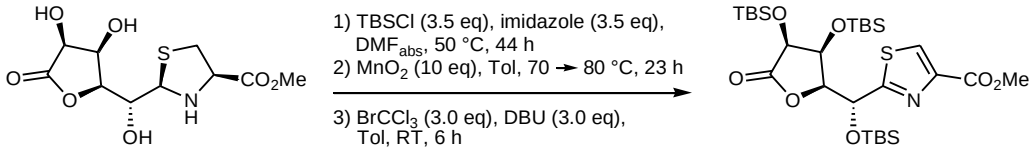

100 **131** M = 632.04

Preparation:

Compound **100**	M = 293.29 g mol^{-1}	1.0 eq	36.7 mmol	10.8 g
TBSCl	M = 150.72 g mol^{-1}	3.5 eq	128 mmol	19.3 g
Imidazole	M = 68.08 g mol^{-1}	3.5 eq	128 mmol	8.71 g
DMF_{abs}				21 mL
MnO_2, activated (*Fluka*)	M = 86.94 g mol^{-1}	10 eq	367 mmol	31.9 g
$BrCCl_3$	M = 198.28 g mol^{-1}, ρ = 2.01	3.0 eq	110 mmol	10.9 mL (21.8 g)
DBU	M = 152.24 g mol^{-1}, ρ = 1.02	3.0 eq	110 mmol	16.4 mL (16.7 g)
Tol				200 mL

10.8 g of the thiazolidine triol **100** (36.7 mmol, 1.0 eq), 19.3 g of TBSCl (128 mmol, 3.5 eq) and 8.71 g of imidazole (128 mmol, 3.5 eq) were dissolved in 21 mL of DMF_{abs} in a nitrogen atmosphere. The solution was stirred for 44 h at 50 °C, diluted with 700 mL of pentane, and 50 mL of 5% aq. $NaHCO_3$ were added. The pentane phase was reextraced with 20 mL MeOH in order to remove the precipitate, and the MeOH phase was reextracted with pentane. The combined pentane phases were dried over $MgSO_4$, filtered, concentrated *in vacuo*, and dried *in vacuo* at 40 °C for 24 h in order to remove the TBSOH.

The resulting waxy yellow solid was dissolved in 200 mL of Tol, 31.9 g of MnO_2 (activated, *Fluka*; 367 mmol, 10 eq) were added and the suspension was vigorously stirred for 6 h at 70 °C. Further 16.0 g of (activated, *Fluka*; 184 mmol, 5.0 eq) were added and the solution was heated to 80 °C until TLC (Tol/EtOAc 7:1) showed complete consumption of the thiazolidine (13 h). After cooling to RT, 10.9 mL of $BrCCl_3$ (21.8 g, 110 mmol, 3.0 eq) and 16.4 mL of DBU (16.7 g, 110 mmol, 3.0 eq) were added and the suspension was stirred at RT until no thiazoline intermediate **133** (section 5.4.23) was shown any more by TLC (approx. 6 h, Tol/EtOAc 7:1). After filtration over Celite, the suspension was extracted once with sat. $NaHCO_3$ and once with sat. NH_4Cl, dried with brine and over $MgSO_4$, and concentrated *in vacuo*. Purification by flash chromatography (CH_2Cl_2/pentane 4:1) yielded 34% of the thiazole **131** (7.77 g, 13.0 mmol) as a colorless oil.

TLC: R_f = 0.71 (Tol/EtOAc 7:1).

ESI-MS: m/z = 654 $[M+Na]^+$.

HRMS: $[M+Na]^+$: $C_{28}H_{53}NO_7SSi_3Na$, calculated: 654.2743, found: 654.2758.

IR: pellet; $\tilde{\nu}$ = 2952, 2929, 2886, 2857, 1804, 1731, 1471, 1362, 1249, 1212, 1124, 1026, 987, 948, 893, 859, 836, 809, 778, 753 cm^{-1}.

^{1}H-NMR: 300 MHz, $CDCl_3$: δ = 0.09, 0.18, 0.18, 0.21, 0.23, 0.24 (each s, 3 H, $SiCH_3$), 0.83, 0.95, 0.79 (each s, 9 H, $SiC(CH_3)_3$), 3.92 (s, 3 H, CO_2CH_3), 4.25 (dd, 1 H, $^3J_{3\text{-H}/4\text{-H}}$ = 2.0 Hz, $^3J_{3\text{-H}/2\text{-H}}$ = 9.3 Hz, 3-H), 4.41 (d, 1 H, $^3J_{5\text{-H}/4\text{-H}}$ = 3.6 Hz, 5-H), 4.94 (dd, 1 H, $^3J_{4\text{-H}/3\text{-H}}$ = 2.0 Hz, $^3J_{4\text{-H}/5\text{-H}}$ = 3.6 Hz, 4-H), 5.40 (d, 1 H, $^3J_{2\text{-H}/3\text{-H}}$ = 9.3 Hz, 2-H), 8.16 (s, 1 H, Thz-H).

^{13}C-NMR: 75 MHz, $CDCl_3$: δ = –5.1, –5.0, –4.9, –4.3, –4.2, –4.0, (each $SiCH_3$), 18.6, 18.6, 18.9 (each $SiC(CH_3)_3$), 26.0, 26.2, 26.2 (each $SiC(CH_3)_3$), 52.2 (CO_2CH_3), 70.2 (C-2), 73.3 (C-4), 74.5 (C-5), 81.3 (C-2), 128.2 (Thz-HC=C), 147.2 (Thz-HC=C), 161.8 (CO_2CH_3), 172.6 (C-1), 174.0 (C-5).

Melting point: 45 °C.

Opt. rotation: $[\alpha]_{589}^{23}$ = –11.1, $[\alpha]_{578}^{23}$ = –11.4, $[\alpha]_{546}^{23}$ = –12.3, $[\alpha]_{436}^{23}$ = –15.0, $[\alpha]_{365}^{23}$ = –10.4 (c = 0.81 g/100 mL $CHCl_3$).

5.4.22 [(3*S*,4*S*)-bis[(triethylsilyl)oxy]-5-oxo-tetrahydro-furan-(2*S*)-yl)-(1*R*)-(triethylsilyl)oxymethyl]-1,3-thiazole-carboxylic acid methyl ester (132)

Method A) oxidation of purified thiazolidine **128**

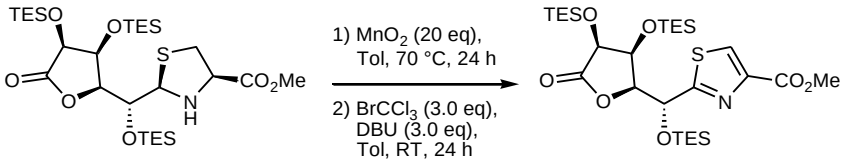

128 **132** M = 632.04

Preparation:

Compound **128**	M = 632.04 g mol^{-1}	1.0 eq	0.14 mmol	87 mg
MnO_2, activated (*Fluka*)	M = 86.94 g mol^{-1}	20 eq	2.74 mmol	238 mg
$BrCCl_3$	M = 198.28 g mol^{-1}, ρ = 2.01	3.0 eq	0.41 mmol	40 µL (81 mg)
DBU	M = 152.24 g mol^{-1}, ρ = 1.02	3.0 eq	0.41 mmol	61 µL (63 mg)
Tol				4 mL

To a solution of 87 mg thiazolidine **128** (0.14 mmol, 1.0 eq) in 4 mL of Tol were added 238 mg of MnO_2 (activated, *Fluka*; 2.74 mmol, 20 eq) and the suspension was vigorously stirred at 70 °C until TLC (Tol/EtOAc 7:1) showed complete consumption of the thiazolidine (24 h). After cooling to RT, 40 µL of $BrCCl_3$ (81 mg, 0.41 mmol, 3.0 eq) and 61 µL of DBU (63 mg, 0.41 mmol, 3.0 eq) were added and the suspension was stirred at RT until no thiazoline intermediate **134** (section 5.4.23) was shown any more by TLC (approx. 24 h, Tol/EtOAc 7:1). After filtration over Celite, the suspension was extracted once with sat. $NaHCO_3$ and once with sat. NH_4Cl, dried with brine and over $MgSO_4$, and concentrated *in vacuo*. The resulting colorless solid was dissolved in pentane/H_2O, the phases were separated and the aqueous phase was extracted with pentane. The combined organic phases were dried with brine and over $MgSO_4$, filtered, and concentrated *in vacuo* to yield 53% of the thiazole **132** (46 mg, 72.8 µmol) as a colorless oil.

Method B) three-step protection/oxidation of **100**

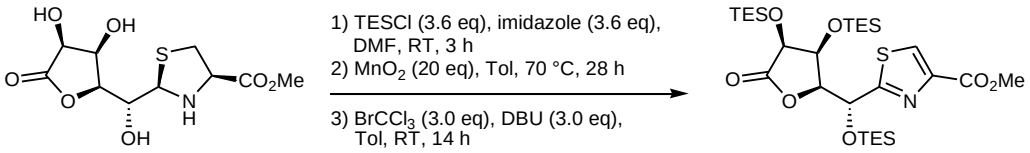

100 **132** M = 632.04

Preparation:

Compound **100**	M = 293.29 g mol^{-1}	1.0 eq	22.6 mmol	6.64 g
TESCl	M = 150.72 g mol^{-1}, ρ = 0.90	3.6 eq	81.5 mmol	13.7 mL (12.3 g)
Imidazole	M = 68.08 g mol^{-1}	3.6 eq	81.5 mmol	5.55 g
DMF				14 mL
MnO_2, activated (*Fluka*)	M = 86.94 g mol^{-1}	20 eq	453 mmol	39.4 g
$BrCCl_3$	M = 198.28 g mol^{-1}, ρ = 2.01	3.0 eq	67.8 mmol	6.69 mL (13.5 g)
DBU	M = 152.24 g mol^{-1}, ρ = 1.02	3.0 eq	67.8 mmol	10.1 mL (10.3 g)
Tol				200 mL

6.64 g of the thiazolidine triol **100** (22.6 mmol, 1.0 eq) were dissolved in 14 mL of DMF and 5.55 g of imidazole (81.5 mmol, 3.6 eq) were added. 12.3 mL of TESCl (12.3 g, 81.5 mmol, 3.6 eq) were slowly added and the solution was stirred for 3 h at RT, diluted with 500 mL of CH_2Cl_2, and 40 mL of 5% aq. $NaHCO_3$ were added. The phases were separated and the aqueous phase was extracted once with CH_2Cl_2. The combined organic phases were dried with brine and over $MgSO_4$, filtered, concentrated *in vacuo*, and dried *in vacuo* for 24 h in order to remove the TESOH.

The resulting pale yellow oil was dissolved in 200 mL of Tol, 39.4 g of MnO_2 (activated, *Fluka*; 453 mmol, 20 eq) were added and the suspension was vigorously stirred at 70 °C until TLC (Tol/EtOAc 7:1) showed complete consumption of the thiazolidine (28 h). After cooling to RT, 6.69 mL of $BrCCl_3$ (13.5 g, 67.8 mmol, 3.0 eq) and 10.1 mL of DBU (10.3 g, 67.8 mmol, 3.0 eq) were added and the suspension was stirred at RT until no thiazoline intermediate **134** (section 5.4.23) was shown any more by TLC (Tol/EtOAc 7:1). After filtration over Celite, the suspension was extracted once with sat. $NaHCO_3$ and once with sat. NH_4Cl, dried with brine and over $MgSO_4$, and concentrated *in vacuo*. Purification by flash chromatography (CH_2Cl_2/pentane 4:1) yielded 48% of the thiazole **132** (6.91 g, 10.9 mmol) as a colorless oil.

TLC: R_f = 0.61 (Tol/EtOAc 7:1).

ESI-MS: m/z = 654 $[M+Na]^+$.

HRMS: $[M+Na]^+$: $C_{28}H_{53}NO_7SSi_3Na$, calculated: 654.2743, found: 654.2744.

IR: film; $\tilde{\nu}$ = 2954, 2911, 2877, 1803, 1727, 1458, 1414, 1239, 1207, 1135, 1004, 987, 947, 892, 855, 830, 787, 725 cm^{-1}.

^{1}H-NMR: 500 MHz, $CDCl_3$: δ = 0.73-0.78 (m, 18 H, 9 x $SiC\underline{H}_2CH_3$), 0.90 (t, 9 H, $^3J_{SiCH2CH\underline{3}/SiCH\underline{2}CH3}$ = 8.0 Hz, 3 x $SiCH_2C\underline{H}_3$), 0.97-1.01 (m, 18 H, 6 x $SiCH_2C\underline{H}_3$), 3.91 (s, 3 H, CO_2CH_3), 4.28 (dd, 1 H, $^3J_{3\text{-}H/4\text{-}H}$ = 2.2 Hz, $^3J_{3\text{-}H/2\text{-}H}$ = 9.1 Hz, 3-H), 4.36 (d, 1 H, $^3J_{5\text{-}H/4\text{-}H}$ = 3.8 Hz, 5-H), 4.76 (dd, 1 H, $^3J_{4\text{-}H/3\text{-}H}$ = 2.2 Hz, $^3J_{4\text{-}H/5\text{-}H}$ = 3.8 Hz, 4-H), 5.42 (d, 1 H, $^3J_{2\text{-}H/3\text{-}H}$ = 9.1 Hz, 2-H), 8.18 (s, 1 H, Thz-H).

^{13}C-NMR: 125 MHz, $CDCl_3$: δ = 4.9, 5.1, 5.2 (each $SiCH_2CH_3$), 6.8, 6.8, 6.9 (each $SiCH_2CH_3$), 52.3 (CO_2CH_3), 70.5 (C-2), 72.8 (C-4), 73.5 (C-5), 81.7 (C-2), 128.4 (Thz-HC=C), 147.3 (Thz-HC=C), 162.0 (CO_2CH_3), 172.5 (C-1), 174.2 (C-6).

Opt. rotation: $[\alpha]_{589}^{20}$ = –8.9, $[\alpha]_{578}^{20}$ = –9.2, $[\alpha]_{546}^{20}$ = –10.2, $[\alpha]_{436}^{20}$ = –13.9, $[\alpha]_{365}^{20}$ = –13.4 (c = 2.40 g/100 mL $CHCl_3$).

5.4.23 [(3*S*,4*S*)-bis[(*tert*-butyl-dimethylsilyl)oxy]-5-oxo-tetrahydro-furan-(2*S*)-yl)-(1*R*)-(*tert*-butyl-dimethylsilyl)oxymethyl]-1,3-thiazoline-(4*R*)-carboxylic acid methyl ester (133) and [(3*S*,4*S*)-bis[(triethylsilyl)oxy]-5-oxo-tetrahydro-furan-(2*S*)-yl)-(1*R*)-(triethylsilyl)oxymethyl]-1,3-thiazoline-(4*R*)-carboxylic acid methyl ester (134)

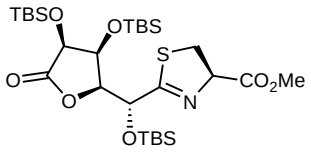

133
M = 634.06

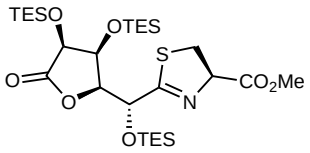

134
M = 634.06

The thiazolines **133** and **134** occur as intermediates in the oxidation of the thiazolidines **124** (section 5.4.21) and **128** (section 5.4.22), respectively. As they were not isolated as pure compounds, they were not further analyzed.

TLC: **133**: R_f = 0.62 (Tol/EtOAc 7:1).
134: R_f = 0.55 (Tol/EtOAc 7:1).

^{1}H-NMR (133): 600 MHz, DMSO-d_6: δ = 0.08, 0.08, 0.12, 0.12, 0.13, 0.15 (each s, 3 H, $SiCH_3$), 0.83, 0.84, 0.92 (each s, 9 H, $SiC(CH_3)_3$), 3.81 (s, 3H, CO_2CH_3), 4.08 (dd, 1 H, $^2J_{\beta\text{-}H^u/\beta\text{-}H^d}$ = 16.9 Hz, $^3J_{\beta\text{-}H^u/\alpha\text{-}H}$ = 6.3 Hz, β-H^u), 4.21 (d, 1 H, $^3J_{2\text{-}H/3\text{-}H}$ = 9.3 Hz, 2-H), 4.22 (dd, 1 H, $^2J_{\beta\text{-}H^d/\beta\text{-}H^u}$ = 16.9 Hz, $^3J_{\beta\text{-}H^d/\alpha\text{-}H}$ = 3.1 Hz, β-H^d), 4.60 (dd, 1 H, $^3J_{3\text{-}H/4\text{-}H}$ = 2.1 Hz, $^3J_{3\text{-}H/2\text{-}H}$ = 9.3 Hz, 3-H), 4.71 (dd, 1 H, $^3J_{4\text{-}H/3\text{-}H}$ = 2.1 Hz, $^3J_{4\text{-}H/5\text{-}H}$ = 3.7 Hz, 4-H), 4.90 (d, 1 H, $^3J_{5\text{-}H/4\text{-}H}$ = 3.7 Hz, 5-H).

^{13}C-NMR (134): 150 MHz, DMSO-d_6: δ = 42.3 (C-β), 52.5 ($CO_2\underline{C}H_3$), 72.2 (C-4), 72.9 (C-5), 73.0 (C-2), 79.1 (C-3), 82.8 (C-α), 161.6 ($\underline{C}O_2CH_3$), 163.7 (C-1), 174.2 (C-6); determined from HSQC and HMBC; the exact positions of the TBS carbon signals cannot be given due to signal overlap.

5.4.24 [(3*S*,4*S*)-bis[(*tert*-butyl-dimethylsilyl)oxy]-5-oxo-tetrahydro-furan-(2*S*)-yl)-(1*R*)-(*tert*-butyl-dimethylsilyl)oxymethyl]-formonitrile (135)

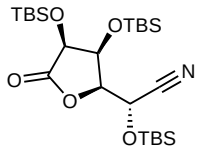

135
M = 515.91

The overoxidation product **135** was obtained in 4.3% yield (65 mg, 1.26 mmol) from the oxidation reaction of **124** (section 5.4.21) as a colorless oil.

TLC: R_f = 0.82 (Tol/EtOAc 7:1).

ESI-MS: m/z = 538 $[M+Na]^+$.

HRMS: $[M+Na]^+$: $C_{24}H_{49}NO_5SSi_3Na$, calculated: 538.2811, found: 538.2815.

IR: film; $\tilde{\nu}$ = 2954, 2930, 2887, 2858, 1807, 1756, 1726, 1472, 1390, 1362, 1253, 1180, 1126, 1029, 1006, 988, 945, 886, 836, 806, 777 cm^{-1}.

^{1}H-NMR: 300 MHz, DMSO-d_6: δ = 0.12, 0.14, 0.15, 0.16, 0.16, 0.17 (each s, 3 H, $SiCH_3$), 0.87, 0.91, 0.93 (each s, 9 H, $SiC(CH_3)_3$), 4.60 (dd, 1 H, $^3J_{4\text{-H}/3\text{-H}}$ = 2.3 Hz, $^3J_{4\text{-H}/5\text{-H}}$ = 3.8 Hz, 4-H), 4.66 (dd, 1 H, $^3J_{3\text{-H}/4\text{-H}}$ = 2.3 Hz, $^3J_{3\text{-H}/2\text{-H}}$ = 8.6 Hz, 3-H), 4.85 (d, 1 H, $^3J_{5\text{-H}/4\text{-H}}$ = 3.8 Hz, 5-H), 4.88 (d, 1 H, $^3J_{2\text{-H}/3\text{-H}}$ = 8.6 Hz, 2-H).

^{13}C-NMR: 75 MHz, DMSO-d_6: δ = –5.6, –5.5, –4.9, –4.9, –4.8, –4.0 (each $SiCH_3$), 17.9, 18.0, 18.3 (each $SiC(CH_3)_3$), 25.3, 25.7, 25.8 (each $SiC(CH_3)_3$), 60.9 (C-2), 71.8 (C-4), 72.8 (C-5), 78.1 (C-2), 117.1 (C-1), 173.4 (C-6).

Melting point: 82 °C.

5.4.25 (9*aR*)H-bis-(6*S*,7*S*)-(8*S*,9*R*)-*O*-isopropylidene-5-oxo-octahydro-thiazolo [3,2-*a*]azepine-(3*R*)-carboxylic acid methyl ester (136)

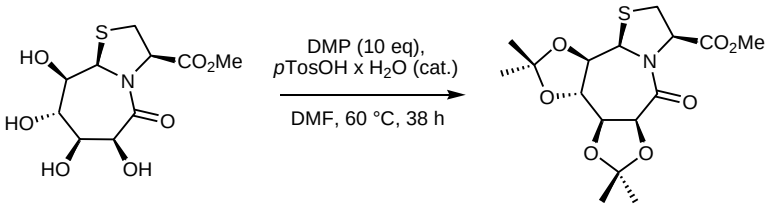

105 **136**
M = 373.42

Preparation:

Compound **105**	M = 293.29 g mol^{-1}	1.0 eq	40.9 mmol	12.0 g
DMP	M = 104.15 g mol^{-1}, ρ = 0.85	10 eq	409 mmol	50.3 mL (42.6 g)
*p*TosOH x H_2O	M = 190.22 g mol^{-1}			cat.
DMF_{abs}				120 mL

Under a nitrogen atmosphere, 12.0 g of the tetraol **105** (40.9 mmol, 1.0 eq) were dissolved in 120mL of DMF_{abs}. After the addition of 50.3 mL of DMP (42.6 g, 409 mmol, 10 eq) and a catalytic amount of *p*TosOH x H_2O, the solution was stirred for 38 h at 60 °C, cooled to RT, neutralized by addition of NEt_3, and concentrated *in vacuo*. Residual amounts of DMF were removed by coevaporation with Tol. The crude product was subjected to flash chromatography (EtOAc/Tol/NEt_3 300:50:1) to obtain 93% (14.19 g, 38.0 mmol) of the bisacetonide **136** as a colorless powder.

TLC: R_f = 0.54 (EtOAc/Tol 4:1).

ESI-MS: m/z = 396 $[M+Na]^+$.

HRMS: $[M+Na]^+$: $C_{16}H_{23}NO_7SNa$, calculated: 396.1087, found: 396.1089.

IR: pellet; $\tilde{\nu}$ = 2985, 2939, 2888, 1752, 1647, 1372, 1302, 1213, 1165, 1076, 998, 851 cm^{-1}.

^{1}H-NMR: 300 MHz, DMSO-d_6: δ = 1.34 (s, 3 H, Isopr-CH_3), 1.38 (s, 6 H, 2 x Isopr-CH_3), 1.44 (s, 3 H, Isopr-CH_3), 3.09 (dd, 1 H, $^2J_{2\text{-}H^u/2\text{-}H^d}$ = 12.3 Hz, $^3J_{2\text{-}H^u/3\text{-}H}$ = 1.8 Hz, 2-H^u), 3.26 (dd, 1 H, $^2J_{2\text{-}H^d/2\text{-}H^u}$ = 12.3 Hz, $^3J_{2\text{-}H^d/3\text{-}H}$ = 7.3 Hz, 2-H^d), 3.65 (s, 3 H, CO_2CH_3), 4.29 (dd, 1 H, $^3J_{9\text{-}H/9a\text{-}H}$ = 7.1 Hz, $^3J_{9\text{-}H/8\text{-}H}$ = 9.4 Hz, 9-H), 4.36 (dd, 1 H, $^3J_{7\text{-}H/6\text{-}H}$ = 5.9 Hz, $^3J_{7\text{-}H/8\text{-}H}$ = 8.2 Hz, 7-H), 4.52 (dd, 1 H, $^3J_{8\text{-}H/7\text{-}H}$ = 8.2 Hz, $^3J_{8\text{-}H/9\text{-}H}$ = 9.4 Hz, 8-H), 4.78 (dd, 1 H, $^3J_{3\text{-}H/2\text{-}H^u}$ = 1.8 Hz, $^3J_{3\text{-}H/2\text{-}H^d}$ = 7.3 Hz, 3-H), 4.84 (d, 1 H, $^3J_{6\text{-}H/7\text{-}H}$ = 5.9 Hz, 6-H), 5.46 (d, 1 H, $^3J_{9a\text{-}H/9\text{-}H}$ = 7.1 Hz, 9a-H).

^{13}C-NMR: 75 MHz, DMSO-d_6: δ = 26.2, 26.2, 26.9, 27.0 (each Isopr-CH_3), 30.6 (C-2), 52.2 ($CO_2\underline{C}H_3$), 62.0 (C-9a), 63.5 (C-3), 73.5 (C-9), 75.1 (C-6), 75.3 (C-8), 76.9 (C-7), 111.8, 111.9 (each Isopr-$C_{quart.}$), 166.4, 170.1 ($\underline{C}O_2CH_3$, C-5).

Melting point: 224 °C.

Opt. rotation: $[\alpha]_{589}^{23}$ = +57.1, $[\alpha]_{578}^{23}$ = +59.7, $[\alpha]_{546}^{23}$ = +67.8, $[\alpha]_{436}^{23}$ = +116.1, $[\alpha]_{365}^{23}$ = +176.8 (c = 1.02 g/100 mL $CHCl_3$).

5.4.26 (9*aR*)H-bis-(6*S*,7*S*)-(8*S*,9*R*)-*O*-isopropylidene-5-oxo-octahydro-thiazolo [3,2-*a*]azepine-(3*S*)-carboxylic acid methyl ester (137)

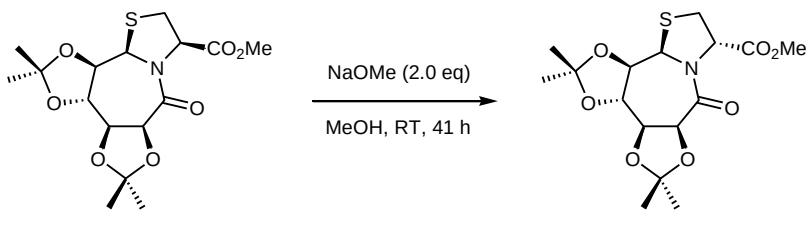

136 **137**
M = 373.42

Preparation:

Compound **136**	M = 373.42 g mol^{-1}	1.0 eq	80.3 µmol	30 mg
NaOMe (30% in MeOH)	M = 54.02 g mol^{-1}, ρ = 0.95	1.0 eq	80.3 µmol	15.3 µL (14.5 mg)
$MeOH_{abs}$				2.0 mL

30 mg of the bisacetonide **136** (80.3 µmol, 1.0 eq) were dissolved in 2.0 mL of $MeOH_{abs}$ in a nitrogen atmosphere and the solution was cooled to 0°C. After treatment with 1.0 eq of NaOMe (30% in MeOH, 15.3µL, 14.5 mg, 80.3 µmol) the solution was stirred for 16 h at 0 °C. Another equivalent of NaOMe was subsequently added, the solution was allowed to warm to RT and stirred for further 25h. The reaction was quenched with 5 mL of ice, 15 mL of Tol/EtOAc (3:1) were added and the phases were separated. The aqueous phase was extracted with Tol/EtOAc (3:1), the combined organic phases were dried with brine and over $MgSO_4$, filtered, and concentrated *in vacuo*. Flash chromatography (EtOAc/Tol 4:1) yielded 30% (9 mg, 24.1 µmol) of the epimeric bisacetonide **137** as a colorless solid, and 63% (19 mg, 50.9 µmol) of the starting material **136.**

TLC: R_f = 0.51 (EtOAc/Tol 4:1).

ESI-MS: m/z = 396 $[M+Na]^+$.

HRMS: $[M+Na]^+$: $C_{16}H_{23}NO_7SNa$, calculated: 396.1087, found: 396.1079.

^{1}H-NMR: 300 MHz, DMSO-d_6: δ = 1.34 (s, 3 H, Isopr-CH_3), 1.39 (s, 6 H, 2 x Isopr-CH_3), 1.44 (s, 3 H, Isopr-CH_3), 2.97 (dd, 1 H, $^2J_{2\text{-}H^u/2\text{-}H^d}$ = 11.9 Hz, $^3J_{2\text{-}H^u/3\text{-}H}$ = 6.7 Hz, 2-H^u), 3.27-3.33 (m, 1 H, 2-H^d and s, H_2O), 3.64 (s, 3 H, CO_2CH_3), 3.88 (dd, 1 H, $^3J_{8\text{-}H/7\text{-}H}$ = 8.1 Hz, $^3J_{8\text{-}H/9\text{-}H}$ = 9.4 Hz, 8-H), 4.39 (dd, 1 H, $^3J_{7\text{-}H/6\text{-}H}$ = 6.1 Hz, $^3J_{7\text{-}H/8\text{-}H}$ = 8.1 Hz, 7-H), 4.82 (dd, 1 H, $^3J_{9\text{-}H/9a\text{-}H}$ = 6.5 Hz, $^3J_{9\text{-}H/8\text{-}H}$ = 9.4 Hz, 9-H), 4.95 (d, 1 H, $^3J_{6\text{-}H/7\text{-}H}$ = 6.1 Hz, 6-H), 4.99 (pt, 1 H, $^3J_{3\text{-}H/2\text{-}H^u}$ = $^3J_{3\text{-}H/2\text{-}H^d}$ = 6.7 Hz, 3-H), 5.20 (d, 1 H, $^3J_{9a\text{-}H/9\text{-}H}$ = 6.5 Hz, 9a-H).

5.4.27 bis-(6*S*,7*S*)-(8*S*,9*R*)-*O*-isopropylidene-5-oxo-(2,2,3,6,7,8)-hexahydro-thiazolo [3,2-*a*]azepine-(3*R*)-carboxylic acid methyl ester (138)

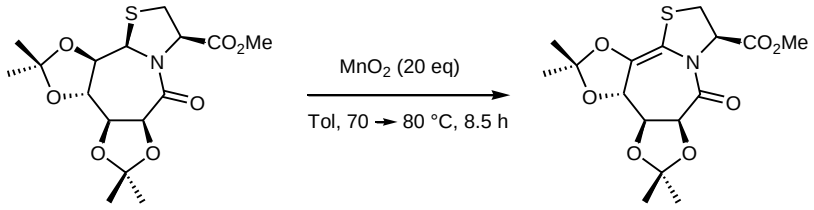

136 **138**
M = 371.41

Preparation:

Compound **136**	M = 373.42 g mol^{-1}	1.0 eq	7.90 mmol	2.95 g
MnO_2, activated (*Fluka*)	M = 86.94 g mol^{-1}	20 eq	15.8 mmol	13.7 g
Tol				60 mL

To a solution of 2.95 g thiazolidine **136** (7.90 mmol, 1.0 eq) in 60 mL Tol were added 13.7 g MnO_2 (activated, *Fluka*; 15.8 mmol, 20 eq). The suspension was vigorously stirred for 6.5 h at 70 °C and further 2 h at 80 °C, cooled to RT, filtered over Celite, and concentrated. After purification with flash chromatography (Tol/EtOAc 3:1) 40% of the oxidized [7,5]-bicycle **138** (1.18 g, 3.19 mmol) were obtained as a colorless foam.

TLC: R_f = 0.74 (EtOAc/Tol 4:1).

ESI-MS: *m/z* = 372 $[M+H]^+$, 394 $[M+Na]^+$

HRMS: $[M+H]^+$: $C_{16}H_{21}NO_7SH$, calculated: 372.1111, found: 372.1123.
$[M+Na]^+$: $C_{16}H_{21}NO_7SNa$, calculated: 394.0931, found: 394.0938.

IR: pellet; $\tilde{\nu}$ = 2997, 2894, 1751, 1679, 1374, 1203, 1136, 1102, 1060, 1001, 855, 841.

^{1}H-NMR: 600 MHz, DMSO-d_6: δ = 1.34, 1.34, 1.38, 1.43 (each s, 3 H, Isopr-CH_3), 3.38 (dd, 1 H, $^2J_{2\text{-H}^{proS}/2\text{-H}^{proR}}$ = 11.2 Hz, $^3J_{2\text{-H}^{proS}/3\text{-H}}$ = 2.0 Hz, 2-H^{proS}), 3.51 (dd, 1 H, $^2J_{2\text{-H}^{proR}/2\text{-H}^{proS}}$ = 11.2 Hz, $^3J_{2\text{-H}^{proR}/3\text{-H}}$ = 7.7 Hz, 2-H^{proR}), 3.71 (s, 3 H, CO_2CH_3), 4.80 (m, 2 H, 6-H, 8-H), 4.86 (dd, 1 H, $^3J_{7\text{-H}/6\text{-H}}$ / $^3J_{7\text{-H}/8\text{-H}}$ = 2.3/4.8 Hz, 7-H), 4.99 (dd, 1 H, $^3J_{3\text{-H}/2\text{-H}^{proS}}$ = $^3J_{3\text{-H}/2\text{-H}^{proR}}$ = 7.7 Hz, 3-H).

^{13}C-NMR: 150 MHz, DMSO-d_6: δ = 25.1, 25.6, 25.7, 27.0 (each Isopr-CH_3), 31.1 (C-2), 52.6 ($CO_2\underline{C}H_3$), 58.3 (C-3), 75.2 (C-7), 77.0, 86.8 (C-6, C-8), 105.5 (C-9a), 111.0, 114.6 (each Isopr-$C_{quart.}$) , 137.3 (C-9), 166.7 (C-6), 169.3 ($\underline{C}O_2CH_3$).

Melting point: 84 °C.

Opt. rotation: $[\alpha]_{589}^{24}$= –294.5, $[\alpha]_{578}^{24}$= –309.5, $[\alpha]_{546}^{24}$= –359.2, $[\alpha]_{436}^{24}$= –693.4 (c = 1.09 g/100 mL $CHCl_3$).

5.4.28 (6*S*,7*S*)-dihydroxy-(8*S*,9*R*)-*O*-isopropylidene-5-oxo-(2,2,3,6,7,8)-hexahydro-thiazolo [3,2-*a*]azepine-(3*R*)-carboxylic acid methyl ester (139)

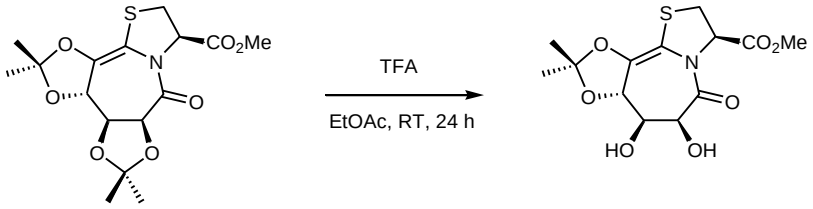

138 **139**
M = 331.34

Preparation:

Compound **138**	M = 371.41 g mol^{-1}	1.0 eq	1.80 mmol	667 mg
TFA	M = 114.02 g mol^{-1}, ρ = 1.48			1.0 mL (1.48 g)
EtOAc				10 mL

667 mg of the bisacetonide **138** (1.80 mmol, 1.0 eq) were dissolved in 10 mL of EtOAc and 1.0 mL of TFA (1.48 g) were added dropwise. Another 2 mL of TFA (2.96 g) were added after 20 h stirring at RT, and again after further 2 h. The solution was stirred at RT for another 2 h and 5 mL H_2O were subsequently added. The phases were separated, the aqueous phase was extracted with EtOAc and the combined organic phases were dried with brine and over $MgSO_4$. After evaporation of the solvents *in vacuo* the product was purified with flash chromatography (EtOAc/Tol 4:1) to yield 36% of the monoacetonide **139** (215 mg, 0.65 mmol) as a pale yellow oil.

TLC: R_f = 0.33 (EtOAc/Tol 4:1).

ESI-MS: m/z = 354 $[M+Na]^+$

HRMS: $[M+Na]^+$: $C_{13}H_{17}NO_7SNa$, calculated: 354.0618, found: 354.0620.

^{1}H-NMR: 600 MHz, DMSO-d_6: δ = 1.38, 1.52 (each s, 3 H, Isopr-CH_3), 3.38-3.40 (m, 1 H, 2-H^u and s, H_2O), 3.44 (dd, 1 H, $^2J_{2\text{-}H^d/2\text{-}H^u}$ = 11.2 Hz, $^3J_{2\text{-}H^d/3\text{-}H}$ = 7.5 Hz, 2-H^u), 3.69 (s, 3 H, CO_2CH_3), 4.25 (m, 1H, 7-H), 4.35 (m, 1 H, 6-H), 4.63 (d, 1 H, $^3J_{8\text{-}H/7\text{-}H}$ = 3.5 Hz, 8-H), 4.90 (d, 1 H, $^3J_{6\text{-}OH/6\text{-}H}$ = 7.3 Hz, 6-OH), 5.42 (dd, 1 H, $^3J_{3\text{-}H/2\text{-}H^u}$ = 2.9 Hz, $^3J_{3\text{-}H/2\text{-}H^d}$ = 7.5 Hz, 3-H), 5.72 (d, 1 H, $^3J_{7\text{-}OH/7\text{-}H}$ = 4.2 Hz, 7-OH).

5.4.29 [(3*S*,4*S*)-dihydroxy-5-oxo-tetrahydro-furan-(2*S*)-yl)-(1*R*)-hydroxymethyl]-1,3-thiazole-carboxylic acid methyl ester (140)

Method A) deprotection of TBS protected thiazole **131** *using HF*

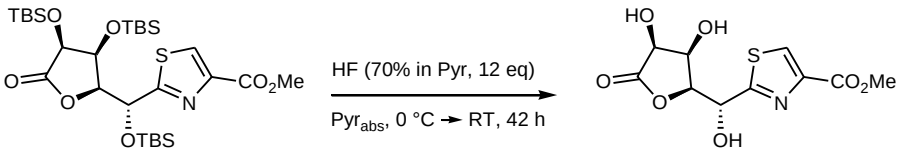

131 **140**
M = 289.26

Preparation:

Compound **131**	M = 632.04 g mol^{-1}	1.0 eq	4.00 mmol	2.52 g
HF (70% in Pyr)	M = 20.01 g mol^{-1}, ρ = 1.10	12 eq	48.0 mmol	1.25 mL (1.37 g)
Pyr_{abs}				12 mL

2.52 g of the thiazole **131** (4.00 mmol, 1.0 eq) were dissolved in 12 mL of Pyr_{abs} in a taper joint PTFE flask in a nitrogen atmosphere and cooled to 0 °C. 1.25 mL of HF (70% in Pyr; 1.37 g, 48.0 mmol, 12 eq) were slowly added and the solution was allowed to warm to RT under stirring. After 19 h, additional 1.25 mL of HF (70% in Pyr; 1.37 g, 48.0 mmol, 12 eq) were added and the solution was stirred for 23h at RT. Aq. sat. $NaHCO_3$ solution was subsequently added dropwise via a pressure-equalizing addition funnel until gas (CO_2) evolution stopped (approx. 80mL required). 250 mL of EtOAc were added and H_2O was added until all residues dissolved. The phases were separated and the aqueous phase was extracted three times with EtOAc. The combined organic phases were dried with brine and over $MgSO_4$, filtered, and concentrated *in vacuo*. The resulting yellow oil is dissolved in EtOAc/MeOH/Tol 1:1:1 and the solution is concentrated *in vacuo* in order to remove residual amounts of Pyr. The thiazole triol **140** is obtained as a colorless solid in 91% yield (1.05 g, 3.63 mmol).

The TBS cleavage can also be carried out using the less toxic hexafluorosilicic acid (H_2SiF_6) as described for the TES analog **132** in the following, although longer reaction times are required.

Method B) deprotection of TES protected thiazole **132** *using* H_2SiF_6

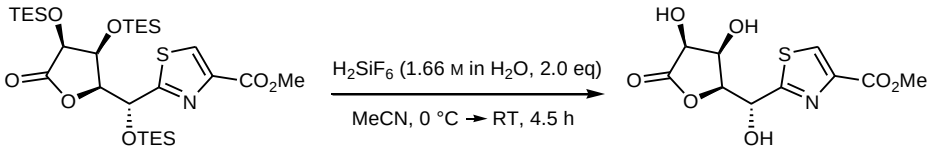

132 **140**
M = 289.26

Preparation:

Compound **132**	M = 632.04 g mol^{-1}	1.0 eq	3.29 mmol	2.08 g
H_2SiF_6 (1.66 M in H_2O)	M = 144.09 g mol^{-1}, ρ = 1.22	2.0 eq	6.58 mmol	3.96 mL (4.83 g)
CH_3CN				35 mL

2.08 g of the thiazole **132** (3.29 mmol, 1.0 eq) were dissolved in 35 mL of CH_3CN and cooled to 0 °C. 3.96 mL of H_2SiF_6 (1.66 M in H_2O; 4.83 g, 6.58 mmol, 2.0 eq) were added and the solution was stirred for 2.5 h at 0 °C and for additional 2 h at RT. Solid $NaHCO_3$ was added in small portions until a pH of approx. 6 was reached, and 20 g of solid $MgSO_4$ were subsequently added. The mixture was filtered over Celite and the residue was washed with approx. 100 mL of CH_3CN. The filtrate was concentrated *in vacuo* to yield 98% of the thiazole triol **140** (933 mg, 3.23 mmol) as a colorless solid.

TLC: R_f = 0.77 (EtOAc/MeOH 5:1).

ESI-MS: m/z = 312 $[M+Na]^+$.

HRMS: $[M+Na]^+$: $C_{10}H_{11}NO_7SNa$, calculated: 312.0148, found: 312.0146.

IR: pellet; $\tilde{\nu}$ = 3380, 3097, 1795, 1780, 1718, 1683, 1477, 1417, 1362, 1254, 1220, 1164, 1136, 1114, 1089, 1001, 992, 955, 858, 780, 769, 729 cm^{-1}.

^{1}H-NMR: 300 MHz, DMSO-d_6: δ = 3.83 (s, 3 H, CO_2CH_3), 4.29-4.32 (m, 1 H, 4-H), 4.55 (dd, 1 H, $^3J_{5\text{-H}/4\text{-H}}$ = 4.6 Hz, $^3J_{5\text{-H}/5\text{-OH}}$ = 7.4 Hz, 5-H), 4.61 (dd, 1 H, $^3J_{3\text{-H}/4\text{-H}}$ = 2.9 Hz, $^3J_{3\text{-H}/2\text{-H}}$ = 7.9 Hz, 3-H), 5.15 (dd, 1H, $^3J_{2\text{-H}/2\text{-OH}}$ = 5.7 Hz, $^3J_{2\text{-H}/3\text{-H}}$ = 7.9 Hz, 2-H), 5.52 (d, 1 H, $^3J_{4\text{-OH}/4\text{-H}}$ = 3.8 Hz, 4-OH), 5.91 (d, 1 H, $^3J_{5\text{-OH}/5\text{-H}}$ = 7.4 Hz, 5-OH), 6.57 (d, 1 H, $^3J_{2\text{-OH}/2\text{-H}}$ = 5.7 Hz, 2-OH), 8.57 (s, 1 H, Thz-H).

^{13}C-NMR: 75 MHz, DMSO-d_6: δ = 52.0 ($CO_2\underline{C}H_3$), 68.5 (C-2), 69.7 (C-4), 70.4 (C-5), 80.9 (C-3), 129.7 (Thz-H$\underline{C}$=C), 145.5 (Thz-HC=$\underline{C}$), 161.2 ($\underline{C}O_2CH_3$), 172.0 (C-1), 175.8 (C-6).

Melting point: 105 °C

Opt. rotation: $[\alpha]_{589}^{24}$= +73.3, $[\alpha]_{578}^{24}$= +77.3, $[\alpha]_{546}^{24}$= +87.7, $[\alpha]_{436}^{24}$= +142.6 (c = 0.84 g/100 mL DMSO).

X-ray: Suitable crystals of **140** were grown from a MeOH solution. See figure 4.12.

5.4.30 [(3*R*,4*S*)-dihydroxy-5-oxo-tetrahydro-furan-(2*S*)-yl)-(1*R*)]-1,3-thiazole-carboxylic acid methyl ester (141)

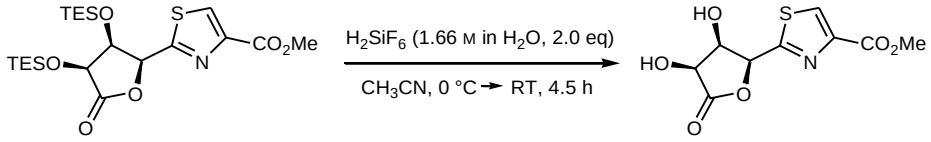

129 **141** M = 259.24

Preparation:

Compound **129**	M = 487.76 g mol^{-1}	1.0 eq	2.47 mmol	1.21 g
H_2SiF_6 (1.66 M in H_2O)	M = 144.09 g mol^{-1}, ρ = 1.22	2.0 eq	4.94 mmol	2.96 mL (3.61 g)
CH_3CN				30 mL

1.21 g of the thiazole **129** (2.47 mmol, 1.0 eq) were dissolved in 30 mL of CH_3CN and cooled to 0 °C. 2.96 mL of H_2SiF_6 (1.66 M in H_2O; 3.61 g, 4.94 mmol, 2.0 eq) were added and the solution was stirred for 2.5 h at 0 °C and for additional 2 h at RT. Solid $NaHCO_3$ was added in small portions until a pH of approx. 6 was reached, and 15 g of solid $MgSO_4$ were subsequently added. The mixture was filtered over Celite and the residue was washed with approx. 100 mL of CH_3CN. The filtrate was concentrated *in vacuo* to yield 94% of the thiazole diol **141** (602 mg, 1.23 mmol) as a colorless solid.

TLC: R_f = 0.22 (pure EtOAc).

ESI-MS: m/z = 282 $[M+Na]^+$.

HRMS: $[M+Na]^+$: $C_9H_9NO_6SNa$, calculated: 282.0043, found: 282.0041.

^{1}H-NMR: 600 MHz, DMSO-d_6: δ = 3.84 (s, 3 H, CO_2CH_3), 4.48 (dpt, 1 H, $^3J_{3\text{-H}/2\text{-H}}$ = 3.0 Hz, $^3J_{3\text{-H}/4\text{-H}}$ = 4.3 Hz, $^3J_{3\text{-H}/3\text{-OH}}$ = 4.6 Hz, 3-H), 4.71 (dd, 1 H, $^3J_{4\text{-H}/3\text{-H}}$ = 4.3 Hz, $^3J_{4\text{-H}/4\text{-OH}}$ = 7.8 Hz, 4-H), 5.85 (dd, 1H, $^3J_{2\text{-H}/3\text{-H}}$ = 3.0 Hz, $^4J_{2\text{-H}/3\text{-OH}}$ = 0.7 Hz, 2-H), 5.95 (d, 1 H, $^3J_{3\text{-OH}/3\text{-H}}$ = 4.6 Hz, $^4J_{3\text{-OH}/2\text{-H}}$ = 0.7 Hz, 3-OH), 6.09 (d, 1 H, $^3J_{4\text{-OH}/4\text{-H}}$ = 7.8 Hz, 4-OH), 8.62 (s, 1 H, Thz-H).

^{13}C-NMR: 125 MHz, DMSO-d_6: δ = 52.0 ($CO_2\underline{C}H_3$), 70.6 (C-3), 70.8 (C-4), 78.3 (C-2), 130.6 (Thz-H$\underline{C}$=C), 145.2 (Thz-HC=$\underline{C}$), 161.1 ($\underline{C}O_2CH_3$), 165.4 (C-1), 175.2 (C-5).

Melting point: 185 °C.

Opt. rotation: $[\alpha]_{589}^{19}$ = –5.4, $[\alpha]_{578}^{19}$ = –5.6, $[\alpha]_{546}^{19}$ = –6.4, $[\alpha]_{436}^{19}$ = –10.9, $[\alpha]_{365}^{19}$ = –16.7 (c = 1.03 g/100 mL MeOH).

5.4.31 2-((1*R*,2*S*,3*S*,4*S*)-4-(methoxycarbonyl)-1,2,3,4-tetrahydroxybutyl)-1,3-thiazole-4-carboxylic acid methyl ester (142)

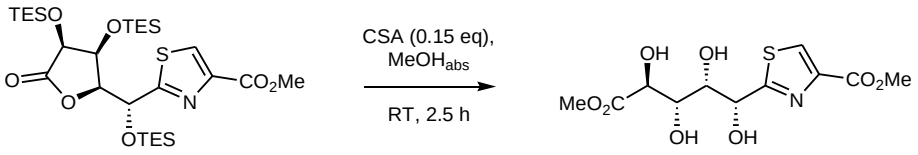

132 **142**
M = 321.30

Preparation:

Compound **132**	M = 632.04 g mol^{-1}	1.0 eq	2.77 mmol	1.75 g
CSA	M = 232.30 g mol^{-1}	0.15 eq	0.43 mmol	100 mg
$MeOH_{abs}$				50 mL

1.75 g of the lactone **132** (2.77 mmol, 1.0 eq) were dissolved in 50 mL of $MeOH_{abs}$ in a nitrogen atmosphere. 100 mg of CSA (0.43 mmol, 0.15 eq) were added and the mixture was stirred at RT for 2.5 h. 600 mg of solid $NaHCO_3$ and 250 mg of solid $MgSO_4$ were subsequently added, the mixture was stirred for 30 min at RT, and filtered over a short Celite column. The solvent was removed *in vacuo* to afford a 54:46 mixture of the tetraol **142** and the lactone **140** (section 5.4.29) in quantitative yield.

TLC: R_f = 0.58 (EtOAc/MeOH 5:1).

ESI-MS: m/z = 344 $[M+Na]^+$.

HRMS: $[M+Na]^+$: $C_{11}H_{15}NO_8SNa$, calculated: 344.0411, found: 344.0412.

^{1}H-NMR: 300 MHz, DMSO-d_6: δ = 3.61 (m, 4 H, 4-H, 6-CO_2CH_3), 3.82 (m, 4 H, 3-H, Thz-CO_2CH_3), 4.03 (dd, 1 H, $^3J_{5\text{-H}/5\text{-OH}}$ = 6.5 Hz, $^3J_{5\text{-H}/4\text{-H}}$ = 7.7 Hz, 5-H), 4.77 (d, 1 H, $^3J_{4\text{-OH}/4\text{-H}}$ = 7.1 Hz, 4-OH), 4.22 (d, 1 H, $^3J_{3\text{-OH}/3\text{-H}}$ = 7.3 Hz, 3-OH), 4.95 (pt, 1 H, $^3J_{2\text{-H}/3\text{-H}}$ = 4.9 Hz, $^3J_{2\text{-H}/2\text{-OH}}$ = 4.9 Hz, 2-H), 5.70 (d, 1 H, $^3J_{5\text{-OH}/5\text{-H}}$ = 6.5 Hz, 5-OH), 6.22 (d, 1 H, $^3J_{2\text{-OH}/2\text{-H}}$ = 4.9 Hz, 2-OH), 8.48 (s, 1 H, Thz-H).

^{13}C-NMR: 75 MHz, DMSO: δ = 51.0 (6-$CO_2\underline{C}H_3$), 51.7 (Thz-$CO_2\underline{C}H_3$), 71.2 (C-5), 71.6 (C-4), 71.7 (C-3), 71.8 (C-2), 128.8 (Thz-H$\underline{C}$=C), 145.2 (Thz-HC=$\underline{C}$), 161.3 (Thz-$\underline{C}O_2CH_3$), 173.2 (C-6), 175.7 (C-1).

5.4.32 2-((1*S*,2*R*,3*S*)-3-(methoxycarbonyl)-1,2,3-trihydroxypropyl)-1,3-thiazole-4-carboxylic acid methyl ester (143)

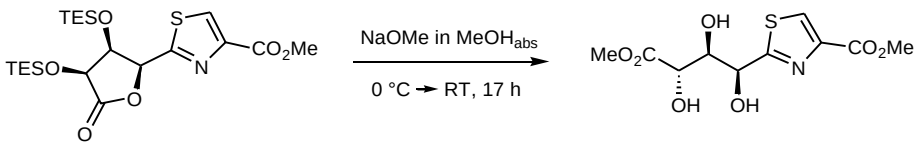

129 **143**
M = 291.28

Preparation:

Compound **129**	M = 487.76 g mol^{-1}	1.0 eq	266 µmol	130 mg
NaOMe (30% in MeOH)	M = 54.02 g mol^{-1}, ρ = 0.95	0.1 eq	26.6 µmol	5.0 µL (4.8 mg)
$MeOH_{abs}$				10 mL

130 mg of the lactone **129** (266 µmol, 1.0 eq) were dissolved in 10 mL of $MeOH_{abs}$ in a nitrogen atmosphere and the solution was cooled to 0 °C. 5.0 µL of NaOMe (30% in MeOH, 0.1 eq, 4.8 mg) were added and the mixture was stirred at 0 °C for 1.5 h. Another 10.0 µL of NaOMe (30% in MeOH, 0.1 eq, 4.8 mg) were added and the mixture was allowed to warm to RT under stirring for 15.5 h. The mixture was subsequently neutralized with 1 N aq. HCl, EtOAc was added and the MeOH was removed under reduced pressure. The residual solution was extracted with H_2O, the phases were separated, and the aqueous phase was extracted two times with EtOAc. The combined organic phases were dried with brine and over $MgSO_4$, filtered, and concentrated *in vacuo* to yield 50% of the triol **143** (39 mg, 134 µmol) as a pale yellow solid.

TLC: R_f = 0.69 (EtOAc/MeOH 5:1).

ESI-MS: m/z = 314 $[M+Na]^+$.

HRMS: $[M+Na]^+$: $C_{10}H_{13}NO_7SNa$, calculated: 314.0305, found: 314.0304.

^{1}H-NMR: 600 MHz, DMSO-d_6: δ = 3.63 (s, 3 H, 5-CO_2CH_3), 3.82 (s, 3 H, Thz-CO_2CH_3), 3.95 (ddd, 1 H, $^3J_{3\text{-H}/2\text{-H}}$ = 1.7 Hz, $^3J_{3\text{-H}/3\text{-OH}}$ = 8.2 Hz, $^3J_{3\text{-H}/4\text{-H}}$ = 9.3 Hz, 3-H), 4.10 (dd, 1 H, $^3J_{4\text{-H}/4\text{-OH}}$ = 7.1 Hz, $^3J_{4\text{-H}/3\text{-H}}$ = 9.3 Hz, 4-H), 5.02 (d, 1 H, $^3J_{3\text{-OH}/3\text{-H}}$ = 8.2 Hz, 3-OH), 5.06 (dd, 1 H, $^3J_{2\text{-H}/3\text{-H}}$ = 1.7 Hz, $^3J_{2\text{-H}/2\text{-OH}}$ = 6.7 Hz, 2-H), 5.92 (d, 1 H, $^3J_{4\text{-OH}/4\text{-H}}$ = 7.1 Hz, 4-OH), 6.28 (d, 1 H, $^3J_{2\text{-OH}/2\text{-H}}$ = 6.7 Hz, 2-OH), 8.43 (s, 1 H, Thz-H).

^{13}C-NMR: 150 MHz, DMSO: δ = 51.2 (5-$CO_2\underline{C}H_3$), 51.8 (Thz-$CO_2\underline{C}H_3$), 65.5 (C-2), 71.0 (C-4), 74.2 (C-3), 128.9 (Thz-H$\underline{C}$=C), 145.4 (Thz-HC=$\underline{C}$), 161.6 (Thz-$\underline{C}O_2CH_3$), 173.6 (C-5), 177.2 (C-1).

5.4.33 2-((1*S*,2*R*,3*S*)-3-(benzyloxycarbonyl)-1,2,3-trihydroxypropyl)-1,3-thiazole-4-carboxylic acid methyl ester (148)

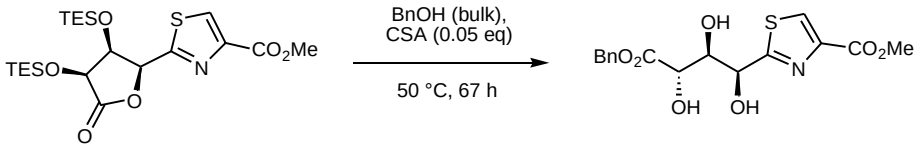

129 **148**
M = 367.37

Preparation:

Compound **129**	M = 487.76 g mol^{-1}	1.0 eq	8.14 mmol	3.97 g
CSA	M = 232.30 g mol^{-1}	0.05 eq	0.40 mmol	93 mg
BnOH				20 mL

3.97 g of the lactone **129** (8.14 mmol, 1.0 eq) were dissolved in 20 mL of BnOH, 93 mg of CSA (0.40 mmol, 0.05 eq) were added and the mixture was stirred at 50 °C for 67 h during which a colorless solid precipitated. The mixture was allowed to cool to RT and filtered, the solid was washed with Tol and dried *in vacuo* to afford 81% of the triol **148** (2.42 g, 6.59 mmol) as a colorless solid.

TLC: R_f = 0.72 (EtOAc/MeOH 5:1).

ESI-MS: m/z = 390 $[M+Na]^+$.

HRMS: $[M+Na]^+$: $C_{16}H_{17}NO_7SNa$, calculated: 390.0618, found: 390.0625.

IR: pellet; $\tilde{\nu}$ = 3427, 3237, 2960, 1712, 1495, 1389, 1318, 1294, 1232, 1200, 1124, 1090, 1045, 979, 914, 834, 726, 672, 648 cm^{-1}.

^{1}H-NMR: 600 MHz, DMSO-d_6: δ = 3.82 (s, 3 H, CO_2CH_3), 3.98-4.01 (m, 1 H, 3-H), 4.16 (dd, 1 H, $^3J_{4\text{-H}/4\text{-OH}}$ = 7.1 Hz, $^3J_{4\text{-H}/3\text{-H}}$ = 9.1 Hz, 4-H), 5.08 (d, 1 H, $^3J_{3\text{-OH}/3\text{-H}}$ = 8.2 Hz, 3-OH), 5.08 (dd, 1 H, $^3J_{2\text{-H}/3\text{-H}}$ = 1.4 Hz, $^3J_{2\text{-H}/2\text{-OH}}$ = 6.7 Hz, 2-H), 5.11 (d, 1 H, ^2J = 12.8 Hz, $CO_2C\underline{H}_2Ph^u$), 5.16 (d, 1 H, ^2J = 12.8 Hz, $CO_2C\underline{H}_2Ph^d$), 6.00 (d, 1 H, $^3J_{4\text{-OH}/4\text{-H}}$ = 7.1 Hz, 4-OH), 6.30 (d, 1 H, $^3J_{2\text{-OH}/2\text{-H}}$ = 6.7 Hz, 2-OH), 7.32-7.41 (m, 5 H, $CO_2CH_2\underline{Ph}$), 8.43 (s, 1 H, Thz-H).

^{13}C-NMR: 150 MHz, DMSO: δ = 51.8 ($CO_2\underline{C}H_3$), 65.4 ($CO_2\underline{C}H_2Ph$), 69.6 (C-2), 71.3 (C-4), 74.3 (C-3), 127.6, 127.8, 128.3 (each Bn-$CH_{arom.}$), 128.9 (Thz-H$\underline{C}$=C), 136.1 (Bn-$C_{arom., quart.}$), 145.4 (Thz-HC=$\underline{C}$), 161.5 ($\underline{C}O_2CH_3$), 172.8 (C-5), 177.0 (C-1).

Melting point: 104 °C.

Opt. rotation: $[\alpha]_{589}^{18}$ = –23.3, $[\alpha]_{578}^{18}$ = –29.4, $[\alpha]_{546}^{18}$ = –33.6, $[\alpha]_{436}^{18}$ = –59.0, $[\alpha]_{365}^{18}$ = –94.2 (c = 1.03 g/100 mL MeOH).

5.4.34 2-((1*S*,2*R*,3*S*)-3-(hydroxycarbonyl)-1,2,3-trihydroxypropyl)-1,3-thiazole-4-carboxylic acid methyl ester (149)

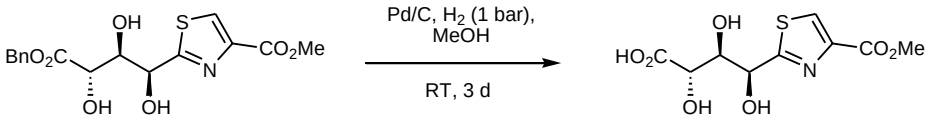

148 **149**
M = 277.25

Preparation:

Compound **148**	M = 367.37 g mol^{-1}	1.0 eq	0.57 mmol	200 mg
Pd/C (5%, wet, *Degussa*)				400 mg
MeOH				60 mL

200 mg of the benzyl ester **148** (0.57 mmol, 1.0 eq) were dissolved in 60 mL of MeOH, 400 mg of Pd/C (5%, wet, *Degussa*) were added and the mixture was stirred at RT for 3 h in a H_2 atmosphere at 1 bar. Over the following 3 d the H_2 atmosphere was renewed three times and additional 200 mg of Pd/C (5%, wet, *Degussa*) were added each time. The mixture was filtered over Celite and concentrated *in vacuo*. Residual amounts of H_2O were removed by coevaporation with $CHCl_3$. This afforded afford 90% of the carboxylic acid **149** (141 mg, 0.51 mmol) as a colorless solid.

TLC: R_f = 0.05 (EtOAc/MeOH 5:1).

ESI-MS: m/z = 276 $[M-H]^-$.

HRMS: $[M-H]^-$: $C_9H_{10}NO_7S$, calculated: 276.0183, found: 276.0186.

^{1}H-NMR: 300 MHz, DMSO-d_6: δ = 3.82 (CO_2CH_3), 3.90 (dd, 1 H, $^3J_{3\text{-H}/2\text{-H}}$ = 1.6 Hz, $^3J_{3\text{-H}/4\text{-H}}$ = 8.8 Hz, 3-H), 3.97 (d, 1 H, $^3J_{4\text{-H}/3\text{-H}}$ = 8.8 Hz, 4-H), 5.05 (d, 1 H, $^3J_{2\text{-H}/3\text{-H}}$ = 1.6 Hz, 2-H), 8.43 (s, 1 H, Thz-H). OH- and CO_2H signals are strongly broadened.

600 MHz, D_2O: δ = 3.98 (CO_2CH_3), 4.21 (dd, 1 H, $^3J_{3\text{-H}/2\text{-H}}$ = 2.8 Hz, $^3J_{3\text{-H}/4\text{-H}}$ = 7.2 Hz, 3-H), 4.40 (d, 1 H, $^3J_{4\text{-H}/3\text{-H}}$ = 7.2 Hz, 4-H), 5.35 (d, 1 H, $^3J_{2\text{-H}/3\text{-H}}$ = 2.8 Hz, 2-H), 8.47 (s, 1 H, Thz-H). OH- and CO_2H signals are strongly broadened.

^{13}C-NMR: 150 MHz, D_2O: δ = 52.7 ($CO_2\underline{C}H_3$), 70.4 (C-2), 71.3 (C-4), 74.4 (C-3), 129.7 (Thz-H$\underline{C}$=C), 145.3 (Thz-HC=$\underline{C}$), 163.4 ($\underline{C}O_2CH_3$), 175.3 (C-1), 176.3 (C-5).

5.4.35 [(3*S*,4*S*)-*O*-isopropylidene-5-oxo-tetrahydro-furan-(2*S*)-yl)-(1*R*)-hydroxymethyl]-1,3-thiazole-carboxylic acid methyl ester (157)

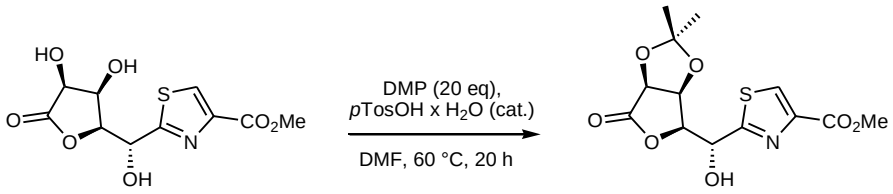

140 **157**
M = 329.33

Preparation:

Compound **140**	M = 293.29 g mol^{-1}	1.0 eq	4.21 mmol	1.22 g
DMP	M = 104.15 g mol^{-1}, ρ = 0.85	20 eq	84.2 mmol	10.3 mL (8.77 g)
*p*TosOH x H_2O	M = 190.22 g mol^{-1}			cat.
DMF				12 mL

1.22 g of the triol **140** (4.21 mmol, 1.0 eq) were dissolved in 12 mL of DMF and 10.3 mL of DMP (8.77 g, 84.2 mmol, 20 eq). After the addition of a catalytic amount of *p*TosOH x H_2O the solution was stirred for 20 h at 60 °C. The reaction mixture was neutralized by addition of NEt_3, filtered over Celite and concentrated *in vacuo*. Residual amounts of DMF were removed by coevaporation with Tol. In the obtained yellow oil, the product crystallized, and after filtration, washing with pentane/Tol (1:1), and drying *in vacuo* 23% of the acetonide **157** (316 mg, 0.96 mmol) were obtained as pale yellow crystals. The filtrate was concentrated *in vacuo*, and by addition of EtOAc/Tol (1:1) another 12% of the product (160 mg, 0.49 mmol) were isolated by the same procedure as a pale yellow solid. The filtrate was concentrated *in vacuo* and subjected to flash chromatography (EtOAc/Tol 1:1) which yielded another 24% of the product (339 mg, 1.03 mmol) as a pale yellow solid. In total, 59% of **157** were obtained (815 mg, 2.47 mmol).

TLC: R_f = 0.66 (EtOAc/Tol 7:1).

ESI-MS: m/z = 352 $[M+Na]^+$.

HRMS: $[M+Na]^+$: $C_{13}H_{15}NO_7SNa$, calculated: 352.0461, found: 352.0458.

IR: pellet; $\tilde{\nu}$ = 3525, 3122, 1791, 1704, 1494, 1387, 1320, 1269, 1252, 1234, 1196, 1155, 1107, 1072, 1004, 977, 942, 918, 908, 880, 862, 790, 744, 651 cm^{-1}.

^{1}H-NMR: 300 MHz, $CDCl_3$: δ = 1.45 (s, 3 H, Isopr-CH_3^{proR}), 1.57 (s, 3 H, Isopr-CH_3^{proS}), 3.81 (d, 1 H, $^3J_{2\text{-OH}/2\text{-H}}$ = 2.2 Hz, 2-OH), 3.95 (s, 3 H, CO_2CH_3), 4.91 (d, 1 H, $^3J_{5\text{-H}/4\text{-H}}$ = 5.2 Hz, 5-H), 5.04 (pt, 1 H, $^3J_{3\text{-H}/2\text{-H}}$ = 3.0 Hz, $^3J_{3\text{-H}/4\text{-H}}$ = 3.6 Hz, 3-H), 5.09 (dd, 1 H, $^3J_{4\text{-H}/3\text{-H}}$ = 3.6 Hz, $^3J_{4\text{-H}/5\text{-H}}$ = 5.2 Hz, 4-H), 5.54 (dd, 1 H, $^3J_{2\text{-H}/2\text{-OH}}$ = 2.2 Hz, $^3J_{2\text{-H}/3\text{-H}}$ = 3.0 Hz, 2-H), 8.22 (s, 1 H, Thz-H).

500 MHz, DMSO-d_6: δ = 1.27 (s, 3 H, Isopr-CH_3^{proR}), 1.34 (s, 3 H, Isopr-CH_3^{proS}), 3.83 (s, 3 H, CO_2CH_3), 4.87 (dd, 1 H, $^3J_{3\text{-H}/4\text{-H}}$ = 3.5 Hz, $^3J_{3\text{-H}/2\text{-H}}$ = 8.1 Hz, 3-H), 4.92 (dd, 1 H, $^3J_{4\text{-H}/3\text{-H}}$ = 3.5 Hz, $^3J_{4\text{-H}/5\text{-H}}$ = 5.3 Hz, 4-H), 5.02 (d, 1 H, $^3J_{5\text{-H}/4\text{-H}}$ = 5.3 Hz, 5-H), 5.11 (dd, 1 H, $^3J_{2\text{-H}/2\text{-OH}}$ = 6.5 Hz, $^3J_{2\text{-H}/3\text{-H}}$ = 8.1 Hz, 2-H), 6.76 (d, 1 H, $^3J_{2\text{-OH}/2\text{-H}}$ = 6.5 Hz, 2-OH), 8.58 (s, 1 H, Thz-H).

^{13}C-NMR: 125 MHz, DMSO-d_6: δ = 25.6 (Isopr-CH_3^{proR}), 26.6 (Isopr-CH_3^{proS}), 52.0 ($CO_2\underline{C}H_3$), 68.1 (C-2), 76.2 (C-5), 76.5 (C-4), 80.2 (C-3), 112.7 (Isopr-$C_{quart.}$), 129.9 (Thz-H$\underline{C}$=C), 145.5 (Thz-HC=$\underline{C}$), 161.1 ($\underline{C}O_2CH_3$), 171.7 (C-1), 174.1 (C-6).

Melting point: 168 °C.

Opt. rotation: $[\alpha]_{589}^{23}$ = +28.4, $[\alpha]_{578}^{23}$ = +29.7, $[\alpha]_{546}^{23}$ = +33.9, $[\alpha]_{436}^{23}$ = +58.4, $[\alpha]_{365}^{23}$ = +59.8 (c = 1.00 g/100 mL DMSO/EtOAc 1:1).

5.4.36 [(3*S*,4*S*)-*O*-isopropylidene-5-oxo-tetrahydro-furan-(2*S*)-yl)-(1*R*)-(methoxydimethyl)methoxymethyl]-1,3-thiazole-carboxylic acid methyl ester (158)

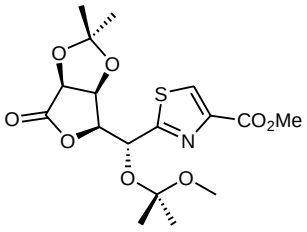

158
M = 401.43

The fully protected acetonide **158** was isolated as side product of the synthesis of **157** (section 5.4.35). By flash chromatography (EtOAc/Tol 1:1), less than 5% were obtained in all cases as a colorless solid.

TLC: R_f = 0.80 (EtOAc/Tol 7:1).

ESI-MS: m/z = 424 $[M+Na]^+$.

HRMS: $[M+Na]^+$: $C_{17}H_{23}NO_8SNa$, calculated: 424.1037, found: 424.1037.

^{1}H-NMR: 300 MHz, DMSO-d_6: δ = 1.33 (s, 6 H, 2 x Isopr-CH_3), 1.43, 1.59 (each s, 3 H, Isopr-CH_3), 3.18 (s, 3 H, $C(CH_3)_2OC\underline{H}_3$), 3.84 (s, 3 H, CO_2CH_3), 4.76-4.78 (m, 2 H, 3-H, 4-H), 4.95 (d, 1 H, $^3J_{5\text{-H}/4\text{-H}}$ = 3.5 Hz, 5-H), 5.72 (d, 1 H, $^3J_{2\text{-H}/3\text{-H}}$ = 1.9 Hz, 2-H), 8.56 (s, 1 H, Thz-H).

5.4.37 2-((*S*)-((3*aS*,6*S*,6*aS*)-2-ethoxy-tetrahydro-4-oxofuro[3,4-*d*][1,3]dioxol-6-yl)(hydroxy)methyl)-1,3-thiazole-4-carboxylic acid methyl ester (159)

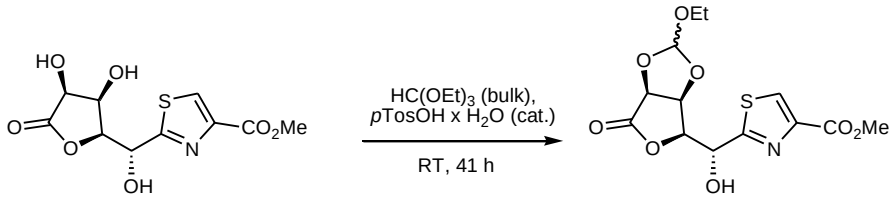

140 **159**
M = 345.33

Preparation:

Compound **140**	M = 289.23 g mol^{-1}	1.0 eq	8.02 mmol	2.32 g
$HC(OEt)_3$	M = 148.20 g mol^{-1}, ρ = 0.90			29.0 mL (26.1 g)
*p*TosOH x H_2O	M = 190.22 g mol^{-1}			cat.

40 mg of the triol **140** (8.02 mmol, 1.0 eq) were suspended in 29.0 mL of $HC(OEt)_3$ (26.1 g) and a catalytic amount of *p*TosOH x H_2O was added. The suspension was stirred at RT for 41 h under which complete solution occurred. The mixture was subsequently transferred onto a silica gel filter column, eluted with pure EtOAc, and concentrated *in vacuo*. Purification by flash chromatography yielded 94% of the orthoester **159** (2.61 g, 7.56 mmol, 8:1 epimeric mixture) as a colorless foam.

ESI-MS: *m/z* = 368 $[M+Na]^+$.

HRMS: $[M+Na]^+$: $C_{13}H_{15}NO_8SNa$, calculated: 368.0411, found: 368.0411.

Major epimer:

TLC: R_f = 0.28 (EtOAc/Tol 1:1).

^{1}H-NMR: 300 MHz, DMSO-d_6: δ = 1.13 (t, 3 H, $^3J_{OCH2CH3/OCH2CH3}$ = 7.0 Hz, OCH_2CH_3), 3.46-3.53 (m, 2 H, OCH_2CH_3), 3.83 (s, 3 H, CO_2CH_3), 4.90-4.94 (m, 1 H, 4-H), 4.91 (d, 1 H, $^3J_{5\text{-}H/4\text{-}H}$ = 8.1 Hz, 5-H), 5.04-5.13 (m, 2 H, 2-H, 3-H), 6.03 (s, 1 H, orthoester-CH), 6.75 (d, 1 H, $^3J_{2\text{-}OH/2\text{-}H}$ = 6.5 Hz, 2-OH), 8.59 (s, 1 H, Thz-H).

Minor epimer: the amount of the minor epimer was determined by the 2-OH signal δ = 6.85 (s, 1 H, $^3J_{2\text{-}OH/2\text{-}H}$ = 6.5 Hz); the other NMR shifts were not determined due to overlap with the signals of the major epimer.

5.4.38 2-((*S*)-((3*aS*,6*S*,6*aS*)-2-ethoxy-tetrahydro-4-oxofuro[3,4-*d*][1,3]dioxol-6-yl)(diethoxymethoxy)methyl)-1,3-thiazole-4-carboxylic acid methyl ester (160)

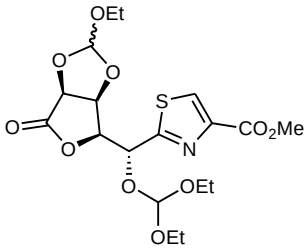

160
M = 447.46

The fully protected orthoester **160** was isolated in traces (< 5%) the synthesis of **159** (section 5.4.37) as a colorless oil.

TLC: R_f = 0.60 (EtOAc/Tol 1:1).

ESI-MS: m/z = 470 $[M+Na]^+$.

HRMS: $[M+Na]^+$: $C_{18}H_{25}NO_{10}SNa$, calculated: 470.1091, found: 470.0195.

^{1}H-NMR: 300 MHz, DMSO-d_6: δ = 1.03-1.13 (m, 9 H, 3 x $OCH_2C\underline{H}_3$), 3.46-3.53 (m, 6 H, 3 x $OC\underline{H}_2CH_3$), 3.84 (s, 3 H, CO_2CH_3), 4.75 (dd, 1 H, $^3J_{4\text{-H}/5\text{-H}}$ = 6.4 Hz, $^3J_{4\text{-H}/3\text{-H}}$ = 4.5 Hz, 4-H), 5.04-5.13 (m, 1 H, 5-H), 5.15 (dd, $^3J_{3\text{-H}/4\text{-H}}$ = 4.5 Hz, $^3J_{3\text{-H}/2\text{-H}}$ = 9.5 Hz, 1 H, 3-H), 5.29 (d, 1 H, $^3J_{2\text{-H}/3\text{-H}}$ = 9.5 Hz, 2-H), 5.32 (s, 1 H, $C\underline{H}(OEt)_2$), 6.03 (s, 1 H, orthoester-CH), 8.64 (s, 1 H, Thz-H).

5.4.39 [(3*S*,4*S*)-*O*-isopropylidene-5-oxo-tetrahydro-furan-(2*S*)-yl)-1-acetoxymethyl]-1,3-thiazole-carboxylic acid methyl ester (1*R*: 161, 1*S*: 165)

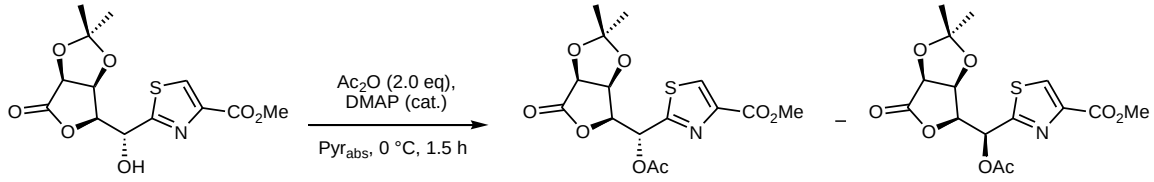

157 | **161** M = 371.36 | **165** M = 371.36

Preparation:

Compound **157**	M = 329.33 g mol^{-1}	1.0 eq	2.36 mmol	777 mg
Ac_2O	M = 102.09 g mol^{-1}, ρ = 1.08	2.0 eq	4.72 mmol	446 µL (482 mg)
DMAP	M = 122.17 g mol^{-1}			cat.
Pyr_{abs}				22 mL

777 mg of the acetonide **157** (2.36 mmol, 1.0 eq) were dissolved in 22 mL of Pyr_{abs} in a nitrogen atmosphere and cooled to 0 °C. A catalytical amount of DMAP and 446 µL of Ac_2O (482 mg, 4.72 mmol, 2.0 eq) were added and the solution was stirred for 1.5 h at 0 °C. The reaction was diluted with CH_2Cl_2, quenched with ice, and 5% aq. $NaHCO_3$ was added. The phases were separated and the aqueous phase was extracted two times with CH_2Cl_2. The combined organic phases were dried with brine and over $MgSO_4$, filtered, and concentrated *in vacuo*. Flash chromatography (Tol/EtOAc 3:1) yielded 88% of a mixture of the acetates **161**/**165** (767 mg, 2.07 mmol, 39:1 epimeric mixture) as a colorless foam.

TLC: R_f = 0.78 (EtOAc/Tol 5:1).

ESI-MS: m/z = 394 $[M+Na]^+$.

HRMS: $[M+Na]^+$: $C_{15}H_{17}NO_8SNa$, calculated: 394.0567, found: 394.0573.

Opt. rotation: $[\alpha]_{589}^{24}$ = +47.0, $[\alpha]_{578}^{24}$ = +49.3, $[\alpha]_{546}^{24}$ = +56.1, $[\alpha]_{436}^{24}$ = +97.6, $[\alpha]_{365}^{24}$ = +152.1 (c = 1.33 g/100 mL $CHCl_3$).

Major epimer (1R, **161***):*

^{1}H-NMR: 300 MHz, DMSO-d_6: δ = 1.24 (s, 3 H, Isopr-CH_3^{proR}), 1.36 (s, 3 H, Isopr-CH_3^{proS}), 2.13 (s, 3 H, Ac-CH_3), 3.85 (s, 3 H, CO_2CH_3), 4.83 (dd, 1 H, $^3J_{4\text{-H}/3\text{-H}}$ = 3.7 Hz, $^3J_{4\text{-H}/5\text{-H}}$ = 5.5 Hz, 4-H), 5.04 (d, 1 H, $^3J_{5\text{-H}/4\text{-H}}$ = 5.5 Hz, 5-H), 5.31 (dd, 1 H, $^3J_{3\text{-H}/4\text{-H}}$ = 3.7 Hz, $^3J_{3\text{-H}/2\text{-H}}$ = 7.8 Hz, 3-H), 6.29 (d, 1 H, $^3J_{2\text{-H}/3\text{-H}}$ = 7.8 Hz, 2-H), 8.67 (s, 1 H, Thz-H).

^{13}C-NMR: 125 MHz, DMSO-d_6: δ = 20.5 (Ac-<u>C</u>H_3), 25.5 (Isopr-CH_3^{proR}), 26.5 (Isopr-CH_3^{proS}), 52.2 (CO_2<u>C</u>H_3), 68.7 (C-2), 76.1 (C-4), 76.2 (C-5), 77.6 (C-3), 113.2 (Isopr-$C_{quart.}$), 131.1 (Thz-H<u>C</u>=C), 145.8 (Thz-HC=<u>C</u>), 160.8 (<u>C</u>O_2CH_3), 164.2 (C-1), 169.4 (Ac-<u>C</u>O), 173.4 (C-6).

Minor epimer (1S, **165***):*

^{1}H-NMR: 300 MHz, DMSO-d_6: δ = 1.37, 1.57 (each s, 3 H, Isopr-CH_3), 1.96 (s, 3 H, Ac-CH_3), 3.84 (s, 3 H, CO_2CH_3), 4.71 (dd, 1 H, $^3J_{4\text{-H}/3\text{-H}}$ = 2.3 Hz, $^3J_{4\text{-H}/5\text{-H}}$ = 7.0 Hz, 4-H), 4.91 (d, 1 H, $^3J_{5\text{-H}/4\text{-H}}$ = 7.0 Hz, 5-H), 5.24 (dd, 1 H, $^3J_{3\text{-H}/2\text{-H}}$ = 1.3 Hz, $^3J_{3\text{-H}/4\text{-H}}$ = 2.3 Hz, 3-H), 6.23 (d, 1 H, $^3J_{2\text{-H}/3\text{-H}}$ = 1.3 Hz, 2-H), 8.65 (s, 1 H, Thz-H).

^{13}C-NMR: Due to weak signal intensities, the ^{13}C signals cannot be unambiguously assigned.

5.4.40 [(3*S*,4*S*)-*O*-isopropylidene-5-oxo-tetrahydro-furan-(2*S*)-yl)-(1*R*)-(*tert*-butyl-dimethylsilyl)oxymethyl]-1,3-thiazole-carboxylic acid methyl ester (163)

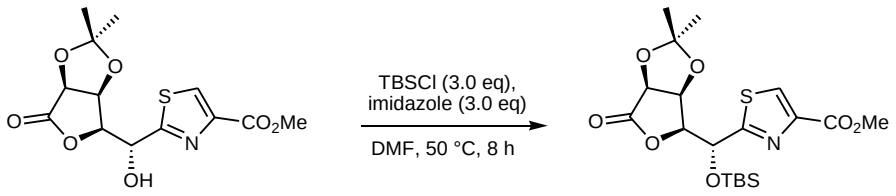

157 **163**
M = 443.59

Preparation:

Compound **157**	M = 329.33 g mol^{-1}	1.0 eq	437 µmol	144 mg
TBSCl	M = 150.72 g mol^{-1}	3.0 eq	1.31 mmol	198 mg
Imidazole	M = 68.08 g mol^{-1}	3.0 eq	1.31 mmol	89 mg
DMF				2.0 mL

144 mg of the thiazole **157** (437 µmol, 1.0 eq) were dissolved in 2.0 mL of DMF, 198 mg of imidazole (1.31 mmol, 3.0 eq) and 89 mg of TBSCl (1.31 mmol, 3.0 eq) were added and the solution was stirred for 8 h at 50 °C. After cooling to RT and dilution with CH_2Cl_2 the reaction was quenched with 5% aq. $NaHCO_3$, the phases were separated and the aqueous phase was extracted two times with CH_2Cl_2. The combined organic phases were dried with brine and over $MgSO_4$, filtered, and concentrated *in vacuo*. Residual amounts of DMF were removed by coevaporation with Tol. The crude product was purified by flash chromatograohy (EtOAc/Tol 1:1) to yield 90% of the silyl ether **163** (174 mg, 392 µmol) as a colorless solid.

TLC: R_f = 0.77 (EtOAc/Tol 3:2).

ESI-MS: m/z = 466 $[M+Na]^+$.

HRMS: $[M+Na]^+$: $C_{19}H_{29}NO_7SSiNa$, calculated: 466.1326, found: 466.1326.

IR: pellet; $\tilde{\nu}$ = 2960, 2030, 2854, 1790, 1734, 1385, 1374, 1333, 1305, 1249, 1211, 1170, 1114, 1092, 1015, 977, 966, 873, 694 cm^{-1}.

^{1}H-NMR: 500 MHz, DMSO-d_6: δ = 0.08, 0.14 (each s, 3 H, $SiCH_3$), 0.88 (s, 9 H, $SiC(CH_3)_3$), 1.28 (s, 3 H, Isopr-CH_3^{proR}), 1.35 (s, 3 H, Isopr-CH_3^{proS}), 3.84 (s, 3 H, CO_2CH_3), 4.77 (dd, 1 H, $^3J_{4\text{-H}/3\text{-H}}$ = 3.3 Hz, $^3J_{4\text{-H}/5\text{-H}}$ = 5.0 Hz, 4-H), 4.79 (dd, 1 H, $^3J_{3\text{-H}/4\text{-H}}$ = 3.3 Hz, $^3J_{3\text{-H}/2\text{-H}}$ = 8.7 Hz, 3-H), 5.00 (d, 1 H, $^3J_{5\text{-H}/4\text{-H}}$ = 5.0 Hz, 5-H), 5.30 (d, 1 H, $^3J_{2\text{-H}/3\text{-H}}$ = 8.7 Hz, 2-H), 8.60 (s, 1 H, Thz-H). All signals correspond to the major epimer.

^{13}C-NMR: 125 MHz, DMSO-d_6: δ = −5.1, −4.8 (each $SiCH_3$), 17.9 ($SiC(CH_3)_3$), 25.5 ($SiC(CH_3)_3$), 25.8 (Isopr-CH_3^{proR}), 26.7 (Isopr-CH_3^{proS}), 52.1 (CO_2CH_3), 70.3 (C-2), 76.0 (C-4), 76.4 (C-5), 80.1 (C-3), 112.8 (Isopr-$C_{quart.}$), 130.2 (Thz-HC=C), 145.7 (Thz-HC=C), 161.0 (CO_2CH_3), 170.2 (C-1), 173.9 (C-6). All signals correspond to the major epimer.

Melting point: 79 °C.

Opt. rotation: $[\alpha]_{589}^{15}$ = +10.9, $[\alpha]_{578}^{15}$ = +11.6, $[\alpha]_{546}^{15}$ = +13.1, $[\alpha]_{436}^{15}$ = +21.8, $[\alpha]_{365}^{15}$ = +31.8 (c = 1.00 g/100 mL EtOH).

5.4.41 2-((*S*)-((3*aS*,6*S*,6*aS*)-2-ethoxy-tetrahydro-4-oxofuro[3,4-*d*][1,3]dioxol-6-yl)-(acetoxy)methyl)-1,3-thiazole-4-carboxylic acid methyl ester (162)

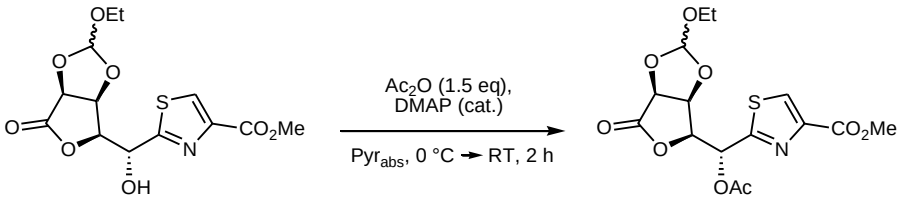

159 **162**
M = 387.36

Preparation:

Compound **159**	M = 331.33 g mol^{-1}	1.0 eq	0.55 mmol	182 mg
Ac_2O	M = 102.09 g mol^{-1}, ρ = 1.08	1.5 eq	0.83 mmol	78.4 µL (84.7 mg)
DMAP	M = 122.17 g mol^{-1}			cat.
Pyr_{abs}				3.0 mL

182 mg of the orthoester **159** (0.55 mmol, 1.0 eq) were dissolved in 3.0 mL of Pyr_{abs} in a nitrogen atmosphere and cooled to 0 °C. A catalytical amount of DMAP and 78.4 µL of Ac_2O (84.7 mg, 0.83 mmol, 1.5 eq) were added, the solution was stirred for 30 min at 0 °C and for 1.5 h at RT. The reaction was diluted with CH_2Cl_2, quenched with ice, and 5% aq. $NaHCO_3$ was added. The phases were separated and the aqueous phase was extracted two times with CH_2Cl_2. The combined organic phases were dried with brine and over $MgSO_4$, filtered, and concentrated *in vacuo*. Flash chromatography (Tol/EtOAc 2:1) yielded 65% of the acetate **162** (119 mg, 0.31 mmol) as a colorless foam (13:1 epimeric mixture of 2*R*/2*S*).

TLC: R_f = 0.30 (Tol/EtOAc 2:1).

ESI-MS: *m*/*z* = 410 $[M+Na]^+$.

HRMS: $[M+Na]^+$: $C_{15}H_{17}NO_9SNa$, calculated: 410.0516, found: 410.0519.

^{1}H-NMR: 300 MHz, DMSO-d_6: δ = 1.08 (t, 3 H, $^3J_{OCH2CH3/OCH2CH3}$ = 7.0 Hz, OCH_2CH_3), 2.12 (s, 3 H, Ac-CH_3), 3.42-3.53 (m, 2 H, OCH_2CH_3), 3.85 (s, 3 H, CO_2CH_3), 4.85 (dd, 1 H, $^3J_{4\text{-}H/3\text{-}H}$ = 4.7 Hz, $^3J_{4\text{-}H/5\text{-}H}$ = 6.4 Hz, 4-H), 5.10 (d, 1 H, $^3J_{5\text{-}H/4\text{-}H}$ = 6.4 Hz, 5-H), 5.40 (dd, 1 H, $^3J_{3\text{-}H/4\text{-}H}$ = 4.7 Hz, $^3J_{3\text{-}H/2\text{-}H}$ = 9.1 Hz, 3-H), 6.04 (s, 1 H, orthoester-CH), 6.30 (d, 1 H, $^3J_{2\text{-}H/3\text{-}H}$ = 9.1 Hz, 2-H), 8.67 (s, 1 H, Thz-H). All signals correspond to the major epimer.

5.4.42 2-((*S*)-((3*aS*,6*S*,6*aS*)-2-ethoxy-tetrahydro-4-oxofuro[3,4-*d*][1,3]dioxol-6-yl)[(*tert*-butyl-dimethylsilyl)oxyl]methyl)-1,3-thiazole-4-carboxylic acid methyl ester (164)

159

164
M = 459.59

Preparation:

Compound **159**	M = 329.33 g mol^{-1}	1.0 eq	7.56 mmol	2.61 g
TBSCl	M = 150.72 g mol^{-1}	2.0 eq	15.1 mmol	2.28 g
Imidazole	M = 68.08 g mol^{-1}	2.0 eq	15.1 mmol	1.03 g
DMF				25 mL

2.61 g of the orthoester **159** (7.56 mmol, 1.0 eq) were dissolved in 25 mL of DMF, 1.03 g of imidazole (15.1 mmol, 2.0 eq) and 2.28 g of TBSCl (15.1 mmol, 2.0 eq) were added and the solution was stirred for 7 h at 50 °C. After cooling to RT and dilution with CH_2Cl_2 the reaction was quenched with 5% aq. $NaHCO_3$, the phases were separated and the aqueous phase was extracted two times with CH_2Cl_2. The combined organic phases were dried with brine and over $MgSO_4$, filtered, and concentrated *in vacuo*. Residual amounts of DMF were removed by coevaporation with Tol. Purification by flash chromatography (EtOAc/Tol 1:1) yielded 86% of the silyl ether **164** (2.99 g, 6.51 mmol, 12:1 epimeric mixture) as a colorless foam.

TLC: R_f = 0.64 (EtOAc/Tol 3:2).

ESI-MS: m/z = 482 $[M+Na]^+$.

HRMS: $[M+Na]^+$: $C_{19}H_{29}NO_8SSiNa$, calculated: 482.1275, found: 482.1284.

IR: film; $\tilde{\nu}$ = 2955, 2930, 2887, 2857, 1791, 1726, 1483, 1473, 1341, 1322, 1249, 1215, 1183, 1117, 1063, 1011, 983, 956, 911, 838, 778, 676 cm^{-1}.

^{1}H-NMR: 600 MHz, DMSO-d_6: δ = 0.09, 0.14 (each s, 3 H, $SiCH_3$), 0.87 (s, 9 H, $SiC(CH_3)_3$), 1.05 (t, 3 H, $^3J_{OCH2CH3/OCH2CH3}$ = 7.1 Hz, OCH_2CH_3), 3.42-3.57 (m, 2 H, OCH_2CH_3), 3.84 (s, 3 H, CO_2CH_3), 4.78 (dd, 1 H, $^3J_{4\text{-}H/3\text{-}H}$ = 4.4 Hz, $^3J_{4\text{-}H/5\text{-}H}$ = 6.2 Hz, 4-H), 4.88 (dd, 1 H, $^3J_{3\text{-}H/4\text{-}H}$ = 4.4 Hz, $^3J_{3\text{-}H/2\text{-}H}$ = 9.2 Hz, 3-H), 5.08 (d, 1 H, $^3J_{5\text{-}H/4\text{-}H}$ = 6.2 Hz, 5-H), 5.28 (d, 1 H, $^3J_{2\text{-}H/3\text{-}H}$ = 9.2 Hz, 2-H), 6.06 (s, 1 H, orthoester-CH), 8.62 (s, 1 H, Thz-H).

^{13}C-NMR: 150 MHz, DMSO-d_6: δ = −5.1, −4.6 (each $SiCH_3$), 17.9 ($SiC(CH_3)_3$), 18.3 (OCH_2CH_3), 25.6 ($SiC(CH_3)_3$), 52.1 (CO_2CH_3), 55.7 (OCH_2CH_3), 70.8 (C-2), 73.6 (C-5), 76.0 (C-4), 81.8 (C-3), 115.3 (orthoester-CH), 130.3 (Thz-HC=C), 145.6 (Thz-HC=C), 161.0 (CO_2CH_3), 168.8 (C-1), 174.1 (C-6).

5.4.43 [(3*S*,4*S*)-dihydroxy-5-oxo-tetrahydro-furan-(2*S*)-yl)-(1*R*)-acetoxymethyl]-1,3-thiazole-carboxylic acid methyl ester (166)

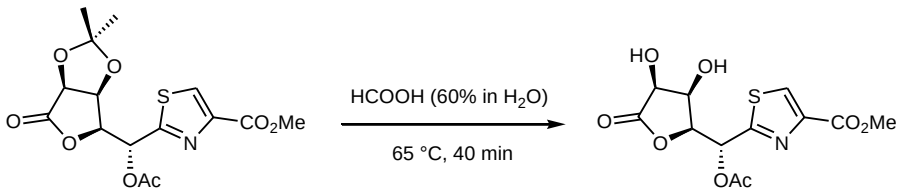

161 **166**
M = 331.30

Preparation:

Compound **161**	M = 371.36 g mol^{-1}	0.17 mmol	63 mg
HCOOH (60% in H_2O)			1.5 mL

63 mg of the acetonide **161** (0.17 mmol) were dissolved in 1.5 mL of HCOOH (60% in H_2O) and the solution was stirred for 40 min at 65 °C under regular control by TLC. Upon completion of the reaction the mixture was cooled to RT and the HCOOH/H_2O was removed under reduced pressure. Residual amounts of H_2O were removed by coevaporation with $CHCl_3$. Purification of the raw product by flash chromatography (EtOAc/Tol 5:1) yielded 77% of the diol **166** (43mg, 0.13 mmol) as a colorless solid. Small amounts of acyl migration products (**167** and **168**, section 5.4.44) were also detected (ratio **166**/**167**/**168** 90:8:2).

TLC: R_f = 0.27 (EtOAc/Tol 5:1).

ESI-MS: m/z = 354 $[M+Na]^+$.

HRMS: $[M+Na]^+$: $C_{12}H_{13}NO_8SNa$, calculated: 354.0254, found: 354.0254.

^{1}H-NMR: 500 MHz, DMSO-d_6: δ = 2.11 (s, 3 H, Ac-CH_3), 3.85 (s, 3 H, CO_2CH_3), 4.09 (dpt, 1 H, $^3J_{4\text{-H}/3\text{-H}}$ = 3.1 Hz, $^3J_{4\text{-H}/4\text{-OH}}$ = 4.4 Hz, $^3J_{4\text{-H}/5\text{-H}}$ = 4.4 Hz, 4-H), 4.60 (dd, 1 H, $^3J_{5\text{-H}/4\text{-H}}$ = 4.4 Hz, $^3J_{5\text{-H}/5\text{-OH}}$ = 7.4 Hz, 5-H), 5.06 (ddd, 1 H, $^3J_{3\text{-H}/4\text{-H}}$ = 3.1 Hz, $^3J_{3\text{-H}/2\text{-H}}$ = 9.0 Hz, $^4J_{3\text{-H}/4\text{-OH}}$ = 0.9 Hz, 3-H), 5.64 (d, 1 H, $^3J_{4\text{-OH}/4\text{-H}}$ = 4.4 Hz, $^4J_{4\text{-OH}/3\text{-H}}$ = 0.9 Hz, 4-OH), 5.98 (d, 1 H, $^3J_{5\text{-OH}/5\text{-H}}$ = 7.4 Hz, 5-OH), 6.24 (d, 1 H, $^3J_{2\text{-H}/3\text{-H}}$ = 9.0 Hz, 2-H), 8.65 (s, 1 H, Thz-H).

^{13}C-NMR: 125 MHz, DMSO-d_6: δ = 19.5 (Ac-$\underline{C}H_3$), 51.2 ($CO_2\underline{C}H_3$), 67.9 (C-4), 68.3 (C-2), 69.3 (C-5), 77.3 (C-3), 130.1 (Thz-H$\underline{C}$=C), 144.9 (Thz-HC=$\underline{C}$), 160.1 ($\underline{C}O_2CH_3$), 162.9 (C-1), 168.7 (Ac-$\underline{C}$O), 174.6 (C-6).

5.4.44 [(3*S*)-acetoxy-(4*S*)-hydroxy-5-oxo-tetrahydro-furan-(2*S*)-yl)-(1*R*)-hydroxymethyl]-1,3-thiazole-carboxylic acid methyl ester (167) and [(3*S*)-hydroxy-(4*S*)-acetoxy-5-oxo-tetrahydro-furan-(2*S*)-yl)-(1*R*)-hydroxymethyl]-1,3-thiazole-carboxylic acid methyl ester (168)

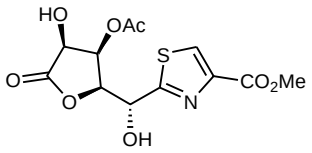

167
M = 331.36

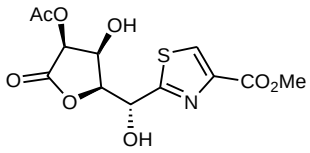

168
M = 331.30

The diols **167** and **168** were identified in the purified product obtained after acetonide cleavage (section 5.4.43) in small amounts (8% of **167** and 2% of **168**, respectively).

Compound **167**:

^{1}H-NMR: 500 MHz, DMSO-d_6: δ = 2.04 (s, 3 H, Ac-CH_3), 3.82 (s, 3 H, CO_2CH_3), 4.72 (dd, 1 H, $^{3}J_{3\text{-H}/4\text{-H}}$ = 3.2 Hz, $^{3}J_{3\text{-H}/2\text{-H}}$ = 7.9 Hz, 3-H), 4.79 (dd, 1 H, $^{3}J_{5\text{-H}/4\text{-H}}$ = 5.1 Hz, $^{3}J_{5\text{-H}/5\text{-OH}}$ = 8.0 Hz, 5-H), 5.11 (dd, 1 H, $^{3}J_{2\text{-H}/2\text{-OH}}$ = 5.8 Hz, $^{3}J_{2\text{-H}/3\text{-H}}$ = 7.9 Hz, 2-H), 5.25 (dd, 1 H, $^{3}J_{4\text{-H}/3\text{-H}}$ = 3.2 Hz, $^{4}J_{4\text{-H}/5\text{-H}}$ = 5.1 Hz, 4-H), 6.17 (d, 1 H, $^{3}J_{5\text{-OH}/5\text{-H}}$ = 8.0 Hz, 5-OH), 6.90 (d, 1 H, $^{3}J_{2\text{-OH}/2\text{-H}}$ = 5.8 Hz, 2-OH), 8.57 (s, 1 H, Thz-H).

^{13}C-NMR: 125 MHz, DMSO-d_6: δ = 20.2 (Ac-$\underline{C}H_3$), 51.7 ($CO_2\underline{C}H_3$), 68.2 (C-5), 68.7 (C-2), 70.3 (C-4), 79.6 (C-3), 129.6 (Thz-H$\underline{C}$=C), 145.4 (Thz-HC=$\underline{C}$), 160.9 ($\underline{C}O_2CH_3$), 168.7 (Ac-$\underline{C}$O), 170.9 (C-1), 174.7 (C-6).

Compound **168**:

^{1}H-NMR: 500 MHz, DMSO-d_6: δ = 3.83 (s, 3 H, CO_2CH_3), 5.18 (dd, 1 H, $^3J_{2\text{-H}/2\text{-OH}}$ = 6.0 Hz, $^3J_{2\text{-H}/3\text{-H}}$ = 8.6 Hz, 2-H), 5.90 (d, 1 H, $^3J_{4\text{-OH}/4\text{-H}}$ = 4.8 Hz, 4-OH), 6.72 (d, 1 H, $^3J_{2\text{-OH}/2\text{-H}}$ = 6.0 Hz, 2-OH), 8.58 (s, 1 H, Thz-H). The other ^{1}H and the ^{13}C chemical shifts can not be given due to signal overlap and weak intensity.

5.4.45 2-((1*R*,2*S*,3*S*,4*S*)-4-(methoxycarbonyl)-1-(*tert*-butyl-dimethylsilyloxy)-2,3,4-trihydroxy-butyl)-1,3-thiazole-4-carboxylic acid methyl ester (170)

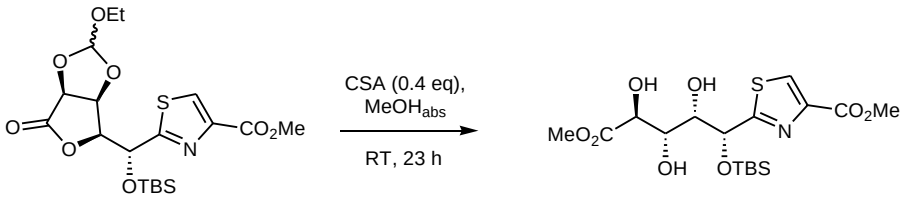

164 **170**
M = 435.56

Preparation:

Compound **164**	M = 459.59 g mol^{-1}	1.0 eq	70.0 µmol	32 mg
CSA	M = 232.30 g mol^{-1}	0.4 eq	28.0 mmol	6.5 mg
$MeOH_{abs}$				3.0 mL

32 mg of the orthoester **164** (70.0 µmol, 1.0 eq) were dissolved in 3.0 mL of $MeOH_{abs}$ in a nitrogen atmosphere. 6.5 mg of CSA (28.0 µmol, 0.4 eq) were added and the mixture was stirred at RT for 23 h. 23 mg of solid $NaHCO_3$ and 18 mg of solid $MgSO_4$ were subsequently added, the mixture was stirred for 1 h at RT, filtered, and the raw products were adsorbed on Celite. After purification by flash chromatography (EtOAc/Tol 3:2) 18% of the triol **170** (5.4 mg, 12.4 µmol) were obtained as a colorless oil. In addition, 16% of the orthoester deprotected lactone **169** (4.6 mg, 11.4 µmol) were isolated as a colorless oil (further protocols and analytics in section 5.4.46).

TLC: R_f = 0.19 (EtOAc/MeOH 5:1).

ESI-MS: m/z = 458 $[M+Na]^+$.

HRMS: $[M+Na]^+$: $C_{17}H_{29}NO_8SSiNa$, calculated: 458.1275, found: 485.1278.

Storage in DMSO effects a rapid silyl migration from 2-OH to 5-OH which is obtained as main species.

^{1}H-NMR: 600 MHz, DMSO-d_6: δ = –0.02, 0.03 (each s, 3 H, $SiCH_3$), 0.80 (s, 9 H, $SiC(CH_3)_3$), 3.60-3.63 (m, 4 H, 4-H, 6-CO_2CH_3), 3.78 (dpt, 1 H, $^3J_{3\text{-H}/4\text{-H}}$ = 1.9 Hz, $^3J_{3\text{-H}/2\text{-H}}$ = 6.7 Hz, $^3J_{3\text{-H}/3\text{-OH}}$ = 6.7 Hz, 3-H), 3.82 (s, 3 H, Thz-CO_2CH_3), 4.16 (dd, 1 H, $^3J_{5\text{-H}/4\text{-H}}$ = 8.1 Hz, 5-H), 4.83 (d, 1 H, $^3J_{4\text{-OH}/4\text{-H}}$ = 7.7 Hz, 4-OH), 4.86 (d, 1 H, $^3J_{3\text{-OH}/3\text{-H}}$ = 6.7 Hz, 3-OH), 4.92 (dd, 1 H, $^3J_{2\text{-H}/2\text{-OH}}$ = 5.0 Hz, $^3J_{2\text{-H}/3\text{-H}}$ = 6.7 Hz, 2-H), 6.27 (d, 1 H, $^3J_{2\text{-OH}/2\text{-H}}$ = 5.0 Hz, 2-OH), 8.49 (s, 1 H, Thz-H).

^{13}C-NMR: 125 MHz, DMSO: δ = –5.6, –5.4 (each s, $Si\underline{C}H_3$), 17.5 (s, $Si\underline{C}(CH_3)_3$), 25.5 (s, $SiC(\underline{C}H_3)_3$), 51.2 (6-$CO_2\underline{C}H_3$), 51.9 (Thz-$CO_2\underline{C}H_3$), 71.5 (C-5), 71.4 (C-2, C-4), 71.8 (C-3), 72.5 (C-2), 128.9 (Thz-H$\underline{C}$=C), 145.2 (Thz-HC=$\underline{C}$), 161.3 (Thz-$\underline{C}O_2CH_3$), 172.4 (C-6), 175.4 (C-1).

5.4.46 [(3*S*,4*S*)-dihydroxy-5-oxo-tetrahydro-furan-(2*S*)-yl)-(1*R*)-(*tert*-butyl-dimethylsilyloxy)methyl]-1,3-thiazole-carboxylic acid methyl ester (169)

Method A) with aq. HCl

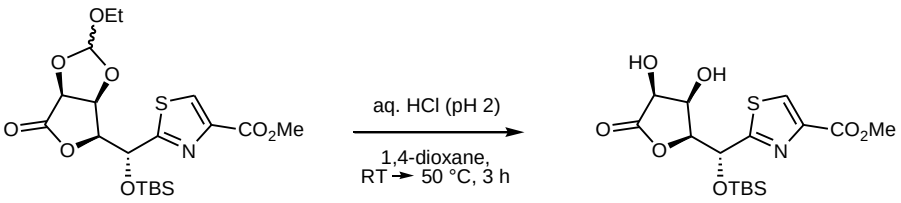

164 **169**
M = 403.52

Preparation:

Compound **164**	M = 459.59 g mol^{-1}	82.7 µmol	38 mg
aq. HCl (pH 2)			2.0 mL
1,4-dioxane			1.0 mL

38 mg of the orthoester **164** (82.7 µmol) were dissolved in 2.0 mL of aq. HCl (pH 2) and 1.0 mL of 1,4-dioxane. The solution was stirred at RT for 1 h and at 50 °C for 2 h, neutralized with basic ion exchange resin, and concentrated *in vacuo* to yield a 72:28 mixture of the diol **169** and the TBS-deprotected triol **140** (analytics in section 5.4.29) as a colorless solid.

Method B) in acidified BnOH (attempt to synthesize the benzyl ester **171***)*

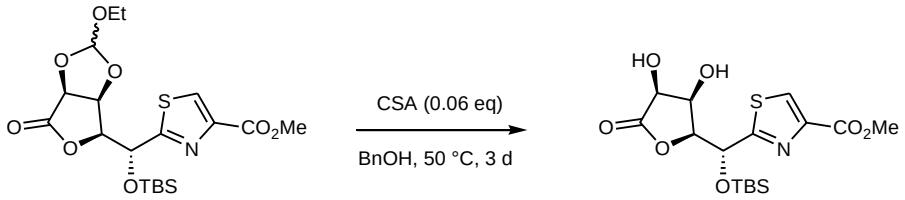

164 **169** M = 403.52

Preparation:

Compound **164**	M = 459.59 g mol^{-1}	1.0 eq	1.63 mmol	751 mg
CSA	M = 232.30 g mol^{-1}	0.06 eq	99.0 µmol	23 mg
BnOH				5.0 mL

751 mg of the orthoester **164** (1.63 mmol, 1.0 eq) were dissolved in 5.0 mL of BnOH and 23 mg of CSA (99.0 µmol, 0.06 eq) were added. The solution was stirred at 50 °C for 3 d, neutralized with NEt_3, and concentrated *in vacuo*. The raw product was purified by flash chromatography (EtOAc/Tol 3:2) to yield 35% of the diol **169** (230 mg, 0.57 mmol) as a colorless oil. As byproduct, 17% of the TBS-deprotected triol **140** (80 mg, 0.28 mmol; analytics in section 5.4.29) were isolated.

TLC: R_f = 0.33 (EtOAc/MeOH 5:1).

ESI-MS: m/z = 426 $[M+Na]^+$.

HRMS: $[M+Na]^+$: $C_{16}H_{25}NO_7SSiNa$, calculated: 426.1013, found: 426.1014.

IR: film; $\tilde{\nu}$ = 3418, 2956, 2930, 2857, 1770, 1723, 1485, 1473, 1333, 1253, 1236, 1184, 1135, 1093, 991, 940, 863, 806, 782, 699 cm^{-1}.

^{1}H-NMR: 500 MHz, DMSO-d_6: δ = 0.06, 0.13 (each s, 3 H, $SiCH_3$), 0.87 (s, 9 H, $SiC(CH_3)_3$), 3.84 (s, 3 H, CO_2CH_3), 4.06-4.10 (m, 1 H, 4-H), 4.50 (dd, 1 H, $^{3}J_{5\text{-H}/4\text{-H}}$ = 4.6 Hz, $^{3}J_{5\text{-H}/5\text{-OH}}$ = 7.2 Hz, 5-H), 4.52-4.57 (m, 1 H, 3-H), 5.31 (d, 1 H, $^{3}J_{2\text{-H}/3\text{-H}}$ = 9.0 Hz, 2-H), 5.45 (d, 1 H, $^{3}J_{4\text{-OH}/4\text{-H}}$ = 3.7 Hz, 4-OH), 5.93 (d, 1 H, $^{3}J_{5\text{-OH}/5\text{-H}}$ = 7.2 Hz, 5-OH), 8.61 (s, 1 H, Thz-H).

^{13}C-NMR: 125 MHz, DMSO: δ = –5.1, –4.7 (each s, $SiCH_3$), 17.9 (s, $SiC(CH_3)_3$), 25.5 (s, $SiC(CH_3)_3$), 52.0 (CO_2CH_3), 69.0 (C-4), 70.6 (C-2), 70.7 (C-5), 81.3 (C-3), 130.0 (Thz-HC=C), 145.7 (Thz-HC=C), 160.5 (CO_2CH_3), 170.5 (C-1), 175.6 (C-1).

5.4.47 2-((1*R*,2*S*,3*S*,4*S*)-4-(benzyloxycarbonyl)-1-(*tert*-butyl-dimethylsilyloxy)-2,3,4-trihydroxy-butyl)-1,3-thiazole-4-carboxylic acid methyl ester (171)

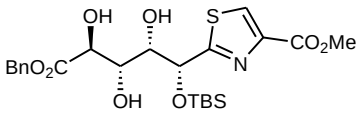

171
M = 511.66

The benzyl ester **171** was obtained in traces (only identifiable in the ESI spectrum) in the synthesis of **169** (section 5.4.46, method B) by coelution with the main product.

ESI-MS: *m*/*z* = 534 $[M+Na]^+$.

HRMS: $[M+Na]^+$: $C_{23}H_{33}NO_8SSiNa$, calculated: 534.1588, found: 534.1594.

5.4.48 2-((1*S*,2*R*,3*S*)-3-(benzyloxycarbonyl)-1,2-dihydroxy-3-(*tert*-butyl-dimethylsilyloxy)-propyl)-1,3-thiazole-4-carboxylic acid methyl ester (174)

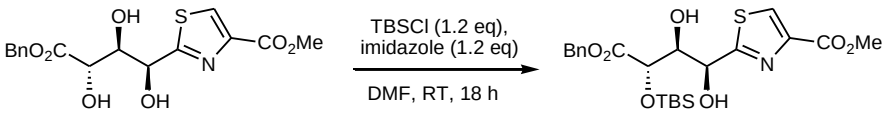

148 **174**
M = 481.63

Preparation:

Compound **148**	M = 367.37 g mol^{-1}	1.0 eq	9.77 mmol	3.59 g
TBSCl	M = 150.72 g mol^{-1}	1.2 eq	11.7 mmol	1.77 g
Imidazole	M = 68.08 g mol^{-1}	1.2 eq	11.7 mmol	798 mg
DMF				24 mL

3.59 g of the triol **148** (9.77 mmol, 1.0 eq) were dissolved in 24 mL of DMF, 1.77 g of imidazole (11.7 mmol, 1.2 eq) and 798 mg of TBSCl (11.7 mmol, 1.2 eq) were added and the solution was stirred for 18 h at RT. After cooling to RT and dilution with CH_2Cl_2 the reaction was quenched with 5% aq. $NaHCO_3$, the phases were separated and the aqueous phase was extracted two times with CH_2Cl_2. The combined organic phases were dried with brine and over $MgSO_4$, filtered, and concentrated *in vacuo*. Residual amounts of DMF were removed by coevaporation with Tol. The raw product was dissolved in Tol/EtOAc 4:1 for flash chromatographic purification upon which residual starting material **148** precipitated and was isolated by filtration (16%, 585 mg, 1.59 mmol). The filtrate was subjected to flash chromatographic purification (Tol/EtOAc 4:1→3:1) which yielded 74% of the silyl ether **174** (3.49 g, 6.83 mmol) as a colorless oil.

TLC: R_f = 0.36 (EtOAc/Tol 1:1).

ESI-MS: m/z = 504 $[M+Na]^+$.

HRMS: $[M+Na]^+$: $C_{22}H_{31}NO_7SSiNa$, calculated: 504.1483, found: 504.1486.

IR: film; $\tilde{\nu}$ = 3446, 3118, 2954, 2930, 2887, 2857, 1724, 1486, 1461, 1435, 1389, 1348, 1326, 1251, 1170, 1099, 1049, 989, 837, 780, 750, 697 cm^{-1}.

^{1}H-NMR: 600 MHz, DMSO-d_6: δ = –0.01, 0.06 (each s, 3 H, $SiCH_3$), 0.83 (s, 9 H, $SiC(CH_3)_3$), 3.82 (s, 3 H, CO_2CH_3), 3.95 (ddd, 1 H, $^3J_{3\text{-H}/2\text{-H}}$ = 1.9 Hz, $^3J_{3\text{-H}/3\text{-OH}}$ = 8.1 Hz, $^3J_{3\text{-H}/4\text{-H}}$ = 8.9 Hz, 3-H), 4.32 (d, 1 H, $^3J_{4\text{-H}/3\text{-H}}$ = 8.9 Hz, 4-H), 4.98 (dd, 1 H, $^3J_{2\text{-H}/3\text{-H}}$ = 1.9 Hz, $^3J_{2\text{-H}/2\text{-OH}}$ = 6.4 Hz, 2-H), 5.09 (d, 1 H, ^2J = 12.5 Hz, $CO_2C\underline{H}_2Ph^u$), 5.16 (d, 1 H, ^2J = 12.5 Hz, $CO_2C\underline{H}_2Ph^d$), 5.31 (d, 1 H, $^3J_{3\text{-OH}/3\text{-H}}$ = 8.1 Hz, 3-OH), 6.33 (d, 1 H, $^3J_{2\text{-OH}/2\text{-H}}$ = 6.4 Hz, 2-OH), 7.32-7.40 (m, 5 H, $CO_2CH_2\underline{Ph}$), 8.45 (s, 1 H, Thz-H).

^{13}C-NMR: 150 MHz, DMSO-d_6: δ = –4.8, –4.7 (each $SiCH_3$), 18.5 ($Si\underline{C}(CH_3)_3$), 26.2 ($SiC(\underline{C}H_3)_3$), 52.7 ($CO_2\underline{C}H_3$), 66.5 ($CO_2\underline{C}H_2Ph$), 70.3 (C-2), 73.3 (C-4), 75.4 (C-3), 128.0, 128.1, 128.3 (each Bn-$CH_{arom.}$), 129.7 (Thz-H$\underline{C}$=C), 135.7 (Bn-$C_{arom.,\ quart.}$), 146.3 (Thz-HC=$\underline{C}$), 162.2 ($\underline{C}O_2CH_3$), 172.2 (C-5), 177.4 (C-1).

Opt. rotation: $[\alpha]_{589}^{18}$ = –45.5, $[\alpha]_{578}^{18}$ = –47.4, $[\alpha]_{546}^{18}$ = –54.1, $[\alpha]_{436}^{18}$ = –94.9, $[\alpha]_{365}^{18}$ = –151.3 (c = 1.08 g/100 mL EtOH).

RT (HPLC): 20.86 min (linear gradient of 0 to 60% A over 10 min→60 to 99% A over 15 min, A = CH_3CN, B = 0.08% TFA/H_2O).

5.4.49 2-((1*S*,2*R*,3*S*)-3-(benzyloxycarbonyl)-1,3-bis(*tert*-butyl-dimethylsilyloxy)-2-hydroxy-propyl)-1,3-thiazole-4-carboxylic acid methyl ester (175)

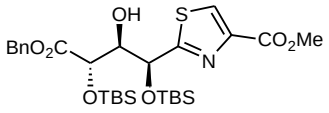

175
M = 595.90

The silyl ether **175** was obtained as byproduct in the synthesis of the single protected thiazole triol **174** (section 5.4.48). By flash chromatographic purification 9.6% of **175** (561 mg, 0.94 mmol) were obtained as a colorless oil.

TLC: R_f = 0.62 (EtOAc/Tol 1:1).

ESI-MS: m/z = 618 $[M+Na]^+$.

HRMS: $[M+Na]^+$: $C_{28}H_{45}NO_7SSi_2Na$, calculated: 618.2347, found: 618.2354.

IR: film; $\tilde{\nu}$ = 3498, 2953, 2930, 2886, 2857, 1724, 1497, 1471, 1463, 1435, 1389, 1348, 1324, 1250, 1212, 1095, 991, 834, 778, 751, 696 cm^{-1}.

^{1}H-NMR: 600 MHz, DMSO-d_6: δ = –0.13, –0.08. –0.06, 0.06 (each s, 3 H, $SiCH_3$), 0.78, 0.85 (each s, 9 H, $SiC(CH_3)_3$), 3.82 (s, 3 H, CO_2CH_3), 3.73 (ddd, 1 H, $^3J_{3\text{-H}/2\text{-H}}$ = 5.0 Hz, $^3J_{3\text{-H}/4\text{-H}}$ = 5.2 Hz, $^3J_{3\text{-H}/3\text{-OH}}$ = 7.4 Hz, 3-H), 4.51 (d, 1 H, $^3J_{4\text{-H}/3\text{-H}}$ = 5.2 Hz, 4-H), 5.16 (d, 1 H, $^3J_{2\text{-H}/3\text{-H}}$ = 5.0 Hz, 2-H), 5.08-5.17 (m, 3 H, 2-H, $CO_2C\underline{H}_2Ph$), 5.71 (d, 1 H, $^3J_{3\text{-OH}/3\text{-H}}$ = 7.4 Hz, 3-OH), 7.34-7.42 (m, 5 H, $CO_2CH_2\underline{Ph}$), 8.52 (s, 1 H, Thz-H).

^{13}C-NMR: 150 MHz, DMSO-d_6: δ = –5.4, –5.1, –5.0, –4.6 (each $SiCH_3$), 17.8, 18.6 (each $Si\underline{C}(CH_3)_3$), 25.5, 26.6 (each $SiC(\underline{C}H_3)_3$), 51.9 ($CO_2\underline{C}H_3$), 65.9 ($CO_2\underline{C}H_2Ph$), 72.2 (C-2), 73.1 (C-4), 76.6 (C-3), 128.0, 128.2, 128.3 (each Bn-$CH_{arom.}$), 129.8 (Thz-H$\underline{C}$=C), 135.6 (Bn-$C_{arom., quart.}$), 145.0 (Thz-HC=$\underline{C}$), 161.2 ($\underline{C}O_2CH_3$), 170.8 (C-5), 173.2 (C-1).

Opt. rotation: $[\alpha]_{589}^{23}$ = –34.5, $[\alpha]_{578}^{23}$ = –36.0, $[\alpha]_{546}^{23}$ = –41.3, $[\alpha]_{436}^{23}$ = –71.2, $[\alpha]_{365}^{23}$ = –109.7 (c = 1.23 g/100 mL $CHCl_3$).

5.4.50 2-((1*S*,2*R*,3*S*)-3-(benzyloxycarbonyl)-1,2-*O*-isopropylidene-3-(*tert*-butyl-dimethylsilyloxy)-propyl)-1,3-thiazole-4-carboxylic acid methyl ester (176)

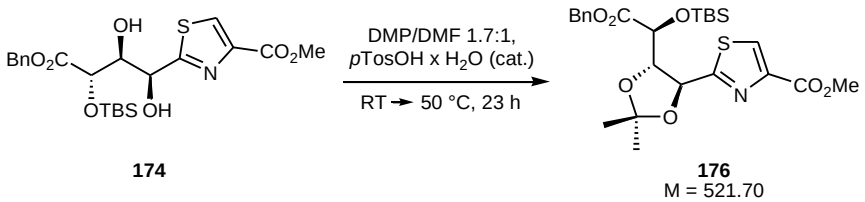

174 **176**
M = 521.70

Preparation:

Compound **174**	M = 481.63 g mol^{-1}	1.0 eq	56.1 µmol	27 mg
DMP	M = 104.15 g mol^{-1}, ρ = 0.85			1.7 mL
*p*TosOH x H_2O	M = 190.22 g mol^{-1}			cat.
DMF				1.0 mL

27 mg of the diol **174** (56.1 µmol, 1.0 eq) were dissolved in 1.0 mL of DMF and 1.7 mL of DMP. After the addition of a catalytic amount of *p*TosOH x H_2O, the solution was stirred for 16 h at RT and for further 7 h at 50 °C. The reaction mixture was cooled to RT, neutralized by addition of NEt_3, and concentrated *in vacuo*. Residual amounts of DMF were removed by coevaporation with Tol. The crude product was subjected to flash chromatography (Tol/EtOAc 5:1) to obtain 75% (22 mg, 42.2 µmol) of the acetonide **176** as a colorless oil.

TLC: R_f = 0.70 (Tol/EtOAc 4:1).

ESI-MS: *m*/*z* = 544 $[M+Na]^+$.

HRMS: $[M+Na]^+$: $C_{25}H_{35}NO_7SSiNa$, calculated: 544.1796, found: 544.1796.

^{1}H-NMR: 300 MHz, $CDCl_3$: δ = 0.05, 0.06 (each s, 3 H, $SiCH_3$), 0.87 (each s, 9 H, $SiC(CH_3)_3$), 1.46, 1.49 (each s, 3 H, Isopr-CH_3), 3.84 (s, 3 H, CO_2CH_3), 4.57 (dd, 1 H, $^3J_{3\text{-H}/2\text{-H}}$ = 7.4 Hz, $^3J_{3\text{-H}/4\text{-H}}$ = 2.4 Hz, 3-H), 4.70 (d, 1 H, $^3J_{4\text{-H}/3\text{-H}}$ = 2.4 Hz, 4-H), 5.23 (s, 2 H, $CO_2C\underline{H}_2Ph$), 5.49 (d, 1 H, $^3J_{2\text{-H}/3\text{-H}}$ = 7.4 Hz, 2-H), 7.31-7.35 (m, 5 H, $CO_2CH_2\underline{Ph}$), 8.13 (s, 1 H, Thz-H).

^{13}C-NMR: 75 MHz, $CDCl_3$: δ = –5.1, –5.0 (each $SiCH_3$), 18.4 ($Si\underline{C}(CH_3)_3$), 25.8 ($SiC(\underline{C}H_3)_3$), 26.8, 27.0 (each Isopr-CH_3), 52.3 ($CO_2\underline{C}H_3$), 67.4 ($CO_2\underline{C}H_2Ph$), 71.5 (C-4), 75.1 (C-2), 83.5 (C-3), 111.3 (Isopr-$C_{quart.}$), 128.1 (Thz-H$\underline{C}$=C), 128.4, 128.6, 128.8 (each Bn-$CH_{arom.}$), 135.7 (Bn-$C_{arom., quart.}$), 147.3 (Thz-HC=$\underline{C}$), 161.8 ($\underline{C}O_2CH_3$), 170.4, 171.8 (C-1, C-5).

5.4.51 2-((1*S*,2*R*,3*S*)-3-(benzyloxycarbonyl)-1,2-diacetoxy-3-(*tert*-butyl-dimethylsilyloxy)-propyl)-1,3-thiazole-4-carboxylic acid methyl ester (177)

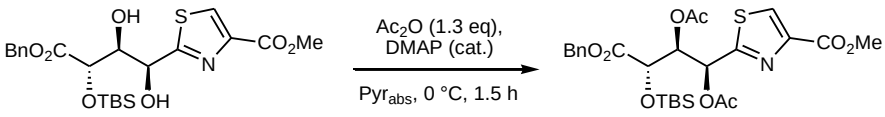

174 **177**
M = 565.71

Preparation:

Compound **174**	M = 481.63 g mol^{-1}	1.0 eq	139 µmol	67 mg
Ac_2O	M = 102.09 g mol^{-1}, ρ = 1.08	2.5 eq	348 µmol	32.9 µL (35.5 mg)
DMAP	M = 122.17 g mol^{-1}			cat.
Pyr_{abs}				2.0 mL

67 mg of the diol **174** (139 µmol, 1.0 eq) were dissolved in 2.0 mL of Pyr_{abs} in a nitrogen atmosphere. A catalytical amount of DMAP and 32.9 µL of Ac_2O (35.5 mg, 348 mmol, 2.5 eq) were added and the solution was stirred for 1.5 h at 0 °C. The reaction was diluted with Tol, quenched with ice, and 5% aq. $NaHCO_3$ was added. The phases were separated and the aqueous phase was extracted two times with Tol. The combined organic phases were dried with brine and over $MgSO_4$, filtered, and concentrated *in vacuo*. Flash chromatography (Tol/EtOAc 4:1) yielded 85% of the diacetate **177** (67 mg, 118 µmol) as a colorless oil.

TLC: R_f = 0.51 (Tol/EtOAc 4:1).

ESI-MS: *m/z* = 588 $[M+Na]^+$.

HRMS: $[M+Na]^+$: $C_{26}H_{35}NO_9SSiNa$, calculated: 588.1694, found: 588.1686.

^{1}H-NMR: 600 MHz, $CDCl_3$: δ = –0.01, 0.01 (each s, 3 H, $SiCH_3$), 0.88 (each s, 9 H, $SiC(CH_3)_3$), 1.89 (s, 3 H, 3-Ac-CH_3), 2.13 (s, 3 H, 2-Ac-CH_3), 3.91 (s, 3 H, CO_2CH_3), 4.45 (d, 1 H, $^3J_{4\text{-H}/3\text{-H}}$ = 6.3 Hz, 4-H), 5.05 (d, 1 H, ^2J = 12.5 Hz, $CO_2C\underline{H}_2Ph^u$), 5.07 (d, 1 H, ^2J = 12.5 Hz, $CO_2C\underline{H}_2Ph^d$), 5.82 (dd, 1 H, $^3J_{3\text{-H}/2\text{-H}}$ = 4.6 Hz, $^3J_{3\text{-H}/4\text{-H}}$ = 6.3 Hz, 3-H), 6.42 (d, 1 H, $^3J_{2\text{-H}/3\text{-H}}$ = 4.6 Hz, 2-H), 7.32-7.38 (m, 5 H, $CO_2CH_2\underline{Ph}$), 8.15 (s, 1 H, Thz-H).

^{13}C-NMR: 150 MHz, $CDCl_3$: δ = –5.5, –5.0 (each $SiCH_3$), 18.2 ($SiC(CH_3)_3$), 20.5 (3-Ac-CH_3), 20.9 (2-Ac-CH_3), 25.7 ($SiC(CH_3)_3$), 52.6 (CO_2CH_3), 67.5 (CO_2CH_2Ph), 70.4 (C-2), 71.6 (C-4), 74.2 (C-3), 128.6 (Thz-HC=C), 128.7, 128.7, 128.9 (each Bn-$CH_{arom.}$), 135.2 (Bn-$C_{arom., quart.}$), 147.2 (Thz-HC=C), 161.7 (CO_2CH_3), 166.4 (C-1), 169.1 (3-Ac-CO), 169.5 (2-Ac-CO), 170.2 (C-5).

Opt. rotation: $[\alpha]_{589}^{18}$ = –35.8, $[\alpha]_{578}^{18}$ = –37.5, $[\alpha]_{546}^{18}$ = –42.6, $[\alpha]_{436}^{18}$ = –73.8, $[\alpha]_{365}^{18}$ = –115.4 (c = 1.00 g/100 mL EtOH).

5.4.52 2-((4*S*,5*R*)-5-((*S*)-(methoxycarbonyl)(hydroxy)methyl)-2-ethoxy-1,3-dioxolan-4-yl)-1,3-thiazole-4-carboxylic acid methyl ester (179)

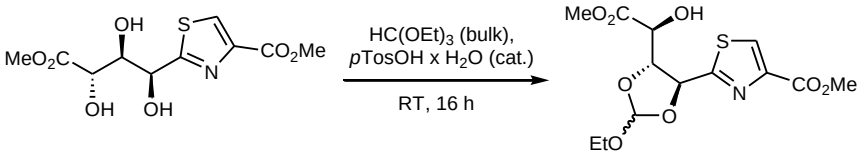

143 **179**
M = 347.34

Preparation:

Compound **143**	M = 291.28 g mol^{-1}	1.0 eq	1.34 mmol	391 mg
$HC(OEt)_3$	M = 148.20 g mol^{-1}, ρ = 0.90			20.0 mL (18.0 g)
*p*TosOH x H_2O	M = 190.22 g mol^{-1}			cat.

391 mg of the triol **143** (1.34 mmol, 1.0 eq) were suspended in 20.0 mL of $HC(OEt)_3$ (18.0 g) and a catalytic amount of *p*TosOH x H_2O was added. The suspension was stirred at RT for 16 h under which complete solution occurred. The mixture was neutralized with NEt_3, directly transferred onto a flash chromatography column and eluted with EtOAc/Tol 1:1 to yield 83% of the orthoester **179** (387 mg, 1.11 mmol, 65:35 epimeric mixture) as a colorless oil.

TLC: R_f = 0.41 (EtOAc/Tol 3:2).

ESI-MS: *m/z* = 370 $[M+Na]^+$.

HRMS: $[M+Na]^+$: $C_{13}H_{17}NO_8SNa$, calculated: 370.0567, found: 370.0566.

Major epimer:

^{1}H-NMR: 500 MHz, DMSO-d_6: δ = 1.12 (t, 3 H, $^3J_{OCH2CH3/OCH2CH3}$ = 7.0 Hz, OCH_2CH_3), 3.57-3.64 (m, 2 H, OCH_2CH_3), 3.65 (s, 3 H, 5-CO_2CH_3), 3.83 (s, 3 H, Thz-CO_2CH_3), 4.46 (dd, 1 H, $^3J_{4\text{-}H/3\text{-}H}$ = 4.0 Hz, $^3J_{4\text{-}H/4\text{-}OH}$ = 5.7 Hz, 4-H), 4.57 (dd, 1 H, $^3J_{3\text{-}H/4\text{-}H}$ = 4.0 Hz, $^3J_{3\text{-}H/2\text{-}H}$ = 5.9 Hz, 3-H), 5.38 (d, 1 H, $^3J_{2\text{-}H/3\text{-}H}$ = 5.9 Hz, 2-H), 6.10 (s, 1 H, orthoester-CH), 6.20 (d, 1 H, $^3J_{4\text{-}OH/4\text{-}H}$ = 5.7 Hz, 4-OH), 8.56 (s, 1 H, Thz-H).

^{13}C-NMR: 125 MHz, DMSO-d_6: δ = 14.5 (OCH_2CH_3), 51.3 (CO_2CH_3), 51.6 (Thz-CO_2CH_3), 59.5 (OCH_2CH_3), 69.1 (C-4), 74.3 (C-2), 81.2 (C-3), 115.4 (orthoester-CH), 129.9 (Thz-HC=C), 145.4 (Thz-HC=C), 160.8 (Thz-CO_2CH_3), 170.6 (C-5), 170.8 (C-1).

Minor epimer:

^{1}H-NMR: 500 MHz, DMSO-d_6: δ = 1.15 (t, 3 H, $^3J_{OCH2CH3/OCH2CH3}$ = 7.0 Hz, OCH_2CH_3), 3.57-3.64 (m, 2 H, OCH_2CH_3), 3.65 (s, 3 H, 5-CO_2CH_3), 3.84 (s, 3 H, CO_2CH_3), 4.41 (dd, 1 H, $^3J_{4\text{-}H/4\text{-}OH}$ = 6.1 Hz, $^3J_{4\text{-}H/3\text{-}H}$ = 7.1 Hz, 4-H), 4.41 (dd, 1 H, $^3J_{3\text{-}H/2\text{-}H}$ = 4.8 Hz, $^3J_{3\text{-}H/4\text{-}H}$ = 7.1 Hz, 3-H), 5.54 (d, 1 H, $^3J_{2\text{-}H/3\text{-}H}$ = 4.8 Hz, 2-H), 6.14 (s, 1 H, orthoester-CH), 6.32 (d, 1 H, $^3J_{4\text{-}OH/4\text{-}H}$ = 6.1 Hz, 4-OH), 8.59 (s, 1 H, Thz-H).

^{13}C-NMR: 125 MHz, DMSO-d_6: δ = 14.5 (OCH_2CH_3), 51.3 (5-CO_2CH_3), 51.6 (Thz-CO_2CH_3), 59.5 (OCH_2CH_3), 70.2 (C-4), 75.1 (C-2), 81.2 (C-3), 115.2 (orthoester-CH), 129.8 (Thz-HC=C), 145.8 (Thz-HC=C), 160.8 (Thz-CO_2CH_3), 169.6 (C-1), 171.2 (C-5).

5.4.53 2-((4*S*,5*R*)-5-((*S*)-(methoxycarbonyl)(diethoxymethoxy)methyl)-2-ethoxy-1,3-dioxolan-4-yl)-1,3-thiazole-4-carboxylic acid methyl ester (181)

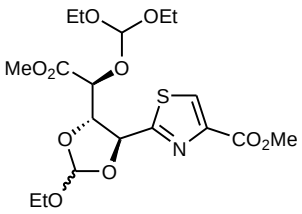

181
M = 449.47

The fully protected orthoester **181** was isolated in 5.5% yield (33 mg, 73.7 µmol) in the synthesis of the orthoester **179** (section 5.4.52) as a colorless oil. The yield of **181** is considerably increased if the reaction is run at higher temperature.

ESI-MS: *m*/*z* = 472 $[M+Na]^+$.

HRMS: $[M+Na]^+$: $C_{18}H_{27}NO_{10}SNa$, calculated: 472.1248, found: 472.1252.

TLC: R_f = 0.68 (EtOAc/Tol 3:2).

Major epimer:

^{1}H-NMR: 300 MHz, DMSO-d_6: δ = 1.04-1.20 (m, 9 H, 3 x $OCH_2C\underline{H}_3$), 3.48-3.63 (m, 6 H, 3 x $OC\underline{H}_2CH_3$), 3.69 (s, 3 H, 5-CO_2CH_3), 3.83 (s, 3 H, Thz-CO_2CH_3), 4.57 (d, 1 H, $^3J_{4\text{-H}/3\text{-H}}$ = 4.7 Hz, 4-H), 4.63 (dd, 1 H, $^3J_{3\text{-H}/4\text{-H}}$ = 4.7 Hz, $^3J_{3\text{-H}/2\text{-H}}$ = 5.6 Hz, 3-H), 5.36 (s, 1 H, $C\underline{H}(OEt)_2$), 5.43 (d, 1 H, $^3J_{2\text{-H}/3\text{-H}}$ = 5.6 Hz, 2-H), 6.13 (s, 1 H, orthoester-CH), 8.59 (s, 1 H, Thz-H).

Minor epimer:

^{1}H-NMR: 300 MHz, DMSO-d_6: δ = 1.04-1.20 (m, 9 H, 3 x $OCH_2C\underline{H}_3$), 3.48-3.63 (m, 6 H, 3 x $OC\underline{H}_2CH_3$), 3.67 (s, 3 H, 5-CO_2CH_3), 3.84 (s, 3 H, Thz-CO_2CH_3), 4.45-4.51 (m, 2 H, 3-H, 4-H), 5.38 (s, 1 H, $C\underline{H}(OEt)_2$), 5.56 (d, 1 H, $^3J_{2\text{-H}/3\text{-H}}$ = 4.3 Hz, 2-H), 6.16 (s, 1 H, orthoester-CH), 8.61 (s, 1 H, Thz-H).

5.4.54 2-((4S,5R)-5-((S)-(benzyloxycarbonyl)(hydroxy)methyl)-2-ethoxy-1,3-dioxolan-4-yl)-1,3-thiazole-4-carboxylic acid methyl ester (180) and 2-((4*S*,5*R*)-5-((*S*)-(methoxycarbonyl)(diethoxymethoxy)methyl)-2-ethoxy-1,3-dioxolan-4-yl)-1,3-thiazole-4-carboxylic acid methyl ester (182)

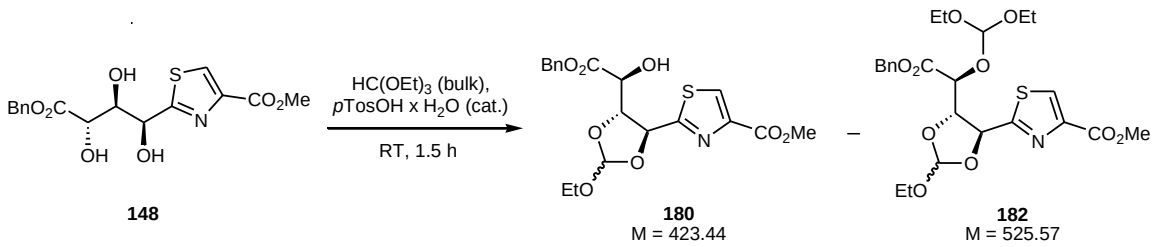

Preparation:

Compound **148**	M = 367.37 g mol^{-1}	1.0 eq	28.3 µmol	10 mg
$HC(OEt)_3$	M = 148.20 g mol^{-1}, ρ = 0.90			1.0 mL (0.9 g)
*p*TosOH x H_2O	M = 190.22 g mol^{-1}			cat.

10 mg of the triol **148** (28.3 µmol, 1.0 eq) were suspended in 1.0 mL of $HC(OEt)_3$ (0.9 g) and a catalytic amount of *p*TosOH x H_2O was added. The suspension was stirred at RT for 1.5 h under which complete solution occurred. The mixture was neutralized with NEt_3, directly transferred onto a silica gel filter column, and eluted with EtOAc/Tol 3:1 to obtain a 61:39 mixture of the orthoesters **180** and **182** (each as 55:45 epimeric mixture) in quantitative yield as a colorless oil.

Compound **180***:*

ESI-MS: *m*/*z* = 446 $[M+Na]^+$.

HRMS: $[M+Na]^+$: $C_{19}H_{21}NO_8SNa$, calculated: 446.0880, found: 446.0888.

TLC: R_f = 0.58 (EtOAc/Tol 3:1).

Major epimer:

^{1}H-NMR: 500 MHz, DMSO-d_6: δ = 1.03-1.13 (m, 3 H, $OCH_2C\underline{H}_3$), 3.48-3.61 (m, 2 H, $OC\underline{H}_2CH_3$), 3.82 (s, 3 H, CO_2CH_3), 4.40 (dd, 1 H, $^3J_{4\text{-H}/4\text{-OH}}$ = 6.1 Hz, $^3J_{4\text{-H}/3\text{-H}}$ = 7.3 Hz, 4-H), 4.45 (dd, 1 H, $^3J_{3\text{-H}/2\text{-H}}$ = 4.6 Hz, $^3J_{3\text{-H}/4\text{-H}}$ = 7.3 Hz, 3-H), 5.11-5.21 (m, 2 H, $CO_2C\underline{H}_2Ph$), 5.56 (d, 1 H, $^3J_{2\text{-H}/3\text{-H}}$ = 4.6 Hz, 2-H), 6.14 (s, 1 H, orthoester-CH), 6.40 (d, 1 H, $^3J_{4\text{-OH}/4\text{-H}}$ = 6.1 Hz, 4-OH), 8.57 (s, 1 H, Thz-H).

Minor epimer:

^{1}H-NMR: 500 MHz, DMSO-d_6: δ = 1.03-1.13 (m, 3 H, $OCH_2C\underline{H}_3$), 3.48-3.61 (m, 2 H, $OC\underline{H}_2CH_3$), 3.83 (s, 3 H, CO_2CH_3), 4.48 (dd, 1 H, $^3J_{3\text{-H}/2\text{-H}}$ = 4.5 Hz, $^3J_{3\text{-H}/4\text{-H}}$ = 7.7 Hz, 3-H), 4.51-4.55 (m, 1 H, 4-H), 5.11-5.21 (m, 2 H, $CO_2C\underline{H}_2Ph$), 5.57 (d, 1 H, $^3J_{2\text{-H}/3\text{-H}}$= 4.5 Hz, 2-H), 6.16 (s, 1 H, orthoester-CH), 6.26 (d, 1 H, $^3J_{4\text{-OH}/4\text{-H}}$ = 5.7 Hz, 4-OH), 8.59 (s, 1 H, Thz-H).

Compound **182***:*

TLC: R_f = 0.81 (EtOAc/Tol 3:1).

ESI-MS: m/z = 548 $[M+Na]^+$.

HRMS: $[M+Na]^+$: $C_{24}H_{31}NO_{10}SNa$, calculated: 548.1561, found: 548.1566.

Major epimer:

^{1}H-NMR: 500 MHz, DMSO-d_6: δ = 1.03-1.13 (m, 9 H, 3 x $OCH_2C\underline{H}_3$), 3.48-3.61 (m, 6 H, 3 x $OC\underline{H}_2CH_3$), 3.79 (s, 3 H, CO_2CH_3), 4.51-4.55 (m, 1 H, 4-H), 4.62 (dd, 1 H, $^3J_{3\text{-H}/4\text{-H}}$ = 4.0 Hz, $^3J_{3\text{-H}/2\text{-H}}$ = 5.8 Hz, 3-H), 5.11-5.21 (m, 2 H, $CO_2C\underline{H}_2Ph$), 5.39 (s, 1 H, $C\underline{H}(OEt)_2$), 5.41 (d, 1 H, $^3J_{2\text{-H}/3\text{-H}}$ = 5.8 Hz, 2-H), 6.09 (s, 1 H, orthoester-CH), 8.55 (s, 1 H, Thz-H).

Minor epimer:

^{1}H-NMR: 500 MHz, DMSO-d_6: δ = 1.03-1.13 (m, 9 H, 3 x $OCH_2C\underline{H}_3$), 3.48-3.61 (m, 6 H, 3 x $OC\underline{H}_2CH_3$), 3.80 (s, 3 H, CO_2CH_3), 4.62 (d, 1 H, $^3J_{4\text{-H}/3\text{-H}}$ = 4.5 Hz, 4-H), 4.66 (dd, 1 H, $^3J_{3\text{-H}/4\text{-H}}$ = 4.5 Hz, $^3J_{3\text{-H}/2\text{-H}}$ = 5.5 Hz, 3-H), 5.11-5.21 (m, 2 H, $CO_2C\underline{H}_2Ph$), 5.37 (s, 1 H, $C\underline{H}(OEt)_2$), 5.45 (d, 1 H, $^3J_{2\text{-H}/3\text{-H}}$ = 5.5 Hz, 2-H), 6.10 (s, 1 H, orthoester-CH), 8.57 (s, 1 H, Thz-H).

5.4.55 2-((1*S*,2*R*,3*S*)-3-(benzyloxycarbonyl)-1,2-dihydroxy-3-(methoxydimethylmethoxy)-propyl)-1,3-thiazole-4-carboxylic acid methyl ester (183)

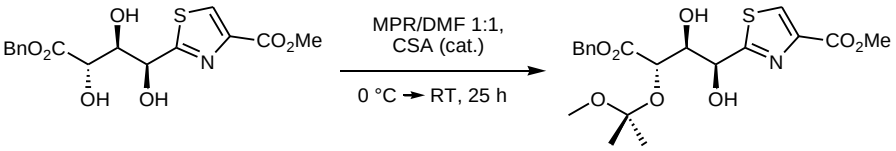

Preparation:

Compound **148**	M = 367.37 g mol^{-1}	1.0 eq	272 µmol	100 mg
MPR	M = 72.11 g mol^{-1}, ρ = 0.75			1.5 mL
CSA	M = 232.30 g mol^{-1}			cat.
DMF				1.5 mL

100 mg of the triol **148** (272 µmol, 1.0 eq) were dissolved in 1.5 mL of DMF and 1.5 mL of MPR and the solution was cooled to 0 °C. After the addition of a catalytic amount of CSA, the solution was stirred for 7 h at 0 °C and for further 18 h at RT. The reaction mixture was neutralized by addition of NEt_3, and concentrated *in vacuo*. Residual amounts of DMF were removed by coevaporation with Tol. The crude product was subjected to flash chromatography (EtOAc/Tol 1:1) to obtain 33% (40 mg, 91.0 µmol) of the MOP-protected compound **183** as yellow oil.

TLC: R_f = 0.31 (EtOAc/Tol 1:1).

ESI-MS: *The compound is not visible as it cyclizes to an acetonide* (m/z = 430 $[M+Na]^+$) *under the applied ESI conditions* .

^{1}H-NMR: 500 MHz, $CDCl_3$: δ = 1.26, 1.34 (each s, 3 H, Isopr-CH_3), 3.02 (s, 3 H, $C(CH_3)_2OC\underline{H}_3$), 3.82 (s, 3 H, CO_2CH_3), 3.97 (ddd, 1 H, $^3J_{3\text{-H}/2\text{-H}}$ = 1.6 Hz, $^3J_{3\text{-H}/3\text{-OH}}$ = 8.5 Hz, $^3J_{3\text{-H}/4\text{-H}}$ = 9.2 Hz, 3-H), 4.29 (d, 1 H, $^3J_{4\text{-H}/3\text{-H}}$ = 9.2 Hz, 4-H), 4.98 (dd, 1 H, $^3J_{2\text{-H}/3\text{-H}}$ = 1.6 Hz, $^3J_{2\text{-H}/2\text{-OH}}$ = 6.8 Hz, 2-H), 5.11 (s, 2 H, $CO_2C\underline{H}_2$Ph), 5.30 (d, 1 H, $^3J_{3\text{-OH}/3\text{-H}}$ = 8.5 Hz, 3-OH), 6.34 (d, 1 H, $^3J_{2\text{-OH}/2\text{-H}}$ = 6.8 Hz, 2-OH), 7.31-7.41 (m, 5 H, $CO_2CH_2\underline{Ph}$), 8.44 (s, 1 H, Thz-H).

^{13}C-NMR: 125 MHz, $CDCl_3$: δ = 24.1, 24.2 (each Isopr-CH_3), 48.6 ($C(CH_3)_2O\underline{C}H_3$), 51.5 ($CO_2\underline{C}H_3$), 65.4 ($CO_2\underline{C}H_2$Ph), 69.3 (C-2), 70.4 (C-4), 73.6 (C-3), 101.0 ($\underline{C}(CH_3)_2OCH_3$), 128.8 (Thz-H$\underline{C}$=C), 127.8, 127.9, 127.9 (each Bn-$CH_{arom.}$), 135.9 (Bn-$C_{arom.,\ quart.}$), 145.1 (Thz-HC=$\underline{C}$), 161.0 ($\underline{C}O_2CH_3$), 171.6 (C-5), 176.4 (C-1).

5.4.56 2-((3*aS*,6*S*,6*aR*)-tetrahydro-2,2-dimethyl-4-oxofuro[3,4-*d*][1,3]dioxol-6-yl)-1,3-thiazole-4-carboxylic acid methyl ester (184)

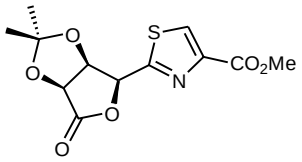

184
M = 299.30

The acetonide protected lactone **184** was obtained as byproduct in the synthesis of **183** (section 5.4.55) in 18% yield (15 mg, 50.1 µmol) as a pale yellow oil.

TLC: R_f = 0.36 (EtOAc/Tol 1:1).

ESI-MS: m/z = 322 $[M+Na]^+$.

HRMS: $[M+Na]^+$: $C_{12}H_{13}NO_6SNa$, calculated: 322.0356, found: 322.0354.

^{1}H-NMR: 500 MHz, DMSO-d_6: δ = 1.30, 1.33 (each s, 3 H, Isopr-CH_3), 3.85 (s, 3 H, CO_2CH_3), 5.17 (d, 1 H, $^3J_{4\text{-H}/3\text{-H}}$ = 5.2 Hz, 4-H), 5.21 (dd, 1 H, $^3J_{3\text{-H}/2\text{-H}}$ = 3.5 Hz, $^3J_{3\text{-H}/4\text{-H}}$ = 5.2 Hz, 2-H), 6.08 (d, 1 H, $^3J_{2\text{-H}/3\text{-H}}$ = 3.5 Hz, 2-H), 8.64 (s, 1 H, Thz-H).

5.4.57 2-((1*S*,2*R*,3*S*)-3-(benzyloxycarbonyl)-1,2-*O*-isopropylidene-3-hydroxy-propyl)-1,3-thiazole-4-carboxylic acid methyl ester (185)

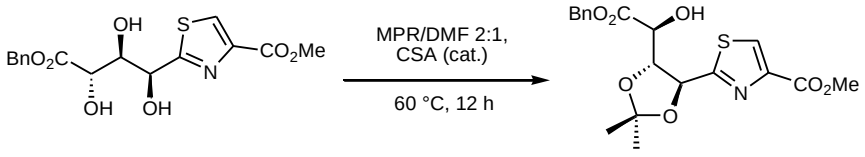

148 **185**
M = 407.44

Preparation:

Compound **148**	M = 367.37 g mol^{-1}	1.0 eq	544 µmol	200 mg
MPR	M = 72.11 g mol^{-1}, ρ = 0.75			4.0 mL
CSA	M = 232.30 g mol^{-1}			cat.
DMF				2.0 mL

200 mg of the triol **148** (544 µmol, 1.0 eq) were dissolved in 2.0 mL of DMF and 4.0 mL of MPR. After the addition of a catalytic amount of CSA, the solution was stirred for 12 h at 60 °C. The reaction mixture was neutralized by addition of NEt_3, and concentrated *in vacuo*. Residual amounts of DMF were removed by coevaporation with Tol. The crude product was subjected to flash chromatography (Tol/EtOAc 3:1→1:1) to obtain 81% (179 mg, 439 µmol) of the acetonide **185** as pale red oil. The lactone **184** (section 5.4.56) was obtained as byproduct in 14% yield (22 mg, 73.5 µmol).

TLC: R_f = 0.64 (EtOAc/Tol 1:1).

ESI-MS: m/z = 430 $[M+Na]^+$.

HRMS: $[M+Na]^+$: $C_{19}H_{21}NO_7SNa$, calculated: 430.0931, found: 430.0933.

^{1}H-NMR: 500 MHz, DMSO-d_6: δ = 1.40, 1.41 (each s, 3 H, Isopr-CH_3), 3.79 (s, 3 H, CO_2CH_3), 4.45-4.50 (m, 2 H, 3-H, 4-H), 5.10 (d, 1 H, ^2J = 12.5 Hz, $CO_2C\underline{H}_2Ph^u$), 5.16 (d, 1 H, ^2J = 12.5 Hz, $CO_2C\underline{H}_2Ph^d$), 5.37 (d, 1 H, $^3J_{2\text{-H}/3\text{-H}}$ = 6.5 Hz, 2-H), 6.12 (d, 1 H, $^3J_{4\text{-OH}/4\text{-H}}$ = 5.8 Hz, 4-OH), 7.30-7.36 (m, 5 H, $CO_2CH_2\underline{Ph}$), 8.54 (s, 1 H, Thz-H).

^{13}C-NMR: 125 MHz, DMSO-d_6: δ = 26.8 (2 x Isopr-CH_3), 52.0 ($CO_2\underline{C}H_3$), 66.1 ($CO_2\underline{C}H_2Ph$), 69.8 (C-4), 75.3 (C-2), 82.6 (C-3), 110.9 (Isopr-$C_{quart.}$), 127.9, 128.0, 128.3 (each Bn-$CH_{arom.}$), 129.9 (Thz-H$\underline{C}$=C), 135.7 (Bn-$C_{arom.,\ quart.}$), 145.8 (Thz-HC=$\underline{C}$), 161.0 ($\underline{C}O_2CH_3$), 170.6 (C-5), 170.7 (C-1).

Opt. rotation: $[\alpha]_{589}^{24}$ = –0.6, $[\alpha]_{578}^{24}$ = –0.7, $[\alpha]_{546}^{24}$ = –0.2
(c = 1.77 g/100 mL $CHCl_3$).

5.4.58 2-((4*S*,5*R*)-5-((*S*)-((benzyloxy)carbonyl)(hydroxy)methyl)-2,2-dimethyl-1,3-dioxolan-4-yl)-1,3-thiazole-4-carboxylic acid methyl ester (186)

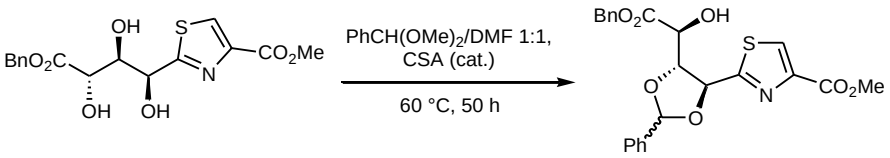

148 **186**
M = 455.48

Preparation:

Compound **148**	M = 367.37 g mol^{-1}	1.0 eq	408 µmol	150 mg
$PhCH(OMe)_2$	M = 152.19 g mol^{-1}, ρ = 1.02			2.0 mL (2.04 g)
CSA	M = 232.30 g mol^{-1}			cat.
DMF				2.0 mL

150 mg of **148** (408 µmol, 1.0 eq) were suspended in 2.0 mL of DMF and 2.0 mL of $PhHC(OMe)_2$ (2.04 g). A catalytic amount of CSA was added and the solution was stirred at 60 °C for 50 h. The mixture was neutralized with NEt_3 and concentrated *in vacuo*. Residual amounts of DMF were removed by coevaporation with Tol. Flash chromatography (Tol/EtOAc 3:1) yielded 68% of the benzylidene acetal **186** (127 mg, 279 µmol) as a colorless oil (70:30 mixture of epimers).

ESI-MS: *m/z* = 478 $[M+Na]^+$.

HRMS: $[M+Na]^+$: $C_{23}H_{21}NO_7SNa$, calculated: 478.0931, found: 478.0932.

IR: film; $\tilde{\nu}$ = 3467, 3115, 3034, 2954, 1725, 1496, 1456, 1434, 1404, 1322, 1272, 1213, 1114, 1091, 1069, 1026, 977, 914, 863, 751, 696 cm^{-1}.

Major epimer:

TLC: R_f = 0.71 (EtOAc/Tol 1:1).

^{1}H-NMR: 400 MHz, $CDCl_3$: δ = 3.84 (s, 3 H, CO_2CH_3), 4.69 (d, 1 H, $^3J_{4\text{-H}/3\text{-H}}$ = 3.5 Hz, 4-H), 4.76 (dd, 1 H, $^3J_{3\text{-H}/4\text{-H}}$ = 3.5 Hz, $^3J_{3\text{-H}/2\text{-H}}$ = 5.8 Hz, 3-H), 5.21 (d, 1 H, ^2J = 12.3 Hz, $CO_2C\underline{H}_2Ph^u$), 5.28 (d, 1 H, ^2J = 12.3 Hz, $CO_2C\underline{H}_2Ph^d$), 5.57 (d, 1 H, $^3J_{2\text{-H}/3\text{-H}}$ = 5.8 Hz, 2-H), 6.04 (s, 1 H, C<u>H</u>Ph), 7.30-7.50 (m, 10 H, $CH_{arom.}$), 8.12 (s, 1 H, Thz-H). 4-OH signal invisible.

^{13}C-NMR: 100 MHz, $CDCl_3$: δ = 52.5 ($CO_2\underline{C}H_3$), 68.2 ($CO_2\underline{C}H_2Ph$), 70.5 (C-4), 75.8 (C-2), 84.0 (C-3), 105.6 (<u>C</u>HPh), 127.0 ($CH_{arom.}$), 128.1 (Thz-H<u>C</u>=C), 128.6, 128.6, 128.7, 129.1, 129.9 (each $CH_{arom.}$), 135.0 (Bn-$C_{arom.,\ quart.}$), 135.8 (Ph-$C_{arom.,\ quart.}$), 147.7 (Thz-HC=<u>C</u>), 161.2 (Thz-<u>C</u>O_2CH_3), 171.3 (C-5), 171.4 (C-1).

Minor epimer:

TLC: R_f = 0.68 (EtOAc/Tol 1:1).

^{1}H-NMR: 400 MHz, $CDCl_3$: δ = 3.80 (s, 3 H, CO_2CH_3), 4.60 (d, 1 H, $^3J_{3\text{-H}/4\text{-H}}$ = 3.4 Hz, $^3J_{3\text{-H}/2\text{-H}}$ = 5.7 Hz, 3-H), 4.73 (d, 1 H, $^3J_{4\text{-H}/3\text{-H}}$ = 3.4 Hz, 4-H), 5.29 (d, 1 H, ^2J = 12.2 Hz, $CO_2C\underline{H}_2Ph^u$), 5.34 (d, 1 H, ^2J = 12.2 Hz, $CO_2C\underline{H}_2Ph^d$), 5.60 (d, 1 H, $^3J_{2\text{-H}/3\text{-H}}$ = 5.7 Hz, 2-H), 6.15 (s, 1 H, C<u>H</u>Ph), 7.30-7.50 (m, 10 H, $CH_{arom.}$), 8.08 (s, 1 H, Thz-H). 4-OH signal invisible.

^{13}C-NMR: 100 MHz, $CDCl_3$: δ = 52.4 ($CO_2\underline{C}H_3$), 68.4 ($CO_2\underline{C}H_2Ph$), 71.6 (C-4), 76.3 (C-2), 83.6 (C-3), 106.2 ($\underline{C}HPh$), 127.0 ($CH_{arom.}$), 128.1 (Thz-H$\underline{C}$=C), 128.6, 128.7, 129.1, 130.1 (each $CH_{arom.}$), 135.0 (Bn-$C_{arom., quart.}$), 135.8 (Ph-$C_{arom., quart.}$), 147.2 (Thz-HC=$\underline{C}$), 161.2 (Thz-$\underline{C}O_2CH_3$), 171.0 (C-5), 171.5 (C-1).

5.4.59 2-((4*S*,5*R*)-5-((*S*)-((benzyloxy)carbonyl)(methoxy(phenyl)methoxy)methyl)-2,2-dimethyl-1,3-dioxolan-4-yl)-1,3-thiazole-4-carboxylic acid methyl ester (187)

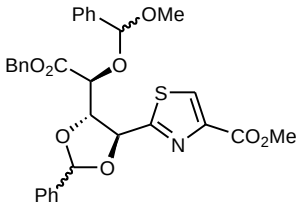

187
M = 575.63

The benzylidene acetal **187** was obtained as byproduct in the preparation of **186** (section 5.4.58) as a colorless oil in 25% yield (59 mg, 102 µmol, mixture of four diastereomers).

ESI-MS: *m*/*z* = 598 $[M+Na]^+$.

HRMS: $[M+Na]^+$: $C_{31}H_{29}NO_8SNa$, calculated: 598.1506, found: 598.1507.

IR: film; $\tilde{\nu}$ = 3033, 2951, 2830, 1739, 1723, 1495, 1454, 1434, 1351, 1312, 1243, 1207, 1100, 1070, 1051, 1027, 978, 911, 862, 745, 697 cm^{-1}.

5.4.60 2-((4*S*,5*R*)-5-((*S*)-((benzyloxy)carbonyl)(t*ert*-butyl-dimethylsilyloxy)methyl)-2,2-dimethyl-1,3-dioxolan-4-yl)-1,3-thiazole-4-carboxylic acid methyl ester (188)

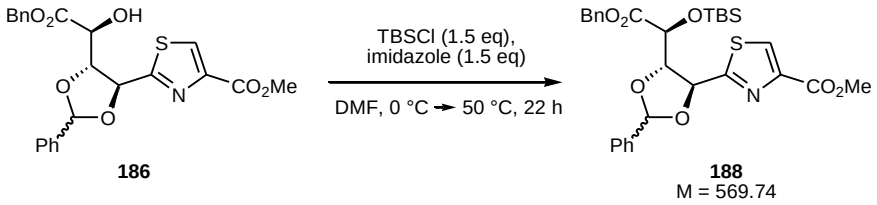

Preparation:

Compound **186**	M = 455.48 g mol^{-1}	1.0 eq	274 µmol	125 mg
TBSCl	M = 150.72 g mol^{-1}	1.5 eq	411 µmol	62 mg
Imidazole	M = 68.08 g mol^{-1}	1.5 eq	411 µmol	28 mg
DMF_{abs}				1.0 mL

125 mg of the benzylidene acetal **186** (274 µmol, 1.0 eq) were dissolved in 1.0 mL of DMF_{abs} in a nitrogen atmosphere, cooled to 0 °C, and 62 mg of TBSCl (411 µmmol, 1.5 eq) as well as 28 mg of imidazole (411 µmmol, 1.5 eq) were added. The solution was allowed to warm to RT, stirred for 8 h, and subsequently stirred at 50 °C for another 14 h. After cooling to RT and dilution with CH_2Cl_2 the reaction was quenched with 5% aq. $NaHCO_3$, the phases were separated and the aqueous phase was extracted two times with CH_2Cl_2. The combined organic phases were dried with brine and over $MgSO_4$, filtered, and concentrated *in vacuo*. Residual amounts of DMF were removed by coevaporation with Tol. Flash chromatographic purification (Tol/EtOAc 5:1) yielded 72% of the silyl ether **188** (113 mg, 198 µmol) as a colorless oil (70:30 mixture of epimers). In addition, 17% of the starting material **186** (21 mg, 46.0 µmol) were reisolated.

TLC: R_f = 0.76 (Tol/EtOAc 3:1).

ESI-MS: m/z = 592 $[M+Na]^+$.

HRMS: $[M+Na]^+$: $C_{22}H_{35}NO_7SSiNa$, calculated: 592.1796, found: 592.1798.

IR: film; $\tilde{\nu}$ = 2955, 2930, 2886, 2857, 1722, 1499, 1459, 1435, 1323, 1251, 1213, 1156, 1091, 1068, 1026, 985, 916, 838, 804, 781, 754, 697 cm^{-1}.

Major epimer:

^{1}H-NMR: 400 MHz, $CDCl_3$: δ = 0.03, 0.05 (each s, 3 H, $SiCH_3$), 0.88 (s, 9 H, $SiC(CH_3)_3$), 3.86 (s, 3 H, CO_2CH_3), 4.77 (d, 1 H, $^{3}J_{4\text{-H}/3\text{-H}}$ = 2.7 Hz, 4-H), 4.83 (dd, 1 H, $^{3}J_{3\text{-H}/4\text{-H}}$ = 2.7 Hz, $^{3}J_{3\text{-H}/2\text{-H}}$ = 5.9 Hz, 3-H), 5.25 (d, 1 H, ^{2}J = 12.1 Hz, $CO_2C\underline{H}_2Ph^{u}$), 5.28 (d, 1 H, ^{2}J = 12.1 Hz, $CO_2C\underline{H}_2Ph^{d}$), 5.67 (d, 1 H, $^{3}J_{2\text{-H}/3\text{-H}}$ = 5.9 Hz, 2-H), 6.06 (s, 1 H, C<u>H</u>Ph), 7.18-7.56 (m, 10 H, $CH_{arom.}$), 8.15 (s, 1 H, Thz-H).

^{13}C-NMR: 100 MHz, $CDCl_3$: δ = −5.0, −4.9 (each $SiCH_3$), 18.4 ($Si\underline{C}(CH_3)_3$), 25.7 ($SiC(\underline{C}H_3)_3$), 52.3 ($CO_2\underline{C}H_3$), 67.6 ($CO_2\underline{C}H_2Ph$), 71.6 (C-4), 74.9 (C-2), 84.3 (C-3), 104.6 (<u>C</u>HPh), 127.2 ($CH_{arom.}$), 128.1 (Thz-H<u>C</u>=C), 128.4, 128.6, 128.7, 129.9 (each $CH_{arom.}$), 135.6 (Bn-$C_{arom.,\ quart.}$), 135.9 (Ph-$C_{arom.,\ quart.}$), 147.8 (Thz-HC=<u>C</u>), 161.8 (<u>C</u>O_2CH_3), 170.4 (C-5), 171.5 (C-1).

Minor epimer:

^{1}H-NMR: 400 MHz, $CDCl_3$: δ = 0.12, 0.13 (each s, 3 H, $SiCH_3$), 0.96 (s, 9 H, $SiC(CH_3)_3$), 3.83 (s, 3 H, CO_2CH_3), 4.67 (dd, 1 H, $^{3}J_{3\text{-H}/4\text{-H}}$ = 2.7 Hz, $^{3}J_{3\text{-H}/2\text{-H}}$ = 5.8 Hz, 3-H), 4.82 (d, 1 H, $^{3}J_{4\text{-H}/3\text{-H}}$ = 2.7 Hz, 4-H), 5.30 (d, 1 H, ^{2}J = 12.1 Hz, $CO_2C\underline{H}_2Ph^{u}$), 5.34 (d, 1 H, ^{2}J = 12.1 Hz, $CO_2C\underline{H}_2Ph^{d}$), 5.80 (d, 1 H, $^{3}J_{2\text{-H}/3\text{-H}}$ = 5.8 Hz, 2-H), 6.21 (s, 1 H, C<u>H</u>Ph), 7.18-7.56 (m, 10 H, $CH_{arom.}$), 8.13 (s, 1 H, Thz-H).

^{13}C-NMR: 100 MHz, $CDCl_3$: δ = −5.0, −4.8 (each $SiCH_3$), 18.4 ($Si\underline{C}(CH_3)_3$), 25.9 ($SiC(\underline{C}H_3)_3$), 52.3 ($CO_2\underline{C}H_3$), 67.7 ($CO_2\underline{C}H_2Ph$), 73.4 (C-4), 75.9 (C-2), 83.8 (C-3), 106.3 (<u>C</u>HPh), 127.0 ($CH_{arom.}$), 128.1 (Thz-H<u>C</u>=C), 128.4, 128.6, 128.7, 128.7, 130.0 (each $CH_{arom.}$), 135.7 (Bn-$C_{arom.,\ quart.}$), 136.4 (Ph-$C_{arom.,\ quart.}$), 147.8 (Thz-HC=<u>C</u>), 161.8 (<u>C</u>O_2CH_3), 170.1 (C-5), 170.8 (C-1).

5.4.61 2-((1*S*,2*R*,3*S*)-3-(benzyloxycarbonyl)-1-hydroxy-2-benzyloxy-3-(*tert*-butyl-dimethylsilyloxy)-propyl)-1,3-thiazole-4-carboxylic acid methyl ester (189)

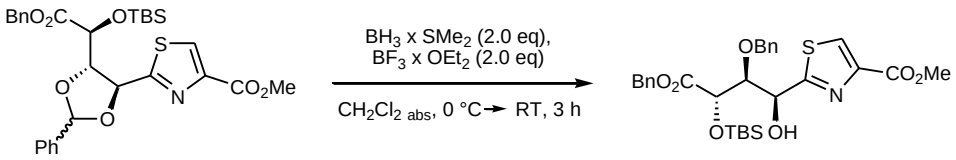

188 **189**
M = 571.76

Preparation:

Compound **188**	M = 569.74 g mol^{-1}	1.0 eq	149 µmol	85 mg
BF_3 x OEt_2	M = 141.93 g mol^{-1}, ρ = 1.15	2.0 eq	298 µmol	36.8 µL (42.3 mg)
BH_3 x SMe_2	M = 75.97 g mol^{-1}, ρ = 0.80	2.0 eq	298 µmol	28.3 µL (22.6 mg)
$CH_2Cl_{2\ abs}$				4.0 mL

85 mg of the benzylidene acetal **188** (149 µmol, 1.0 eq) were dissolved in 4.0 mL of $CH_2Cl_{2\ abs}$ in a nitrogen atmosphere and cooled to 0 °C. 18.4 µL of BF_3 x OEt_2 (21.2 mg, 1.0 eq) and, after 5 min, 14.2 µL of BH_3 x SMe_2 (11.3 mg, 1.0 eq) were added, the solution was allowed to warm to RT, and stirred for 1.5 h. Another 18.4 µL of BF_3 x OEt_2 (21.2 mg, 1.0 eq) and, after 5 min, 14.2 µL of BH_3 x SMe_2 (11.3 mg, 1.0 eq) were added and the solution was stirred for further 1.5 h at RT. The reaction was carefully quenched with 1.0 mL of MeOH (vigorous gas evolution), and concentrated *in vacuo*. By flash chromatographic purification (Tol/EtOAc 5:1) 27% of the product **189** (23.1 mg, 40.2 µmol) were obtained as a colorless oil. In addition, 10% of the starting material **188** (8.7 mg, 15.3 µmol) were reisolated.

TLC: R_f = 0.59 (Tol/EtOAc 3:1).

ESI-MS: m/z = 594 $[M+Na]^+$.

HRMS: $[M+Na]^+$: $C_{22}H_{37}NO_7SSiNa$, calculated: 594.1952, found: 594.1955.

IR: film; $\tilde{\nu}$ = 3469, 1952, 2929, 2886, 2857, 1736, 1497, 1455, 1326, 1242, 1212, 1170, 1095, 989, 913, 837, 779, 734, 696 cm^{-1}.

^{1}H-NMR: 500 MHz, DMSO-d_6: δ = –0.01, 0.06 (each s, 3 H, $SiCH_3$), 0.84 (s, 9 H, $SiC(CH_3)_3$), 3.80 (d, 1 H, ^2J = 10.9 Hz, 3-$OC\underline{H}_2Ph^u$), 3.83 (s, 3 H, CO_2CH_3), 4.01 (dd, 1 H, $^3J_{3\text{-}H/2\text{-}H}$ = 2.7 Hz, $^3J_{3\text{-}H/4\text{-}H}$ = 8.0 Hz, 3-H), 4.17 (d, 1 H, ^2J = 10.9 Hz, 3-$OC\underline{H}_2Ph^d$), 4.51 (d, 1 H, $^3J_{4\text{-}H/3\text{-}H}$ = 8.0 Hz, 4-H), 5.07 (dd, 1 H, $^3J_{2\text{-}H/3\text{-}H}$ = 2.7 Hz, $^3J_{2\text{-}H/2\text{-}OH}$ = 6.1 Hz, 2-H), 5.10 (d, 1 H, ^2J = 12.2 Hz, $CO_2C\underline{H}_2Ph^u$), 5.14 (d, 1 H, ^2J = 12.2 Hz, $CO_2C\underline{H}_2Ph^d$), 6.56 (d, 1 H, $^3J_{2\text{-}OH/2\text{-}H}$ = 6.1 Hz, 2-OH), 6.93-6.95 (m, 2 H, $CH_{arom.}$), 7.20-7.22 (m, 3 H, $CH_{arom.}$), 7.31-7.36 (m, 5 H, $CH_{arom.}$), 8.49 (s, 1 H, Thz-H).

^{13}C-NMR: 125 MHz, DMSO-d_6: δ = –5.5, –5.4 (each $SiCH_3$), 17.7 ($Si\underline{C}(CH_3)_3$), 25.4 ($SiC(\underline{C}H_3)_3$), 51.9 ($CO_2\underline{C}H_3$), 66.3 ($CO_2\underline{C}H_2Ph$), 69.2 (C-2), 71.4 (C-4), 73.9 (3-$O\underline{C}H_2Ph$), 83.5 (C-3), 127.5, 127.6, 127.9, 128.2, 128.4, 128.5 (each $CH_{arom.}$), 129.3 (Thz-$H\underline{C}$=C), 135.3 (Bn-$C_{arom.,\ quart.}$), 137.3 (3-OBn-$C_{arom.,\ quart.}$), 145.6 (Thz-HC=$\underline{C}$), 161.2 ($\underline{C}O_2CH_3$), 171.2 (C-5), 176.4 (C-1).

Opt. rotation: $[\alpha]_{589}^{21}$ = –5.2, $[\alpha]_{578}^{21}$ = –5.5, $[\alpha]_{546}^{21}$ = –6.2, $[\alpha]_{436}^{21}$ = –10.8, $[\alpha]_{365}^{21}$ = –17.1 (c = 1.15 g/100 mL $CHCl_3$).

5.4.62 2-((3*aS*,6*S*,6*aR*)-2-ethoxy-tetrahydro-4-oxofuro[3,4-*d*][1,3]dioxol-6-yl)-1,3-thiazole-4-carboxylic acid methyl ester (190)

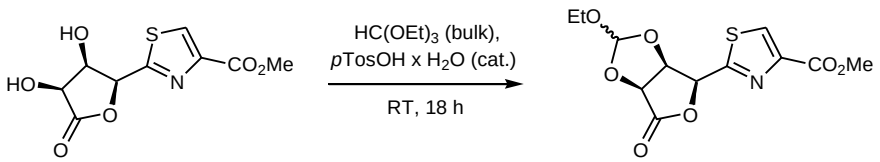

141 **190**
M = 315.30

Preparation:

Compound **141**	M = 259.24 g mol^{-1}	1.0 eq	154 µmol	40 mg
$HC(OEt)_3$	M = 148.20 g mol^{-1}, ρ = 0.90			1.5 mL (1.35 mg)
*p*TosOH x H_2O	M = 190.22 g mol^{-1}			cat.

40 mg of the diol **141** (154 µmol, 1.0 eq) were suspended in 1.5 mL of $HC(OEt)_3$ (1.35 mg) and a catalytic amount of *p*TosOH x H_2O was added. The suspension was stirred at RT until complete solution (approx. 15 min), and the solution was stirred at RT for further 18 h. The mixture was subsequently transferred onto a silica gel filter column and eluted with pure EtOAc. After removal of the solvents and drying *in vacuo*, the orthoester **190** was obtained as a colorless oil in quantitative yield (49 mg, 154 µmol, 12:1 epimeric mixture).

ESI-MS: m/z = 338 $[M+Na]^+$.

HRMS: $[M+Na]^+$: $C_{12}H_{13}NO_7SNa$, calculated: 338.0305, found: 338.0306.

Major epimer:

TLC: R_f = 0.53 (EtOAc/Tol 3:2).

^{1}H-NMR: 300 MHz, DMSO-d_6: δ = 1.21 (t, 3 H, $^3J_{OCH2CH3/OCH2CH3}$ = 7.1 Hz, OCH_2CH_3), 3.49-3.65 (m, 2H, OCH_2CH_3), 3.97 (s, 3 H, CO_2CH_3), 5.05 (d, 1 H, $^3J_{4\text{-}H/3\text{-}H}$ = 6.0 Hz, 4-H), 5.19 (dd, 1 H, $^3J_{3\text{-}H/2\text{-}H}$ = 4.6 Hz, $^3J_{3\text{-}H/4\text{-}H}$ = 6.0 Hz, 3-H), 5.91 (s, 1 H, orthoester-CH), 6.04 (d, 1 H, $^3J_{2\text{-}H/3\text{-}H}$ = 4.6 Hz, 2-H), 8.28 (s, 1 H, Thz-H).

^{13}C-NMR: 150 MHz, DMSO: δ = 14.5 (OCH_2CH_3), 52.7 (CO_2CH_3), 61.8 (OCH_2CH_3), 73.8 (C-4), 77.4 (C-3), 79.6 (C-2), 116.4 (orthoester-CH), 129.4 (Thz-HC=C), 146.7 (Thz-HC=C), 161.7 (CO_2CH_3), 164.6 (C-1), 171.9 (C-5).

Minor epimer:

TLC: R_f = 0.73 (EtOAc/Tol 3:2).

^{1}H-NMR: 300 MHz, DMSO-d_6: δ = 1.21 (t, 3 H, $^3J_{OCH2CH3/OCH2CH3}$ = 7.1 Hz, OCH_2CH_3), 3.46-3.65 (m, 2H, OCH_2CH_3), 3.97 (s, 3 H, CO_2CH_3), 5.15 (d, 1 H, $^3J_{4\text{-}H/3\text{-}H}$ = 5.3 Hz, 4-H), 5.29 (dd, 1 H, $^3J_{3\text{-}H/2\text{-}H}$ = 3.8 Hz, $^3J_{3\text{-}H/4\text{-}H}$ = 5.3 Hz, 3-H), 5.96 (s, 1 H, orthoester-CH), 6.03-6.05 (m, 1 H, 2-H), 8.28 (s, 1 H, Thz-H).

^{13}C-NMR: 150 MHz, DMSO: δ = 61.5 (O<u>C</u>H$_2$CH$_3$), 75.4 (C-4), 76.1 (C-3), 77.8 (C-2), 117.3 (orthoester-CH). Due to weak signal intensities and signal overlap, the other ^{13}C signals cannot be unambiguously assigned.

5.4.63 (4*S*,5*S*)-5-((1*S*,2*R*)-2-(4-(methoxycarbonyl)thiazol-2-yl)-2-(*tert*-butyl-dimethylsilyloxy)-1-hydroxyethyl)-2-ethoxy-1,3-dioxolane-4-carboxylic acid (191)

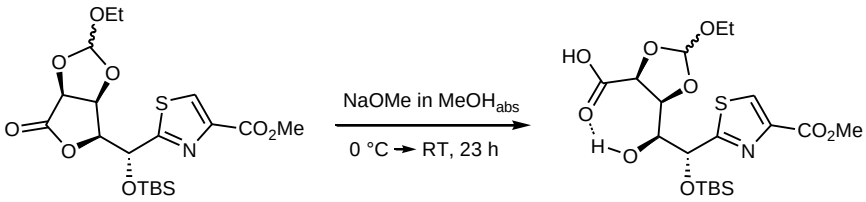

164 **191**
M = 477.15

Preparation:

Compound **164**	M = 459.59 g mol^{-1}	1.0 eq	152 µmol	70 mg
NaOMe (30% in MeOH)	M = 54.02 g mol^{-1}, ρ = 0.95			9.3 µL (8.8 mg)
MeOH$_{abs}$				3.0 mL

70 mg of the lactone **164** (152 µmol, 1.0 eq) were dissolved in 3.0 mL of MeOH$_{abs}$ in a nitrogen atmosphere and the solution was cooled to 0 °C. 9.3 µL of NaOMe (30% in MeOH, 8.8 mg) were added and the solution was stirred at RT for 5 h. The mixture was subsequently neutralized with acidic ion exchange resin, filtered, and concentrated *in vacuo* to yield a 53:47 mixture of the carboxylic acid **191** and the starting material **164** (69 mg) as colorless powder. No isolated yield was determined as the highly polar product proved difficult to purify.

TLC: R_f = 0.00 (EtOAc/MeOH 5:1).

ESI-MS: m/z = 500 [M+Na]$^+$.

HRMS: [M+Na]$^+$: $C_{19}H_{31}NO_9SSiNa$, calculated: 500.1381, found: 500.1385.

The product could not be identified in the ESI(–).

^{1}H-NMR: 600 MHz, DMSO-d_6: δ = 0.09, 0.10 (each s, 3 H, $SiCH_3$), 0.84 (s, 9 H, $SiC(CH_3)_3$), 1.08-1.11 (m, 3 H, $OCH_2C\underline{H}_3$), 3.57-3.59 (m, 1 H, 3-H), 3.81-3.84 (m, 5 H, $OC\underline{H}_2CH_3$, CO_2CH_3), 3.93 (dd, 1 H, $^3J_{4\text{-H}/3\text{-H}}$ = 1.7 Hz, $^3J_{4\text{-H}/5\text{-H}}$ = 7.7 Hz, 4-H), 4.13 (d, 1 H, $^3J_{5\text{-H}/4\text{-H}}$ = 7.7 Hz, 4-H), 5.03 (d, 1 H, $^3J_{2\text{-H}/3\text{-H}}$ = 7.4 Hz, 2-H), 5.66 (s, 1 H, orthoester-CH), 6.41 (br s, 1 H, 3-OH), 8.50 (s, 1 H, Thz-H). CO_2H signal invisible.

^{13}C-NMR: 150 MHz, DMSO: δ = −4.6, −4.5 (each $SiCH_3$), 15.4 ($OCH_2\underline{C}H_3$), 18.0 ($Si\underline{C}(CH_3)_3$), 25.5 ($SiC(\underline{C}H_3)_3$), 51.9 ($CO_2\underline{C}H_3$), 57.2 ($O\underline{C}H_2CH_3$), 73.7 (C-2), 74.3 (C-4), 74.8 (C-3), 78.6 (C-5), 113.6 (orthoester-CH), 129.5 (Thz-H$\underline{C}$=C), 145.1 (Thz-HC=$\underline{C}$), 161.3 ($\underline{C}O_2CH_3$), 170.2 (C-5), 174.2 (C-1).

The NMR signals of the minor epimer could not be assigned unambiguously due to low intensity and signal overlap.

5.4.64 (4*S*,5*R*)-5-((*S*)-(4-(methoxycarbonyl)thiazol-2-yl)(methoxy)methyl)-2-ethoxy-1,3-dioxolane-4-carboxylic acid (192)

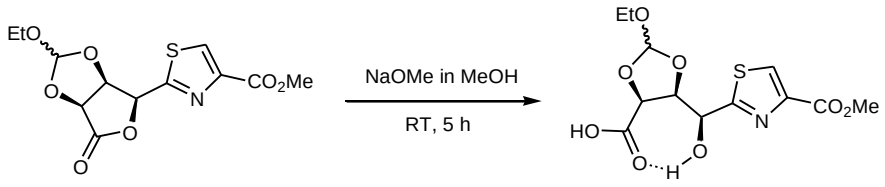

190 **192**
M = 355.30

Preparation:

Compound **190**	M = 315.30 g mol^{-1}	1.0 eq	159 µmol	50 mg
NaOMe (30% in MeOH)	M = 54.02 g mol^{-1}, ρ = 0.95			9.3 µL (8.8 mg)
$MeOH_{abs}$				3 mL

50 mg of the lactone **190** (159 µmol, 1.0 eq) were dissolved in 3 mL of $MeOH_{abs}$ in a nitrogen atmosphere and the solution was cooled to 0 °C. 9.3 µL of NaOMe (30% in MeOH, 8.8 mg) were added and the mixture was stirred at RT for 5 h. The mixture was subsequently neutralized with acidic ion exchange resin, filtered, and concentrated *in vacuo* to yield 49 mg of the carboxylic acid **192** as pale yellow powder. No isolated yield was determined as the highly polar product proved difficult to purify.

TLC: R_f = 0.00 (EtOAc/MeOH 5:1).

ESI-MS: m/z = 332 $[M-H]^-$.

HRMS: $[M-H]^-$: $C_{12}H_{14}NO_8S$, calculated: 332.0446, found: 332.0447.

^{1}H-NMR: 600 MHz, DMSO-d_6: δ = 1.11 (t, 3 H, $^3J_{OCH2CH3/OCH2CH3}$ = 7.1 Hz, OCH_2CH_3), 3.75-3.90 (m, 5 H, OCH_2CH_3, CO_2CH_3), 4.42 (d, 1 H, $^3J_{4\text{-}H/3\text{-}H}$ = 7.7 Hz, 4-H), 4.52 (dd, 1 H, $^3J_{3\text{-}H/2\text{-}H}$ = 1.5 Hz, $^3J_{3\text{-}H/4\text{-}H}$ = 7.7 Hz, 3-H), 5.06 (d, 1 H, $^3J_{2\text{-}H/3\text{-}H}$ = 1.5 Hz, 2-H), 5.70 (s, 1 H, orthoester-CH), 8.60 (br s, 1 H, 2-OH), 8.43 (s, 1 H, Thz-H). CO_2H signal invisible.

^{13}C-NMR: 150 MHz, DMSO: δ = 15.3 (OCH_2CH_3), 51.9 (CO_2CH_3), 58.3 (OCH_2CH_3), 70.8 (C-2), 77.8 (C-4), 78.3 (C-3), 114.0 (orthoester-CH), 128.8 (Thz-HC=C), 145.4 (Thz-HC=C), 161.4 (CO_2CH_3), 171.4 (C-5), 175.8 (C-1).

The NMR signals of the minor epimer could not be unambiguously assigned due to signal overlap.

5.4.65 *(R)*-(4-(methoxycarbonyl)thiazol-2-yl)((3*aS*,6*S*,6*aS*)-tetrahydro-2,2-dimethyl-4-oxofuro[3,4-*d*][1,3]dioxol-6-yl)methyl 4-methylbenzenesulfonate (215)

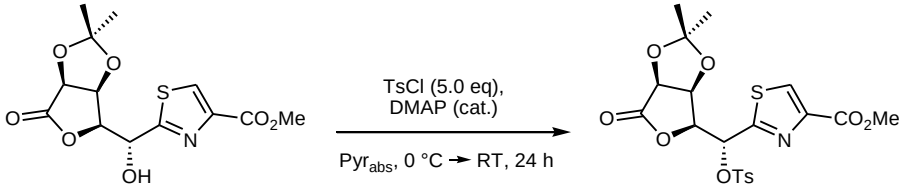

157 **215**
M = 483.51

Preparation:

Compound **157**	M = 329.33 g mol^{-1}	1.0 eq	60.7 µmol	20 mg
TsCl	M = 190.65 g mol^{-1}	5.0 eq	304 µmol	58 mg
DMAP	M = 122.17 g mol^{-1}			cat.
Pyr$_{abs}$				1.0 mL

20 mg of the acetonide **157** (60.7 µmol, 1.0 eq) were dissolved in 1.0 mL of Pyr_{abs} in a nitrogen atmosphere and cooled to 0 °C. A catalytical amount of DMAP and 58 mg of TsCl (304 µmol, 5.0 eq) were added, the solution was allowed to warm to RT and stirred for 24 h. The reaction was diluted with CH_2Cl_2, quenched with ice, and the phases were separated. The aqueous phase was extracted two times with CH_2Cl_2. The combined organic phases were dried with brine and over $MgSO_4$, filtered, and concentrated *in vacuo* to obtain the tosylate **215** in quantitative yield (29 mg) as a pale yellow oil.

TLC: R_f = 0.65 (EtOAc/Tol 3:2).

ESI-MS: *m/z* = 506 $[M+Na]^+$.

HRMS: $[M+Na]^+$: $C_{20}H_{21}NO_9S_2Na$, calculated: 506.0561, found: 506.0555.

^{1}H-NMR: 300 MHz, DMSO-d_6: δ = 1.18, 1.27 (each s, 3 H, Isopr-CH_3), 3.18 (s, 3 H, Ts-CH_3), 3.84 (s, 3 H, CO_2CH_3), 4.61 (dd, 1 H, $^3J_{4\text{-H}/3\text{-H}}$ = 3.7 Hz, $^3J_{4\text{-H}/5\text{-H}}$ = 5.5 Hz, 4-H), 4.97 (d, 1 H, $^3J_{5\text{-H}/4\text{-H}}$ = 5.5 Hz, 5-H), 5.21 (dd, 1 H, $^3J_{3\text{-H}/4\text{-H}}$ = 3.7 Hz, $^3J_{3\text{-H}/2\text{-H}}$ = 9.2 Hz, 3-H), 5.80 (d, 1 H, $^3J_{2\text{-H}/3\text{-H}}$ = 9.2 Hz, 2-H), 7.39 (d, 2 H, $^3J_{\text{Ts-CH/CH'}}$ = 8.4 Hz, Ts-$CH_{arom.}$), 7.72 (d, 2 H, $^3J_{\text{Ts-CH'/CH}}$ = 8.4 Hz, Ts-$CH'_{arom.}$), 8.65 (s, 1 H, Thz-H).

5.4.66 *(R)*-(4-(methoxycarbonyl)thiazol-2-yl)((3*aS*,6*S*,6*aS*)-tetrahydro-2,2-dimethyl-4-oxofuro[3,4-*d*][1,3]dioxol-6-yl)methyl methylsulfonate (216)

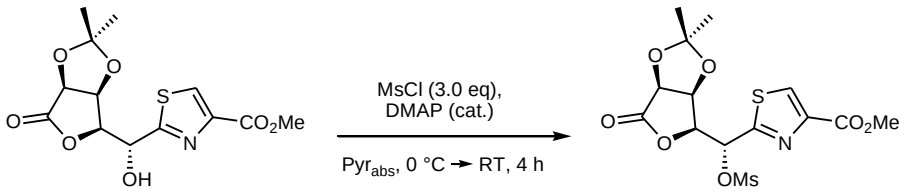

157 **216**
M = 407.42

Preparation:

Compound **216**	M = 329.33 g mol^{-1}	1.0 eq	0.73 mmol	240 mg
MsCl	M = 114.55 g mol^{-1}, ρ = 1.48	3.0 eq	2.19 mmol	170 µL (250 mg)
DMAP	M = 122.17 g mol^{-1}			cat.
Pyr_{abs}				10 mL

240 mg of the acetonide **157** (0.73 mmol, 1.0 eq) were dissolved in 10 mL of Pyr_{abs} in a nitrogen atmosphere and cooled to 0 °C. A catalytical amount of DMAP and 170 µL of MsCl (250 mg, 2.19 mmol, 3.0 eq) were added, the solution was stirred for 3 h at 0 °C and for another 1 h at RT. The reaction was diluted with CH_2Cl_2, quenched with ice, and the phases were separated. The aqueous phase was extracted two times with CH_2Cl_2. The combined organic phases were dried with brine and over $MgSO_4$, filtered, and concentrated *in vacuo*. Flash chromatographic purification (EtOAc/Tol 1:1) afforded 84% of the mesylate **216** (250 mg, 0.61 mmol) as a colorless oil.

TLC: R_f = 0.67 (EtOAc/Tol 3:2).

ESI-MS: m/z = 430 $[M+Na]^+$.

HRMS: $[M+Na]^+$: $C_{14}H_{17}NO_9S_2Na$, calculated: 430.0248, found: 430.0242.

^{1}H-NMR: 500 MHz, DMSO-d_6: δ = 1.23 (s, 3 H, Isopr-CH_3^{proR}), 1.38 (s, 3 H, Isopr-CH_3^{proS}), 3.27 (s, 3 H, Ms-CH_3), 3.86 (s, 3 H, CO_2CH_3), 4.74 (dd, 1 H, $^3J_{4\text{-H}/3\text{-H}}$ = 3.7 Hz, $^3J_{4\text{-H}/5\text{-H}}$ = 5.5 Hz, 4-H), 5.04 (d, 1 H, $^3J_{5\text{-H}/4\text{-H}}$ = 5.5 Hz, 5-H), 5.30 (dd, 1 H, $^3J_{3\text{-H}/4\text{-H}}$ = 3.7 Hz, $^3J_{3\text{-H}/2\text{-H}}$ = 8.7 Hz, 3-H), 6.04 (d, 1 H, $^3J_{2\text{-H}/3\text{-H}}$ = 8.7 Hz, 2-H), 8.74 (s, 1 H, Thz-H).

^{13}C-NMR: 125 MHz, DMSO-d_6: δ = 25.5 (Isopr-CH_3^{proR}), 26.4 (Isopr-CH_3^{proS}), 38.6 (Ms-$\underline{C}H_3$), 52.2 ($CO_2\underline{C}H_3$), 75.5 (C-2), 75.7 (C-4), 76.2 (C-5), 77.7 (C-3), 113.4 (Isopr-$C_{quart.}$), 131.9 (Thz-H$\underline{C}$=C), 146.0 (Thz-HC=$\underline{C}$), 160.8 ($\underline{C}O_2CH_3$), 162.5 (C-1), 173.1 (C-6).

5.4.67 [(3*S*,4*S*)-dihydroxy-5-oxo-tetrahydro-furan-(2*S*)-yl)-(1*S*)-hydroxymethyl]-1,3-thiazole-carboxylic acid methyl ester (218)

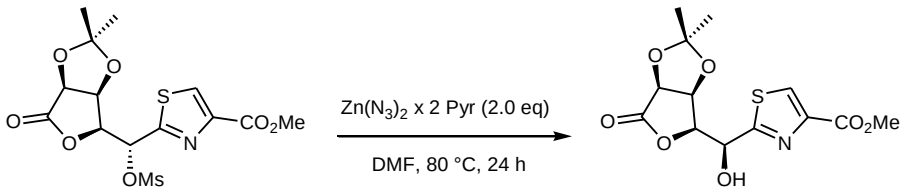

216 **218**
M = 329.33

Preparation:

Compound **218**	M = 407.42 g mol^{-1}	1.0 eq	245 µmol	100 mg
$Zn(N_3)_2$ x 2 Pyr	M = 307.63 g mol^{-1}	2.0 eq	490 µmol	151 mg
DMF				10 mL

100 mg of the mesylate **216** (245 µmol, 1.0 eq) were dissolved in 10 mL of DMF and 151 mg of $Zn(N_3)_2$ x 2 Pyr (491 µmol, 2.0 eq) were added. The solution was stirred for 24 h at 80 °C, cooled to RT, and concentrated *in vacuo*. 10 mL of H_2O and 35mL of $CHCl_3$ were added and the phases were separated. The aqueous phase was extracted two times with $CHCl_3$. The combined organic phases were dried with brine and over $MgSO_4$, filtered, and concentrated *in vacuo*. Flash chromatographic purification (EtOAc/Tol 3:2) afforded 26% of the alcohol **218** (21 mg, 63.8 µmol) as a colorless foam. In addition, 41% of the alcohol **157** with unchanged configuration were obtained (41 mg, 100 µmol).

TLC: R_f = 0.34 (EtOAc/Tol 3:2).

ESI-MS: *m/z* = 352 $[M+Na]^+$.

HRMS: $[M+Na]^+$: $C_{13}H_{15}NO_7SNa$, calculated: 352.0461, found: 352.0463.

^{1}H-NMR: 500 MHz, $CDCl_3$: δ = 1.40 (s, 3 H, Isopr-CH_3^{proR}), 1.55 (s, 3 H, Isopr-CH_3^{proS}), 3.95 (s, 3 H, CO_2CH_3), 4.09 (d, 1 H, $^{3}J_{2\text{-OH}/2\text{-H}}$ = 7.8 Hz, 2-OH), 4.89 (d, 1 H, $^{3}J_{5\text{-H}/4\text{-H}}$ = 5.2 Hz, 5-H), 4.97 (dd, 1 H, $^{3}J_{3\text{-H}/4\text{-H}}$ = 3.5 Hz, $^{3}J_{3\text{-H}/2\text{-H}}$ = 6.6 Hz, 3-H), 5.01 (dd, 1 H, $^{3}J_{4\text{-H}/3\text{-H}}$ = 3.5 Hz, $^{3}J_{4\text{-H}/5\text{-H}}$ = 5.2 Hz, 5-H), 5.40 (dd, 1 H, $^{3}J_{2\text{-H}/3\text{-H}}$ = 6.6 Hz, $^{3}J_{2\text{-H}/2\text{-OH}}$ = 7.8 Hz, 2-H), 8.24 (s, 1 H, Thz-H).

^{13}C-NMR: 125 MHz, $CDCl_3$: δ = 26.0 (Isopr-CH_3^{proR}), 26.9 (Isopr-CH_3^{proS}), 52.7 ($CO_2\underline{C}H_3$), 70.2 (C-2), 76.3 (C-5), 76.8 (C-4), 78.2 (C-3), 115.2 (Isopr-$C_{quart.}$), 129.0 (Thz-H$\underline{C}$=C), 147.0 (Thz-HC=$\underline{C}$), 161.7 ($\underline{C}O_2CH_3$), 171.0 (C-1), 172.7 (C-6).

5.4.68 [(3*S*,4*S*)-dihydroxy-5-oxo-tetrahydro-furan-(2*R*)-yl)-(1*S*)-hydroxymethyl]-1,3-thiazole-carboxylic acid methyl ester (219)

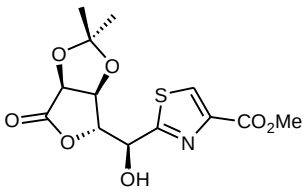

219
M = 329.33

The alcohol **219** was obtained as another diastereomer from the hydrolysis of the mesylate **216** (section 5.4.67). By flash chromatographic purification (EtOAc/Tol 3:2) 5.0% of **219** (4.0 mg, 12.1 µmol) were obtained as a colorless solid.

TLC: R_f = 0.23 (EtOAc/Tol 3:2).

ESI-MS: m/z = 352 $[M+Na]^+$.

HRMS: $[M+Na]^+$: $C_{13}H_{15}NO_7SNa$, calculated: 352.0461, found: 352.0464.

^{1}H-NMR: 600 MHz, $CDCl_3$: δ = 1.40 (s, 3 H, Isopr-CH_3^{proR}), 1.46 (s, 3 H, Isopr-CH_3^{proS}), 3.94 (s, 3 H, CO_2CH_3), 4.23 (d, 1 H, $^{3}J_{2\text{-OH}/2\text{-H}}$ = 4.9 Hz, 2-OH), 4.91 (d, 1 H, $^{3}J_{5\text{-H}/4\text{-H}}$ = 5.7 Hz, 5-H), 4.95 (d, 1 H, $^{3}J_{4\text{-H}/5\text{-H}}$ = 5.7 Hz, 4-H), 4.96 (d, 1 H, $^{3}J_{3\text{-H}/2\text{-H}}$ = 2.0 Hz, 3-H), 5.40 (dd, 1 H, $^{3}J_{2\text{-H}/3\text{-H}}$ = 2.0 Hz, $^{3}J_{2\text{-H}/2\text{-OH}}$ = 4.9 Hz, 2-H), 8.19 (s, 1 H, Thz-H).

^{13}C-NMR: 150 MHz, $CDCl_3$: δ = 25.8 (Isopr-CH_3^{proR}), 26.9 (Isopr-CH_3^{proS}), 52.8 ($CO_2\underline{C}H_3$), 71.4 (C-2), 75.5 (C-5), 78.3 (C-4), 83.8 (C-3), 113.8 (Isopr-$C_{quart.}$), 129.1 (Thz-H$\underline{C}$=C), 146.4 (Thz-HC=$\underline{C}$), 161.6 ($\underline{C}O_2CH_3$), 170.7 (C-1), 174.2 (C-6).

5.4.69 [(3*S*)-4-methylbenzenesulfonyl-(4*S*)-hydroxy-5-oxo-tetrahydro-furan-(2*S*)-yl)-(1*R*)-(4-methylbenzenesulfonyl)methyl]-1,3-thiazole-carboxylic acid methyl ester (222)

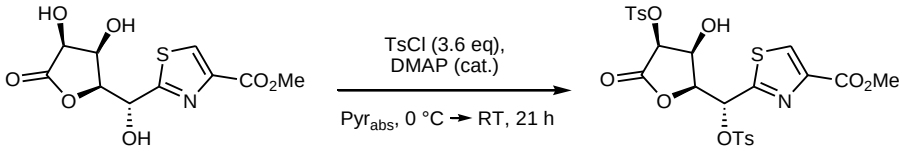

140 **222**
M = 597.63

Preparation:

Compound **140**	M = 289.26 g mol^{-1}	1.0 eq	0.69 mmol	200 mg
TsCl	M = 190.65 g mol^{-1}	3.6 eq	2.48 mmol	473 mg
DMAP	M = 122.17 g mol^{-1}			cat.
Pyr_{abs}				8.0 mL

200 mg of the triol **140** (0.69 mmol, 1.0 eq) were dissolved in 8.0 mL of Pyr_{abs} in a nitrogen atmosphere and cooled to 0 °C. A catalytical amount of DMAP and 473 mg of MsCl (2.48 mmol, 3.6 eq) were added, the solution was allowed to warm to RT and stirred for 21 h. The reaction was diluted with CH_2Cl_2, quenched with ice and 5% $NaHCO_3$, and the phases were separated. The aqueous phase was extracted two times with CH_2Cl_2. The combined organic phases were dried with brine and over $MgSO_4$, filtered, and concentrated *in vacuo*. Flash chromatographic purification (Tol/EtOAc 2:1→1:1) afforded 48% of the ditosylate **222** (196 mg, 0.32 mmol) as a colorless solid.

TLC: R_f = 0.71 (EtOAc/Tol 1:1).

ESI-MS: m/z = 620 $[M+Na]^+$.

HRMS: $[M+Na]^+$: $C_{24}H_{23}NO_{11}S_3Na$, calculated: 620.0325, found: 620.0325.

^{1}H-NMR: 600 MHz, DMSO-d_6: δ = 2.37, 2.41 (each s, 3 H, Ts-CH_3), 3.85 (s, 3 H, CO_2CH_3), 4.04 (m, 1 H, 4-H), 5.15 (dd, 1 H, $^3J_{3\text{-H}/4\text{-H}}$ = 2.8 Hz, $^3J_{3\text{-H}/2\text{-H}}$ = 9.1 Hz, 3-H), 5.60 (d, 1 H, $^3J_{5\text{-H}/4\text{-H}}$ = 4.6 Hz, 5-H), 5.86 (d, 1 H, $^3J_{2\text{-H}/3\text{-H}}$ = 9.1 Hz, 2-H), 6.46 (d, 1 H, $^3J_{4\text{-OH}/4\text{-H}}$ = 5.6 Hz, 4-OH), 7.37, 7.47 (each d, 2 H, $^3J_{\text{Ts-CH}/\text{CH}'}$ = 8.3 Hz, Ts-$CH_{arom.}$), 7.68, 7.82 (each d, 2 H, $^3J_{\text{Ts-CH}'/\text{CH}}$ = 8.3 Hz, Ts-$CH'_{arom.}$), 8.63 (s, 1 H, Thz-H).

^{13}C-NMR: 150 MHz, DMSO-d_6: δ = 21.0, 21.1 (each Ts-$\underline{C}H_3$), 51.9 ($CO_2\underline{C}H_3$), 67.5 (C-4), 75.1 (C-5), 76.0 (C-2), 79.0 (C-3), 127.7, 127.9 (each Ts-$CH'_{arom.}$), 129.9, 130.1 (each Ts-$CH_{arom.}$), 131.9 (Thz-H$\underline{C}$=C), 131.3, 131.4, 145.4, 145.5 (each Ts-$C_{arom.,\ quart.}$), 145.9 (Thz-HC=$\underline{C}$), 160.6 (C-1), 160.9 ($\underline{C}O_2CH_3$), 168.8 (C-6).

Melting point: 184 °C.

Opt. rotation: $[\alpha]_{589}^{24}$ = +47.7, $[\alpha]_{578}^{24}$ = +49.6, $[\alpha]_{546}^{24}$ = +56.7, $[\alpha]_{436}^{24}$ = +99.5
(c = 0.73 g/100 mL EtOAc).

5.4.70 [(3*S*)-4-methylbenzenesulfonyl-(4*S*)-hydroxy-5-oxo-tetrahydro-furan-(2*S*)-yl)-(1*R*)-hydroxymethyl]-1,3-thiazole-carboxylic acid methyl ester (221)

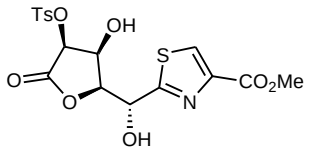

221
M = 443.45

The tosylate **221** was obtained as byproduct in the synthesis of **222** (section 5.4.69) as a pale yellow solid in 19% yield (57 mg, 129 µmol).

TLC: R_f = 0.41 (EtOAc/Tol 1:1).

ESI-MS: m/z = 466 $[M+Na]^+$.

HRMS: $[M+Na]^+$: $C_{17}H_{17}NO_9S_2Na$, calculated: 466.0237, found: 466.0220.

IR: pellet; $\tilde{\nu}$ = 3417, 2958, 2929, 2859, 1802, 1727, 1497, 1460, 1377, 1351, 1224, 1191, 1119, 1072, 1002, 976, 891, 847, 818, 773, 743, 706 cm^{-1}.

^{1}H-NMR: 600 MHz, DMSO-d_6: δ = 2.43 (s, 3 H, Ts-CH_3), 3.84 (s, 3 H, CO_2CH_3), 4.44 (ddd, 1 H, $^3J_{4\text{-H}/3\text{-H}}$ = 2.6 Hz, $^3J_{4\text{-H}/5\text{-H}}$ = 4.5 Hz, $^3J_{4\text{-H}/4\text{-OH}}$ = 5.0 Hz, 4-H), 4.74 (dd, 1 H, $^3J_{3\text{-H}/4\text{-H}}$ = 2.6 Hz, $^3J_{3\text{-H}/2\text{-H}}$ = 8.5 Hz, 3-H), 5.12 (dd, 1 H, $^3J_{2\text{-H}/2\text{-OH}}$ = 6.2 Hz, $^3J_{2\text{-H}/3\text{-H}}$ = 8.5 Hz, 2-H), 5.66 (d, 1 H, $^3J_{5\text{-H}/4\text{-H}}$ = 4.5 Hz, 5-H), 6.16 (d, 1 H, $^3J_{4\text{-OH}/4\text{-H}}$ = 5.0 Hz, 4-OH), 6.71 (d, 1 H, $^3J_{2\text{-OH}/2\text{-H}}$ = 6.2 Hz, 2-OH), 7.50 (d, 2 H, $^3J_{\text{Ts-CH}/\text{CH}'}$ = 8.3 Hz, Ts-$CH_{arom.}$), 7.87 (d, 2 H, $^3J_{\text{Ts-CH}'/\text{CH}}$ = 8.3 Hz, Ts-$CH'_{arom.}$), 8.57 (s, 1 H, Thz-H).

^{13}C-NMR: 150 MHz, DMSO-d_6: δ = 21.1 (Ms-$\underline{C}H_3$), 52.0 ($CO_2\underline{C}H_3$), 67.8 (C-2), 68.3 (C-4), 75.8 (C-5), 81.8 (C-3), 127.9 (Ts-$CH'_{arom.}$), 130.1 (each Ts-$CH_{arom.}$), 130.0 (Thz-H$\underline{C}$=C), 132.3, 145.6 (each Ts-$C_{arom.,\ quart.}$), 145.4 (Thz-HC=$\underline{C}$), 161.1 ($\underline{C}O_2CH_3$), 169.8 (C-6), 171.6 (C-1).

Melting point: 188 °C.

Opt. rotation: $[\alpha]_{589}^{21}$ = +30.1, $[\alpha]_{578}^{21}$ = +31.4, $[\alpha]_{546}^{21}$ = +36.1, $[\alpha]_{436}^{21}$ = +64.2
(c = 0.94 g/100 mL DMSO/MeOH 9:1).

5.4.71 (5*Z*)-5-((4-methoxycarbonyl-1,3-thiazole-2-yl)methylene)-3-methylsulfonyloxy-furan-2-one (223)

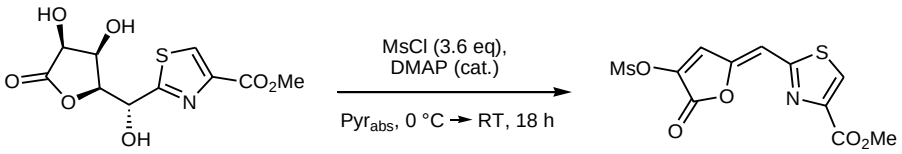

140 **223** M = 331.32

Preparation:

Compound **140**	M = 289.26 g mol^{-1}	1.0 eq	0.69 mmol	200 mg
MsCl	M = 114.55 g mol^{-1}, ρ = 1.48	3.6 eq	2.48 mmol	193 µL (285 mg)
DMAP	M = 122.17 g mol^{-1}			cat.
Pyr_{abs}				8.0 mL

200 mg of the triol **140** (0.69 mmol, 1.0 eq) were dissolved in 8.0 mL of Pyr_{abs} in a nitrogen atmosphere and cooled to 0 °C. A catalytical amount of DMAP and 193 µL of MsCl (285 mg, 2.48 mmol, 3.6 eq) were added, the solution was stirred for 1 h at 0 °C and for another 17 h at RT. The precipitate was filtered, washed with cold Pyr, and dried *in vacuo* which afforded 73% of the butenolide **223** (168 mg, 0.51 mmol) as a pale yellow solid.

TLC: R_f = 0.52 (EtOAc/Tol 7:1).

ESI-MS: m/z = 332 $[M+H]^+$.

HRMS: $[M+H]^+$: $C_{11}H_9NO_7SH$, calculated: 331.9893, found: 331.9892.

IR: pellet; $\tilde{\nu}$ = 3120, 3036, 2960, 1775, 1726, 1609, 1548, 1490, 1449, 1419, 1249, 1219, 1188, 1142, 1078, 1032, 1021, 991, 965, 945, 908, 795, 752, 679 cm^{-1}.

^{1}H-NMR: 500 MHz, DMSO-d_6: δ = 3.67 (s, 3 H, Ms-CH_3), 3.85 (s, 3 H, CO_2CH_3), 6.97 (d, 1 H, $^4J_{2\text{-H}/4\text{-H}}$ = 1.1 Hz, 2-H), 7.93 (d, 1 H, $^4J_{4\text{-H}/2\text{-H}}$ = 1.1 Hz, 4-H), 8.73 (s, 1 H, Thz-H).

^{13}C-NMR: 125 MHz, DMSO-d_6: δ = 38.4 (Ms-$\underline{C}H_3$), 52.2 ($CO_2\underline{C}H_3$), 107.2 (C-2), 126.0 (C-4), 132.7 (Thz-H$\underline{C}$=C), 146.3 (Thz-HC=$\underline{C}$), 147.8 (C-3), 159.8 (C-1), 161.0 ($\underline{C}O_2CH_3$, C-5), 161.5 (C-6).

Melting point: 152 °C.

5.4.72 (5*E*)-5-((4-methoxycarbonyl-1,3-thiazole-2-yl)methylene)-3-methylsulfonyloxy-furan-2-one (224)

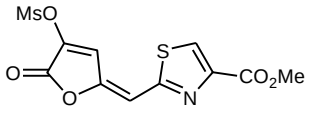

224
M = 331.32

The butenolide **224** is generated by *Z*→*E* isomerization of the C-2/C-3 double bond of **223** if dissolved in DMSO-d_6 at RT:

time	223	224
2 h	99%	1%
13 d	68%	32%
32 d	35%	65%

^{1}H-NMR: 500 MHz, DMSO-d_6: δ = 2.07 (s, 3 H, Ms-CH_3), 3.83 (s, 3 H, CO_2CH_3), 6.49 (d, 1 H, $^{4}J_{2\text{-H}/4\text{-H}}$ = 1.2 Hz, 2-H), 6.74 (d, 1 H, $^{4}J_{4\text{-H}/2\text{-H}}$ = 1.2 Hz, 4-H), 8.57 (s, 1 H, Thz-H).

^{13}C-NMR: 125 MHz, DMSO-d_6: δ = 36.7 (Ms-$\underline{C}H_3$), 52.1 ($CO_2\underline{C}H_3$), 101.0 (C-2), 110.7 (C-4), 130.9 (Thz-H$\underline{C}$=C), 145.7 (Thz-HC=$\underline{C}$), 150.7 (C-3), 161.0 (C-1), 161.2 ($\underline{C}O_2CH_3$, C-5), 164.0 (C-6).

5.4.73 [(3*S*,4*S*)-*O*-isopropylidene-5-oxo-tetrahydro-furan-(2*S*)-yl)-1-oxomethyl]-1,3-thiazole-carboxylic acid methyl ester (225)

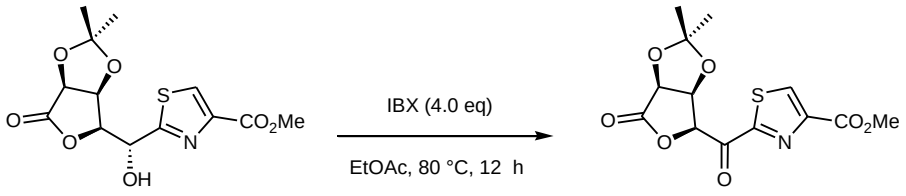

157 **225**
M = 327.31

Preparation:

Compound **157**	M = 331.34 g mol^{-1}	1.0 eq	1.14 mmol	377 mg
IBX	M = 280.02 g mol^{-1}	4.0 eq	4.58 mmol	1.28 g
EtOAc				40 mL

To a solution of 377 mg of the alcohol **157** (1.14 mmol, 1.0 eq) in 40 mL of EtAOc were added 1.28 g of IBX (4.58 mmol, 4.0 eq) and the suspension was refluxed at 80 °C for 12 h under vigorous stirring. After cooling to RT the suspension was filtered over Celite and concentrated *in vacuo* to obtain 99% of the ketone **225** (370 mg, 1.13 mmol) as a colorless solid.

TLC: R_f = 0.73 (EtOAc/Tol 4:1).

ESI-MS: m/z = 350 $[M+Na]^+$.

HRMS: $[M+Na]^+$: $C_{13}H_{13}NO_7SNa$, calculated: 350.0305, found: 350.0411.

IR: pellet; $\tilde{\nu}$ = 3090, 2970, 2932, 1786, 1716, 1461, 1377, 1317, 1254, 1226, 1188, 1103, 1070, 986, 928, 862, 829, 769, 709 cm^{-1}.

^{1}H-NMR: 500 MHz, $CDCl_3$: δ = 1.31, 1.39 (each s, 3 H, Isopr-CH_3), 3.99 (s, 3 H, CO_2CH_3), 4.95 (d, 1 H, $^3J_{5\text{-H}/4\text{-H}}$ = 5.8 Hz, 5-H), 5.54 (dd, 1 H, $^3J_{4\text{-H}/3\text{-H}}$ = 4.6 Hz, $^3J_{4\text{-H}/5\text{-H}}$ = 5.8 Hz, 4-H), 6.15 (d, 1 H, $^3J_{2\text{-H}/3\text{-H}}$ = 2.2 Hz, $^3J_{3\text{-H}/4\text{-H}}$ = 4.6 Hz, 3-H), 8.52 (s, 1 H, Thz-H).

^{13}C-NMR: 125 MHz, $CDCl_3$: δ = 26.3, 26.6 (each Isopr-CH_3), 52.9 ($CO_2\underline{C}H_3$), 75.8 (C-5), 77.1 (C-4), 80.8 (C-3), 115.4 (Isopr-$C_{quart.}$), 133.8 (Thz-H$\underline{C}$=C), 148.9 (Thz-HC=$\underline{C}$), 161.0 ($\underline{C}O_2CH_3$), 163.9 (C-1), 172.6 (C-6), 182.4 (C-2).

Melting point: 108 °C.

Opt. rotation: $[\alpha]_{589}^{23}$ = –98.4, $[\alpha]_{578}^{23}$ = –102.9, $[\alpha]_{546}^{23}$ = –117.3, $[\alpha]_{436}^{23}$ = –202.4 (c = 0.97 g/100 mL $CHCl_3$).

5.4.74 (9*aR*)H-(6*S*,7*R*)-*O*-isopropylidene-(8*R*,9*R*)-epoxy-(9*R*)-5-oxo-octahydro-thiazolo[3,2-*a*]azepine-(3*R*)-carboxylic acid methyl ester (231)

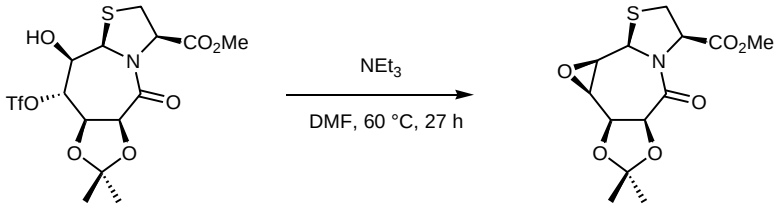

235 **231**
M = 315.34

Preparation:

Compound **235**	M = 465.42 g mol^{-1}	1.0 eq	23.2 mmol	10.8 g
NEt_3	M = 101.19 g mol^{-1}, ρ = 0.79	7.0 eq	164 mmol	21.0 mL (16.6 g)
DMF				300 mL

12.0 g of the triflate **235** (1.0 eq, 23.2 mmol) were dissolved in 300 mL of DMF and 21 mL of NEt_3 (16.6 g, 7.0 eq, 164 mmol) were added. The mixture was stirred for 27 h at 60 °C, cooled to RT and concentrated *in vacuo*. Residual amounts of DMF were removed by coevaporation with Tol. 50 mL of EtOAc/Tol 1:1 were added and the resulting suspension was stored in the fridge overnight, filtered, and the precipitate was washed with cold Tol to yield 81% (5.95 g, 18.9 mmol) of the epoxide **231** as colorless powder.

TLC: R_f = 0.31 (EtOAc/Tol 7:1).

ESI-MS: *m/z* = 338 $[M+Na]^+$.

HRMS: $[M+Na]^+$: $C_{13}H_{17}NO_6SNa$, calculated: 338.0669, found: 338.0671.

^{1}H-NMR: 500 MHz, DMSO-d_6: δ = 1.33, 1.42 (each s, 3 H, Isopr-CH_3), 3.11 (dd, 1 H, $^2J_{2\text{-}H^u/2\text{-}H^d}$ = 11.8 Hz, $^3J_{2\text{-}H^u/3\text{-}H}$ = 3.5 Hz, 2-H^u), 3.22 (dd, 1 H, $^2J_{2\text{-}H^d/2\text{-}H^u}$ = 11.8 Hz, $^3J_{2\text{-}H^d/3\text{-}H}$ = 6.7 Hz, 2-H^d), 3.33 (d, 1 H, $^3J_{9\text{-}H/8\text{-}H}$ = 4.4 Hz, 9-H), 3.42 (dd, 1 H, $^3J_{8\text{-}H/7\text{-}H}$ = 3.0 Hz, $^3J_{8\text{-}H/9\text{-}H}$ = 4.4 Hz, 8-H), 3.62 (s, 3 H, CO_2CH_3), 4.56 (dd, 1 H, $^3J_{7\text{-}H/8\text{-}H}$ = 3.0Hz, $^3J_{7\text{-}H/6\text{-}H}$ = 6.5 Hz, 7-H), 4.74 (dd, 1 H, $^3J_{3\text{-}H/2\text{-}H^u}$ = 3.5 Hz, $^3J_{3\text{-}H/2\text{-}H^d}$ = 6.7 Hz, 3-H), 4.68 (d, 1 H, $^3J_{6\text{-}H/7\text{-}H}$ = 6.5 Hz, 6-H), 4.74 (dd, 1H, $^3J_{3\text{-}H/2\text{-}H^u}$ = 3.5 Hz, $^3J_{3\text{-}H/2\text{-}H^d}$ = 6.7 Hz, 3-H), 5.53 (s, 1 H, 9a-H).

^{13}C-NMR: 125 MHz, DMSO-d_6: δ = 25.8, 26.9 (each Isopr-CH_3), 31.4 (C-2), 51.5 (C-8), 51.8 ($CO_2\underline{C}H_3$), 54.7 (C-9), 56.2 (C-9a), 63.3 (C-3), 73.6 (C-6), 73.7 (C-7), 108.3 (Isopr-$C_{quart.}$), 166.8, 169.1 ($\underline{C}O_2CH_3$, C-5).

Melting point: 189 °C.

5.4.75 (9*aR*)H-(6*S*,7*R*)-*O*-isopropylidene-(8*S*)-hydroxy-(9*S*)-azido-5-oxo-octahydro-thiazolo[3,2-*a*]azepine-(3*R*)-carboxylic acid methyl ester (232)

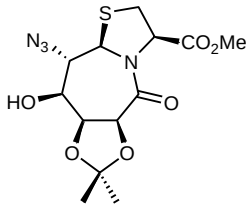

232
M = 358.37

The thiazolidine lactam **232** occurs as intermediate in the formation of the thiazolidine lactone **233** (section 5.4.76) and it was obtained in 33% yield as mixture with byproduct **236** and starting material. If the flash chromatographic purification (section 5.4.76) was carried out with EtOAc/Tol 2:1 → 5:1 → 9:1 the pure compound was isolated.

TLC: R_f = 0.41 (EtOAc/Tol 7:1).

ESI-MS: m/z = 381 $[M+Na]^+$.

HRMS: $[M+Na]^+$: $C_{13}H_{18}N_4O_6SNa$, calculated: 381.0839, found: 381.0842.

^{1}H-NMR: 300 MHz, DMSO-d_6: δ = 1.30, 1.41 (each s, 3 H, Isopr-CH_3), 3.21 (dd, 1 H, $^{2}J_{2\text{-H}^u/2\text{-H}^d}$ = 11.7 Hz, $^{3}J_{2\text{-H}^u/3\text{-H}}$ = 5.1 Hz, 2-H^u), 3.37 (dd, 1 H, $^{2}J_{2\text{-H}^d/2\text{-H}^u}$ = 11.7 Hz, $^{3}J_{2\text{-H}^d/3\text{-H}}$ = 7.0 Hz, 2-H^d), 3.67 (s, 3 H, CO_2CH_3), 4.00 (dd, 1 H, $^{3}J_{9\text{-H}/8\text{-H}}$ = 1.3 Hz, $^{3}J_{9\text{-H}/9a\text{-H}}$ = 10.4 Hz, 9-H), 4.07 (m, 1 H, 8-H), 4.47 (dd, 1 H, $^{3}J_{7\text{-H}/8\text{-H}}$ = 1.7 Hz, $^{3}J_{7\text{-H}/6\text{-H}}$ = 8.8 Hz, 7-H), 4.86 (dd, 1 H, $^{3}J_{3\text{-H}/2\text{-H}^u}$ = 5.1 Hz, $^{3}J_{3\text{-H}/2\text{-H}^d}$ = 7.0 Hz, 3-H), 4.96 (d, 1H, $^{3}J_{6\text{-H}/7\text{-H}}$ = 8.8 Hz, 6-H), 4.99 (d, 1 H, $^{3}J_{9a\text{-H}/9\text{-H}}$ = 10.4 Hz, 9a-H), 5.05 (d, $^{3}J_{8\text{-O-H}/8\text{-H}}$ = 4.9 Hz, 8-OH).

^{13}C-NMR: 150 MHz, DMSO-d_6: δ = 23.6, 25.6 (each Isopr-CH_3), 31.0 (C-2), 52.4 ($CO_2\underline{C}H_3$), 61.8 (C-9a), 62.0 (C-3), 67.3 (C-9), 71.3 (C-8), 74.2 (C-6), 74.6 (C-7), 107.9 (Isopr-$C_{quart.}$), 166.6 (C-5), 170.6 ($\underline{C}O_2CH_3$).

5.4.76 (2*R*)-[(3*S*,4*S*)-*O*-isopropylidene -5-oxo-tetrahydro-furan-(2*R*)-yl)-(1*S*)-azidomethyl]-1,3-thiazolidine-(4*R*)-carboxylic acid methyl ester (233)

Method A) from epoxide **231**

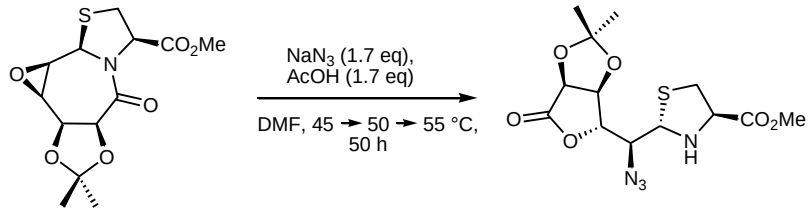

231 **233**
M = 358.37

Preparation:

Compound **231**	M = 315.34 g mol^{-1}	1.0 eq	8.44 mmol	2.66 g
NaN_3	M = 65.01 g mol^{-1}	1.7 eq	14.3 mmol	950 mg
DMF/AcOH 130:1			38 ml DMF	0.29 mL AcOH

2.66 g of epoxide **231** (1.0 eq, 8.44 mmol) and 950 mg of NaN_3 (1.7 eq, 14.3 mmol) were dissolved in 38 mL of DMF. After the addition of 0.29 mL AcOH (DMF/AcOH 130:1) the mixture was stirred for 23 h at 45 °C, then for 4 h at 50 °C and for additional 47 h at 55 °C. After cooling to RT, the solution was neutralized with NEt_3 and concentrated *in vacuo*. Residual amounts of DMF were removed by coevaporation with Tol. 200 mL of EtOAc and 50 mL of H_2O were added and the phases were separated. The aqueous phase was extracted with EtOAc and the combined organic phases were dried with brine and over $MgSO_4$, filtered, and concentrated *in vacuo*. Flash chromatography (EtOAc/Tol 1:1) yielded 39% (1.17 g, 3.26 mmol) of the thiazolidine lactone **233** as a colorless solid. After complete elution of **233** all other species were obtained by elution with pure EtOAc which yielded 33% of the reaction intermediate **232** (section 5.4.75), 12% of the byproduct **236** (section 5.4.79), and 4% of educt as mixture (1.448 g, yellow foam). This was recycled in order to yield more thiazolidine lactone **233** (method B).

Method B) from intermediate **232**

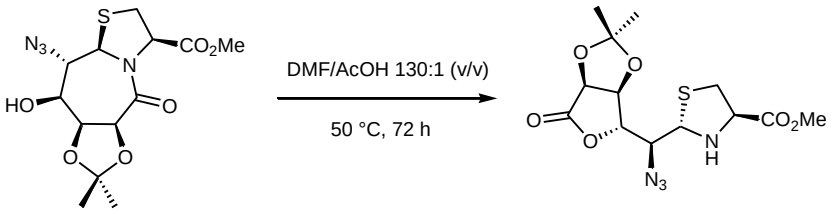

232 **233** M = 358.37

Preparation:

Compound **232** (as mixture, section 5.4.75)	M = 358.37 g mol^{-1}	1.0 eq	4.91 mmol	1.76 g
DMF/AcOH 130:1			50 mL DMF	0.38 mL AcOH

2.66 g of the thiazolidine lactam **231** (1.0 eq, 4.91 mmol) were dissolved in 50 mL of DMF and 0.38 mL of AcOH were added (DMF/AcOH 130:1). The mixture was stirred for 72 h at 50 °C, allowed to cool to RT, neutralized with NEt_3 and concentrated *in vacuo*. Residual amounts of DMF were removed by coevaporation with Tol. 200 mL of EtOAc and 50 mL of H_2O were added and the phases were separated. The aqueous phase was extracted with EtOAc and the combined organic phases were dried with brine and over $MgSO_4$, filtered, and concentrated *in vacuo*. Flash chromatography (EtOAc/Tol 1:1) yielded 33% (587 mg, 1.64 mmol) of the thiazolidine lactone **233** as a colorless solid. After complete elution of **233** the other species were obtained by elution with pure EtOAc as mixture which again could be recycled.

TLC: R_f = 0.83 (EtOAc/Tol 7:1) / 0.40 (Tol/EtOAc 5:1).

ESI-MS: m/z = 381 $[M+Na]^+$.

HRMS: $[M+Na]^+$: $C_{13}H_{18}NO_6SNa$, calculated: 381.0839, found: 338.0840.

IR: pellet; $\tilde{\nu}$ = 3323, 3296, 2115, 1786, 1735, 1381, 1349, 1294, 1269, 1216, 1176, 1145, 1017, 993, 967, 945, 923, 864, 785, 764 cm^{-1}.

^{1}H-NMR: 500 MHz, $CDCl_3$: δ = 1.38, 1.45 (each s, 3 H, Isopr-CH_3), 2.94 (dd, 1 H, $^2J_{\beta\text{-}H^u/\beta\text{-}H^d}$ = 10.6 Hz, $^3J_{\beta\text{-}H^u/\alpha\text{-}H}$ = 8.5 Hz, β-H^u), 3.09 (br s, 1 H, NH), 3.34 (dd, 1 H, $^2J_{\beta\text{-}H^d/\beta\text{-}H^u}$ = 10.6 Hz, $^3J_{\beta\text{-}H^d/\alpha\text{-}H}$ = 6.4 Hz, β-H^d), 3.48 (dd, 1 H, $^3J_{2\text{-}H/3\text{-}H}$ = 1.7 Hz, $^3J_{2\text{-}H/1\text{-}H}$ = 9.6 Hz, 2-H), 3.81 (s, 3 H, CO_2CH_3), 3.95 (dd, 1 H, $^3J_{\alpha\text{-}H/\beta\text{-}H^d}$ = 6.4 Hz, $^3J_{\alpha\text{-}H/\beta\text{-}H^u}$ = 8.5 Hz, α-H), 4.66 (d, 1 H, $^3J_{4\text{-}H/5\text{-}H}$ = 5.8 Hz, 4-H), 4.77 (d, 1 H, $^3J_{3\text{-}H/2\text{-}H}$ = 1.7 Hz, 3-H), 4.86 (d, 1 H, $^3J_{5\text{-}H/4\text{-}H}$ = 5.8 Hz, 5-H), 4.98 (d, 1H, $^3J_{1\text{-}H/2\text{-}H}$ = 9.6 Hz, 1-H).

^{13}C-NMR: 125 MHz, $CDCl_3$: δ = 25.7, 26.8 (each Isopr-CH_3), 38.3 (C-β), 53.0 ($CO_2\underline{C}H_3$), 63.6 (C-α), 66.3 (C-2), 69.6 (C-1), 75.0 (C-5), 79.0 (C-4), 81.1 (C-3), 113.8 (Isopr-$C_{quart.}$), 171.1 ($\underline{C}O_2CH_3$), 173.5 (C-6).

Melting point: 175 °C.

Opt. rotation: $[\alpha]_{589}^{22}$ = –78.5, $[\alpha]_{578}^{22}$ = –81.6, $[\alpha]_{546}^{22}$ = –93.1, $[\alpha]_{436}^{22}$ = –162.8, $[\alpha]_{365}^{22}$ = –267.6 (c = 1.08 g/100 mL $CHCl_3$).

5.4.77 (9*aR*)H-(6*S*,7*S*)-dihydroxy-(8*S*,9*R*)-*O*-isopropylidene-5-oxo-octahydro-thiazolo [3,2-*a*]azepine-(3*R*)-carboxylic acid methyl ester (234)

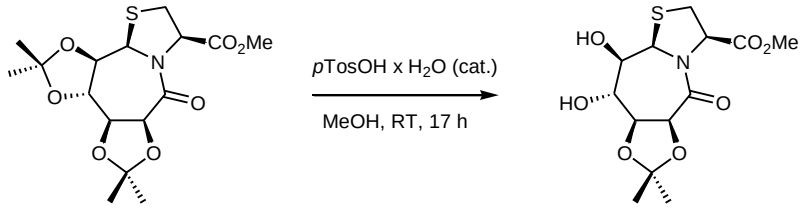

136 **234**
M = 333.36

Preparation:

Compound **136**	M = 373.42 g mol^{-1}	1.0 eq	38.0 mmol	14.2 g
*p*TosOH x H_2O	M = 190.22 g mol^{-1}			cat.
MeOH				150 mL

A solution of 14.2 g of the bisacetonide **136** (38.0 mmol, 1.0 eq) in 150 mL MeOH was treated with a catalytic amount of *p*TosOH x H_2O and the solution was stirred for 17 h at RT. A part of the product had crystallized from the reaction mixture and was it separated by filtration, washing with cold MeOH, and drying *in vacuo*. This yielded 21% of the monoacetonide **234** (2.70 g, 8.10 mmol) as colorless powder. The filtrate was neutralized by addition of NEt_3 and adsorbed on Celite by evaporation of the solvent *in vacuo*. Flash chromatography (CH_2Cl_2/MeOH 10:1) yielded 46% (5.84 g, 17.5 mmol) of the monoacetonide **234** as a colorless solid which resulted in an overall yield of 67% (8.54 g, 25.6 mmol).

TLC: R_f = 0.58 (CH_2Cl_2/MeOH 10:1).

ESI-MS: m/z = 356 $[M+Na]^+$.

HRMS: $[M+Na]^+$: $C_{13}H_{19}NO_7SNa$, calculated: 356.0774, found: 356.0767.

IR: pellet; $\tilde{\nu}$ = 3503, 3434, 3000, 2936, 2897, 1754, 1650, 1434, 1204, 1170, 1143, 1081, 1068, 1034, 1007, 829 cm^{-1}.

^{1}H-NMR: 300 MHz, DMSO-d_6: δ = 1.32, 1.38 (each s, 3 H, Isopr-CH_3), 3.26 (dd, 1 H, $^2J_{2\text{-}H^u/2\text{-}H^d}$ = 10.7 Hz, $^3J_{2\text{-}H^u/3\text{-}H}$ = 8.8 Hz, 2-H^u), 3.26 (dd, 1 H, $^2J_{2\text{-}H^d/2\text{-}H^u}$ = 10.7 Hz, $^3J_{2\text{-}H^d/3\text{-}H}$ = 7.6 Hz, 2-H^d), 3.33-3.39 (m, 1 H, 9-H), 3.55 (ddd, 1 H, $^3J_{8\text{-}H/8\text{-}OH}$ = 5.4 Hz, $^3J_{8\text{-}H/9\text{-}H}$ = 7.3 Hz, $^3J_{8\text{-}H/7\text{-}H}$ = 9.9 Hz, 8-H), 3.63 (s, 3 H, CO_2CH_3), 4.24 (dd, 1 H, $^3J_{7\text{-}H/6\text{-}H}$ = 8.0 Hz, $^3J_{7\text{-}H/8\text{-}H}$ = 9.8 Hz, 7-H), 4.50 (dd, 1 H, $^3J_{3\text{-}H/2\text{-}H^d}$ = 7.6 Hz, $^3J_{3\text{-}H/2\text{-}H^u}$ = 8.8 Hz, 3-H), 5.01 (d, 1 H, $^3J_{6\text{-}H/7\text{-}H}$ = 8.0 Hz, 6-H), 5.24 (d, 1 H, $^3J_{9a\text{-}H/9\text{-}H}$ = 3.2 Hz, 9a-H), 5.32 (pt, 2 H, 8-OH, 9-OH).

^{13}C-NMR: 75 MHz, DMSO-d_6: δ = 24.7, 26.9 (each Isopr-CH_3), 32.4 (C-2), 52.0 ($CO_2\underline{C}H_3$), 62.3 (C-3), 62.4 (C-9a), 74.6 (C-8), 74.8 (C-9), 75.0 (C-6), 76.8 (C-7), 108.6, (Isopr-$C_{quart.}$), 165.8, 169.6 ($\underline{C}O_2CH_3$, C-5).

Melting point: 207 °C.

Opt. rotation: $[\alpha]_{589}^{22}$ = –95.4, $[\alpha]_{578}^{22}$ = –99.8, $[\alpha]_{546}^{22}$ = –114.2, $[\alpha]_{436}^{22}$ = –204.2, $[\alpha]_{365}^{22}$ = –334.9 (c = 0.95 g/100 mL DMSO).

5.4.78 (9*aR*)H-(6*S*,7*R*)-*O*-isopropylidene (8*S*)-trifuoromethanesulfonyl-(9*R*)-hydroxy-5-oxo-octahydro-thiazolo[3,2-*a*]azepine-(3*R*)-carboxylic acid methyl ester (235)

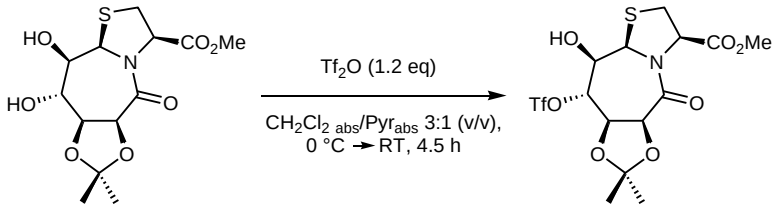

234 **235**
M = 465.42

Preparation:

Compound **234**	M = 333.36 g mol^{-1}	1.0 eq	24.7 mmol	8.24 g
Tf_2O	M = 282.13 g mol^{-1}, ρ = 1.68	1.2 eq	32.1 mmol	4.98 mL (8.37 g)
$CH_2Cl_{2\ abs}$				140 mL
DMF_{abs}				47 mL

8.24 g of the diol **234** (24.7 mmol, 1.0 eq) were dissolved in 140 mL of $CH_2Cl_{2\ abs}$ and 47 mL of DMF_{abs} (approx. 3:1) under a nitrogen atmosphere and cooled to 0 °C. 4.98 mL of Tf_2O (8.37 g, 1.2 eq, 32.1 mmol) were added dropwise over 15 min. and the deep red solution was stirred for 1 h at 0 °C and another 3.5 h at RT. The reaction was quenched with 170 mL of ice, the phases were separated and the aqueous phase was extracted two times with CH_2Cl_2. The combined organic phases were dried with brine and over $MgSO_4$, filtered and concentrated *in vacuo*. Residual DMF was removed by coevaporation with Tol and the raw product was obtained as yellow solid. After addition of EtOAc/Tol 2:1 the solution was filtered and 52% of the triflate **235** (6.06 g, 13.0 mmol) were isolated as a pale yellow solid. The residual amount was subjected to flash chromatography (EtOAc/Tol 2:1) which yielded additional 42% (4.79 g, 10.3 mmol) of **235**, resulting in an overall yield of 94% (10.9 g, 23.3 mmol).

TLC: R_f = 0.59 (EtOAc/Tol 10:1).

ESI-MS: m/z = 488 $[M+Na]^+$.

HRMS: $[M+Na]^+$: $C_{14}H_{18}F_3NO_9SNa$, calculated: 488.0267, found: 488.0269.

IR: pellet; $\tilde{\nu}$ = 3328, 2992, 2950, 1747, 1661, 1436, 1411, 1397, 1376, 1352, 1329, 1246, 1199, 1141, 1069, 954, 888 cm^{-1}.

^{1}H-NMR: 600 MHz, DMSO-d_6: δ = 1.35, 1.36 (each s, 3 H, Isopr-CH_3), 3.30 (dd, 1 H, $^2J_{2\text{-}H^u/2\text{-}H^d}$ = 10.9 Hz, $^3J_{2\text{-}H^u/3\text{-}H}$ = 8.9 Hz, 2-H^u), 3.37 (dd, 1 H, $^2J_{2\text{-}H^d/2\text{-}H^u}$ = 10.9 Hz, $^3J_{2\text{-}H^d/3\text{-}H}$ = 7.3 Hz, 2-H^d), 3.63 (s, 3 H, CO_2CH_3), 3.91 (dd, 1 H, $^3J_{9\text{-}H/9a\text{-}H}$ = 3.2 Hz, $^3J_{9\text{-}H/8\text{-}H}$ = 7.8 Hz, 9-H), 4.64 (dd, 1 H, $^3J_{3\text{-}H/2\text{-}H^d}$ = 7.3 Hz, $^3J_{3\text{-}H/2\text{-}H^u}$ = 8.9 Hz, 3-H), 4.74 (dd, 1 H, $^3J_{7\text{-}H/6\text{-}H}$ = 8.2 Hz, $^3J_{7\text{-}H/8\text{-}H}$ = 10.5 Hz, 7-H), 4.94 (dd, 1 H, $^3J_{8\text{-}H/9\text{-}H}$ = 7.8 Hz, $^3J_{8\text{-}H/7\text{-}H}$ = 10.5 Hz, 8-H), 5.28 (d, 1 H, $^3J_{6\text{-}H/7\text{-}H}$ = 8.2 Hz, 6-H), 5.30 (d, 1 H, $^3J_{9a\text{-}H/9\text{-}H}$ = 3.2 Hz, 9a-H), 6.33 (br s, 1 H, 9-OH).

^{13}C-NMR: 125 MHz, DMSO-d_6: δ = 25.0, 26.1 (each Isopr-CH_3), 32.1 (C-2), 52.1 ($CO_2\underline{C}H_3$), 61.9 (C-9a), 62.2 (C-3), 71.2 (C-9), 72.7 (C-7), 75.3 (C-6), 92.2 (C-8), 110.2 (Isopr-$C_{quart.}$), 164.4, 169.2 ($\underline{C}O_2CH_3$, C-5).

Melting point: 85 °C.

Opt. rotation: $[\alpha]_{589}^{20}$ = –78.5, $[\alpha]_{578}^{20}$ = –82.1, $[\alpha]_{546}^{20}$ = –94.0, $[\alpha]_{436}^{20}$ = –166.7, $[\alpha]_{365}^{20}$ = –269.1 (c = 1.00 g/100 mL $CHCl_3$).

5.4.79 (9*aR*)H-(6*S*,7*R*)-*O*-isopropylidene-(8*S*)-hydroxy-(9*R*)-azido-5-oxo-octahydro-thiazolo[3,2-*a*]azepine-(3*R*)-carboxylic acid methyl ester (236)

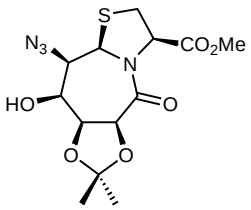

236
M = 358.37

The thiazolidine lactam **236** occurs as byproduct in the formation of the thiazolidine lactone **233** (section 5.4.76) and was obtained in 12% yield as mixture with intermediate **232** and starting material. If the flash chromatographic purification was carried out with EtOAc/Tol 2:1 → 5:1 → 9:1 the pure compound was isolated.

TLC: R_f = 0.63 (EtOAc/Tol 7:1).

ESI-MS: *m/z* = 381 $[M+Na]^+$.

HRMS: $[M+Na]^+$: $C_{13}H_{18}N_4O_6SNa$, calculated: 381.0839, found: 381.0841.

^{1}H-NMR: 600 MHz, DMSO-d_6: δ = 1.32, 1.54 (each s, 3 H, Isopr-CH_3), 3.12 (dd, 1 H, $^2J_{2\text{-}H^u/2\text{-}H^d}$ = 12.2 Hz, $^3J_{2\text{-}H^u/3\text{-}H}$ = 1.0 Hz, 2-H^u), 3.36 (m, 1 H, 8-H), 3.56 (dd, 1 H, $^2J_{2\text{-}H^d/2\text{-}H^u}$ = 12.2 Hz, $^3J_{2\text{-}H^d/3\text{-}H}$ = 7.9 Hz, 2-H^d), 3.62 (s, 3 H, CO_2CH_3), 4.00 (dd, 1 H, $^3J_{9\text{-}H/9a\text{-}H}$ = 3.7 Hz, $^3J_{9\text{-}H/8\text{-}H}$ = 8.0 Hz, 9-H), 4.58 (dd, 1 H, $^3J_{7\text{-}H/8\text{-}H}$ = 1.7 Hz, $^3J_{7\text{-}H/6\text{-}H}$ = 9.3 Hz, 7-H), 4.67 (d, 1H, $^3J_{6\text{-}H/7\text{-}H}$ = 9.3 Hz, 6-H), 4.86 (dd, 1 H, $^3J_{3\text{-}H/2\text{-}H^u}$ = 1.0 Hz, $^3J_{3\text{-}H/2\text{-}H^d}$ = 7.9 Hz, 3-H), 5.66 (d, 1 H, $^3J_{9a\text{-}H/9\text{-}H}$ = 3.7 Hz, 9a-H), 5.99 (d, $^3J_{8\text{-}O\text{-}H/8\text{-}H}$ = 6.3 Hz, 8-OH).

^{13}C-NMR: 125 MHz, DMSO-d_6: δ = 22.3, 25.1 (each Isopr-CH_3), 32.1 (C-2), 52.2 ($CO_2\underline{C}H_3$), 59.3 (C-9a), 62.4 (C-3), 70.1 (C-9), 71.9 (C-8), 77.1 (C-7), 77.6 (C-6), 109.9 (Isopr-$C_{quart.}$), 165.3 (C-5), 196.3 ($\underline{C}O_2CH_3$).

5.4.80 2-[(3*S*,4*S*)-*O*-isopropylidene-5-oxo-tetrahydro-furan-(2*R*)-yl)-(1*S*)-azidomethyl]-1,3-thiazole-4-carboxylic acid methyl ester (241)

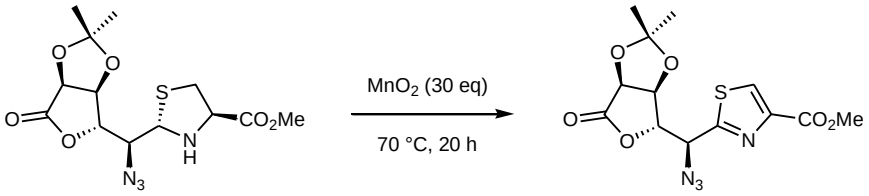

233 **241**
M = 354.34

Preparation:

Compound **233**	M = 358.37 g mol^{-1}	1.0 eq	1.84 mmol	661 mg
MnO_2, activated (*Fluka*)	M = 86.94 g mol^{-1}	30 eq	55.3 mmol	4.81 g
CH_3CN				40 mL

To a solution of 661 mg of the thiazolidine **233** (1.84 mmol, 1.0 eq) in 40 mL of CH_3CN were added 4.81 g of MnO_2 (activated, *Fluka*; 55.3 mmol, 30 eq). The suspension was vigorously stirred for 20 h at 70 °C, filtered over Celite, and concentrated *in vacuo*. The yellow residue was dissolved in EtOAc/Tol 2:1, adsorbed on Celite, and subjected to purification by flash chromatography (EtOAc/Tol 5:1 → 3:1) to yield 31% of the thiazole **241** (203 mg, 0.58 mmol) as colorless/pale yellow solid. 27% of the starting material **233** were also obtained (179 mg, 0.50 mmol), resulting in an overall yield of 58% b.r.s.m.

TLC: R_f = 0.16 (Tol/EtOAc 5:1).

ESI-MS: m/z = 377 $[M+Na]^+$.

HRMS: $[M+Na]^+$: $C_{13}H_{14}N_4O_6SNa$, calculated: 377.0526, found: 377.0527.

IR: KBr; $\tilde{\nu}$ = 3098, 2990, 2114, 1790, 1717, 1474, 1377, 1346, 1276, 1244, 1223, 1210, 1166, 1103, 1084, 1065, 1032, 991, 980, 964, 947, 928, 913, 864, 780 cm^{-1}.

^{1}H-NMR: 600 MHz, $CDCl_3$: δ = 1.41, 1.46 (each s, 3 H, Isopr-CH_3), 3.98 (s, 3 H, CO_2CH_3), 4.87-4.88 (m, 2 H, 3-H, 4-H), 4.96 (d, 1 H, $^3J_{5\text{-H}/4\text{-H}}$ = 5.8 Hz, 5-H), 5.35 (d, 1 H, $^3J_{2\text{-H}/3\text{-H}}$ = 2.6 Hz, 2-H), 8.30 (s, 1 H, Thz-H).

^{13}C-NMR: 150 MHz, $CDCl_3$: δ = 25.7, 26.7 (each Isopr-CH_3), 52.8 ($CO_2\underline{C}H_3$), 63.5 (C-2), 75.2 (C-5), 78.8 (C-4), 82.2 (C-3), 109.9 (Isopr-$C_{quart.}$), 129.9 (Thz-H$\underline{C}$=C), 147.1 (Thz-HC=$\underline{C}$), 161.4 ($\underline{C}O_2CH_3$), 164.9 (C-1), 173.1 (C-6).

Melting point: 142 °C.

Opt. rotation: $[\alpha]_{589}^{20}$ = –103.8, $[\alpha]_{578}^{20}$ = –108.7, $[\alpha]_{546}^{20}$ = –124.5, $[\alpha]_{436}^{20}$ = –225.3
(c = 0.99 g/100 mL $CHCl_3$).

5.4.81 2-aminocarbonyl-1,3-thiazole-4-carboxylic acid methyl ester (242)

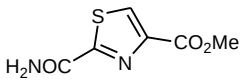

242
M = 186.19

The thiazole carbamic acid **242** was isolated as over-oxidation product in the synthesis of **241** in varying yields (< 12%). It could be isolated by filtration of the raw product solution prior to flash chromatographic purification (section 5.4.80).

TLC: R_f = 0.40 (pure EtOAc).

^{1}H-NMR: 300 MHz, $CDCl_3$: δ = 3.98 (s, 3 H, CO_2CH_3), 5.79 (br s, 1 H, $CONH_2^u$), 7.30 (br s, 1 H, $CONH_2^d$), 7.38 (s, 1 H, Thz-H).

X-ray: Suitable crystals of **242** were grown from a $CHCl_3$ solution. See figure 4.18.

5.4.82 2-((1*R*,2*S*,3*S*,4*S*)-4-(methoxycarbonyl)-1-azido-2,3,4-trihydroxybutyl)-1,3-thiazole-4-carboxylic acid methyl ester (243)

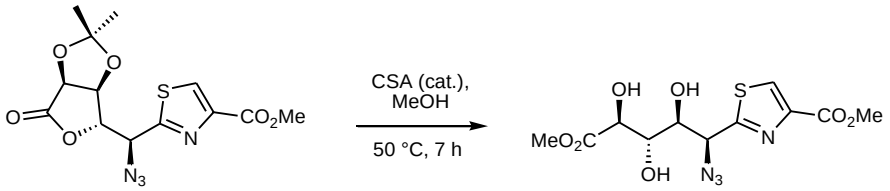

241 **243**
M = 346.32

Preparation:

Compound **241**	M = 354.34 g mol^{-1}	1.0 eq	138 µmol	49 mg
CSA	M = 232.30 g mol^{-1}			cat.
$MeOH_{abs}$				5.0 mL

49 mg of the lactone **241** (138 µmol, 1.0 eq) were dissolved in 5.0 mL of MeOH. A catalytical amount of CSA was added and the mixture was stirred at 50 °C for 7 h. The solution was neutralized with NEt_3, and concentrated *in vacuo*. Flash chromatographic purification ($CHCl_3$/MeOH 9:1) afforded 38% of the triol **243** (18 mg, 50.8 µmol) as a colorless oil. In addition, 12% of the diol lactone **246** (5.4 mg, 17.2 µmol) were obtained (section 5.4.85).

TLC: R_f = 0.39 ($CHCl_3$/MeOH 9:1).

ESI-MS: m/z = 369 $[M+Na]^+$.

HRMS: $[M+Na]^+$: $C_{11}H_{14}N_4O_7SNa$, calculated: 369.0475, found: 369.0483.

^{1}H-NMR: 300 MHz, $CDCl_3$: δ = 3.13 (br s, 1 H, 4-OH), 3.70 (s, 3 H, 6-CO_2CH_3), 3.91 (s, 3 H, Thz-CO_2CH_3), 4.07 (br s, 1 H, 3-OH), 4.31-4.34 (m, 1 H, 4-H), 4.68 (d, 1 H, $^3J_{5\text{-H}/4\text{-H}}$ = 3.0 Hz, 5-H), 4.88-4.93 (m, 1 H, 3-H), 5.18 (d, 1 H, $^3J_{2\text{-H}/3\text{-H}}$ = 2.0 Hz, 2-H), 5.98 (br s, 1 H, 5-OH), 8.14 (s, 1 H, Thz-H).

^{13}C-NMR: 125 MHz, $CDCl_3$: δ = 52.7 (6-$CO_2\underline{C}H_3$, Thz-$CO_2\underline{C}H_3$), 63.8 (C-2), 71.6 (C-3), 72.0 (C-5), 72.7 (C-4), 128.6 (Thz-H$\underline{C}$=C), 146.6 (Thz-HC=$\underline{C}$), 161.6 (Thz-$\underline{C}O_2CH_3$), 170.0 (C-1), 173.5 (C-1).

5.4.83 2-((1*R*,2*S*,3*S*,4*S*)-4-(benzyloxycarbonyl)-1-azido-2,3,4-trihydroxybutyl)-1,3-thiazole-4-carboxylic acid methyl ester (244)

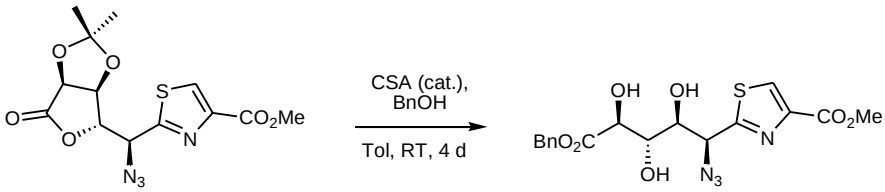

241 **244**
M = 422.41

Preparation:

Compound **241**	M = 354.34 g mol^{-1}	1.0 eq	56.4 µmol	20 mg
CSA	M = 232.30 g mol^{-1}			cat.
BnOH				1.0 mL
Tol				1.0 mL

20 mg of the lactone **241** (56.4 µmol, 1.0 eq) were dissolved in 1.0 mL of Tol and 1.0 mL of BnOH. A catalytical amount of CSA was added and the mixture was stirred at RT for 4 d. The solution was neutralized with NEt_3, and concentrated *in vacuo* at 40 °C. Flash chromatographic purification ($CHCl_3$/MeOH 9:1) afforded a 70:30 mixture of the triol **244** and the starting material **241**. The yield cannot be given due to residual amounts of BnOH which were coeluted.

TLC: R_f = 0.33 ($CHCl_3$/MeOH 9:1).

ESI-MS: *m*/*z* = 445 $[M+Na]^+$.

HRMS: $[M+Na]^+$: $C_{17}H_{18}N_4O_7SNa$, calculated: 445.0788, found: 445.0792.

^{1}H-NMR: 300 MHz, $CDCl_3$: δ = 3.97 (s, 3 H, CO_2CH_3), 4.21 (br s, 1 H, 3-OH), 4.38 (dd, 1 H, $^3J_{4\text{-H}/5\text{-H}}$ = 2.9 Hz, $^3J_{4\text{-H}/3\text{-H}}$ = 9.6 Hz, 4-H), 4.73 (d, 1 H, $^3J_{5\text{-H}/4\text{-H}}$ = 2.9 Hz, 5-H), 4.95-5.00 (m, 1 H, 3-H), 5.04 (d, 1 H, ^2J = 12.1 Hz, $CO_2C\underline{H}_2Ph^u$), 5.14 (d, 1 H, $^3J_{2\text{-H}/3\text{-H}}$ = 2.9 Hz, 2-H), 5.15 (d, 1 H, ^2J = 12.1 Hz, $CO_2C\underline{H}_2Ph^d$), 5.98 (br s, 1 H, 5-OH), 8.11 (s, 1 H, Thz-H).

5.4.84 (4*S*,5*S*)-5-((1*S*,2*S*)-2-(4-(methoxycarbonyl)thiazol-2-yl)-2-azido-1-hydroxyethyl)-2-ethoxy-1,3-dioxolane-4-carboxylic acid (245)

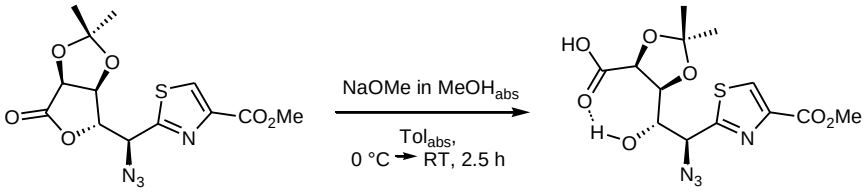

241 **245** M = 372.35

Preparation:

Compound **241**	M = 354.34 g mol^{-1}	1.0 eq	56.4 µmol	20 mg
NaOMe (30% in MeOH)	M = 54.02 g mol^{-1}, ρ = 0.95			6.2 µL (5.9 mg)
$MeOH_{abs}$				1.5 mL
Tol_{abs}				0.5 mL

20 mg of **241** (56.4 µmol, 1.0 eq) were dissolved in 1.5 mL of $MeOH_{abs}$ and 0.5 mL of Tol_{abs} in a nitrogen atmosphere and the solution was cooled to 0 °C. 6.2 µL of NaOMe (30% in MeOH, 5.9 mg) were added and the solution was stirred at 0 °C for 2.5 h. The mixture was subsequently neutralized with acidic ion exchange resin, filtered, and concentrated *in vacuo* to yield the carboxylic acid **245** as pale yellow powder. No isolated yield was determined as the highly polar product proved difficult to purify.

TLC: R_f = 0.00 (EtOAc/MeOH 5:1).

ESI-MS: m/z = 500 $[M-H]^-$.

HRMS: $[M-H]^-$: $C_{13}H_{15}N_4O_7S$, calculated: 371.0667, found: 371.0672.

^{1}H-NMR: 600 MHz, DMSO-d_6: δ = 1.33, 1.48 (each s, 3 H, Isopr-CH_3), 3.85 (s, 1 H, CO_2CH_3), 4.10-4.15 (m, 2 H, 2-H, 5-H), 4.61 (br s, 1 H, 4-H), 5.21 (dd, 1 H, ^3J = 6.6 Hz, ^3J = 8.9 Hz, 3-H), 6.41 (br s, 1 H, 3-OH), 8.60 (s, 1 H, Thz-H). CO_2H signal invisible.

^{13}C-NMR: 150 MHz, DMSO: δ = 25.5, 27.5 (each Isopr-CH_3), 52.1 ($CO_2\underline{C}H_3$), 63.9, 67.3 (C-2, C-5), 71.4 (C-3), 78.0 (C-4), 109.2 (Isopr-$C_{quart.}$), 130.4 (Thz-H$\underline{C}$=C), 145.8 (Thz-HC=$\underline{C}$), 160.6 ($\underline{C}O_2CH_3$), 162.5 (C-1), 173.5 (C-6).

5.4.85 2-[(3*S*,4*S*)-dihydroxy-5-oxo-tetrahydro-furan-(2*R*)-yl)-(1*S*)-azidomethyl]-1,3-thiazole-4-carboxylic acid methyl ester (246)

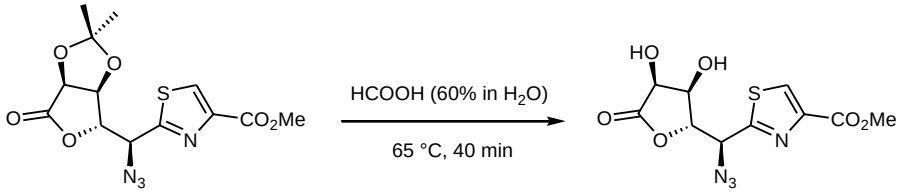

241 **246**
M = 314.27

Preparation:

Compound **241**	M = 354.34 g mol^{-1}	0.31 mmol	110 mg
HCOOH (60% in H_2O)			11 mL

110 mg of the acetonide **241** (0.31 mmol) were dissolved in 11 mL of HCOOH (60% in H_2O) and the solution was stirred for 40 min at 65 °C under regular control by TLC. Upon completion of the reaction the mixture was cooled to RT and the HCOOH/H_2O was removed under reduced pressure. Residual amounts of H_2O were removed by coevaporation with $CHCl_3$. Purification of the raw product by flash chromatography (EtOAc/MeOH 5:1) yielded 69% of the diol **246** (67 mg, 0.21 mmol) as grey solid.

TLC: R_f = 0.23 (EtOAc/MeOH 5:1).

ESI-MS: m/z = 337 $[M+Na]^+$.

HRMS: $[M+Na]^+$: $C_{10}H_{10}N_4O_6SNa$, calculated: 337.0213, found: 337.0207.

IR: pellet; $\tilde{\nu}$ = 3365, 3117, 2956, 2111, 1781, 1716, 1480, 1435, 1323, 1221, 1132, 1061, 979, 956, 922, 905, 863, 843, 757 cm^{-1}.

^{1}H-NMR: 400 MHz, DMSO-d_6: δ = 3.84 (s, 3 H, CO_2CH_3), 4.29 (dd, 1 H, $^3J_{4\text{-H}/3\text{-H}}$ = 1.2 Hz, $^3J_{4\text{-H}/5\text{-H}}$ = 5.5 Hz, 4-H), 4.57 (d, 1 H, $^3J_{5\text{-H}/4\text{-H}}$ = 5.5 Hz, 5-H), 4.60 (dd, 1 H, $^3J_{3\text{-H}/4\text{-H}}$ = 1.2 Hz, $^3J_{3\text{-H}/2\text{-H}}$ = 6.2 Hz, 3-H), 5.75 (d, 1 H, $^3J_{2\text{-H}/3\text{-H}}$ = 6.2 Hz, 2-H), 8.63 (s, 1 H, Thz-H). 4-OH and 5-OH signals are strongly broadened.

^{13}C-NMR: 100 MHz, DMSO-d_6: δ = 52.6 ($CO_2\underline{C}H_3$), 61.9 (C-2), 68.4 (C-5), 69.1 (C-4), 85.5 (C-3), 131.0 (Thz-H$\underline{C}$=C), 146.2 (Thz-HC=$\underline{C}$), 161.5 ($\underline{C}O_2CH_3$), 166.4 (C-1), 175.7 (C-6).

Opt. rotation: $[\alpha]_{589}^{21}$ = –98.8, $[\alpha]_{578}^{21}$ = –103.1, $[\alpha]_{546}^{21}$ = –117.7, $[\alpha]_{436}^{21}$ = –206.3, $[\alpha]_{365}^{21}$ = –335.3 (c = 0.60 g/100 mL $CHCl_3$).

5.4.86 2-((2S,3S,4S,5S)-3-hydroxy-4,5-*O*-isopropylidene-6-oxopiperidin-2-yl)-1,3-thiazole-4-carboxylic acid methyl ester (252)

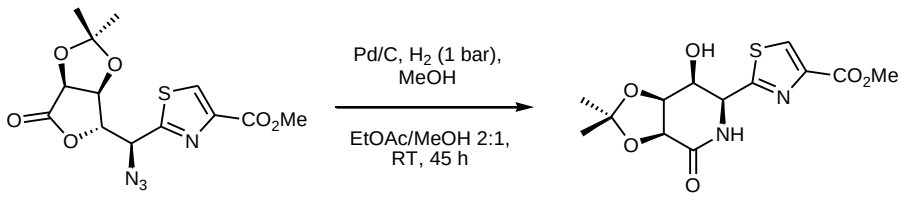

241 **252**
M = 328.34

Preparation:

Compound **241**	M = 354.34 g mol^{-1}	1.0 eq	0.57 mmol	203 mg
Pd/C (5%, wet, *Degussa*)				400 mg
EtOAc				10 mL
MeOH				5 mL

203 mg of the azide **241** (0.57 mmol, 1.0 eq) were dissolved in 10 mL of EtOAc and 5 mL of MeOH, 400 mg of Pd/C (5%, wet, *Degussa*) were added and the mixture was stirred at RT for 45 h in a H_2 atmosphere at 1 bar. During this time period the H_2 atmosphere was renewed two times. The mixture was filtered over a Celite column and concentrated *in vacuo*. Residual amounts of H_2O were removed by coevaporation with $CHCl_3$. This afforded 88% of the lactam **252** (165 mg, 0.50 mmol) as a pale yellow solid.

TLC: R_f = 0.36 ($CHCl_3$/MeOH 9:1).

ESI-MS: m/z = 351 $[M+Na]^+$.

HRMS: $[M+Na]^+$: $C_{13}H_{16}N_2O_6SNa$, calculated: 351.0621, found: 351.0621.

^{1}H-NMR: 600 MHz, DMSO-d_6: δ = 1.44 (s, 3 H, Isopr-CH_3^{proR}), 1.51 (s, 3 H, Isopr-CH_3^{proS}), 3.95 (CO_2CH_3), 4.36 (m, 1 H, 3-H), 4.64-4.65 (m, 2 H, 4-H, 5-H), 5.03 (m, 1 H, 2-H), 6.39 (br s, 1 H, CONH), 8.24 (s, 1 H, Thz-H). 3-OH invisible.

^{13}C-NMR: 150 MHz, DMSO-d_6: δ = 24.4 (Isopr-$\underline{C}H_3^{proR}$), 26.0 (Isopr-$\underline{C}H_3^{proS}$), 52.7 ($CO_2\underline{C}H_3$), 55.5 (C-2), 66.3 (C-3), 72.2 (C-5), 74.6 (C-4), 111.4 (Isopr-$C_{quart.}$), 129.3 (Thz-H$\underline{C}$=C), 146.4 (Thz-HC=$\underline{C}$), 161.5 ($\underline{C}O_2CH_3$), 167.4 (C-1), 168.8 (C-6).

5.4.87 2-((2*S*,3*S*,4*S*,5*S*)-3,4,5-trihydroxy-6-oxopiperidin-2-yl)-1,3-thiazole-4-carboxylic acid methyl ester (255) and 2-((1*S*,2*S*,3*S*,4*S*)-4-(methoxycarbonyl)-1-amino-2,3,4-trihydroxybutyl)-1,3-thiazole-4-carboxylic acid methyl ester (256)

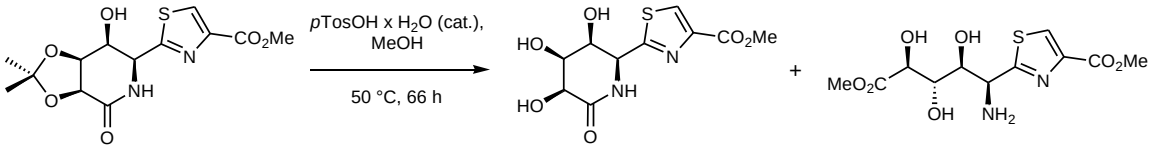

252 **255** M = 288.28 **256** M = 320.32

Preparation:

Compound **252**	M = 328.34 g mol^{-1}	1.0 eq	0.35 mmol	115 mg
*p*TosOH x H_2O	M = 190.22 g mol^{-1}			cat.
MeOH				15 mL

A solution of 115 mg of the acetonide **252** (0.35 mmol, 1.0 eq) in 15 mL MeOH was treated with a catalytic amount of *p*TosOH x H_2O and the solution was stirred for 7 h at 60 °C and overnight at RT. The mixture was neutralized with NEt_3 upon which the amine **256** precipitated. The solution was filtered and concentrated *in vacuo*, and the solid was dried *in vacuo* to afford 13% of the amine **256** (14.2 mg, 44.3 µmol) as colorless powder. The filtrate contained the starting material **252** and the triol **255** in a 60:40 ratio. This mixture was dissolved in 4 mL of MeOH together with a catalytic amount of *p*TosOH x H_2O and stirred at 50 °C for another 18 h. By neutralization with NEt_3 and subsequent filtration, additional 8.9% of the amine **256** (10.0 mg, 31.2 µmol) were isolated as colorless powder. This resulted in an overall 22% yield of **256** (24.2 mg, 75.5 µmol). The filtrated was concentrated *in vacuo* to afford a pale red oil which was identified as a 70:30 mixture of the triol **255** and starting material **252** and which was not further purified.

Compound **255***:*

TLC: R_f = 0.19 (EtOAc/MeOH 5:1).

ESI-MS: m/z = 311 $[M+Na]^+$.

HRMS: $[M+Na]^+$: $C_{10}H_{12}N_2O_6SNa$, calculated: 311.0308, found: 311.0312.

^{1}H-NMR: 300 MHz, DMSO-d_6: δ = 3.80-3.89 (m, 4 H, 4-H/5-H, CO_2CH_3), 3.97 (d, 1 H, ^3J = 3.8 Hz, 4-H/5-H), 4.21 (pt, 1 H, $^3J_{3\text{-H}/2\text{-H}}$ = 6.0 Hz, $^3J_{3\text{-H}/3\text{-OH}}$ = 6.0 Hz, 3-H), 4.91 (dd, 1 H, $^3J_{2\text{-H}/\text{CONH}}$ = 2.3 Hz, $^3J_{2\text{-H}/2\text{-OH}}$ = 6.0 Hz, 2-H), 5.14-5.20 (m, 2 H, 4-OH, 5-OH), 5.54 (d, 1 H, $^3J_{3\text{-OH}/3\text{-H}}$ = 6.0 Hz, 3-OH), 8.17 (d, 1 H, $^3J_{\text{CONH}/2\text{-H}}$ = 2.3 Hz, CONH), 8.48 (s, 1 H, Thz-H).

Compound **256***:*

TLC: R_f = 0.09 (EtOAc/MeOH 5:1).

ESI-MS: m/z = 343 $[M+Na]^+$.

HRMS: $[M+Na]^+$: $C_{11}H_{16}N_2O_7SNa$, calculated: 343.0570, found: 343.0570.

IR: pellet; $\tilde{\nu}$ = 3419, 3341, 3275, 3118, 1741, 1719, 1713, 1495, 1468, 1433, 1396, 1346, 1318, 1265, 1240, 1205, 1166, 1115, 1084, 1071, 1043, 995, 973, 946, 908, 871, 847, 827, 773 cm^{-1}.

^{1}H-NMR: 600 MHz, DMSO-d_6: δ = 2.28 (br s, 2 H, 2-NH_2), 3.61 (s, 3 H, 6-CO_2CH_3), 3.82 (m, 4 H, 4-H, Thz-CO_2CH_3), 4.21 (ddd, 1 H, ^3J = 1.6 Hz, $^3J_{3\text{-H}/3\text{-OH}}$ = 6.9 Hz, ^3J = 8.9 Hz, 3-H), 4.27-4.29 (m, 2 H, 2-H, 5-H), 4.82 (d, 1 H, $^3J_{3\text{-OH}/3\text{-H}}$ = 6.9 Hz, 3-OH), 5.26 (d, 1 H, $^3J_{4\text{-OH}/4\text{-H}}$ = 6.1 Hz, 4-OH), 5.41 (d, 1 H, $^3J_{5\text{-OH}/5\text{-H}}$ = 6.0 Hz, 5-OH), 8.35 (s, 1 H, Thz-H).

^{13}C-NMR: 150 MHz, DMSO-d_6: δ = 51.1 (6-$CO_2\underline{C}H_3$), 51.7 (Thz-$CO_2\underline{C}H_3$), 54.0 (C-2), 72.0 (C-5), 72.5 (C-3), 73.3 (C-4), 128.8 (Thz-H$\underline{C}$=C), 145.6 (Thz-HC=$\underline{C}$), 161.6 (Thz-$\underline{C}O_2CH_3$), 172.6 (C-6), 180.2 (C-1).

Melting point: 168 °C.

Opt. rotation: $[\alpha]_{589}^{30}$ = –42.3, $[\alpha]_{578}^{30}$ = –43.7, $[\alpha]_{546}^{30}$ = –50.4, $[\alpha]_{436}^{30}$ = –101.0, $[\alpha]_{365}^{30}$ = –172.5 (c = 0.37 g/100 mL DMSO).

5.4.88 2-((2*R*,3*S*)-3-(benzyloxycarbonyl)-1-oxo-2-hydroxy-3-(*tert*-butyl-dimethylsilyloxy)-propyl)-1,3-thiazole-4-carboxylic acid methyl ester (260)

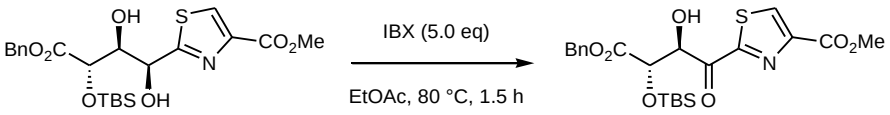

174 **260**
M = 479.62

Preparation:

Compound **174**	M = 481.63 g mol^{-1}	1.0 eq	2.12 mmol	1.02 g
IBX	M = 280.02 g mol^{-1}	5.0 eq	10.6 mmol	2.97 g
EtOAc				60 mL

To a solution of 1.02 g of the diol **174** (2.12 mmol, 1.0 eq) in 60 mL of EtAOc were added 2.97 g of IBX (10.6 mmol, 5.0 eq) and the suspension was refluxed at 80 °C for 1.5 h under vigorous stirring. After cooling to RT the suspension was filtered over Celite and concentrated *in vacuo*. Flash chromatographic purification (Tol/EtOAc 5:1→3:1) afforded 29% of the ketone **260** (294 mg, 0.61 mmol) as a pale yellow oil. Furthermore, 53% of the starting material **174** (543 mg, 1.13 mmol) were reisolated.

TLC: R_f = 0.59 (Tol/EtOAc 3:1).

ESI-MS: m/z = 502 $[M+Na]^+$.

HRMS: $[M+Na]^+$: $C_{22}H_{29}NO_7SSiNa$, calculated: 502.1326, found: 502.1325.

IR: pellet; $\tilde{\nu}$ = 3485, 3113, 2954, 2930, 2887, 2857, 1726, 1697, 1492, 1336, 1250, 1216, 1186, 1140, 990, 938, 864, 837, 779, 748, 697 cm^{-1}.

^{1}H-NMR: 600 MHz, $CDCl_3$: δ = 0.08, 0.12 (each s, 3 H, $SiCH_3$), 0.88 (s, 9 H, $SiC(CH_3)_3$), 3.92 (s, 3 H, CO_2CH_3), 4.00 (br s, 1 H, 3-OH), 5.12 (d, 1 H, ^2J = 12.1 Hz, $CO_2C\underline{H}_2Ph^u$), 5.15 (d, 1 H, $^3J_{4\text{-H}/3\text{-H}}$ = 2.5 Hz, 4-H), 5.22 (d, 1 H, ^2J = 12.1 Hz, $CO_2C\underline{H}_2Ph^d$), 5.42 (br s, 1 H, 3-H), 7.31-7.35 (m, 5 H, $CO_2CH_2\underline{Ph}$), 8.45 (s, 1 H, Thz-H).

^{13}C-NMR: 150 MHz, $CDCl_3$: δ = –5.3, –4.6 (each $SiCH_3$), 18.4 ($SiC(CH_3)_3$), 25.8 ($SiC(CH_3)_3$), 52.6 (CO_2CH_3), 67.5 (CO_2CH_2Ph), 76.0 (C-5), 78.4 (C-4), 128.5, 128.6, 128.7 (each Bn-$CH_{arom.}$), 133.7 (Thz-HC=C), 135.4 (Bn-$C_{arom., quart.}$), 148.6 (Thz-HC=C), 161.0 (CO_2CH_3), 164.5 (C-1), 170.2 (C-5), 189.9 (C-2).

Opt. rotation: $[\alpha]_{589}^{25}$ = –8.6, $[\alpha]_{578}^{25}$ = –9.0, $[\alpha]_{546}^{25}$ = –10.8, $[\alpha]_{436}^{25}$ = –23.9 (c = 1.00 g/100 mL $CHCl_3$).

5.4.89 2-((1*R*,2*R*,3*S*)-3-(benzyloxycarbonyl)-1,2-dihydroxy-3-(*tert*-butyl-dimethylsilyloxy)-propyl)-1,3-thiazole-4-carboxylic acid methyl ester (261)

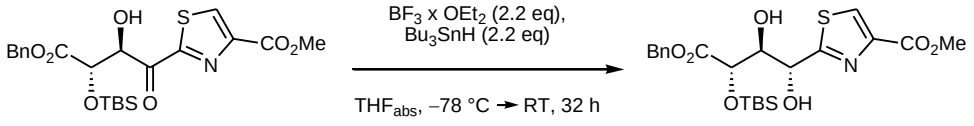

260 **261**
M = 481.63

Preparation:

Compound **260**	M = 479.62 g mol^{-1}	1.0 eq	0.60 mmol	290 mg
BF_3 x OEt_2	M = 141.93 g mol^{-1}, ρ = 1.15	2.2 eq	1.32 mmol	163 µL (187 mg)
Bu_3SnH	M = 291.02 g mol^{-1}, ρ = 1.09	2.2 eq	1.32 mmol	352 µL (384 mg)
Tol_{abs}				20 mL

290 mg of the ketone **260** (0.60 mmol, 1.0 eq) were dissolved in 20 mL of Tol_{abs} in a nitrogen atmosphere and cooled to –78 °C. 89.5 µL of BF_3 x OEt_2 (103 mg, 0.73 mmol, 1.2 eq) were added dropwise and, after 7 min, 194 µL of Bu_3SnH (211 mg, 0.73 mmol, 1.2 eq) were added. The solution was allowed to warm to 0 °C overnight under stirring. After 12 h, additional 73.5 µL of BF_3 x OEt_2 (84 mg, 0.60 mmol, 1.0 eq) and, after 7 min, additional 158 µL of Bu_3SnH (173 mg, 0.60 mmol, 1.0 eq) were added. The solution was allowed to warm to RT and stirred for additional 20 h. The reaction was subsequently quenched with 5% aq. $NaHCO_3$ (15 mL) and vigorously stirred for 4 h. The mixture was extracted three times with EtOAc, the combined organic phases were dried with brine and over $MgSO_4$, filtered, and concentrated *in vacuo*. The raw product was subjected to flash chromatographic purification (Tol/EtOAc 4:1→2:1) which yielded 75% of the diol **261** (219 mg, 0.45 mmol) as a colorless oil.

TLC: R_f = 0.21 (Tol/EtOAc 3:1).

ESI-MS: m/z = 504 $[M+Na]^+$.

HRMS: $[M+Na]^+$: $C_{22}H_{31}NO_7SSiNa$, calculated: 504.1483, found: 504.1484.

IR: film; $\tilde{\nu}$ = 3446, 3118, 2953, 2928, 2895, 2856, 1724, 1486, 1461, 1435, 1388, 1346, 1326, 1248, 1214, 1145, 1099, 1072, 991, 837, 780, 751, 697 cm^{-1}.

^{1}H-NMR: 400 MHz, DMSO-d_6: δ = 0.00, 0.08 (each s, 3 H, $SiCH_3$), 0.83 (s, 9 H, $SiC(CH_3)_3$), 3.81 (s, 3 H, CO_2CH_3), 4.06 (ddd, 1 H, $^3J_{3\text{-H}/2\text{-H}}$ = 4.2 Hz, $^3J_{3\text{-H}/3\text{-OH}}$ = 5.7 Hz, $^3J_{3\text{-H}/4\text{-H}}$ = 6.8 Hz, 3-H), 4.35 (d, 1 H, $^3J_{4\text{-H}/3\text{-H}}$ = 6.8 Hz, 4-H), 4.99 (dd, 1 H, $^3J_{2\text{-H}/3\text{-H}}$ = 4.2 Hz, $^3J_{2\text{-H}/2\text{-OH}}$ = 5.0 Hz, 2-H), 5.10 (s, 2 H, $CO_2C\underline{H}_2Ph$), 5.62 (d, 1 H, $^3J_{3\text{-OH}/3\text{-H}}$ = 5.7 Hz, 3-OH), 6.48 (d, 1 H, $^3J_{2\text{-OH}/2\text{-H}}$ = 5.0 Hz, 2-OH), 7.32-7.41 (m, 5 H, $CO_2CH_2\underline{Ph}$), 8.47 (s, 1 H, Thz-H).

^{13}C-NMR: 100 MHz, DMSO-d_6: δ = −5.3, −5.2 (each $SiCH_3$), 17.9 ($Si\underline{C}(CH_3)_3$), 25.6 ($SiC(\underline{C}H_3)_3$), 51.8 ($CO_2\underline{C}H_3$), 65.7 ($CO_2\underline{C}H_2Ph$), 70.3 (C-2), 73.3 (C-4), 75.6 (C-3), 128.0, 128.1, 128.3 (each Bn-$CH_{arom.}$), 129.2 (Thz-H$\underline{C}$=C), 135.8 (Bn-$C_{arom.,\ quart.}$), 145.0 (Thz-HC=$\underline{C}$), 161.4 ($\underline{C}O_2CH_3$), 171.3 (C-5), 174.4 (C-1).

Opt. rotation: $[\alpha]_{589}^{24}$ = +16.0, $[\alpha]_{578}^{24}$ = +17.4, $[\alpha]_{546}^{24}$ = +20.4, $[\alpha]_{436}^{24}$ = +36.5, $[\alpha]_{365}^{24}$ = +59.6 (c = 0.48 g/100 mL $CHCl_3$).

5.4.90 2-((1*R*,2*R*,3*S*)-3-(benzyloxycarbonyl)-1-methanesulfonyloxy-2-hydroxy-3-(*tert*-butyl-dimethylsilyloxy)-propyl)-1,3-thiazole-4-carboxylic acid methyl ester (262)

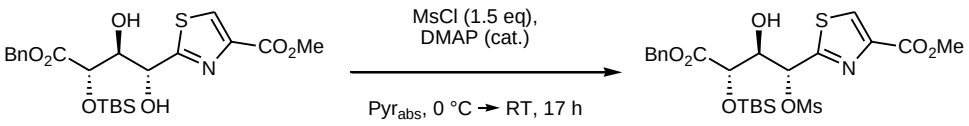

261 **262**
M = 559.72

Preparation:

Compound **261**	M = 481.63 g mol^{-1}	1.0 eq	405 µmol	195 mg
MsCl	M = 114.55 g mol^{-1}, ρ = 1.48	1.5 eq	608 µmol	47.0 µL (69.9 mg)
DMAP	M = 122.17 g mol^{-1}			cat.
Pyr_{abs}				6.0 mL

195 mg of the diol **261** (405 µmol, 1.0 eq) were dissolved in 6.0 mL of Pyr_{abs} in a nitrogen atmosphere and cooled to 0 °C. A catalytical amount of DMAP and 31.3 µL of MsCl (46.4 mg, 405 µmol, 1.0 eq) were added and the solution was allowed to warm to RT under stirring. After 14 h, the solution was cooled to 0 °C and another 15.7 µmol of MsCl (23.5 mg, 203 µmol, 0.5 eq) were added. The solution was allowed to warm to RT and stirred for another 3 h. The reaction was diluted with CH_2Cl_2, quenched with ice, and the phases were separated. The aqueous phase was extracted two times with CH_2Cl_2. The combined organic phases were dried with brine and over $MgSO_4$, filtered, and concentrated *in vacuo*. Flash chromatographic purification (Tol/EtOAc 5:1) afforded 73% of the mesylate **262** (165 mg, 295 µmol) as a colorless oil.

TLC: R_f = 0.23 (CH_2Cl_2/MeOH 35:1).

ESI-MS: m/z = 582 $[M+Na]^+$.

HRMS: $[M+Na]^+$: $C_{23}H_{33}NO_9S_2SiNa$, calculated: 582.1258, found: 582.1267.

IR: film; $\tilde{\nu}$ = 3463, 2954, 2930, 2857, 1727, 1462, 1435, 1412, 1361, 1249, 1216, 1175, 1099, 956, 836, 781, 751, 697 cm^{-1}.

^{1}H-NMR: 600 MHz, DMSO-d_6: δ = –0.05, 0.05 (each s, 3 H, $SiCH_3$), 0.84 (s, 9 H, $SiC(CH_3)_3$), 3.16 (s, 3 H, Ms-CH_3), 3.84 (s, 3 H, CO_2CH_3), 4.16 (d, 1 H, $^3J_{4\text{-H}/3\text{-H}}$ = 6.2 Hz, 4-H), 4.38 (m, 1 H, 3-H), 5.11 (d, 1 H, ^2J = 12.3 Hz, $CO_2C\underline{H}_2Ph^u$), 5.18 (d, 1 H, ^2J = 12.3 Hz, $CO_2C\underline{H}_2Ph^d$), 5.87 (d, 1 H, $^3J_{2\text{-H}/3\text{-H}}$ = 4.8 Hz, 2-H), 6.40 (d, 1 H, $^3J_{3\text{-OH}/3\text{-H}}$ = 6.0 Hz, 3-OH), 7.35-7.42 (m, 5 H, $CO_2CH_2\underline{Ph}$), 8.65 (s, 1 H, Thz-H).

^{13}C-NMR: 150 MHz, DMSO-d_6: δ = −5.6, −5.4 (each $SiCH_3$), 17.8 ($SiC(CH_3)_3$), 25.5 ($SiC(CH_3)_3$), 38.3 (Ms-CH_3), 52.1 (CO_2CH_3), 66.3 (CO_2CH_2Ph), 73.4 (C-4), 73.5 (C-3), 77.7 (C-2), 128.2, 128.3, 128.4 (each Bn-$CH_{arom.}$), 131.2 (Thz-HC=C), 135.4 (Bn-$C_{arom., quart.}$), 145.2 (Thz-HC=C), 161.0 (CO_2CH_3), 165.0 (C-1), 170.5 (C-5).

Opt. rotation: $[\alpha]_{589}^{22}$ = +26.5, $[\alpha]_{578}^{22}$ = +27.7, $[\alpha]_{546}^{22}$ = +31.7, $[\alpha]_{436}^{22}$ = +56.6
(c = 2.38 g/100 mL $CHCl_3$).

RT (HPLC): 22.05 min (linear gradient of 0 to 60% A over 10 min→60 to 99% A over 15 min, A = CH_3CN, B = 0.08% TFA/H_2O).

5.4.91 2-((1*R*,2*R*,3*S*)-3-(benzyloxycarbonyl)-1,2-dimethanesulfonyloxy-3-(*tert*-butyl-dimethylsilyloxy)-propyl)-1,3-thiazole-4-carboxylic acid methyl ester (263)

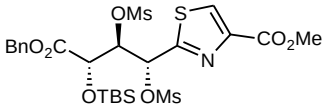

263
M = 637.82

The dimesylate **263** was obtained as byproduct in the mesylation reaction of the diol **261** (section 5.4.89). The flash chromatographic purification (Tol/EtOAc 5:1) afforded 25% of **263** (64 mg, 100 µmol) as a colorless oil.

TLC: R_f = 0.51 (CH_2Cl_2/MeOH 35:1).

ESI-MS: m/z = 660 $[M+Na]^+$.

HRMS: $[M+Na]^+$: $C_{24}H_{35}NO_{11}S_3SiNa$, calculated: 660.1034, found: 660.1041.

IR: film; $\tilde{\nu}$ = 3033, 2954, 2933, 2894, 2858, 1728, 1472, 1362, 1251, 1215, 1176, 1107, 955, 836, 799, 782, 754, 720, 698 cm^{-1}.

^{1}H-NMR: 600 MHz, DMSO-d_6: δ = 0.03, 0.09 (each s, 3 H, $SiCH_3$), 0.85 (s, 9 H, $SiC(CH_3)_3$), 3.03, 3.22 (each s, 3 H, Ms-CH_3), 3.85 (s, 3 H, CO_2CH_3), 4.80 (d, 1 H, $^{3}J_{4\text{-H}/3\text{-H}}$ = 3.4 Hz, 4-H), 5.15 (d, 1 H, ^{2}J = 12.1 Hz, $CO_2C\underline{H}_2Ph^{u}$), 5.23 (d, 1 H, ^{2}J = 12.1 Hz, $CO_2C\underline{H}_2Ph^{d}$), 5.46 (dd, 1 H, $^{3}J_{3\text{-H}/4\text{-H}}$ = 3.4 Hz, $^{3}J_{3\text{-H}/2\text{-H}}$ = 7.0 Hz, 3-H), 6.09 (d, 1 H, $^{3}J_{2\text{-H}/3\text{-H}}$ = 7.0 Hz, 2-H), 7.36-7.46 (m, 5 H, $CO_2CH_2\underline{Ph}$), 8.71 (s, 1 H, Thz-H).

^{13}C-NMR: 150 MHz, DMSO-d_6: δ = −5.6, −5.3 (each $SiCH_3$), 17.9 ($Si\underline{C}(CH_3)_3$), 25.4 ($SiC(\underline{C}H_3)_3$), 38.1, 38.2 (each Ms-$\underline{C}H_3$), 52.2 ($CO_2\underline{C}H_3$), 67.1 ($CO_2\underline{C}H_2Ph$), 72.0 (C-4), 73.6 (C-2), 80.6 (C-3), 128.4, 128.5, 128.5 (each Bn-$CH_{arom.}$), 131.8 (Thz-H$\underline{C}$=C), 135.1 (Bn-$C_{arom., quart.}$), 145.6 (Thz-HC=$\underline{C}$), 160.8 ($\underline{C}O_2CH_3$), 164.1 (C-1), 168.8 (C-5).

Opt. rotation: $[\alpha]_{589}^{23}$ = +30.1, $[\alpha]_{578}^{23}$ = +31.4, $[\alpha]_{546}^{23}$ = +35.9, $[\alpha]_{436}^{23}$ = +63.9, $[\alpha]_{365}^{23}$ = +104.7 (c = 2.00 g/100 mL $CHCl_3$).

RT (HPLC): 22.91 min (linear gradient of 0 to 60% A over 10 min→60 to 99% A over 15 min, A = CH_3CN, B = 0.08% TFA/H_2O).

5.4.92 2-((1*S*,2*R*,3*S*)-3-(benzyloxycarbonyl)-1-methanesulfonyloxy-2-hydroxy-3-(*tert*-butyl-dimethylsilyloxy)-propyl)-1,3-thiazole-4-carboxylic acid methyl ester (264)

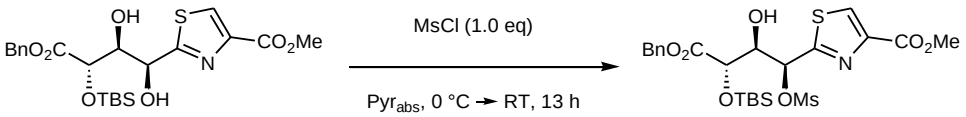

174 **264** M = 559.72

Preparation:

Compound **174**	M = 481.63 g mol^{-1}	1.0 eq	2.05 mmol	988 mg
MsCl	M = 114.55 g mol^{-1}, ρ = 1.48	1.0 eq	2.05 mmol	159 µL (235 mg)
Pyr_{abs}				40 mL

988 mg of the diol **174** (2.05 mmol, 1.0 eq) were dissolved in 40 mL of Pyr_{abs} in a nitrogen atmosphere and cooled to 0 °C. 159 µL of MsCl (235 mg, 2.05 mmol, 1.0 eq) were added and the solution was allowed to warm to RT under stirring. After 13 h the reaction was diluted with CH_2Cl_2, quenched with ice, and the phases were separated. The aqueous phase was extracted three times with CH_2Cl_2. The combined organic phases were dried with brine and over $MgSO_4$, filtered, and concentrated *in vacuo*. Flash chromatographic purification (Tol/EtOAc 5:1→4:1) afforded 48% of the mesylate **264** (547 mg, 0.98 mmol) as a colorless oil. In addition, 23% of the starting material **174** (225 mg, 0.47 mmol) were reisolated.

TLC: R_f = 0.53 (CH_2Cl_2/MeOH 35:1).

ESI-MS: m/z = 582 $[M+Na]^+$.

HRMS: $[M+Na]^+$: $C_{23}H_{33}NO_9S_2SiNa$, calculated: 582.1258, found: 582.1263.

IR: film; $\tilde{\nu}$ = 3472, 2953, 2931, 2857, 1725, 1472, 1435, 1359, 1250, 1217, 1174, 1120, 987, 963, 910, 836, 780, 752, 697 cm^{-1}.

^{1}H-NMR: 600 MHz, DMSO-d_6: δ = –0.04, 0.05 (each s, 3 H, $SiCH_3$), 0.84 (s, 9 H, $SiC(CH_3)_3$), 3.15 (s, 3 H, Ms-CH_3), 3.83 (s, 3 H, CO_2CH_3), 4.16 (ddd, 1 H, $^3J_{3\text{-H}/2\text{-H}}$ = 4.4 Hz, $^3J_{3\text{-H}/4\text{-H}}$ = 6.0 Hz, $^3J_{3\text{-H}/3\text{-OH}}$ = 7.0 Hz, 3-H), 4.32 (d, 1 H, $^3J_{4\text{-H}/3\text{-H}}$ = 6.0 Hz, 4-H), 5.02 (d, 1 H, ^2J = 12.3 Hz, $CO_2C\underline{H}_2Ph^u$), 5.07 (d, 1 H, ^2J = 12.3 Hz, $CO_2C\underline{H}_2Ph^d$), 5.86 (d, 1 H, $^3J_{2\text{-H}/3\text{-H}}$ = 4.4 Hz, 2-H), 6.39 (d, 1 H, $^3J_{3\text{-OH}/3\text{-H}}$ = 7.0 Hz, 3-OH), 7.36-7.41 (m, 5 H, $CO_2CH_2\underline{Ph}$), 8.66 (s, 1 H, Thz-H).

^{13}C-NMR: 150 MHz, DMSO-d_6: δ = –5.4, –5.3 (each $SiCH_3$), 17.8 ($Si\underline{C}(CH_3)_3$), 25.5 ($SiC(\underline{C}H_3)_3$), 38.7 (Ms-$\underline{C}H_3$), 52.1 ($CO_2\underline{C}H_3$), 66.3 ($CO_2\underline{C}H_2Ph$), 73.2 (C-4), 74.0 (C-3), 77.6 (C-2), 128.1, 128.3, 128.4 (each Bn-$CH_{arom.}$), 131.3 (Thz-H$\underline{C}$=C), 135.4 (Bn-$C_{arom.,\ quart.}$), 145.5 (Thz-HC=$\underline{C}$), 161.0 ($\underline{C}O_2CH_3$), 165.5 (C-1), 170.3 (C-5).

Opt. rotation: $[\alpha]_{589}^{18}$ = –42.4, $[\alpha]_{578}^{18}$ = –44.3, $[\alpha]_{546}^{18}$ = –50.6, $[\alpha]_{436}^{18}$ = –88.9, $[\alpha]_{365}^{18}$ = –142.0 (c = 1.04 g/100 mL $CHCl_3$).

RT (HPLC): 21.85 min (linear gradient of 0 to 60% A over 10 min→60 to 99% A over 15 min, A = CH_3CN, B = 0.08% TFA/H_2O).

5.4.93 2-((1*S*,2*R*,3*S*)-3-(benzyloxycarbonyl)-1,2-dimethanesulfonyloxy-3-(*tert*-butyl-dimethylsilyloxy)-propyl)-1,3-thiazole-4-carboxylic acid methyl ester (265)

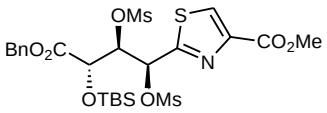

265
M = 637.82

The dimesylate **265** was obtained as byproduct in the mesylation reaction of the diol **174** (section 5.4.92). The flash chromatographic purification (Tol/EtOAc 5:1→4:1) afforded 20% of **265** (258 mg, 0.40 mmol) as a colorless oil.

TLC: R_f = 0.68 (CH_2Cl_2/MeOH 35:1).

ESI-MS: m/z = 660 $[M+Na]^+$.

HRMS: $[M+Na]^+$: $C_{24}H_{35}NO_{11}S_3SiNa$, calculated: 660.1034, found: 660.1040.

IR: film; $\tilde{\nu}$ = 3033, 2954, 2933, 2887, 2858, 1760, 1725, 1471, 1361, 1250, 1217, 1175, 1104, 952, 833, 782, 751, 698 cm^{-1}.

^{1}H-NMR: 500 MHz, DMSO-d_6: δ = –0.04, 0.03 (each s, 3 H, $SiCH_3$), 0.86 (s, 9 H, $SiC(CH_3)_3$), 3.19, 3.32 (each s, 3 H, Ms-CH_3), 3.81 (s, 3 H, CO_2CH_3), 4.72 (d, 1 H, $^3J_{4\text{-H}/3\text{-H}}$ = 1.6 Hz, 4-H), 4.96 (d, 1 H, ^2J = 12.2 Hz, $CO_2C\underline{H}_2Ph^u$), 5.01 (d, 1 H, ^2J = 12.2 Hz, $CO_2C\underline{H}_2Ph^d$), 5.50 (dd, 1 H, $^3J_{3\text{-H}/4\text{-H}}$ = 1.6 Hz, $^3J_{3\text{-H}/2\text{-H}}$ = 8.9 Hz, 3-H), 6.02 (d, 1 H, $^3J_{2\text{-H}/3\text{-H}}$ = 8.9 Hz, 2-H), 7.35-7.39 (m, 5 H, $CO_2CH_2\underline{Ph}$), 8.74 (s, 1 H, Thz-H).

^{13}C-NMR: 125 MHz, DMSO-d_6: δ = –5.9, –5.5 (each $SiCH_3$), 17.8 ($Si\underline{C}(CH_3)_3$), 25.4 ($SiC(\underline{C}H_3)_3$), 38.5, 38.8 (each Ms-$\underline{C}H_3$), 52.2 ($CO_2\underline{C}H_3$), 67.0 ($CO_2\underline{C}H_2Ph$), 72.2 (C-4), 73.8 (C-2), 82.0 (C-3), 128.3, 128.3, 128.4 (each Bn-$CH_{arom.}$), 132.4 (Thz-H$\underline{C}$=C), 135.0 (Bn-$C_{arom., quart.}$), 146.2 (Thz-HC=$\underline{C}$), 160.7 ($\underline{C}O_2CH_3$), 161.7 (C-1), 167.9 (C-5).

Opt. rotation: $[\alpha]_{589}^{21}$ = –32.2, $[\alpha]_{578}^{21}$ = –33.6, $[\alpha]_{546}^{21}$ = –38.2, $[\alpha]_{436}^{21}$ = –64.9 (c = 1.92 g/100 mL $CHCl_3$).

RT (HPLC): 22.76 min (linear gradient of 0 to 60% A over 10 min→60 to 99% A over 15 min, A = CH_3CN, B = 0.08% TFA/H_2O).

5.4.94 2-((1*S*,2*R*,3*S*)-3-(benzyloxycarbonyl)-1-hydroxy-2-methanesulfonyloxy-3-(*tert*-butyl-dimethylsilyloxy)-propyl)-1,3-thiazole-4-carboxylic acid methyl ester (266)

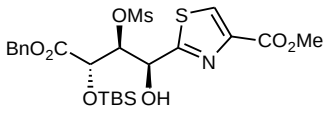

266
M = 559.72

The mesylate **266** was obtained as byproduct (13% isolated yield, colorless oil) in the mesylation reaction of the diol **174** (section 5.4.92) if the MsCl was added in small portions chosen over a long period of time (table 4.18, section 4.4.9.3).

TLC: R_f = 0.60 (CH_2Cl_2/MeOH 35:1).

ESI-MS: *m*/*z* = 582 $[M+Na]^+$.

HRMS: $[M+Na]^+$: $C_{23}H_{33}NO_9S_2SiNa$, calculated: 582.1258, found: 582.1260.

IR: film; $\tilde{\nu}$ = 3459, 2953, 2931, 2858, 1726, 1498, 1472, 1349, 1250, 1216, 1174, 1127, 1099, 959, 922, 836, 781, 751, 697 cm^{-1}.

^{1}H-NMR: 600 MHz, DMSO-d_6: δ = –0.04, 0.00 (each s, 3 H, $SiCH_3$), 0.81 (s, 9 H, $SiC(CH_3)_3$), 2.97 (s, 3 H, Ms-CH_3), 3.82 (s, 3 H, CO_2CH_3), 4.86 (d, 1 H, $^3J_{4\text{-H}/3\text{-H}}$ = 4.3 Hz, 4-H), 4.96 (dd, 1 H, $^3J_{3\text{-H}/4\text{-H}}$ = 4.3 Hz, $^3J_{3\text{-H}/2\text{-H}}$ = 6.1 Hz, 3-H), 5.06 (d, 1 H, ^2J = 12.3 Hz, $CO_2C\underline{H}_2Ph^u$), 5.12 (d, 1 H, ^2J = 12.3 Hz, $CO_2C\underline{H}_2Ph^d$), 5.21 (pt, 1 H, $^3J_{2\text{-H}/3\text{-H}}$ = 6.1 Hz, $^3J_{2\text{-H}/2\text{-OH}}$ = 6.1 Hz, 2-H), 7.03 (d, 1 H, $^3J_{2\text{-OH}/2\text{-H}}$ = 6.1 Hz, 2-OH), 7.36-7.41 (m, 5 H, $CO_2CH_2\underline{Ph}$), 8.55 (s, 1 H, Thz-H).

^{13}C-NMR: 150 MHz, DMSO-d_6: δ = –5.8, –5.5 (each $SiCH_3$), 17.8 ($SiC(CH_3)_3$), 25.3 ($SiC(CH_3)_3$), 38.4 (Ms-CH_3), 52.0 (CO_2CH_3), 66.7 (CO_2CH_2Ph), 67.9 (C-2), 71.6 (C-4), 84.6 (C-3), 128.2, 128.3, 128.4 (each Bn-$CH_{arom.}$), 130.0 (Thz-HC=C), 135.3 (Bn-$C_{arom., quart.}$), 145.8 (Thz-HC=C), 161.1 (CO_2CH_3), 169.2 (C-5), 172.1 (C-1).

Opt. rotation: $[\alpha]_{589}^{18}$ = –38.8, $[\alpha]_{578}^{18}$ = –40.4, $[\alpha]_{546}^{18}$ = –45.8, $[\alpha]_{436}^{18}$ = –75.9, $[\alpha]_{365}^{18}$ = –111.4 (c = 1.46 g/100 mL $CHCl_3$).

5.4.95 2-((*S*)-4-(tert-butyl-dimethylsilyl)-2,5-dihydro-5-oxofuran-2-yl)thiazole-4-carboxylic acid methyl ester (267)

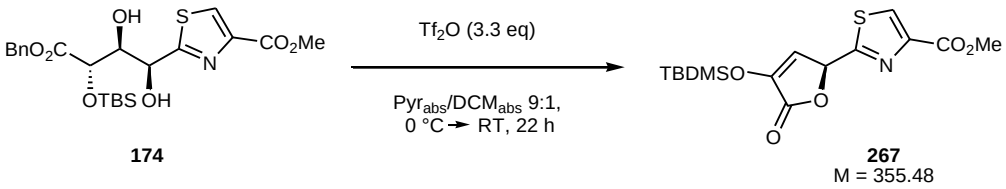

Preparation:

Compound **174**	M = 481.63 g mol^{-1}	1.0 eq	66.4 µmol	32 mg
Tf_2O	M = 282.13 g mol^{-1}, ρ = 1.68	3.3 eq	219 µmol	36.6 µL (61.8 mg)
$CH_2Cl_{2\ abs}$				0.9 mL
DMF_{abs}				0.1 mL

32 mg of the diol **174** (66.4 µmol, 1.0 eq) were dissolved in 0.9 mL of $CH_2Cl_{2\ abs}$ and 0.1 mL of Pyr_{abs} under a nitrogen atmosphere and cooled to 0 °C. 12.2 µL of Tf_2O (20.6 mg, 1.1 eq, 73.0 µmol) were slowly added, the solution was stirred for 1 h at 0 °C and for another 12 h at RT. The reaction was subsequently cooled to 0 °C and additional 24.4 µmol of Tf_2O (41.2 mg, 2.2 eq, 146 µmol) were slowly added. The reaction was allowed to warm to RT and stirred for another 9 h. The solvents were removed under reduced pressure and to the residue were added CH_2Cl_2 and 5% aq. $NaHCO_3$, the phases were separated and the aqueous phase was extracted once with CH_2Cl_2. The combined organic phases were dried with brine and over $MgSO_4$, filtered and concentrated *in vacuo*. Purification by flash chromatography (Tol/EtOAc 5:1) yielded 30% (7.1 mg, 20.0 µmol) of the butenolide **267** as a colorless oil.

TLC: R_f = 0.41 (Tol/EtOAc 3:1).

ESI-MS: m/z = 378 $[M+Na]^+$.

HRMS: $[M+Na]^+$: $C_{15}H_{21}NO_5SSiNa$, calculated: 378.0802, found: 378.0807.

IR: film; $\tilde{\nu}$ = 3115, 3033, 2955, 2935, 2859, 1783, 1727, 1651, 1472, 1345, 1239, 1215, 1174, 1098, 1054, 989, 954, 868, 839, 783, 753, 698 cm^{-1}.

^{1}H-NMR: 500 MHz, DMSO-d_6: δ = 0.25, 0.26 (each s, 3 H, $SiCH_3$), 0.97 (s, 9 H, $SiC(CH_3)_3$), 3.97 (s, 3 H, CO_2CH_3), 6.21 (d, 1 H, $^3J_{2\text{-H}/3\text{-H}}$ = 2.3 Hz, 2-H), 6.52 (d, 1 H, $^3J_{3\text{-H}/2\text{-H}}$ = 2.3 Hz, 3-H), 8.21 (s, 1 H, Thz-H).

^{13}C-NMR: 125 MHz, DMSO-d_6: δ = −5.5, −5.5 (each $SiCH_3$), 17.6 ($SiC(CH_3)_3$), 25.2 ($SiC(CH_3)_3$), 51.7 (CO_2CH_3), 62.3 (C-2), 66.1 (CO_2CH_2Ph), 73.4, 73.7 (C-3, C-4), 127.9, 128.0, 128.1 (each Bn-$CH_{arom.}$), 130.4 (Thz-HC=C), 135.5 (Bn-$C_{arom.,\ quart.}$), 145.0 (Thz-HC=C), 160.9 (CO_2CH_3), 165.9 (C-1), 170.4 (C-5).

Opt. rotation: $[\alpha]_{589}^{18}$ = +6.0, $[\alpha]_{578}^{18}$ =+6.6, $[\alpha]_{546}^{18}$ = +7.5, $[\alpha]_{436}^{18}$ = +14.5, $[\alpha]_{365}^{18}$ = +26.7 (c = 0.32 g/100 mL $CHCl_3$).

5.4.96 2-((1*R*,2*S*,3*S*)-3-(benzyloxycarbonyl)-1-azido-2-hydroxy-3-(*tert*-butyl-dimethylsilyloxy)-propyl)-1,3-thiazole-4-carboxylic acid methyl ester (268)

Method A) azidation of **262** *under stereoinversion*

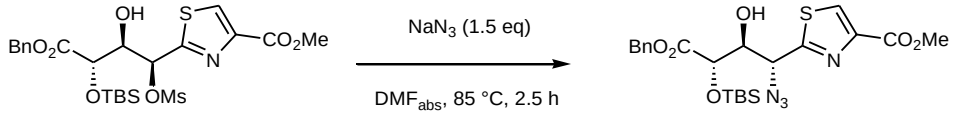

262 **268**
M = 506.65

Preparation:

Compound **262**	M = 559.72 g mol^{-1}	1.0 eq	39.3 µmol	22 mg
NaN_3	M = 65.01 g mol^{-1}	1.5 eq	59.0 mmol	3.8 mg
DMF_{abs}				0.4 mL

22 mg of the mesylate **262** (1.0 eq, 39.3 µmol) and 3.8 mg of NaN_3 (1.5 eq, 59.0 µmol) were dissolved in 0.4 mL of DMF_{abs} in a nitrogen atmosphere. The mixture was stirred for 2.5 h at 85 °C (TLC/HPLC control). The solution was allowed to cool to RT and the DMF was removed *in vacuo*. To the resulting colorless residue were added CH_2Cl_2 and H_2O, the phases were separated and the aqueous phase was extracted two times with CH_2Cl_2. The combined organic phases were dried with brine and over $MgSO_4$, filtered, and concentrated *in vacuo*. Flash chromatography (Tol/EtOAc 6:1) yielded 10% (2.42 mg, 4.78 µmol) of the azide **268** as a colorless oil.

Method B) azidation of **264** *under stereoretention*

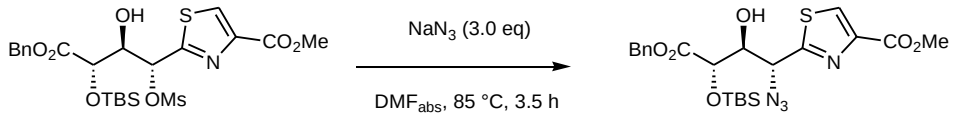

264 **268**
M = 506.65

Preparation:

Compound **264**	M = 559.72 g mol^{-1}	1.0 eq	60.7 µmol	34 mg
NaN_3	M = 65.01 g mol^{-1}	1.5 eq	91.1 µmol	5.9 mg
DMF_{abs}				1.0 mL

34 mg of the mesylate **264** (1.0 eq, 60.7 µmol) and 5.9 mg of NaN_3 (1.5 eq, 91.1 µmol) were dissolved in 1.0 mL of DMF_{abs} in a nitrogen atmosphere. The mixture was stirred for 2.5 h at 85 °C (HPLC control), allowed to cool to RT, and additional 5.9 mg of NaN_3 (1.5 eq, 91.1 µmol) were added. The solution was stirred for another 1 h at 85 °C, allowed to cool to RT and concentrated *in vacuo*. To the resulting colorless residue were added CH_2Cl_2 and H_2O, the phases were separated and the aqueous phase was extracted two times with CH_2Cl_2. The combined organic phases were dried with brine and over $MgSO_4$, filtered, and concentrated *in vacuo* to obtain 17 mg of a 75:25 mixture of the azides **268** and **269** as a pale yellow oil. The raw product was directly subjected to TBS deprotection (sections 5.4.103 and 5.4.104).

TLC: R_f = 0.58 (Tol/EtOAc 3:1).

ESI-MS: m/z = 529 $[M+Na]^+$.

HRMS: $[M+Na]^+$: $C_{22}H_{30}N_4O_6SSiNa$, calculated: 529.1548, found: 529.1554.

^{1}H-NMR: 500 MHz, DMSO-d_6: δ = −0.05, 0.00 (each s, 3 H, $SiCH_3$), 0.82 (s, 9 H, $SiC(CH_3)_3$), 3.83 (s, 3 H, CO_2CH_3), 4.24-4.27 (m, 2 H, 3-H, 4-H), 5.03 (d, 1 H, $^3J_{2\text{-H}/3\text{-H}}$ = 5.4 Hz, 2-H), 5.15 (s, 2 H, $CO_2C\underline{H}_2Ph$), 6.26 (d, 1 H, $^3J_{2\text{-OH}/2\text{-H}}$ = 5.6 Hz, 3-OH), 7.33-7.41 (m, 5 H, $CO_2CH_2\underline{Ph}$), 8.58 (s, 1 H, Thz-H).

^{13}C-NMR: 125 MHz, DMSO-d_6: δ = −5.5, −5.5 (each $SiCH_3$), 17.6 ($Si\underline{C}(CH_3)_3$), 25.2 ($SiC(\underline{C}H_3)_3$), 51.7 ($CO_2\underline{C}H_3$), 62.3 (C-2), 66.1 ($CO_2\underline{C}H_2Ph$), 73.4, 73.7 (C-3, C-4), 127.9, 128.0, 128.1 (each Bn-$CH_{arom.}$), 130.4 (Thz-H$\underline{C}$=C), 135.5 (Bn-$C_{arom.,\ quart.}$), 145.0 (Thz-HC=$\underline{C}$), 160.9 ($\underline{C}O_2CH_3$), 165.9 (C-1), 170.4 (C-5).

Opt. rotation: $[\alpha]_{589}^{18}$ = +6.0, $[\alpha]_{578}^{18}$ =+6.6, $[\alpha]_{546}^{18}$ = +7.5, $[\alpha]_{436}^{18}$ = +14.5, $[\alpha]_{365}^{18}$ = +26.7 (c = 0.32 g/100 mL $CHCl_3$).

RT (HPLC): 24.46 min (linear gradient of 0 to 60% A over 10 min→60 to 99% A over 15 min, A = CH_3CN, B = 0.08% TFA/H_2O).

5.4.97 2-((1*R*,2*S*,3*S*)-3-(benzyloxycarbonyl)-1-azido-2-(*tert*-butyl-dimethylsilyloxy)-3-hydroxy-propyl)-1,3-thiazole-4-carboxylic acid methyl ester (269)

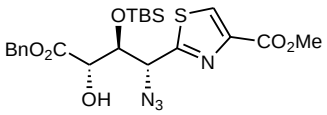

269
M = 506.65

The azide **269** was obtained as a second product in the azidation reactions of the mesylates **262** and **264** (section 5.4.96) as result of the migration of the TBS group. By flash chromatographic purification (Tol/EtOAc 6:1) 8.4% of **269** were isolated as a colorless oil (yield obtained from the azidation of **262**).

TLC: R_f = 0.47 (Tol/EtOAc 3:1).

ESI-MS: m/z = 529 $[M+Na]^+$.

HRMS: $[M+Na]^+$: $C_{22}H_{30}N_4O_6SSiNa$, calculated: 529.1548, found: 529.1542.

^{1}H-NMR: 500 MHz, DMSO-d_6: δ = –0.07, 0.04 (each s, 3 H, $SiCH_3$), 0.72 (s, 9 H, $SiC(CH_3)_3$), 3.84 (s, 3 H, CO_2CH_3), 4.19 (pt, 1 H, $^3J_{4\text{-H}/3\text{-H}}$ = 5.1 Hz, $^3J_{4\text{-H}/4\text{-OH}}$ = 5.1 Hz, 4-H), 4.40 (dd, 1 H, $^3J_{3\text{-H}/4\text{-H}}$ = 5.1 Hz, $^3J_{3\text{-H}/2\text{-H}}$ = 5.7 Hz, 3-H), 5.12 (d, 1 H, ^2J = 12.5 Hz, $CO_2C\underline{H}_2Ph^u$), 5.18 (d, 1 H, ^2J = 12.5 Hz, $CO_2C\underline{H}_2Ph^d$), 5.33 (d, 1 H, $^3J_{2\text{-H}/3\text{-H}}$ = 5.7 Hz, 2-H), 6.10 (d, 1 H, $^3J_{4\text{-OH}/4\text{-H}}$ = 5.1 Hz, 4-OH), 7.34-7.40 (m, 5 H, $CO_2CH_2\underline{Ph}$), 8.58 (s, 1 H, Thz-H).

^{13}C-NMR: 125 MHz, DMSO-d_6: δ = –5.2, –4.9 (each $SiCH_3$), 17.7 ($Si\underline{C}(CH_3)_3$), 25.2 ($SiC(\underline{C}H_3)_3$), 51.8 ($CO_2\underline{C}H_3$), 62.2 (C-2), 65.6 ($CO_2\underline{C}H_2Ph$), 71.6 (C-4), 75.4 (C-3), 127.8, 128.0, 128.1 (each Bn-$CH_{arom.}$), 130.3 (Thz-H$\underline{C}$=C), 135.8 (Bn-$C_{arom.,\ quart.}$), 145.4 (Thz-HC=$\underline{C}$), 161.0 ($\underline{C}O_2CH_3$), 165.8 (C-1), 171.0 (C-5).

RT (HPLC): 24.01 min (linear gradient of 0 to 60% A over 10 min→60 to 99% A over 15 min, A = CH_3CN, B = 0.08% TFA/H_2O).

5.4.98 2-((1*S*,2*R*,3*S*)-3-(benzyloxycarbonyl)-1,2-dimethanesulfonyloxy-3-hydroxypropyl)-1,3-thiazole-4-carboxylic acid methyl ester (278)

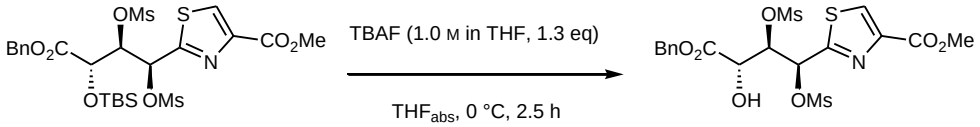

264 **278**
M = 523.55

Preparation:

Compound **264**	M = 637.82 g mol^{-1}	1.0 eq	332 µmol	212 mg
TBAF (1.0 M in THF)	M = 261.47 g mol^{-1}	2.0 eq	432 µmol	432 µL
THF_{abs}				10 mL

121 mg of the dimesylate **264** (332 µmol, 1.0 eq) were dissolved in 10 mL of THF_{abs} in a nitrogen atmosphere and cooled to 0 °C. 432 µL of TBAF (1.0 M in THF_{abs}; 432 µmol, 1.3 eq) were added and the solution was stirred for 2.5 h at 0 °C. The reaction mixture was diluted with EtOAc and the THF was removed *in vacuo*. The remaining solution was extracted two times with aq. NaCl, dried with brine and over $MgSO_4$, filtered, and evaporated. After flash chromatographic purification (EtOAc/Tol 1:1) 38% of the dimesylate **278** (67 mg, 128 µmol) were obtained as a pale yellow foam.

TLC: R_f = 0.49 (EtOAc/Tol 1:1).

ESI-MS: m/z = 546 $[M+Na]^+$.

HRMS: $[M+Na]^+$: $C_{18}H_{21}NO_{11}S_3Na$, calculated: 546.0169, found: 546.0175.

IR: pellet; $\tilde{\nu}$ = 3468, 3115, 3033, 2938, 1726, 1498, 1456, 1434, 1353, 1218, 1173, 1100, 1056, 953, 876, 818, 784, 752, 698 cm^{-1}.

^{1}H-NMR: 500 MHz, DMSO-d_6: δ = 3.12, 3.29 (each s, 3 H, Ms-CH_3), 3.83 (s, 3 H, CO_2CH_3), 4.46 (dd, 1 H, $^3J_{3\text{-H}/4\text{-H}}$ = 4.7 Hz, $^3J_{3\text{-H}/2\text{-H}}$ = 6.2 Hz, 3-H), 5.01 (d, 1 H, ^2J = 12.3 Hz, $CO_2C\underline{H}_2Ph^u$), 5.11 (d, 1 H, ^2J = 12.3 Hz, $CO_2C\underline{H}_2Ph^d$), 5.34 (dd, 1 H, $^3J_{4\text{-H}/3\text{-H}}$ = 4.7 Hz, $^3J_{4\text{-H}/4\text{-OH}}$ = 6.0 Hz, 4-H), 6.16 (d, 1 H, $^3J_{2\text{-H}/3\text{-H}}$ = 6.2 Hz, 2-H), 6.73 (s, 1 H, $^3J_{4\text{-OH}/4\text{-H}}$ = 6.0 Hz, 4-OH), 7.37-7.41 (m, 5 H, $CO_2CH_2\underline{Ph}$), 8.69 (s, 1 H, Thz-H).

^{13}C-NMR: 125 MHz, DMSO-d_6: δ = 38.2, 38.5 (each Ms-$\underline{C}H_3$), 52.2 ($CO_2\underline{C}H_3$), 66.7 ($CO_2\underline{C}H_2Ph$), 69.7 (C-3), 74.9 (C-2), 81.0 (C-4), 128.2, 128.2, 128.4 (each Bn-$CH_{arom.}$), 131.6 (Thz-H$\underline{C}$=C), 135.2 (Bn-$C_{arom., quart.}$), 146.0 (Thz-HC=$\underline{C}$), 160.8 ($\underline{C}O_2CH_3$), 163.9 (C-1), 169.5 (C-5).

Melting point: 62 °C.

Opt. rotation: $[\alpha]_{589}^{19}$ = –35.1, $[\alpha]_{578}^{21}$ = –36.7, $[\alpha]_{546}^{19}$ = –41.8
(c = 1.08 g/100 mL $CHCl_3$).

RT (HPLC): 19.27 min (linear gradient of 0 to 60% A over 10 min→60 to 99% A over 15 min, A = CH_3CN, B = 0.08% TFA/H_2O).

5.4.99 2-((1*R*,2*R*,3*S*)-3-(benzyloxycarbonyl)-1,2,3-trihydroxypropyl)-1,3-thiazole-4-carboxylic acid methyl ester (279)

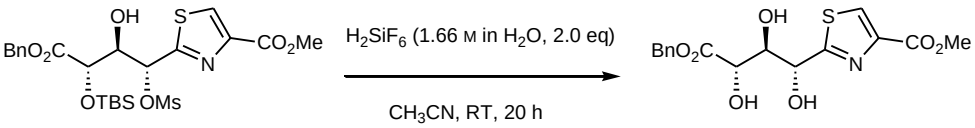

262 **279**
M = 367.37

Preparation:

Compound **262**	M = 559.72 g mol^{-1}	1.0 eq	150 µmol	84 mg
H_2SiF_6 (1.66 M in H_2O)	M = 144.09 g mol^{-1}, ρ = 1.22	2.0 eq	300 µmol	180 µL
CH_3CN				4.0 mL

84 mg of the TBS ether **262** (150 µmol, 1.0 eq) were dissolved in 4.0 mL of CH_3CN, 180 µL of H_2SiF_6 (1.66 M in H_2O; 300 µmol, 2.0 eq) were added and the solution was stirred for 20 h at RT. Solid $NaHCO_3$ was added in small portions until a pH of approx. 6 was reached, and approx. 0.8 g of solid $MgSO_4$ were subsequently added. The mixture was filtered over Celite and the residue was washed with CH_3CN. The filtrate was concentrated *in vacuo* and subjected to flash chromatographic purification (EtOAc/Tol 1:1) which yielded 67% of the thiazole triol **279** (37 mg, 101 µmol) as a colorless solid.

TLC: R_f = 0.17 (EtOAc/Tol 1:1).

ESI-MS: m/z = 390 $[M+Na]^+$.

HRMS: $[M+Na]^+$: $C_{16}H_{17}NO_7SNa$, calculated: 390.0618, found: 390.0628.

IR: pellet; $\tilde{\nu}$ = 3391, 2951, 1719, 1492, 1455, 1434, 1323, 1259, 1194, 1115, 1072, 1047, 991, 919, 861, 781, 742, 696 cm^{-1}.

^{1}H-NMR: 500 MHz, DMSO-d_6: δ = 3.82 (s, 3 H, CO_2CH_3), 3.99-4.03 (m, 1 H, 3-H), 4.21 (dd, 1 H, $^3J_{4\text{-H}/4\text{-OH}}$ = 6.1 Hz, $^3J_{4\text{-H}/3\text{-H}}$ = 6.6 Hz, 4-H), 5.03 (pt, 1 H, $^3J_{2\text{-H}/3\text{-H}}$ = 5.1 Hz, $^3J_{2\text{-H}/2\text{-OH}}$ = 5.1 Hz, 2-H), 5.09 (d, 1 H, ^2J = 12.5 Hz, $CO_2C\underline{H}_2Ph^u$), 5.12 (d, 1 H, ^2J = 12.5 Hz, $CO_2C\underline{H}_2Ph^d$), 5.50 (d, 1 H, $^3J_{3\text{-OH}/3\text{-H}}$ = 5.9 Hz, 3-OH), 5.72 (d, 1 H, $^3J_{4\text{-OH}/4\text{-H}}$ = 6.1 Hz, 4-OH), 6.41 (d, 1 H, $^3J_{2\text{-OH}/2\text{-H}}$ = 5.1 Hz, 2-OH), 7.32-7.40 (m, 5 H, $CO_2CH_2\underline{Ph}$), 8.46 (s, 1 H, Thz-H).

^{13}C-NMR: 125 MHz, DMSO: δ = 51.8 ($CO_2\underline{C}H_3$), 65.3 ($CO_2\underline{C}H_2Ph$), 70.7 (C-2), 71.6 (C-4), 75.5 (C-3), 127.7, 127.8, 128.3 (each Bn-$CH_{arom.}$), 128.9 (Thz-H$\underline{C}$=C), 136.1 (Bn-$C_{arom., quart.}$), 144.9 (Thz-HC=$\underline{C}$), 161.4 ($\underline{C}O_2CH_3$), 172.2 (C-5), 174.8 (C-1).

Melting point: 54 °C.

Opt. rotation: $[\alpha]_{589}^{19}$ = +30.2, $[\alpha]_{578}^{19}$ =+31.4, $[\alpha]_{546}^{19}$ = +36.1, $[\alpha]_{436}^{19}$ = +63.7

(c = 0.71 g/100 mL MeOH).

5.4.100 2-((1*S*,2*R*,3*S*)-3-(benzyloxycarbonyl)-1,2-epoxy-3-hydroxypropyl)-1,3-thiazole-4-carboxylic acid methyl ester (280)

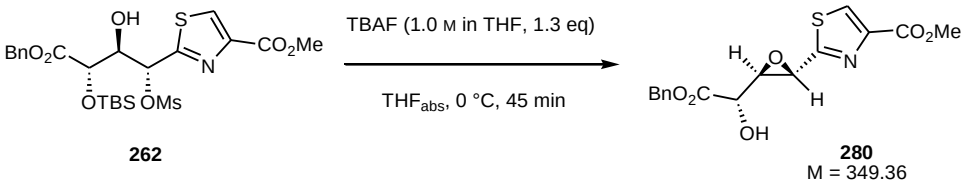

262 **280** M = 349.36

Preparation:

Compound **262**	M = 559.72 g mol^{-1}	1.0 eq	156 µmol	87 mg
TBAF (1.0 M in THF)	M = 261.47 g mol^{-1}	1.3 eq	203 µmol	203 µL
THF_{abs}				10 mL

121 mg of the mesylate **262** (156 µmol, 1.0 eq) were dissolved in 10 mL of THF_{abs} in a nitrogen atmosphere and cooled to 0 °C. 203 µL of TBAF (1.0 M in THF_{abs}; 203 µmol, 1.3 eq) were slowly added and the solution was stirred for 45 min at 0 °C. The reaction mixture was diluted with EtOAc and the THF was removed *in vacuo*. The remaining solution was extracted two times with aq. NaCl, dried with brine and over $MgSO_4$, filtered, and evaporated. Flash chromatographic purification (Tol/EtOAc 3:1) yielded 42% of the *trans*-epoxide **280** (23 mg, 65.8 µmol) as a colorless solid.

TLC: R_f = 0.36 (EtOAc/Tol 1:1).

ESI-MS: m/z = 372 $[M+Na]^+$.

HRMS: $[M+Na]^+$: $C_{16}H_{15}NO_6SNa$, calculated: 372.0512, found: 372.0510.

IR: pellet; $\tilde{\nu}$ = 3478, 3111, 2958, 1732, 1715, 1496, 1455, 1440, 1392, 1274, 1237, 1205, 1124, 1093, 1028, 984, 933, 911, 882, 851, 753, 698 cm^{-1}.

^{1}H-NMR: 500 MHz, DMSO-d_6: δ = 3.84 (s, 3 H, CO_2CH_3), 3.62 (dd, 1 H, $^3J_{3\text{-H}/2\text{-H}}$ = 2.0 Hz, $^3J_{3\text{-H}/4\text{-H}}$ = 4.2 Hz, 3-H), 4.39 (dd, 1 H, $^3J_{4\text{-H}/3\text{-H}}$ = 4.2 Hz, $^3J_{4\text{-H}/4\text{-OH}}$ = 6.5 Hz, 4-H), 4.45 (d, 1 H, $^3J_{2\text{-H}/3\text{-H}}$ = 2.0 Hz, 2-H), 5.21 (s, 1 H, $CO_2C\underline{H}_2Ph$), 6.18 (d, 1 H, $^3J_{4\text{-OH}/4\text{-H}}$ = 6.5 Hz, 4-OH), 7.33-7.37 (m, 5 H, $CO_2CH_2\underline{Ph}$), 8.56 (s, 1 H, Thz-H).

^{13}C-NMR: 125 MHz, DMSO-d_6: δ = 52.1 ($CO_2\underline{C}H_3$), 52.2 (C-2), 66.1 ($CO_2\underline{C}H_2Ph$), 62.4 (C-3), 68.8 (C-4), 127.8, 128.1, 128.4 (each Bn-$CH_{arom.}$), 129.7 (Thz-H$\underline{C}$=C), 135.7 (Bn-$C_{arom., quart.}$), 146.0 (Thz-HC=$\underline{C}$), 160.9 ($\underline{C}O_2CH_3$), 167.9 (C-1), 170.5 (C-5).

Melting point: 89 °C.

Opt. rotation: $[\alpha]_{589}^{18}$ = –0.7, $[\alpha]_{578}^{18}$ = –0.3, $[\alpha]_{546}^{18}$ = +0.4, $[\alpha]_{436}^{18}$ = +8.8
(c = 1.77 g/100 mL $CHCl_3$).

RT (HPLC): 13.95 min (linear gradient of 0 to 60% A over 10 min→60 to 99% A over 15 min, A = CH_3CN, B = 0.08% TFA/H_2O).

5.4.101 2-((1*R*,2*R*,3*S*)-3-(benzyloxycarbonyl)-1,2-epoxy-3-hydroxypropyl)-1,3-thiazole-4-carboxylic acid methyl ester (282)

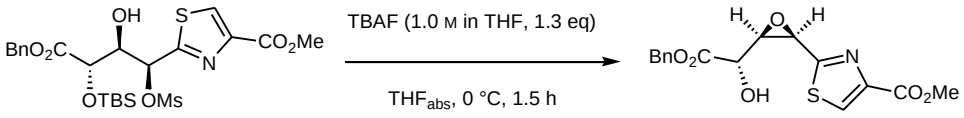

264 **282**
M = 349.36

Preparation:

Compound **264**	M = 559.72 g mol^{-1}	1.0 eq	393 µmol	220 mg
TBAF (1.0 M in THF)	M = 261.47 g mol^{-1}	1.3 eq	511 µmol	511 µL
THF_{abs}				25 mL

220 mg of the mesylate **264** (393 µmol, 1.0 eq) were dissolved in 25 mL of THF_{abs} in a nitrogen atmosphere and cooled to 0 °C. 511 µL of TBAF (1.0 M in THF_{abs}; 511 µmol, 1.3 eq) were slowly added and the solution was stirred for 1.5 h at 0 °C. The solvent was removed under rotary evaporation at 30 °C and the resulting red oil was subjected to flash chromatographic purification (EtOAc/Tol 1:1) which yielded 26% of the *cis*-epoxide **282** (16 mg, 45.8 µmol) as a colorless solid.

TLC: R_f = 0.30 (EtOAc/Tol 1:1).

ESI-MS: m/z = 372 $[M+Na]^+$.

HRMS: $[M+Na]^+$: $C_{16}H_{15}NO_6SNa$, calculated: 372.0512, found: 372.0509.

IR: pellet; $\tilde{\nu}$ = 3237, 3130, 3102, 2956, 2926, 1725, 1495, 1455, 1436, 1322, 1289, 1261, 1242, 1229, 1193, 1096, 1083, 1071, 981, 921, 882, 837, 759, 744, 696 cm^{-1}.

^{1}H-NMR: 600 MHz, DMSO-d_6: δ = 3.84 (s, 3 H, CO_2CH_3), 3.59 (dd, 1 H, $^3J_{3\text{-H}/2\text{-H}}$ = 4.0 Hz, $^3J_{3\text{-H}/4\text{-H}}$ = 8.5 Hz, 3-H), 3.93 (dd, 1 H, $^3J_{4\text{-H}/4\text{-OH}}$ = 6.5 Hz, $^3J_{4\text{-H}/3\text{-H}}$ = 8.5 Hz, 4-H), 4.62 (d, 1 H, $^3J_{2\text{-H}/3\text{-H}}$ = 4.0 Hz, 2-H), 5.21 (d, 1 H, ^2J = 12.7 Hz, $CO_2C\underline{H}_2Ph^u$), 5.25 (d, 1 H, ^2J = 12.7 Hz, $CO_2C\underline{H}_2Ph^d$), 6.11 (d, 1 H, $^3J_{4\text{-OH}/4\text{-H}}$ = 6.5 Hz, 4-OH), 7.33-7.42 (m, 5 H, $CO_2CH_2\underline{Ph}$), 8.58 (s, 1 H, Thz-H).

^{13}C-NMR: 150 MHz, DMSO-d_6: δ = 52.1 ($CO_2\underline{C}H_3$), 53.8 (C-2), 59.0 (C-3), 66.0 ($CO_2\underline{C}H_2Ph$), 67.5 (C-4), 127.1, 128.1, 128.4 (each Bn-$CH_{arom.}$), 129.6 (Thz-H$\underline{C}$=C), 135.8 (Bn-$C_{arom., quart.}$), 146.4 (Thz-HC=$\underline{C}$), 160.9 ($\underline{C}O_2CH_3$), 165.3 (C-1), 171.3 (C-5).

Melting point: 101 °C.

Opt. rotation: $[\alpha]_{589}^{13}$ = +68.5, $[\alpha]_{578}^{13}$ = +72.2, $[\alpha]_{546}^{13}$ = +81.8, $[\alpha]_{436}^{13}$ = +144.0 (c = 1.14 g/100 mL $CHCl_3$).

RT (HPLC): 14.10 min (linear gradient of 0 to 60% A over 10 min→60 to 99% A over 15 min, A = CH_3CN, B = 0.08% TFA/H_2O).

5.4.102 2-((1*S*,2*R*,3*S*)-3-(benzyloxycarbonyl)-1-methanesulfonyloxy-2,3-dihydroxybutyl-dimethylsilyloxy)-propyl)-1,3-thiazole-4-carboxylic acid methyl ester (281)

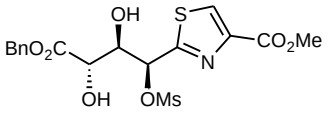

281
M = 445.46

The mesylate **281** was obtained as a second product in the TBS cleavage step starting with **264** (section 5.4.100). By flash chromatographic purification (EtOAc/Tol 1:1) 21% of **281** (36 mg, 80.8 µmol) were isolated as a pale yellow oil.

TLC: R_f = 0.15 (EtOAc/Tol 1:1).

ESI-MS: *m*/*z* = 468 $[M+Na]^+$.

HRMS: $[M+Na]^+$: $C_{17}H_{19}NO_9S_2Na$, calculated: 468.0393, found: 468.0398.

IR: film; $\tilde{\nu}$ = 3435, 3117, 3029, 2955, 1722, 1496, 1485, 1455, 1435, 1351, 1217, 1174, 1095, 964, 908, 854, 812, 787, 751, 734, 697 cm^{-1}.

^{1}H-NMR: 300 MHz, DMSO-d_6: δ = 3.27 (s, 3 H, Ms-CH_3), 3.84 (s, 3 H, CO_2CH_3), 4.08-4.13 (m, 2 H, 3-H, 4-H), 5.12 (d, 1 H, ^2J = 12.6 Hz, $CO_2C\underline{H}_2Ph^u$), 5.16 (d, 1 H, ^2J = 12.6 Hz, $CO_2C\underline{H}_2Ph^d$), 5.99 (d, 1 H, $^3J_{2\text{-H}/3\text{-H}}$ = 1.0 Hz, 2-H), 6.04, 6.39 (each br s, 1 H, 3-OH, 4-OH), 7.35-7.42 (m, 5 H, $CO_2CH_2\underline{Ph}$), 8.61 (s, 1 H, Thz-H).

Opt. rotation: $[\alpha]_{589}^{19}$ = –27.9, $[\alpha]_{578}^{19}$ = –29.1, $[\alpha]_{546}^{19}$ = –33.1, $[\alpha]_{436}^{19}$ = –58.0
(c = 1.54 g/100 mL $CHCl_3$).

RT (HPLC): 13.26 min (linear gradient of 0 to 60% A over 10 min→60 to 99% A over 15 min, A = CH_3CN, B = 0.08% TFA/H_2O).

5.4.103 2-((1*R*,2*S*,3*S*)-3-(benzyloxycarbonyl)-1-azido-2,3-dihydroxy-propyl)-1,3-thiazole-4-carboxylic acid methyl ester (272)

Method A) opening of the epoxide **280**

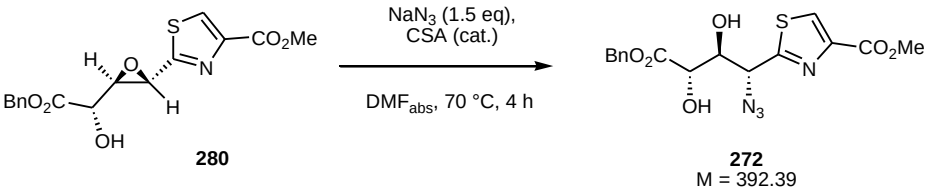

Preparation:

Compound **280**	M = 349.36 g mol^{-1}	1.0 eq	54.4 µmol	19 mg
NaN_3	M = 65.01 g mol^{-1}	1.5 eq	272 µmol	18 mg
CSA	M = 232.30 g mol^{-1}			cat.
DMF_{abs}				2.0 mL

19 mg of the epoxide **280** (1.0 eq, 54.4 µmol) and 18 mg of NaN_3 (5.0 eq, 272 µmol) were dissolved in 2.0 mL of DMF_{abs} in a nitrogen atmosphere, and a catalytical amount of CSA was added. The mixture was stirred for 4 h at 85 °C (TLC control), allowed to cool to RT, neutralized with NEt_3, and the DMF was removed *in vacuo*. EtOAc and H_2O were added, the phases were separated and the aqueous phase was extracted three times with EtOAc. The combined organic phases were dried with brine and over $MgSO_4$, filtered, and concentrated *in vacuo* to obtain the raw product as a pale yellow oil.

NMR monitoring of the reaction with DMSO-d_6 instead of DMF_{abs} as solvent showed a > 90% conversion after 3.5 h under otherwise identical conditions.

Method B) azidation of **281** *under stereoinversion*

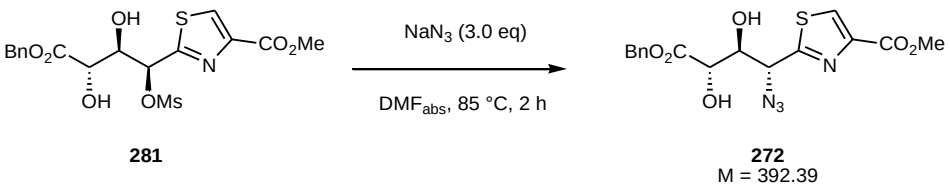

Preparation:

Compound **281**	M = 445.46 g mol^{-1}	1.0 eq	171 µmol	76 mg
NaN_3	M = 65.01 g mol^{-1}	3.0 eq	513 µmol	33 mg
DMF_{abs}				6.5 mL

19 mg of the mesylate **281** (1.0 eq, 171 µmol) and 33 mg of NaN_3 (3.0 eq, 513 µmol) were dissolved in 6.5 mL of DMF_{abs} in a nitrogen atmosphere. The mixture was stirred for 2 h at 85 °C (TLC control), allowed to cool to RT, and the DMF was removed *in vacuo*. EtOAc and H_2O were added, the phases were separated and the aqueous phase was extracted three times with EtOAc. The combined organic phases were dried with brine and over $MgSO_4$, filtered, and concentrated *in vacuo* to obtain the raw product as a pale yellow oil. Flash chromatography (EtOAc/Tol 1:1) yielded 70% (47 mg, 120 µmol) of the azide **272** as a pale yellow oil.

Method C) azidation of **264** *under stereoretention and subsequent TBS cleavage*

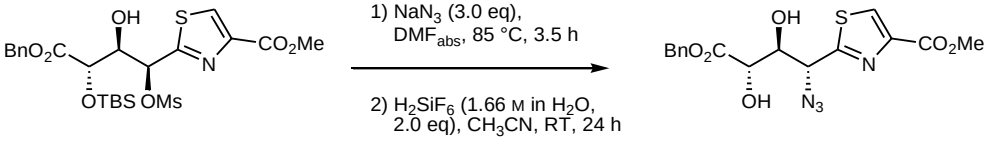

264 **272** M = 392.39

Preparation:

Compound **264**	M = 559.72 g mol^{-1}	1.0 eq	60.7 µmol	34 mg
NaN_3	M = 65.01 g mol^{-1}	1.5 eq	91.1 µmol	5.9 mg
DMF_{abs}				1.0 mL
H_2SiF_6 (1.66 M in H_2O)	M = 144.09 g mol^{-1}, ρ = 1.22	2.0 eq[1)]	67.1 µmol[1)]	40.4 µL
CH_3CN				1.0 mL

1) in relation to the amount of azidation raw product

34 mg of the mesylate **264** (1.0 eq, 60.7 µmol) and 5.9 mg of NaN_3 (1.5 eq, 91.1 µmol) were dissolved in 1.0 mL of DMF_{abs} in a nitrogen atmosphere. The mixture was stirred for 2.5 h at 85 °C (HPLC control), allowed to cool to RT, and additional 5.9 mg of NaN_3 (1.5 eq, 91.1 µmol) were added. The solution was stirred for another 1 h at 85 °C, allowed to cool to RT and concentrated *in vacuo*. To the resulting colorless residue were added CH_2Cl_2 and H_2O, the phases were separated and the aqueous phase was extracted two times with CH_2Cl_2. The combined organic phases were dried with brine and over $MgSO_4$, filtered, and concentrated *in vacuo* to obtain 17 mg of a 75:25 mixture of the azides **268** and **269** (sections 5.4.96 and 5.4.97) as a pale yellow oil (33.6 µmol).

The raw product was dissolved in 1.0mL of CH_3CN, 40.4 µL of H_2SiF_6 (1.66 M in H_2O; 67.1 µmol, 2.0 eq) were added and the solution was stirred for 24 h at RT. The reaction mixture was diluted with CH_3CN, solid $NaHCO_3$ was added in small portions until a pH of approx. 6 was reached, and approx. 0.2 g of solid $MgSO_4$ were subsequently added. The mixture was filtered over Celite and the residue was washed with CH_3CN. The filtrate was concentrated *in vacuo* and subjected to flash chromatographic purification (Tol/EtOAc 2:1) which yielded 12% of the azide **272** (2.8 mg, 7.2 µmol) as a colorless oil. In addition, 13% of the epimeric azide **273** (3.0 mg, 7.7 µmol) were also obtained (section 2.4.104).

TLC: R_f = 0.31 (EtOAc/Tol 3:2).

ESI-MS: m/z = 415 $[M+Na]^+$.

HRMS: $[M+Na]^+$: $C_{16}H_{16}N_4O_6SNa$, calculated: 415.0683, found: 415.0689.

IR: film; $\tilde{\nu}$ = 3435, 3115, 2954, 2925, 2854, 2108, 1724, 1482, 1456, 1435, 1324, 1216, 1095, 989, 915, 854, 753, 697 cm^{-1}.

^{1}H-NMR: 300 MHz, DMSO-d_6: δ = 3.83 (s, 3 H, CO_2CH_3), 3.99-4.03 (m, 1 H, 4-H), 4.18-4.22 (m, 1 H, 3-H), 5.11 (d, 1 H, ^2J = 12.6 Hz, $CO_2C\underline{H}_2Ph^u$), 5.16 (d, 1 H, ^2J = 12.6 Hz, $CO_2C\underline{H}_2Ph^d$), 5.17 (d, 1 H, $^3J_{2\text{-H}/3\text{-H}}$ = 4.8 Hz, 2-H), 6.06 (d, 1 H, $^3J_{4\text{-OH}/4\text{-H}}$ = 6.2 Hz, 4-OH), 6.28 (d, 1 H, $^3J_{3\text{-OH}/3\text{-H}}$ = 6.2 Hz, 3-OH), 7.34-7.39 (m, 5 H, $CO_2CH_2\underline{Ph}$), 8.58 (s, 1 H, Thz-H).

600 MHz, $CDCl_3$: δ = 3.49 (br s, 1 H, 4-OH), 3.77 (br s, 1 H, 3-OH), 3.93 (s, 3 H, CO_2CH_3), 4.34 (dd, 1 H, $^3J_{3\text{-H}/4\text{-H}}$ = 3.9 Hz, $^3J_{3\text{-H}/2\text{-H}}$ = 7.6 Hz, 3-H), 4.42 (d, 1 H, $^3J_{4\text{-H}/3\text{-H}}$ = 3.9 Hz, 4-H), 5.06 (d, 1 H, $^3J_{2\text{-H}/3\text{-H}}$ = 7.6 Hz, 2-H), 5.26 (d, 1 H, ^2J = 12.1 Hz, $CO_2C\underline{H}_2Ph^u$), 5.30 (d, 1 H, ^2J = 12.1 Hz, $CO_2C\underline{H}_2Ph^d$), 7.34-7.39 (m, 5 H, $CO_2CH_2\underline{Ph}$), 8.21 (s, 1 H, Thz-H).

^{13}C-NMR: 150 MHz, $CDCl_3$: δ = 52.7 ($CO_2\underline{C}H_3$), 62.6 (C-2), 68.2 ($CO_2\underline{C}H_2Ph$), 71.9 (C-4), 75.0 (C-3), 128.8 (Thz-H$\underline{C}$=C), 128.8, 128.9, 128.9 (each Bn-$CH_{arom.}$), 134.8 (Bn-$C_{arom., quart.}$), 147.1 (Thz-HC=$\underline{C}$), 161.5 ($\underline{C}O_2CH_3$), 168.8 (C-1), 171.8 (C-5).

Opt. rotation: $[\alpha]_{589}^{21}$ = +10.5, $[\alpha]_{578}^{21}$ = +10.9, $[\alpha]_{546}^{21}$ = +13.2, $[\alpha]_{436}^{21}$ = +26.4 (c = 0.26 g/100 mL $CHCl_3$).

RT (HPLC): 14.04 min (linear gradient of 0 to 60% A over 10 min→60 to 99% A over 15 min, A = CH_3CN, B = 0.08% TFA/H_2O).

5.4.104 2-((1*S*,2*S*,3*S*)-3-(benzyloxycarbonyl)-1-azido-2,3-dihydroxy-propyl)-1,3-thiazole-4-carboxylic acid methyl ester (273)

Method A) opening of the epoxide **282**

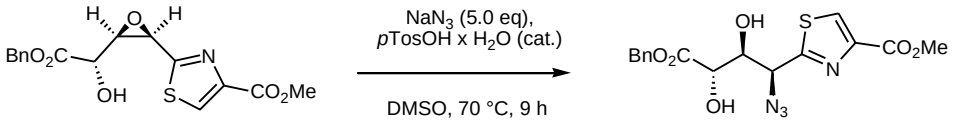

282
M = 349.36

273
M = 392.39

Preparation:

Compound **282**	M = 349.36 g mol^{-1}	1.0 eq	48.7 µmol	17 mg
NaN_3	M = 65.01 g mol^{-1}	5.0 eq	244 µmol	16 mg
*p*TosOH x H_2O	M = 190.22 g mol^{-1}			cat.
DMSO				1.0 mL

17 mg of the epoxide **282** (1.0 eq, 48.7 µmol) and 16 mg of NaN_3 (5.0 eq, 244 µmol) were dissolved in 1.0 mL of DMSO in a nitrogen atmosphere, and a catalytical amount of *p*TosOH x H_2O was added. The mixture was stirred for 9 h at 70 °C (TLC control), allowed to cool to RT, and 0.6 mL of H_2O as well as 10mL of CH_2Cl_2 were added. The phases were separated and the aqueous phase was extracted three times with CH_2Cl_2. The combined organic phases were dried with brine and over $MgSO_4$, filtered, and concentrated *in vacuo*. Flash chromatographic purification (Tol/EtOAc 2:1) yielded 16% of the azide **273** (3.0 mg, 7.6 µmol) as a pale yellow oil. NMR monitoring of the reaction in DMSO-d_6 showed a > 90% conversion after 13.5 h under identical conditions.

Method B) azidation of **264** *under stereoretention and subsequent TBS cleavage and epimerization*

The azide **273** was also obtained as epimerization product in the two-step azidation/ deprotection sequence starting with the mesylate **264** (section 5.4.103, method C). By flash chromatographic purification (Tol/EtOAc 2:1) 13% of **273** (3.0 mg, 7.7 µmol) were obtained as a colorless oil.

TLC: R_f = 0.41 (EtOAc/Tol 3:2).

ESI-MS: m/z = 415 $[M+Na]^+$.

HRMS: $[M+Na]^+$: $C_{16}H_{16}N_4O_6SNa$, calculated: 415.0683, found: 415.0688.

IR: film; $\tilde{\nu}$ = 3436, 3116, 3012, 2954, 2925, 2108, 1723, 1625, 1498, 1456, 1435, 1319, 1214, 1095, 986, 918, 864, 828, 783, 748, 697 cm^{-1}.

^{1}H-NMR: 300 MHz, $CDCl_3$: δ = 3.95 (s, 3 H, CO_2CH_3), 4.32 (dd, 1 H, $^3J_{3\text{-H}/2\text{-H}}$ = 3.1 Hz, $^3J_{3\text{-H}/4\text{-H}}$ = 7.4 Hz, 3-H), 4.41 (d, 1 H, $^3J_{4\text{-H}/3\text{-H}}$ = 7.4 Hz, 4-H), 5.24-5.27 (m, 3 H, 2-H, $CO_2C\underline{H}_2Ph$), 7.36-7.38 (m, 5 H, $CO_2CH_2\underline{Ph}$), 8.22 (s, 1 H, Thz-H).

500 MHz, DMSO-d_6: δ = 3.83 (s, 3 H, CO_2CH_3), 4.16 (dd, 1 H, $^3J_{4\text{-H}/3\text{-H}}$ = 2.9 Hz, $^3J_{4\text{-H}/4\text{-OH}}$ = 6.9 Hz, 4-H), 4.25 (dpt, 1 H, $^3J_{3\text{-H}/4\text{-H}}$ = 2.9 Hz, $^3J_{3\text{-H}/2\text{-H}}$ = 7.3 Hz, $^3J_{3\text{-H}/3\text{-OH}}$ = 7.3 Hz, 3-H), 5.11 (d, 1 H, $^3J_{2\text{-H}/3\text{-H}}$ = 7.3 Hz, 2-H), 5.13 (d, 1 H, ^2J = 12.6 Hz, $CO_2C\underline{H}_2Ph^u$), 5.17 (d, 1 H, ^2J = 12.6 Hz, $CO_2C\underline{H}_2Ph^d$), 5.58 (d, 1 H, $^3J_{4\text{-OH}/4\text{-H}}$ = 6.9 Hz, 4-OH), 6.04 (d, 1 H, $^3J_{3\text{-OH}/3\text{-H}}$ = 7.3 Hz, 3-OH), 7.35-7.40 (m, 5 H, $CO_2CH_2\underline{Ph}$), 8.56 (s, 1 H, Thz-H).

^{13}C-NMR: 125 MHz, DMSO-d_6: δ = 52.1 ($CO_2\underline{C}H_3$), 63.1 (C-2), 65.9 ($CO_2\underline{C}H_2Ph$), 71.2 (C-4), 74.4 (C-3), 127.8, 128.0, 128.4 (each Bn-$CH_{arom.}$), 130.3 (Thz-H$\underline{C}$=C), 135.9 (Bn-$C_{arom., quart.}$), 145.7 (Thz-HC=$\underline{C}$), 161.0 ($\underline{C}O_2CH_3$), 167.1 (C-1), 171.8 (C-5).

Opt. rotation: $[\alpha]_{589}^{21}$ = –30.9, $[\alpha]_{578}^{21}$ = –32.4, $[\alpha]_{546}^{21}$ = –37.8, $[\alpha]_{436}^{21}$ = –66.4 (c = 0.28 g/100 mL $CHCl_3$).

RT (HPLC): 14.04 min (linear gradient of 0 to 60% A over 10 min→60 to 99% A over 15 min, A = CH_3CN, B = 0.08% TFA/H_2O).

5.4.105 2-((1*R*,2*S*,3*S*)-3-(benzyloxycarbonyl)-1,2-epoxy-3-(*tert*-butyl-dimethylsilyloxy)propyl)-1,3-thiazole-4-carboxylic acid methyl ester (270)

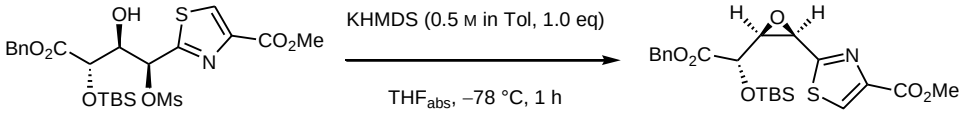

264 **270** M = 463.62

Preparation:

Compound **264**	M = 559.72 g mol^{-1}	1.0 eq	94.7 µmol	53 mg
KHMDS (0.5 M in Tol)	M = 199.49 g mol^{-1}	1.0 eq	94.7 µmol	189 µL
THF_{abs}				9.0 mL

53 mg of the mesylate **264** (94.7 µmol, 1.0 eq) were dissolved in 9.0 mL of THF_{abs} in a nitrogen atmosphere and cooled to −78 °C. 189 µL of TBAF (1.0 M in THF_{abs}; 94.7 µmol, 1.0 eq) were added dropwise and the solution was stirred for 1 h at −78 °C. MeOH was slowly added (0.2 mL) and the reaction mixture was allowed to warm to 0 °C under stirring. After dilution with EtOAc the solution was extracted with 10% aq. citric acid, dried with brine and over $MgSO_4$, filtered, and concentrated *in vacuo*. By flash chromatographic purification (Tol/EtOAc 2:1) 16% of the *cis*-epoxide **270** (7.2 mg, 15.5 µmol) were obtained as a colorless solid.

TLC: R_f = 0.75 (EtOAc/Tol 3:2).

ESI-MS: *m*/*z* = 486 $[M+Na]^+$.

HRMS: $[M+Na]^+$: $C_{22}H_{29}NO_6SSiNa$, calculated: 486.1377, found: 486.1376.

^{1}H-NMR: 600 MHz, DMSO-d_6: δ = −0.37, −0.22 (each s, 3 H, $SiCH_3$), 0.66 (s, 9 H, $SiC(CH_3)_3$), 3.66 (dd, 1 H, $^{3}J_{3\text{-H}/2\text{-H}}$ = 3.9 Hz, $^{3}J_{3\text{-H}/4\text{-H}}$ = 8.4 Hz, 3-H), 3.84 (s, 3 H, CO_2CH_3), 4.22 (d, 1 H, $^{3}J_{4\text{-H}/3\text{-H}}$ = 8.4 Hz, 4-H), 4.67 (d, 1 H, $^{3}J_{2\text{-H}/3\text{-H}}$ = 3.9 Hz, 2-H), 5.23 (d, 1 H, ^{2}J = 12.5 Hz, $CO_2C\underline{H}_2Ph^{u}$), 5.28 (d, 1 H, ^{2}J = 12.5 Hz, $CO_2C\underline{H}_2Ph^{d}$), 7.35-7.42 (m, 5 H, $CO_2CH_2\underline{Ph}$), 8.60 (s, 1 H, Thz-H).

^{13}C-NMR: 100 MHz, DMSO-d_6: δ = −6.0, −5.4 (each $SiCH_3$), 17.6 ($Si\underline{C}(CH_3)_3$), 25.2 ($SiC(\underline{C}H_3)_3$), 52.1 ($CO_2\underline{C}H_3$), 53.4 (C-2), 59.1 (C-3), 66.5 ($CO_2\underline{C}H_2Ph$), 69.0 (C-4), 128.0, 128.2, 128.4 (each Bn-$CH_{arom.}$), 129.8 (Thz-H$\underline{C}$=C), 135.5 (Bn-$C_{arom.,\ quart.}$), 146.6 (Thz-HC=$\underline{C}$), 160.8 ($\underline{C}O_2CH_3$), 164.9 (C-5), 170.3 (C-1).

6 References

[1] K. Tatemoto, M. Carlquist, V. Mutt, *Nature* **1982**, *296*, 659.
[2] C. Cabrele, A. G. Beck-Sickinger, *J. Pept. Sci.* **2000**, *6*, 97.
[3] T. Pedrazzini, F. Pralong, E. Grouzmann, *Cell. Mol. Life Sci.* **2003**, *60*, 350.
[4] D. Larhammar, *Regulatory Peptides* **1996**, *62*, 1.
[5] A. G. Blomqvist, C. Söderberg, I. Lundell, R. J. Milner, D. Larhammar, *Proceedings of the National Academy of Sciences of the United States of America* **1992**, *89*, 2350.
[6] J. A. Bard, M. W. Walker, T. A. Branchek, R. L. Weinshank, *J. Biol. Chem.* **1995**, *270*, 26762.
[7] D. R. Gehlert, D. A. Schober, L. Beavers, R. Gadski, J. A. Hoffman, D. L. Smiley, R. E. Chance, I. Lundell, D. Larhammar, *Mol. Pharmacol.* **1996**, *50*, 112.
[8] M. C. Michel, A. G. Beck-Sickinger, H. Cox, H. N. Doods, H. Herzog, D. Larhammar, R. Quirion, T. Schwartz, T. Westfall, *Pharmacol Rev* **1998**, *50*, 143.
[9] V. K. Gribkoff, R. L. Pieschl, T. A. Wisialowski, A. N. van den Pol, F. D. Yocca, *J. Neurosci.* **1998**, *18*, 3014.
[10] D. K. Sindelar, R. D. Palmiter, S. C. Woods, M. W. Schwartz, *Peptides* **2005**, *26*, 2597.
[11] E. Carro, L. M. Seoane, R. Senaris, R. V. Considine, F. F. Casanueva, C. Dieguez, *Neuroendocrinology* **1998**, *68*, 187.
[12] L. L. Anderson, S. Jeftinija, C. G. Scanes, *Experimental Biology and Medicine* **2004**, *229*, 291.
[13] S. P. Kalra, P. S. Kalra, *Peptides* **2004**, *25*, 465.
[14] T. E. Thiele, D. J. Marsh, S. L. Marie, I. L. Bernstein, R. D. Palmiter, *Nature* **1998**, *396*, 366.
[15] T. E. Thiele, M. T. Koh, T. Pedrazzini, *J. Neurosci.* **2002**, *22*, 1.
[16] M. W. Schwartz, S. C. Woods, P. D. Jr., R. J. Seeley, D. G. Baskin, *Nature* **2000**, *404*, 661.
[17] A. Inui, *Trends Pharmacol. Sci.* **1999**, *20*, 43.
[18] T. Kelly, W. Yang, C.-S. Chen, K. Reynolds, J. He, *International Journal of Obesity* **2008**, *32*, 1431.
[19] K. Palczewski, T. Kumasaka, T. Hori, C. A. Behnke, T. Okada, R. E. Stenkamp, M. Yamamoto, M. Miyano, *Science* **2000**, *289*, 739.
[20] S. G. F. Rasmussen, H.-J. Choi, D. M. Rosenbaum, T. S. Kobilka, F. S. Thian, P. C. Edwards, M. Burghammer, V. R. P. Ratnala, R. Sanishvili, R. F. Fischetti, G. F. X. Schertler, W. I. Weis, B. K. Kobilka, *Nature* **2007**, *450*, 383.
[21] V. Cherezov, D. M. Rosenbaum, M. A. Hanson, S. G. F. Rasmussen, F. S. Thian, T. S. Kobilka, H.-J. Choi, P. Kuhn, W. I. Weis, B. K. Kobilka, R. C. Stevens, *Science* **2007**, *318*, 1258.
[22] S. Luca, J. F. White, A. K. Sohal, D. V. Filippov, J. H. van Boom, R. Grisshammer, M. Baldus, *Proceedings of the National Academy of Sciences of the United States of America* **2003**, *100*, 10706.
[23] J. J. Lopez, A. K. Shukla, C. Reinhart, H. Schwalbe, H. Michel, C. Glaubitz, *Angewandte Chemie International Edition* **2008**, *47*, 1668.
[24] T. L. Blundell, J. E. Pitts, I. J. Tickle, S. P. Wood, C. W. Wu, *Proceedings of the National Academy of Sciences of the United States of America* **1981**, *78*, 4175.
[25] I. Glover, J. Haneef, J. E. Pitts, S. P. Wood, D. Moss, J. Tickle, T. L. Blundell, *Biopolymers* **1983**, *22*, 293.
[26] A. D. MacKerell, *Journal of Computer-Aided Molecular Design* **1988**, *2*, 55.
[27] J. Allen, J. Novotny, J. Martin, G. Heinrich, *Proceedings of the National Academy of Sciences of the United States of America* **1987**, *84*, 2532.

[28] V. Saudek, J. T. Pelton, *Biochemistry* **1990**, *29*, 4509.
[29] S. A. Monks, G. Karagianis, G. J. Howlett, R. S. Norton, *Journal of Biomolecular NMR* **1996**, *8*, 379.
[30] D. J. Cowley, J. M. Hoflack, J. T. Pelton, V. Saudek, *European Journal of Biochemistry* **1992**, *205*, 1099.
[31] H. Minakata, J. W. Taylor, M. W. Walker, R. J. Miller, E. T. Kaiser, *Journal of Biological Chemistry* **1989**, *264*, 7907.
[32] D. F. Mierke, H. Dürr, H. Kessler, G. Jung, *European Journal of Biochemistry* **1992**, *206*, 39.
[33] H. Darbon, J.-M. Bernassau, C. Deleuze, J. Chenu, A. Roussel, C. Cambillau, *European Journal of Biochemistry* **1992**, *209*, 765.
[34] A. Nordmann, M. J. J. Blommers, H. Fretz, T. Arvinte, A. F. Drake, *European Journal of Biochemistry* **1999**, *261*, 216.
[35] A. Bettio, M. C. Dinger, A. G. Beck-Sickinger, *Protein Science* **2002**, *11*, 1834.
[36] D. Sakakibara, A. Sasaki, T. Ikeya, J. Hamatsu, T. Hanashima, M. Mishima, M. Yoshimasu, N. Hayashi, T. Mikawa, M. Walchli, B. O. Smith, M. Shirakawa, P. Guntert, Y. Ito, *Nature* **2009**, *458*, 102.
[37] K. Inomata, A. Ohno, H. Tochio, S. Isogai, T. Tenno, I. Nakase, T. Takeuchi, S. Futaki, Y. Ito, H. Hiroaki, M. Shirakawa, *Nature* **2009**, *458*, 106.
[38] M. Haack, S. Enck, H. Seger, A. Geyer, A. G. Beck-Sickinger, *Journal of the American Chemical Society* **2008**, *130*, 8326.
[39] A. Chattopadhyay, E. London, *Analytical Biochemistry* **1984**, *139*, 408.
[40] M. Peric, M. Alves, B. L. Bales, *Chemistry and Physics of Lipids* **2006**, *142*, 1.
[41] S. Enck, F. Kopp, M. A. Marahiel, A. Geyer, *Organic and Biomolecular Chemistry* **2010**, *8*, 559.
[42] T.-L. Hwang, A. J. Shaka, *Journal of Magnetic Resonance, Series A* **1995**, *112*, 275.
[43] R. Bader, A. Bettio, A. G. Beck-Sickinger, O. Zerbe, *J. Mol. Biol.* **2001**, *305*, 307.
[44] E. T. Kaiser, F. J. Kezdy, *Science* **1984**, *223*, 249.
[45] R. Bader, O. Zerbe, *ChemBioChem* **2005**, *6*, 1520.
[46] M. Fabry, M. Langer, B. Rothen-Rutishauser, H. Wunderli-Allenspach, H. Höcker, A. G. Beck-Sickinger, *European Journal of Biochemistry* **2000**, *267*, 5631.
[47] C. Zou, S. Kumaran, S. Marcovic, R. Walser, O. Zerbe, *ChemBioChem* **2008**, *9*, 2276.
[48] M. B. Doughty, L. Hu, *Biopolymers* **1993**, *33*, 1195.
[49] L. Hu, P. Balse, M. B. Doughty, *J. Med. Chem.* **1994**, *37*, 3622.
[50] S. S. Chu, D. V. Velde, D. Shobe, P. Balse, M. B. Doughty, *Biopolymers* **1995**, *35*, 583.
[51] M. Mutter, T. Wohr, S. Gioria, M. Keller, *Biopolymers* **1999**, *51*, 121.
[52] I. Langmuir, *Journal of the American Chemical Society* **1919**, *41*, 1543.
[53] E. Riedel, *Anorganische Chemie*, 4th ed., de Gruyter, Berlin, New York, **1999**.
[54] C. D. Siebert, *Chemie in unserer Zeit* **2004**, *38*, 320.
[55] C. Eckard, C. Cabrele, H. Wieland, A. Beck-Sickinger, *Molecules* **2001**, *6*, 448.
[56] S. P. Sheikh, R. Håkanson, T. W. Schwartz, *FEBS Letters* **1989**, *245*, 209.
[57] J.-C. Martel, S. St-Pierre, R. Quirion, *Peptides* **1986**, *7*, 55.
[58] A. G. Beck-Sickinger, G. Jung, *Biopolymers* **1995**, *37*, 123.
[59] B. Rist, N. Ingenhoven, L. Scapozza, G. Schnorrenberg, W. Gaida, H. A. Wieland, A. G. Beck-Sickinger, *European Journal of Biochemistry* **1997**, *247*, 1019.
[60] R. M. Söll, M. C. Dinger, I. Lundell, D. Larhammer, A. G. Beck-Sickinger, *European Journal of Biochemistry* **2001**, *268*, 2828.
[61] K. Rudolf, W. Eberlein, W. Engel, H. A. Wieland, K.-D. Willim, M. Entzeroth, W. Wienen, A. G. Beck-Sickinger, H. N. Doods, *Eur. J. Pharmacol.* **1994**, *271*, R11.
[62] H. A. Wieland, W. Engel, W. Eberlein, K. Rudolf, H. N. Doods, *British Journal of Pharmacology* **1998**, *125*, 549.

[63] H. Doods, W. Gaida, H. A. Wieland, H. Dollinger, G. Schnorrenberg, F. Esser, W. Engel, W. Eberlein, K. Rudolf, *European Journal of Pharmacology* **1999**, *384*, R3.
[64] B. Rist, O. Zerbe, N. Ingenhoven, L. Scapozza, C. Peers, P. F. T. Vaughan, R. L. McDonald, H. A. Wieland, A. G. Beck-Sickinger, *FEBS Letters* **1996**, *394*, 169.
[65] C. Gerald, M. W. Walker, L. Criscione, E. L. Gustafson, C. Batzl-Hartmann, K. E. Smith, P. Vaysse, M. M. Durkin, T. M. Laz, D. L. Linemeyer, A. O. Schaffhauser, S. Whitebread, K. G. Hofbauer, R. I. Taber, T. A. Branchek, R. L. Weinshank, *Nature* **1996**, *382*, 168.
[66] Y. Hu, B. T. Bloomquist, L. J. Cornfield, L. B. DeCarr, J. R. Flores-Riveros, L. Friedman, P. Jiang, L. Lewis-Higgins, Y. Sadlowski, J. Schaefer, N. Velazquez, M. L. McCaleb, *Journal of Biological Chemistry* **1996**, *271*, 26315.
[67] C. Cabrele, M. Langer, R. Bader, H. A. Wieland, H. N. Doods, O. Zerbe, A. G. Beck-Sickinger, *Journal of Biological Chemistry* **2000**, *275*, 36043.
[68] C. Cabrele, H. A. Wieland, M. Langer, C. E. Stidsen, A. G. Beck-Sickinger, *Peptides* **2001**, *22*, 365.
[69] C. Cabrele, H. A. Wieland, N. Koglin, C. Stidsen, A. G. Beck-Sickinger, *Biochemistry* **2002**, *41*, 8043.
[70] L. Criscione, P. Rigollier, C. Batzl-Hartmann, H. Rueger, A. Stricker-Krongrad, P. Wyss, L. Brunner, S. Whitebread, Y. Yamaguchi, C. Gerald, R. O. Heurich, M. W. Walker, M. Chiesi, W. Schilling, K. G. Hofbauer, N. Levens, *J. Clin. Invest.* **1998**, *102*, 2136.
[71] H. Rueeger, P. Rigollier, Y. Yamaguchi, T. Schmidlin, W. Schilling, L. Criscione, S. Whitebread, M. Chiesi, M. W. Walker, D. Dhanoa, I. Islam, J. Zhang, C. Gluchowski, *Bioorganic & Medicinal Chemistry Letters* **2000**, *10*, 1175.
[72] C. Drahl, *Chemical and Engineering News* **2009**, *April 13*, 11.
[73] A. G. Beck-Sickinger, H. A. Weland, H. Wittneben, K.-D. Willim, K. Rudolf, G. Jung, *European Journal of Biochemistry* **1994**, *225*, 947.
[74] D. A. Kirby, J. H. Boublik, J. E. Rivier, *Journal of Medicinal Chemistry* **1993**, *36*, 3802.
[75] J. C. Reubi, M. Gugger, B. Waser, J. C. Schaer, *Cancer Res.* **2001**, *61*, 4636.
[76] I. U. Khan, D. Zwanziger, B. I., M. Javed, H. Naseer, S. W. Hyder, A. G. Beck-Sickinger, *Angewandte Chemie International Edition* **2010**, *49*, 1155.
[77] N. Koglin, C. Zorn, R. Beumer, C. Cabrele, C. Bubert, N. Sewald, O. Reiser, A. G. Beck-Sickinger, *Angewandte Chemie International Edition* **2003**, *42*, 202.
[78] P. Tremmel, A. Geyer, *Eur. J. Org. Chem.* **2005**, 3475.
[79] H. Seger, A. Geyer, *Synthesis* **2006**, 3224.
[80] M. E. Vazquez, M. Nitz, J. Stehn, M. B. Yaffe, B. Imperiali, *Journal of the American Chemical Society* **2003**, *125*, 10150.
[81] G. Loving, B. Imperiali, *Journal of the American Chemical Society* **2008**, *130*, 13630.
[82] R. Y. Tsien, *Angewandte Chemie International Edition* **2009**, *48*, 5612.
[83] V. Sharma, D. S. Lawrence, *Angewandte Chemie International Edition* **2009**, *48*, 7290.
[84] C. Moser, G. Bernhardt, J. Michel, H. Schwarz, A. Buschauer, *Can. J. Physiol. Pharmacol.* **2000**, *78*, 134.
[85] K. Wüthrich, *Angewandte Chemie International Edition* **2003**, *42*, 3340.
[86] HyperChem, release 6.03 ed., Hypercube, Inc., Gainesville, FL, **2000**.
[87] P. Stanley, V. Koronakis, C. Hughes, *Microbiol. Mol. Biol. Rev.* **1998**, *62*, 309.
[88] E. M. Driggers, S. P. Hale, J. Lee, N. K. Terrett, *Nature Reviews Drug Discovery* **2008**, *7*, 608.
[89] E. M. Nolan, C. T. Walsh, *ChemBioChem* **2009**, *10*, 34.
[90] H. Kessler, *Angewandte Chemie International Edition* **1982**, *21*, 512.
[91] J. Rizo, L. M. Gierasch, *Annual Review of Biochemistry* **1992**, *61*, 387.
[92] D. G. Udugamasooriya, M. R. Spaller, *Biopolymers* **2008**, *89*, 653.
[93] D. E. Koshland, *Proceedings of the National Academy of Sciences of the United States of America* **1958**, *44*, 98.

[94] J. Clardy, C. T. Walsh, *Nature* **2004**, *432*, 829.
[95] J. Blankenstein, J. Zhu, *European Journal of Organic Chemistry* **2005**, 1949.
[96] C. T. Walsh, *Science* **2004**, *303*, 1805.
[97] F. Kopp, M. A. Marahiel, *Natural Product Reports* **2007**, *24*, 735.
[98] A. Tanovic, S. A. Samel, L.-O. Essen, M. A. Marahiel, *Science* **2008**, *321*, 659.
[99] C. Gilon, D. Halle, M. Chorev, Z. Selincer, G. Byk, *Biopolymers* **1991**, *31*, 745.
[100] H. D. Mootz, M. A. Marahiel, *Journal of Bacteriology* **1997**, *179*, 6843.
[101] J. W. Trauger, R. M. Kohli, H. D. Mootz, M. A. Marahiel, C. T. Walsh, *Nature* **2000**, *407*, 215.
[102] R. M. Kohli, C. T. Walsh, M. D. Burkart, *Nature* **2002**, *418*, 658.
[103] E. J. Prenner, R. N. A. H. Lewis, R. N. McElhaney, *Biochimica et Biophysica Acta* **1999**, *1462*, 201.
[104] K. Shin-ya, K. Wierzba, K.-i. Matsuo, T. Ohtani, Y. Yamada, K. Furihata, Y. Hayakawa, H. Seto, *Journal of the American Chemical Society* **2001**, *123*, 1262.
[105] M.-Y. Kim, H. Vankayalapati, K. Shin-ya, K. Wierzba, L. H. Hurley, *Journal of the American Chemical Society* **2002**, *124*, 2098.
[106] B. K. Hubbard, C. T. Walsh, *Angewandte Chemie International Edition* **2003**, *42*, 730.
[107] A. Blond, J. Péduzzi, C. Goulard, M. J. Chiuchiolo, M. Barthélémy, Y. Prigent, R. A. Salomón, R. N. Farías, F. Moreno, S. Rebuffat, *European Journal of Biochemistry* **1999**, *259*, 747.
[108] M. J. Bayro, J. Mukhopadhyay, G. V. T. Swapna, J. Y. Huang, L.-C. Ma, E. Sineva, P. E. Dawson, G. T. Montelione, R. H. Ebright, *Journal of the American Chemical Society* **2003**, *125*, 12382.
[109] K. J. Rosengren, R. J. Clark, N. L. Daly, U. Goransson, A. Jones, D. J. Craik, *Journal of the American Chemical Society* **2003**, *125*, 12464.
[110] K.-A. Wilson, M. Kalkum, J. Ottesen, J. Yuzenkova, B. T. Chait, R. Landick, T. Muir, K. Severinov, S. A. Darst, *Journal of the American Chemical Society* **2003**, *125*, 12475.
[111] H.-D. Arndt, S. Schoof, J.-Y. Lu, *Angewandte Chemie International Edition* **2009**, *48*, 6770.
[112] R. P. Morris, J. A. Leeds, H. U. Naegeli, L. Oberer, K. Memmert, E. Weber, M. J. LaMarche, C. N. Parker, N. Burrer, S. Esterow, A. E. Hein, E. K. Schmitt, P. Krastel, *Journal of the American Chemical Society* **2009**, *131*, 5946.
[113] L. C. Wieland Brown, M. G. Acker, J. Clardy, C. T. Walsh, M. A. Fischbach, *Proceedings of the National Academy of Sciences* **2009**, *106*, 2549.
[114] R. Liao, L. Duan, C. Lei, H. Pan, Y. Ding, Q. Zhang, D. Chen, B. Shen, Y. Yu, W. Liu, *Chemistry and Biology* **2009**, *16*, 141.
[115] W. L. Kelly, L. Pan, C. Li, *Journal of the American Chemical Society* **2009**, *131*, 4327.
[116] L. A. Wessjohann, E. Ruijter, D. Garcia-Rivera, W. Brandt, *Molecular Diversity* **2005**, *9*, 171.
[117] C. A. Lipinski, F. Lombardo, B. W. Dominy, P. J. Feeney, *Advanced Drug Delivery Reviews* **2001**, *46*, 3.
[118] G. S. Tillotson, *Expert Review of Clinical Pharmacology* **2009**, *2*, 119.
[119] R. C. Moellering, Jr., *Clinical Infectious Diseases* **2006**, *42*, S3.
[120] D. A. P. Levine, *Clinical Infectious Diseases* **2006**, *42*, S5.
[121] P. J. Loll, A. E. Bevivino, B. D. Korty, P. H. Axelsen, *Journal of the American Chemical Society* **1997**, *119*, 1516.
[122] K. C. Nicolaou, R. Hughes, S. Y. Cho, N. Winssinger, H. Labischinski, R. Endermann, *Chemistry - A European Journal* **2001**, *7*, 3824.
[123] M. Baginski, J. Czub, *Current Drug Metabolism* **2009**, *10*, 459.
[124] N. Matsumori, N. Yamaji, S. Matsuoka, T. Oishi, M. Murata, *Journal of the American Chemical Society* **2002**, *124*, 4180.

[125] G. Weckbecker, I. Lewis, R. Albert, H. A. Schmid, D. Hoyer, C. Bruns, *Nature Reviews Drug Discovery* **2003**, *2*, 999.
[126] J. Van Op den bosch, D. Adriaensen, L. Van Nassauw, J.-P. Timmermans, *Regulatory Peptides* **2009**, *156*, 1.
[127] D. F. Veber, R. M. Freidinger, D. S. Perlow, W. J. Paleveda, F. W. Holly, R. G. Strachan, R. F. Nutt, B. H. Arison, C. Homnick, W. C. Randall, M. S. Glitzer, R. Saperstein, R. Hirschmann, *Nature* **1981**, *292*, 55.
[128] W. Bauer, U. Briner, W. Doepfner, R. Haller, R. Huguenin, P. Marbach, T. J. Petcher, J. Pless, *Life Sciences* **1982**, *31*, 1133.
[129] E. Nogales, S. G. Wolf, I. A. Khan, R. F. Luduena, K. H. Downing, *Nature* **1995**, *375*, 424.
[130] J. Goodman, V. Walsh, *The Story of Taxol: Nature and Politics in the Pursuit of an Anti-Cancer Drug*, Cambridge University Press, Cambridge, **2001**.
[131] F. Feyen, F. D. R. Cachoux, J. R. Gertsch, M. Wartmann, K.-H. Altmann, *Accounts of Chemical Research* **2007**, *41*, 21.
[132] T. Rezai, B. Yu, G. L. Millhauser, M. P. Jacobson, R. S. Lokey, *Journal of the American Chemical Society* **2006**, *128*, 2510.
[133] T. Rezai, J. E. Bock, M. V. Zhou, C. Kalyanaraman, R. S. Lokey, M. P. Jacobson, *Journal of the American Chemical Society* **2006**, *128*, 14073.
[134] D. Lamarre, P. C. Anderson, M. Bailey, P. Beaulieu, G. Bolger, P. Bonneau, M. Bos, D. R. Cameron, M. Cartier, M. G. Cordingley, A.-M. Faucher, N. Goudreau, S. H. Kawai, G. Kukolj, L. Lagace, S. R. LaPlante, H. Narjes, M.-A. Poupart, J. Rancourt, R. E. Sentjens, R. St George, B. Simoneau, G. Steinmann, D. Thibeault, Y. S. Tsantrizos, S. M. Weldon, C.-L. Yong, M. Llinas-Brunet, *Nature* **2003**, *426*, 186.
[135] M. Llinas-Brunet, M. D. Bailey, G. Bolger, C. Brochu, A.-M. Faucher, J. M. Ferland, M. Garneau, E. Ghiro, V. Gorys, C. Grand-Maitre, T. Halmos, N. Lapeyre-Paquette, F. Liard, M. Poirier, M. Rheaume, Y. S. Tsantrizos, D. Lamarre, *Journal of Medicinal Chemistry* **2004**, *47*, 1605.
[136] R. Flisiak, A. Parfieniuk, *Expert Opinion on Investigational Drugs* **2010**, *19*, 63.
[137] R. J. Cherney, L. Wang, D. T. Meyer, C.-B. Xue, Z. R. Wasserman, K. D. Hardman, P. K. Welch, M. B. Covington, R. A. Copeland, E. C. Arner, W. F. DeGrado, C. P. Decicco, *Journal of Medicinal Chemistry* **1998**, *41*, 1749.
[138] L. Ruzicka, *Helvetica Chimica Acta* **1926**, *9*, 230.
[139] K. Ziegler, H. Eberle, H. Ohlinger, *Justus Liebig's Annalen der Chemie* **1933**, *504*, 94.
[140] K. Ziegler, *Methoden der Organischen Chemie (Houben-Weyl), Vol. 4/II*, 4th ed., Thieme, Stuttgart, **1955**.
[141] J.-M. Lehn, *Chemistry - A European Journal* **1999**, *5*, 2455.
[142] S. J. Rowan, S. J. Cantrill, G. R. L. Cousins, J. K. M. Sanders, J. F. Stoddart, *Angewandte Chemie International Edition* **2002**, *41*, 898.
[143] R. B. Woodward, E. Logusch, K. P. Nambiar, K. Sakan, D. E. Ward, B. W. Au-Yeung, P. Balaram, L. J. Browne, P. J. Card, C. H. Chen, *Journal of the American Chemical Society* **1981**, *103*, 3210.
[144] R. B. Woodward, B. W. Au-Yeung, P. Balaram, L. J. Browne, D. E. Ward, P. J. Card, C. H. Chen, *Journal of the American Chemical Society* **1981**, *103*, 3213.
[145] R. B. Woodward, E. Logusch, K. P. Nambiar, K. Sakan, D. E. Ward, B. W. Au-Yeung, P. Balaram, L. J. Browne, P. J. Card, C. H. Chen, *Journal of the American Chemical Society* **1981**, *103*, 3215.
[146] N. Sayyadi, D. Skropeta, K. A. Jolliffe, *Organic Letters* **2005**, *7*, 5497.
[147] R. B. Silverman, *The Organic Chemistry of Drug Design and Drug Action*, Elsevier Academic Press, Oxford, **2004**.
[148] H. J. Jacobson, W. H. Stockmayer, *Journal of Chemical Physics* **1950**, *18*, 1600.
[149] P. J. Flory, *Statistical Mechanics of Chain Molecules*, Wiley-Interscience, New York, **1969**.

[150] G. Illuminati, L. Mandolini, *Accounts of Chemical Research* **1981**, *14*, 95.
[151] C. Galli, L. Mandolini, *European Journal of Organic Chemistry* **2000**, 3117.
[152] T. Caruso, C. Donnamaria, A. Artillo, A. Peluso, A. Spinella, G. Monaco, *Journal of Physical Organic Chemistry* **2009**, *22*, 978.
[153] F. C. Lightstone, T. C. Bruice, *Bioinorganic Chemistry* **1998**, *26*, 193.
[154] F. C. Lightstone, T. C. Bruice, *Journal of the American Chemical Society* **1996**, *118*, 2595.
[155] F. C. Lightstone, T. C. Bruice, *Journal of the American Chemical Society* **1997**, *119*, 9103.
[156] R. Cacciapaglia, S. Di Stefano, L. Mandolini, *Journal of the American Chemical Society* **2005**, *127*, 13666.
[157] T. Matsumoto, E. Morishita, T. Shioiri, *Tetrahedron* **2007**, *63*, 8571.
[158] R. F. Service, *Science* **2008**, *321*, 784.
[159] E. H. Cordes, W. P. Jencks, *Journal of the American Chemical Society* **1962**, *84*, 832.
[160] R. W. Layer, *Chemical Reviews* **1963**, *63*, 489.
[161] C. Godoy-Alcántar, A. K. Yatsimirsky, J.-M. Lehn, *Journal of Physical Organic Chemistry* **2005**, *18*, 979.
[162] D. Voet, J. G. Voet, C. W. Pratt, *Lehrbuch der Biochemie*, Wiley-VCH, Weinheim, **2002**.
[163] H. Nakamichi, T. Okada, *Angewandte Chemie International Edition* **2006**, *118*, 4376.
[164] M. Kono, P. W. Goletz, R. K. Crouch, *Biochemistry* **2008**, *47*, 7567.
[165] N. E. Borisova, M. D. Reshetova, Y. A. Ustynyuk, *Chemical Reviews* **2007**, *107*, 46.
[166] R. L. Zuckerman, S. W. Krska, R. G. Bergman, *Journal of the American Chemical Society* **2000**, *122*, 751.
[167] I. M. Goldman, J. K. Larson, J. R. Tretter, E. G. Andrews, *Journal of the American Chemical Society* **1969**, *91*, 4941.
[168] D. C. R. Hockless, L. F. Lindoy, G. F. Swiegers, S. B. Wild, *J. Chem. Soc., Perkin Trans. 2* **1998**, 117.
[169] T. Golakoti, W. Y. Yoshida, S. Chaganty, R. E. Moore, *Journal of Natural Products* **2001**, *64*, 54.
[170] H. Luesch, D. Hoffmann, J. M. Hevel, J. E. Becker, T. Golakoti, R. E. Moore, *The Journal of Organic Chemistry* **2002**, *68*, 83.
[171] R. E. Schwartz, C. F. Hirsch, D. F. Sesin, J. E. Flor, M. Chartrain, R. E. Fromtling, G. H. Harris, M. J. Salvatore, J. M. Liesch, K. Yudin, *Journal of Industrial Microbiology and Biotechnology* **1990**, *5*, 113.
[172] T. Golakoti, J. Ogino, C. E. Heltzel, T. Le Husebo, C. M. Jensen, L. K. Larsen, G. M. L. Patterson, R. E. Moore, S. L. Mooberry, *Journal of the American Chemical Society* **1995**, *117*, 12030.
[173] D. Panda, K. DeLuca, D. Williams, M. A. Jordan, L. Wilson, *Proceedings of the National Academy of Sciences of the United States of America* **1998**, *95*, 9313.
[174] J. E. Becker, R. E. Moore, B. S. Moore, *Gene* **2004**, *325*, 35.
[175] D. E. Ehmann, A. M. Gehring, C. T. Walsh, *Biochemistry* **1999**, *38*, 6171.
[176] N. Gaitatzis, B. Kunze, R. Müller, *Proceedings of the National Academy of Sciences of the United States of America* **2001**, *98*, 11136.
[177] L. Li, W. Deng, J. Song, W. Ding, Q.-F. Zhao, C. Peng, W.-W. Song, G.-L. Tang, W. Liu, *Journal of Bacteriology* **2008**, *190*, 251.
[178] F. Kopp, C. Mahlert, J. Grünewald, M. A. Marahiel, *Journal of the American Chemical Society* **2006**, *128*, 16478.
[179] S. Enck, F. Kopp, M. A. Marahiel, A. Geyer, *ChemBioChem* **2008**, *9*, 2597.
[180] *Novabiochem catalog (applications)*, p. 3.38, application 3-12, **2006/2007**.
[181] A. C. Murphy, M. I. Mitova, J. W. Blunt, M. H. G. Munro, *Journal of Natural Products* **2008**, *71*, 806.
[182] T.-L. Wang, A. J. Shaka, *Journal of Magnetic Resonance Series A* **1995**, *112*, 275.
[183] Y. A. Bare, A. Friedrich, H. Kessler, M. Molter, *Chemische Berichte* **1978**, *111*, 1045.

[184] A. Sandström, H. Baumann, L. Kenne, *J. Chem. Soc., Perkin Trans. 2* **1998**, 809.
[185] I. Ivarsson, C. Sandström, A. Sandström, L. Kenne, *J. Chem. Soc., Perkin Trans. 2* **2000**, 2147.
[186] S. Bekiroglu, L. Kenne, C. Sandström, *The Journal of Organic Chemistry* **2003**, *68*, 1671.
[187] J. N. S. Evans, *Biomolecular NMR spectroscopy*, Oxford University Press, **1995**.
[188] M. Karplus, *Journal of Chemical Physics* **1959**, 11.
[189] *Thieme Roempp Online: Karplus equation*, Thieme, **2007**.
[190] M. Hesse, H. Meier, B. Zeeh, *Spektroskopische Methoden in der organischen Chemie*, 7th ed., Thieme, Stuttgart, **2005**.
[191] V. F. Bystrov, *Progr. NMR Spec.* **1976**, *10*, 41.
[192] G. Govil, R. V. Hosur, *Conformation of Biological Molecules, New Results from NMR*, Springer, Berlin, Heidelberg, New York, **1982**.
[193] K. G. R. Pachler, *Spectrochimica Acta* **1964**, *20*, 581.
[194] M. T. Cung, M. Marraud, *Biopolymers* **1982**, *21*, 953.
[195] G. Melacini, Q. Zhu, M. Goodman, *Biochemistry* **1997**, *36*, 1233.
[196] V. Pavone, G. Gaeta, A. Lombardi, F. Nastri, O. Maglio, C. Isernia, M. Saviano, *Biopolymers* **1996**, *38*, 705.
[197] P. W. Atkins, *Physikalische Chemie*, 2nd ed., VCH, Weinheim, New York, **1996**.
[198] K. K. Frederick, M. S. Marlow, K. G. Valentine, A. J. Wand, *Nature* **2007**, *448*, 325.
[199] R. M. Levy, L. Y. Zhang, E. Gallicchio, A. K. Felts, *Journal of the American Chemical Society* **2003**, *125*, 9523.
[200] B. Lu, C. F. Wong, *Biopolymers* **2005**, *79*, 277.
[201] Y. Harano, R. Roth, M. Kinoshita, *Chemical and Physical Letters* **2006**, *79*, 275.
[202] H. Gohlke, G. Klebe, *Angewandte Chemie International Edition* **2002**, *41*, 2644.
[203] J. Dolenc, R. Baron, J. H. Missimer, M. O. Steinmetz, W. F. van Gunsteren, *ChemBioChem* **2008**, *9*, 1749.
[204] L. Mandolini, *Journal of the American Chemical Society* **1978**, *100*, 550.
[205] L. M. Amzel, *Proteins: Structure, Function, and Genetics* **1997**, *28*, 144.
[206] M. Mammen, E. I. Shakhnovich, G. M. Whitesides, *Journal of Organic Chemistry* **1998**, *63*, 3168.
[207] G. Ercolani, *Journal of Organic Chemistry* **1999**, *64*, 3350.
[208] M.-C. Kuo, W. A. Gibbons, *Biochemistry* **1979**, *18*, 5855.
[209] M.-C. Kuo, W. A. Gibbons, *The Journal of Biological Chemistry* **1979**, *254*, 6278.
[210] M.-C. Kuo, W. A. Gibbons, *Biophysical Journal* **1980**, *32*, 807.
[211] M.-C. Kuo, T. Drakenberg, W. A. Gibbons, *Journal of the American Chemical Society* **1980**, *102*, 520.
[212] N. Zhou, P. Mascagni, W. A. Gibbons, N. Niccolai, C. Rossi, H. Wyssbrod, *J. Chem. Soc., Perkin Trans. 2* **1985**, 581.
[213] A. P. Tonge, P. Murray-Rust, W. A. Gibbons, L. K. McLachlan, *Journal of Computational Chemistry* **1988**, *9*, 522.
[214] J. W. Trauger, R. M. Kohli, C. T. Walsh, *Biochemistry* **2001**, *40*, 7092.
[215] X. Bu, X. Wu, G. Xie, Z. Guo, *Organic Letters* **2002**, *4*, 2893.
[216] C. Qin, X. Bu, X. Wu, Z. Guo, *Journal of Combinatorial Chemistry* **2003**, *5*, 353.
[217] C. Qin, X. Bu, X. Zhong, N. L. J. Ng, Z. Guo, *Journal of Combinatorial Chemistry* **2004**, *6*, 398.
[218] H. Lin, D. A. Thayer, C.-H. Wong, C. T. Walsh, *Chemistry and Biology* **2004**, *11*, 1635.
[219] H. Hu, J. Xue, B. M. Swarts, Q. Wang, Q. Wu, Z. Guo, *Journal of Medicinal Chemistry* **2009**, *52*, 2052.
[220] S. Laiken, M. Printz, L. C. Craig, *The Journal of Biological Chemistry* **1969**, *244*, 4454.
[221] R. M. Kohli, J. W. Trauger, D. Schwarzer, M. A. Marahiel, C. T. Walsh, *Biochemistry* **2001**, *40*, 7099.

[222] S. K. Arora, *The Journal of Antibiotics* **1981**, *34*, 462.
[223] V. Helmetag, S. A. Samel, M. G. Thomas, M. A. Marahiel, L.-O. Essen, *FEBS Journal* **2009**, *276*, 3669.
[224] F. Yokokawa, A. Inaizumi, T. Shioiri, *Tetrahedron Letters* **2001**, *42*, 5903.
[225] C. Wagner, W. Graninger, E. Presterl, C. Joukhadar, *Pharmacology* **2006**, *78*, 161.
[226] L. Forlani, E. Marianucci, P. E. Todesco, *J. Chem. Res.* **1984**, 126.
[227] J. A. Chudek, R. Foster, D. Young, *J. Chem. Soc., Perkin Trans. 2* **1985**, 1285.
[228] D. A. Evans, G. Borg, K. A. Scheidt, *Angewandte Chemie International Edition* **2002**, *41*, 3188.
[229] R. J. Hooley, T. Iwasawa, J. Rebek, *Journal of the American Chemical Society* **2007**, *129*, 15330.
[230] A. Stern, W. A. Gibbons, L. C. Craig, *Journal of the American Chemical Society* **1969**, *91*, 2794.
[231] H. Morita, Y. Yun, K. Takeya, H. Itokawa, *Tetrahedron Letters* **1994**, *35*, 9593.
[232] H. Itokawa, Y. Yun, H. Morita, K. Takeya, K. Yamada, *Plant. Med.* **1995**, *61*, 561.
[233] H. Morita, Y. Sook Yun, K. Takeya, H. Itokawa, M. Shiro, *Tetrahedron* **1995**, *51*, 5987.
[234] P. Sonnet, L. Petit, D. Marty, J. Guillon, J. Rochette, J.-D. Brion, *Tetrahedron Letters* **2001**, *42*, 1681.
[235] *Novabiochem catalog (methods)*, p. 3.38, method 3-49, **2006/2007**.
[236] A. Moulin, J. Martinez, J.-A. Fehrentz, *J. Pept. Sci.* **2007**, *13*, 1.
[237] B. Hu, K. Xiao, J. K. Shen, *Chinese Chemical Letters* **2006**, *17*, 1162.
[238] S. Chandrasekhar, M. S. Kumar, B. Muralidhar, *Tetrahedron Letters* **1998**, *39*, 909.
[239] C. Douat, A. Heitz, J. Martinez, J.-A. Fehrentz, *Tetrahedron Letters* **2000**, *41*, 37.
[240] F. Diness, J. Beyer, M. Meldal, *QSAR Comb. Sci.* **2004**, *23*, 130.
[241] J. C. Kappel, G. Barany, *J. Pept. Sci.* **2005**, *11*, 525.
[242] M. S. Scott, A. C. Lucas, C. A. Luckhurst, J. C. Prodger, D. J. Dixon, *Organic & Biomolecular Chemistry* **2006**, *4*, 1313.
[243] T. A. Knappe, U. Linne, L. Robbel, M. A. Marahiel, *Chemistry & Biology* **2009**, *16*, 1290.
[244] S. Everts, *Chemical and Engineering News* **2010**, *88*, 38.
[245] S. Hiller, G. Wider, L. L. Imbach, K. Wüthrich, *Angewandte Chemie International Edition* **2008**, *47*, 977.
[246] C. T. Walsh, E. M. Nolan, *Proceedings of the National Academy of Sciences* **2008**, *105*, 5655.
[247] B. Johnson, H. Anker, F. Meleney, *Science* **1945**, *102*, 376.
[248] K. J. Stone, J. L. Strominger, *Proceedings of the National Academy of Sciences of the United States of America* **1971**, *68*, 3223.
[249] D. R. Storm, J. L. Strominger, *Journal of Biological Chemistry* **1973**, *248*, 3940.
[250] A. M. Gehring, E. DeMoll, J. D. Fetherston, I. Mori, G. F. Mayhew, F. R. Blattner, C. T. Walsh, R. D. Perry, *Chemistry & Biology* **1998**, *5*, 573.
[251] D. A. Miller, C. T. Walsh, *Biochemistry* **2001**, *40*, 5313.
[252] R. S. Roy, A. M. Gehring, J. C. Milne, P. J. Belshaw, C. T. Walsh, *Natural Product Reports* **1999**, *16*, 249.
[253] D. Schwarzer, R. Finking, M. A. Marahiel, *Natural Product Reports* **2003**, *20*, 275.
[254] B. Silakowski, H. U. Schairer, H. Ehret, B. Kunze, S. Weinig, G. Nordsiek, P. Brandt, H. Blöcker, G. Höfle, S. Beyer, R. Müller, *Journal of Biological Chemistry* **1999**, *274*, 37391.
[255] L. Tang, S. Shah, L. Chung, J. Carney, L. Katz, C. Khosla, B. Julien, *Science* **2000**, *287*, 640.
[256] L. Du, M. Chen, C. Sanchez, B. Shen, *FEMS Microbiology Letters* **2000**, *189*, 171.
[257] H. Onaka, M. Nakaho, K. Hayashi, Y. Igarashi, T. Furumai, *Microbiology* **2005**, *151*, 3923.
[258] S. W. Lee, D. A. Mitchell, A. L. Markley, M. E. Hensler, D. Gonzalez, A. Wohlrab, P. C. Dorrestein, V. Nizet, J. E. Dixon, *Proceedings of the National Academy of Sciences* **2008**, *105*, 5879.

[259] O. A. Pierrat, A. Maxwell, *Biochemistry* **2005**, *44*, 4204.
[260] G. Rosendahl, S. Douthwaite, *Nucl. Acids Res.* **1994**, *22*, 357.
[261] D. E. Vanderwall, S. M. Lui, W. Wu, C. J. Turner, J. W. Kozarich, J. Stubbe, *Chemistry & Biology* **1997**, *4*, 373.
[262] A. Bertram, G. Pattenden, *Natural Product Reports* **2007**, *24*, 18.
[263] E. M. Webb, A. Marquet, R. R. Mendel, F. Rebeille, A. G. Smith, *Natural Product Reports* **2007**, *24*, 988.
[264] T. P. Begley, A. Chatterjee, J. W. Hanes, A. Hazra, S. E. Ealick, *Current Opinion in Chemical Biology* **2008**, *12*, 118.
[265] A. Hazra, A. Chatterjee, T. P. Begley, *Journal of the American Chemical Society* **2009**, *131*, 3225.
[266] F. J. Leeper, A. G. Smith, *Natural Product Reports* **2007**, *24*, 923.
[267] H. Steinmetz, N. Glaser, E. Herdtweck, F. Sasse, H. Reichenbach, G. Höfle, *Angewandte Chemie International Edition* **2004**, *43*, 4888.
[268] R. Preusentanz, O. Pando, L. A. Wessjohann, *Nachrichten aus der Chemie* **2010**, *58*, 526.
[269] G. Kaur, M. Hollingshead, S. Holbeck, V. Schauer-Vukasinovic, R. F. Camalier, A. Dömling, S. Agarwal, *Biochemistry Journal* **2006**, *396*, 235.
[270] M. W. Khalil, F. Sasse, H. Lünsdorf, Y. A. Elnakady, H. Reichenbach, *ChemBioChem* **2006**, *7*, 678.
[271] A. Ullrich, Y. Chai, D. Pistorius, Y. A. Elnakady, J. E. Herrmann, K. J. Weissmann, U. Kazmaier, R. Müller, *Angewandte Chemie International Edition* **2009**, *48*, 4422.
[272] A. W. Patterson, H. M. Peltier, J. A. Ellman, *The Journal of Organic Chemistry* **2008**, *73*, 4362.
[273] I. R. Vlahov, Y. Wang, P. J. Kleindl, C. P. Leamon, *Bioorganic & Medicinal Chemistry Letters* **2008**, *18*, 4558.
[274] T. Schluep, P. Gunawan, L. Ma, G. S. Jensen, J. Duringer, S. Hinton, W. Richter, J. Hwang, *Clin. Cancer Res.* **2009**, *15*, 181.
[275] B. Han, K. L. McPhail, H. Gross, D. E. Goeger, S. L. Mooberry, W. H. Gerwick, *Tetrahedron* **2005**, *61*, 11723.
[276] Z. Jin, *Natural Product Reports* **2006**, *23*, 464.
[277] B. L. Marquez, K. S. Watts, A. Yokochi, M. A. Roberts, P. Verdier-Pinard, J. I. Jimenez, E. Hamel, P. J. Scheuer, W. H. Gerwick, *Journal of Natural Products* **2002**, *65*, 866.
[278] A. V. Ramaswamy, C. M. Sorrels, W. H. Gerwick, *Journal of Natural Products* **2007**, *70*, 1977.
[279] A. Bayer, S. Freund, G. Nicholson, G. Jung, *Angewandte Chemie International Edition* **1993**, *32*, 1336.
[280] Y.-M. Li, J. C. Milne, L. L. Madison, R. Kolter, C. T. Walsh, *Science* **1996**, *274*, 1188.
[281] J. C. Milne, R. S. Roy, A. C. Eliot, N. L. Kelleher, A. Wokhlu, B. Nickels, C. T. Walsh, *Biochemistry* **1999**, *38*, 4768.
[282] N. L. Kelleher, C. L. Hendrickson, C. T. Walsh, *Biochemistry* **1999**, *38*, 15623.
[283] J. L. Vizan, Hernandez-Chico, I. del Castillo, F. Moreno, *EMBO Journal* **1991**, *10*, 467.
[284] T. Takita, T. Muraoka, T. Nakatani, A. Fujii, Y. Umezawa, H. Naganawa, *J. Antibiot.* **1978**, *31*, 801.
[285] M. J. Absalon, W. Wu, J. W. Kozarich, J. Stubbe, *Biochemistry* **1995**, *34*, 2076.
[286] R. M. Burger, *Chemical Reviews* **1998**, *98*, 1153.
[287] S. M. Hecht, *Journal of Natural Products* **1999**, *63*, 158.
[288] C. M. Ireland, A. R. Durso, R. A. Newman, M. P. Hacker, *The Journal of Organic Chemistry* **1982**, *47*, 1807.
[289] B. M. Degnan, C. J. Hawkins, M. F. Lavin, E. J. McCaffrey, D. L. Parry, A. L. van den Brenk, D. J. Watters, *J Med. Chem.* **1989**, *32*, 1349.

[290] E. W. Schmidt, J. T. Nelson, D. A. Rasko, S. Sudek, J. A. Eisen, M. G. Haygood, J. Ravel, *Proceedings of the National Academy of Sciences of the United States of America* **2005**, *102*, 7315.
[291] B. F. Milne, P. F. Long, A. Starcevic, D. Hranueli, M. Jaspars, *Organic & Biomolecular Chemistry* **2006**, *4*, 631.
[292] M. S. Donia, B. J. Hathaway, S. Sudek, M. G. Haygood, M. J. Rosovitz, J. Ravel, E. W. Schmidt, *Nat. Chem. Biol.* **2006**, *2*, 729.
[293] M. C. Bagley, J. W. Dale, E. A. Merritt, X. Xiong, *Chemical Reviews* **2005**, *105*, 685.
[294] R. A. Hughes, C. J. Moody, *Angewandte Chemie International Edition* **2007**, *46*, 7930.
[295] M. A. Ciufolini, D. Lefranc, *Natural Product Reports* **2010**, *27*, 330.
[296] O. Delgado, H. M. Müller, T. Bach, *Chemistry - A European Journal* **2008**, *14*, 2322.
[297] S. Baumann, S. Schoof, S. D. Harkal, H.-D. Arndt, *Journal of the American Chemical Society* **2008**, *130*, 5664.
[298] S. Baumann, S. Schoof, M. Bolten, C. Haering, M. Takagi, K. Shin-ya, H.-D. Arndt, *Journal of the American Chemical Society* **2010**, online; DOI: 10.1021/ja909317n.
[299] S. E. Heffron, F. Jurnak, *Biochemistry* **1999**, *39*, 37.
[300] A. Parmeggiani, I. M. Krab, S. Okamura, R. C. Nielsen, J. Nyborg, P. Nissen, *Biochemistry* **2006**, *45*, 6846.
[301] J. F. Pagano, M. J. Weinstein, H. A. Stout, R. Donovick, *Antibiot. Annu.* **1955-1956**, 554.
[302] T. Prange, A. Ducruix, C. Pascard, J. Lunel, *Nature* **1977**, *265*, 189.
[303] C. Zhang, J. Occi, P. Masurekar, J. F. Barrett, D. L. Zink, S. Smith, R. Onishi, S. Ha, O. Salazar, O. Genilloud, A. Basilio, F. Vicente, C. Gill, E. J. Hickey, K. Dorso, M. Motyl, S. B. Singh, *Journal of the American Chemical Society* **2008**, *130*, 12102.
[304] T. Sasaki, T. Otani, H. Matsumoto, N. Unemi, *The Journal of Antibiotics* **1998**, *51*, 715.
[305] H. Jayasuriya, K. Herath, J. G. Ondeyka, C. Zhang, D. L. Zink, M. Brower, F. P. Gailliot, J. Greene, G. Birdsall, J. Venugopal, M. Ushio, B. Burgess, G. Russotti, A. Walker, M. Hesse, A. Seeley, B. Junker, N. Connors, O. Salazar, O. Genilloud, K. Liu, P. Masurekar, J. F. Barrett, S. B. Singh, *J Antibiot* **2007**, *60*, 554.
[306] C. Zhang, K. Herath, H. Jayasuriya, J. G. Ondeyka, D. L. Zink, J. Occi, G. Birdsall, J. Venugopal, M. Ushio, B. Burgess, P. Masurekar, J. F. Barrett, S. B. Singh, *Journal of Natural Products* **2009**, *72*, 841.
[307] K. C. Nicolaou, J. S. Chen, D. J. Edmonds, A. A. Estrada, *Angewandte Chemie International Edition* **2009**, *48*, 660.
[308] A. Hantzsch, *Berichte der deutschen chemischen Gesellschaft* **1888**, *21*, 942.
[309] M. Jesberger, T. P. Davis, L. Barner, *Synthesis* **2003**, 1929.
[310] U. Schmidt, P. Gleich, R. Utz, *Synthesis* **1986**, *12*, 992.
[311] G. R. Pettit, P. S. Nelson, C. W. Holzapfel, *The Journal of Organic Chemistry* **1985**, *50*, 2654.
[312] M. W. Bredenkamp, C. W. Holzapfel, W. J. van Zyl, *Synthetic Communications* **1990**, *20*, 2235.
[313] E. Aguilar, A. I. Meyers, *Tetrahedron Letters* **1994**, *35*, 2473.
[314] E. A. Merritt, M. C. Bagley, *Synthesis* **2007**, 3535.
[315] K. C. Nicolaou, B. S. Safina, M. Zak, S. H. Lee, M. Nevalainen, M. Bella, A. A. Estrada, C. Funke, F. J. Zecri, S. Bulat, *Journal of the American Chemical Society* **2005**, *127*, 11159.
[316] K. C. Nicolaou, M. Zak, B. S. Safina, A. A. Estrada, S. H. Lee, M. Nevalainen, *Journal of the American Chemical Society* **2005**, *127*, 11176.
[317] Y. Hamada, M. Shibata, T. Sugiura, S. Kato, T. Shioiri, *The Journal of Organic Chemistry* **1987**, *52*, 1252.
[318] K. Ninomiya, H. Satoh, T. Sugiyama, M. Shinomiya, R. Kuroda, *Chemical Communications* **1996**, 1825.
[319] L. M. Martin, B.-H. Hu, *Tetrahedron Letters* **1999**, *40*, 7951.

[320] H. Sugiyama, F. Yokokawa, T. Shioiri, *Tetrahedron* **2003**, *59*, 6579.
[321] E. B. Veale, J. E. O'Brien, T. McCabe, T. Gunnlaugsson, *Tetrahedron* **2008**, *64*, 6794.
[322] F. Yokokawa, H. Sameshima, Y. In, K. Minoura, T. Ishida, T. Shioiri, *Tetrahedron* **2002**, *58*, 8127.
[323] F. Yokokawa, H. Sameshima, D. Katagiri, T. Aoyama, T. Shioiri, *Tetrahedron* **2002**, *58*, 9445.
[324] M. Sani, G. Fossati, F. Huguenot, M. Zanda, *Angewandte Chemie International Edition* **2007**, *46*, 3526.
[325] A. J. Fatiadi, *Synthesis* **1976**, 65.
[326] A. J. Fatiadi, *Synthesis* **1976**, 133.
[327] E. N. Silva da Junior, *Synlett* **2008**, 149.
[328] D. L. Evans, D. K. Minster, U. Jordis, S. M. Hecht, A. L. Mazzu, Jr., A. I. Meyers, *The Journal of Organic Chemistry* **1978**, *44*, 497.
[329] M. Groarke, M. A. McKervey, H. Moncrieff, M. Nieuwenhuyzen, *Tetrahedron Letters* **2000**, *41*, 1279.
[330] B. Wagner, D. Schumann, U. Linne, U. Koert, M. A. Marahiel, *Journal of the American Chemical Society* **2006**, *128*, 10513.
[331] S.-L. You, J. W. Kelly, *Journal of Organic Chemistry* **2003**, *68*, 9506.
[332] M. Z. A. Badr, M. M. Aly, A. M. Fahmy, M. E. Y. Mansour, *Bulletin of the Chemical Society of Japan* **1981**, *54*, 1844.
[333] D. R. Williams, P. D. Lowder, Y.-G. Gu, D. A. Brooks, *Tetrahedron Letters* **1997**, *38*, 331.
[334] K. C. Nicolaou, B. Zou, D. H. Dethe, D. B. Li, D. Y.-K. Chen, *Angewandte Chemie International Edition* **2006**, *118*, 7950.
[335] Y. Huang, H. Gan, S. Li, J. Xu, X. Wu, H. Yao, *Tetrahedron Letters* **2010**, *51*, 1751.
[336] D. Castagnolo, M. Pagano, M. Bernardini, M. Botta, *Synlett* **2009**, 2093.
[337] M. Yoshimatsu, T. Yamamoto, A. Sawa, T. Kato, G. Tanabe, O. Muraoka, *Organic Letters* **2009**, *11*, 2952.
[338] P. Wipf, S. Venkatraman, *Journal of Organic Chemistry* **1996**, *61*, 8004.
[339] M. Riedrich, S. Harkal, H.-D. Arndt, *Angewandte Chemie International Edition* **2007**, *46*, 2701.
[340] J.-Y. Lu, M. Riedrich, M. Mikyna, H.-D. Arndt, *Angewandte Chemie International Edition* **2009**, *48*, 8137.
[341] E. Riego, D. Hernández, F. Albericio, M. Álvarez, *Synthesis* **2005**, 1907.
[342] E. Biron, J. Chatterjee, H. Kessler, *Organic Letters* **2006**, *8*, 2417.
[343] J. R. Davies, P. D. Kane, C. J. Moody, *Tetrahedron* **2004**, *60*, 3967.
[344] T. D. Gordon, J. Singh, P. E. Hansen, B. A. Morgan, *Tetrahedron Letters* **1993**, *34*, 1901.
[345] R. A. Hughes, S. P. Thompson, L. Alcaraz, C. J. Moody, *Journal of the American Chemical Society* **2005**, *127*, 15644.
[346] M. C. Bagley, K. Chapaneri, J. W. Dale, X. Xiong, J. Bower, *The Journal of Organic Chemistry* **2005**, *70*, 1389.
[347] P. Lafargue, P. Guenot, J.-P. Lellouche, *Synlett* **1995**, 171.
[348] T. Sakamoto, H. Nagata, Y. Kondo, M. Shiraiwa, H. Yamanaka, *Chemical and Pharmaceutical Bulletin* **1987**, *35*, 823.
[349] A. Spieß, G. Heckmann, T. Bach, *Synlett* **2003**, 131.
[350] O. Delgado, G. Heckmann, H. M. Müller, T. Bach, *Journal of Organic Chemistry* **2006**, *71*, 4599.
[351] H. M. Müller, O. Delgado, T. Bach, *Angewandte Chemie International Edition* **2007**, *46*, 4771.
[352] A. Dondoni, G. Fantin, M. Fogagnolo, A. Medici, P. Pedrini, *The Journal of Organic Chemistry* **1988**, *53*, 1748.
[353] C. J. Moody, *Chemical Communications* **2004**, 1341.

[354] A. Dömling, W. Richter, *Molecular Diversity* **2005**, *9*, 141.
[355] H. M. Peltier, J. P. McMahon, A. W. Patterson, J. A. Ellman, *Journal of the American Chemical Society* **2006**, *128*, 16018.
[356] U. Schöllkopf, *Angewandte Chemie International Edition in English* **1977**, *16*, 339.
[357] B. Henkel, B. Beck, B. Westner, B. Mejat, A. Dömling, *Tetrahedron Letters* **2003**, *44*, 8947.
[358] A. Dömling, B. Beck, U. Eichelberger, S. Sakamuri, S. Menon, Q.-Z. Chen, Y. Lu, L. A. Wessjohann, *Angewandte Chemie International Edition* **2006**, *45*, 7235.
[359] A. Dömling, I. Ugi, *Angewandte Chemie* **2000**, *39*, 3168.
[360] T. Belhadj, A. Nowicki, C. J. Moody, *Synlett* **2006**, 3033.
[361] M. C. Kimber, C. J. Moody, *Chemical Communications* **2008**, 591.
[362] L. C. Vishwakarma, O. D. Stringer, F. A. Davis, *Organic Syntheses* **1988**, *66*, 203.
[363] S. Hanessian, B. Vanasse, *Canadian Journal of Chemistry* **1993**, *71*, 4101.
[364] K. C. Nicolaou, B. S. Safina, M. Zak, A. A. Estrada, S. H. Lee, *Angewandte Chemie International Edition* **2004**, *43*, 5087.
[365] K. C. Nicolaou, M. Zak, B. S. Safina, C. E. Lee, A. A. Estrada, *Angewandte Chemie International Edition* **2004**, *43*, 5092.
[366] K. C. Nicolaou, M. Nevalainen, M. Zak, S. Bulat, M. Bella, B. S. Safina, *Angewandte Chemie International Edition* **2003**, *42*, 4318.
[367] P. T. Nyffeler, C.-H. Liang, K. M. Koeller, C.-H. Wong, *Journal of the American Chemical Society* **2002**, *124*, 10773.
[368] A. Geyer, F. Moser, *European Journal of Organic Chemistry* **2000**, 1113.
[369] P. Tremmel, Ph.D. thesis, University of Regensburg **2004**.
[370] S. Eckhardt, Ph.D. thesis, Phillips-University (Marburg), **2009**.
[371] T. Kubota, *Journal of Biochemistry* **1941**, *34*, 119.
[372] S. I. F. S. Martins, W. M. F. Jongen, M. A. J. S. van Boekel, *Trends in Food Science & Technology* **2000**, *11*, 364.
[373] D. R. Cremer, M. Vollenbroeker, K. Eichner, *Eur. Food Res. Technol.* **2000**, *211*, 400.
[374] P. Tremmel, A. Geyer, *Journal of the American Chemical Society* **2002**, *124*, 8548.
[375] P. Tremmel, A. Geyer, *Angewandte Chemie International Edition* **2004**, *16*, 5913.
[376] B. Eckhardt, Ph.D. thesis, Philipps-University (Marburg), **2009**.
[377] B. Eckhardt, W. Grosse, L.-O. Essen, A. Geyer, *Proceedings of the National Academy of Science of the United States of America* **2010**, *accepted*.
[378] P. Tremmel, J. Brand, V. Knapp, A. Geyer, *European Journal of Organic Chemistry* **2003**, 878.
[379] T. F. Braish, P. L. Fuchs, *Synthetic Communications* **1986**, *16*, 111.
[380] E. J. Corey, A. Venkateswarlu, *Journal of the American Chemical Society* **1972**, *94*, 6190.
[381] R. West, P. Nowakowski, P. Boudjouk, *Journal of the American Chemical Society* **1976**, *98*, 5620.
[382] T. P. Mawhinney, M. A. Madson, *The Journal of Organic Chemistry* **1982**, *47*, 3336.
[383] H. Sugiyama, F. Yokokawa, T. Shioiri, *Organic Letters* **2000**, *2*, 2149.
[384] K. S. Ramasamy, R. Bandaru, D. Averett, *The Journal of Organic Chemistry* **2000**, *65*, 5849.
[385] R. S. Brown, J. Dowden, C. Moreau, B. V. L. Potter, *Tetrahedron Letters* **2002**, *43*, 6561.
[386] S. Chandrasekhar, B. Mahipal, M. Kavitha, *The Journal of Organic Chemistry* **2009**, *74*, 9531.
[387] I. M. Goldman, *The Journal of Organic Chemistry* **1969**, *34*, 1979.
[388] C. Hilf, F. Bosold, K. Harms, M. Marsch, G. Boche, *Chemische Berichte* **1999**, *130*, 1213.
[389] S.-L. You, H. Razawi, J. W. Kelly, *Angewandte Chemie International Edition* **2003**, *42*, 83.
[390] N. Nakajima, M. Ubukata, *Tetrahedron Letters* **1997**, *38*, 2099.
[391] H. Seger, Ph.D. thesis, Philipps-University (Marburg), **2008**.
[392] R. Hörger, Ph.D. thesis, Philipps-University (Marburg), **2007**.

[393] M. T. Molina, C. del Valle, A. M. Escribano, J. Ezquerra, C. Pedregal, *Tetrahedron* **1993**, *49*, 3801.
[394] M. Lauz, Ph.D. thesis, Philipps-University (Marburg), **2009**.
[395] Y.-Y. Yeung, S. Hong, E. J. Corey, *Journal of the American Chemical Society* **2006**, *128*, 6310.
[396] B. Danieli, G. Lesma, P. D., A. Sacchetti, A. Silvani, A. Virdis, *Organic Letters* **2004**, *6*, 493.
[397] D. Stead, P. O'Brien, A. J. Sanderson, *Organic Letters* **2005**, *7*, 4459.
[398] A. T. Khan, E. Mondal, *Synlett* **2003**, 694.
[399] S. Kim, S. M. Jacobo, C.-T. Chang, S. Bellone, W. S. Powell, J. Rokach, *Tetrahedron Letters* **2004**, *45*, 1973.
[400] A. Iida, H. Okazaki, T. Misaki, M. Sunagawa, T. Sasaki, Y. Tanabe, *Journal of Organic Chemistry* **2006**, *71*, 5380.
[401] C. M. König, K. Harms, U. Koert, *Organic Letters* **2007**, *9*, 4777.
[402] K. C. Nicolaou, S. E. Webber, *Synthesis* **1986**, *1986*, 453.
[403] E. B. Segal, *Chemical Health and Safety* **2000**, *January/February*, 18.
[404] S. J. Shimshock, R. E. Waltermire, P. DeShong, *Journal of the American Chemical Society* **1991**, *113*, 8791.
[405] A. S. Pilcher, D. K. Hill, S. J. Shimshock, R. E. Waltermire, P. DeShong, *The Journal of Organic Chemistry* **1992**, *57*, 2492.
[406] K. N. Houk, A. Jabbari, H. K. Hall, C. Aleman, *The Journal of Organic Chemistry* **2008**, *73*, 2674.
[407] T. W. Greene, P. G. M. Wuts, *Protective groups in organic synthesis.*, 3rd ed., Wiley, New York, **1999**.
[408] A. Dondoni, A. Marra, *Chemical Reviews* **2004**, *104*, 2557.
[409] D. M. Clode, *Chemical Reviews* **1979**, *79*, 491.
[410] C. B. Reese, *Tetrahedron* **1978**, *34*, 3143.
[411] R. Albert, K. Dax, R. Pleschko, A. E. Stütz, *Carbohydrate Research* **1985**, *137*, 282.
[412] S. Hanessian, Ed., *Preparative Carbohydrate Chemistry*, Marcel Dekker, Inc., New York, **1997**.
[413] S. Saito, A. Kuroda, K. Tanaka, R. Kimura, *Synlett* **1996**, 231.
[414] P. Magnus, T. Gallagher, *Journal of the Chemical Society, Chemical Communications* **1984**, 389.
[415] W. Braje, J. Frackenpohl, H. M. R. Hoffmann, *Tetrahedron* **1998**, *54*, 3495.
[416] M. Daumas, Y. Vo-Quang, L. Vo-Quang, F. Le Goffie, *Synthesis* **1989**, 64.
[417] F. Sarabia, A. Sanchez-Ruiz, S. Chammaa, *Bioorganic and Medicinal Chemistry* **2005**, *13*, 1691.
[418] E. J. Corey, E. Winter, *Journal of the American Chemical Society* **1963**, *85*, 2677.
[419] E. J. Corey, P. B. Hopkins, *Tetrahedron Letters* **1982**, *23*, 1979.
[420] M. Adiyaman, S. P. Khanapure, S. W. Hwang, J. Rokach, *Tetrahedron Letters* **1995**, *36*, 7367.
[421] M. Adiyaman, Y.-J. Jung, S. Kim, G. Saha, W. S. Powell, G. A. Fitzgerald, J. Rokach, *Tetrahedron Letters* **1999**, *40*, 4019.
[422] M. Ando, H. Ohhara, K. Takase, *Chemistry Letters* **1986**, 879.
[423] J. L. King, B. A. Posner, K. T. Mak, N.-C. Yang, *Tetrahedron Letters* **1987**, *28*, 3919.
[424] F. W. Eastwood, K. J. Harrington, J. S. Josan, J. L. Pura, *Tetrahedron Letters* **1970**, *11*, 5223.
[425] S. Hanessian, A. Bargiotti, M. LaRue, *Tetrahedron Letters* **1978**, *19*, 737.
[426] H. Weidmann, W. Timpe, N. Wolf, *Carbohydrate Research* **1972**, *25*, 67.
[427] H. Itoh, K. Aoki, T. Matsumoto, *Bulletin of the Chemical Society of Japan* **1985**, *58*, 777.
[428] J. A. J. M. Vekemans, G. A. M. Franken, C. W. M. Dapperens, E. F. Godefroi, G. J. F. Chittenden, *The Journal of Organic Chemistry* **1988**, *53*, 627.

[429] P. J. Garegg, B. Samuelsson, *Synthesis* **1979**, 469.
[430] P. J. Garegg, B. Samuelsson, *Synthesis* **1979**, 813.
[431] J. A. J. M. Vekemans, C. W. M. Dapperens, R. Claessen, A. M. J. Koten, E. F. Godefroi, G. J. F. Chittenden, *The Journal of Organic Chemistry* **1990**, *55*, 5336.
[432] O. Mitsunobu, M. Wada, T. Sano, *Journal of the American Chemical Society* **1972**, *94*, 679.
[433] O. Mitsunobu, *Synthesis* **1981**, 1.
[434] M. C. Viaud, P. Rollin, *Synthesis* **1990**, 130.
[435] C. J. Schwörer, M. Oberthür, *European Journal of Organic Chemistry* **2009**, *2009*, 6129.
[436] S. Bräse, C. Gil, K. Knepper, V. ZImmermann, *Angewandte Chemie International Edition* **2005**, *44*, 5188.
[437] D. H. R. Barton, M. Bénéchie, F. Khuong-Huu, P. Potier, Reyna-Pinedo, *Tetrahedron Letters* **1982**, *23*, 651.
[438] O. J. Varela, A. Fernández Cirelli, R. M. De Lederkremer, *Carbohydrate Research* **1982**, *100*, 424.
[439] J. Bigorra, J. Font, C. Ochoa de Echagüen, R. M. Ortuno, *Tetrahedron* **1993**, *49*, 6717.
[440] J. D. More, S. N. Finney, *Organic Letters* **2002**, *4*, 3001.
[441] N. Umino, T. Iwakuma, M. Ikezaki, N. Itoh, *Chem. Pharm. Bull.* **1978**, *26*, 2897.
[442] M. Krishnamurty, W. Li, B. M. Moore II, *Bioorganic and Medicinal Chemistry* **2004**, *12*, 393.
[443] D. G. Brown, R. A. Urbanek, T. M. Bare, F. M. McLaren, C. L. Horchler, M. Murphy, G. B. Steelman, J. R. Empfield, J. M. Forst, K. J. Herzog, W. Xiao, M. C. Dyroff, C.-M. C. Lee, S. Trivedi, K. L. Neilson, R. A. Keith, *Bioorganic & Medicinal Chemistry Letters* **2003**, *13*, 3553.
[444] D. Enders, H. Eichenauer, *Tetrahedron Letters* **1977**, *18*, 191.
[445] S. Martinez, E. Trepat, M. Moreno-Manas, R. Sebastián, A. Vallribera, I. Mata, E. Molins, *ARKIVOC* **2007**, 170.
[446] T. S. Cooper, A. S. Larigo, P. Laurent, C. J. Moody, A. K. Takle, *Synlett* **2002**, 1730.
[447] F. Yokokawa, H. Sameshima, T. Shioiri, *Synlett* **2001**, 986.
[448] J. Rush, C. R. Bertozzi, *Organic Letters* **2005**, *8*, 131.
[449] O. Berteau, A. Guillot, A. Benjdia, S. Rabot, *Journal of Biological Chemistry* **2006**, *281*, 22464.
[450] I. S. Carrico, B. L. Carlson, C. R. Bertozzi, *Nat Chem Biol* **2007**, *3*, 321.
[451] B. Junker, A. Walker, M. Hesse, M. Lester, J. Christensen, N. Connors, *Biotechnology Progress* **2009**, *25*, 176.
[452] P. Hrnciar, Y. Ueda, S. Huang, J. E. Leet, J. J. Bronson, *Journal of Organic Chemistry* **2002**, *67*, 8789.
[453] A. Regueiro-Ren, Y. Ueda, *Journal of Organic Chemistry* **2002**, *67*, 8699.
[454] A. Regueiro-Ren, B. N. Naidu, X. Zheng, T. W. Hudyma, T. P. Connolly, J. D. Matiskella, Y. Zhang, O. K. Kim, M. E. Sorenson, M. Pucci, J. Clark, J. J. Bronson, Y. Ueda, *Bioorganic & Medicinal Chemistry Letters* **2004**, *14*, 171.
[455] B. N. Naidu, M. E. Sorenson, T. Hudyma, X. Zheng, Y. Zhang, J. J. Bronson, M. J. Pucci, J. M. Clark, Y. Ueda, *Bioorganic & Medicinal Chemistry Letters* **2004**, *14*, 3743.
[456] B. N. Naidu, M. E. Sorenson, Y. Zhang, O. K. Kim, J. D. Matiskella, J. A. Wichtowski, T. P. Connolly, W. Li, K. S. Lam, J. J. Bronson, M. J. Pucci, J. M. Clark, Y. Ueda, *Bioorganic & Medicinal Chemistry Letters* **2004**, *14*, 5573.
[457] B. N. Naidu, M. E. Sorenson, J. J. Bronson, M. J. Pucci, J. M. Clark, Y. Ueda, *Bioorganic & Medicinal Chemistry Letters* **2005**, *15*, 2069.
[458] B. N. Naidu, M. E. Sorenson, J. D. Matiskella, W. Li, J. B. Sausker, Y. Zhang, T. P. Connolly, K. S. Lam, J. J. Bronson, M. J. Pucci, H. Yang, Y. Ueda, *Bioorganic & Medicinal Chemistry Letters* **2006**, *16*, 3545.

[459] W. Li, S. Huang, X. Liu, J. E. Leet, J. L. Cantone, K. S. Lam, *Bioorganic & Medicinal Chemistry Letters* **2008**, *18*, 4051.
[460] L. Xu, A. K. Farthing, J. F. Dropinski, P. T. Meinke, C. McCallum, P. S. Leavitt, E. J. Hickey, L. Colwell, J. Barrett, K. Liu, *Bioorganic & Medicinal Chemistry Letters* **2009**, *19*, 3531.
[461] S. N. Fischer, Diploma thesis, Philipps-University (Marburg), **2010**.
[462] K. C. Nicolaou, A. A. Estrada, G. C. Freestone, S. H. Lee, X. Alvarez-Mico, *Tetrahedron* **2007**, *63*, 6088.
[463] K. L. Constantine, L. Mueller, S. Huang, S. Abid, K. S. Lam, W. Li, J. E. Leet, *Journal of the American Chemical Society* **2002**, *124*, 7284.
[464] K. L. Constantine, L. Mueller, S. Huang, S. Abid, K. S. Lam, W. Li, J. E. Leet, *Journal of the American Chemical Society* **2002**, *124*, 14810.
[465] X. S. Huang, X. Liu, K. L. Constantine, J. E. Leet, V. Roongta, *Magnetic Resonance in Chemistry* **2007**, *45*, 447.
[466] T. Y. S. But, P. H. Toy, *Chemistry - An Asian Journal* **2007**, *2*, 1341.
[467] M. Saiah, M. Bessodes, K. Antonakis, *Tetrahedron Letters* **1992**, *33*, 4317.
[468] B. H. Lipshutz, T. A. Miller, *Tetrahedron Letters* **1990**, *31*, 5253.
[469] O. Mitsunobu, R. Kimura, Y. Fujisawa, *Bulletin of the Chemical Society of Japan* **1972**, *45*, 245.
[470] T. Tsunoda, Y. Yamamiya, Y. Kawamura, S. Ito, *Tetrahedron Letters* **1995**, *36*, 2529.
[471] A. Dondoni, G. Fantin, M. Fogagnolo, A. Medici, P. Pedrini, *The Journal of Organic Chemistry* **1989**, *54*, 702.
[472] T. Ooi, D. Uraguchi, J. Morikawa, K. Maruoka, *Organic Letters* **2000**, *2*, 2015.
[473] M. Oba, S. Koguchi, K. Nishiyama, *Tetrahedron* **2004**, *60*, 8089.
[474] Y. G. Gololobov, I. N. Zhumurova, L. F. Kasukhin, *Tetrahedron* **1981**, *37*, 437.
[475] Y. G. Gololobov, *Tetrahedron* **1992**, *48*, 1353.
[476] M. Tamaki, G. Han, V. J. Hruby, *Journal of Organic Chemistry* **2001**, *66*, 1038.

Aus is‘
und gar is‘
und schad‘ is‘
dass‘ wahr is‘

(bavarian saying)

Danksagung

Diese Arbeit wäre nicht möglich gewesen ohne die Unterstützung einer Menge Menschen auf fachlicher und nichtfachlicher Ebene. Deswegen möchte ich mich an dieser Stelle ganz herzlich bedanken:

Prof. Dr. Armin Geyer danke ich für die hervorragende Betreuung dieser Arbeit. Er hat mir die Möglichkeit gegeben, mehrere Themen aus verschiedenen Bereichen parallel bearbeiten zu können, und mir dabei große Freiheit in der Planung und Durchführung gewährt. Vielen Dank auch für die spontane Behebung des Druckluft-Lärmproblems in unserem Labor sowie für alle nicht-chemischen Gespräche über Bergwandern, über Fahrräder (insbesondere Fahrradunfälle), über die Nachteile von vollgefederten Mountainbikes, über den Halbmarathon, und vieles mehr.

Prof. Dr. Mohamed A. Marahiel danke ich für die erfolgreiche Kooperation auf dem Gebiet der Cycloiminopeptide, die vielen hilfreichen Tipps und für die Übernahme des Zweitgutachtens.

Prof. Dr. Karl-Michael Weitzel sowie *Prof. Dr. Paultheo von Zezschwitz* danke ich dafür, dass sie sich als Prüfer für die Disputation zur Verfügung gestellt haben.

Prof. Dr. Annette G. Beck-Sickinger (Universität Leipzig) danke ich für die erfolgreiche Kooperation auf dem Gebiet der Neuropeptid Y-Analoga und für die Einladung zum Arbeitstreffen in Leipzig.

Prof. Dr. Indrapal Singh Aidhen (IITM Madras) sei herzlich gedankt für die vielen fachlichen und nichtfachlichen Gespräche, die vielen nützlichen Tips bei Syntheseproblemen sowie für seine regelmäßigen Versuche, uns „Zusammenschreiber“ zu beruhigen. *Just relax!*

Prof. Dr. Martha C. Lux-Steiner (Helmholtz-Zentrum Berlin/Freie Universität Berlin) danke ich für die engagierte Leitung unserer Südtiroler Retina-Arbeitsgruppe der Studienstiftung, viele hervorragende fachliche Diskussionen und für das tolle Arbeitstreffen samt Verköstigung in Berlin.

Dr. Markus Oberthür danke ich für das Korrekturlesen eines großen Teils dieser Arbeit und für die vielen hilfreichen Synthesetipps.

Dr. Uwe Linne danke ich herzlich für die große und geduldige Hilfe bei unzähligen problematischen HPLC-MS- und ESI-MS-Messungen der Cycloiminopeptide, sowie für die Durchführung der präparativen HPLC-Läufe.

Dr. Michael Haack (Universität Leipzig) danke ich für die Synthesen der NPY-Analoga sowie für die Aktivitätsmessungen.

Michael Marsch danke ich für die tolle Betreuung der Computer bei uns im Arbeitskreis und für die schnelle Behebung aller Probleme. Ein großes Dankeschön auch für die schnelle Bestellung und Installation des Farblasers sowie für die unendliche Geduld, mit der er meine „Kristalle“ (die Anführungszeichen waren in den meisten Fällen berechtigt) begutachtet und zu messen versucht hat.

Dr. Florian Kopp muss an dieser Stelle ganz besonders hervorgehoben werden - er hat mit unglaublichem Gespür die Kooperation auf dem Gebiet der Cycloiminopeptide ins Rollen gebracht und damit sehr viel zum Gelingen dieser Arbeit beigetragen.

Den Mitarbeitern der Dienstleistungs- und Serviceabteilungen des Fachbereichs danke ich für die Versorgung mit Labormaterial und Chemikalien jeder Art sowie für die Durchführung einer Unmenge verschiedener analytischer Messungen.

Ganz herzlich möchte ich mich bei den aktuellen und ehemaligen Mitgliedern der Arbeitsgruppen *Geyer* und *Oberthür* bedanken:

Ferdinand Bosold, der auch tapfer täglich und wetterunabhängig mit dem Fahrrad anreist (sehr motivierend!) danke ich für den morgendlichen Aufschließdienst. Ich habe dafür in Deinem Labor abends immer alles ausgeschaltet. Nochmals Entschuldigung dafür, dass ich bei unserer Aufführung von „Rudolph the Red-Nosed Reindeer“ so lachen musste.

Nikolas Bugdahn danke ich für seine gesunde, ruhige Einstellung zu alltäglichen Problemen mit den Molekülen (*„What shall's!“*), und für die wunderbare regelmäßige Aktualisierung der lebensnotwendigen Kaffee- und Milchvorräte.

Björn Eckhardt danke ich für die Klettergeschichten, für die nützlichen Tipps zum Bewältigen längerer Laufstrecken und wie man dabei am besten nicht angeleinte Hunde umbringt, sowie dafür dass ich seinen Bachelorstudenten betreuen durfte.

Sebastian Fischer und *Frauke Messik* danke ich für die Gesellschaft in den Kaffeepausen und für die Versorgung mit etlichen Chemikalien.

Rolf Hörger, dem Hardcore-FC-Bayern-Fan und wandelndem Lexikon an Polt-Sprüchen, danke ich für die Aufnahme in sein Labor zu Beginn der Diplomarbeit, für die spektakuläre Zerstörung einer vollen 2L-Rotweinflasche, sowie für die Einladung nach Würzburg.

Anita Jansen de Salazar, am Schluss meine Leidensgenossin im 34 °C heißen Schreibraum, danke ich für die geduldige Einweisung in die Festphasensynthese und für diverse Chemikalien und Säulen.

Christoph Klotz danke ich für die zuverlässigen regelmäßigen Fußball-Updates und für die Entdeckung desjenigen Menschen in der Mensa, der nur einen Arm zum Essen benutzt, was bei vielen Mensabesuchen über die Qualität des Essens hinweghalf.

Matthias Körling, während der heißen Schlussphase mein Laborkollege, danke ich für die vielen Gespräche über Fahrräder, sowie weitere wichtige Dinge des Lebens und für die vielen guten Sprüche sowie Bilder (ich will den Kraken sehen!).

Dominik Kohr danke ich ebenfalls für die tollen Fahrradgeschichten (wir sind hier halt mal der Arbeitskreis der Fahrradverrückten - es gibt bei uns sogar einen Verbandkasten für Fahrräder!) und für die Erheiterung aller durch etliche „nach-der-Feier“-Katastrophen mit Langzeitfolge für die Gesundheit sowie für die Ausstattung der Wohnung.

Markus Pfitzenmaier, mit dem ich mir ganz am Anfang das Labor und ganz am Schluss den Schreibraum geteilt habe, danke ich für… (wo fange ich nur an?) das gewissenhafte Korrekturlesen des NPY-Kapitels dieser Arbeit (alle Fehler, die man dort jetzt noch findet, gehen auf seine Kappe), die vielen Hilfestellungen bei NMR-Messungen, das Einweisen in die Geheimnisse des AV-600-Spektrometers und der Wasserunterdrückung. Außerdem für unzählige Diskussionen über Klassiker aus Film und Filmmusik, über spezifische Oxidationszahlen (und warum sie etwas mit dem Backen von Waffeln zu tun haben) sowie für die stundenlangen philosophische Betrachtungen der Spezies der Dauerurlauber. Die Sprüche sind schon jetzt legendär! Um nochmal auf die Fahrräder zu sprechen zu kommen: Nur das Fahrrad ist ein forschungskonformes Fortbewegungsmittel, denn der Last Bus fährt zu früher Stunde!

Yana Raeva danke ich für die schnelle Durchführung etlicher analytischer Messungen.

Andreas Roeder, der sich mit mir die Aufgabe des Blödchen-Kurierdienstes teilte, danke ich für das oftmalige abendliche mit-Durchhalten am Fachbereich und für die spektakulären Demonstrationen von *Kohr*scher Krankheit.

Susanne Schellenberg, der heimlichen Chefin auf A6, sei hier ganz herzlich gedankt für die hervorragende und unkomplizierte Organisation jeglichen „Papierkrams“ bei uns im Arbeitskreis. Ich hoffe dass ich mich für die viele Arbeit mit meinem regelmäßigem Blödchen-Kurierdienst etwas revanchieren konnte! Habe auch extra immer die Blödchen mit „parma Schinken“ gekauft (aber einmal Schinken hätte doch auch gereicht…).

Peter Schüler danke ich für das sehr hilfreiche Korrekturlesen, für die Gesellschaft in den Kaffeepausen und dafür, dass er mit seiner unerschütterlichen Ruhe Panikattacken abwenden oder zumindest lindern kann.

Timm Schlosser, mit dem ich zwei spektakuläre Praktika betreut und überlebt habe, danke ich für seine vielen tollen Sprüche und dafür dass er sich bereit erklärt hat, in den nächsten Jahren den leuchtenden Nikolaus am Gebäude außen anzubringen. Vielen Dank auch für die ganzen Gespräche über Fachliches und nicht-Fachliches sowie für die sehr realistischen (= pessimistisch-ironischen) Einschätzungen von Situationen jeder Art.

Clemens Schwörer, dem Herrn der Pullover-Querstreifen, danke ich für das gewissenhafte Korrekturlesen sowie für hilfreiche Synthesetipps. Du warst der Einzige, der meine Bärenmarke-Bär-Prophezeihung uneingeschränkt lustig fand, vielen Dank für diese Unterstützung!

Harald Seger danke ich für die Synthese der Dha=Tap-Bausteine, für die vielen tollen Vertiefergeschichten (die Boc-Schutzgruppe wird durch Behandlung mit B_2O_3 und Aktivkohle (C) angebracht, sind ja schon mal die richtigen Buchstaben), für das gemeinsame bayerische Fluchen und das Krachmachen mit Blechblasinstrumenten.

Felix Weiher, der zum Glück die Ehre der Fahrradfahrer sehr hoch hält, danke ich für das regelmäßige Auffüllen der Getränke im Kaffeeraum, für die Mit-Durchsetzung der erlösenden MULL-Liste und für die tollen Geschichten aus dem Viehtransporter.

Ralph Wieneke, dem „Mann mit Privatleben“ und mit dem lustigen Doktorhut, danke ich für das oftmalige abendliche Mit-Durchhalten am Fachbereich und für diverse Synthesetipps. Ein tolles Erlebnis war der Überfall von A.K.H. („Hallllooo!“) auf Dich nach dem Hartmann-Symposion. Falsche Zeit, falscher Ort, falsches Reiseziel!

Meinen Vertiefungsstudenten *Philipp Bron*, *Sebastian Fischer*, *Fabian Fries*, *Peter Göbel*, *Markus Hellmund*, *Jan Kirchberg* und *Romina Sütterlin* sei herzlich gedankt für ihre engagierte Arbeit im Labor, mit der sie alle zum Gelingen dieser Arbeit beigetragen haben.

Ganz besonders hervorgehoben werden müssen meine beiden Laborkolleginnen (ich würde Euch gerne auch weiter unten nochmal erwähnen, aber dann schafft es der Drucker heute nicht mehr bis zur Schließung des Kopierladens):

Sonja Eckhardt und *Miriam Lauz*, meine Laborkolleginnen (die beiden müssen hier zusammen genannt werden) haben sich hier ein riesengroßes Dankeschön verdient: für die tolle Laborzeit mit Musik und dem ganzen QUAKorama, für die Ausflüge nach München und Würzburg, für die Spieleabende mit Phase 10 - gefrusteten Mitspielern, für das geduldige Anhören meines Genöles, für die Verköstigung mit Lasagne und Schweizer Schokolade, etliche Mitfahrgelegenheiten und vieles mehr. Die Spruchwand in Labor 6216 wird nachfolgende Generationen an diese Zeit erinnern. Danke für Eure selbstlosen Last-Minute-Einsätze zur Formatierung gewisser Word-Dateien. Jetzt ist das Drama schon zweimal passiert. Ich verspreche, dass ich bei der nächsten Gelegenheit einen VHS-Kurs belegen werde!

Je mehr gearbeitet wird, desto mehr ist es notwendig, für den notwendigen Ausgleich zu sorgen, und ohne meine Freunde wäre das nicht möglich gewesen:

Andreas Jacob danke ich für die stets frischen Gerüchte, die ich dann immer ausgeschmückt sowie dramatisiert und sie dann dem gesamten Arbeitskreis weitererzählt habe, und für die vielen Ausflüge zur Geologen-Cafete.

Christian König danke ich für das tägliche und wetterunabhängige Fahrradfahren rauf zur Uni, für den Spaß im Stockkampf-Kurs, für unzählige Abende in diverse Kneipen, für die Feiern in Offenbach und für die vielen hilfreichen Synthesetipps. Unvergessen sind auch die Hardcore-Trekking-Urlaube zusammen mit *Andreas Schlecker* in Schweden, auf Kreta und auf Korsika sowie der Toskana-Urlaub. Alles wird aber getoppt von der dreitägigen Odyssee Korsika→Marburg mit diversen NICHT-fliegenden Verkehrsmitteln. *I believe I can fly…*

Florian und *Katharina Kopp* - vielen Dank auch für die die tolle Woche in San Diego, die Klavier+Geige-Aktionen im Musizierhaus und was alles sonst so während des Studiums unternommen wurde. Wir sehen uns bald beim Wildmoser!

Angela und *Roland Raabe* danke ich für das tolle Wochenende in Düsseldorf und für die Feuerzangenbowlen-Abende.

Regina Reul danke ich dafür, dass sie unseren regelmäßigen Konsum überwürzter Speisen, knoblauchgesättigter Soßen und wirklich schlechter Filmklassiker (aber es sind Klassiker) in ihrer Wohnung bereitwillig ertragen hat.

Anne Rieß danke ich für die Versorgung mit Schweizer Schokolade, die ganzen Kindergartengeschichten und für das kurzfristige Einspringen am Klavier.

Andreas Schlecker danke ich für die Organisation der Trekking-Urlaube, für diverse lustige Kneipenabende mit und ohne Fanta sowie für seine Halte-durch-Mails.

Martina Werner danke ich für die regelmäßigen Touren durch Geheimtipps der Münchner Café-Szene.

Christian und *Nadine Wirges* danke ich für die Verköstigung in Darmstadt und - ebenfalls - für das Mitwirken bei etlichen abendfüllenden Veranstaltungen.

Inga Bödeker, *Matthias Edén*, *Thomas Hede*, *Christine Kipfer* och *Martje van Bruggen*: tack ska ni ha för de fantaskiska månader i Stockholm på studenthemmet och universitet med ondsdagspubar, många turer med tunnelbanan och bussen till slussen, alla långa timmar där vi satte och snackade på caféet, och framför allt för den helt otroliga resan till norrskenens land!

Meinen Mitbewohnern während der Doktorarbeit *Stephan Becker*, *Christina Heine*, *Matthias Klune* und *Sandra Mahler* danke ich sehr herzlich für die WG-Abende und diverse Freizeitaktionen, welche das (ab und zu notwendige) Abschalten von der Arbeit ermöglicht haben.

Für inspirierenden musikalischen Ausgleich haben besonders folgende Freunde gesorgt:

Katharina Vogt (Universität Dresden) - danke für die Vermittlung einer Stelle bei der JSB in der Spielzeit 2008. Die Arbeitsphase und der Auftritt in der Berliner Philharmonie waren fantastische Erlebnisse und sind eigentlich nicht zu toppen.

Meine 8-Minuten-Ruhm-Bandcrew: *Benjamin Cassel*, *Alex Cevolani*, *Anne-Sophie Sättler* und *Johanna Schwarz* - vielen Dank für die schöne gemeinsame Zeit mit gelungenen Bandkonzerte und tollen Proben.

Nicola Niehage, meiner „Pult-Ehefrau“ im SSO, danke ich für die lustige Zeit während unzähliger Proben und Konzerte sowie für das spontane Geigenduo zur Begleitung schwedisch Tanzender.

Jan-Sebastian Kittel, *Tina Kremer*, *Emily Stehling* und *Vera Vaßmann* von ROAM Mainz - vielen Dank für Eure Organisation der Mainzer Arbeitsphasen mit unvergesslichen Wochenenden, sowie für die unkomplizierte Unterbringung bei Euch.

Das Wichtigste zum Schluss - Bei meiner Familie möchte ich mich ganz herzlich für die schönen Wochenenden in München und für die große Unterstützung während des gesamten Studiums und der Doktorarbeit danken. Liebe(r) *Leonhard*, *Norbert*, *Renate* und *Severin*: Danke dass Ihr es mir nie übelgenommen habt, dass die viele Arbeit sowie mein „Zweitberuf“ des Musikers dazu geführt haben, dass ich ich allzuselten zu Besuch war.